

Subhransu Sekhar Dash
M. Arun Bhaskar
Bijaya Ketan Panigrahi
Swagatam Das *Editors*

Artificial Intelligence and Evolutionary Computations in Engineering Systems

Proceedings of ICAIECES 2015

Advances in Intelligent Systems and Computing

Volume 394

Series editor

Janusz Kacprzyk, Polish Academy of Sciences, Warsaw, Poland
e-mail: kacprzyk@ibspan.waw.pl

About this Series

The series “Advances in Intelligent Systems and Computing” contains publications on theory, applications, and design methods of Intelligent Systems and Intelligent Computing. Virtually all disciplines such as engineering, natural sciences, computer and information science, ICT, economics, business, e-commerce, environment, healthcare, life science are covered. The list of topics spans all the areas of modern intelligent systems and computing.

The publications within “Advances in Intelligent Systems and Computing” are primarily textbooks and proceedings of important conferences, symposia and congresses. They cover significant recent developments in the field, both of a foundational and applicable character. An important characteristic feature of the series is the short publication time and world-wide distribution. This permits a rapid and broad dissemination of research results.

Advisory Board

Chairman

Nikhil R. Pal, Indian Statistical Institute, Kolkata, India
e-mail: nikhil@isical.ac.in

Members

Rafael Bello, Universidad Central “Marta Abreu” de Las Villas, Santa Clara, Cuba
e-mail: rbellop@uclv.edu.cu

Emilio S. Corchado, University of Salamanca, Salamanca, Spain
e-mail: escorchado@usal.es

Hani Hagrass, University of Essex, Colchester, UK
e-mail: hani@essex.ac.uk

László T. Kóczy, Széchenyi István University, Győr, Hungary
e-mail: koczy@sze.hu

Vladik Kreinovich, University of Texas at El Paso, El Paso, USA
e-mail: vladik@utep.edu

Chin-Teng Lin, National Chiao Tung University, Hsinchu, Taiwan
e-mail: ctlin@mail.nctu.edu.tw

Jie Lu, University of Technology, Sydney, Australia
e-mail: Jie.Lu@uts.edu.au

Patricia Melin, Tijuana Institute of Technology, Tijuana, Mexico
e-mail: epmelin@hafsamx.org

Nadia Nedjah, State University of Rio de Janeiro, Rio de Janeiro, Brazil
e-mail: nadia@eng.uerj.br

Ngoc Thanh Nguyen, Wroclaw University of Technology, Wroclaw, Poland
e-mail: Ngoc-Thanh.Nguyen@pwr.edu.pl

Jun Wang, The Chinese University of Hong Kong, Shatin, Hong Kong
e-mail: jwang@mae.cuhk.edu.hk

More information about this series at <http://www.springer.com/series/11156>

Subhransu Sekhar Dash · M. Arun Bhaskar
Bijaya Ketan Panigrahi · Swagatam Das
Editors

Artificial Intelligence and Evolutionary Computations in Engineering Systems

Proceedings of ICAIECES 2015

Editors

Subhransu Sekhar Dash
Department of Electrical and Electronics
Engineering
SRM Engineering College
Kattankulathur, Tamil Nadu
India

Bijaya Ketan Panigrahi
IIT Delhi
New Delhi
India

M. Arun Bhaskar
Department of Electrical and Electronics
Engineering
Velammal Engineering College
Chennai, Tamil Nadu
India

Swagatam Das
Indian Statistical Institute
Kolkata
India

ISSN 2194-5357

ISSN 2194-5365 (electronic)

Advances in Intelligent Systems and Computing

ISBN 978-81-322-2654-3

ISBN 978-81-322-2656-7 (eBook)

DOI 10.1007/978-81-322-2656-7

Library of Congress Control Number: 2015951771

Springer New Delhi Heidelberg New York Dordrecht London

© Springer India 2016

This work is subject to copyright. All rights are reserved by the Publisher, whether the whole or part of the material is concerned, specifically the rights of translation, reprinting, reuse of illustrations, recitation, broadcasting, reproduction on microfilms or in any other physical way, and transmission or information storage and retrieval, electronic adaptation, computer software, or by similar or dissimilar methodology now known or hereafter developed.

The use of general descriptive names, registered names, trademarks, service marks, etc. in this publication does not imply, even in the absence of a specific statement, that such names are exempt from the relevant protective laws and regulations and therefore free for general use.

The publisher, the authors and the editors are safe to assume that the advice and information in this book are believed to be true and accurate at the date of publication. Neither the publisher nor the authors or the editors give a warranty, express or implied, with respect to the material contained herein or for any errors or omissions that may have been made.

Printed on acid-free paper

Springer (India) Pvt. Ltd. is part of Springer Science+Business Media (www.springer.com)

Preface

This AISC volume contains the papers presented at the International Conference on Artificial Intelligence and Evolutionary Computations in Engineering Systems (ICAIECES) held during 22 and 23 April, 2015 at Velammal Engineering College, Chennai, India. ICAIECES 2015 received 312 paper submissions from various countries across the globe. After a rigorous peer-review process, 123 full length articles were accepted for oral presentation at the conference. This corresponds to an acceptance rate of 42 % and is intended for maintaining the high standards of the conference proceedings. The papers included in this LNAISC volume cover a wide range of topics on Genetic Algorithms, Evolutionary Programming, and Evolution Strategies such as AIS, DE, PSO, ACO, BFA, HS, SFLA, Artificial Bees and Fireflies Algorithm, Parallel Computation, Membrane, Grid, Cloud, DNA, Mobile Computing, Computer Networks and Security, Data Structures and Algorithms, Data Compression, Data Encryption, Data Mining, Digital Signal Processing, Digital Image Processing, Watermarking, Security and Cryptography, AI methods in Telemedicine and eHealth, Document Classification and Information Retrieval, Optimization Techniques, and their applications for solving problems in these areas.

In the conference, separate sessions were arranged for delivering the keynote address by eminent members from various academic institutions and industries. Four keynote lectures were given on 22 and 23 April, 2014. On the first day, Dr. Bale V. Reddy, Professor and Chair, Faculty of Engineering and Applied Science, University of Ontario, Canada gave a talk on “Research Advances in Natural Gas, Biomass and Solar Power Generation Systems and Energy Management” and in the post-lunch session, Dr. B.K. Panigarhi, Associate Professor, Department of Electrical Engineering, IIT Delhi, gave a lecture on “Optimization of Relay Operation” and covered various optimization techniques and their applications to power systems. On the second day, Dr. Ramazan Bayindir, Professor, Department of Electrical and Electronics Engineering, Gazi University, Turkey, gave a talk on “A Comprehensive Study on Microgrid: Modelling, Control, Stability” and in the post-lunch session, Dr. Swagatam Das, Assistant Professor, Electronics and Communication Sciences Unit, Indian

Statistical Institute, Kolkata, gave a lecture on “Differential Evolutionary Algorithm and its Application to Engineering Systems” and clarified the queries raised by the participants. All these lectures generated great interest among the participants of ICAIECES 2014 in paying more attention to these important topics in their research work.

We take this opportunity to thank the authors of all the submitted papers for their hard work, adherence to the deadlines, and for suitably incorporating the changes suggested by the reviewers. The quality of a refereed volume depends mainly on the expertise and dedication of the reviewers. We are indebted to the Program Committee members for their guidance and coordination in organizing the review process.

We are indebted to the Chairman, Chief Executive Officer, Advisor, Principal, Faculty members, and Administrative Personnel of Velammal Engineering College, Chennai, for encouraging us to organize the conference on such a grand scale. Also, we thank Mr. Aninda Bose, Springer India, for the suggestions in bringing out this AISC series. We thank all the participants for their interest and enthusiastic involvement. Finally, we thank all the volunteers whose tireless efforts in meeting the deadlines and arranging every detail meticulously made sure that the conference could run smoothly. We hope the readers of these proceedings find the papers useful, inspiring, and enjoyable.

Contents

Content-Based Load Balancing Using Web Clusters and Service Rankings	1
T.N. Anitha and R. Balakrishna	
A Fast Adaptive Kalman Filtering Algorithm for Speech Enhancement Under Stationary Noise Environment.	11
C.N. Prabhavathi and K.M. Ravikumar	
Reliability Assessment and Economic Evaluation of Offshore Wind Farm Using Stochastic Probability	25
Ahmed M. Atallah, Almoataz Y. Abdelaziz, Mohamed Ali, R.K. Saket and O.P. Bharti	
Charge Pump with Improved High-Swing Cascode Current Source for Accurate Current Matching in DPLL.	39
D.S. Rajeshwari, P.V. Rao and V. Rajesh	
Recent Research and Various Techniques Available for Efficiency Improvement of IGCC Power Plants	49
Ruchi Pandey, V.K. Sethi, Mukesh Pandey and Maneesh Choubey	
An Involuntary Data Extraction and Information Summarization Expending Ontology	59
R. Deepa and R. Manicka Chezian	
DWT–SVD-Based Watermarking Scheme Using Optimization Technique.	69
Sarthak Nandi and V. Santhi	
Fireworks Algorithm-Based Maximum Power Point Tracking for Uniform Irradiation as Well as Under Partial Shading Condition	79
K. Sangeetha, T. Sudhakar Babu and N. Rajasekar	

Design of Low Power Efficient Median Filter for Noise Reduction in Image	89
M. Vinothini and B. Syed Ibrahim	
A Cycle Detection-Based Efficient Approach for Constructing Spanning Trees Directly from Nonregular Graphic Sequences.	97
Prantik Biswas, Shahin Shabnam, Abhisek Paul and Paritosh Bhattacharya	
Differential Illumination Enhancement Technique for a Nighttime Video	111
G. Abirami and S. Padmavathi	
Low-Cost Appliance Control System for Home Automation and Energy Management Using Image Processing	125
Nagaraj Shet, C. Shreesh, P.V. Rao and Abdullah Gubbi	
Design of Wireless Sensor Network for Submarine Detection	135
Anjali Arunan and R.D. Aryadevi	
Underground Tunnel Detection Across Border Areas	151
K.V. Nibi, K.A. Unnikrishna Menon and Preeja Pradeep	
Communication Network of Wide Area Measurement System for Real-Time Data Collection on Smart Micro Grid	163
Varma C. Prakash, P. Sivraj and K.K. Sasi	
Accoustic Modeling for Development of Accented Indian English ASR.	173
Partho Mandal, Gaurav Ojha, Anupam Shukla and S.S. Agrawal	
Improved Identity Anonymization Using Hashed-TOR Network	185
Gaurav Ojha, Rakesh Singh and Anupam Shukla	
A Tokenized Binding Update Scheme for Next Generation Proxy IP Mobility	193
P.N. Anbarasi and Senthilkumar Mathi	
VLSI Implementation and Analysis of Kidney Stone Detection from Ultrasound Image by Level Set Segmentation and MLP-BP ANN Classification	209
K. Viswanath and R. Gunasundari	
Simulation Framework for Modeling Magnetic Induction Based Wireless Underground Channel	229
P. Ajith, K.A. Unnikrishna Menon and Vrinda N. Menon	
A Generic Algorithm for Segmenting a Specified Region of Interest Based on Chanvese's Algorithm and Active Contours.	239
Pranshu Agrawal, Gaurav Ojha and Mahua Bhattacharya	

Static Noise Margin Analysis of 6T SRAM Cell 249
 Abinkant A. Jose and Nikhitha C. Balan

Topology Preserving Map Generation for Multiple Mobile Fishing Vessels 259
 N. Sruthi, P. Divya and Maneesha Vinodini Ramesh

Accumulator Design in Cadence 90 nm Technology 273
 Nikhitha C. Balan and Abinkant A. Jose

Placement Chance Prediction: Clustering and Classification Approach 285
 M.V. Ashok, A. Apoorva and V. Chethan

Cluster-Based Distributed Key Architecture Scheme for MANETs 295
 B. Rajanna and R. Rajeswara Rao

Design and Implementation of 270-Tap Finite Impulse Response Filter 307
 T. Vandana Raj and S. Sreelakshmi

Implementation of 18-Bit High-Speed Binary Multipliers 315
 S. Sreelakshmi and T. Vandana Raj

A New Approach to Object-Oriented Programming Language for Remote Power Quality Monitoring and Analysis Considering Harmonics 323
 Vidula S. Jape and D.G. Bharadwaj

Dynamic Programming Parallelization of Matrix Chain Multiplication on GPU: A Comparative Study 333
 Tausif Diwan and S.R. Sathe

Data Mining for Healthy Tomorrow with the Implementation of Software Project Management Technique. 345
 K. Venkata Rao, R. Balakrishna, H. Aditya Pai and Piyush Kumar Pareek

Real-time Implementation of Electromyography for Hand Gesture Detection Using Micro Accelerometer. 357
 Subhendu Roy, Sraboni Ghosh, Aratrika Barat, Madhurima Chattopadhyay and Debjyoti Chowdhury

RSA Public Key Acceleration on CUDA GPU 365
 Jitendra V. Tembhurne and S.R. Sathe

Low-Power Home Embedded Surveillance System Using Image Processing Techniques. 377
 K. Arathi and Anju S. Pillai

Performance Analysis of a Software Defined Network Using Mininet	391
Chaitra N. Shivayogimath and N.V. Uma Reddy	
Comparative Analogy on Classification and Clustering of Genomic Signal by a Novel Factor Analysis and F-Score Method	399
R.C. Barik and R. Mishra	
Planar Crossover Using Microstrip Patch Antenna for Beamforming Networks	411
Mirav Mehta, K.A. Naveen, Vishnu Rajan, Rahul R. Pillai and Sreedevi K. Menon	
Energy-Efficient Communication in Wireless Sensor Network for Precision Farming	417
T.V. Aneeth and R. Jayabarathi	
Design and Evaluation of 3D NoC Routers with Quality-of-Service (QoS) Mechanism for Multi-core Systems	429
Pournamy Mohan and K. Somasundaram	
Single-Stage Boost Rectifier for Wireless Charging of Portable Devices Through Magnetic Resonant Coupling	443
Ria George, M. Sreekala and K. Deepa	
Big Data Analytics for Network Congestion Management Using Flow-Based Analysis	453
Yasmeen Arafath and R. Ranjith Kumar	
A Real-Time Intelligent Microcontroller-Based Harmonic Computing with Smart Phone Connectivity	459
Haripriya H. Kulkarni, D.G. Bharadwaj, Dipti B. Yeolekar and Sheetal B. Mhetre	
Performance Improvement of Compressed Sensing Reconstruction Using Modified-AMP Algorithm	471
Nissy Sara Mathai and R. Gandhiraj	
Diagnosis of Corneal Arcus Using Statistical Feature Extraction and Support Vector Machine	481
S.V. Mahesh Kumar and R. Gunasundari	
Hospital-Based Screening for Osteoporosis in Both Sexes Aged Above 50 Years Using Prototype US Bone Densitometer	493
Moataz Samir and M. Anburajan	
Real-Time ECG Acquisition and Detection of Anomalies	503
S. Kalaivani, I. Shahnaz, Shaikh Rizwana Shirin and C. Tharini	

Weight-Based Data Center Selection Algorithm in Cloud Computing Environment 515
 Sunny Nandwani, Mohit Achhra, Raveena Shah, Aditi Tamrakar, Kiran Joshi and Sowmiya Raksha

Real-Time Remote Monitoring of Indoor Air Quality Using Internet of Things (IoT) and GSM Connectivity 527
 Siva V. Girish, R. Prakash and A. Balaji Ganesh

Energy Conservation in Multi-storey Buildings at Indian Cities by Daylighting Control—A Study 535
 M. Abdul Rahman Rafi and N. Albert Singh

Enhancement in the Performance of Routing Protocols for Wireless Communication Using Clustering, Encryption, and Cryptography 547
 Kanchan Dhote and G.M. Asutkar

Design and Implementation of an Efficient Level Set Segmentation and Classification for Brain MR Images 559
 C.M. Naveen Kumar, B. Ramesh and J. Chandrika

Robotic Imitation of Human Hand Using RGB Color Gradient Mapping 569
 T. Thyagaraj, Kumar Abhishek, N.S. Brunda, Rakesh Ranjan and Nikita Kini

A Data Activity-Based Server-Side Cache Replacement for Mobile Devices 579
 Kottilingam Kottursamy, Gunasekaran Raja and K. Saranya

Privilege-Based Scoring System Against Cross-Site Scripting Using Machine Learning 591
 N. Shyam Sunder and T. Gireeshkumar

Content-Based Cricket Video Shot Classification Using Bag-of-Visual-Features 599
 M. Ravinder and T. Venugopal

HDTCV: Hybrid Detection Technique for Clickjacking Vulnerability 607
 D. Kavitha, S. Chandrasekaran and S.K. Rani

QUANCE: Quality-Driven Automated Negotiation for Composite Web Services 621
 Kanchana Rajaram and Chitra Babu

The Analysis of PQ Sequences Generated from Continued Fractions for Use as Pseudorandom Sequences in Cryptographic Applications 633
 Jayashree S. Pillai and T. Padma

A Novel Approach to Adopt Scrum by an Enterprise 645
 B. Reddaiah, R. Pradeep Kumar Reddy, C. Nagaraju
 and V. Harsha Sree

**Review on Security Attacks and Mechanism in VANET
 and MANET.** 655
 S. Balasubramani, S.K. Rani and K. Suja Rajeswari

**Security of Networks Using Efficient Adaptive Flow Counting
 for Anomaly Detection in SDN** 667
 Gagandeep Garg and Roopali Garg

**A Novel Low Power Multiply–Accumulate (MAC) Unit Design
 for Fixed Point Signed Numbers** 675
 N. Jithendra Babu and Rajkumar Sarma

Optimizing Technical Ecosystem of Digital Marketing 691
 Smitha Rao, V. Srivatsala and V. Suneetha

**An Efficient Image Encryption Technique Based on Optimized Key
 Generation in ECC Using Genetic Algorithm** 705
 K. Shankar and P. Eswaran

**Optimization of Fuel Consumption and Emission for Hybrid
 Electric Vehicle.** 715
 Soham Dey, Sushma Kamlu and Sudhansu Kumar Mishra

Classification Scheme for Software Reliability Models. 723
 Dalbir Kaur and Monika Sharma

**Secure Spectrum Leasing in Cognitive Radio Networks via Secure
 Primary–Secondary User Interaction** 735
 Meenakshi Malhotra and Inderdeep Kaur Aulakh

**Traffic Signal Synchronization Using Computer Vision and Wireless
 Sensor Networks.** 743
 Shivani Desai and Param Trivedi

**Nature-Inspired Moving Sink Energy Efficient Data Gathering
 Protocol for Wireless Sensor Network** 753
 Biswaranjan Swain and Siddhartha S. Satapathy

**Mining Frequent Itemsets in Association Rule Mining Using Improved
 SETM Algorithm** 765
 D. Kerana Hanirex and K.P. Kaliyamurthie

**An Efficient Approach for Evolution of Functional Requirements
 to Improve the Quality of Software Architecture** 775
 M. Sunil Kumar and A. Rama Mohan Reddy

Pitch Frames Classification in a Cricket Video Using Bag-of-Visual-Words 793
 M. Ravinder and T. Venugopal

Retinal Abnormality Risk Prediction Model: A Hybrid Approach Based on Vessel Characteristics and Exudates 803
 M. Aiswarya Raj and Shinu Acca Mani

BER and RSSI Analysis-Based Frequency Adaptive Technique for Radio Frequency Transceiver. 819
 A. Balasubramanian, A. Ahamad Meeran Mydeen and P.K. Dhal

A Two-Stage 0.18 μm CMOS Differential Low-Noise Amplifier with Integrated LC Balun for 2.4 GHz Applications 831
 J.L. Lakshmi and Premanand V. Chandramani

Energy Harvesting in Wireless Sensor Networks. 841
 R. Ramya, G. Saravanakumar and S. Ravi

Implementation of Z-Ternary Content-Addressable Memory Using FPGA 855
 G.P. Mullai and C. Sheeba Joice

Design of Visual Aid for Blind People 865
 Rajalakshmi Pushparaman

Implementing Fusion to Improve the Efficiency of Information Retrieval Using Clustering and Map Reduction 879
 B. Gomathi and P. Sakthivel

Cellular Automata-Based LDPC Decoder. 885
 C. Abisha Queen, M. Anbuselvi and S. Salivahanan

A Game Theoretic Model to Detect Cooperative Intrusion Over Multiple Packets 895
 Purbita Chakraborty, Koushik Majumder and Anurag Dasgupta

Filtration of Noise in Images Using Median Filter. 909
 Vigya and Tirthadip Ghose

PVDF Polymer-Based MEMS Cantilever for Energy Harvesting 917
 G. Dinesh Ram and S. Praveenkumar

Separation of Blood Cells Using Silicon-Based Microfilter. 925
 K. Swarnalatha, T. Sripriya and S. Praveenkumar

Optimal Image Enhancement Method Based on Histogram Analysis 933
 S.J. Monisha Selas and E.T. Jaba Jasphin

Epileptic Seizure Characterization Using Transform Domain	941
Sushree Sangita Biswal, Itishree Biswal and Mihir Narayan Mohanty	
WSN Backbone Formation Using Non-probabilistic Spanning Tree Algorithm	953
Rachita Nagpal and Roopali Garg	
Design Specifications of Reversible Logic Using CMOS and Quantum Dot Cellular Automata	961
Shaik Shabeena and Jyotirmoy Pathak	
Effective Models for Segmentation and Shape Tracking of Cells	973
J. Himayavardhini and R. Ramesh	
Real-Time Rule-Based Scheduling System for Integrated Delivery in a Semiconductor Manufacturing Using Evolutionary Algorithm-Based Simulation Approach	981
V.K. Manupati, A.S. Revanth, K.S.S.L. Srikanth, A. Maheedhar and M.B.S. Sreekara Reddy	
Least Square Mean Optimization-Based Real Object Detection and Tracking	991
Sanjay Rao, Deepak Jhanwar, Diwakar Gautam and Anand Choudhary	
Improving Efficiency and Fairness in Mobile Ad Hoc Networks	1001
Varun Manchikalapudi and Sk. Khadar Babu	
A Novel Content-Based Image Indexing and Retrieval Framework Using Clockwise Local Difference Binary Pattern (CWLDBP)	1009
M. Ravinder and M. Tirupathamma	
Self-organization Strategies for Hierarchical Network Structure in Wireless Ad Hoc Networks: A Short Survey	1019
Dinesh A. Kulkarni and Suhas H. Patil	
Efficient-Fused Architectures for FFT Processor Using Floating-Point Arithmetic	1029
D. Tamil Eniyan and J. Harirajkumar	
Design, Test and Evaluation of Trace-Buffer Inserted FPGA System	1039
R.S. Karpagam and B. Viswanathan	
Mining-Based Device Control for Home Automation	1049
C. Ganesh Kumar, S. Januja Josephine and Premanand V. Chandramani	
Methods and Materials for Adsorbing the Benzene Molecule Based on Micro Electro Mechanical System	1059
D. Lingaraja and S. Praveen Kumar	

A Multi-parametric Hybrid Cooperative Localization Scheme for Mobile Communication Network 1067
 D. Pavankumar and H.R. Mahadevaswamy

Interface and Control of Appliances by the Analysis of Electrooculography Signals 1075
 S.V. Arthi and Suresh R. Norman

An Advanced Magnetic Resonance Imaging Technique for the Detection of Abnormal Changes Using Artificial Neural Network 1085
 P. Balasubramanian and S. Manju

Implementation of a Hybrid Renewable Energy Plant with Remote Monitoring Feature 1093
 Ersan Kabalci and Ramazan Bayindir

Artificial Neural Network Control Strategy for Multi-converter Unified Power Quality Conditioner for Power Quality Improvements in 3-Feeder System 1105
 Karthikrajan Senthilnathan and K. Iyswarya Annapoorani

Investigations on Multidimensional Maximum Power Point Tracking in Partially Shaded Photovoltaic Arrays with PSO and DE Algorithms 1113
 R. Sridhar, S. Jeevananthan and B. Sai Pranahita

Study on Effect of Series Compensation on Double-Circuit Transmission Lines 1127
 S. Radha Krishna Reddy, J.B.V. Subrahmanyam and A. Srinivasula Reddy

Optimal Scheduling of Microgrid with Energy Storage System Considering Islanding Constraints 1145
 N. Jayalakshmi and B. Ashokvannan

Voltage Sensitivity-Based Reactive Power Injection Using Fuzzy Inference System in Power System 1169
 Prem Pratik, Prem Prakash and R.C. Jha

Residential House Electrical Energy Audit Case Study with ETAP 1181
 K. Keerthi Jain, N. Kishore Kumar, S. Muralikrishnan and L. Ramesh

Bidirectional Buck–Boost Converter-Fed DC Drive 1195
 P. Karthikeyan and V. Siva Chidambaranathan

Asymmetrical Multilevel Inverter Using Renewable Energy System	1205
V. Kala and C. Bhuvaneshwari	
High Efficient Power Supply for Ozone Generator System with Input Power Factor Correction Converter	1215
G. Udhayakumar, M.R. Rashmi, K. Patel and A. Suresh	
Performance Comparison for Feed Forward, Elman, and Radial Basis Neural Networks Applied to Line Congestion Study of Electrical Power Systems	1227
Pradyumna K. Sahoo, Ramaprasad Panda, Prasanta K. Satpathy and Mihir N. Mohanty	
Design and Analysis of PEM Fuel Cell with Multilevel Inverter Using Multicarrier PWM Techniques.	1239
M. Muthuselvi and K. Antony Samson	
Power Quality Enhancement in a Distribution System Using Inductive Active Filtering Technique.	1253
K. Naresh Kumar, R. Siva and S. Srinath	
Optimization of Impedance Mismatch in Distance Protection of Transmission Line with TCSC.	1265
M. Arun Bhaskar, A. Indhirani and S. Premalatha	
Reconfigurable WSN Interface for Water Quality Measurement	1279
Ajin Mathew Sam and C. Balaji	
Optimization of Micro Thermoelectric Generator for Renewable Source of Energy	1287
Y. Jeyashree, A. Vimala Juliet, C. Prantik Barua, J. Sree Harsha and Abhilash Mallick	
Optimal Design of a Fuzzy PID Controller for Inverted Pendulum System	1297
Sadhna Malik and Sudhansu Kumar Mishra	
Kalman Filter Based MPC with Dead Band for a Ball Mill.	1309
Punit Krishna, M. Guruprasath, K. Ramkumar, S. Venkatesh and G. Balasubramanian	
Design of Optimal Controller for Magnetic Levitation System Using Brownian Bat Algorithm	1321
K. Sundaravadivu, C. Ramadevi and R. Vishnupriya	
Meta-Heuristics Based Approach for Workflow Scheduling in Cloud Computing: A Survey	1331
Poonam, Maitreyee Dutta and Naveen Aggarwal	

Brain MRI Segmentation for Lesion Detection Using Clustering with Fire-Fly Algorithm	1347
Pramita Manna and Tapas Si	
Author Index	1357

About the Editors

Dr. Subhransu Sekhar Dash is presently Professor in the Department of Electrical and Electronics Engineering, SRM Engineering College, SRM University, Chennai, India. He received his Ph.D. degree from College of Engineering, Guindy, Anna University. He has more than seventeen years of research and teaching experience. His research areas are Power Electronics and Drives, Modeling of FACTS Controller, Power Quality, Power System Stability and Smart Grid. He is a Visiting Professor at Francois Rabelais University, POLYTECH, France. He is the chief editor of International Journal of Advanced Electrical and Computer Engineering.

Dr. M. Arun Bhaskar is presently Assistant Professor in the Department of Electrical and Electronics Engineering, Velammal Engineering College, Chennai. He has received his Ph.D. degree from SRM University, Chennai. He has more than nine years of research and teaching experience. He has published more than 30 papers in national conferences, 36 papers in international conferences, 8 papers in IEEE CPS, and in 9 international journals. His research areas are modeling of FACTS Controller, Voltage stability improvement, Design of nonlinear controllers for FACTS devices. He is a life member of Indian Society of Technical Education and member of Institution of Electrical and Electronics Engineering.

Dr. Bijaya Ketan Panigrahi is Associate Professor of Electrical and Electronics Engineering Department in Indian Institute of Technology Delhi, India. He received his Ph.D. degree from Sambalpur University. He is a chief editor in the International Journal of Power and Energy Conversion. His interests focus on Power Quality, FACTS Devices, Power System Protection, and AI Application to Power System.

Dr. Swagatam Das received the B.E. Tel. E., M.E. Tel. E (Control Engineering specialization) and Ph.D. degrees, all from Jadavpur University, India, in 2003, 2005, and 2009, respectively. Currently, he is Assistant Professor at the Electronics and Communication Sciences Unit of Indian Statistical Institute, Kolkata. His research interests include evolutionary computing, pattern recognition, multi-agent

systems, and wireless communication. Dr. Das has published one research monograph, one edited volume, and more than 150 research articles in peer-reviewed journals and international conferences. He is the founding co-editor-in-chief of “Swarm and Evolutionary Computation,” an international journal from Elsevier. He serves as associate editor of the IEEE Trans. on Systems, Man, and Cybernetics: Systems and Information Sciences (Elsevier). He is an editorial board member of Progress in Artificial Intelligence (Springer), Mathematical Problems in Engineering, International Journal of Artificial Intelligence and Soft Computing, and International Journal of Adaptive and Autonomous Communication Systems. He is the recipient of the 2012 Young Engineer Award from the Indian National Academy of Engineering (INAE).

Content-Based Load Balancing Using Web Clusters and Service Rankings

T.N. Anitha and R. Balakrishna

Abstract Web servers have gained immense popularity currently due to its nature to cater to a huge number of user requests, where any number of users can get service from Web-based applications. As it comes with global accessibility, servers hosting popular websites tend to get massive load that deteriorates in efficiency to provide quality service. Currently, most servers use load balancing techniques that distribute load among multiple virtual servers hosting a website. Generally, these load balancing techniques concentrate on balancing user request load on server and ignore the type of content requested. The reason behind it is overhead on dispatcher for analyzing content request and assigning appropriate rank. This process consumes additional time for dispatcher to allocate server and users face little delay in viewing their site; however it is helpful in the long run as heavy bandwidth consuming services such as multimedia requests can be catered efficiently by high priority servers only. The priority of servers can be defined as per their configuration and capabilities. Through experimental results on J Meter software it is proved that this concept can be helpful in providing better Quality of Service (QOS) to the website users.

Keywords Content-based load balancing · Clusters and Web servers · Content-wise service ranking

T.N. Anitha (✉)
Department of CSE, RajaRajeswari College of Engineering,
Mysore Road, Bangalore, India
e-mail: anithareddytn72@gmail.com

R. Balakrishna
Department of ISE, RajaRajeswari College of Engineering,
Mysore Road, Bangalore, India
e-mail: rayankibala@yahoo.com

1 Introduction

Highly developed Web-service delivery possesses considerable influence on organizations that are making use of it as a means to facilitate deliverance of their content to users. Similar to web pages, downloads, one-to-one communications, digital media and electronic-commerce need the latest and advanced tactics for content delivery. Simultaneously, size and dimensions of content rising widely need to convene ease of use. QOS and scalability is a gauge of the aptitude of the application to spread out to fulfill user requirements [1]. So as to convene service excellence specification sooner or later it is needed to affix more servers to convene rising needs. Cluster computing provides an influential setting to measure Web apps. Here in Web-service settings, users are able to notice merely the service and not the infrastructure needed for service deliverance. The content-based delivery services are explicit for content. Load balancing over the web offers newer prospects and efficiency of bandwidth usage [2].

Load balancing is a technique to share out workload through one or more servers. Here, even sharing of the load on many processors should get better the entire corresponding computation recital in clusters. In support of Web apps, load unprovoked situation happens often although the workload was disseminated time after time previously. As a result, vigorously and intermittently regulating workload sharing is necessary to ensure that every executive assignment at diverse sites would end their implementation at practically the same instance, reducing the inactivating time. On the other hand, active strategies to Web-services contain numerous confines [3, 4].

For getting better so that they do not tie together manifold services, there is a shortage of holdup for active and custom-made content formation and sharing and right to use. They do not shore up laterally content deliverance. There is shortage of flexibility in furnishing QOS access and practice [5]. The option of routing has too a huge influence on sharing requests as this sort of information accessible at the Web-server is fairly dissimilar. The sender is able to direct the requests in two ways; non-content-oriented and content-oriented techniques.

In this study, we talk about our idea, the limitations, and the study aims for sustaining upcoming generation streamed, interactive, and combined elevated resolution on content-oriented Web-services. We authenticated our application via content-wise service ranking (CWSR) adaptation. Additionally, we conducted a set of experiments to demonstrate the functionality of CWSR. Finally, we evaluate the content-oriented services sustained by CWSR to existing non-content-oriented service alongside the envisaged is of CWSR [6].

2 Related Works

The research on how to apply resource distribution of web system can be traced back to an auction since the last 20 years, there has been a noteworthy study attempt in load balancing. The fundamental supposition in most of this research is that the service scopes of the different requests are administered by an exponential supply. Contrary to the above statement, on the other hand, there is pretty tough evidence that the dimension of a web text, and for that reason its service scope, is administered in its place by heavy-tail sharing [7]. This entails that, to curtail reply time in that type of multi-base station method, “small” and “extensive” tasks must be allocated to diverse queues. In extremely variable workloads, software recital perks up significantly if comprehensive data regarding the action of every backend base station is accessible to the frontend sender. Therefore, a majority of investigators have considered and repeat in mock traces the area of web references and area conscious distribution rules that use the knowledge to widen the Web service accessibility [8]. Chuang Lin and associates largely concentrate on ventures assurance to provide the accessibility of operation services utilizing the stochastic high level Petri net of Web-server-clusters. Diverse classifications of requests are allocated diverse precedences [9]. These precedence intensities are employed and used into the load balancing algorithms to adopt precedence-oriented sending, i.e., QOS-alert load balancing. They calculated accessibility making use of MTBF and MTTR by means of the HTTP server scheduling and QOS alert load balancing to guesstimate accessibility of services [8].

In order to improve the competency of service, a set of Web-servers could be configured to make available Web service in a group to clientele. Load balancing is vital for a Web-service mechanism to ensure even sharing of inward requests on the Web-servers. Many approaches are there for load balancing over shared Web servers. The classification in [10, 11] divides the approaches of load balancing into four classes, namely client-oriented, DNS-oriented, dispatcher-oriented, and server-oriented approaches [12, 13]. From the above, we are able to discover that all load balancing mechanisms for shared Web servers entail recurrent message interactions among the request dispenser (DNS server or sender) and servers or clients to identify and swap over load data. The message interactions augment the network traffic in a Web-service method. A majority of the mechanisms also reveal the issue of restricted access in the routing and rerouting of requests. Generally, these mechanisms work only on load balancing without checking further consequences. Nonetheless content-based load balancing is obviously needed these days to cater to user requests more efficiently for high bandwidth usage services such as multimedia viewing or file downloading [14, 15].

3 Content-Wise Service Ranking

The load balancer dispatches the requests in two ways as content-based and non-content-based methods. In non-content-based the dispatcher dispatches the request to Web server without verifying the incoming request information. This method causes load imbalance and overhead on the Web servers. But in content-based method the dispatcher verifies the incoming request information, according to which a specific server providing that service is allocated. This leads to certain overhead on the dispatcher to match the requested service; to avoid this we provide ranking to the Web services. Ranks are assigned based on the highest hit rate of the service. For example, Rank1 to Multimedia Services, Rank2 to File Services, Rank3 to Text-based services, etc. Based on this, the priority of serving the requests is taken care of by the dispatcher here (Table 1).

3.1 Methodology for Content-Based Load Balancing in Clusters

1. Give rank to servers as per its service;
2. Create three major clusters combining similar ranking servers;
3. Receive URL requests from user;
4. Keep incoming requests in a queue;
5. For any request, analyze type of content requested;
6. Get list of clusters and search content matching ranking cluster;
7. Get server list within the cluster;
8. Find load status of each server
9. Locate server with minimum load;
10. Verify availability of the least load server
11. If available, then forward user request to that server;
12. Else except this as down server and locate server with minimum load;
13. Go to Step 10.

Table 1 Notation table

Notation	Description	Notation	Description
R	Ranking of server as per configuration	n	Upper bound of server list
C	Cluster of same ranking servers	LDS DS	List of down servers down server
UR	User request	A	Availability of server
Q	Queue	A_{s_i}	Availability of i th server, where $i \geq 1$ and $i \leq n$
m	Upper bound of user request	$L L_{s_i}$	Load load on particular server
UR_k	Particular user request in queue	L_{\min}	Minimum load
LS S	List of servers server	$L_{\min_{s_i}}$	Server with minimum load


```

1.  LS = {S1, S2, ..., Sn}
2.  {S1, S2, Sn} ∈ R1, {S1, S2, Sn} ∈ R2, {S1, S2, Sn} ∈ R3
3.  C1 = {LS(R1)}, C2 = {LS(R2)}, C3 = {LS(R3)}
4.  DS ← ∅, Lmin ← 1000
5.  Q = {UR1, UR2, ..., URm}
6.  for all UR ∈ Q do
7.      Rx ≡ SR(UR)
8.      Cx = Rx
9.      for all S ∈ Cx and i ≤ n do
10.         LSi ← ∑ UR ∈ Si
11.         if LSi ≤ Lmin then
12.             Lmin ← LSi
13.             LminSi ← Si
15.         end if
16.     end for
17.     ASi ← INetAddress.isAvailable(LminSi)
18.     if ASi ≡ true then
19.         URk → LminSi
20.     end if
21.     else
22.         DS ← LminSi
23.         LDS ← LDS ∪ {DS}
24.         LS ← LS - LDS
25.     Repeat Step 9
26.     end else
27. end for

```

The above algorithm explains the complete mechanism involved in internal processing of dispatch action. The very first step here is to obtain a list of all available servers and keep the names in temporary storage. Then as per the specific service of systems allot ranks to them such that multimedia service server gets Rank1 and Text Service server gets Rank3. Next, combine all the same rank servers in one cluster and form multiple clusters, so that for each rank there would be individual clusters. Now, down servers list can be initialized with null and min load server with 1000, assuming maximum load would be less than 1000 on any server. All the user requests can be placed in a queue with a queue limit and would be replaced with new ones after certain intervals. Now, for each user request dispatcher has to find the type of content requested so that the appropriate rank cluster can be found. Once cluster is found, the server inside has to be checked for minimum load. If minimum load server appears to be down then it should be kept in the list of down serves and again minimum load server should be searched, except servers listed in down server list. After it is found, the user request is forwarded to the respective server.

4 Experimental Results

For the experimental results generation J Meter tool is used, which is one of the most popular tools used for testing web applications. The speciality of this tool is it can generate any number of user requests considered as load for the web

Table 2 Content-based load balancing system sample data

Id	Sample time (Ms)	Label	Response code	Status	Thread name	Service	Reached	Bytes	Latency
1411839684493	1347	User requests	200	Ok	Users 1-10	Text	True	9461	1344
1411839683821	1321	User requests	200	Ok	Users 1-5	Text	True	9461	2038
1411839683820	1339	User requests	200	Ok	Users 1-4	Text	True	9461	2039
1411839684658	1325	User requests	200	Ok	Users 1-11	Text	True	9461	1324
1411839684826	1242	User requests	200	Ok	Users 1-12	Text	True	9461	1240
1411839685009	1242	User requests	200	Ok	Users 1-13	Text	True	9461	1238
1411839685170	1230	User requests	200	Ok	Users 1-14	Text	True	9461	1228
1411839685347	1184	User requests	200	Ok	Users 1-15	Text	True	9461	1183
1411839685497	1399	User requests	200	Ok	Users 1-16	Text	True	9459	1390
1411839685665	1303	User requests	200	Ok	Users 1-17	Text	True	9459	1296

Table 3 Non-content-based load balancing system sample data

ID	Sample time (ms)	Label	Response code	Status	Thread name	Service	Reached	Status	Latency
1411839691853	1180	User requests	200	Ok	Users 1-54	Text	True	9459	1172
1411839692027	1188	User requests	200	Ok	Users 1-55	Text	True	9459	1182
1411839692194	1172	User requests	200	Ok	Users 1-56	Text	True	9459	1165
1411839692362	1154	User requests	200	Ok	Users 1-57	Text	True	9459	1149
1411839692529	1162	User requests	200	Ok	Users 1-58	Text	True	9459	1152
1411839692687	1146	User requests	200	Ok	Users 1-59	Text	True	9459	1140
1411839692864	1208	User requests	200	Ok	Users 1-60	Text	True	9461	1207
1411839693021	1228	User requests	200	Ok	Users 1-61	Text	True	9461	1227
1411839693188	1186	User requests	200	Ok	Users 1-62	Text	True	9461	1185
1411839693355	1173	User requests	200	Ok	Users 1-63	Text	True	9461	1172

application. In order to work with J Meter there are minimum prerequisites that have to be done such as settings and making decision about parameters that have to be evaluated.

4.1 Settings

Before getting the results, a few configurations need to be done which are listed below:

1. Install server, database, and web application in the PCs.
2. Set rank of PCs (for example, Rank1 for multimedia service and Rank3 for text service).
3. Create cluster after grouping PCs of the same rank.
4. Creation of test project in J Meter.
5. Set the URL of application and parameters.
6. Set the number of user threads as 300 and ramp time as 60 s.
7. Add listeners on HTTP request results so that test results can be recorded.

Run the test and save the result file. Tables 2 and 3 demonstrate the sample data from J Meter which shows sample time taken for each user request in content-based proposed system.

Tables 2 and 3 demonstrate the sample data for content-based and non-content-based systems are generated from J Meter.

Figures 1 and 2 show content-based system takes 1185 or 1.2 ms and non-content-based system takes 1117 or 1.1 ms to serve the requests.

Figure 3 indicates there is a 0.1 ms latency comparison between non-content and content-based request processing. Figure 4 shows that content-based system has 26 % additional throughput compared to non-content-based system.

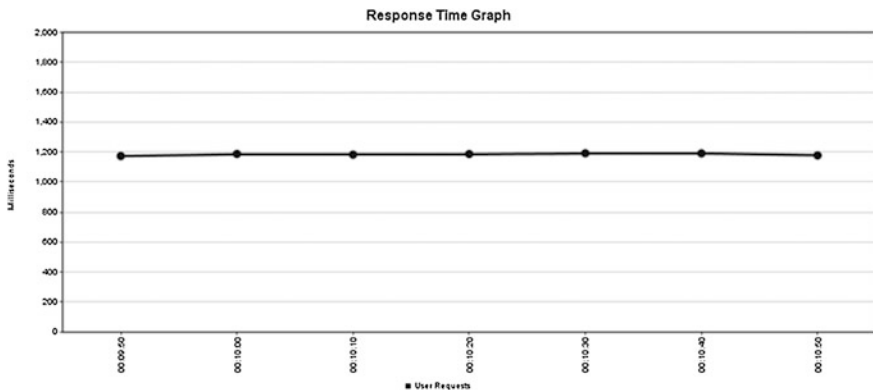


Fig. 1 Content-based response time

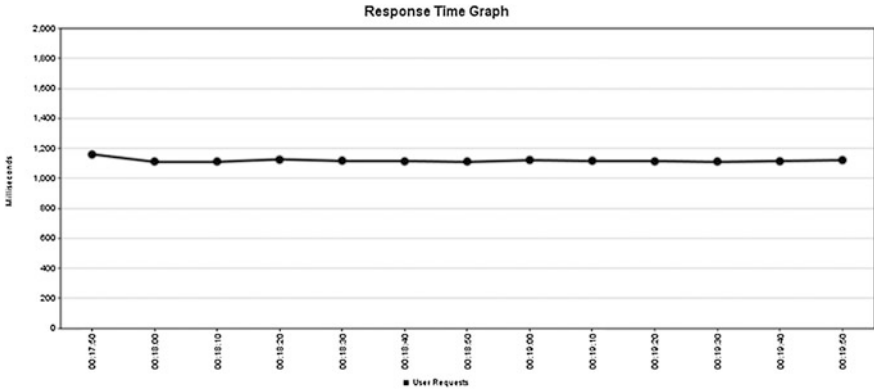


Fig. 2 Non-content-based response time

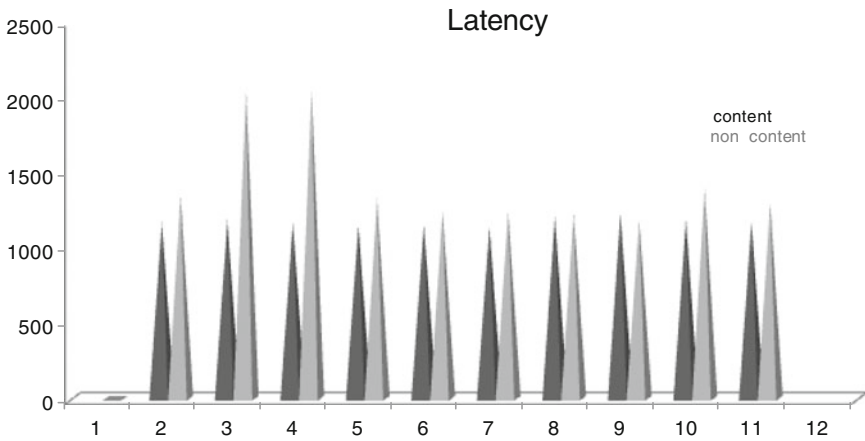
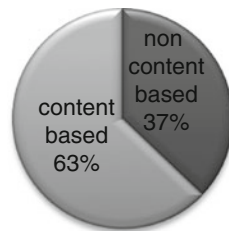


Fig. 3 Latency of content and non-content-based load balancing systems

Fig. 4 Throughput comparison

Throughput Comparison



5 Conclusion

The above comparisons of sample requests show that non-content-based dispatcher obviously takes 0.1–0.2 ms time compared to proposed content aware dispatcher. This test was done for text-based service but can be treated as generic for any kind of service as current non-content-based dispatcher cannot make differentiating while redirecting requests at the time of load balancing. The difference comes when actual service is used by user such as viewing multimedia content. Here, if proper server is not allocated there are chances that user may fail to get quality service and this may result in huge latency and bad throughput.

References

1. Sachin Kumar C, Singhal N. A priority based dynamic load balancing approach in a grid based distributed computing network. *Int J Comput Appl.* (0975–8887) 2012;49:5.
2. Mehta MA. A hybrid dynamic load balancing algorithm for distributed systems. *J Comput.* 2014;9:8 (Academy Publishers).
3. Ciardo G, Riska A, Smiri E. *EquiLoad: a load balancing policy for clustered web servers.* Performance Evaluation, Elsevier; 2001. p. 101–24.
4. Aversa L, Bestavros A. Load balancing a cluster of web servers using distributed packet rewriting. *IEEE*; 2003.
5. Gilly K, Juit C, Puljaner R. *An up-to-date survey in web load balancing.* Springer; 2011. P. 699–706.
6. Hussain J, Mishra DK. Performance evaluation of diffusion method for load balancing in distributed environment. *Int J Adv Res Comput Communication Eng.* 2013;2:12.
7. Menascè DA. QOS issues in web services. *IEEE Internet Computing* (November–December 2002).
8. Conti M, Gregori E, Lapenn W. A content delivery policies in replicated web services: client-side versus server-side. *Cluster Comput.* 2005;8:47–60 (Springer Science+Business Media, Inc. Manufactured in The Netherland).
9. Li J, Lin C. Availability analysis of web-server clusters with QOS-aware load balancing. In: *International Symposium on Computational Intelligence and Design, IEEE*; 2010.
10. Deshmukh AP, Pamu K. Applying load balancing: a dynamic approach. *Int J Adv Res Comput Sci Softw Eng.* 2012;2:6.
11. Zou S, Sha J. Analysis and algorithm of load balancing strategy of the web server cluster system. In: *ICCIP 2012.* Springer 2012.
12. Ayyasamy S, Sivanandam SN. A cluster based replication architecture for load balancing in peer-to-peer content distribution. *Int J Comput Netw Commun (IJCNC).* 2010;2:5.
13. Roussopoulos M, Baker M. *Practical load balancing for content requests in peer-to-peer network.* Berlin: Springer; 2006.
14. Dümmler J, Rauber T, Rüniger G. Semi-dynamic scheduling of parallel tasks for heterogeneous clusters. In: *10th international symposium on parallel and distributed computing*; 2011.
15. Tian C, Jiang H, Iyengar A, Liu X, Wu Z, Chen J, Liu W. Improving application placement for cluster-based web applications. *IEEE Trans Netw Serv Manag.* 2011;8:2.

A Fast Adaptive Kalman Filtering Algorithm for Speech Enhancement Under Stationary Noise Environment

C.N. Prabhavathi and K.M. Ravikumar

Abstract Kalman Filtering is one of the time domain speech-enhancement techniques. The conventional Kalman filtering technique involves more number of matrix operations. The complexity of matrix operations is reduced by fast adaptive Kalman Filtering technique. The proposed method of fast adaptive filtering technique is simple and gives best results for stationary noises. From the simulation results, it is seen that the proposed method of Kalman filtering is more effective in obtaining the clean speech signal. The performance of this filter is compared with the conventional method with respect to the signal to noise ratio and the execution time.

Keywords Speech enhancement · SNR · Execution time

1 Introduction

In voice communication, speech signals can be contaminated by environmental noise-like babble noise, mall noise, traffic noise, etc., and as a result the communication quality will be affected with less intelligibility. The quality of such speech signals can be improved using speech-enhancement techniques. One such technique is the Kalman filtering technique. There are many applications based on Kalman filtering algorithm as seen in [1–6]. These method models noisy speech signals in terms of state space equation and observation equation. The computational complexity is high as it needs the calculation of Linear prediction coding (LPC) coefficient and inverse matrix calculations [7].

C.N. Prabhavathi (✉)
Department of ECE, CERSSE, Hebbal Campus, Jain University, Bangalore
Karnataka, India
e-mail: prabhacngowda@gmail.com

K.M. Ravikumar
Department of ECE, SJGIT, VTU (Research Guide Jain University),
Chickballapur, Karnataka, India
e-mail: kmravikumar@rediffmail.com

The Kalman Filtering algorithm can be categorized as follows:

1. Conventional (Matrix) Kalman Filtering algorithm.
2. An improved filtering algorithm.
3. Modified fast adaptive Kalman filtering algorithm.

A brief of above algorithm is as follows:

Conventional Kalman filtering method is purely a matrix method, which involves matrix multiplications and matrix inversions. This method contains large number of redundant data and it is less adaptive. An improved filtering method reduces some matrix operations, and hence reduces the complexity of the conventional method. The proposed method which is the modified fast adaptive filtering is less complex and eliminates most of the matrix operations. This algorithm adapts for any type of environmental noise and works better with stationary type of background noises [8]. It has been observed that the intelligibility of speech signal is much better in the proposed method than with the conventional method.

This paper is organized as follows: Sect. 2 describes conventional filtering algorithm, improved filtering algorithm, and modified fast adaptive filtering algorithm. Section 3 provides the implementation steps with the results and conclusion is drawn in Sect. 4.

2 Fast Adaptive Kalman Filter Algorithm

2.1 Conventional Kalman Filtering Algorithm

The conventional method involves matrix operations and matrices and is created for covariance, variance, Kalman coefficient, Kalman gain, noise coefficient, etc. [7].

The noisy speech signal $y(n)$ is given by

$$y(n) = s(n) + v(n) \quad (1)$$

where $s(n)$ is a clean speech signal and $v(n)$ is a noise signal.

The state equation and observation equation in matrix form is expressed as
[State equation]

$$X(n) = F(n) \times x(n - 1) + Gw(n) \quad (2)$$

[Observation equation]

$$Y(n) = Hx(n) + v(n)$$

where $F(n)$ is a $L \times L$ transition matrix, G is the input vector and H is the observation vector.

The recursion equation of conventional Kalman filtering algorithm is as given below. The following set of equations provides the procedure for the implementation.

[Initialization]

$$\begin{aligned} X(0|0) &= 0, P(0|0) = I \\ R_v(n) &= \delta_v^2, G = [10 \dots 0] \\ R_s(n)[I,j] &= \begin{cases} E(y(n) \times y(n) - \delta_v^2), (i,j) & 1 \\ 0 & \text{otherwise} \end{cases} \end{aligned} \quad (3)$$

[Iteration]

$$P\left(\frac{n}{n-1}\right) = F \times P\left(\frac{n-1}{n-1}\right) F^T + G \times R_s(n) \times G^T \quad (4)$$

$$K(n) = P\left(\frac{n}{n-1}\right) G^T / (G \times P\left(\frac{n}{n-1}\right) G^T + R_v(n)) \quad (5)$$

$$X\left(\frac{n}{n-1}\right) = F \times X\left(\frac{n-1}{n-1}\right) \quad (6)$$

$$X\left(\frac{n}{n}\right) = X\left(\frac{n}{n-1}\right) + K \times X\left(y(n) - G \times X\left(\frac{n}{n-1}\right)\right) \quad (7)$$

$$P\left(\frac{n}{n}\right) = (I - K(n) \times G) \times P\left(\frac{n}{n-1}\right) \quad (8)$$

where X : State Vector, P : Parity matrix, R_v : Variance of noise (matrix), R_s : variance of noisy speech (matrix), K : Kalman Gain matrix, G : Input vector

Thus in the implementation of conventional method, each of the above parameters are realized using separate matrices which are then used to perform matrix operations including matrix inversions which are extremely time consuming.

2.2 Improved Filtering Algorithm

During the whole process of filtering, only the value of noisy speech $y(n)$ is useful. Hence in improved filtering algorithm very few matrix operations are done. This has much lesser execution time when compared to conventional method. Here even though the enhancement efficiency is lesser, the quality of required speech signal is not compromised. It is much more basic and simpler to understand than the conventional method. Here the matrix inversion is totally avoided [7].

Algorithm for the improved filtering method is given in the following steps:

[Initialization]

$$\begin{aligned} S(0) &= 0, \quad R_v = \delta_v^2, \\ R_s(n) &= E(y(n) \times y(n)) - \delta_v^2. \end{aligned}$$

[Iteration]

$$K(n) = \frac{R_s(n)}{(R_s(n) + R_v(n))} \quad (9)$$

$$S(n) = K(n) \times y(n) \quad (10)$$

2.3 Modified Fast Adaptive Kalman Filtering Algorithm

It is observed that in conventional filtering, any changes in the environmental noise due to the surrounding environment, it could be difficult to update the estimation of noise regularly. Hence it is required to estimate the noise regularly and obtain the filter algorithm which adapts to environmental noise change. This adaptation of filter is the fast adaptive Kalman filter which is useful in speech enhancement.

In order to update the estimation of noise constantly, a threshold level has to be set to determine whether current speech frame is noise or not. The environmental noise is updated with the following steps (a) update the variance of environmental noise. (b) Obtaining the SNR.

(a) Update the variance of environmental noise by [7],

$$R_v(n) = (1 - d) \times R_v(n) + d \times R_u(n), \quad (11)$$

In “(11),” d is the loss factor and it is given by

$$d = \frac{1 - b}{(1 - b^{t+1})} \quad (12)$$

b is a constant and it is assumed as 0.99.

Here before updating the variance of environmental noise, the variance of current speech frame $R_u(n)$ is compared with the threshold U “(13).” If $R_u(n)$ is less than or equal to U , the current speech frame can be considered as noise and then the algorithm will reestimate the noise variance.

$$U = (1 - d) \times U + d \times R_u(n) \quad (13)$$

(b) Obtaining the SNR

When the noise is very large “(13),” the updating threshold cannot be used directly and hence the SNRs are calculated by determining the variance of pure speech signal, variance of input degraded speech signal, and variance of background noise. The two SNRs are calculated, one for current speech frame ($SNR_I(n)$) and another for whole speech signal ($SNR_o(n)$) and are compared. According to [6]

$$SNR_I(n) = 10 \times \log_{10} \left(\frac{\delta_r^2(n) - \delta_v^2(n)}{\delta_v^2(n)} \right) \quad (14)$$

$$SNR_o(n) = 10 \times \log_{10} \left(\frac{\delta_x^2(n) - \delta_v^2(n)}{\delta_v^2(n)} \right) \quad (15)$$

In “(14)” and “(15),” n is the number of speech frames. The speech frame is noise when $SNR_I(n)$ is $\leq SNR_o(n)$. If $SNR_I(n)$ is $> SNR_o(n)$, the noise estimation will be attenuated to avoid damaging of speech signals. According to [9], noise attenuation can be expressed as

$$R_v(n) = \frac{R_v(n)}{1.2} \quad (16)$$

Updating Amplitude Threshold

Along with the above two steps, an extra condition is set by determining an amplitude threshold for the noisy speech signal. This condition is sufficient to have the updating of background noise constantly. Here an amplitude threshold Z of 0.008 is set for the noise samples taken for simulation. Here all the sample values less than 0.008 has been considered as only noise and been processed such that their enhanced amplitude is 0. The implementation steps are described with the following set of equations:

Let

$$Y(n) = S(n) + v(n)$$

$$R_s(n) = \delta_x^2(n)$$

$$R_v(n) = \delta_v^2(n)$$

[Initialization]

$$S(0) = 0, \quad R_v(1) = \delta_v^2(1)$$

[Iteration]

If

$$SNR_I(n) \leq SNR_o(n) \parallel SNR_o(n) < 0$$

then

If $R_s(n) < Z$

Then

$$\delta_r^2(n) = 0$$

Else

$$R_s(n) = \delta_x^2(n)$$

End

$$K(n) = \frac{R_s(n)}{R_s(n) + R_v(n)}$$

$$S(n) = K(n)Xy(n)$$

where $R_s(n)$ = Variance of noisy speech, $R_v(n)$ = Variance of noise, $\delta_r^2(n)$ = variance of speech frame, $K(n)$ = Kalman gain, $S(n)$ = Enhanced speech.

3 Implementation Steps and Results

The prerequisite for the implementation of the algorithm is the creation of the database for the noise and the speech. The noise database is created by considering various acoustic environmental noises. For the implementation purpose, the database includes stationary noises like white noise, traffic noise, canteen noise, shop mall noise, etc. All these noises are recorded using a microphone and an i-phone for duration of 60 s [8].

Similarly, a separate speech database is created by recording a sentence, which is taken from a TSP speech database. This database includes hundreds of sentences of which a sentence "A king ruled the state in early days" is recorded by various age groups. The age group includes the ages <12 years, between 12 and 19, 20 and 29, 30 and 40, and above 40. All the age groups include a male and a female. The above sentence is recorded in a closed silence room.

The purpose of creating separate database is that, in this paper, the degraded speech is assumed to be additive, and hence the noise and speech are added separately to obtain a degraded or corrupted noisy speech signal [8]. The simulation is

done for all the groups mentioned and the modified fast adaptive algorithm works better for the various age groups.

The performance results are categorized into three different sections: (i) In the form of waveform (ii) Compared with respect to SNR values and (iii) Compared with respect to execution time.

3.1 Performance Results in the Form of Waveform

Here the performance is compared in the form of time waveform for all the three methods for the noises like traffic noise and shop mall noise. The waveform is as shown in Figs. 1, 2, 3, 4, 5, 6, 7, and 8. Each figure has the waveform for clean speech signal, noisy speech signal, and enhanced speech signal.

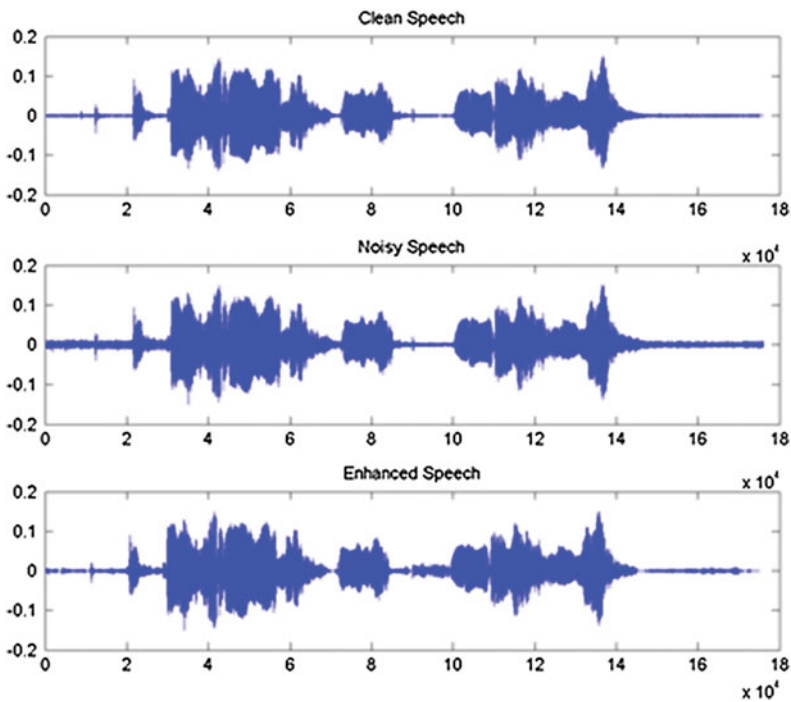


Fig. 1 Filtering results for male voice under traffic noise

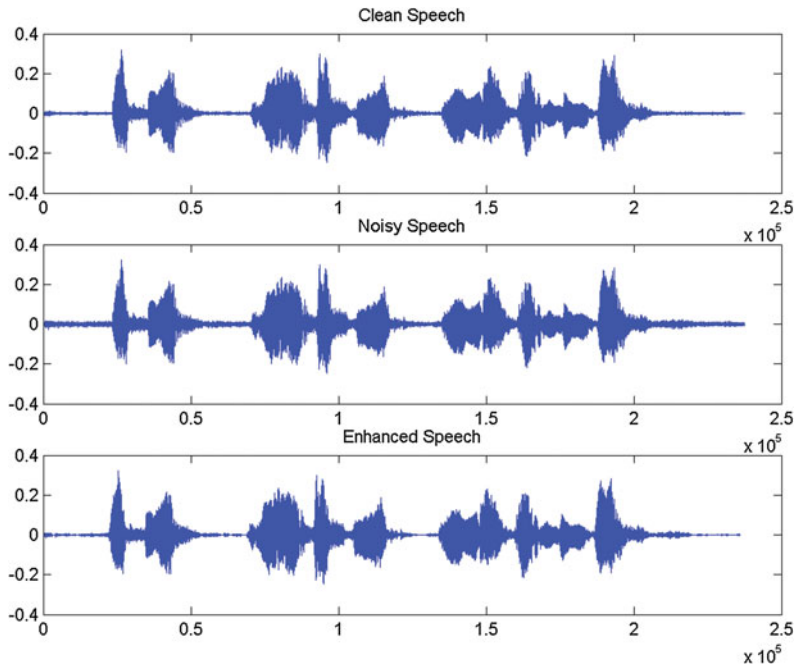


Fig. 2 Filtering results for female voice under traffic noise

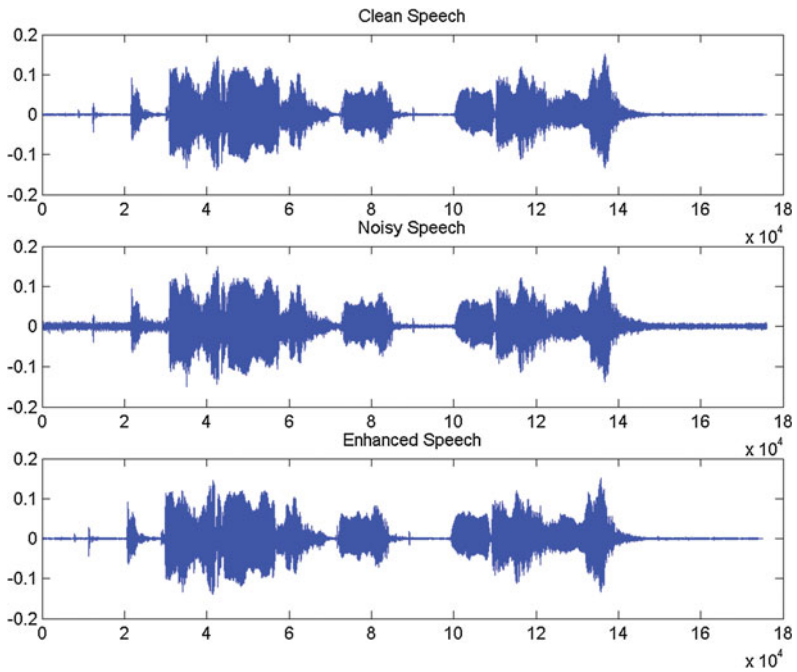


Fig. 3 Filtering results for male voice under traffic noise

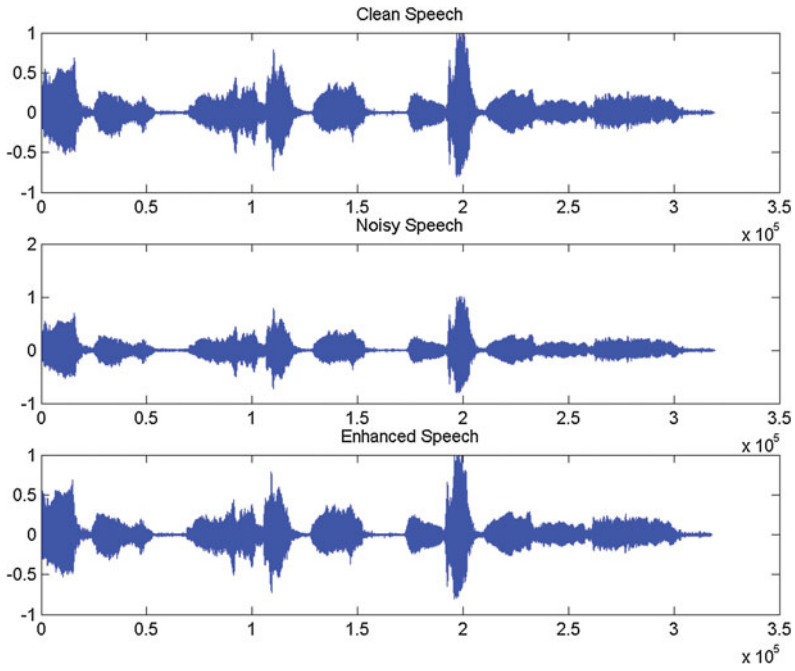


Fig. 4 Filtering results for female voice under traffic noise

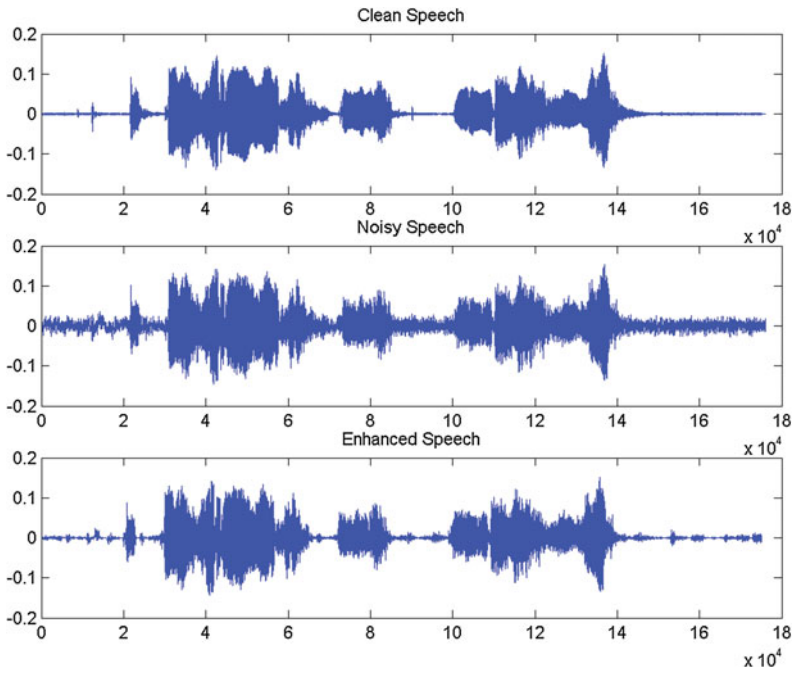


Fig. 5 Filtering results for male voice under shop mall noise

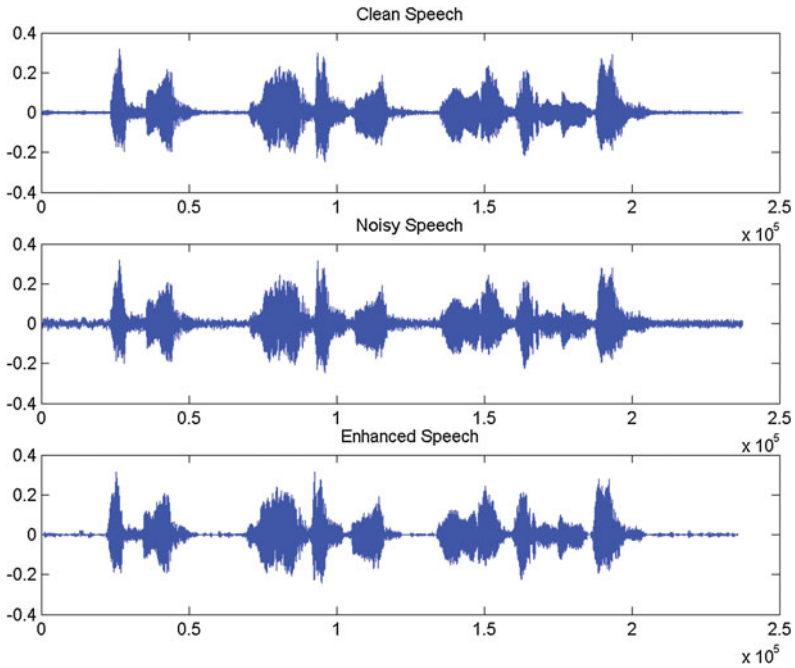


Fig. 6 Filtering results for female voice under shop mall noise

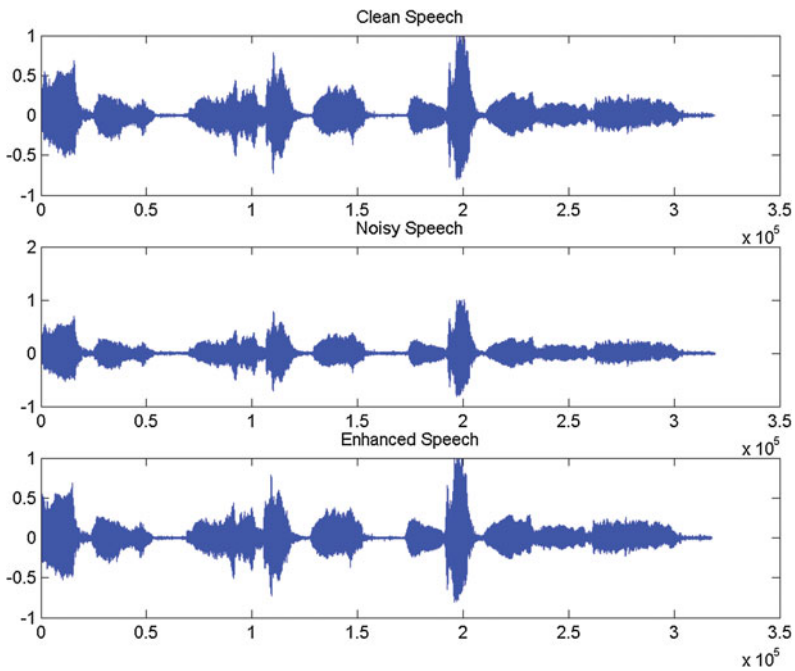


Fig. 7 Filtering results for male voice under shop mall noise

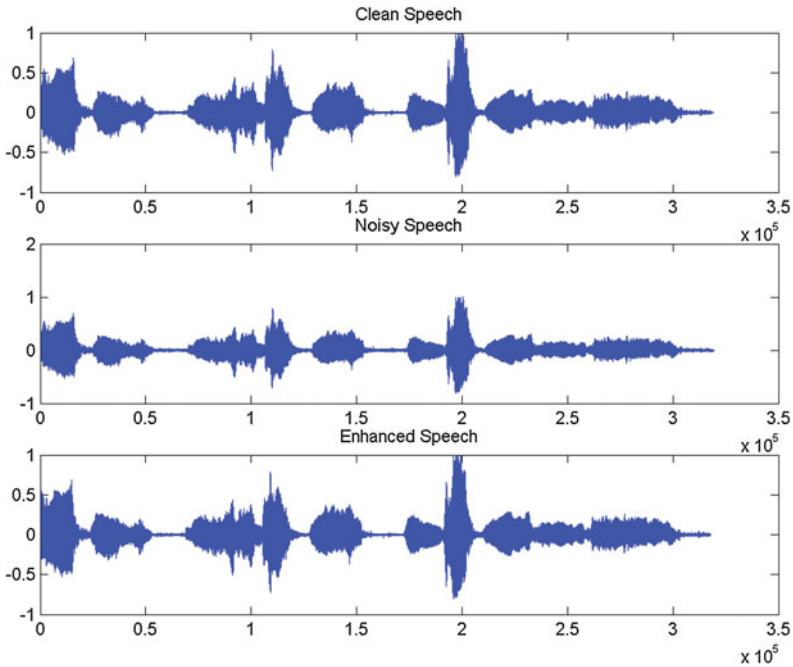


Fig. 8 Filtering results for female voice under shop mall noise

3.1.1 Traffic Noise

A. Conventional method

From the observation of all the three signal waveforms, the intelligibility of the enhanced speech signal is same as clean speech signal and it is much better in fast adaptive algorithm than the conventional and adaptive filter algorithm (see Figs. 1 and 2).

B. Modified Fast adaptive Kalman Filter

See Figs. 3 and 4.

3.1.2 Shopmall Noise

A. Conventional method

See Figs. 5 and 6.

B. Modified Fast adaptive Kalman Filter

In all the above figures, the results of modified fast adaptive filtering method have better enhanced waveform which resembles the original clean signal. Here the simulation results are shown for male speaker and a female speaker with an average

Table 1 Comparison table for SNR

Sl. No	Methods	SNR(in)db	SNR(out)db
1	Conventional method	-10.2081	-3.288
2	Adaptive filtering method	-11.8536	-3.2067
3	Modified fast adaptive filtering method	-10.2171	-3.2054

Table 2 Comparison table for execution time

Methods	Execution time (s)
Conventional method	29.9
Adaptive filtering method	0.055
Modified fast adaptive filtering method	1.3068

age of 35 years. The simulation results for adaptive filtering resemble almost the conventional method, and hence the plots for the adaptive filtering are not shown.

The results are also compared with respect to the SNRs as described below (see Figs. 7 and 8).

3.2 Performance Results with Respect to SNR Values

Here the input SNR of noisy speech and output SNR of enhanced speech is tabulated in Table 1 for all the three methods.

Here the SNR values are not normalized. The results show that there is an improvement in the SNR (out) of the modified fast adaptive filtering method when compared with the conventional method and adaptive filtering method.

3.3 Performance Results with Respect to Execution Time

The execution time of all the three methods is tabulated in Table 2. The execution time for adaptive filter is less and it is more for conventional method. Hence the adaptive filtering algorithm is faster than the conventional method and fast adaptive filtering algorithm.

4 Conclusions

This paper has presented Kalman filtering with conventional method, adaptive filtering method and fast adaptive filtering method for stationary noise. The listening test and the simulation results show that fast adaptive Kalman filtering is more efficient in obtaining the clean speech signal. The SNR values obtained for

fast adaptive filtering is better than the other two methods. But the execution time required for the fast adaptive filter is more than the adaptive filtering technique and lesser than the conventional method. Hence the proposed modified fast adaptive filtering is more efficient.

References

1. Zhang X, Fu X, Wang X. Improved filter method for speech enhancement. *Comput Appl.* 2008; 28:363–5.
2. Tanabe N., Furukawa T., Matsue H, Tsujii S. Fast noise suppression algorithm with Kalman filter theory. In: *Second International Symposium on universal communication*, 2008, pp. 411–5.
3. Tanabe N, Furukawa T, Matsue H, Tsujii S. Kalman Filter for robust noise suppression in white and colored noise. In: *IEEE International Symposium on Circuits and Systems*, 2008.
4. Wu C, Han C. Square—root quadrature filter. *Acta Electronica Sinica.* 2009;37(5):987–92.
5. Su W, Huang C, Liu P, Ma M. Application of adaptive Kalman filter technique in initial alignment of inertial navigation system. *J. Chin. Inertial Technol.* 2010;18 1:44–47.
6. Gao Y, Zhang J. Kalman filter with wavelet based unknown measurement noise estimation and its application for information fusion. *Acta Electronica Sinica* 2007;35 1:108–111.
7. Mai Q, He D, Hou Y, Huang Z. A fast adaptive Kalman filtering algorithm for speech enhancement. In: *IEEE International Conference on Automatic Science and Engineering Trieste, Italy*, 2011.
8. Prabhavathi CN, Ravikumar KM. Acoustic noise classification and characterisation using statistical properties. *IJETAE*, 2014;4 6:638.
9. Hua X. Adaptive speech enhancement based on discrete cosine transform in high noise environment. Harbin: Harbin Engineering University; 2006.

Reliability Assessment and Economic Evaluation of Offshore Wind Farm Using Stochastic Probability

Ahmed M. Atallah, Almoataz Y. Abdelaziz, Mohamed Ali,
R.K. Saket and O.P. Bharti

Abstract This paper shortly introduced the electric power transmission system for offshore wind farms (OWF). The transmission system components are demonstrated. Each component cost and reliability are studied and tabulated. An evaluation of the transmission system reliability of OWF is performed to increase the dependence on the OWF as a power source in the future. Reliability assessment is performed on a proposed site in Zafarana, Egypt and results are tabulated and simulated for different distances from the shore. The cost of the transmission system is studied using the stochastic probability method; optimization is performed on the investment cost, unavailability cost, and ohmic cost losses. Optimization results on the proposed site are done using different electrical power transmission system schemes. Losses due to the wind unavailability and ohmic losses are studied and simulated.

Keywords Reliability assessment · Economic evaluation · Offshore wind farm · Stochastic probability

A.M. Atallah (✉) · A.Y. Abdelaziz · M. Ali
Electrical Power & Machines Department, Faculty of Engineering
Ain Shams University, Cairo, Egypt
e-mail: atallah_eg@yahoo.com

A.Y. Abdelaziz
e-mail: almoatazabdelaziz@hotmail.com

M. Ali
e-mail: mohamed_ali_mohamed_ali86@yahoo.com

R.K. Saket · O.P. Bharti
Electrical Engineering Department, Indian Institute of Technology (BHU),
Varanasi (UP), India
e-mail: drrksaket@gmail.com

O.P. Bharti
e-mail: opiitbhu@gmail.com

1 Introduction

More than one technique was discussed to calculate the OWF system reliability. The analytic reliability uses the probability of availability and unavailability of each item of OWF subsystems [1–3]. Monte Carlo technique has been used to simulate system availability to conclude total system reliability [4]. In this paper, a stochastic model is used to optimize OWF electric power system by considering the power boundaries, investment cost, system efficiency, and reliability.

The electric system design of OWF must be efficient, reliable, economic to provide OWFs adequacy, and increase reliance on OWFs as a new source of power. The OWF electric system should be optimized to provide lower cost and better efficiency. The OWFs adequacy, efficiency, and reliability depend on the electrical system design and the wind speed distribution.

A good electric power system design reduces the repair time and failure rate, which increase the OWFs reliability. Also, some redundancies should be available in the electrical system to increase the system reliability. The limit of using redundant equipment is the OWF investment cost.

The problem is to optimize the investment cost, ohmic losses, power not served due to component failure or repair, and increase performance and efficiency for a known OWF location and the proposed site wind speed distribution (Table 1).

Table 1 Symbols and abbreviations

(I)	The interest rate (p.u). $I = 4\%$
(L)	The OWF life span (year). $L = 20$ years
(K)	The MV cables type between turbines and between turbines and CCP
(C_k)	The cost of the MV cables (\$/m) (does not include the cable installation cost)
$ij, i'j'$	The generic turbines coordinate
$D_{ij'i'j'}$	Distance between wind turbines (ij) and ($i'j'$) (m). $D_{ij'i'j'} = 500$ m
$x_{ij'i'j'k}$	Equal (1) or (0) if there is one cable type (K) between wind turbines (ij) and ($i'j'$) or not
$(i_a j_a)$	The coordinates of the CCP
$D_{ij_i a j_a}$	Distance between wind turbines and CCP (m). $D_{ij_i a j_a} = 500$ m
$x_{ij_i a j_a k}$	Equal (1) or (0) if there is one (K) type cable between wind turbines (ij) and CCP or not
$r_{ij_i a j_a k}$	Equal (1) or (0) if there is redundant (K) type cable between wind turbines (ij) and CCP or not
$(i^* j^*)$	The PCC coordinates
(h)	The HV cables type between CCP and PCC
(C_h)	The HV cables cost (\$/m)
$D_{i_a j_a i^* j^*}$	Distance between CCP and PCC (m). $D_{i_a j_a i^* j^*} = 50,000$ m
$x_{i_a j_a i^* j^* h}$	Equal (1) or (0) if there is one cable of the type (h) between CCP and PCC or not

(continued)

Table 1 (continued)

$r_{i_a i_a' j'}$	Equal (1) or (0) if there is redundant cable of the type (h) between CCP and PCC or not
(t)	Substation transformer type (MVA rating)
(C_t)	Transformer cost (\$). $C_t = 0.9$ million\$
(x_t)	Equal (1) or (0) if there is a transformer of the type (t) used or not
(r_t)	Equal (1) or (0) if there is a redundant transformer of the type (t) used or not
(C)	Cost of non-served energy (\$/MWh). $C = 100$ \$/MWH
(e)	Wind speed scenario
(s)	System state
(T^e)	Period duration of the scenario (hours)
$P - E^s$	Probability of system state
pns_{ij}^{es}	Power not served by wind turbine (ij) in scenario (e) and system state (s) (MW)
$\left(f_{ij'j'k}^{es} \right)$	The active power flows in cable type (K) from wind turbine (ij) to turbine ($i'j'$) in wind speed scenario (e) for system state (s)
$f_{ij'aj'k}^{es}$	The active power flows in cable type (K) from wind turbine (ij) to CCP in wind speed scenario (e) for system state (s)
$f_{i'j' i_a j_a h}^{es}$	Active power flows in cable type (h) from CCP to PCC in wind speed scenario (e) for system state (s)
$Pt(v)$	The turbine output power in Watts
ρ	The air density (is considered 1.225 kg/m ³ at an average atmospheric pressure at sea level).
R	The radius of the rotor measured in meters (63 m)
v_{wind}	The velocity of the wind measured in m/s
C_p	The turbine coefficient of performance (0.44)
n	The number of turbines in the wind farm assumed 10 turbines
$f(v)$	Turbine's output power variation as a function of wind speed variation

2 Transmission System

The electrical system contains medium-voltage (MV) cables between turbines and high-voltage (HV) cables to deliver power to the onshore grid. The submarine cables are usually buried 1–2 m deep the seabed. HV submarine cables can be buried at deeper depth. For low distance to shore between 50 and 80 km, HVAC transmission is the most economical option. For longer distances, HVDC will be likely lower cost and better performance [5]. The AC transmission system components are shown in Figs. 1 and 2.

Fig. 1 The electric power system when OWF is far from shore and substation is installed

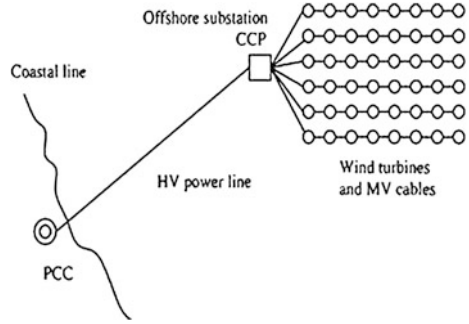
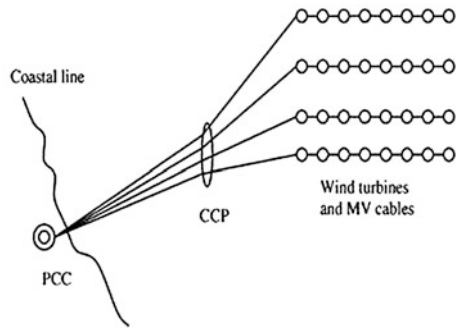


Fig. 2 The electric power system when OWF is near the shore and there is no offshore substation



3 Performance Data and Costs

3.1 Cable Cost

Cable prices are highly different between companies, especially for smaller C.S.A., Table 2, which has posted some burden and uncertainty during our calculations (Table 3).

3.2 Transformers Cost

At each turbine base, there is a (690 V/36 kV) transformer. Offshore transformer steps up the voltage to transmission voltage level (150 kV). This transmission voltage level is the most used voltage level in currently installed operating OWFs. Transformer cost is simplified to $(Cost_{transf.} = 0.041MVA_{rating}^{0.7513})$ M\$. The transformer cost is given in Fig. 3 [8].

Table 2 Equations

$\sum_{ijl'jk} (C_k D_{ijl'jk} x_{ijl'jk})$	The cost of the MV cables between OWF turbines
$\sum_{ijaak} (C_k D_{ijaak} (x_{ijaak} + r_{ijaak}))$	Cost of MV cables between turbines and CCP
$\sum_{iajah} (C_h D_{iajah} (x_{iajah} + r_{iajah}))$	Cost of HV cables between CCP and PCC
$\sum_t C_t (x_t + r_t)$	The substation transformer cost
$\left(\sum_{ijl'jkes} C \cdot T^e \cdot P - E^s \cdot 3 \left(\frac{f_{ijl'jk}^{cs}}{\sqrt{3}V_{MV}} \right)^2 R_k D_{ijl'jk} \right)$	Cost losses due to power losses in MV cables between turbines for the power generated in each wind speed scenario (<i>e</i>) and each system state (<i>s</i>)
$\left(\sum_{ijaakes} C \cdot T^e \cdot P - E^s \cdot 3 \left(\frac{f_{ijaak}^{cs}}{\sqrt{3}V_{MV}} \right)^2 R_k D_{ijaak} \right)$	Cost losses due to power losses in MV cables between turbines and CCP for the power generated in each wind speed scenario (<i>e</i>) and each system state (<i>s</i>)
$\left(\sum_{i'j'iajahes} C \cdot T^e \cdot P - E^s \cdot 3 \left(\frac{f_{i'j'iajah}^{cs}}{\sqrt{3}V_{HV}} \right)^2 R_h D_{i'j'iajah} \right)$	Cost losses due to power losses in HV cables between CCP and PCC for the power generated in each wind speed scenario and each system state (<i>s</i>)

Table 3 Comparison between different C.S.A cable prices for two companies [6, 7]

Conductor size (mm ²)	Company A	Company B
	Cost \$/m	Cost \$/m
<i>Collection system within the turbines (MV cables)</i>		
95	152	455
150	228	494
400	381	609
630	571	635
800	600	731
<i>HV cables transmission to the onshore grid</i>		
630	755	860

3.3 Cable Installation Cost

The cable installation cost includes cable shipping, transportation, route survey, planning, installation vessels, cable’s burial, and protection procedures. Cable installation is given in Table 4. Reference [9] considered that the HVAC cable installation cost is 125,000\$/km.

3.4 Compensators Cost

Reactive power compensation is to avoid the effect of the reactive power generated by cable capacitance. As assumed in Ref. [10], compensator cost is (2/3) of the transformer cost for the same MVA rating.

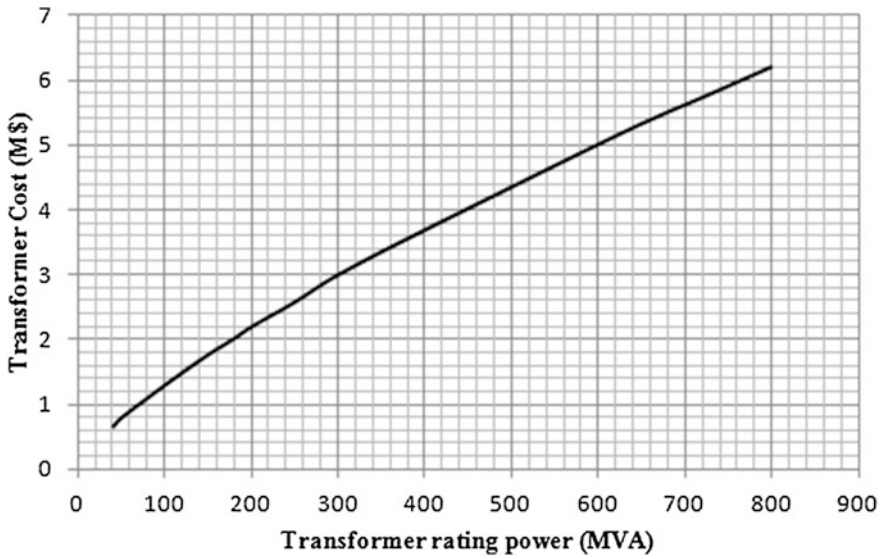


Fig. 3 The transformer cost fitting curve

Table 4 Cables installation breakdown

Marine route survey and planning	2,000,000\$
Cable transport	70\$/m
Mobilization/demobilization of ships	5,500,000\$
Cable laying process	98\$/m

4 Stochasticity

Study OWF reliability according to wind speed variation and electric system availability

4.1 Variation of Wind Turbines Output Power Due to Wind Speed Variation [11]

In the proposed site, the wind speed is distributed according to Rayleigh probability density function (c) and average speed (\bar{v}).

$$f(v) = 2\left(\frac{v}{c^2}\right)e^{-\left(\frac{v}{c}\right)^2} \tag{1}$$

$$\bar{v} = \frac{c}{1.128} \tag{2}$$

4.2 Reliability Assessment Due to Failure and Repair of Electrical System Component

Each component in the electrical system has two probabilities either available or unavailable which can be represented by Markov discrete model [12]. With the failure rate (λ) and repair rate (μ) of the component, (p) available and (q) unavailable can be calculated:

$$p = \frac{\mu}{\mu + \lambda} \qquad q = \frac{\lambda}{\mu + \lambda} \qquad p + q = 1 \qquad (3)$$

In the stochastic optimization problem, in this case there are two variables [13]: 1—Wind speed, 2—Reliability of each component.

The two variables change over two stages as shown in Fig. 4 which call scenario tree.

Branches of this tree are composed of each wind speed scenario and each system state scenario. The duration of each branch is obtained from multiplying the period of each wind speed scenario by the system state probability (Fig. 5).

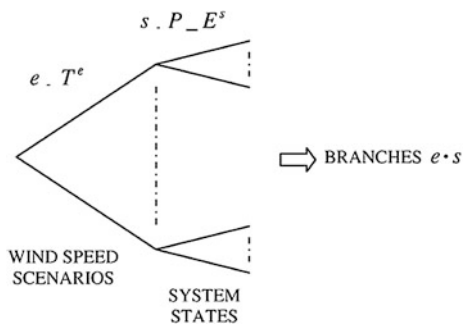
5 The Optimization Function

To optimize OWF transmission cost, there are three components that must be optimized [14].

5.1 The Capital Cost Investment (C_{inv})

The cost of electrical system components and the redundant components is expressed by (Table 5)

Fig. 4 Scenario tree, the changes of the stochastic problem variables over two stages



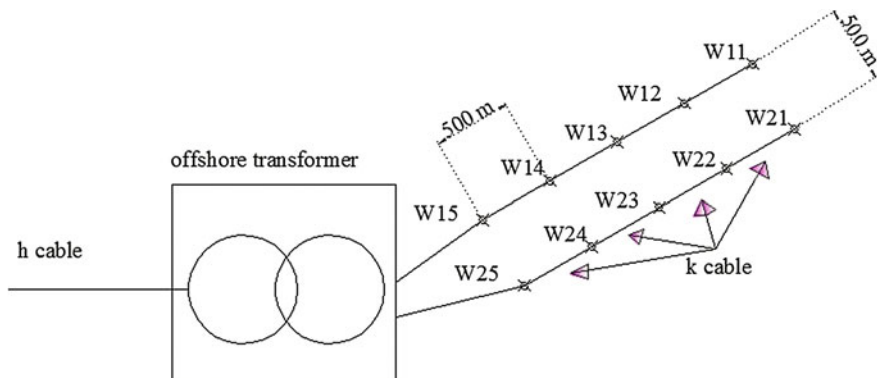


Fig. 5 The proposed OWF electric system layout

Table 5 The compensator cost for 150 kV transmission voltage level for different distances to shore

Distance to shore (km)	50	100	150	200	250	300
Compensation at 150 kV (MVAR)	32.5	65	97.5	130	162.5	195
Cost M\$	0.373	0.63	0.852	1.06	1.25	2.04

$$\begin{aligned}
 C_{\text{inv}} = & \left(\frac{I(1+I)^L L}{(1+I)^L - 1} \right) * \sum_{ijl'j'k} (C_k D_{ijl'j'k} x_{ijl'j'k}) + \sum_{ija_ajk} (C_k D_{ija_ajk} (x_{ija_ajk} + r_{ija_ajk})) \\
 & + \sum_{ija_ah} (C_h D_{ija_ah} (x_{ija_ah} + r_{ija_ah})) + \sum_t C_t (x_t + r_t)
 \end{aligned} \quad (4)$$

5.2 Cost of Power not Served (Unavailable) Because of a Component Failure (C_{unav})

$$C_{\text{unav}} = \sum_{ijes} C \cdot T^e \cdot P - E^s \cdot \text{pns}_{ij}^{\text{es}} \quad (5)$$

where System States are

- All the components are available.
- One cable of the type (K) is unavailable.
- One cable of the type (h) between CCP and PCC is unavailable.
- The transformer (t) is unavailable.

5.3 Cost Losses Due to the Power Losses in the Electric System Components (C_{loss})

$$\begin{aligned}
 C_{\text{loss}} = & \sum_{ijj'kes} C \cdot T^e \cdot P - E^s \cdot 3 \left(\frac{f_{ijjk}^{\text{es}}}{\sqrt{3}V_{\text{MV}}} \right)^2 R_k D_{ijj} \\
 & + \sum_{iji_ajakes} C \cdot T^e \cdot P - E^s \cdot 3 \left(\frac{f_{iji_ajak}^{\text{es}}}{\sqrt{3}V_{\text{MV}}} \right)^2 R_k D_{iji_aj} \quad (6) \\
 & + \sum_{i'j'i_aj_ahes} C \cdot T^e \cdot P - E^s \cdot 3 \left(\frac{f_{i'j'i_aj_ah}^{\text{es}}}{\sqrt{3}V_{\text{HV}}} \right)^2 R_h D_{i'j'i_aj_ah}
 \end{aligned}$$

5.4 The Objective Function of This Paper Is How to Optimize

$$C_{\text{inv}} + C_{\text{unav}} + C_{\text{loss}}$$

6 Case Study

Apply the previous explained stochastic equations on a proposed case study in Zafarana shore (Egypt). Studying different OWF layouts to asses power losses, system reliability, and cost, some assumptions are used (Table 6):

- OWF location is 50 km from shore (distance between CCP and PCC).
- Total number of turbines $N = 10$.
- Turbines are distributed in two rows, two rows with five turbines in each row.
- Distance between turbines is (500 m) and the distance between the rows is also (500 m). The distance between turbines is usually 5–7 times of the rotor diameter.

Table 6 Cables characteristics which used in the power transmission for the proposed OWF [16–18]

Cable type	V_{rated} (KV)	I_n (A)	$R_{a,c}$ (Ω/Km)	L (mH/Km)	C ($\mu\text{f}/\text{Km}$)	C.S.A (mm^2)	Cost
K	36	911	0.0341	0.294	0.331	400	553 \$/m
h	150	1088	0.0416	0.352	0.233	630	710 \$/m

Table 7 Electric system components repair rate and failure rate [15]

Failure rate	MV cable	HV cable	Transformer
Failure rate (λ)	0.0001486 failure/m	0.000179 failure/m	0.688 failure
Repair rate (μ)	912.5 repairs	347.6 repairs	347.6 repairs

- The rated power of each turbine is (5 MW); the total installed power is (50 MW).
- An offshore substation of (60 MVA) has a step-up transformer (150/36 kV). The transformer cost is 0.9 million \$/unit [15].
- Cables characteristics used for power transmission are shown in Table 7.

In the optimization case for simplification:

- Five wind speed scenarios will be taken into account.
- Each system state might have at most one component unavailable.

Input data: Mean wind speed at hub height 9 m/s. The wind speed distribution through the Rayleigh density function of parameter $c = 10.152$, Eq. 2.

6.1 System Reliability Assessment Study

By knowing the failure and repair rate of each component of the OWF electrical system, transmission system reliability can be evaluated. For our case study, assuming the OWF is located at different distances from shore (10, 20, 30, 40, 50 km) (Table 8).

Assumptions:

- No change in MV cables.
- Only variation has been taking place on HV cable distance to shore.
- One transformer is used (no redundancy used in both cables and transformers).

6.1.1 Series and Parallel Components Handling of the Proposed System

For series-connected component, if any component failure, the entire system fails. $R1$ and $R2$ are the probabilities of component availability (reliability). $Q1$ and $Q2$

Table 8 The electrical transmission system reliability variation with the distance to shore variation

$P_{\text{system}10 \text{ km}}$	$P_{\text{system}20 \text{ km}}$	$P_{\text{system}30 \text{ km}}$	$P_{\text{system}40 \text{ km}}$	$P_{\text{system}50 \text{ km}}$
0.99289	0.9878	0.9828	0.9778	0.973

are the probabilities of component unavailability. $R_s = R1R2$ is the system reliability and $Q_s = 1 - R1R2$ is the probability of the system unavailability.

In parallel-connected components, if all connected components fail, the entire system fails.

$Q_s = Q1Q2$ is the probability of system unavailability. $R_s = 1 - Q1Q2$ is the system reliability.

The system reliability will be

$$P_{system} = P_{MVcables} * P_{transformer} * P_{HV cable}$$

6.2 Cost of Losses Due to the Wind Speed Unavailability and Ohmic Losses

Wind speed of OWF changes in seasons and day time. There are two costs, the cost of losses due to the wind unavailability as the OWF does not generate its installed power capacity, besides the ohmic losses' cost due to power losses in the cable.

In the proposed site, the wind changes from 7 to 13 m/s. At each wind speed, the generated power, the power not served because of wind unavailability, the cost of wind unavailability, and cost of ohmic losses will be calculated (Table 9).

We proposed that the wind turbine capacity is 5 MW.

- The output power of OWF can be calculated from Eq. (7):

$$P_t(v) = \frac{1}{2} * \rho * \pi * R^2 * v_{wind}^3 * C_p * n \tag{7}$$

The cost loss variation due to the wind unavailability is calculated from Eq. (5). The cost losses variation due to the ohmic losses variation with the variation of the cable's power loading is calculated from Eq. (6).

Table 9 Cost of losses variation due to wind unavailability and ohmic losses against variation of wind speed

Wind speed	P_{in} HV cable	$P_{not served}$	$I_{flow in}$ HV cable	$I_{flow in}$ MV cable	P_{losses} HV cable	P_{losses} MV cable	P_{losses} total	C_{unavi} (M\$)	C_{losses} (M\$)	Total losses (M\$)
7	11.53	38.4	52.210	26.105	0.0170	0.0003	0.0173	2.71	0.001	2.718
8	17.21	32.7	77.930	38.965	0.0378	0.0007	0.0386	2.31	0.003	2.318
9	24.5	25.5	110.94	55.470	0.0768	0.0015	0.0783	1.8	0.006	1.806
10	33.6	16.4	152.14	76.074	0.1444	0.0029	0.1474	1.16	0.01	1.168
11	44.73	5.27	202.54	101.27	0.256	0.0052	0.2612	0.37	0.018	0.390
12	50	0	226.41	113.20	0.3198	0.0065	0.3264	0	0.023	0.023
13	50	0	226.41	113.20	0.3198	0.0065	0.3264	0	0.023	0.023

Table 10 The proposed average wind system generation during the year

Number of months	Power generated (MW)
10	50
1	43
1	23

7 Cost Optimization

7.1 The Investment Cost

Considering the following values and using Eq. (4),

$$C_k = 553\$/m, r_{ijaja} = 0, r_{iaja i*j*} = 0, C_h = 710\$/m, r_t = 0.$$

We obtained that $C_{inv} = 39.165$ million \$ (No redundant cables or redundant transformer).

7.2 The Cost Losses Due to System Unavailability

We propose that the wind system produces power as given in Table 10. Substituting these values in Eq. (5), we get that $C_{unav} = 1.4688$ million \$.

7.3 The Ohmic Losses Costs

Considering the transmission, the voltages are $V_{MV} = 36$ kV, $V_{HV} = 150$ kV. The results of Eq. (6) shows that $C_{loss} = 1.24$ million \$.

8 Conclusion

To depend on the OWF as a source of the power, the reliability assessment of the system components must be performed. The transmission system reliability assessment decreases with the increase of the distance to shore. Not only the electrical transmission system component reliability is the only factor which affects on the usage of the OWF as a power source, but also the wind speed variation and wind unavailability are the main factors. As studied when the wind speed reduced, the power output from the OWF is rapidly decreased and the cost of losses due to the wind unavailability is highly increased.

In case 1, the investment cost is high because higher C.S.A. cables are used for future expansions.

References

1. Shahinpour A, Moghani JS, Gharehpetian GB, Abdi B. High gain high-voltage z-source converter for offshore wind energy systems. In: IEEE conference, power electronics, 5th drive systems and technologies conference (PEDSTC). Tehran, Iran; 2014.
2. Sannino A, Breder H, Nielsen EK. Reliability of collection grids for large offshore wind parks. In: Proceedings of the 9th international conference on probabilistic methods applied to power systems; 2006. p. 1–6.
3. Underbrink A, Hanson J, Osterholt A, Zimmermann W. Probabilistic reliability calculations for the grid connections of an offshore wind farm. In: Proceedings of the 9th international conference on probabilistic methods applied to power systems; 2006. p. 1–5.
4. Zhao M, Chen Z, Blaabjerg F. Generation ratio availability assessment of electrical systems for offshore wind farms. IEEE Trans Energy Convers. 2007;22(3):755–63.
5. Shin J-S, Kim J-O, Cha ST, Wu Q. Reliability evaluation considering structures of a large scale wind farm. Power electronics and applications (EPE), 15th IEEE European conference on Lille, France; 2013.
6. Negra NB, Holmstrøm O, Bak-Jensen B, Sorensen P. Aspects of relevance in offshore wind farm reliability assessment. IEEE Trans Energy Convers. 2007;22(1):159–66.
7. Tastu J, Pinson P, Trombe P-J, Madsen H. Probabilistic forecasts of wind power generation accounting for geographically dispersed information. IEEE Trans Smart Grid. 2014.
8. Ackermann T. Transmission systems for offshore wind farms. In: Ackermann T, editor. Wind power in power systems. West Sussex, England: Wiley; 2005. p. 479–503.
9. Lumbreras S, Ramos A. Optimal design of the electrical layout of an offshore wind farm applying decomposition strategies. Power Syst IEEE Trans IEEE Power Energy Soc. 2013.
10. Wright SD, Rogers AL, Manwell JF, Ellis A. Transmission options for offshore wind farms in the united states. In: Proceedings of the AWEA annual conference; 2002. p. 1–12.
11. McShane P. Vegetable-oil-based dielectric coolants. IEEE Ind Appl Mag. 2002;8(3):34–41.
12. Nielson P. Offshore wind energy projects feasibility study guidelines. [Online document], 2003 June (Ver 3.0), [cited 2006 Aug 07]. <http://www.emd.dk/Projects/Projekter/Seawind/OTHER%20RELEVANT%20DOCOPPERMENTS/Feasibility%20Study%20Guidelines.pdf>. (2003)
13. Gerdes G, et al. Case study: european offshore wind farms – a survey for the analysis of the experiences and lessons learnt by developers of offshore wind farms—final report. Published by the EU project “POWER—Pushing Offshore Windfarm Regions”.
14. Ionescu A, Brkic S. Report on the implementation of CBT mechanism in SEE region. Power point presentation prepared for ETSO, 4th Athens Forum. http://www.seerecon.org/infrastructure/sectors/energy/documents/3ew/cbt_mechanism_implementation.ppt(2004).
15. Caramanis T, Associates. Cost and risk analysis for a Norway-Netherlands HVDC interconnector. Power point presentation, tabors caramanis and associates. http://www.dte.nl/nl/Images/12_24732.pdf (2004).
16. Lumbreras S, Ramos A, Cerisola S. A progressive contingency incorporation approach for stochastic optimization problems. IEEE Trans Power Syst. 2013.
17. Brown T. Transmission network loading in Europe with high shares of renewables. IET Renew Power Gener. 2015.
18. Banzo M, Ramos A. Stochastic optimization model for electric power system planning of offshore wind farms. IEEE Trans Power Syst. 2013;26(3).

Charge Pump with Improved High-Swing Cascode Current Source for Accurate Current Matching in DPLL

D.S. Rajeshwari, P.V. Rao and V. Rajesh

Abstract In loop dynamics of charge pump phase-locked loop, the charge pump current plays predominate role to loop bandwidth. Different charge pump architectures suffer from charge sharing, clock feed-through, channel charge injection, and current mismatch. Due to this, charge pump phase-locked loop can have more reference spur. Improved high-swing current source is proposed to obtain nearest current matching characteristics. 0.01 % of current mismatch is achieved with 3.3 V, 90 nm CMOS technology. The circuit is verified at process voltage temperature corners.

1 Introduction

Phase-locked loops are the implementations of clock generation for SOC processor. Charge pump-based phase-locked loop (CPPLL) is adequate because of its wide capture range and zero systematic phase offset. In CPPLL, the phase frequency detector (PFD) generates to output pulse UP and DOWN proportional to phase difference of two input pulses ω_{ref} (ω_{in}) and ω_{fb} . Charge pump either charges or discharges according to UP and DOWN. The charge pump current through loop filter generates VCO control output voltage V_{ctrl} . The loop stability ensures locking

D.S. Rajeshwari (✉)

Electronics & Communication Department, Jain University & SiCon Design Technologies Pvt. Ltd, Bengaluru 560024, India
e-mail: dsrajeshwari@gmail.com

P.V. Rao

Electronics & Communication Department, RajaRajeshwari College of Engineering, Bengaluru 560074, India
e-mail: pachararao@rediffmail.com

V. Rajesh

SiCon Design Technologies Pvt. Ltd, Bengaluru 560037, India

© Springer India 2016

S.S. Dash et al. (eds.), *Artificial Intelligence and Evolutionary Computations in Engineering Systems*, Advances in Intelligent Systems and Computing 394, DOI 10.1007/978-81-322-2656-7_4

to input ω_{ref} . Thus charge pumps current proportional to vary the lock time and capture time. Any nonidealities in charge pump degrade performance of PLL.

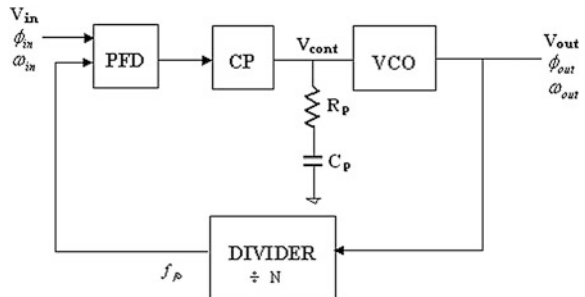
Several single-ended common source charge pump architecture were proposed in the literature [1–2]. Charge sharing effect is greatly minimized using two switches NMOS-Mn and PMOS-Mp. Opamp restricts output range, need good stability by itself, and also the PSSR can reflect largely on PLL spur. Careful design of opamp, inverter delays match, and switch size are required in [1]. The implementation of switch using TG and folded cascode opamp makes careful design, but the TGs have to be scaled up to drive the current mirror, which results in larger Δt_{on} and worsens the reference spur level of CPPLL as charge pump proposed in [3]. Literature [4] exploits rail-to-rail operational amplifier and self-biased high-swing cascode current source to implement charge pump. Since the gain of rail-to-rail opamp varies for input voltage variation across full power supply makes less attraction for charge pump even though stability analysis is obliged. Literature [5] proposed that charge pump circuit uses opamp, cascode reference current source, and charge removal transistor. It backs with supporting any or zero current in cascode current mirror mean startup circuit, which may not turn ON to provide current through current mirror. Proposed charge pump in [2] as gate drain overlap capacitance of NMOSs is not equal to PMOSs, TGs do not avoid clock feed-through effectively. The current mismatch is avoided in literature [2] by deriving charging and discharging of current from the same current reference.

Section 2 covers PLL loop dynamics. Section 3 discusses conventional charge pump nonidealities. Section 4 shows proposed charge pump structure with results. Section 5 draws conclusion from this work.

2 CPPLL Loop Dynamics

CPPLL block diagram is shown in Fig. 1. PFD in loop increases the acquisition range and wide acquisition range. It is necessary because voltage-controlled oscillator (VCO) center frequency can vary considerably with process and temperature.

Fig. 1 CPPLL block diagram



The PLL open-loop transfer function [6] including the divider which is equal to

$$\frac{\phi_{\text{out}}}{\phi_{\text{in}}}(s)|_{\text{open}} = \frac{I_P}{2\pi} \left(R_P + \frac{1}{C_P s} \right) \cdot \frac{K_{\text{VCO}}}{s} \cdot \frac{1}{N} \quad (1)$$

The closed-loop transfer function is compared with the standard response of second-order system.

$$H(s) = \frac{\frac{I_P K_{\text{VCO}}}{2\pi C_P} (R_P C_P s + 1)}{s^2 + \frac{I_P K_{\text{VCO}} R_P s}{2\pi N} + \frac{I_P K_{\text{VCO}}}{2\pi C_P N}} = \frac{2\zeta\omega_n s + \omega_n^2}{s^2 + 2\zeta\omega_n s + \omega_n^2} \quad (2)$$

Thus

$$\omega_n = \sqrt{\frac{I_P K_{\text{VCO}}}{2\pi C_P N}} \quad (3)$$

$$\zeta = \frac{R_P}{2} \sqrt{\frac{I_P C_P K_{\text{VCO}}}{2\pi N}} \quad (4)$$

ζ is proportional to charge pump current I_P , K_{VCO} , and $1/N$. The poles are at zero for $I_P = 0$. For $I_P K_{\text{VCO}} > 0$ which is small, the poles are complex. As $I_P K_{\text{VCO}} > \infty$ system becomes more stable, the closed-loop system contains zero at $S_Z = -1/(R_P C_P)$. The settling time is inversely proportional to ζ . Thus the design challenges loop bandwidth with charge pump current, VCO gain, and divider factor. Manipulating (3) and (4), the loop filter values are

$$C_P = \sqrt{\frac{I_P K_{\text{VCO}}}{2\pi\omega_n N}} \quad (5)$$

$$R = \frac{2\zeta}{\omega_n C_P} \quad (6)$$

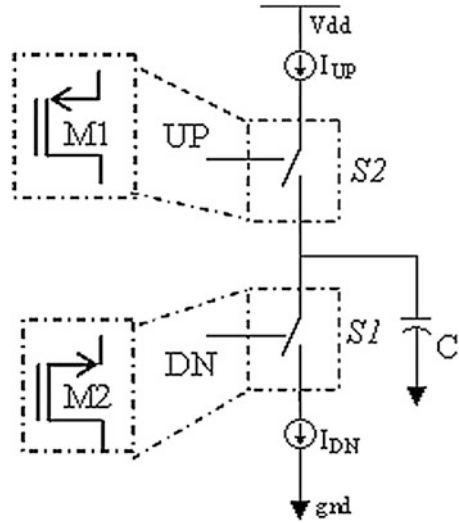
Depending on the VCO output frequency to be locked, the divider factor is chosen and is given as

$$N = \frac{f_{\text{out}}}{f_{\text{ref}}} \quad (7)$$

The settling time [7] for 2 % tolerance as

$$t_s = \frac{3}{\zeta\omega_n} \quad (8)$$

Fig. 2 Block diagram of charge pump



3 Basic Charge Pump Considerations and Its Nonidealities

Block diagram of charge pumps is as shown in Fig. 2. It consists of two switches and two current sources, correspondingly, for UP and DOWN. The switch can be placed at different terminals of current source. The switch S2 charges when switch UP is low, S1 discharges when switch DN is low and the mechanism ensures both switches are OFF as shown in Fig. 3. The MOS switch implementation favors error due to MOS transistor operation when the switch turns OFF/ON.

When MOS switch turns ON to OFF, the total charge in the inversion layer exits through the source and drain terminals. The charge injected on terminals introduces error in the voltage stored in the capacitor. The phenomenon is channel charge injection. Due to rise and fall transition, the output of PFD UP and DOWN pulse signals is coupled to output node via gate to source and gate to drain overlap capacitances. Resulting variation in capacitor voltage refers as clock feed-through. When the MOS switch is OFF, the output capacitor is floating. Later on MOS switch turns OFF to ON state, then charge shares among output capacitance and

Fig. 3 States **a** Charging **b** Discharging **c** No change

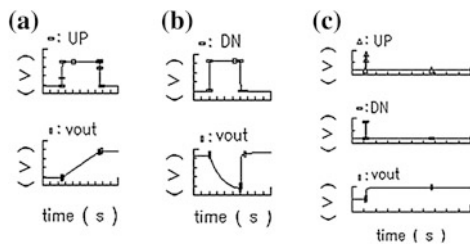
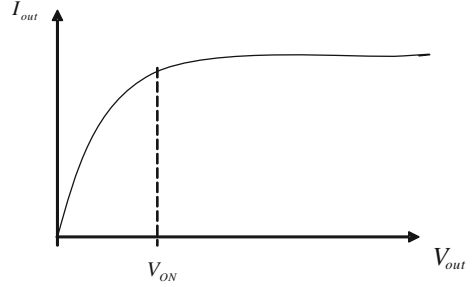


Fig. 4 I_{out} across V_{out}


parasitic capacitance of switch causing deviation output capacitor voltage. Charge sharing, clock feed-through, and channel charge injection contributes gain error, dc offsets, and nonlinearity. The MOS switch errors and MOS implementation determine significant role in reference spur of PLL.

The current sources should be properly biased. The minimum voltage required to obtain constant current in V_{MIN} or V_{ON} is as shown in Fig. 4. The high output impedance minimizes the current variation for V_{DS} variation.

$$V_{DS}(\text{sat}) = V_{GS} - V_T = V_{ON} \quad (9)$$

The constant current depends on the value of V_{ON} [6, 8]. Lesser the V_{ON} faster the constant current can be achieved. MOS switch and current source results phase offset due to leakage mismatch $\phi_{\epsilon, \text{leakage}}$, current mismatch $\phi_{\epsilon, \text{mismatch}}$, and timing mismatch $\phi_{\epsilon, \text{timing}}$. The total phase error due to these mismatches

$$\phi_{\epsilon, \text{tot}} = \phi_{\epsilon, \text{leakage}} + \phi_{\epsilon, \text{mismatch}} + \phi_{\epsilon, \text{timing}} \quad (10)$$

$$\phi_{\epsilon, \text{tot}} = \frac{2\pi I_{\text{leak}}}{I_{CP}} + 2\pi \frac{\Delta t_{\text{on}}}{T_{\text{REF}}} \frac{\Delta I}{I_{CP}} + 2\pi \frac{\Delta t_{\text{on}}}{T_{\text{REF}}} \frac{\Delta t_d}{I_{CP}} \quad (11)$$

where Δt_{on} , Δt_d , T_{REF} , and ΔI are the turn on time of the PFD, the delay mismatch, the period of reference clock, and current mismatch of the charge pump, respectively.

4 Proposed Charge Pump

The charge pump proposed has an excellent current matching using improved cascode swing current source with a startup circuit. Charge sharing occurs when switch turns ON to OFF state. The charge stored during ON state is provided by definite path. Transistors MSUP2 and MSDN2 takes away stored Charge. These transistors are sized to turn ON fast. The charge pump has self-bias circuit with high output impedance and low turn on voltage to give constant bias voltage.

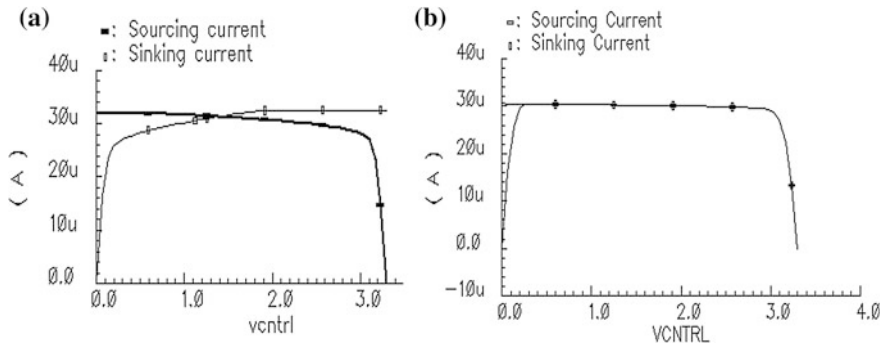


Fig. 6 Charge pump current matching characteristics A. V_{cntrl} versus Charge pump sourcing and sinking current B. current matching characteristics of proposed high-swing cascode CP

power supply 0–3.3 V are plotted comparing with conventional charge pump as shown in Fig. 6. From the proposed improved charge pump with improved high-swing cascode current source obtains nearest 0.01 % of current mismatch is achieved with 3.3 V, CMOS 90 nm *technology* [9, 10].

5 Layout Design and Simulation Results

CPLL consists of Digital blocks as PFD, Divider, and analog blocks as VCO. The placement is taken care to avoid ground bounce and supply bounce effects. The symmetry routing is provided in PFD so that it has minimum dead zone due to PFD and CP performance in loop. In layout of charge pump, symmetry affects the performance of CP. The proposed structure provides better matching in terms of layout performance. The entire transistors unit sized to the other on both N and P side. The structure makes routing very simple. The inter-digitization matching techniques are used to do current matching in cascode structure.

The output results of VCO are shown in Fig. 7. The VCO output signal ranges 1.65–3.1 V [11, 12]. The design is simulated for temperature range -40° to 125° .

Fig. 7 VCO waveforms, before and after Level shifter ($V_{ctrl} = 1.65$ V)

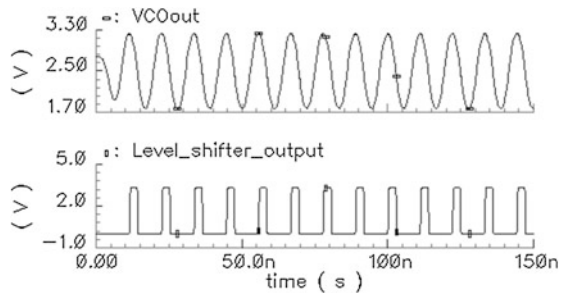
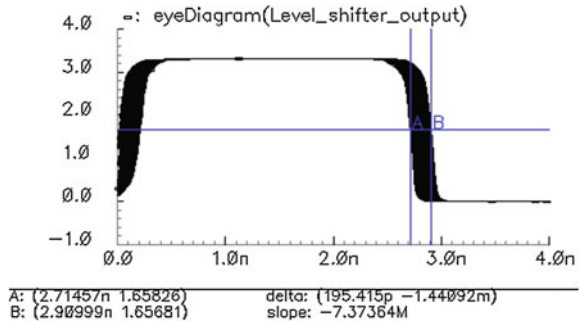


Fig. 8 VCO jitter calculation using “eye diagram” function in Cadence tool. Peak jitter = 195 ps at 85 MHz ($V_{ctrl} = 1.65\text{ V}$)



The VCO output ranges to supply rails 0–3.3 V. The peak jitter is measured as shown in Fig. 8. The third-order CPPLL is simulated with proposed new architecture results as shown in Fig. 9. In Fig. 9, the waveform VCTR can be observed charging and discharging and settle down once it locks to reference input frequency. The loop parameters are modeled using octave to observe the stability. The V_{ctrl} (VCTR) plot can be observed to see verge of critically damped.

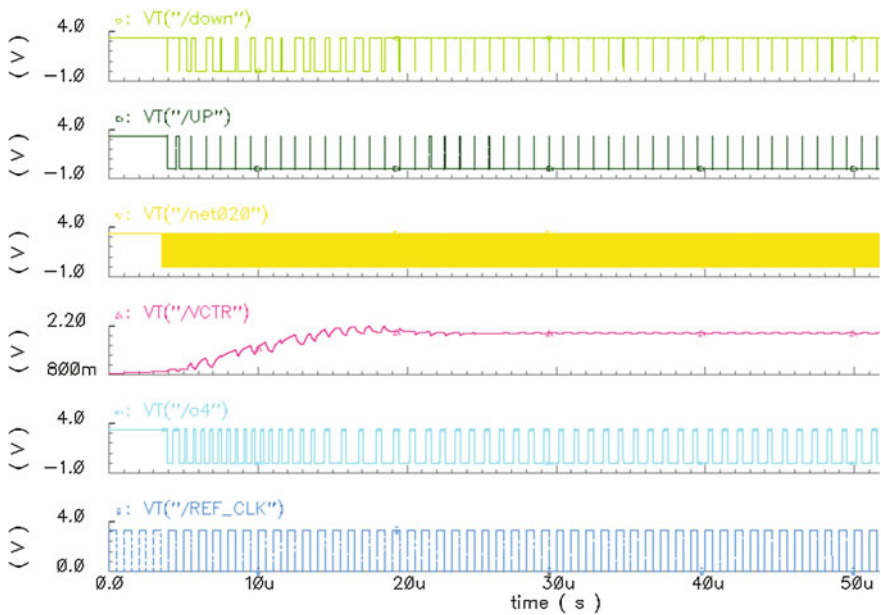


Fig. 9 Charge pump PLL Simulation results

6 Conclusion

The charge pump with improved high-swing cascode current source for accurate current matching is designed and analyzed using tsmc 90 nm technology. The proposed charge pump architecture provides 0.01 % current matching and provides stable current for voltage range 0–3.63. The dependence of ζ on loop parameters charge pump current I_{CP} , VCO Gain K_{VCO} , divider factor N , and its effects on settling time, lockin range, and loop bandwidth is discussed. Feature implementation can make programmable charge pump, so that the current source can be shutdown to avoid power consumption.

References

1. Shi X, Imfeld K, Tanner S, Ansoorge M. A low-jitter and low-power CMOS PLL for clock multiplication. Published in IEEE Esscirc—Mixed Signal, High Voltage & High Power Circuits 7, 2006.
2. Nanda U, Acharya DP, Patra SK. A new transmission gate cascode current mirror charge pump for fast locking low noise PLL. Circuits Systems and Signal Processing, © Springer Science Business Media New York, Apr. 2014.
3. Zhou J, Wang Z. A high-performance CMOS charge-pump for phase-locked loops. International conference on Microwave and millimeter wave technology ICMMT 2008, vol. 2, Apr 2008. pp. 839–842.
4. Zhiqun L, Shuangshuang Z, Ningbing H. Design of a high performance CMOS charge pump for phase-lockedloop synthesizers. J Semicond 14 February 2011;32(7):209–212.
5. Sujatha V, Dwahida banu RS. High performance charge pump phase locked loop with low current mismatch. IJCSI Jan 2012;9(Issue 1, NO. 2):442–446.
6. Razavi B. Design of analog CMOS integrated circuits. Tata McGraw Hill; 2002.
7. Fahim AM. Clock generators for SOC processors- circuits and architectures. Boston: Kluwer academic publishers.
8. Allen PE, Holberg DR. CMOS analog circuit design. Oxford: Oxford University Press; 2002.
9. Rhee W. Design of high-performance CMOS charge pumps in phase-locked loops. 1999 IEEE International Symposium on Circuits and Systems, ISCAS'99, vol. 2, 30 May–2 June 1999. pp. 545–548.
10. Lee J-S, Keel M-S, Lim S-I, Kim S. Charge pump with perfect current matching characteristics in phase-locked loops. Electron Lett. 2000;36(23):1907–8.
11. Prutchi D, Norris M. Design & development of medical electronic instrumentation—practical perspective of the design, construction, and test of medical devices. Wiley; 2005.
12. Rajeshwari DS, Rao PV. 3.3 V low power, low peak jitter Voltage controlled oscillator for MICS applications. National conference on VLSI signal processing, communication and soft computing, 2014. pp. 331–336.

Recent Research and Various Techniques Available for Efficiency Improvement of IGCC Power Plants

Ruchi Pandey, V.K. Sethi, Mukesh Pandey and Maneesh Choubey

Abstract This paper mainly focuses on the various technological improvements that need to be made for the current-integrated gasification combined cycle (IGCC)-based power plants in the near future through which efficiency of above 50 % would be achievable. This paper also elaborates about the working and the parts of an IGCC-based power plant. A discussion on the premier technologies that make IGCC the foremost prominent and promising technology for power generation today and tomorrow has been done, such as the advanced turbine technology, hot-gas cleanup technology, and the efficiency enhancement of the process, while taking into account the various aspects of each of these. If all of these novel technologies are adopted, then not only this will make the process very efficient, but also will be a promising solution for the years to come.

Keywords IGCC · SGS and CO

1 Introduction to an IGCC Plant

In an integrated combustion combined cycle power plant, the heating and partial oxidation of coal is done, such as synthesis gas or syngas (primarily hydrogen and carbon monoxide) is produced, which is subjected to the mechanisms of cooling and cleaning and then it is fired in a gas turbine generator. Whatever exhaust gases are produced, they are led through a heat recovery steam generator (HRSG), which

R. Pandey (✉) · M. Pandey
School of Energy & Environment Management, RGPV, Bhopal
Madhya Pradesh, India
e-mail: ruchipandey@ggits.org

V.K. Sethi
RKDF University, Bhopal, Madhya Pradesh, India

M. Choubey
Gyan Ganga Group, Jabalpur, Madhya Pradesh, India

forms steam that is sent to a steam turbine generator. The Oxygen that is required for the gasifier section is produced in an air separation unit (ASU). And from both the gas and steam turbines, while working in a combined cycle, power is produced. Given above is the block schematic of an integrated gasification combined cycle (IGCC). And the description of the above has been given below, while illustrating the functions of all of the above.

Slurry Preparation Unit Initially, the feed material, slag and fines water, viscosity modifier, and grinding water are ground into slurry. Additional large particles are removed. Further slurry is heated in order to reduce the amount of fuel necessary for gasification of the coal. The slurry so produced is led to the gasifier.

Air Separation Unit The air feed to the ASU is supplied from a stand-alone main air compressor and supplemented by pressurized air extracted from the gas turbine. The air separation plant is designed to produce 95 mol.% O₂ for use in the gasifier and Claus Plants. Inside the distillation column, the air is separated into oxygen and nitrogen products.

Gasifiers The gasifier vessel is a refractory-lined, high-pressure reaction chamber. The coal slurry feedstock and oxygen are fed through a fuel injector at the top of the gasifier vessel. The coal slurry and the oxygen react in the gasifier at 5.6 MPa (815 psia) and approximately 1,316 °C (2,400 °F) to produce syngas.

Syngas Scrubbers The purpose of the syngas scrubbers is to clean the syngas by separating the solids and entrained liquids from the syngas. The syngas scrubber system also collects and recycles the quench water used in the gasifier quench ring and dip tube. In addition, it controls the level of chlorides and other contaminants in the scrubber water system by bleeding some of the water off to the vacuum flash system.

Shift Reactors The conversion of CO to CO₂ for this plant is achieved by sour gas shift (SGS), where the water–gas (CO–) shift reaction occurs prior to removal of the acid gas from the synthesis gas. The shift reactors also serve to hydrolyze COS, which eliminates the need for a separate COS hydrolysis reactor. They also decompose metal carbonyls, formic acid, and hydrogen cyanide.

Gas Cooling and MP and LP Steam Generation Syngas is sent to a two-stage heat exchanger, wherein the first stage of cooling lowers the temperature by 70 °F and in the second stage the temperature of the syngas is lowered by 115 °F. The syngas is further sent to a knockout drum to collect any remaining liquid.

Mercury Removal Syngas is now heated by 5 °F in a preheater to prevent condensation within the activated carbon beds, wherein the Mercury is removed, removal of which is necessarily important so as to avoid the corrosion of heat exchangers.

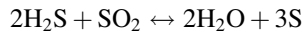
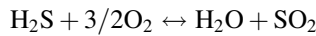
Selexol Acid Gas Removal The shifted raw syngas stream is sent to a removal chamber which removes the Hydrogen Sulfide (H₂S) and Carbon Dioxide (CO₂) which results in the formation of three product streams, namely clean syngas for the combustion turbine, H₂S rich acid gas for use in the Claus Plant, and CO₂ for

sequestration. The Syngas is flashed off at high temperatures for CO₂ stripping. Further in order to remove the H₂S, reboiling and recirculation actions are used.

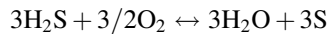
CO₂ Compression The compressor raises the pressure level of CO₂ to about 2200 psi during which it becomes a supercritical fluid. Also CO₂ is dried by mixing with Tri-ethylene Glycol, thereby minimizing the possibility of corrosion in the transport piping due to moisture being present.

Syngas Reheat and Expansion This stage involves the heating of a mixture of clean syngas from AGR system and clean gas from the CO₂ compression process to about 465 °F and then passing the above to an expansion turbine.

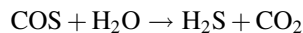
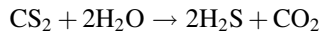
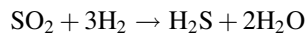
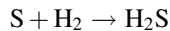
Claus Plant This stage involves the conversion of H₂S to elemental Sulphur using an exothermic reaction.



The Claus reaction:



Hydrogenation Reactor and Gas Cooler The following hydrogenation and hydrolysis reactions occur in the hydrogenation reactor:



The reactions are exothermic, and heat is removed from the gas in the gas cooler, which produces LP steam.

Combustion Turbine and Generators The combustion turbine is often coupled to a generator via a compressor shaft. Further, the combustion turbine utilizes Hydrogen-rich syngas derived from coal gasification in the aforesaid stages. Also a HRSG recovers the energy from the exhaust gas of the combustion turbine.

HRSGs and the Steam Turbine Generator The exhaust gas from the Combustion Turbine is fed to a HRSG where the heat transfer takes place across a heat transfer surface which reduces the exhaust gas temperature and raises the temperature of the steam and water inside the heat transfer surfaces.

Steam Turbine Generator The function of turbine models is to convert the thermodynamic energy of main and reheat steam into mechanical energy used to drive the generator rotor.

2 Next Generation IGCC Technology

Technological developments which are expected to be achieved by the next generation of IGCC projects and contribute to such cost reductions include:

1. Utilization of dry coal feed system instead of slurry;
2. “Warm” or hot-gas cleanup systems; warm gas cleaning processes are important to the overall IGCC system because at higher temperatures the gas maintains moisture content and some sensible heat.
3. Improvement of gasifier refractory properties, resulting in longer life cycle;
4. Ion transport membranes for air separation;
5. Gas turbine inlet chilling where appropriate and effective;
6. Advanced syngas turbines to increase efficiency and reduce NO_x emissions;
7. Improved reliability of key components and the overall system in general; and
8. Reduced use of water.

Advanced technologies are also being developed to improve the IGCC performance: new technologies for air separation and oxygen production, high-temperature gas cleaning methods, advanced gas turbines, and fuel cells. These technologies are being developed with the goal of raising thermal efficiency (higher heating value) to 50–60 %. An important new system developed incorporates the latest GT improvements for a high-efficiency quench (HEQ) design [1].

3 Advanced Turbines

The advanced syngas turbines provide the greatest performance improvements as the result of air integration, increased turbine firing temperature and pressure ratio, and increased inlet temperature. For example, the advanced “F” frame, 2010-AST, and 2015-AST syngas turbines result in the most significant capital cost reductions of all technologies (by \$304/kW, \$382/kW, and \$429/kW, respectively). These reductions are due to more increased net power generated than from any change in turbine equipment cost. The turbine section itself contributes only \$28/kW, \$32/kW, and \$44/kW reduction to the total plant cost, respectively.

The efficiency of a gas turbine depends on inlet temperature to the turbine. Turbines are designed for high inlet temperature by making improvements in coatings, film, and materials capabilities. Optimization between cooling air consumption and aerodynamic efficiency is an iterative process and thus the best designs need to be put into operation such that economy and efficiency are at their best.

When syngas is combusted in the gas turbine compressor, a pollutant namely NO_x is produced due to the high temperature and pressure, which is not a desirable feature. Thus NO_x emissions need to be controlled in the following ways:

1. Premixed combustion improvement by employing dry low NO_x burners and catalytic combustion. This technology holds importance as it creates a uniform air to fuel ratio to avoid localized high temperatures. Also catalytic combustion mechanism is employed so as to allow the fuel to burn at low temperatures, which also directly affects the reduction in the NO_x formation.
2. Addition of inerts to gas turbine flame to reduce flame temperature such as steam, water, and N₂ helps reduce NO_x to 9–25 ppm. This is done because the aforesaid technique is not very effective for syngas containing high amounts of H₂ which has a high reaction rate. Thus fuel dilution is further required for NO_x control.
3. Further NO_x reduction to 5–9 ppm is possible by selective catalytic reduction (SCR), wherein Ammonia is injected into the exhaust gas so that NO_x after chemical reactions with Ammonia and Oxygen forms Nitrogen and Water.

The major components of a gas turbine are the compressor, combustor, and the turbine. The materials of an entire gas turbine unit are under the influence of various operating conditions, and thus the materials to be used for an advanced turbine need lot of thoughts. The blades of the compressor are made from hardenable stainless steels generally. Coatings are also done on the compressor sections so as to reduce the surface roughness and thus the friction losses, which can be abradable and abrasive coatings. In the combustor section, coatings are provided for an insulation barrier from the hot-gas stream and the combustor parts. The materials for combustors must be easily formed and welded, should have resistance to high-temperature oxidation, good compatibility with thermal barrier coatings, and must have fatigue strength. The material for the combustor liner and transition piece can be a Nickel-based alloy such as Alloy X. For the advanced turbine materials, it is an extensive research and development area to find the optimum mix between mechanical properties, environmental resistance, and manufacturability. For that the options that are generally considered are Nickel-based alloys and single-crystal superalloys.

By making use of high temperature, high strength materials, new and novel approaches in sealing and cooling, advanced aerodynamic flow path optimization may help increase the efficiency of IGCC process to more than 50 %, which will reduce fuel consumption, reduce emissions, and will meet future ever-increasing energy demands.

In the present scenario, even H Class turbines are being preferred taking into account the advantages like

1. Increase of combined cycle net efficiency to over 60 %
2. Reduced emissions per produced kWh
3. High efficiency and low emissions also in part-load operation
4. Fast startup capability and operational flexibility
5. Reduced investment costs per kW
6. High reliability and availability
7. Lowest in lowest life cycle costs

The F-class gas turbine and combined cycle technology have been into successful operation for about two decades, but the new advanced H-class represents the most advanced and modern technology for economic and environmental friendly gas fired power generation.

The new generation H-class turbine provides a mix of environmental protection and economic effectiveness and is an advanced turbine technology while making use of innovative design, enhancement of process of manufacturing, and materials of high class. For the objective of high output and high efficiency, certain parameters namely compressor mass flow, firing temperature, exhaust temperature, and corresponding combined cycle parameters such as steam temperatures and pressure levels are used. In the present era of industrialization and power generation requirements, another issue that has been addressed is the choice of the engine cooling method so that the components in the turbine which have to withstand the massively high temperatures do not undergo any harm. And for this, making use of certain optimization methods, it has been realized that completely air-cooled method is the best.

Taking into account the above, the expectations from the H Class turbines are given as follows:

1. Combined cycle net efficiency over 60 %, resulting in approximately 3 % of fuel savings for improved operating expense.
2. Significantly reduced emissions per kWh produced combined with the lower heat rate and 25 ppm NO_x, 10 ppm CO.
3. Increased turn-down for achievement of high efficiency and low emissions also in part-load operation from 100 to 50 % load.
4. Quick startup capability of less than 15 min and operational flexibility to meet immediate needs in power grids.
5. Lower specific investment costs (EUR/kW) for reduced specific capital expenditure.
6. Reliability of over 99 %, availability of over 94 % and serviceability comparable to today's proven F-class technology.
7. Minimized life cycle costs for increased net present value for the owner of at least 7–8 %.

4 Hot-Gas Cleanup Technology

Basically, when it comes to the efficiency improvement of IGCC, there is requirement of the cleanup of the syngas that is produced at the gasifier, and thus there are two major techniques employed for the gas cleanup namely the cold gas cleanup at temperatures below 300 °C for the removal of particulate matter and Sulphur species, but the major limiting factor is that this process is very energy intensive and thus it reduces the overall process efficiency of IGCC.

Before the steps of particulate removal and desulphurization, a hot-gas cleanup is done of the syngas so produced in the gasifier section of an IGCC Power plant, such that the process can be done without the heat exchangers and the process condensate systems.

Since we know that in an IGCC plant, air is directly used as the oxidant, thus there is no need of an oxygen plant. Also, in this method, for the particulate removal, it is possible to use high-efficiency cyclones. There are two approaches to desulphurization, when inside the gasifier itself, limestone is used, which results in about 90 % Sulphur removal; and when done outside the gasifier, a high-temperature removal process is done using the Zinc Ferrite desulphurization process and this helps in reducing the levels of sulphur to about 10 ppmv, which not only helps reduce the SO₂ emissions from the gas turbine, but also the sulphur captured is recycled, and due to which additional sulphur recovery mechanism does not need to be set up. Also the Zinc Ferrite sorbent is recycled and reprocessed. The syngas that is available at the gasifier outlet needs to be cooled and for that water quench is made use of and thus no knockout drum is required for removal of process condensate.

Hot-gas cleanup offers the potential for higher plant thermal efficiencies and lower cost. A key subsystem of hot-gas cleanup is hot-gas desulfurization using regenerable sorbents. Sorbents based on zinc oxide are currently the leading candidates and are being developed for moving- and fluidized-bed reactor applications. Zinc oxide sorbents can effectively reduce the H₂S in coal gas to around 10 ppm levels and can be regenerated for multicycle operation. Advanced IGCC power plants require advanced particle filters and hot-gas desulfurization (HGD) following gasification in order to achieve high thermal efficiency (Figs. 1 and 2, Tables 1 and 2).

Some of the major factors affecting the performance of desulphurization are pressure and temperature of the gas, syngas composition, contaminants, and particulate matter in the gas [2].

5 Efficiency Optimization of IGCC Power Plants

Another improvement that can be made is the efficiency improvement of the IGCC power plants which can be done in a manner as to increase the efficiency of the individual gas and steam turbine efficiencies which is quite possible taking into account the various research and development efforts in progression and achieved till date. Another aspect that needs to be addressed is the increase in the temperature of the syngas reaching the gas turbine. This hike in temperature is required so as to control the presence of alkali metals in the syngas such that the corrosion of the turbine blades does not occur. A hike in temperature also increases the process efficiency. Again there is another limit to the high range of the temperature because the Indian coals are high in ash content such as Silica or Alumina, whose sintering occurs at temperatures beyond a certain limit and that again is not a desirable feature. Thus, it is of utmost importance that the efficiency improvement with the

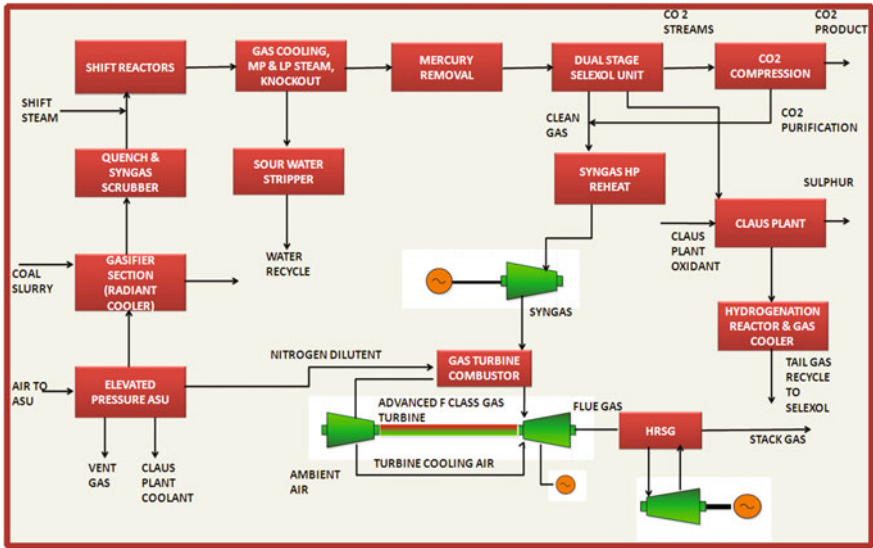


Fig. 1 Schematic of an IGCC power plant. Source Volume 2: IGCC Process Descriptions, NETL, 2008

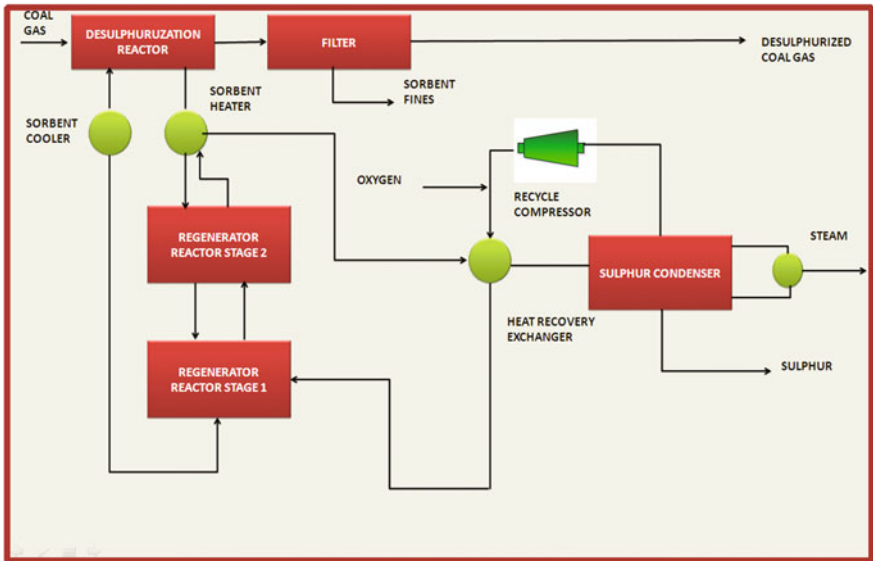


Fig. 2 Schematic of a hot-gas desulphurization plant. Source Volume 2: Hot-Gas Desulphurization With Sulfur Recovery, Research Triangle Park

Table 1 Performance comparison between GE 7FA turbine for syngas and natural gas as a fuel

Manufacturer model	General electric frame 7FA	
Fuel: type heating value (LHV)	Syngas 115 BTU/SCF	Natural gas 910 BTU/SCF
Power output @ 59 °F	197 MWe	172 MWe
Heat rate, LHV	8,840 BTU/kW-h	9,420 BTU/kW-h
Efficiency	37.5 %	35.2 %
Exhaust temperature	1091 °F	1116 °F
NO _x control	Nitrogen injection	Dry low NO _x burner
NO _x (@ 15 % O ₂ dry)	9 ppmv	9 ppmv
CO (dry)	25 ppmv	9 ppmv

Source Gasification, Gasification Workshop, September 11–13, 2001 Indianapolis, Indiana

Table 2 General electric H class turbine performance rating

Performance rating	SGT5-8000H	SGT6-8000H
Gas turbine power output	375 MW	274 MW
Gas turbine efficiency	40 %	40 %
Combined cycle (1 × 1) power output	570 MW	410 MW
Combined cycle (1 × 1) efficiency	>60 %	>60 %

Source <http://www.Ge-Energy.Com>

hike in temperature does not yield issues which cause an increase in the maintenance costs. Another factor of concern is the efficiency of fuel conversion.

Controlling the temperature of the syngas reaching the gas turbine is of utmost importance, and this is carried out by making use of a radiant syngas cooler stage just after the gasifier, wherein the raw syngas is cooled down to various temperatures as per the process requirement. When the outlet temperature of the radiant syngas cooler is varied, the efficiency increases, with increase in temperature; but after certain temperature range the electrical power output decreases, thus, creating the need of an optimization mechanism, which finds the optimum temperature range of operation which yields maximum efficiency and maximum power output from the IGCC.

6 Conclusions

1. Though IGCC present efficiency is up to 40 %, still if the further improvements in the process are made, then the efficiencies can reach up to and more than 50 % in the near future.
2. Out of the various improvements that can work, one of the major technological advancements is the advanced gas turbines, wherein the major factors that can help are reduction in flame temperature, increase in turbine inlet temperature, and fuel dilution.

3. Warm gas cleanup systems are beneficial, as before the steps of particulate removal and desulphurization, a hot-gas cleanup is done of the syngas so produced in the gasifier section, such that the process can be done without the heat exchangers and the process condensate systems. This increases the overall efficiency of the system.
4. As far as the improvement in efficiency is concerned, apart from the efficiency of the gas and the steam turbine cycles, another factor that needs focus is that alkali metals in the syngas may corrode the turbine blades; so the temperature needs to be kept beyond a specific temperature and also there is a limit to the higher range of temperature as it can cause sintering of the Silica, which is present in huge quantities in Indian coal.
5. The outlet temperature of the syngas exiting from the radiant syngas cooler stage, after the gasifier section needs to be controlled in a manner as to find the optimum temperature at which the power and efficiency of the IGCC is maximum.

References

1. Todd DM. Gas turbine improvements. In: Enhance IGCC Viability 2000. Gasification Technologies Conference.
2. Atimtay AT, Harrison DP. Desulfurization of hot coal gas. Nato Asi Series G.

An Involuntary Data Extraction and Information Summarization Expending Ontology

R. Deepa and R. Manicka Chezian

Abstract The World Wide Web is a repository of huge data that are the web pages. The web pages are acquired using a query given by the user. The web pages may sometimes be unstructured and unequal. The main objective of the study is information extraction and summarization using ontology. The system proposes a new method named as Structural Semantic Domain Ontology (SSDO) for effective information retrieval. The proposed system automatically extracts the unstructured information from the repository and stores it in the search buffer. The information extraction will be performed using domain ontology. The main disadvantage of the existing system is, the information which is extracted from various sources is not aligned properly. The system may fail to know, where the exact information is located on the website. The current proposal overcomes the above problem by adopting the technologies that are named as pair alignment, top-down alignment, and loop structure algorithms. The proposed system will acquire things such as if the user needs to know any data, then the user will type the detail known as a label. Then the web page will extract the information with a proper description and additional details.

Keywords SSDO · Ontology domain storage · DELTA · Information retrieval · Pair Alignment · Technologies

1 Introduction

This paper focuses on to overcome the existing approaches and it works based on a new method called Structural Semantic Domain Ontology (SSDO) [1] for extracting the regulated data from the web pages that are generated relevant to the

R. Deepa (✉) · R.M. Chezian
Research Department of Computer Science, NGM College, Pollachi, Coimbatore, India
e-mail: deepaharini2015@gmail.com

R.M. Chezian
e-mail: Chezian_r@yahoo.co.in

users' [2] query with the use of ontology. It performs unit level data extraction that successfully extracts data units and aligns them in an ordered format, finally summarizes the data by means of clustering. Auxiliary information which was eliminated in the existing method is maintained and stored by means of ontology domain storage.

The main idea of data extraction is to extract the SR (search result) from the query [3] result pages and align them in tabular format based on the criteria that the tag and values are similar to tables assigned to the data units. It aims to provide higher precision and extraction results compared with the existing state-of-the-art methods.

This study aims to automatically extract wrappers, tags, and values from a raw HTML file by introducing a semantic method called Structural Semantic Domain Ontology (SSDO), which automatically assigns meaningful labels to the data units in the SRs [4]. It has a main objective of finding relative labels for SR result set alignment.

- This Study provides a solution against three major problems in dealing with SR.
- The query result records extracted from result pages may have lots of unwanted data.
- The web page extraction may vary based on the construction of web pages.
- Another problem is the alignment and summarization of the needed results into an ordered form.

The implementation of SSDO aims to provide optimal extraction, alignment, and summarization of the SR data attributes. The extraction time and memory usage can be minimized to enable the fully automatic extraction and summarization. The result pages have to be automatically obtained and the SRs need to be automatically extracted [5].

2 Methodology

2.1 *Structural Semantic Domain Ontology (SSDO)*

The proposed system extracts and summarizes the SRs in web databases if there are at least two records in the page. The new technique is proposed to handle the case when there are no contiguous data in the dataset, then it extracts the available data and calculates a priority and makes it as an outline for the fast summarization. The result shows that noncontiguous data region problem can be addressed easily due to the presence of auxiliary information such as a comment, recommendation, and advertisement. Data can be referenced further if needed. Existing DELTA eliminates the auxiliary information for data labeling. Compared with existing data

extraction methods, SSDO improves data extraction accuracy in many ways as follows:

- A data region identification technique is proposed to identify the noncontiguous SRs that have the same parents according to their tag similarities, followed by a data region merge, that merges the data region that contains similar data records into one. Tag identification and classification methods are used to identify similar tags [6].
- A new method is proposed to align the data values in the identified SRs first pairwise, then top-down, and finally after prioritizing they can be put into a table with the data values belonging to the same attribute arranged into the same table column. Both tag structure similarity and data value similarity are used in the pair-wise alignment.
- Dissimilar existing nested structure processing algorithms rely on the tag information only [6], but SSDO uses both tag and data value similarity information to improve the accuracy of middle out ontology structure processing.
- This approach considers other important features shared between data units, such as their priority- based information. Finally the system integrates the interface schema over multiple web databases with the common cluster to enhance data summarization.

2.2 *Search Result Extraction*

Search result records are obtained from the result pages by identifying the data regions in the web pages followed by merging the data regions that exist in several pages. For a query result page, the tag tree construction module constructs a tag tree for the page rooted in the HTML tag [7]. Every node within the tag tree represents a tag within the hypertext markup language page, its derivatives are tags authorized within it. Each internal node n of the tag tree includes a tag string (tsn) and a tag path (tpn) [8], which integrates the tags from the basis node to n . Next, information region identification module identifies all potential knowledge regions in websites that contain dynamically generated data, prime down ranging from the basis node to n . The information region merges section helps to merge totally different data regions that contain similar records into one. The record segmentation section then segments the known knowledge regions into knowledge records in step with the tag patterns within the knowledge regions. Query result sets identification part helps to pick one, among united regions that contains the SR and eventually SRs are extracted from this region [7]. Earlier works on webpage segmentation were on free texts and intended on rising performances of the knowledge retrieval. In information retrieval, documents are extracted with the values of the linguistics of a web page to the queries [3, 6, 9, 10].

2.3 Middle Out Ontology Structure Processing

Top-down data value alignment constraints a data value in a SR to be aligned to atmost one data value from another SR. If SR contains middle out ontology structure such that an attribute has several values, then certain values may not be associated with any other values [6].

The middle out ontology structure identification algorithm steps are as follows:

- Step1:** Identifies the nested column set C and creates a replacement row for every combination of a repetitive part.
- Step 2:** For all found SRs, the tag tree for the question result page and also the SRs' prime down aligned columns as input.
- Step 3:** For each SR with a record root node t in T, the procedure nest column determines is invoked to spot any nested columns within the SR.
- Step 4:** After all the nested columns are known, a new row is generated by bridging the remaining components additionally because the repetitive information is worthful.
- Step 5:** Given n records with atmost m data values and atmost tag string length of 1, the time complexity of the middle out ontology structure processing algorithm is $O(nl2m2)$ [7].

Middle out Ontology Structure Processing Algorithm [7]

Procedure nets processing (SRs, T, Top Down Align)

1. $C == \Phi$
2. for each SR with record root t
3. nest column identify (t,T, Top down align, C)
4. for each column pattern cp in C do
5. create a new row for each repeated subpart
- Procedure nest processing (SRs, T, Top down align)
6. if(t contains more than one data value) then
7. for each child ti of t do
8. nest column identify(ti, T, Top down align, C)
9. for each repetition p of any consecutive maximum repetitive tag pattern found in t's children
10. Cp= data columns for p in the Top down align
11. if cp \in C and nested (cp, Snest) then

```

12. add nested column (cp, C)
   Function Boolean nested (cp, Snest)
13. Simintra== intra- column similarity within cp
14. Siminter==inter- column similarity with in cp
15. if(Siminter/Simintra>Snest) then
16. return true
17. else return false
Procedure add nested column (cp, C)
18. for each element ci in C do
19. if( $cp \cap ci \neq \phi$ ) then
20.  $C == C - ci + cp \cup ci$ 
21. break
22. if no element in C shares a common column with cp then  $C == C + cp$ 

```

2.4 Data Summarization

In this data summarization technique clustering algorithms are used. The first identifies all information units within the SRs to organize them into totally different teams with every cluster equivalent [11] to a distinct conception.

Grouping data units of the same semantic can help in identifying the common patterns and features among these data units. These common features are the basis of the labeling technique for summarization. A tag node corresponds to an HTML tag surrounded by “<” and “>” in HTML source, while text node is the text outside the “<” and “>.” `stero`

2.5 Process Included in Data Summarization

The proposed enhanced data alignment rule is predicated on the idea that attributes seem within the same order across all SRs on the identical result page though the SRs might contain completely different sets of attributes. The following are the steps involved in the enhanced alignment for data summarization [12].

Step 1: Merge text nodes. This step detects and removes decorative tags from each search result record to allow the text nodes corresponding to the same attribute (separated by decorative tags) to be merged into a single text node.

Step 2: Align the text nodes. This step aligns the text nodes into groups so that eventually each group contains the text nodes with the same concept (for atomic nodes) or the same set of concepts. (For merged nodes)

- Step 3:** Split composite text nodes. This step aims to split the values in composite text nodes into character data units. This step is processed out based on the text nodes in the same group top-down. A group whose values need to be split is called composite group.
- Step 4:** Align data units. This step is to separate each composite group into multiple aligned groups with each containing the data units of the same concept [1].

Data Summarization Algorithm [1]

Grouping Data Units

Input: a set of query terms T , A data section block B

Output: a set of data Record R

1. set R , a set of leaf nodes NI , a set of starting leaf nodes Ns , a set of data unit groups G , a set of leaf nodes groups $G1$ and a set of horizontally expanded data unit groups G all to $\{\}$
2. Add every text nodes in B to NI
3. for every leaf node $nl \in NI$ do
4. if nl contains a query term $t \in T$ then
5. Add nl to NS
6. remove nl from NI
7. for every starting leaf node $ns \in Ns$ do
8. set a data unit group g to $\{ns\}$
9. for every leaf node $nl \in NI$ do
10. if nl is horizontally aligned with ns then
11. Add nl to g
12. remove nl from NI
13. Add g to G
14. repeat
15. remove a leaf node nl from NI
16. set a leaf node group $gl = \{nl\}$
17. for each leaf node $nl \in NI$ do
18. if nl is horizontally aligned with nl then
19. add nl to gl
20. remove nl from NI
21. add gl to $G1$
22. until $NI = \{\}$
23. repeat
24. remove a data unit group g from G
25. for each data unit group $g \in G$ do

26. if g is horizontally aligned with g then
27. set g to $g \cup g$
28. remove g from G
29. add g to G
30. Until $G = \{ \}$
31. Repeat
32. Remove a horizontally expanded data unit group g from G
33. for each horizontally expanded data not group $g \in G$ do
34. if g is vertically adjacent of g then
35. set g to $g \cup g$
36. Remove g from G
37. for each leaf node group $g_l \in G_l$ do
38. if g_l vertically adjacent to g then
39. set g to $g \cup g_l$
40. remove g_l from G_l
41. Add g to R
42. Until $G = \{ \}$
43. Return to R

A set of query terms- as T , Data section block- as B , Set of data records- as R

3 Results and Discussion

3.1 Data Summarization

SR results will be summarized by highlighting the data attributes. Based on the details such as Author Edition, Publication Date, the links extract the necessary data. In case of mobile dataset, model, version, and prices are summarized. In case of laptop, price, configuration, name, and brand are described [7].

3.2 Performance Evaluation

Performance evaluation of the proposed approach is conducted based on the working of SRs context scenario. Precision, Recall, and F1 Score plays an important role in the ontology-based semantic web query matching performance.

$$\text{Precision} = \frac{tp}{tp + fp}. \quad (1)$$

$$\text{Recall} = \frac{tp}{tp + fp}. \quad (2)$$

$$\text{Accuracy} = \frac{tp + tn}{tp + tn + fp + fn} \tag{3}$$

$$F - \text{Measure} = 2 \cdot \frac{\text{precision} \cdot \text{recall}}{\text{precision} + \text{recall}} \tag{4}$$

where

- tp True Positive (Correct result)
- tn True Negative (Correct absence of result)
- fp False Positive (Unexpected result)
- fn False Negative (Missing result)

Noncontiguous SR analysis compares the performance for query result pages during which the SRs area unit for contiguous and noncontiguous [13]. Fig. 1 compares the contiguous and noncontiguous search results for the existing DELTA and the proposed SSDO Methods. The Comparison notifies that SSDO performs better as it provides the SRs needed result (Table 1).

The simulation results for the evaluation of the proposed approach against the existing approach for various performance measures like Precision, Recall, and F-Measure are shown in the Table 2. The results of the performance measures are plotted in Fig. 2.

Fig. 1 The extracted results and currently extracted SRs for DELTA and SSDO are compared

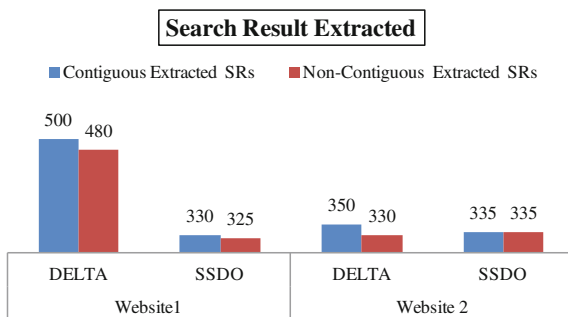


Table 1 Search result extracted

	Website1		Website 2	
	DELTA	SSDO	DELTA	SSDO
Contiguous extracted SRs	500	330	350	335
Noncontiguous extracted SRs	480	325	330	335

Table 2 Performance Analysis

	Website1		Website 2	
	DELTA	SSDO	DELTA	SSDO
Record level precision (%)	72.6	81	76.6	91.9
Record level recall (%)	83	89.5	86.3	96.9
Accuracy (%)	91.8	94.5	93.8	94.3
F-measure	77.4	85	81	94.3

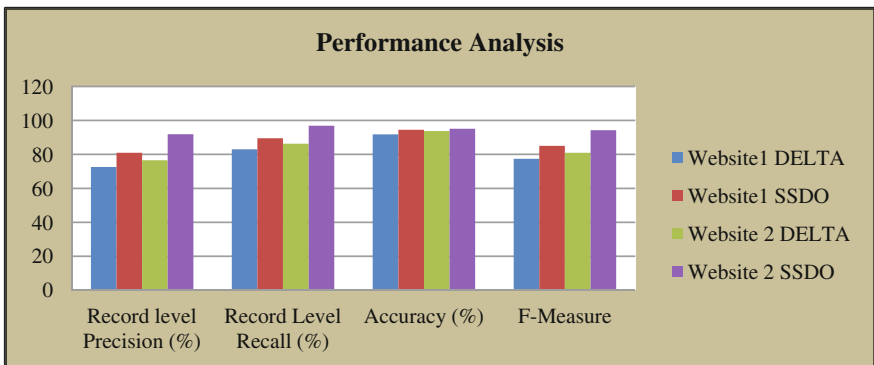


Fig. 2 Performance analysis measure for the existing DELTA and the proposed SSDO for the factors Precision, Recall, Accuracy, and F-Measure

From Table 2 of the performance measures, it is seen that the accuracy of the proposed system is 94 %, which is high in comparison with the available approaches in the literature. Then SSDO shows the best recommendation to users. The recommendation results are shown in Fig. 2.

4 Conclusion

A new design of query-based recommendation system based on improved Structural Semantic Domain Ontology (SSDO) with nested structure and data alignment using improved clustering algorithms, has been proposed for the implementation of an efficient web search [14]. The salient feature of this proposed approach is that it is based on semantic domain ontology, which decides the relevance between keyword and user query words. SSDO first discovers the data regions from multiple pages and merges the data region that contains similar data records. Finally, it aligns the data values in SR by the following methods: pairwise, top-down, priority basis, and middle out ontology structure processing. SRs with a similar tag and value will be stored in the tables. The ontology domain storage technique is used to store the supporting information [15].

SSDO extracts desired data from various SR pages. The experiments on many collections of SR, drawn from several well-known knowledge wealthy sites, this means that SSDO is extraordinarily smart in extracting and orienting the information from the online page sources. The opposite fascinating feature of the planned system is that's doesn't complexes, fail to extract any knowledge even once, a number of the ideas created by non mandatory tag aren't met by the input

assortment. SSDO inclines to offer higher accuracy compared with the prevailing ways.

References

1. Suresh Babu A, Premchand P, Govardhan A. Record-level information extraction from a web page based on visual features. *Int J Comput Technol Electron Eng. (IJCTEE)*. 2012;2 2:99–105. ISSN 2249-6343.
2. Arasu A, Garcia-Molina H. Extracting structured data from web pages. In: *SIGMOD 2003*, pp. 337–348, San Diego, CA, 9–12 June 2003.
3. Su W, Wang J, Lochovsky FH. ODE: ontology-assisted data extraction. *ACM Trans Database Syst.* 2009;34 2. Article 12, Publication date: June 2009.
4. Chen K, Zhang F, He FL. Extracting data records based on global schema. *Appl Mech Mater. (AMM)*. 2010;20–23:553–558.
5. Bing L, Lam W, Gu Y. Towards a unified solution: data record region detection and segmentation. In: *CIKM'11*, Glasgow, Scotland, UK, 24–28 Oct 2011.
6. Su W, Wang J, Lochovsky FH, Liu Y. Combining tag and value similarity for data extraction and alignment. *IEEE Trans Knowl. Data Eng.* 2012;24 7:1186–1200.
7. Deepika J. Non-duplicate data extraction in web databases by combining tag and value similarity. *Int J Adv Inform Sci Technol. (IJAIST)*. 2013;9 9:16–22. ISSN: 2319:2682.
8. Jude Victor M, John Aravindhar D, Dheepa V. Web data extraction and alignment. *Int J Sci Res. (IJSR)*. 2013;2 3:129–132. India Online ISSN: 2319-7064.
9. Manonmani K, Kalidass M. Automated data extraction and arrangement using segmentation based tag and value resemblance analysis. *Int J Comput Sci Manag Res.* 2013;2 4:2211–2216. ISSN 2278-733X.
10. da Costa MG, Zhiguo J. Web structure mining: an introduction. In: *Proceedings of the 2005 IEEE International Conference on Information Acquisition*, Hong Kong and Macau, China, 27 June–July 3 2005.
11. Oro E, Ruffolo, M. Sila: a spatial instance learning approach for deep webpages. *Proceedings of the 20th ACM international conference on Information and knowledge management*. ACM, 2011.
12. Ruiz EJ, Hristidis V, Ipeirotis PG. Facilitating document annotation using content and querying value. *IEEE Trans Knowl Data Eng.* 2014;26 2:336–349.
13. Vinod Kumar R, Kumar Somayajula SP. Automatic template extraction from heterogeneous web pages. *Int J Adv Res Comput Sci Softw Eng.* 2012;2 8:408–418. ISSN: 2277 128X,.
14. Baldonado M, Chang C-CK, Gravano L, Paepcke A. The stanford digital library metadata architecture. *Int J Digit Libr.* 1997;1:108–21.
15. Bruce KB, Cardelli L, Pierce BC. Comparing object encodings. In: Abadi M, Ito T editors. *Theoretical aspects of computer software*. Lecture notes in computer science, vol. 1281. Berlin: Springer; 1997. pp. 415–438.

DWT–SVD-Based Watermarking Scheme Using Optimization Technique

Sarthak Nandi and V. Santhi

Abstract In this paper, a watermarking scheme has been proposed for embedding a digital watermark in images. The process of inserting a watermark is carried out in invisible mode. The proposed watermarking algorithm utilizes particle swarm optimization technique to obtain the scaling and embedding factors which are required to carry out the watermarking process, thus the proposed methodology is adaptive. The embedding and extraction processes are carried out using discrete wavelet transform and singular value decomposition (SVD) techniques. The proposed scheme finds application in curbing the copyright infringement of images by inserting an invisible watermark in the image, which can be colour or greyscale. The watermarked images are tested with various attacks in order to ensure the robustness of the proposed technique. The results obtained are tabulated to verify and prove the efficiency of the proposed technique.

Keywords Digital watermarking · Discrete wavelet transform · Invisible · Particle swarm optimization · Singular value decomposition

1 Introduction

Internet and the availability of affordable smart phones, laptops, etc. has enabled people to share images with millions of other people at the click of a button, as it is extremely easy to produce and distribute unlimited number of copies of any digital information. This has also increased the possibility of copyright infringement of images. Digital watermarking is considered as a security mechanism, which is used to curb the illegal practices.

S. Nandi (✉) · V. Santhi
SCSE, VIT University, Vellore 632014, India
e-mail: sarthakn@gmail.com

V. Santhi
e-mail: vsanthinathan@gmail.com

Digital watermarking is a process through which any secret data, called a digital watermark, is inserted in a digital signal which can be images, audio clips, video sequences, etc. In general, the inserted digital watermark can then be used to identify the authorized owner of the signal. Based on perceptibility, watermarking schemes could be classified as visible and invisible. Security threat is very minimal in perceptible watermarking schemes compared to imperceptible schemes, because of the visibility of the watermark. However, it might be possible to remove a visible watermark using some image editing applications. Also, perceptible watermarking schemes may not be suitable for all kinds of applications, because the existence of visible watermark obscures the underlying content. Thus it is required to propose a new, robust imperceptible watermarking scheme to protect the digital signal. The unauthorized users might not suspect whether an image contains an invisible watermark or not, and if any copyright infringement is found, the violator may be prosecuted with relative ease. The important components of any watermarking scheme consist of cover data, secret data to be hidden and algorithms to insert/extract watermark [1–3].

The process of inserting a watermark could be carried out either by modifying sample intensity values or frequency components of the signal. The former is called spatial domain processing, whereas the latter is known as frequency domain processing [4]. In order to obtain frequency components of the signal, any transformation techniques such as, discrete cosine transformation (DCT), discrete wavelet transformation (DWT), discrete Hadamard transformation (DHT) and discrete Fourier transform (DFT) could be used [5].

In earlier days, least significant bit (LSB)-based undetectable electronic watermark was inserted in greyscale images as proposed in [6]. In this, instead of considering logo or any image as watermark, a pseudorandom sequence is generated and used as an electronic watermark. The pseudorandom sequence is generated using linear shift register. In [7], a new watermarking scheme is proposed for medical images. The proposed scheme uses singular value decomposition, contourlet transform and discrete cosine transform. The obtained watermarked images are tested against various attacks and its efficiency is proved. In [8], Yenhui has proposed a watermarking scheme based on particle swarm optimization technique and multi-wavelet technique. This proposal considers human visual system characteristics for inserting a watermark. In [9], a blind watermarking algorithm is proposed. It is based on the significant differences of wavelet coefficients. However, it is pointed out in [10], that the scheme proposed is potentially insecure. In order to alleviate this security issue, an intelligent watermarking is proposed using particle swarm optimization technique in wavelet domain [11]. In [12], Meghdut has proposed an algorithm that inserts a watermark using SVD and PSO with multiple scaling factors. Jianzhong Li has proposed a watermarking scheme using an encrypted gyrator transform computer generated hologram, which uses PSO to find the optimal embedding parameter in [13]. Irshad Ahmed Ansari has shown that incorporating PSO improves the results in an SVD-based watermarking technique [14].

Based on the literature review, it is observed that above PSO-based watermarking techniques have included the attacked watermarked images in the fitness function, leading to higher computational complexity. The complexity of an algorithm is magnified when it is running higher number of iterations. This paper aims to simplify the fitness function so as to reduce the time taken to perform watermarking an image while performing at par with other algorithms. In this paper, Sect. 2 discusses the proposed algorithm in detail. The performance analysis is carried out in Sect. 3. Section 4 concludes the work.

2 Proposed Watermarking Scheme

2.1 Adaptive Calculation of Scaling and Embedding Factors

In this section, the adaptive calculation of scaling and embedding factors using particle swarm optimization is discussed. The scaling factor is represented as α and embedding factor is represented as β . The proposed algorithm could be used to embed a watermark in colour images as well as in grayscale images. If the colour image is to be watermarked, then it needs to be transformed into YIQ domain in order to insert the watermark in the luminance components otherwise greyscale values can be considered directly for inserting the same. In order to increase robustness in watermarked images, the watermarking procedure could be carried in the frequency domain of Y components. The luminance component Y is transformed into frequency components using DWT. The multi-resolution capability of DWT decomposes the signal into low frequency, middle frequency and high frequency bands. As low frequency components are more significant and robust to attacks, it is selected for inserting the secret data. The identified low-frequency band is decomposed into singular matrix, left orthogonal and right orthogonal matrices. In order to calculate the scaling factor using PSO, four particles are considered. The maximum number of iterations is set to 100. The fitness function to be maximized is

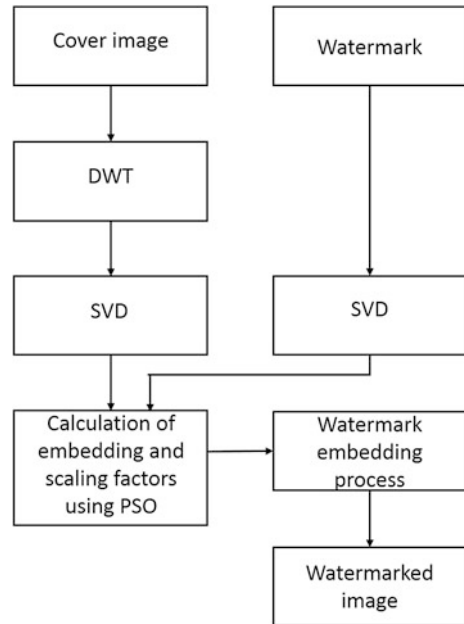
$$f = NCC_w + NCC_{img} \quad (1)$$

where NCC_w denotes the normalized correlation coefficient (NCC) of the extracted watermark and NCC_{img} denotes the NCC of the watermarked image. Once the scaling factor α is calculated, the embedding factor β is calculated as

$$\beta = 1 - \alpha \quad (2)$$

The use of embedding factor β is to reduce the strength of the image for inserting the watermark. Thus, the strength of the image is reduced in proportion to the strength of the inserted watermark. The calculated values of both parameters should range between 0 and 1 ($0 < \alpha < 1$, $0 < \beta < 1$).

Fig. 1 Watermark embedding process



2.2 Watermark Embedding Process

This section discusses the watermark embedding process. The pictorial representation of a watermark embedding process is shown in Fig. 1. The image to be watermarked is called the cover image. The luminance component of the cover image is converted into frequency components. The low-frequency band is decomposed into singular values. From these singular values, the embedding and scaling factors are calculated. As the parameters are calculated adaptively from the content of the cover image, the inserted watermark does not distort the quality of the cover image.

2.3 Watermark Extraction Process

During the extraction process, the original image is used to obtain the embedding and scaling factors. The watermarked image is transformed into frequency components, and the band in which the watermark was embedded is transformed into SVD domain. The S'_w matrix of the watermark is extracted from here and the orthogonal components obtained from the original watermark are used to retrieve the watermark.

3 Performance Analysis

The performance of the proposed watermarking algorithm is tested in this section. To test the performance of the proposed algorithm, the test images considered in Fig. 2 are used. The original watermark used is shown in Fig. 3. The watermarked images are shown in Fig. 4.

The adaptively calculated scaling and embedding factors are shown in Table 1. The extracted watermark without any attack is compared with the original watermark and it is observed that the similarity is more than 99 %. These are shown in Table 2. In order to test the robustness of the watermarked images, they are tested against various attacks. The obtained results are tabulated. The watermarking is carried out on both greyscale and colour images. The obtained results for a colour image are given in Table 3.



Fig. 2 Test images

Fig. 3 Original watermark





Fig. 4 Watermarked images

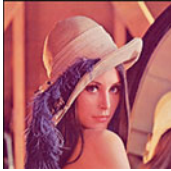
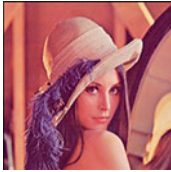


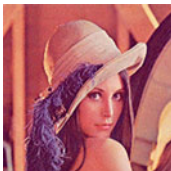

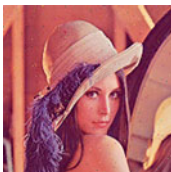



Table 1 Calculated scaling and embedding parameters

S. no.	Type	Name of the image	Scaling parameter	Embedding parameter
1	Colour	Lena	0.067301964	0.932698036
2	Colour	Airplane	0.062420516	0.937579484
3	Colour	Baboon	0.060040078	0.939959922
4	Colour	Pepper	0.06004	0.93996
5	Greyscale	Barbara	0.061199138	0.938800862
6	Greyscale	Boat	0.068389376	0.931610624
7	Greyscale	Cameraman	0.064473887	0.935526113
8	Greyscale	Houses	0.062390292	0.937609708

Table 2 Similarity measure between original and extracted watermark

S. no.	Type	Name of the image	NCC of extracted watermark
1	Colour	Lena	0.9999963
2	Colour	Airplane	0.9999948
3	Colour	Baboon	0.9999961
4	Colour	Pepper	0.9999895
5	Greyscale	Barbara	0.9999967
6	Greyscale	Boat	0.9999966
7	Greyscale	Cameraman	0.9999905
8	Greyscale	Houses	0.9999959

Table 3 Results obtained after extracting the watermark from the attacked watermarked image

Type of attack	Attacked watermarked image	PSNR	Retrieved watermark	Similarity between the original and retrieved watermark
Translation	 Translated by (2,2)	68.12781274		0.999742036
Resize	 Resized to 1/2 of original	83.27870673		0.984478661
Compression	 Compressed to 10% of original size	80.68531116		0.996606628
Gaussian noise	 M=0, V=0.001	77.92357249		0.997033494
Salt and pepper noise	 D=0.005	75.75283476		0.994545254
Gaussian filter	 hsize=3 sigma=0.5	86.66201722		0.993890348

As per the results obtained, the proposed watermarking algorithm is robust against various attacks. Moreover, the hidden information is not recognizable as it is inserted using scaling and embedding factors obtained using particle swarm optimization.

4 Conclusion

A novel adaptive invisible watermarking scheme has been proposed in this paper, which uses the PSO technique to calculate the embedding and scaling factors. The proposed scheme embeds the watermark in the transform domain using DWT and SVD techniques. The proposed methodology can be used to prevent copyright infringement of images in the public or private domain by securely inserting a watermark into the colour or greyscale images. The efficiency of the proposed algorithm is verified by the results obtained through various attacks implemented on watermarked images.

Acknowledgments The authors would like to thank VIT University for permitting us to make use of the facilities for implementing and testing this work.

References

1. Chen YC, Yu WY, Feng JC. A digital watermarking based on discrete fractional Fourier transformation DWT and SVD. In: 24th Chinese Control and Decision Conference (CCDC), 2012. IEEE; 2012.
2. Kankanhalli MS, Ramakrishnan KR. Adaptive visible watermarking of images. In: IEEE international conference on multimedia computing and systems, 1999. IEEE; 1999. vol. 1.
3. Berghel H, O’Gorman L. Protecting ownership rights through digital watermarking. *Computer*. 1996;29(7):101–3.
4. Manoharan JS, Vijila KC Dr, Sathesh A. Performance analysis of spatial and frequency domain multiple data embedding techniques towards Geometric attacks. *Int J Sec (IJS)* 2010;4 3:28–37.
5. Wang B et al. An image watermarking algorithm based on DWT DCT and SVD. In: IEEE international conference on network infrastructure and digital content, 2009. IC-NIDC 2009. IEEE; 2009.
6. Van Schyndel RG, Tirkel AZ, Osborne CF. A digital watermark. In: IEEE international conference image processing, 1994. Proceedings. ICIP-94. IEEE; 1994. vol. 2.
7. Manoharan S. An efficient reversible data embedding approach in medical images for health care management. 2013.
8. Yinghui P. Digital watermarking particle swarm optimization based on multi-wavelet. *J Conver Inf Technol*. 2010;5 3.
9. Lin W-H, Horng S-J, Kao T-W, Fan P, Lee C-L, Pan Yi. An efficient watermarking method based on significant difference of wavelet coefficient quantization. *IEEE Trans Multimedia*. 2008;10(5):746–57.
10. Meerwald P, Koidl C, Uhl A. Attack on “watermarking method based on significant difference of wavelet coefficient quantization”. *IEEE Trans Multimedia*. 2009;11(5):1037–41.

11. Wang Y-R, Lin W-H, Yang Ling. An intelligent watermarking method based on particle swarm optimization. *Expert Syst Appl.* 2011;38(7):8024–9.
12. Roychowdhury M, Sarkar S, Laha S, Sarkar S. Efficient digital watermarking based on SVD and PSO with multiple scaling factor. In: *Proceedings of the 3rd international conference on Frontiers of Intelligent Computing: Theory and Applications (FICTA) 2014.* Springer International Publishing; 2015. p. 791–6.
13. Li J. An optimized watermarking scheme using an encrypted gyrator transform computer generated hologram based on particle swarm optimization. *Opt Express.* 2014;22(8):10002–16.
14. Ansari IA, Pant M. SVD watermarking: particle swarm optimization of scaling factors to increase the quality of watermark. In: *Proceedings of fourth international conference on soft computing for problem solving.* Springer India; 2015. p. 205–14.

Fireworks Algorithm-Based Maximum Power Point Tracking for Uniform Irradiation as Well as Under Partial Shading Condition

K. Sangeetha, T. Sudhakar Babu and N. Rajasekar

Abstract Harnessing of maximum power from solar PV with the aid of maximum power point tracking (MPPT) methods is of significant importance as it contributes to better utilization of the system. Amidst the conventional MPPT methods, hill climbing (HC) and incremental conductance methods are widely recognized but they yield maximum power only under constant irradiation and utterly fail when exposed to conditions of varying irradiation levels. Besides these, they exhibit wide power fluctuations even under steady state along with poor transient characteristics under partial shading conditions which is quite probable. Therefore, a recently developed optimization technique namely, fireworks algorithm is utilized for global MPPT. Extensive simulations are performed for constant irradiation as well as partial shading condition. The obtained results are compared with existing methods to highlight the superiority of the method used in this work.

Keywords Boost converter · Maximum power point tracking (MPPT) · Fireworks algorithm (FWA) · Incremental conductance (Inc. cond.) · Hill climbing (HC) · Photovoltaic (PV) module

1 Introduction

The widespread usage of solar energy for diverse range of applications like water pumping, communications, satellites and space vehicles and large-scale power plants can be noticed in the recent past [1]. Even though solar power is employed in

K. Sangeetha · T. Sudhakar Babu · N. Rajasekar (✉)
Solar Energy Research Centre, School of Electrical Engineering,
VIT University, Vellore, Tamil Nadu, India
e-mail: natrajanrajasekar@gmail.com

K. Sangeetha
e-mail: sangukrish21@gmail.com

T. Sudhakar Babu
e-mail: sudhakarbabu66@gmail.com

many areas, the main shortcomings vested with it includes low energy conversion efficiency, huge initial expense incurred and reduction in power output during varying atmospheric conditions. In order to operate the system effectively and to harvest maximum power output from solar PV, maximum power point tracking (MPPT) algorithms are essential [2].

A lot of MPPT algorithms can be noticed on performing a thorough literature survey, which includes the well-accepted ones such as fractional open circuit voltage [3], fractional short-circuit current [4], perturb and observe (P&O) [5], incremental conductance (Inc. Cond.) [6] and hill climbing (HC) algorithm [7]. As already mentioned above, identification of maximum power point (MPP) is not possible by aforementioned methods owing to increased power loss due to steady-state oscillations, which in turn paves way for lowered efficiency. To mitigate these ill effects, artificial intelligence (AI) methods including neural network (NN) [8] and fuzzy logic control (FLC) [9] have been put forward for MPPT. Even though their performance is better than conventional methods, they are complex as they need periodic training, ability to handle large volume of data for training, computational burden as well as high memory capacity.

As an alternate approach, bio-inspired methods were utilized for MPP tracking [10, 11]. Amongst different methods, PSO is widely used for solar MPPT since it yields better results. However, system performance is tampered in consequence to its random nature. Even though many modifications were incorporated to conventional PSO method, the improvement in performance was not significant. Moreover, it requires definite parameter tuning which is cumbersome along with prolonged settling time.

Hence, with an aim to accurately track the global peak power even under partial shading conditions without much complexities and modifications, a recently developed meta-heuristics algorithm namely fireworks algorithm is used for global MPP tracking. This stochastic optimization technique is capable of solving nonlinear and complex numerical computation problems effectively and is successfully applied in various fields of practical optimization problems. This algorithm simulates the process of fireworks explosion in night sky to search the optimal solution of the given problem. This method assures faster convergence, reduced steady-state oscillations and minimal power fluctuations. The ability of this algorithm to perform exploration along with exploitation makes it distinct from the existing optimization techniques. This method is well efficient to carry out global as well as local search simultaneously, which is essential for global MPP tracking and henceforth it is chosen in this work.

2 Modelling of PV Module

2.1 Single Diode Model

The conventional way employed to depict the nonlinear characteristics of solar cell is to portray it with the photovoltaic power modelled as current source in parallel with a single diode along with a series and shunt resistance as it can be seen in

Fig. 1 Single-diode model for PV modeling

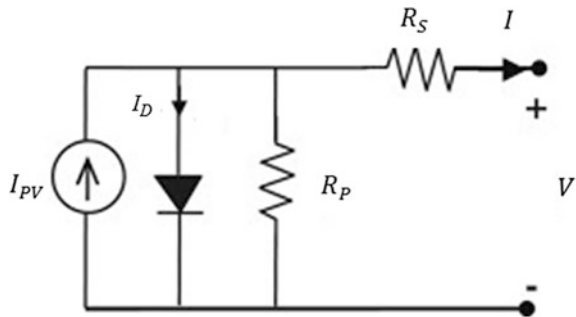


Fig. 1. This topology is termed single-diode model which is simple and moderately accurate [12]. The resistances R_s and R_p represent the voltage drop due to metal grid, contacts and leakage losses, respectively.

The output current of solar PV module obtained according to this model can be formulated using KCL and is given below:

$$I = I_{pv} - I_D - \frac{V + IR_s}{R_p} \quad (1)$$

where

I_D is the diode current, and

assuming the diode to be ideal, its current equation is given by

$$I_D = I_0(e^{V_D/aV_t} - 1) \quad (2)$$

where a is the ideality constant of diode, and V_t is the thermal voltage defined by the following equation for any value of temperature T :

$$V_t = N_s kT/q \quad (3)$$

where k is the Boltzmann constant = 1.3805×10^{-23} J/K, T is the cell temperature in Kelvin, q is the electron charge which is equal to 1.6×10^{-19} C, N_s is the number of cells in series constituting the PV module.

3 Overview of Fireworks Algorithm

Fireworks algorithm FWA which falls under the category of meta-heuristic algorithms was developed by Tan Y. and Zhu Y. in 2010. It is a powerful global optimization technique and is based on intelligent behaviour of swarms. This algorithm simulates the process of fireworks explosion in night sky to search the optimal solution of the given problem [13]. In FWA, numbers of fireworks

(particles) are generated in the search space and a stochastic explosion process is initiated for each firework. On completion of the explosion process, a shower of sparks that are generated as a result of firework explosion fills the local space surrounding the exploded firework. Both the fireworks as well as the newly generated sparks represent the potential solutions in the desired search space. For effectively searching the global optimum in the problem space, the algorithm makes use of explosion sparks generated by explosion operator and Gaussian mutation sparks by Gaussian mutation operator. The key feature of this algorithm is its ability to properly balance between exploration as well as exploitation. Exploration refers to the ability of the method to explore various regions of the search space in order to locate promisingly good solutions, whereas exploitation is the feature to conduct a thorough search within smaller area to obtain the best solution. Further, it is characterized by global search capability at beginning followed by effective local search at the end. Gaussian mutation sparks are generated to enhance the local search capability as well as to ensure the diversity of the swarm.

The equations involved in the calculation of sparks and amplitude are listed below:

$$S_i = m * \frac{f_{\max} - f(x_i) + \varepsilon}{\sum_{j=1}^p (f_{\max} - f(x_j)) + \varepsilon} \quad (4)$$

$$A_i = A * \frac{f(x_i) - f_{\min} + \varepsilon}{\sum_{j=1}^p (f(x_j) - f_{\min}) + \varepsilon} \quad (5)$$

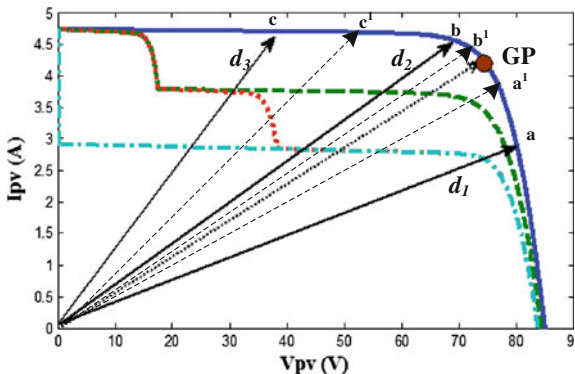
$$S_i = \begin{cases} S_{\min} & S_i < S_{\min} \\ S_{\max} & \text{else if } S_i > S_{\max} \\ S_i & \text{else} \end{cases} \quad (6)$$

where m is a parameter for controlling the total number of sparks generated by the fireworks, A is the amplitude of maximum explosion which is used in order to balance the global and local search, p is the size of the swarm, f_{\max} and f_{\min} are the maximum and minimum objective values among the p fireworks, ε is a constant to avoid zero-division error. The lower and upper bounds are defined for S_i to avoid overwhelming effects of splendid fireworks.

3.1 Problem Formulation

The ultimate objective of every MPPT technique is to maximize the amount of power drawn from a solar PV array by adjusting the duty cycle of the power converter. In this work, FWA is implemented with a focus on global peak power tracking. Hence, the objective function to be maximized given in [10] is followed for implementing MPPT using FWA which is given as:

Fig. 2 Identification of partial shading condition under different duty cycles



$$P(d_i^t) > P(d_i^{t-1}) \tag{7}$$

where, $P(d_i^t)$ present power of i th particle at t th iteration. $P(d_i^{t-1})$ old power of i th particle at $(t - 1)$ th iteration.

Subject to the constraints $V_i^{\min} \leq V_i^{t+1} \leq V_i^{\max}$, $0.05 < d_i^{t+1} < 0.95$

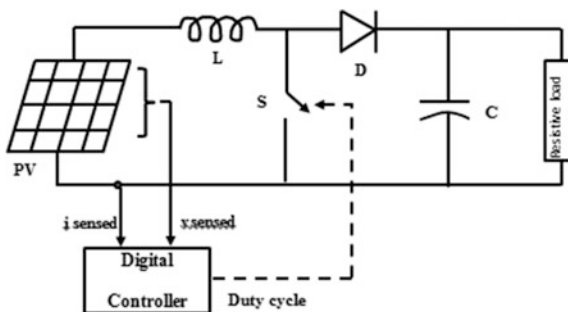
The process involved in identifying the optimal duty cycle with the aid of FW is thoroughly explained below.

To begin the search process, three randomly generated duty cycles (d_1, d_2, d_3) are sent to the power converter and the corresponding power values are noted. The respective duty cycles are marked as a, b and c in the curve shown in Fig. 2. The duty cycle with highest power value will be regarded the best duty cycle which is retained, whereas other duty cycles are suitably adjusted according to the calculated values of amplitude and sparks of explosion given in Eq. (5). To ensure the diversity among sparks and to enhance local search capability, two new duty cycles are generated with the help of Gaussian mutation operator applied to the best values. The updated duty cycles (particle position) at this stage are again sent to the power converter and corresponding power values are recorded. Further, duty cycles are sorted according to their powers and the two worst values are deleted so as to maintain the population size constant after the first iteration. In the second iteration, the same steps are repeated after computing the new values of amplitude and sparks. This process is continued until all the particles converge to the MPP. Similar procedure is followed for partial shading condition as well.

4 Simulation Results

The system configuration is depicted in Fig. 3. It comprises of a DC–DC boost converter, digital controller, voltage and current sensors connected at the input end of the boost converter. Digital controller is used to code the proposed as well as conventional MPPT algorithms. For simulation, a dedicated MATLAB/SIMULINK

Fig. 3 System configuration



model is developed for FW method along with the other two conventional algorithms. DC–DC boost converter is operated at a switching frequency of 10 kHz with L and C values of 1 mH and 100 μ F, respectively. The boost converter is operated in continuous conduction mode and the algorithms are tested for two different conditions: (1) uniform irradiation (2) partial shading. The chosen FW parameter values are $p = 3$, $A = 0.3$ and $\varepsilon = 0.001$. In this work, the sampling time is chosen as 0.06 s for simulation. The panel selected for study is Kotak KM80 whose rated maximum power is 80 W and a string comprising of four such modules (4S configuration) is chosen.

4.1 Uniform Irradiation Condition

Simulation results showing voltage, current, duty cycle and tracked power waveforms under uniform irradiation (1000 W/m^2) using HC method, Inc. Cond, and FWA are presented in Fig. 4. For HC and Inc. cond. Method, a fixed step size of 0.02 is applied at an interval of 0.06 s. From Fig. 4a, b, it is clearly evident that steady-state oscillations persist around MPP for HC and Inc. Cond. method. Whereas in case of FW algorithm, three randomly generated initial duty cycles are sent to the boost converter. These duty cycle values are updated applying FW algorithm until global peak is reached. Further, it indicates after two iterations, FW algorithm settles at MPP with zero steady-state oscillations.

4.2 Partial Shading Condition

Simulation results are taken for HC, Inc. Cond and FW considering partial shading conditions of 1000–800–600–400 irradiation. The simulation result of all the three methods for the chosen shading pattern is shown in Fig. 5. From the obtained simulation results shown above, the following conclusions can be made. HC method utterly fails to track the global peak power value and converges to one of

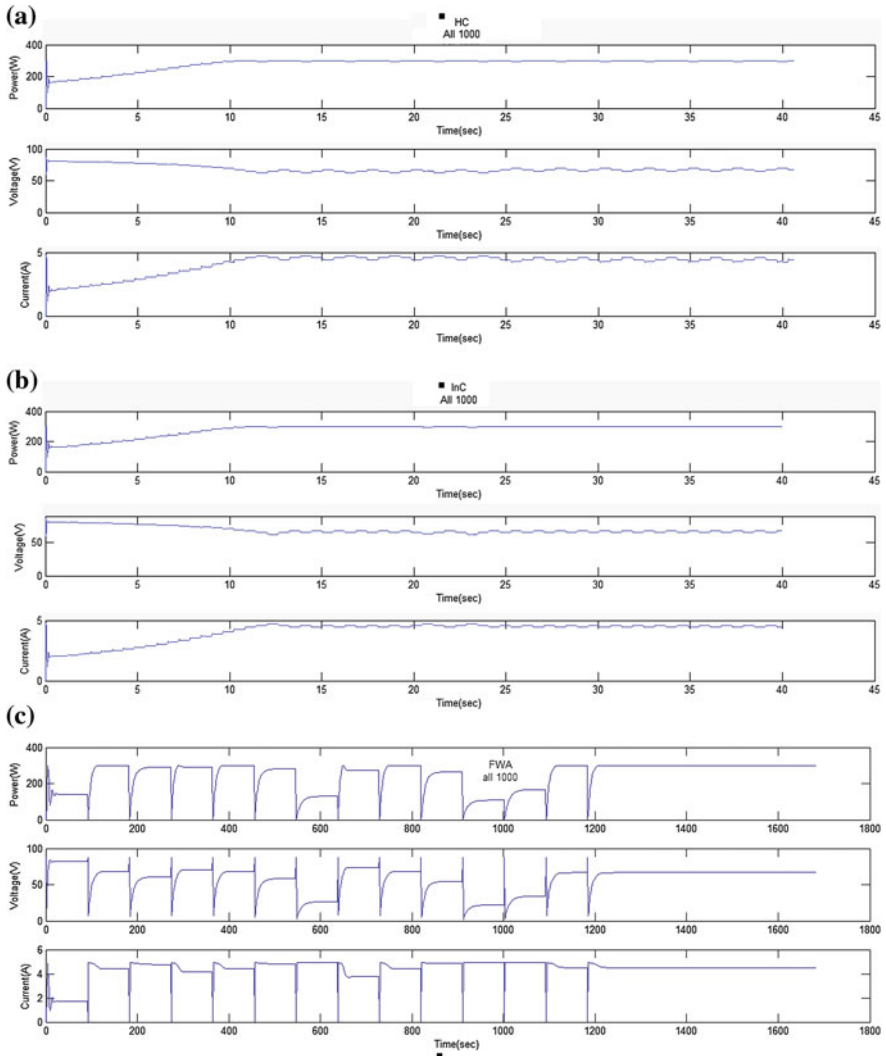


Fig. 4 **a** Simulated results of voltage, current and power using HC algorithm for constant irradiation. **b** Simulated results of voltage, current and power for Inc. Cond. constant irradiation condition. **c** Simulated results of voltage, current and power tracked for FW algorithm constant irradiation

the local peak values around 60 W. This as clearly noticed in Fig. 5a is purely inadmissible since it results in significant power loss. In addition, there exists a steady-state oscillation which adds to the existing power loss. Moreover, it takes longer time to settle even at the local peak. While analyzing the performance of InC method under partial shading condition, it is seen that the method yields higher power value of 120 W which is still not the global peak. This is due to the reason

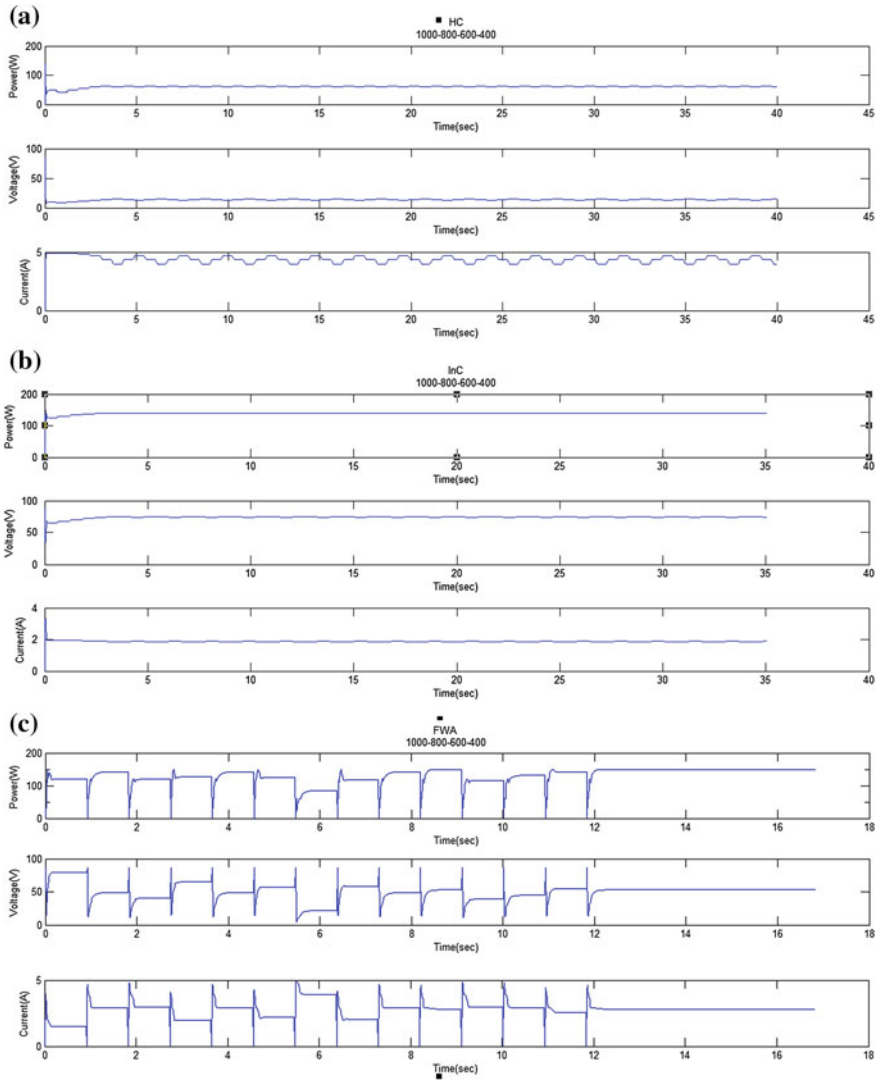


Fig. 5 a Variation in irradiation level, voltage, current, duty cycle, power using HC algorithm for the shading pattern. b Variation in irradiation level, voltage, current, duty cycle, power using Inc. Cond. for the shading pattern. c Variation in irradiation level, voltage, current, duty cycle, power using FW algorithm for the shading pattern

that the initial duty cycle value chosen is closer to the corresponding local peak. This is expected since there is no information about the optimal duty cycle value that yields maximum power for the shaded pattern. From FWA simulation results shown in Fig. 5c, it is apparently evident that the method converges to the global peak power of 150 W. This provides proof for the statement that FWA possess

excellent global search capacity along with well-defined local search. Further, the power fluctuations are nullified once the method has converged to the optimal value. In addition, the method takes fewer steps to converge to the best possible solution yielding good dynamic performance as well. The obtained results ensure the effectiveness of the chosen FWA for accurate global MPP tracking.

5 Conclusion

In this paper, a recent optimization technique, fireworks algorithm, was utilized for global MPP tracking was presented. The Proposed method along with HC and incremental conductance were tested using simulation for uniform as well as partial shading conditions. Based on simulation results, the following conclusions were obtained. Fireworks method was found to have good tracking ability even under varying environmental conditions, with almost zero steady-state oscillations, providing good tracking speed along with ease in implementation.

References

1. Eltawil MA, Zhao Z. MPPT techniques for photovoltaic applications. *Renew. Sustain. Energy Rev.* 2013;25:793–813.
2. Reisi AR, Moradi MH, Jamasb S. Classification and comparison of maximum power point tracking techniques for photovoltaic system: a review. *Renew. Sustain. Energy Rev.* 19:433–43.
3. Kobayashi K, Matsuo H, Sekine Y. A novel optimum operating point tracker of the solar cell power supply system. In: *Proceedings' 35th annual IEEE power electronics specialists conference*; 2004. p. 2147–51.
4. Mutoh N, Matuo T, Okada K, Sakai M. Prediction-data-based maximum power-point-tracking method for photovoltaic power generation systems. In: *2002 IEEE 33rd annual power electronics specialists conference*; 2002. vol. 1483, p. 1489–94.
5. Moacyr AGB, Galotto L, Poltronieri Sampaio L, Guilherme AM. Evaluation of the main MPPT techniques for photovoltaic applications, *IEEE Trans. Ind. Electron.* (2013);60:1156–67.
6. Zhou X, Song D, Ma Y. The simulation and design for MPPT of PV system based on incremental conductance method. In: *2010 WASE international conference, information engineering (ICIE)*; 2010. p. 314–7.
7. Wolfs PJ, Tang L. A single cell maximum power point tracking converter without a current sensor for high performance vehicle solar arrays. *IEEE Power Electron. Specialists Conf.* 2005;36:165–71.
8. Rai K, Kaushika ND, Singh B, Agarwal N. Simulation model of ANN based maximum power point tracking controller for solar PV system. *Solar Energy Mater. Solar Cells.* 2011;95:773–8.
9. Alajmi N, Ahmed KH, Finney SJ, Williams BW. Fuzzy logic-control approach of a modified hill-climbing method for maximum power point in microgrid standalone photovoltaic system. *IEEE Trans Power Electron.* 2011;26:1022–30.
10. Sudhakar Babu T, Rajasekar N, Sangeetha K. Modified particle swarm optimization technique based maximum power point tracking for uniform and under partial shading condition. *Appl. Soft Comput.* 2015;34:613–24.

11. Kobayashi K, Ichiro T. A study on a two stage maximum power point tracking control of a photovoltaic system under partially shaded insolation conditions. *IEEE Trans.* 2003.
12. Rajasekar N, Neeraja KK, Rini V. Bacterial foraging algorithm based solar PV parameter estimation. *Solar Energy.* 2013;97:255–65.
13. Tan Y, Zhu Y. Fireworks algorithm for optimization advances in swarm intelligence. *Lecture Notes in Computer Science* (2010);6145:355–64.

Design of Low Power Efficient Median Filter for Noise Reduction in Image

M. Vinothini and B. Syed Ibrahim

Abstract In this paper, designing of the median filter is done with help of the comparator and multiplexer. In image processing, as median filter is an important factor to reduce salt and pepper noise, it is essential to develop a new design technique to reduce the power consumption. So the comparator and multiplexer design used in the median filter is designed using various styles of the full adder with help of DSCH and Microwind tool.

Keywords Multiplexer · Full adder (FA) · Comparator · Power

1 Introduction

Digital images play an important role in various applications such as astronomy, magnitude resonance imaging, and mathematical morphology. These images get often corrupted by factors such as channel transmission error, from noisy sensors. Smoothing of these images leads to destroy of edge and instance details of the images, while sharpening will lead to unwanted intensification of noise. Since the image enhancement through noise cleansing is the fundamental problems in the image processing. So, the depending upon the imagery and the restoration technique will make more assumption, this technique is not useful for application.

Thus various filtering method are used depending upon whether the noise is nonadditive or not. Linear filtering method fails when the noise is nonadditive and not effective in removing impulsive noise in the images. This has given importance to the use of nonlinear filtering.

The most commonly used nonlinear filter is the median filter because of its superior and edge preservation compared to linear filters. The block diagram of n -bit median filter is shown in Fig. 1.

M. Vinothini (✉) · B. Syed Ibrahim
ECE Department, Chettinad College of Engineering, Karur, India
e-mail: vinothini.1505@gmail.com

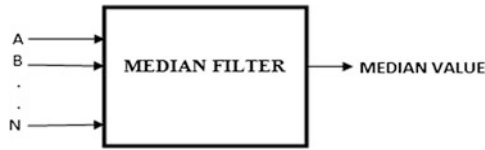


Fig. 1 Block diagram of n -bit median filter

Here the median filter is designed using comparator and multiplexer. The comparator design is implemented by full adder design which is the basic building block of the many digital VLSI circuits. In this paper, the design technique is implemented using the microwind software. The combination of the comparator and multiplexer, which is the basic block of the median filter, is shown in Fig. 2.

2 Design Implementation

First, discussion about the median's basic block such as the comparator and multiplexer is done. In this paper, 3bit 3input are used where the median value are displayed as output. Here the implementations of the median filter are mainly based

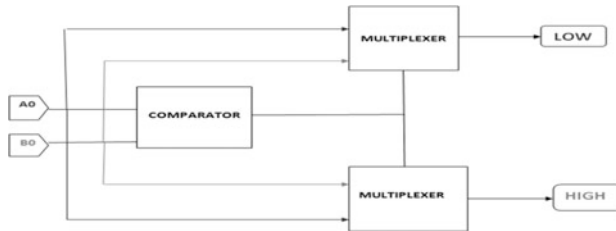


Fig. 2 Combination of comparator and multiplexer

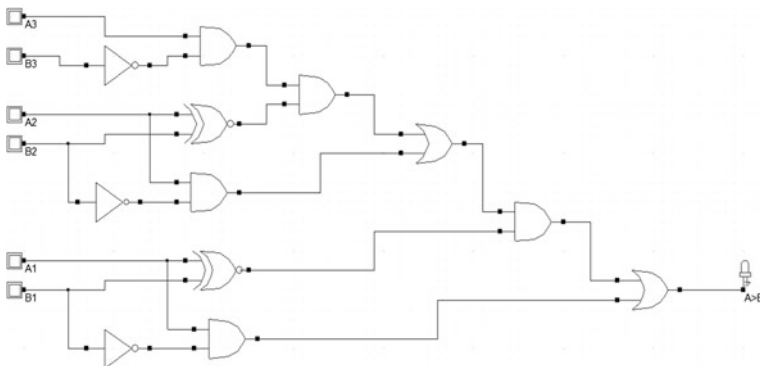


Fig. 3 Basic comparator design

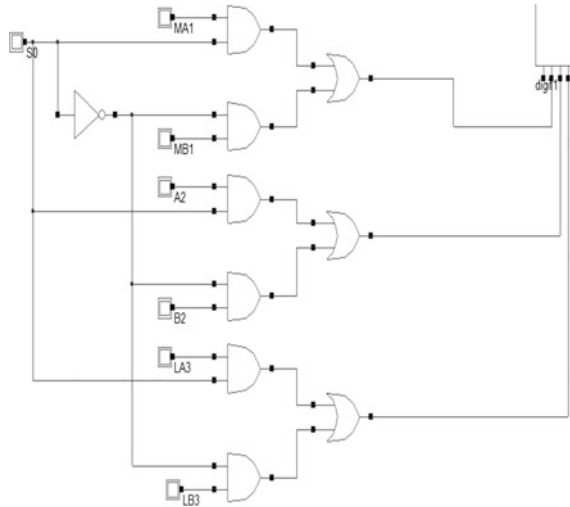


Fig. 4 Basic multiplexer design

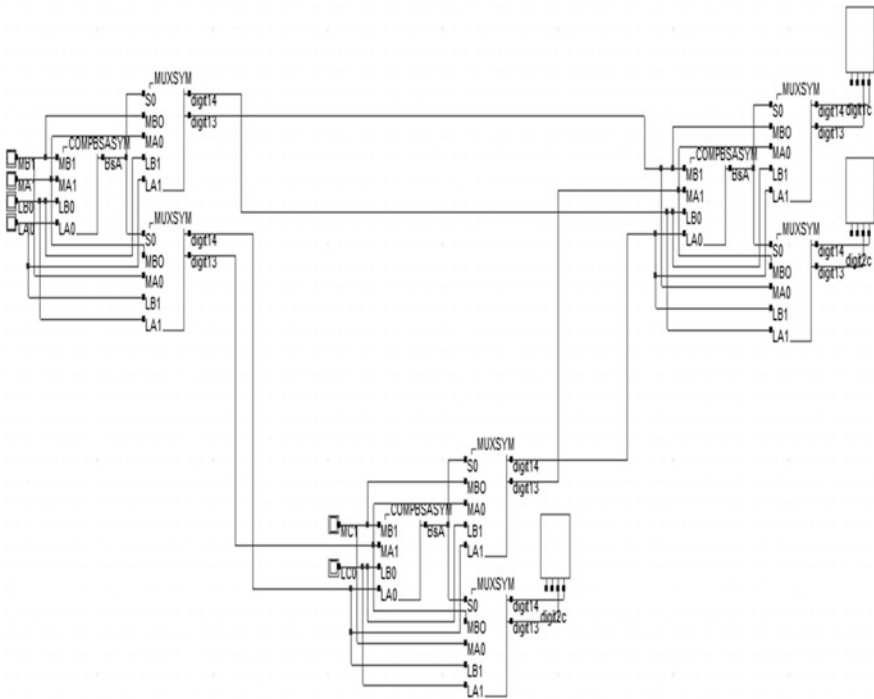


Fig. 5 Basic median filter design

on the reduction of the power consumption. The comparator is implemented using various gates as AND, OR, EX-NOR, and NOT, where the output is given as $A > B$. The multiplexer are implemented with help of AND, OR, and NOT gates where output are mainly concerned with selection line S0. The basic comparator and multiplexer design used for implementation of basic median filter is shown in Figs. 3 and 4.

(a)



(b)

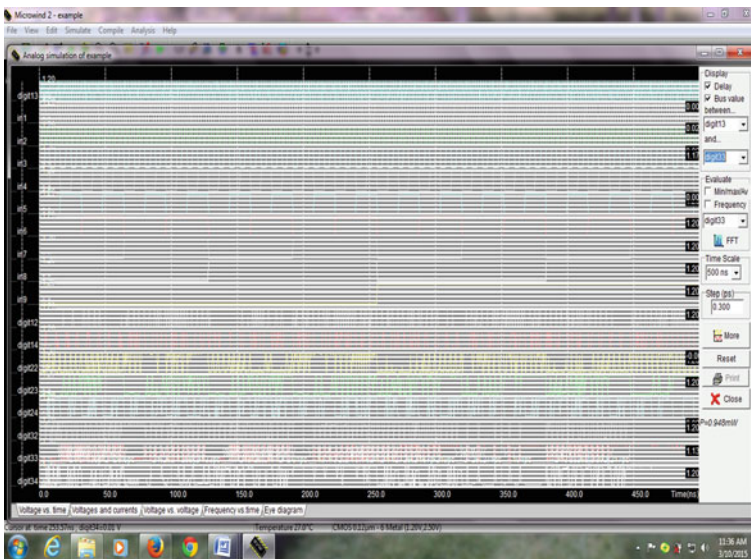


Fig. 6 a Layout diagram. b Analog simulation of basic median filter design

The basic median filter design is shown in Fig. 5.

The layout design of the basic median filter is shown in Fig. 6a and its analog simulation in Fig. 6b.

Then another design of low power median filter using hybrid full adder is shown in Fig. 8 using Figs. 7 and 9.

Fig. 7 Multiplexer design

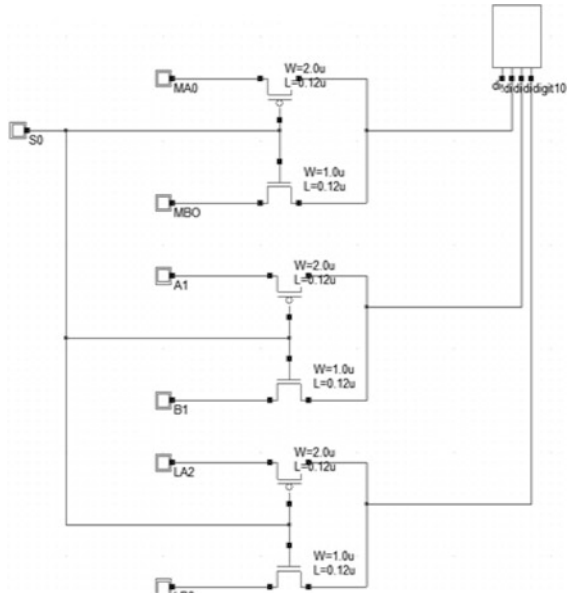
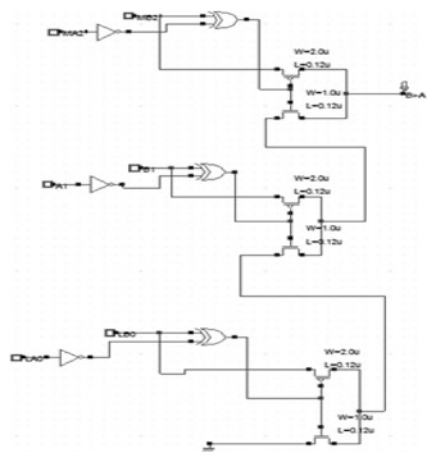


Fig. 8 Comparator using hybrid full adder design



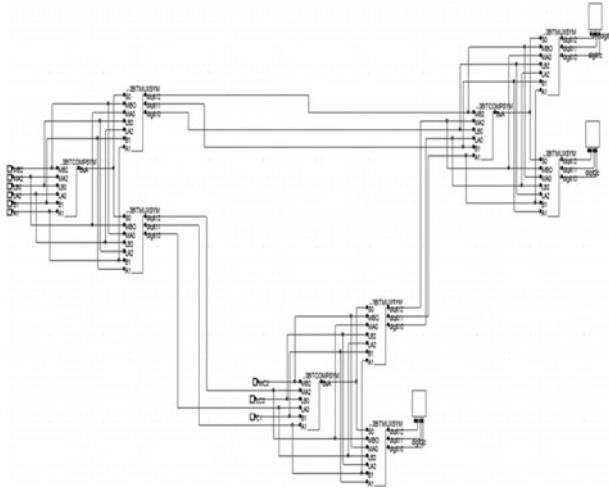


Fig. 9 Low-power median filter

The layout design of low power median filter is shown in Fig. 10a and its analog simulation shown in Fig. 10b.

3 Result Analysis

Here the analysis and the comparison of the median filter using hybrid full adder is shown in Table 1 based on the simulation obtained from the microwind software.

The simulation is done in the following steps. As to obtain simulation, compile the verilog file in the microwind and that verilog file is created from the schematic circuit diagram which is designed using DSCH part of the microwind software.

The analysis is shown in graphical form by means of chart as follows (see Chart 1).

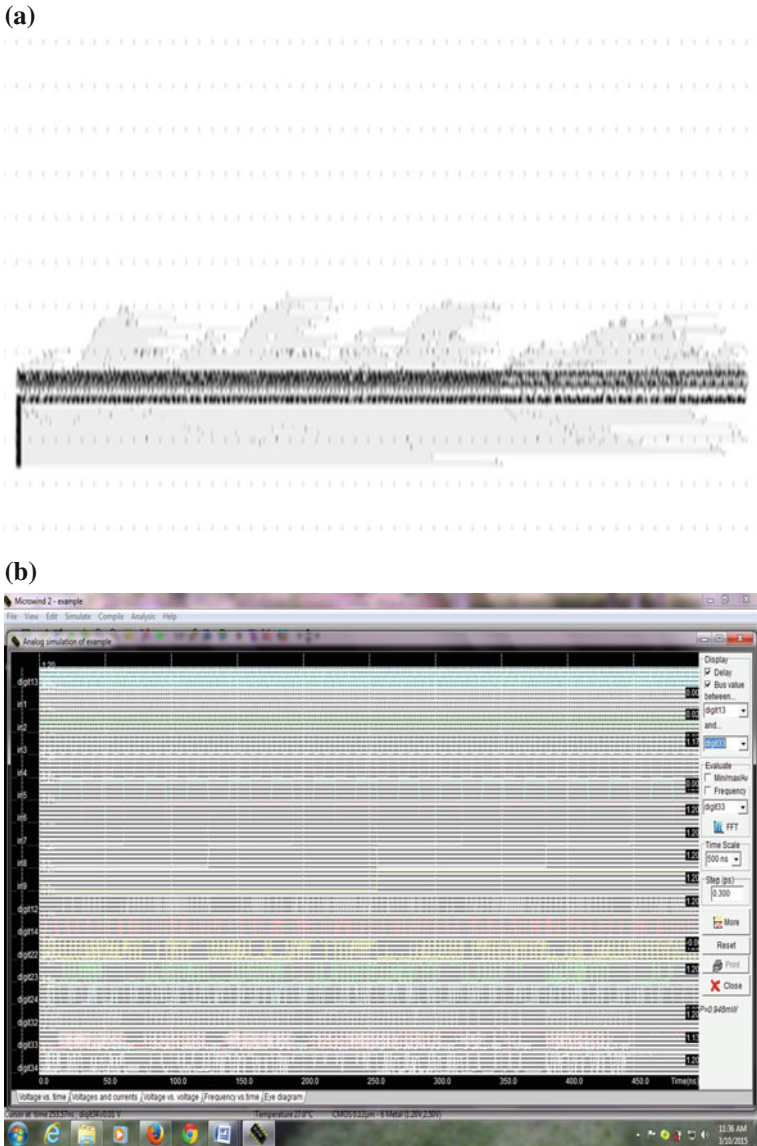
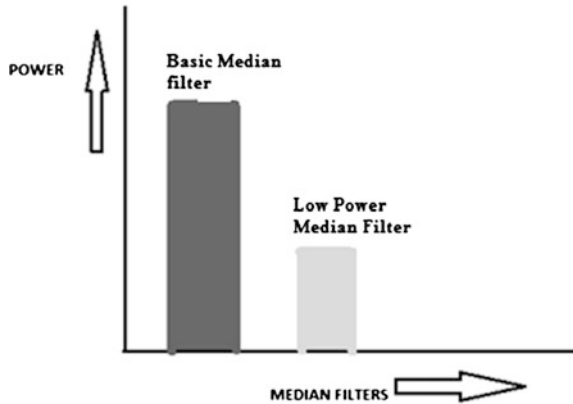


Fig. 10 a Layout diagram. b Analog simulation of low-power median filter design

Table 1 Comparison of median filters

S. no.	Median filter design	Power (W)
1.	Basic median filter	0.3336 m
2.	Low-power median filter using hybrid full adder	55.490 μ

Chart 1 Power analysis of the median filter



4 Conclusions

This paper discuss about the various styles of the median filter using hybrid full adder. And from the result obtained, it is found that the low-power median filter has reduced power consumption compared to the basic median filter.

Bibliography

1. Lu C-T, Chou T-C. Denoising of salt and pepper noise corrupted image using modified directional-weighted-median filter. Taiwan, ROC; 2011.
2. Meher SK. Recursive and noise-exclusive fuzzy switching median filter for impulse noise reduction. Bangalore; 2013.
3. Horng S-J, Hsu L-Y, Li T, Khan MK. Using sorted switching median filter to remove high-density impulse noises. Chengdu; 2012.
4. Toh KKV, Isa NAM. Cluster based adaptive fuzzy based salt and pepper noise removal using adaptive switching median filter. Proc Eng. 2010;38:2858–65.
5. Bai T, Tan J, Hu M, Wang Y. A novel algorithm for removal of salt and pepper noise using continued fractions interpolation. Hefei; 2013.
6. Toprak A, Guler I. Impulse noise reduction in medical images with use of switch mode fuzzy adaptive median filter. Turkey; 2007. p. 711–723.
7. Zhang J. An efficient median filter based method for removing random valued impulse noise. Shanghai; 2009.
8. Luo W. An efficient detail-preserving approach for removing impulse noise in images. IEEE Signals Process Lett. 2006;13:413–6.
9. Luo W. An efficient algorithm for the removal of impulse noise from corrupted images. USA; 2006. p. 78228–8534.
10. Pattnaik A, Agarwal S, Chand S. A new and efficient method for removal of high density salt and pepper noise through cascade decision based filtering algorithm' Rourkela, India. Procedia Technol. 2012. 6:108–117.

A Cycle Detection-Based Efficient Approach for Constructing Spanning Trees Directly from Nonregular Graphic Sequences

Prantik Biswas, Shahin Shabnam, Abhisek Paul
and Paritosh Bhattacharya

Abstract Realization of graphic sequences and finding the spanning tree of a graph are two popular problems of combinatorial optimization. A simple graph that realizes a given nonnegative integer sequence is often termed as a realization of the given sequence. In this paper, we have proposed a method for obtaining a spanning tree directly from a degree sequence by applying cycle detection algorithm, provided the degree sequence is graphic and nonregular. The proposed method is a two-step process. First, we apply an algorithm to check whether the input sequence is realizable through the construction of an adjacency matrix corresponding to the degree sequence. Then we apply the cycle detection algorithm separately to generate the spanning tree from it.

Keywords Spanning tree · Graph · Algorithms · Cycle detection · Graphic realization · Degree sequence · Adjacency matrix

1 Introduction

Spanning trees problems form the core of a numerous set of problems in graph theory. It has a wide range of application in various fields of science and technology ranging from computer and communication networks, wiring connections, VLSI circuit designs to traveling salesman problem, multiterminal flow problem, etc.

P. Biswas (✉) · A. Paul · P. Bhattacharya
Department of Computer Science and Engineering, National Institute of Technology,
Agartala, India
e-mail: pranmasterbi@gmail.com

S. Shabnam
Department of Computer Science, Assam University, Silchar, India

At present, problems in biology and medicine such as cancer detection, medical imaging, and proteomics, and national security and bioterrorism such as detecting the spread of toxins through populations in the case of biological/chemical warfare are analyzed with the aid of spanning trees.

A spanning tree of a connected undirected graph $G = (V, E)$, is defined as a tree T consisting of all the vertices of the graph G . If the graph G is disconnected, then every connected component will have a spanning tree T_i the collection of which forms the spanning forest of the graph G . A graph may have many spanning trees.

Although a large variety of algorithms exists, that can compute the spanning tree from a given graph, determining it from a given degree sequence has not yet been tried. Popular algorithms were proposed by Kruskal [1] and Prim [2] that can successfully compute the minimal spanning tree of a given graph. In this paper, we have applied a variant of Prim's [2] algorithm to determine the spanning tree directly from a given degree sequence of nonregular simple graphs.

A finite sequence $d: d_1, d_2, d_3, \dots, d_n$ of nonnegative integers is said to be graphical if there exists some finite simple graph G , having vertex set $V = \{v_1, v_2, v_3, \dots, v_n\}$ such that each v_i has degree d_i ($1 \leq i \leq n$). Although it is quite easy to determine the degree sequence of a given graph, the converse procedure is potentially difficult. This problem is closely linked with the other branches of combinatorial analysis such as threshold logic, integer matrices, enumeration theory, etc. The problem also has a wide range of application in communication networks, structural reliability, stereochemistry, etc.

Two necessary conditions for a sequence to be graphical are: (1) $d_i < n$ for each i , and (2) $\sum_{i=1}^n d_i$ is even. However, none of these are sufficient conditions for the sequence to be graphic. The first known solutions were proposed independently by Havel [3] and Hakimi [4] in the mid twentieth- century. Although they provided separate proofs yet their work is jointly known as the Havel–Hakimi theorem.

With the advent of time, well-known necessary and sufficient conditions were published. Erdős and Gallai [5], Ryser [6], Berge [7], Fulkerson, Hofman and McAndrew [8], Bollobás [9], Grünbaum [10], and Hässelbarth [11] independently proposed the sufficient condition for a degree sequence to be graphic. Sierksma and Hoogeveen [12] listed the seven well-known characterizations of a degree sequence and their equivalence. The works of Havel–Hakimi were further extended by Kleitman and Wang [13], and that of Erdős and Gallai by Eggleton [14] and Tripathi and Vijay [15]. Dahl and Flatberg [16] proposed a direct way of obtaining Tripathy and Vijay's result from a simple geometrical observation involving weak majorization. Tripathy and Tyagi [17] provided two elegant proofs of Havel–Hakimi and Erdős and Gallai.

Our proposed algorithm is based on the cycle detection algorithm. Various elegant cycle detection algorithm of almost linear order can be easily found [18, 19]. A major advantage of using cycle detection for breaking a cycle is that removal of a single edge may result in breaking of multiple cycles thereby reducing the execution time of the algorithm.

In this paper, we have taken the problem of determining a spanning tree from a given degree sequence provided the degree sequence is graphic and nonregular. Here the term nonregular implies that the given sequence is graphic and its realization gives a nonregular graph. We first check whether the input sequence satisfies the basic criteria for having a realization. Next we design a sufficient condition by constructing the adjacency matrix corresponding to the input sequence. Finally, we apply cycle detection algorithm on the matrix to obtain a spanning tree.

In Sect. 2 we have given a brief definition of the problem. Section 3 describes our proposed approach while Sect. 4 illustrates the working of the proposed method. Section 5 discusses the results obtained. We draw a concise conclusion in Sect. 6.

2 Problem Definition

The proposed problem can be divided into two subproblems. The first part is to determine whether the degree sequence is graphic and nonregular and to construct the corresponding adjacency matrix if the given degree sequence is graphic and nonregular. The second part is to construct the spanning tree from the resultant adjacency matrix

- Determination of graphic sequences

Let $G = (V, E)$ be a finite simple graph with vertex set V and order n . Let each vertex v_i has a degree d_i where $1 \leq i \leq n$. Then the finite sequence $d: d_1, d_2, d_3, \dots, d_n$ of nonnegative integers is called a degree sequence of the graph G . The problem statement can be formally stated as follows.

Given a finite degree sequence $d: d_1, d_2, d_3, \dots, d_n$ of nonnegative integers, whether there exists a graph G of order n with vertex set V such that each vertex v_i has a degree d_i where $1 \leq i \leq n$.

- Construction of spanning tree

Let $G = (V, E)$ be a given graph of order n and size m . A spanning tree T of G is defined as a connected graph spanning all the vertices of the vertex set V with exactly $n - 1$ edges belonging to the edge set E . The construction of spanning tree requires us to eliminate $m - n + 1$ edges from the given graph G in order to obtain a subgraph T of G such that it has an order n and size $n - 1$.

3 Proposed Approach

In this section, we demonstrate our proposed approach to solve the problem. In the first part, we present an algorithm that determines whether a given degree sequence is graphic by applying some basic criteria and constructing the adjacency matrix corresponding to the input sequence. In the next part, we present how the BFS and DFS algorithm can be applied to obtain the spanning tree from the adjacency matrix obtained in the earlier part.

- Determination of graphic sequence through the construction of adjacency matrix

Here we propose an algorithm that determines whether the given degree sequence is graphical by constructing the adjacency matrix corresponding to the given degree sequence. The degree sequence is stored in a vector $\text{degree}[n]$ of length n . The vector $\text{Allocated}[n]$ of length n helps us to determine whether a given position in the adjacency matrix can be allocated to 1, based on checking the number of positions allocated in the j th column of the i th row with respect to the degree of vertex j . The $n \times n$ vector $\text{Adj}[n][n]$ is the adjacency matrix that we construct using the algorithm. Once the entire matrix is constructed, the algorithm then checks whether the resultant matrix is symmetric. The input to the algorithm is the given degree sequence in a nonincreasing order and its output is the decision (i.e., graphic or nongraphic). If the decision of the algorithm is graphic, then we return the adjacency matrix $\text{Adj}[n][n]$ thus constructed for further operations.

```

ALGORITHM-ADJ-CONST( $d: d_1, d_2, d_3, \dots, d_n$ )
for  $i \leftarrow 1$  to  $n$ 
    Allocated[ $i$ ]  $\leftarrow 0$ ;
    degree[ $i$ ]  $\leftarrow d_i$ ;
 $r \leftarrow$  degree[0];
sum  $\leftarrow 0$ , flag  $\leftarrow 0$ , rflag  $\leftarrow 0$ ;
for  $i \leftarrow 1$  to  $n$ 
    if degree[ $i$ ]  $\geq n$ 
        return Non-Graphic;
    if degree[ $i$ ]  $\neq r$ 
        rflag  $\leftarrow$  rflag + 1;
    sum  $\leftarrow$  sum + degree[ $i$ ];
if sum mod 2  $\neq 0$ 
    return Non-Graphic;
if sum mod 2 = 0 and rflag = 0
    return Graphic and regular;
for  $i \leftarrow 1$  to  $n$ 
     $k \leftarrow$  degree[ $i$ ];
    for  $j \leftarrow 1$  to  $n$ 
        if  $k > 0$ 
            if  $i = j$ 
                Adj[ $i$ ][ $j$ ]  $\leftarrow 0$ 
            else
                if Allocated[ $j$ ] < degree[ $j$ ]
                    Adj[ $i$ ][ $j$ ]  $\leftarrow 1$ ;
                    Allocated[ $j$ ]  $\leftarrow$  Allocated[ $j$ ] + 1;
                     $k \leftarrow k - 1$ ;
                else
                    Adj[ $i$ ][ $j$ ]  $\leftarrow 0$ ;
            else
                Adj[ $i$ ][ $j$ ]  $\leftarrow 0$ ;
        if  $k > 0$ 
            return Non-Graphic;
for  $i \leftarrow 1$  to  $n$ 
    for  $j \leftarrow 1$  to  $n$ 
        if Adj[ $i$ ][ $j$ ]  $\neq$  Adj[ $j$ ][ $i$ ]
            flag  $\leftarrow$  flag + 1;
if flag > 0
    return Non-Graphic;
else
    return Graphic and Adj[ $n$ ][ $n$ ];

```

- Construction of the spanning tree from the adjacency matrix

In this part, we show how to apply cycle detection algorithm to obtain the spanning tree from the adjacency matrix $Adj[n][n]$ obtained in the previous section. The algorithm takes the adjacency matrix as input and processes it to obtain the spanning tree.

We randomly select a vertex u from the set of unmarked vertices ($V-S$), where S is the set of marked vertices. We then check if the chosen vertex is a member of a cycle/knot. If it is so, we then identify any edge e_x and delete it from the cycle as well as from the list of edges E . We repeat this process with the selected vertex u until the vertex becomes free of all the cycles it is involved with. Whenever a node becomes free of all the cycles it was associated with, we add it to the set of marked vertices S . We then select another vertex and continue the process. The algorithm terminates when the number of edges $|E|$ becomes equal to $|V|-1$, since a tree with $|V|$ vertices contains $|V|-1$ edges. The algorithm is given below

INPUT: A weighted undirected graph $G = (V, E)$.

OUTPUT: A MST T of G .

MST_Algo (G, V, E, T)

```
{
  T=G;
  while(|E| > |V|-1)
  {
    SELECT  $u \in (V-S)$ 
    while (TRUE)
    {
      if ( $u$  is a member of a cycle/knot in  $T$ )
      {
        Remove any edge  $e_x$  from the cycle/knot containing the vertex  $u$ 
        from  $T$ ;
         $E = E - e_x$ ;
      }
      else
      {
         $S = S \cup u$ ;
        break;
      }
    }
  }
  return  $T$ ;
}
```

4 Illustration

In this section, we illustrate how the algorithm generates the spanning tree. Suppose that we enter the degree sequence: 5,3,3,3,3,2,2,1.

In the first part, the algorithm generates the adjacency matrix shown in Fig. 1.

The graph corresponding to the above matrix is shown below (Fig. 2).

Suppose the algorithm chooses V_6 . It finds that V_6 is a member of the cycle $V_6-V_5-V_1-V_6$. It chooses the edge V_1V_6 and removes it from the edge set of the graph, as shown by the dotted blue lines in Fig. 3. Now, V_6 is not a member of any cycle and hence it is added to the list of marked vertices, S . Next, the algorithm chooses vertex V_2 and detects that it is a member of multiple cycles. It removes the edge V_2V_3 as shown in Fig. 4. The removal of edge V_2V_3 results in breaking multiple cycles like $V_2-V_3-V_1-V_2$, $V_2-V_3-V_4-V_2$, $V_2-V_3-V_1-V_4-V_2$, $V_2-V_3-V_4-V_1-V_2$ etc.

After the removal of the edge V_2V_3 , the vertex V_2 is still a member of other cycles like $V_2-V_4-V_3-V_1-V_2$, etc. Hence, the edge V_2V_4 is removed which makes V_2 cycle free as shown in Fig. 5. Now V_2 is added to S . Next the algorithm chooses V_3

Fig. 1 Adjacency matrix

	V_1	V_2	V_3	V_4	V_5	V_6	V_7	V_8	V_9
V_1	0	1	1	1	1	1	0	0	0
V_2	1	0	1	1	0	0	0	0	0
V_3	1	1	0	1	0	0	0	0	0
V_4	1	1	1	0	0	0	0	0	0
V_5	1	0	0	0	0	1	1	0	0
V_6	1	0	0	0	1	0	0	0	0
V_7	0	0	0	0	1	0	0	1	0
V_8	0	0	0	0	0	0	1	0	1
V_9	0	0	0	0	0	0	0	1	0

Fig. 2 Graph corresponding to Fig. 1

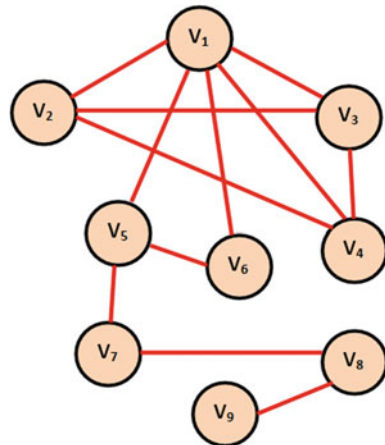


Fig. 3 V_1V_6 deleted

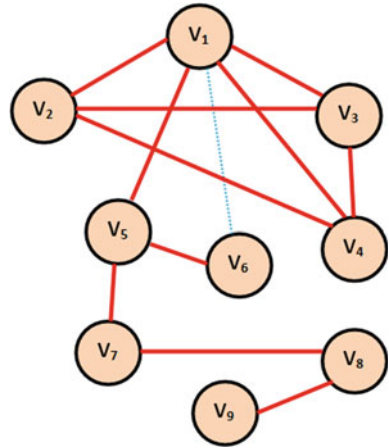


Fig. 4 V_2V_3 deleted

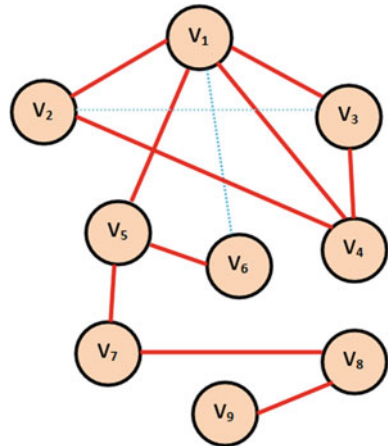
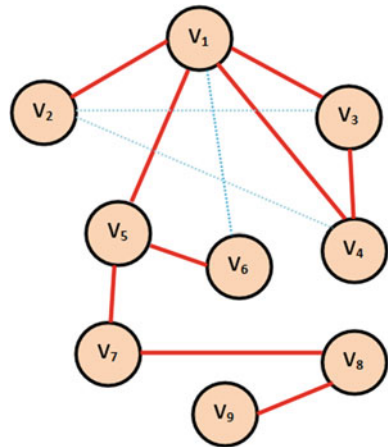


Fig. 5 Edge V_2V_4 deleted



and finds that it is a member of the cycle $V_3-V_1-V_4-V_3$. Next, the edge V_1V_3 is eliminated thereby making V_3 cycle free and adding it to S (Fig. 6). At this point, the condition $|E| > |V|-1$ is satisfied and the algorithm terminates thereby returning the output spanning tree T (Fig. 7).

The set of marked vertices S is used to keep a track of the vertices that have been made cycle free.

Fig. 6 Edge V_1V_3 deleted

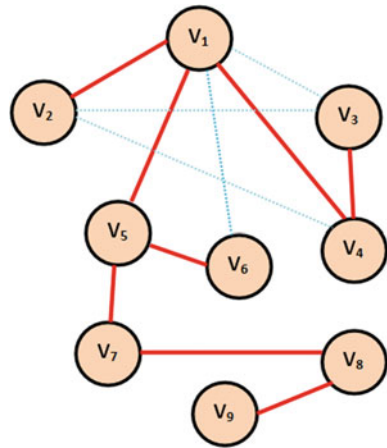


Fig. 7 Final spanning tree

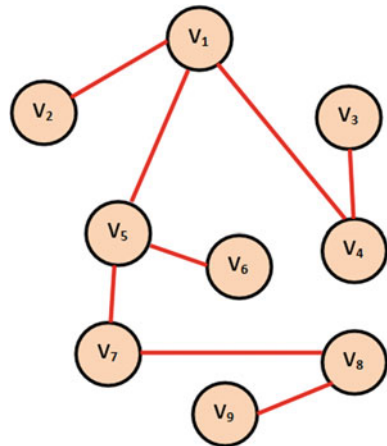
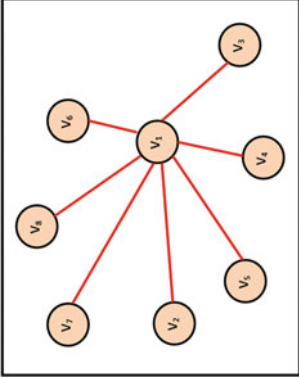


Table 1 Results of the proposed work

Input sequence	Matrix	Spanning tree																																																																																																				
5,3,3,3,3,2,2,2,1	<table border="1"> <thead> <tr> <th></th> <th>V₁</th> <th>V₂</th> <th>V₃</th> <th>V₄</th> <th>V₅</th> <th>V₆</th> <th>V₇</th> <th>V₈</th> <th>V₉</th> </tr> </thead> <tbody> <tr> <th>V₁</th> <td>0</td> <td>1</td> <td>1</td> <td>1</td> <td>1</td> <td>1</td> <td>0</td> <td>0</td> <td>0</td> </tr> <tr> <th>V₂</th> <td>1</td> <td>0</td> <td>1</td> <td>1</td> <td>0</td> <td>0</td> <td>0</td> <td>0</td> <td>0</td> </tr> <tr> <th>V₃</th> <td>1</td> <td>1</td> <td>0</td> <td>1</td> <td>0</td> <td>0</td> <td>0</td> <td>0</td> <td>0</td> </tr> <tr> <th>V₄</th> <td>1</td> <td>1</td> <td>0</td> <td>0</td> <td>0</td> <td>0</td> <td>0</td> <td>0</td> <td>0</td> </tr> <tr> <th>V₅</th> <td>1</td> <td>0</td> <td>0</td> <td>0</td> <td>1</td> <td>1</td> <td>0</td> <td>0</td> <td>0</td> </tr> <tr> <th>V₆</th> <td>1</td> <td>0</td> <td>0</td> <td>0</td> <td>1</td> <td>0</td> <td>0</td> <td>0</td> <td>0</td> </tr> <tr> <th>V₇</th> <td>0</td> <td>0</td> <td>0</td> <td>0</td> <td>1</td> <td>0</td> <td>0</td> <td>1</td> <td>0</td> </tr> <tr> <th>V₈</th> <td>0</td> <td>0</td> <td>0</td> <td>0</td> <td>0</td> <td>0</td> <td>1</td> <td>0</td> <td>1</td> </tr> <tr> <th>V₉</th> <td>0</td> <td>0</td> <td>0</td> <td>0</td> <td>0</td> <td>0</td> <td>0</td> <td>1</td> <td>0</td> </tr> </tbody> </table>		V ₁	V ₂	V ₃	V ₄	V ₅	V ₆	V ₇	V ₈	V ₉	V ₁	0	1	1	1	1	1	0	0	0	V ₂	1	0	1	1	0	0	0	0	0	V ₃	1	1	0	1	0	0	0	0	0	V ₄	1	1	0	0	0	0	0	0	0	V ₅	1	0	0	0	1	1	0	0	0	V ₆	1	0	0	0	1	0	0	0	0	V ₇	0	0	0	0	1	0	0	1	0	V ₈	0	0	0	0	0	0	1	0	1	V ₉	0	0	0	0	0	0	0	1	0	
	V ₁	V ₂	V ₃	V ₄	V ₅	V ₆	V ₇	V ₈	V ₉																																																																																													
V ₁	0	1	1	1	1	1	0	0	0																																																																																													
V ₂	1	0	1	1	0	0	0	0	0																																																																																													
V ₃	1	1	0	1	0	0	0	0	0																																																																																													
V ₄	1	1	0	0	0	0	0	0	0																																																																																													
V ₅	1	0	0	0	1	1	0	0	0																																																																																													
V ₆	1	0	0	0	1	0	0	0	0																																																																																													
V ₇	0	0	0	0	1	0	0	1	0																																																																																													
V ₈	0	0	0	0	0	0	1	0	1																																																																																													
V ₉	0	0	0	0	0	0	0	1	0																																																																																													
4,4,2,2,2	<table border="1"> <thead> <tr> <th></th> <th>V₁</th> <th>V₂</th> <th>V₃</th> <th>V₄</th> <th>V₅</th> </tr> </thead> <tbody> <tr> <th>V₁</th> <td>0</td> <td>1</td> <td>1</td> <td>1</td> <td>1</td> </tr> <tr> <th>V₂</th> <td>1</td> <td>0</td> <td>1</td> <td>1</td> <td>1</td> </tr> <tr> <th>V₃</th> <td>1</td> <td>1</td> <td>0</td> <td>0</td> <td>0</td> </tr> <tr> <th>V₄</th> <td>1</td> <td>1</td> <td>0</td> <td>0</td> <td>0</td> </tr> <tr> <th>V₅</th> <td>1</td> <td>1</td> <td>0</td> <td>0</td> <td>0</td> </tr> </tbody> </table>		V ₁	V ₂	V ₃	V ₄	V ₅	V ₁	0	1	1	1	1	V ₂	1	0	1	1	1	V ₃	1	1	0	0	0	V ₄	1	1	0	0	0	V ₅	1	1	0	0	0																																																																	
	V ₁	V ₂	V ₃	V ₄	V ₅																																																																																																	
V ₁	0	1	1	1	1																																																																																																	
V ₂	1	0	1	1	1																																																																																																	
V ₃	1	1	0	0	0																																																																																																	
V ₄	1	1	0	0	0																																																																																																	
V ₅	1	1	0	0	0																																																																																																	

(continued)

Table 1 (continued)

<p>Input sequence 7,6,5,4,4,3,2,1</p>	<p>Matrix</p> <table border="1" data-bbox="218 869 448 1245"> <thead> <tr> <th></th> <th>V_1</th> <th>V_2</th> <th>V_3</th> <th>V_4</th> <th>V_5</th> <th>V_6</th> <th>V_7</th> <th>V_8</th> </tr> </thead> <tbody> <tr> <th>V_1</th> <td>0</td> <td>1</td> <td>1</td> <td>1</td> <td>1</td> <td>1</td> <td>1</td> <td>1</td> </tr> <tr> <th>V_2</th> <td>1</td> <td>0</td> <td>1</td> <td>1</td> <td>1</td> <td>1</td> <td>1</td> <td>0</td> </tr> <tr> <th>V_3</th> <td>1</td> <td>1</td> <td>0</td> <td>1</td> <td>1</td> <td>1</td> <td>0</td> <td>0</td> </tr> <tr> <th>V_4</th> <td>1</td> <td>1</td> <td>1</td> <td>0</td> <td>1</td> <td>0</td> <td>0</td> <td>0</td> </tr> <tr> <th>V_5</th> <td>1</td> <td>1</td> <td>1</td> <td>1</td> <td>0</td> <td>0</td> <td>0</td> <td>0</td> </tr> <tr> <th>V_6</th> <td>1</td> <td>1</td> <td>1</td> <td>0</td> <td>0</td> <td>0</td> <td>0</td> <td>0</td> </tr> <tr> <th>V_7</th> <td>1</td> <td>1</td> <td>0</td> <td>0</td> <td>0</td> <td>0</td> <td>0</td> <td>0</td> </tr> <tr> <th>V_8</th> <td>1</td> <td>0</td> <td>0</td> <td>0</td> <td>0</td> <td>0</td> <td>0</td> <td>0</td> </tr> </tbody> </table>		V_1	V_2	V_3	V_4	V_5	V_6	V_7	V_8	V_1	0	1	1	1	1	1	1	1	V_2	1	0	1	1	1	1	1	0	V_3	1	1	0	1	1	1	0	0	V_4	1	1	1	0	1	0	0	0	V_5	1	1	1	1	0	0	0	0	V_6	1	1	1	0	0	0	0	0	V_7	1	1	0	0	0	0	0	0	V_8	1	0	0	0	0	0	0	0	<p>Spanning tree</p>  <pre> graph TD v1((v1)) --- v2((v2)) v1 --- v3((v3)) v1 --- v4((v4)) v1 --- v5((v5)) v1 --- v6((v6)) v1 --- v7((v7)) v8((v8)) </pre>
	V_1	V_2	V_3	V_4	V_5	V_6	V_7	V_8																																																																											
V_1	0	1	1	1	1	1	1	1																																																																											
V_2	1	0	1	1	1	1	1	0																																																																											
V_3	1	1	0	1	1	1	0	0																																																																											
V_4	1	1	1	0	1	0	0	0																																																																											
V_5	1	1	1	1	0	0	0	0																																																																											
V_6	1	1	1	0	0	0	0	0																																																																											
V_7	1	1	0	0	0	0	0	0																																																																											
V_8	1	0	0	0	0	0	0	0																																																																											

5 Results and Discussion

The output of the algorithm when applied to the test sequences of Table 1, clearly justifies the correctness of the algorithm. For every nonregular graphic sequence, we can obtain the spanning tree.

However, an important observation is that the spanning tree generated by the algorithm may not be unique. This is a well-known fact since a different choice of initial vertex will result in a different spanning tree and does not deviate from the problem statement. Another point about the algorithm is that the matrix generated in the first step can be linearly permuted over rows and columns to obtain different adjacency matrices thereby varying the spanning trees thus constructed. But in all the scenarios, the algorithm ends up giving the spanning tree corresponding to the final matrix fed to the final matrix fed to the second part of our approach.

6 Conclusion

From the above discussions, we can easily conclude that the algorithm is an efficient approach to construct a spanning tree directly from the degree sequence of nonregular graphs. It is easy to understand and simple to code. Further, we can also obtain all the spanning trees corresponding to a given input sequence by applying the algorithm repeatedly over the various linearly permuted matrices and by choosing a new starting vertex. Moreover, removal of certain edges sometimes results in breaking of multiple cycles thereby reducing the execution time. Hence, we can infer that it is a good approach to determine the spanning tree directly from the degree sequence of a graph.

References

1. Kruskal JB. On the shortest spanning subtree of a graph and the travelling salesman problem. *Proc Am Math Soc.* 1956;7:48–50.
2. Prim RC. Shortest connection networks and some generalizations. *Bell Syst Tech J.* 1957;4:53–7.
3. Havel V. A remark on the existence of finite graphs. (Czech.) *Casopis Pest Mat.* 1955;80:477–80.
4. Hakimi SL. On the realizability of a set of integers as degrees of the vertices of a graph. *SIAM J Appl Math.* 1962;10:496–506.
5. Erdős P, Gallai T. Graphs with prescribed degree of vertices. (Hungarian) *Math Lapok.* 1960;11:264–74.
6. Ryser HJ. Combinatorial properties of matrices of zeros and ones. *Can J Math.* 1957;9:371–7.
7. Berge C. *Graphs and hypergraphs.* Amsterdam: North Holland and New York: American Elsevier; 1973.
8. Fulkerson DR, Hofman AJ, McAndrew MH. Some properties of graphs with multiple edges. *Can J Math.* 1965;17:166–77.

9. Bollobás B. *Extremal graph theory*. New York: Academic Press; 1978.
10. Grönbaum B. *Graphs and complexes*. Report of the university of Washington, Seattle, Math. 572B, (1969) (private communication).
11. Hässelbarth W. Die Verzweigteit von Graphen. *Match*. 1984;16:3–17.
12. Sierksma G, Hoogeveen H. Seven criteria for integer sequences being graphic. *J Graph Theory*. 1991;15(2):223–31.
13. Kleitman DJ, Wang DL. Algorithms for constructing graphs and digraphs with given valences and factors. *Discrete Math*. 1973;6:79–88.
14. Czajkowski, Eggleton RB. Graphic sequences and graphic polynomials: a report. *Infinite Finite Sets*. 1973;1:385–92.
15. Tripathi A, Vijay S. A note on theorem on Erdős and Gallai. *Discrete Math*. 2003;265:417–20.
16. Dahl G, Flatberg T. A remark concerning graphical sequences. *Discrete Math*. 2005;304:62–4.
17. Tripathi A, Taygi H. A simple criterion on degree sequences of graphs. *Discrete Appl Math*. 2008;156:3513–7.
18. Boukerche A, Tropper C. A distributed graph algorithm for the detection of local cycles and knots. *IEEE Trans Parallel Distrib Syst*. 1998;9:748–57.
19. Manivannan D, Singhal M. An efficient distributed algorithm for detection of knots and cycles in a distributed graph. *IEEE Trans Parallel Distrib Syst*. 2003;14:961–72.

Differential Illumination Enhancement Technique for a Nighttime Video

G. Abirami and S. Padmavathi

Abstract Video surveillance has become a common security need in the present-world scenario. The nighttime video surveillance becomes more challenging due to the presence of extreme illumination conditions, which is not uniform in a frame. Pedestrian detection would be very difficult under such illumination condition. The system proposes a method to identify and segregate the differently illuminated regions with the help of day-time reference image. Various enhancement techniques are applied on these regions separately and the results are combined to obtain the enhanced frame. Results of these techniques are summarized and appropriate methods are suggested for specific cases.

Keywords Nighttime video enhancement · Video surveillance · Illumination

1 Introduction

A nighttime video lacks the surrounding scene context due to poor illumination and also sensor noise. More background noises are caused by the environmental weather conditions. In high light/dark regions the scene information cannot be seen clearly by the observers. These characteristics increase the necessity of nighttime video enhancement. Nighttime video enhancement will be useful for both visual and machine perception.

Nighttime video enhancement is a crucial step in nighttime video surveillance. Identification of persons, animals in dark regions is a major requirement in the nighttime videos. It helps human monitoring in a better way due to the enhancement

G. Abirami (✉) · S. Padmavathi
CSE Department, Amrita Vishwa Vidyapeetham, Amrita Nagar, Ettimadai, Coimbatore
641112, India
e-mail: abiramigovindarajan@ymail.com

S. Padmavathi
e-mail: s_padmavathi@cb.amrita.edu

of the dark regions. The frames are not uniformly dark due to the presence of different light sources ranging from stationary street lights to moving vehicle lights. A global illumination enhancement technique fails in such a scenario. It only degrades the image further. Hence identifying the differently illuminated regions in a frame will lead to precise enhancement of the regions.

Video enhancement improves the visual appearance and produces a better representation for higher level processing such as detection, identification, recognition, and analysis. Video-enhancement technique is categorized into two major groups [1]: Self-enhancement and context-based fusion enhancement. Self-enhancement deals with enhancing the nighttime video without any external reference but context-based fusion enhancement needs external information for enhancement.

Self-enhancement of nighttime video introduces small distortions which produces unrealistic effects. Even though objects are visible, it does not reveal the contour thereby making foreground extraction a difficult task. Due to presence of light sources at few locations, the dark regions lose their actual information. Context-based fusion enhancement is done with the help of daytime image so that the finer image details can be preserved and made visible. The daytime reference video has a rich background context that is almost uniformly illuminated with high brightness values. The lack of nighttime video characteristics can be resolved with a daytime reference video. The real-time application environment for this system would be nighttime surveillance and home security. The paper is structured as follows: Sect. 2 deals with the literature survey, Sect. 3 explains about the proposed work, Sect. 4 depicts experimental results and Sect. 5 concludes the paper.

2 Literature Survey

The existing nighttime video-enhancement techniques are global in nature and perform the enhancement with or without a reference daytime image. The self-enhancement techniques adopt tone mapping, histogram equalization, contrast-based methods, etc., globally for the nighttime frames without the reference frame. These techniques results in small distortions as they are uniformly applied to the bright and the dark regions. The context-based fusion video-enhancement aims to detect, recognize, and track objects (including pedestrians and vehicles) from video/image, while being aware of existing surrounding context from the daytime reference video/image. Various fusion methods are adopted for different illumination enhancement. Context-based fusion enhancement is categorized into three major divisions

1. Color-based method
2. Gradient-based method
3. Intensity-based method

These methods are briefly discussed in the Table 1 with their pros and cons.

Table 1 Comparison between context-based fusion methods

Category	Description	Pros	Cons
Color-based method [2]	Method for applying daytime colors to nighttime imagery in real time can improve situational awareness	The target image need not represent the same scene as the source image	Lack of color constancy
Gradient-based method [3]	Aims to capture the gradient information from the nighttime image/video	Achieves a smooth blend of the input images, preserves their important features	Observable color shift. Difficult to maintain high contrast in single image
Intensity-based method	Background fusion Foreground extraction. Fusion by logical OR operation [4]	Maintain the proper quality of the image	If proper value is not detected then the proper change occurring in the image is not determined
	<i>Hybrid method</i> —high contrast in local part of the image which is stable in the night images [5]	Gives better visibility	It works well with the indoor environment
	<i>Denighting method</i> —Fusion method based on the illumination ratio of daytime background and nighttime background [6]	Maintains intrainage coherence by using the weighting ratio	Due to uneven illumination ratio, the enhanced results will lose illumination information of nighttime videos
	Enhance nighttime background using illumination images of day/night for determining weights. Enhancement performed by a combination of illumination [7]	Maintains high contrast in the image	Works well for nighttime images that are uniformly dark. It can produce false background problem
	Motion detection is carried out by Gaussian mixture model. Illumination is estimated by Retinex theory weighted sum fusion technique is used [8]	Retains information density and helps in high-level behavior analysis and understanding	The important region information in nighttime image may not be maintained

3 Proposed Work

In this paper, a nonglobal method for enhancing the nighttime video with the daytime reference image is proposed. The differentially lighted regions in the video frames are segregated using illumination segmentation method. The luminance values of these regions are adjusted to with the help of daytime reference image.

The segregation of differentially lighted regions is based on the assumption that the luminance value of the dark regions is less than the daytime reference. The regions of the nighttime video frames that are illuminated by street lights, vehicle lights, etc., have a higher luminance value than that of a daytime reference image.

3.1 Methodology

3.1.1 Illumination Segmentation

Based on the assumption, the pixels in a nighttime video frame is said to be part of region under street light or head light of a vehicle based on the following condition

```

If( $N_t(x, y) > DB(x, y)$ )
 $N_t(x, y) = 1$ ;
Else  $N(x, y) = 0$ ;
end

```

$N_t(x,y)$ —intensity image of nighttime video frame

$DB(x,y)$ —intensity image of daytime background image.

We obtain a binary image BDB with dark regions represented by 0 and high light regions are represented by 1. These regions are treated separately by various enhancement techniques.

3.1.2 Illumination Adjustment

The illumination segmentation module yields the output as a binary image BDB of the particular nighttime frame which represents both highlight regions and dark regions. The bright regions are segmented and a homomorphic filtering is applied to it. Histogram equalization technique is applied to the dark regions. The results are then combined to give the enhanced frame.

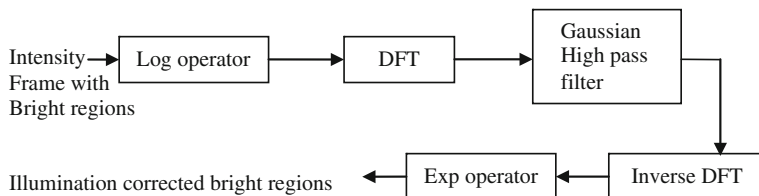


Fig. 1 Design of homomorphic filter

3.2 Bright Regions

3.2.1 Illumination adjustment using homomorphic filtering

Homomorphic filtering [9] is a technique for removing multiplicative noise and most commonly used for correcting illumination effect in images; it assumes that illumination is uniform and illumination varies slowly across the image as compared to reflectance. Reflectance changes abruptly at object edges. The homomorphic filtering is explained with the block diagram given in Fig. 1.

The bright regions segmented from the binary image BDB is given to Log operator to convert the multiplicative noise to additive noise. Discrete Fourier transform (DFT) is applied to convert the frame to frequency domain. The Gaussian high-pass filter function as given in Eq. (1) is applied to enhance the bright regions. Then inverse DFT and exponential operator are applied on the filtered frame to obtain the illumination corrected bright regions.

The filter function is represented as follows:

$$H(u, v) = (\gamma H - \gamma L) [1 - \exp(-c^* D^2(u, v)/D^2)] + \gamma L. \quad (1)$$

$$D(u, v) = \left[(u - P/2)^2 + (v - Q/2)^2 \right]^{(1/2)}. \quad (2)$$

$D(u, v)$ is the distance between the point (u, v) in the frequency domain and the centre of frequency rectangle.

P, Q is the size of the image.

$\exp(\cdot)$ is the exponential function.

c is the constant which controls the slope between the transitions of γL and γH .

D is the cut off frequency.

3.3 Dark Regions

The dark regions are enhanced using histogram equalization [9] which stretches the intensity levels to fit the dynamic range 0–255. This converts the low-contrast dark image into the high-contrast image and further the distribution of pixels is not too far from uniform.

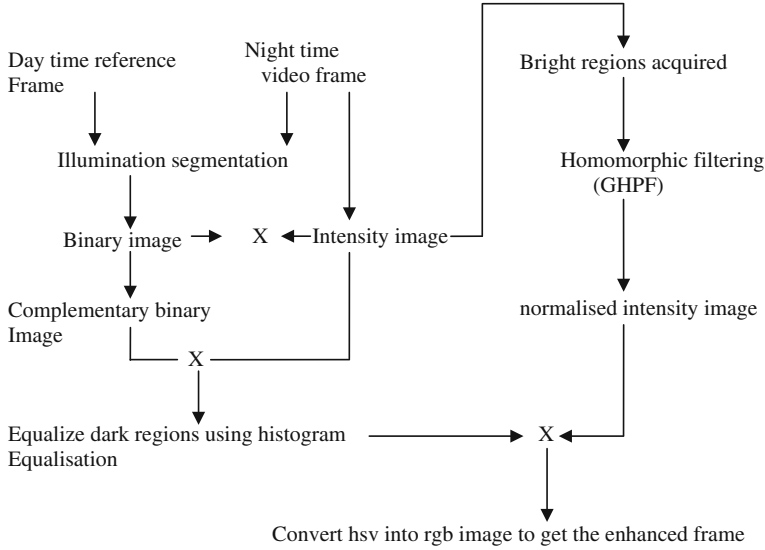


Fig. 2 Overall flow diagram of illumination segmentation and adjustment for the differentially illuminated areas of the nighttime video

The probability of occurrence of the intensity level r_k in the image is approximated by

$$\Pr(r_k) = nk/MN. \quad k = 0, 1, 2, \dots, L - 1 \quad (3)$$

where MN is the total number of pixels in the image.

nk is the number of pixels that have intensity r_k .

L is the number of possible intensity levels in the image (e.g., 256 for an 8-bit image).

Fig. 2 explains the differential illumination-enhancement method. Here the binary image that indicates the bright and dark region is obtained as specified in Sect. 3.1.1. Once the differential regions are segmented in the intensity frame, enhancement methods are performed accordingly as specified in the Sect. 3.1.2. The regions after enhancement are combined and normalized to fit into the range of 0–255. The enhanced intensity frame is concatenated with hue, saturation components of the nighttime frame, which is converted back to an enhanced RGB video frame.

4 Experimental Results

The Experimental dataset includes an indoor video which is collected from the website: <http://web.media.mit.edu/~raskar/NPAR04/>. The video has a person walking from one place to another in indoor environment. Two outdoor surveillance videos are collected from the Amrita Vishwa Vidyapeetham University campus for a day, is also considered for experimentation. Videos taken in Amrita Vishwa

Table 2 List of several night and daytime videos among the dataset

Name of the video	Day/night	Category	Time in min	No. of frames	Frame rate (fps)
Nite_outdoor.avi	Night	Outdoor	60	89,982	25
Nite_indoor.avi	Night	Indoor	5 s	154	29
Nite_outdoor1.avi	Night	Outdoor	30	43,293	25
day_outdoor2.avi	Day	Outdoor	60	89,982	25

Vidyapeetham is freely available for Amrita students and staff for the research purpose and is approved by the University heads. The outdoor video datasets are taken from same view point, same location but at different times such as day and night without manipulating camera parameters. The camera specification is as follows: Common CCD Outdoor Camera, Vari Focal lens (2.8–12 mm) (2 mega pix), Horizontal Resolution 700 TV Lines, 36 IR LED, IR Distance-20 m. The outdoor videos have huge number of pedestrians and vehicles crossing the security post. These videos are cut to 1 h videos for experimentation which are listed in Table 2. Among the videos the nighttime videos are used for testing the algorithm. A daytime image is considered as a background reference frame for computing the bright and dark regions. The implementation is performed on MATLAB R2013a platform.

Indoor environment

Figure 3 shows a sample of indoor nighttime frame with the person and daytime background image. Figure 4 depicts the enhanced frame corresponding to Fig. 3. Another enhanced night frame without the person is shown in Fig. 5.

Outdoor environment

Figures 6 and 8 show a sample of outdoor nighttime frame and the daytime background image taken as reference. Illumination segmentation algorithm as specified in Sect. 3.1.1 is applied to Fig. 6 which gives the mask with light regions specified in white and dark

Fig. 3 Nighttime frame and daytime background image

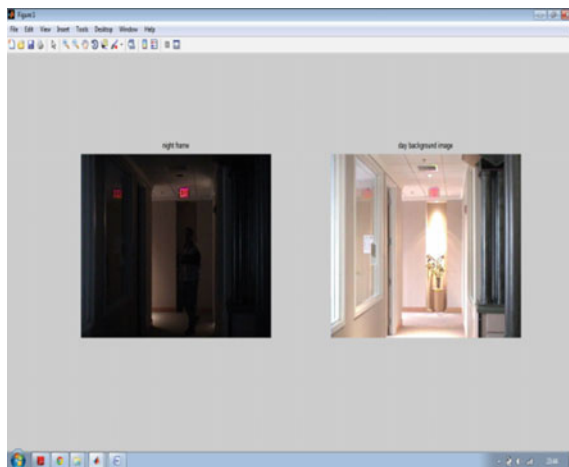


Fig. 4 Enhanced nighttime frame

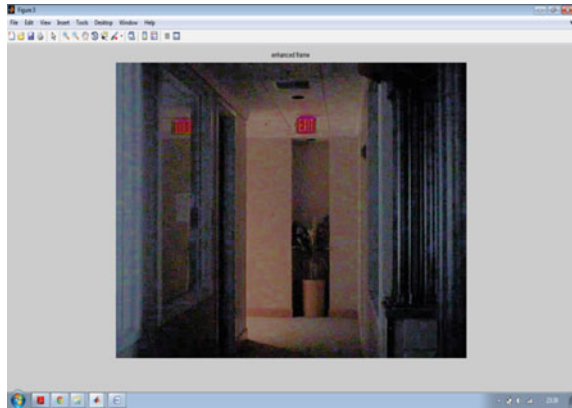
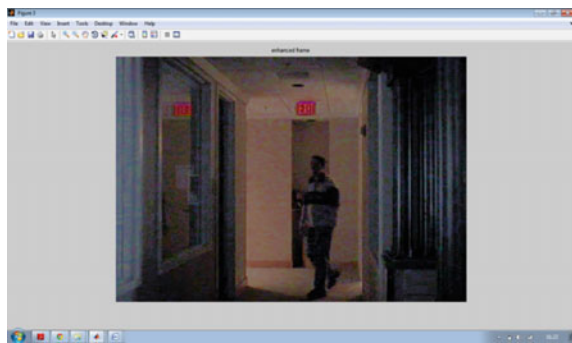


Fig. 5 Enhanced frame with the presence of person



regions specified in black as in Fig. 7. Figure 8 depicts the corresponding enhanced frame, obtained through the algorithm as specified in the Sect. 3.1.2.

The proposed illumination enhancement method reduces the luminance levels around the bright regions but did not expose the details in the darker region (Fig. 9).

Fig. 6 Screen shot of nighttime video



Fig. 7 Illumination segmentation mask for a frame

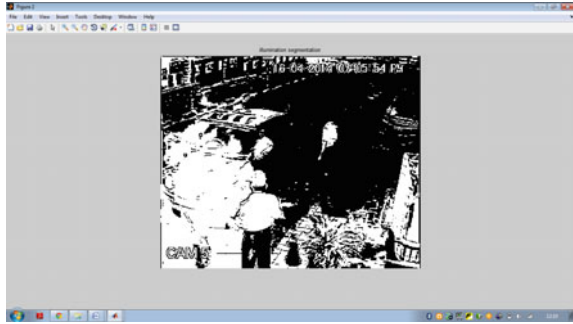


Fig. 8 Daytime reference background image



To exhibit those details, methods like histogram equalization, contrast-enhancement functions like log, exponential operators, and also histogram matching, homomorphic filtering for both dark and bright regions were experimented and

Fig. 9 Enhanced nighttime frame obtained from the proposed work

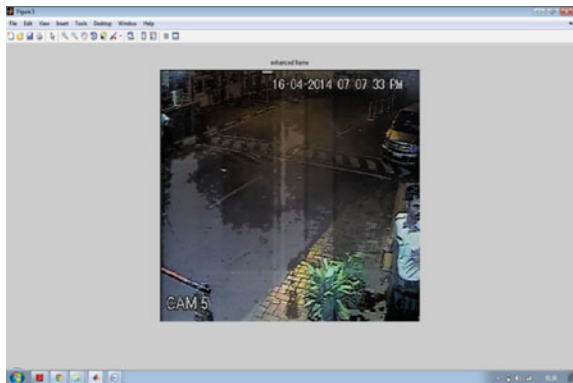



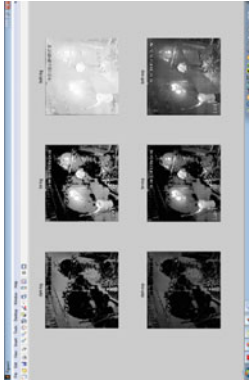




Table 3 Experimentation on different illumination methods for the differential regions

Method	Region segments	Output result	Inference
Histogram equalization-worked on intensity image alone	For dark region		Dark regions enhanced
	For bright region		Bright regions not fully discovered
	Both combined	<p data-bbox="635 776 664 1120">Combined intensity on taking inverse</p> 	Sharpness reduced, and bright regions can still be reduced


(continued)

Table 3 (continued)

Method	Region segments	Output result	Inference
Contrast enhancement	Using log and exp operator		Dark regions log operator better. Bright regions exp operator better. Whole image exp operator comparatively better but bright light not suppressed
Histogram match	For dark region-match saturation and intensity		Slight increase in dark regions
	For bright region-match Intensity alone		Light around the vehicle lights reduced but complete bright regions not exposed

(continued)

Table 3 (continued)

Method	Region segments	Output result	Inference
	Both regions		Comparatively better enhancement

summarized in Table 3. The daytime reference background image and illumination segmentation are similar to the previous method.

Observation

From the experimental analysis, it could be seen that certain techniques produce better result for the bright regions and certain other techniques are better for dark regions. These are summarized in the following paragraph.

For bright regions Homomorphic filter reduces the effect of luminance values with γ^L as 0.25 and γ^H as 1. Histogram matching reduces the intensities around the bright light areas. Exponential operator when used to enhance the image, the regions around the head lights was darkened.

For dark regions Enhancing the dark regions with log operator produces a better result than histogram equalization and histogram matching.

These methods work better on the individual regions. The quality of the combined image after the independent enhancement of the regions was poor. Histogram matching when applied on the regions independently and the results when combined give a better result than the above-specified methods. The regions from the daytime reference frame are considered for matching the histogram of the nighttime regions.

5 Conclusion and Future Work

Nighttime video enhancement is required to identify people, object in the dark regions. It is a challenging task due to the presence of different illumination sources. In this paper, the highly illuminated areas are identified and segregated with the help of daytime reference image. Various enhancement techniques are experimented on the bright areas and dark areas separately, whose results are combined to get the enhanced frames. After a detailed experimentation, it could be summarized that homomorphic filtering, and exponential filters enhance the bright regions; log filters enhance the dark regions and histogram matching for the combined regions are found better than the other methods.

Histogram matching between the nighttime regions and daytime regions is performed with various combinations of HSV and RGB components. It can be concluded that matching between intensity and saturation component provides better-enhanced image than others. The effect of the headlights in the surrounding regions is reduced and the darker regions are enhanced to see the finer details present there. But the illumination equivalent to the daytime could not be achieved.

References

1. Pallavi, Reecha S. Study of the night time context enhancement algorithms. Int J Sci Mod Eng (IJISME). 2013;1(6). ISSN:2319-6386

2. Hogervorst MA, Toet A. Method for applying daytime colors to night time imagery in real time. Multisensor, multisource information fusion: architectures, algorithms, and applications. Proc. SPIE 2008;6974-2.
3. Ubhi JS, Kaur J. Enhancement of context by image fusion. Proc World Congr Eng. 2011;II.
4. Rao Y, Lin W, Chena L. Image-based fusion for video enhancement of night-time surveillance. Opt Eng 2010;49(12). © SPIE. 120501-1.
5. Cai Y, Huang K, Tan T, Wang Y. Context enhancement of nighttime surveillance by image fusion. IEEE. 2006.
6. Singh A, Banga VK. Enhancement of contrast of image using daytime and nighttime image. Int J Electron Commun Eng (IJECE). 2013;2(2):153–160. © IASET. ISSN:2278-9901.
7. Jing L, Tao Y, Quan P, Yongmei C. Combining scene model and fusion for night video enhancement. J Electron (China). 2009;26(1).
8. Jin H, Tu L, Deng X. Night image enhancement algorithm based on retinex theory. Int J Adv Comput Technol (IJACT). 2011;3(10).
9. Gonzalez RC, Woods RE. Digital image processing. Person Prentice Hall.

Low-Cost Appliance Control System for Home Automation and Energy Management Using Image Processing

Nagaraj Shet, C. Shreesha, P.V. Rao and Abdullah Gubbi

Abstract In the stressful life, enhancing the quality of life at home is the need of the hour. Smart home automation is being incorporated with an intelligent system. Existing systems are creating major challenges in terms of cost and energy management. In a home network environment, keeping the sensors and devices always on consumes more electrical power and increases the cost paid for consumption of power. In the proposed work, energy management has been carried out with an intelligent algorithm. Image processing has a very big potential to do virtually anything. The challenges of cost have been overcome using image processing. Algorithm is developed for image processing-based appliance control system. The method proposed in this paper reduces the cost of sensors used in home automation. With image processing-based home automation there is less energy consumption, reduction in number of sensors, and also optimized maintenance cost of home automation networks.

Keywords Electric power · Sensors · Energy management · Image processing · Home automation · Appliance control

N. Shet (✉) · P.V. Rao · A. Gubbi
Department of ECE, VTU Belgaum, India
e-mail: shet_nagaraj@yahoo.co.in

P.V. Rao
e-mail: pachararao@rediffmail.com

A. Gubbi
e-mail: abduallahgubbi@yahoo.com

C. Shreesha
Department I&CE, MIT Manipal, India
e-mail: shreesha.c@manipal.edu

1 Introduction

Due to improvement in living standards, everyone loves to have all the facilities without difficulty and at the earliest. This resulted in the use of advanced technology for home automation. So home automation has become the center of research. People want all the things to be automated from very simple tasks to many complex tasks. User satisfaction and comfort is the main criteria for home automation. There are plenty of electrical appliances in every modern household. Automating the operation of all the electronic and electrical equipments and providing security improves the quality of life and provides more comfort to the dwellers. User requirements for home automations [1] are broadly classified into the following groups:

- (1) Efficient automation of routine tasks
- (2) Security of automation systems
- (3) Ease of use
- (4) Local and remote access
- (5) Telemonitoring
- (6) System cost and flexibility.

When we look in a wider extent, gestures came out from human body is natural. From Concise Oxford English Dictionary, gesture is a movement of part of the body, especially a hand or head, to express an idea or meaning. As for this work, the development portion is to develop a new practical technology for alternative human interface. This gesture definition has been narrowed down to only hand and is given particular attention on details that Indian hands has. We aim to design technique that reduces the number of sensors are being used for different applications. Image processing is a branch of knowledge that tries to reach the same goal as human vision does. The process will not be the same but the objective is. The concept may or may not differ, depends on what subtask of the whole system is to be accomplished first. Machine look on something through segregated details to do matching based on system's hardware capability. Human on the other hand, used as much information as possible and will decide at that instance, fulfilling directly to the objective of the vision task itself. That is why trying to have the same par with human capability especially from the recognition accuracy perspective is impossible with current technology advancement available. Image processing consists of various processes like image enhancement, image segmentation, and image perception. These processes help the designer to extract the proper input from images.

(ii) Image Thresholding: Image thresholding is a part of image processing that converts the intensity or grayscale image to binary image. In binary image, high-intensity values are represented as white colour and low-intensity values are represented as black colour. This process helps us to identify the objects from images by eliminating the background of the image. Finally to summarize, the objective of this work is

- i. Human detection system using surveillance camera or PIR sensor to detect the human
- ii. To develop a hand gesture recognition system
- iii. To develop a system that can translate snapshot of hand gesture to a set of actions.

The organization of the paper is as follows. In Sect. 2, literature survey is described. Proposed architecture of the system is discussed in Sect. 3. In Sect. 4, methodology is discussed. In Sect. 5, results are shown. In Sect. 6, the conclusion is discussed, and future work is discussed in Sect. 7.

2 Literature Survey

Home automation is also popular as digital home, e-home, and intelligent house or smart home. For building the home automation system, automation technology, computer technology, telecommunication technology along with electromechanical technology is used. Quality of entertainment, security, and safety has been improved using home automation. It helps people with less work and better management of household work with automation and interactive closed-loop system. Home automation technology and smart home was considered science fiction during 1920s. We do not have details about exact date of the invention of home automation. Based on available facts home automation, one of smart technology, evolved over a period of time but did not happen with immediate invention. It happened step-by-step with significant improvement in recent years. There was a gradual change to the next step in development of home automation technologies compared to previous step. At the earlier stages, people noticed the use of high technology in dwelling. Slowly, electrical equipments were controlled through wired connections. That home automation in 1960s called as “wired homes.” It was built by some hobbyist. Official name of home automation was used by the American Association of House Builders only during 1984. That became the key development to the modern smart homes. People at that time were able to make difference between interactive home automation technologies used in smart home [2] and technologies that were used to build better homes by effectively using space with environment friendly features. Home can be considered to be smart home depend on to what extent interactive technologies are used in it. Those are still useful rules for home automation technology today.

According to Mitra [6], gesture recognition is an image-processing technique. Man-made gestures are captured and system recognizes it. This technique can be easily used to interact with machines by making different gestures according to required message to be conveyed. Database of different messages for different environment according to application syntax is stored. System is made to give them particular message according to the environment and application syntax. Even people who cannot communicate orally (sick, old, or young child), they would also

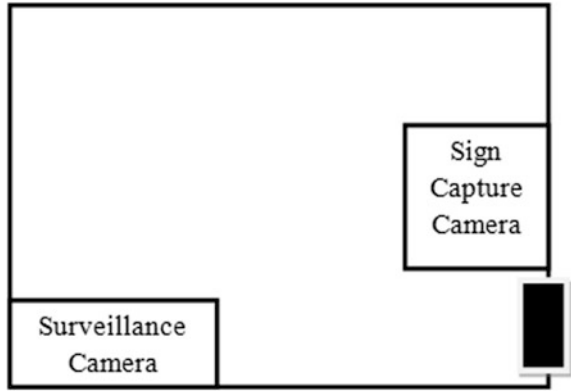
get benefit from this technology. During 1960s, hardly there were any interactive technologies. It is possible to make a gesture recognition system for these people. For the people who cannot speak due to disability from birth or old age problems, a mechanism can be provided to express themselves using gesture-based systems. Gesture-based systems can be connected to speech processing systems to generate oral messages from stored database after selecting suitable message for particular type of gesture. Nowadays, mobile companies are trying to make handsets which can recognize gesture and could operate from little distance also. Here we are focusing on human-to-machine interaction (HMI), in which machine would be able to recognize the gesture made by human. Even though Stanford University researched a lot of this kind of technology, they did not become so successful. They concluded some principal reason for not succeeding is scientific research. (a) Lacking of motivation to increase productivity in domestic work. (b) Less involvement of users of the technology in the design process. (c) The view held by product designers that domestic technology is unexciting. (d) A continued focus on stand-alone appliances in the design of new technology. Today smart energy management is very important for energy saving [3]. Due to lot of popularity of mobile communication, GSM-based home automation [4] is popular. But lot of sensors and GSM-based communication itself is not consistent, becomes unreliable [5]. FPGA-based home automation system does not make a universally acceptable solution [6]. Zigbee-based HAM becomes very costly with increase in number of functionalities and devices [7]. Simulation is not close to practical things. Two types of approaches to HGR are discussed.

- i. Appearance-based approaches where hand image is reconstructed using the image properties and extraction.
- ii. Model-based approaches where different models are used to model image using different models to represent in computers. In this paper, we proposed a new algorithmic-based technique in two possible combinations as follows: (1) Sign based (2) Person detection and shown that it is a cost effective and energy efficient.

3 Proposed System Architecture

Many researchers proposed methods like hand gloves fitted with flex sensors or wires. Variation in resistive values with movements of gloves is analyzed to match with the required response. But contact less gesture recognition became a research area in machine vision or computer vision and is as natural as human to human interaction. In proposed algorithm, enhancement of home automation system has been focus for appliance control system with a real-time scenario. The real-time scenario has been defined in Fig. 1. Here two cameras are placed in a room. One camera is used for capturing the sign to turn on the appliances. Another camera is used for capturing whether any person has entered in the room to turn on the

Fig. 1 Appliance control scenario for home automation



appliances or come out of the room to turn off the appliances. The functional block diagram of proposed algorithm for appliance control system is shown in Fig. 2. First it is capturing inputs from sign capture camera and surveillance camera. Captured images are not suitable for appliance control. Therefore, image processing has been carried out using thresholding method.

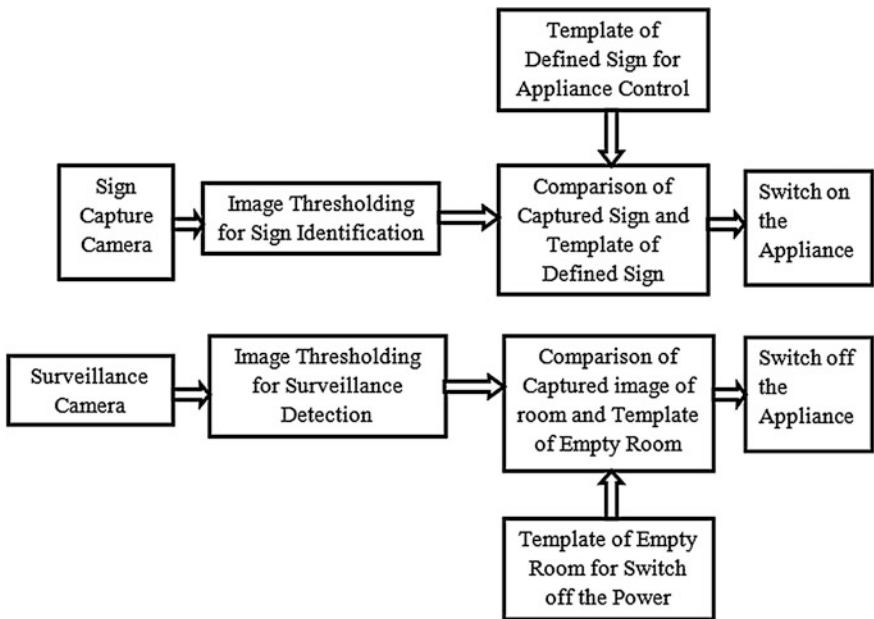


Fig. 2 Functional block diagram of appliance control system

After thresholding, threshold images are taken for template matching to identify the sign for turning on different appliances. Simultaneously, same template matching will happen for person identification to turning off the appliances.

4 Methodology

Natural hand gesture recognition (HGR) is hot research areas in the computer vision. Hands-free operation of machines is possible using hand gesture recognition systems. Using NHGR can help people to interact with machines without using any extra device. Such systems are also useful if the users do not have much technical knowledge about the system. Machines can be operated without physically touching, but just by indicating hand gestures. They still will be able to use the system with their normal hands. Gesture made using human hand can be any, but few have a special meaning. Human hand can have movement in any direction and can bend to any angle. For human face detection, the Voila Jones code which is available from MATLAB latest version is used. Once the face or human is detected in the room than hand sign camera is activated, that will capture the hand gesture. The captured image is a color image. First color image is converted to grayscale image, then followed by binarization of image is done. In order to convert the image to binary image, proper threshold should be selected.

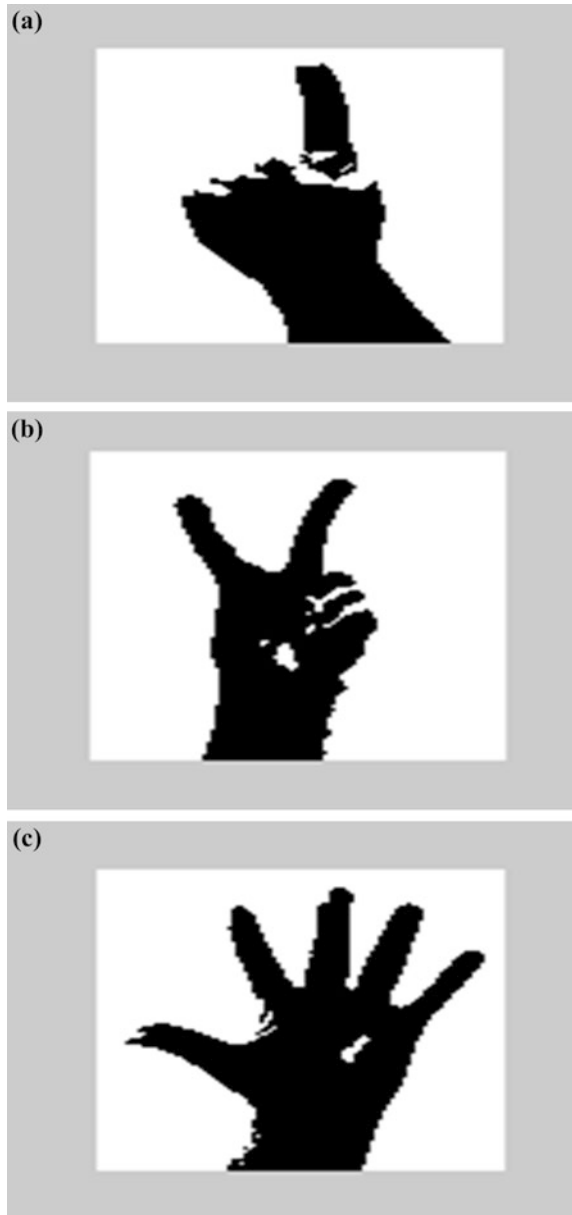
The steps are involved for the carrying out the work is as follows. (i) Most important thing is the presence of human being in the room that is carried out by voila Jones code. Voila Jones code is based on the Haar wavelet transform. (ii) Take the input sign image. (iii) Threshold the sign image to capture the sign from image. (iv) Take the Threshold template of all the sign. (v) Then count the number of ones in captured sign. (vi) Match the count with template sign. (vii) The match is found by 80 % then turn on the appliance else switch off the appliance. (viii) For turn off, the appliance match the surveillance image with template of empty rooms. (ix) If it matches with template of empty room then turn off the appliances.

5 Results

For tuning on light, fan, and high-volt AC three templates have been taken. The threshold images of template are shown in Fig. 3a–c. Figure 3a is for turning on the lighting appliance. Figure 3b is for turning on the fan and Fig. 3c is for turning on high-volt AC appliance.

Real-time input is shown in Fig. 4. In Fig. 4 five fingers are shown that all are indicating to turn on the high-volt AC appliance.

Fig. 3 **a** Template for light control. **b** Template for fan control. **c** Template for HVAC control

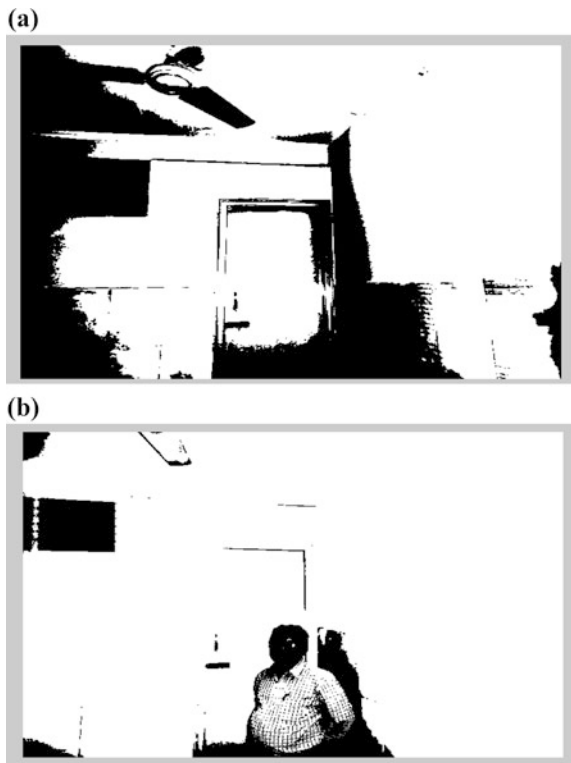


For tuning off light, fan, and high-volt AC empty room template has been taken. The threshold images of template are shown in Fig. 5a. Figure 5a is for turning off the lighting appliance, fan, and high-volt AC appliance. Real-time input is shown in Fig. 5b. In Fig. 5b human being is present. Therefore, the appliances are kept in same state.

Fig. 4 Real-time input capture by algorithm

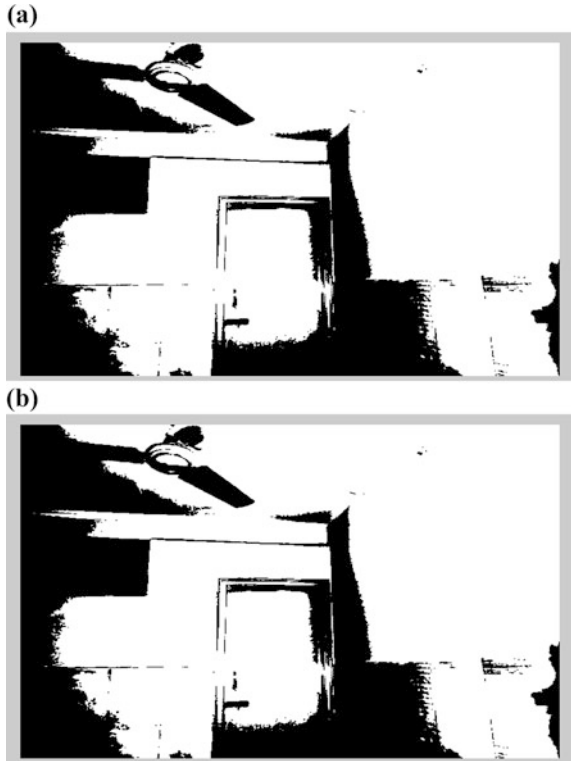


Fig. 5 **a** Template for turning off appliance. **b** Real-time input for person detection



For tuning off light, fan, and high-volt AC empty room template has been taken. The threshold images of template are shown in Fig. 3a. Figure 6a is for turning off the lighting appliance, fan, and high-volt AC appliance. Real-time input is shown in Fig. 6b. In Fig. 6b human being is not present. Therefore, the appliances are turned off.

Fig. 6 **a** Template for turning off appliance. **b** Real-time input for person detection



6 Conclusion

Hand gesture-based electronic device control is gaining more importance nowadays. Different applications of hand gesture recognition have been implemented in different domains from simply game inputs to critical applications. Hand gesture recognitions is natural to interact with vision-enabled computers and other machines. This paper primarily focused on the study of work done in the area of natural hand gesture recognition using computer vision techniques. From the results obtained in this work, that the proposed algorithmic-based methodology has been reduced the complexity of controlling appliances and energy management has been carried out with intelligent algorithm. The number of sensors is required in a home automation system is also reduced and which in turn reduces the maintenance cost of home automation. The number of devices is reduced by approximately by 10 % and almost the cost by 5 %.

7 Future Scope

In this proposed work, home automation can be done by adopting the image-processing techniques. The implementation becomes cost effective, consumes less power, and can be easily converted to security-based home automation system along with controlling home appliances. Further work can be carried out to analyze individual finger position, figure bending detection, and finger movements. Works carried out with such implementations are few. Present investigations are carried out with full hand position detection or the fingertip position detection to generate or match required response. With additional enhancements, better security and surveillance system can be developed with improved features and characteristics in home automation while considering the cost, power consumption, security along with main task of automation.

References

1. Maikowski M. X 10 Home security systems. Jefferson Technology Press; 2006. pp 190. ISBN:10:096789171X.
2. Park W-K, Choi C, Jang J. Energy efficient multi-function home gateway in always-on home environment. 2010 IEEE, Consumer Electronics, IEEE Transactions; 2010. ISBN:978-1-4244-4316-1/10/\$25.00.
3. Al-saedi FAT. Peak saving energy management system for smart house. IJCSET. 2013;3 (10):359–366. ISSN:2231-0711.
4. Gopu S, Kishore GS. Monitoring of home & activation of automated system via GSM through FPGA. Int J New Trends Electron Commun IJNTEC. 2014;2(1):11–14. ISSN:2347-7334.
5. Debono CJ, Abela K. Implementation of a home automation system through a central FPGA controller. IEEE; 2012. p. 641–644. ISBN:978-1-4673-0784-0/12/\$31.00.
6. Gill K, Yang SH, Yao F, Lu X. A ZigBee-based home automation system. IEEE Trans Consum Electron. 2009;55(2):422–430.
7. Coral Lozada MA, Fernando De la Rosa R. Simulation platform for domotic systems. IEEE; 2014. ISBN:978-1-4799-4340-1/14/.

Design of Wireless Sensor Network for Submarine Detection

Anjali Arunan and R.D. Aryadevi

Abstract The coastline of India extends up to nearly 12 Nautical miles which increase the possibility of intruders into the coastline of country (Barr et al. Barrier coverage for underwater sensor networks. IEEE Military communications conference. MILCOM; 2008. p. 1–7) [1]. This work looks into the intrusion of the other submarine to coastline of the country. Most of the existing submarine intrusion detection systems use sonar-based technologies. As submarine hulls can absorb the sonar waves, it can effectively hide from the detection system (Heidemann et al. Research challenges and applications for underwater sensor networking. IEEE Wireless Commun Netw Conf (WCNC). 2006;1:228–35) [2]. The proposed submarine detection system described in this paper helps to avoid this issue. The proposed system uses a wireless sensor network which provides an effective submarine detection and localization. In this work, a new MAC protocol and Routing Protocol is proposed for efficient working of the system.

Keywords Connectivity · Coverage · Coverage degree · Localization · Protocol · Sensing range

1 Introduction

Indian coasts are vulnerable to criminals and anti-national activities, sea-born threats, and activities. The cases like people smuggling and human trafficking; terrorism has been reported over years. The existence of vital strategic installation, and increased marine traffic causes these problems. India has a 7516.6 km long

A. Arunan (✉) · R.D. Aryadevi
Amrita Center for Wireless Networks and Applications, Amrita Vishwa Vidyapeetham,
Kollam, Kerala, India
e-mail: anjali.a27@gmail.com

R.D. Aryadevi
e-mail: aryadevird@am.amrita.edu

coastline, which includes 5422 km of coastline in mainland and 2094 km of coastline bordering islands [3]. Indian coastline extends up to nearly 12 Nautical miles has intense maritime activity. Hence huge areas need to be kept under surveillance to prevent the intrusion of the other submarines to the coastline of the country. This requires the development of antisubmarine capabilities to prevent the intrusion of the other submarines. These antisubmarine methods boosted the Indian Navy to exercise the sea control.

Antisubmarine methods are introduced to detect the intruder and enemy submarines. Early sonar systems were used to detect, classify, and tracking the target submarine. A submarine can effectively hide from the sonar and by its direction the submarine can deviate the reflected wave away from the receiver. This scenario can be excluded by deploying a system which has an array of acoustic sensors that can detect the reflected signal and determine and track the position of the target [4]. However, tracking the position of target is challenging due to the difficulty in the data acquisition under water.

In this paper, an effective method is proposed which can detect and locate the submarine using an array of acoustic sensors. The proposed method is evaluated and compared with other existing methods. The Sect. 2 describes the related work in the research area and Sect. 3 presents the challenges faced during data acquisition under water. In Sect. 4, the approach to the design is discussed and Sect. 5 presents the system and protocol design.

2 Related Works

Antisubmarine technology was performed earlier with several concepts like Optical detection [5], Radio intercept [6], Radar [7], sonar [8] and other nonacoustic methods. Many of these developments have been used by the naval operation. The Navy has named this as the Cat and Mouse game between submarine and surface combatants. Antisubmarine warfare is a branch of navy for the submarine detection [8].

Underwater echo detection method was first developed by the American, British, French scientist in order to detect the submarines during the First World War. But these systems worked only at high frequencies and have a small detection range. Hence advanced technology has been developed. Military and industry made profit on these developments [4].

In [9], Barr et al. proposes an auction algorithm to deploy sensors by providing optimal coverage. A three-dimensional barrier is constructed using magnetic or acoustic mobile sensors to form the barrier. According to the proposed algorithm when the number of sensors in the network increases, the computational time of the network and delay of the network also increases due to the increase of back off timer value.

Peng et al. proposed a scheme which uses the node's proximity to overhear the other transmission, in order to increase the packet delivery by selectively cloning

the packet. In the paper, they describe about the various challenges faced in the design of the network and protocols. The presented data delivery scheme uses cloning packet to have a high-packet delivery ratio, but using these clones the energy and cost of the system will increase and the chances of collisions are also increasing [10].

3 Challenges in Underwater Communication

Underwater sensors will provide real-time data, but they faces a number of challenges such as floating node mobility, large propagation delay, low communication bandwidth, high error probability, and limited battery capacity and the sensors themselves are prone to corrosion [2].

The terrestrial network has low-cost nodes and they can utilize the solar energy in order to recharge the nodes and have a dense multihop network. There are significant difference between the terrestrial network and the underwater sensor network. In terrestrial application, most of the nodes will be static but the nodes in the underwater network will be mobile due to the water movements. It is a great challenge for the design of an underwater sensor network and the cost for constructing the underwater network is very high comparable to the terrestrial network. The deployment of the underwater network and its maintenance is also a huge challenge.

RF communication and optical communication is not possible for the underwater network. RF signal experience attenuation due to the salt water and optical waves may not be selected because they suffer scattering and need large precision to point to the target [2]. When low-frequency waves are used, it may lead to high transmission power. When comparing with terrestrial wireless sensor networks, the underwater WSN will be less dense and more costly. The underwater network deployment cost is high, since it has to ensure the reliability of the network communication through water, rock, and sand. The battery power is limited and hence energy usage can be conserved by implementing network data aggregation and multihop optimal routing. Underwater environment is mobile and localization of the sensors is very challenging. There are many factors which affect the spatial distribution of the sensor nodes such as depth, salinity, current, temperature, and pressure.

Acoustic communication will have so many challenges like, signal fading, propagation delay and low bandwidth, high channel error, and sensor node mobility (most terrestrial sensor will be stationary). Battery power is limited and solar energy cannot be exploited. Underwater sensor is exposed to more failure like corrosion and fouling.

4 Design of Underwater Wireless Sensor Network

In this paper, an interesting application has been taken for the deployment of underwater sensor network. The application scenario focuses on the military target tracking system for submarine detection. In earlier days, sonar system was used for the detection of the submarine but it is observed that modern submarines are built with rubber antisonar protection tiles which help the submarine to be undetected by the sonar system. They have the capability to prevent the active probing and reduce the submarine noise, thus avoids the passive listening.

When a source continuously emits probing signal, the reflected signal from the submarine can be used to detect the submarines which are below the periscope depth. The probing signal will be acoustic signal having frequency between 10 Hz and 1 kHz [2]. The receiver in a particular location can only detect the presence of the target, if and only if the reflected signal traverses toward the location of receiver. Thus the submarine can hide from the system. To avoid this situation, the target position is determined using the large distribution of the sensor network.

The detection system uses a passive method for the detection of submarine where the propellant sound and flow sounds are used for the detection method. The position of the target is uncertain and the reflected wave direction is also unpredictable. Hence a network of sensors (receivers) will be deployed and a small part of sensor field will be strobed by the acoustic signals from the submarine. The sensor network may be connected as ad hoc [11].

The underwater sensor nodes will detect the propeller noise and flow sound from the submarine. The flow noise is around 350 Hz and the propeller harmonics are in range of 500 Hz [1]. Sensor nodes are capable of signal processing and communication. It will estimate the direction of arrival (DOA) and time of arrival (TOA) of the signals from the submarine. DOA will be estimated and using that the receiver determines the direction and location of the target and report the detection. The sensor nodes collect and process the information then transmit to the base station. Base station helps interference with user and web.

4.1 Sensor Subsystem

Sensing subsystem consist of sensors to monitor submarine presence, data acquisition device, etc. One of the requirements for detection of foreign submarines is to capture the sound under the water. The sensor network should be capable to detect the propeller noise and flow noise of the submarine. With help of the signal processing unit, the sensor should be able to calculate the DOA and TOA. Using this information, it is able to find the location and direction of movement of submarine. This can be achieved through hydrophones.

Hydrophones are basically piezoelectric material or magnetostatic material. In the case of piezoelectric material produce a voltage output according to the input

pressure. When the sound wave propagates causing compression and dilation, which causes the pressure variation, the hydrophone will produce an electric potential.

Selection of Sensors The sensor network should be capable to detect the propeller noise and flow noise of the submarine. With help of the signal processing unit, the sensor should be able to calculate the DOA and TOA. Using this information, it is able to find the location and direction of movement of submarine. The main requirement of the application is to capture the sound waves; hence, hydrophones are used as the sensors in the network. Hydrophones are piezoelectric material which can detect the sound waves underwater and can produce a voltage output corresponding to it.

For the selection of the sensor, several hydrophones have been compared for different parameters. Hydrophone TC4013 is a hydrophone which works in a frequency range of about 1 Hz–170 kHz. It can work up to a depth of about 700 m. WHS 3000 series is a hydrophone works in the frequency range of 416.7 kHz. RESON is another hydrophone having sensitivity about -170 dB and operates about a depth of 900 m. Its operating frequency is about 5–120 kHz and cost about 17.887 DKK. Aquarian H2a is a hydrophone, which operates in 10–100 Hz frequency range, and has a sensitivity of about -180 dB. It operates at a depth which is less than 80 m [7].

Dolphin Ear is another hydrophone that works in the frequency range of 7 Hz–22 kHz. JS-B100-C4DS-PA is a hydrophone operating between 50 Hz and 100 kHz and have a sensitivity about -180 dB. The cheap and reliable sensor is preferred in the application. The cheaper sensor is the Aquarian H2a. By comparing all characteristics, it is better option to have Aquarian H2a as the sensor for the application. The sensor input is fed to the Analog to Digital Converter. The analog to digital converter converts the analog signal sensed by the sensor to digital signal by quantization methods. The discretization level is decided based on the value of frequency and processing storage.

The minimum bit resolution required for capturing the sensor data from Aquarian H2A is 16 bit. The ADC provides a 16 bit resolution, 4 acquisition channel, and simultaneous sampling. The input bias current of NI WLS 9125 is 10 nA.

4.2 Processing Subsystem

Processing subsystem mainly consists of ROM (nonvolatile), RAM, internal clock, and other device. The selection of the processing subsystem is performing based on the cost, flexibility, energy consumption, efficiency, and performance. Several processors are available on the market. The processors available in the market are listed are compared.

Microcontroller is a single integrated circuit with high-speed bus, memory unit. It uses high-level programming which in turn increases the programming speed and helps in debugging. But microcontrollers are not much powerful; for example, Atmel AVR 8, Atmel AVR 32, AVR UC3, and AVR XMEGA. Digital signal processor chips are special purpose processors which can perform mathematical operations. The DSP chips are complex hardware. Complex hardware increases the cost of the device; moreover devices used for underwater is already expensive. When complex operations are to be involved, the overhead of the whole system increases. Hence, it cannot be used for underwater application scenario; for example, ARM Cortex-A8, OMAP3, and C6000.

According to features of sensor, that sensor platform will use a microcontroller-based processor. Since it is program flexible, small sized, low cost, low power consumption, and CPU core ranges from 4 to 32 bit. All these features supports for underwater application scenario. Hence Microcontroller is used as the processor for the system. For the evaluation of the processor, three microcontrollers were compared which include ATMEGA48, ARM920T, and MSP430 against their various characteristics. From the comparison of the microcontroller-based processor, ARM920T is chosen.

ARM920T can support 32-bit architecture also 8- and 16-bit architecture and provides advantages of RISC and functionality of CISC. It uses 3.7 V rechargeable 720 mAh lithium-ion battery. They have low power consumption about 30.4 mA on VDDCORE, 3.1 mA in standby mode. It have 200 MIPS at 180 MHz, 16 KB cache, 16 Kbyte SRAM, 2 on-chip oscillator with two PLL, 20 channel peripheral data controller, and 7 external interrupt source and 1 fast interrupt source. The hydrophones need a preprocessing hence the microcontroller ARM920T provides the sufficient processing and provides necessary characteristics which is suitable for the application scenario.

4.3 Communication Subsystem

The data transfer between the sensor nodes is critical for reliability and efficiency of the wireless sensor network. The communication can be possible through different ways; one is through the serial buses and other through the parallel buses. When parallel buses are used it affects the size of node but when comparing with serial buses, parallel buses are faster than them.

The wireless sensor implementation can be done using the several technologies such as Bluetooth, Zig-Bee, Wi-Fi, etc. The transmission medium for the underwater communication channel can be sound for acoustic channel, electromagnetic waves for radio communication, optical communication, and magnetic anomaly detection. The electromagnetic wave can travel faster than acoustic waves but they are highly attenuated in salt water. They can transmit at low frequency about 30–300 Hz. In case of optical communication, they have high data rate, but affected

by absorption and scattering by salt water. Hence, they are not suitable for the underwater communication.

The submerged submarine can be detected using the magnetic anomaly detection. The presence of the submarine in the underwater disturbs the magnetic lines of force of the earth. When a submarine heads the magnetic field of the earth get changed and cause an induced field. But the magnetic field gets reduced substantially using the degaussing coils.

The acoustic channel offers a better performance than other methods. But the design of the acoustic channel in under water is challenging due to its large propagation delay, limited bandwidth, high bit error rate, and temporary loss of connectivity. Underwater channel experience impairment is due to multipath and fading. This absorption, fading, and multipath will cause the limitation for the acoustic channel bandwidth. Since the bandwidth is limited, its data rate also reduces. It is found that the acoustic channel provides a data rate up to 10 kbps which is greater than the data rate offered by the optical communication and RF.

4.4 Power Subsystem

The lifespan of the wireless sensor network mainly depends on the battery used to power up. The main requirement is that it should work at least for 6 months without the human interference. The power management should be done automatically, when there is no work to process or does it should automatically switch to the power saving mode.

Processor The Processor ARM9 generally provides three power modes of operation. In active mode (Run), the power drawn by the sensor platform is in the range of 70–120 mA and in idle the processor shut off the power to the radio and clock. Power consumption is about 24 mA. In sleep mode, the processor will consume less power. During deep sleep, the processor clock is stopped and restarts when interrupts occur, but this mode consumes more power. In this mode, the power consumption is about 32 μA [7]. ARM9200T have peripherals operate in the range of 1.65–1.95 V and external bus interface I/O uses 1.65–3.6 V. Current consumption is about 7.98×10^{-3} MA. Hence the total power from the processor is 0.13167 m W.

CC2420 Chipcon ZigBee RF transceiver Transceiver uses about 2.1–3.6 V with integrated voltage regulator and current consumption is about 18.8 MA. The power consumption is about 39.48 m W.

Sensor Aquarian H2A hydrophone Sensitivity of -180 dB 1 V/ μ Pa and power is about 0.3 m. The ADC ADT7411 uses a voltage in the range of 2.7–5.5 V and the current is about 10 μA .

The power management can be performed using a voltage limiter or a potential divider to provide sufficient voltage for processor, transceiver, and sensor part.

4.5 Operating System

The operating system is an important factor in wireless sensor network. It provides an interface for hardware and software and bridge. The main criterion for choosing an OS for underwater application is that it should withstand with the challenging underwater environment. In underwater, environmental data acquisition and processing are complicated. Some of the algorithm used may be complex, time consuming, and expensive energy. Hence, while choosing an OS for the submarine detection we have to consider all these.

Study of Operating System This section discusses and compares the features of different OS in the market. There are so many OS used for wireless sensor network. They include:

TinyOS is a single-threaded operating system. It uses an event-driven mechanism. The main characteristics of the TinyOS are that it consumes lower power and the resources (memory) used is less. Non-preemptive event-driven mechanism of the OS is not suitable for submarine detection for the application is real time. While performing an experiment to find the performance of sensor mote with TinyOS, it shows that the energy consumption and execution time is much higher.

MANTIS is a multithreaded operating system which needs only a small footprint for memory and is less 500 bytes. It provides multitasking and virtual memory management. MANTIS cannot be used for underwater sensor network because it does not consider the special characteristics of the underwater environment and diverse characteristic of the underwater environment. The underwater sensor network involves a set of distributed sensors for monitoring and collecting data and has an acoustic modem for communication. It is difficult to handle all these hardware components and it causes a challenge for the operating system. Hence it cannot be used for underwater sensor network. Contiki OS is network-embedded OS and can support IP communication IPV4 and IPV6. It is not suited for underwater environment, because it does not consider the characteristics of the underwater environment. Underwater environments are harsh and both hardware and software are prone to errors. The most important factor is that it does not provide dynamic power management to control and save the limited energy supplied for the underwater sensor nodes.

Operating System Requirement An operating system for submarine detection should be robust, energy efficient, fully utilize the available resource, highly customizable, tackle to the harsh environment, work efficiently in the underwater environment, reconfigurable, and handle failures in hardware and software components.

Haining Mo, Son Le and coworkers, University of Connecticut has developed an operating system Aqua OS, which provides all features and requirements mentioned above. Aqua OS provides robustness by handling both failures in hardware and software and malicious user attack [12]. The main feature of Aqua OS is that it has a system status updating component and emergency handling component. Updating

component will be running periodically. The emergency handling component can handle the exception that can arise due to failures. Aqua OS is highly customizable and reconfigurable before and after installment, respectively. The OS provides dynamic power management and hence provide energy efficiency. In underwater application as submarine detection, the network traffic can be reduced by performing preprocessing the collected data before sending it. This can accomplish by Aqua OS. It can be event-based or preemptive scheduler.

5 Coverage and Connectivity

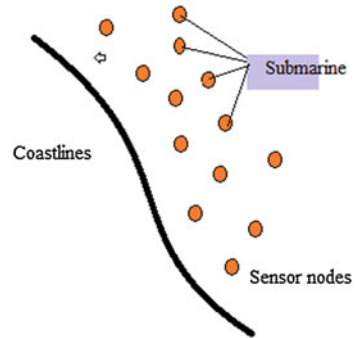
Types of Deployment The deployment for underwater application can be done in two ways, randomly deploying the sensor on ocean surface which is scattered from the airplane, and next is that sensors can be accurately placed when it is released from a vessel. The deployment is chosen to be two linear arrays of acoustic sensor because the position of the submarine cannot be predicted. But in under water, the nodes deployed will be mobile due to movement of water, aquatic animals, etc. Hence, even though the deployment is deterministic it will be dispersed due to the mobility of the water. When the deployed nodes become random due to the mobility, it is important that the deployed nodes should communicate with each other to decide their position and identify their neighbors and the gateway node. So that communication should be reliable and efficient.

Types of Coverage The coverage of sensors can be classified as point coverage, area coverage, barrier coverage. In area coverage, an area is monitored using the sensor network. In point coverage, a set of points is covered by the sensor network and monitored. Barrier coverage considers reducing the probability of a target to be undetected through the barrier.

Sensing range and Coverage Degree In submarine detection, the submarine should be detected by any of the sensor which is in barrier coverage. So the sensor placement should be such that submarine should be detected by at least one active sensor node and report it to the base station. Hence the deployed sensors which are three barriers covered, in order to detect the submarine at least two node should be active to detect the submarine and report to base station. While considering the power consumption, it is difficult to have two sensors to be active at same time.

Transmission range and Connectivity Degree The network uses a distributed architecture in order to detect the submarine detection. The topology for the application uses a hybrid of tree topology and cluster-based approach in which, at each round a cluster head is selected and each leaf node report to the cluster head nearer to it. The cluster head will collect the data from its leaf node and perform the data aggregations and forward the data toward the next nearest cluster head. Through the multihop communication, each cluster head forward the data toward the base station (Fig. 1).

Fig. 1 System architecture of the sensor network



The distributed sensors forms a cluster and each cluster will have a cluster head. Each cluster head will collect the data from each node in its cluster and it forwards the data toward the base station. Each time the cluster head is changed and they are chosen dynamically. Main advantages include: it can communicate in a hierarchal manner, large coverage area, and uses only less power.

6 Design of MAC Protocol

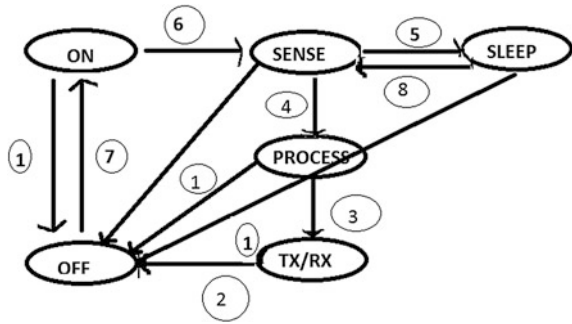
The scenario taken into account has a barrier of several 10 km. In order to provide integrated coverage and connectivity considers sensors within 10 km. One node can communicate with adjust node surrounded by a radius greater than two times the sensing range R_s .

Total area monitored by 80 m sensor node is $10 \text{ km} \times 0.08 \text{ km}$. The sensing range is 80 m, then 1 km needs about 26 sensors. Since $R_c > 2R_s$ the sensors remain connected, even if sensors are separated by a distance greater or equal to $2R_s$ [11]. 26 sensors for 1 km hence 10 km needs about 260 or more sensors. 260 sensor nodes are randomly deployed on the $10 \times 0.08 \text{ km}^2$. The expected transmission range is 90 m. The available bandwidth of acoustic channel is less than 15 kHz.

6.1 State Transition Diagram

The main consideration of design is to have energy-efficient system so that the power will last. In order to have power saving, during sleep period, the energy is saved and there should be at least one node to be active at a time. During ON period, the communication between the nodes will happen. During POWER ON period, power subsystem is active and during SENSING period, power and sensing subsystem is active. In TRANSMIT period, power and communication subsystem

Fig. 2 State transition diagram



is active and in RECEIVE period, power and communication subsystem is active. During SLEEP period, power subsystem is only active and during POWER OFF period, all the subsystem will be inactive (Fig. 2).

6.2 Cyclic MAC Protocol

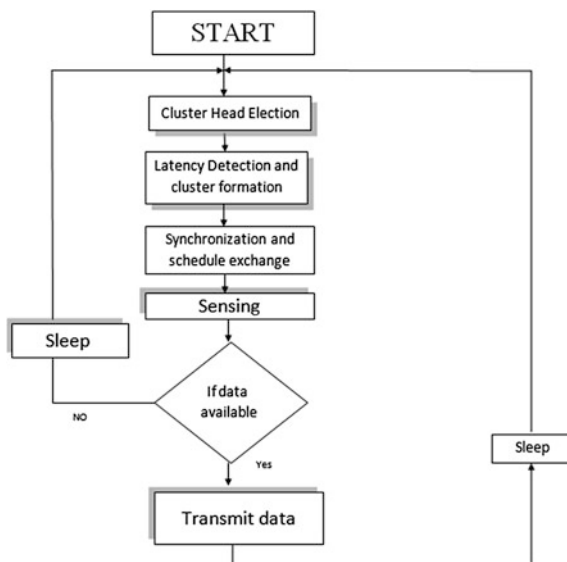
In general, MAC protocol is divided as contention-based protocol and contention free protocol. In contention-free protocol, includes TDMA, FDMA and CDMA. In TDMA, channels are separated based on the time slots. Since the bandwidth is limited, FDMA is not suited for the underwater application. The near far problem makes CDMA not suited for this application. Contention-based protocol includes random access and collision avoidance method. In random access, the collision will be higher but in collision avoidance, such as RTS/CTS mechanism, the energy consumption will be higher.

The proposed cyclic MAC protocol reduces the wastage of energy by avoiding overhearing and making listening and sleep modes to be periodically.

Initially, each node assumes a random number and compares with a threshold value. The threshold value is selected based on the energy of the node. After the initial round, each cluster head of the previous round will select the cluster head of the next round. Each cluster head upon selection will send beacons with its timestamp. When the child node receives the beacon, each node compare its local time with the timestamp on the beacon and find which cluster node is closer and sends a joining request to that node with its battery level. Each cluster uses a set of frequency in bandwidth of 150 kHz. A frequency among the set is used by each node for the transmission to its cluster head. The same set of frequency is reused by another cluster. Each cluster is considered as a cell called as a femtocell. But adjacent nodes in different femtocell will use different frequency to avoid interference.

Next phase is the periodic operation phase in which each node reserves the channel whenever it wants to transmit a data. These are done using reservation and acknowledgment packets. A node send reservation packet when it have a data to

Fig. 3 Cyclic MAC protocol



send, to its cluster head. If the cluster head is not busy, it will send the Acknowledgement packet which notifies its neighbor about the reserved slot. After that the data is exchanged. The control packet used will be much smaller than the data packet. Hence the overhead is lesser (Fig. 3).

The cyclic MAC guarantees data delivery without collision and solves the exposed terminal problem. The complexity in the system is that it considers more control packet. The overhead of the packet is much higher, it has to be avoided using coding technique. For N node network, there will be complexity of about $O(N)$.

When certain number of nodes die, the network becomes useless hence we need redeploy of the sensors; suppose we have N sensors which died due to lack of energy then redeployment of N nodes will not help because the nodes will not be redeployed at the same place where the previous node was. Hence inorder to have connectivity between the nodes, the number of nodes redeployed should be greater than N .

6.3 Hybrid Protocol

The proposed protocol uses the concept of distributed cluster-based routing and localization protocol.

In this application, each node in a cluster have to communicate with the cluster head of that cluster and each cluster head have to communicate with other cluster head to transfer the data toward the gateway node. The cluster head has to handle

the data aggregation and the communication with the base station. Since the network contains a hierarchal topology and grouping of nodes into cluster, it uses a hierarchal routing protocol. This concept is used for distributed underwater clustering scheme.

In this each node sends the data collected to its responsible cluster head using single hop and each cluster head perform the data aggregation and communicate with the base station using multihop network. The cluster head is not fixed; it is selected based on the remaining energy in the node. The propagation delay is a major drawback for the underwater sensor network can be avoided by advancing the transmission relative to the reception. The timing advance is calculated by each cluster head for the each node of its own cluster.

The application uses a location-based routing protocol in which the node will checks its route cache whenever it has a data to send. If the node has no route toward that destination, it will find the route to its destination using a control packet which incorporates its own position and a threshold distance to have energy-efficient communication, node ID, and the destination node. When a node receives this packet, it computes its own position with respect to the packet arrived and position of the sender. If the received node is within the specified range, it will forward the packet (within a hop count) and incorporates its own position. Each intermediate node will record the position of nodes mentioned in the packet and forwarder of the packet. When the packet is received by the intended destination, the received node can contact with the sender based on the position of the forwarders of that packet. Thus the whole network will learn the position of other nodes.

Any node can contact to every node whenever they want. Each node sends a Hello packet periodically to find its neighbors and they store the list of neighbor nodes. Whenever a node find that its neighbor node absence, it will initiate the route discovery. Since the control packet used for the route discovery is much less, the overhead is also reduced. Each node learns its own position based on the anchor nodes.

Features of the protocol are self-organizing protocol, integrates the localization, reactive routing protocol, it is robust and scalable. The route discovery is done with less number of nodes and can achieve very high-packet delivery ratio. It has randomized rotation of the cluster head. In this protocol, the cluster head estimates the timing delay using GPS at each node and eliminates by timing advances. The routing overhead is minimum and can handle dynamic network.

7 Conclusion

The paper focuses on the various challenging aspect of both underwater communications and the detection of the submarine. The main design issues of the underwater sensor network were the effectiveness of the sensor network, reliable

communication, maximization of the lifetime of the network, and reduced delay for the detection system.

In this paper, an effective method for the tracking of the submarine has been proposed. The proposed system considers a suitable MAC protocol, routing protocol, for the system. The proposed protocols were compared with the existing protocols and evaluated.

Acknowledgments We would like to express our sincere gratitude to Prof. K.A. Unnikrishna Menon for the time he dedicated to help us solving doubts at various stages of this research. We also take this opportunity to thank Dr. Maneesha V. Ramesh for her support in completing this paper. We would also like to express our gratitude for the immeasurable motivation and guidance provided by Sri. (Dr.) Mata Amritanandamayi Devi (AMMA), Chancellor of Amrita University.

References

1. Barr S, Liu B, Wang J. Barrier coverage for underwater sensor networks. IEEE military communications conference. MILCOM; 2008. p. 1–7. doi:[10.1109/MILCOM.2008.4753077](https://doi.org/10.1109/MILCOM.2008.4753077).
2. Heidemann J, Ye W, Wills J, Syed A, Li Y. Research challenges and applications for underwater sensor networking. IEEE Wireless Commun Netw Conf (WCNC). 2006;1:228–235. doi:[10.1109/WCNC.2006.1683469](https://doi.org/10.1109/WCNC.2006.1683469).
3. Ambadiyil S, Mahadevan Pillai VP, Praveen V, Jayan KG, Sudheer SK: Holographic registration plates with GPRS (HRPG) network for sea-going vessels to augment the coastal security. International conference on ultra modern telecommunications & workshops, ICUMT '09; 2009. p. 1–4.
4. Been R, Hughes DT, Potter JR, Strode C. Cooperative anti-submarine warfare at NURC moving towards a net-centric capability. IEEE OCEANS. 2010;1–10. (Sydney). doi:[10.1109/OCEANSSYD.2010.5603637](https://doi.org/10.1109/OCEANSSYD.2010.5603637).
5. El Kouche A, Hassanein HS, Obaia K. WSN platform plug-and-play (PnP) customization. IEEE ninth international conference on intelligent sensors, sensor networks and information processing (ISSNIP); 2014. p. 1–6. doi:[10.1109/ISSNIP.2014.6827642](https://doi.org/10.1109/ISSNIP.2014.6827642).
6. Zhou Z, Cui J-H, Zhou S. Efficient localization for large-scale underwater sensor networks. Ad Hoc Netw. 2010;8(3):267–279. doi:[10.1016/j.adhoc.2009.08.005](https://doi.org/10.1016/j.adhoc.2009.08.005) <http://dx.doi.org/10.1016/j.adhoc.2009.08.005>.
7. Forney C, Manii E, Farris M, Moline MA, Lowe CG, Clark CM. Tracking of a tagged leopard shark with an AUV: sensor calibration and state estimation. IEEE international conference on robotics and automation (ICRA); 2012. p. 5315–21. doi:[10.1109/ICRA.2012.6224991](https://doi.org/10.1109/ICRA.2012.6224991).
8. Encarnacao LM, Barton RJ, III, Zeltzer D. Interactive exploration of the underwater sonar space. OCEANS, 2001. MTS/IEEE Conf Exhib. 2001;3:1945–1952. doi:[10.1109/OCEANS.2001.968144](https://doi.org/10.1109/OCEANS.2001.968144).
9. Manjula RB, Manvi SS. Coverage optimization based sensor deployment by using PSO for anti-submarine detection in UWASNs. Ocean electronics (SYMPOL); 2013. p. 15–22. doi:[10.1109/SYMPOL.2013.6701906](https://doi.org/10.1109/SYMPOL.2013.6701906).
10. Sun P, Seah WK-G, Lee PWQ. Efficient data delivery with packet cloning for underwater sensor networks. Symposium on underwater technology and workshop on scientific use of submarine cables and related technologies; 2007. p. 34–41. doi:[10.1109/UT.2007.370944](https://doi.org/10.1109/UT.2007.370944).

11. Wang X, Xing G, Zhang Y, Lu C, Pless R, Gill C. Integrated coverage and connectivity configuration in wireless sensor networks. In Proceedings of the 1st international conference on embedded networked sensor systems (SenSys '03). ACM, New York, NY, USA; 2013. p. 28–9. doi:[10.1145/958491.958496](https://doi.org/10.1145/958491.958496) <http://doi.acm.org/10.1145/958491.958496>.
12. Hisamatsu T, Ogawa A, Sugiura K, Nakamura O, Murai J. Software compatibility and human interface for DV over IP. Proceedings of the 2003 symposium on applications and the internet workshops; 2003. p. 188–91. doi:[10.1109/SAINTW.2003.1210153](https://doi.org/10.1109/SAINTW.2003.1210153).

Underground Tunnel Detection Across Border Areas

K.V. Nibi, K.A. Unnikrishna Menon and Preeja Pradeep

Abstract Tunnels are considered as the oldest method of passageway. Underground tunnels are popular from olden eras for connecting places, travelling, and aid for various surface threats. They are also used for illegal activities like smuggling of unlicensed drugs, weapons, currency, gold, explosives, and even human trafficking is being done through these tunnels. These immoral activities are concentrated in national border areas in order to escape from the border security measures. Hence the detection processes of such tunnels in the national security border areas are necessary in order to protect our homeland security systems. The geology plays an important role in the detection of the underground tunnel system procedures. There is no perfect system for the tunnel detection and localization and even today the tunnels revealed in coincidence. The basic principle to find the hollow space (tunnel) is, by sending an ultrasonic frequency signal into the ground, and study the reflected beam from the tunnel or the hollow space. By analyzing the reflected signal characteristics, preliminary detection of a tunnel/void is possible. Basic idea of the detection is to perform the range estimation algorithm (REA) by pulse echo method. From these, we can estimate the depth of the tunnel. The characteristics of the signal at the soil-tunnel (air) reflection interface are to be investigated.

Keywords Cross correlation · Peak detection · Pulse echo method · Range estimation · Ultrasonic frequency

K.V. Nibi (✉) · K.A.U. Menon · P. Pradeep
Amrita Center for Wireless Networks and Applications, Amrita Vishwa Vidyapeetham,
Amritapuri, Kollam 690525, India
e-mail: nibikv@gmail.com

K.A.U. Menon
e-mail: kaumenon@amritapuri.amrita.edu

P. Pradeep
e-mail: preejapradeep@am.amrita.edu

1 Introduction

Underground tunnels are used as both offensive and defensive aid. Cross-border tunnels are used for terrorist activities and purposes like smuggling illegal materials such as drugs, firearms, etc., with the intention of avoiding border security force. It is a serious offense especially in national border areas. Weapons, currency, drugs, and gold are also transported through these tunnels. The security of a nation can be completely threatened by these actions. It is important to locate such tunnels for enforcement of law and maintaining national security. In olden days, the underground tunnel and mine detection was done by echo mechanisms, like using hammers for hitting the ground and by measuring the echo that reflect back, the underground tunnels and mines could be identified. Pulsed electromagnetic search system (PEMSS), ground penetration radar (GPR), seismic sensor technology, brillouin optical time reflectometry (BOTR) [1], and GPDR (Ground Penetration Radar and RF microwave tomography) [2] are some of the methods that were used to detect the tunnels. Some of them are destructive methods and others are non-destructive methods. The tunnel is actually a hollow space compared to the other materials around it. One of the principles to find the hollow space is, by sending a narrow ultrasonic beam of suitable frequency to the ground and study the reflected beam from the tunnel or the hollow space. By analyzing the reflected signal characteristics, detection of a tunnel or a void is possible.

2 Related Work

Electromagnetic wave gradiometer [3]: Electromagnetic waves are transmitted to the ground and the conducting property of the tunnel or any other material inside the tunnel that enhances the conductivity and produce secondary electromagnetic fields around the conductor. These secondary fields will be received by the gradiometer. The gradiometer is synchronized in such a way that low signal strength secondary signal can be easily received. A low-frequency electromagnetic signal is generated (around 100 Hz) in order to illuminate the area where the tunnel probably resides. The tunnels have more conductivity as compared to the surrounding medium due to conducting elements present in the tunnels. The transmitted EM wave will induce a current flow in conductors associated with the tunnel and develop a secondary electromagnetic field (EMF). The secondary emf can be observable from the tunnel. Compared to the illuminating signal, the secondary emf is so small in magnitude. This system is efficient since it can suppress the primary signal by 70 dB and enhance the secondary signal by the use of a synchronized receiver (BW = 1 Hz).

Pulsed-electromagnetic search system (PEMSS) [4]: It is a cross-hole ground probing radar instrument. In intrusive and complex metamorphic terrain regions,

PEMSS is used as the primary instrument for the search system for clandestine tunnels. The operating frequency is from 20 kHz to 100 MHz. In this method, boreholes are used to locate the tunnels. If the transmitting signals are 30–40 MHz range, and the distance between the tunnel and the borehole is 20 m, then the received signal strength exhibit maximum power. Basically, PEMSS is a tool for rock mass characterization. PEMSS is a destructive detection method. With the help of the boreholes drilled in linear spacing, we can characterize the geology and lithological and structural rock mass discontinuities. The antenna array will be kept in these boreholes and are capable of transmitting signals of 20–100 MHz range. The received signals are processed for velocity (arrival time), attenuation, and dispersion using wiggle-trace, tomography, and signature analysis techniques [5]. As in gradiometer, this system has electromagnetic signal sensitivity to conductive mineral assemblages and to hydrogeological conditions. Characteristics of certain features can be recognized by detailed examination of travel time, attenuation, and a measure of dispersion. Discrete ground features, on the order of 2 meters can be detected if holes are no more than approximately 20 m apart. Probability of detection is high for planar structures at greater transmitter–receiver separations. Both theoretical considerations and empirical evidences suggest that signal propagation range is limited by structural, mineralogical, and hydrogeological conditions in the rock mass. The more acute the angle between a tunnel and a borehole pair straddling its axis, the greater the magnitude and the prominence of the PEMSS arrival-time anomaly. Detecting and imaging the underground tunnels using seismic waves [6]: Seismic reflections and synthetic aperture time delay from back projection algorithm can create the 3D images of the buried tunnel. Radon transform for the tool for detecting curves in the images. The previous work was designed and development of data collection system for electromagnetic waves with cross-hole tomography and seismic waves. Data acquisition and signal generation accomplished at 32,000 points per seconds with four second chirp excitation signal of 100 samples and 8 kHz signals. Low SNR tunnels can locate using 2D and 3D radon transform. This paper is an experimental study for underground tunnel detection and imaging using seismic waves. The seismic reflections are converted to 3D images using synthetic aperture time delay back projection algorithm. Radon transform is applied to these reflections to localize the linear features of the tunnel. They studied the performance of the radon transform in various noise levels. Radon transformed back projected images can show the lines which cannot visually seen in the reflected images. Probability of detection is higher for longer lines as compared to shorter lines. Simulation results compare with the experimental result in order to measure the performance accuracy of the Radon transform. The relation between the probability of detection and SNR as a function of the line length is analyzed in this work. Furthermore, the line detection in the presence of the white Gaussian noise with zero mean and variance is also analyzed. In this [7], authors considered uncorrelated signal and noise. Ground-penetrating radar (GPR) and seismic sensors are used in multimodal detection of subsurface targets. Seismic sensors were tested

in bistatic configuration and the GPR are expanded to multistatic configuration to provide improved performance. These two systems will measure entirely different properties that are GPR electrical property and seismic system mechanical properties.

3 System Architecture

The architecture for the underground tunnel detection using nondestructive method includes the ultrasonic transceivers and range estimation algorithm (REA). The proposed architecture of the underground tunnel detection system consists of one transmitter for transmitting the ultrasonic frequency pulse and one receiver for receiving the reflected signal from the target. The system mainly uses the two ultrasonic sensors which can produce a frequency from 1 to 60 kHz. The system architecture, Fig. 1, shows the placement of transmitter and receiver to estimate the velocity of ultrasonic signal and calculate the depth of the tunnel.

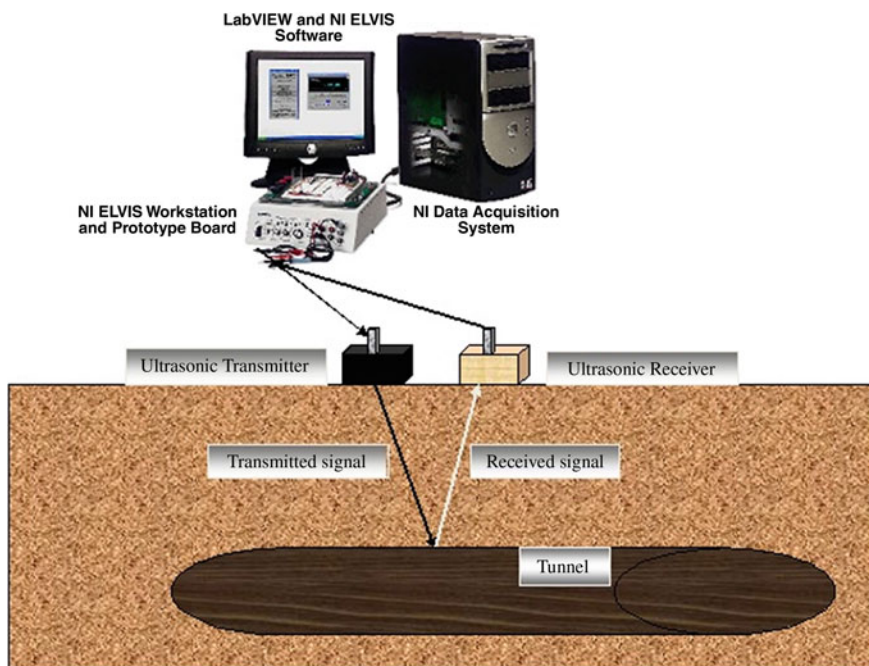


Fig. 1 System architecture

3.1 Ultrasonic Sensors

Ultrasonic sensors are mainly used for generating and receiving sound waves. They are either made of piezoelectric material or magnetostrictive material. Piezoelectric materials have the property of generating and gathering voltage output according to the variations in the input pressure. Transmitter will convert the electrical signal to an ultrasonic sound signal and the receiver will convert the ultrasonic signal to an electrical signal. Parameters for the sensor selection are linear frequency range, sensitivity, directivity, and change in the sensitivity with the temperature, etc. The frequency range shows the range in which the sensors work. The directivity implies whether the sensor is omnidirectional or not. Cost and ease of use are the other parameters for sensor selection criteria [8].

3.2 Principle of Operation

In ultrasonic testing (UT), high-frequency ultrasound energy will be used for detection. Typical pulse/echo principle will use for general inspection purposes. An ultrasonic testing and inspection system consists of different functional units, such as the transmitter/receiver, display devices, and processor. The transducer generates high-frequency ultrasonic energy which propagates through the materials in the form of waves and their wave motion is due to compression and rarefaction. When there is a void (discontinuity) in the wave path, part of the energy will get reflected back from the void surface. The receiving transducer will convert received reflected signal into an electrical signal. From the travelling time of the signal, the distance traveled by the signal can be estimated. From the analysis of received signal, information about the reflector location, size of the reflector, orientation, and other features can easily be achieved [9]. Figure 2 Block diagram describes the steps of the tunnel detection process.

$$D = v_s * t/2 \quad (1)$$

D : Distance from the ground to tunnel

v_s : Velocity of the ultrasonic sound in the soil

t : Round trip time.

4 LabVIEW Implementation

The system mainly consists of three sections, i.e., signal generation section, signal acquisition section, range estimation algorithm (Time delay estimation) section. The first section includes creating the input signals with the accurate frequency

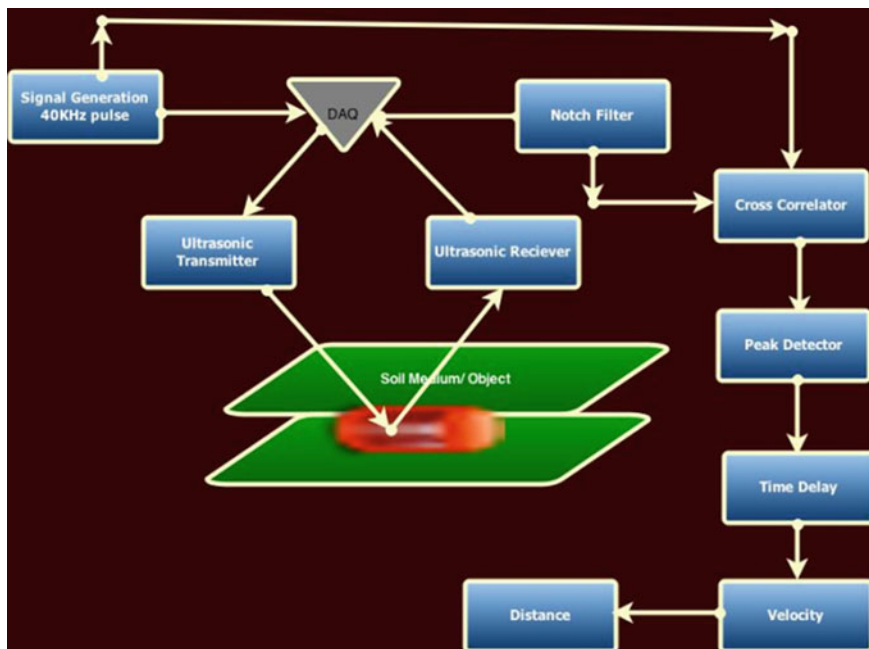


Fig. 2 Block diagram

(40 kHz) amplitude and pulse width. This signal should be capable of penetrating through the soil up to 20 m. The second section involves the acquisition of the ultrasonic signals received by the reflection from the object (tunnel). The third section involves the cross-correlation of the input and output signal of the ultrasonic transmitter and receiver. Cross-correlation is used to estimate the time delay between the signals.

LabVIEW signal express was used for data collection and recording. It is an interactive logging, software for acquiring, analyzing, and presenting data from various acquisition devices.

4.1 Frequency Selection

First step is to identify the optimum frequency. Ultrasonic frequency range is between 20 kHz and 200 MHz. As the frequency increases, the resolution increases but penetration power decreases. At low frequencies, the resolution decreases but penetration power increases. So low frequencies can cover large distances than high frequencies. Frequency selection is medium dependent, here medium is homogeneous soil.

4.2 System Overview Software

LabVIEW is using the programming language *G* which is a data flow programming language. LabVIEW signal express was used for data collection and recording. It is an interactive logging, software for acquiring, analyzing, and presenting data from various acquisition devices. It is virtual instrumentation application software. It can create user-defined system software instrumentation systems [10]. NI ELVIS uses LabVIEW and NI data acquisition hardware creates a virtual instrumentation system.

4.3 Signal Generation Block

Signal generation part consists of DAQ Assistant Express VI which creates edits and runs tasks using NI-DAQmx. Data contains the samples to write the task, number of samples specifies the number of samples to generate for the finite task. We have to generate a 40 kHz pulse in order to drive the ultrasonic sensor. In order to create this, pulse signal is multiplied by the sine wave. Here normalization of the signal obtained. This 40 kHz 50,000 sample sine pulses will be fed to the ultrasonic transmitter through the NI Elvis DAQ block. Figure 3 shows the input generations

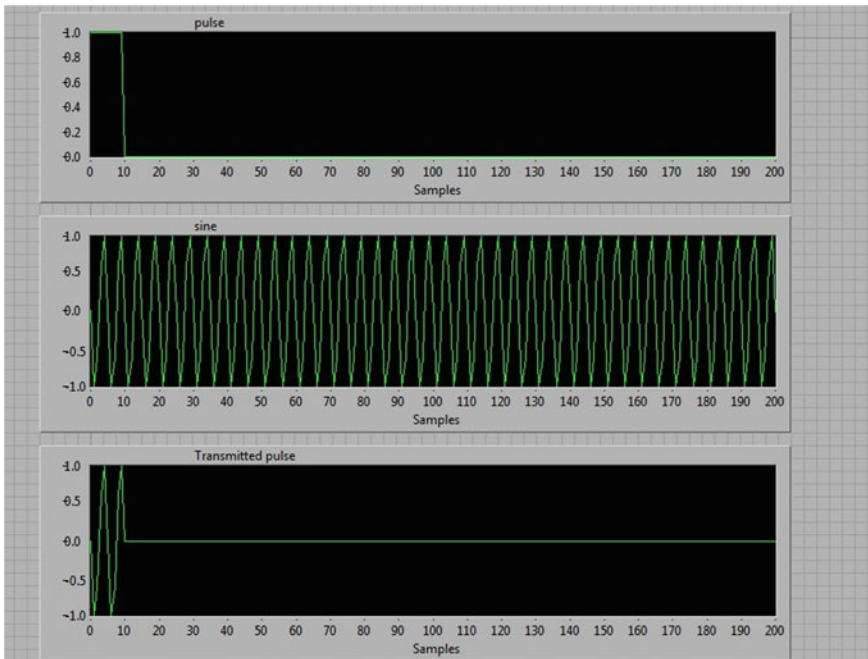


Fig. 3 Generated input

block output which consists of a signal pulse which acts as a window for the continuous sine waves.

The signal generation is an important part of UT or any other measurement system. When the real-world signals are not available to simulate the test algorithm, two applications examples are used. For example, DAQ device is unavailable for obtaining real-world signals or when it is not possible to access to real-world signals then generate signals to apply to a digital-to-analog (D/A) converter.

Frequency Normalization: In the analog systems, the unit of signal frequency is hertz (Hz), or cycles per second. A digital system uses digital frequency and is the ratio of the modulating frequency and the sampling frequency. It is also known as the normalized frequency and its unit in cycles per sample. The normalized frequency ranges from zero to one which equivalent to analog frequency range of zero to the sampling frequency f_s .

4.4 Signal Acquisition Block

The ultrasonic receiver receives the reflected signal and applied it to the LabVIEW system. The reflected signal is the delayed version of the transmitted signal. It also has the attenuation in its amplitude. There will be multiple echoes means signals with time delay and amplitude reductions are also present. The signal path contains the other noise signals too. In all these noise, the DC content or power-line interference is the predominant one. So in order to avoid the noise, we will use the notch filter with cutoff frequencies 40 and 60 Hz. Figure 4 shows the received signal and the filtered signal.

Notch filters are band stop filters and the main function of the notch filter is to eliminate the power line interferences and noise signals. Digital notch filters can be designed in both infinite impulse response (IIR) and finite impulse response (FIR) structures. As compared to the FIR filters, IIR filters have the advantage that for a given set of specifications, at lower order itself it gets an efficient approximation. The disadvantages of the IIR filters are they potentially unstable and do not provide linear phase characteristics. But FIR filters are unconditionally stable and can be designed for linear phase characteristics.

4.5 Time Delay Estimation

For time delay estimation [11] the range estimation algorithm is used. TDE has significant practical importance in many fields like radar, sonar, seismology, ultrasonic, etc. It is the first stage for identifying, localizing, and tracking radiating sources or reflecting targets.

Cross-correlation: The transmitted signal and the received signal output from the sensor are correlated with each other. After correlating the two signals, the



Fig. 4 Received output

correlation peak is detected using the peak detector. The time axis of the peak in correlation corresponds to the time delay. In this case, 500,000 samples are taken at a time to correlate.

So the correlation output has 1,000,000 values. If any delay is present between the correlated signals, then the peak will deviate from the 49,999th position by the value equivalent to that delay.

Cross-correlation is the tool for determining the time delay between two signals. The signals are correlated positively then the maximum value will obtain or if correlated negatively then correlated then will get the minimum values. The significance of the cross-correlation is that it gives point of time at signals aligned perfectly. Argument of maximum of the cross-correlation will give the time delay between two signals.

$$TimeDelay = argmax((f * g(t))) \tag{2}$$

The correlation technique presented offers a good possibility for measuring the distance between the ground and the tunnel by the time delay between two signals. Cross-correlation gives equivalent of power spectral density. Hence cross-correlation a well-suited tool for analyzing time invariant systems, where spurious signals or noise interfere with the output measured signal.

- R_T : Transmitted signal = $A(t)$
- R_X : Received signal = $B(t + \tau)$
- $R_{IX}(\tau)$: Cross-correlated signal

$$R_{ix}(\tau) = \int_{-\infty}^{\infty} A(t)B(t+\tau) \quad (3)$$

5 Testing and Analysis

Compare the results from simulated scenario to the DAQ acquisition method. Ultrasonic velocity in soil is varying according to the frequency. An ultrasonic wave has lowest speed in gaseous medium, moderate speed in liquid medium, and highest in solid medium. Hence in soil medium, it has high frequency. Table 1 shows the experimental results of velocity of ultrasonic sound in air and wood. The velocity of ultrasonic signal in one medium depends on the density of the material. The main soil parameters affecting the speed of propagation is the density, impedance, water content, transducer impedance matching, etc. Transmission of waves in a material is models with two parameters: velocity and attenuation. Ultrasonic velocity can be correlated to mechanical properties of a material, whereas ultrasonic attenuation can be correlated to microstructural properties of a material. Here we avoid all these parameters and considered soil as homogeneous and even medium. The reflected signal should be amplitude attenuated and delayed in time. This model will give the real-world values of the distance compared to the ideal values from the unattenuated signal. Table 2 shows the time delay and the velocity at different noise power levels at a constant distance of 0.01 m. Table 3 shows the distance of the object at various depths and the time delay with the average velocity

Table 1 Experimental results velocity for different depths

Medium	Distance (cm)	Velocity (m s ⁻¹)
Air	1	332.163
Air	5	339.358
Wood	6	3800
Wood	9	3500

Table 2 Time delay and velocity at different noise levels

Noise level (dB)	Time delay (ms)	Distance (m)	Velocity (m s ⁻¹)
0.0	0.021075	0.01	948.99
0.20	0.017031	0.01	1176.25
0.40	0.022439	0.01	891.29
0.60	0.001679	0.01	1195
0.80	0.00987	0.01	2025
1	0.0212854	0.01	939.6

Table 3 Distance and time delay with constant velocity 1000 m/s

Time delay (μs)	Distance (m)
20	0.01
100	0.05
200	0.1
300	0.15
400	0.2
500	0.25

1000 m/s from Table 2. We can obtain the values which similar to the real lossy environment. Cross-correlation is a powerful tool it will automatically nullify the environmental noise content from the result.

6 Conclusion

Cross-border underground tunnels are threat to our homeland security. These tunnels are the main migration path for the terrorists. So the detection of such tunnels is necessary for our security. The pulse echo technique with round trip time is a better method for the distance estimation and hence we can find the depth of such clandestine tunnels.

By range estimation algorithm, we calculated the velocity for the soil sample and then estimate the unknown depth at which the tunnel resides. With this experimental result (velocity), the depth of the tunnel easily discovered. Due to the noise present in the transmission and reception process, we get velocity values slightly different from the actual results which cause deviation in estimated value of depth. Penetration capability of the signal or the maximum distance estimation is limited by the power of the signal.

7 Future Works

The aim of the project was to estimate the depth of the tunnel. Using the frequency estimation and the range estimation algorithm, we calculate the depth of the tunnel from the ground. The power of the generated signal is too low to penetrate up to the required distance. So amplification using a high-power amplifier and robust algorithm for the localization of the tunnel are considered as future work. The system with a single transmitter and receiver can extended to an array of transmitters and receivers with mobility for surveillance of user area.

Acknowledgments We would like to express our sincere gratitude to Ms. Vrinda N Menon for the time she dedicated to help us solving doubts at various stages of this research. We also take this opportunity to thank Dr. Maneesha V. Ramesh for her support in complete this paper. We would also like to express our gratitude for the immeasurable motivation and guidance provided by Sri. (Dr.) Mata Amritanandamayi Devi (AMMA), Chancellor of Amrita University.

References

1. Klar A, Linker R. Feasibility study of the automated detection and localization of underground tunnel excavation using Brillouin optical time domain reflectometer. *Fiber Opt Sens Appl VI, Proc. SPIE.* 2009;7316:731603.
2. Lo Monte L, Erricolo D, Soldovieri F, Wicks MC. Radio frequency tomography for tunnel detection. *IEEE Trans Geosci Rem Sens.* 2010;48(3).
3. Cameron KCSBWWCP, Mitchell KD. Pemss characterization of metamorphic environments in the central korean peninsula. Fourth tunnel detection symposium on subsurface. 1993.
4. Christos Orfanos GA. Analysis of different geophysical methods in the detection of an underground opening at a controlled test site. *Balkan Geophys. Soc.* 2012;15(1):7–18.
5. Gurbuz A, McClellan J, Scott W, Larson G. Seismic tunnel imaging and detection, in image processing. *IEEE international conference on;* 2006. p. 3229–32.
6. Tegan Counts ACGJHM, Larson G, WRS Jr. Investigation of the detection of shallow tunnels using electromagnetic and seismic waves. *SPIE.* 2007;6553, 65531G.
7. Ryan Dobbins BS, Garcia S. Software defined radio localization using 802.11-style communications. Worcester Polytechnic Institute; 2008.
8. <https://www.ndeed.org/Ultrasonics/Introduction/.html>.
9. <http://en.wikipedia.org/wiki/Cross-correlation>.
10. Location of illegal tunnels in the south west border. <http://content.time.com/time/photogallery/0,29307,1895418,00.html> (2012).
11. http://eecs.vanderbilt.edu/courses/eece258/Lab1/Lab1_Identification_Virtual%20Instrumentation.htm.

Communication Network of Wide Area Measurement System for Real-Time Data Collection on Smart Micro Grid

Varna C. Prakash, P. Sivraj and K.K. Sasi

Abstract This paper deals with communication architecture employing appropriate communication technologies for distribution side Wide Area Measurement System (WAMS). The different communication technologies like WiredLAN, WLAN, ZigBee protocol are simulated in ns2 considering a 5-bus smart micro-grid topology and the performance metrics are compared and analysed based on the standard requirements in order to suggest the apt technology. The study shows that in comparison with a homogeneous network, a heterogeneous network provides a better result considering the operational demands at different levels of the smart distribution grid architecture.

Keywords WAMS · Smart grid · Communication technologies

1 Introduction

The conventional power system faces many significant challenges like meeting the demand of energy, environmental issues, deregulation, security issues and integrating renewable and distributed sources to the system. To overcome these challenges the existing power system needs to undergo considerable amount of change. To ensure that the system stability is maintained even in the heavily loaded conditions real-time measurements must be taken from throughout the grid. These measurements must be taken in a distributed as well as synchronised manner. This is achieved through Wide Area Measurement System (WAMS) [1]. WAMS provides real-time knowledge of various issues and events as and when they occur. This on-time warning helps the operators in taking the necessary control action. In the transmission side of the grid Phasor Measurement Units (PMU) are used to take the real-time measurements [1]. With the help of a GPS unit the real-time data taken

V.C. Prakash (✉) · P. Sivraj · K.K. Sasi
Electrical and Electronics Engineering, Amrita School of Engineering, Coimbatore, India
e-mail: varna1312@gmail.com

by the distributed PMUs are synchronised [1]. For real-time monitoring in distribution side Real-Time Data Collection Units (RTDCU) [2] are introduced to mimic the synchronized and distributed real-time data collection of PMU. The data collected by the RTDCUs are transmitted to the server either directly or via a Data Concentrator (DC). A reliable communication system, which enables this message passing, forms the backbone of WAMS [1].

This paper focuses on developing communication architecture for WAMS in smart distribution network focusing on the selection of communication technologies that can be used for data transmission. The selection of the communication technology depends on many performance indices like delay, bandwidth, throughput, cost, packet delivery ratio, etc. A suitable communication technology has to be selected for the distribution side WAMS by comparing the performance of various technologies for the selected topology. Different communication technologies are simulated in a network simulator for a selected topology for the 5-bus smart micro-grid laboratory simulator [3] and their performance metric values are compared, based on which the selection of the communication technology is done.

The paper consists of three sections. The second section gives an overall idea about the WAMS and the different communication technologies used in WAMS. The next section deals with the system description and then finally the results and conclusion.

2 WAMS for Distribution System

As the real-time condition of the grid changes dynamically with dynamic variations in supply and demand, WAMS began playing a significant role in acquiring the real-time status of the grid as well as maintaining its stability. WAMS helps in monitoring the grid in a more real-time and synchronous manner [2]. In the earlier stages SCADA was used in WAMS for taking measurements. SCADA has a few drawbacks like measurements taken are analogue, has a low resolution of 2–4 samples per cycle, dynamic observability is not possible and the measurements taken are not synchronised [4]. To overcome these drawbacks faced by SCADA, PMU was introduced. In PMU the measurements taken are digital in nature, the resolution increased to a maximum of 60 samples per cycle, the observability became dynamic in a wide range and the measurements are taken in a synchronised manner which helped in knowing current status of the grid. By introducing a GPS unit to the PMUs, synchronised data acquisition with time stamp was made possible. The PMUs are deployed in the transmission side of the grid [2]. For a similar function in the distribution side RTDCUs can be used [2]. For streaming of the data collected by the RTDCUs to the server a reliable communication system is needed. The communication system of WAMS for distribution side is responsible for the transmission of data from RTDCUs to the server and the control messages from the server to the RTDCUs. The selection of the communication technology mainly depends on lot of factors like performance of the communication technology,

requirements from power system, operational conditions, etc. A few of the characteristics that are considered for the selection of the communication technologies are delay, bandwidth, throughput, packet delivery ratio, etc. [5–8]. Delay is the time taken to deliver the message at the destination from the source. For transmitting data from RTDCU to DC the delay should be within a range of 20–50 ms [9]. But in real-time applications it can go up to 10 s [9]. Throughput is the number of bits transmitted per second expressed in kilobits per second. The RTDCU has to transmit 10–60 frames per second [9]. Since in WAMS data being transmitted is of a large size, the communication technology selected from RTDCU to DC should have a minimum bandwidth of 25.39 kbps [9] and the communication technology selected from DC to server should have even a higher bandwidth because the DC collects the measurements from many RTDCUs and transmit it to the server; so the data size increases. To transmit data in the transmission side of the grid PMUs rely mainly on fibre optic communication [10]. Implementing fibre optic communication in a power distribution network results in high infrastructure and deployment cost because of the large number of nodes that are part of the network. Also latency increases when using fibre optic communication [10]. Depending upon the scenario either the same communication technology can be used throughout the different links of the communication network creating a homogenous communication system or a combination of technologies can be used at different links of the communication network creating a heterogeneous communication system. The different communication technologies that are available are Wired LAN, WLAN, ZigBee protocol, WiMaX, Optical Fibre, PLC, etc. [5, 11].

There are different software simulators using which the communication technologies can be simulated for the required application and their performance metrics can be compared. A few of the software simulators available are ns2, ns3, OPNET, OmNet++, GNS3, Qualnet, etc. [12, 13].

3 System Description

The block diagram depicted in Fig. 1 gives an overall idea about the different communication scenarios that are needed in the smart distribution grid. The smart metres are used to collect data from the consumers. The data collected by the smart metres are either transmitted directly to the cloud or via a data collector depending on the distance of the smart metre from the cloud gateway. The RTDCUs are employed to take the real-time measurements from the primary distribution side of the grid. The data from the RTDCUs are also sent to the cloud for analysis. Based upon the data received and analysed the cloud takes necessary control actions which is implemented in real time by the different control units. For distributed decision-making cloud computing is used [14].

Figure 2 is a schematic representation of the communication system of WAMS for smart distribution network. The real-time data collected by the RTDCUs are

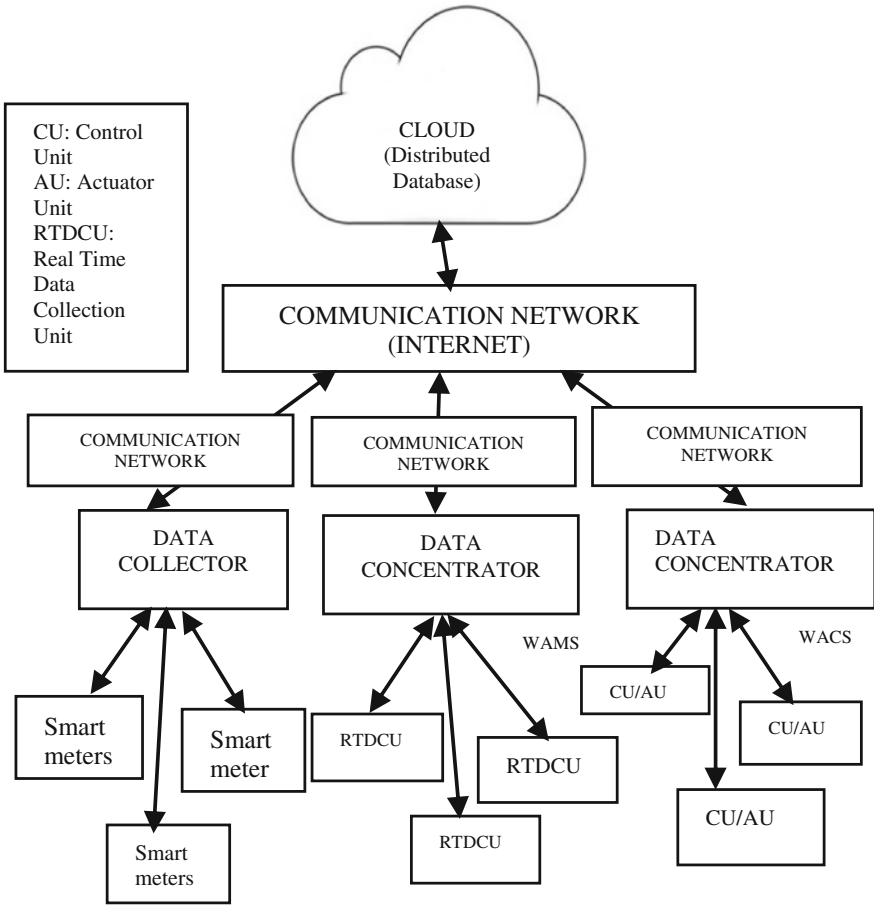


Fig. 1 Communication scenario in a smart micro-grid

transmitted to the cloud. Depending upon the position of the RTDCU the data is either sent directly or through a DC.

The DC accumulates the data received from different RTDCUs and sends it to the cloud. In the cloud the data will be analysed. The cloud sends command messages back to the RTDCUs. These commands can be messages asking the RTDCU to start transmitting the data or stop transmitting the data or asking the RTDCU to vary the time interval between the consecutive data messages [9]. Hence an efficient bidirectional communication is necessary for the proper monitoring and control of the grid.

Figure 3 depicts the topology of the WAMS system being implemented in the laboratory model of a 5-bus smart micro-grid [3, 13]. The server is kept at the centre since it will be equidistant from all nodes. The DCs are placed nearer to server because the size of the data being transmitted will be large when it reaches near the server.

Fig. 2 WAMS communication system

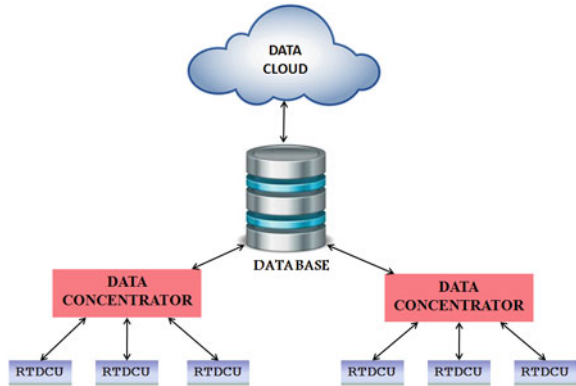
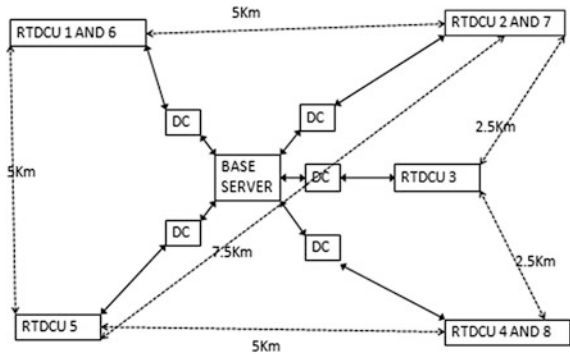


Fig. 3 Topology of the communication network



4 Simulation Results

Different available communication technologies for the implementation in a 5-bus smart micro-grid are PLC, Bluetooth, ZigBee protocol, WiredLAN, WLAN, etc. Due to restriction or overhead posed by several communication technologies, only WiredLAN, WLAN and ZigBee protocol are selected for simulation in ns2 [1, 5]. Communication technology was selected considering the performance metrics delay, throughput and packet delivery ratio.

The communication scenario in this selected topology can be divided into two segments. First, the communication from RTDCU to DC and second the communication from DC to server. The communication between all RTDCU-DC pair is similar, the only difference being the distance from each RTDCU to its corresponding DC. The performance metrics like delay, throughput and packet delivery ratio was analysed for the communication link between RTDCU-DC, DC-server and for the overall topology.

Table 1 Simulation result for WiredLAN

	Throughput (kbps)	Delay (ms)	Packet delivery ratio
DC to Server	12849.92	3.50372	74.56

**Fig. 4** Simulation of WiredLAN in ns2

Table 1 contains the performance metrics for WiredLAN. Since implementing WiredLAN in a new area over large distance causes unnecessary overhead in infrastructure and deployment cost, the performance metrics for WiredLAN was found out only from DC to server. Figure 4 depicts the simulation of WiredLAN from DC to server.

Table 2 contains the simulation result of ZigBee protocol. ZigBee protocol is based on low power transmission. By analysing the results obtained it is observed that ZigBee protocol has the required range and the throughput and delay obtained are within the satisfactory range. Figure 5 shows the simulation of ZigBee protocol in the overall topology.

The simulation results of WLAN are tabulated in Table 3. The delay for the data being transmitted from RTDCU to DC in each link was found to be outside the desired limit. So WLAN was not simulated in the overall topology. Figure 6 shows the simulation of WLAN in a single link.

Table 2 Simulation result for ZigBee protocol

	Throughput (kbps)	Delay (ms)	Packet delivery ratio	Number of intermediate nodes
Server to DC	1456.42	2.4133	75.02	0
RTDCU1 to DC	2021.63	3.94	74.48	3
RTDCU2 to DC	2299.40	3.441	75.05	3
RTDCU3 to DC	3743.59	2.0133	76.61	0
RTDCU4 to DC	1723.84	2.519	74.27	2
RTDCU5 to DC	2123.35	4.158	76.04	3
Overall topology	48807.4	18.19	76.28	11

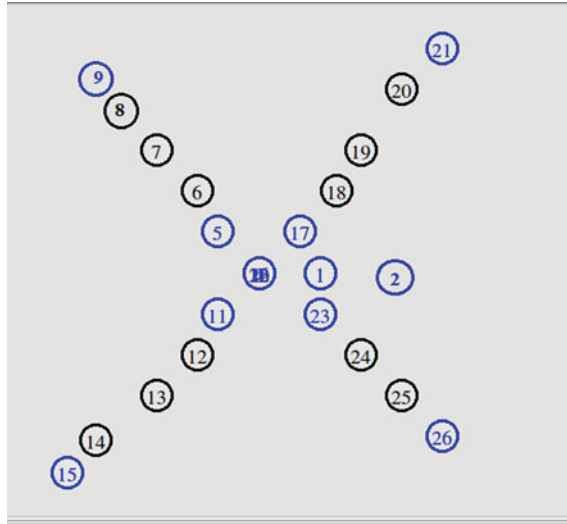


Fig. 5 Simulation of ZigBee protocol in ns2

Table 3 Simulation result for WLAN

	Throughput (kbps)	Delay (ms)	Packet delivery ratio	Number of intermediate nodes
Server to DC	612	218.36	86.90	5
RTDCU1 to DC	1742.06	230.29	85.10	16
RTDCU2 to DC	1643.28	230.32	86.90	17
RTDCU3 to DC	600.22	218.11	86.64	5
RTDCU4 to DC	1642.46	230.15	86.90	13
RTDCU5 to DC	1763.05	237.92	86.64	21

ZigBee protocol has more range when compared to WLAN. So the number of intermediate nodes decreases in case of ZigBee protocol. It can be seen that WLAN has more throughput than ZigBee protocol but the bandwidth of ZigBee protocol satisfies the WAMS requirement. The delay of WLAN is more than that of ZigBee protocol. So ZigBee protocol is an apt technology to be implemented from RTDCU to DC. The main requirement for the selection of communication technology from DC to the server is that it should have high bandwidth because the size of the data increases and the loss of data must be restricted up to a certain point. Also the data must be delivered within the required frame of time. From the performance metrics tabulation it can be seen that WiredLAN has the largest bandwidth when compared

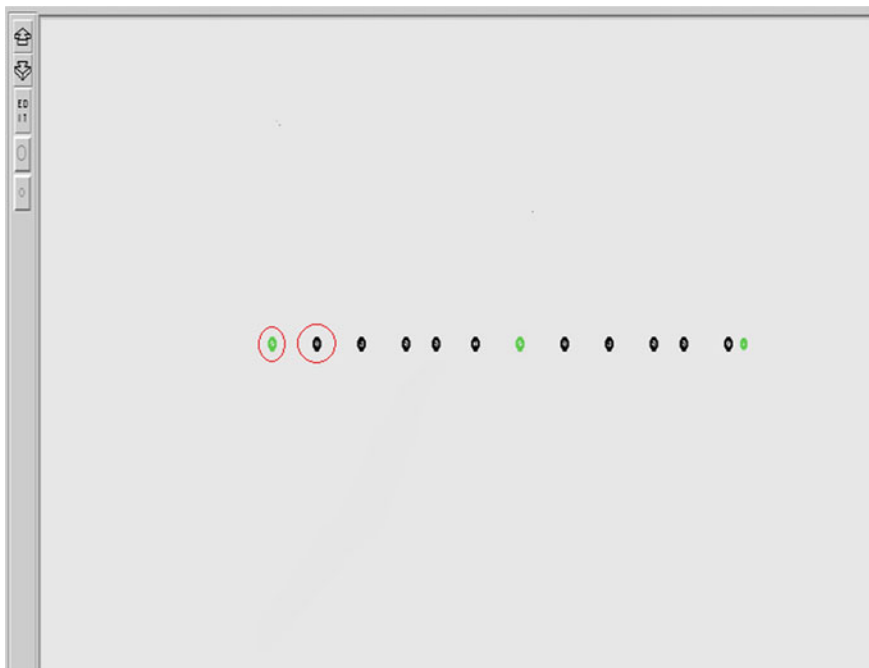


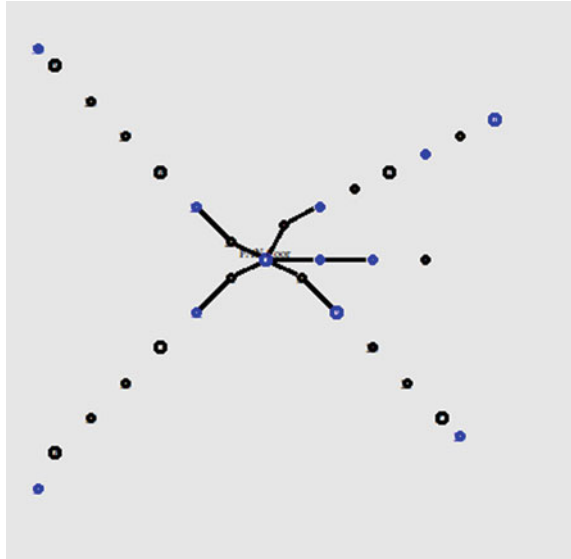
Fig. 6 Simulation of WLAN in ns2

Table 4 Simulation result for heterogeneous communication system

	Throughput (kbps)	Number of intermediate nodes
Server to DC	12812.92	0
RTDCU1 to DC	104.06	3
RTDCU2 to DC	104.28	3
RTDCU3 to DC	60.22	0
RTDCU4 to DC	104.46	2
RTDCU5 to DC	106.05	3

to ZigBee protocol and WLAN. Also WiredLAN delivers data within the desired time. So WiredLAN can be implemented from DC to server. A combination of ZigBee protocol and WiredLAN is best suited for implementation in the topology that has been selected. The heterogeneous communication was simulated in ns2. The delay was found to be 15 ms and throughput was within the desired range. Table 4 contains the performance metrics of the heterogeneous system. Figure 7 shows the simulation of the heterogeneous communication in ns2.

Fig. 7 Simulation of heterogeneous network in ns2



5 Conclusion

Different communication technologies like WiredLAN, WLAN and ZigBee protocol were simulated in ns2 considering a 5-bus smart micro-grid topology and the results were analysed. It was analysed that due to physical constraints, WiredLAN could not be implemented from RTDCU-DC, however, it serves as one of the better options to be implemented from DC-server. From the simulation results it was evaluated that WLAN was not able to meet requirements set by the performance metrics. ZigBee protocol meets all the criteria set by the performance metrics in RTDCU-DC link but due to low bandwidth does not satisfy the bandwidth requirement from DC-server. In comparison with a homogeneous network, a heterogeneous network provides a better result. Hence a heterogeneous network comprising of ZigBee protocol from RTDCU-DC and WiredLAN from DC-server is proposed for the selected topology.

This work can be further extended by analysing the data received at the server and taking the necessary control action thereby developing a wide area monitoring, protection and control system for distribution side automation. Also all the messages transmitted by the RTDCU can be standardised based on IEEE C37.118 standards.

References

1. Sahraeini M, Javidi MH. Wide area measurement systems. In: Md. ZahurulHaq, editor. Advanced topics in measurements.
2. Nithin S, Sivraj P, Sasi KK, Lagerstom R. Development of a real time data collection unit for distribution network in a smart grid. International conference on power and energy systems: towards sustainable energy, ASE Bangalore, India, 15 March 2014.
3. Nithin S, Sasi KK, Nambiar TNP. Development of smart grid simulator. Proceedings of national conference on power distribution, CPRI, India, 2012.
4. Singh B, Sharma NK, Tiwari AN, Verma KS, Singh SN. Applications of phasor measurement units (PMUs) in electric power system networks incorporated with FACTS controllers. *Int J Eng Sci Technol*. 2011;3(3):64–82.
5. Gungör VC, Sahin D, Kocak T, Ergüt S, Buccella C, Cecati C, Hancke GP. Smart grid technologies: communication technologies and standards. *IEEE Trans Ind. Inf.* November 2011;7(4):529–539.
6. Gajrani K, Sharma KG, Bhargava A. Performance assessment of communication network in WAMS. *Int J Distrib Parallel Syst (IJDP)*. November 2012;3(6).
7. Eissa MM, Allam AM, Mahfouz MMA, Gabbar H. Wireless communication requirements selection according to PMUs data transmission standard for smart grid. IEEE international conference on smart grid engineering (SGE'12). 27–29 August 2012, UOIT, Oshawa, ON, Canada.
8. Kansal P, Bose A. Bandwidth and latency requirements for smart transmission grid applications. *IEEE Trans Smart Grid*. September 2012;3(3):1344–1352.
9. Martin KE, Hamai D, Adamiak MG, Anderson S, Begovic M, Benmouyal G, Brunello G, Burger J, Cai JY, Dickerson B, Gharpure V, Kennedy B, Karlsson D, Phadke AG, Salj J, Skendzic V, Sperr J, Song Y, Huntley C, Kasztenny B, Price E. Exploring the IEEE Standard C37.118–2005. *Synchrophasor for Power Systems*. IEEE standards, October 2008.
10. Phasor Measurement Unit. http://en.wikipedia.org/wiki/Phasor_measurement_unit#Phasor_networks.
11. Gungor VC, Lambert FC. A survey on communication networks for electric system automation. *Comput Netw*. 2006;50:877–897.
12. Chhimwal MP, Rai DS, Rawat D. Comparison between different wireless sensor simulation tools. *IOSR J Electron Commun Eng (IOSR-JECE)*. March–April 2013;5(2):54–60.
13. Sarath TV, Sivraj P. Simulation and analysis of communication technology for a smart grid framework. International conference on communication and computing. Elsevier Publications; 2014.
14. Simmhan Y, et al. Cloud-based software platform for data-driven smart grid management. *IEEE/AIP computing in science and engineering*; 2013.

Acoustic Modeling for Development of Accented Indian English ASR

Partho Mandal, Gaurav Ojha, Anupam Shukla and S.S. Agrawal

Abstract This paper investigates Indian English from the point of view of a speech recognition problem. A novel approach towards building an Automated Speech Recognition System (ASR) for Indian English using PocketSphinx has been proposed. The system was trained with a database of English words spoken by Indians in three different accents using continuous as well as semi-continuous models. We have compared the performances in each case and the optimum case performance comes close to 98 % accurate. Based on this study, we tweaked the original PocketSphinx Android application in order to incorporate our results and present it as an Indian English-based SMS sending application. We are working further on this approach to identify ways of successfully training a speech recognition system to recognize a much wider variety of Indian accents with much more significant accuracy.

Keywords Automatic speech recognition · Indian English · Discrete HMMs

1 Introduction

Nowadays, the application of information processing machines have become widespread. From desktop computers to handheld devices and even web applications can do a fair bit of speech processing. But most of this speech recognition technology has become more of an adjust-to-available-options rather than speak-however-you-feel-convenient. Speech recognition technology currently supports English spoken in a rather peculiar way. This leaves a lot of people still fumbling to make the device understand what they are speaking [1]. Given that

P. Mandal · G. Ojha (✉) · A. Shukla
Department of Information Technology, ABV-IIITM, Gwalior, India
e-mail: ojha.iiitm@gmail.com

S.S. Agrawal
KIIT Group of Colleges, Gurgaon, India

English is an official language of India, and over 200 million English speakers exist in India, it becomes essential to modify the speech recognition systems accordingly rather than try to adapt to the ones currently in use which support British or American accents more comfortably. We are highly motivated by this and wish to build something that caters to the need of Indians since they form the second largest country of English-speaking people [2].

Many institutions are working on making speech recognition more and more effortless for people across the globe and we have attempted to do our bit in this research. In this project, we are working on developing a system that performs better speech recognition for Indian accents. Our approach involves studying outputs of various methods and trying to find the optimal approach for training by simply varying the inputs till we get to the point where results could not be further optimized.

2 Previous Work

Quite a few studies have been done in this field of customized speech recognition for regional accents and languages.

One of the initial studies in this context [3, 4] provides a good idea about how speech recognition works and how to get an automatic speech recognition (ASR) system up from scratch. They give a lot of relevant information regarding the working of a speech recognition system and two models for the same, viz., acoustic model and language model. Relevant work in this scenario has been done in [5] and a lot more can still be done.

Researchers at Carnegie Mellon University have developed PocketSphinx [6] which proves to be a boon for speech recognition systems especially in handheld devices. PocketSphinx happens to be the first such system and it comes with an open-source license. They had used a 1000-word vocabulary system which worked quite well on a handheld device operating at 206 MHz. PocketSphinx is revolutionary in that it is nearly real time and several times faster than the baseline system under consideration.

Further work in ASR for accented Indian English has been done at Siemens collaboratively at Bangalore and Germany [7]. The results show the effect of variability in accents on the performance of a system processing Indian English and are quite impressive. The test vocabularies were trained using Hidden Markov Models (HMMs) specifically on accent-specific data. The study suggests that the first task should be to identify the accent and then use the selected accent for further speech recognition. This approach maybe effective but the primary task, viz., identifying the accent still remains somewhat ambiguously mysterious.

In a study contemporary with that done at Siemens, researchers at Carnegie Mellon University proposed that currently available speech recognition systems can be improved using additional data [8] which can be used to create new duration and

pronunciation models. They have essentially tried to build a better sounding Indian English voice with some additional speech data over the existing systems. The technique can prove to be effective but that is something yet to be examined.

A more recent study in the domain has been done on the phonetic segmentation of Hindi speech using HMMs [9]. The system mimics the way humans understand and identify spoken words. The study concludes that best performance was obtainable through a combination of two different Gaussian mixtures and five HMM states. Although there are certain errors in the automatic segmentation process especially concerning some consonants, the study throws light on the fact that it is possible to work on the idea to develop more friendly recognition systems which can outperform the current ones. On similar lines, [10] attempts to highlight the significance of appropriate selection of Gaussian mixtures toward improving the results of a speech recognition problem. The experimental results of the study have proven an improvement of 3–4 % over the current recognition rates due to the inclusion of a third-order derivative of the speech features. Further it states that for a medium-sized vocabulary of about 600 words, the system required 8 Gaussian components to give the optimal results.

In this paper, we have used the CMU PocketSphinx and trained an Indian English database spoken by speakers of various dialects using the continuous as well as the semi-continuous models by changing various parameters and comparing their performance.

3 Proposed Methodology

We start by analyzing the ASR architecture and the procedure of speech analysis and feature extraction. After that we discuss the Continuous Density Hidden Markov Model (CDHMM) for speech recognition and then we state our experiments.

3.1 ASR Architecture

A conventional ASR system is made up of four primary structures which comprise of the following—a. Speech analysis and feature extraction, b. Feature reduction, c. Phonetic transcription, and d. Acoustic model. Figure 1 explains this structure.

3.1.1 Speech Analysis and Feature Extraction

The module for feature extraction computes the various acoustic feature vectors that are used to state the speech signal. Empirical studies in speech analysis [11] have shown that since a speech signal evolves from the lungs with the help of the vocal

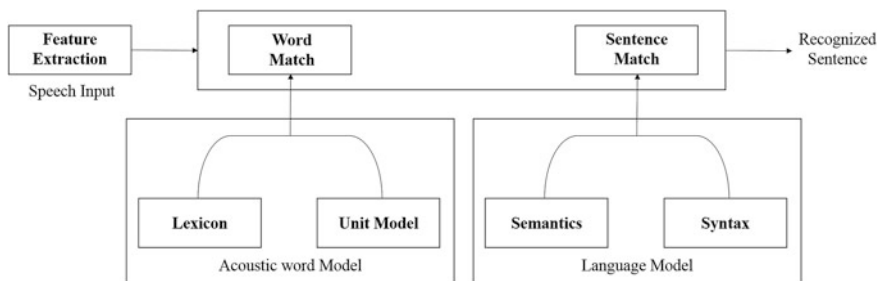


Fig. 1 Working of a continuous speech recognizer

tract, it is best to discriminate between sounds based on the response of the vocal tract component. It has also been observed that including the psychophysical process attributes of how humans perceive speech improves the accuracy of recognition. We have used the mel frequency cepstral coefficients (MFCC) which is a widely used feature based on how humans hear and perceive pitch. The samples of speech are divided into several overlapping frames of small durations, usually 20–30 ms and the frame rate is 10 ms. Hamming window is then used and the log magnitude of each frame is calculated. In order to simulate the human auditory system, the subject spectrum is filtered using triangular band-pass filters which are based on the mel scale. This gives the vector of log energies, a relation which is governed by the following equation where f is the normal frequency and $\text{mel}(f)$ is its counterpart on the mel scale:

$$\text{mel}(f) = 2595 \times \log_{10} \left(1 + \frac{f}{700} \right) \quad (1)$$

3.1.2 Feature Reduction

Feature reduction refers to the methods and techniques which utilize mathematical and statistical tools to reduce the complexity of features while attempting to retain as much information as possible [12]. Majority of these methods rely on schemes involving linear transformation such as the Linear Discriminate Analysis (LDA) and Maximum Likelihood Linear Transform (MLLT). LDA focuses on much more significant differences in variance along a specific direction which helps achieve an optimum value of the probability that all training data in the transformed space and every training sample is an equal contributor to the final objective function. MLLT supposes one transformation matrix to be tied with a group of covariance matrices (CM) belonging to (an) individual state(s) of a HMM. It introduces a new form of a CM which allows sharing a few full CM over many distributions [13].

3.1.3 Phonetic Transcription

The next task is to write down a phonetic structure of the recorded signal. This includes whole word models, syllable-based models, and phone-based models. The former is the simplest of all and often yields good results for small databases which are usually utilized in closed vocabulary systems. Phone-based models are complex but are more flexible and are called context-independent (CI) models. Each phoneme can have one of many possible acoustic realizations which is context-dependent (CD). For a properly trained system, it is essential to take into consideration this co-articulation effect as well. Senones are generated to model these CD sub-word units, which are combinations of phonemes with their preceding and succeeding phonemes. These senones are then represented using the HMMs. In our study, we have used the Arpabet [14] phonetic transcription code.

3.1.4 Acoustic Model

During this modeling process, HMMs which represent the basic phonetic units of the training data are created which are free from quantization errors and model continuous signal representation in a much better and useful way than other techniques. For each model it is necessary to evaluate the highest likelihood of the observation sequence. This is done using the forward algorithm. Given a set of feature vectors, it is possible to find the highest likely word sequence by mapping all possible state sequences that could be generated from all possible word sequences. This can be done using the Baum–Welch algorithm. Finally, the forward–backward algorithm is used to solve the learning problem. In this, the HMM corresponding to the sequence of words in each spoken sentence is found out and another HMM is generated which represents the statement. The system then utilizes the results from the language model to understand the sequence of words which is most likely to occur. In the end, the recognizer takes the final decision as to what word was spoke by taking into consideration the results given out by the previous blocks, viz., the word sequences which are likely and ones which have the highest matching score.

3.2 CDHMM and SCHMM

The continuous density HMMs come into picture here and are based on some probability density functions (PDFs). The multivariate Gaussian mixture density function has been employed for the requirement of a probability density function in our analysis. It is a parametric probability density function represented as a weighted sum of Gaussian component density [15] which can be expressed using the following equation:

$$p(x|\gamma) = \sum_{i=1}^M w_i g\left(x|\mu_i, \sum i\right) \quad (2)$$

Here, γ is a D-dimensional continuous feature vector, w_i where $i = 1 \dots M$ are the mixture weights and $g(x|\mu_i, \sum i)$ represents component Gaussian densities from $i = 1 \dots M$. The component densities are D-variate Gaussian functions which can be represented by the following equation:

$$g\left(x|\mu_i, \sum i\right) = \frac{e^{-\left(\frac{1}{2(x - \mu_i)' \sum_i^{-1} (x - \mu_i)}\right)}}{\sqrt{(2\pi)^D |\sum i|}} \quad (3)$$

Here μ_i represents the mean, $\sum i$ represents the covariance and $\sum_{i=1}^M w_i = 1$ represents the constraint on the mixture weight where covariance can be full or diagonal. To initialize the estimation of the GMM parameters, maximum a posteriori parameter estimation (MAP) is used. The number of mixture components per state which is given by M forms an important parameter for the overall performance of ASR.

The semi-continuous HMM models, a mixture of Gaussians is shared by all the HMM state densities with different mixture weights assigned to them. The weights are further shared by the senones in these models [16].

The likelihood that state s would be observed for frame \bar{X} is represented by the following:

$$L_s(\bar{X}) = \sum_{i=1}^N \lambda_{s_i} \times N_i(\bar{X}) \quad (4)$$

Wherein N is the size of the Gaussian set, λ_{s_i} is the weight for the i th Gaussian in the state s and $N_i(\bar{X})$ represents the likelihood of that Gaussian [17].

4 Results and Discussion

We have used an Indian English database with three speakers (D1, D2, and D3) for our ASR system. Each speaker data consists of 620 sentences. A short description of these speakers is as follows:

D1: The speaker is female, native language is Hindi. It consists of a vocabulary of 1267 words.

D2: The speaker is female, native language is Kannada. It consists of a vocabulary of 1228 words.

D3: The speaker is male, native language is Punjabi. It consists of a vocabulary of 1300 words.

The speech utterances were recorded in 16 kHz through two recording channels: a headset and a desktop-mounted microphone. The speech data was recorded in 16 kHz stereo 16-bit format.

The recognition system is an HMM-based speaker dependent speech recogniser. We have used three—state HMMs for each model, these models are left to right with no skip state. For all the speakers, n-gram statistical language model was used with a language weight of 11.5. We tried experimenting with both open set models and closed set models.

For the open set, we used 80 % of the data, i.e., 496 sentences as training data, and 20 %, i.e., 124 sentences as testing data. The acoustic model uses HMMs as explained earlier. We trained the data using both continuous (Table 1) as well as semi-continuous (Table 2) model.

For the closed set, we used all the 620 sentences as training data, and 20 %, i.e., 124 sentences as testing data for each of the speaker utterances. HMMs were used and the data was trained using both continuous (Table 3) as well as semi-continuous (Table 4) models.

In case of the Continuous model, the input features consisted of a single independent stream “1s_c_d_dd”. The initial tied Gaussian density was 1. The initial tied Gaussian density should be less than final tied Gaussian density. The data was trained using both 8 as well as 16 tied Gaussian densities. The accuracy was tested by comparing the data trained using different tied Gaussian Mixture Models (Senones).

Table 1 Error rates of all speaker utterances in open set continuous model

Database name	Error (%)	Senones: tied Gaussian density				
		70:8	100:8	100:16	120:8	120:16
D1	SER	37.1	37.1	27.4	40.3	32.3
	WER	7.5	7.5	5.4	8.9	6.5
D2	SER	36.3	36.3	31.5	35.5	33.1
	WER	7.2	7.2	5.2	7.7	6.2
D3	SER	29.0	29.0	27.4	30.6	28.2
	WER	3.9	3.9	3.5	4.3	3.9

Table 2 Error rates in the open set semi-continuous model

Database name	Error (%)	Senones: tied Gaussian density	
		100:128	100:256
D1	SER	31.5	24.2
	WER	7.2	5.2
D2	SER	29.0	28.2
	WER	5.8	5.3
D3	SER	30.6	27.4
	WER	5.2	4.6

Table 3 Error rates of all speaker utterances in closed set continuous model

Database name	Error (%)	Senones: tied Gaussian density	
		100:8	100:16
D1	SER	35.0	20.2
	WER	5.5	3.4
D2	SER	37.1	25.0
	WER	7.4	4.5
D3	SER	25.8	12.1
	WER	3.2	1.5

Table 4 Error rates in the closed set semi-continuous model

Database name	Error (%)	Senones: tied Gaussian density	
		100:128	100:256
D1	SER	22.6	21.7
	WER	4.9	4.2
D2	SER	23.4	20.2
	WER	3.5	2.8
D3	SER	21.0	17.7
	WER	2.7	2.2

In case of the semi-continuous model, the input features consisted of feature vector with four independent streams “s2_4x”. The initial tied Gaussian density is same as final tied Gaussian density. The data was trained using both 128 as well as 256 tied Gaussian densities and accuracy was tested by comparing data trained using different Senones.

It was observed that the optimal number of senones to be used for training data should be 100. As it can be seen that in each database the result of data trained using 70 senones and 100 senones gave the same accuracy, senones less than 100 were not used. The more senones the model has, the more precisely it discriminates the sounds. But on the other hand if we have too many senones, it may not be generic enough to recognize any unseen (new) speech. That means that the WER will be higher on unseen data. That is why it is important to not overtrain the models. This is evident from experiments—as the number of senones is increased from 100 to 120, both SER as well as WER increase. Formula used for calculating the recognition score is as follows:

$$\frac{\text{No. of Recognized Words/Sentences}}{\text{Total no. of Words/Sentences in the Testing Set}} \times 100 \quad (5)$$

It was also observed that more the number of final tied Gaussian density, better is the accuracy. Usually, 8–32 densities are used for each mixture in a typical CDHMM system but in the experiments they have been limited to 16, as increasing

the number of densities also increases the computational time. Another interesting feature observed is that the accuracy of the male speaker is better than that of the female speakers. Here, the data has been considered as having 100 senones and 16 tied Gaussian states.

It has been observed that the optimal number of senones to be used for training data should be 100 in continuous model. So we took the number of senones as 100 for semi-continuous model as well. It has also been observed that in the continuous model, greater number of final tied Gaussian density is better for accuracy. The number of mixture Gaussians is usually 128–2048 in SCHMM system, which is much larger than the 16–32 densities used for each mixture in a typical CDHMM system. The number of Gaussian densities was thus limited to 256, as increasing the number of densities also increases the computational time. Here, the data has been considered as having 100 senones and 256 tied Gaussian states.

Table 5 shows the overall comparison between the models discussed earlier. These are error % change b/w 8 tied Gaussian states and 16 tied Gaussian states in continuous and b/w 128 tied Gaussian states and 256 tied Gaussian states in semi-continuous when the number of senones is 100. The summary of overall database accuracy is shown in Table 6.

Experiments were repeated with inclusion of LDA/MLLT along with MFCC. LDA/MLLT was utilized to improve the accuracy of the results and those observations were recorded as well. The LDA dimension used is 32. For semi-continuous models, LDA/MLLT feature transform is not supported in PocketSphinx. The data of MFCC+LDA/MLLT is summarized in Table 7.

Table 5 Overall comparison of tested models

DB/model	D1		D2		D3	
	Δ SER	Δ WER	Δ SER	Δ WER	Δ SER	Δ WER
O/C	26.14	28.00	13.22	27.77	5.54	10.23
O/S-C	23.17	27.77	2.76	8.62	10.46	11.54
C/C	42.28	38.18	32.61	39.18	53.11	53.12
C/S-C	3.98	14.28	13.67	20.0	15.71	18.52

Table 6 Overall best % accuracy for each database using MFCC

DB/model	D1		D2		D3	
	S-A	W-A	S-A	W-A	S-A	W-A
O/C	72.6	94.6	68.5	94.8	73.4	96.5
O/S-C	75.8	94.8	71.8	94.7	72.6	95.4
C/C	79.8	96.6	75.0	95.5	87.9	98.5
C/S-C	78.3	95.8	79.8	97.2	82.3	97.8

Table 7 Best % accuracy using MFCC+LDA/MLLT

DB/model	D1		D2		D3	
	S-A	W-A	S-A	W-A	S-A	W-A
O/C	78.9	95.9	76.4	96.1	79.5	97.3
C/C	84.6	97.4	81.2	96.6	90.9	98.3

5 Conclusion and Future Work

It can be concluded that in terms of accent, the Punjabi accented HMMs (i.e., database D3) gives the best performance compared to other two accented HMMs. The percentage change in error is higher in continuous models when data is trained from 8 tied Gaussian states to 16 tied Gaussian states than in semi-continuous models when data is trained from 128 tied Gaussian states to 256 tied Gaussian states. Better improvement in terms of change in percentage error is seen in the case of continuous models based on closed data set (SER in the range of 32–56 %) as compared to continuous models based on open data set (SER in the range of 5–26 %). Overall, the optimum number of senones for each of the database is found to be 100 and the optimal number of final tied Gaussian for continuous model chosen is 16. For semi-continuous model, the number of final tied Gaussian is found to be 256.

It can also be deduced that the accuracy of a male speaker is overall better than that of female speakers, with exception in semi-continuous model in open set data where SER of female speaker is more than male speakers. Also, on an average, the overall accuracy of closed set data is better than the accuracy of open set data. The sentence accuracy of closed set data is 7–15 % more than open set data in case of continuous model and 3–10 % more than open set data in case of semi-continuous model. The word accuracy of closed set data is 0.7–2 % more than open set data in case of continuous model and 1–3.5 % more than open set data in case of semi-continuous model. It was observed that LDA/MLLT could bring about nearly a 6–8 % improvement in sentence accuracy and 1–2 % in word accuracy. LDA/MLLT brought more improvement in data sets that had less sentence and word accuracy compared to data sets that had more sentence and word accuracy.

Based on this study, we tweaked the original PocketSphinx Android application in order to incorporate our results and present it as an Indian English-based SMS sending application [18].

These are only the initial results and more work needs to be done in order to completely implement these ideas in practical applications.

References

1. Discussion Forum about Siri on the official website of Apple Inc. <https://discussions.apple.com/thread/3390280?tstart=0>.
2. List of Countries by English Speaking Population—Wikipedia. http://en.wikipedia.org/wiki/List_of_countries_by_English-speaking_population.

3. Samudravijaya K. Automatic Speech Recognition. Tata Institute of Fundamental Research Archives. 2004.
4. Samudravijaya K. Speech and speaker recognition—a tutorial. Tata Institute of Fundamental Research Archives. 2004.
5. Samudravijaya K, Rao PVS, Agrawal SS. Hindi speech database. In: the Proceedings of the International Conference on Spoken Language Processing ICSLP00, Beijing, 2000; CDROM: 00192.pdf.
6. Huggins-Daines D, Kumar M, Chan A, Black AW, Ravishankar M, Rudnicky AI. Pocketsphinx: a free, real-time continuous speech recognition system for hand-held devices. In: The proceedings of the IEEE international conference on acoustics, speech and signal processing (ICASSP), France, 2006.
7. Kulkarni K, Sengupta S, Ramasubramanian V, Bauer JG, Stemmer G. Accented Indian english ASR: some early results. In: The proceedings of the IEEE spoken language technology workshop, India, 2008.
8. Kumar R, Gangadharaiiah R, Rao S, Prahallad K, Rosé CP, Black AW. Building a better Indian english voice using ‘more data’. In: The proceedings of the 6th ISCA workshop on speech synthesis, Germany, 2007.
9. Balyan A, Agrawal SS, Dev A. Automatic phonetic segmentation of Hindi speech using hidden Markov model 27:543–549, AI & Soc, Springer: London; 2012.
10. Sinha, S, Agrawal, SS, Jain, A. Continuous density hidden markov model for context dependent hindi speech recognition. In: The proceedings of the international conference on advances in computing, communication and informatics (ICACCI), India, 2013.
11. Picone J. Signal modeling techniques in speech recognition. In: Proceedings of the IEEE international conference, June 1993.
12. Geirhofer S. Feature reduction with linear discriminant analysis and its performance on phoneme recognition. Department of Electrical and Computer Engineering: University of Illinois at Urbana-Champaign; 2004.
13. Psutka JV. Benefit of maximum likelihood linear transform (MLLT) used at different levels of covariance matrices clustering in ASR systems., Lecture Notes in Computer ScienceBerlin Heidelberg: Springer; 2007.
14. Arpabet. <http://en.wikipedia.org/wiki/Arpabet>.
15. Reynolds DA. A Gaussian mixture modeling approach to text-independent speaker identification. Ph.D. thesis, Georgia Institute of Technology, 1992.
16. Raux A, Singh R. Maximum-likelihood adaptation of semi-continuous HMMs by latent variable decomposition of state distributions. In: The proceedings of the 8th international conference on spoken language processing (ICSLP), South Korea, 2004.
17. Duchateau J, Demuynck K, Van Compernelle D. Fast and accurate acoustic modelling with semi-continuous HMMs. Speech Commun. 1998;24(1):5–17.
18. Indian English SMS Sending App—PocketSphinx Derivative. <https://github.com/parthoiiitm/smsforindeng>.

Improved Identity Anonymization Using Hashed-TOR Network

Gaurav Ojha, Rakesh Singh and Anupam Shukla

Abstract At present, the modern world has been computerized to a huge extent because of the increasing penetration of the Internet. There is a plethora of services available on the web platform these days. Services available may be either legitimate or illegitimate. International borders have been effectively eliminated with the help of the internet and so more and more companies are offering their services across the globe. The physical location of the service provider does not matter anymore. Since every request that is sent to the WWW, every message that is relayed and, in fact, every click is logged somewhere on the internet, it gives rise to a huge knowledge base of user data. This knowledge base can be manipulated and exploited in a number of ways. This poses a great threat to any individual user who wants to utilize the services available on the internet anonymously. A mechanism is required using which individuals can maintain their own privacy from global organizations such as the NSA, Google, etc., which are believed to collect huge amounts of personal user data. The TOR network goes a long way in doing that and abstracts the user from the conventional internet. But TOR itself is not free from vulnerabilities. In this paper, a vulnerability with the ONION routing protocol, which is the spine of the TOR network, has been presented. It has been analyzed and a technique to overcome it has also been discussed to make the TOR network safer for anonymous use on the World Wide Web.

Keywords TOR · ONION routing · Internet

G. Ojha (✉) · R. Singh · A. Shukla
Department of ICT, ABV-IIITM, Gwalior, India
e-mail: ojha.iiitm@gmail.com

R. Singh
e-mail: f25527180@gmail.com

A. Shukla
e-mail: dranupamshukla@gmail.com

1 Introduction

Privacy problems exist on the Internet because data has to pass through a long route before it reaches from its source to destination. Every single packet of data sent by a casual Internet user passes through a number of “checkpoints”, where there exists a possibility of it being sniffed, modified, deleted, or lost. Contiguous data has a potential to define a subject, i.e., a real human being and his/her actions. When vast amounts of such personal information lie with one single entity or group, it gives rise to hegemony. This is an immense threat to the world of Internet users—essentially the whole world by mammoth companies like Google, Facebook, etc., or dominant government establishments such as the NSA (PRISM). There exists a huge list of such organizations who are trying to prey on personal user information.

This makes it necessary to implement some mechanism to prevent privacy of individuals using the Internet. In general, techniques to achieve anonymity can be broadly classified into two categories which are described as follows.

1.1 Anonymity by Policy

In this technique, anonymity is granted with an accord. All the policies and rules are defined by a third party and the user needs to agree with them to be able to use the service. For, e.g., if one wants to use Google’s Gmail, one has to agree with their rules and policies. If any of the policies change, it puts one’s privacy at risk and nobody can be blamed for it. The same applies for a lot of major services on the internet today, which are offered by huge companies including Facebook, Yahoo!, etc.

1.2 Anonymity by Design

Anonymity by design is a concept in which privacy is ensured without any rules. In fact, privacy itself is the service. For, e.g., a typical proxy provider sets up a server somewhere on the internet and allows users to relay traffic through it [1]. All users enter and leave through it. The provider may charge a fee for providing this service or may allow advertisements on the site to gather funds for its maintenance. From the users’ end, it looks as if they are connecting to a random website, while from the destinations’ end, it looks as if a random source is trying to connect to them. Such simple proxy providers are good enough if all that the user requires is to protect his privacy and the service provider can be trusted to refrain from misusing the users’ data. Some of them also encourage the use of SSL/TLS to prevent users against local eavesdroppers like those at a public place with free Wi-Fi.

The problem with simple proxy providers is that they create a single point of failure. The provider usually knows who the user is and what content is being accessed. This is possible simply because the traffic passes through their servers. In some cases, it is also possible to peek inside encrypted traffic, such as banking transactions or payment gateway transactions, as it is passively intercepted by them. The only thing the user can do is trust the provider who could actually be doing a number of things such as watching user traffic, injecting advertisements into their traffic stream, or recording their personal information.

1.3 Onion Routing

Onion routing means successively encrypting a plaintext message at each node during transit such that each layer of encryption can be decrypted only by a specific node in the transit path. Just like layers of an onion, encryption layers are arranged and can be removed to disclose the message to the recipient. Every node in the network only knows about the node it has to send the packet next to, as rest of the information is encrypted in a layer which the current node cannot decrypt.

1.4 TOR

TOR is an acronym for “The Onion Router.” The TOR network is one of the best free anonymization techniques available today for the casual internet user. TOR passes user traffic through at least three different servers before sending it to the destination. Since there are separate layers of encryption for each of the relays used, TOR does not modify or even know what the user is sending through it. It merely relays user traffic, which is completely encrypted, through itself and sends it out somewhere else ensuring that everything is intact.

The TOR client manages the encryption and the path (which can sometimes be dynamic) followed by the network for a specific user. There are relays located all over the world and they merely pass encrypted packets between themselves before finally ejecting them to the destination. This is shown in Fig. 1, which also illustrates the cryptographic architecture of the path by showing the communication between the relays. It is very clear that the sender (TOR client on user’s PC) knows the complete path and creates the virtual circuit as described.

TOR is based on the onion routing protocol. NSA dubbed it as “the King of high security, low-latency Internet anonymity” [2] owing to its free nature, ease of use, and strong network, which gives users their personal privacy and freedom to browse the internet and perform confidential transactions without having to worry about the risk of being monitored [3].

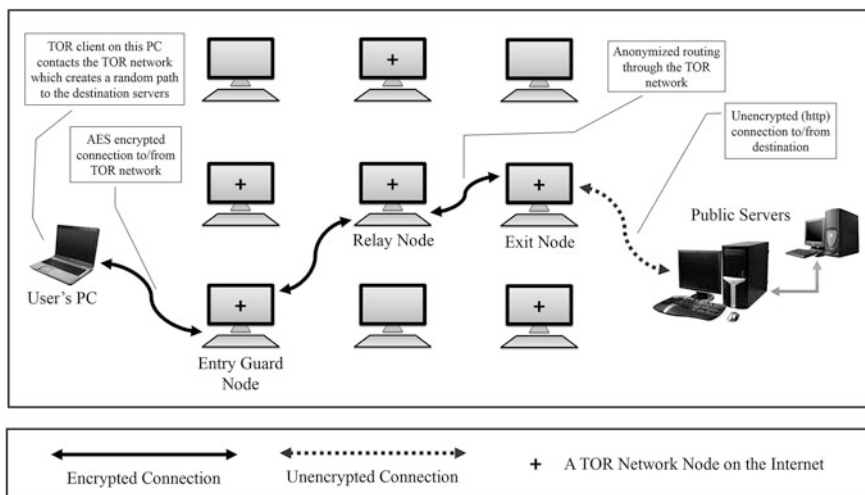


Fig. 1 Working of the TOR network

1.5 The Problem

Anonymity in the TOR network can be compromised if there is simultaneous sniffing at the entry and exit nodes, because this would reveal the IP of the user by guessing the flow of packets [4]. Regardless of the fact that data was encrypted throughout its lifetime in the TOR network, the user can be identified if simultaneous sniffing exposes consistent information flows. Figure 2 shows this possibility, for example, if the request is received at a specific time and a response is received within milliseconds, an intelligent attacker can interpret that it is from a specific user as sniffing is being done at both input and output nodes.

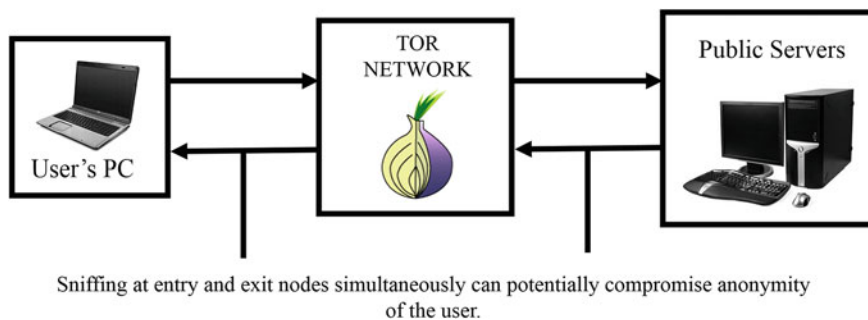


Fig. 2 The vulnerability in TOR

2 Previous Work

Not much has been written about the identified vulnerability but some security methods have been proposed earlier, which can be implemented outside or instead of TOR in some or the other way.

In [1], two anonymity models had been proposed to ensure the privacy of the communicating parties and to protect the sender's address during the routing process. This ensured that the communicating parties were rendered unidentifiable and untraceable from the other end of the network. The results are amazing and demonstrate that the proposed models have antispooofing capabilities as well. A high anonymity degree was ensured even if some of the nodes on the path are compromised. In one of the two proposed models, the request and response cannot be linked and there is no additional overhead cost. The measurements showed that additional incurred delay on each collaborative router varies between 1.35 and 3.5 ms, which means that end-to-end delay is negligible for a typical internet path.

Using traffic analysis [5], it is possible to infer who is talking to whom over a public network. Onion routing comes into the picture here as it is resistant to traffic analysis and lives just beneath the application layer. It is designed to interact with a wide variety of unmodified Internet services by means of proxies. Onion routing had been implemented on various platforms and services including the Sun Solaris 2.4 operating System, HTTP proxies for browsing the World Wide Web [6], RLOGIN for remote logins, SMTP for e-mail, and FTP for file transfers.

But onion routing can only be effective at complicating traffic analysis if its infrastructure is widely deployed and widely used. One of the reasons for this is simple is that the applications utilizing it need not be modified. TOR [7] is presented as a circuit-based, low-latency anonymous communication service. Its based on the second-generation onion routing system that addresses limitations in the original design by adding perfect forward secrecy, congestion control, directory servers, integrity checking, configurable exit policies, and a practical design for location-hidden services via rendezvous points.

In this paper, we are proposing a technique to overcome this vulnerability of TOR, which has been identified by using an additional anti-espionage layer (AEL) in order to prevent synchronized sniffing from both ends. This effectively patches the vulnerability.

3 Proposed Methodology

We are assuming that everything is encrypted and we have this predefined setup of network (having relays and client proxy) [8] as shown previously in Fig. 1. We propose to add a middle layer AEL to solve the existing vulnerability after which TOR becomes completely anonymous. The steps involved are as follows:

1. Sender client searches randomly for an available PC in the middle layer and sends a request to it.
2. The selected PC gets an encrypted request which does not reveal the content of the request and it simply sends it further. This PC does not even know the ultimate exit address. It uses some sort of hash with the IP of the sender which is unique for every request. This PC in the AEL which goes ahead and establishes a circuit with the TOR Network.
3. When the TOR network sends the response to the AEL, another random PC receives it and is responsible for sending the response back to the client who sent it. For this it needs to know the sender's IP address.
4. The sender's IP address is included in the hash that was sent back by TOR along with the response. This hash is broadcasted in the AEL in order to retrieve the sender's IP address.
5. Once the sender's IP address is retrieved, the response is sent back to it.

The proposed architecture can be represented in Fig. 3.

In the AEL, the request and response are separated and are made to appear to be coming/going from/to different locations. This makes it impossible to guess a pattern among the packets being transmitted and thus curbs the existing vulnerability.

The flowchart of requests from client and from the recipient is shown in Fig. 4.

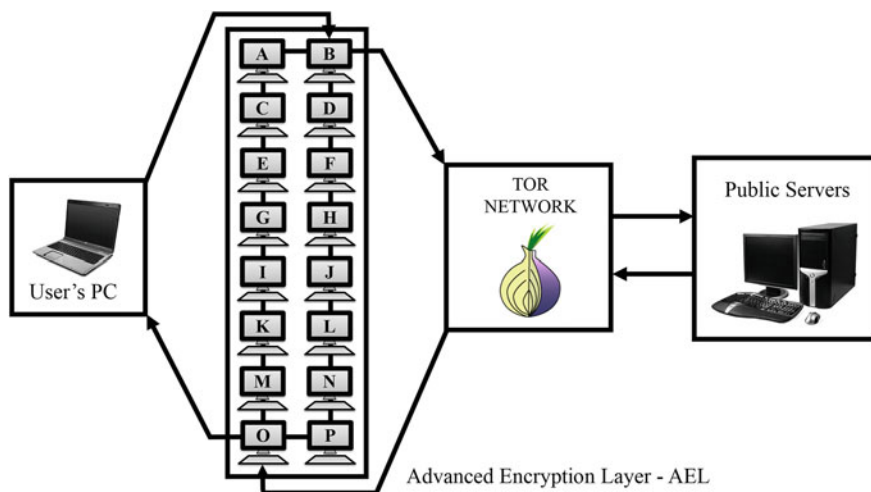


Fig. 3 Proposed solution—the advanced encryption layer (AEL)

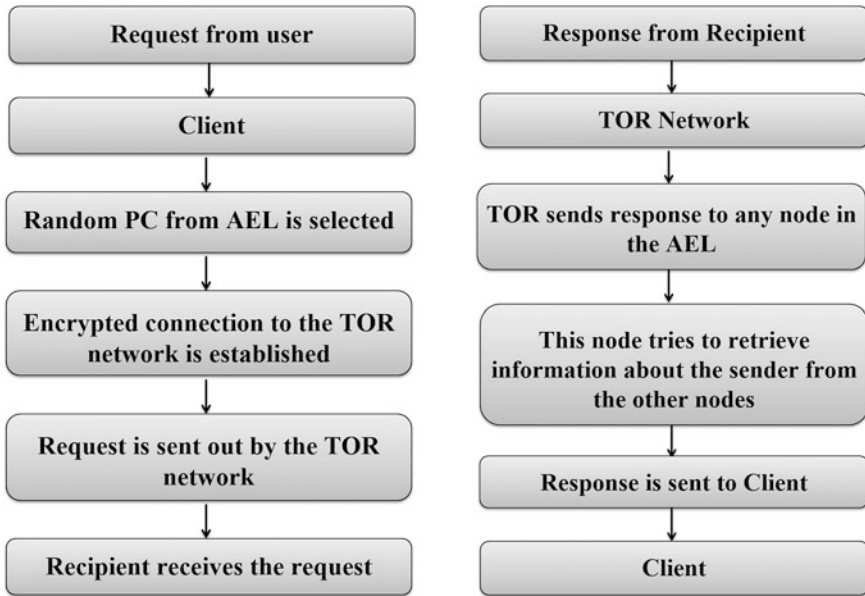


Fig. 4 Flowcharts showing the steps in communication between the user and recipient

4 Conclusion

In this paper, a vulnerability was identified in the TOR network, which can be violated by sniffing simultaneously at the entry and exit nodes. This poses a significant threat to the security of an individual attempting to maintain anonymity using the TOR network or onion routing. A solution was proposed to overcome the said vulnerability and make overall communication, using TOR, more secure. Implementation of an AEL between the TOR network and the sender has been proposed. The AEL effectively abstracts the sender by responding to a request through a separate channel. Secrecy is maintained through hashing within the AEL. The overall implementation has the potential to make TOR completely anonymous.

Further work can be done on the same lines by creating an interface which can link the AEL theory to Vidalia. Also, the link between the encryption keys used in TOR and those used in AEL needs to be securely implemented. [9, 10].

References

1. Sarji I, Kayssi A, Chehab, A. Low overhead anonymous routing. In: The proceedings of the 3rd international conference on communications and information technology (ICCIT-2013): Networks and Internet Technologies, Beirut.
2. About TOR. http://en.wikipedia.org/wiki/Tor_anonymity_network.

3. Simon D. Anonymous communication and anonymous cash. In: *Advances in cryptology, CRYPTO 2006*, (LNCS vol. 1109), Kobitz N editor. New York: Springer; 2006, pp. 61–73, 2006.
4. Reed MG, Syverson PF, Goldschlag DM. *Anonymous connections and onion routing*. IEEE: Naval Research Laboratory; 1998.
5. Barker J, Hannay P, Szewczyk P. Using traffic analysis to identify the second generation onion router. Melbourne: VIC IEEE; 2011. p. 72–8.
6. Berners-Lee T, Fielding R, Frystyk H. Presented at the hypertext transfer protocol HTTP/1.0, Available FTP: <ftp://ds.internic.net/rfc/rfc1945.txt> (19xx).
7. The Tor Project, Inc., Tor metrics portal: users. <https://metrics.torproject.org/users.html> (2011). Accessed June 2011.
8. The Anonymizer. <http://www.anonymizer.com>.
9. The TOR Project and related documents. <https://www.torproject.org/>.
10. The TOR Source Code. <https://github.com/grabhive/Tor.framework>.

A Tokenized Binding Update Scheme for Next Generation Proxy IP Mobility

P.N. Anbarasi and Senthilkumar Mathi

Abstract At present, the users are apparently high for wireless networks. In proxy mobile IPv6, the mobility management among the networks is tedious for the location update of mobile node and the secrecy plays a tremendous role. Here, the messages are exchanged via a localized mobility anchor between the communicants. Consequently, the data traffic is high due to the centralized feature of local mobility anchor. Also there is a single point of failure and increase in the network cost. Therefore, the efficacy of the network is increased by distributing the functionality of local mobility anchor among the mobile access gateways present in the network. However, there are several security challenges such as denial-of-service, man-in-the-middle attack, etc. Thus, the network needs an enhancement for prevention of threat and location update of mobile node. Hence, the presented paper proposes a new tokenized binding update scheme by sharing a routing table. Here, the token of mobile node is incorporated in the routing table and shared among the mobile access gateways. In addition, the proposed scheme decreases the cost of signaling and traffic overhead by eliminating unnecessary queries for binding update and acknowledgment. The security of the scheme is validated using AVISPA—the model checker. From the security and numerical analyses, the proposed scheme shows the enhancement of security and significant reduction in the connection cost and data delivery cost when compared to the existing schemes.

Keywords Mobile IP · Proxy Care-of-Address · Mobile access gateway · Local mobility anchor · Distributed mobility management · Token · Routing table update · Proxy binding update · Proxy binding query

P.N. Anbarasi (✉) · S. Mathi
Department of Computer Science and Engineering, Amrita School of Engineering,
Amrita Vishwa Vidyapeetham (University), Coimbatore, Tamilnadu, India
e-mail: anbarasipn@gmail.com

S. Mathi
e-mail: m_senthil@cb.amrita.edu

1 Introduction

Usage of various wireless networks arises at high cause with the increase in security and efficiency of the network [1]. The standard protocol developed for nonintervention of internet services, while moving is called mobile internet protocol (MIP). In this protocol, various IP addresses are used for message exchange among the communicants. When a host moves to other network called foreign network, an address called care-of-address (CoA) is assigned to the host as temporary address for further communication [2]. Here the hand-off latency is high and it is a client-based protocol; thus [3, 4] a network-based standard procedure is proposed and it is called as proxy mobile internet protocol version 6 (PMIPv6). Here the mobility of the host is managed by the network.

As shown in Fig. 1 in PMIPv6, the mobile node (MN) gets an IP address from the mobility anchor gateway (MAG) as the prefix. The MAG sends the location of MN to local mobility anchor (LMA). Here, the MN moves from one MAG to another MAG in a distributed environment called hand-off. Thus, sends an proxy care-of-address (PCoA) of MN to LMA via MAG as proxy binding update (PBU). Subsequently, proxy binding acknowledgment (PBA) is sent as response after updating the location of MN in the binding cache (BC). Consequently, the communication is sent between MN and correspondent node (CN) via LMA through MAGs of the hosts. Here, the LMA is centralized thus every MN belonging to the same network has to be sent through the same LMA.

Subsequently, alternative methods were proposed in terms of reduction in traffic and signaling cost. Here a scheme was proposed for finding the optimal path for data packets called localized routing for PMIPv6 [4, 5]. Before finding an optimal path for exchange of message, the control packets such as localized routing information (LRI) and localized routing acknowledgment (LRA) is exchanged between LMA and the hosts of the network, (i.e., mobile node and correspondent node) [5]. Therefore, there is an issue before finding optimal path and the traffic cost is high since all MN in the network has to propel the control packets through the same LMA. But here also a single point of failure arises and efficiency of the network does not meet the requirement. Thus, a scheme called partially distributed PMIPv6 was introduced. Here, also a control packet is forwarded through LMA. Thus, fully distributed PMIPv6 [6] was developed where the functionality of LMA was distributed among the MAGs in the network. However, due to the multicasting of queries for location update among MAGs in the network, the signaling cost is high. However, it is impossible to prevent several attacks such as false binding update, man-in-the-middle attack, replay attack, etc.

The rest of the paper is organized as follows; Sect. 2 emphasizes about the related work. The proposed scheme is explained in Sect. 3. Section 4 describes the security validation using AVISPA and security analysis. The performance evaluation of the proposed scheme is presented in Sect. 5. Then the conclusion of the paper is discussed in Sect. 6.

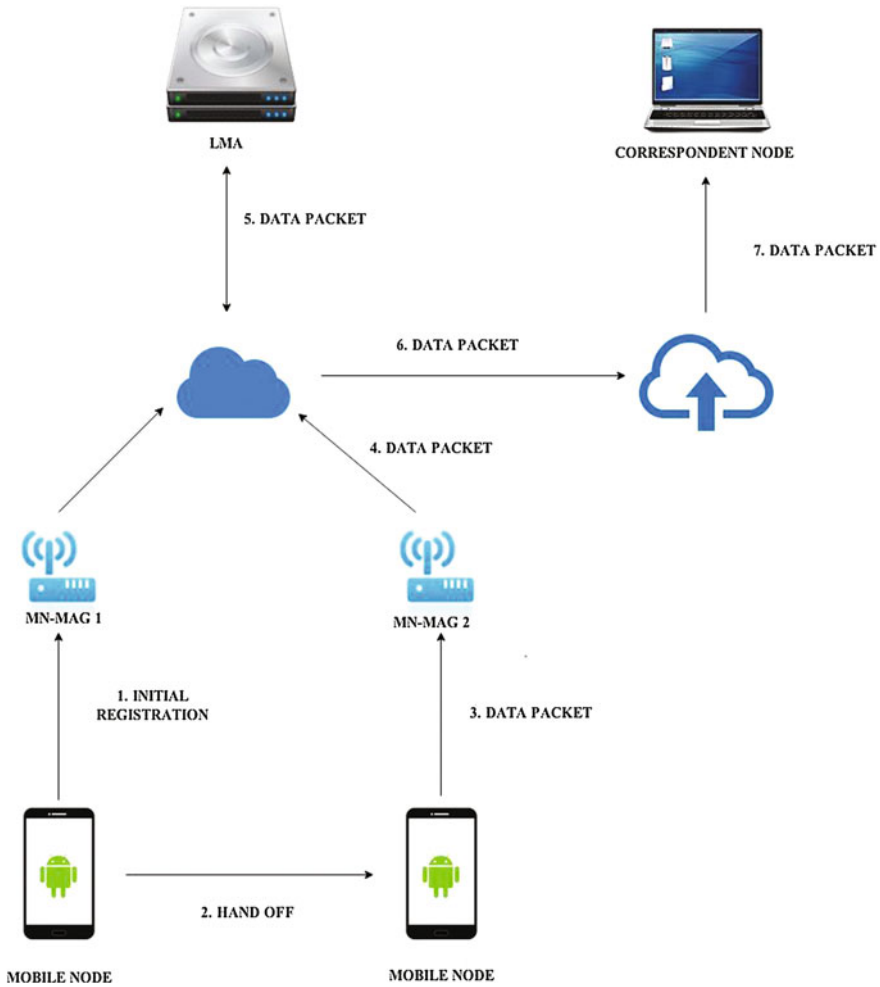


Fig. 1 An overview of proxy mobile IPv6

2 Related Works

In conventional Proxy Mobile IPv6, the network is responsible for the functionality of the nodes in the network, thus the protocol is called network-based protocol investigated by Gundavelli et al. [3]. Here, on behalf of mobile node the packet exchange is done by the MN's MAG [3]. Subsequently, the MAG of MN sends proxy binding update to LMA after the initial registration of MN. Thus, the LMA updates the PBU in the proxy binding cache for further communication. However,

the MN and CN communicate through LMA via MAG. Hence, here occurs single point of failure due to centralized LMA results in high data traffic and latency cost.

Accordingly, Liebsch et al. [4] proposed an alternative protocol named localized routing for finding the optimal path while exchanging messages in PMIPv6 (localized routing for PMIPv6). Here, after the initial registration of MN with MAG, extra control packets are exchanged between MAGs of MN and CN to LMA called localized routing information (LRI) and acknowledgment. The LRI contains the request for finding the optimal path between MN and CN for message exchange without the intervention of LMA. Subsequently, [5] the LMA sends localized routing acknowledgment (LRA) containing the optimal path between the communicants. Even though the path is optimized, the control packets such as LRI and LRA are forwarded via LMA a centralized feature. Thus, there exists a nonoptimal path before optimized routing and high signaling cost.

Bernardos et al. [7] proposed partially distributed PMIPv6 for reducing the signaling cost. Here, the MN sends the IP address of MAG to LMA for communication. Subsequently, the CN sends request to know the location update of MN by forwarding proxy binding query packet to LMA. The LMA acknowledges with the location update of MN [7]. After, the exchange of PBQ and PBA, MN and CN directly communicates with each other. Nevertheless, here exists single point of failure due to the centralized behavior of LMA.

Bernardos and Coworkers [8] proposed an enhanced technique for distributed PMIPv6 called fully distributed PMIPv6. Here, the functionality of LMA is distributed among the MAGs in the network. Thus, in this scheme centralization is avoided. After the initial registration of MN, the CN requests for the location of MN by multicasting the proxy binding query to all MAGs in the network. The corresponding MN responses with the proxy binding update for the query. Consequently, the CN forwards/exchanges the message to MN via MAGs. Nevertheless, multicasting [8] of query packet to all MAGs imposes high signaling cost and denial-of-service attack is possible.

Thus, this paper presents a new tokenized scheme in distributed environment to know the location of MN. Here, the security and efficiency of the scheme are enhanced by stipulating reduced latency and signaling cost.

3 Proposed Scheme

3.1 Notations

Table 1 show the terminologies used in the proposed scheme.

Table 1 Notations used in the tokenized scheme

Symbols	Description
$PCoA_{MN}, PCoA'_{MN}$	Proxy care-of address and new proxy care-of address of MN
$N_{MN}, N_{MNMAG1}, N_{MNMAG2}, N_{CNMAG}, N'_{CN}, N'_{MN}, N'_{MNMAG1}, N'_{MNMAG2}$	Nonces of MN, old MAG, new MAG CN-MAG, new nonce of CN and MN, and new nonce of old MAG and new MAG, respectively
$E_{SK}, E_{SK1}, E_{SK2}, E_{PU-MN}$	Secret keys of MN and old MAG, MN and new MAG and old MAG and new MAG, and public key of MN, respectively
σ_{CN}	Digital signature by CN's private key
HASH and	Hash function and concatenation
MSG	Data packet sent between MN and CN via MAGs

3.2 Detailed Description of the Proposed Scheme

In the proposed scheme, the entities involved are MN, CN, MAGs of MN and CN, and other MAGs in the network. The MN-MAG forwards the routing table incorporated with the token of MN after initial registration of MN. Accordingly, the CN checks the routing table for the token to know the location of MN. Here, the routing table is encrypted using the public key of the recipient thus, the token and PCoA of MN is not known by every other node present in the network. After verifying the token, the CN sends the message packet to MN via MAGs. Due to the frequent mobility nature of MN, the location gets drastic change. Thus, whenever the MN changes the location, the respective MAG forwards/updates the routing table to all MAG in the network as shown in Fig. 2.

Following steps show the message flow of tokenization using routing table for location update,

Step 1: MN performs initial registration with MN-MAG1.

$$MN-MAG1 \rightarrow MN: M_1 = MNMAG1_{ADDR}, MN_{ADDR}, N_{MN}, N_{MNMAG1}, E_{SK} [PCoA_{MN}, N_{MNMAG1}], HASH[N_{MN} || N_{MNMAG1}]$$

The message M_1 contains nonce of MN and MN-MAG, PCoA of MN, source address, and destination address. The IP address of MAG and nonce of MAG is encrypted using the secret key shared between MN and MN-MAG1. Here, pre-sharing of nonce is performed by hashing the nonce of MN and MAG (N_{MN}, N_{MNMAG1}).

Step 2: After performing hand-off, solicitation is performed by MN with the new MAG.

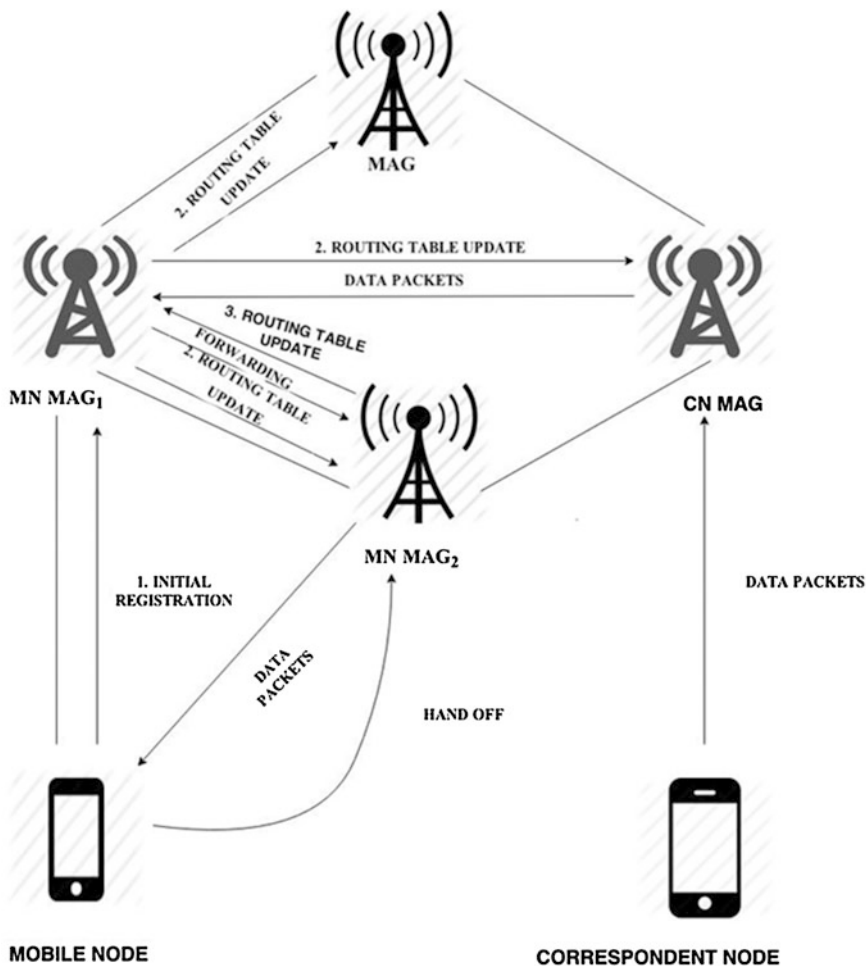


Fig. 2 Architecture of the proposed tokenized binding update scheme

$$MN \rightarrow MN-MAG_2: M_2 = MN_{ADDR}, MNMAG_{2ADDR}, E_{SK1}[PCoA_{MN}]$$

Step two states that the solicitation message sent by MN to MN-MAG₂ after performing the hand-off. Here, the old PCoA is sent to new MAG. The old PCoA of MN is encrypted using the secret key. The M_2 contains the solicitation of MN sent to new MAG for connection setup.

Step 3: Registration process is done between MN and MN-MAG₂

$$MN \rightarrow MN-MAG_2: M_3 = MN_{ADDR}, MNMAG_{2ADDR}, N_{MN}, E_{SK1}[PCoA_{MN}, N_{MN}], HASH[N_{MN}]$$

Subsequently, the MN performs the hand-off operation with new MAG (MN-MAG2). The MN sends the old PCoA address by encrypting the address with the secret key shared between MN and MN-MAG2.

Step 4: Proxy binding update (PBU) is performed after registration.

$$\text{MN-MAG2} \rightarrow \text{MN}:M_4 = \text{MN}_{\text{MAG2}}\text{ADDR}, \text{MN}_{\text{ADDR}}, N'_{\text{MN}}, N_{\text{MN}_{\text{MAG2}}}, E_{\text{PU-MN}} \\ \left[\text{PCoA}'_{\text{MN}}, N'_{\text{MN}}, N_{\text{MN}_{\text{MAG2}}} \right] \text{HASH}[N'_{\text{MN}} || N_{\text{MN}_{\text{MAG2}}}]$$

The new MAG sends new PCoA of MN to MN after completing the registration process with new MAG. It attaches the new nonce of MN (N'_{MN}) and its own nonce ($N_{\text{MN}_{\text{MAG2}}}$). These nonces are shared using hashing operation.

Step 5: Internally, the token (T_{MN}) is distributed among all MAGs in the network by incorporating the token in the routing table by the MN's MAG.

Step 6: PBU is sent to MN's old MAG.

$$\text{MN-MAG2} \rightarrow \text{MN-MAG1}:M_5 = \text{MN}_{\text{MAG2}}\text{ADDR}, \\ \text{MN}_{\text{MAG1}}\text{ADDR}, N_{\text{MN}_{\text{MAG2}}}, N'_{\text{MN}_{\text{MAG1}}}, \\ E_{\text{SK2}} \left[\text{PCoA}'_{\text{MN}}, N'_{\text{MN}_{\text{MAG1}}} \right] \text{HASH}[N_{\text{MN}_{\text{MAG2}}} || N'_{\text{MN}_{\text{MAG1}}}]$$

Here, the new MAG sends PBU to old MAG before updating the routing table among all MAGs in the network. The M_5 contains PBU sent to old MAG by new MAG for further communication. Here, the address PCoA'_{MN} is encrypted using the secret key shared between old MAG and new MAG and the nonce of both MAGs are concatenated using hash function.

Step 7: Proxy binding acknowledgement (PBA) is sent to MN-MAG₂ by MN-MAG₁.

$$\text{MN-MAG1} \rightarrow \text{MN-MAG2}:M_6 = \text{MN}_{\text{MAG1}}\text{ADDR}, \text{MN}_{\text{MAG2}}\text{ADDR}, N'_{\text{MN}_{\text{MAG2}}}, N'_{\text{MN}_{\text{MAG1}}}, \\ E_{\text{SK2}} \left[\text{PCoA}'_{\text{MN}}, N'_{\text{MN}_{\text{MAG1}}} \right] \text{HASH}[N'_{\text{MN}_{\text{MAG2}}} || N'_{\text{MN}_{\text{MAG1}}}]$$

Subsequently, step seven sends response for PBU as PBA, which contains the new address and the new nonce of new MAG generated by old MAG (PCoA'_{MN} , $N'_{\text{MN}_{\text{MAG2}}}$, and $N_{\text{MN}_{\text{MAG1}}}$), respectively. The nonce of both MAG is hashed ($\text{HASH}[N'_{\text{MN}_{\text{MAG2}}} || N_{\text{MN}_{\text{MAG1}}}]$) and PCoA'_{MN} and $N'_{\text{MN}_{\text{MAG1}}}$ are encrypted using the secret key ($E_{\text{SK2}}[\text{PCoA}'_{\text{MN}}, N'_{\text{MN}_{\text{MAG1}}}]$).

Step 8: Message is exchanged between MAGs' of MN and CN

$$\text{CN-MAG} \rightarrow \text{MN-MAG1}:M_7 = \text{CN}_{\text{MAG}}\text{ADDR}, \text{MN}_{\text{MAG1}}\text{ADDR}, N_{\text{CN}}, N_{\text{CN}_{\text{MAG}}}, \\ \sigma_{\text{CN}}[\text{MSG}], \text{HASH}[N_{\text{MN}} || N_{\text{CN}}]$$

Finally, CN sends the data packet and digital signature directly to MN's old MAG because the routing table is not updated yet.

Step 9: MN-MAG₁ forwards the message packet to PCoA of MN.

$$\text{MN-MAG1} \rightarrow \text{MN-MAG2}: M_8 = \text{MN}_{\text{MAG1ADDR}}, \text{MN}_{\text{MAG2ADDR}}, \\ N_{\text{CN}}, N_{\text{CNMAG}}, \sigma_{\text{CN}}[\text{MSG}], \text{HASH}[N_{\text{MN}}||N_{\text{CN}}]$$

Probably, the old MAG forwards the message packet to new MAG by incorporating its address as source address.

Step 10: Message is finally passed to MN via MN-MAG₂.

$$\text{MN-MAG2} \rightarrow \text{MN}: M_9 = \text{MN}_{\text{MAG2ADDR}}, \text{MN}_{\text{ADDR}}, \\ N_{\text{CN}}, N_{\text{CNMAG}}, \sigma_{\text{CN}}[\text{MSG}], \text{HASH}[N_{\text{MN}}||N_{\text{CN}}].$$

4 Security Validation and Analysis

Section 4 focuses on security validation of the proposed scheme using automated validation of internet security protocols and applications (AVISPA)—the model checker [9]. Additionally, the informal security analysis is discussed here.

4.1 Formal Validation Using AVISPA

The security properties of any protocol are validated using the AVISPA tool. In AVISPA, the protocol is written in high-level protocol specification language (HLPSL), which is later converted to low level intermediate format (IF) using hlp2if as translator. Here, there are four backends which are used to trace attacks present in the network. The low-level IF language is passed to the following backends to trace the attack or safe summary of the protocol specified in HLPSL. (1) OFMC—On-the-fly model-checker [9, 10] is used to find the falsify protocol; estimate the knowledge of intruder, and efficient search heuristics. Here, the OFMC finds bounded number of session and falsify protocol using demand drive way. (2) CL-AtSe—constraint-logic-based attack searcher is used for constraint solving by performing [11] bounded session and falsify protocols and it is useful to trace the sequence of events. Here, the proposed scheme is written in HLPSL and validated for backend results of AVISPA. The simulation consists of the roles MN, MN-MAG1, MN-MAG2, CN, and CN-MAG. The attack validation results of the HLPSL for the proposed scheme using AVISPA backends are as follows:

- Figure 3 shows, OFMC backend summary that checks the bounded number of sessions and summarized as safe. Here, it shows the search time as 0.07 s, number of visited nodes as 14 nodes and the depth it reaches is 4 plies.

Fig. 3 Backend results of OFMC

```
% OFMC
% Version of 2006/02/13
SUMMARY
SAFE
DETAILS
BOUNDED_NUMBER_OF_SESSIONS
PROTOCOL
D:\Program Files\SPAN\testsuite\results\miniproject.if
GOAL
as_specified
BACKEND
OFMC
COMMENTS
STATISTICS
parseTime: 0.00s
searchTime: 0.07s
visitedNodes: 14 nodes
depth: 4 plies
```

- CL-AtSe states the bounded number of session using constraints solving and summarizes the proposed protocol as safe (as shown in Fig. 4). Subsequently, the number of analyzed state is 6, reachable state is 4, and the translation time is 0.04 s.

Fig. 4 Backend results of CL-ATSE

```
SUMMARY
SAFE
DETAILS
BOUNDED_NUMBER_OF_SESSIONS
TYPED_MODEL
PROTOCOL
D:\Program Files\SPAN\testsuite\results\miniproject.if
GOAL
As Specified
BACKEND
CL-AtSe
STATISTICS
Analysed : 6 states
Reachable : 4 states
Translation: 0.04 seconds
Computation: 0.00 seconds
```

4.2 Data Confidentiality

Data confidentiality is to provide [12] or check the confidentiality of the message while exchanging between the nodes. In the proposed scheme, the privacy of the data is checked while sharing the PCoA of MN to the old MAG. As shown in M_5 packet the address of MN is encrypted using the secret key shared between MN and old MAG ($MN_{MAG2ADDR}$, $MN_{MAG1ADDR}$, N_{MNMAG2} , N'_{MNMAG1} , $E_{SK2} [PCoA'_{MN}$, N'_{MNMAG1} , $HASH[N_{MNMAG2}||N'_{MNMAG1}]$). Here, the decryption is done using the same secret key, which is shared between MN and MN-MAG1, thus the intruder cannot change the PCoA of MN. Hence, the confidentiality of the packet is ensured in the proposed scheme.

4.3 False Binding Update Attack Prevention

False binding update is an attacker tries to send false or his address as BU to the legitimate user [13]. Hence, the false BU is prevented by encrypting the PCoA of MN using the public key of MN sent by new MAG (see message M_4). Consequently, the PBU is decrypted using the private key of the recipient. This is impossible for the intruder to know the private key of MN which is not shared among anyone.

4.4 Authentication

Authentication of a user plays an important role in network to identify the legitimist of the user. The mutual authentication can be achieved by the hash function, authentication code hash-based message authentication, and digital signature. Here, in the proposed scheme the CN sends data packets to MN via MAG using digital signature and hashing the nonce of MN and CN as follows: $M_9 = MN_{MAG2ADDR}$, MN_{ADDR} , N_{CN} , N_{CNMAG} , $\sigma_{CN} [MSG]$, $HASH[N_{MN}||N_{CN}]$. The nonce of MN and CN is secretly shared between the communicants as the process of mutual authentication. Here, the CN uses digital signature technique for sharing message packet.

4.5 Data Integrity

The consistency of the data packet is ensured between the sender and the receiver for data integrity [10, 14]. Integrity of a data packet is ensured or achieved using hash function. Thus, in the proposed scheme the integrity of the packets is achieved

during the exchange of PBU between MN, MN-MAG1, and MN-MAG2. Here, an intruder cannot hack the PCoA and the token of MN because of the random numbers such as N'_{MN} , N_{MNMAG2} . In case if an intruder tries to change the random number then the hash value changes, when the recipient performs hashing using same hash function. If the hash value changes then the recipient ignores the packet. Thus, the chance of modification by an intruder is not possible.

4.6 Man-in-the-Middle Attack Prevention

Man-in-the-middle attack is an attacker monitors and injects malicious packets in the channel [15]. Here, there is a private connection maintained by the attacker as the communicants communicate directly to each other. This attack is prevented using nonce and encryption method while sharing the packets. Thus, the interception of intruder is impossible.

4.7 Replay Attack Prevention

The data transmission is intercepted by the attacker and redirects it to the user as the legitimate user in replay attack. This attack is avoided through nonce. In the proposed scheme, the nonce is used when updates and acknowledgments are shared. As shown in steps 6 and 7, the nonce of the MAG's such as N'_{MNMAG2} , N_{MNMAG1} , N_{MNMAG2} , N'_{MNMAG1} are used for updating PCoA of MN and PBA via MAGs. Additionally, the nonce is generated and updated at the recipient side for sharing communication.

5 Performance Evaluation

The performance of the proposed scheme is analyzed and compared with the existing four PMIPs in the current section. In conventional PMIPv6, the location updates of MN and message transfer are sent through the centralized feature LMA. Except fully distributed PMIPv6, the location update of MN is through LMA. In fully distributed environment, the location update query, i.e., PBQ is distributed among all MAGs in the network. The respective MAG sends PBU to the CN via MAG. In our proposed scheme, the multicasting of query exchange and location update control packets is avoided. Here, the location update is incorporated in the routing table and it is shared among all MAGs by the MN's MAG. The total cost [16] is the sum of connection cost and data delivery cost (Table 2).

In the proposed scheme, when MN initially registers with MAG the token of MN is incorporated in the routing table and shared among all the MAGs in the network.

Table 2 Variables used for performance evaluation

Variables	Description
t_{m-1}, t_{m-m}	Transmission time between MAG's of CN and MN to LMA and MAGs, respectively
$d_{mm}, d_{cm}, d_{m-1}, d_{m-m}$	Transmissions cost and hop count of data transfer between MN to MN-MAG, CN to CN-MAG, MAGs to LMA, MAG of MN, and CN to MAG, respectively

Hence, the cost of sharing routing table is $R_t(n_{m-1})$. Consequently, the response contains the token of MN for verification is sent by the respective CN via MAG (because the token is preshared between MN and CN). Thus, the cost of token response is $R_{tr} \log n_h$. So, the connection cost of proposed scheme (CC_{PS}) is mentioned as

$$CC_{PS} = C_{setup} + C_p(2t_{m-m}) * n_m + R_t(n_{m-1}) + R_{tr} \log n_h \tag{1}$$

The data is delivered to MN via MAGs. Thus, the CN gets the location update of MN from the cache. So, CN forwards the message to MN via MAG. The data delivery cost of proposed scheme (DC_{PS}) is expressed as follows,

$$DC_{PS} = d_s(d_{cm} + 2d_{m-m} + d_{mm}) + R_{tr} \log n_h \tag{2}$$

Figures 5 and 6 exhibits the comparison of number of hosts per MAG and number of hops between the existing schemes and PMIPv6, localized routing for PMIPv6, partially distributed PMIPv6, fully distributed PMIPv6, and the proposed scheme. The cost of number of hosts is proportional to the binding cache lookup

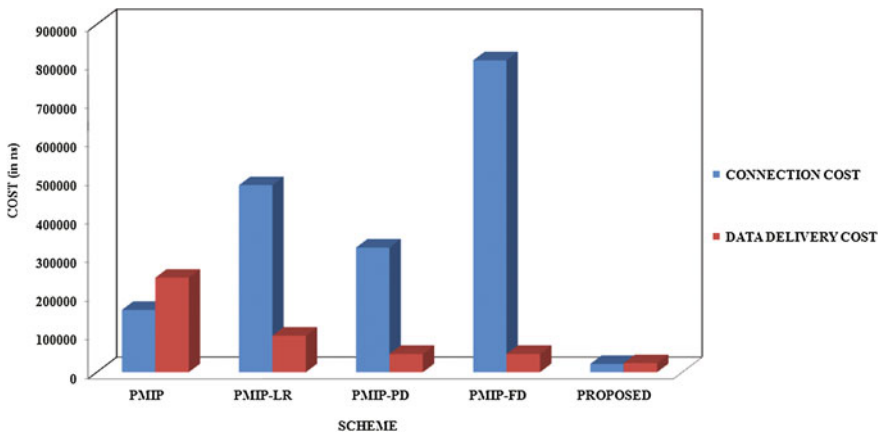


Fig. 5 Comparison of total cost with respect to number of hosts per MAG

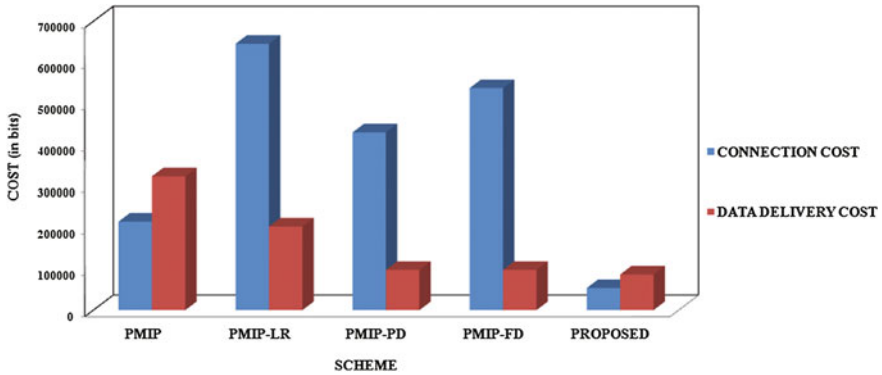


Fig. 6 Comparison of total cost with respect to number of hops

and update for finding the location of MN. Figure 5 shows that the fully distributed PMIPv6 and PMIPv6-LR scheme has high connection cost when compared with other scheme. The fully distributed PMIPv6 has high connection cost since the PBQ control packet is sent to all MAGs in the network to know the location update of MN. In addition, the connection cost of Localized Routing PMIPv6 is second highest because extra control packets such as LRI and LRA are shared to find the optimal path between the communicants and the LMA for further communication between them. Nevertheless, the proposed scheme shows significant reduction in connection cost as well as data delivery cost since, the additional control packets are avoided. The token response is sent by the respective MAG and unwanted lookups to know the token are prevented because the token is encrypted using private key of the recipient.

Figure 6 depicts the comparison of number of hops required for initial connection setup and transmitting data between the existing and proposed scheme. Here, the PMIP-FD has high connection cost because multicasting of control packets is present and the data delivery cost of PMIP is high since, the PBU and PBA is sent via LMA to CN and vice versa. However, the proposed scheme shows minimal number of hops due to sharing of token via routing table distribution. Additionally, the control plane and data plane are directly shared between the communicants.

Figure 7 shows the comparison of packet size among the scheme. Here, the packet size of PMIP-PD and PMIP-FD is similar since both share PBQ packets to LMA and MAG, respectively. However, the proposed scheme shows least packet size since the request for location update and response is not present. It contains PCoA of MN in routing table and it is encrypted using the recipient’s private key, thus the recipient only can view the token and address of MN.

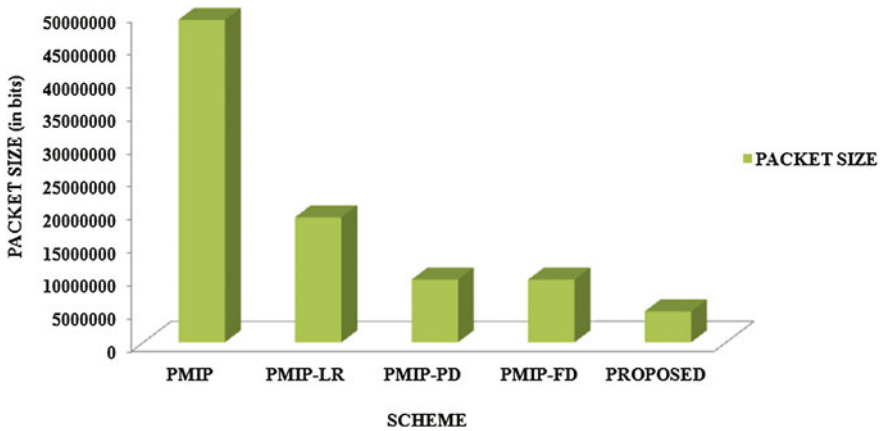


Fig. 7 Total cost with respect to packet size

6 Conclusion

In this paper, a tokenized binding update is proposed by reducing the cost while increasing the efficiency and secrecy of the scheme. Here, to identify the location of a MN the token is incorporated in routing table and it is distributed among all the MAGs in the network. The routing table is encrypted using the private key of the recipient. Thus, the respective node can only respond with the token. Further, as there is no exchange of extra control packets such as PBU, PBA, PBQ, and PQA, the efficiency of the proposed scheme is also increased. From the numerical analysis, the proposed scheme shows significant reduction in data and control packet exchange. The security of the scheme is validated using AVISPA—model checker.

References

1. Mathi S, Valarmathi ML. A secure and decentralized registration scheme for IPv6 network-based mobility. *Int J Eng Technol.* 2013;5:5.
2. Elgoarany K, Eltoweissy M. Security in mobile IPv6: a survey. *Inf. Secur. Tech. Rep.* 2007;12(1):32–43.
3. Gundavelli S, Leung K, Devarapalli V, Chowdhury K, Patil B. Proxy mobile IPv6. RFC 5213, August 2008.
4. Liebsch M, Jeong S. Proxy Mobile IPv6 (PMIPv6) localized routing problem statement (2011).
5. Lei J, Fu X. Evaluating the benefits of introducing PMIPv6 for localized mobility management. In: *Wireless Communications and Mobile Computing Conference, 2008. IWCMC'08. International.* IEEE, 2008.
6. Krishnan S, et al. Localized routing for proxy mobile IPv6. draft-ietf-netext-pmIP-lr-01 (2010).

7. Bernardos CJ, De la Oliva A, Giust F. A PMIPv6-based solution for distributed mobility management. 2013.
8. Giust F, Bernardos CJ, de la Oliva A. Analytic evaluation and experimental validation of a network-based IPv6 distributed mobility management solution; 2014.
9. Viganò L. Automated security protocol analysis with the AVISPA tool. *Electron Notes Theor Comput Sci.* 2006;155:61–86.
10. Mathi S, Valarmathi ML. An efficacious and secure registration for internet protocol mobility. *Def Sci J.* 2013;63 5:502–507.
11. Olsen, AA. Extended AnB for Web Services; 2012.
12. Aura Tuomas. *Mobile IPv6 Security*. Security Protocols. Berlin: Springer; 2004.
13. Alsaliyh WAHA, Alsayfi MSS. Integrating identity-based encryption in the return routability protocol to enhance signal security in mobile IPv6. *Wirel Pers Commun.* 2013;68 3:655–669.
14. Ali-Ahmad H, et al. Comparative performance analysis on dynamic mobility anchoring and proxy mobile IPv6. In: 15th international symposium on wireless personal multimedia communications (WPMC), IEEE; 2012.
15. Moravejosharieh A, Modares H, Salleh R. Overview of mobile IPv6 security. In: Third international conference on intelligent systems, modelling and simulation (ISMS), IEEE; 2012.
16. Kim, JI, Koh SJ. Distributed mobility management in proxy mobile IPv6 using hash function. In: International conference on information networking (ICOIN), IEEE; 2013.

VLSI Implementation and Analysis of Kidney Stone Detection from Ultrasound Image by Level Set Segmentation and MLP-BP ANN Classification

K. Viswanath and R. Gunasundari

Abstract In recent years, there is an increase in the count of individuals suffering from kidney abnormalities. Kidney stone prevalence has increased both in men and women, across all age groups, racial/ethnic groups. According to the recent statistics report, the vulnerability of kidney stone abnormality even surpasses the effects of several chronic diseases, including diabetes, coronary heart disease, and stroke. This inflicts a need for early detection and accurate diagnosis of kidney stones. Urologists undergo enormous stress at the time of surgery related to stone removal in order to precisely locate the stones, which may be scattered. Kidney abnormality may also indicate the formation of stones, cysts, cancerous cells, and blockage of urine, etc. Currently available scanning approaches in hospitals such as Ultrasound (US) imaging, MRI, and CT scanners, do not help in easy and quick diagnosis of the minute stones in the initial stage, as well as multiple stones present in the scanned images due to low contrast and speckle noise. Thus, to remove speckle noise in ultrasound images preprocessing is applied. Reaction and diffusion (RD) level set segmentation is applied two times, first to the segment kidney portion and second to segment the stone portion. The extracted region of the kidney stone after segmentation is applied with Symlets, Biorthogonal, and Daubechies lifting scheme wavelet subbands with higher vanishing moments to extract energy levels. These energy levels give an indication about the presence of stone, which significantly vary from that of normal energy level. These energy levels are trained by multilayer perceptron (MLP) and back propagation (BP) ANN to identify the type of stone with an accuracy of 97.8 % and real time implementation is done using Verilog on Vertex-2Pro FPGA.

K. Viswanath (✉)

Pondicherry Engineering College, Pondicherry, India

e-mail: viswa_kv@pec.edu

R. Gunasundari

Department of ECE, Pondicherry Engineering College, Pondicherry, India

e-mail: gunasundari@pec.edu

© Springer India 2016

S.S. Dash et al. (eds.), *Artificial Intelligence and Evolutionary Computations in Engineering Systems*, Advances in Intelligent Systems and Computing 394, DOI 10.1007/978-81-322-2656-7_19

209

Keywords Kidney stone database • RD level set segmentation • Multilayer perceptron (MLP) and back propagation (BP) • Lifting scheme wavelet transform • Ultrasound imaging • Verilog and Vertex-2Pro FPGA

1 Introduction

Kidney stone disease is one of the risks for life throughout the world, and majority of people with stone formation in kidney initially do not notice it as disease and it damages the limbs (organ) slowly. Many people are affected by continual kidney failure due to diabetes mellitus and hypertension, glomerulonephritis, etc. Since kidney malfunctioning can be life threatening, diagnosis of diseases in the earlier stages is crucial. Currently available options include Ultrasound (US) image which is one of the noninvasive, low cost, widely used imaging techniques for diagnosing kidney diseases [1]. Shock wave lithotripsy (SWL), percutaneous nephrolithotomy (PCNL), and relative super saturation (RSS) are the techniques to test urine. The Robertson risk factor algorithms (RRFA) are open and are used for laparoscopic surgery; these algorithms are reserved for uncommon [2]. special cases. Hyaluronan is a large (>106 Da) linear glycosaminoglycan composed of repeating units of glucuronic acid (GlcUA) and *N*-acetyl glucosamine (GlcNAc) disaccharides [3]. Hyaluronan has a central role in a number of processes that can ultimately lead to renal stone disease, including urine concentration, uric acid, salt form crystal, crystallization inhibition, crystal retention, magnesium ammonium phosphate, and amino acid.

Tanzila Rahman, Mohammad Shorif Uddin proposed reduction of speckle noise and segmentation from US image is discussed. It not only detects the kidney region, but also enhances the image quality [1]. Wan Mahani Hafizah proposed kidney US images were divided into four dissimilar categories: normal, bacterial infection and cystic disease, kidney stones, based on gray-level cooccurrence matrix (GLCM). From these categories, doctors identify whether the kidney is normal or abnormal [4]. Gladis Pushpa had proposed hierarchical self-organizing map (HSOM) for brain tumours using segmentation, wavelets packets, and the results were correct up to maximum of 97 % [5]. Norihiro Koizumi proposed high-intensity focused ultrasound (HIFU) technique, used for destroying tumours and stones [6, 7]. K. Viswanath and R. Gunasundari proposed a content descriptive of multiple stone detection using level set segmentation, wavelets processing for identification of kidney stone, and artificial neural network (ANN) for classification and the results indicate that a maximum accuracy of 98.66 % only [8]. The MLP-BP ANN is found to have better performance in terms of accuracy with 92 %, speed is 0.44 s and is very sensitive [9, 10]. The noninvasive combination of renal using pulsed cavitation US therapy proposed shock wave lithotripsy (ESWL) has become a standard for the treatment of calculi located in the kidney and ureter [11]. P.R. Tamilselvi proposed seeded region growing based on segmentation and classification of kidney images

with stone sizes using computer-aided diagnosis system [12]. Mohammad E. Abou EI-Ghar proposed location of urinary stones with unenhanced computed tomography (CT) using half radiation (low) dose compared with the standard dose and of the 50 patients, 35 patients had a single stone while the rest of them had multiple stones [13]. In order to solve the local minima and segmentation problem Thord Andersson, Gunnar Lathen proposed modified gradient search and level set segmentation [14]. For 3-D detection of kidneys and their pathology in real time, the Emmanouil Skounakis proposed *templates-based technique* with accuracy of 97.2 % and abnormalities in kidneys at an accuracy of 96.1 % [7]. For sharpening and smoothening of 2-D images, the Gabor function is used and also to achieve optimality both in time and frequency resolution [15]. Xinjian Chen proposed finite element method-based 3-D tumor growth prediction using longitudinal kidney tumor images [16]. For calculating the depth of shock wave scattering by a kidney stone in water, the Neil R. Owen proposed pressure finding in fluid by using linear elastic theory [17]. Dirk J. Kok proposed that prevalence of stone formation due to urinary, epidemiological is based on pH values [18]. Dinesh S. Datar proposed that the segmentation of required portion is done by initial seed selection, growing, and region merging which do not use any edge detection [19]. Multilayer Perceptron and back propagation implementation on FPGA and ASIC design is carried out by Cyril Prasanna Raj P [20].

This research paper proceeds as follows: In Sect. 2, the problem statement is defined, Sect. 3 describes the proposed method, in Sect. 4 image segmentation to locate the kidney stone is described, in Sect. 5 calculation of energy optimization for segmentation is described, in Sect. 6 wavelets based energy extraction is described, Sect. 7 describes the artificial neural networks classifiers used, in Sect. 8 experimental results are discussed and in the last section we conclude the paper with future work.

2 Problem Statement

Kidney malfunctioning can be life threatening, thus detection of kidney stone in the earlier stages is crucial. In order to carry out the surgical operation to remove kidney stone, it is important to locate the kidney stone. The ultrasound images of kidney contain speckle noise and are of low contrast, which makes the detection of kidney abnormalities a challenging task. As a result, the doctors may have problems in identifying the small kidney stones and their type properly. To address this issue, a modified level set segmentation, to identify location of the stone, lifting scheme wavelets subbands to extract the energy levels of the stone and MLP-BP ANN algorithms for classification is proposed and analyzed [21].

3 Methodology

Figure 1 shows the overall block diagram of the proposed method. It consists of the following blocks: kidney image database, image preprocessing, image segmentation, wavelet processing, and ANN Classification.

3.1 Kidney Image Database

The 500 US kidney images of both normal and abnormal kidneys are collected from different hospitals from different patients and are stored in a database. One of the images is taken from the database and subjected to stone detection.

3.2 Image Preprocessing

The acquired ultrasound (US) image consists of speckle noise and is of low contrast. Due to this, the image quality may not be good for analyzing. For surgical operations, it is very important to identify the location of kidney stone. To overcome

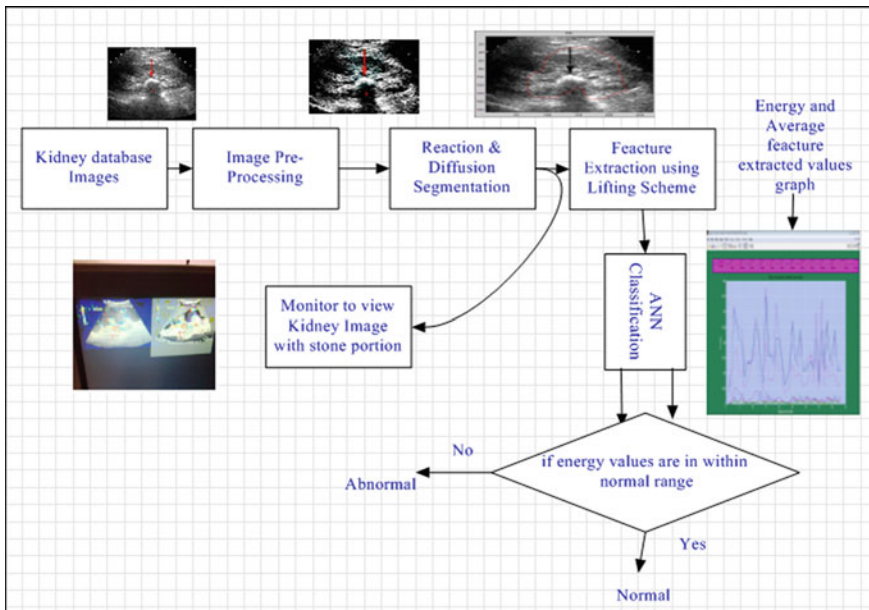
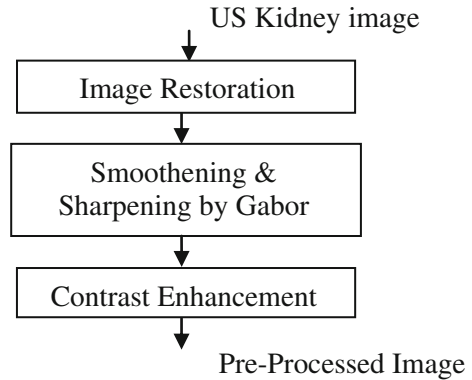


Fig. 1 Proposed block diagram for kidney stone detection

Fig. 2 Preprocessing of kidney image



speckle noise and low contrast, preprocessing of US image needs to be done. Figure 2 shows preprocessing of US image, which consists of the following steps:

- Image restoration
- Smoothing and sharpening
- Contrast enhancement

3.2.1 Image Restoration

The purpose of image restoration is to reduce the degradations that are caused during acquisition of US scanning. In this system for proper orientation, level set function is used.

$$f(x) = \begin{cases} \max(k, 0), & \text{if } a(x, y) < G(x, y) \\ \min(k, 0), & \text{otherwise} \end{cases} \quad (1)$$

By the use of planar curve motion, curve smoothers, shrinks will eventually disappear [1]. Thus Merriman and Sethian proposed evolution between $\max(k, 0)$ and $\min(k, 0)$.

Where $a(x, y)$: Average intensity small neighborhood

$G(x, y)$: median in the same neighborhood

3.2.2 Smoothing and Sharpening

To obtain optimal resolution in both spatial and frequency domains, Gabor filter is used which acts as band-pass filter for the local spatial frequency distribution [6]. Image smoothing and removal of noise is done by convolution operator. The

standard deviation of the Gaussian function can be varied by adjusting the degree of smoothing.

3.2.3 Contrast Enhancement

To improve the contrast and to obtain uniform intensity, histogram equalization is used. This approach can be used on whole image or part of an image. In this system, enhancing the contrast of the images is done by transforming the values in an intensity image, such that the histogram of the output image approximately matches a specified histogram. The output signal is of same data type as the input signal.

4 Image Segmentation

Figure 3 shows the level set segmentation method used, first to segment the location of kidney from US scanned image and the segmented kidney portion output is applied again for level set segmentation to segment only stone portion, so that processing time will be reduced and image storage memory utilization is also reduced. Proposed work

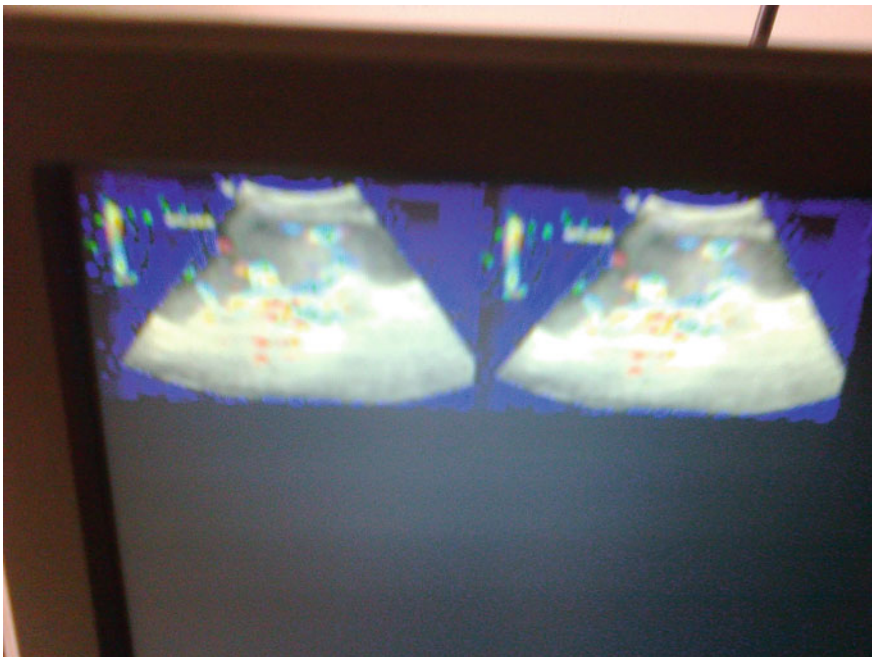


Fig. 3 Level set segmentation of kidney and stone detection on FPGA

consists of two modified gradient descent methods. First is using a momentum term and second is based on resilient propagation (R_{prop}) term. The intention of the segmentation is to overcome the difficulties involved in energy function. The energy function depends on the properties of the image such as gradients, curvatures, intensities, and regularization terms, e.g., smoothing constraints. These are simple, but effective modifications of the basic method and are directly compatible with any type of level set implementation. The first proposed method is based on a modification, which essentially adds a momentum to the motion in solution space [2, 22]. This simulates the physical properties of momentum and often allows the search to disregard local optima and take larger steps in positive directions. In order to avoid the typical problems of gradient descent search, R_{prop} provides a modification, which uses individual adaptive step sizes and the signs of the gradient components.

4.1 Momentum Term

Spinning to gradient descent with momentum will adopt the machine learning community and choose a search vector according to

$$\mathbf{a}_1 = -\eta(1 - w)\nabla f_1 + w\mathbf{a}_{1-1} \quad (2)$$

where η is the *learning rate* and $\omega \in [0, 1]$ is the *momentum*. Note that $w = 0$ gives standard gradient descent $\mathbf{a}_1 = -\eta\nabla f_1$, while $w = 1$ gives “infinite momentum” $\mathbf{a}_1 = \mathbf{a}_{1-1}$.

4.2 R_{prop} Term

The disadvantages of standard gradient descent (SGD) is overcome by incorporating adaptive stepsizes ∇_1 called *update-values* in which each dimension will have one update value, i.e., $\dim(\nabla_1) = \dim(\mathbf{x}_1)$. The gradient size is never used in R_{prop} . The update rule considers only the signs of the partial derivatives. Another advantage of R_{prop} , which is very important in practical use, is the stoutness of its parameters; R_{prop} will work out of the box in many applications using only the standard values of its parameters [23, 24].

We will now describe the R_{prop} algorithm briefly; however, for implementation details of R_{prop} we refer to [25, 26]. For R_{prop} , we choose a search vector \mathbf{s}_1 according to

$$\mathbf{s}_1 = -\text{sign}(\nabla f_1) * \nabla_1 \quad (3)$$

where ∇_1 is a vector containing the current update-values and $\text{sign}(\cdot)$ the element-wise sign function.

4.3 Reaction and Diffusion Level Set Segmentation

The level set function (LSF) always considers the zero level set on object contour, with the same initial zero level set, different embedded LSF will give the same final stable interface for phase transition theory [18, 24]. Reaction diffusion equation is derived by adding a diffusion term into the conventional LSE equation. Such an introduction of diffusion to LSE will make LSE stable without reinitialization.

The RD equation is constructed by adding a diffusion term into the conventional LSE equation. Such an introduction of diffusion to LSE will make LSE stable without reinitialization. The diffusion term

“ $\varepsilon\Delta$ ” added to the LSE equation in Eq. (2) we get the following equation for RD.

$$\begin{cases} \phi_t = \varepsilon\Delta\phi - \frac{1}{\varepsilon}L(\phi), x \in \Omega \subset R^n \\ \text{Subject} \longrightarrow \phi(x, t = 0, \varepsilon) = \phi_0(x) \end{cases} \quad (4)$$

where ε is a small positive constant, $L(\phi)$ for PDE-based LSM or $L(\phi) = -F \delta(\phi)$ for variational LSM, Δ is the laplacian operator defined by $\Delta(\cdot) = \sum_{i=1}^n \frac{\partial^2(\cdot)}{\partial x_i^2}$ and $\phi_0(x)$ is the initial LSF. Eq. (4) has two dynamic processes, the diffusion term $\varepsilon\Delta\phi$ gradually regularizes the LSF to be piecewise constant in each segment domain Ω_i and the reaction term “ $-\varepsilon^{-1}L(\phi)$ ” forces the final stable solution of Eq. (4) to $L(\phi) = 0$, which determines Ω_i .

Figure 3 shows the FPGA output displayed in the monitor through VGA, the first image is the kidney portion and second image is kidney with stone indicated with red color

5 Lifting Scheme Wavelets Processing

The segmented image (only stone) from the previous block is sent to the lifting scheme wavelet processing block. It consists of Daubechies filter (Db12), Symlets filter (sym20), and Biorthogonal filter (bio3.7, bio3.9, and bio4.3). Daubechies filter (Db12) in this is the number 12 refers to the number of vanishing moments. Basically, the higher the number of vanishing moments, the smoother the wavelet (and longer the wavelet filter) and the length of the wavelet (and scaling) filter is two times that number [5]. Symlets filter (sym20) extracts features of kidney image and analyze discontinuities and abrupt changes contained in signals, one of the 20th-order Symlets wavelets is used. Biorthogonal filter’s (bio3.7, bio3.9, and bio4.4) wavelet energy signatures were considered and averages of horizontal and vertical coefficients’ details were calculated. Figure 4 shows each filter will give different energy levels or energy features. These energy features will show significant difference, if there is any stone present in the particular region or location. The identification of type of stone is described in the next section.

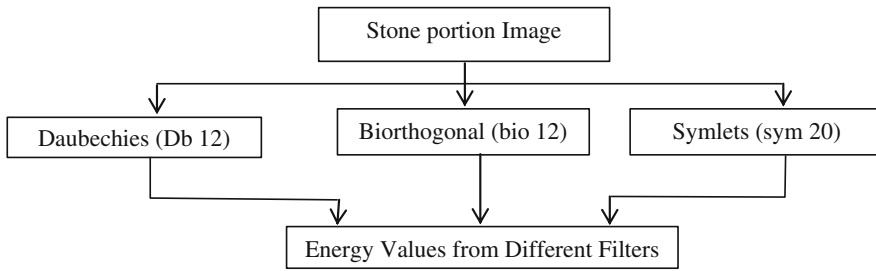


Fig. 4 Wavelet filters to extract energy features

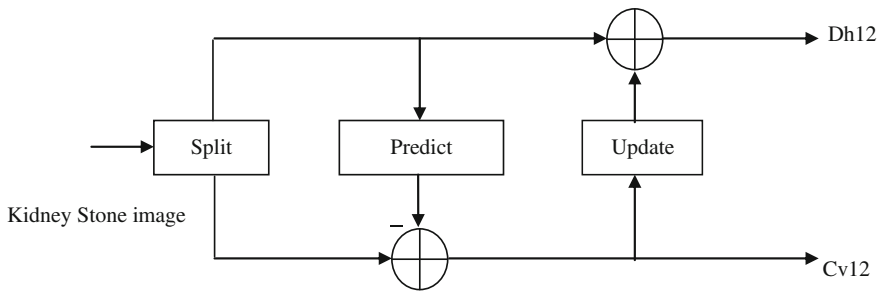


Fig. 5 2-D lifting scheme DWT

In 2-D lifting scheme wavelets transformation consists of update and predictor to get Db12, sym20, bio3.7, bio3.9, and bio4.3 as shown in Fig. 5.

The equations of predict and update is given as

$$d_i^1 = \alpha(x_{2i} + x_{2i+2}) + x_{2i+1} \tag{5}$$

$$a_i^1 = \beta(d_i^1 + d_{i-1}^1) + x_{2i} \tag{6}$$

$$d_i^2 = \gamma(a_i^1 + a_{i+1}^1) + d_i^1 \tag{7}$$

$$a_i^2 = \delta(d_i^2 + d_{i-1}^2) + a_i^1 \tag{8}$$

$$d_i = \frac{d_i^2}{\epsilon} \tag{9}$$

$$a_i = \epsilon a_i^2 \tag{10}$$

where x_{2i} and x_{2i+2} are even pixels, x_{2i+1} are odd pixels of stone image and $\alpha, \beta, \gamma, \delta, \epsilon$ are the constants.

6 ANN Classification

In ANN Classification two architectures are used namely, multilayer perceptron and back propagation, which are described in detail in the following sections.

6.1 Multilayer Perceptron (MLP)

A multilayer perceptron is a feed-forward artificial neural network algorithm that maps sets of energy values obtained from wavelets subbands energy extraction shown in the Table 1. These energy values are fed to input layer and multiplied with initial weights as in Eq. (13). The back propagation is a modified version of linear perceptron in which it uses three or more hidden layers with nonlinear activation function. The back propagation is the most widely applied learning algorithm for multilayer perceptron in neural networks, and it employs gradient descent to minimize the squared error between the network output value and desired output value as in Eq. (14). These error signals are used to calculate the weight updates, which represent power of knowledge learnt in the network [27]. Multilayer perceptron with back propagation (MLP-BP) are the main algorithms. Based on the literature survey, MLP-BP algorithm was found to be better than the others in terms of accuracy, speed, and performance [28].

Figure 6 shows the phases involved in ANN are forward phase and backward phase. In back propagation, weights are updated after each pattern and by taking one pattern m at a time as follows:

6.1.1 Forward Phase

Apply the pattern $X_j^{(l)}$ to the input layer and propagate the signal forward through the network until the final outputs X_j^L have been calculated for each i and L

$$X_j^{(l)} = \theta(s_j^{(l)}) = \theta\left(\sum_{i=0}^{D(L-1)} x_j^i w_j^i + w_j^l\right) \quad (11)$$

where $D(L-1)$ is the number of neurons in layer $(L-1)$, $X_j^{(l-1)}$ output of the j th neuron in the $(l-1)$ th layer, $W_{ij}(l)$ synaptic weight contained in the current neuron, $W_{ij}(l)$ current neuron's bias weight, $X_j^{(l)}$ output of the current neuron.

Table 1 Enlarged table of the table in the GUI of lifting scheme wavelets

Dh12 Dh1 average	Dh12 cV energy	Sym20 Dh1 average	Sym20 cV energy	rbio3.7 Dh1 average	rbio3.7 cD energy	rbio3.7 cV energy	rbio3.7 Dh1 average	rbio3.9 cD energy	rbio3.9 cV energy	rbio3.9 average	rbio4.4 Dh1 average	rbio4.4 cH energy	rbio4.4 cV energy
0.0026	5.5953e-05	0.0026	5.5953e-05	0.0052	1.3895e-04	1.6450e-04	0.0043	1.0764e-04	1.0719e-04	0.0039	1.7720e-04	9.9153e-05	9.0838e-05
0.0059	7.0192e-05	0.0059	7.0192e-05	0.0127	2.2286e-04	1.8849e-04	0.0128	1.7324e-04	1.5039e-04	0.0129	3.9994e-04	1.6002e-04	1.3280e-04
0.0163	9.1629e-04	0.0163	9.1629e-04	0.0316	0.0010	0.0021	0.0306	7.6544e-04	0.0023	0.0303	0.0051	6.9376e-04	0.0022
0.0179	3.9806e-04	0.0179	3.9806e-04	0.0255	5.4659e-04	4.8874e-04	0.0263	3.9515e-04	3.5478e-04	0.0267	0.0051	3.5862e-04	5.7644e-04
0.0093	2.7436e-04	0.0093	2.7436e-04	0.0249	6.8200e-04	9.5594e-04	0.0214	5.2108e-04	8.9330e-04	0.0198	0.0031	4.9557e-04	9.0662e-04
0.0111	9.0990e-04	0.0111	9.0990e-04	0.0239	5.5269e-04	0.0033	0.0197	4.1572e-04	0.0023	0.0179	0.0031	3.8182e-04	0.0019
0.0050	1.3049e-04	0.0050	1.3049e-04	0.0094	5.6388e-04	3.4976e-04	0.0087	3.9534e-04	2.5024e-04	0.0085	7.2749e-04	3.4186e-04	2.1581e-04
0.0073	7.8642e-05	0.0073	7.8642e-05	0.0136	2.6317e-04	2.4022e-04	0.0132	1.8109e-04	1.5338e-04	0.0133	8.1203e-04	1.5963e-04	1.2771e-04
0.0105	2.3515e-04	0.0105	2.3515e-04	0.0137	7.1012e-04	4.0684e-04	0.0131	5.2176e-04	3.7809e-04	0.0133	0.0013	4.5959e-04	4.0670e-04
0.0145	1.3983e-04	0.0145	1.3983e-04	0.0154	6.6207e-04	3.3536e-04	0.0144	4.8498e-04	2.4507e-04	0.0184	0.0018	4.3049e-04	2.1859e-04
0.0173	2.1550e-04	0.0173	2.1550e-04	0.0278	6.2009e-04	4.9155e-04	0.0262	4.7615e-04	4.1534e-04	0.0260	0.0042	4.4141e-04	4.0481e-04
0.0128	3.7797e-04	0.0128	3.7797e-04	0.0256	5.8045e-04	5.3523e-04	0.0234	4.5160e-04	5.7497e-04	0.0238	0.0038	4.1888e-04	6.8299e-04
0.0074	0.0018	0.0074	0.0018	0.0132	8.6715e-04	0.0043	0.0133	6.7642e-04	0.0040	0.0140	8.5301e-04	6.2365e-04	0.0040
0.0043	2.0368e-04	0.0043	2.0368e-04	0.0072	6.4413e-04	4.8808e-04	0.0066	5.2519e-04	3.7235e-04	0.0065	4.2114e-04	4.8302e-04	3.3005e-04
0.0204	3.3482e-04	0.0204	3.3482e-04	0.0379	7.3661e-04	9.6556e-04	0.0353	5.1190e-04	8.2002e-04	0.0344	0.0043	4.3896e-04	7.5465e-04
0.0077	0.0012	0.0077	0.0012	0.0169	5.8343e-04	0.0030	0.0158	4.5069e-04	0.0028	0.0153	6.8829e-04	4.1780e-04	0.0027
0.0080	1.7951e-04	0.0080	1.7951e-04	0.0161	5.8455e-04	3.1453e-04	0.0155	4.8010e-04	2.9501e-04	0.0154	0.0017	4.4850e-04	3.1878e-04
0.0079	2.9445e-04	0.0079	2.9445e-04	0.0151	4.5209e-04	0.0010	0.0134	3.6543e-04	9.2231e-04	0.0126	0.0011	3.3598e-04	8.9855e-04
0.0171	5.9446e-04	0.0171	5.9446e-04	0.0325	0.0010	8.2026e-04	0.0214	8.0706e-04	8.5152e-04	0.0180	0.0016	7.2994e-04	9.7450e-04
0.0111	1.3944e-04	0.0111	1.3944e-04	0.0224	4.9967e-04	3.9034e-04	0.0211	3.9642e-04	3.4776e-04	0.0202	0.0021	3.7177e-04	3.4225e-04
0.0074	2.6753e-04	0.0074	2.6753e-04	0.0153	3.5545e-04	8.2306e-04	0.0141	2.8304e-04	7.1102e-04	0.0136	0.0011	2.7166e-04	8.4002e-04
0.0036	2.0845e-04	0.0036	2.0845e-04	0.0065	5.9656e-04	5.5595e-04	0.0061	4.5940e-04	4.5326e-04	0.0061	4.0954e-04	4.1321e-04	4.4339e-04
0.0048	1.6351e-04	0.0048	1.6351e-04	0.0083	6.4050e-04	4.1405e-04	0.0086	5.0618e-04	3.0850e-04	0.0085	5.2424e-04	4.5489e-04	1.7296e-04
0.0056	8.0388e-05	0.0056	8.0388e-05	0.0106	1.5185e-04	2.4317e-04	0.0115	9.1844e-05	1.8853e-04	0.0139	6.2159e-04	7.8351e-05	1.7249e-04
0.0128	2.9260e-04	0.0128	2.9260e-04	0.0255	2.4498e-05	0.0019	0.0272	1.0831e-05	0.0024	0.0258	7.3530e-04	7.3841e-06	0.0022
0.0087	6.3554e-04	0.0087	6.3554e-04	0.0157	0.0013	0.0021	0.0143	5.8765e-04	0.0014	0.0146	0.0018	3.7878e-04	0.0012

(continued)

Table 1 (continued)

Dh12 average	Dh12 cV energy	Sym20 Dh1 average	Sym20 cV energy	rbio3.7 Dh1 average	rbio3.7 cD energy	rbio3.7 cV energy	rbio3.7 Dh1 average	rbio3.9 cD energy	rbio3.9 cV energy	rbio3.9 cV average	rbio4.4 Dh1 average	rbio4.4 cH energy	rbio4.4 cV energy
0.0099	8.3973e-04	0.0099	8.3973e-04	0.0123	3.7739e-04	7.3807e-04	0.0163	1.9745e-04	9.0590e-04	0.0189	7.7251e-04	1.4336e-04	0.0010
0.0094	0.0011	0.0094	0.0011	0.0219	0.0015	0.0028	0.0239	0.0010	0.0024	0.0247	0.0015	8.7336e-04	0.0024
0.0059	2.5405e-04	0.0059	2.5405e-04	0.0112	4.3833e-04	7.4134e-04	0.0105	2.6179e-04	6.1060e-04	0.0105	6.9152e-04	2.1206e-04	5.9138e-04
0.0063	7.7728e-04	0.0063	7.7728e-04	0.0124	6.3668e-04	0.0024	0.0112	4.0345e-04	0.0020	0.0109	0.0011	3.3200e-04	0.0019
0.0074	8.2789e-04	0.0074	8.2789e-04	0.0152	8.4256e-04	0.0020	0.0128	6.0219e-04	0.0019	0.0118	0.0011	5.2250e-04	0.0018
0.0167	4.1325e-04	0.0167	4.1325e-04	0.0156	5.3976e-04	4.7820e-04	0.0140	2.9495e-04	4.2729e-04	0.0136	0.0018	2.1938e-04	5.2332e-04
0.0069	5.5092e-04	0.0069	5.5092e-04	0.0122	0.0010	0.0018	0.0113	6.9704e-04	0.0016	0.0119	0.0012	5.8484e-04	0.0014
0.0148	9.2528e-04	0.0148	9.2528e-04	0.0298	8.8080e-04	0.0017	0.0214	5.8155e-04	0.0015	0.0163	0.0011	4.8485e-04	0.0016
0.0045	2.3998e-04	0.0045	2.3998e-04	0.0080	3.3799e-04	6.2947e-04	0.0069	2.5098e-04	5.5864e-04	0.0065	4.1366e-04	2.1907e-04	5.0073e-04
0.0169	0.0011	0.0169	0.0011	0.0336	5.8337e-04	0.0016	0.0241	3.8469e-04	0.0016	0.0182	8.5080e-04	3.4381e-04	0.0018
0.0056	8.0388e-05	0.0056	8.0388e-05	0.0106	1.5185e-04	2.4317e-04	0.0115	9.1844e-05	1.8853e-04	0.0139	6.2159e-04	7.8351e-05	1.7249e-04
0.0128	2.9260e-04	0.0128	2.9260e-04	0.0255	2.4498e-05	0.0019	0.0272	1.0831e-05	0.0024	0.0258	7.3530e-04	7.3841e-06	0.0022
0.0087	6.3554e-04	0.0087	6.3554e-04	0.0157	0.0013	0.0021	0.0143	5.8765e-04	0.0014	0.0146	0.0018	3.7878e-04	0.0010
0.0099	8.3973e-04	0.0099	8.3973e-04	0.0123	3.7739e-04	7.3807e-04	0.0163	1.9745e-04	9.0590e-04	0.0189	7.7251e-04	1.4336e-04	0.0012
0.0094	0.0011	0.0094	0.0011	0.0219	0.0015	0.0028	0.0239	0.0010	0.0024	0.0247	0.0015	8.7336e-04	0.0024
0.0059	2.5405e-04	0.0059	2.5405e-04	0.0112	4.3833e-04	7.4134e-04	0.0105	2.6179e-04	6.1060e-04	0.0105	6.9152e-04	2.1206e-04	5.9138e-04
0.0063	7.7728e-04	0.0063	7.7728e-04	0.0124	6.3668e-04	0.0024	0.0112	4.0345e-04	0.0020	0.0109	0.0011	3.3200e-04	0.0019

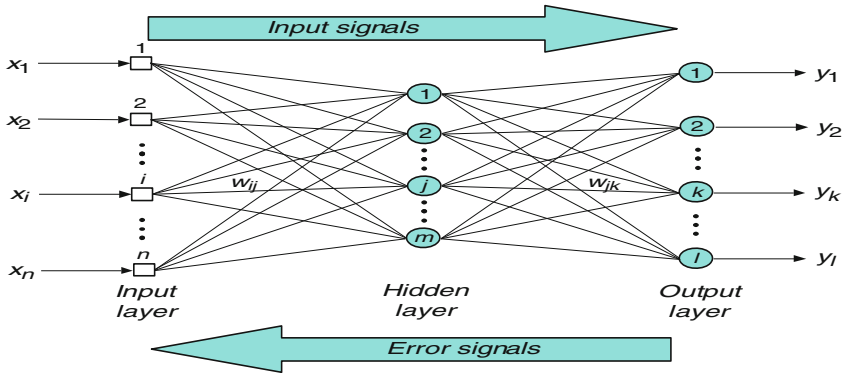


Fig. 6 Multilayer perceptron architecture

6.1.2 Backward Phase

In this phase, the weight and biases are updated according to the error gradient descent vector. After an input vector is applied during the forward computation phase, a network output vector is obtained. A target vector t is provided to the network, to drive the network’s output toward the expected targeted value [11, 28].

Starting with the output layer, and moving back toward the input layer, calculate the error terms and gradient as follows:

$$e_j^{(l)} = \begin{cases} (u - x_j^{(1)}) & \text{for } l = L \\ \sum w_{ij}^{(l+1)} s_j^{(l+1)} & \text{for } l = 1, 2, 3, \dots, L - 1 \end{cases} \quad (12)$$

where $e_j^{(l)}$ is the error term for j th neuron in the l th layer

$$s_j^{(l=1)} = e_j^{(l+1)} \theta(s_j^{(l)}) \quad \text{for } l = 1, 2, \dots \quad (13)$$

where $\theta(s_j^{(l)})$ is the derivative in the activation function.

Calculate the changes for all the weights as follows:

$$\Delta w_{ij}^{(l)} = \eta s_j^{(l)} x_i^{(l-1)} \quad l = 1, 2, \dots, L \quad (14)$$

where η is the learning rate. Update all the weights as follows:

$$w_{ij}^{(l)}(L + 1) = w_{ij}^{(l)}(L) + \Delta w_{ij}^{(l)}(L) \quad (15)$$

where $l = 1, 2 \dots L^{(1)}$ and $j = 0, 1 \dots L^{(l-1)}$, $W_{ij}^{(l)}(L)$ is the current synaptic weight.

$W_{ij}^{(l)}(L + 1)$ is the updated synaptic weights to be used in the next feed-forward iteration. Figure 4 shows the complete cycle of period, in neural networks training

the term period is used to describe a complete pass through all of the training patterns. The weight in the neural net may be updated after each pattern is presented to the net, or they may be updated just once at the end of the period.

7 Implementation and Results

The implementation is done using Verilog on Vertex-2Pro FPGA and Matlab 2012A. The graphical user interface (GUI) is created as shown in Fig. 7. From the database of the US kidney images, one kidney image is loaded through the GUI. The loaded image is preprocessed and is shown in the GUI. The image segmentation option given in the GUI is selected next to get segmented image. The segmented image is applied for wavelet processing by selecting one of the lifting wavelet filters shown in the GUI. After selecting the particular filter, that particular wavelet code will be invoked to get resultant image. Then the feature extraction option is selected to get list of energy levels extracted from the segmented image (Figs. 8, 9, and 10).

In the GUI shown in Fig. 7 there is another table which lists energy levels of all the kidney images present in the database. This is done to test the accuracy of MLP-BP ANN system in identifying the kidney images as normal or abnormal and the stone type. Essentially in the database, we have both normal and abnormal images, which we already know how many of them are normal and abnormal. During the test, it is found that our system can classify the kidney images as normal and abnormal almost

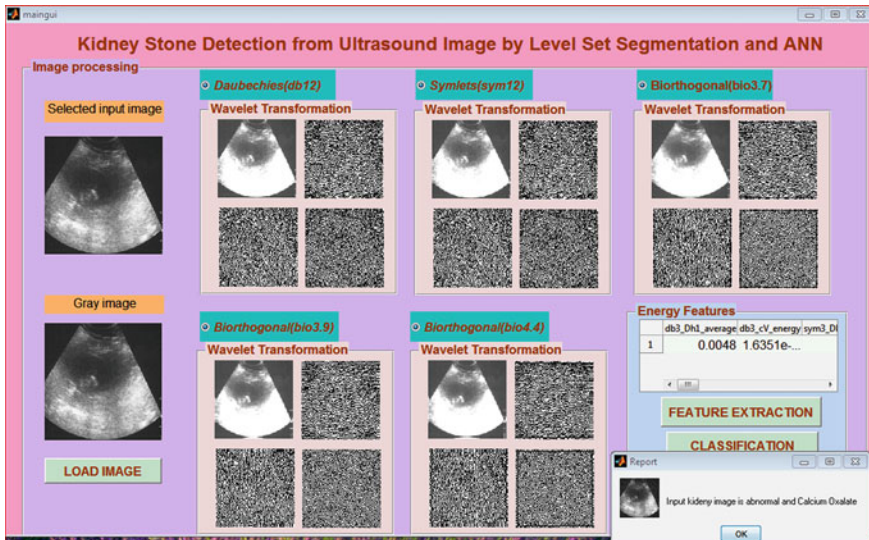


Fig. 7 Wavelets subbands energy extraction

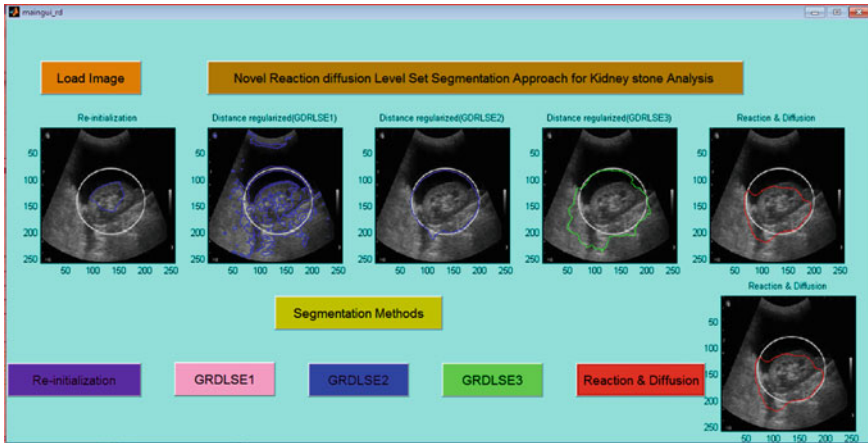


Fig. 8 Kidney stone segmentation methods results from different image from database

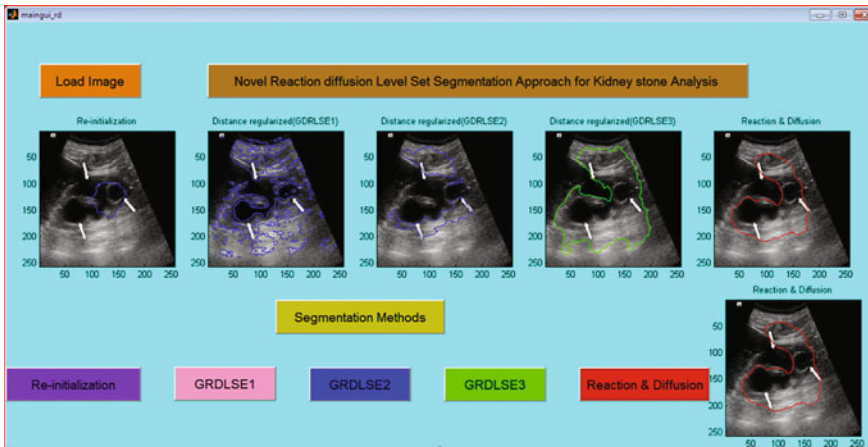


Fig. 9 Kidney stone segmentation methods results from different image from database

with an accuracy of 98.8 %. In Fig. 11 is the Chipscope hardware implementation, the first rows show the pixel values of kidney stone, second rows show the kidney pixel values, and third row shows the original kidney image.

Table 1 shows the lists of energy levels extracted from the segmented image. This table is the enlarged version of the table shown in the GUI. The rows of the table are individual energy level of each kidney images of database. The columns of the table show energy levels extracted from the images of database with respect to each wavelet filter. First two columns are corresponding to Daubechies filter, the third and fourth columns are corresponding to symlets20. The fifth, sixth, and seventh columns are corresponding to Biorthogonal filter (Bio3.7). The eighth,

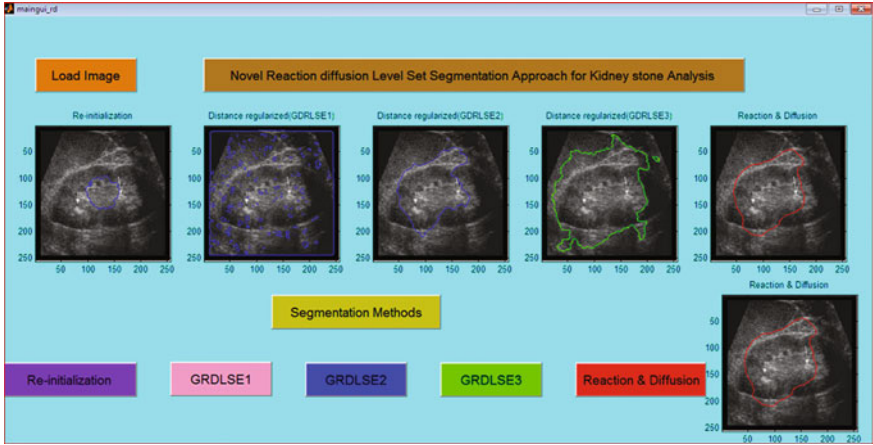


Fig. 10 Kidney stone segmentation methods results from different image from database

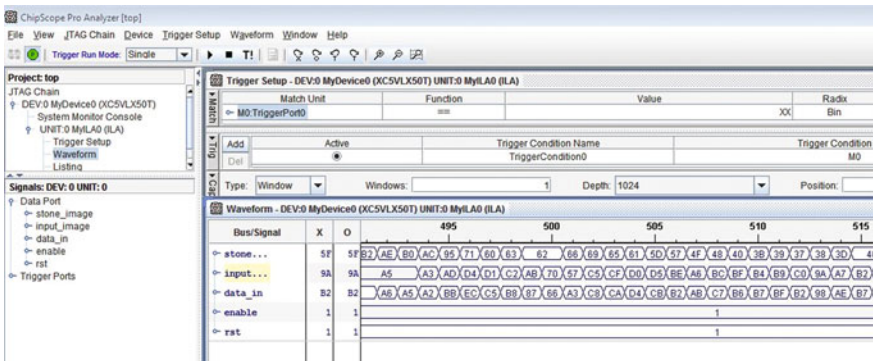


Fig. 11 FPGA hardware implementation using Chipscope, ILA and ICON of segmentation for kidney and stone pixel values

Device Utilization Summary				Number of LUT Flop pairs used	617
Logic Utilization	Used	Available	Utilization	Number with an unused Flop Pair	740
Number of Slice Registers	277	28,800	1%	Number with an unused LUT	110
Number used as Flop Pairs	376			Number of fully used LUT/Flop pairs	267
Number used as Latches	1			Number of unique control sets	58
Number of Slice LUTs	507	28,800	1%	Number of slice register sites left to control and restrictors	139
Number used as logic	424	28,800	1%	Number of bonded I/Os	3
Number using O5 output only	262			Number of L0Ced I/Os	3
Number using O5 output and O6	119			Number of BlockRAMs	60
Number using O5 and O6	43			Number using BlockRAM ports	10
Number used as Memory	56	7,680	1%	Number of 36k BlockRAM used	10
Number used as Shift Register	56			Number of 18k BlockRAM used	10
Number using O6 output only	50			Total Memory used (KB)	360
Number using O5 output only	1			Number of BRAMs/BlockRAMs	2
Number used as exclusive route thru	27			Number used as Buffer	2
Number of route-thrus	146			Number of SIOs	1
Number using O6 output only	146			Number of SRM macros	4
Number of occupied Slices	225	7,000	3%	Average Fanout of Non-Clock Nets	3.13

Fig. 12 Design summary of the proposed hardware implementation

ninth, and tenth columns are corresponding to Biorthogonal filter (Bio3.9). The eleventh, twelfth, and thirteenth columns are corresponding to Biorthogonal filter (Bio4.4).

The proposed work is implemented on Vertex-2Pro FPGA and speed was increased by 35 % with gate delay of 3.765 ns and number of slices LUT's are decreased by 23 % as compared to existing methods, the design summary table is shown in Fig. 12.

8 Conclusion and Future Work

The proposed work is implemented on Vertex-2Pro FPGA using level set segmentation with momentum and resilient propagation and is very effective in identifying the region of stones in the US kidney image with very less utilization of resources. The energy levels extracted from the lifting scheme wavelet subbands, i.e., Daubechies (Db12), Symlets (sym20), and Biorthogonal filterers (bio3.7, bio3.9, and bio4.4), give the clear indication of difference in the energy levels compared to that of normal kidney image if there is a stone. The ANN trained with normal kidney image and classified image input into normal or abnormal by considering extracted energy levels from wavelets filters. The system was tested with different kidney images from the database and has classified successfully with the accuracy of 98.8 %. So this system can be readily used in the hospitals for detecting the abnormality of an individual's US kidney image. Thus in this work, it is proved that the combination level set segmentation, lifting scheme wavelet filters, multi-layer perceptron with back propagation are the better approaches for the detection of stones in the kidney. In the future work, the system will be designed and implemented in real time by placing biomedical sensors near the abdomen to capture the kidney portion and the captured kidney image is subjected to the proposed algorithm to process and detect stone on FPGA using hardware description language (HDL) and display the kidney stone image with color for easy identification and visibility of stone on monitor.

References

1. Rahman T, Uddin MS. Speckle noise reduction and segmentation of kidney regions from ultrasound image, 978-1-4799-0400-6/13, IEEE;.2013
2. Robertson WG. Methods for diagnosing the risk factors of stone formation 2090–598X, Arab Association of Urolog. Production and hosting by Elsevier B.V, 2012;10:250–257.
3. Bernhard Hess, "Metabolic syndrome, obesity and kidney stone", 2090–598X, 2012 Arab Association of Urolog, Production and hosting by Elsevier B.V, 10,258-264.
4. Hafizah WM. Feature Extraction of Kidney Ultrasound Images based on Intensity Histogram and Gray Level Co-occurrence Matrix 2012, sixth Asia Modeling Symposium, 978-0-7695-4730-5/12, 2012 IEEE.

5. Gladis Pushpa Rathi VP. Detection and characterization of brain tumor using segmentation based on HSOM, wavelet packet feature spaces and ANN", 978-1-4244-8679-3/11, 2011 IEEE.
6. Koizumi N. Robust kidney stone tracking for a non-invasive ultrasound theragnostic system—servoing performance and safety enhancement, In: 2011 IEEE international conference on robotics and automation shanghai international conference center, May 9–13, Shanghai, China; 2011.
7. Abou El-Ghar ME. Low-dose unenhanced computed tomography for diagnosing stone disease in obese patients. 2090–598X, Arab Association of Urolog. Production and hosting by Elsevier B.V., 2012;10:279–283.
8. Viswanath K, Gunasundari R. Kidney stone detection from ultrasound images by level set segmentation and multilayer perceptron ANN, Elsevier publisher. In: Proceedings of the international Conference on Communication and Comuting, IMCIET-ICCE-2014, p. 38–48, ISBN:978-93-5107-270-6.
9. Dheepa N. Automatic seizure detection using higher order moments and ANN. In: IEEE—international conference on advance in engineering science and management (ICAESM-2012) March 30, 31, 2012 with ISBN: 978-81-909042-2-3, 2012 IEEE.
10. Kumar K. Artificial neural network for diagnosis of kidney stone disease. I.J. Inf Technol Comput Sci. 2012;7:20–25.
11. Morse PM, Feshbach H. The variational integral and the Euler equations. In: Proceedings of the Methods of Theoretical Physics Part I, May 1953, p. 276–280.
12. Tamilselvi PR. Computer aided diagnosis system for stone detection and early detection of kidney stones. J Comput Sci. 2011;7 2:250–254, ISSN:1549-3636.
13. Bagly DH, Healy KA. Ureteroscopic treatment of larger renal calculi (>2 cm)". Arab J Urol. 2012;10:296–300 production and hosting by Elsevier.
14. RobertsonWG. Methods for diagnosing the risk factors of stone formation. Arab J Urol. 2012;10:296–300 production and hosting by Elsevier.
15. Shen L, Jin S. Three-dimensional gabor wavelets for pixels-based hyperspectral imagery classification. IEEE Trans Geosci Remote Sens. 2011;49:12.
16. Chen X. FEM-based 3-D tumor growth prediction for kidney tumor. IEEE Trans Biomed Eng 2011;58:3.
17. Owen NR. Use of acoustic scattering to monitor kidney stone fragmentation during shock wave lithotripsy. In: 2006 IEEE Ultrasonics Symposium, 1051–0117/06.
18. Kok DJ. Metaphylaxis, diet and lifestyle in stone disease. In: 2012 Arab association of urology, production and hosting by Elsevier B.V., 2012;10:240–249.
19. Datar DS. Color image segmentation based on initial seed selection, seeded region growing and region merging. In: International journal of electronics, communication and soft computing science and engineering, vol. 2 Issue 1. ISSN:2277–9477.
20. Cyril Prasanna Raj P. Design and analog VLSI implementation of neural network architecture for signal processing. Eur J Sci Res. 2009;27 2:199–216. ISSN:1450–216X.
21. Martinez-Carballido J. Metamyelocyte nucleus classification uses a set of morphologic templates. In: 2010 Electronics, Robotics And Automatic Mechanics Conference 978-0-7695-4204-1/10, 2010 IEE.
22. Zhang W. Mesenteric vasculature-guided small bowel segmentation on 3-D CT. IEEE Trans Med Image. 2013;32:11.
23. Law MWK, Chung ACS. Segmentation of intracranial vessel and aneurysms in phase contrast magnetic resonance angiography using multirange filters and local variances. IEEE Trans Image Process. 2013;22:3.
24. Law YN, Huan H. A multiresolution Stochastic Level set method for Mumford-shah image segmentation. IEEE Trans Image Process. 2013;17:12.
25. Kimmel R. Fast edge integration. In: Geometric Level Set Methods in Imaging, Vision and Graphics. New York: Springer; 2003.

26. Andersson T, Lathen G. Modified gradient search for level set based image segmentation. *IEEE Trans Image Process.* 2013;22:2.
27. Stevenson M, Weinter R, Widow B. sensitivity of feedforward neural networks to weight errors. *IEEE Trans Neural Networks.* 1990;1(2):71–80.
28. M. Riedmiller and H. Braun, “A direct adaptive method for faster backpropagation learning: The RPROP algorithm,” in *Proc. IEEE Int. Conf. Neural Netw.*, vol. 1. Jun. 1993, p. 586–591.

Simulation Framework for Modeling Magnetic Induction Based Wireless Underground Channel

P. Ajith, K.A. Unnikrishna Menon and Vrinda N. Menon

Abstract Wireless underground communication is a challenging task when electromagnetic (EM) waves are used. The communication has to face many limitations like spreading loss, fading, and attenuation. The existing solution for this problem is magnetic induction (MI) based communication. The performance of this method depends on many factors like the distance between the transmitter and receiver, placement of relay coils, moisture content, permeability, seasonal changes, and the depth at which the system is deployed. There are no proper MI channel model which incorporates all these soil parameters and geometrical parameters for predicting the signal quality at the receiver. We propose a simulation model using MATLAB to predict the signal quality at the receiver by optimizing the placement of relay coils, taking into consideration the soil parameters, geometrical parameters of coils, and geological parameters.

Keywords Wireless underground communication · Magnetic induction · Geometric parameters · Geological parameters · MATLAB · Simulation platform

1 Introduction

Nowadays wireless underground communication [1] has a prominent role in the communication field. In the areas of intelligent irrigation, environmental monitoring, border patrol, etc., the performance of wireless underground communication is

P. Ajith (✉) · K.A. Unnikrishna Menon · V.N. Menon
Amrita Centre for Wireless Networks and Applications,
Amrita Vishwa Vidyapeetham, Amritapuri, Kollam, Kerala 690525, India
e-mail: ajithvatsan@gmail.com

K.A. Unnikrishna Menon
e-mail: kaumenon@gmail.com

V.N. Menon
e-mail: vrindanm@gmail.com

many times better than above ground communication and wired underground communication, in terms of cost, complexity, and maintenance.

MI based communication and shortwave communication. When we consider the parameters like soil composition, permeability of soil, depth, moisture content, and seasonal changes, EM waves will undergo high degradation [2]. But in the case of magnetic induction [3], these types of signal fading and attenuation will be very less. The losses and attenuation in shortwave communication are very less. But the main restriction to this method is its difficulty in implementation. The main parameters which restrict the underground communication are antenna size [4] and power consumption. Otherwise this can be used as an efficient method for underground communication. In case of efficient power transfer, we cannot use short-wave communication.

There are no proper MI channel models which incorporate various soil parameters and geometric parameters for predicting the signal quality at receiver. No underground simulation model talks about effective placement of relay coils and its effect on the communication. Dynamic modeling of the underground channel, according to the geological parameters, soil composition, and seasonal changes, is the main research challenge. Mainly, the factors that can affect the propagation are innumerable, which makes it difficult to model. One of the major constraints is the heterogeneous nature of soil, because the presence of rock in the soil and the characteristics of the rock, even its composition affect the communication. We assumed the soil characteristics are homogeneous throughout the deployment site and the characteristics of coils considered (transmitter, receiver, and relay) are same.

This paper focuses more on modeling the wireless underground communication channel, by including parameters like permeability of soil, moisture content, seasonal changes, and geometrical parameters like depth. This will help to predict the output signal quality at sink node, and effective placement of relay coils.

The paper is organized as follows: The Sect. 2 describes about the related works. The detailed system architecture is given in Sect. 3. Implementation steps are described in Sect. 4. Results are discussed in Sect. 5 and finally the Sect. 6 concludes this work.

2 Related Work

In this research work, the main focus is to develop a simulation framework for predicting signal quality at the output and effective placement of coils. The literature study was mainly aimed at collecting details related to wireless underground communication techniques, parameters which are affecting the wireless underground communication and how they are affecting the communication.

A detailed study of the wireless underground communication network (WUCN) is given in [5]. It mainly focuses on WUCNs and the possibilities of placement of coils in underground medium such as buried completely under dense soil and

placed within a bounded open underground space. It stated that the multipath fading would be strong up to two meters depth and would be considerably less below two meters. They also noted that the permeability of soil and water will be approximately same. But they did not mention about the effect of seasonal changes on wireless underground communication, and the need of a simulation platform to predict the signal quality and relay coils.

The difference between WUSNs and terrestrial wireless networks are explained in [6]. They pointed out the importance of a wireless underground communication and its communication principle, over a terrestrial wireless network. The paper projected the demerits of EM wave communication like high path loss, dynamic channel condition, and large antenna size. They mainly concentrated their studies on the performance comparison of three communication techniques, namely traditional EM wave system, ordinary MI system, and MI waveguide system. But they did not consider the seasonal changes, geological parameters, geometrical parameters, and moisture content in their model.

A detailed description about the parameters which affect the magnetic induction is given in [7]. Here, they studied the theoretical details and mentioned that the soil type, moisture content, and soil composition would not affect the communication and then calculated the effect of the geometrical parameters on received signal strength.

Operating frequency, details of MI technique, and placements of coils were discussed in [8]. They have not considered placing of a core inside the coils to improve communication range, high data rate, two-way communication, and simulation part.

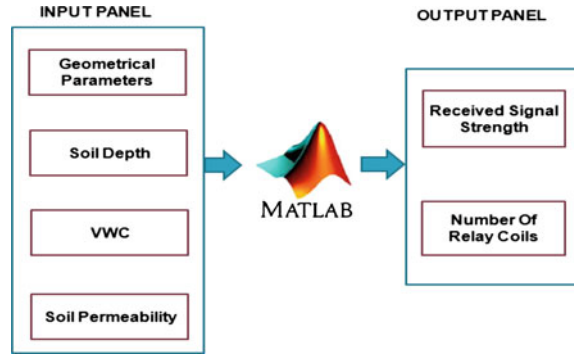
The importance of simulation for wireless underground transmission is described in [9]. This paper introduced different types of underground communication scenarios like underground to underground communication, underground to above ground communication, and above ground to underground communication.

We focus to enhance the existing underground MI propagation models, by including geometrical, geological, and soil parameters. A simulation platform has been developed based on this model to predict the signal quality as well as the effective placement of the coils in the system.

3 System Architecture

The system architecture is shown in Fig. 1. The input panel included parameters which usually affect the underground communication. Various geometrical parameters like number of turns in coils, operating frequency, coil radius, lower loop resistance, angle between two axes, distance between coils, and permeability of soil were included in the model. In addition to these parameters, this work included many other geological parameters, like depth and volumetric water content (VWC), which affects the wireless underground communication. These geological parameters, especially VWC, indirectly depended on seasonal changes. MATLAB was the platform for developing the model and the output panel showed the received signal

Fig. 1 System architecture



quality at the output/sink node. It verifies whether the received signal is above the minimum detectable signal (MDS), if so, it will display the received signal strength in the output panel along with the number of relay coils required for efficient communication. Otherwise it will show the message, 'signal is too weak.'

The work was started with the classification of input parameters into seasonal changes related, VWC related, depth related, and efficiency needed. Then we identified that if the 'seasonal change' related parameter is rainy, summer, or winter. Based on this parameter, its effect on communication is represented on the output. Then based on VWC and depth, how much reduction might occur for the signal strength is predicted. Calculation of distance between coils is purely based on the expected efficiency. The next output, number of relay coils needed, is calculated from distance parameters and expected efficiency. After that, received signal strength calculation is done. If the received signal strength was less than -60 dB, this simulation platform would print the result as 'signal is too weak.' Otherwise it would print the signal strength. At last, plotting of this received signal strength is done. The plot gave a clear comparison between wireless underground communication with relay coils and without relay coils.

4 Implementation

The simulation platform for WUCN mainly concentrated on predicting the received signal strength at the receiver and effective placement of relay coils [10] according to the desired efficiency. The efficiency in magnetic induction is defined as the ratio between the quantities of flux produced to the signal strength given to the coil.

4.1 Seasonal Changes

By observation, we found that there was only light rainfall or no rainfall in summer season. The moisture content is initially at high level and it dropped down to low

level gradually with respect to time. There was continuous rainfall in rainy season. When a heavy rainfall occurs, moisture level rises from low amplitude to high and falls back to low level. There was a moderate or no rainfall in winter season. As winter season is followed by rainy season, volumetric water content or moisture content in the soil will be low when compared to rainy season.

4.2 Curve Fitting

The effect of depth and moisture content were studied and formulated equations [11] for both the curves, according to curve-fitting rules.

The values that were taken from the above graphs [12], shown in Fig. 2, are listed in Tables 1 and 2.

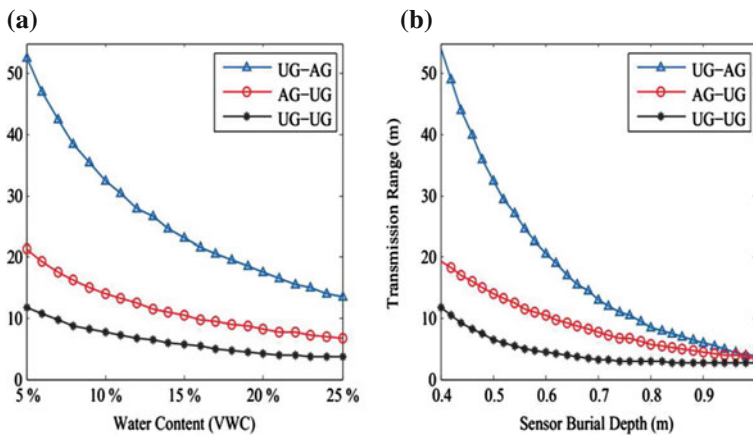


Fig. 2 Relation between VWC versus transmission range and sensor burial depth versus transmission range

Table 1 Depth versus transmission range

Depth in cm (x)	Transmission range in cm (y)
40	1175
50	670
60	450
70	330
74	300
84	270
90	270
100	270

Table 2 VWC versus transmission range

VWC in percentage (x)	Transmission range in cm (y)
5	1150
6	1075
7	980
10	800
15	600
20	425
25	400

The Table 1, indicated that the increment in deployment depth would adversely affect the transmission range as well as the signal strength. Depth difference of 10 cm made 43 % reduction in transmission range. After that transmission range showed a gradual reduction along with the increment in depth. Equation from Table 1 is

$$y = 3300.36 - 71.88x + 0.4212x^2. \quad (1)$$

The Table 2 showed inverse relation between VWC and transmission range. Around 5 % increment in VWC indicated 30 % reduction of transmission range. Then the rate of reduction in transmission range decreased after 10 % VWC. Equation from Table 2 is

$$y = 1568.24 - 95x + 1.93x^2 \quad (2)$$

Both Eqs. (1) and (2) contributed to the simulation platform of prediction of signal quality reduction due to depth and VWC.

4.3 Efficient Placement of Coils

From Table 3 [13], according to the efficiency needed by the user, we could select the correct distance between coils. From the information of total distance between source and sink, and distance between two relay coils, the total number of relay coils needed to achieve that expected efficiency could also be calculated.

Table 3 Distance between coils versus efficiency

Distance in cm	Efficiency in percentage
1.5	99
2	98
4	97
8	94
16	77
32	70

5 Result

Figure 3 shows result of this research work. Here the input panel is divided into three panels: geometrical parameters, deployment requirements, and ambient conditions. The geometrical parameters mainly included the geometrical features of coils in the deployment. Ambient conditions included the soil permeability, VWC, and seasonal changes. The section, ‘Deployment requirements’ included all other parameters like transmission power, depth, frequency, distance between source and sink, angle between coils, and expected efficiency. The output window has two outputs namely, received signal strength and relay coils. Received signal strength showed the output power at the sink node and relay coils showed the number of relay coils needs to fulfill the expected efficiency of user. The effect of different parameters like seasonal changes, depth and VWC are shown in ‘effect of parameters’ part of the output panel.

Figure 3 represents the sample result with the following conditions:

- Receiver and Transmitter turns = 5
- Coil radius = 2 cm
- Lower loop resistance = 100 Ω
- Transmission power = 20 W

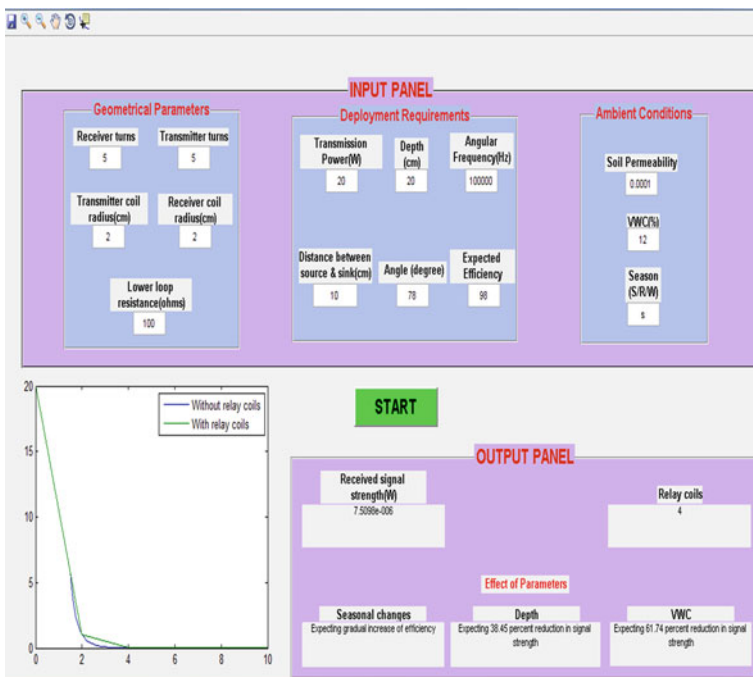
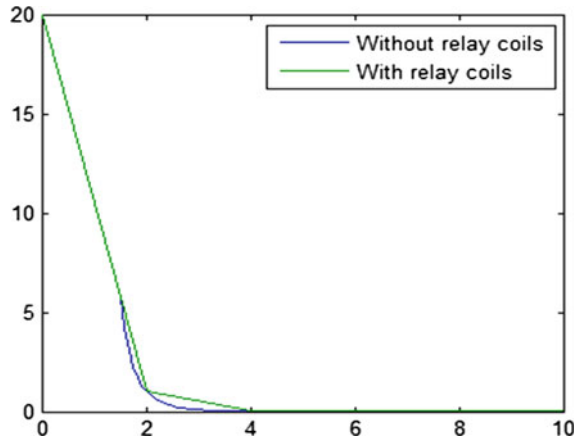


Fig. 3 Simulation platform

Fig. 4 Signal strength variation in communication with relay coils and without relay coils



- Depth of deployment = 20 cm
- Angular frequency = 100 kHz
- Distance between source and sink = 10 cm
- Angle between adjacent coils = 78°
- Expected efficiency = 98 %
- Soil permeability = 0.0001
- VWC = 12 %
- Season = Summer

The received signal strength and the number of relay coils needed to accomplish the expected efficiency, for the given inputs were $7.5098e-006$ and 4 respectively. Figure 4 shows the difference between direct communication without relay coils and with relay coils. This resulted that the reduction rate of signal strength in relay coil communication has reduced when compared to direct communication.

6 Conclusion

Currently there is no simulation framework to predict the signal quality at output node as well as the effective placement of relay coils. This work is a detailed study on the geometrical parameters, geological parameters, seasonal changes, and soil parameters, which might affect the wireless underground communication. Formulated all the effect of these parameters on underground communication and included in simulation framework. This work could be used as user-friendly simulation framework for signal quality prediction and effective placement of coils. Based on all the input parameters, the model predicted the received signal strength at the sink node and number of relay coils needed to accomplish the expected efficiency. As additional information, this model analyzed and displayed the effect of 'seasonal changes,' 'depth of deployment,' and 'VWC.'

Acknowledgments This project is fully funded by a grant from Ministry of Earth Sciences (MoES) and this work is fulfilled under the guidance and support from Amrita Centre for Wireless Networks and Applications. We would also like to express our gratitude for the immeasurable motivation and guidance provided by Sri. (Dr.) Mata Amritanandamayi Devi (AMMA), Chancellor of Amrita University.

References

1. Ashwini R, Dr. Mukesh DP. Magnetic induction-based wireless underground waveguide modelling and its parameters. IJECCT, May 2014.
2. Vuran MC, Angelo RS. Communication through soil in wireless underground sensor networks —theory and practice. In: Ferrari G, editor. Sensor networks, signals and communication technology. Berlin Heidelberg: Springer-Verlag; 2010.
3. Johnson IA. Investigation of near field inductive communication system models, channels and experiments. Progs Electromagnet Res B. 2013;49:129–53.
4. Maneesha VR, Nirmala V. The deployment of deep-earth sensor probes for landslide detection. Springer-Verlag. Landslides. 2011;. doi:10.1007/s10346-011-0300-x.
5. Akyildiz IF, Zhi S, Vuran MC. Signal propagation techniques for wireless underground communication networks. Phys Commun (Elsevier) 2009; 2.
6. Akyildiz IF, Zhi S. Magnetic induction communications for wireless underground sensor networks. IEEE Trans Antennas Propag 2010; 58, 7.
7. Mittu M, Lenin J. Study on the parameters affecting magnetic induction waveguide for underground communication. IC—IASET 2014; 3, Special Issue 5.
8. Menon KA, Gungi A, Hariharan B. Efficient wireless power transfer using underground relay coils. In: IEEE 2014 international conference on computing, communication and networking technologies (ICCCNT), 2014.
9. Conceicao SDL. NS-3 simulation model for underground networks. Master thesis, Faculdade de Engenharia da Universidade do Porto, 2014.
10. Yu X, Wu P, Zhang Z, Wang N, Han W. Electromagnetic wave propagation in soil for wireless underground sensor networks. Progs Electromag Res M 2013; 30:11–23.
11. Gurley: Numerical methods lecture 5—curve fitting techniques. CGN 3421—Computer Methods, p 89–102.
12. Gungi, A.: Inductively powered underground wireless communication system. Master thesis. Amrita Vishwa Vidyapeetham, Kollam, India, 2014.
13. Wireless high power transfer under regulatory constraints. <http://www.google.com/patents/EP2301133A1?cl=en>.

A Generic Algorithm for Segmenting a Specified Region of Interest Based on Chanvese's Algorithm and Active Contours

Pranshu Agrawal, Gaurav Ojha and Mahua Bhattacharya

Abstract Image processing and recognition is a modern field which is gaining popularity due to its capability to automate certain mundane object recognition tasks and provide unparalleled accuracy and precision. Computer graphics have evolved sufficiently so as to cater to a wide array of applications ranging from categorizing mechanical parts of a machine to identify foreign objects/tumors inside the human body [1]. In this particular application, we are working toward identifying cotton plants from a heap. Traditionally, this task has been performed by laborers who identify the cotton plants from a collection and classify them based on certain characteristics. This task can take anywhere from a day to a week depending upon how good the yield is. We propose that this entire task from identifying cotton to classifying it based on the prerequisite characteristics can be performed automatically. We have developed an algorithm that can provide the exact position of cotton buds from pictures of the harvested plant. From the hardware aspect, this is the scope of automating the harvesting task. We have used the techniques of image acquisition, segmentation, and feature extraction. A highly modified iterative version of Chanvese's algorithm is utilized to chalk out a starting boundary (contour) and then work successively on it to reach at a final segment that defines the cotton buds.

Keywords Chanvese · Matlab · Feature extraction · Artificial neural network · Cotton buds

P. Agrawal · G. Ojha (✉) · M. Bhattacharya
Indian Institute of Information Technology and Management, Gwalior, India
e-mail: ojha.iiitm@gmail.com

P. Agrawal
e-mail: pranshu.a.11@gmail.com

M. Bhattacharya
e-mail: mb@iiitm.ac.in

1 Introduction

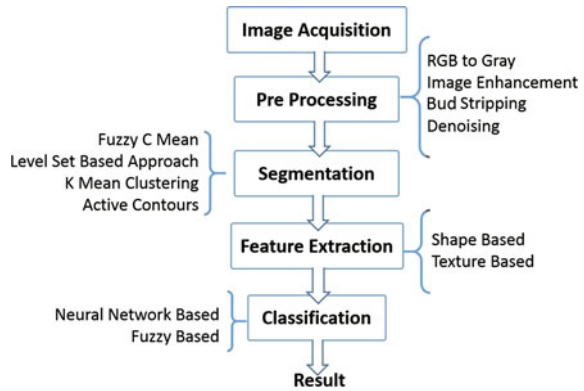
A number of studies [4–10] performed in the field of image segmentation, feature extraction and identification throw light on the fact that it has huge potential for widespread applications. A major contribution in flower classification is given by Nilsback and Zisserman [11–13] which covers wide variety of aspects to consider for flower classification process. Nilsback and Zisserman [11], in their fruitful study in flower classification took the benefit of three classes for feature extraction, i.e., shape, color, and texture. A dataset provided by Oxford university was used which contains information of 10 species, and 40 images of each species of flower. For shaped-based features, SIFT descriptor is used and achieved performance is 75.3 % with 800 clusters. The features considered for texture is MR8 filter which was proposed in [12]. The performance of features extracted for color turns out to an efficiency level of 49 %. Another color space, i.e., Hue, saturation value (HSV) is applied in order to study the impact of illumination alterations. The result shows that using color vocabulary achieves the best extraction. In another attempt by same authors [12], graph cut segmentation was employed to get boundary of a flower. In this research, a large number of classes of flower were considered, also the features used were a little different, i.e., boundary shape, petal spatial distribution, color, and shape/texture. For classification, support vector machine (SVM) [2, 3] is used which results into a total accuracy of above 70 %. Further a method for two-step model for segmentation of flower is proposed by the same authors, Nilsback and Zisserman [13]. The two steps correspond to separation of foreground and background, and extracting petal structure of the flower.

2 Methodology

An image of the cotton plants has to be procured by means of capturing it via digital equipment specifically designed to generate high-contrast images.

Given an image of cotton plants, now the objective which we need to accomplish is to find whether that image of the plants has cotton buds in it or not. This is a step-by-step procedure in which the first step is preprocessing. In this step, we make a digital image ready for future analysis. Preprocessing mainly includes denoising the captured plant images, feature sharpening, bud-stripping, and image enhancement. The second step is segmentation in which we will compare fuzzy C Mean algorithm and level set-based approach and K Mean clustering algorithm and their combination so as to achieve best segmentation in time efficient manner. The third phase is feature extraction in which we will extract the feature of the cotton buds' segmented part which will act as the input to the classifier and the final decision will be made according to the features present in the segmented plant Image. The methodology can be denoted by a process flowchart as shown in Fig. 1.

Fig. 1 Process flowchart



2.1 Preprocessing

Preprocessing is a mandatory step required to make the plant image ready for further analysis. In preprocessing, we will denoise the image using either median filter or combination median and mean filtering. Then we will sharpen the features of the denoised image by adjusting the contrast and brightness to an optimum level. The next step is bud-stripping which is needed to be done so as to delineate the plant boundary and to extract the effective part containing cotton. Then the denoised, sharpened and bud-stripped image will be enhanced by removing the green leaves surrounding the cotton buds which will make the further image analysis more accurate.

2.2 Segmentation

After the preprocessing step, the image of cotton plants is segmented either by active contours or by fuzzy C Means or by level set-based approach or by K-means clustering algorithm. In K Means clustering algorithm, K cluster centers are randomly chosen from image data. Then distance is computed for each pixel with the K cluster centers. The pixel belongs to that cluster center which gives us the minimum distance. Then the K—cluster centers are recomputed and this process is repeated until the centers converge. In FCM algorithm, the arguments used are data set to be clustered. The output arguments are the matrix representing final cluster centers. Each row provides the center coordinates, fuzzy partition matrix, and values of the objective function in different iterations. The clustering process stops when the specified numbers of iterations are achieved or when the objective function improvement between two consecutive iterations is less than the minimum amount of the improvement specified. Level set methods utilize dynamic variation boundaries for image segmentation. The parameters are set on a trial and error basis.

2.3 Classification

Classification uses the output of the segmented image as input and tells about the presence of the cotton buds in the image of the whole plant. In this we need to design a classifier which can be done by using two approaches. The first one is by using a neural network-based classifier and the second one is by using a fuzzy-based classifier. In case of the ANN (Artificial Neural Network)-based classifier, there are varied types of neural networks like the probabilistic neural network and the back-propagation neural network. All these classifiers need to be compared so as to choose the best one in case of detecting cotton buds from the plant images.

3 Implementation

There are two phases involved in the implementation of designing a system which detects cotton buds in images of a cotton plant.

The first phase is the preprocessing of the plant images, which deals basically with the visual representation of the image. Modifying the visual representation of the digital plant image mainly involves denoising the image. Denoised images are smooth versions of the original digital plant image. Then, the parts containing cotton buds are stripped from these images using a Bud-stripping algorithm specifically designed for this purpose.

The second phase involves the segmentation of the cotton buds from the main plant image. To do this, we have introduced a highly modified method for segmenting images which is based on the algorithm developed by Chan and Vese in [x]. This is a very powerful, flexible method which can successfully segment many types of images, including some that would be difficult or even impossible to segment using classical thresholding or gradient-based methods. The derivation of this method has been outlined and an algorithm is presented for segmenting images and it examines performances on some sample images.

The code implementation includes converting the input image to grayscale using the following code snippet

```
% Input the image
RGB = imread('img1.jpg');
I = rgb2gray(RGB);
```

For the image input, we have used the `imread()` function supplied with the argument of the image file location. Then, using the `rgb2gray()` function supplied with the argument of the image object, the image is converted to grayscale.

The next step is to adjust the contrast values of the image. The code snippet for the contrast adjustment operation is given below

```
% Change the contrast values of the image
I = imadjust(I);
```

This is used to enhance the image. The `imadjust()` function is supplied with the argument of the Image object and it performs the optimal adjustments in the contrast of the image.

The next step is the implement of the bud-stripping part. This is done using the following code

```
% Bud Stripping Code
subplot(1,2,1);
imshow(I);
BW=im2bw(I,graythresh(I));
cc = bwconncomp(BW);
s = regionprops(cc, 'Perimeter');
sum=0;
t=size(s);
t=t(1);
fori=1:t
if(s(i).Perimeter>sum)
m=i; sum=s(i).Perimeter;
end
end
BW2 = ismember(labelmatrix(cc), 1);
[m n]=size(I);
fori=1:m
for j=1:n
if(BW2(i,j)==1)
I(i,j)=0;
end
end
end
subplot(1,2,2);
imshow(I);
```

Bud stripping implementation is required as it provides a part of the image with the stripped buds. To strip the buds, we are using the enhanced image and then converting it to Binary. The binary value is stored in a variable named BW. Here `graythresh(I)` computes a global threshold (level) that can be used to convert the intensity image to a binary image with `im2bw`. Level is a normalized intensity value that lies in the range [0,1]. Then, we use the `bwconncomp()` function supplied with the binary image as the argument to find the connected components in the binary image.

After this, we are using the function `regionprops(CC, properties)` to measure a set of properties for each connected component (object) in CC, which is a structure returned by `bwconncomp` is stored in S. The next for loop finds the largest parameter. Then, we calculate `labelmatrix(CC)`. A label matrix is essentially an image which is the same size as the input image in which the objects

in the input image are distinguished by different integer values in the output matrix. Then, we pass it in the `ismember()` function which gives Array elements that are members of the set array. Next, we replace the pixels (i, j) with the value 1 which are 1 in BW2, which finally results in the bud-stripped image.

The implementation of the bud-stripping filter is done using the following code snippet

```
% Gaussian Filter
H = fspecial('gaussian');
GaussianFilter = imfilter(I,H);
```

The step for designing the mask for the modified Chan Vese algorithm is given below

```
%Segmented Tumor from the MR Image
seg = chenvese(I, 'small', 300, 0.02, 'chan');
```

`Chenvese()` is the function used to apply the Chan-veese algorithm for the calculation of segmented image. The function has three arguments. The first argument is the preprocessed image. The second argument is the size of the initial mask. The third argument is the number of iterations, on each iteration the mask size increases.

Once we get the segmented cotton bud, we can calculate its features to find out where the bud lies.

```
%---- Dimension of segmented image
[x,y]=size(seg);

%---- Area of the bud inside the segmented image
labeledImage = bwlabel(seg);
measurements = regionprops(labeledImage, 'Area');
allAreas = [measurements.Area];
totalAreaOfAllBlobs = sum(allAreas);

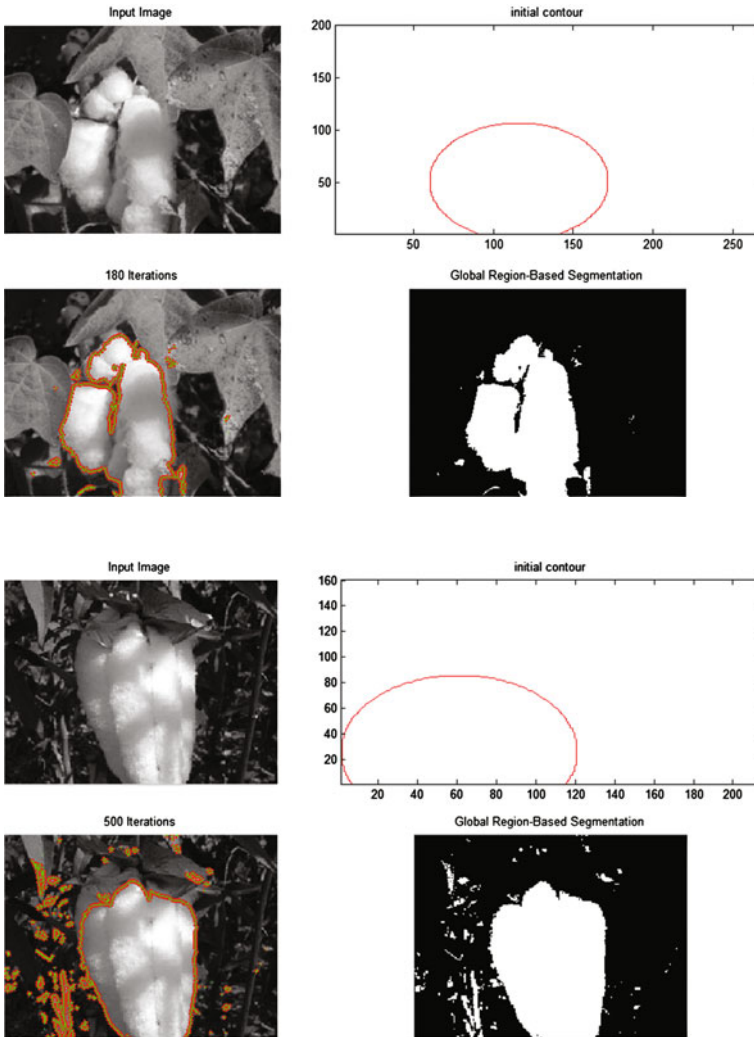
%---- Percentage of budarea in the segmented image
pertumor = totalAreaOfAllBlobs*100/(x*y);
segPerm = bwperim(seg);
[a,b]= find(segPerm==1);

fprintf('Resolution of segmented image %dpx X %dpx\n',
x,y);
fprintf('Total area of the ROI %d sqPixels\n',
totalAreaOfAllBlobs);
fprintf('ROI Occupancy %f percent\n\n', pertumor);
fprintf('List of cordinates of ROI Perimeter\n');
fprintf('%f %f\n', a,b);
```

This will give us the exact coordinates of perimeter of cotton in the heap which is a very precise measure to identify its exact location.

4 Results and Discussion

We tested the approach on a variety of cases and the results we have got are more than reassuring.



Resolution of segmented image 200px × 267px
Total area of the ROI 14521 sqPixels
ROI Occupancy 27.192884 percent
List of coordinates of ROI Perimeter

136.000000 137.000000
 140.000000 150.000000

 138.000000 139.000000
 140.000000 141.000000
 159.000000 164.000000

5 Conclusion

In this study, we have used a highly modified version of the Chan vese algorithm to identify cotton buds from cotton plants. In accordance with recent researches [14–18], our results are very motivating. We have tested the algorithm on our samples and the detection accuracy is $\sim 90\%$. We are highly optimistic about working on this to improve the accuracy further.

References

1. Bhatia N. et al. Survey of nearest neighbor techniques. arXiv preprint [arXiv:1007.0085](https://arxiv.org/abs/1007.0085), 2010.
2. Cai H, Yang Z, Cao X, Xia W, Xiaoyin X. A new iterative triclass thresholding technique in image segmentation. *IEEE Trans Image Process.* 2014;23(3):1038–46.
3. Cortes C, Vapnik V. Support-vector networks. *Mach Learn* 1995; 20(3):273–297, ISSN 0885-6125. doi: [10.1007/BF00994018](https://doi.org/10.1007/BF00994018). <http://dx.doi.org/10.1007/BF00994018>.
4. Costa AF, Humpire-Mamani G, Traina AJM. An efficient algorithm for fractal analysis of textures. In: *IEEE 2012 25th SIBGRAPI conference on graphics, patterns and images (SIBGRAPI) 2012*; p 39–46.
5. Das M, Manmatha R, Riseman EM. Indexing flower patent images using domain knowledge. *Intell Syst Appl, IEEE* 1999; 14(5):24–33.
6. Guru DS, Sharath YH, Manjunath S. Texture features and knn in classification of flower images. *IJCA, Special Issue on RTIPPR.* 2010;1:21–9.
7. Hartigan JA, Wong MA. Algorithm as 136: A k-means clustering algorithm. *Appl Statistics* 1979; 100–8.
8. Li CH, Yuen PC. Tongue image matching using colour content. *Pattern Recogn.* 2002;35(2):407–19.
9. Liao P-S, Chen T-S, Chung P-C. A fast algorithm for multilevel thresholding. *J Inf Sci Eng.* 2001;17(5):713–27.
10. McCulloch WS, Pitts W. A logical calculus of the ideas immanent in nervous activity. *Bull Math Biophys.* 1943;5(4):115–33.
11. Nilsback M-E, Zisserman A.. A visual vocabulary for flower classification. In: *2006 IEEE computer society conference on computer vision and pattern recognition 2006*; vol. 2, p. 1447–54.
12. Nilsback M-E, Zisserman A. Automated flower classification over a large number of classes. In: *Sixth Indian conference on computer vision, graphics & image processing ICVGIP'08; 2008*, p. 722–9.
13. Nilsback M-E, Zisserman A. Delving deeper into the whorl of flower segmentation. *Image Vis Comput.* 2010;28(6):1049–62.

14. Saitoh T, Aoki K, Kaneko T. Automatic recognition of blooming flowers. In: Proceedings of the 17th international conference on pattern recognition, 2004. ICPR 2004; vol. 1, p. 27–30.
15. Sari YA, Suciati N. Flower classification using combined a* b* color and fractal-based texture feature, 2014.
16. Sural S, Qian G, Pramanik S. Segmentation and histogram generation using the hsv color space for image retrieval. In: Proceedings of 2002 international conference on image processing, IEEE, 2002, vol. 2, p. II-589.
17. Tan WN, Tan YF, Koo AC, Lim YP. Petals' shape descriptor for blooming flowers recognition. In: Fourth international conference on digital image processing (ICDIP 2012), International Society for Optics and Photonics 2012, p. 83343K–83343K.
18. Woods K, Bowyer K, Kegelmeyer WP Jr. Combination of multiple classifiers using local accuracy estimates. In: Proceedings of 1996 IEEE computer society conference on computer vision and pattern recognition, CVPR'96, 1996; p. 391–6.

Static Noise Margin Analysis of 6T SRAM Cell

Abinkant A. Jose and Nikhitha C. Balan

Abstract This report describes the SNM calculation and analysis of SRAM cell which are obtained from simulations performed in Cadence Virtuoso 90 nm technology. The SRAM cell structure is implemented with a compact structure of six transistors. Static noise margin is found from the butterfly curve obtained for read, write, and hold modes of operation.

Keywords SNM · Butterfly · Cadence

1 Introduction

Importance of SRAM—static random access memory—is increasing as it is used for a wide range of VLSI application circuits. Two aspects which are important for SRAM cell design are the cell area and the stability of the cell. The cell stability is discussed with butterfly curve analysis which shows graphical representation of the SNM. Cell area is reduced by using 6T implementation. SRAM cell should be able to provide data in read mode, accept data in write mode, and hold the accepted data during hold mode. SRAM cell holds the written data in the cell until the power is on. An ordinary flip-flop also does the same, but the area of the flip-flop is large in comparison to the SRAM. The area, capacitance, and hence the power dissipation is less as the design of SRAM uses only six transistors.

A.A. Jose (✉) · N.C. Balan
Amrita Vishwa Vidyapeetham, Amritapuri, Kollam 690525, India
e-mail: abin.kant@gmail.com

N.C. Balan
e-mail: nikhithacbalan34@gmail.com

2 Overall Design Is Divided into the Following

2.1 Write Driver Circuitry

The 6T SRAM cell contains a latch in order to store the state and two access transistors to enable writing/reading to the SRAM cell, the state. The noise/disturbances are eliminated by the feedback of the latch (Fig. 1).

A. Read Operation

Bit and Bit_b is at logic high state initially. Logic state of Q is low and of Q b is high initially. While WL (Word line) is activated, logic state of bit is lowered by M1 and M5. Now, the logic state of Q begins to rise. M1 lowers the logic state of Q whereas M5 opposes it. So, M1 is sized stronger than M5. The transistors are sized in such a way that the voltage at Q is less than the threshold value of M2/M4 transistor which is known as read stability. Waveforms for the read operation are shown in Fig. 10.

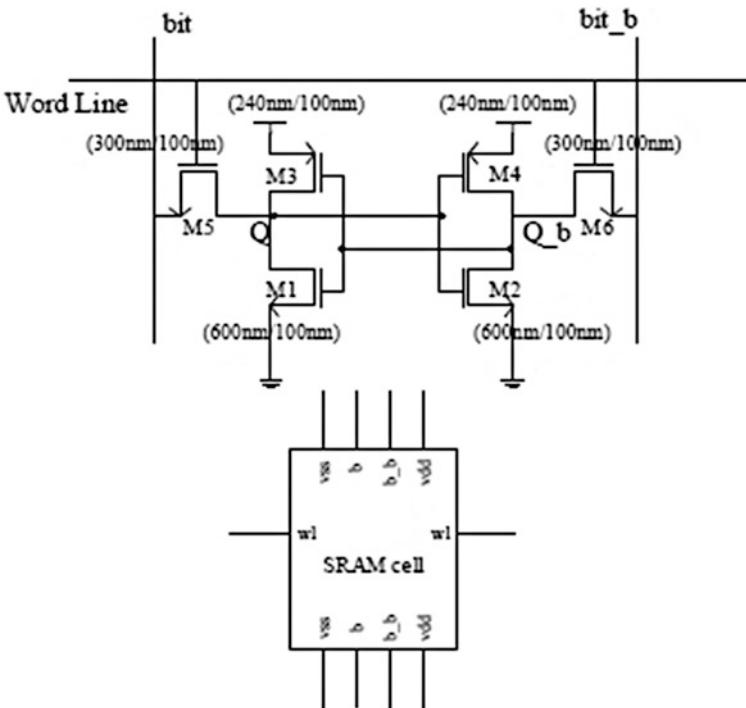


Fig. 1 Schematic and symbol of SRAM cell

B. Write Operation

Logic state of Q is 0. Signal “Bit” is in high state. The write operation happens by forcing Q_b to logic low state through M6. M4 is sized weaker than M6 in order to pull Q_b low enough, which is known as writability (Fig. 2).

C. Cell Stability

To ensure proper read and write operation, the transistors must satisfy cell ratio as well as pull-up ratio. The nMOS pull down transistor, access transistor, and the pMOS pull-up transistor should be the decreasing order of strength for proper operation of the SRAM cell.

Sizing of transistors M1–M6: Consider length of all the transistors as 100 nm, supply voltage as 1.2 V, and mobility ratio as 2.

- Read Operation—Region of operation

M1-Linear, M2-Cut-off, M3-Cut-off, M4-Linear, M5-Saturation, M6-Cut-off. The transistor M1 should be strong enough in order to prevent the read failure (Table 1).

Linear Current (M1) is greater than saturation current (M5).

$$u_n C_{ox} W/L_{(M1)} [(V_{gs} - V_{thn}) V_{ds} - 0.5 * V_{ds}^2] > = 0.5 * u_n C_{ox} W/L_{(M5)} [V_{gs} - V_{thn}]^2$$

Fig. 2 Schematic of SRAM write cell

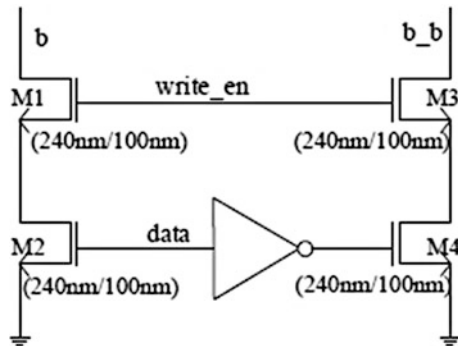


Table 1 Threshold values of transistors in SRAM cell

Transistor	Vth (mV)
M1	237.9
M5	99.28
M3	99.98
M2	-217.1
M4	-230.9
M6	-216.69

$$\text{Cell Ratio (CR)} = W1/W5 \geq 6.7131$$

Hence,

$$W1/L1 = W2/L2 = 600 \text{ nm}/100 \text{ nm}$$

$$W5/L5 = 300 \text{ nm}/100 \text{ nm}$$

- Write Operation—Region of operation

M1—Linear, M2—Cut-off, M3—Cut-off, M4—Linear, M5—Saturation, M6—Linear

Linear current (M6) is greater than linear current (M4).

$$U_n C_{ox} (W/L)_{M6} \left[(V_{gs} - V_{thn}) V_{ds} - \left(\frac{V_{ds}^2}{2} \right) \right] > U_p C_{ox} (W/L)_{M4} \left[(V_{sg} - |V_{thp}|) V_{sd} - 0.5 * (V_{sd})^2 \right]$$

$$\text{Pull-up ratio (PR)} = W_4/W_6 = 4.5$$

$$\text{Hence, } W4/L4 = W3/L3 = 240 \text{ nm}/100 \text{ nm, } W6/L6 = 300 \text{ nm}/100 \text{ nm}$$

2.2 Write Driver Circuitry

The data applied will be written to bit by forcing the qb and bitb to low state.

The transistors in the write driver circuitry are sized minimum.

$$W/L_{M10} = W/L_{M11} = 240 \text{ nm}/100 \text{ nm}$$

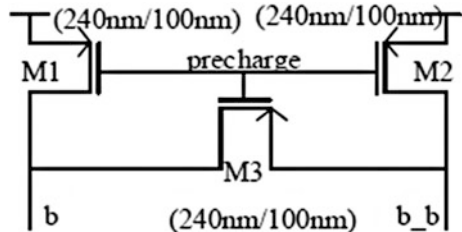
$$W/L_{M12} = W/L_{M13} = 240 \text{ nm}/100 \text{ nm}$$

2.3 Precharge Circuitry

The circuit precharges the bit and bitb signals to logic high state when the clock is logic low state. It includes an equalizing pmos transistor also apart from the two pmos transistors to which the clock signal is applied. The precharge transistors are sized minimum (Fig. 3).

$$W/L_{M7} = W/L_{M9} = W/L_{M7} = 240 \text{ nm}/100 \text{ nm}$$

Fig. 3 Schematic of SRAM precharge cell



2.4 *Simulation of Write and Read Operation into a Single SRAM Cell*

For analyzing the operation of a single SRAM-6T cell, the cell is connected to the precharge circuitry as well as the write driver circuitry. Initially, the bit and bit bar lines are precharged to logic high state by enabling the clock. At this time, of precharge the access transistors will be in off-condition controlled by the word lines. Then, the write-enable signal as well as the word line is activated and data is fed through which it is written into the bit. Again after precharge, the word lines connected to the nmos pair gets into high state which enables the read operation (Fig. 4).

During this time, the write driver will be in off-state which is controlled by activating the write-enable signal to low state. Voltage pulse (V_{pulse}) is applied as input for the clock and word line whose period is 50 ns. Period of data input applied is 60 ns and piece wise linear voltage (V_{pwl}) input is applied for enabling the write operation. Transient analysis simulation is performed for a stop time of 200 ns.

2.5 *SNM Calculation for Read, Write, and Hold Modes of Operation*

Amount of noise that can be applied to the latch before losing the stable state is the Static Noise Margin (SNM) (Figs. 5 and 6).

Hold margin is the static noise margin in the SRAM cell when it is in hold mode, during which either read or write takes place (Fig. 7). The SNM is found from the butterfly curves (Fig. 8).

The SNM for the read margin is smaller than that of hold margin as the access transistors try to pull the low state node to high state. Figure 7 shows the results.

The write margin is the measure of smallest square that can be made between the two curves in Fig. 9.

A. Simulation of Butterfly Diagrams for Hold, Read, and Write Modes of Operation

The circuit diagrams shown are realized in cadence by using a “pvcvs2” source. The corresponding polynomial coefficients are entered in the object properties of pvcvs2.

- Hold state

Access transistors are made off-state by setting word line to V_{ss} . Four pvcvc2 are used to generate V1 and V2 and is plotted with respect to U varying from $-V_{dd}/\sqrt{2}$ to $V_{dd}/\sqrt{2}$, i.e., -848.5 to $+848.5$ m (Fig. 10).

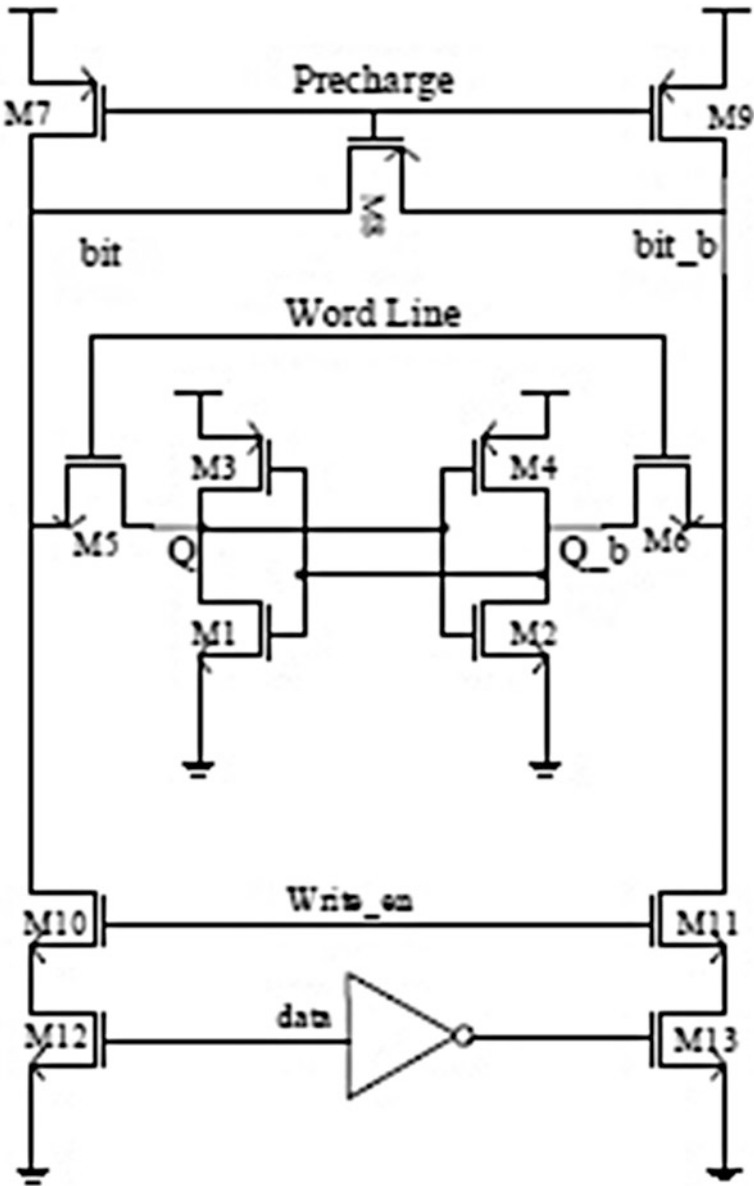


Fig. 4 Schematic of SRAM cell for read and write operation

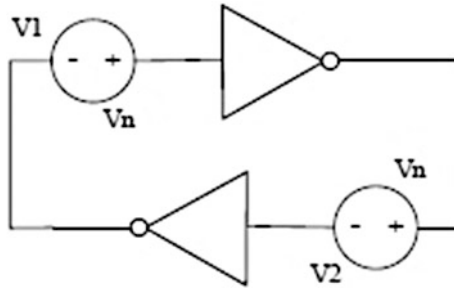


Fig. 5 Cross-coupled inverters with noise sources for hold margin

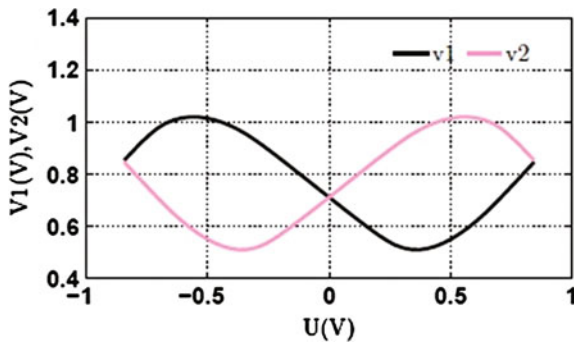


Fig. 6 Butterfly curve for hold margin 45° rotated

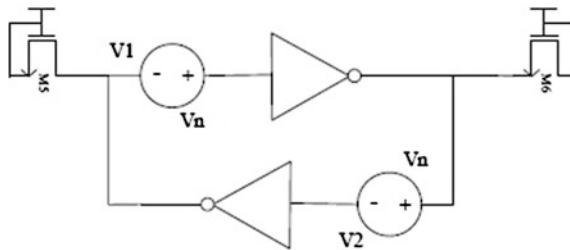


Fig. 7 Cross-coupled inverters with noise sources for read margin

- Read state

Access transistors are made on-state by setting word line to V_{dd} . The bit and bitbar signals are made V_{dd} which is the initial state for read operation. Four pvcvc2 are used to generate V_1 and V_2 and is plotted with respect to U varying from $-V_{dd}/\sqrt{2}$ to $V_{dd}/\sqrt{2}$, i.e., -848.5 to $+848.5$ m (Fig. 11).

Fig. 8 Butterfly curve for hold margin

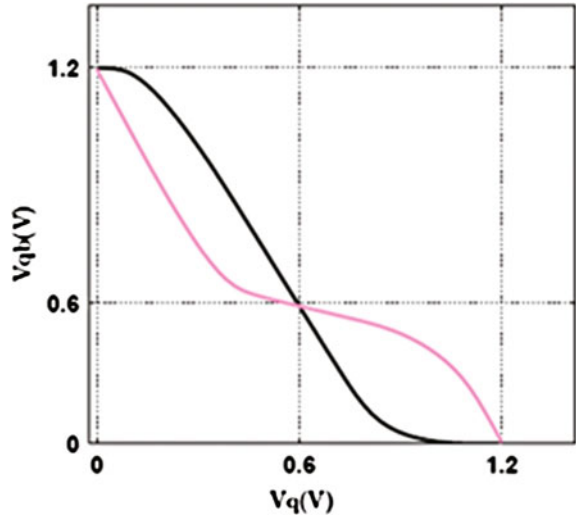


Fig. 9 Cross-coupled inverters with noise sources for write margin

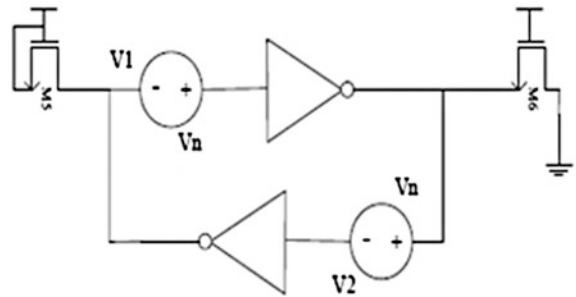


Fig. 10 Butterfly curve for write margin

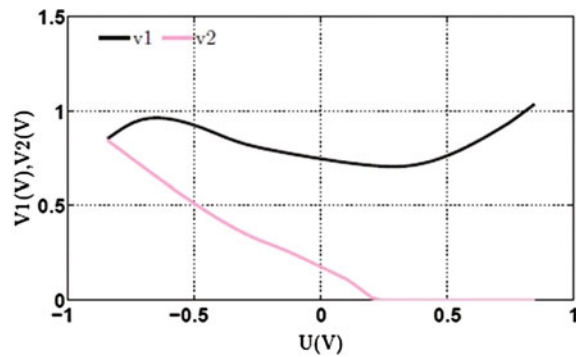
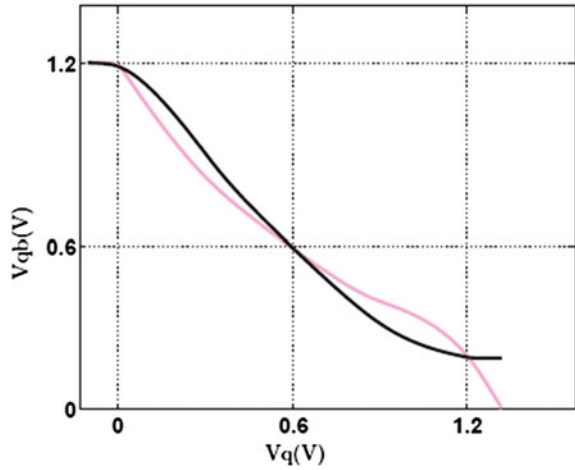


Fig. 11 Butterfly curve for read margin



- Write state

Access transistors are made on-state by setting word line to V_{dd} . The bit and bitbar signals are made V_{dd} and V_{ss} , respectively which is the initial state for write operation (Table 2).

Four pvcvc2 are used to generate V_1 and V_2 and is plotted with respect to U varying to $V_{dd}/\sqrt{2}$ (2), i.e., -848.5 to $+848.5$ m (Figs. 12 and 13).

Table 2 Static noise margin

Corner	Hold margin (m)	Read margin (m)	Write margin (m)
NN	298	130	732
SF	329	217	743
FS	264	122	723
SS	310	141	743
FF	286	121	723

Fig. 12 Butterfly curve for read margin 45° rotated

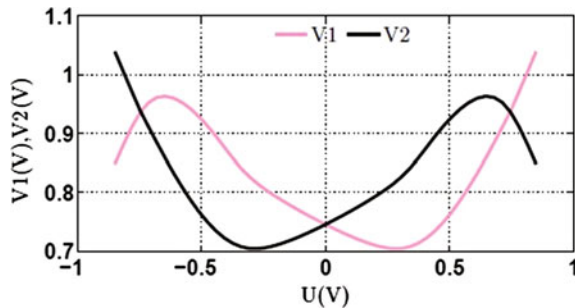
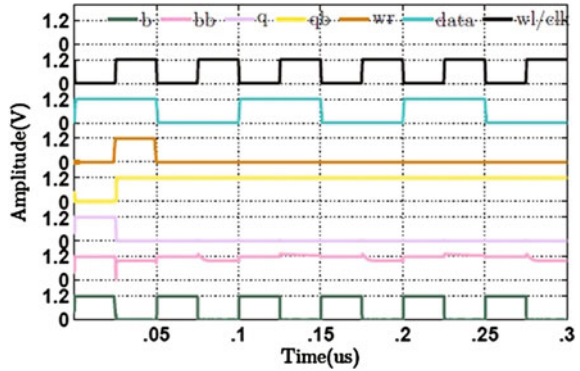


Fig. 13 Output waveform of read and write for a SRAM cell



3 Conclusion

The butterfly diagram simulation as well as the SNM calculation is obtained for all corners. The 6T SRAM CELL is designed, simulated, and analyzed in cadence (virtuoso).

References

1. Grossar E. Read stability and write-ability analysis of SRAM cells for nanometer technologies. IEEE J Solid-State Circuits, vol. 41(11):2577–88.
2. Calhaun BH, Chandrakasan AP. Static noise margin variation for sub-threshold SRAM in 65 nm CMOS. IEEE J Solid-State Circuits 2006; 41:1673–1679.
3. Weste NHE, Harris DM. CMOS VLSI design (fourth edition).
4. Birla S. et al. Static noise margin analysis of various SRAM topologies. IACSIT 2011;3 (3):304–9.
5. Rabaey JM, Chandrakasan A, Nikolic B. Digital integrated circuits (2nd edition).

Topology Preserving Map Generation for Multiple Mobile Fishing Vessels

N. Sruthi, P. Divya and Maneesha Vinodini Ramesh

Abstract In Indian coastal zone, real-time tracking of fishing vessels is nonexistent. This leads to numerous challenges in search and rescue operation, communicating emergency messages, etc. A quick solution for this is to install GPS devices, which is costly. In our research work, we designed and developed a low-cost hybrid solution with minimum number of location aware nodes. Real-time relative location information of mobile sensor nodes was developed by integrating mobility management, virtual coordinate system (VCS), and topology preserving map (TPM). The architecture is implemented in MATLAB and is tested with a rectangular network scenario with up to five mobile nodes and is able to track the relative location trace of mobile nodes at a particular interval of time. The effect of various simulation parameters such as communication range, node placement, number of mobile nodes, and sampling rate selection in tracking the mobile nodes with our system is also performed.

Keywords Virtual coordinate system • Singular value decomposition • Topology preserving maps • Fishing vessels • Mobility management • Tracking

1 Introduction

Wireless sensor network (WSN) is a fast growing technology due to its advantages including portability, low cost, flexibility, and the ease of instantaneous network installation. WSN has diverse applications including precision agriculture, healthcare

N. Sruthi (✉) · P. Divya · M.V. Ramesh
Amrita Center for Wireless Networks and Applications, Amrita Vishwa Vidyapeetham,
Kollam, Kerala, India
e-mail: sruthinnampoothiri@gmail.com

P. Divya
e-mail: divyap@am.amrita.edu

M.V. Ramesh
e-mail: maneesha@am.amrita.edu

monitoring, disaster monitoring, habitat monitoring, border security, fish vessel monitoring, etc. The type of sensed data, accuracy, and the scalability depends on the application of WSN. Efficient localization techniques have to be developed for wide area monitoring, real-time detection, tracking of nodes, etc.

Accurate localization can be performed with GPS-based systems. This is extensively used for object tracking and monitoring in wide area networks. But the main problem with GPS-based systems is the cost and complexity associated with it. Alternate localization techniques are based on RSSI (received signal strength indication) and connectivity information. But RSSI can easily be affected by interference. Connectivity information method is based on number of hops to a subset of nodes having location information. Virtual coordinate system (VCS) is a recent technique based on connectivity information for localization [3]. However, VCS lacks the directional information and therefore an enhanced location map is needed. TPM (topology preserving map) is used to include directional information without the need of physical distance information.

Applications such as disaster management, habitat monitoring, border security, fish vessel monitoring, etc., would involve mobility of a few nodes. Tracking of a moving object effectively by considering both localization of the target and navigation of mobile sensors is a major challenge in wireless sensor network. This research work deals with localization and tracking of multiple mobile nodes. In this work, we propose a tracking algorithm called topological coordinate-based tracking for multiple mobile nodes (TCTM), which considers the impact on tracking based on anchor placement, transmission range, density of mobile nodes, etc. To our best of knowledge, the proposed algorithm is the first demonstration for efficient tracking of multiple mobile nodes using TPM. Our objective is to implement this work for monitoring the fishing vessels in Indian coastal zone.

Section 2 provides a comprehensive study and background information on existing techniques and its problems in this area. Section 3 explains the system architecture and design. Then the algorithm is explained in Sect. 4. The simulation and the results have been presented and analyzed in Sect. 5. Finally the paper is concluded, and the future scope of the presented work is described in Sect. 6.

2 Related Works

Target tracking and sensor routing is necessary when a mobile object does not follow a predictable path. Various target localization approaches based on different approaches are raised in which each can be used according to the applications. Localization in wireless sensor networks [1] can be explained as the problem of getting individual sensors awareness with respect to a coordinate system of the entire network. The sensor localization problem or finding out location information can be through actual distance metrics or through relative metrics [2].

MDS-MAP [1] is having comparatively high accuracy, but its algorithm complexity is very high since every node has to find the distance to every other node.

TOA or RSSI-based methods are better for low-cost applications. Virtual coordinates (VC)-based localization scheme is developed using a subset of nodes called anchor nodes where each virtual coordinate represent the minimum hop distance to anchors. VCS is one of the best alternatives in terms of cost [3].

Physical layout information includes physical voids, sensor node's relative physical position, etc. VCS lacks this layout information since it loses the directionality of node position in virtual coordinate domain. If information on physical topology is available, lost directionality can be regained. Topology preserving maps [4] is one of the best methods to regain the directionality of VCS. Due to the calculation complexity, MDS cannot be used for generating topology preserving maps (TPM). Singular value decomposition (SVD) technique can be used to generate TPM from VC [4].

Detection and tracking of mobile sensor node in a network commonly exploit physical location information using GPS or RSSI. The predictive location tracking (PLT) scheme for mobile devices [5] is a tracking method that uses predictive location information obtained from Kalman filter in the deficient signal sources environment. All these methods need GPS and having the negative consequences of high cost, high energy consumption, poor routability under concave physical voids, etc. In order to avoid the cost and complexity associated with existing detection and tracking systems, mobile target detection, prediction and tracking (TCTP) algorithm [6] is proposed that uses the concept of TPM for localization.

Mobility models [7] help in describing the movement pattern of users and their location, velocity, and acceleration change over time.

Both VCS and TPM are generated based on the hop distances and therefore not having negative consequences like cost, fading, and low-signal strength. Since VCS and TPM does not rely upon analog measurements, they are free of the cumulative errors and can maintain the quality in large networks.

Existing work only focused on the TPM generation of a single mobile node in a static network. But in our work, we focus on the monitoring and tracking of mobility of multiple mobile sensor nodes based on VCS technique in a static network.

3 Design of Tracking Fishing Vessels

There are numerous fishing vessels, each of different sizes, are present in Indian coastal zone. These vessels engage in fishing in the sea for duration of a day to a maximum of 15 days. Even though some of the fishing vessels are equipped with wireless devices, they do not receive connectivity beyond 20 km, but they have to travel a maximum of 200 km in the sea. Also all the fishing vessels do not have GPS to inform about their location when they are in a distress, or they see any abnormal behavior. Due to the nonavailability of connectivity, accurate location information, etc., emergency management in the sea, locating and tracking fishing vessels, search and rescue operation after some mishap etc., becomes very tedious job to accomplish.

This work aims in developing relative location awareness among the fishing vessels that will aid in developing effective emergency management in sea, search and rescue operations, etc. Monitoring, localizing, and tracking in the sea are very challenging, due to the higher density of mobile nodes with very low connectivity. Hence, we have to develop a tracking system which is scalable and cater to the challenges of very large adhoc network with mobility.

In this work, we have considered a network consisting of both static and mobile nodes which are connected to the base station using multihop communication. GPS-enabled base stations are considered to be on the shore. We assume that there exists a small number of location aware primary nodes which act as the anchor nodes for this application. The primary nodes can be buoys or relatively static boats that could communicate with the base station.

Sea has several fishing zones and these zones change with respect to the time, climatic condition, wind direction, water quality, etc. The fishing vessels reach the fishing zones mostly in groups, and they remain in the same fishing zone for long duration. After that they may return to the fishing port for selling the fish, or they may continue to travel to another fishing zone.

For fishing, the fisherman form their own 'buddy group' who will engage in fishing in the same zone, move to and from the shore almost at the same time. We can call these groups of fishing vessels as 'buddy groups,' since they share their trade secrets also. For a particular fishing zone, we assume that the fishing vessels in the buddy groups are static for a predefined time δ . These static fishing vessels in buddy groups can be considered as secondary boats. Within δ time, some vessels will finish fishing and start moving or some other vessels may enter into this fishing zone. During that time period, they can form adhoc network in that fishing zone. Our aim is to track the movement of these mobile fishing vessels.

The moving fishing vessels may not be in the connectivity range of the BS. However, they will establish the connectivity through the primary nodes or secondary nodes. In our system, we consider the tracking of mobile boats in a particular fishing zone within the δ time. The proposed system architecture for multiple mobile nodes connected to one base station is shown in Fig. 1.

4 Topological Coordinate-Based Tracking Algorithm for Multiple Mobile Nodes (TCTM)

In large scale monitoring applications, GPS-based localization and tracking of multiple mobile nodes will increase the total cost of the system. And most of the times, GPS-based localization will not be an economically viable solution for the individual nodes. In this work, we aim to develop a tracking algorithm for multiple mobile nodes which are unaware of their locations. The relative locations of these nodes based on their anchor nodes are developed using the proposed algorithm.

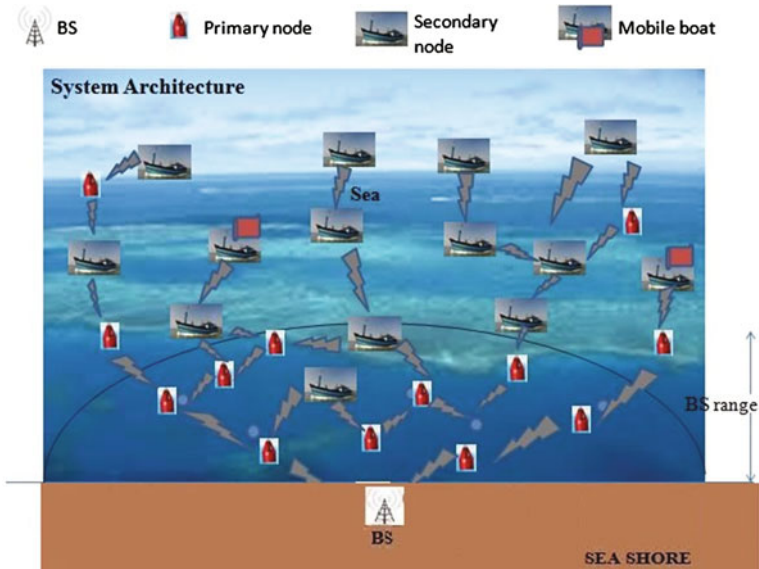


Fig. 1 System architecture

The major assumptions are most of the nodes are static and a percentage of mobile nodes are present in the network. The number of anchors nodes will be very less than total density of nodes. The communication range of all nodes is same. The communication delay among sensors is considered to be negligible in our system. Centralized topology is maintained by the network of nodes.

As explained earlier, very few nodes are aware of its location such as anchor nodes, and the majority of nodes are unaware of their own location. Under the above-mentioned conditions, the proposed algorithm is designed to identify the relative location of mobile nodes, to track the mobile nodes, to identify the buddy nodes, and to identify the area of operation by mobile nodes.

An algorithm is developed to implement the tracking of multiple mobile nodes in a static network. Proposed model and algorithm details are explained in this section. Proposed model involves different input parameters and three main phases. The phases in the proposed model are explained below and its block diagram is shown in Fig. 2.

Initialization Phase This phase is intended for identifying the hop distance from each anchor node to each of the static and mobile nodes. As discussed earlier, our network includes primary nodes or buoys and static secondary boats. Initially, base station will inform to all nodes about the input parameters such as total number of nodes in the network and total number of anchor nodes. Every node will send beacons, in which all anchor nodes are set as the destination address, and this beacon will be heard by neighbor nodes in its range. Thereby a single node will get

TPM Generation Phase Physical domain to virtual domain transformation is a one to many mapping. Here the coordinates are concentrated around anchor nodes. So in virtual coordinate domain, directionality of a node loses. Some information on the physical topology is needed to regain the directional information. So to obtain topological or directional information, VCS to any other domain is needed. The main two methods for this transformation are directional virtual coordinate (DVC) system and topology preserving map (TPM). TPM is less complex than DVC and is more economical. So we use TPM in our work to generate the network.

VC matrix contains higher dimensional information of the network and its connectivity. So it will not contain the topological information and has to be extracted from virtual coordinates. This transformational map is similar to the actual Cartesian coordinate map and is a distorted version of physical map. Singular value decomposition (SVD) is used to create the TPM from VCS. TPM is homeomorphic to the physical network and preserves internal and external boundaries of the network. SVD helps to decompose the higher-dimensional VC matrix into lower-dimensional matrices which can then be used to extract the topological information. If our network has N nodes and M anchor nodes. Then SVD of the VC matrix [4], P is given as:

$$P = U \cdot S \cdot V^T, \tag{1}$$

where U , S , and V are $N * N$, $N * M$, and $N * N$ matrices, respectively.

Here U and V are unitary matrices because $U^T \cdot U = I_{M * M}$ and $V^T \cdot V = I_{N * N}$ and S is the diagonal matrix. The optimal basis for the matrix P^T is V and with this basis, $U \cdot S$ will give the coordinates for the dataset P . Elements in S are the singular vales arranged in descending order and provides unequal weights on columns of U . Singular vales are nothing but the square root values of Eigen values. So the principal component matrix is:

$$P_{SVD} = U \cdot S \tag{2}$$

Since the principal component matrix can be generated with the projection of P on to V , we can write P_{SVD} as:

$$P_{SVD} = P \cdot V \tag{3}$$

Principal component matrix, P_{SVD} contains the information about the original coordinate set and is arranged in its descending order. That is first column or the first ordinate contains the most important information especially the radial information. But this ordinate will not give us enough information to identify nodes distinctly. So we go for second and third ordinates for generating TPM. Since SVD provides orthonormal basis, all ordinates are orthogonal to each other. Second and third ordinates provide a set of two-dimensional Cartesian coordinates for node

positions. That means each node will have an x -topology coordinate (TC) from the second ordinate and y -TC from the third ordinate which is given by:

$$[X_T, Y_T] = [P_{SVD}^{(2)}, P_{SVD}^{(3)}] \quad (4)$$

Thus, we get the topology information without any physical layout information other than hop count from anchors. With this method, base station generates TPM of the network after generating VC matrix.

The number of anchors and their placement in the network is critical for generating better topological maps [8]. Increase in number of anchors will increase routability and decrease probability of having identical coordinates for different nodes. But over placement of anchors degrades routing performance. Also an increase in anchor nodes will increase the VC generation cost and an increase in the length of address field of packet. This in turn increases energy consumption. Under placement of anchors causes identical coordinates. Thus, the determination of the number of anchor together with their placement remains a challenge for generating TPM.

Updation Phase If there are external mobile nodes come into the network, the network will updates its network size and will create VC matrix of network including mobile nodes. Then this VC matrix is used to create TPM of the network.

Tracking Phase Here an administrator at the sea shore can trace the location of a fishing vessel while it is moving or static using the TPM network map. We generate VC and TPM at every sampling time to track the mobile node. Due to the movement of mobile nodes, its hop distance to anchor nodes changes, and this will change virtual coordinate of mobile nodes at every sampling interval. Thus, VC matrix and accordingly topology coordinate (TC) of mobile nodes also changes during every sampling interval. By comparing the TC of mobile nodes with that of other nodes, we get the idea of nearest neighbors and its residing area. Thus, the connectivity can be established through the neighbors and can track the mobile node from the shore station. Based on the proposed model, we developed the TCTM algorithm of our network.

5 Simulation and Results

MATLAB R2011a is used as the simulation environment since it has both the support of linear algebra and mobility. MATLAB codes are developed for generating TPM for multiple mobile nodes. The steps involved in the simulation environment of TCTM algorithm as follows.

- Step 1: Input number of nodes and number of anchor nodes.
- Step 2: Create actual network of static nodes.
- Step 3: Input the number of mobile nodes as next input.

Step 4: Simulate the mobility model (e.g., Random waypoint mobility model) to generate the trace of mobile nodes by taking various mobility parameters including speed, axes, pause time, simulation time, etc. Random waypoint model allows each node to randomly select a particular node as the destination and travels to that destination with a constant speed.

Step 5: Update the network size by adding external mobile nodes (if any) into the network.

Step 6: Create VC matrix of the network by performing dijkstras algorithm which is a distance vector routing algorithm. Dijkstras algorithm helps in finding minimum number of hop counts from each and every node (source) to all anchor nodes (destination).

Step 7: Generate TPM from VC using SVD.

Step 8: Repeat Step 5, 6 and Step 7 in every sampling period.

Step 9: Modify the network size into the default size of the network by removing the number of mobile nodes.

The performance of our proposed system is evaluated using ‘Rectangular grid network.’ We generate TPM for the network and are able to track the area residing by the mobile node. Analysis of tracking is performed by comparing the TPM with the actual network map. We have also performed analysis of the effect of various simulation parameters that affect tracking and TPM.

5.1 TPM Generation and Tracking of Mobile Fishing Vessels

In our network, system fishing vessels are not GPS equipped. Topological coordinate generation of network helps to track the fishing vessels in sea in the absence of GPS. In δ time, base station generates TPM for the whole network and estimates the neighbors of each fishing vessel and also its connectivity information. When external mobile fishing vessels come, network size must get updated. TPM generation has to be done in each sampling interval in order to trace the track of mobile node. Sampling interval should be very small than δ . For the connectivity with the mobile fishing vessels in the absence of GPS in a particular sampling period, the neighborhood information based on the range of fishing vessels is needed and will get from the TPM. Thus, the tracking of mobile fishing vessels and connectivity with them can be achieved without using GPS in the fishing vessels.

The rectangular grid network consists of 100 nodes which represents primary nodes and secondary fishing vessels. The TPM generation result with multiple mobile fishing vessels during different sampling intervals with a communication range of 6 units is shown in Fig. 3.

Analysis To evaluate the amount of clarity, we have performed the mobility model in actual network map, and this serves as a baseline for comparison for TPM

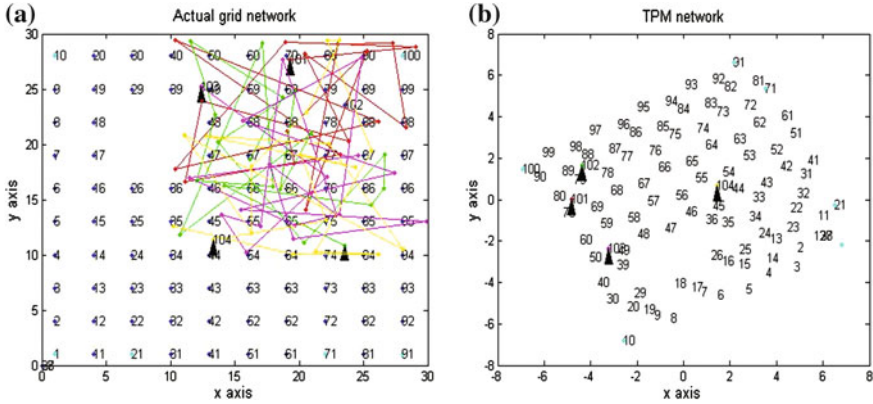


Fig. 3 First trace position of four mobile nodes in static network (a) and in TPM (b)

map. Actual map is shown in Figs. 3a and 4a. It is clear from Figs. 3b and 4b that TPM is the distorted version of actual map. In all our figures, we use the color code as: red for first mobile node, green for second mobile node, magenta for third mobile node, yellow for fourth mobile node, and black for fifth mobile node. Triangular pointer shown in the trace of all our figures gives the present position of mobile nodes. From the TPM map, we can say that the mobile node is nearer to which static fishing vessel or anchor node in a particular sampling period.

From Table 1, we can see that the nearest neighbors of a mobile node in physical map and the TPM map are almost same. With this understanding, we can search a mobile node in the range of that static fishing vessel or anchor node in that particular sampling period. We can communicate with that boat from the base station through the anchor node and through the secondary node. Thus, we get connectivity with the boat without using GPS in the fishing vessels.

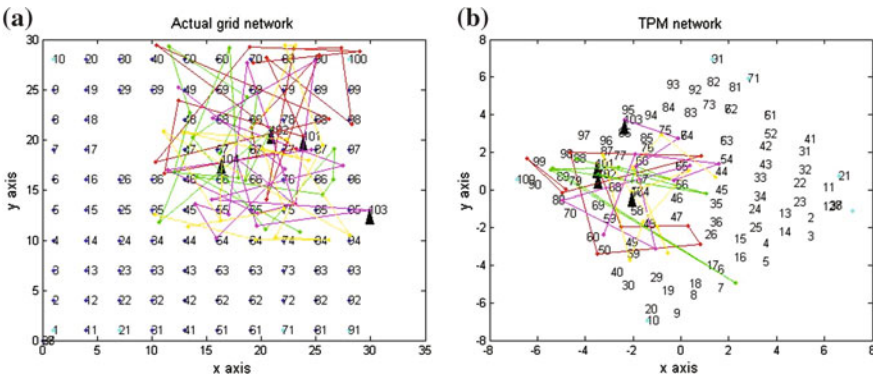


Fig. 4 Tenth trace position of four mobile nodes in static network (a) and in TPM (b)

Table 1 Nearest neighbors of mobile node in actual network and TPM from Fig. 5

Mobile nodes	Nearest neighbor during sampling period 1		Nearest neighbor during sampling period 10	
	Actual network	TPM	Actual network	TPM
4 mobile nodes	60, 69, 70,80	69, 70, 80	77, 78, 87, 88	77,78,87, 88
	78, 79, 88, 89	78, 79, 88, 89	67, 68, 77, 78	68, 78
	39, 48, 49, 50	39, 49, 50	95	95
	44, 45	44, 45	56, 57	57

5.2 Analysis of Effect of Simulation Parameters

Tracking accuracy, complexity, and delay in a network that consist of mobile nodes and vary with change in simulation parameters. The main simulation parameters considered in our system are anchor placement, communication range of nodes, number of mobile nodes, and sampling interval.

Effect of Anchor Node Placement We consider two different anchor node placements in the system. According to the shape of the anchor node placement, we call each placement as half bucket shape placement and full bucket shape placement. From Figs. 5 and 6, it is clear that full bucket shape placement gives good results compared to the half bucket shape placement. We consider nodes in the upper half of the network as anchor nodes only in the full bucket shape placement. When we consider the boundary nodes as anchor nodes, better TPM can be obtained [8] and is evident from our results. It is difficult to use top level nodes as buoys in sea. So we select full bucket shape placement for our system for better TPM generation.

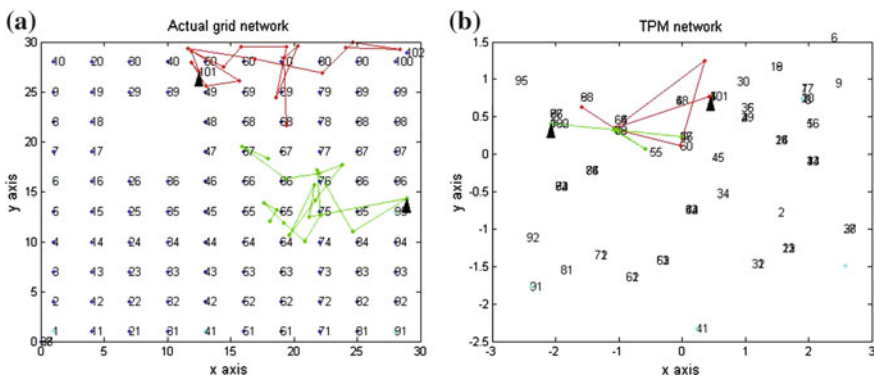


Fig. 5 Half bucket shape anchor placement in actual network (a) and in TPM (b) with two mobile nodes during tenth sampling interval with range 10

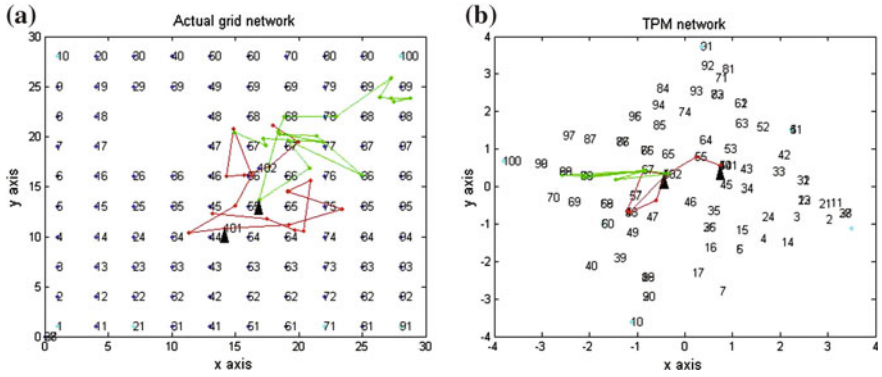


Fig. 6 Full bucket shape anchor placement in actual network (a) and in TPM (b) with two mobile nodes during tenth sampling interval with range 10

Effect of Node Range Different communication ranges considered in our system for evaluation are 6 and 10. The evaluation results in Figs. 7 and 8 show that communication range has a high impact on TPM performance. When the range of a node is very high or too small, the accuracy and performance of TPM degrades. When range is medium, we get good performance. TPM degradation in a high-range network is due to the small hop count to all anchor nodes from a node. Here node has high range and thus anchor nodes are reachable with one or two hops. This will result in a less accurate VC matrix and will result in a bad TPM with so many overlapping of nodes. In the case of small range, nodes cannot reach to all anchor nodes. So a node has to generate virtual coordinate with small set of anchor nodes and will end up in less accurate TPM. If TPM accuracy is less, this will adversely affect the tracking accuracy. So it is essential to select an optimum range for better tracking accuracy in VCS-based tracking. This optimum range selection shows the fact that our system performs well in a multihop system.

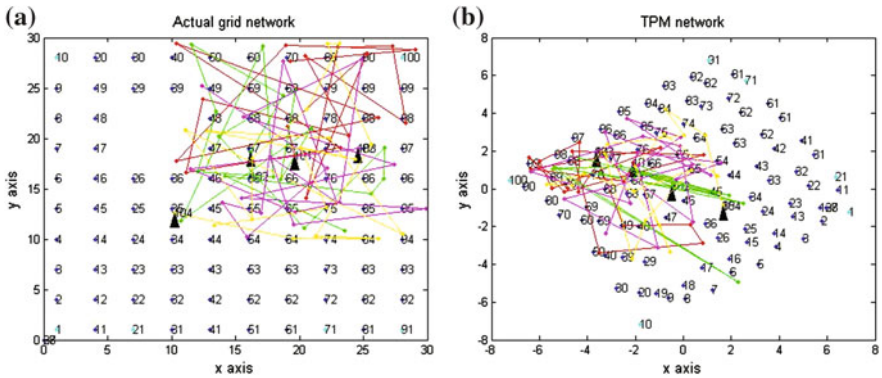


Fig. 7 Actual network (a) and TPM (b) with four mobile nodes during final sampling interval with range 6

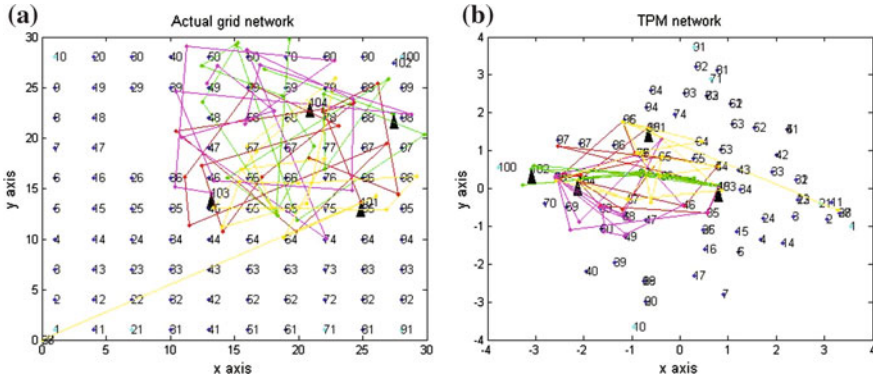


Fig. 8 Actual network (a) and TPM (b) with four mobile nodes during final sampling interval with range 10

Effect of Number of Mobile Nodes We have showed the evaluation results with different number of mobile nodes in figures of this paper. Even though the effect of number of mobile nodes has qualitatively less impact, it has a high impact on the system performance when we have done a quantitative analysis. When number of mobile node in the network increases, overhead to the base station becomes high and thereby increases the system complexity. Chance of sending data to a wrong destination- mobile node by mistake is very high in a network having large number of mobile nodes moving with less distance between them. Also the delay in communication in such a network is high. Thus, a proper ratio between number of mobile nodes, and number of base stations should be there for the efficient handling of tracking of mobile fishing vessels in sea.

Effect of Sampling Interval An average speed of mobile fishing vessel in sea is approximately 8–12 km/hr. For an effective tracking by considering the speed of mobile node, a proper sampling interval is needed. If sampling interval is very large, the tracking performance degrades because of the failure in updating tracking information in time. If it is too small, overhead given to the base station in computation is very large. So it is better to take an optimum sampling interval.

6 Conclusion and Future Works

Present techniques for monitoring and tracking of mobile fishing vessels in sea faces the problem of high cost and complexity because of the use of GPS. In our work, we presented an algorithm for generating TPM for multiple mobile fishing vessels and performed its tracking in a fishing zone which remains static for a predefined time. We also performed a detailed analysis on tracking of mobile

fishing vessels and the various simulation parameters such as anchor node placement, communication range, density of mobile nodes, and sampling interval that will affect the quality of TPM. Our simulation results show that the tracking of multiple mobile fishing vessels can be accomplished even without any geographic information. When communication range and anchor placements are optimum, we can track the mobile nodes with high accuracy using the TPM technique. Future work can be the mobility consideration of fishing vessels, which remained static for a predefined time, between two fishing zones and the methods to optimize the simulation and operation parameters with a view of real-time monitoring and tracking the fishing vessels in sea.

Acknowledgments We would like to express our sincere gratitude to Dr. Anura P. Jayasumana, Professor, Colorado State University, USA, for the time he dedicated to help us in our research work and the seamless guidance and support. Also we would like to express our gratitude for the immeasurable motivation and guidance provided by Sri. (Dr) Mata Amritanandamayi Devi (AMMA), Chancellor of Amrita University. This project is partly funded by a grant from Information Technology Research Agency (ITRA), Department of Electronics and Information Technology (DeitY), Govt. of India.

References

1. Wang J, Ghosh R, Das S. A survey on sensor localization. *J Control Theory Appl.* 2010;8(1): 2–11.
2. Tse D, Viswanath P. Localization in wsn. In: *Fundamentals of wireless communications.* Cambridge University Press; 2005.
3. Chen M, Wang X, Leung VC, Yuan Y. Virtual coordinates based routing in wireless sensor networks. *J Control Theory Appl.* 2006;4:325–30.
4. Dhanapala DC, Jayasumana AP. Topology preserving maps from virtual coordinates for wireless sensor networks. In: *Proceedings of the 2010 IEEE 35th conference on local computer networks, ser. LCN'10, Washington, DC, USA, IEEE Computer Society; 2010.* pp. 136–43.
5. Zou Y, Chakrabarty K. Distributed mobility management for target tracking in mobile sensor networks. *IEEE Trans Mob Comput.* 2007;6(8):872–87.
6. Jiang Y, Dhanapala DC, Jayasumana AP. Tracking and prediction of mobility without physical distance measurements in sensor networks. In: *Communications (ICC), IEEE international conference; 2013.* pp. 1845–50, June 2013.
7. Bai F, Helmy A. Chapter 1 a survey of mobility models in wireless adhoc networks.
8. Dhanapala DC, Jayasumana AP. Anchor selection and topology preserving maps in wsns; a directional virtual coordinate based approach. In: *Local computer networks (LCN), IEEE 36th conference; 2011.* pp. 571–79, Oct 2011.

Accumulator Design in Cadence 90 nm Technology

Nikhitha C. Balan and Abinkant A. Jose

Abstract This paper describes the characteristics and analysis of accumulator which are obtained from simulations performed in Cadence (Virtuoso) and done the layout. The sizing strategy used for sizing the standard cell blocks used to build the accumulator result in a minimum propagation delay between input and output.

Keywords Accumulator · D-FF · Sizing strategy · Adders

1 Introduction

An accumulator is designed which accumulates the inputs provided at each clock and provide the added result as the output. Addition is done with the aid of full and half adders. The memory for storing the previous result to be added with the new input is done with the aid of D FFs. The Design and Layout of the accumulator is carried out in cadence virtuoso gpdk90 nm technology.

2 Used Standard Cells

2.1 Half Adder

Inputs to the half adder A and B produce a 2-bit output represented by the sum (S) and carry (C) bits. From the circuit schematic (Fig. 1), inputs as well as their complements are used to generate the C and S. In order to implement sum and carry

N.C. Balan (✉) · A.A. Jose

Amrita Vishwa Vidyapeetham, Amritapuri, Kollam 690525, India
e-mail: nikhithacbalan34@gmail.com

A.A. Jose
e-mail: abin.kant@gmail.com

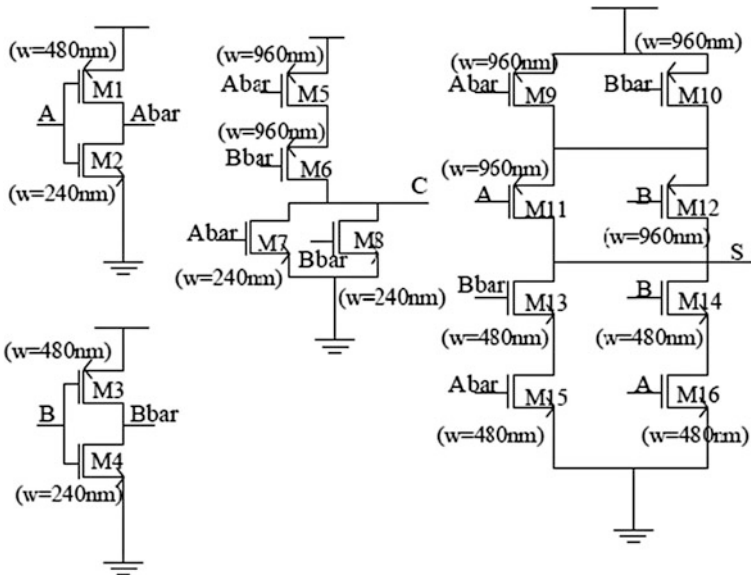


Fig. 1 Schematic of half adder

Table 1 Truth table of half adder

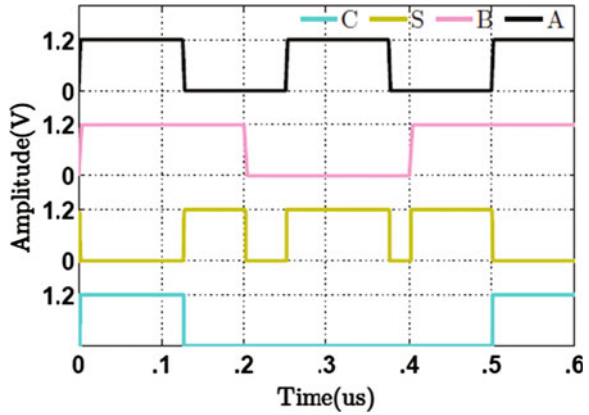
A	B	Carry	Sum
0	0	0	0
0	1	0	1
1	0	0	1
1	1	1	0

expressions (logic functions) using CMOS, carry expression $A \cdot B$ is converted to $(A'+B)'$ and sum expression $(A \oplus B)$ to $(A'B'+AB)'$. For gpdk 90; $W_{min} = 240$ nm and $L_{min} = 100$ nm [1].

Carry (C) Generating Circuit: Carry generating circuit is a NOR gate. On considering the pull-down path, equivalent resistance of M7 and M8 is R_n which is same as the equivalent pull-down resistance of the UNIT INVERTER. Size of M7, M8 = size of nMOS (Unit inverter) = 240 nm/100 nm. On considering the pull-up path, equivalent resistance is $2 R_p$ (as M5 and M6 are in series). Equivalent resistance of UNIT INVERTER is R_p with a pMOS device size of 480 nm/100 nm. In order to equalize the equivalent resistances, Size of M5, M6 = 2 size of pMOS_{Unitinverter} = 2×480 nm/100 nm = 960 nm/100 nm (Table 1).

Sum (S) Generating Circuit: Pull-down path consists of 2 branches. One path includes transistors M14 and M16 while the other path comprises of transistors M13 and M15. Each path contributes an equivalent resistance of $2R_n$ compared to R_n (Equivalent resistance of pull-down nMOS in the Unit inverter). As the size of the nMOS in the unit inverter is 240 nm/100 nm, to equalize the equivalent

Fig. 2 Transient response of half adder



resistances, Size of M13, M14, M15, M16 = 480 nm/100 nm. Similarly, we can find size of M10, M12, M9, M11 = 960 nm/100 nm.

Sizing of Inverters: Output of the inverter which produce Abar is connected to the gates of M5, M7 (carry circuit) and M9, M15 (sum circuit). Output capacitance of the inverter is equal to the sum of input capacitances offered by the different gates connected to the inverter output which is equivalent to the sum of all gate sizes (M5, M7, M9, M15) = 960 nm + 960 nm + 240 nm + 480 nm = 2640 nm. Input capacitance of the inverter equal to output capacitance of inverter/4. Input capacitance of inverter is 3C (2C of pmos and 1C of nmos). Then, Size of the nMOS device (M2) = 2640/(4 × 3) = 220 nm. This value is below 240 nm, so we can take $W_n/L_n(M2) = 240 \text{ nm}/100 \text{ nm}$; $W_p/L_p(M1) = 2 \times W_n/L_nM2$; $W_p/L_p(M1) = 480 \text{ nm}/100 \text{ nm}$. Apply same approach to Bbar generating inverter. Then, $W_n/L_n(M4) = 240 \text{ nm}/100 \text{ nm}$; $W_p/L_p(M3) = 2 \times W_n/L_nM4 = W_p/L_pM3 = 480 \text{ nm}/100 \text{ nm}$.

Voltage pulse (V pulse) of periods 250 and 400 nm is applied as inputs A and B. To plot the outputs Sum and Carry, transient analysis simulation is performed for a stop time of 600 ns (Figs. 2 and 3).

2.2 Full Adder

A full adder circuit accepts 3 inputs, performs the addition of the 3 signal states and produce 2 outputs. From the circuit schematic shown in Fig. 4 A, B, C are the 3 inputs and Sbar, Cbar are the outputs of the full adder circuit. It requires a total of 24 transistors to produce the Cbar and Sbar outputs. The Cbar generating circuit is a part of Sbar generation also (Table 2).

This circuit also knows as mirror adder. It is easy to draw layout because of the beauty of the circuit.

Sizing Strategy: We can size the pull-up paths up to Cbar node. Pull-up path consists of three branches. These paths include transistors (M1, M3), (M2, M3) and

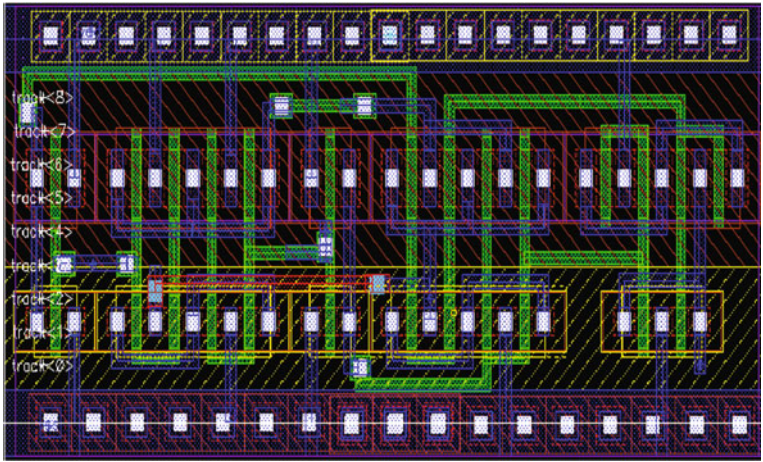


Fig. 3 Layout of half adder

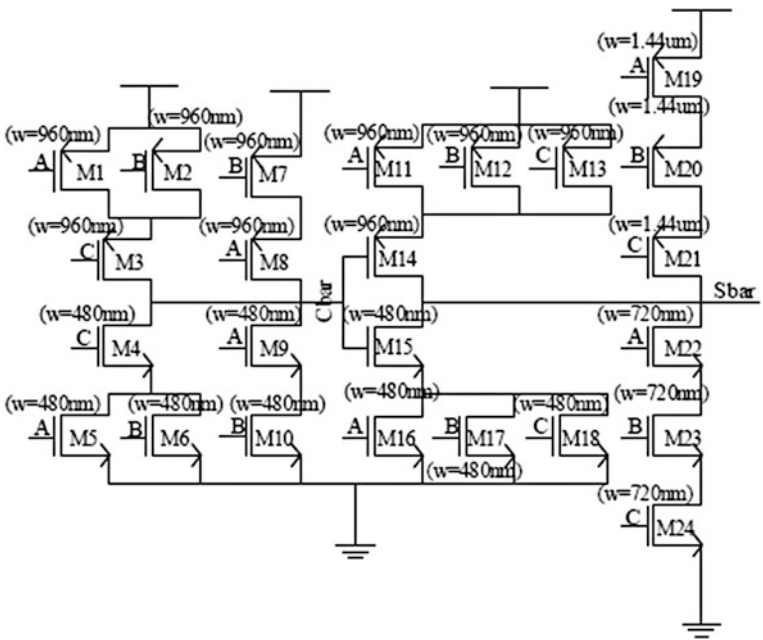


Fig. 4 Schematic of full adder

(M7, M8). Each path contributes an equivalent resistance of $2R_p$, compared to R_p , (Equivalent resistance of pull-up pMOS in the Unit inverter). As the size of the pMOS in the unit inverter is 480 nm/100 nm, to equalize the equivalent resistances,

Table 2 Truth table of full adder

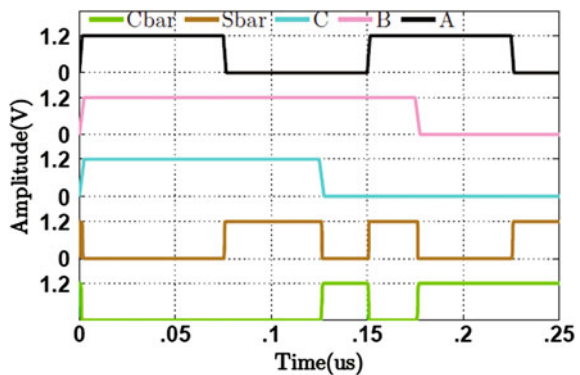
A	B	C	Carry	Sum
0	0	0	0	0
0	0	1	0	1
0	1	0	0	1
0	1	1	1	0
1	0	0	0	1
1	0	1	1	0
1	1	0	1	0
1	1	1	1	1

Size of M1, M2, M3, M7, M8 = 960 nm/100 nm. By applying same concept we can find the size of pull-down path transistors.

As the size of the nMOS in the unit inverter is 240 nm/100 nm, to equalize the equivalent resistances, Size of M4, M5, M6, M9, M10 = 480 nm/100 nm. Now we can size the pull-up path up to Sbar node. Pull-up path consist of four branches. On considering the first 3 paths which include transistors (M11, M14), (M12, M14) and (M13, M14), each path contributes an equivalent resistance of $2R_p$ compared to R_p (Equivalent resistance of pull-up pMOS in the Unit inverter). As the size of the pMOS in the unit inverter is 480 nm/100 nm, to equalize the equivalent resistances, Size of M11, M12, M13, M14 = 960 nm/100 nm. Considering the fourth path, which include transistors (M19, M20, M21) each path contributes an equivalent resistance of $3R_p$ compared to R_p (Equivalent resistance of pull-up pMOS in the Unit inverter). As the size of the pMOS in the unit inverter is 480 nm/100 nm, to equalize the equivalent resistances, Size of M19, M20, M21 = 1440 nm/100 nm. Pull-down path size can be found by same approach. The size of M15, M16, M17, M18 = 480 nm/100 nm and Size of M22, M23, M24 = 720 nm/100 nm.

Simulation: Voltage pulse (V pulse) is applied as inputs A and B and C. To plot the outputs Sbar and Cbar, transient analysis simulation is performed (Figs. 5 and 6).

Fig. 5 Transient response of full adder



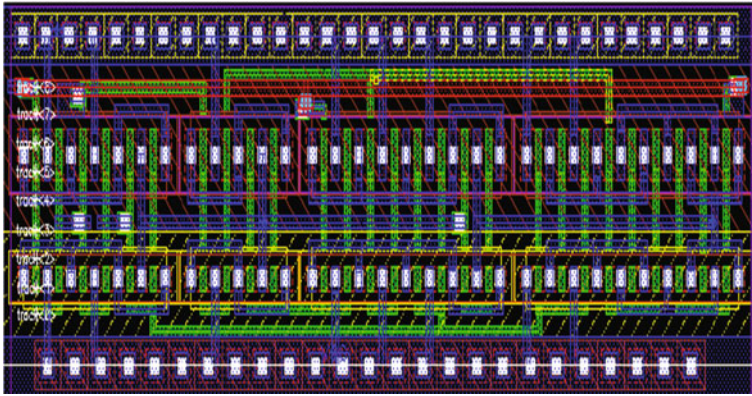


Fig. 6 Layout of full adder

2.3 D Flip-Flop

CMOS Flip-Flops are built from a pair of back-to-back Latches. The flip-flop implemented in the circuit schematic shown in Fig. 7 is a positive edge triggered flip-flop. Transmission gate, tristate inverter and inverters are used to build the D-FF. Clock (clk), data (d) are the inputs to the D-FF, q and qb are the outputs of

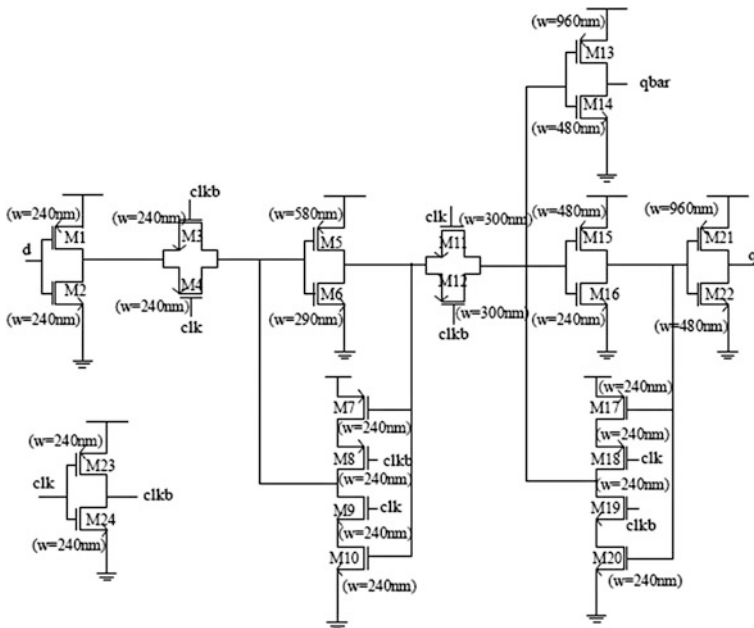


Fig. 7 Schematic of D flip-flop

the D-FF. Transitions occur in the output only for the positive edges of the clock (clk) signal. When the clock signal is in low state (logic-0), the 1st latch circuit is in ON state which allows the passage of the data to the middle node between the two latches. When clk is in high state (logic-1), the 2nd latch circuit turns ON which allows the transfer of data from the middle node to the output. Before the clock gets into high state, a certain logic state (0 or 1) should be available at the middle node in a stable state. Only then during the positive edge of the clock, the D-FF will be able to change the output in accordance with the stable state value. The data should be available at the middle node some time before the clock gets into high state, and this time is said to be the SETUP time of the D-FF [2].

Sizing Strategy: Sizing for D flip-flop is done from Sizing of Inv5 (M21, M22) is as follows. The Load at the output node of this inverter is INVX8. To size inv5 (M21, M22), Input capacitance of last inverter = Output capacitance (inv5)/fan-out.

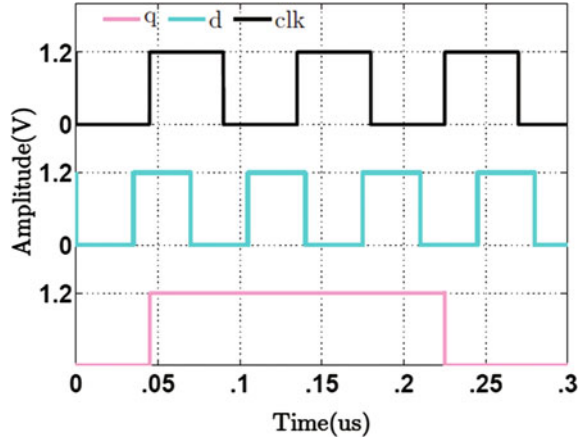
Output Capacitance (inv5) = Capacitance offered by gates of pMOS and nMOS of INVX8 (equivalent to the sum of transistor sizes). The input capacitance of the inv5 is also equal to 3C (2C-pMOS, C-nMOS—Unit inverter). Therefore the size of nMOS device $W_{nM22} = 3.84 \mu\text{m} + 1.92 \mu\text{m}/(4 \times 3) = 480 \text{ nm}$; So $W_n/L_{nM22} = 480 \text{ nm}/100 \text{ nm}$ (minimum length = 100 nm). Double will be the size of the pMOS device $W_{pM21} = 2 \times W_{nM22} = 2 \times 480 \text{ nm} = 960 \text{ nm}$; $W_p/L_{pM21} = 960 \text{ nm}/100 \text{ nm}$. Similarly, sizes of M13, M14, M15 and M16 can be found and it is noted in Fig. 7.

The transmission gate (tg2) drives inv3, inv4 and also the output of the tristate inverter. The output capacitance of transmission gate is the sum of input capacitance of inv3 (equivalent to the sum of M13 and M14 transistor sizes = (960 nm + 480 nm)), the input capacitance of inv4 (equivalent to the sum of M15 and M16 transistor sizes = (480 nm + 240 nm)) and the capacitance at the output of tristate inverter. Capacitance at output of tristate inverter = C_d (pMOS-M18) + C_d (nMOS-M19) = $[0.5C_{g(M18)}] + [0.5C_{g(M19)}] = [0.5 \times 240 \text{ nm}] + [0.5 \times 240 \text{ nm}] = 240 \text{ nm}$; Input capacitance of the TG = 2C (C-pMOS, C-nMOS). Input capacitance (TG) = output capacitance (TG)/4 Size of nMOS device (M12), $W_n = [(960 \text{ nm} + 480 \text{ nm} + 480 \text{ nm} + 240 \text{ nm} + 240 \text{ nm})/(4 \times 2)] = 300 \text{ nm}$, i.e. $W_n/L_n = [\text{min width}/100 \text{ nm}] = 300 \text{ nm}/100 \text{ nm}$. Size of pMOS device (M11), $W_p = W_n = 300 \text{ nm}$.

Inv2 is driving the transmission gate 2 (tg2), inv3 (M13, M14), inv4 (M15, M16) and the output of the tristate inverter. The output capacitance of inv2 is the sum of input capacitance of inv3 (equivalent to the sum of M13 and M14 transistor sizes = (960 nm + 480 nm)), input capacitance of inv4 (equivalent to the sum of M15 and M16 transistor sizes = (480 nm + 240 nm)), the capacitance at the output of tristate inverter (240 nm) and the capacitance offered by the transmission gate.

Capacitance of transmission gate at either side, $[C_{s(M11)} + C_{s(M12)}] + [C_d(M11) + C_d(M12)] = [0.5C_{g(M11)} + 0.5C_{g(M12)}] + [0.5C_{g(M11)} + 0.5C_{g(M12)}] = [2 \times 0.5C_{g(M11)}] + [2 \times 0.5C_{g(M12)}] = 2 \times [0.5C_{g(M11)}] + [0.5C_{g(M12)}] = 2 \times [(0.5 \times 300 \text{ nm}) + (0.5 \times 300 \text{ nm})] = 600 \text{ nm}$. Input capacitance of the inverter = 3C (2C-pMOS, C-nMOS). Input capacitance (inv2) = output capacitance (inv2)/4, Size of nMOS device (M6) = (960 nm + 480 nm + 480 nm + 600 nm +

Fig. 8 Transient response of D flip-flop



$480 \text{ nm} + 240 \text{ nm} + 240 \text{ nm})/4 = 290 \text{ nm}$; So $W_n/L_{nM6} = 290 \text{ nm}/100 \text{ nm}$. Size of pMOS devices (M5) = $2 \times W_n/L_{nM6} = 580 \text{ nm}$, i.e. $W_p/L_p (M5) = 580 \text{ nm}/100 \text{ nm}$.

The sizing strategy of TRANSMISSION GATE (tg1) and inv1 is as follows. The transmission gate (tg1) drives inv2 and the output of the tristate inverter. Calculate the output capacitance and follow the same approach done for tg2. Inv1 is driving the transmission gate (t_{g1}), inv2, and the output of the tristate inverter and follow the same approach done for inv2. Clkb generating inverter drives M3, M8, M12 and M19. Output capacitance = capacitance offered by M3, M8, M12 and M19. Hence, size of nMOS device (M24) = $W_n = 960 \text{ nm}/(4 \times 3) = 80 \text{ nm}$. Size of pMOS device (M23) = $2 \times W_n = 160 \text{ nm}$. As sizes of both transistors M23 and M24 are below 240 nm, $W_p/L_{pM23} = 240 \text{ nm}/100 \text{ nm}$ and $W_n/L_{nM24} = 240 \text{ nm}/100 \text{ nm}$.

Simulation: Voltage pulse of periods 70 ns, 90 ns are applied as inputs 'd' and 'clk' respectively to the latch. Output 'q' is plotted by performing transient analysis simulation for a stop time of 300 ns (Fig. 8). The propagation delay (t_{pcq}) between the clock (clk) and the output (q) is measured to be 87.36 ns. The Set up time (t_{setup}) to be provided at the negative edge of the latch is measured to be 27.4 ps (Fig. 9).

An Inverter

One of the primary functions in digital logic is the NOT operation. A CMOS inverter circuit does this operation and is considered as the nucleus of all digital designs. As the high and low output levels of an inverter are VDD and GND, the voltage swing is equal to the supply voltage. Therefore, noise margin of inverter is very high. The Output impedance of the inverter is low, hence inverters are more immune to disturbances and noise. The resistance at the input of the inverter is large as input is directly connected to the gates of the two transistors (M1) and (M2) which draws zero current (Fig. 10, Table 3) [3, 4].

When V_{in} is high (VDD) the NMOS Transistor (M2) is on, while the PMOS (M1) is off. As a path forms between V_{out} and the ground, the output get pulled down to logic zero state. When the input voltage (V_{in}) is low (0 V), PMOS and

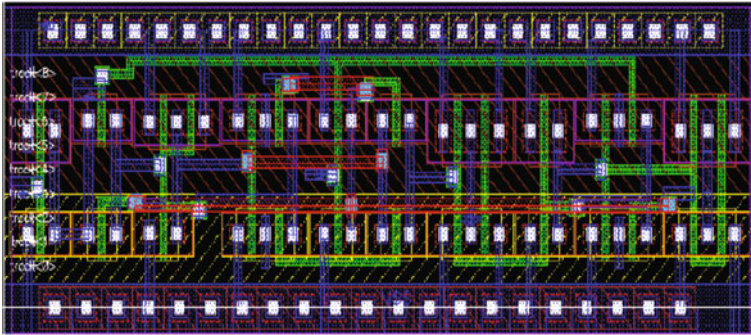


Fig. 9 Layout of D flip-flop

Fig. 10 Schematic and symbol of inverter

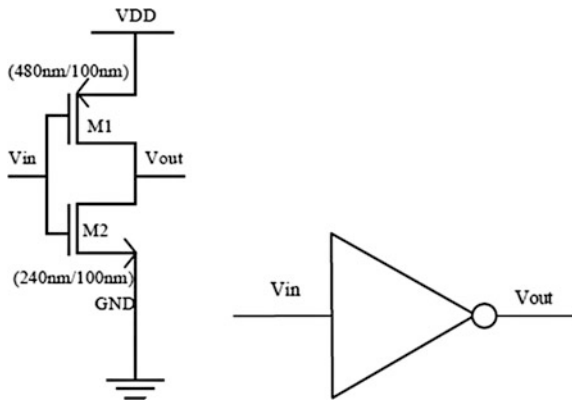


Table 3 Truth table of inverter

V _{in}	V _{out}
0	1
1	0

NMOS are on and off respectively. So, a path exists between VDD and V_{out} to yield a high output voltage. $W/L_{nmos} = 240 \text{ nm}/100 \text{ nm}$. For equal Rise time and Fall time, resistance of PMOS and NMOS should be equal ($R_n = R_p$).

$$1/(\mu_n C_{ox} (W/L)_n (V_{gs} - V_{thn})) = 1/(\mu_p C_{ox} (W/L)_p (V_{SG} - |V_{thp}|))$$

$$V_{GS} = V_{SG} = V_{DD}; V_{thn} = |V_{thp}|$$

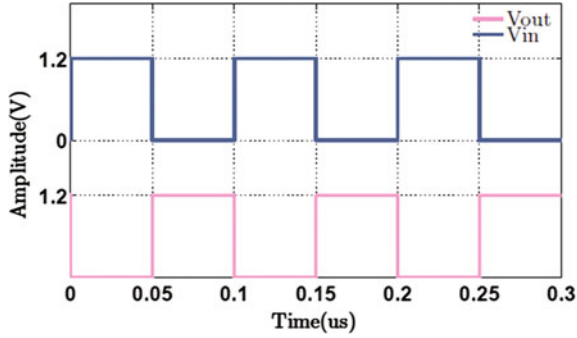


Fig. 11 Transient response of inverter

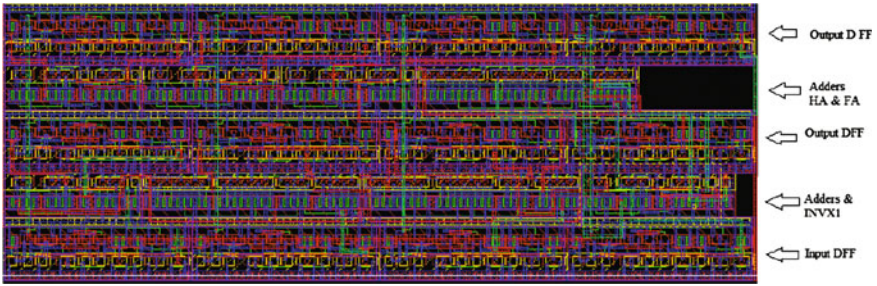


Fig. 12 Layout of accumulator

$$\mu_n(W/L)_{(nmos)} = \mu_p(W/L)_{(pmos)}$$

Since $\mu_n/\mu_p = 2$; $L_n = L_p = 100$ nm

$$W_p = 2W_n = 480$$
 nm

A pulse input is applied to the input of the inverter to obtain an inverted pulse wave output as shown in the transient response (INV X1) obtained by performing transient analysis simulation (Figs. 11 and 12).

3 Accumulator

The accumulator (ripple carry adder) circuit schematic shown in Fig. 13 uses Asynchronous reset D-FFs, Asynchronous set D-FFs, half adders, full adders and one inverter. The 4-bit input (a3, a2, a1, a0) produces a 9-bit output (q9, q8, q7, q6, q5, q4, q3, q2, q1, q0). Set and reset flip-flops are used in order to initialize the

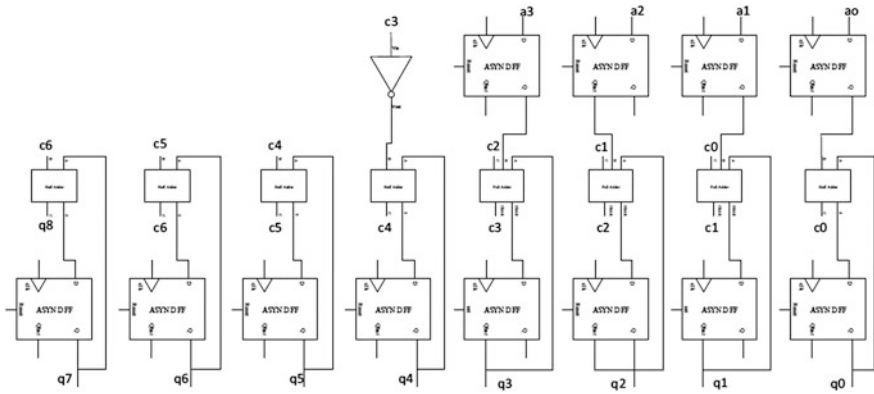


Fig. 13 Schematic of accumulator

flip-flop states. Set flip-flops are used in the case where the output is taken from qb (qbar-compliment of the FF output), so that the output remains at logic -0 itself while setting the FFs. An inverter is used in order to convert the output of full adder to positive logic as it is connected to input of half adder which expects a positive logic input. The full adders used produces Sbar and Cbar at its outputs, so the connections (both input and output) to the adders and other FFs are in such a way that additions and propagation of added signals to output take place in the required manner. Some of the standard cell circuits (Asynchronous reset D-FF, Asynchronous set D-FF, half adder, full adder, and inverter) discussed early are instantiated to build the accumulator.

Sizing Strategy: FFs (both reset and set), half adder, full adder, inverter used for the accumulator are of x_1 size (basic size).

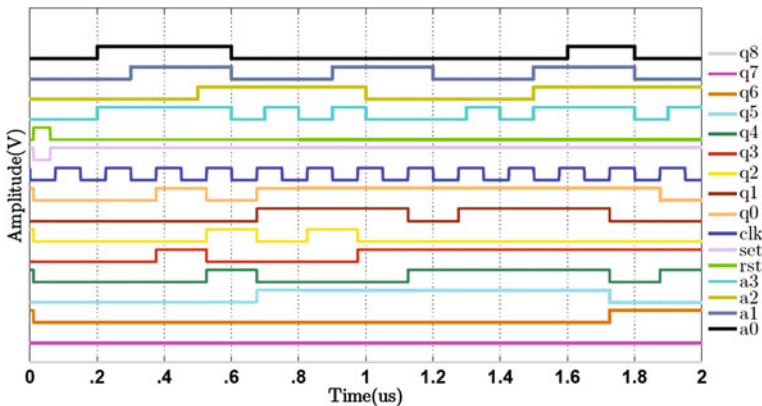


Fig. 14 Transient response of accumulator

Simulation: Rand-bit-stream which is available in the ahdLib is applied as the inputs (a3, a2, a1, a0) to produce random input patterns for each time the simulation is being run. Time periods (T_{period}) given for the inputs a0, a1, a2, a3 are 200, 300, 500, 100 ns respectively. For all the inputs (a3, a2, a1, a0), $v_{\text{high}} = 1.2$ V, $V_{\text{low}} = 0.0$ V, rise time (t_{rise}) = 30 ps, falltime (t_{fall}) = 30 ps. The period of the clock (clk) signal applied is 150 ns. Transient analysis with a stop time of 2 s is performed in order to plot the outputs as shown in Fig 14 [5].

4 Conclusion

We have sized, simulated and analysed the accumulator schematic and layout in Cadence (Virtuoso) 90 nm. The propagation delay between input and output of the standard cells being analysed are low as the VDD applied is 1.2 V and by optimizing the sizing strategy by using a fan-out of 4.

References

1. Weste NH, Harris D. CMOS VLSI design: a circuit and system perspective, 4th ed. Addison-Wesley.
2. Razavi B. Design of analog CMOS integrated circuits. McGraw-Hill.
3. Rabaey J, Chandrakasan A, Nikolic B. Digital integrated circuits, 2nd edn. Prentice Hall.
4. Morris Mano M. Digital design, 4th edn. Prentice Hall.
5. Brown S, Vranesic Z. Fundamentals of digital logic with verilog design. McGraw-Hill.

Placement Chance Prediction: Clustering and Classification Approach

M.V. Ashok, A. Apoorva and V. Chethan

Abstract Educational data mining is an area wherein a combination of techniques, such as data mining, machine learning and statistics, is applied on educational data to get valuable information. The purpose of this paper is to help prospective FAD students in selecting or choosing the right undergraduate course, viz., accessory design, fashion design, textile, fashion communication, etc., based on the entrance exam ranking for admission to the UG course. A clustering and classification approach is applied to solve the placement chance prediction problem. Two classification algorithms, viz., decision tree and Naïve Bayes and a clustering algorithm K-means are applied on the same data set. Algorithms applied are compared and it was found that clustering algorithm K-means predicts better in terms of precision, accuracy, and true positive rate. This work will help students in selecting the best course suitable for them that ensures best placement chance.

Keywords Educational data mining · Naive Bayes · K-means · Decision tree · Prediction and models

Abbreviations

FAD Fashion and Apparel Designing

NIFT National Institute of Fashion Technology

1 Introduction

Fashion designing is the valuable art of designing clothes and lifestyle trimmings. Hence there is lot of demand for this specialization. Success relies on choosing the right specialization during graduation. Decision in this regard is arrived at by

M.V. Ashok · A. Apoorva (✉) · V. Chethan
Global Institute of Management Sciences, Bangalore, India
e-mail: a.apoorva89@gmail.com

accessing the previous year's admission records of Fashion Technology Institute and manually going through the database. The objective of doing this is to predict the future choice of the course. So huge data need to be processed and patterns need to be compared manually, which is tedious and cumbersome. Data were obtained from Fashion Technology Institute in Excel format from 2010 to 2014. Data in the Excel format were fed to MYSQL in the form of queries and two databases were constructed, one containing historic data from 2010 to 2013 and another test data, i.e., 2014.

1.1 Background and Related Work

Many scientists have been working to explore the best mining techniques for solving placement chance prediction problems. Various works have been done in this regard. A few of the similar works are listed below:

Krishna and Murty [1] propose a novel hybrid genetic algorithm (GA) viz., genetic K-means algorithm that finds worldwide optimal partition of a given data into a specified number of clusters. It is also observed that GKA searches quicker than some of the other evolutionary algorithms used for clustering. Huang [2] focuses on the practical issues of extending the K-means algorithm to cluster data with categorical value. The outstanding property of the K-means algorithm in data mining is its efficiency in clustering large datasets. However, it only works on numeric data and limits its use in many data mining applications because of the involvement of categorical data. Bottou and Bengio [3] study the convergence properties of the well-known K-means clustering algorithm. It minimizes the quantization error using the very fast Newton algorithm. Ting and Zheng [4] introduce tree structures into naive Bayesian classification to improve the performance of boosting when working with naive Bayesian classification. Yong Wang and Botang [5] focus upon three aspects of this approach: different event models for the Naive Bayes method, disparate chance of smoothing method, and dissimilar feature assortment methods. In the above research paper is described the performance of each method in terms of recall, precision, and F-measures. Tang and Xu [6] present a method to detect a fuzzy model from data by means of the fuzzy Naive Bayes and a real-valued genetic algorithm. The detection of a fuzzy model is comprises the mining of "if-then" rules followed by the estimation of their parameters. Murthy [7] survey the existing work on decision tree construction, attempting to recognize the important issues implicated, the directions the work has taken, and the present state of the art. Murray [8] conducted studies in a similar area, such as understanding student data. There he applies and evaluates a decision tree algorithm to university records, producing graphs that are useful both for predicting graduation and verdict factors that lead to graduation. It has always been an active discussion over which engineering branch is in demand. So this work gives a scientific solution to answer these. Safavian and Landgrebe [9] present a survey of the current methods for DTC designs and various existing issues. Past

considerations of potential advantages of DTCs over single-stage classifiers, the subjects of tree structure design, characteristic selection at each inner node, decision and search strategy are discussed. Some remarks concerning the relation between decision trees and neural networks (NN) are also made. Mingers [10] method involves three main stages—creating a complete tree able to classify all the examples, considering this tree to give statistical reliability, and processing the considered tree to develop understandability. This paper is concerned with the initial stage—tree creations that depend on a measure for goodness of split, that is, how well the attributes distinguish between classes. Some problems encountered at this stage are lost data and multi-valued attribute. Elayidom et al. [13] proved that the technology named data mining can be effectively applied to the domain called employment prediction, which helps students to select a good branch that may fetch them placement. A global framework for similar concerns has been proposed. Pal and Pal [14] present a proposed model based on classification approach to find an enhanced evaluation method for predicting the placement for students. This replica of a model can determine the associations between academic achievement of students and their placement in campus selection. Pal and Pal [15] frequently studied classifiers and experiments are conducted to find the best classifier for predicting the students' performance. Bharadwaj and Pal [16] provide work to identify those students who need special attention to reduce their fail ratio and taking appropriate action for the next semester examination. Yadav et al. [17] focus on identifying the dropouts and students who need special attention and allow the teacher to provide appropriate advising/counselling.

1.2 Problem Statement

Every student dreams to be successful in life. For him to be successful, choosing the right courses while studying is important. Here student will enter Rank, Gender, Category, and Sector. Among the fields or attributes that he enters, the result would be displayed in terms of Excellent [E], Good [G], Average [A], and Poor [P] for the data entered. Each and every course offered is associated with one of the above answers, viz., E, G, A, P such as, Fashion communication with—E, Knitwear design with—P, and so on. Various mining algorithms from different models are applied on the processed data and tested accordingly. Algorithms are compared based on certain criteria such as accuracy, precision, and true positive rate.

2 Data Description

Name—name of the student. It takes only the alphabetical values from A to Z.

Category—it is the category of the student that he belongs to. It takes string values. The possible values that it can take are 2A, 3A, 2B, 3B, SC/ST, and GM.

Age—it is the age of the student and it takes only numeric values from 0 to 9.

Sector—represents the sector that the student belongs to and the possible values that it can take are URBAN and RURAL.

Rank—rank that a student gets in the entrance exam and can take values from 0 to 9.

Address—it is the address of the student. It can take alphanumeric values from A to Z, 0 to 9.

Ph. no—it is the contact number of the student and it takes numerical values from 0 to 9.

Gender—it is the gender of the student and the possible values are male, female.

Specialization—it is the specialization that the student chooses and the possible values are Textile design, Fashion design, etc.

3 Methodology

3.1 Data Preprocessing

The number of attributes that were found to be contributing to the result, after applying the chi-square test, is as follows:

Rank: obtained by student in the UG entrance examination Range: (1–800)

Category: social background Range (2A, 2B, 3A, 3B, GM, SC, ST, OBC).

Gender: Range (male, female).

Sector: Range (urban, rural).

Specialization: Range (A–F).

All the input values would be mapped between 0 and 1 as given above.

The same data preprocessing steps are applied to all the three algorithms.

4 Data Mining Algorithms Applied

4.1 Brief Description of the K-Means Algorithm

K-means: K-means is the clustering algorithm. Concept used is partitioned clustering. Its working is shown in terms of the steps below.

Application of K-means algorithm on the dataset:

Step 1: Initialize the value of k either manually or systematically.

Step 2: The database provided will be divided into a number of groups based on the attributes as follow: Rank, Category, Gender, Specialization, and Sector.

Step 3: Table 2 is obtained from Table 1 based on the application of numerical formulae. In the table 0.25 in the rank attribute will be compared with all other

Table 1 Mapping input values to numeric values

Category	Input values	Numeric values
Gender	Female, male	0 and 1
Category	2A, 2B, 3A, 3B OBC, GM, SC, ST	0 and 1
Rank	1–N	0 and 1
Sector	Rural, urban	0 and 1
Specialization	A–F	0 and 1
Chances	E, G, A, P	0 and 1

Table 2 Input for K-means algorithm

Rank	Sector	Gender	Category
0.25	0	1	0.25
0.35	1	0	0.50
0.30	1	1	0.75
0.90	0	0	1

values in the same column and the differences between the values are noted (0.25–0.35). Similarly, the second value, i.e., 0.35 will be compared with the rest of the values in the column (0.35–0.30). The same process continues for other values and differences are obtained in each case. A column headed by difference is obtained and values that are close to each other are grouped as a cluster which forms a centroid.

$$0.25 - 0.35 = 0.10, 0.35 - 0.30 = 0.5$$

0.10 and 0.5 forms a centroid provided there are no numbers less than the above values mentioned.

Step 4: while (! EOF)

{If (next value in the difference column is nearest to centroid) {

Include in the cluster

}Else {Form a new cluster}

After each step the cluster sets gets updated, which results in the formation of classified knowledge dataset. The student enters the data that would be compared with the classified knowledge dataset that predicts the specialization to be selected (Tables 3 and 4).

Table 3 Output table

Gender	Sector	Rank	Branch	Chance
Male	Rural	52	Textile design	E
Female	Urban	100	Fashion communication	E
Male	Rural	200	Textile design	E
Male	Urban	150	Fashion communication	E

Table 4 Input for Naïve Bayes

Name	Age	Gender	Sector	Category	Rank	Specialization
Shiva	21	M	Rural	2a	52	Textile design
John	22	M	Urban	3b	100	Fashion communication
Rani	22	F	Rural	SC	200	Textile design

Distribution (D) for the k-Means algorithm is calculated using

$$N$$

$$D = \sum_1 (\text{dataset } (i) - \text{center } (\text{dataset } (i)))^2$$

If the value of D is close to 0 then

Algorithm performance is good

Else

Below average performance.

4.2 Naive Bayes

It is a classifier modeled on Bayes theorem which is probabilistic.

The procedure to be followed while applying this method is as follows:

- Data preprocessing
- Finding positive and negative knowledge data
- Application of Bayes theorem

Step 1: Data preprocessing: Filling of the missing values and the dependency check on the attributes listed in Table 8 is performed using chi-square test and Table 5 is a resultant after preprocessing.

Table 5 After preprocessing

Gender	Sector	Category	Rank	Specialization
M	Rural	2a	52	Textile design
M	Urban	3b	100	Fashion communication
F	Rural	SC	200	Textile design
M	Rural	3a	150	Fashion communication

Step 2: Finding positive and negative knowledge data: selection constructs are applied on a rank attribute to get positive and negative knowledge data.

If (rank <= 800)//the maximum limit of the possible rank

{Positive knowledge data}

Else

{Negative knowledge data}

The above process is repeated for all the attributes listed in Table 9 to get the positive knowledge data as given below.

Step 3: Application of Bayes theorem in Table 10 gives the resultant output table. At the first instance, data in Table 10 is converted into numeric data.

Formulae listed under are used to get the below output table as the resultant.

$$\begin{aligned}
 h_{MAP} &= \arg \max_{heH} P(h/D) \\
 &= \arg \max_{heH} \\
 &= \arg \max_{heH} P(D|h)P(h)
 \end{aligned}$$

where,

P(h) ≡ Prior Probability of (Correctness of) Hypothesis h

P(h|D) ≡ Probability of h Given Training Data D

P(D) ≡ Probability of D

P(D|h) ≡ Probability of D Given h

4.3 Decision Tree

Decision tree is the classification method that makes use of the top-down tree construction approach, which results in a tree-like structure where each node represents an attribute to be tested and the branch will be the outcome of the test on an attribute. The objective of this algorithm is to generate

- a. Knowledge database.
- b. Output based on knowledge database for the user input.

Step 1: Priorities are set for the attributes based on the dataset. For our dataset rank is taken as the attribute with the topmost priority and then sector, category, and so on.

Step 2: based on the conditions set, the prioritized attribute, i.e., rank will be divided basically into two, one with positive values and the other with negative values.

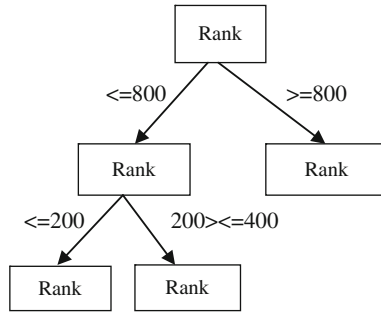
Step 3: If the tree contains all the nodes that are positive, then create results as yes and then exit the step.

If the tree contains all the nodes that are negative, then create result as no and exit the loop.

The partial view of a tree after the application of Step 3 for Rank attributes

Step 4:

If Step 3 fails; expand the tree by selecting the next attribute (F) sector or gender.



Step 5:

Repeat Step 4 until all the nodes are visited at least once.

Output: The table represents the knowledge database obtained after the application of the decision tree algorithm on the resultant of Table 2, after preprocessing.

For the following user input (Rank, Gender, sector, etc.) Table 5 represents the possibilities of choice of specialization as the final output, after processing the knowledge data (Tables 6, 7, 8, 9, 10, and 11).

Table 6 Positive knowledge data

Name	Age	Gender	Sector	Category	Rank	Specialization
Shiva	21	M	Rural	2a	52	Textile design
John	22	M	Urban	3b	100	Fashion communication
Rani	22	F	Rural	SC	200	Textile design

Table 7 Output table

Rank	Gender	Sector	Category	Specialization	Chance
1–200	M	Rural	Any	Textile design	E
1–200	M	urban	Any	Fashion communication	E
1–200	F	Rural	Any	Fashion design	E

Table 8 Input for the algorithm

Name	Category	Age	Sector	Rank	Address	Ph. no	Gender	Specialization
Ravi	2A	30	Urban	150	Jayanagar	9812346754	Male	Fashion communication
Raj	3B	38	Urban	1	Nagarabhavi	9440213456	Male	Fashion communication
Rani	2A	21	Rural	200	Bannikuppe	8050214356	Female	Textile design

Table 9 Representation of the knowledge database

Rank	Sector	Gender	Category	Specialization
1<==>200	Rural	Female	2A	Fashion communication
400<==>600	Urban	Male	2A, 3B	Textile design, fashion design

Table 10 Output table for the user input

Id	Specialization	Chance	Possibilities (%)
1	Textile design	E	90
2	Fashion communication	E	85
3	Fashion design	E	70

Table 11 Confusion matrix table

Algorithms	TPR	Accuracy (%)	Precision
K-means	0.83	83	0.83
Naïve Bayes	0.80	77	0.75
Decision tree	0.81	81	0.81

5 Implementation

All the algorithms used were implemented and the front end was developed using PHP and MYSQL as a database.

6 Testing

Results obtained after the tests for each algorithm were modeled as confusion matrix. Confusion matrix explains the performance of three algorithms expressed in terms of True Positive rate, Accuracy, and Precision.

From Table 9 it is clear that the K-means algorithm is more accurate with 83 % compared to other algorithms, viz., Decision Tree (81 %) and Naïve Bayes (77 %). K-means algorithm leads with respect to true positive rate (TPR) with 0.83 correct instances and precision (0.83). Thus the clustering algorithm K-means predicts the results better than the other algorithms used.

7 Conclusion and Future Enhancement

Applying data mining techniques on educational data is concerned with developing methods for exploring the unique types of data; in this study, two classification algorithms, viz., Naïve Bayes and decision Tree and a clustering algorithm, K-means were applied. Among these algorithms, K-means proved to be the best

predicting algorithm representing cluster model, for solving placement chance prediction problems. Hence, having the information generated through our study, students would be able to select the appropriate specialization with the best chances of getting placed. Furthermore, the work can be extended to solve problems on predictions, using different approaches on data of different disciplines.

References

1. Krishna K, Murty MN. Genetic k-means algorithm. 1999;29(3):435–9.
2. Huang Z. Extensions to the k-means algorithm for clustering large data sets with categorical values. 1998;2(3):283–304.
3. Bottou L, Bengio Y. Convergence properties of the k-means algorithms. Denver: MIT Press; 1995.
4. Ting KM, Zheng Z. Improving the performance of boosting for Naïve Bayesian classification, vol. 1574. 1999. p. 296–305.
5. Wang Y, Hodges J, Tang B. Classification of web documents using a Naïve Bayes method, 2003. Germany; 2005. p. 560–564.
6. Tang Y, Xu Y. Application of fuzzy Naïve Bayes and a real-valued genetic algorithm in identification of fuzz model. 2005;169(3–4): 205–226.
7. Murthy SK. Automatic construction of decision trees from data: a multi-disciplinary survey. *Data Min Knowl Discov*. 1998;2:345–389.
8. Murray E. Using decision trees to understand student data. In: *Proceedings of the 22nd international conference on machine learning*. Germany: Bonn; 2005.
9. Safavian SR, Landgrebe D. A survey of decision tree classifier methodology. *IEEE Trans Syst Man Cybern*. 1991;21(3):660–674.
10. Mingers J. An empirical comparison of selection measures for decision-tree induction. 1989;3(4):319–342.
11. Quinaln JR. *C4.5: Programs for machine learning*. Morgan Kaufmann: San Francisco; 1993.
12. Wu X, Kumar V. *The top ten algorithms in data mining*. Boca Raton: Chapman and Hall; 2009.
13. Elayidom S, Idikkula SM, Alexander J. A generalized data mining framework for placement chance prediction problems. *Int J Comput Appl* (0975–8887). 2011;31(3):40–47.
14. Pal AK, Pal S. Classification model of prediction for placement of students. *Int J Mod Educ Comput Sci*. 2013;11:49–56.
15. Pal AK, Pal S. Analysis and mining of educational data for predicting the performance of students. *Int J Electron Commun Comput Eng (IJECCE)*. 2013;4(5):1560–1565. ISSN: 2278-4209.
16. Bharadwaj BK, Pal S. Mining educational data to analyze students' performance. *Int J Adv Comput Sci Appl (IJACSA)*. 2011;2(6):63–9.
17. Yadav SK, Bharadwaj BK, Pal S. Data mining applications: a comparative study for predicting student's performance. *Int J Innovative Technol Creative Eng (IJITCE)*. 2011;1(12):13–9.

Cluster-Based Distributed Key Architecture Scheme for MANETs

B. Rajanna and R. Rajeswara Rao

Abstract Security deployment in data communication is very vital, where authentication is most obvious prerequisite. However, similar authentication procedures are not appropriate in hierarchical mobile ad hoc networks as it is characterized by infrastructure less. We develop and evaluate security method based on multilevel key distribution, called cluster-based distributed key architecture for MANETs, which addresses two important characteristics: authentication and authorization. It considers cluster head selection based on novel metric called “optimized packet processing capacity” and multilevel key distribution process with the help of diffie-Hellman Key distribution. We evaluated the availability of the security infrastructure, and its overhead using NS2. Results show that it is possible to deploy security architecture with an acceptable performance and overhead.

Keywords MANETs · Routing · Knapsack · Cluster · Security

1 Introduction

Wireless mobile ad hoc networks on-the fly are characterized by infrastructure less network. Heterogeneous mobile nodes present in a network have to perform the operations of routing as well as hosting, well suited for a situation where infrastructure is hard to setup or time/cost effective. Due to its self configuration and maintenance characteristics, MANETs gains wide range of applications include military, disaster recovery, and law enforcements.

B. Rajanna (✉)

Computer Science & Engineering, JNTUH, Hyderabad, Telangana, India
e-mail: raj1math@yahoo.co.in

R. Rajeswara Rao

Computer Science & Engineering, JNTUK University College of Engineering,
Vijayanagaram, A.P., India
e-mail: raob4u@yahoo.com

© Springer India 2016

S.S. Dash et al. (eds.), *Artificial Intelligence and Evolutionary Computations in Engineering Systems*, Advances in Intelligent Systems and Computing 394, DOI 10.1007/978-81-322-2656-7_26

Due to its characteristics, security is very much challenging task in MANETs. Peer-to-peer networks are a fundamental vulnerability MANETs regarding security deployment, there is no clear cutline of defense in security design and no well-defined place is available to develop security solutions. An energy and computation constraint characteristic makes MANETs to challenging to perform cryptographic operations.

In this work, we present security architecture for securing mobile ad hoc networks communication. Where network is divided into number of clusters, and cluster head selection is based on metric called optimized packet processing capacity and we assign a multilevel authentication with the help of diffie-Hellman key exchange. The remaining paper is organized as follows: Next section discusses about related work. In Sect. 1.2, we discuss a process of finding optimized packet processing capacity of node. Section 1.3 describe cluster head selection. Section 1.5 discuss the intercluster communication and our work end with simulation and conclusion.

1.1 Related Work

In past decades, number of key management protocols has been proposed to secure group communication in MANETs, which mainly divided into two categories, i.e., distributed and centralized protocols [1]. In work [2, 3, 4] are distributed protocols based on Group diffie-Hellman Key Method, but main overhead in this approach is number of public key operations. Due to overhead, these approaches are not well suited for real-time applications and delay-sensitive operations. Work [5, 6] are centralized key distribution protocols based on the concept of key predistribution (KPS), where trusted third party needs to share secrete information before group communication; in which only those privileged users can compute certain keys. Work [7] presented a key management based on shared key solution for scalable ad hoc networks, which assumes each node in a network good node with proper behavior. This approach combines the adaptive clustering with mobility and selects a key generation node based on probabilistically, key updating done periodically. But this assumption is not always true in hostile environment like MANETs.

The idea behind our work is based on work [7, 8]. Main aim of our method is to provide secure communication along with security goals: authentication and authorization in MANETs. Providing security is the most vital issue as MANETs as it is infrastructure less. In our work, we provide multilevel secure authentication; if secure authentication is achieved, one can easily realize the methods to ensure integrity, nonrepudiation, and confidentiality in communication. Another aim is to

cope with dynamic network characteristics of MANETs and finally support network scalability.

In order to achieve our goals, we partition the networks to number of clusters similarly based on existing CGSR [9]. Where CH (cluster head) is responsible for cluster organization GW (gate way) is responsible for intercluster communication with adjacent clusters. Our work is on the top of extension of CGSR with security concept and some additional features. Cluster head selection is based on metric called optimized packet processing capacity. The idea behind the metric optimized packet processing capacity is come from work [8], which calculates the optimized information processing capacity in multi hop MANETs. At the same time, we are not limiting our method with particular routing protocol. Every node in a network agrees a key used for end-to-end security, with the help of diffie-Hellman [10, 11], which introduced the concept of two person key exchange technique that allows two participants to exchange two public keys through an unsecured channel and generate a shared secured key between them.

Our contribution of work mainly as follows:

1. Optimization of packet processing capacity of node with respect to residual energy and current traffic
2. Cluster head selection
3. Key distribution
4. Intercluster communication

1.2 Optimized Packet Processing Capacity of Node with Respect to Residual Energy and Current Traffic (AK)

In a network, to calculate packet processing capacity of every node says 'AS' with respect to residual energy and current traffic. Let node 'k' has ' C_e ' joules of energy. In which we are considering ' n ' kbps packets to process through it in a current traffic conditions. Where, node 'k' takes total $e(x)$ energy to process $[x]$ kbps packets. In order to calculate optimization, we require to process as much as packets through node 'k' within a residual energy and current traffic. Which in turn require calculating subset of packets such that below conditions needs to satisfy.

1. All processing packets have combined with size (bytes) at most of ' C_e ' joules
2. Node needs to process as much as possible packets
3. Node in a network cannot process a part of packet (which should either hole/nothing)

Total energy required by a node to process the $[x]$ kbps packet within a multi hop MANETs from node u to node v , is given by [8]

$$e(x) = T(x) + R(x) + D(X)$$

where $T(x), R(x), D(X)$ are transmitting, receiving, processing energies of node, respectively, to transmit, receive, and process $[x]$ kbps packets.

In order to calculate optimized packet processing capacity of node 'K' with current energy ' C_e ' joules and buffer size of ' B ' kilo bytes and can process ' n ' kbits packets say $\{I_1, I_2, I_3, \dots\}$. We assume that in given number of packets which needs to be process through node 'K' in a network, the packets need to process completely, and partial packets process is not possible (either complete or nothing). We assumes n -Topples of positive values as follows

1. Total number of packets need to be process from the given node 'K' let $(I_1, I_2, I_3, \dots, I_n)$ and each of these packets contain the size of x [kbits]
2. Energy required by node to process x [kbits] packet is $e(x)$, include transmit, process and receive x [kbits] packet

We want to determine the energy required by node to process packets in k bits

$$T \{I_1, I_2, I_3, \dots, I_n\} \text{ so as to Maximize } \sum 1 (I_i)$$

where $I \in T$ Subject to $\sum e(I) \leq C_e$

To get maximum packet processed by a node 'K' for given residual energy capacity ' C_e ', one solution is to try all 2^n possible subsets of ' T '. Here we apply Knapsack algorithm to get the optimizing solution, where it construct two dimensional arrays

$$S[0..n, 0..C_e] \forall 1 \leq i \leq n \& 0 \leq e(I) \leq C_e$$

Such that $S[I, C_e]$ will process maximum packets of any subset of flows with I kbits of data $\{1, 2, 3, \dots, i\}$ of energy required to process at most ' $e(I)$ '. Where array entries $S[n, C_e]$ will contain maximum packets process from given number of packets. At the same time, array entries should not follow below two conditions.

$$S[0, e(I)] = 0 \forall. 0 \leq e(I) \leq C_e \text{ no packet process from node}$$

$$S[i, e(I)] = -\infty \forall e(I) < 0, \text{ illegal statement.}$$

Optimization as below

$$S[i, e] = \max(S[i-1, e(x)], S_i + S[i-1, e(x) - e(x)i]) \forall 1 \leq I \leq n \text{ and } 0 \leq e(x) \leq C_e$$

The algorithm to calculate optimized packet process strength of a node with an available energy capacity of nodes is shown in algorithm 2.5 [12].

1.3 Cluster Head Selection

Cluster head is one which is responsible for cluster organization needs to be in a good condition regarding computation and energy capacity. Where metric ‘AK’ is calculated in previous section address both the features of nodes. In order to select cluster head, we are considering the heterogeneous nodes present in a network, each node in a network proactively maintain a table with entry of its optimized packet processing capacity ‘AK’. Depending on the optimized packet processing capacity of nodes with respect to current energy and traffic present in a node is used as a metric to find the cluster head, shown in Fig. 1. We are considering the threshold value AKmax depending on the optimized process capacity of node in ideal conditions.

AKmax, the value of nodes packet processing capacity when its residual energy equal to half of ‘ C_e ’ with minimum current traffic condition. If nodes are optimized, packet process capacity greater than AKmax act as a cluster head. Remaining network formation follows existing network setup given in [9].

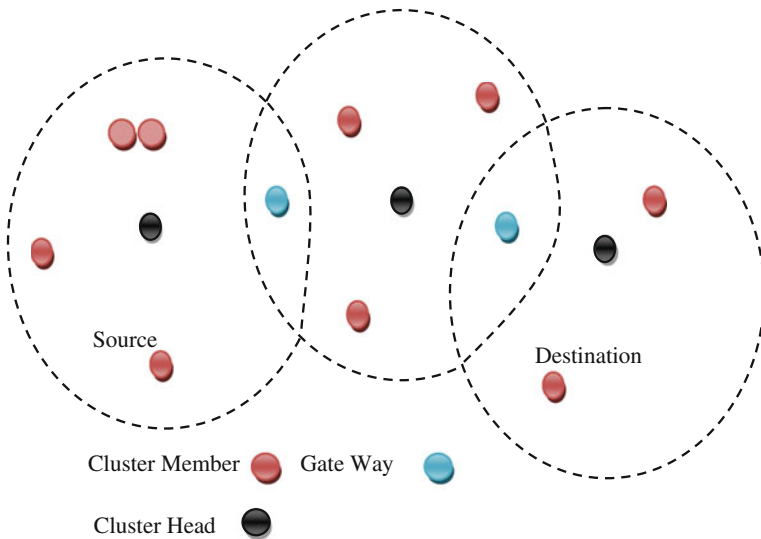


Fig. 1 Cluster network

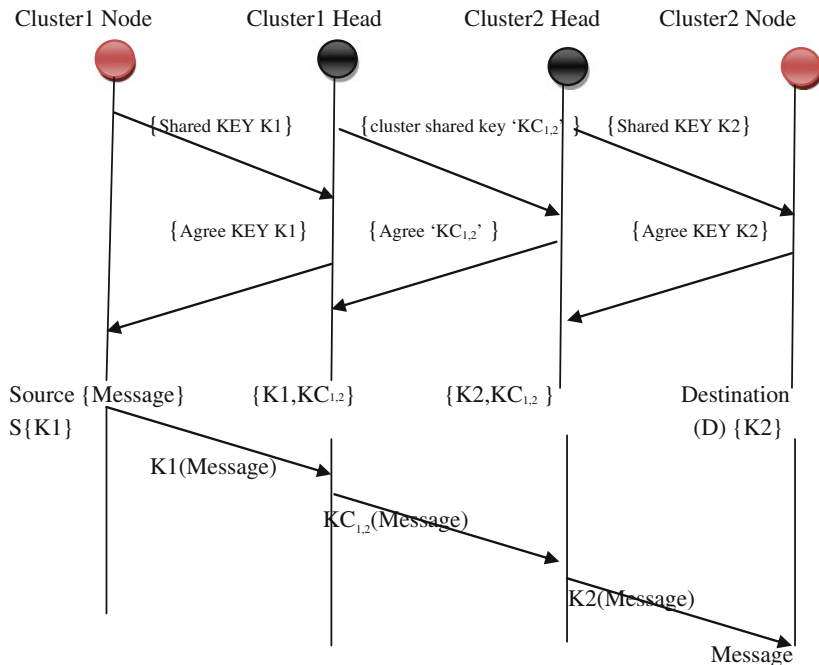


Fig. 2 Key distribution and intercluster communication

1.4 Key Distribution

Each node in a cluster agrees a shared key ‘k’ with cluster head using diffie–Helman [10, 11] key algorithm. Every cluster maintains a shared key with its cluster head. Whenever cluster form or new node enters into a cluster, it needs to agree a shred key ‘K’ with cluster head. Each cluster head of any cluster need to agree with adjacent cluster’s cluster head with a cluster shared key ($KC_{1,2}, KC_{1,3}, KC_{2,3} \dots KC_{m,n}$) with group diffie-hellman key algorithm. Cluster shared key value varies depending upon the number of adjacent cluster. Each cluster head shares their adjacent cluster shared key with its neighbor cluster head. For encryption, we used the data encryption standard algorithm. Figure 2 shows the Key distribution & Inter cluster communication of proposed work.

Where shared key (K) ensures the intracluster authentication, shared cluster key (KC) is used for intercluster authentication. As cluster head selection is based on metric ‘AK’, it can hold more keys and compute the cryptographic operations.

1.5 Intercluster Communication

Let us consider a situation that source 'S' in a cluster one want to communicate with destination 'D' in a cluster three. Where source and destination contain a share key of respected clusters, and their cluster heads contain shared keys of cluster as well as all the cluster shared keys.

1. Source 'S' encrypt the message with shared key ' K_n ' and transmit it to cluster head, Where ' n ' is cluster number
2. Cluster head decrypt the message and conforms the authentication of Source. It contains shred key of respective cluster
3. Cluster head again encrypt the message with destination cluster's cluster shared key ' $K_{m,n}$ ' and forward it to adjacent cluster
4. Whenever it reaches the destination cluster head, it decrypts the message to ensure the authentication of source's cluster
5. And encrypt with shared key of respective cluster and forward to destination node
6. Destination decrypts the message with shared key.

2 Performance Calculations

We evaluate the performance of proposed work using the network simulator-2 with the necessary changes and evaluated the availability of the security infrastructure, and its overhead with respect to random way point mobility. In our simulations, we used a fixed transmission range of node as two fifty meters, and delay as 120 ms per hop count. All mobile nodes are randomly distributed across square area of $800\text{ m} \times 800\text{ m}$. We used the "random waypoint" mobility model with speed of mobile nodes is uniformly distributed between minimum of 0 to maximum speed of 20 m/s with pause time value of 35 s. All nodes of network arranged with IEEE 802.11 network interface card and data rates of 2 Mbps. The initial energy of all the mobile nodes is set to 10 J and transmission power is 600 mW, the receiving power is 300 mW. Finally, source nodes generate CBR (constant bit rate) traffic. Traffic sessions are generated randomly on selected different source-destinations with a packet size of 512 bytes. Every node in a network has to run our algorithm to become the cluster head. Cluster heads broadcasted their beacons over 2 hops every 20 s. The lifetime of key was chosen randomly between 200 and 300 s.

Our aim is mainly to investigate the node's optimized packet processing capacity with respect to residual battery as well as current traffic condition, and according to

it select the cluster head. We therefore measure the availability and communication overhead security architecture. As availability is important parameter of any security architecture, we calculated it by dividing number of full member nodes by total number of available nodes. Communication overhead is another important parameter as security protocols always makes extra overhead, which affect both network as well as system. Figs. 3, 4, 5 and 6, clearly shows that it is possible to deploy security architecture with an acceptable performance and overhead.

Fig. 3 Availability (Hop count)

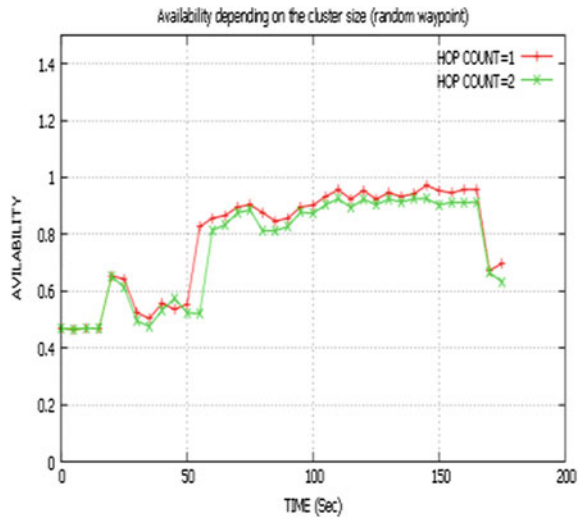


Fig. 4 Availability (CH interval)

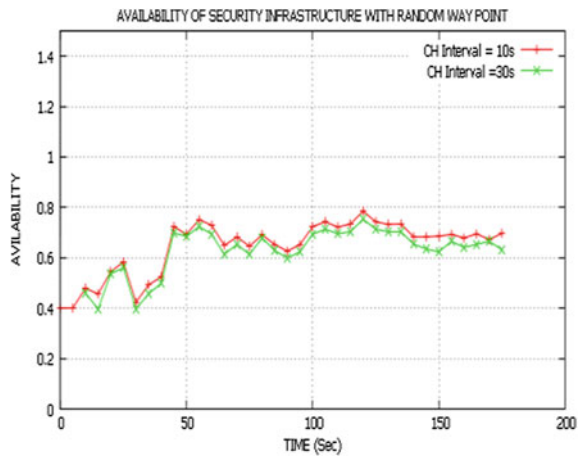


Fig. 5 Overhead (CH interval)

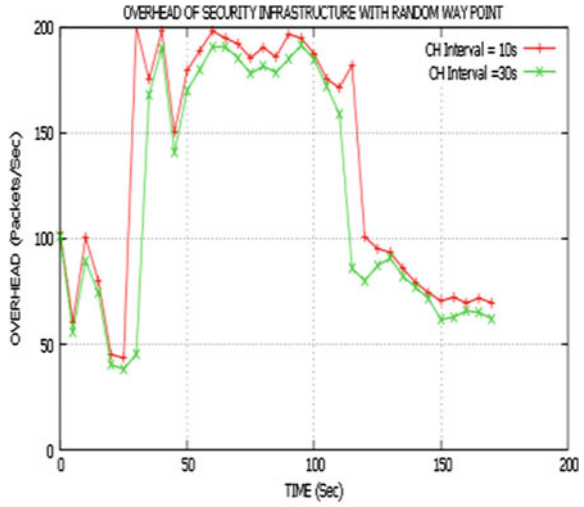
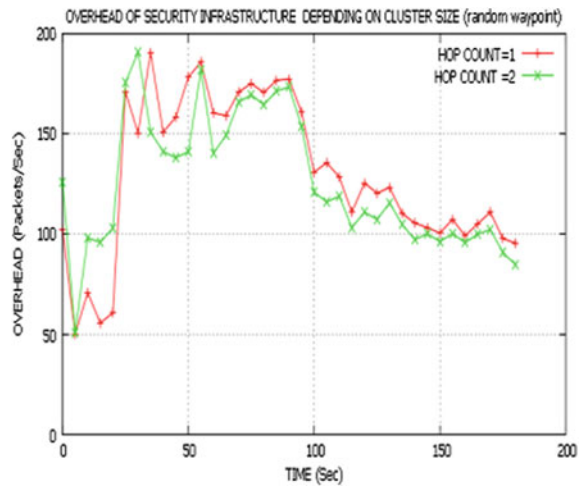


Fig. 6 Overhead (HOP count)



2.1 Algorithm

```

Knapsack (L, e, n, Ce) {
  for (e=0 to Ce) S[0, e]=0;
  for (i=1 to n)
    for (e=0 to Ce)
      If ((e[i] ≤ e) and (l[i]+S[i-1, e-e[i]] > S[i-1, e])) {
        S[i, e]=l[i]+V[i-1, e-e[i]]; Keep[i, e]=1; }
      else {S[i, e]=S[i-1, e]; Keep[i, e]=0; }
    K=Ce; For (I=ndownto1)
      If (keep[i, K]==1) {
        Output i;
        K=K-e[i]; }
  Return S[n, Ce];

```

3 Conclusion

In this work, we introduced a dynamic cluster-based distributed key architecture scheme for MANETs. In order to adopt the MANETs characteristics, we avoided centralized coordinator instead network is considered as cluster and cluster head selection is based on proactive metric called optimized packet processing capacity with respect to residual energy and current traffic. Our concept uses dieffi-Helman key exchange protocol for key agreement between “cluster head and cluster nodes” and between cluster heads instead of registration central authority. These keys are used for multilevel authentication for interlevel cluster communication. Performance evaluation has done with random waypoint mobility model with ns2 simulator. We evaluated the availability of the security infrastructure, and its overhead. Results show that it is possible to deploy security architecture with an acceptable performance and overhead.

References

1. Rafaeli S, Hutchison D. A survey of key management for secure group communication. *ACM computing surveys*; 2003. p. 309–29.
2. Kim Y, Perrig A, Tsudik G. Simple and fault-tolerant keyagreement for dynamic collaborative groups. In: *Proceedings of the ACM conference on computer and communications security*; 2000. p. 235–44.
3. Ateniese G, Steiner M, Tsudik G. Authenticated group key agreement and friends. In: *Proceedings of the 5th ACM conference on computer and communications security*, New York, NY, USA, San Francisco, California, United States: ACM Press; 1998. p. 17–26.
4. Burmester M, Desmedt Y. Efficient and secure conference key distribution. In: *Proceedings of the security protocols. Workshop*, Cambridge, UK: Springer-Verlag; 1996. pp. 119–129. Taormina: Communications (ISCC); 2002.
5. Blundo C, Santis AD, Herzberg A, Kutten S, Vaccaro U, Yung M. Perfectly-secure key distribution for dynamic conferences. *Inf Comput.* 1998;146(1):1–23.
6. Fiat A, Naor M. Broadcast encryption. In: *CRYPTO'93, Lecture notes in computer science*, vol. 773. New York, Inc., Santa Barbara, California, United States: Springer-Verlag; 1994. p. 480–91.
7. Basagni S, Herrin K, Bruschi D, Rosti E. Secure pebblenets. In: *Proceedings of the 2nd ACM international symposium on Mobile ad hoc networking and computing*, New York, NY, USA: ACM Press; 2001. p. 156–63.
8. Mohammad AAK, Mirza A, Razzak MA. Reactive energy aware routing selection based on Knapsack. *Emergency ICT for bridging the future*, vol. 2. Switzerland: Springer International Publishing; 2015.
9. Chiang CC et al. Routing in cluster Multi hop ad hoc networks with fading channel. In: *Proceeding of IEEE SICON*; 1997. p. 197–211.
10. Murthyl NVES, Naresh VS. Extended diffie-hellman technique to generate multiple shared keys at a time with reduced keos and its polynomial time complexity. *IJCSI Int J Comput Sci Issues*. May 2010;7(Issue 3, No. 3).
11. Bresson E, Chevassut O, Pointcheval D. Dynamic group diffie-Hellman Key exchange under standard assumption. In: *IACR*; 2002. p. 321–36.
12. Martello S, Toth P. Knapsack problems, catalog.enu.kz, 1990.

Design and Implementation of 270-Tap Finite Impulse Response Filter

T. Vandana Raj and S. Sreelakshmi

Abstract Filtering is processing of a time domain signal and hence results in changing the original spectral components. The process involves reducing or filtering out some of the unwanted input spectral contents, where it allows certain frequencies to pass while attenuating some other frequencies. Filters are basically of two types— analog and digital, where analog filter operates on continuous signal, while digital filter operates on discrete sample values. Digital filters are basically of two types, finite impulse response (FIR) and infinite impulse response (IIR) filters. FIR filter uses only present and past input samples and none of the past output values for obtaining the present output sample value. This paper is about the implementation of a 270-tap low-pass FIR filter. The paper implements a direct form of FIR filter with given passband, stop-band specifications using MATLAB and Verilog codes. Specifications of the FIR filter are passband frequency = 100 kHz, stop-band frequency = 500 kHz, passband attenuation = 0.01 dB, stop-band attenuation = 120 dB, sampling frequency = 20 MHz.

Keywords Finite impulse response filter · Finite precision · Quantization · Multi-tone sine wave

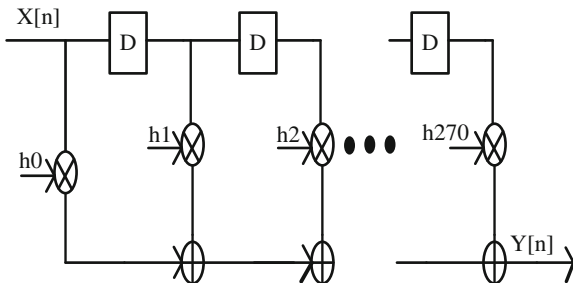
1 Introduction

In signal processing a finite impulse response (FIR) filter is a type of filter whose impulse response has finite duration and it takes a finite time to settle to zero value. Infinite impulse response (IIR) filter has an internal feed-back and responds in

T. Vandana Raj (✉) · S. Sreelakshmi
Electronics and Communication Department,
Amrita Viswa Vidyapeedom Amrita School of Engineering,
Amritapuri, Kollam, Kerala, India
e-mail: vandanatt@gmail.com

S. Sreelakshmi
e-mail: sreelakshmi.sree001@gmail.com

Fig. 1 FIR 270-tap block diagram



indefinite time. The impulse response of an N th-order discrete-time filter lasts for $N + 1$ samples and eventually settles to zero. For a discrete-time FIR filter, the output is the weighted sum of the current and a finite number of previous values of inputs. An FIR filter has a lot of distinct properties, which makes it preferable to an IIR filter.

1. No feedback is required.
2. Stability is high.
3. They can easily be designed to be linear phase by making the coefficient sequence symmetric.

The difference equation of an FIR output in terms of it inputs is

$$Y[n] = h_0x[n] + h_1x[n - 1] + h_2x[n - 2] + \dots + h_nx[n - N] \tag{1}$$

where $x[n]$ is the input signal, $y[n]$ is the output signal, h_i is the filter coefficient is the filter order. The block diagram of a 270-tap FIR filter is shown in Fig. 1.

2 Building Blocks

2.1 Multiplier

In a DSP system, the multiplier must be fast and have sufficient precision to support the desired application. For fast multiplication, modified Booth multiplication algorithm is used.

2.2 Adder

Additions are required in combination with multiplications, hence a multiply accumulate system needs to be implemented.

2.3 Unit Delay

It provides a unit sample delay. A sample value is stored in memory slot for one sample clock cycle and then made available as an input to the next processing stage.

3 Implementation and Results

3.1 Coefficient Quantization

Using FDA tool in MATLAB we get the 270 filter coefficients. These are copied to the MATLAB workspace. The 270 coefficients need to be quantized in such a way that the error in frequency response obtained using finite precision quantized coefficients is less than 0.01 dB. While quantizing we have to take into consideration the sensitivity of each coefficient. For e.g., while quantizing the first coefficient we will keep all other coefficients with their golden value and quantize to a particular number of bits for which the error is less than 0.01 dB. Now the first coefficient is fixed and the procedure is carried out for the second coefficient. This process is continued for all the coefficients in such a way that they are quantized to less than 0.01 dB error.

3.2 Input Sine Wave Generation

Three sine waves for passband, transition band, and stopband were chosen. NFFT was taken as 2^{14} and sine wave was generated using the equation:

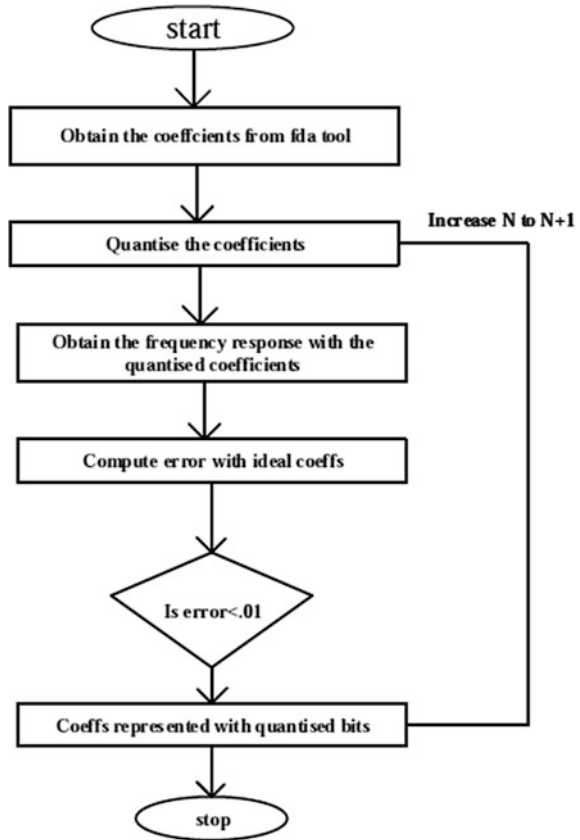
$$x = \text{sine}(2 \times \pi i \times N \times f_s / \text{NFFT}) \quad (2)$$

Here the N value should be chosen in such a way that both the N and NFFT should be co-primes. f_s corresponds to the sampling frequency. The flowchart of the input quantization procedure is as in Fig. 2.

3.3 Multiplication

In order to reduce the number of partial products, we employ radix-4 Booth multiplication for the input sample and coefficient multiplication. The multiplication with proposed algorithm was implemented to reduce the complexity in multiplication. For radix-4 modified Booth multiplication, in order to reduce the hardware complexity (for proper results the partial products have to be sign extended to the

Fig. 2 Coefficient quantization procedure



number of bits of the multiplicand and this results in additional half adders and full adders), in cases where $-A$ and $-2A$ (A is the multiplicand) are the required partial products, only the 1's complement value is taken in order to avoid the extra adder required prior to the Wallace tree accumulation. In order to reduce the sign extension the algorithm is implemented to modify the partial products by sign extending by 2 the MSB of the first partial product, then extending the complement of the MSB and placing it as the LSB of the next partial product so that if the previous partial product was negative, i.e., either $-A$ or $-2A$, then 1 is added to it which generates the 2's complement, else it simply adds bit '0'. From the second partial product onwards the complement of the MSB is sign extended by 1 bit and the second bit is extended as '1' and the MSB is appended as the LSB of the next partial product. The advantage of modified Booth method is that the number of partial products is reduced by half. The modified partial products are then accumulated using the Wallace tree adder. An algorithmic implementation for an 8-bit number is shown in Fig. 3. The s_1, s_2 , etc., correspond to the MSBs in each of the partial products generated.

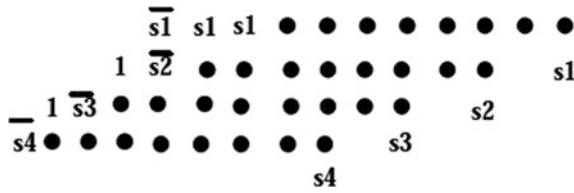


Fig. 3 Modified Booth multiplication partial products generation algorithm to reduce the hardware complexity otherwise needed for sign extension

3.4 Multiplication Quantization

The multiplier outputs obtained from the 270 multipliers are also quantized in such a way that the result in error (non-quantized product–quantized product) is less than 0.01 dB. Initially the first multiplier output is quantized while all other multiplier outputs are kept at golden value. Then the error is computed and the first multiplier is quantized until the condition is met. Once the quantized value is fixed, it is the same process; the first multiplier output bit is fixed and then the second multiplier bits are quantized while keeping other multiplier outputs as golden value. The same process is repeated for all the multipliers. In this way a perfectly optimized multiplier output is obtained. Table 1 shows the quantized bits of the first 7 multipliers as an instance.

3.5 Adder Quantization

The 269 adder outputs have to be quantized to obtain a more optimized filter response. The adder optimization is more complex than that of multipliers, but is done in the same way. The first adder outputs are quantized while the remaining are kept at golden value and quantized till the error (non-quantized sum–quantized sum) is less than 0.01 dB. Once the quantized bits satisfy the error condition, it is fixed and the same process is repeated for the remaining adder outputs. The number of bits to which each adder is quantized is obtained and the quantized number of bits for a few adders is given as an instance in Table 2. The flowchart of adder quantization is shown in Fig. 4.

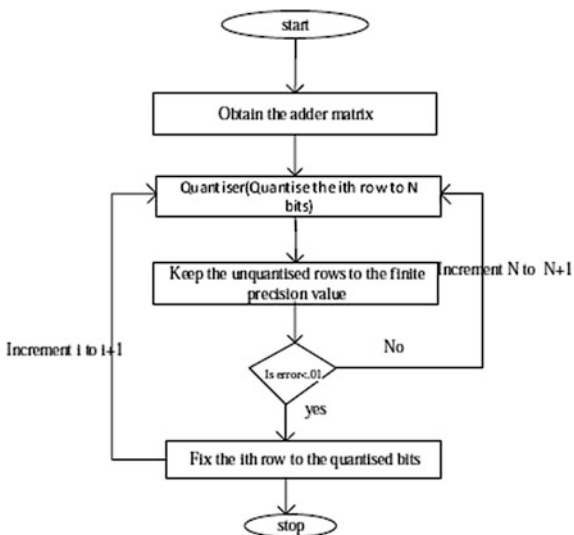
Table 1 The optimized number of bits in the product of first 7 multipliers

Multiplier	1	2	3	4	5	6	7
Non-quantized number of bits in product	35	33	33	30	31	29	36
Quantized number of bits in product with error exactly less than 0.01 dB	32	34	31	29	31	28	32

Table 2 The optimized number of bits in the sum of first 6 adders

Adder	1	2	3	4	5	6
Non-quantized number of bits in sum output	35	35	35	35	35	36
Quantized number of bits in sum output with error exactly less than 0.01 dB	34	34	34	34	34	34

Fig. 4 The flowchart of adder quantization



3.6 Results

The response obtained for the passband, stopband, and transition band input sine wave to the FIR filter are shown in Fig. 5.

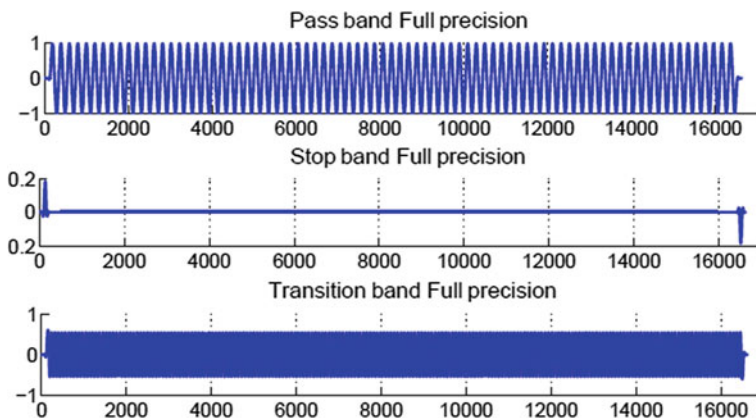


Fig. 5 The response of the 270-tap filter at different input frequencies

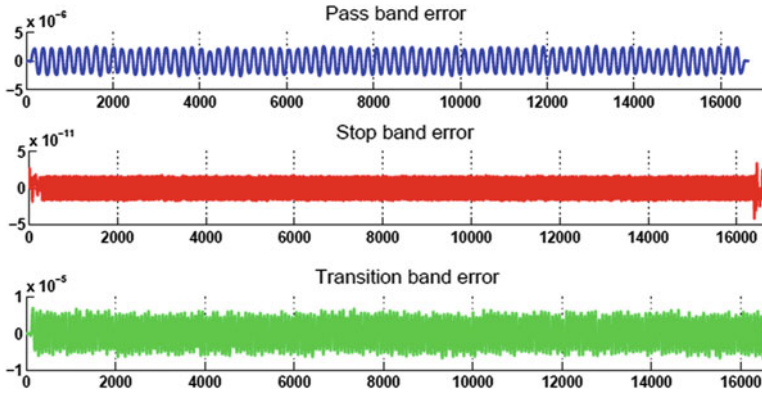


Fig. 6 Error plot for different bands of input sine waves



Fig. 7 Verilog implementation result

The error is plotted by taking the difference between finite precision and golden response. Figure 6 plots the error obtained for the different bands of input sine waves (passband, stopband, transition band).

The 270-tap FIR filter is implemented in Verilog and the output obtained is shown in Fig. 7.

4 Conclusion

Multi-tone sine wave containing passband, stopband, and transition band frequencies were given as inputs to the FIR filter module created in Verilog and output response is stored in a file and is plotted in MATLAB and the response is verified.

Acknowledgments The authors would like to thank Amrita Vishwa Vidya Peedom for providing effective tools for the work and the support of the faculty throughout the completion of the work.

References

1. Efficient Implementation of Real-Valued FIR Filters on the TMS320C55x DSP David M. Alter Application Report SPRA655—April 2000.
2. Proakis J, Manolakis D. Digital signal processing: principles, algorithms, and applications. 3rd ed. Upper Saddle River: Prentice Hall; 1996.
3. Parhi KK. VLSI digital signal processing systems: design and Implementation. Chapter 3. New York: Wiley; 1999.
4. Jagadeshwar Rao M, Dubey S. A High speed wallace tree multiplier using modified booth algorithm for fast arithmetic circuits. IOSR J Electron Commun Eng (IOSRJECE). (Sep-Oct 2012);3(1). ISSN: 2278-2834, ISBN No: 2278-8735.
5. Cho KJ, Lee KC, Chung JG, Parhi KK. Design of low-error fixed-width modified Booth multiplier. IEEE Trans Very Large Scale Integr (VLSI) Syst. 2004;12(5):522-31.
6. Yeh WC, Jen CW. High speed booth encoded parallel multiplier design. IEEE Trans Comput. 2000;49(7):692-701.
7. Booth AD. A signed binary multiplication technique. Q J Mech Appl Math. 1951;4:236-40 (Reprinted in [8, p. 100-104]).
8. Song MA, Van LD, Kuo SY. Adaptive low-error fixed-width booth multipliers. IEICE Trans Fundam. 2007;E90-A(6):1180-7.
9. Madrid PE, Millar B, Swartzlander EE. Modified booth algorithm for high radix fixed point multiplication. IEEE Trans VLSI Syst. 1993;1(2):164-7.
10. Vignesh Kumar R, Kamala J. High accuracy fixed width multipliers using modified booth algorithm. In: International conference on modeling optimization and computing, Procedia Engineering vol. 38; 2012. p. 2491-8.
11. Koren I. Computer arithmetics algorithms. A.K. Peters Ltd. ISBN 1568811608.

Implementation of 18-Bit High-Speed Binary Multipliers

S. Sreelakshmi and T. Vandana Raj

Abstract Multiplication is an extensively used arithmetic operation that has immense usage in signal processing and scientific applications. Multiplication is hardware intensive, and the main criteria of interests are less VLSI area, higher speed, and lower cost. Multiplication involves basically two operations, first is generating the partial products and then their accumulation, where the partial product is shifted by one bit to the right and adding with the previous partial product. The speed of multiplication can be enhanced by reducing the number of partial products or by enhancing the speed of the accumulation. Hence, in this paper, the novel study of the different fast multipliers like radix-2 or Booth algorithm, radix-4 or modified Booth algorithm is done, and implementation of 18-bit multiplier is done in Verilog (Modelsim) and compared the results in MATLAB. The SNR analysis of the multiplier of finite precision product, truncation, and rounding is done. Algorithms for reducing the hardware complexity in partial product sign extension are implemented for both radix-2 Booth multiplication and radix-4 modified Booth multiplication. The Wallace tree adder is implemented for increasing the speed of the accumulation of the partial products.

Keywords Radix-2 Booth algorithm · Radix-4 modified Booth algorithm · Wallace tree · Biased rounding · Unbiased rounding

S. Sreelakshmi (✉) · T. Vandana Raj
Electronics and Communication Department,
Amrita Viswa Vidyapeedom Amrita School of Engineering,
Amritapuri, Kollam, Kerala, India
e-mail: sreelakshmi.sree001@gmail.com

T. Vandana Raj
e-mail: vandanatt@gmail.com

1 Introduction

In hardware, multiplication is performed in its binary format. So the multiplier and multiplicand both have to be converted to its two's complement representation in 0's and 1's. The MSB in both corresponds to the signed bit. Each partial product generated is '0' if the multiplier bit is '0' and otherwise the partial product will be the multiplicand itself. So if the multiplier bit is a '0' then it results only in a shift operation. Hence, the number of partial products generated depends on the number of 1's in the multiplier. The shift/add multiplication algorithm is implemented in a such a way, where each bit of the multiplicand is multiplied with the multiplier so as to generate the partial products and then accumulating them in order to get the result. As the number of partial products increases, this method becomes very slow. Hence algorithms like Booth multiplier, modified Booth multiplier, etc., are used in which more than 1 bit of the multiplier is used simultaneously and recoded in another way, which will reduce the number of partial products [1, 2].

2 Booth Multiplication Algorithms

2.1 Radix-2 Booth Multiplication Algorithm

In Booth algorithm, the multiplier is recoded in a way so as to reduce the total number of partial products generated. An extra '0' bit is appended to the LSB (Least Significant Bit) of the multiplier and then y_i and y_{i-1} of the multiplier are considered for recoding. If the bits are 1 1 or 0 0 then recoded as bit '0' and only shift operation is performed. If the bits are 1 0 then recoded as -1 and the subtract and shift operation are performed. If the bits are 0 1 then recoded as 1 and performs an addition followed by shifting. The radix-2 Booth recoding is explained in Table 1. For instance, if the multiplier is 1 1 1 0, then 3 partial products are generated as it depends on the number of 1's in the multiplier. While recoding by appending a '0' to the LSB, the recoded multiplier becomes 0 0 -1 0 and thus reduces the partial products from 3 to 1. Multiplication starts from the LSB otherwise longer adder/subtraction is required to allow carry propagation. The disadvantage of Booth algorithm is that the recoding results in increased number of partial products in a series of isolated 1's. ,i.e., if the number is 01010101 then recoded as 1 -1 1 -1 1 -1 1 -1 . So 8 partial products are required instead of 4.

Table 1 Radix-2 Booth multiplication recoding table

X_i	X_{i-1}	Operation	Y_i
0	0	Shift only	0
1	1	Shift only	0
0	1	Add and shift	1
1	0	Subtract and shift	-1

This problem is solved by considering three bits at a time which is the method in modified Booth algorithm [3].

2.2 Radix-4 Modified Booth Multiplication Algorithm

It is possible to reduce the number of partial products by half by this method. It will compare three bits at a time with overlapping technique. Grouping starts from LSB and the first block only uses two bits of the multiplier and assumes a ‘0’ for the third bit ,i.e., x_1, x_0, x_{-1} then x_3, x_2, x_1 and so on. The recoding of the radix-4 modified Booth multiplication is explained in Table 2 in which A corresponds to the multiplicand. In this method, the isolated 1’s results in the same number of the partial products, while recoding and 2’s complement multiplications are handled correctly. If the multiplier is odd then a sign extension is required at the MSB (Most Significant Bit) for the proper grouping of the multiplier bits. For instance, if the multiplier is 0 1 0 1 0 1 0 1, then it is recoded as 01 01 01 01 and results in 4 partial products which was 8 in the case of radix-2 Booth multiplication [4, 5].

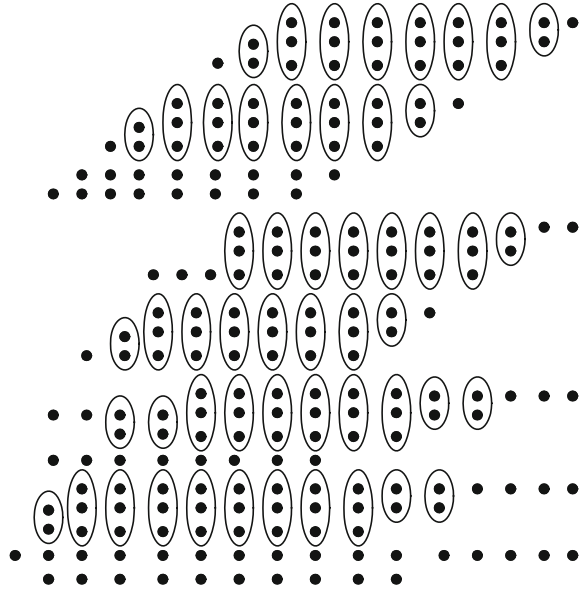
2.3 Wallace Tree Adder

Wallace tree adder method is used for enhancing the speed of the accumulation of the partial products. The first step involved in this process involves grouping the partial products into sets of 3. ,i.e., if there are ‘a’ rows of partial products, then $3 \times (a/3)$ rows are grouped together and the rest $a \bmod 3$ rows are used in the next stage of accumulation. Half adders are used for the addition of the 3 rows if there are only 2 elements in the column, and otherwise full adders are used. The resulting sum and carry signals are passed to the next stage where two more rows of partial products are considered, and the same process is repeated. Finally, when only two rows are left to be added, then implementation is using fast carry propagate adder. An instance of Wallace tree accumulation is illustrated in Fig. 1 [6].

Table 2 Radix-4 modified Booth multiplication recoding table

X_i	X_{i-1}	X_{i-2}	Y_i	Y_{i-1}	Operation
0	0	0	0	0	+0
0	1	0	0	1	+A
1	0	0	-1	0	-2A
1	1	0	0	-1	-A
0	0	1	0	1	+A
0	1	1	1	0	+2A
1	0	1	0	-1	-A
1	1	1	0	0	+0

Fig. 1 Wallace tree addition of partial products



3 Experiments and Results

3.1 MATLAB Implementation

The implementation is done for floating point numbers between ‘-1’ and ‘1’. The floating point number is represented in two’s complement form where 16 bits represents the decimal and 2 bits for the integer part, where one bit is for integer and the MSB as the sign bit. Initially the binary conversion of the number to two’s complement is done and then multiplier bits are recoded, and the partial products are generated based on the recoded multiplier starting from the LSB. The shifting operation is done by sign extending the MSB of the partial products. The result contains $m + n$ bits where m is number of bits of the multiplicand and n is the number of bits of the multiplier. The finite precision value obtained by the Booth multiplication is of 36 bits (18 + 18).

The finite precision result obtained is truncated to the first 18 bits. Similarly the rounding of the bits to first 18 bits based on the 19th bit is also done, where both biased and unbiased rounding are implemented.

3.1.1 Unbiased Rounding

The steps involved are:

- (a) Add $\frac{1}{2}$ LSB normally.
- (b) Do not add a $\frac{1}{2}$ LSB when result is negative.
- (c) Then truncate the result.

For unbiased rounding, if number is positive then add 1 to the 19th bit and then truncate to 18 bits and if negative number, then truncate to 18 bits.

3.1.2 Biased Rounding

The steps involved are:

- (a) Add $\frac{1}{2}$ LSB irrespective of whether a positive or a negative number.
- (b) Then truncate the result.

In biased rounding for both positive and negative numbers, add 1 to the 19th bit and then truncate to 18 bits. The exception in both cases is that if the 19th bit is 1 and the remaining bits are all 0, then no addition of 1 and only truncate to 18 bits. Unbiased rounding is symmetric i.e., rounding the same positive and negative number gives the same result.

3.1.3 SNR (Signal to Noise Ratio) Calculation

The SNR is a measure of how much the signal is affected by noise. In this method, 10,000 samples of random values between -1 and 1 are taken as the multiplier and multiplicand and the SNR in different cases are considered. SNR is the ratio of signal power to noise power where the rms value of the amplitude is taken. The signal power corresponds to the power obtained in direct multiplication. Here, 10,000 samples are taken for getting a proper mean, i.e., if random values are generated within -1 and 1 then mean should be 0 or if between 0 and 1 then mean should be 0.5 . Then the noise power is computed for finite precision, truncation, and unbiased rounding.

$$\text{SNR} = 10 \log_{10} \left(\frac{P_{\text{signal}}}{P_{\text{noise}}} \right), \quad (1)$$

where P_{signal} and P_{noise} are the rms power of signal and noise.

$$\begin{aligned} \text{SNR} &= 10 \log_{10} \left(\frac{A_{\text{signal}}}{A_{\text{noise}}} \right)^2 \\ &= 20 \log_{10} \left(\frac{A_{\text{signal}}}{A_{\text{noise}}} \right), \end{aligned} \quad (2)$$

where A_{signal} and A_{noise} are the rms amplitude of signal and noise.

$$SNR = 20 \log 10 \sqrt{\frac{1/n(A_{sig,0}^2 + A_{sig,1}^2 + \dots + A_{sig,n}^2)}{1/n(A_{noise,0}^2 + A_{noise,1}^2 + \dots + A_{noise,n}^2)}}, \tag{3}$$

where n is the number of the random inputs, A_{sig} is the amplitude of the decimal value (non-quantized) and

$$A_{noise} = A_{sig; \text{ Non-quantized}} - A_{sig; \text{ quantized}} \tag{4}$$

The SNR values obtained for the finite precision, truncation, and unbiased rounding are in Table 3.

3.2 Hardware Implementation

The multipliers are implemented in Verilog using the Wallace tree method for the accumulation of the partial products. The partial products are generated using the recoded value of the multiplicand using multiplexers. In radix-2 multiplication, the partial products generated has to be sign extended (MSB is sign extended to the number of bits in the multiplicand) in order to get the expected product which requires additional hardware in the form of full adders or half adders. In order to optimize the hardware complexity the algorithm used in radix-2 Booth multiplication is sign extending the MSB of the first partial product by one bit and extending the complement of the MSB as the next bit. In the remaining partial products, the MSB itself is replaced by the complement of the MSB. In this way, the additional hardware is reduced. For example, if the multiplicand is 5 bits then there are 5 partial products and the algorithm is applied as in Fig. 2 in which s_1, s_2, \dots , corresponds to the MSB in each of the partial products [7].

Table 3 SNR values obtained for different cases

Method	Finite precision	Truncation	Unbiased rounding
SNR value	90.8784	88.8363	89.6236

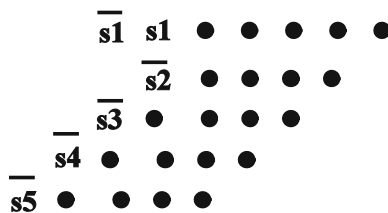


Fig. 2 The algorithm for radix-2 Booth multiplication without sign extension of partial products (considering the multiplicand as 5 bits)

The multiplication is performed for 18-bit multiplicand and multipliers, where the 16 bits corresponds to the decimal part and 2 bits corresponds to the multiplicand. The 18 partial products are generated, and the algorithm is applied before accumulation is done through Wallace tree. The final result of the Wallace tree which gets reduced to two rows are then accumulated using fast adder like vector merging array. The vector matching is checked using 1000 random vectors and matched with the result generated from MATLAB.

For radix-4 modified Booth multiplication, in order to reduce the hardware complexity due to the sign extension of partial products, in cases where $-A$ and $-2A$ are the required partial products, only the 1's complement value is taken in order to avoid the extra adder required prior to the Wallace tree accumulation. In order to reduce the sign extension, the algorithm implemented to modify the partial products by sign extending by 2 the MSB of the first partial product, then extend the complement of the MSB and then placing the MSB as the LSB of the next partial product, so that if the previous partial product was negative, i.e., either $-A$ or $-2A$, then 1 is added with it and thus generating the 2's complement else it simply adds bit '0.' From the second partial product onward the complement of the MSB is sign extended by 1 bit and the second bit extended as '1' and the MSB is appended as the LSB of the next partial product. The advantage of modified Booth method is that for 18 bit numbers only 9 partial products are generated. The modified partial products are then accumulated using the Wallace tree adder. An algorithmic implementation for an 8-bit multiplicand is in Fig. 3 in which s1, s2, etc., correspond to the MSB in each of the partial products.

The modified Booth multiplication result obtained in Verilog for the 18-bit random inputs is in Fig. 4.

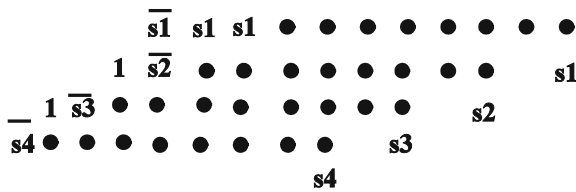


Fig. 3 The algorithm for radix-4 modified Booth multiplication without sign extension of the partial products (Shown for 8×8 multiplication)

Messages					
BOOTH_MUL_TB/in...	-127165	-97179	-7423	-3722	22509
BOOTH_MUL_TB/in...	43704	-44526	-13043	118077	128908
BOOTH_MUL_TB/f...	11915869160	4326992154	96818189	-439482594	2901590172

Fig. 4 The multiplication result obtained in Verilog

Table 4 Vector matching result

Multiplicand	Multiplier	Product
-0.6555634	-0.8500214	0.5572429
-0.865234	0.12939445	-0.1119566
0.2721252	0.7992706	0.2175017
0.2444763	-0.2809601	0.6868809
0.2189484	-0.1627960	-0.3564392
0.7002106	-0.7935791	-0.5556725
0.80766477	-0.07116699	-0.05747786

The result obtained in Verilog is verified by matching with the results obtained in MATLAB by generating 1000 vectors. The vector matching results for some combinations are in Table 4.

4 Conclusion

The radix-2 and radix-4 multiplication of 18 bit numbers in both MATLAB and Verilog are perfectly matched for random floating point inputs between -1 and 1 . The implementation using the algorithm without sign extension of the partial products results in reducing the hardware complexity otherwise required. The accumulation of the partial products using the Wallace tree adder also enhances the speed of accumulation.

Acknowledgments The authors would like to thank Amrita Viswa Vidyapeedom for providing effective tools for the work and the support of the faculty throughout the completion of the work.

References

1. Cho KJ, Lee KC, Chung JG, Parhi KK. Design of Low- error fixed-width modified Booth multiplier. *IEEE Trans Very Large Scale Integr VLSI Syst.* 2004;12(5):522–31.
2. Yeh WC, Jen CW. High speed booth encoded parallel multiplier design. *IEEE Trans Comput.* July 2000;49(7):692–701.
3. Booth AD. A signed binary multiplication technique. *Quart J Mech Appl Marh.* 1951;4:236–240. (Reprinted in [8, pp. 100-104]).
4. Song MA, Van LD, Kuo SY. Adaptive low-error fixed-width Booth multipliers. *IEICE Trans Fundam.* June 2007;E90-A(6):11180–1187.
5. Madrid PE, Millar B, Swartzlander EE. Modified booth algorithm for high radix fixed point multiplication. *IEEE Trans.* 1993.
6. Fadavi-Ardekani J, “M X N Booth encoded multiplier generator using optimized Wallace trees. *IEEE Trans Very Large Scale Integr VLSI Syst.* June 1993;1(2):120–125.
7. Koren I. *Computer arithmetics algorithms.* A.K. Peters Ltd. ISBN 1568811608.

A New Approach to Object-Oriented Programming Language for Remote Power Quality Monitoring and Analysis Considering Harmonics

Vidula S. Jape and D.G. Bharadwaj

Abstract Use of micro processed technology enhances the power system operation and control tasks, but at the same time resulting into power quality problems for utility as well as consumers. One of the major issues of power quality is harmonics in power system. Through mandatory regulations, harmonics in the power system must be prevented to ensure good power quality. This paper presents a new approach of object-oriented programming for remote power quality monitoring and analysis with harmonic considerations. The real-time monitoring and analysis of power system parameters is inherently complex due to large data handling process. Object-oriented programming tool has been used as computational tool which performs monitoring and analysis in substation related to power quality, and gives subsequent analysis for the residual life assessment of substation equipment due to power quality. A GUI is created in java to create user-friendly environment. Data can be transmitted from remote stations to the central server and authority sharing has been developed as per the process. This is an innovative approach in electrical field in terms of substation monitoring which thereby improves power quality. A case study of distribution network supplying linear and nonlinear loads is presented which encompasses the effects of harmonics on substation equipments to find out the solution to be implemented.

Keywords Distribution network · IEEE standard · Harmonics · Life expectancy · Lightning arrester (LA) · Penalty factor · Power quality · Substation monitoring system (SMS) · System interruption · Total harmonic distortion (THD)

V.S. Jape (✉) · D.G. Bharadwaj
BVDUCOE, Pune, Maharashtra, India
e-mail: jape_swati@yahoo.co.in

© Springer India 2016
S.S. Dash et al. (eds.), *Artificial Intelligence and Evolutionary Computations in Engineering Systems*, Advances in Intelligent Systems and Computing 394,
DOI 10.1007/978-81-322-2656-7_29

323

1 Introduction

In deregulation era, more emphasis is given to meet the customer expectations and maintaining their confidence as they are the predominant contributors of the power industries as well as the nation's economy. Up to now, the regulatory entities attended to cope up with system interruption only give the idea about reliability of the system. No attention is paid to power quality of the system which requires attributing the responsibilities for the deterioration of the power quality. IEEE standard 519-1992 provides the basis for limiting harmonics [1]. The main objective of IEEE standard 519-1992 is to limit the harmonic injection from individual consumer and to limit the overall harmonic distortion in the voltage and current supplied by the utility. This standard emphasizes the responsibility for limiting the harmonics on both customer and utility. Customer will be responsible for limiting the current harmonic injection and utility will be responsible for limiting the voltage harmonic distortion in the supply system which will further deteriorate the power quality of the system. The gradual rise in awareness the of effect of power quality disturbances on substation equipments has led to many utilities, taking much proactive approach toward the measurement of power quality levels on their networks [2]. In this paper, power quality monitoring and its analysis is proposed through substation monitoring system (SMS) with object-oriented programming which gives aspect of the effects of harmonic distortion on the behavior and performance of several important electrical equipments such as transformer, lightning arrestors, and the ill-effects of harmonics on life expectancy of substation equipment as key parameters are also discussed.

2 Effects of Harmonics on Substation Equipments

To support the theoretical study, survey for the measurement of power quality has been done by using an Advanced Power Analyzer "Yokogawa" (model CW240) at different substations feeding power to various categories of nonlinear consumers. This survey highlights study and analysis of the effects of harmonics on winding losses and core losses of transformer, and life expectancy of lightning arrestor. The developed relation between voltage level, harmonics, and distance from nonlinear load summarizes the overall adverse effect on substation equipments.

2.1 Transformers

Transformers are designed to deliver the required power to the connected loads with minimum losses at fundamental frequency. The effect of harmonics on transformer is twofold, current harmonics cause an increase in copper losses and voltage harmonics cause an increase in iron losses. Transformer losses, categorized as load

losses and no-load losses, may be further divided by I^2R (Winding loss) and stray losses.

$$P_T = P_L + P_{NL} \quad (1)$$

No-load loss: This loss is independent of the load and is caused by the induced voltage in the core. It comprises two components: hysteresis and eddy current losses [3]. The core losses such as iron loss and eddy current loss, being the functions of frequency, are higher at higher harmonics.

$$P_{NL} = H + E = k_h \times f \times B_m^n + k_e f^2 \times B_m^2 \quad (2)$$

where k_e and k_h are constants of the core material, B_m is the maximum flux density, and $n = [1.5, 2.5]$ is material dependent. The effect of harmonic loads on no-load loss is often insignificant since the voltage harmonics are dominated by the fundamental component and hence V_{THD} usually does not exceed 5 %.

2.2 Lightning Arrestor (LA)

It is observed from survey that the failure of lightning arrestor takes place in the vicinity of harmonic prone area. The healthiness of lightning arrestors is determined on the basis of internal resistance of the arrestor and its leakage current. The internal resistance of EHV LA should be more than 20 M Ω [1]. This can be ascertained by recording Megger values of LAs. For example, the internal resistance of a 220 kV LA should be more than 25 M Ω . The second important parameter to ensure the healthiness of LA is the measurement of leakage current. In normal practice, the leakage current of the LA should be less than 300 μ A. Usually, it is found that the leakage current of the LA (I_L) is about four times the third harmonic current I_3 , passing through LA [4] $I_L = 4 \times I_3$.

In harmonic prone area, the magnitude of the third harmonic current I_3 is very high. This results in very high magnitude of leakage current. If it is more than 300 μ A, the chances of failure of LA is more [5].

3 Case Study and Analysis

A survey was conducted at 33 kV substation feeding power to six nonlinear consumers, as shown in Fig. 1.

Table 1 shows the relations between voltage level and harmonics and distance from nonlinear load. As shown in Fig. 2, it is observed that as the voltage level increases, the effect of I_{THD} decreases. Similarly, as the distance from nonlinear load increases the effect of I_{THD} decreases. Hence, I_{THD} observed at substation is less as compared to the consumer end.

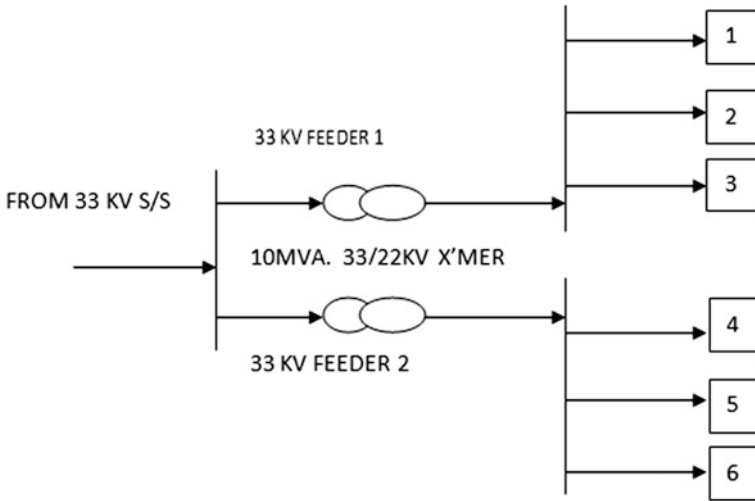
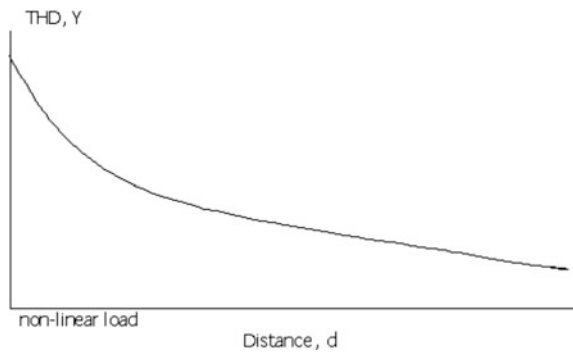


Fig. 1 Single line diagram of substation

Table 1 Observations at consumer end, feeders, and substation

Location where measurements are taken	I_{THD} (%)
Substation	5.8
Feeder-1	8.5
Feeder-2	8.8
Consumer-1	10.1
Consumer-2	10.2
Consumer-3	9.83
Consumer-4	11.12
Consumer-5	11.28
Consumer-6	12.41

Fig. 2 Relation between distance and THD



With reference to the above observations, power quality monitoring and analysis was performed and results are calculated in the form of indices. Objective of derived power quality indices is to qualify the distribution network against the distortion index. In this regard, a new procedure is presented that evaluates the distortion index introduced by different types of nonlinear loads connected to the power distribution network [6]. In the presence of harmonics, the voltage and current functions with respect to time can be expressed as

$$V(t) = V_0 + \sqrt{2 \sum_{H \neq 0}^{\infty} V_H \sin(H\omega t + \alpha_H)} \tag{3}$$

where $V(t)$ is instantaneous voltage, V_0 is the average value,

$V_{H,rms}$ is the value of voltage harmonics H , and α_H is phase angle of voltage harmonic H .

$$i(t) = I_0 + \sqrt{2 \sum_{H \neq 0}^{\infty} I_h \sin(H\omega t + \beta_H)} \tag{4}$$

β_H is the phase angle of current harmonic H

Separating the fundamental component V_1 and I_1 from the harmonic component V_H and I_H gives $V = \sqrt{V_1^2 + V_H^2}$ $I = \sqrt{I_1^2 + I_H^2}$

$$\text{Total Harmonic Distortion Voltage } V_{THD} = V_H / V_1 \tag{5}$$

$$\text{Total Harmonic Distortion Current } I_{THD} = I_H / I_1 \tag{6}$$

$$\text{Fundamental Apparent Power, FAP } V_1 I_1 \tag{7}$$

$$\text{Current Distortion Power, CDP} = V_1 I_H \tag{8}$$

$$\text{Voltage Distortion Power, VDP} = V_H I_1 \tag{9}$$

$$\text{Harmonic Distortion Power, HDP} = V_H I_H \tag{10}$$

$$\text{NAP: Non-linear Apparent Power; NAP} = \sqrt{\text{CDP}^2 + \text{VDP}^2 + \text{HDP}^2} \tag{11}$$

$$\text{TAP: Total Apparent Power; TAP} = \sqrt{\text{FAP}^2 + \text{NAP}^2} \tag{12}$$

$$\text{DI: Distortion Index; DI} = \text{NAP} / \text{FAP} * 100 \tag{13}$$

DI is improved power quality index as it directly relates to the distortion in power. As compared with the available THD as the power quality parameter, it reflects either the voltage or the current distortion only. Hence, it is important to include DI

as major index which measures the levels of the harmonic pollution present to evaluate the power quality performance of the network. This index can also be used as “Quality factor” or “Penalty Factor” [7].

4 Operation of Substation Monitoring System (SMS)

In the present work, object-oriented programming language has been used to develop the Substation Monitoring System (SMS) [5] as shown in Fig. 3. It comprises two main applications, substation client application and substation server application. Which will install on each substation? This application will show all the substations along with the monitoring report of each substation as per the selected time period. This monitoring report includes the PQ parameters, power quality indices, and power quality distortion index as per first to ninth harmonics.

Server side web applications deployed in web server are accessible through internet. To deploy this server application, cloud server on the internet is used. User administrator or substation manager will access this application through browsers

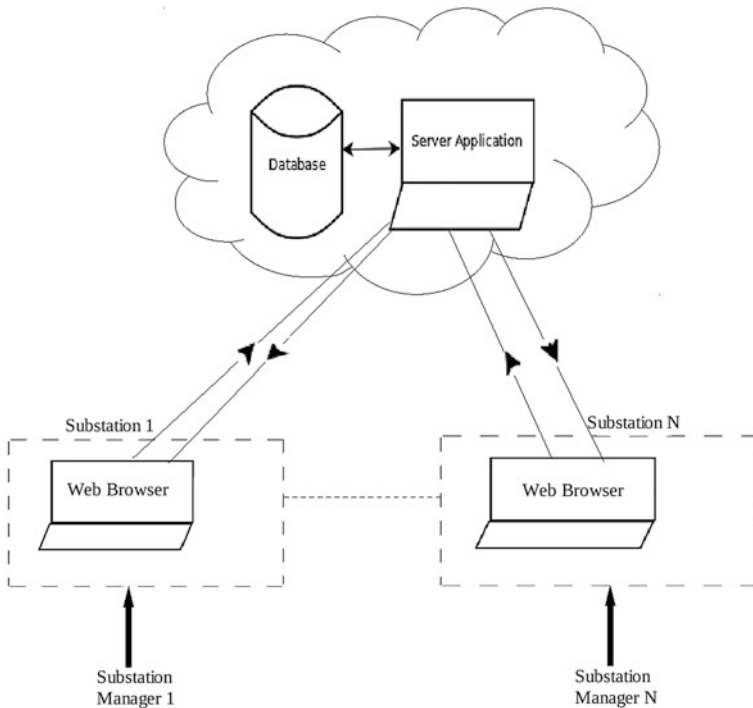


Fig. 3 Block diagram of substation monitoring system

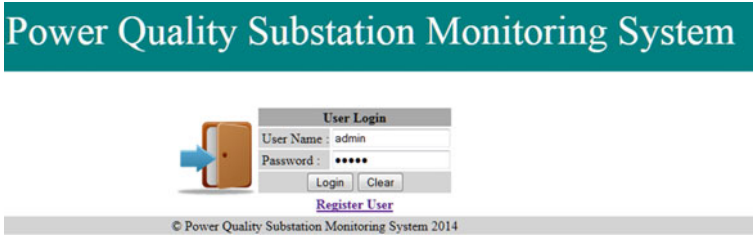


Fig. 4 Web page set up for log in

like, Internet Explorer/Mozilla Firefox/Google Chrome as web application so that nontechnical authority can access or login into web. Figure 4 shows the web page set up for log in into SMS.

4.1 Flow of Substation Server Application

There are two types of users, Administrator and Substation Manager, who can access substation server application; administrator of server application will be single whereas substation managers will be multiple depending on the number of substation. Administrator can create virtual information of substation. This procedure will create list of substations and provide access to the particular user. It also creates users for each substation that will be available in a database to maintain the list of substations. Each substation’s information contains substation name, address (location), and single line diagram description. This system will monitor and analyze the power quality parameters of each substation as per IEEE standards.

Table 2 % Average voltage harmonic distortion measured at nonlinear consumers

Industry no.	AVG VR _{THD} (%)	AVG VY _{THD} (%)	AVG VB _{THD} (%)
1	2.56	2.42	2.48
2	0.243	0.044	0.12
3	0.165	0.045	0.0098
4	49.4	19.9	19.4
5	0.845	2.25	0.486
6	1.97	1.79	1.89
7	0.886	0.929	0.643
8	0.09	0.0714	0.946

Table 3 % average current harmonic distortion measured at nonlinear consumers

Industry no.	AVG IR _{THD} (%)	AVG IY _{THD} (%)	AVG IB _{THD} (%)
1	20.9	18.7	20.1
2	42.7	45.9	47.6
3	0.81	0.527	0.42
4	20.7	19.9	19.4
5	6.89	5.7	6.32
6	20.1	18	19.3
7	6.74	4.7	5.7
8	6.03	6.01	5.79

Table 4 Calculated indices for industry no. 4

Indices	R	Y	B
V _{THD} (%)	1.68905	0.99535	1.389165
I _{THD} (%)	17.17866	15.65746	15.66782
FAP	125.2349	136.9234	134.6265
CDP	21.51368	21.43872	21.09304
VDP	2.115275	1.362867	1.870183
HDP	0.363376	0.21339	0.293017
NAP	21.62048	21.48306	21.17781
TAP	127.0875	138.5985	136.282
DI	17.26393	15.68984	15.73079

5 Conclusion

From the result of the harmonic survey done at various voltage levels in power system networks as shown in (Tables 2, 3 and 4), it is observed that current harmonic levels are substantial. The higher level of current harmonic distortion causing overloading, overheating of transformer, and other substation equipments, adversely affects the life expectancy of these equipments. This paper presents the work based on the new approach of object-oriented programming language in the field of electrical power distribution system. This transmits the data from remote station to central station in user-friendly environment.

SubStation Monitoring system (SMS) displays the reports regarding power quality represents the harmonic indices that gives contribution of each load on the total distortion of the power system. It includes distortion of voltage, current, power, total apparent power, and also nonlinear apparent power. Therefore, this system set the basis of monitoring and analysis of power quality for distribution network.

The case studies presented here are the examples and it is necessary to improve the existing situation of power quality. The study leads to the following conclusions.

1. Electric utility must be able to evaluate, characterize, and access the system performance to plan the system improvements for satisfying the power quality needs.
2. To track the performance of the system, it is important to consider power quality indices as one of the method of deciding the power quality.
3. The consumers who are polluting the power quality are required to be penalized logically through smart metering system. In short, it is necessary to test the validity of power system networks with particular reference to Indian context. Such study makes it possible to rectify and correct the system.

Acknowledgments The project work is being carried out in Bharati Vidyapeeth Deemed University COE, Pune. The authors wish to thank authorities of BVDUCOE, Pune for granting permission to publish the work. Special thanks to MSEDCL and MSETCL for collection of data at substation and consumer end.

References

1. IEEE Std. 519-1992:-IEEE recommended practices and requirements for harmonic control in electrical power systems.
2. Dugan RC, Mc Granghan MF. A book on Electrical power system quality. 2nd ed. Tata Mcgraw Hill.
3. Arrilaga J, Watson NR. A book on Power system harmonics. 1st ed. Wiley.
4. MPEB Technical Report No. 124, Research Scheme on Power, June 2000. Study of harmonic present in the system and determination of permissible limits of harmonics.
5. IEEE STD. 1159-1995, IEEE recommended practice for monitoring electric power quality.
6. IEEE Working Group. Practical definitions for powers in systems with non-sinusoidal waveforms and unbalanced load: a discussion. IEEE Trans Power Delivery. 1996;11(1).
7. Vlahinic S, Brnobic D, Stojkovic N. Indices for harmonic distortion monitoring of power distribution systems. Instrumentation. 2008:12–15.

Dynamic Programming Parallelization of Matrix Chain Multiplication on GPU: A Comparative Study

Tausif Diwan and S.R. Sathe

Abstract The dynamic programming paradigm involves various important optimization problems. The set of optimization problems includes optimal binary search tree, longest common subsequence, binary knapsack, Matrix chain multiplication (MCM), and many more. In dynamic programming problems, the MCM of n matrices comprises the computation of the parenthesization for an optimal matrix product, which requires the computation time of $O(n^3)$ using $O(n^2)$ table size. We propose the MCM parallelization techniques for thread-level of multi-core CPU and group of threads on NVIDIA GPU. The prime objective of this paper is to present and analyze massively parallel implementations of MCM algorithm using OpenMP and CUDA on parallel systems such as Intel Xeon CPU and NVIDIA GPU. The implemented parallel MCM algorithm achieved a speedup of $10\times$ on an Intel Xeon using OpenMP and a speedup of $7\times$ on NVIDIA Quadro FX 3800 GPU with reference to its serial implementation. So the speedup achieved on multi-core CPU dominates the speedup achieved by the GPU. This paper also presents performance comparisons for OpenMP, when chunk size of iterations of a loop and scheduling techniques of those chunks among core changes.

Keywords GPU · Dynamic programming · CUDA · OpenMP · Matrix chain multiplication

1 Introduction

Today is an era of parallel programming. There are various parallel programming tools available such as OpenMP, CUDA, OpenCL, OpenAcc, MPI, etc. In this paper, we present parallel implementations, analysis, and comparisons among those

T. Diwan (✉) · S.R. Sathe
Department of Computer Science and Engineering, Visvesvaraya National
Institute of Technology, Nagpur, Maharashtra, India
e-mail: tausifdiwan.tausif@gmail.com

S.R. Sathe
e-mail: srsathe@cse.vnit.ac.in

implementations for a non-deterministic dynamic programming (NPDP) problem matrix chain multiplication (MCM) using OpenMP and CUDA parallel programming languages.

Dynamic programming (DP) is one of the Berkley 13 dwarfs, where a dwarf can be defined as a methodology or protocol for communication and distributed computation. Dynamic programming has two distinguished features (1) Overlapping subproblems: A subproblem is overlapped on some other subproblem, partially or fully. (2) Optimal substructure: every subproblem is optimal. While solving a particular problem using dynamic programming, we get a recurrence equation and terminating conditions for that recurrence equation. A problem is divided into subproblems and those subproblems are divided further until we reach to the terminating condition of the recurrence. Based on the characteristics of the recurrence equation, dynamic programming classification is done. If characteristics equation contains only single recursive term on the right-hand side, then DP is called monadic otherwise it is called polyadic. If terms of right-hand side of equation depend only on the terms calculated in the immediate previous level, then DP is called serial, otherwise it is called non-serial. Based on this, there are four categories; (1) Serial monadic DP, (2) Serial polyadic DP, (3) Non-serial monadic DP, and (4) Non-serial polyadic DP. We will target for parallelization the most complex among these four that is non-serial polyadic DP. Examples of this category are MCM and Zukar's Algorithm.

Matrix chain multiplication is defined, formulated, and solved by Godbole [1]. His solution is based on the fact that matrix multiplication is associative in nature. If we are given with N matrices which are compatible for multiplication for each consecutive pair of matrices, order of multiplication affects a lot to the total number of scalar multiplication. This problem pursues inherent parallelism available in the algorithm itself. In [2], the authors have parallelized this algorithm on shared memory-based parallel computer. They showed that the best performance can be achieved when we minimize communication among processors. In [3], the authors have applied several optimization techniques such as tiling, memory coalescing for the performance improvements of the Smith Waterman algorithm on the GPU. Nishida et al. [4] implemented the matrix chain product in parallel, which achieved a significantly good speedup over a conventional CPU. They employ thread, block, and several blocks of threads for calculation of a subproblem of MCM and compare the performance. Wu et al. [5] proposed methodology for load balancing of MCM over GPU cores. The authors addressed the problem of nonuniform load distribution and proposed a technique for load balancing. In the recent trend of parallel computing, NVIDIA's GPUs [6] are heavily used for general-purpose computations.

The main contributions of this research work are as follows;

1. We present the parallel implementation of MCM using OpenMP and CUDA.
2. We present the performance analysis of parallel MCM using parallel programming for multi-core CPU and GPU with reference to classical serial implementation of MCM.

3. We present the performance comparisons of OpenMP implementations, when we change the scheduling policy of chunks of iterations over processing cores.

The remaining paper is organized as follows. Problem formulation is described in Sect. 2. Section 3 gives a brief introduction of existing parallel programming technologies such as OpenMP and CUDA. Parallel implementations of MCM are presented in Sect. 4. In Sect. 5, the results of these parallel implementations are elaborated. Conclusions and future work are discussed in Sect. 6.

2 Problem Formulation

The matrix chain problem is defined as given n matrices $m_1 \dots m_n$ and each consecutive pair is compatible for multiplication that is m_i and m_{i+1} can be multiplied. We can easily identify that matrix multiplication is associative in nature and total number of possibilities for parenthesization of all matrices are a Catalan number. For a large number of matrices, it becomes tedious to find the optimal order such that the total number of scalar multiplications would come out to be minimized. In this problem, we have to find the optimal order of MCM such that the total number of scalar multiplications would be optimal. Equation (1) gives the mathematical representation of MCM. Algorithm 1 [7] takes the input array $p[0 \dots n]$ of size $(n + 1)$. The dimension of matrix m_i is $p_{i-1} \times p_i$ and $m[i, j]$ indicates minimum number of multiplications required for actual multiplication of the sequence from m_i to m_j . The final entry that is to be calculated is $m[1, n]$. Algorithm 2 [7] is used for printing an optimal paranthesization.

$$m[i, j] = \begin{cases} 0 & \text{if } (i = j) \\ \min_{i \leq k < j} \{m[i, k] + m[k + 1, j] + p_{i-1} p_k p_j\} & \text{if } (i < j) \end{cases} \quad (1)$$

Algorithm 1. MATRIX-CHAIN-ORDER(p)

1. $n \leftarrow \text{length}[p] - 1$
 2. for $i \leftarrow 1$ to n
 3. do $m[i, i] \leftarrow 0$
 4. for $l \leftarrow 2$ to n /* l is the chain length */
 5. do for $i \leftarrow 1$ to $n - l + 1$
 6. do $j \leftarrow i + l - 1$
 7. $m[i, j] \leftarrow \infty$
 8. for $k \leftarrow i$ to $j - 1$
 9. do $q \leftarrow m[i, k] + m[k + 1, j] + p_{i-1} p_k p_j$
 10. if $q < m[i, j]$
 11. then $m[i, j] \leftarrow q$
 12. $s[i, j] \leftarrow k$
 13. return m and s
-

Algorithm 2. PRINT-OPTIMAL-PARENS(s, i, j)

```

1 if  $i = j$ 
2   then print "A" $i$ 
3   else print "("
4     PRINT-OPTIMAL-PARENS( $s, i, s[i, j]$ )
5     PRINT-OPTIMAL-PARENS( $s, s[i, j] + 1, j$ )
6   print ")"

```

3 Parallel Programming Paradigm

3.1 OpenMP

OpenMP is one of the favorite APIs used for parallelization of a code segment on multi-core architecture due to its higher programming efficiency. OpenMP is based on shared memory parallel architecture where the higher level cache is shared between processor cores. The lower level cache memory of each processing element is dedicated to that core itself [8, 9] (Fig. 1).

We can exploit the inherent parallelism available in the algorithm using OpenMP very easily. We can distribute the iterations of a loop over the cores to get the maximum performance benefits of all processing elements (cores). User can also specify what should be the distribution policy for iterations over threads. Load balancing techniques can be used for improving the performance. The complete specification of OpenMP can be found in [10].

OpenMP is based on fork join model. Initially, one master thread starts execution of the serial portion of the code. Whenever OpenMP runtime encounters a *pragma* for parallelization, a team of threads is created and load is distributed among the cores automatically or manually as well. We can also control the accessibility of each and every variable through private and shared clauses. A lot of built-in variables and libraries are available for managing all this stuff. Using schedule clause, we can manually define the chunk size of iterations of any loop and distribute chunks over the cores.

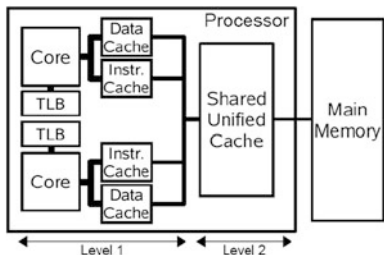


Fig. 1 Block diagram of a generic, cache-based dual-core processor [9]

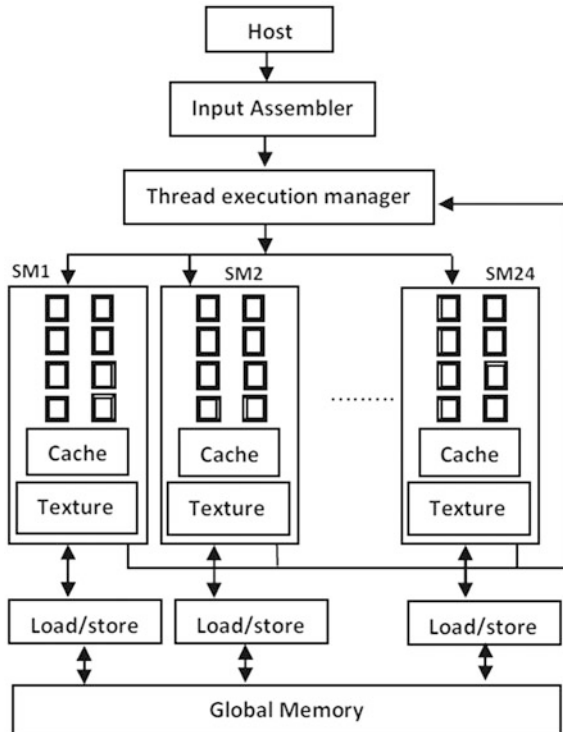
3.2 CUDA

This is an era of graphics processing units (GPUs) where general-purpose scientific computation can be carried out on the graphic processors. The speed of such system is very high as compared to CPUs. NVIDIA GeForce GTX series graphics processors provide more than 1500 GFLOPS/s [6] and memory bandwidth in such processor is about more than 200 GB/s.

In GPU computing architecture, a number of streaming multiprocessors (SM) are available on a device. In one SM, a number of streaming processors (SP) or cores are present [11]. Figure 2 shows the schematic configuration of NVIDIA CUDA Quadro FX 3800 with 24 SMs, 8 SPs in each SM, presents a huge compute engine.

CUDA was introduced by NVIDIA Corporation in 2007 as a general-purpose parallel computing architecture along with its own instruction set architecture. CUDA provides a programming interface and environment for software developers to write parallel programs using high-level languages such as C, C++, and FORTRAN. Data parallel computations are sent to the GPU via kernel launching. Kernel is a function that executes on a device. While launching the kernel, we have to specify the grid size and block size [12]. In CUDA architecture, a logical set of

Fig. 2 NVIDIA CUDA Quadro FX 3800 with 192 CUDA cores organized as 24 SMs, 8 SPs in each SM



32 threads is created, scheduled, and executed in parallel, called as Warp. Threads executing an instance of a kernel can be accessed using built-in variables.

Memory hierarchy in CUDA is very important. In CUDA software model, every thread is having its own private memory. A very small amount of shared memory is also available for each block of threads; since it is on-chip memory, it is very fast. For a set of blocks, called as grid, global memory is available. Since it is off-chip memory, it is very much slow as compared to shared memory. We can take benefit of using shared memory instead of expensive global memory to get improved performance.

4 Parallel Implementation

Matrix chain multiplication is one of the most likely problems that can be solved using dynamic programming. Algorithm 1 has an inherent parallelism which suits for parallel implementation on the available parallel hardware system. In Algorithm 1, line 4 indicates the total number of passes, and line 5 calculates the total number of $m[i, j]$ for that particular pass. This algorithm needs a total of $(n - 1)$ passes to compute the optimal number of multiplications required. In a pass l , $(n - l + 1)$ entries are calculated. As we can see in the algorithm 1, innermost loop will run $(j - i)$ times for the optimal computation of one $m[i, j]$. All $m[i, j]$ entries of a particular pass l can be computed in parallel. Loop-carried dependencies exist among passes for the calculation of $m[i, j]$. So we target line 5 of Algorithm 1 for parallelization.

In OpenMP implementation of MCM, we target line 5 of Algorithm 1 wherein we have distributed the iterations among the cores using different scheduling techniques such as static, dynamic, guided, and runtime. In static scheduling technique, the size of each chunk is fixed and it is calculated as the total number of iterations divided by number of threads generated. Assignments of chunks to processing cores are done statically according to round-robin method. This is the simplest method for assigning chunks to cores because very little overhead is involved. In dynamic scheduling, chunk size is fixed as is in static scheduling technique. Threads request for new chunk for execution as they finish the execution of assigned chunk. Guided seems to be more practical and beneficial clause due to the methodology for calculation of chunk size. A thread request for a chunk and chunk size is calculated dynamically as the number of remaining iterations that are to be executed divided by number of threads. A much overhead is involved in the computation of chunk size for each and every request of the chunk. In runtime scheduling technique, chunk assignments are done at runtime, depending on the assigned load for each core.

In Listing 1, we present a pseudocode of MCM implementation using OpenMP, and compiler directive is inserted for parallelization of second for loop. The runtime scheduling scheme is chosen here for the distribution of chunks among cores. In OpenMP, by default, the number of threads generated is same as the number of cores available on CPU side that is 12 threads for Intel Xeon 5650 Quad Core processor.

Listing 1 OpenMP implementation of MCM

```

void MCM(int *p, int **m, int **s, int n, int cSize){
.....
for(l=2; l<=n; l++){
#pragma omp parallel for schedule(runtime) \
private(i, j, k, q) shared(m, s, l, p)
for(i=0; i<=n-l; i++){/* Parallel region begins */
j = i + l - 1;
m[i][j]= inf;
for(k=i; k <= j-1; k++){
q = m[i][k] + m[k+1][j] + p[i]*p[k+1]*p[j+1];
if(q < m[i][j]){
m[i][j] = q; s[i][j] = k;}/* end if */
}/* for loop ends */
}/* Parallel region ends */
}
}

```

Listing 2 High-level description of MCM using CUDA on GPU

```

__global__ void MCM(int *p,int n,int l,int *m,int *s){
int tid = blockDim.x * blockIdx.x + threadIdx.x;
int j, k, q;
if(tid <= n-l){
j = tid + l - 1;
m[tid*n+j] = inf;
for(k=tid; k<=j-1; k++){
q = m[tid*n+k]+m[(k+1)*n+j]+p[tid]*p[k+1]*p[j+1];
if(q < m[tid*n+j]){
m[tid*n+j] = q; s[tid*n+j] = k;
}/* end if */
}/* for loop ends */
}/* end if */
}/* kernel ends */

int main(){
.....
for(l=2; l<=n; l++)
MCM<<<blocks, threads>>>(p, n, l, m, s);
.....
}

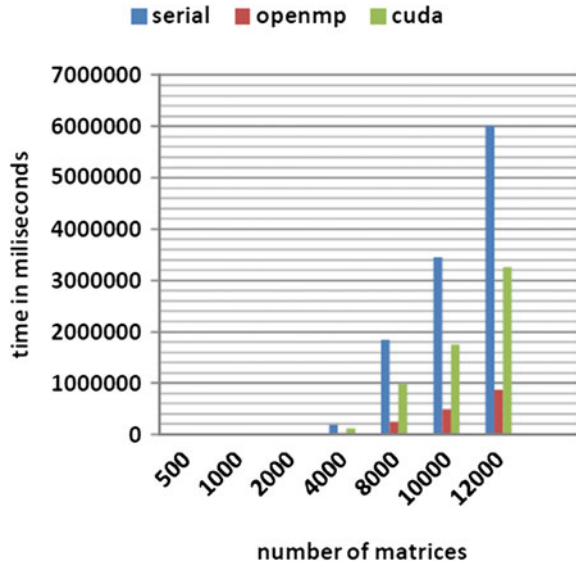
```

In CUDA, we focused same code block as the construct for parallelization that is calculations of all $m[i, j]$ belonging to same pass. For each and every pass, a new kernel is launched. One of the kernel parameters indicates pass number being executed. Listing 2 shows CUDA implementation of Algorithm 1 on the GPU side. Each thread computes tid and other variables accordingly using built-in variables such as *blockDim*, *blockIdx*, and *threadIdx*. One $m[i, j]$ is computed by one thread in our implementation. To keep the GPU busy, we have chosen the different block sizes to carry threads such as 128, 256, and 512 threads per block.

5 Results

We have evaluated the performance of MCM on Intel Xeon 5650 Quad Core processor with CPU clock 2.67 GHz, 12 CPU cores, and 4 GB of RAM. On the GPU side, we have NVIDIA CUDA Quadro FX 3800 with CUDA driver version 5.0, 192 CUDA cores, and global memory of 1 GB. The operating system used for performance evaluation is openSUSE 11.4 32-bit Linux with GNU GCC compiler

Fig. 3 Comparisons of computation time for calculation of optimal parenthesization of MCM among OpenMP, CUDA, and serial implementation



4.5.1, OpenMP 3.1. To compile MCM for execution on GPU side, we have NVIDIA Nsight Eclipse Edition 2.0 with CUDA 5.0 SDK.

Figure 3 shows a pictorial representation of comparisons of parallel implementations of MCM using OpenMP and CUDA with reference to its serial implementation. Time taken for the computation using OpenMP is much better as compared to its GPU implementation.

Figure 4 provides a graphical representation between times taken for the MCM versus the number of matrices for the GPU implementation for different block sizes. We observed in Fig. 4 that no significant performance benefit is achieved, if we

Fig. 4 Comparison based on number of threads per block on the GPU side in the implementation of MCM

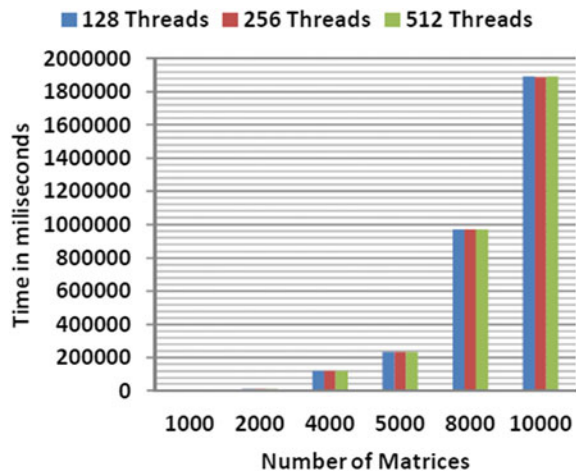
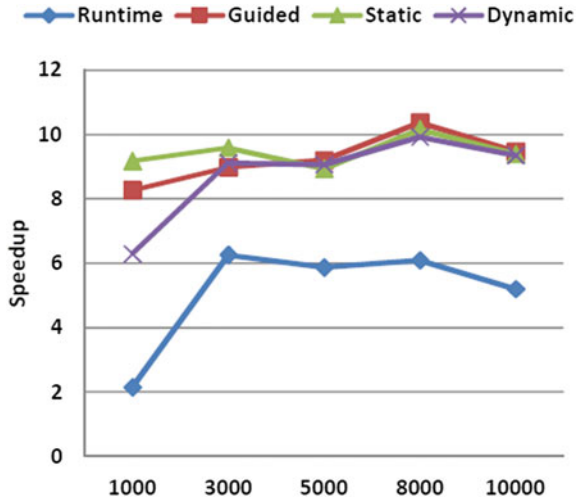


Fig. 5 Comparisons of speedup among various chunk scheduling techniques in OpenMP



increase block size. The reason is that only increasing the numbers of threads in each block would not produce any performance improvements, if we do not work on effective scheduling of warps. Ultimately, increasing the block size would not produce any improvements in the mapping between processing elements and the warps.

Figure 5 gives a basic idea for different scheduling policies of chunks of iterations among cores in OpenMP. Here, we compare the speedup among static, guided, dynamic, and runtime scheduling for different numbers of matrices. The *x*-axis represents the number of matrices and *y*-axis represents the speedup achieved. Runtime scheduling produces a less speedup as compared to other scheduling policies because the OpenMP runtime distributes the chunks over the cores very easily but does not assure the optimal load balancing. Among the rest of the three policies, guided produces better speedup.

6 Conclusion and Future Scope

From Fig. 3, we see that if we increase the number of matrices, then only we achieve a measurable speedup. For a small number of matrices, we do not get any significant speedup. OpenMP performs better as compared to CUDA because in OpenMP there is no intervention of GPU device. All computations are performed on the host side. Moreover, CPU threads are more powerful than those of GPU threads. CUDA may perform better as compared to OpenMP if we apply several optimization techniques, but here OpenMP dominates significantly over CUDA. In GPU evolved computations, if we can reduce the amount of data transfer between host and device, GPU performance will be significantly improved. In

future work, we can apply more optimization techniques for both, CPU as well as for GPU device.

Conclusions from Fig. 4 can be drawn as if we increase the number of threads on GPU side, then we will not get significant performance improvement. This is because warp size is fixed. We can improve the warp scheduling scheme to get much performance benefit.

Figure 5 shows that static scheduling scheme performs much better as compared to other scheduling policies. Guided scheduling may perform better for a large number of matrices, and compensates incurred overhead in the calculation of chunk size. In future, we can also try to implement some mixed scheme for scheduling of chunks over processing cores. The following points can also be noted down in the context of OpenMP:

1. Irrespective of the number of cores available, the speedup is large when input size as well as the size of the computation is large.
2. If the program runs on dual-core machine, there is no much speedup as compared to multi-core machines.
3. As the number of threads increases after a certain limit, computational time stabilizes.
4. Time for the execution of a program takes more time on m core architecture as compared to n core architecture where ($m > n$), while using the same number of threads.
5. Implied barrier after every construct also affects the performance.

In this paper, we proposed the parallel implementation and performance comparison of MCM algorithm on multi-core and many-core parallel architecture systems. The suggested improvements can be applied, such as memory coalescing, efficient utilization of shared memory, effective warp scheduling, and load balancing.

References

1. Godbole SS. On efficient computation of matrix chain products. *IEEE Trans Comput.* 1973;22(9):864–6.
2. Dash T, Nayak T. Chain multiplication of dense matrices: proposing a shared memory based parallel algorithm. *Int J Comput Appl.* 2012;8(1):11–6.
3. Xiao S, Aji AM, Feng WC. On the robust mapping of dynamic programming onto a graphics processing unit. In: *Proceeding of the 15th international conference on parallel and distributed systems (ICPADS)*; 2009. p. 26–33.
4. Nishida K, Ito Y, Nakano K. Accelerating the dynamic programming for matrix chain product on the GPU. In: *2nd international conference on networking and computing (ICNC)*; 2011. p. 320–6.
5. Wu CC, Ke JY, Lin H, Feng WC. Optimizing dynamic programming on graphics processing units via adaptive thread-level parallelism. In: *17th international conference on parallel and distributed systems (ICPADS)*; 2011. p. 96–103.
6. The CUDA Zone. http://www.nvidia.com/object/cuda_home_new.html.

7. Cormen TH, Leiserson CE, Rivest RL, Stein C. Introduction to algorithms. 2nd ed. PHI Learning Private Limited; 2008.
8. Broquedis F, Diakhaté F, Thibault S, Aumage O, Namyst R, Wacrenier PA. Scheduling dynamic OpenMP applications over multicore architectures. In: OpenMP in a new era of parallelism. Lecture notes in computer science, vol. 5004; 2008. p. 170–180.
9. Chapman B, Jost G, Van Der Pas R. Using OpenMP: portable shared memory parallel programming. The MIT Press; 2007.
10. OpenMP specifications. <http://www.openmp.org/specs/>.
11. Nickolls J, Dally WJ. The GPU computing era. Micro IEEE. 2010;30(2):56–69.
12. NVIDIA Corporation. CUDA C Programming Guide. Version 3.1.1.

Data Mining for Healthy Tomorrow with the Implementation of Software Project Management Technique

K. Venkata Rao, R. Balakrishna, H. Aditya Pai
and Piyush Kumar Pareek

Abstract In the current scenario, we find many data mining-related projects being used. These projects are being used very widely and very effectively for the extraction of data in the organization. The usage of data mining has helped in a big way in terms of getting information where the nature of database retrieval is humongous. In this paper, we are seeing how to carry out these data mining projects by using the project management technique. The project management technique makes the project to be carried out very effectively and very efficiently by properly planning the project, organizing according to the objectives, controlling, or coordinating the projects. Hence making the project reach the objectives being framed or formulized.

Keywords Data mining · Project management techniques · Scenario

1 Introduction

The project management technique is primarily a mechanism in which each project can be planned, organized, and controlled or monitored properly. There are various types of projects in the real-world scenarios which can be related to handling disaster management, managing events in the production management, etc. (viz.,

K. Venkata Rao (✉)

Computer Science and Engineering, JAIN University, Bengaluru, India

e-mail: kothapallivenkat@yahoo.co.in

K. Venkata Rao · H. Aditya Pai · Piyush Kumar Pareek

Department of Computer Science and Engineering, Kammavari Sangham Institute of Technology, Bengaluru, India

e-mail: piyushpareek88@gmail.com

R. Balakrishna

Department of Information Science and Engineering, RajaRajeswari College of Engineering, Bengaluru, India

e-mail: rayankibala@yahoo.com

© Springer India 2016

S.S. Dash et al. (eds.), *Artificial Intelligence and Evolutionary Computations in Engineering Systems*, Advances in Intelligent Systems and Computing 394, DOI 10.1007/978-81-322-2656-7_31

345

where software products and machinery tools being manufactured). The way of applying management principles to the project were introduced way back in 1800s during the period of Industrial Revolution. There were many contributors to these like Fredric Taylor, Henry Fayol (1826–1915), Vytautas Andrius Graicunas (1841–1925), Peter F. Drucker (1909–2005), etc., whose contributions were immense in the field of management.

The main emphasis of my paper is to implement the project management technique to the project using data mining technologies. Here, data mining is used for extracting information from the software where it has all the details about the health care units like hospitals, clinics, and fitness centers (viz., Yoga Ashrams, Gyms, etc.). The patient residing in the nearby locality will have access to the nearest health care units. Also, they can choose the health care units as per their choice if the nearest health care unit is not their primary choice.

Now, we are trying to implement the software project management techniques primarily on how to carry out developing such software. Here, the project goes through numerous phases: right from conceptualization phase, analysis and design phase, implementation phase, and the deployment and testing phases. During the process, we carry out the project according to the need of the major stake holders. There are various people involved in the project which also depends on the type of project we carry out. The paper explains how we are going to carry out the data mining project, how many stages are included, who are the beneficiaries, and how many people are involved in doing the project.

2 Problem Identification

The paper titled “Data Mining for Healthy Tomorrow with the implementation of Software Project Management technique” requires data mining technique to be used for extracting information about the location of the health care fields. To carry out this project, we are first going to find out the beneficiaries involved in the project. The beneficiaries are the users who are actually searching the information about the health centers and second the health care units who will get benefit from the software being developed. Now, the problem involved in the project to be carried out is that what steps we are going to undertake to carry out this project. How do we begin with? What are the people’s choices to remain fit? To collect the information of the nearest specialty or super specialty hospitals for the people who are in real emergency.

Now, there are causes for the problem, i.e., the funding of the projects. Who are the people investing in these types of projects which require millions of investment to implement the software in the first place? How to make the software cost-effective so that common people can access the software for free and to provide all the information he/she wants about the health care units.

To carry out these, we need to find out the stake holders through survey and then collect the facts and data, ask the beneficiaries' opinions and accordingly we carry out assumptions. What are the risk factors involved?

Another main thing about the project is how we carry out this project in a team. Who is the client we are searching for? How we are going to plan the objectives? How are we going to formulate them to carry out such tasks? How are we going to divide the task among the individuals in the team and carry out the project in time without much delay?

3 Literature Survey

Literature survey is done on few papers related to the thesis of this paper. The first paper that I surveyed is "Project management: key tool for implementing strategy," by Ngoc Se, March 2010. Here, the author describes how to use project management technique during conferences or any programs where a large number of people are attending. The paper tells about Plan-> Do-> Check-> Act which is similar to the paper that I am publishing on software project management technique used for data mining projects.

The second paper I surveyed is "A literature review of the role of project management in post-disaster reconstruction," by Benny Hidayat and Charles Egbu. The author, in the paper, describes how to use project management technique during natural calamities. Thus, the points discussed are crucial for bringing the human life and their environment back to normal which when not done will affect their life. Now, when it comes to the project that I do which is based on the project management techniques used for the data mining projects, we require techniques like mitigation and preparation which in this case, during the course of doing the project if the stake holders withdraw or demand major changes, we have to be prepared for it. Recovery too is needed for the project as the project phase is stuck in any point can use this technique to recover the current project process.

Next, project management: key tool for implementing strategy by Andrew Longman and Jim Mullins. This paper explains about essential ways where software project can be done effectively by a team with the support from team leaders and project managers. The project I am using is also related to developing the code in the front end and using data mining in the back end, but to manage the project I am using software project management technique. Thus, the steps mentioned in the description are useful for any software engineer to do the project but the same steps are not used in my project.

4 Data Collection and Analysis

(A) Selection of organization

- 50 Indian, small- and medium-level, software firms are selected on the basis of convenient sampling of Bengaluru region during January 2014–December 2014.
- These companies are also selected on the basis of top 100 companies ranked by Just Dial rating.

(B) Sampling population

- As many as 500 samples were included as part of the data for study. These samples were collected from middle management executives

(C) Data collection

- An exhaustive questionnaire was prepared and data was collected with regard to six sigma in the firm.

(D) Stages of Data collection (Fig. 1).

5 Results

The following tables and figures show the opinion of the participants. SPSS software package is used for statistical analysis (Tables 1, 2, 3, 4, 5, 6, 7 and Figs. 2, 3, 4, 5, 6, 7, and 8).

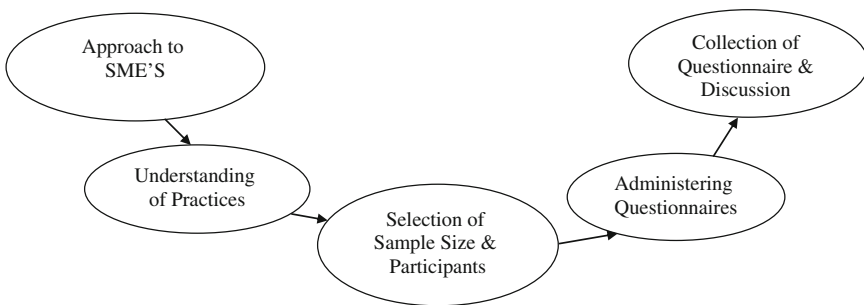


Fig. 1 Stages of data collection followed by author

Table 1 How much time does it require to carry out the project on data mining where it requires to extract all the health care unit in the nearby locality or in a city?

		Frequency	%	Valid %	Cumulative %
Valid	6 months	100	20.0	20.0	20.0
	9 months	250	50.0	50.0	70.0
	12 months	100	20.0	20.0	90.0
	More than 12 months	50	10.0	10.0	100.0
	Total	500	100.0	100.0	

Table 2 After successful completion of this project, will the patients or the users find it easier to access the data of all the health care units in the nearby locality?

		Frequency	%	Valid %	Cumulative %
Valid	Agree	201	40.2	40.2	40.2
	Strongly agree	149	29.8	29.8	70.0
	Disagree	100	20.0	20.0	90.0
	Strongly disagree	50	10.0	10.0	100.0
	Total	500	100.0	100.0	

Table 3 The main concern of the data mining techniques project management is to maintain it and the cost involved for the project

		Frequency	%	Valid %	Cumulative %
Valid	Agree	207	41.4	41.4	41.4
	Strongly agree	144	28.8	28.8	70.2
	Disagree	99	19.8	19.8	90.0
	Strongly disagree	50	10.0	10.0	100.0
	Total	500	100.0	100.0	

Table 4 Is there a high risk involved in terms of security of the server?

		Frequency	%	Valid %	Cumulative %
Valid	Agree	199	39.8	39.8	39.8
	Strongly agree	145	29.0	29.0	68.8
	Disagree	102	20.4	20.4	89.2
	Strongly disagree	54	10.8	10.8	100.0
	Total	500	100.0	100.0	

Table 5 Project management technique keeps check of the frequency in doing the project also and finds out the reason why there is more delay in carrying out the project by Pareto chart?

		Frequency	%	Valid %	Cumulative %
Valid	Agree	204	40.8	40.8	40.8
	Strongly agree	147	29.4	29.4	70.2
	Disagree	99	19.8	19.8	90.0
	Strongly disagree	50	10.0	10.0	100.0
	Total	500	100.0	100.0	

Table 6 Data is collected and dotted over period of time and over that run chart is drawn to find out where the problem had occurred while carrying out the project?

		Frequency	%	Valid %	Cumulative %
Valid	Agree	201	40.2	40.2	40.2
	Strongly agree	147	29.4	29.4	69.6
	Disagree	102	20.4	20.4	90.0
	Strongly disagree	50	10.0	10.0	100.0
	Total	500	100.0	100.0	

Table 7 To meet or exceed user’s expectations and to build in order service, we require quality control

		Frequency	%	Valid %	Cumulative %
Valid	Agree	200	40.0	40.0	40.0
	Strongly agree	147	29.4	29.4	69.4
	Disagree	103	20.6	20.6	90.0
	Strongly disagree	50	10.0	10.0	100.0
	Total	500	100.0	100.0	

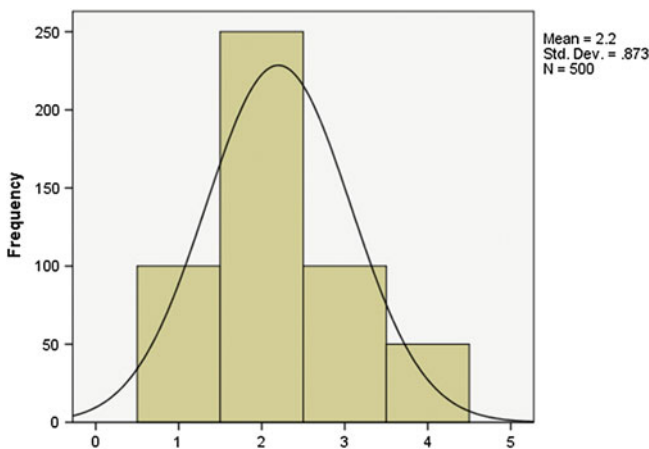


Fig. 2 How much time does it require to carry out the project on data mining where it requires to extract all the health care unit in the nearby locality or in a city?

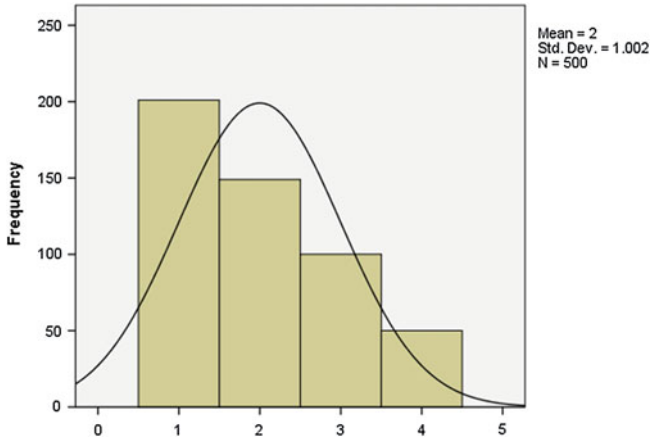


Fig. 3 After successful completion of this project will the patients or the users find it easier to access the data of all the health care units in the nearby locality?

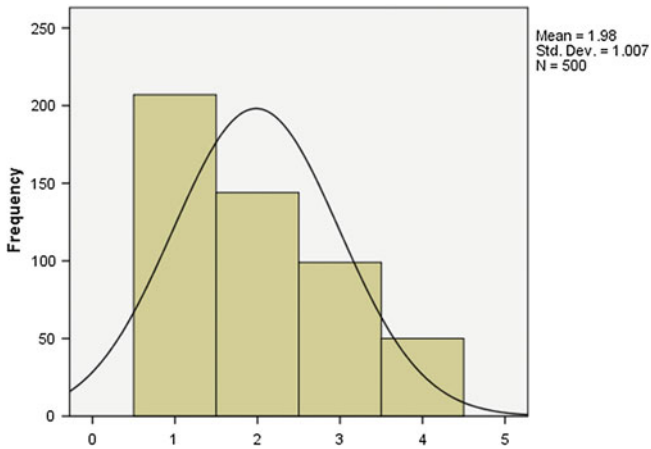


Fig. 4 The main concern of the data mining techniques project management is to maintain it and the cost involved for the project

A. Histograms

Analysis and Interpretation:

- The data collected has been primarily tabulated and master table was prepared
- Sample was tested for reliability using Cronbach's alpha

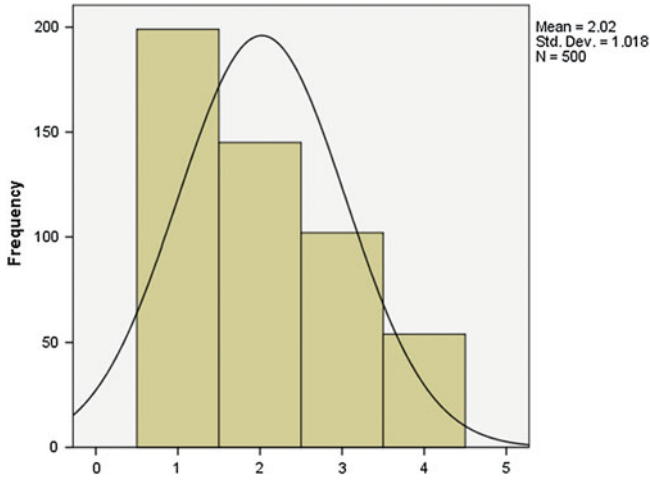


Fig. 5 Is there a high risk involved in terms of security of the server?

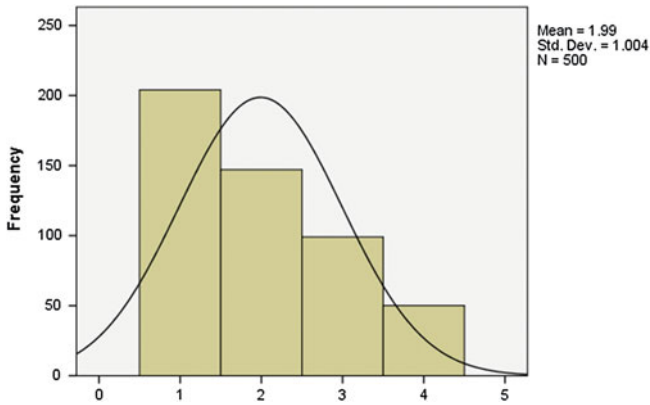


Fig. 6 Project management technique keeps check of the frequency in doing the project and also finds out the reason why there is more delay in carrying out the project by Pareto chart

- Percentage analysis is the basic tool for analysis
- Regression analysis, a statistical process for estimating the relationships among variables, is used

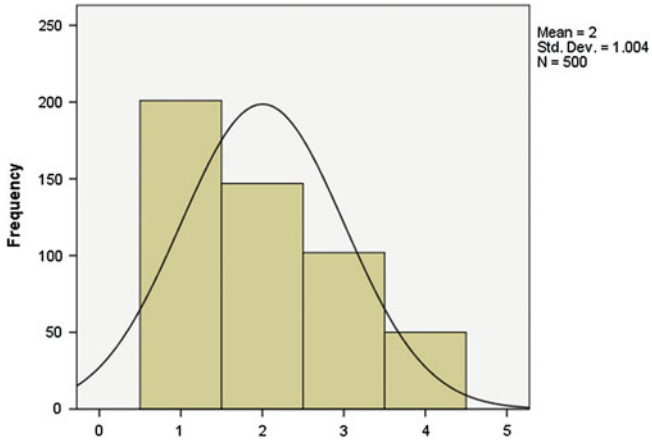


Fig. 7 Data is collected and dotted over period of time and over that run chart is drawn to find out where the problem had occurred while carrying out the project?

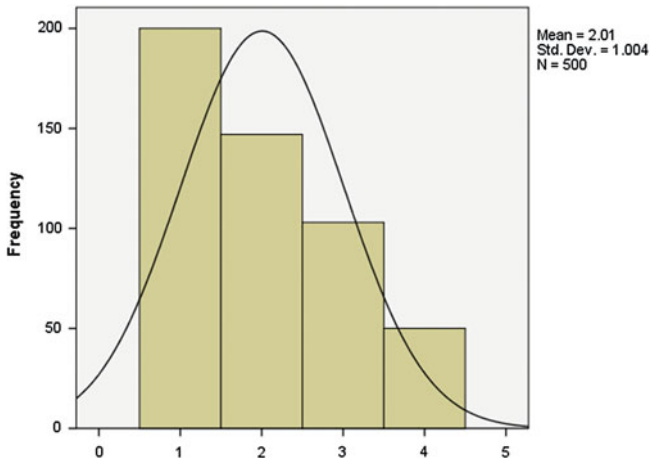


Fig. 8 To meet or exceed user's expectations and to build in order service, we require quality control

Reliability statistics

Cronbach's alpha	No. of items
0.941	7

Limitation of the study

- The sample size is only 500 respondents, much more elaborate study could be done.
- There may be some positive and negative biases of the respondent.

6 Conclusion

- For research question—How much time does it require to carry out the project on data mining, where it requires to extract all the health care unit in the nearby locality or in a city? It has been found that 70 % of population agrees 9 months as average duration on data mining.
- For research question—After successful completion of this project, will the patients or the users find it easier to access the data of all the health care units in the nearby locality? It has been observed that 69.8 % of the sample population cumulatively agrees to it.
- For research question—The main concern of the data mining techniques project management is to maintain it and the cost involved for the project: It has been observed that 68 % of the sample population agrees to the above factors.
- For research question—Is there a high risk involved in terms of security of the server? 30 % of the sample population disagrees to the above factors.
- For research question—Data is collected and dotted over period of time and over that run chart is drawn to find out where the problem had occurred while carrying out the project? It has been observed that 70 % of the sample population agrees to it.
- For research question—To meet or exceed user's expectations and to build in order service, we require quality control: It has been that 20 % disagree for the quality control services.

Acknowledgments This research was supported by Research and Development Lab of Computer Science Department of Kammavari Sangham Institute of Technology affiliated to Visvesvaraya Technological University under the able leadership of Professor Rekha B Venkatapur, Dynamic Dr. Naveen N C, and Professor Harshavardhan J R. We thank our colleagues from Department of CSE who provided insight and expertise that greatly assisted the research.

We would also like to show our gratitude to Shri Y Ramachandra Naidu, Honorable President, Kammavari Sangham; Shri K Venkatesh Naidu, Honorable Secretary, Kammavari Sangham; Shri D Rukmangada, and Honorable Treasurer, Kammavari Sangham for sharing their pearls of wisdom with us during the course of this research. We are also immensely grateful to Dr. T.V. Govindaraju, Honorable Principal/Director, KS Institute of Technology for tremendous support during our Research in all the possible ways.

Real-time Implementation of Electromyography for Hand Gesture Detection Using Micro Accelerometer

Subhendu Roy, Sraboni Ghosh, Aratrika Barat,
Madhurima Chattopadhyay and Debjyoti Chowdhury

Abstract This paper focuses on the development of a novel approach for identification of various hand movements of a person that involves actions like fist opening, closing, and arm roll. The system consists of an electromyogram (EMG) sensor coupled with a digital MEMS accelerometer (full scale range of ± 2 g, ± 4 g, ± 8 g, and ± 16 g) for detection of hand gestures; this system is mounted over a strip strapped on the limb of its user. Based on the analysis of the EMG signals that are coupled with the MEMS accelerometer data from the limb, innumerable hand gestures are identified. Six-point-based calibration of the accelerometer data is done to eliminate mounting errors. The hand movements involving roll are better identified using this sensor topology, which is based on EMG sensor coupled with MEMS accelerometer than a system which just uses an EMG sensor to find out hand gestures because the accelerometer data gives precise information about the orientation of the limb in three-dimensional spaces.

Keywords Electromyography · Hand gesture recognition · MEMS accelerometer · Hand gesture · Six-point calibration

S. Roy (✉) · S. Ghosh · A. Barat · M. Chattopadhyay · D. Chowdhury
Applied Electronics and Instrumentation Engineering Department, Heritage Institute
of Technology, Kolkata 700107, India
e-mail: subhenduroy4@gmail.com

S. Ghosh
e-mail: sraonighosh26@gmail.com

A. Barat
e-mail: barataratrika5@gmail.com

M. Chattopadhyay
e-mail: madhurima.chattopadhyay@heritageit.edu

D. Chowdhury
e-mail: djbabai.debjyoti@gmail.com

1 Introduction

The electromyography is the measure of electrical activity produced by the muscles which is usually represented as a function of time. This electromyography can be used in abundant applications including identifying neuromuscular diseases and control signal for prosthetic devices, controlling machines, robots. Hand gesture identification has numerous applications hence it has become an active research theme because of its use in human-machine interface (HMI) and it has got a focus in the sense that it will help the disabled people or aged people. The gesture recognition is to create a system that recognizes the gestures and use them for controlling the device. There is a significant body of research describing the use of pattern recognition of myoelectric signals to control prosthetic devices.

The surface electromyogram has the advantage of easy recording and noninvasive procedure. The hand gestures are captured by sensors through EMG signals [1]. When compared with the other biosignals, EMG is a noisy signal and it contains complicated types of noises that are caused by environment, electromagnetic induction, motion artifacts, interaction of different tissues, and sometimes it is difficult to get the useful information from the muscles that is left over by any disabled person. This paper presents an approach to detect, analyze, and classify EMG signals generated by the limb.

Accelerometers can measure acceleration from vibrations and the gravity [2–4]. Since both accelerometers and EMG sensors have their own advantages in capturing hand gestures, the combination of both the sensing approaches may improve the performance of hand gesture recognition. In this paper, a wearable gesture-based real-time interaction prototype using the fusion of accelerometer and EMG signals are presented.

The combination of EMG and accelerometers has previously been used by Roy et al. [5] for monitoring patients with stroke and by Li et al. [6] for sign language detection and game control. To the best of our knowledge, the combination of EMG and accelerometers has not been used in conjunction with prosthesis control. This study is an example of a general trend toward including more sensor types to maximize the environmental and intent information provided to the control system.

2 System Architecture

This gesture-based interaction prototype enables operating a mobile phone without touching it. It consists of a custom-wearable gesture-capturing device and an interaction application program running on a smartphone, worn on an user's forearm. The gesture-capturing device records EMG and accelerometer signals, and

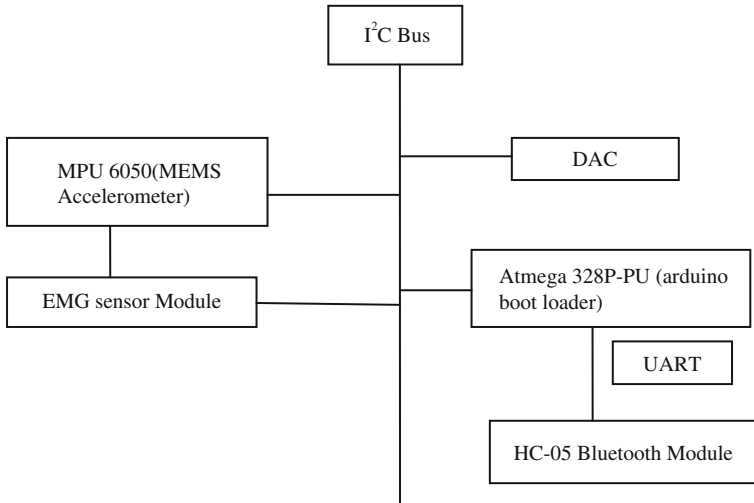


Fig. 1 Gesture capturing device (proposed)

sends them to the phone through a wireless connection. The interaction application program processes these signals, translates each gesture into instructions, and then provides feedback [7].

2.1 *Gesture-Capturing Device*

The proposed device comes as a wrist mountable belt, with the triaxial accelerometer MPU6050 mounted at the center of the band. An onboard processor, Atmega 328 reads the accelerometer data and sends it over to the bluetooth module after calibrating with the six-point algorithm as shown in Fig. 1. It consists of three dry EMG sensors connected via a main board embedded with an accelerometer. These three EMG sensors are attached to the main board in order to share the battery and the controller. The main board consists of a 1000 mAh lithium battery, a charging circuit, and a power circuit. After acquiring the signal by each EMG sensor, it passes through a band-pass filter.

2.2 *EMG Sensor Design*

In Fig. 2, the EMG sensor along with the associated circuitry is described. The signals from instrumentation amplifiers are used. The output of this amplifier passes through first-order low-pass filter (500 Hz) and high-pass filter (50 Hz), and finally

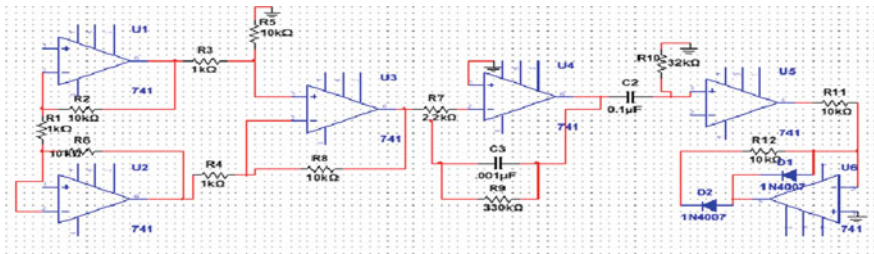


Fig. 2 EMG sensor design in MultiSIM

the filtered value is passed through the precision rectifier. Input of the instrumentation amplifier is connected with the electrode which is placed in the forearm of the user. The output of the precision rectifier is connected to the cathode ray oscilloscope (CRO) for observing the corresponding waveform.

2.3 Six-Point Calibration of Digital Accelerometer

Measurement accuracy of the accelerometer’s can be improved by calibrating the sensor’s output, the two deciding parameters in the sensor calibration are:

1. ZeroG: This number tells which voltage reading corresponds to zeroG’s on an axis
2. Sensitivity: This tells by how much the voltage changes per G in an axis

The MEMS accelerometer calibration arrangement using six-point analogy for Z-axis, is (a) Not inverted (+1G) and (b) Inverted (−1G). Table 1 represents data read from the sensor [8].

The sensor read out for 0 g corresponds to digital 512; the zeroG and sensitivity values for Z-axis is shown here

$$m_z = (618 + 413)/2 = 515.2 \tag{1}$$

$$\delta_z = (618 - 413)/2 = 102.5 \tag{2}$$

Table 1 Values for six-point calibration of accelerometer (MPU-6050)

(a)				(b)			
Sample no.	X-axis	Y-axis	Z-axis	Sample no.	X-axis	Y-axis	Z-axis
1	512	513	619	1	511	514	413
2	511	512	617	2	513	512	412
3	512	511	618	3	512	513	411

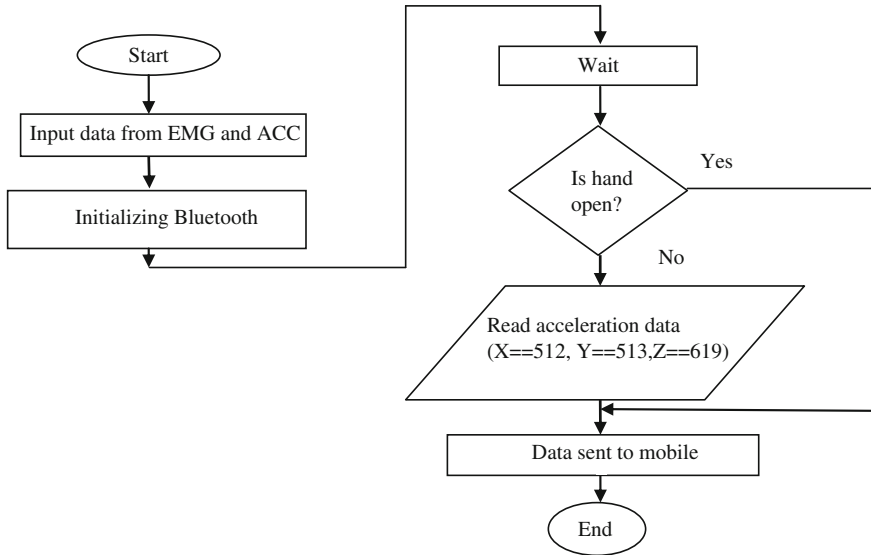


Fig. 3 Proposed algorithm flow sequence

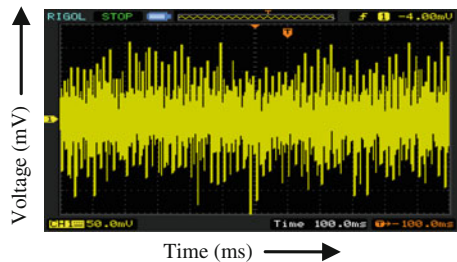
3 Algorithm of the Design

3.1 Results and Discussion

Figure 3 shows the raw EMG signal after passing through an instrumentation amplifier. The raw EMG signal passes through filters to remove the noise as shown in Fig. 4. Finally, the filtered EMG signal is fed to the precision rectifier as shown in Fig. 5 for high-precision signal processing. When an electrode is connected to the user’s limb, the waveforms of Figs. 6 and 7 are obtained with palm in opening and closing positions, respectively [9].

Figure 8 shows the output waveform of the EMG circuit designed in MultiSIM using two out of phase sine wave, sampled at 60 Hz [10].

Fig. 4 Raw EMG signal



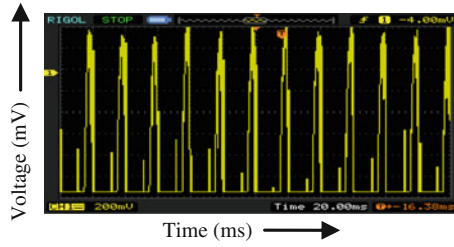


Fig. 5 Filtered EMG signal

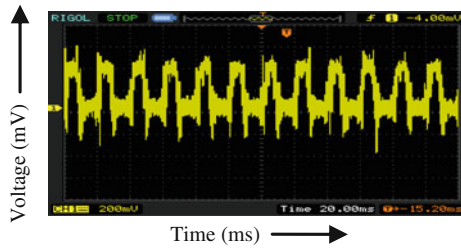


Fig. 6 Rectified EMG output with electrodes

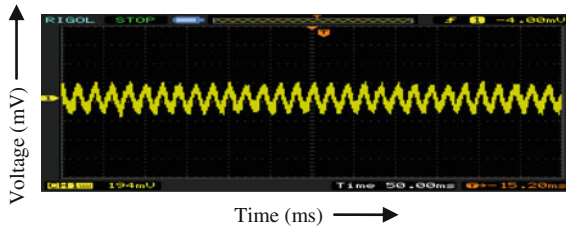


Fig. 7 EMG signal (while palm is open)

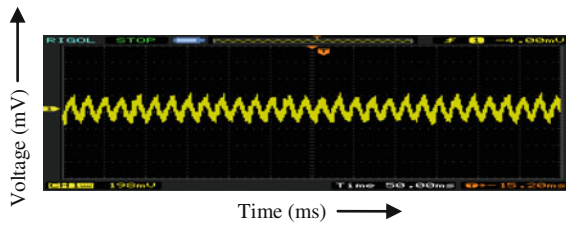


Fig. 8 EMG signal (while palm is close)

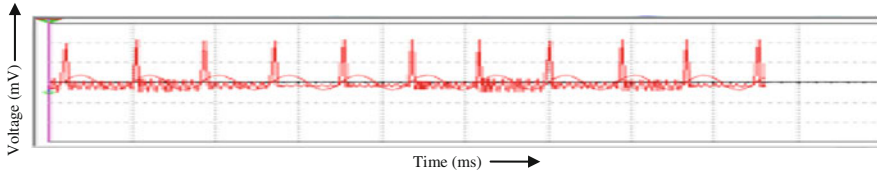


Fig. 9 EMG signal result in MultiSIM

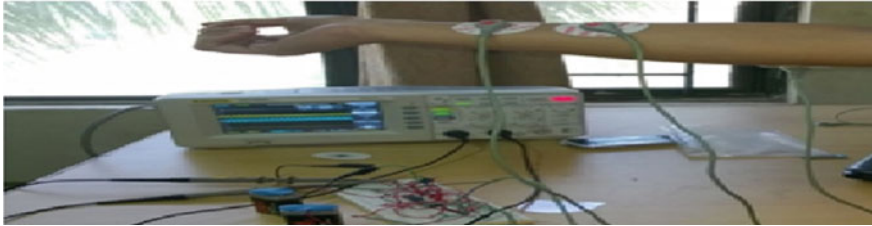


Fig. 10 Real-time implementation of acquiring EMG signal

4 Conclusion

In this paper, an accelerometer coupled electromyogram-based gesture recognition method is presented. The real-time implementation of hardware is shown in Fig. 9 [11]. Different from the popular sensor-based gesture recognition approaches found in the literature that uses only accelerometer to identify user hand movements cannot distinctly classify palm close and open movements. The proposed technique uses electromyogram signal coupled with accelerometer data to better identify hand gestures. The developed gesture recognition algorithm effectively reduces the need for extensive hardware to process the sensor data, so making it extremely efficient for mobile applications. To tackle the issue of sensor bias and installation error at gesture feature extraction, the six-point calibration is applied on the sensor data (Fig. 10).

References

1. Subasi MY, Ozcalik HR. Classification of EMG signals using wavelet neural network. *J Neurosci Methods*. 2006;156:360–7.
2. Liu J, Zhong L, Wickramasuriya J, Vasudevan V. uWave—accelerometer-based personalized gesture recognition and its applications. *Pervasive Mobile Comput*. 2009;5:657–75.
3. Chong MK, Marsden G, Gellersen H. Gesture PIN: using discrete gestures for associating mobile devices. In *Proceedings of the 12th international conference human computer interaction mobile devices services*; 2010, p. 261–4.

4. Wang J, Chuang F. An accelerometer-based digital pen with a trajectory recognition algorithm for handwritten digit and gesture recognition. *IEEE Trans Ind Electron.* 2012;59(7):2998–3007.
5. Zhu C, Sheng W. Wearable sensor-based hand gesture and daily activity recognition for robot-assisted living. *IEEE Trans Syst Man Cybern A Syst Humans.* 2011;41(3):569–573.
6. Saponas TS, Tan DS, Morris D, Balakrishnan R. Demonstrating the feasibility of using forearm electromyography for muscle-computer interfaces. In: *Proceedings of the SIGCHI Conference Human Factors Computing Systems*; 2008, p. 515–24.
7. Lu Z, Chen X, Member, IEEE, Li Q, Zhang X, Member, IEEE, Zhou P, Member, IEEE. A hand gesture recognition framework and wearable gesture-based interaction prototype for mobile devices. *IEEE Trans Human-Machine Syst.* 2014;44(2):293.
8. Chowdhury D, Banerjee S, Sanyal K, Chattopadhyay M. A real time gesture recognition with wrist mounted accelerometer. *Inf Adv Intell Syst Comput.* 2015;340:245–53.
9. Roy SH, Cheng MS, Chang S, Moore J, De Luca G, Nawab SH, Luca JE. Combined SEMG and accelerometer system for monitoring functional activity in stroke. *IEEE Trans. Neural Syst Rehabil Eng.* 2009;17(6):585–94.
10. Li Y, Chen X, Tian J, Zhang X, Wang K, Yang J. Automatic recognition of sign language subwords based on portable accelerometer and EMG sensors, *ICMI-MLMI'10*, Beijing; 2010.
11. Fougner A, Member, IEEE, Scheme E, Student Member, IEEE, Chan ADC, Senior Member, IEEE, Englehart ØK, Senior Member, IEEE. Resolving the Limb Position Effect in Myoelectric Pattern Recognition.

RSA Public Key Acceleration on CUDA GPU

Jitendra V. Tembhurne and S.R. Sathe

Abstract Cryptography is a technique of using number theoretical mathematics for the key generation, encryption and decryption of confidential information. Cryptography has many uses in real-world applications such as Digital Right Management, E-Commerce, Secret Broadcasting and Financial Cryptography, etc. In this paper, we mainly focus on the speedup of the RSA public-key cryptosystem algorithm. We proposed the high-performance parallel RSA algorithms on parallel hardware such as Graphics Processing Units (GPUs). We used NVIDIA GPU Quadro FX 3800 to exploit the many-core parallelism for the implementation of highly parallel and efficient RSA algorithm on Compute Unified Device Architecture (CUDA). The experiments conducted on many-core GPUs show the enhanced speedup of proposed parallel RSA algorithms compared to single CPU RSA algorithm implementation. We observed that the speedup achieved by the GPU dominates the single CPU RSA implementation.

Keywords CUDA · GPU · RSA · Parallel algorithm

1 Introduction

In network security and cryptography, RSA is an algorithm that uses public key for encryption and private key for decryption of giving secret message. The RSA was publicly provided in 1978 by Rivest et al. [1]. This algorithm was a great advancement in the public-key cryptography and best suitable for message signing

J.V. Tembhurne (✉) · S.R. Sathe
Department of Computer Science and Engineering, Visvesvaraya National
Institute of Technology, Nagpur, Maharashtra, India
e-mail: dt11cse077@cse.vnit.ac.in

S.R. Sathe
e-mail: srsathe@cse.vnit.ac.in

and encryption. RSA is widely used in electronic commerce such as financial transaction with the use of sufficient long key size.

For more security, RSA requires longer key size such as 1024, 2048 and 4096 bits, etc. As we know, RSA involved more integer mathematics for the conversion of plaintext to ciphertext and ciphertext back to the original message in the process of encryption and decryption. Moreover, RSA heavily performs the computation of integer modular exponentiation on the product of selected large integer (chosen to be large prime) which makes it computationally more expensive and performance-wise more slow. Due to these bottlenecks it restricts wider use of this algorithm in different security applications. The researches [2–4] worked on this issue of algorithm optimization and higher performance on computation of more integer arithmetic mathematics.

With the advent of parallel architectures; multi-core and many-core technology, more computation power is available with computer systems. The technologies such as Pthreads [5], OpenMP [6], UPC [7], message passing interface (MPI) [8], we can create the multiple threads on the CPU and threads perform the assigned task independently on different cores available on the CPU, enhancing the computational efficiency of the procedure or task. These threads concurrently complete the computation in order to shorten the execution of operations.

The parallel implementation and performance evaluation of the RSA cryptographic algorithm using CUDA [9], which significantly improves the task of encryption and decryption, is the main focus of this paper. The test and experimentation, analysis shows the significantly enhanced speedup achieved for the parallel RSA algorithm on the GPU as compared to the original RSA algorithm on the CPU.

The research objective of this work is to speed up the RSA encryption and decryption process using parallel programming CUDA. The specific aims are identified as; first, design and develop a parallel RSA algorithm. Second, measure the performance of RSA on the GPU.

The remaining part of this paper focused as follows; Sect. 2 presents in brief the principle of public-key cryptosystem and the functionality of the RSA cryptography algorithm. In Sect. 3, we demonstrate the parallel architecture used for the implementation of RSA and discussed the parallel implementation of the RSA algorithm. In Sect. 4, we show the results obtained by the parallel implementation on the GPU and in Sect. 5 we conclude the paper with some suggested future implementation.

2 Related Work

The attempts have been started by the researchers in past years to accelerate the cryptography applications by proposing new, efficient algorithm implementation on software as well as hardware. In 1993 Shand [10] introduced the fast implementation of RSA for Programmable Active Memory (PAM) on the technology called Programmable Gate Array (PGA). The speedup achieved by the hardware

implementation matches the software implementation and both were analysed. In [11], Pearson et al. proposed an efficient and highly parallel implementation of RSA on parallel computers. The RSA implementation used the new modular multiplication algorithm based on the Residue Number System (RNS) and Montgomery's method. The Field Programmable Gate Array (FPGA) based implementation of a public-key cryptosystem was proposed in [12]. The proposed unified architecture in [12] was implemented on the FPGA to speed up the RSA GM (2^m) multiplication and modular exponentiation. In cryptography, the exponentiation is the major operation performed to encrypt or decrypt the message. The parallel implementation of modular exponentiation was proposed in [13] is faster than the [14] with improved time complexity and efficiency for the RSA.

But in the recent years, new parallel hardware platforms were provided by the Intel and NVIDIA. These platforms are feasible for different general purposes, scientific computation, in our case RSA cryptosystem. The parallelization of RSA on the GPU using JCUDA and Hadoop was proposed in [15], which supports 64-bit arithmetic operations. This was the primitive and unoptimized implementation of RSA on CUDA. An efficient parallelized RSA for decryption on the GPU was demonstrated by Lin et al. in [16], focused on the integer factorization using the Pollard Rho algorithm and decryption of RSA on the CUDA with supporting key size ranging from RSA-41 to RSA-64. The speedup achieved by the GPU-based RSA implementation on the CPU-based implementation was significantly high.

3 Public-Key Cryptosystem and RSA

In a public-key cryptosystem each user has his own encryption and decryption methods, E and D , wherein E is public and D is secret. These methods use different keys and specifically in RSA, sets of two special numbers. The message is symbolized by M , to be encrypted. There are four essential steps to be followed by public-key cryptosystem;

- Deciphering an enciphered message gives you the original message

$$D(E(M)) = M \tag{1}$$

- Reversing the procedures returns M

$$E(D(M)) = M \tag{2}$$

- E and D are easily computed.
- Publicize the E and keep secret D .

With the availability of E , it is very difficult to compute D . If $C = E(M)$ is the ciphertext, then finding out D on satisfy M in $E(M) = C$ is more complex and time consuming task.

The RSA algorithm consists of three major steps for the secure transmission and reception of confidential data through a communication channel on the end terminals/systems. The RSA basic steps are key generating, encryption and decryption.

3.1 Key Generation

RSA involves two keys; a public key and a private key. The public key is known to everyone and used to encrypt the confidential messages. The encrypted message is decrypted using the private key in a reasonable amount of time. The RSA keys are generated as;

- Select two non-identical prime integers p and q , with same bit-length.
- Calculate $n = p \times q$. Where n is the modulus for public and private keys with same key length.
- Calculate $\phi(n) = \phi(p) \times \phi(q) = (p - 1) \times (q - 1)$.
- Select an integer e such that $1 < e < \phi(n)$ with $\gcd(e, \phi(n)) = 1$. Where, e is the exponent for public key. Commonly, e can be $2^{16} + 1 = 65,537$ (for more details see [17]).
- Find d as $d^{-1} \equiv e \pmod{\phi(n)}$. The exponent d is used for private key.

The public key (n, e) , a private key (n, d) , p , q , and $\phi(n)$ must also be kept secret because they are used to calculate d .

3.2 Encryption and Decryption

Encryption

Bob receives the public key pair (n, e) , transmitted by the Alice through communication channels. Bob first, represents original message M , the plaintext into non-negative integer m , where $0 \leq m < n$ and uses agreed-upon padding scheme. Then Bob computes $c \equiv m^e \pmod{n}$, the ciphertext from m , and transmit the ciphertext c to Alice.

Decryption

Alice at the other end decode the ciphertext c by using his secret key called private key pair (n, d) and computes $m \equiv c^d \pmod{n}$. On finding m , Alice can apply reverse padding scheme to generate original message M .

4 Parallel Architecture

NVIDIA Corporation invented the new computing architecture called as Compute Unified Device Architecture (CUDA) in 2006 to support general purpose computing on the Graphic Processing Units (GPUs). CUDA [18] enables the parallel computing infrastructure with highly increased computational performance for software developer to write or develop parallel programmes using C, C++, FORTRAN, OpenCL, etc., which can easily be ported on the GPU. A typical architecture of CUDA enables GPU as shown in Fig. 1. The GPU is organized as a

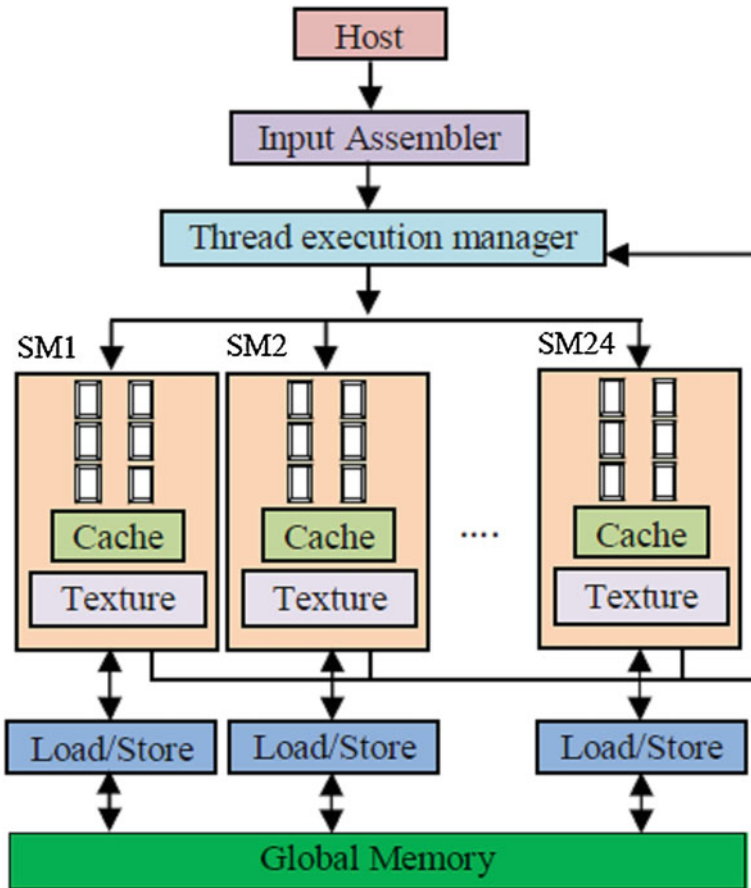


Fig. 1 General CUDA GPU architecture for Quadro FX 3800

multithreaded array of Streaming Multiprocessors (SMs) which performs the real computations. Each of the SMs has a collection of Streaming Processors (SPs) and its own set of registers, cache, control units and execution pipeline. The memory on the GPU is accessed by SMs consists of thousands of threads has specified memory access hierarchy. The thread has registers and its own limited local memory. Threads in blocks have shared memory and all blocks have global memory. GPU also supports constant memory to store the programme constant and texture memory for the 2D, 3D graphics processing. Shared memory is a faster memory than global memory and can be used to gain more performance for the application on the GPU.

The main advantage of the GPU is that it hides the computation latency from other threads warps. A typical computation flow of the GPU is to copy data from CPU memory to the GPU memory, load GPU kernel code from the CPU to the GPU and execute, and at last transfer data from the GPU to the CPU. The GPU we used in this work is NVIDIA Quadro FX 3800 has 24 SMs and 8 SPs per SMs (i.e. 192 parallel computing cores) with 462.3 GFLOPS of computational horsepower. CUDA support the heterogeneous model of computation, where the CPU and GPU work together to accomplish the computation.

5 Parallel RSA Implementation

RSA performs heavy mathematical computations, handles long numbers and computes expensive modular exponentiation and multiplication operations. Thus, the parallelism can be achieved by dividing the modular operations and performed them independently. To implement RSA in parallel, in this paper, we adopt the thread-level parallelism, where all the computation is divided among the threads.

Parallel RSA implementation using multithreaded programming language CUDA, we follow the strategy of dividing the plaintext message into different chunks of the same size. To get the same size of chunks out of plaintext message, we padded the original message for dividing the plaintext message. All of these checks are stored in an array and encryption, operation performed on each of these stored chunks available in an array. Each chunk is handled by different threads and performs the encryption as well as decryption of messages. The encryption and decryption operation are independent of any data access while the computation is carried on. Hence, they are highly suitable for parallel implementation.

In CUDA-based RSA implementation, the plaintext message is divided into chunks of multiple of the warp size. The warp is the basic unit of execution in the GPU. For our GPU it is 32 threads per warp. Multiple threads are allocated to each chunk to perform encryption as well as decryption operations in parallel, the same have been demonstrated by Fig. 2. To keep the GPU busy we have chosen the block dimension 256 threads per block which we found after conducting several experimentations.

C CUDA implementation of the RSA algorithm for the computation of encryption and decryption on the GPU is shown in the programme Listing 1.

```

// Main function
int main(){
//Initialization and memory allocation on the CPU and
GPU.
    . . . . .

//Encryption kernel call
    enckernel<<<N/THREADS, THREADS>>>(devmsg, devenc, n,
                                        ekey, N);
    . . . . .

/ Decryption kernel call
    deckernel<<<N/THREADS, THREADS>>>(devenc, devdec, n,
                                        dkey, N);
    . . . . .

    return 0;
}
// Encryption kernel
__global__ void enckernel(long int *devmsg,
                          long int *devenc,
                          long int nn, long int enckey,
                          int nN){
    int tid = blockIdx.x * blockDim.x + threadIdx.x;
    if(tid < nN)
        devenc[tid] = encryptMsg(&devmsg[tid], enckey, nn);
}
// Decryption kernel
__global__ void deckernel(long int *devenc,
                          long int *devdec,
                          long int nn,
                          long int deckey,
                          int nN){
    int tid = blockIdx.x * blockDim.x + threadIdx.x;
    if(tid < nN)
        devdec[tid] = decryptMsg(&devenc[tid], deckey, nn);
}

```



```

// Device function for encrypting message
__device__ long int encryptMsg(long int *msg,
                               long int enckey,
                               long int nn){

    int i, k;
    int tid = threadIdx.x;
    __shared__ long int pt;
    pt = msg[tid];
    pt = pt - 96;
    k = 1;
    for(i = 0; i < enckey; i++){
        k = k * pt;
        k = k % nn;
    }
    return(k + 96);
}

// Device function for decrypting message
__device__ long int decryptMsg(long int *encmsg,
                               long int deckey,
                               long int nn){

    __shared__ long int pt;
    int i, k;
    int tid = threadIdx.x;
    pt = encmsg[tid];
    k = 1;
    for(i = 0; i < deckey; i++){
        k = k * pt;
        k = k % nn;
    }
    return(k + 96);
}

```

Listing 1 C CUDA programme code for encryption and decryption on the GPU.

6 Experimentation and Performance Evaluation

All the experimentations were performed on parallel workstation, HP Z600 with configuration, Intel Xeon Quad-core processor of 2.60 MHz clock speed, 4 GB RAM with GNU GCC 4.8.2 C compiler, running under OpenSuse 13.1 × 86_64 operating system. On the GPU side, NVIDIA CUDA Quadro FX 3800 with CUDA driver 6.0, number of CUDA cores 192, 51.2 GB/s memory bandwidth, 1.2 GHz

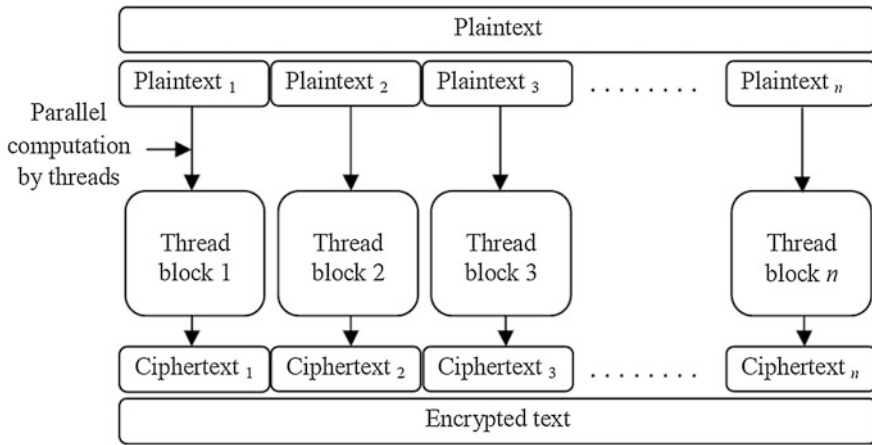


Fig. 2 Parallel encryption of partitioned plaintext by block of threads on the CUDA GPU

Table 1 CPU and GPU timing in ms to compute encryption and decryption of given message. Also, data transfer time in ms from CPU to GPU with GPU speedup is shown for both encryption and decryption techniques

Bytes	Data transfer time	Encryption		Decryption		GPU speedup	
		CPU	GPU	CPU	GPU	Encryption	Decryption
16,384	0.0775	188.14	4.98	46509.50	1305.15	37.72	35.63
32,768	0.1213	376.31	9.51	93335.47	2499.24	39.56	37.34
65,536	0.2227	753.15	17.62	185349.60	4641.55	42.74	39.93
131,072	0.4633	1504.87	34.78	375471.28	9159.14	43.26	40.99
262,144	0.7409	2876.59	67.99	734584.12	18810.21	42.30	39.05

GPU clock rate, 1 GB device memory, 512 threads per block, warp size of 32 threads and execution environment NVIDIA Nsight Eclipse Edition 6.0 and CUDA 6.0 SDK.

Table 1 illustrates the CPU and GPU timing performance measurement for encryption and decryption of different byte size data. Table 1, also shows the speedup achieved for encryption and decryption of different byte size data on NVIDIA GPU. The maximum speedup achieved for encryption is 43.26× and decryption is 40.99× on the GPU.

7 Conclusion and Future Work

In this paper, we proposed our experimentation on RSA algorithm using CUDA for 64-bit double precision operations. We implemented and analysed the RSA algorithm in parallel by thread-level technique. The CUDA implementation of RSA shows the performance gain over single CPU RSA implementation.

Moreover, the proposed implementation has some drawbacks which have to be improved. It is known to us that, the GPU does not support multi-precision integer arithmetic. To perform efficient RSA computations for large size keys such as 1024 bits and more, we have to implement multi-precision integer arithmetic operation on the GPU. CPU already has an efficient multi-precision library called GMP. In the future, we will work to implement efficiently and highly parallel multi-precision RSA algorithm on GPU to support key sizes of 1024 bits and more.

Acknowledgments This work was financially supported by the TEQIP-II scheme (2011–2012) for technical quality improvement by Ministry of Human Resource Development (MHRD), Government of India.

References

1. Rivest RL, Shamir A, Adleman L. A method for obtaining digital signatures and public-key cryptosystems. *Commun ACM*. 1978;21(2):120–6 New York, NY.
2. Kunth DE. *Seminumerical algorithms: the art of computer programming*, 3rd edn. vol. 2. Reading: Addison-Wesley; 2008.
3. Gathen J, Gerhard J. *Modern computer algebra*, 3rd edn. Cambridge University Press: Cambridge; 1999.
4. Menezes AJ, Oorschot PC, Vanstone SA. *Handbook of applied cryptography*, CRC Press: Boca Raton; 1996.
5. Buttlar D, Farrell J, Nichols B. *Pthreads programming: a POSIX standard for better multiprocessing*, O'Reilly Media, 1996.
6. OpenMP Application Program Interface, Version 4.0, July 2013.
7. Berkeley UPC—Unified Parallel C, <http://upc.lbl.gov/>.
8. Open MPI: Open Source High Performance Computing, <http://www.open-mpi.org/>.
9. Sanders J, Kandrot E, *CUDA by example: an introduction to general-purpose GPU programming*, 1st edn. Addison-Wesley: Upper Saddle River; 2010.
10. Shand M, Vuillemin J. Fast implementations of RSA cryptography. In: 11th symposium on computer arithmetic, Windsor, Ontario, p. 252–9, July 1993.
11. Pearson D. A parallel implementation of RSA. Computer Science Department, Cornell University, Ithaca, NY, Technical Report, July 1996.
12. Cilaro A, Mazzeo A, Mazzocca N, Romano L. A novel unified architecture for public-key cryptography. In: *Proceedings of the design, automation and test in Europe, Italy, 2005*, vol. 3, p. 52–7.
13. Wu C-L, Lou D-C, Lai J-C, Chang T-J. Fast parallel exponentiation algorithm for RSA public-key cryptosystem. *Informatica*. 2006;17(3):445–62.
14. Savas E, Tenca AF, Koc CK. A scalable and unified multiplier architecture for finite field GF(p) and GF(2 m). In: *International workshop on cryptographic hardware and embedded systems*, Worcester, MA, USA, LNCS, Springer, vol. 1965, pp. 277–292, August 2000.

15. Fan W, Chen X, Li X. Parallelization of RSA algorithm based on compute unified device architecture. In: 9th international conference on grid and cooperative computing (GCC-2010), Nanjing, pp. 174–8, Nov 2010.
16. Lin Y-S, Lin C-Y, Lou D-C. Efficient parallel RSA decryption algorithm for many-core GPUs with CUDA. In: Proceeding of the international conference on telecommunication systems, modeling and analysis, American telecommunications systems management association, Czech Technical University, Prague, Czech Republic, May 2012.
17. Boneh D. Twenty years of attacks on the RSA cryptosystem. *Not Am Math Soc.* 1999;46(2):203–13.
18. NVIDIA Corporation, CUDA C Programming guide, Version 6.0, February 2014.

Low-Power Home Embedded Surveillance System Using Image Processing Techniques

K. Arathi and Anju S. Pillai

Abstract The need for surveillance systems are increasing due to safety and security requirements. And there exists an ample amount of challenging work yet to be explored in this domain. The current work proposes design, development and implementation of a low-power home embedded surveillance system. Such systems being operated throughout the day, consumes considerable amount of power. Power consumption being a crucial design parameter affects the utility of the system. In the proposed system to consume power, use of low-power sensor groups and controlling the activation of surveillance camera is incorporated through the M-bed microcontroller. Presence of a person is detected and face recognition is carried out using various image processing techniques.

Keywords Surveillance system · PIR sensor · Ultrasonic sensor · Image processing · Viola–Jones detection · PCA algorithm · Gamma correction

1 Introduction

There is a wide popularity of surveillance system everywhere due to the increased threats and burglaries. Most of the modern automated home supports surveillance systems for security reasons. Security systems with CCD cameras are commercially used in all places where security is essential. These systems are powered all the time and they capture video continuously. This results in large amount of electricity consumption. Sometimes it may take long time to detect the presence of an intruder. The major reason for power consumption in such systems is standby electricity. According to the statistics, approximately 3–12 % of residential electricity usage is

K. Arathi (✉) · A.S. Pillai
Amrita Vishwa Vidyapeetham (University), Coimbatore, India
e-mail: aarathijayakrishnan@gmail.com

A.S. Pillai
e-mail: s_anju@cb.amrita.edu

due to standby power [1]. To improve the power efficiency, accurate control of hardware and software is necessary.

A home surveillance system is an essential part of most of the modern automated home embedded surveillance systems which are frequently used in home, office or image detection, but this application requires a very high performance matrix, that will work against some advantages of embedded systems, such as low cost and low power consumption.

The main objective of the project work is to develop a home embedded surveillance system with low power consumption and facilitates accurate and reliable techniques for intruder identification. Power consumption of the proposed system is minimized by using low power consuming sensors and turning ON the surveillance camera only when a valid intruder enters the surveillance area and image processing techniques are used for accurate face detection and recognition.

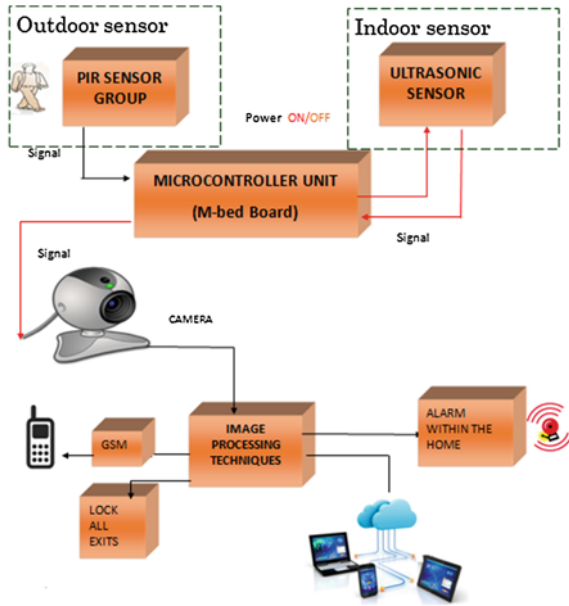
The rest of the paper is organized as follows. Architecture of the proposed surveillance system is given in Sect. 2. Face detection method is explained in Sect. 3. Details of face recognition is explained in Sect. 4. Section 5 contains database storage details. Implementation results in Sect. 6 and conclusion in Sect. 7.

2 Proposed Surveillance System

This paper proposes the design, development and implementation of a low-power home surveillance system with the use of low power consuming sensors and face recognition technique. The proposed system has two group of sensors; alert sensor group and detection sensor group. Alert sensor group consists of PIR sensors which are placed outdoors, near doors and windows. These sensors are always kept ON to identify the presence of an intruder. During standby condition it consumes only very less power in the order of mW. Power consumption of PIR sensor HC-SR205 is only 7.35 mW [2]. Detection sensors are ultrasonic sensors which are placed inside the house. These sensors will turn ON only when the alert sensor group senses the presence of an intruder. Role of detection sensor group is to confirm the presence of intruder which is detected by the alert state. When the detection sensor group detects the presence of an unknown person, decision signal is passed to the microcontroller to turn ON the web camera. Camera helps to capture the video or images. Faces are detected from the still images (or live video sequences). Face recognition is done by comparing the captured image to a set of known images in the database. A decision is then made regarding the identity of the person as an authenticated person or as an intruder.

If the presence of an intruder is detected, then the system uploads that image to an authenticated web page by means of web server through Internet. Authorized person in the house can view the images captured by the surveillance system through Internet [3]. Figure 1 shows the system architecture.

Fig. 1 Proposed surveillance system architecture



2.1 Hardware Modules

Microcontroller unit: Entire surveillance system is controlled by LPC1768 ARM processor [M-bed board]. It has an online compiler through which programming can be done. It is a 100 MHz ARM controller with 64 Kb of SRAM and 512 Kb of flash. It offers high performance and low power consumption.

PIR Sensors: PIR sensors are used in the alert state to reduce the power consumption. It measures infrared (IR) light radiating from humans in its field of view.

Ultrasonic sensors: Generates high-frequency sound wave and evaluates the echo which is received back by sensor, by measuring the time interval between sending the signal and receiving the echo to determine the distance to an object [4, 5].

USB Camera: Camera used is USB camera of 30MP, 30FP. It is a true plug and play easy USB interface. High-quality CMOS sensor is used. Camera is ideally designed to work with both laptops and desktops. Image resolution of this camera is 30 MP and frame rate is up to 30 fps. Focal distance is 4 cm and lens view angle is 54 degree. Image format is RGB24 and power consumption is only 1600 mW.

2.2 Software Modules

The surveillance control is implemented using the microcontroller. The programme for control is executed and downloaded into the M-bed board. Code is written in C language and compiled using M-bed compiler. The flow chart of the front end functioning is shown in Fig. 2.

At the beginning of the program, M-bed board is initialized and the ports used are set. When an intruder passes the sensing area, alert sensor group detect the presence of intruder. When an intruder has been detected by the alert sensor group, it gives signal to wake up the microcontroller unit (MCU). When MCU woke up, it turns ON the power supply for the indoor sensors. If indoor sensors do not detect any intruder presence, then MCU turns OFF the supply to the indoor sensors and goes back to the alert state. In case, the indoor sensors also detect the presence of an intruder, MCU will turn on the web camera.

Web camera starts recording the images and then face detection and recognition algorithms are run to identify the person. A decision is made about the identity of the person. If the recognized face is not belonging to the database, that image will

Fig. 2 Software flow chart of front end

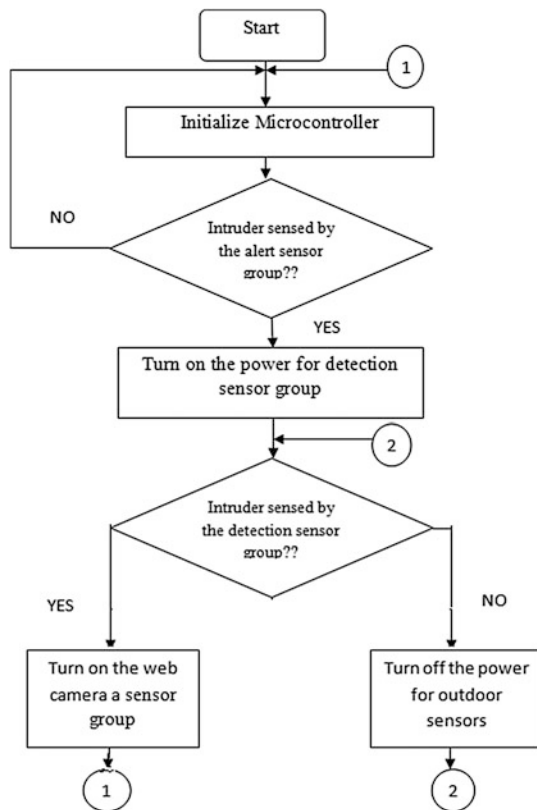
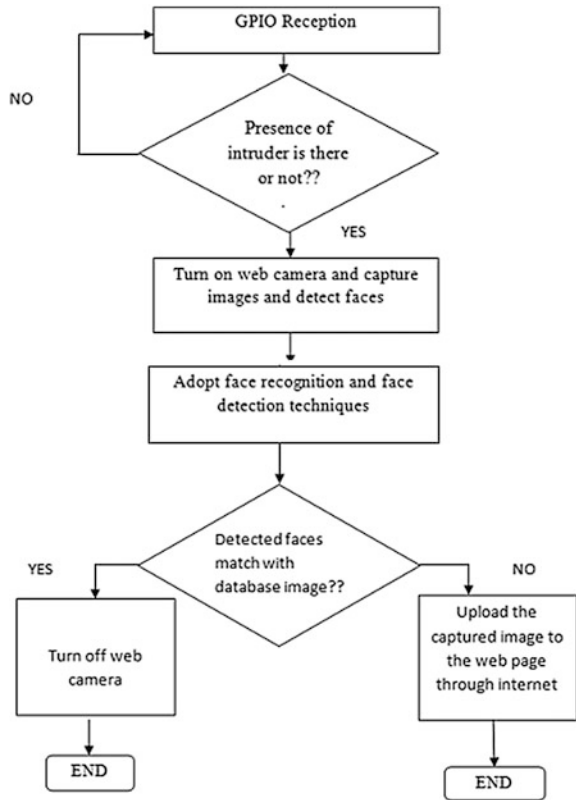


Fig. 3 Software flow chart of back end



be uploaded in the web page and authorized person (member of the house) can access the image from the web page. If the recognized face is one of the faces in the database, then the system goes to the idle state.

The flow chart describing the system functioning at the back end is shown in Fig. 3.

3 Face Detection

Face detection is the initial step of detecting a face in the image or video frame. Face detection can be achieved using various methods, of which Viola–Jones method [6] is the popular and most widely used one. There are three key contributions for this approach. The first is the introduction of a new image representation called the “Integral Image” which allows the features to be computed very fast. The second is a very simple and efficient classifier which is built using the AdaBoost learning algorithm in order to select a small number of critical visual features from a

very large set of potential features. The last contribution is a method for combining classifiers in a “cascade” which allows background regions of the image to be quickly discarded while spending more computation on promising face-like regions.

First the real-time video is captured, then each frame is taken and then the YUY2 format of the image obtained is converted to RGB since most of the MATLAB functions are compatible with RGB. This RGB image is then converted to grayscale for easy calculation. Then the image is enhanced and then passed on to face detection part. The input image was first converted to integral image; the integral image was calculated as shown in Fig. 4. This is done by making each pixel equal to the entire sum of all pixels above and to the left of the concerned pixel.

The second step in face detection is feature extraction. The integral image makes feature extraction faster and is easier to calculate. The white areas in the image are subtracted from the black ones. So after feature extraction these features are passed to the classifier section where the classification of these extracted features takes place, whether they are positive or negative features (that is if the features belong to that of a face or not). Thus a face is detected from the image. But there will be a lot of features extracted. But a single classifier becomes insufficient to evaluate so we go for a method called AdaBoosting [6, 7]. So using viola Jones method the face detection was carried out and faces were detected as shown in Fig. 5. But some problems were encountered when the images captured from the real time video were not in frontal upright positions and due to illumination problems.

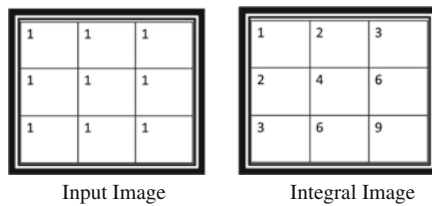


Fig. 4 a Input image, b integral image

Fig. 5 Face detection

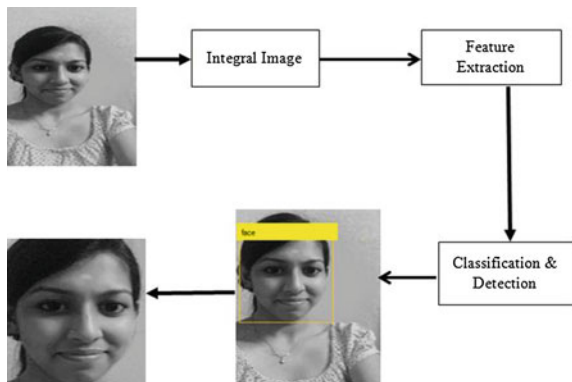
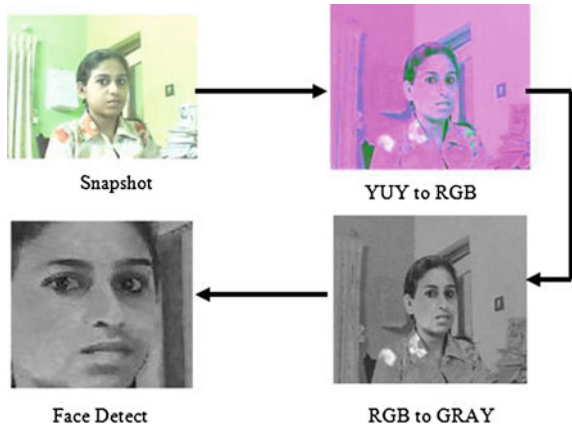


Fig. 6 Stage output



Once the face has been detected using the Viola–Jones face detection method, the face portion is then cropped from the image by specifying its aspect ratio and this face image will be passed over to perform the recognition function (Fig. 6).

4 Face Recognition

After detection, the next step is the recognition of the detected face. Face recognition involves extracting selected features from the image and then classifying them for recognition. The required features can be extracted from an image using image processing algorithms. The extracted features are fed to a classifier where feature classification takes place and face is recognized. The feature extraction can be done by Principle Component Analysis (PCA) algorithm and classification can be achieved by geometrical similarity measurement [8, 9]. There are two phases in face recognition, namely *training phase* and *recognition phase*. The training phase involves obtaining the projected images of the train images and the recognition phase involves first obtaining the projected image of the input image and then determining the Euclidean distance or geometrical similarity measure. The train image with the minimum Euclidean distance with the input image is the recognized image.

Training phase, the training set is taken and the mean face is computed. Using this mean face, the deviation vector for each image is computed by subtracting the mean from each face to obtain the difference matrix. Then the eigenfaces are calculated by finding the covariance matrix C of the training image vectors by [8, 10].

$$C = AA^T \tag{1}$$

where A is the difference matrix.



Fig. 7 Train dataset

Now the eigenvectors of C are obtained by:

$$U_i = AV_i \quad (2)$$

where V is the covariance matrix with reduced dimensions of size $M \times M$.

Now the Eigenfaces are:

$$\text{Eigen Faces} = [U_1, U_2, \dots, U_m] \quad (3)$$

The projected image or the signature matrix of the whole set is then computed.

In the recognition phase, the projected image of the input image is obtained and Euclidean distance of the image is computed with all the signatures in the database or train set [8] (Fig. 7).

5 Database Storage

In this stage, the information attained according to the recognition is stored in the database initially. If the detected face is recognized as an individual in the database, then the details of the individual in the database is retrieved and stored in another database (excel sheet) along with the login time as shown in Fig. 8. Otherwise the detected face will be stored in the database along with entered time and uploaded in the web page (Fig. 9).

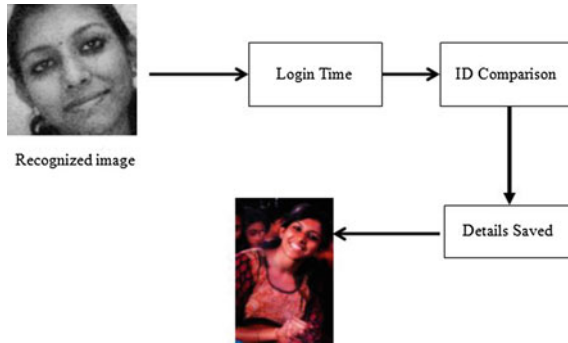


Fig. 8 Member database storage

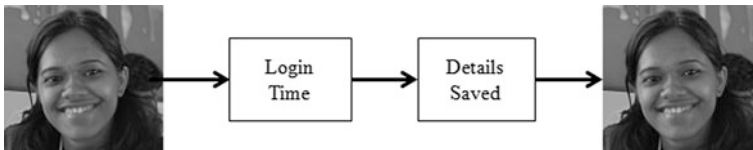


Fig. 9 Non-member database storage

6 Simulation Results













Extensive simulations are run in MATLAB to verify the performance of the proposed surveillance system.

6.1 Threshold Setting and System Efficiency

The face recognition system was developed by using Viola–Jones method and PCA algorithm. The system gave satisfactory results of more than 70 % true recognition. The main problem is the threshold setting which depends on the Euclidean distance. Threshold setting is required to distinguish between the authority and an outsider.

The experiment was done by providing different images of 3 persons in the database so that they represent the authorities (members). From Fig. 10, out of 6 recognitions of the employees 4 true recognitions were achieved. It was noted that under similar illuminations and with similar pose, the minimum Euclidean distance took the lowest value of $0.886e+15$. However, as the pose and illuminations are varied the value increased to a maximum of $3.3e+15$. Also for false recognitions the values were $2.33e+15$ and $2.8e+15$. Moreover for outsider detection the recognition values were high under different illuminations but low for similar illuminations.

Fig. 10 Threshold setting and system efficiency result

Input Image	Recognized Image	Euclidean Distance (*e+15)	True / False
		0.886	True
		2.5	True
		2.04	True
		3.3	True
		2.33	False
		2.8	False

This introduces high difficulty to threshold setting and also the recognition efficiency is reduced to 50–60 %.

6.2 Reducing Illumination Variation Effects for Better Recognition

6.2.1 Introducing Bilateral Filter

From Fig. 11 out of 6 recognitions of the members, 4 were true recognitions. So the recognition efficiency is not much increased. The improvement is that minimum Euclidean distance of the true recognitions ranged from 1.37e+15 to 2.09e+15 which is a narrow range and also that for false recognitions were 3.56e+15 and 3.43e+15. So the threshold setting will be easy since there is a proper gap between true and false recognitions. Therefore it can be concluded that introducing bilateral filter eliminates the threshold setting problem but the efficiency can be increased only to about 70 %.

6.2.2 Introducing Gamma Correction

Gamma correction is, in the simplest cases, defined by the following power-law expression:

$$V_{out} = AV_{in}^\gamma \tag{4}$$

This method of enhancement changes the intensity of the input image according to the value of ‘gamma’. Gamma can be any value greater than 0. Setting a value greater than 1 for gamma enhances the highly illuminated image but spoils low illuminations and vice versa. To eliminate this, gamma value can be made adaptive to the illuminations. This is done by first taking the mean intensity of the image and then applying suitable gamma value according to the mean. This enables the enhancement of both high and low illumination images. As a result the recognition efficiency is increased to a certain extend [11].

From the comparison chart (Fig. 11) it can be observed that for recognition without any enhancement the geometrical similarity measure or Euclidean distance range is wide and for recognition with gamma correction and bilateral filter the

Fig. 11 Results after the introduction of bilateral filter












Input Image	Recognized Image	Euclidean Distance (*e+15)	True / False
		3.4352	False
		1.9795	True
		1.374	True
		2.095	True
		3.5652	False
		1.9895	True

Fig. 12 Threshold comparison chart

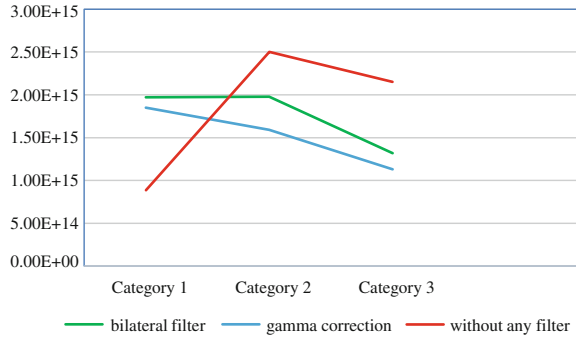
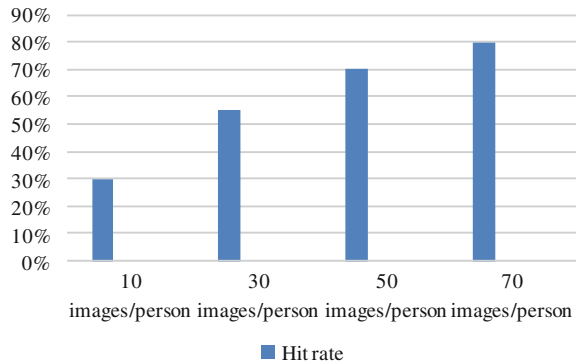


Fig. 13 Efficiency chart



range is narrow, where the categories represent true recognitions [12]. As a result the threshold setting can be done efficiently with enhancement methods.

The efficiency chart shows that increasing train dataset increases the efficiency of recognition. The train dataset was created with 10 images per person. As the images per person were increased to 30, the efficiency was increased to 55–60 % (Figs. 12 and 13).

7 Conclusion

Design and implementation of an advanced low-power home surveillance system is carried out in this project work. A user interactive system is created using MATLAB GUI. Automatic capturing of the image with time tag is carried out. Face detection can be effectively performed by using Viola–Jones method. The first contribution of Viola–Jones method is a new technique for computing a rich set of image features using the integral image. Integral image makes the face detection fast. The second contribution is a simple and efficient classifier built from computationally efficient features using AdaBoost for feature selection. This classifier is

clearly an effective one for face detection. The third contribution is a technique for constructing a cascade of classifiers which radically reduces computation time while improving detection accuracy. Face recognition can be done by Principle Component Analysis (PCA) algorithm and classification can be achieved by geometrical similarity measurement. PCA algorithm for feature extraction gives good recognition efficiency and also in the training phase, the time required for training is less compared to neural network. Geometrical similarity measurement gives the best hit rate when used with Adaptive Histogram Equalization. Pose invariant technique is used before the classification which enables the classifier to recognize face for varied poses. This improves the efficiency of the face recognition system.

References

1. Meier AK. A worldwide review of standby power use in homes. Lawrence Berkeley National Laboratory, Dec 2001, p. 1–5.
2. Bai Y-W, Shen L-S, Li Z-H. Design and implementation of an embedded home surveillance system by use of multiple ultrasonic sensors. *IEEE Trans Consum Electron.* 2010;56:1.
3. Bai Y-W, Xie Z-L, Li Z-H. Design and implementation of a home embedded surveillance system with ultra-low alert power. *IEEE Trans Consum Electron.* 2011;57:1.
4. Nahatkar S, Gaur A, Pattewar TM. Design of a home embedded surveillance system with pyroelectric infrared sensor and ultra-low alert power. *Int J Adv Res Electron Commun Eng (IJARECE).* 2012;1:3.
5. <https://en.wikipedia.org>.
6. Viola P, Jones MJ. Robust real-time face detection. *Int J Comput Vision.* 2004;57:2.
7. Arandjelovic O, Cipolla R. An illumination face recognition system for access control using video, Department of engineering University of Cambridge, Cambridge, CB2 IPPZ, UK.
8. Abdullah M, Wazzan M, Bo-saeed S. Optimizing face recognition using PCA. *Int J Artif Intell Appl.* 2012;3:2 (Faculty of Computer Sciences and Information Technology, King Abdullaziz University, Jeddah, KSA).
9. Ahmad F, Najam A, Ahmed Z. Image-based face detection and recognition. *IJCSI Int J Comput Sci.* 2012;9(6):1.
10. Shankar Kartik J, Ram Kumar K, Srimadhavan VS. Security system with face recognition, SMS alert and embedded network video monitoring terminal. *Int J Secur Priv Trust Manag (IJSPTM)* 2013;2:5 (Department of Electronics and Communication Engineering, SRM Easwari Engineering College, Anna University).
11. Susan Varghese S, Godwin Premi MS. User-controlled low power home surveillance system. *Int J Emerg Technol Adv Eng.* 2013;3:3 (Department of ETCE, Sathyabama University, Chennai).
12. Tasleem Mandrupkar Dept of Computer Engg, Dept of ComputerEngg Manisha Kumari Rupali Mane, Dept of Computer Engg, Pune University, Pune, India. Smart video security surveillance with mobile remote control. *Int J Adv Res Comput Sci Softw Eng.* 2013;3:3.

Performance Analysis of a Software Defined Network Using Mininet

Chaitra N. Shivayogimath and N.V. Uma Reddy

Abstract Network is growing day by day. New devices are getting added into the network making it very difficult for an IT administrator to configure the ACLs and the other network parameters in the devices. Flexibility and programmability are the key factors in the present day scenario. Software Defined Networks (SDN) is the evolving network technology which provides the two factors mentioned. The latency in the packet delivery is less compared to the legacy Hardware Defined Networks (HDN) and in turn the throughput is also high. The work done in this paper provides a Proof of Concept (POC) for the better throughput of SDN-based routing.

Keywords SDN · Mininet · Throughput · Latency · HDN

1 Introduction

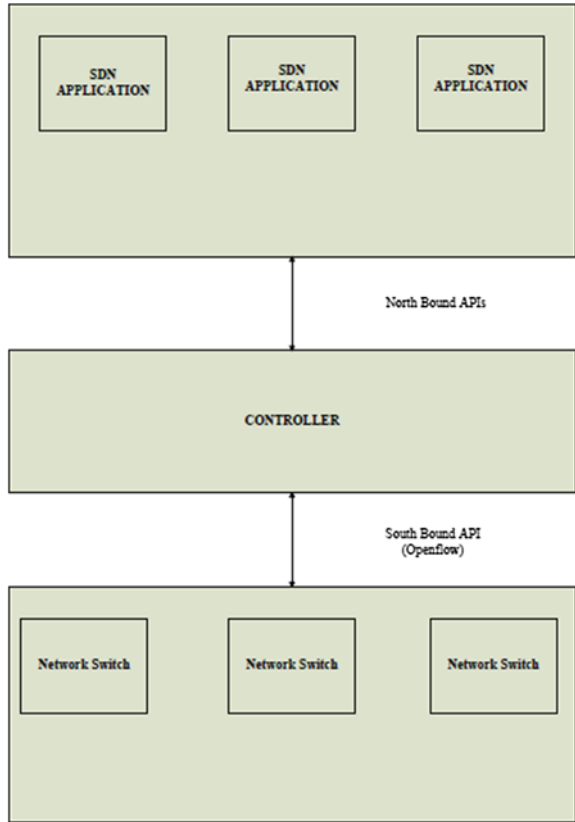
An evolving networking technology coming into prominence is “Software Defined Networking” (SDN) [1]. SDN separates the control plane and data plane in networking devices such as routers and switches with the help of an API. All the routing decisions are done by a centralized device called controller and the forwarding done by a dumb device, such as a switch.

A controller talks to the underlying network device, i.e. the forwarding switch via the “Southbound API”, this is a protocol which talks from switch to controller and vice versa. One such popular protocol is, OpenFlow protocol by the Open Network Foundation (ONF) [2]. This is a flow-based protocol. The routing

C.N. Shivayogimath (✉) · N.V. Uma Reddy
Department of E&C, AMC Engineering College, Bangalore, India
e-mail: chaishivyogi@gmail.com

N.V. Uma Reddy
e-mail: nvumareddy@gmail.com

Fig. 1 SDN architecture



decisions from the controller are inserted into the forwarding switch, which is now called as OpenFlow switch as flow rules into the flow table of the switch. The applications are the “Northbound APIs” which sit on the controller for various applications as shown in Fig. 1. An analogy to a computer would better explain what SDN is. Similar to the way we install programmes on the OS of our computer (e.g. Browsers, text editors, softwares IDEs, etc.), APIs are written to the NOS (Network Operating System) of the controller.

There is a huge need for flexibility and programmability of network in the present day world. Due to virtualization, a single machine can be partitioned into many servers. A virtual instance of a server can be modified, cloned and can be used as another virtual server by starting it as another new instance. So it is easy for migration of server from one machine to another. But it creates a problem in the legacy Hardware Defined Networks (HDN). A major problem will be caused with VLANs whenever a VM moves, VLAN has to be reconfigured. In general terms, to match the flexibility of server virtualization, the network manager needs to be able to dynamically add, drop and change network resources and profiles. This process is difficult to do with legacy network switches, in which the control logic for each

switch is co-located with the switching logic. Another need is, rapidly increasing mobile devices such as smartphones, PDAs, tablets, notebooks accessing the network. Network managers must be able to respond to the changing QoS and security requirements [3].

2 Analysis of Latency of Packets in SDN

The traditional way of measuring a network's performance is the packet latency and the throughput. The later is dependent on the foster. An SDN-based network has less latency per packet and hence an increased throughput compared to the legacy HDN. Since hardware testbeds are time-consuming and costlier, simulators are used. The emulation for SDN is done using Mininet [4], an SDN emulator and for HDN, the emulator used is GNS3.

2.1 Hardware Defined Network

A network emulated in GNS3 is shown in Fig. 1.

GNS3 is a network emulating software used to design networks in lab environments for testing and study purpose [5]. A sample network as shown in Fig. 2 is created. Once the network is up and running, the latency of the packets can be determined by conducting a ping test between the hosts. Figure 3 shows the time taken for a ping packet to reach from host H1 to Host H3.

Figure 4 shows the ping test conducted from H3 to H1. On observing the time taken by a packet, it can be analysed that the latency is consistently more and same for every packet.

Analysis

- On observing Figs. 3 and 4, the latency for every packet from H3 to H1 is either same or more.
- When the first packet from the source arrives at switch, the switch registers in its CAM table (or MAC table) the MAC and IP address of the source host corresponding to the port at which the packet arrives.
- The switch checks its CAM table for the destination address in the CAM table. Since this is the first packet and there is no entry for the address, the switch forwards the packet to the router for the routing decisions.
- The router makes the routing decisions and sends the routing decision entry to switch. The switch forwards the packet accordingly and flushes the entry.
- This process repeats for every packet that arrives consecutively to the switch leading to high latency of every packet.

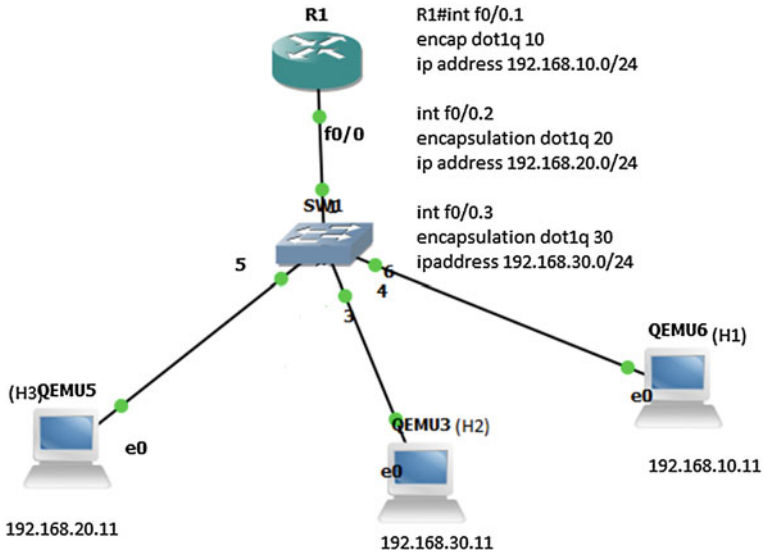


Fig. 2 A legacy hardware defined network emulated in GNS3

```
QEMU
22 packets transmitted, 21 packets received, 4% packet loss
round-trip min/avg/max = 5.087/8.974/19.094 ms
root@qemu6:~# ping 192.168.10.11
PING 192.168.10.11 (192.168.10.11): 56 data bytes
64 bytes from 192.168.10.11: seq=0 ttl=63 time=10.408 ms
64 bytes from 192.168.10.11: seq=1 ttl=63 time=8.098 ms
64 bytes from 192.168.10.11: seq=2 ttl=63 time=8.264 ms
64 bytes from 192.168.10.11: seq=3 ttl=63 time=7.043 ms
64 bytes from 192.168.10.11: seq=4 ttl=63 time=8.108 ms
64 bytes from 192.168.10.11: seq=5 ttl=63 time=5.122 ms
64 bytes from 192.168.10.11: seq=6 ttl=63 time=7.989 ms
64 bytes from 192.168.10.11: seq=7 ttl=63 time=6.944 ms
64 bytes from 192.168.10.11: seq=8 ttl=63 time=6.156 ms
64 bytes from 192.168.10.11: seq=9 ttl=63 time=5.004 ms
64 bytes from 192.168.10.11: seq=10 ttl=63 time=8.117 ms
64 bytes from 192.168.10.11: seq=11 ttl=63 time=5.052 ms
64 bytes from 192.168.10.11: seq=12 ttl=63 time=6.058 ms
64 bytes from 192.168.10.11: seq=13 ttl=63 time=4.949 ms
64 bytes from 192.168.10.11: seq=14 ttl=63 time=8.054 ms
64 bytes from 192.168.10.11: seq=15 ttl=63 time=8.151 ms
^C
--- 192.168.10.11 ping statistics ---
16 packets transmitted, 16 packets received, 0% packet loss
round-trip min/avg/max = 4.949/7.094/10.408 ms
root@qemu6:~#
```

Fig. 3 Ping test conducted from H1 to H3

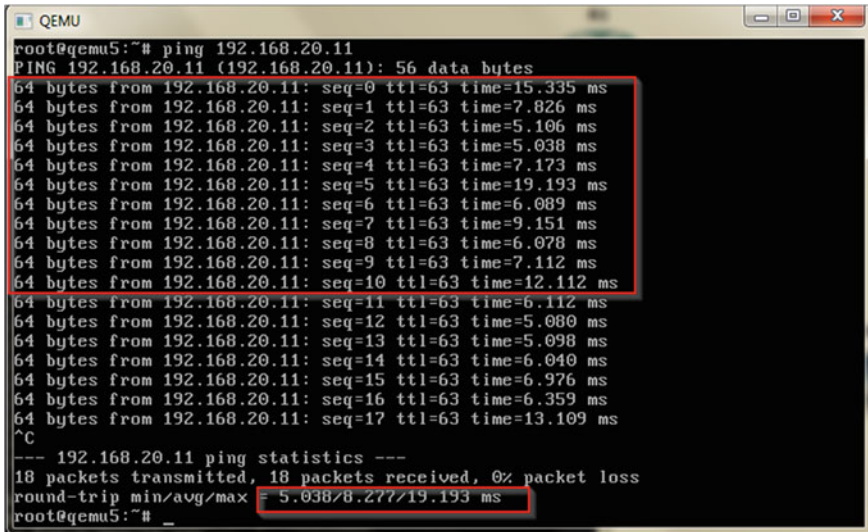


Fig. 4 Ping test conducted from H3 to H1

2.2 Software Defined Network

Mininet is an emulator for rapid prototyping of SDN with limited resource. Mininet creates virtual networks as shown in Fig. 5. A Controller (Control Plane), for making routing decisions, a switch for forwarding the packets based on the controller’s routing decisions. The switch buffers the flow entry inserted by the controller into the flow table of the switch. This eliminates the necessity of contacting the controller for routing decision for every packet, thus reducing the latency of the consecutive packets after the first packet.

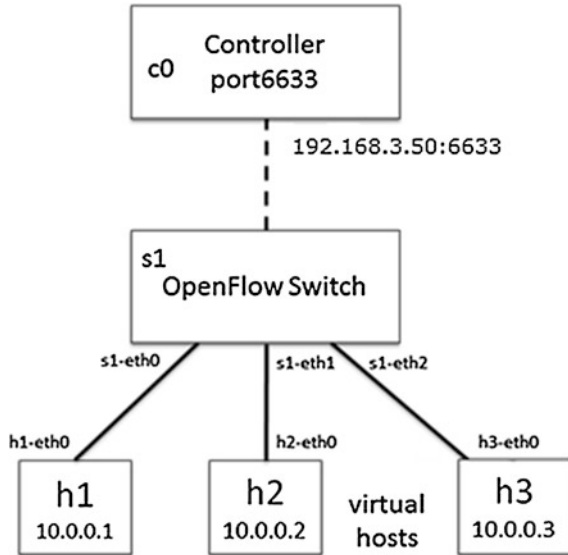
The topology shown in Fig. 5 is created in the Mininet network emulator by issuing the following command:

```
sudo mn -topo=single,3 -mac -switch=ovsk-
controller=remote,ip=192.168.3.50,port=6633
```

The controller chosen is POX controller [6]. Once the network is created, the controller has to be instantiated. This controller is a remote controller on the IP address 192.168.3.50 over port 6633. Figure 6 shows the information of the OpenFlow switch connected to the controller.

The controller is up and now connected to the OpenFlow switch, which is on IP address 192.168.3.32. The virtual hosts H1, H2 and H3 that are created are connected to the OpenFlow switch via virtual Ethernet links. Conducting a ping all the tests determine the connectivity of all the hosts to the network. To determine the latency of packets in SDN, a ping test from H1 to H2 is conducted as shown in Fig. 7.

Fig. 5 SDN single topology with three hosts, simulated in Mininet



Analysis

- On observing from Fig. 7, the first packet takes 21.8 ms, i.e. more time compared to the consecutive packets. All the consecutive packets take very less time compared to the first packet.
- The reason for first packet to take longer is, the routing decision happens only for first packet. Once the controller inserts the flow rule for the first packet, the switch buffers the flow rule in its flow table for 30 s.

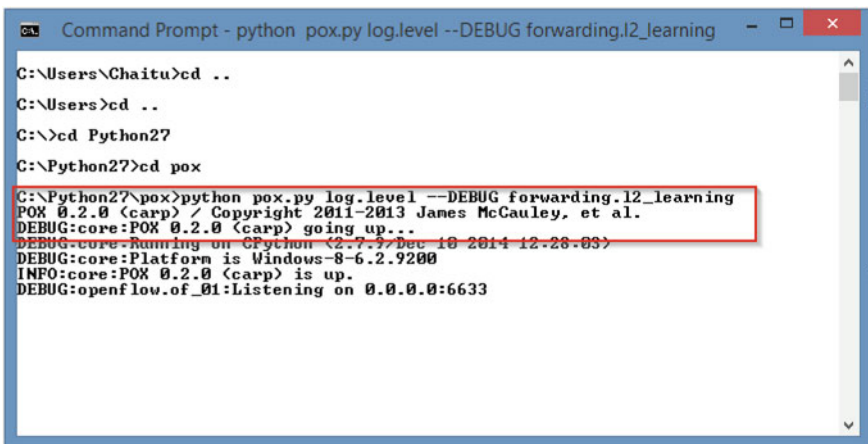


Fig. 6 POX controller on the IP address 192.168.3.50

```

mininet@mininet-vm: ~
*** Configuring hosts
h1 h2 h3
*** Starting controller
c0
*** Starting 1 switches
s1
*** Starting CLI:
mininet> h1 ping -c10 h2
PING 10.0.0.2 (10.0.0.2) 56(84) bytes of data:
64 bytes from 10.0.0.2: icmp_seq=1 ttl=64 time=36.5 ms
64 bytes from 10.0.0.2: icmp_seq=2 ttl=64 time=1.02 ms
64 bytes from 10.0.0.2: icmp_seq=3 ttl=64 time=0.063 ms
64 bytes from 10.0.0.2: icmp_seq=4 ttl=64 time=0.113 ms
64 bytes from 10.0.0.2: icmp_seq=5 ttl=64 time=0.065 ms
64 bytes from 10.0.0.2: icmp_seq=6 ttl=64 time=0.118 ms
64 bytes from 10.0.0.2: icmp_seq=7 ttl=64 time=0.799 ms
64 bytes from 10.0.0.2: icmp_seq=8 ttl=64 time=0.065 ms
64 bytes from 10.0.0.2: icmp_seq=9 ttl=64 time=0.065 ms
64 bytes from 10.0.0.2: icmp_seq=10 ttl=64 time=0.061 ms

--- 10.0.0.2 ping statistics ---
10 packets transmitted, 10 received, 0% packet loss, time 9005ms
rtt min/avg/max/mdev = 0.061/3.891/36.544/10.889 ms
mininet>
    
```

Fig. 7 Ping test from H1 to H2

- The consecutive packets are forwarded by the switch without contacting the controller for the routing decision.
- After 30 s, the buffer is timed out and the flow table is cleared. Again the same procedure repeats.

Table 1 Comparison of the packet flow in HDN and SDN

Packet no.	HDN	SDN
1	Packet originating from H1 arrives to switch port	Packet originating from H1 arrives to switch port
2	The switch sends the packet to the router for routing decision	Switch checks for a flow rule corresponding to the packet in its flow table. If there is no entry, the packet is forwarded to controller
3	The routing decision from router is received and the switch just forwards the packet correspondingly	The flow rule is inserted in the openflow switch by the controller. The switch buffers this entry for further communication
4	The consecutive packet is again sent to the router for routing decision	All the consecutive packets are forwarded based on the flow table entry until the buffer time expires
5	Packet sent to router again	
6	Packet sent to router again	
:	:	:
n	Packet sent to router again	The buffer time is out and the packet will be sent to controller

3 Conclusion

The work in this paper proves that the latency of the packets in SDN is very much less than that for the legacy networks. Thus the throughput is high comparatively. Many other performance parameters like CPU usage and bandwidth can also be measured using command like *iperf* in Mininet. This command gives the bandwidth usage of the link.

Thus SDN is the future of the networking world with better performance than the legacy HDNs.

Table 1 summarizes the HDN and SDN packet flow.

Acknowledgments The authors would like to thank Mr. Santhosh Sundarasamy, Sr. Architect and Engineering Manager, Cloud Managed Security, Paladion Networks Pvt. Ltd. for his complete support and help in carrying out the experiment at Paladion Networks Pvt. Ltd. as part of the Internship Programme of the first author.

References

1. Lantz B, Heller B, McKeown N. A network in a laptop: rapid prototyping for software-defined networks. In: 9th ACM workshop on hot topics in networks, Monterey, CA, 20–21 October 2010.
2. Openflow White paper by Open Network Foundation, 13 April 2012. <https://www.opennetworking.org/images/stories/downloads/sdn-resources/white-papers/wp-sdn-newnorm.pdf>.
3. Stallings W. Software defined networks and openflow. The Internet Protocol Journal 2013. <http://williamstallings.com/Papers/>.
4. Mininet VM image. <https://github.com/mininet/mininet/wiki/Mininet-VM-Images>.
5. GNS3, Network emulator. <http://www.gns3.com/>.
6. POX controller guide. <https://openflow.stanford.edu/display/ONL/POX+Wiki#POXWiki-InvokingPOX>.

Comparative Analogy on Classification and Clustering of Genomic Signal by a Novel Factor Analysis and F-Score Method

R.C. Barik and R. Mishra

Abstract Data is the centroid in any dimension of scientific research. Most of the research arena is problem specific with respect to its data. In machine learning more and more data samples are used for training a machine for efficient cluster formation, prediction, recognition, classification. Variation between data sample to data sample and data sample from its centroid using Euclidean distance, Mahanalabolis distance for better cluster formation has better focused among computational researchers. In this paper, we proposed a novel loss less feature extraction and selection using feedforward cascaded Factor Analysis and F-score method. Comparative analysis of classification and clustering after efficient feature extraction is applied to life killer cancer disease. Tumor classification is based on multilayer perceptron and clustering is based on k-means clustering method.

Keywords Factor analysis · F-score method · k-means clustering · Artificial neural network · Multilayer perceptron

1 Introduction

Prediction is itself a term of research in machine learning, artificial intelligence, and computational intelligence. The current trend of computation and its application to real world is the ultimate destination of any scientific research. According to artificial intelligence, any computational machine is initially assumed as an infant, who

R.C. Barik (✉) · R. Mishra
Department of Computer Science and Engineering, Vikash Institute of Technology,
Bargarh, Odisha, India
e-mail: ramchbarik@gmail.com

R. Mishra
e-mail: rosymishra93@gmail.com

tries to recognize the real-life object and perform enormous mistakes in prediction. By having more and more examples of training of the pattern to identify the same object again and again, some retention photographic energy will store in the memory which is the feature to predict the object in future encounter. Likewise, a computational machine needs to be trained again and again until a threshold is being satisfied. According to machine learning, there is a great gap between supervised and unsupervised classification, where so many researches are being carried out in the past two decades.

Genomic analysis for cancerous disease prediction is being affected by a well-known issue called curse of dimensionality. Cancer is a life killer disease which requires computational diagnosis because of its variety of classes and their respective drugs. For example, let us take a microarray dataset obtained by DNA chip, which is based on intensity to numeric mapping as leukemia cancer consists of 72 samples of bone marrow and 7129 probes from 6817 human genes [1, 2]. It is a high dimensional data such as 72×7129 . To perform prediction, classification, and clustering, some of the redundant uninformative genes need to be minimized. Brain tumor segmentation is an important procedure for early tumor diagnosis and radiotherapy planning. Although numerous brain tumor segmentation methods have been presented, enhancing tumor segmentation methods is still challenging because brain tumor MRI images exhibit complex characteristics, such as high diversity in tumor appearance and ambiguous tumor boundaries [3]. However, brain tumor segmentation from an image has the inertia of reading the image, alignment of the image as per the number of features by analyzing the grey scale levels from 0 to $L - 1$ and the corresponding pixels which contribute to those levels. histogram and edge feature are based on canny, sobel, and prewitt methods. So, the process of feature extraction is a complex procedure for analysis. But every patient who had been affected by brain cancer has independent neural characteristics and shape. Advancements in microarray technology lead to produce a large number of disease databases, which are being utilized usually in computational biological research arena. Basically it is a laboratory technology which maps grey scale intensity to a matrix of real numbers representing the number of samples or observations and its labeling to identify which classes it belongs. Because there is not any kind of universal drug which gives equal solution or cure for every class. We cannot give a drug of one class of disease to another class which creates side effects or even the patients may die. Computational diagnosis is a major solution than the manual solution in case of these deadliest diseases. Artificial neural network has given significant techniques which are used in various dimensions of science and engineering. But multilayer perceptron is being applied to more diversified and complex areas whereas radial basis function has a simple mathematical model of single hidden layer (φ). The activation function $f(\cdot)$ is application specific such as signum, Gaussian, and multiquadratic.

2 Proposed Method Architecture

Computation for any dimension of science requires an apposite architecture to be followed. Figure 1 describes the detailed view of the architecture.

3 Retained Feature Calculation Using Cascaded Statistical Approach

Among the large amount of genes presented in microarray gene expression data, only a small fraction of them is effective for performing a certain diagnostic test [4]. There are a number of reduction techniques proposed by research communities; some successful techniques are principal component analysis, factor analysis, and linear discriminant analysis, which have been used in multidisciplinary research areas yet. There are a number of research methodologies which prove their

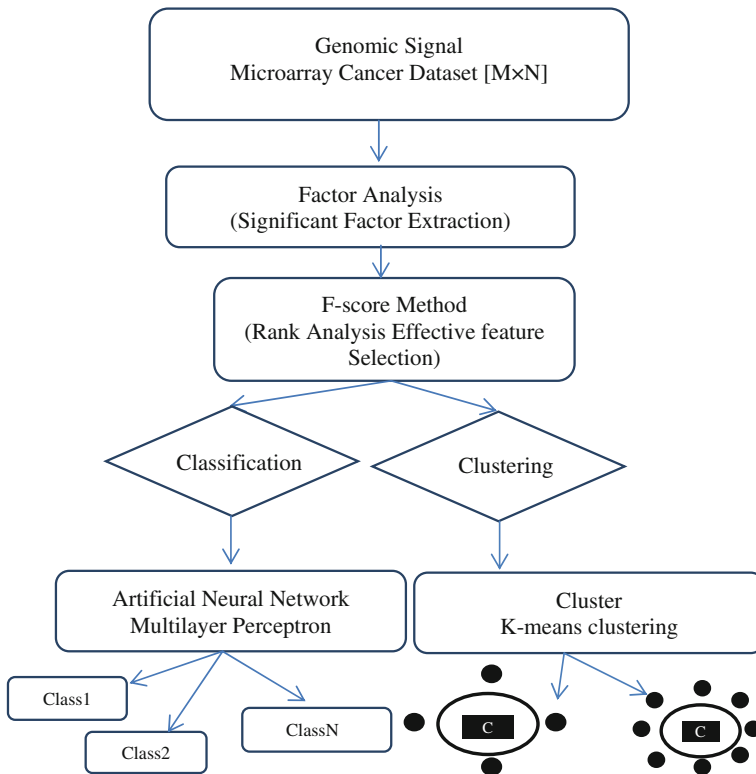


Fig. 1 Detailed view of architecture for the analysis of proposed method

techniques with empirical result analysis. We are proposing a novel cascaded method by combining factor analysis with F-score method for selecting the informative genes architecture; Fig. 1 depicts all of these details. As feature selection using factor analysis has been fed to RBF, SVM works well in EEG signal [5]. So we have given a combined approach of factor analysis and F-score method. There is a quite difference between factor analysis and PCA rather PCA is a kind of factor analysis.

3.1 Factor Analysis

It is a statistical method which describes the variance based on correlation in a set of observed variables to outcome a smallest number of variables called as factors. It finds the joint variation points to be focused with respect to hidden variables or factors. Principal component analysis is a popular method used in versatile research area for factor evaluation. Application of factor analysis is immense in real-time environment such as psychology cognition in child behavior checklist, attitude in sociology and political science, diagnostic criteria in mental health, and many more. Factor analysis with covariance extraction has higher accumulative variances than correlation extraction [5].

$$\begin{aligned}
 Y_1 &= \alpha_{11}F_1 + \alpha_{12}F_2 + \dots + \alpha_{1m}F_m \\
 Y_2 &= \alpha_{21}F_1 + \alpha_{22}F_2 + \dots + \alpha_{2m}F_m \\
 &\dots \\
 &\dots \\
 &\dots \\
 Y_n &= \alpha_{n1}F_1 + \alpha_{n2}F_2 + \dots + \alpha_{nm}F_m
 \end{aligned} \tag{1}$$

where

Y = a variable with known data, α = a constant, F = a function, $f(\cdot)$ of some unknown variables.

3.2 F-Score Method

It is a statistical technique that measures the distinguishing power between two classes with real values [6, 7]. In this method, F-score value of each feature in the dataset is computed to show their discriminative power. The F-score value of k th feature of a two-class problem is defined as:

$$F(k) = \frac{(\bar{x}_k^{c1} - X)^2 + (\bar{x}_k^{c2} - X)^2}{(\sigma_k^{c1})^2 + (\sigma_k^{c2})^2} \quad (2)$$

where X = average of the total samples of the k th feature, \bar{x}_k^{c1} , \bar{x}_k^{c2} = average of the $c1$ and $c2$ class samples of the k th feature and $(\sigma_k^{c1})^2$, $(\sigma_k^{c2})^2$ = variance of the $c1$ and $c2$ class samples of the k th feature.

The numerator of the Eq. 2 shows the discriminating power between the classes and the denominator reveals that within the individual classes. The larger the F-score, the more likely the feature is significant. In order to select the efficient features from entire dataset, a threshold value is employed on the F-scores of all features. If the F-score value of any feature is bigger than threshold value, that feature is added to feature space. Otherwise, that feature is removed from feature space. The threshold value may vary from dataset to dataset depending upon the correlation factor to a minimum and maximum.

4 Classification and Clustering

As the name of this paper reflects, a comparative analogy of classification and clustering are taken into consideration for true empirical analysis. According to machine learning, training of more samples as example is fed to any computational machine which reflects directly the level of classification and prediction. We have taken a popular technique of artificial neural network as multilayer perceptron for classification. Clustering is a natural and artificial process where training is not required. The clusters are being formed automatically by initially taking a random member from a given set of points and computing the distance measure based on correlation between the random member and other members. The process will go on for computing all the remaining members. In this paper for clustering of genome data, we have taken k-means clustering approach.

4.1 *Multilayer Perceptron*

Multilayer perceptron is a popular artificial neural network technique to research communities. MLP can solve linearly inseparable problems. It is a complex technique with comparison to radial basis function, FLANN because of its number of hidden layers. But prediction accuracy is higher than other techniques. Propagation of input signal through the network in a forward direction, on a layer-by-layer basis is the process of multilayer perceptron [8, 9]. The output of MLP can be explained as

$$y_s = f_s \left[\sum_{r=1}^{p2} W_{rs} f_r \left(\sum_{q=1}^{p1} W_{qr} f_q \left\{ \sum_{p=1}^N W_{pq} X_p + b_q \right\} + b_r \right) + b_s \right] \tag{3}$$

The above equation describes that the multilayer network comprises four layers including two hidden layers as represented in Fig. 2 where $x_p(k)$ represents input to the network, $y_s(k)$ is the output of the final layer of the neural network, φ_p, φ_r represents output of the two hidden layers (it is problem dependent to choose the number of layers). The connecting weights between the input to the first hidden layer, first to second hidden layer, and the second hidden layer to the output layers are represented as W_{pq}, W_{qr}, W_{rs} respectively. N is number of Inputs and $f(\cdot)$ is nonlinear activation function in first hidden layer based on threshold function, sigmoid function, piecewise-linear function, hyperbolic tangent function. Here, b_q, b_r, b_s is the threshold to the neurons of the second hidden layer.

For the training, error signal needs to be calculated which is the difference between the actual output and the expected output and accordingly the weight modification using back propagation. Since one of the requirements for the back propagation algorithm is that the activation function is differentiable, a typical activation function used is the sigmoid equation. If the actual activation value of the output node s is y_s , then the expected target output for node s is t_s ; the difference between the actual output and the expected output is given as

$$\Delta_s = t_s - y_s \tag{4}$$

The error signal for node s in the output layer can be calculated as

$$\delta_s = \Delta_s y_s (1 - y_s) \tag{5}$$

$$\delta_s = (t_s - y_s) y_s (1 - y_s) \tag{6}$$

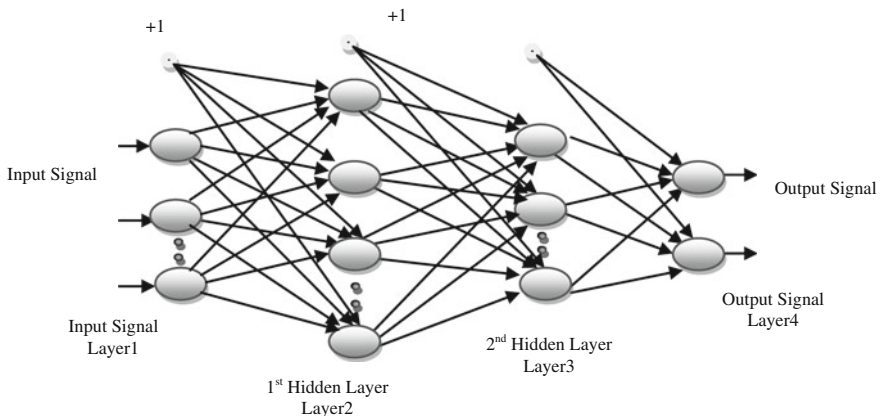


Fig. 2 Structure of MLP with four layers out of which two are hidden layers

where the $y_s(1 - y_s)$ term is the derivative of the sigmoid function.

The formula used to modify the weight, $W_{p,s}$ between the output node, s , and the node, p is:

$$\Delta W_{p,s} = l_r \delta_s x_p \quad (7)$$

$$W_{p,s} = W_{p,s} + \Delta W_{p,s}$$

where $\Delta W_{p,s}$ is the change in the weight between nodes p and s , l_r is the learning rate which synchronizes the network learning. It is desirable to minimize the error on the output nodes over all the patterns presented to the neural network. The following equation is used to calculate the error function, E , for all patterns

$$E = \frac{1}{2} \sum \left(\sum (t_s - y_s)^2 \right) \quad (8)$$

4.2 *k*-Means Clustering

Cluster formation is an old method which has been applied in various real-life scenarios and will be applicable in future. *k*-means algorithm is an unsupervised algorithm that categorizes the input data points into multiple groups or clusters based on their inherent distance from each other (inter-correlation relationship). The algorithm calculates the latent features from the input data or signals as a vector space and performs the natural clustering [10, 11]. The points are categorized around centroids or cluster centers $\mu_i \forall i = 1, 2, \dots, k$ that are obtained by minimizing the objective or distance

$$V = \sum_{i=1}^k \sum_{x_j \in s_i} (x_j - \mu_i)^2 \quad (9)$$

where there are k clusters s_i , $i = 1, 2, \dots, k$ and μ_i is the centroid or mean point of all the points $x_j \in s_i$.

5 Results and Analysis

Result and analysis is the key block of any research paper where the empirical results are being evaluated and analyzed over the specific area of dataset (existing or truly generated) using some existing and proposed techniques. In this paper, we have proposed a hybrid feature selection method based on factor analysis and F-score method.

Table 1 Description of the details of the cancer dataset used

Dataset	Dimension	Class type	Description
Colon	62×2000	Binary	Normal (22), Tumor (40)
SRBCT	83×2308	Multi	Burkitt lymphoma (BL), Ewing family of tumors (EWS), neuroblastoma (NB), rhabdomyosarcoma (RMS)
Brain tumor	$50 \times 10,368$	Multi	Classic Glioblastomas, Classic Anaplastic Oligodendrogliomas, Non-classic Glioblastomas, Non-classic Anaplastic Oligodendrogliomas

The dataset what we have taken for experiments are based on the genome of diseased and normal tissue which has been truly generated by microarray (laboratory technology for mapping grey level intensity to real numbers) DNA database which is described in Table 1.

The cancer dataset which is described in Table 1 is fed to factor analysis to find the significant factor (latent variables) as 500. That means for colon dataset it finds from 62×2000 to 62×500 . After finding factor as unobserved variables it is passed to F-score method which again finds the discriminative feature by rank evaluation as described in Figs. 3 and 4. Which will lead to computation of 62×65 . But F-score method is applied to small round blue cell tumor with a dimension of 62×90 .

Performance of the proposed feature extraction method is tested with the neural network classifiers MLP. The leave-one-out-cross-validation (LOOCV) test or Jackknife test is applied and the result is being analyzed. We can apply fivefold or tenfold cross validation test (Tables 2 and 3).

Fig. 3 Description of discriminative gene selection using F-score method applied on colon dataset in matlab

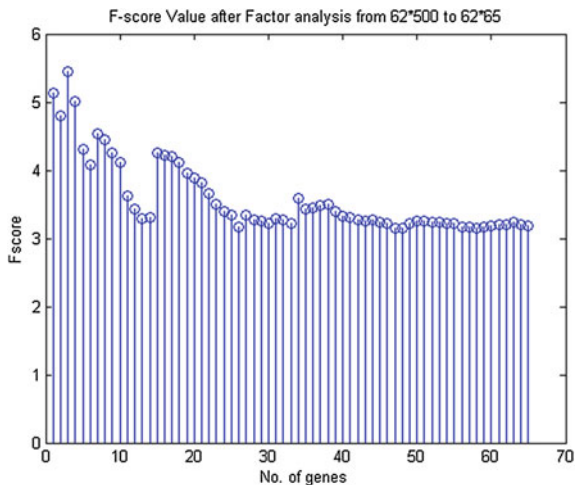


Fig. 4 Description of discriminative gene selection using F-score method applied on SRBCT dataset in matlab

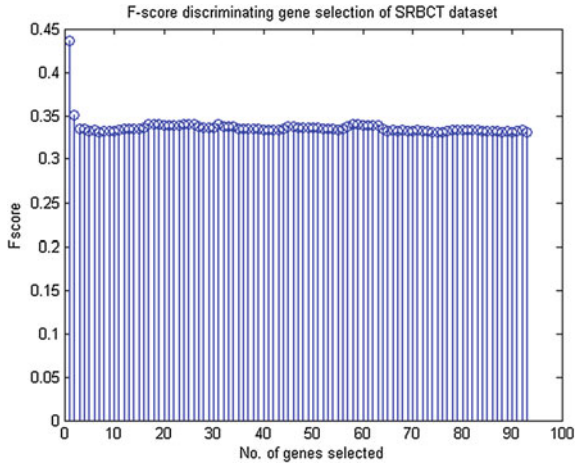


Table 2 Description of the classification accuracy

Methods	Classification accuracy (%)
Colon	98
SRBCT	96.68
Brain tumor	91

Table 3 Comparison study of accuracy of SRBCT dataset

Methods	Classification accuracy
SLDA	100 %
BWNN	96.83 %
C4.5	91.18 %
Bagboost	95.24 %
SVM	93.65 %
TPCR	100 %
Gradient LDA	100 %
Wavelet + F-score + RBFNN	97.59 %
Factor analysis + F-score + MLP	96.68 %
	Promising one

As supervised classification is a machine learning approach, the machine needs to be trained with the data samples, which are being retained after reduction using the proposed cascaded statistical approach. The accuracy may vary from dataset to dataset. The proposed method can be utilized for other types of dataset than genomic dataset, which will definitely give better result for those dataset.

Clustering of microarray cancer data has been implemented using k-means clustering method. Figure 5 explains the K-means clustering of colon data. Figure 6 explains the k-means cluster of small round blue cell tumor (SRBCT). In the similar way, brain tumor factor analysis followed by F-score value is being evaluated.

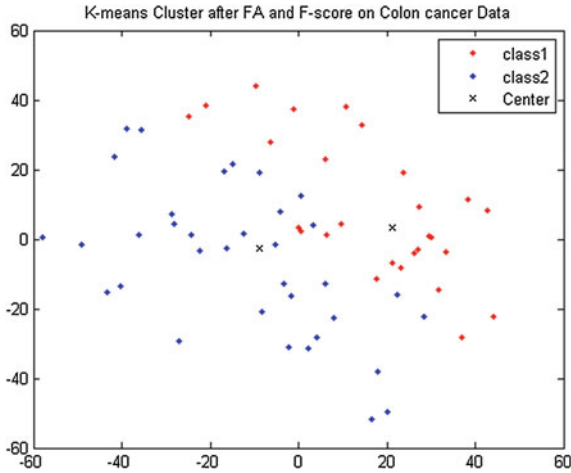


Fig. 5 Description of k-means clustering formation of Colon cancer dataset after the decomposition of factor analysis and F-score method from this very few are non-clustered

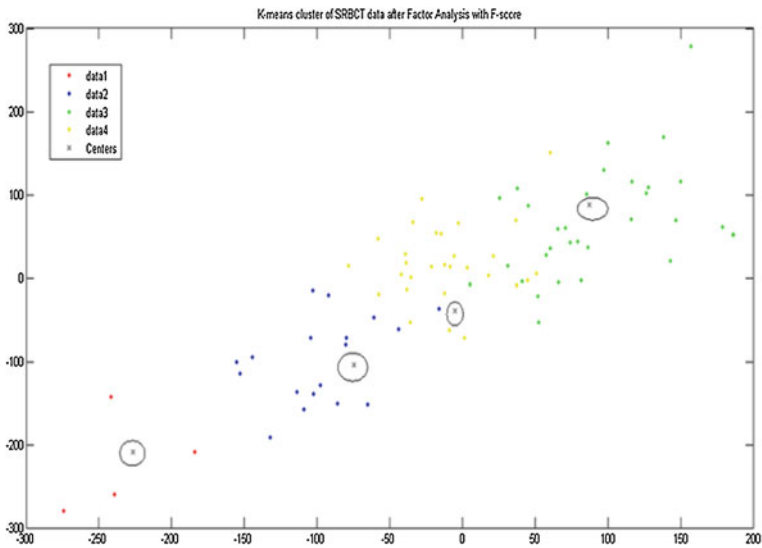


Fig. 6 Description of k-means clustering formation of SRBCT cancer dataset after the decomposition of factor analysis and F-score method describes very few are non-clustered

6 Conclusion

Modern era of scientific research demands laboratory to computational application and vice versa. But for any computation it requires an inherent mathematical model. The proposed method factor analysis with F-score method is a promising one and

works better in classification rather than clustering. Because in multilayer perceptron, the training of the pattern in the data is done with a number of iterations, which is again supervised so the accuracy rate is more. But in case of cluster formation it is based on the closer distance from the centroid to its input signal, which is unsupervised so the input signal are scattered or few are non-clustered. The proposed method can be utilized for other types of dataset than genomic dataset which will definitely give better result for those dataset.

References

1. Golub TR, Slonim DK, Tamayo P, Huard C, Gaasenbeek M, Mesirov JP, Coller H, Loh ML, Downing JR, Caligiuri MA, Bloomfield CD, Lander ES. Molecular classification of cancer: Class discovery and class prediction by gene expression monitoring. *Science*. 1999;286(5439):531–7.
2. Barik RC, Naik B. A novel feature extraction and classification technique for machine learning using time series and statistical approach. In: *Proceeding in Springer “Smart, Innovation and Technologies” Computational Intelligence in Data Mining*, vol-3, 2014.
3. Huang M. Sch. of Biomed. Eng., Southern Med. Univ., Guangzhou, China; Yang W, Wu Y, Jiang J. Brain tumor segmentation based on local independent projection-based classification. *IEEE Trans Biomed Eng* 2014;61 10:2633–45.
4. Maji P, Paul S. Rough set based maximum relevance-maximum significance criterion and Gene selection from microarray data. *Int J Approximate Reasoning Elsevier*. 2011;52(3): 408–26.
5. Wu C-H, Kuo B-C, Tzeng G-H Factor analysis as the feature selection method in an Emotion Norm Database. In: *Springer Proceeding Intelligent Information and Database Systems*, vol. 8398; 2014 p. 332–341.
6. Sahu SS, Panda G, Barik RC. Cancer classification using microarray gene expression data: approached using wavelet transform and f-score method. In: *International conference on electronic systems (ICES-2011)*, Orissa, India: NIT Rourkela, 07–09 Jan 2011.
7. Yang X, Jia L, Qingmao H, Zhijun C. F-score feature selection method may improve texture-based liver segmentation strategies. In: *IEEE International Symposium on IT in Medicine and Education 2008*.
8. Haykin S. *Neural networks: a comprehensive foundation*, 2nd edn. New York: Pearson Education Asia; 2002.
9. Hagan MT, Demuth HB, Beale M. *Neural Network Design*. Singapore: Thomson Asia Pte. Ltd; 2002.
10. Tatiraju S, Mehta A. *Image segmentation using k-means clustering, EM and normalized cuts*. Irvine: University of California.
11. Kanungo T, Mount DM, Netanyahu NS, Piatko CD, Silverman R, Wu AY. An efficient k-means clustering algorithm: analysis and implementation. *IEEE Trans Pattern Anal Mach Intell* 2002;24 7:881–92.

Planar Crossover Using Microstrip Patch Antenna for Beamforming Networks

Mirav Mehta, K.A. Naveen, Vishnu Rajan, Rahul R. Pillai
and Sreedevi K. Menon

Abstract In this paper, a simple planar design for a symmetric four-port crossover is presented. The proposed crossover is derived from a microstrip patch antenna with a set of two orthogonal feeds. Electrical length of the microstrip patch antenna is increased by incorporating slots achieving a frequency shift to the lower side. The slot in the patch antenna is derived from fractal geometry, which allows three stages of iteration. Isolation better than -15 dB and transmission ~ 0 dB is observed in the frequency range of interest. The proposed crossover is a potential candidate for Butler matrix in beamforming applications.

Keywords Crossover · Microstrip components · Sierpinski carpet · Four port devices · Butler matrix · Beamforming

1 Introduction

In an integrated circuit, at high frequency signal, integrity is lost when two signal lines crosses path. Crossover takes place when two transmission lines overlap each other which lead to signal interference. In ideal cases, a given signal is completely received at the output port without any loss. The purity of the signal given to input port of transmission line is lost at output port due to overlapped transmission line. Usually, crossovers are implemented using vias [1] and air wedges [2]. These structures are 3D and consume large volume. To overcome this, planar structures like microstrip patch is used reducing the complexity, improving more isolation, and returns loss giving better performance [3]. Coplanar and microstrip lines are found to be effective as crossovers [3, 4]; moreover, microstrip antenna has been

M. Mehta (✉) · K.A. Naveen · V. Rajan · R.R. Pillai · S.K. Menon
Amrita Vishwa Vidyapeetham, Amritapuri, Kollam 690525, India
e-mail: mirav.mailme@gmail.com

S.K. Menon
e-mail: sreedevikmenon@amritapuri.amrita.edu

effectively used as a crossover [5]. Different approaches for efficient crossovers has been reported [6, 7] which usually leads to the complexity of the system. Recently, a patch antenna with four ports is used with adjacent ports perpendicular to each other as suggested by Henin et al. [3]. This crossover provides good isolation and transmission characteristics.

Crossing over of transmission lines is a major issue in beamforming networks. This is overcome by using Butler matrix [3] which is a key component of the beamforming networks. Butler matrix consists of two or more crossover circuits depending on the number of elements in the phased array network.

In this paper, microstrip patch-based crossover as mentioned in [3] is further modified using Sierpinski carpet to improve the isolation. Three iteration of Sierpinski is analysed and results are discussed in following sections.

2 Square Patch Crossover

The crossover design consists of one square patch with four microstrip lines on the top of the substrate. These microstrip lines which are feeding networks are arranged in such a way that the alternate feeding microstrip lines are parallel to each other. The bottom part of the substrate represents the ground plane. The geometry of the microstrip crossover is shown in Fig. 1.

The patch dimensions is calculated using:

$$f_o = \frac{c}{2l\sqrt{\epsilon_r}}$$

l is length of the patch, c is speed of light, and ϵ_r is the relative permittivity of the substrate. The patch antenna is designed to give orthogonal resonance TM_{010} and TM_{100} at same frequency making the adjacent ports isolated. For a crossover with $L = W = 30$ mm on a material with dielectric constant $\epsilon_r = 4.4$ and thickness $h = 1.6$ mm, the S -parameter variation using a 50Ω microstrip line is shown in Fig. 2. The proposed crossover is Symmetric and reciprocal giving: $S_{11} = S_{22} = S_{33} = S_{44}$, $S_{13} = S_{24}$, and $S_{12} = S_{34}$.

Fig. 1 Square microstrip patch crossover

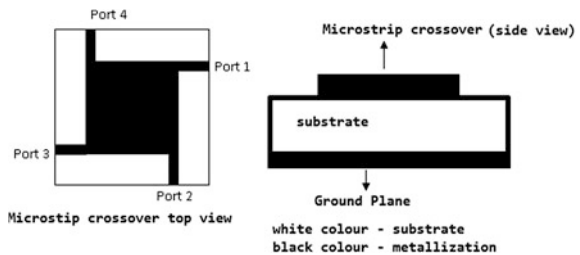
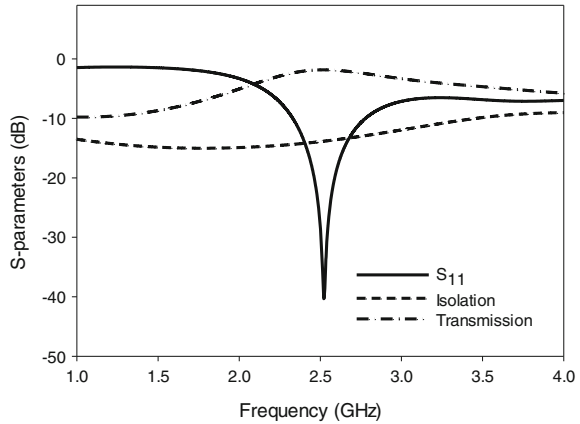


Fig. 2 S parameters of the square patch crossover



The results obtained confirm the utility of the discussed design as an efficient crossover. By varying the length of the patch dielectric constant, the simple square microstrip patch can be used as a crossover for beamforming networks.

In the design discussed, the resonant frequency of the crossover is in inverse proportion with half the guided wavelength. So, for low-frequency applications a large area for crossover is needed. This makes the system very large and can affect the performance of the other components. For obtaining a crossover at lower frequency with less area, a high dielectric constant of the substrate should be considered. As the dielectric constant increases, the losses associated will also increase [8] thus reducing the received power at the through ports.

In the next section, planar crossover is realized at low frequency without altering the dielectric constant of the base geometry.

3 Crossover Using Sierpinski Carpet Fractals

The microstrip crossover is modified to form circular fractal pattern over the patch. Initially, a circular slot of radius ' r ' equal to $L/6$ is etched at the center of the square patch. This gives an additional current path for the signal thus increasing the electrical length shifting the frequency toward the lower side. Further, circular slots with radius ' $r/3$ ' are etched on the square patch as shown in Fig. 3.

These form fractal iterations which are as follows:

$$A_n = (0.888)^n$$

$$N_n = 8^n$$

$$R_n = (0.333)^n$$

Fig. 3 Crossover with circular fractal

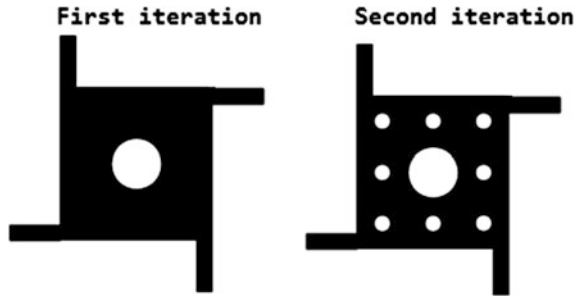


Fig. 4 S parameters of the first order Sierpinski crossover

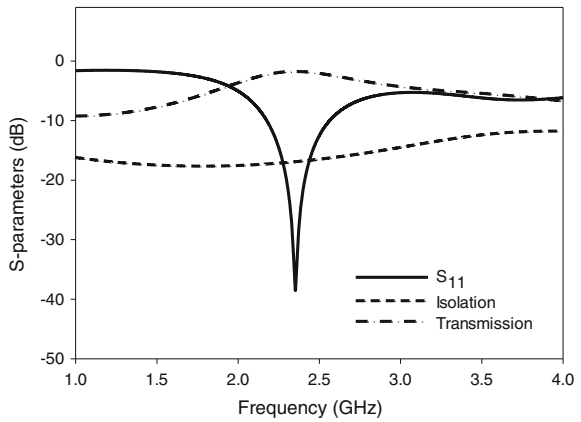
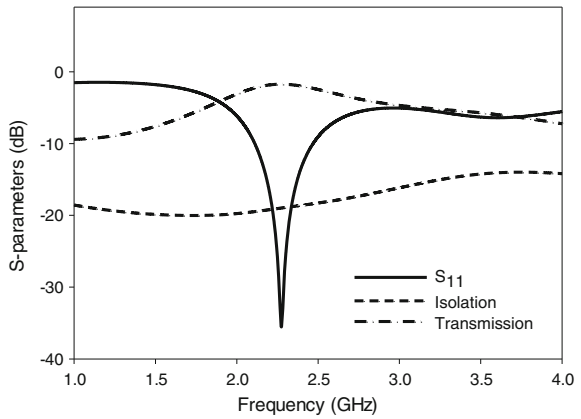


Fig. 5 S parameters of the second order Sierpinski crossover



N_n is the number of black boxes, R_n is the ratio of the radius, and A_n is the ratio for the fractional area after n th iteration [8]. Iterations are initialized without changing the physical structure and orientation by drawing circles from original patch with a factor of one-third. The S-parameters for two iterations are plotted in Figs. 4 and 5.

The crossover characteristics are obtained with a shift in frequency toward the lower side. The circular slots in the Sierpinski fractal acts as inductive elements increasing the current path along the patch with an increase in the effective resonating length. Hence, crossover with fractal slots can be used for a better design as it lowers the resonant frequency. The slots in the microstrip patch are found to shift the resonant frequency to lower side as the effective length increases. For the first iteration of the circular fractal an area reduction of 23 % is achieved, while for second iteration 30 % area reduction is achieved at 2.45 GHz.

4 Conclusion

Planar crossover with Sierpinski carpet on a microstrip patch is presented. The crossover up to two iterations for the fractal is studied. The isolation is found to be better than -20 dB and insertion loss is found better than -1 dB. The fractal geometry is found to give better performance with a frequency shift to lower sides of crossover with fractal slots, which can be used for a better design as it lowers the resonant frequency. Thus, rather than using a patch of larger dimension a smaller patch with fractals and appreciably high dielectric constant can lead to an effective in providing isolation between adjacent ports and transmission between orthogonal ports.

Acknowledgments The project is partially funded by a grant from Information Technology Research Agency (ITRA)-Department of Electronics and Information Technology (Deity), Government of India.

References

1. Chen Y, Poo S-P. A symmetrical 4 port network microstrip coupler for crossover application: *IEEE Trans Microwave Theory Tech.* 2007;55(11):2434–38.
2. Yao J, Lee C, Yeo SP. Microstrip branch-line couplers for crossover application. *IEEE Trans Microwave Theory Tech.* 2011;59(1):2227–2232.
3. Henin B, Abbosh A. Design of compact planar crossover using Sierpinski carpet microstrip patch. *IET Microwaves, Antenna Propag.* 2013;7(1):54–60.
4. Abbosh A, Ibrahim S, Karim M. Ultra-wideband crossover using microstrip-to-coplanar waveguide transition: progress in electromagnetics research, (PIERS-C); 2012.
5. Zhang XY, Guo Q-Y, Wang K-X, Hu B-J, Zhang H-L. Compact filtering crossover using stub-loaded ring resonator. *IEEE Microwave Wirel Compon Lett.* 2014;24(5):327–9.
6. Kusiek A, Marynowski W, Mazur J. Design of a broadband microstrip crossover for ultra-wideband applications. *Micro Opt. Tech. Lett.* 2010;52(5):1100–4.
7. Liu W, Zhang Z, Feng Z, Iskander M. A compact wideband microstrip crossover. *IEEE Microwave Wirel Compon Lett.* 2012;22(5):254–6.
8. Balanis CA. *Antenna theory analysis and design*, 2nd edn. New York: Wiley.

Energy-Efficient Communication in Wireless Sensor Network for Precision Farming

T.V. Aneeth and R. Jayabarathi

Abstract Wireless sensor network is a modern technology used for remotely monitoring the agricultural farms. Sensor network with sensor such as moisture sensor, temperature sensor, and humidity sensor can be used for control of the farm's moisture, temperature, humidity either manually or automatically. In this paper simulation is performed by placing the sensor nodes at various locations in the square-shaped one hectare area. Simulation is performed on four different topologies, namely random, cluster, star with gateway inside, star with gateway outside and the performance of the system is compared for all the four topologies and suitable topologies are proposed for the system. In the selected topology a communication technique is proposed for irrigation application showing the energy efficiency of sensor network. In this application, wireless sensor network uses IEEE 802.15.4/Zigbee communication standard for the topology study. In the selected topology, ad hoc on demand distance vector and dynamic source routing protocol are implemented in star topology with gateway at centre to determine the energy-efficient network.

Keywords Wireless · Sensor network · Topology · Irrigation · Zigbee communication · Routing protocol · Energy-efficient network

1 Introduction

Wireless sensor network is a fast growing research area which has seen a tremendous technological advancement with the latest development in low-cost sensor devices equipped with wireless network interfaces. The creation of sensor

T.V. Aneeth (✉) · R. Jayabarathi
Electrical and Electronics Engineering, Amrita School of Engineering, Coimbatore, India
e-mail: aneethvasu@gmail.com

R. Jayabarathi
e-mail: r_jayabarathi@cb.amrita.edu

network with the large number of sensor nodes has many technical challenges and also it has many application possibilities. Sensor networks find their application in different areas and it includes domain such as process management, health care monitoring, environment monitoring, industrial monitoring and military surveillance. A typical sensor network may have sensor node from a few to few hundreds or few thousands.

The key technical challenges in wireless sensor network is the design of energy-efficient protocols, design of protocol that deals with the scalability of network to large number of nodes, design of data handling technique and development of exciting new application that exploit the potential of wireless sensor networks. Precision agriculture or precision farming is site-based agriculture method which uses new advance method of observation and measurement for the improvement of the agriculture. It employs advanced technical help for better utilization of resource. Water is one of the important resource constraints in agriculture. Wireless sensor network can be used for remotely monitoring the farm. From the farm, different types of data can be sensed using sensor which can be used for improvising the yield from the agriculture land.

The sensor network will be energy efficient if the node placement and networks data routing protocol are selected in the best suited way for communication for the given application. There are some standard routing protocols already in sensor network, which are suited in different application scenarios. Sometimes routing protocol should be slightly modified to get the desired result. Standard ad hoc on demand distance vector (AODV) routing protocol and Dynamic Source Routing (DSR) protocol are compared in this work.

Gutiérrez et al. in 2014 [1] developed automatic irrigation system using wireless sensor network and GPRS module, which was cost-effective and feasible for water optimizing in agriculture. Keshtgary and Deljoo [2] has simulated the wireless sensor network for grid topologies and compared with the performance metric like throughput, load and delay. An efficient wireless sensor network grid topology and random topology are implemented in Wi-fi network [3]. There are many simulation tools which can be used for simulating like NS-2, NS-3, OMNET++, NetSim, Opnet, etc. In this paper, the simulation is done using Opnet for comparing the topology and to study the routing protocol. In this paper, Sect. 2 deals with node placement and Sect. 3 deals with the routing protocol. Section 4 concludes this paper.

2 Node Placement

In wireless sensor network, node deployment pattern makes a good impact on its working of nodes. Sensor node can be randomly deployed or placed in precise location based on the application scenario. For application like remote monitoring of agriculture, sensor node can be placed directly by the human on the field. Depending on the data to be sensed the sensor node can be placed. If the sensor nodes in wireless sensor network are densely deployed, then a single sensor node

will be having many neighbours to which direct communication would be possible when using sufficient transmission power. But this will not be beneficial, because long-range transmission would consume more power and more number of neighbours will add the burden to the Medium Access Control (MAC) protocol. The routing protocol will suffer from volatility in the network if the node positions are changing and frequently creating and breaking many links.

To overcome this problem, topology control should be applied. In topology control main idea is to control the set of nodes that are considered neighbours to a node. In some case, topology control can be done by manually placing the set of nodes to be considered as neighbours. Topology control can also be done by controlling the transmission power, by creating hierarchies in network or cluster formation, etc.

Some of the network topologies which are used are star topology, mesh topology, ring topology, bus topology. Depending on the communication technology used and requirement of the system network, topology is considered. Sometimes a hybrid topology will be best option in some of the scenarios.

2.1 Methodology

Case study for node deployment in precision farming land with dimension $100\text{ m} \times 100\text{ m}$ is considered. Twenty nodes have been used as sensing node and one node has been used as a gateway node. The sensor nodes are assumed to be nodes which sense moisture content of soil. When the moisture content of soil is below the threshold limit set for a crop the sensing node should transmit the information to the gateway node. The gateway node has to pass the information to irrigation valve controlling system. The information which is to be passed to the controlling station will be data about soil's moisture content or temperature, etc. Since the data bandwidth requirement is less it is better to go for low power low-cost wireless standard to form the personal area network. A standard way of node deployment cannot be possible in all practical scenarios because the entire farmer will not be having agriculture land in standard shape and size. So depending on the agriculture land the wireless sensor network suited will differ. Using OPNET simulation tool the Personal Area Network (PAN) can be created. The low power PAN has been created using Zigbee which uses IEEE 802.15.4 standard for the medium access control layer. The star topology with WLAN (Wireless Local Area Network) is considered for the comparison of the AODV and DSR routing protocols. Using the performance metrics route discovery time, the routing protocol is compared.

2.2 System Model

In wireless sensor network a variety of topology have been developed and each scenario has its own advantages and disadvantages. In this paper OPNET simulation tool is used to study four topologies. Four topologies are random, cluster, star with gateway outside and star topology with centred gateway. Figure 1 shows the node deployment pattern of the four topologies mentioned.

In the scenarios considered, there are 20 sensing nodes and a gateway node is placed in the area of 1 Hectare. Figure 2 shows the node placed in a random way. In random topology the sensor node senses the information from the environment, and if it detects the event then the information has to be transmitted to the gateway node. The sensor node can send the information to any neighbour node which is in range. Finally, the information should reach to the gateway node.

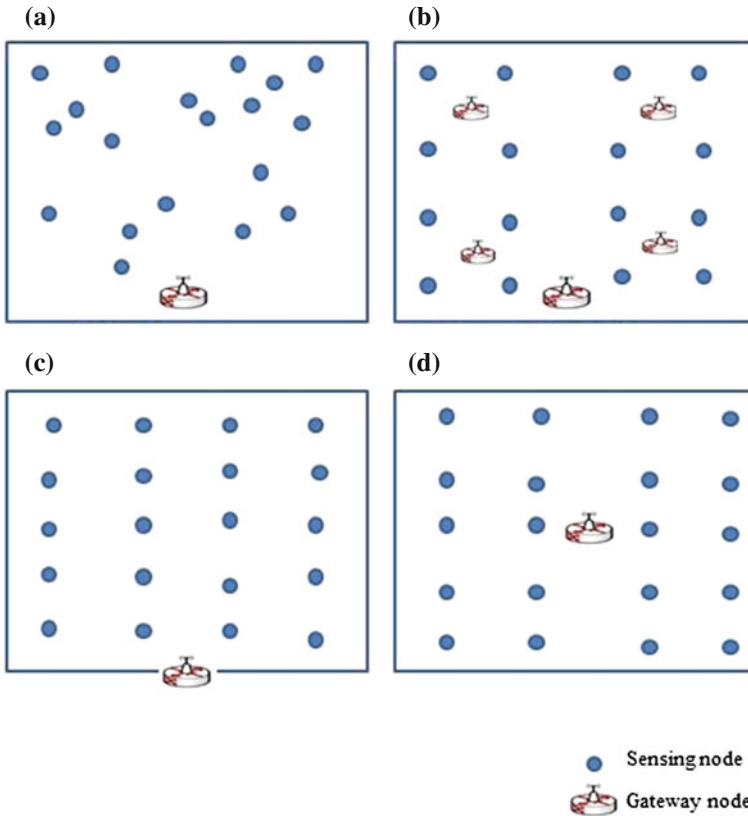
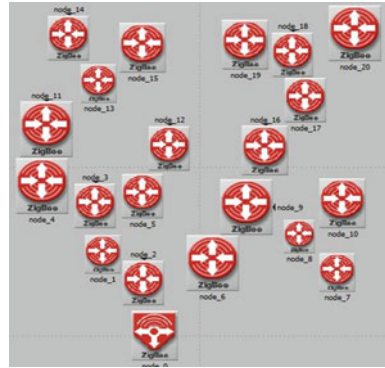


Fig. 1 Network topologies. **a** Random, **b** cluster head topology, **c** star topology with gateway outside, **d** star topology with gateway at centre

Fig. 2 Random topology implemented in OPNET



Second scenario cluster topology considered is shown in Fig. 3. In this, there are four clusters formed in the same farm, each cluster group is of five sensor node with the cluster head as the centre node among the group. In the figure shown, the node 3, node 8, node 13, node 18 are cluster heads and these heads will collect the information from the four sensor nodes of corresponding cluster and then transmit to the gateway node.

Third scenario considered is a star topology with gateway outside as shown in Fig. 4. In this case, all sensor nodes are directly connected to the gateway node. These entire sensor nodes are placed in approximately equal distance from each other.

Fourth topology considered is star topology with the gateway node in the centre of the field as shown in Fig. 5. In this network also all the sensor nodes have to directly communicate to the gateway node.

The node placement for routing protocol comparison is done as explained for the star topology with gateway outside. In this network the route discovery and route maintenance from source to destination is done by the corresponding routing

Fig. 3 Cluster topology implemented in OPNET

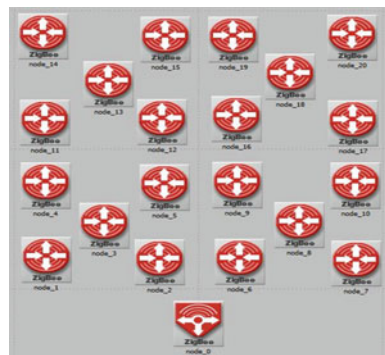


Fig. 4 Star topology with gateway outside implemented in OPNET



Fig. 5 Star topology with gateway at centre implemented in OPNET



protocol. In the same topology, the route discovery time for both scenarios are compared.

2.3 Simulation Results of Topology Comparison

The simulation results are shown for all four topologies. The topologies are compared using a set of performance metrics like MAC throughput, MAC load and application end-to-end delay. Many other performance metrics can be compared using the OPNET software. The definition of the performance metrics used for the comparison of the topologies are:

- MAC throughput: Represents the total number of bits (in bits/s) forwarded from 802.15.4 MAC to higher layer in all WPAN nodes of the network.
- MAC load: Represents the total load (in bits/s) submitted to 802.15.4 by all higher layer to all WPAN nodes of the network.

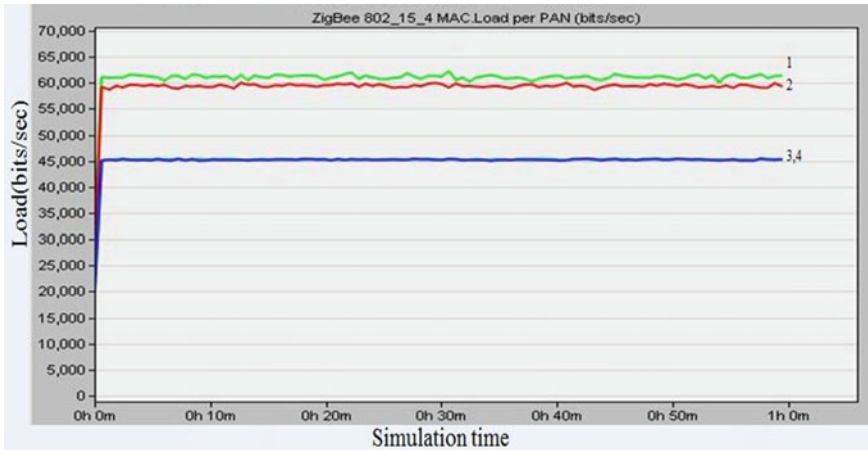


Fig. 6 MAC load

- Application end-to-end delay: Total delay between creation and reception of an application packet.

MAC load for all the four topologies has been shown in Fig. 6. From the figure it is found that load for both star topologies are less than the load of cluster topology and random topology. Random topology has the highest load among all four topologies.

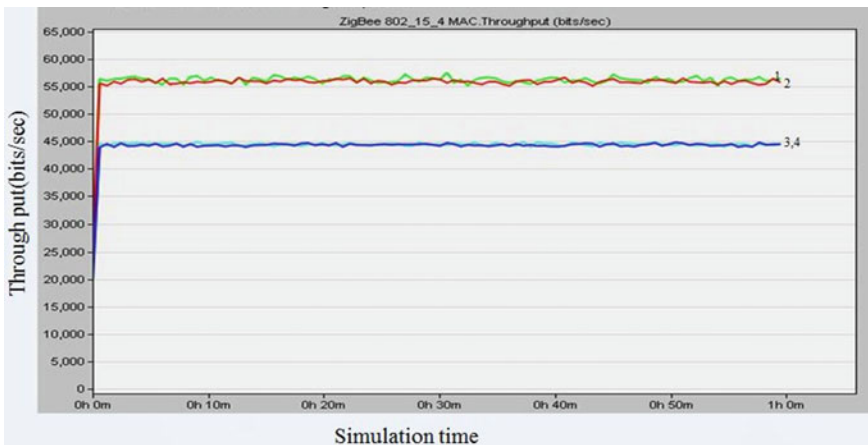


Fig. 7 MAC throughput

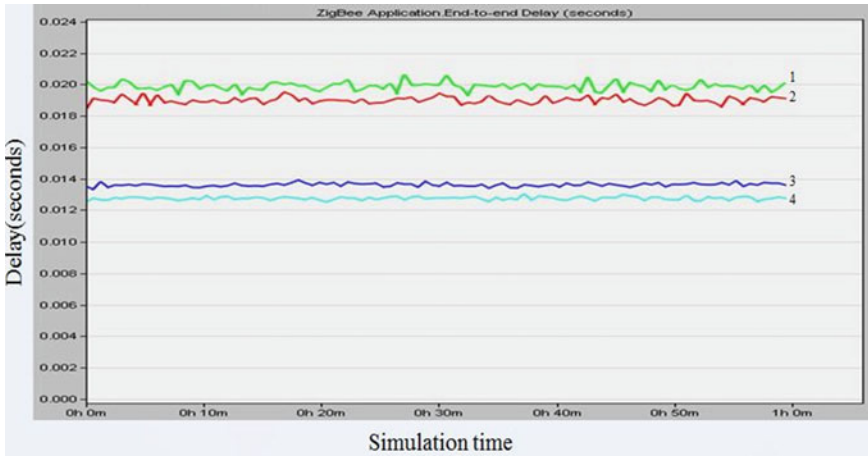


Fig. 8 Application end-to-end delay

Table 1 Performance metrics of topologies compared

Topology	Average MAC load (bits/s)	Average MAC throughput (bits/s)	Average delay (s)
Random	60,500	56,000	0.02
Cluster	58,250	55,000	0.19
Star with gateway outside	45,000	43,250	0.0136
Star with gateway inside	45,000	43,750	0.0128

MAC throughput remains same as that of MAC load for star topologies as shown in Fig. 7. The throughput random topology and cluster topology are more than the throughput of the star topologies.

Application end-to-end delay for the four topologies is shown in Fig. 8. From the figure it is clear that the star topology with gateway node placed in the centre of the sensor node has the lowest application end-to-end delay. The star topology with gateway outside has slightly more delay than star topology with centred gateway. The average values of performance metrics of topologies are listed in Table 1.

In the simulation graph drawn green coloured denoted by 1 is representing random topology, red coloured line denoted with 2 is for clustered topology, light blue denoted with 3 is for star topology with gateway outside and blue coloured graph line denoted with 4 represent star topology with gateway at the centre. The simulation time is 60 min. Data packet size of 1024 bits was generated using constant distribution with mean value of 1 s as the packet inter-arrival time. In the simulation, all the sensor nodes of the four topologies were assigned same distribution for event generation and inter-arrival time.

3 Routing Protocol

The star topology with gateway outside is considered for the routing protocol study. DSR and AODV are demand-driven protocol. In demand-driven routing protocols the route discovery is used to find the active routes between sender and receiver. Route discovery is done by flooding the network with route request and receiving route response. DSR uses route discovery and route maintenance process. AODV uses route discovery and route maintenance from the DSR and hop-by-hop routing, periodic addressing, and sequence numbering from the Destination Sequenced Distance Vector (DSDV) routing protocol. In the scenarios where the nodes are less mobile, the DSR performance is better than the AODV as route to the destination is found quickly in DSR. If the nodes are mobile, then AODV would give better performance than the DSR. DSR has less routing overhead than AODV. In the agriculture monitoring application the nodes are less mobile, so it will be better to use DSR routing protocol than the AODV standard. In most of the low power agricultural monitoring wireless sensor network, Zigbee has been used for communication. Zigbee has Zigbee stack over IEEE 802.15.4, and in Zigbee stack AODV protocol is used.

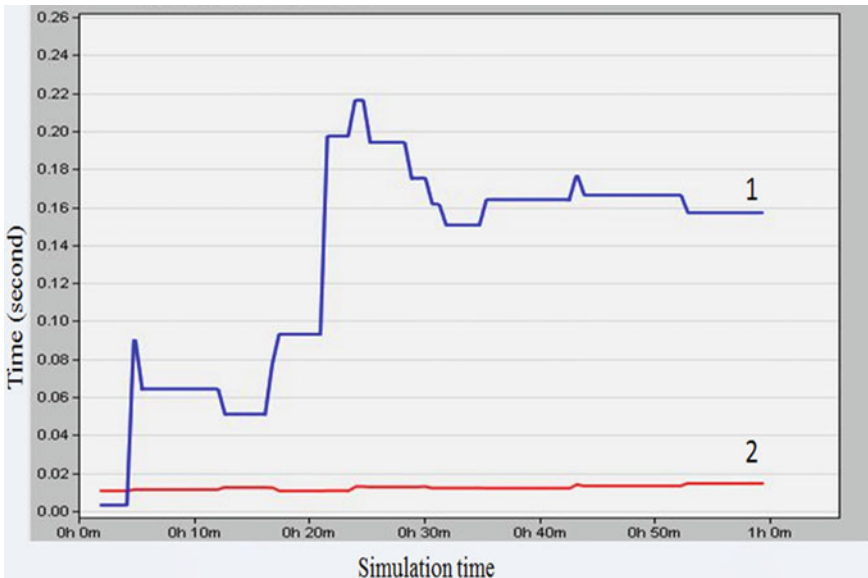


Fig. 9 Route discovery time for AODV and DSR

3.1 Simulation Result of Routing Protocols

Route discovery time The time to discover a route to a specific destination is the time when a route request was sent out to discover a route to that destination until the time a route reply is received with a route to that destination. This statistic represents the time to discover a route to a specific destination.

The route discovery time taken by AODV and DSR protocols are shown in Fig. 9. In simulation graph blue coloured line shown with 1 is showing the route discovery time of AODV protocol and red coloured line shown with 2 is showing the route discovery time of DSR. From the figure it is proved that for sensor network with fixed nodes DSR protocol will perform better than AODV.

4 Conclusions

The paper has highlighted the use of Zigbee wireless technology in four different topologies for farm monitoring. In this paper low-cost, low power consuming Zigbee standard/IEEE 802.15.4 has been used for the simulation. The sensor node has been placed in different topologies like random, cluster, star with gateway outside and star with gateway inside to form wireless sensor network. When application end-to-end delay is used, both star topologies are providing better performance than other two topologies. Star topologies are maintaining approximately same MAC load and MAC throughput for the simulated duration. But random topology and cluster topology give better MAC load and MAC throughput value than star topologies.

Depending on the size of the field, the vegetation type, the agronomist can be consulted for knowing the idea of placement of the sensor in the farm. Then the network topology can selected depending on the requirements from the wireless sensor network deployed.

The two protocol implemented in the work are DSR and AODV protocol. Since DSR protocol has less routing overhead than AODV, implementing DSR protocol stack over the IEEE 802.15.4 standard will reduce the energy consumption of the sensor network for this type of application.

The hardware implementations of DSR protocol over the IEEE 802.15.4 standard are being carried out for wireless sensor network application.

References

1. Gutiérrez J, Villa-Medina JF, Nieto-Garibay A, Porta-Gandara MA. Automated irrigation system using a wireless sensor network and GPRS module. IEEE Trans Instrum Meas. 2014;63(1):166–76.

2. Keshtgary M, Deljoo A. A wireless sensor network solution for precision agriculture based on Zigbee Technology. *Wireless Sens Netw.* 2012;04(1):25–30.
3. Keshtgary M, Deljoo A. An efficient wireless sensor network for precision agriculture. *Canadian J Multimedia Wireless Netw.* 2012;3(1):1–5.

Design and Evaluation of 3D NoC Routers with Quality-of-Service (QoS) Mechanism for Multi-core Systems

Pournamy Mohan and K. Somasundaram

Abstract The importance of on-chip communication interconnects was greatly highlighted with the advent of semiconductor technology at nanoscale domain. As the sizes of semiconductor features are reduced day by day, there occurred problems related to wiring. Network-on-Chip architectures are therefore implemented to overcome the wiring issues and have lately been considered as an important area for research. The communication on NoC is carried out in specific topologies by means of routers. In this paper, Partial Mesh of Grid topology (PMG) is considered. We use the Quality of Service (QoS) mechanism to minimize the area and power. PMG-based NoC will give minimum area and power and it reduces the high chances of redundant connections. Throughput and latency are analysed along with other parameters like packet loss ratio and jitter using network simulator NS-2. Area and power analyses are done using Synopsys Design Compiler and PrimeTime PX tool. Our experimental results show that the architecture with QoS mechanism gives a significant reduction in area and power when compared to Region-based Routing (RBR) mechanism. Moreover, the partial mesh of grid topology gives minimal latency and high throughput when compared to mesh of grid topology.

Keywords Partial mesh of grid · Quality-of-Service · Latency · Throughput · Network-on-chip

P. Mohan (✉)

Department of ECE, Amrita School of Engineering,
Amrita Vishwa Vidyapeetham, Coimbatore 641112, India
e-mail: pournamy2124@gmail.com

K. Somasundaram

Department of Mathematics, Amrita School of Engineering,
Amrita Vishwa Vidyapeetham, Coimbatore 641112, India
e-mail: s_sundaram@cb.amrita.edu

© Springer India 2016

S.S. Dash et al. (eds.), *Artificial Intelligence and Evolutionary Computations in Engineering Systems*, Advances in Intelligent Systems and Computing 394, DOI 10.1007/978-81-322-2656-7_39

429

1 Introduction

To meet the enormous computation-related applications and the requirement for high-performance and low power devices, the amount of resources used for computation on a single on-chip system has massively increased because of the growth in VLSI technology which contains billions of transistors. System on Chip (SoC) at nanoscale domain involves the integration of hundreds of IP cores running numerous processes on a single chip simultaneously.

In the area where the number of cores present in a single SoC is more, the interconnect communication system needs to change significantly as it has to support the new inter-core communication subsystem demands. The interconnection between different IP cores becomes a challenging issue when more number of processing elements like DSP, special hardware circuits, memory blocks are added. Moreover, the global interconnects causes on chip synchronization errors, high power consumption and erratic intervals. On-chip communication thereby plays a vital role in a SoC.

For the communication between various IP cores in a single system on chip, there are mechanisms like bus-based architectures and point-to-point communication. The former had wiring delay problems in addition to bandwidth limitation, whereas the latter roused with scalability issues. In order to overcome such kinds of wired delays and to face the scalability problems in the coming days, there is a need to design and implement network-like interconnections called Network on Chip (NoC) architecture. Network on chip arises as the latest paradigm for communications within large VLSI systems. It is a communication subsystem used for the connection of several multi-core systems. NoCs prove as a promising solution in the future generation and is of great demand in the recent research thrust. NoC architecture consisting of on chip packet switched network better supports the integration of billions of transistors in a single system-on-chip.

NoC improves the scalability, bandwidth limitation and power efficiency of SoCs when compared to other kinds of design architectures. Since the number of cores in a NoC increases, there are high chances of congestion. Congestion while routing has become one of the most crucial factors in any NoC-related SoC. NoCs minimize the number of wires needed to route the data packet and also routing congestion is verified at the back end of the application process. NoC simplifies the complexity of the hardware necessary for routing making SoCs possible to work in a high-frequency environment. NoC has several links through which the data packets are passed from a source IP core to any destination IP core. By the usage of such kinds of communication which includes the insertion of routers in between each communication processing element, the required wiring delays can be minimized. Therefore, the router-based communication prevents scalability issues and provides freedom from the disadvantages of complex wiring. This new approach of NoC has a clear advantage over traditional busses and other communication processes.

Very few NoCs have been designed using silicon. Commercial providers on NoC technology are Arteris, Sonics, etc. Arteris is industry's first network on chip which is commercialised. It also had added advantage of functionality. Arteris Network on Chip (NoC) IP improve performances by reducing power consumption, size of the die and tight time market constraints of system on chip (SoC) devices for several applications mainly consumer electronics devices, automotive devices, mobile, etc. Arteris NoC interconnect communication system is being used in Samsung in its mobile phone applications, modems and processors for easy access and communication. This reduces the risks of IP compatibility. SonicsGN (SGN) is another on-chip network which allows enhanced SoC interconnection network design using a fabric topology of high speed which is also scalable. It is Sonics' fourth generation which is configurable. SGN technology communicates with the highest frequency available nowadays. The outputs delivered are high performance, simultaneous processing of applications for mobile video, smartphones and tablets. NetSpeed Systems also provides coherent, scalable IPs for NoCs to designers of system on chip for applications including networking and high performance-oriented computation.

A NoC has several data links connected with the help of routers in between through point-to-point interconnections. Routers are the back bone of network on chips. Messages can be transmitted from a particular source IP core to a destination IP core with the help of different links, by making routing decisions at each router. The signals are shared between the wires in the links contained in the NoC. As a result, the level of parallelism obtained is high as all links included in the NoC operates in parallel on various data sources.

1.1 Previous Works

The interconnection of different IP cores was possible with the help of specific topologies for various applications. The proposed work of Wang et al. [1] includes a QoS aware and congestion aware router architecture for a 2D Mesh network which is linked with diagonals. The diagonal links reduces the distance between the source and destination nodes and also minimizes the congestion. The problem that aroused was the limitations of a 2D topology which was not able to meet all the requirements necessary for the on-chip communication. In [2], a 3D recursive topology was proposed in which they proved that the topology is connected in Hamiltonian. Brugge et al. [3] proposed a Parameterizable NoC router for mesh topology. The probability of repeated connections and the complexity of the network were the problems faced in this proposed work. Viswanathan et al. [4] proposed different topologies for NoC, namely 3D Recursive Network Topology (3D RNT) and the results were analysed with fully and partially connected mesh topologies. The paper also proves that the topology has a Hamiltonian connectivity. In [5], Ebrahimi et al. proposed a 3D NoC topology to reduce the number of hops

and thus minimize the consumption of power. In [6], an exploration methodology of alternative 3D NoC architectures was presented. The significance of this methodology was to compare and find heterogeneous 3D NoC topologies with the incorporation of 2D, 3D routers and vertical link interconnection patterns that shows best performance to incoming traffic. Dubois et al. [7] proposed a non-regular heterogeneous 3D network topology where there are partially connected planar topologies linked together by only some vertical links in order to reduce the increased number of vertical link connections. In [8], longest linear array between any two distant nodes for interconnection topologies (Hamiltonian connected) was proposed in order to make the congestion and expansions equal to unity.

Palesi et al. [9] used a table-based switching approach that stores the output ports for reaching the destination switch. The main advantage of this approach is that the table is reconfigurable. The same design can be used for implementing any routing algorithm and topology. Mejia et al. [10] proposed a Region-based Routing mechanism for routing packets in 2D structures like meshes with faulty nodes. This consumes very less power and requires lesser area than the conventional method.

In this paper, we propose a Quality of Service (QoS) mechanism based router and is applied to a Partial Mesh of Grid (PMG) topology. We show that area and power is greatly reduced for the proposed work when compared to virtual channel router (VCR) with region based routing (RBR) mechanism. Also, PMG topology will enhance the network performance.

1.2 Basic Ideas

As the number of transistors integrated in a system-on-chip increases day by day, it is important to opt for Three-dimensional (3D) technologies. The disadvantages of on-chip communication with respect to 2D NoCs therefore needs to be overcome by the implementation of 3D NoCs. 3D technologies has different advantages including high packet density, high bandwidth, reduced power consumption, etc. In 3D systems, Through-Silicon Via (TSV) technology is used to implement communication links between different IP cores in the vertical direction. TSVs offers low cost and high interconnection density. The number of layers is not limited by any process, but thermal issues are likely to occur. Moreover, implementation of 3D NoCs require a lot of challenge including the idea of specific routing algorithms and to implement a router architecture for better network performance and to minimize deadlocks. 3D NoC Router with QoS and Congestion aware mechanism in a PMG Topology is proposed here, which when compared with other router architectures shows improved performance.

2 3-D NoC Router for PMG Topology

The topology for any NoC determines the overall cost of the network. The topology should be implemented in such a way that there is minimal hop count and that routing takes place effectively. In order for the packets to route from the source core to the destination core, the topology should be designed efficiently. Since the sizes of devices is shrinking to meet the area requirements, researchers opt more for three dimensional ICs. Such ICs shows higher performance even with increased number of transistors, high packing density, hop count, integration of both homogenous and heterogeneous IP blocks and dissipation of energy.

Hence for 3D ICs, a 3D NoC is to be implemented. An optimal 3D topology is characterized by different trade-off with regard to end-to-end delay, energy consumption, and limited vertical links. For a fully mesh of grid topology, all the links will be interconnected. Figure 1 shows a mesh of grid topology. This results in higher power consumption. A partial mesh of grid network consists of cores arranged in a grid format. Unlike mesh of grid network, the number of interconnections in this topology will be less. This 3D topology has several advantages in terms of latency and throughput. In addition, we can use different traffic patterns like Constant Bit Ratio (CBR) or Transmission Control Protocol (TCP) based on our requirement.

When a 3D mesh of grid topology is used for sending packets, this takes a longer route to send packets, as a result latency increases. In the case of a partial mesh of grid topology, the meshes are partially arranged one above the other and connected with the help of TSVs. Figure 2 depicts a PMG topology. These TSVs makes possible the transfer of packets between different layers of topology and this reduces the distance between the nodes. As a result the latency reduces. Jitter is measured by sending packets from two source nodes to a destination node.

Fig. 1 Mesh of grid topology

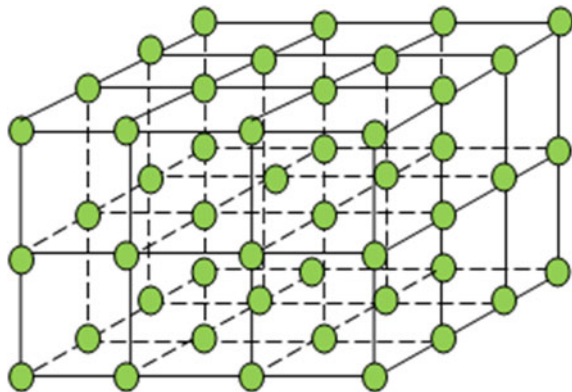
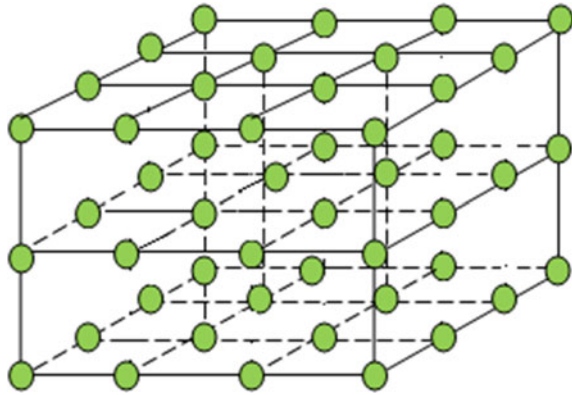


Fig. 2 Partial mesh of grid topology



2.1 Significance of Partial Mesh of Grid Topology

The main aim of designing a partial mesh of grid topology is that the interconnections will be less in number when compared to a fully mesh of grid topology. It thereby reduces the complexity of the network. Moreover the power consumption also gets reduced. The bandwidth performance for a PMG topology is also greatly improved when compared with a fully mesh of grid topology. The redundant connections are also less for this topology. In addition, a mesh topology can withstand high traffic. Even if one of the node fails there is always an alternative present. Therefore data transfer does not get affected. Expansion and modification in topology can be done without disrupting other nodes.

2.2 Partial Mesh of Grid Design

A partial mesh of grid network consists of $3 \times 4 \times 4$ cores arranged in a grid format and another similar layers above it forming a mesh of three layers. Initially, a mesh of grid topology was simulated using a network simulator NS-2 by implementing in TCL scripts. Routing algorithm, topology, applications and protocols are defined in the scripts by taking 48 nodes. In a mesh of grid topology, all the nodes are interconnected by links. Therefore, power consumption is high. Moreover it results in the design complexity also. The bandwidth considered here is 1 Mb and the propagation delay as 50 ms. Different traffic patterns can be used to send packets from a source to a destination. Here, we have used CBR that is, the payload is fixed and the packets are sent in a fixed rate. The traffic is connected to an agent. The agent taken here is User Datagram Protocol.

The following parameters are considered for a design of a mesh of grid topology with fully connected 48 nodes.

- Traffic Pattern: CBR
- Bandwidth of the link: 1 Mb
- Propagation Delay: 50 ms
- Agent: UDP

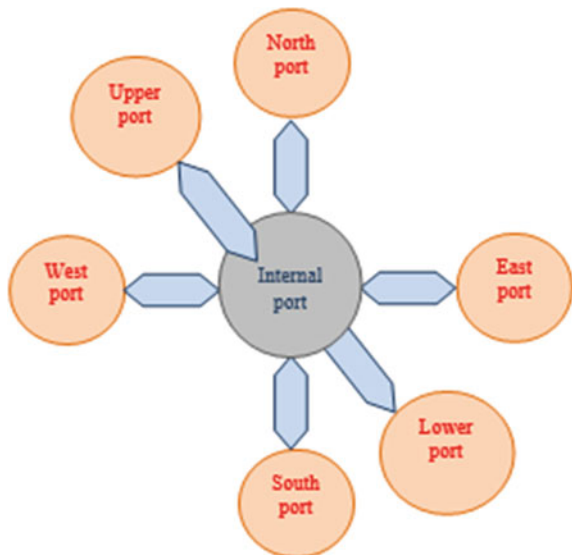
Similarly, for partial mesh of grid topology design, we considered the following with partially linked 48 nodes.

- Bandwidth of the link: 1 Mb
- Propagation delay: 50 ms
- Traffic Pattern: CBR
- Agent: UDP

2.3 Router Design with Loop Back Module

Router is based on a packet-based protocol whose main function is to route packets from source to destination. Here, we are using a seven port model router, that is it has ports in north, south, east, west, up and down directions. It also has a local port which is internal. Figure 3 shows a seven-port router model. Router sends the packet to the output port corresponding to the address contained in the packet. A packet is the basic unit of routing and the packet is divided into flits. Here the flit size used is 128 bits. A flit is the basic unit of bandwidth and storage allocation. Therefore, flits do not contain any routing or sequence information and have to follow the route for the whole packet. The packet is routed through networks

Fig. 3 Seven-port model



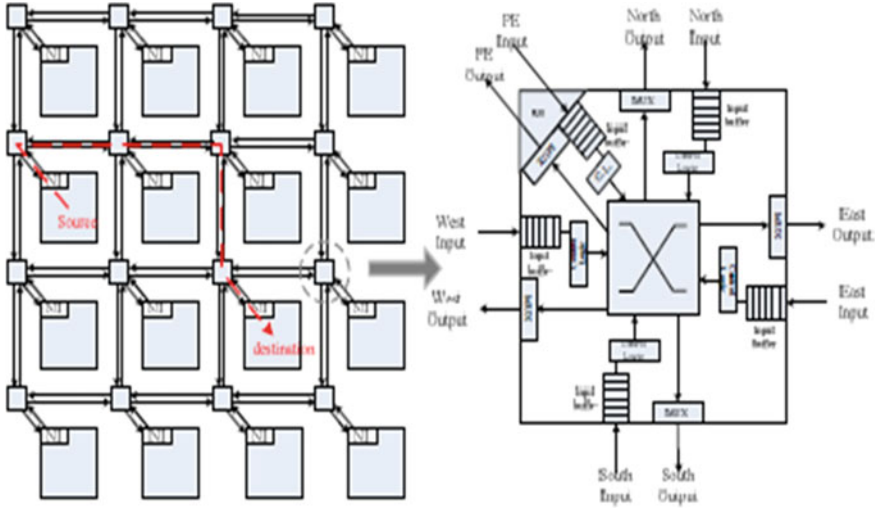


Fig. 4 NoC architecture and router design

depending on a routing strategy. The NoC router is based on shared-buffer architecture and has the advantage of ingress and egress bandwidth decoupling, and better performance as compared with input-buffer router architecture.

Figure 4 illustrates well-known 2D mesh NoC architecture of the size 4×4 . It consists of network interfaces (NI), routers and links. NI is the logic connection between the IP cores and the network. Links are used to connect two routers in a network. Routers are composed of input ports, output ports, switching matrix connecting input and output ports and a local port to connect the IP core to the router.

A loop back module is implemented in each of the ports of a router. The role of a loop back module is that when a processing element or IP emitter sends data packets to a destination IP, and at that point if a router is unavailable, then the data packets in the particular output port will be looped back and rerouted to the destination. This avoids data packets being trapped when a neighbouring switch is detected as permanently faulty, and reduces latency when a neighbour has suffered a dynamic reconfiguration. Figure 5 illustrates the loop back module architecture.

To transmit data packets, the control logic checks the availability of the neighbouring router. The buffer is connected to the data-out signal by means of a crossbar when no loopback mechanism is needed and the out signal made high. The multiplexer also connects the data in signal with the data in bus. The loop back module works when the adjacent router is unavailable or is faulty. At that time, the control logic will configure the semi-crossbar module to take the data packet into the data loopback bus. Therefore, the looped back data will be considered as a new packet. By activating the signal `occ_in`, it shows that the loop back mechanism is

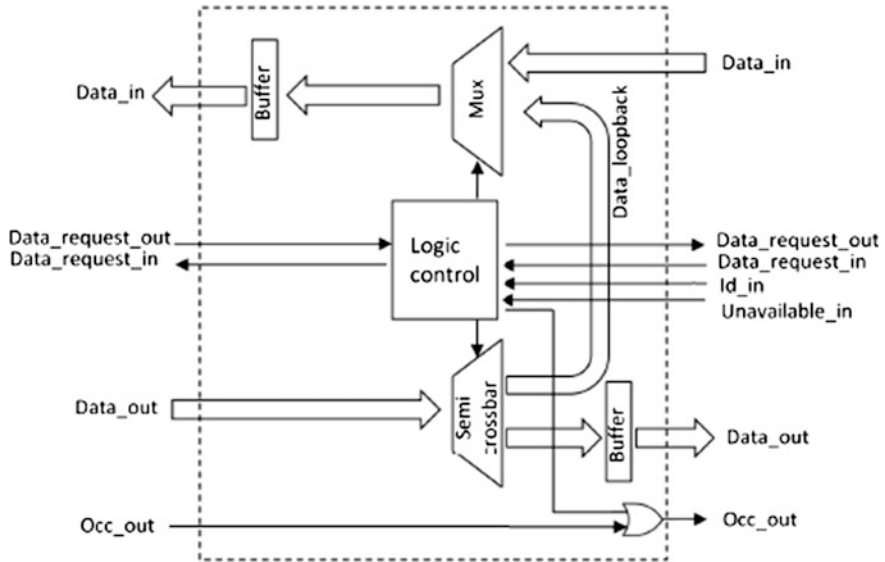


Fig. 5 Loop back module architecture

working and the reception of any other data packet from other switches will be avoided.

2.4 QoS Mechanism

QoS refers to the capability of a network to provide better service to selected network traffic over various technologies. By the incorporation of QoS, the network is assured with quality oriented transmission and also with an implementation cost which is feasible. By doing so, the traffic inside the network is balanced well and also the high traffic is moved to less congested areas. With such a mechanism, the constraints like area and power improves drastically. The cost overhead is also improved.

3 Experimental Results

Our experimental results for PMG are obtained using NS-2, a discrete event network simulator. It is implemented in C++ and TCL Scripts. NS-2 provides a convenient user interface and it includes the Network Animator (NAM), which visualizes the network operation in real time by tracking the data flow.

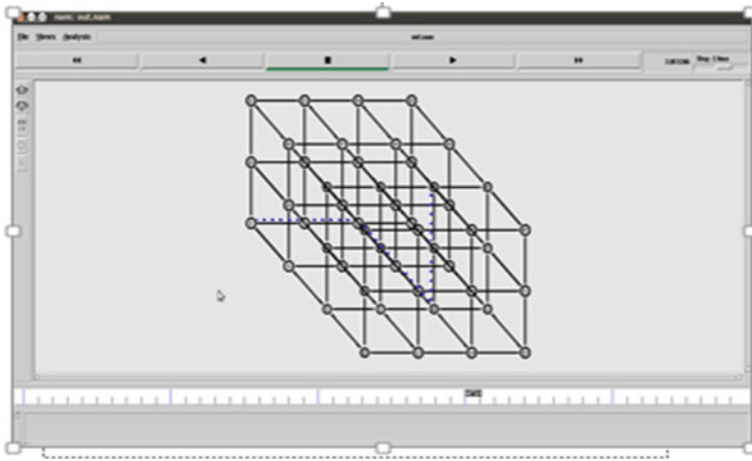


Fig. 6 Simulation result for a mesh of grid topology

Figure 6 shows the simulation result for a fully mesh of grid topology. The routing takes place from node 0 to node 41 as mentioned in the TCL scripts. Similarly in Fig. 7 the simulation for a partial mesh of grid topology is obtained. The same nodes are considered for routing in order to compare and analyse the parameters. Various parameters like throughput, latency and bandwidth are analyzed. Figure 8 shows the bandwidth obtained using X-Graph in NS tool.

Table 1 shows the various parameters for the simulation of PMG topology. For PMG, throughput is 88.31 kbps and the latency is 0.16200 s when sending packets from node 0 to node 41 with the bandwidth of the link being 1 Mb and the propagation of the link being 50 ms. Using the tool NS-2, we obtain the packet

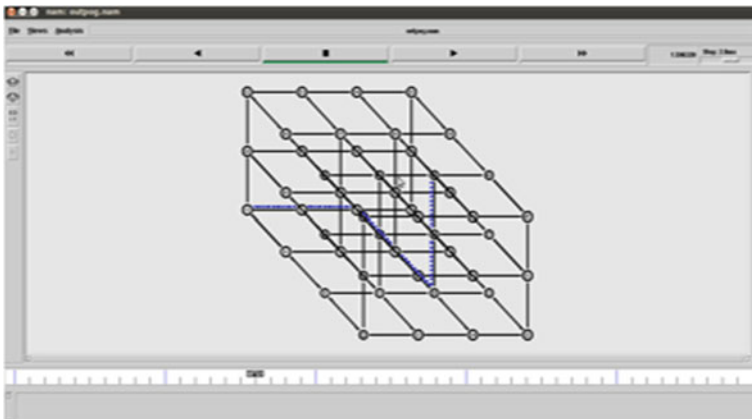


Fig. 7 Simulation result for a partial mesh of grid topology

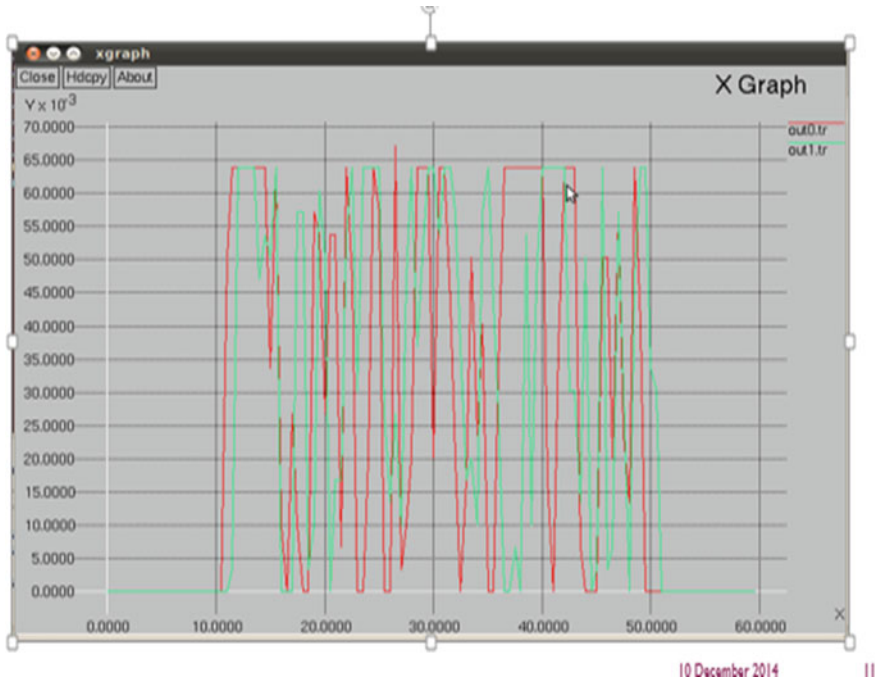


Fig. 8 Graph plotting the bandwidth

Table 1 NS-2 synthesis report

Parameter	Mesh of grid topology	Partial mesh of grid topology
Throughput (kbps)	72.09	88.31
End-to-end delay	0.18300 s	0.16200 s
Total energy	1000	500
No of packets sent	2403	2913
Jitter loss	0	0
Packet delivery ratio	0.9987	1.0009

delivery ratio which is 1.0009 s, jitter loss being 0 and the total energy consumed while sending packets. These results are tabulated and compared with a mesh of grid topology. We observe that there is an improvement in packet delivery ratio and latency using PMG than MoG topology. Moreover, the throughput also increases as the number of packets sent is more for a PMG in comparison with MoG.

Area and power analyses are calculated using Synopsys Design Compiler and PrimeTime- PX tool. Table 2 shows the area and power result analysis of a 3D router, 3D router with the incorporation of loop back module and 3D router with QoS mechanism. It clearly proves that the proposed 3D router with QoS mechanism shows a better performance in terms of both area and power. Table 3 shows the

Table 2 Area and power analysis

Cost metrics	3D router	Router with loop back module	3D router with QoS mechanism
Area (μm^2)	66256.030	102671.791	28673.13
Cell internal power (mW)	0.0240193	0.0127954	0.00218925
Net switching power (mW)	0.00547773	0.0038862	0.000661
Total dynamic power (mW)	0.00144771	0.00051816	0.000145

Table 3 Comparison of 3D router (QoS mechanism) with virtual channel router (RBR mechanism)

Cost metrics	Router with RBR	VCR with RBR	Router with QoS
Area (μm^2)	87424.5	182652.3	28673.13
Cell internal power (mW)	0.00239	0.00156	0.00218925
Net switching power (mW)	0.016104	0.001638	0.000661
Total dynamic power (mW)	0.00255	0.0033	0.000145

comparison results of router with RBR, virtual channel router with RBR and the proposed 3D router with QoS mechanism. The area for the proposed work is $28673.1365 \mu\text{m}^2$ which is considerably lower than the other architectures. The power consumption is also minimized when compared with other router architectures. Moreover, the delay is also reduced when compared to the existing architecture.

4 Conclusion

In this paper, we proposed a 3D NoC router architecture with QoS mechanism and loop back module by applying a Partial Mesh of Grid topology (PMG). We found that this architecture will greatly minimize the area and power constraints when compared to a virtual channel router with RBR mechanism. PMG topology enhances the overall throughput of the network when compared to a fully connected mesh of grid topology. The topology designed is dead-lock free. This PMG-based NoC reduces the high chances of redundant connections. Moreover, the end to end delay is also reduced. This is because of the less number of interconnections and the reduced power consumption. Any routing algorithm with minimal hop count will optimize this result. Different traffic patterns are generated and data transmitted to analyze the performance of this optimized topology. The bandwidth is also improved dramatically.

References

1. Wang C, Bagherzadeh N. Design and evaluation of a high throughput QOS aware and congestion-aware router, architecture for NoC. *Microprocess Microsyst.* 2014;38:304–15.
2. Somasundaram K, Ploaila J, Vishwanathan N. Deadlock free routing algorithm for minimizing congestion in 3D NoCs. *Microelectronic* 2014;45(8):989–1000.
3. Brugge M, Khalid MAS. A parameterizable NoC router for FPGAs. *J Comput.* 2014;9(3):519–28.
4. Viswanathan N, Paramasivam K, Somasundaram K. An optimized 3D topology for on-chip communications. *Int J Parallel Emergent Distrib Syst.* 2014;29(4):346–62.
5. Ebrahimi M, Daneshtalab M, Liljeberg P, Plosila J, Flich J, Tenhunen H. Path based partitioning methods for 3D NoC with minimal adaptive routing. *IEEE Trans Comput* 2014;63(3):718–33.
6. Bartzas A, Skalis N, Siozios K, Soudris D. Exploration of alternative topologies for application specific 3D networks-on-chip. In: *Proceedings of 5th Workshop on Application Specific Processors, 2007*, p. 1–8.
7. Dubois F, Sheibanyard A, Petrot F, Bahmani M. Elevator-first: a deadlock-free distributed routing algorithm for vertically partially connected 3D NoCs. *IEEE Trans Comput.* 2013;62(3):609–15.
8. Fu JS. Hamiltonicity of the WK-recursive network with and without faulty nodes. *IEEE Trans Parallel Distrib Syst.* 2005;16(9):853–65.
9. Palesi M, Kumar S, Holsmarg R. A method for router table compression for application specific routing in mesh topology NoC architectures. In: *Proceedings of SAMOS, 2006*, p. 373–84.
10. Mejia A, Palesi M, Flich J, Kumar S. Region-based Routing: a mechanism to support efficient routing algorithms in NoCs. In: *IEEE Transactions on Very Large Scale Integration (VLSI) Systems*, pp. 356–69.

Single-Stage Boost Rectifier for Wireless Charging of Portable Devices Through Magnetic Resonant Coupling

Ria George, M. Sreekala and K. Deepa

Abstract Advancements in power electronics have aided in the development of inductive power transfer technologies by providing transmitter coil drivers and converters for conditioning the power received at the receiver coil. But the use of traditional two-stage circuit with half wave or full wave rectifiers and boost converter at the receiver side may be inefficient, as it reduces the total power delivered to the load. As an alternative, single-stage boost rectifier can be used, which is compact and more efficient. This paper introduces an efficient wireless charging system based on resonant magnetic coupling that contains single-stage boost rectifier at receiver. Single-stage rectification and boosting is made possible by the bidirectional conduction capability of MOSFETs. The system is designed and simulated in PSIM software. The overall power transfer efficiency of the system is analyzed for different coupling factors of the inductive links and for different loads.

Keywords Wireless power transfer · Inductive links · Magnetic resonant coupling · Single-stage boost rectifier

1 Introduction

With the advancement in technologies, wired connections for powering electronic equipments will soon be replaced with wireless powering techniques. Wireless power transfer would become an inexpensive and practical alternate method to

R. George (✉) · M. Sreekala · K. Deepa
Department of EEE, Amrita Vishwa Vidyapeetham University,
Amrita School of Engineering, Bangalore, India
e-mail: riajoy1991@rediffmail.com

M. Sreekala
e-mail: m_sreekala@blr.amrita.edu

K. Deepa
e-mail: deepa.kaliyaperumal@rediffmail.com

recharge portable electronic devices than traditional methods. In this method, electric energy is transferred from a power source to a target device without connecting wires between them. Also, it can overcome various disadvantages of traditional wired charging, like damage of USB ports, due to constant plugging and unplugging, inconvenience and hazardness of wires, corrosion, etc. When used for powering embedded medical devices or implants, wireless powering avoids the need for risky and cumbersome surgeries.

1.1 Existing Works in the Field of Wireless Power Transfer

Power or energy can be transferred wirelessly through a variety of known techniques, both near-field and far-field. Far-field techniques include radiative transfer in which information is transferred over long distances with more wastage of energy into air. Such inefficient power transfer may be acceptable for data transmission, but cannot be practical in case of transferring useful amounts of electrical energy for powering or charging electrical devices. Near-field technique includes inductive coupling, through which power can be transferred with higher efficiency, but only over very short distance. Also in this scheme, only small offset tolerance is allowed between primary and secondary coils. A better scheme for energy transfer was developed which uses coupled electromagnetic resonators [1]. When coupled through magnetic resonance, high amount of useful energy can be transferred over a distance of several meters. It is because resonant objects transfer energy more efficiently than nonresonant objects.

Most of the works done on wireless power transfer technology focuses on the design and optimization of the resonant inductive coils and the driving circuits for the transmitter [2, 3]. There has been only little research on high frequency and high efficiency rectifiers suitable for this application. As DC loads are more common than AC loads, there is a need to think of better power conditioning circuits for the receiver side. The rectifiers used in wireless power transfer technology are mainly traditional half wave or bridge rectifiers. The major losses in these rectifiers occur due to forward voltage drop of the diodes and also the switching losses [4]. Though synchronous rectifiers are based on bridge configuration, improving the overall efficiency of the system, timing, and control of four switches is difficult especially at high resonant frequencies. Also, the input currents for traditional half wave and bridge rectifiers are non-sinusoidal which may cause a non-sinusoidal current flow in the secondary resonant circuit of the inductive link [5].

2 Modeling of Inductive Links

Two independent circuits are said to be magnetically coupled, if the flux produced by the coil of first circuit enters the coil of the second circuit. Voltage induced in the coil is directly proportional to the number of turns of the coil and rate of change of magnetic flux, according to Faradays law of induction. And Amperes law gives the amount of flux linked with the coil. The voltages induced at the primary and secondary side coils can be given as

$$v_1 = M \frac{di_2}{dt} \quad (1)$$

$$v_2 = L_2 \frac{di_2}{dt} \quad (2)$$

In the above equation, parameter M refers to the mutual inductance existing between two coils having different number of turns and geometries. Mutual inductance indicates the strength of coupling between them and will be a positive quantity. Induced voltages, however, can be positive or negative depending on the windings and orientation of the coils. Mutual inductance and self inductances of the coil can be related through coupling coefficient, k given as

$$k = \frac{M}{\sqrt{L_1 L_2}} \quad (3)$$

In case of perfect coupling, the coupling coefficient will be 1, i.e., all the flux produced by the first coil enters the second one and will be 0 if no flux is linked. In inductive power transfer system, air acts as the core for guiding magnetic flux from one coil to other, and they are not tightly coupled.

2.1 Circuit Model for Resonant Coupling

The coupled coils can be replaced with an equivalent circuit for calculation of induced voltages and currents, and thereby analyzing the circuits containing them. Inserting a matching circuit (such as L-C network) for minimizing power reflection ratio is done in power transfer systems as a technique for impedance matching. A parameter, reflected impedance can be found from the analysis of equivalent circuit for power transfer system. It is a measure of the amount of actual load seen by the source and is a function of mutual inductance. More close the coils are kept, higher is the reflected impedance. Assuming the coils to be ideal (equivalent series resistance is zero) and a resistive load, absolute value of reflected impedance is equal to

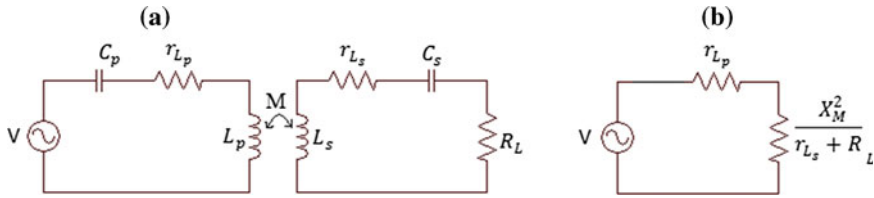


Fig. 1 Circuit with tuned capacitors added to the primary and secondary coils for achieving resonant coupling. 1(b) is the equivalent circuit representation

$$Z_{ref} = \frac{X_M^2}{\sqrt{R_L^2 + X_{L_S}^2}} \tag{4}$$

Eliminating the secondary coils’ reactance would increase the reflected impedance and it can be done by creating resonance at certain frequency. Resonating primary coils can deliver more power to secondary and creating resonance at coils can eliminate reactance of the coils.

In resonant coupling, the total input impedance seen by the voltage source can be given as

$$Z_{in} = r_{L_P} + \frac{X_M^2}{r_{L_S} + R_L} \tag{5}$$

From Eq. (5), it can be noticed that with resonance coupling, the primary coil’s impedance is decreased and reflected impedance is increased. Thus, comparing with nonresonant coupling, more power can be transferred to the load with resonant coupling (Fig. 1).

3 System with Single-Stage Converter at the Receiver

Transferring power via magnetic resonant coupling without radiating electromagnetic waves involves creating LC resonance. The driving current in the primary coil has to be sinusoidal and this can be achieved using resonant converters. The voltage obtained at the receiver coil has to be rectified and boosted so that it can charge or power a DC load. Figure 2 shows the block diagram of the entire system, which is made more compact at the receiver side. Transmitter coils are wound using copper wires with air as core to obtain desired inductance value and are designed to resonate at a particular frequency.

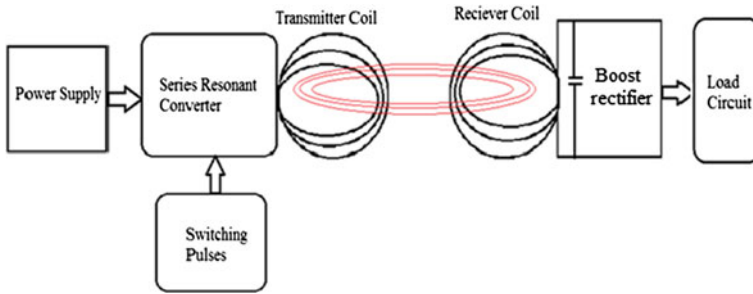


Fig. 2 Block diagram of wireless power transfer system

3.1 DC/AC Inverter for Driving Primary Coil

The DC–AC converter used at the transmitter side is a series resonant converter. As the inductor coils are to be operated at resonance, the current driving the primary coil should be sinusoidal. It can be realized by the inverter using passive networks consisting of inductors and capacitors. The switching frequency is chosen to be lower than the resonant frequency as the converter will be having nearly 100 % theoretical operating efficiency when switching is done at zero voltage. However, efficiency drops practically due to limitations in switches. Class D-type H-bridge resonant inverter is selected as primary coil driver because of its simple principle of operation, wide operating range, and high power efficiency. The passive elements of the inverter are designed for resonant frequency, with selected switching frequency and load quality factor.

3.2 Single-Stage Boost Rectifier at Receiver Side

The voltage obtained at the receiver coil has to be rectified and boosted for providing desirable power to a portable load device. Usually, it is obtained by using traditional half wave or bridge rectifiers and a boost converter. It may be inefficient and reduce the power delivered to the load. Figure 3 shows the circuit containing a two-stage converter used for power conditioning at the receiver side.

In a conventional boost converter topology, the diode is kept in series with the path of power flow which causes voltage drop and reduces reliability by increasing power loss. Also it is required to specially design the DC-side inductor to carry DC current as well as the ripple current which is of high frequency. At all instants, the power flow path contains three semiconductor device drops.

In this work, the receiver side power conditioning is achieved using a single-stage boost rectifier. The single-stage AC-to-DC conversion is made possible by the capability of the MOSFET to conduct in forward and reverse directions (Fig. 4).

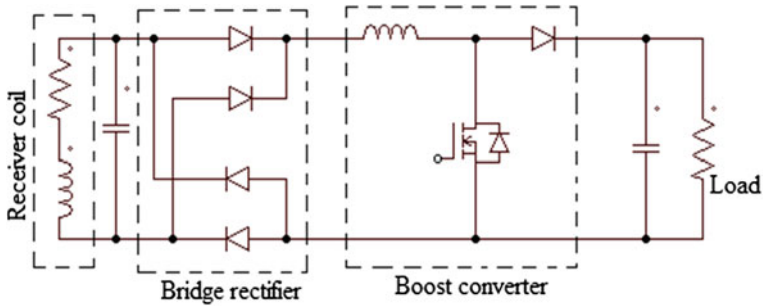


Fig. 3 Two-stage circuit with rectifier and boost converter

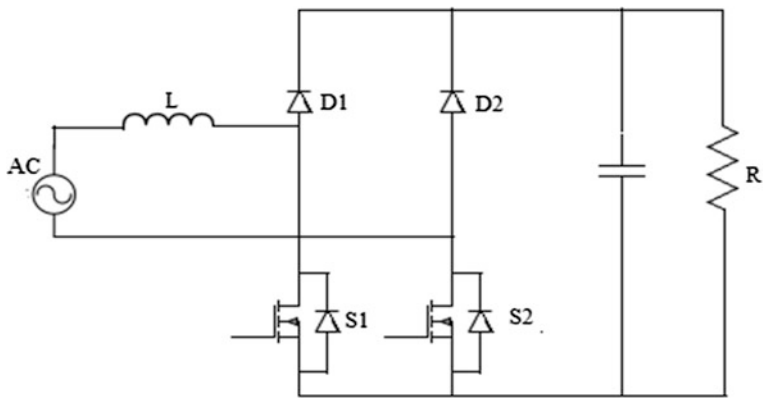


Fig. 4 Single-stage boost rectifier circuit

In this converter topology, the series diode in the boost converter has been eliminated. Also, the DC side inductor is removed and an AC side inductor is introduced for voltage boosting. The location of the inductor at the AC side helps in reduction of electromagnetic interference. Two switches S1 and S2 are realized using n-channel MOSFETs and their bidirectional conduction capability is used for boost operation in both the half cycles of input AC voltage. Their gate drives are referenced to same ground as they are driven by the same pulses. In each half cycle, when the pulses are high for both switches, one MOSFET conducts in forward direction while the other MOSFET conducts in reverse direction. When the gate pulses go low, both the switches are turned off and any circulation current is blocked by the reverse connected body diodes in the MOSFETs. The duty cycle can be varied to maintain the required output voltage.

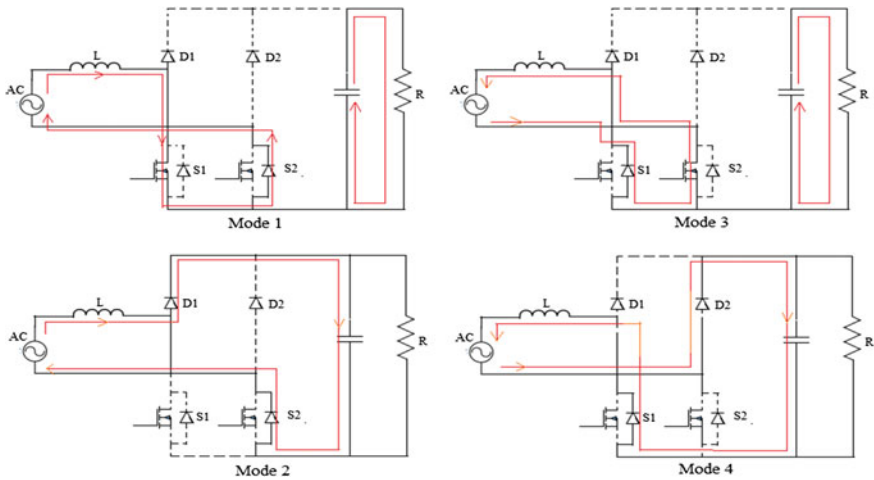


Fig. 5 Modes of operation of the single-stage converter. Modes 1 and 2 occur during the positive input half cycle and Modes 3 and 4 during the negative input half cycle

3.2.1 Modes of Operation

The single-stage converter topology operates mainly in four modes. Assuming the capacitor to be initially in charged state, in mode I the switches S1 and S2 are turned on at the positive half cycle of the input. The input voltage is applied across the boost inductor and the current through it builds up. The capacitor discharges to drive the load. Mode II starts when the gate pulses go low and the switches turn off. Diode D1 is forward biased and the stored energy in the inductor charges the output capacitor.

In mode III, the switches S1 and S2 are closed at the negative half cycle of input voltage. It is similar to mode I, but as the voltage polarity changes, the inductor current builds up in the reverse direction. In mode IV, the switches are made open and flows to the output capacitor and load through diode D2. Figure 7 shows the different modes of operation and current flow through the converter (Fig. 5).

The single-stage boost rectifier is having improved characteristics in terms of sinusoidal shape of AC input current and high input power factor. The number of components used is also reduced as compared to conventional two-stage conversion circuits used for wireless charging circuits.

4 Simulation Results

The whole wireless power transfer circuit was designed and simulations were performed in PSIM software. Initially, the coils of the inductive link were designed. At converter’s switching frequency, the coils must have high quality factor for

achieving maximum efficiency in power transfer. The series resonant converter for driving the primary coil was designed for quality factor 0.5, to obtain a sinusoidal output current. The resonant frequency of the converter is 45 kHz. Primary and secondary coils have a DC resistance of 0.3Ω and inductance of $10 \mu\text{H}$. L-C resonant tank is present in the secondary circuit also, to shape the input to the boost rectifier. The load is assumed to be purely resistive. The circuit is powered by 30 V DC source.

Simulations were carried out for various loads at different values of coupling coefficient, keeping other circuit parameters constant. When coils are perfectly coupled ($k = 1$), maximum power can be transferred and system becomes nearly 100 % efficient. However, for powering portable devices, the source and sink will be kept at an appreciable distance, which reduces the coupling coefficient. It can be observed that, as the value of k increases, the efficiency of the system improves. In wireless charging systems, the maximum value of k that could be practically achieved is less than 0.7. The circuit was simulated for $k = 0.7$ and the waveforms at primary and secondary sides were observed as shown in Fig. 6. After rectification and boosting, the output power obtained is 2.7 W.

The resonant frequency of the coils is based on the values of effective inductance and capacitance. Inductance in the coil is created by the loop, whereas capacitance has to be added to the coils to create resonance at desired frequency. In practical case, size of the capacitance required to induce resonance decreases as the coil diameter increases.

In wireless power transfer with resonant induction technique, efficiency can be improved by determining an optimum load resistance for given Q-factor, L-C ratios, and transmitter source impedance. The optimum loading is found to depend

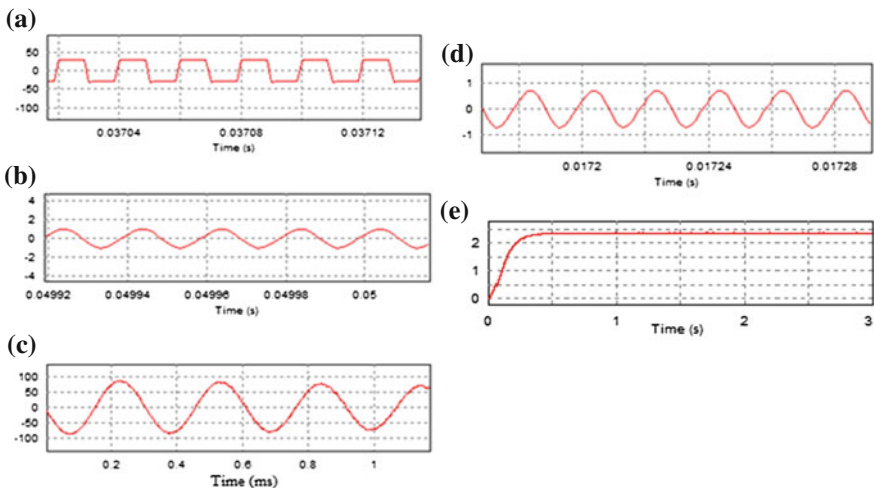


Fig. 6 Waveforms obtained for simulation performed in PSIM. The current driving primary coil is sinusoidal. Also sinusoidal waveforms are obtained at receiver due to LC resonance. **a** Voltage at the primary coil. **b** Current through primary coil. **c** Voltage at the secondary coil. **d** Current through secondary coil. **e** Output power

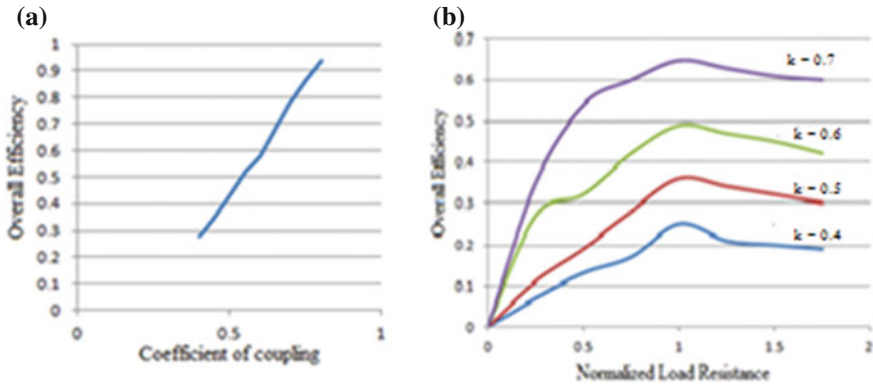


Fig. 7 Plots showing change in efficiency with k and variation in load

on coupling factor k . Also, there exists an optimum value for L-C ratio at receiver side for maximizing efficiency for the given load resistance.

Power is lost mainly in the equivalent series resistance of the coils and also as switching and conduction losses. Efficiency also depends on the system load. Figure 7 shows the variation of system efficiency with change in load for different values of the coefficient of coupling.

At higher loads and loose coupling coefficients ($k < 0.5$), the overall efficiency is reduced. By adjusting the duty cycle and switching frequency of the single-stage converter, it can be tuned to achieve the optimum switching conditions.

5 Conclusion

The wireless power transfer system for charging portable devices using resonant coupling and single-stage boost rectifier was investigated and simulated in this paper. The converter uses lesser number of components and is having improved characteristics and higher efficiency. The simulation results show that the coupling coefficient and loading plays important role in determining system efficiency.

References

1. Canno BL, Hoburg JF, Stancil DD. Magnetic resonant coupling as a potential means for wireless power transfer to multiple small receivers. IEEE Trans Power Electron. 2009;24:7.
2. Robert LS. A comparison of half-bridge resonant converter topologies. IEEE Trans Power Electron. 1999;3:2.
3. Raju S, Wu R, Chan M, Yue CP. Modeling of mutual coupling between planar inductors in wireless power applications. IEEE Trans Power Electron. 2014;29:481–90.

4. Budhia M, Covic GA, Boys JT. Design and optimization of circular magnetic structures for lumped inductive power transfer systems. *IEEE Trans Power Electron.* 2011;26:3096–108.
5. Enjeti PN, Martinez R. A high performance single phase ac to dc rectifier with input power factor correction. In: *IEEE conference on applied power electronics and exposition (APEC)*; 1993. p. 190–5, March1993.

Big Data Analytics for Network Congestion Management Using Flow-Based Analysis

Yasmeen Arafath and R. Ranjith Kumar

Abstract Due to explosive growth of traffic volume, it is hard to accumulate Internet traffic on a single machine. In this paper, a Hadoop-based traffic analysis system accepts input from multiple data traces. Hadoop facilitates scalable data processing and storage services on a distributed computing system. This system accepts input of large scales of trace file generated from traffic measurement tool like Wireshark– identifies flows running on the network from this trace file. Characteristics of flow describe the pattern of network traffic; it helps network operator understand network capacity planning, traffic engineering, and fault handling. The main objective is to design and implement a traffic flow identification system using Hadoop. The traffic flow identification system will be very useful for network administrator to monitor faults and also to plan for the future.

Keywords Traffic analysis · Hadoop · Wireshark

1 Introduction

The proposed system accepts input for large scale to trace the file generated from traffic measurement [1] tool like Wireshark and identifies flows running on the network from this trace file. The system further provides functions of detailed statistical analysis and characteristics mining. With characteristic information of

Y. Arafath (✉) · R. Ranjith Kumar
Department of ECE, AMC Engineering College, 18th, KM Bannerghatta Road,
Kalkere, Bangalore 560083, India
e-mail: yasmeenshaan@gmail.com

R. Ranjith Kumar
e-mail: ranjithocet@gmail.com

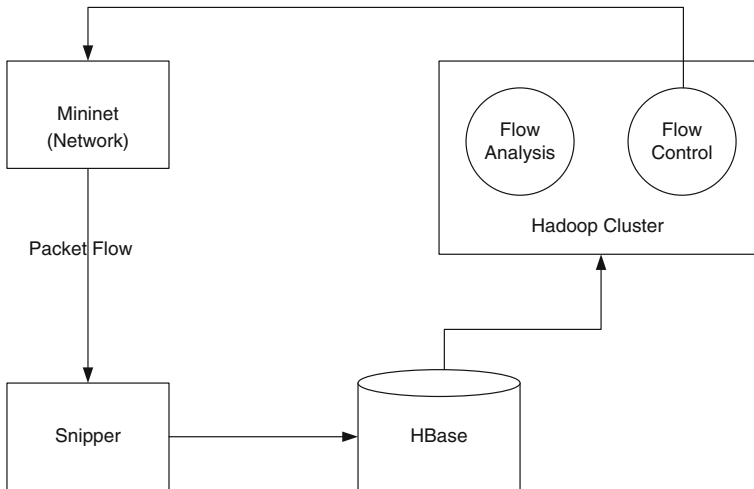


Fig. 1 Block diagram of traffic analysis

individual flow, the controller can provide corresponding resources and services. The controller part will be realized using mininet. Software Defined Network (SDN) is an approach to networking in which control is decoupled from the physical infrastructure,; control plane from individual hardware is collected and given to a centralized software entity called controller.

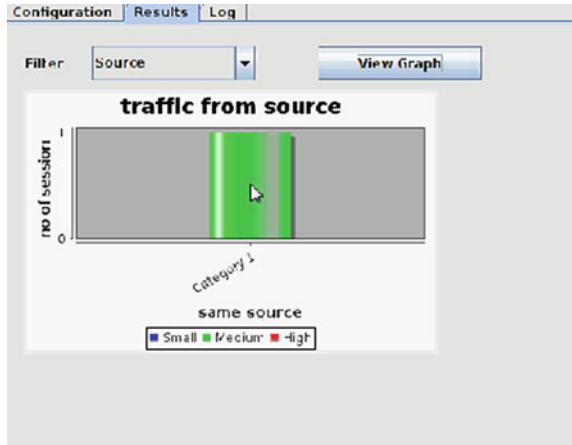
Figure 1 shows the block diagram of traffic analysis system which accepts the input of large-scale trace files generated from traffic measurement tools like Wireshark (network sniffer) that identifies flows running on the network from this trace file.

2 Traffic Analysis in Hadoop

One important component of Hadoop [2] HDFS can split a large file into several blocks and store these blocks on multiple nodes, while MapReduce [3] applications distributes the process job into several tasks and tracks execution of each task on computing nodes. The overall framework of Hadoop makes suitable for flow-level reassembling. Mininet creates a virtual network, running real kernel, switch and application code, on a single machine (VM, cloud, or native), in seconds, with a single command:

```
Cd mininet$ SUDO mn controller ip =
```

Fig. 2 Density graph of traffic from source



3 Flow Analysis

In the input side, collect the log files from Wireshark (network protocol analyzer). Run the script in the terminal window of Ubuntu. Depending on the file size, time requirement for Hadoop is taken into consideration. NetBeans IDE is used to collect the graph. Here, java MapReduce program is written and located in the input side. The jar files are run with the help of a script. Wireshark is used to collect log files. Figure 2 shows the traffic from source. The density of traffic is shown in the form of graph. Similarly, traffic from destination also can be generated by clicking on the drop down destination.

4 Simulation Results

4.1 Mininet and OpenDaylight

SDN [4] Hub VM 32 bit terminal window command is been given as per Fig. 3. Mininet command is given as explained above. OpenDaylight is a software defined network. In the command, window terminal of OS Run batch files and in a browser type 127.0.0.1:8080, OpenDaylight (control switches). By logging into page, we can add flow entry for the switches. Meantime SDN hub [4] terminal is opened given the mininet command for mesh topology. On refreshing SDN four switches should be added in the OpenDaylight. In the command window, open Wireshark capture option, when h1 pings h2, we can collect log summary based on switches added in OpenDaylight. Fig. 3 shows command given in the SDN mininet. In response to the command given, the OpenDaylight will have corresponding switches. Figure 4 shows how to access the switches.

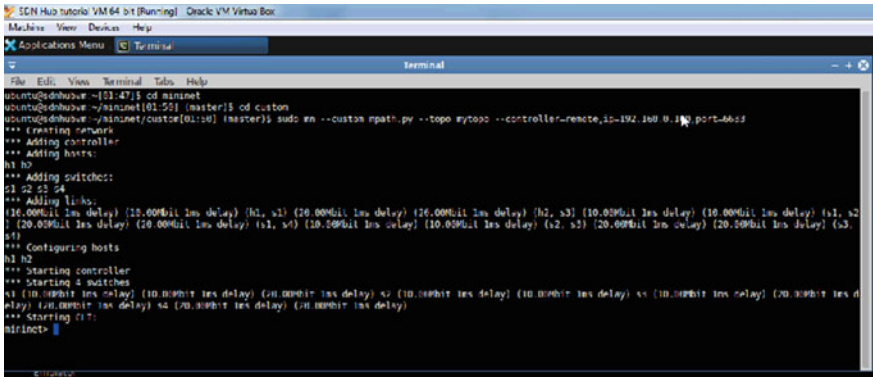


Fig. 3 Mininet command window terminal

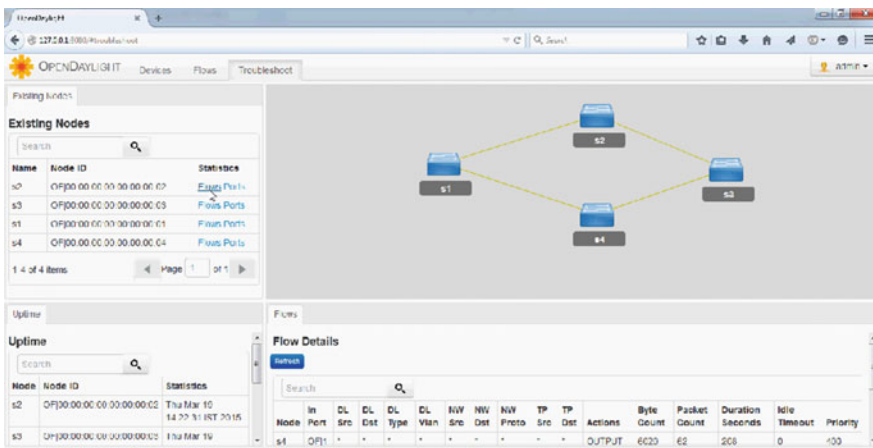


Fig. 4 Accessing switches

4.2 Collect Log

When h1 pings h2, in the Wireshark logs can be collected as from what source to destination IP packets has been transferred. Figure 5 is the block diagram of linear topology. The congestion management mainly takes place when the topology is not linear. The h1 can take path between four switches to reach h2 as shown in Fig. 6.



Fig. 5 Block diagram of linear topology

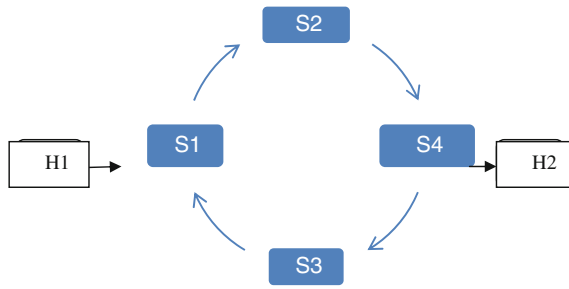


Fig. 6 Block diagram of mesh topology for congestion control

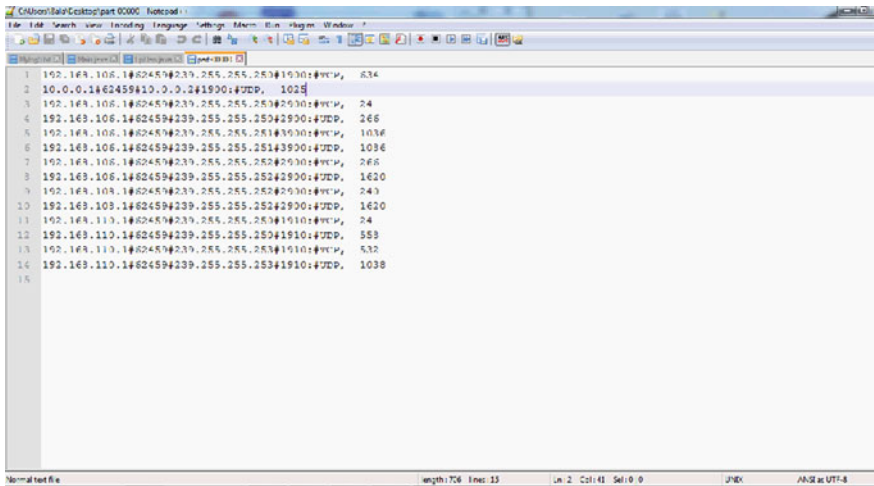


Fig. 7 Details of log from Wireshark

The two paths are bandwidth-oriented. As per the traffic present at that particular time, h1 pings h2 via one of the best path in order to reach the destination. In Wireshark, particular switches are chosen and log summary is collected. Log summary is saved and run on flow analysis input with the java script. We obtain detailed output as from which source IP address to destination IP address, type of protocol, and bytes of data. Figure 7 depicts the log collected from Wireshark.

5 Conclusion

This paper deals on flow identification and characteristics mining from large scale traffic trace on Hadoop platform. It introduces flow identification methodology from packet trace file, and provides detailed statistical information of original trace

packets and flows. The future work includes implementation and evaluation of other clustering algorithm, make efforts to do nearly online traffic analysis.

Acknowledgments The author wish to thank the guide for their moral support.

References

1. Lee Y. Toward scalable internet traffic measurement and analysis with hadoop, ACM SIGCOMM computer communication review, vol. 43;2013, p. 5–13.
2. Lee Y, Kang W. A hadoop-based packet trace processing tool. In: Traffic monitoring and analysis. Springer;2011, p. 51–63.
3. Lee Y, Kang W, Son H. An internet traffic analysis method with mapreduce. In: Network operations and management symposium workshops;2010. p. 357–61.
4. Qian L, Wu B, Zhang RW. Characterization of 3g data-plane traffic and application towards centralized control and management for software defined networking. In: Big data (big data congress);2013. p. 278–85.

A Real-Time Intelligent Microcontroller-Based Harmonic Computing with Smart Phone Connectivity

**Haripriya H. Kulkarni, D.G. Bharadwaj, Dipti B. Yeolekar
and Sheetal B. Mhetre**

Abstract Increased use of nonlinear loads injects current harmonics in electrical distribution networks and creates new problems of power quality in the power system. In today's competitive electrical market, electric utilities strive to supply consumers with reliable and pure sinusoidal electric power that does not represent a damaging threat to their equipment. In the restructured power system, prices of the power are associated to power quality. Hence, it is very important to monitor and ensure power quality. This paper presents an innovative way of real-time harmonic computing using intelligent microcontroller and its assessment with automatic meter reading (AMR) on smart phone. During preparation of this paper, fifty site visits are done covering the nonlinear loads like IT industries, steel industries, paper industries, workshops, etc. It is observed that the current harmonics generated are beyond the tolerable limits. Readings are taken at consumer end with the help of standard power analyzer for a period of 24 h. It is also observed that a good number of researchers have worked on harmonic studies in the power system network; however, their work does not fit into the framework of the standards applicable. The developed solution has the capacity to identify the normal and abnormal presence of harmonics with color code. Through this color coding technique, an unskilled worker can easily identify the objectionable presence of harmonics. The computing results are observed to be satisfactory and promising. It creates awareness in the utility for measurement and control of harmonics which in turn helps to improve the power quality.

Keywords Automatic meter reading (AMR) · Analog to digital converter (ADC) · Central monitoring station (CMS) · Data acquisition system (DAQ) · Data concentrator unit (DCU) · Global system for mobile communication (GSM) · Optical fiber cable (OFC) · Power line carrier communication (PLCC) · Random access memory (RAM) · Remote terminal units (RTU) · Total harmonic distortion (THD) · ZigBee

H.H. Kulkarni (✉) · D.G. Bharadwaj · D.B. Yeolekar · S.B. Mhetre
B.V.D.U.C.O.E, Pune, Maharashtra, India
e-mail: electricalmcoe@yahoo.com

1 Introduction

Power quality is one of the ever growing concerns to utilities and customers. The problem associated with high harmonic content in the power system not only results in poor quality of supply but also the operation of the system will get affected. The modern electronic devices and circuits are mostly nonlinear. According to energy conservation act, demand of energy efficient devices is increased [1]. These energy efficient devices have twofold problems with regard to harmonics. They not only produce harmonics but they are also very sensitive to the resulting harmonic distortion than the traditional power system devices. It is therefore important to measure, analyze, and limit harmonics in power distribution network [2]. This paper illustrates a novice method of reading harmonics from numeric meters installed at remote end using ZigBee at local level and GSM at global level and its processing on smart phone through which the concept of Automatic Meter Reading (AMR) can be implemented [3, 4]. During the late 1990s, the microprocessor-based meters called numeric meters or digital meters were developed. These meters are provided with inbuilt Central Processing Unit (CPU) and Random Access Memory (RAM). These meters also conduct harmonic measurement in terms of total harmonic distortion (THD). In the presented work, meter hardware is developed using ADE 7880 which will measure the harmonics in terms of voltage THD, current THD, and also power THD. In addition to it, it will also measure individual voltage, current, and power harmonics along with its assessment with respect to specified standard. Thus, the proposed system is a complete close loop solution under one roof. However, the existing equipments, viz., cathode ray oscilloscope, harmonic analyzer, and numeric meters do not perform remote measurements and also do not assess harmonics as per the standard. In order to save time in visiting various electrical installations, it was felt necessary to transmit the meter data over a longer distance and meet requirements of AMR [2]. IEEE standard 519-1992, has been used for comparing the presence of harmonics [5]. There are many ill-effects of voltage and current harmonics like creating electromagnetic interference, decrement in the power factor, over heating of cables, transformers and rotating equipment, false tripping of breakers and fuse, additional heating in induction, synchronous motors and generators, weaken insulation in cables, windings, and capacitors, malfunction of different electronic components and circuits that utilize the voltage waveform for synchronization, etc. These ill-effects should be taken into consideration and power quality needs to be improved.

2 Field Visits

Measurement of harmonics [6] has been done by using Advanced Harmonic Analyzer "Yokogawa" (model CW240). Wiring connections for this harmonic analyzer was three-phase four-wire. C.T. ratio is 100/5 amp. Table 2 shows the

harmonic measurement at twenty-four different sites covering various types of nonlinear loads. Total 50 site visits were conducted and readings were taken for 24 hrs. each, but only sample readings are listed in Tables 1 and 2.

It is observed through site visit readings from Tables 1 and 2 that the current harmonics observed are beyond the tolerable limits. Due to harmonic presence, true power factor gets reduced and power consumption only due to harmonics is up to 20 % in Harmonic-rich loads. Hence, the proposed solution of measurement will definitely inculcate the awareness regarding the monitoring and mitigation of harmonics.

Table 1 Observed system parameters at different sites

Sr. no.	Visited site no.	Contract demand (KVA)	Connected load (KW)	CT ratio	PT ratio
1	Site no. 1	15,000	45,000	100 A/1 A	220 kV/110 V
2	Site no. 2	15,000	45,000	100 A/1 A	220 kV/110 V
3	Site no. 3	2500	4000	50 A/1 A	33 kV/110 V
4	Site no. 4	2460	3570	3570 KW	50 A/5 A
5	Site no. 5	1150	1600	1600 KW	50 A/5 A
6	Site no. 6	4800	14,500	14,500 KW	150 A/5 A
7	Site no. 7	4900	14,500	14,500 KW	150 A/5 A
8	Site no. 8	2600	6500	6500 KW	100 A/5 A
9	Site no. 9	1300	3250	3250 KW	75 A/5 A
10	Site no. 10	16,000	29,944	29,944 KW	100 A/1 A
11	Site no. 11	16,000	29,944	29,944 KW	100 A/1 A
12	Site no. 12	2000	5787	5787 KW	50 A/5 A
13	Site no. 13	2500	400	400 KW	50 A/5 A
14	Site no. 14	2000	6800	6800 KW	50 A/5 A
15	Site no. 15	6340	9341	9341 KW	150 A/5 A
16	Site no. 16	6340	9341	9341 KW	150 A/5 A
17	Site no. 17	2400	7000	7000 KW	100 A/5 A
18	Site no. 18	2000	3000	3000 KW	50 A/5 A
19	Site no. 19	7750	12,100	12,100 KW	150 A/5 A
20	Site no. 20	7750	12,100	12,100 KW	150 A/5 A
21	Site no. 21	2250	2790	2790 KW	75 A/5 A
22	Site no. 22	1335	2260	2260 KW	50 A/5 A
23	Site no. 23	1400	1800	1800 KW	50 A/5 A
24	Site no. 24	1050	1733	1733 KW	50 A/5 A

Table 2 Observed harmonic measurement at different sites

Sr. no.	Visited site no.	Voltage harmonic distortion in %			Current harmonic distortion in %		
		R	Y	B	R	Y	B
1	Site no. 1	0.44	0.47	0.67	7.67	8.79	8.79
2	Site no. 2	0.39	0.61	0.67	9.12	9.13	9.13
3	Site no. 3	0.97	1.07	1.09	4.21	4.51	4.51
4	Site no. 4	2.13	1.72	2.16	16.23	18.79	18.79
5	Site no. 5	1.10	1.32	1.31	11.21	16.54	16.54
6	Site no. 6	0.47	0.57	0.56	5.3	8.6	8.6
7	Site no. 7	0.43	0.47	0.41	8.62	7.49	7.49
8	Site no. 8	0.52	0.52	0.61	4.50	5.05	5.05
9	Site no. 9	0.96	0.96	1.06	8.59	5.77	5.77
10	Site no. 10	0.95	0.85	0.90	7.38	5.71	5.71
11	Site no. 11	1.25	1.09	1.04	10.09	8.25	8.25
12	Site no. 12	0.80	0.82	0.63	13.50	15.57	15.57
13	Site no. 13	0.57	0.57	0.45	2.21	1.82	1.82
14	Site no. 14	1.00	1.01	1.06	2.73	3.31	3.31
15	Site no. 15	1.35	1.42	1.55	10.10	18.29	18.29
16	Site no. 16	1.037	1.64	1.71	17.81	17.79	17.79
17	Site no. 17	0.5	0.35	0.63	8.04	9.96	9.96
18	Site no. 18	0.8	0.77	0.69	8.43	10.02	10.02
19	Site no. 19	1.99	2.07	2.04	17.06	17.04	17.04
20	Site no. 20	0.98	1.13	1.01	20.04	20.64	20.64
21	Site no. 21	0.9	0.84	0.87	31.10	27.70	27.70
22	Site no. 22	0.81	0.77	0.78	3.29	2.90	2.90
23	Site no. 23	0.77	0.72	0.76	23.84	21.98	21.98
24	Site no. 24	1.67	1.67	1.64	14.71	14.88	14.88

3 Implemented Hardware System

Today, harmonics are measured with the help of standard power quality analyzer. But the cost of these equipments is very high and is not affordable to every consumer in the distribution sector. A new innovative real-time measurement solution is proposed in this paper. Voltage and current signals are captured through sensors. This data is taken through a DAQ card and connected to a PC for analysis purpose. The developed hardware–software system displays system parameters like KW, KVA, KVAR, KWh, etc., along with harmonics measurement both in terms of V_{THD} and I_{THD} .

- DAQ Card for Data Collection

As shown in Fig. 1, ADE7868 is a high accuracy, 3-phase electrical energy measurement IC with serial interface. ADE7868 consists of analog to digital

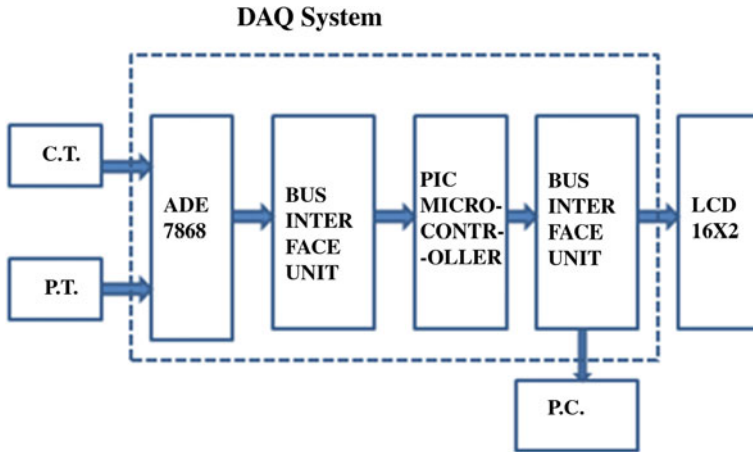


Fig. 1 Block diagram of data acquisition system

Fig. 2 Validation of developed hardware at MAHADISCOM test bench



converter (ADC), digital integrator, reference circuitry and all the signal processing required to perform total (fundamental and harmonic) active, reactive, and apparent energy measurement and RMS calculation for both star and delta connected load, and also for 3-phase 4-wire system. The processed signal is then passed to bus interface unit. The heart of the system is intelligent PIC microcontroller which is used to fetch the data and supply it to the PC for analysis purpose.

Figures 2 and 3 show the actual photograph of developed hardware for measurement of harmonics and other system parameters.

- AMR with Smartphone Communication Using ZigBee

As shown in Fig. 4, data is collected with the ZigBee module and then it is transferred to ZigBee receiver and further to central computer using GSM communication. Automatic meter reading is a process in which meter data is read and processed automatically via special equipment using wireless communication and



Fig. 3 Testing of developed hardware

- AMR WIRELESS COMMUNICATION THROUGH ZIGBEE

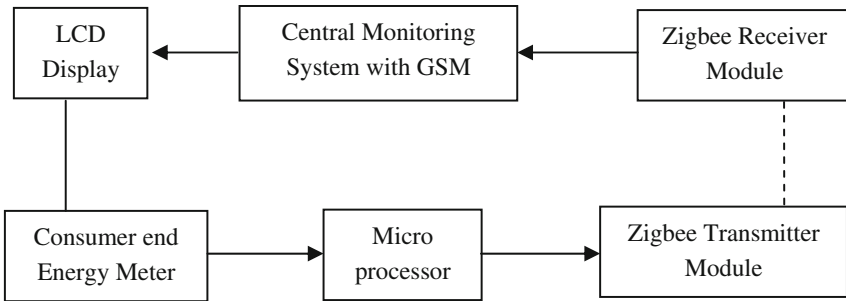


Fig. 4 AMR with ZigBee communication

computer network technology. Compared with the existing meter reading, it effectively saves human resources and can get real-time consumption of every user, helping the management. The communication data rate is set 9.6 kbps and the frequency band is 2.4 GHz. The hardware developed is shown in the following Fig. 5.

4 GUI Developments for Harmonic Assessment

A GUI is developed for harmonic assessment which plays a very important role in an industry. The bar chart shows the identification of abnormal and normal harmonic level presence with RED and GREEN colors, respectively, as shown in Fig. 6. The assessment is done based on IEEE standard 519-1992.

Fig. 5 System hardware for AMR

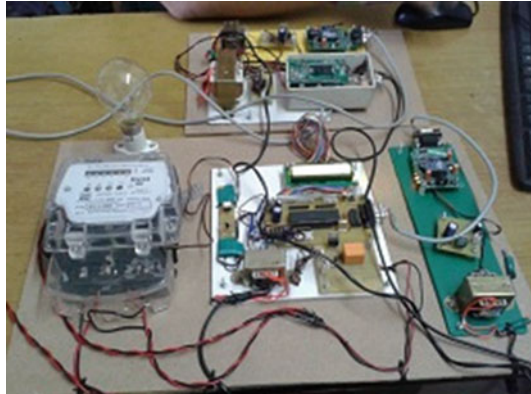
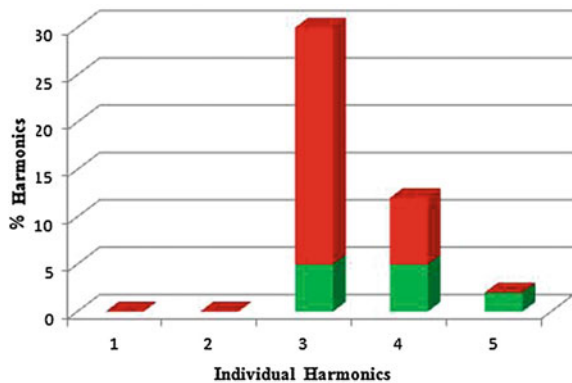


Fig. 6 Bar chart for harmonic level identification



As shown in the above Fig. 6, identifying the presence of harmonics is made simple using color code. A nontechnical person can also identify it, which creates an awareness to maintain the power quality standards.

5 Data Transmission

At the utility substation, numeric meters are installed in a control panel. These numeric meters are connected to modbus through RJ11 connectors. The RJ11 is an Ethernet connector. Modbus is RS485/USB compatible bus. The meter data received at modbus is collected by Data Concentrator Unit (DCU). This data is stored in the local substation server.

As shown in the above Fig. 7; through a wireless internet media, the data is send to the Central Monitoring Station (CMS) via router and other network devices such as modem, bridge, hub, repeater, etc. Data is transmitted through a communication

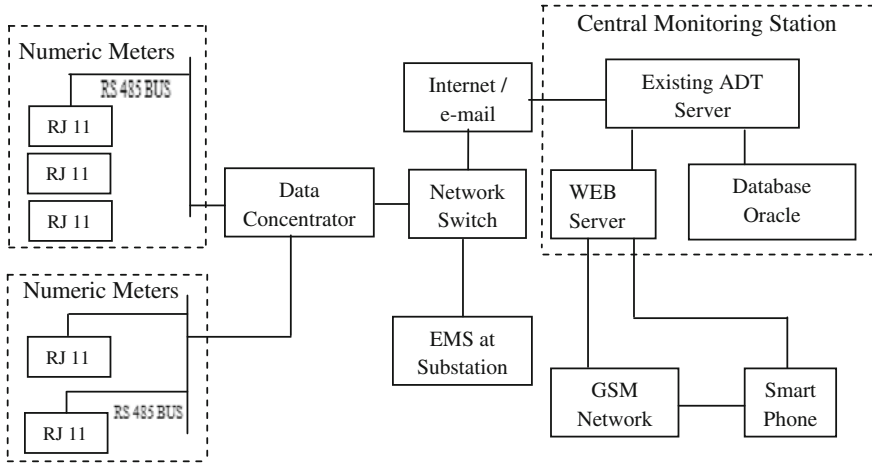


Fig. 7 Functional block diagram of utility substation

satellite named as Very Small Aperture Terminal (VSAT). The data thus received at CMS is stored permanently in the database server. Usually, the RDBMS-based Oracle server is provided. The data is also stored in the local server installed near metering installation. Now, let us understand the working of network components in brief. Modem is the unit comprising of two components—modulator and demodulator. These components perform the function of modulation and demodulation of signals. The repeater amplifies these signals to reduce noise and attenuation. Number of repeaters is combined in a single unit called hub. Bridge is used to connect or disconnect the networks. Another channel of data communication is a wired media. The data is sent through Remote Terminal Units (RTU) data acquisition system or Power Line Carrier Communication (PLCC) network integrated with Optical Fiber Cable (OFC). The wired communication is, however, out of scope of this paper. Both channels, wired and wireless, are used in practice.

6 Connectivity to the Smart Phone

The data received at CMS is also connected to the Web server. It is proposed to connect Web server to the GSM network (Global System for Mobile Communication), as shown in Fig. 7. From GSM network the link is provided to the smart phone. GSM describes protocols for digital cellular networks [7]. The GSM network mainly comprises of GSM/GPRS modems suitable for long duration data transmission. The GSM modem is connected to the microcontroller which would transmit data from meter to cell phone and vice versa [8]. The modem sends unit or pulses (power consumption) on regular interval or on request [9]. Smart phone is a mobile phone built on a mobile operating system having more advanced computing

capability than a feature phone. It is provided within the built CPU and RAM. The mobile operating system used by the smart phones are Google’s Android, Apple’s OS, Nokia’s Symbian, Microsoft’s Windows phone, and HP’s web OS [10]. Data is received at the input port of the smart phone. It is then processed by the inbuilt compiler of smart phone. The Android-based C/C++/Java compilers are available. These compilers are installed in the smart phone. In order to process meter data, the source code is written. This source code written in high-level language is compiled. The compiler translates source code into object code. These file formats are supported by Android or equivalent mobile operating system. Program output is displayed by emulator on the mobile screen [11].

7 Data Processing

The data related to harmonics received by the smart phone from numeric meters is processed. For this purpose, the source code is written in a high-level language such as C/C++ and Java. The source code is compiled by the compiler installed in the smart phone.

An example of Android-based C compiler is shown in Fig. 8. The compiler checks for errors in the program, if any. The programmer has to make respective corrections in the source code. The compiler then translates the source code into object code. The results of data processing are displayed on the mobile screen through an emulator (Fig. 9). The source code can be easily written and compiled in smart phone. For this purpose, click “new” button to enter a source code or click “open” to open the saved code. The “Save” button is clicked to save changes. The program is compiled by clicking on “Compile” button. The program is compiled and errors, if any, are displayed. After removing errors, the “run” button is clicked and the results are displayed. Figure 10 shows smart phone as a compiler [12] [13].

Fig. 8 Text editor of smart phone compiler



Fig. 9 Use of smart phone as compiler

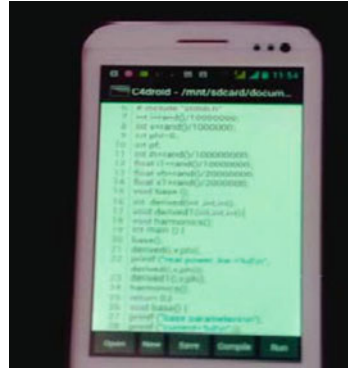
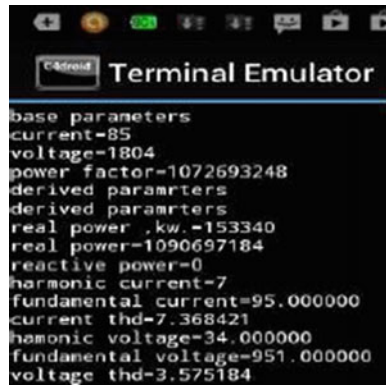


Fig. 10 Emulator of smart phone compiler



8 Conclusion

It is observed through site visits that the current harmonics generated are beyond the tolerable limits. Due to harmonic presence, true power factor gets reduced and power consumption only due to harmonics is up to 20 % in Harmonic-rich loads. Hence, the proposed solution of measurement will definitely inculcate the awareness regarding the measurement and controlling of harmonics.

Much attention is now being paid to the power quality because of increasing use of nonlinear loading. In the process, it is essential to improve the power factor of the system by reactive power compensation and in addition to the harmonics present in the system are required to be almost nullified. The case studies presented here are the sample examples and it is necessary to improve the existing situation of power quality. This paper represents a real-time measurement, assessment, and also communication on smart phone by smarter way. The data related to harmonics collected from meter installed at remote end through automatic meter reading is processed on the compiler installed in the smart phone. The validation is carried out by comparing results with traditional methods of measurements such as harmonic

analyzer and numeric meter. The results are found to be accurate and acceptable. This also results in saving the time required for visiting electrical installations for harmonic measurements. Since processing of the real-time data is carried out on smart phone, the analysis is accurate and speedy. As such, it is concluded that the technique recommended in this paper serves the purpose of harmonic measurements and analysis in electrical network at remote end. Through the color coding technique, an unskilled worker can easily identify the objectionable presence of harmonics. Harmonics can be mitigated by the use of appropriate active or passive filter.

Acknowledgments The project work is being carried out in Bharati Vidyapeeth Deemed University COE, Pune. The authors wish to thank the authorities of BVDUCOE, Pune and PES's Modern College of Engineering for granting permission to publish the work. Special thanks to MSEDCL and MSETCL for collection of data at consumer end.

References

1. Vlahinic S, Brnobic D, Stojkovic N. Indices for harmonic distortion monitoring of power distribution systems. In: IEEE Proceedings on instrumentation and measurement technology conference, IMTC;2009. p. 1771–7.
2. Khalifa T, Naik K, Nayak A. A survey of communication protocols for automatic meter reading applications. IEEE Commun Surv Tutor (2011);13(2):168–82.
3. Yuan SJ. Remote, wireless automatic meter reading system based on GPRS. In: 2011 IEEE third international conference on communication software and networks, Xian;2011. p. 667–69.
4. Mahmood A, Aamir M, Anis MI. Design and implementation of AMR smart grid system. In: IEEE electric power conference, Canada;2008. p. 1–6.
5. IEEE recommended practices & requirements for harmonic controlling electric power system, standard 519-1992.
6. Cuk V, Cobben JFG. Analysis of harmonics current based on field measurements. IEEE Conf Gener Transm Distrib. 2013;7(12):1391–400.
7. Ferrigno L, Paciello V, Pietrosanto A. Visual sensors for remote metering in public network. In: IEEE international conference on instrumentation and measurement technology; 2011. p. 1–6.
8. Wasi-ur-Rahman M, Rahman MT, Khan TH, Kabir SML, Design of an intelligent SMS based remote metering system. In: IEEE Proceedings on information and automation;2009. p. 152–9.
9. Fung CC, Wong KP, Wong KW, Goh OS. Intelligent meters for improved system operation and customer relationship management. In: IEEE Proceedings on power system technology;2002. p. 1758–62.
10. Xu Z, Chen ZD, Nie H. Handheld computers: smartphone centric wireless applications. Microwave Mag, IEEE Microwave Theory Tech Soc. 2014;15(2):36–44.
11. Punithavati R, Duraiswamy K. An optimized solution for mobile computing environment. IEEE Int Conf Comput, Commun Networking. 2008;1:1–10.
12. Tian G, Fang L. A new mobile spatial information system grid computing model based on mobile agent. IEEE Int Conf Commun Mob Comput. 2014;2:596–600.
13. Nhan NQ, Vo MT, Nguyen TD. Improving the performance of data collecting system for electricity meter reading using wireless sensor network. IEEE Int Conf Adv Technol Commun. 2012;1:241–6.

Performance Improvement of Compressed Sensing Reconstruction Using Modified-AMP Algorithm

Nissy Sara Mathai and R. Gandhiraj

Abstract Compressed sensing (CS) is an emerging field which enables the undersampling of sparse signals rather than at the Nyquist rate. But the main computational challenge involved is in the reconstruction process as it is nonlinear in nature and the solution is obtained by solving a set of under determined linear equations. Greedy algorithms offer the solution to these kinds of problems with less computational complexity than the convex relaxations or linear programming methods. The approximate message passing algorithm offers accurate reconstruction of even the approximately sparse signals with reasonable computational intensity. In this paper, we have implemented a modified version of AMP algorithm and obtained a 50 % reduction in mean squared error and an improvement in signal-to-noise ratio.

Keywords Approximate message passing algorithm · Compressed sensing

1 Introduction

Sampling essentially means the projection of the input signal into the measurement matrix to give the output vector. The accurate reconstruction of input signals from the output vector boils down to the solution of linear equations which involves only linear algorithms. The traditional sampling methodology based on Nyquist–Shannon sampling theorem, takes into account the rate of change of signal only. But these methods forget the fact that many natural signals follow a pattern and the dimension of vector does not necessarily imply the actual degrees of freedom of that

N.S. Mathai (✉) · R. Gandhiraj
Department of Electronics and Communication, Amrita Vishwa Vidyapeetham,
Coimbatore, India
e-mail: nissysara@gmail.com

R. Gandhiraj
e-mail: r_gandhiraj@cb.amrita.edu

signal. This notion is defined by a property called sparsity and the signals are called compressible signals [1]. The basic idea is that a compressible signal exhibits sparsity either in time domain or in any transform domain. For example, the natural images can be approximated using only fewer numbers of measurements once we transform code it into another domain like wavelet basis, where it exhibits sufficient sparsity [2]. Generally, the JPEG encoders transform code the signal and then compress it reducing the millions of pixels captured by the sensors into approximately 10 % of its initial quantity. So, a new sensing methodology was put forward that samples only the significant information rather than acquiring large amounts of samples and then discard them afterwards.

The emerging research field called the compressed sensing (CS) enables us to make use of the property called sparsity which basically means that it is possible to represent the signal using fewer nonzero coefficients in some domain. Compressed sensing follows the rate of change of information of the signal. The mathematical foundation is that for a compressible signal, an appropriate random projection provides all the significant information about that signal [3]. Here, the signal is sampled in a compressed manner as opposed to the traditional sampling procedure where the signal is sampled first and then compressed for ease of storage, transmission or processing. Proper reconstruction of the sparse signal can be done from these measurements which are fewer than as required by the Nyquist rate. CS brings in many advantages including area reduction and power reduction, particularly CS lowers the sampling cost involved and has applications in fields including magnetic resonance imaging, image acquisition [4], wearable and wireless body-area networks, bio signal acquisition [5], and spectrum sensing for multiband signals [6].

The CS framework can be divided into two parts, the sensing part and the reconstruction part. Sensing part involves the projection of the sparse signal into the measurement matrix and the reconstruction part includes the reconstruction of the input signal from the knowledge of measurement matrix and the output vector. In the traditional methodology, this involves solving a set of linear equations. But in CS methodology the number of unknowns is more than the number of equations, which is a result of the undersampling of the signal. These kinds of equations have infinite number of solutions and are generally known as ill-posed problem or under-determined set of linear equations. If, however, the signal is known to be sparse, there exists a unique solution under certain conditions. Undersampling of the signal comes at the cost of a computationally expensive algorithm.

Convex programming based on l_1 minimization [7] received lot of attention but is time consuming. Greedy algorithms were later introduced which offers improvement in time required but compromising the reconstruction performance a bit [8]. In this paper, we implement a modified version of the approximate message passing (AMP) algorithm that enables the accurate reconstruction of approximately sparse signals like audio, image and video signals.

2 Compressed Sensing

Compressed sensing is based on the notion that a small collection of nonadaptive linear measurements contains enough information for the reconstruction and processing of a compressible signal. Using far fewer samples or measurements than traditional methods that dictates for the proper reconstruction, CS theory asserts that one can recover certain signals and images. To achieve undersampling, CS depends on two major principles: sparsity, a property defined by the signal of interest and incoherence, which is a characteristic property of the sensing modality.

There are three phases to implement CS [1]: knowing the domain in which the signal is sparse, low dimensional signal acquisition, and the recovery process. The sparse domain is a transform space, typically a set of linear functions, which facilitates a compacted representation of the input. Signal acquisition in CS involves projecting the signal to a lower dimensional domain that is incoherent to the sparse domain. The recovery process exploits the fact that there are only a few information bearing components in the sparse domain in order to identify them.

2.1 Sparsity

When expressed in the appropriate basis, many natural signals can be represented concisely. Let F be a vector $\in R^N$ which we expand in an orthonormal basis Ψ : $F = \Psi X$, where X is the coefficient matrix. The sparse nature of the signal implies that, the small coefficients can be discarded without much perceptual loss. A signal X_s is said to be S sparse, if it consists of utmost S nonzero entries. Simple data compression methods compute X from F and encode the value and position of the nonzero entries adaptively. In CS, sparsity determines how effectively one can sample the signal nonadaptively.

2.2 Incoherence

In CS, the incoherence of matrix used to sample or sense the signal of interest (Ω) and the matrix representing a basis (Ψ), in which the signal of interest is sparse, is of paramount importance. The coherence between sampling and measurement matrices [9] is given as

$$\mu(\Omega, \Psi) = \sqrt{N} \max |\Psi_j, \Omega_k| \text{ where } 1 \leq j, k \leq N \quad (1)$$

The measurements are taken by projecting the signal onto the measurement matrix. In fact, each element of the output vector provides an independent account of all the samples of the input vector X . Hence, to capture maximum amount of

information in each element of the output vector, the input signal should be spread out in the domain in which it is being acquired.

2.3 Sensing Methodology

The sensing methodology used is the linear method that is used conventionally, i.e., if Y is the M dimensional output vector, X the N dimensional input vector, Φ the $M \times N$ measurement matrix, Ψ the sampling domain, and Ω the sparsifying domain, to sparsify the signal X we use transform coding [1], i.e.,

$$X' = \Omega X \quad (2)$$

The output vector Y ,

$$Y = \Psi X' \quad (3)$$

$$Y = \Psi \Omega X \quad (4)$$

$$Y = \Phi X \quad (5)$$

CS captures $M \ll N$ measurements from N samples incoherently achieving a compression ratio C ,

$$C = \frac{N}{M} \quad (6)$$

For accurate reconstruction of the signal, the number of measurements M should be [3] such that

$$M > C \mu^2(\Omega, \Psi) S \log(N) \quad (7)$$

It is an established fact that random matrices and any fixed basis matrices are essentially incoherent with each other. Hence, for accurate reconstruction and ease of designing the system, the measurement matrix can be filled up with random values drawn from different probability density functions including uniform distribution, Bernoulli and Gaussian.

2.4 Reconstruction

Reconstruction of the signal at the receiver end can be performed by solving the equation

$$X' = \Phi^{-1}X \tag{8}$$

We have to solve a nonlinear system of equations as the measurement matrix Φ is of dimension $M \times N$. But the N unknown values in the reconstructed signal X , has to be determined from $N (<M)$ known values in the measured signal Y . As the number of unknowns is greater than the number of equations, this system constitutes an underdetermined set of linear equations which has many possible solutions. With the help of the a priori knowledge that the solution is also a sparse signal, the number of possible solutions is reduced. But still, it is a NP hard problem and computationally intractable. We can relax this problem to a convex optimization problem [10] called as basis pursuit

$$\min \|X'\|_1 \text{ subject to } Y = \Phi X' \tag{9}$$

But the convex optimization algorithms, such as interior point methods, are complex [8] still with the problem sizes occurring in most practical applications. Hence, another class of algorithms was introduced for convergence time improvement.

3 Approximate Message Passing Algorithm

Greedy algorithms iteratively approximate the solution by adding the most correlated element [8] and will iterate till a criterion for convergence based on the residual error is met. But the least square minimization step involved in these algorithms cause considerable computational complexity per iteration. And the residual is calculated generally based on the newly updated approximation of X and the measured vector Y .

Message passing algorithms [11] are another kind of algorithms that employs iterative thresholding [12] in each step to approximate the signal X from the measurement vector Y . Soft thresholding function may be used as the thresholding function and in every iteration threshold is adjusted so as to minimize the residual error.

Approximate message passing algorithm [11] is another algorithm that offers the solution to (9) with reasonable accuracy and fast convergence along with less computational complexity per iteration. AMP algorithms employ soft thresholding function iteratively to approximate the solution. And the residue calculated depends on current approximation of X as well as the previous residue. In the basis, AMP algorithm, as in [13] the threshold, is set as proportional to the regularization parameter λ and the root mean square error of the residual $RMSE = 1/\sqrt{M} * \|r^{i-1}\|_2$. The proportionality factor [13] of the previous residue for calculating the new residue is calculated as the mean of l_0 norm of current X . The basic AMP algorithm is modified

and implemented here. The pseudo code of Modified-AMP algorithm is given in Algorithm 1.

Algorithm 1: Modified-Approximate message passing algorithm

1. Initialize $r^0 = Y$ and $X^0 = 0_{NX1}$
 2. for $i=1$ to I_{MAX}
 3. $\gamma = X^{i-1} + \Phi^T r^{i-1}$
 4. $\theta = \text{arg } e(\gamma, M)$
 5. $X^i = \eta(\gamma, \theta)$
 6. $b = \frac{1}{M} \langle \eta'(\gamma, \theta) \rangle$
 7. $r^i = Y - \Phi X^i + br^{i-1}$
 8. end for
 9. return $X^{I_{MAX}}$
-

Initially, the output vector X is initialized as an N dimensional zero vector and the residue is initialized as the measurement vector Y . First, the γ value is calculated using the transpose of measurement matrix, residue, and the output vector. Using this γ value, the threshold for this particular iteration is calculated. Then, for updating the output vector we perform soft thresholding function in gamma with the threshold value calculated in the previous step. Soft thresholding function is defined mathematically as

$$\eta(\gamma, \theta) = \text{sign}(\gamma) * (|\gamma| - \theta)_+ \quad (10)$$

In soft thresholding function, we multiply the sign of γ either with difference of absolute value of γ and θ or with zero, depending on which value is the maximum. In approximate message passing algorithm, the residue is found by considering not only the output vector and the current estimate of output vector Y , but also we take into account the residue calculated in the previous iteration also. And this additional factor contributes to reduced mean square error and aids in fast convergence of the algorithm. This whole process is repeated continuously till maximum number of iterations is reached.

Modified-AMP algorithm differs from AMP algorithm in two steps: threshold is taken as the M th largest element in γ and the proportionality factor for previous residue is the mean of derivative of soft thresholding function in γ [14]. After completing I_{MAX} iterations, current X value is taken as the reconstructed signal. Also, an early termination method can be applied, i.e., an error tolerance value is predefined and the iterations will be continued till the mean square error goes below

this preset threshold. And finally, the vector X of the last iteration is taken out as the approximated input vector X .

4 Implementation Results

The Modified-AMP algorithm was implemented with $M = 256$ and $N = 64$, using a measurement matrix populated by random values taken from normal distribution with mean zero and standard deviation one, whose matrix dimension is 64×256 .

That is, out of the 256 elements of X vector, 64 measurements are taken randomly achieving compression by a factor of four. This input vector is projected on to the measurement matrix Φ to generate the measurement vector Y of dimension 64. Figure 1 shows the input sparse signal with 256 elements and the measurement vector Y .

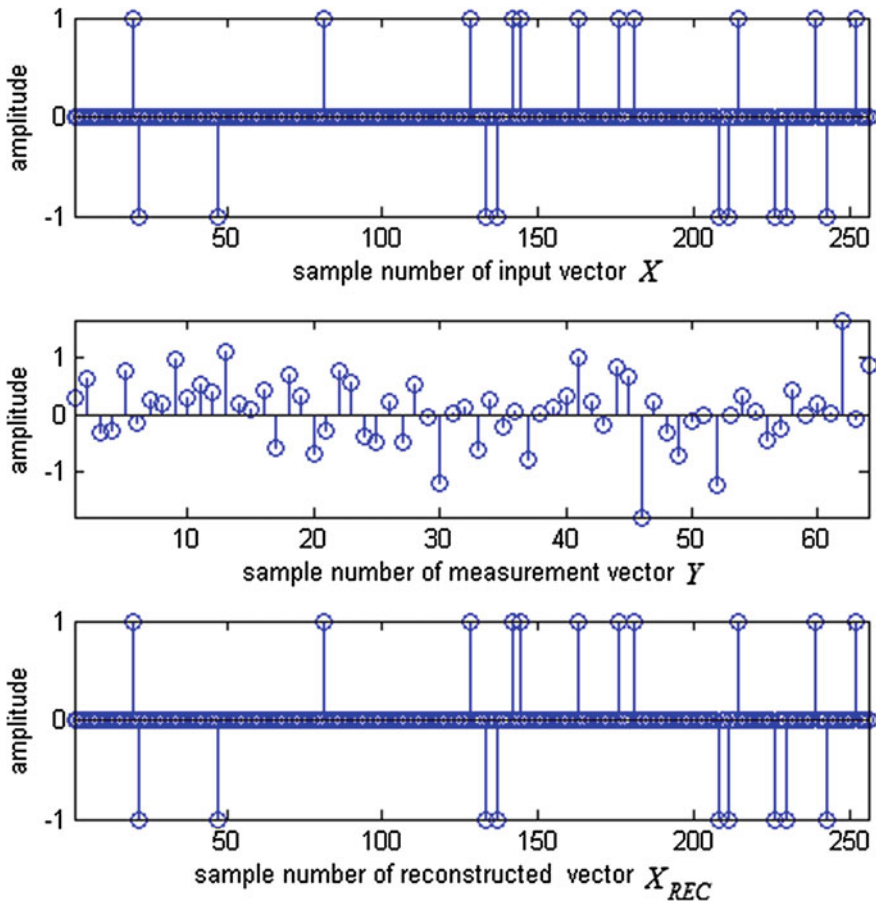


Fig. 1 Input vector, measurement vector, and the reconstructed vector

This measurement vector is given as input to the Modified-AMP reconstruction algorithm and the reconstructed vector is shown in Fig. 1. It is found to be identical to that of the input vector X .

Once the reconstruction was found to be successful for further analysis, the previous version of AMP algorithm is also considered. Both the original AMP algorithm as well as the Modified-AMP algorithm was implemented in MATLAB. Implementation was done for 50 different random data sets and the mean square value and the signal-to-noise ratio was calculated using the equations

$$\text{Mean square value} = \frac{1}{N} * \sum (X - X_{\text{REC}})^2 \tag{11}$$

$$\text{Signal to Noise ratio} = 20 \log \frac{\|X\|}{\|X - X_{\text{REC}}\|} \tag{12}$$

Figure 2 plots the mean square error of each of the data set used for both the algorithms. The average mean square error for all the data sets taken together is 0.1401 for AMP algorithm and is 0.0657 for the Modified-AMP algorithm. Approximately, 50 % reduction in mean square error is observed for reconstructions using the Modified-AMP algorithm.

Figure 3 shows the plot of signal-to-noise ratio for both algorithms using the different random data sets. The average signal-to-noise ratio for all the data sets

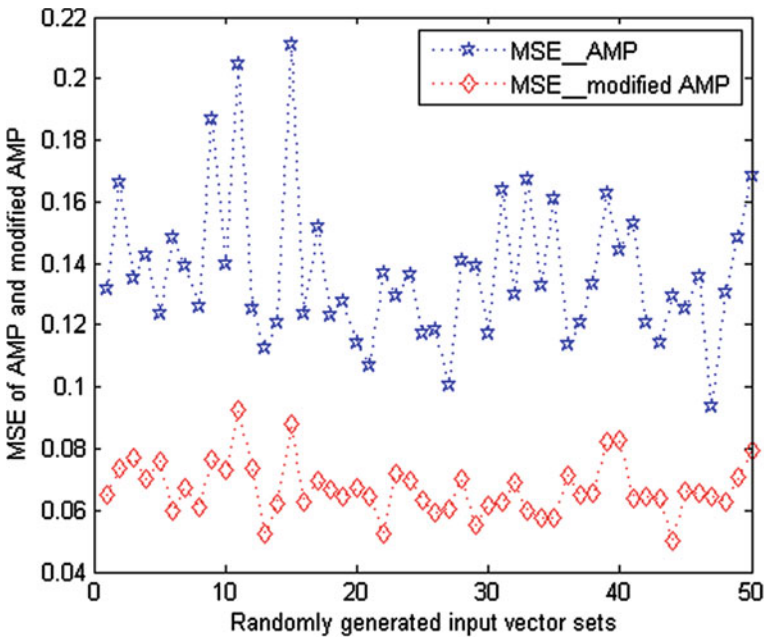


Fig. 2 Mean square error using AMP and Modified-AMP algorithms

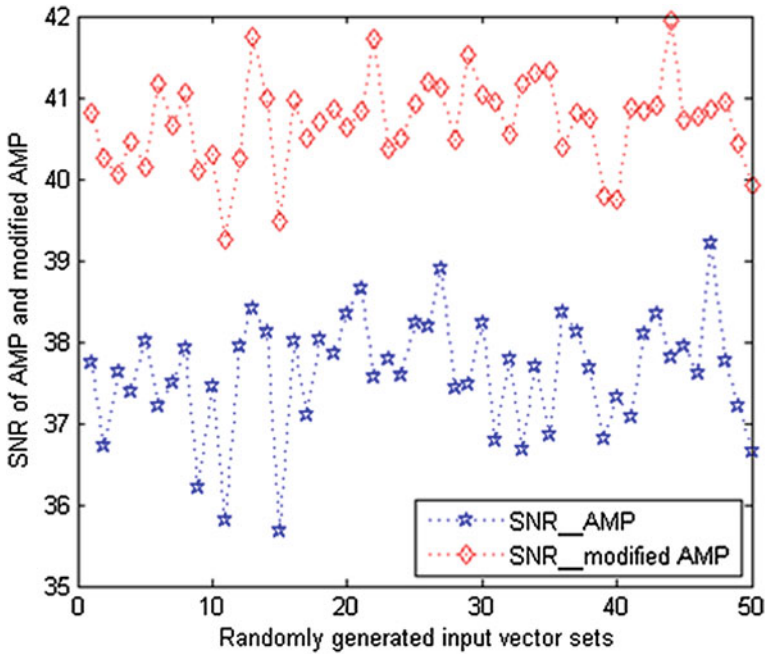


Fig. 3 Signal-to-noise ratio using AMP and Modified-AMP algorithms

Table 1 Comparison of AMP and Modified-AMP algorithm

	MSE	SNR (dB)	Reconstruction time (S)
AMP	0.1401	37.5057	0.001
Modified-AMP	0.0657	40.7837	0.001

taken together is 37.5057 dB for AMP algorithm and is 40.7837 dB for the Modified-AMP algorithm. An SNR improvement of 3 dB is observed when using the improved algorithm.

The reconstruction time taken by both algorithms was also observed and is tabulated in Table 1. For the same reconstruction time, Modified-AMP algorithm offers better recovery performance than the AMP algorithm.

5 Conclusion

Compressed sampling (CS) makes it possible the accurate reconstruction of under-sampled sparse signals and as many natural signals exhibit sparsity in some transfer domain, it has potential applications in fields where sample acquisition is costly, time consuming, and where power saving is of paramount importance like in

mobile biosensors. But to avail the complete benefits of CS, the nonlinear reconstruction algorithms are also required for proper reconstruction of the sensed samples. Many reconstruction algorithms have been developed and continue to be developed. In this paper, we have considered AMP algorithm which has less computational complexity per iteration along with fast convergence and provides an accurate reconstruction of approximately sparse signals also. Here, we have implemented a Modified-AMP algorithm and compared the mean square error and the signal-to-noise ratio of both the algorithms and found that the Modified-AMP algorithm offers a reconstruction with approximately 50 % reduction in mean square error and a 3 dB improvement in signal-to-noise ratio for the same reconstruction time. That is the Modified-AMP algorithm offers better recovery performance than the AMP algorithm utilizing the same amount of time as the AMP algorithm.

References

1. Candès E, Wakin M. An introduction to compressive sampling. *Sig Process Mag IEEE*. 2008;25(2):21–30.
2. Maleki A. Approximate message passing algorithms for compressed sensing. Ph. D. dissertation, Stanford University, 2011.
3. Donoho D. Compressed sensing. *IEEE Trans Inf Theory*. 2006;52(4):1289–306.
4. Subhashini S, Reddy AVS, Janarth M, Vignesh RA, Gandhiraj R, Soman KP. Compressive sensing based image acquisition and reconstruction analysis. In: *IEEE international conference on green computing, communication and electrical engineering (ICGCCEE'14)*, by Dr. N.G. P. Institute of Technology, Coimbatore, 7–8 Mar 2014.
5. Gayathri S, Gandhiraj R. Analysis of ECG signal compression with compressed sensing method. In: *International conference on advance engineering & technology (ICAET)*, Bengaluru, 23 Mar 2014.
6. Avinash P, Gandhiraj R, Soman KP. Spectrum sensing using compressed sensing techniques for sparse multiband signals. *Int J Sci Eng Res*. 2012;3(5).
7. Candès E, Romberg J, Tao T. Robust uncertainty principles: exact signal reconstruction from highly incomplete frequency information. *IEEE Trans Inf Theory*. 2006;52(2):489–509.
8. Tropp J, Gilbert A. Signal recovery from random measurement via orthogonal matching pursuit. *IEEE Trans Inf Theory*. 2007;53(12):4655–66.
9. Candès E, Romberg J. Sparsity and incoherence in compressive sampling. *Inverse Prob*. 2007;23(3):969–85.
10. Candès E, Romberg J, Tao T. Stable signal recovery from incomplete and inaccurate measurements. *Commun Pure Appl Math*. 2006;59:1207–23.
11. Donoho D, Maleki A, Montanari A. Message-passing algorithms for compressed sensing. *Proc. Nat Acad Sci*. 2009;6(45):18914–9.
12. Blumensath T, Davies M. Iterative thresholding for sparse approximations. To appear in *Journal of Fourier Analysis and Applications*, special issue on sparsity, 2008.
13. Maechler P et al. VLSI design of approximate message passing for signal restoration and compressive sensing. *IEEE J Emerg Sel Top Circ Syst*. 2012;2(3):2012.
14. Montanari A. Graphical models concepts in compressed sensing. [arXiv:1011.4328v3](https://arxiv.org/abs/1011.4328v3), Mar 2011.

Diagnosis of Corneal Arcus Using Statistical Feature Extraction and Support Vector Machine

S.V. Mahesh Kumar and R. Gunasundari

Abstract Corneal arcus is a white ring or arc deposited in the corneal region of the human eye. This corneal abnormality is significantly associated with the lipid disorders and atherosclerosis. In this paper, we proposed a computer-aided diagnosis system to detect the corneal arcus. The proposed method detects the corneal arcus using the statistical features extracted from the iris region of the eye image. The iris region is segmented from the other regions of the eye image using circular Hough transform (CHT). In order to achieve the better classification results, a morphological operation-based specular reflection removal and colour transformation-based enhancement methods are also developed in this paper. The proposed method was implemented and evaluated using the abnormal eye images from our own database and normal eye images collected from UBIRIS.v1 database. Our database contains the eye images with different grades of corneal arcus abnormality. The performance of our method was evaluated using the confusion matrix-based metrics. In the training phase, our method achieved a classification accuracy of 1. In the testing phase, our method achieved a classification accuracy of 0.96 with a positive predictive value 0.9791 and negative predictive value 0.9423.

Keywords Corneal arcus · Eye image · Iris segmentation · Statistical features · Classification

1 Introduction

The cornea is the transparent outermost layer of the eye that covers the pupil, iris and anterior chamber regions. Corneal layer has the curvature outer shape and it refracts the light entering into the eye. Due to this refracting nature, cornea plays a key role in human vision. The corneal region is borders with the sclera region by

S.V. Mahesh Kumar (✉) · R. Gunasundari

Department of ECE, Pondicherry Engineering College, Puducherry, India
e-mail: svmaheshkumar@pec.edu

© Springer India 2016

S.S. Dash et al. (eds.), *Artificial Intelligence and Evolutionary Computations in Engineering Systems*, Advances in Intelligent Systems and Computing 394, DOI 10.1007/978-81-322-2656-7_44

481

corneal limbus. Along with the sclera region, the cornea serves as a wall against the harmful particles.

According to the medical research, the abnormalities existing in the corneal region are linked to the lifestyle-related issues [1]. Due to this connection, symptoms of lifestyle-related diseases can be identified during the clinical eye examination. In [2], Urbano reviews the significance of Hyperlipidemia with the corneal abnormality arcus senilis (also known as corneal arcus). Arcus senilis is a yellowish or white ring around the cornea, which is caused by the lipid deposition in the peripheral corneal stroma. The lipid particles in the corneal region are similar to the lipid particles isolated from the atherosclerotic lesions [3]. Medical studies also show that the corneal arcus is significantly associated with the elevated blood total cholesterol, LDL levels and correlated with atherosclerosis [4, 5]. Hence, the screening of corneal arcus is helpful for earlier diagnosis of lipid disorders.

The usual eye examination concentrates on the cornea region, which is easily visible during the slit lamp test. Few computer-aided diagnosis systems are developed to detect the corneal abnormalities automatically using eye images [6–8]. In [9, 10], Ramlee et al. proposed a method to detect the Arcus senilis automatically using iris recognition algorithm [11] combined with Otsu’s threshold method. The iris segmentation module of this method is failed due to the specular reflections in the eye images, and this method was not concentrated about the clinical corneal arcus images with different levels of lipid deposition.

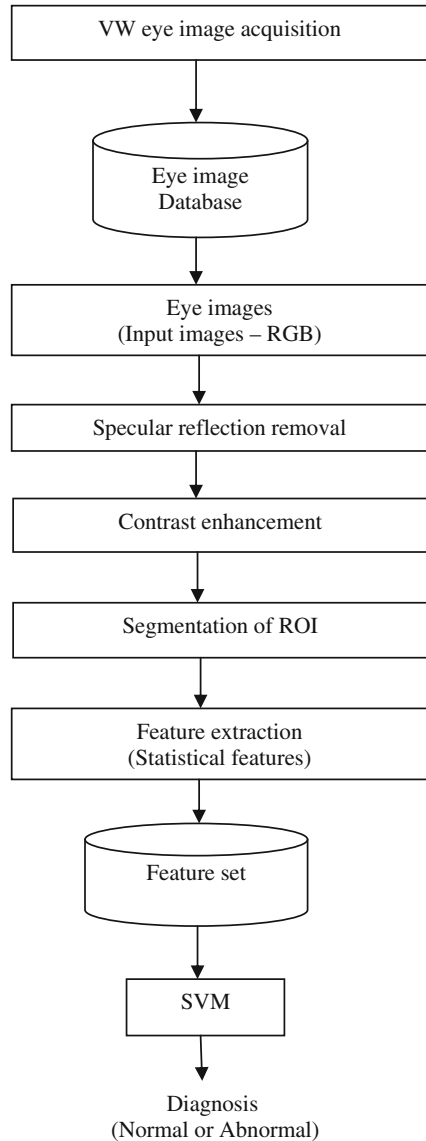
In this paper, we propose a novel classification method, to detect the corneal arcus abnormality. This method can classify the normal and corneal arcus eye images using the statistical features extracted from their iris circle. The proposed method concentrates on the specular reflection removal in the input eye image for accurate diagnosis. In order to implement our method, we have created an eye image database. This database contains the eye images with different grades of corneal arcus. The performance of our method is evaluated using the abnormal (eye with corneal arcus) images from our database and normal images collected from the public eye image database.

The remainder of this paper is organized as follows: In Sect. 2, we present the proposed methodology. The sequential processing step of our methodology is detailed in this section. The database details, experimental details about the learning and testing of support vector machine (SVM) for corneal arcus diagnosis and performance evaluation of the proposed methodology are described in Sect. 3. Finally, Sect. 4 concludes the paper.

2 Methodology

The proposed corneal arcus diagnosis system is illustrated in Fig. 1. The sequential process starts with getting a visible wavelength (VW) eye image from the database. After this, the specular reflection in the input image is removed using the morphological operation. The contrast of the reflection removed image is enhanced for

Fig. 1 Flowchart of the proposed corneal arcus diagnosis method



accurate detection of iris outer boundary. After contrast enhancement process, the circular Hough transform (CHT) is used to segment the iris circle of the enhanced image. The segmented region is considered as the region of interest (ROI) for the feature extraction process. The statistical features are extracted from the ROI. All the training eye images in the database are processed and the features are extracted from their ROI. The extracted features are used to create a training feature set. The SVM is trained using the training feature set. After training process, the SVM

can diagnose the corneal arcus abnormality in the eye image. The sequential steps of our method are described as follows.

2.1 *Specular Reflection Removal*

Specular reflections are appeared as the brightest points in the VW eye image. Specular reflections affect the segmentation process. In our method, the reflections are removed using morphological dilation technique. In the first step of the reflection removal process, the red, green and blue channels of the input image are separated. The higher intensity region in each channel is identified using intensity thresholding. The threshold intensity value of each channel is determined based on the histogram analysis of VW images in the database. The threshold intensity value chosen for R, G and B channels are 230, 235 and 235, respectively. After identification of the higher intensity pixels, a binary image is created using these pixels. In the binary image, the higher intensity regions are represented as the white pixels. The binary image is dilated by the structuring element with size 12 by 12. The dilation operation is represented as

$$\text{dil}(X, B) = X \oplus B \quad (1)$$

In Eq. 1, X is the binary image and B is the structuring element and $X \oplus B$ is defined as

$$X \oplus B = \{x : Bx \cap X \neq \emptyset\}$$

Here, the binary image and structuring elements are represented as sets in two-dimensional Euclidean space. Bx is the translation of B (its origin is located at x) and the intersection is non-empty. After dilation process, the exterior boundaries of the specular reflection regions are identified in the binary image. The specular reflection regions in R, G and B channels are removed by performing the interpolation operation inside their detected boundaries. The intensity of the filled pixels is equal to the maximum intensity of their neighbourhood pixels. Finally, a reflection removed image is created using the specular reflection removed R, G and B channels. Figure 2 shows the example of input eye image with specular reflection and the reflection removed image.

2.2 *Contrast Enhancement*

A minimum contrast level should be maintained for accurate detection of iris outer boundary. Specular reflection removed image is used as an input for the contrast enhancement process. In the first step of this contrast enhancement process, the

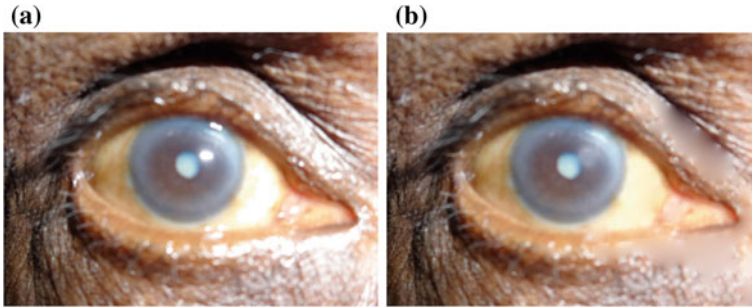
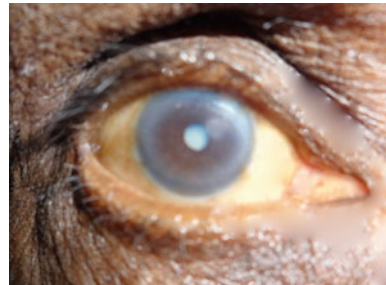


Fig. 2 Specular reflection removal, **a** VW input eye image with specular reflection, **b** reflection removed image

Fig. 3 Enhanced image



reflection removed RGB image is transformed into YUV colour space. After this, the mean value of the luminance (Y) is calculated. The normalized luminance value is calculated from this mean value and it is compared with the threshold value 0.6, to identify the contrast degradation. The luminance of the degraded image is adjusted according to the threshold value using linear transformation. Finally, the YUV colour space is converted to RGB colour space, to create the enhanced image. The enhanced image is shown in Fig. 3.

2.3 Segmentation

In the first step of segmentation process, the enhanced image is converted as a gray-scale image, to create the edge map. Here, the edge map is created using the canny edge detector. After edge detection, the CHT is applied to the edge map, to find the outer circle of the iris. The CHT is scanning the parameters (x_c , y_c and radius), to identify the circles presented in the edge map. The circle scanning process is represented by the equation

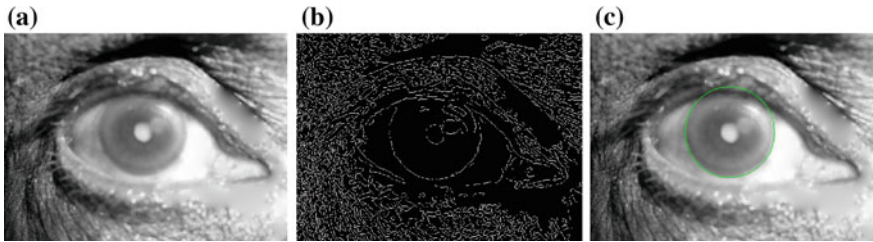


Fig. 4 Segmentation process, **a** gray-scale image, **b** edge map of **(a)**, **c** detected iris boundary using CHT (Region inside the *circle* is ROI)

$$(x - x_c)^2 + (y - y_c)^2 = r^2 \quad (2)$$

Here, x_c and y_c are the center coordinates and r is the radius of the iris circle. After iris circle detection, the region outside the detected circle is masked. The segmented region contains the lipid deposition, if the input eye image is acquired from the subject with corneal arcus abnormality. The segmentation process is mainly concentrated on the isolation of iris circle from the sclera region, which contains white pixels. The various steps involved in the segmentation process are shown in Fig. 4.

2.4 Feature Extraction

The segmented region is used as the ROI for feature extraction. The ROI with corneal lipid deposition contains white pixels. These white pixels differentiate the intensity profile of the ROI of the abnormal image from the ROI of the normal image. Therefore, the normal and abnormal images can be classified using the statistical features extracted from their ROI. We used the first-order statistical features for classification purpose. The first-order statistical features used in our method can be represented as

$$\text{Mean } (\mu) = \sum_{p=0}^{P-1} pH(p) \quad (3)$$

$$\text{Standarddeviation } (\sigma) = \sqrt{\sum_{p=0}^{P-1} (p - \mu)^2 H(p)} \quad (4)$$

$$\text{Entropy } (E) = - \sum_{p=0}^{P-1} H(p) \log_2(H(p)) \quad (5)$$

Table 1 Statistical features of the sample abnormal image

Mean	Standard deviation	Entropy	Skewness	Kurtosis
82.9472	55.6606	6.9067	0.3596	2.6455

$$\text{Skewness } (s) = \frac{\mu_3}{\mu_2^{(3/2)}} \quad (6)$$

$$\text{Kurtosis } (k) = \frac{\mu_4}{\mu_2^2} \quad (7)$$

- Here, $H(p)$ is the probability density function estimated from the histogram $H(p) = n_p/N$ where pixel value $p = 0, 1, 2, \dots, P-1$
- P is the number of gray levels, N is the number of pixels in the image and n_p is the number of pixels with value p .
- μ_3 and μ_4 are computed from $\mu_n = \sum_{p=0}^{P-1} (p - \mu)^n H(p)$

The statistical features are extracted from the ROI of all training images and a training feature set is created using this features. This feature set is used to train the SVM for corneal arcus diagnosis. Table 1 shows the statistical features extracted from the ROI of the sample abnormal image (shown in Fig. 4c).

2.5 Classification

The SVM, a two-class machine learning classifier, is selected for classification purpose. The two-class SVM performs the classification by creating the optimal separating hyper-plane (OSH). The OSH maximizes the margin between the nearest two data points of the normal and abnormal classes. To train the classifier, the training feature set is fed into the classifier. In the testing phase, the statistical features extracted from the ROI of normal and abnormal test images are used for classification. The experimental details about the SVM training and testing are described in Sect. 3.2.

3 Experimental Results

In this section, we describe the experimental details of the proposed method. The database details are first explained and then the effectiveness of the extracted statistical features is evaluated. Training and testing experiments on the SVM classifier using the extracted features are also described. Finally, the performance of our method is evaluated using the confusion matrix-based performance evaluation metrics.



Fig. 5 Example of eye images. **a** Corneal arcus images (abnormal images) from our database. **b** Normal images from UBIRIS.v1 database

3.1 Database

The eye images with and without corneal arcus are used in our experiments. The 100 eye images without corneal arcus were selected from the UBIRIS.v1 database [12]. This database does not have the different grades of corneal arcus images. For this reason, we create our own database in association with Indira Gandhi Medical College and Research Institute, Puducherry. To create this database, a total numbers of 100 images were acquired from the both eyes of the 50 patients, with their permission. The 16.2 Mega Pixel digital camera equipped with a VW illumination was used for image acquisition. The eye images were acquired inside the room environment using user cooperation image acquisition mode. Our database contains the eye images with different grades of corneal arcus. Figure 5 shows the example of abnormal and normal eye images collected from our database and UBIRIS.v1 database.

3.2 SVM Training and Testing Experiments

In the training phase, the training feature set is fed into the SVM classifier. The training feature set contains the first-order statistical features extracted from the ROI of the normal and abnormal eye images. Figures 6 and 7 clearly show that the abnormal images have the higher ranges of mean and standard deviation values compared with the normal images. The kurtosis range of the normal images is greater than the kurtosis range of abnormal images. The entropy range of most of the abnormal images is slightly higher than the entropy range of the normal images. Conversely, the skewness range of most of the normal images is slightly greater than the skewness range of abnormal images. All these observations on the extracted features show that the statistical features vary according to the abnormality presented in the ROI of the eye image and the SVM can be trained using the

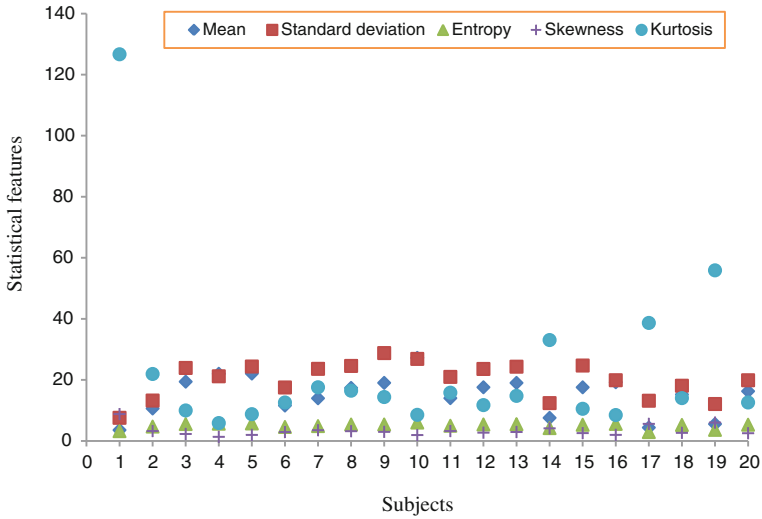


Fig. 6 Statistical features of the sample normal images

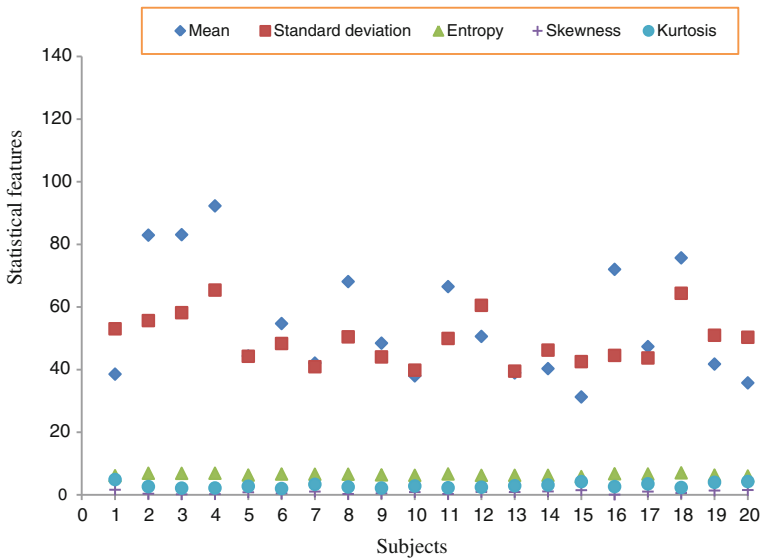


Fig. 7 Statistical features of the sample abnormal images

extracted statistical features. In our experiments, we implemented the SVM using the Kernel Adatron algorithm [13]. Kernel Adatron algorithm maps the inputs into a high-dimensional feature space, after which optimally separates the data points into their respective classes by isolating the inputs, which fall closer to the data

Table 2 Details of training and testing experiments on SVM for corneal arcus diagnosis

Phase	Total number of images	Number of normal images	Number of abnormal images	Feature set size	Maximum epochs
Training	100	50	50	5 features × 100 images	100
Testing	100	50	50	5 features × 100 images	100

boundaries. This algorithm is effective in separating the datasets, which share the complex boundaries. To detect the corneal arcus, the SVM is trained using the training feature set. After the training phase, the testing feature set is fed into the SVM, to measure the classification performance. The experimental details about the training and testing of SVM are summarized in Table 2.

3.3 Performance Evaluation

The classification performance of our method is evaluated using the performance metrics derived from the confusion matrix. The confusion matrixes obtained from the classification experiments of our method are shown in Tables 3 and 4.

From the confusion matrix, we derive the four types of possible results. The possible results are listed as (a) true positive (TP), (b) false positive (FP), (c) true negative (TN), and (d) false negative (FN). For abnormal image, the result is TP if the predicted diagnosis is abnormal and FN if the predicted diagnosis is normal. For normal image, the result is TN if the predicted diagnosis is normal and FP if the predicted diagnosis is abnormal. Using these TP, FP, TN and FN values, we can compute the following performance measures:

$$\text{Sensitivity} = \frac{\text{TP}}{\text{TP} + \text{FN}} \tag{8}$$

Table 3 A confusion matrix of SVM classification using the features extracted from the ROI of training images

Desired classification	Predicted classification	
	Abnormal (%)	Normal (%)
Abnormal (%)	100	0
Normal (%)	0	100

Table 4 A confusion matrix of SVM classification using the features extracted from the ROI of test images

Desired classification	Predicted classification	
	Abnormal (%)	Normal (%)
Abnormal (%)	94	6
Normal (%)	2	98

Table 5 Performance evaluation of the proposed method

Phase	Sensitivity	Specificity	Accuracy	PPV	NPV
Training	1	1	1	1	1
Testing	0.94	0.98	0.96	0.9791	0.9423

$$\text{Specificity} = \frac{\text{TN}}{\text{TN} + \text{FP}} \quad (9)$$

$$\text{Accuracy} = \frac{\text{TP} + \text{TN}}{\text{TP} + \text{FP} + \text{FN} + \text{TN}} \quad (10)$$

$$\text{Positive Predictive value (PPV)} = \frac{\text{TP}}{\text{TP} + \text{FP}} \quad (11)$$

$$\text{Negative Predictive value (NPV)} = \frac{\text{TN}}{\text{TN} + \text{FN}} \quad (12)$$

The performance measures are computed for the training and testing phases separately. These measures are computed from the values in Tables 3 and 4 using the equations 8–12. The computed performance measures are summarized in Table 5.

4 Conclusions

In this paper, a novel approach for corneal arcus diagnosis on VW eye images has been presented. The proposed method detects the corneal arcus abnormality using the statistical features extracted from the segmented iris circle of the eye image. The evaluation of the extracted features shows that the statistical features varied according to the lipid deposition existing in the ROI of the eye image. The learning and testing experiments on the SVM using the normal and abnormal eye images show that our method is efficient to detect the corneal arcus abnormality. The performance evaluation using the confusion matrix-based metrics proved that the classification accuracy of our method is closer to the manual diagnosis. Based on the experimental results and performance evaluation, we concluded that the proposed method is suitable for clinical corneal disease diagnosis systems. This method can also be used to detect the other eye diseases such as cataract and yellow peripheral corneal ring.

Acknowledgments We would like to thank Dr. N. Ezhilvathani, HOD, Department of Ophthalmology, Indira Gandhi Medical College and Research Institute (IGMC&RI), Puducherry for her suggestions and support on the corneal arcus eye image collection for this work.

References

1. Klein BEK, Klein R. Lifestyle exposures and eye diseases in adults. *Am J Ophthalmol.* 2007;144(6):961–9.
2. Urbano FL. Ocular signs of hyperlipidemia. *Rev Clin Signs. Hospital Phys.* 2001;51–53.
3. Gaynor PM, Zhang W-Y, Salehizadeh B, Pettiford B, Kruth HS. Cholesterol accumulation in human cornea: evidence that extracellular cholesteryl ester-rich lipid particles deposit independently of foam cells. *J Lipid Res.* 1996;1849–1861.
4. Moosavi M, Sareshtedar A, Zarei-Ghanavati S, Zarei-Ghanavati M, Ramezanzar N. Risk factors for senile corneal arcus in patients with acute myocardial infarction. *J Ophthalmol Vis Res.* 2010;228–31.
5. Zech LA Jr, Hoeg JM. Correlating corneal arcus with atherosclerosis in familial hypercholesterolemia. *Lipids Health Dis.* 2008. doi:[10.1186/1476-511X-7-7](https://doi.org/10.1186/1476-511X-7-7).
6. Morello R, De Caupa C, Fabbiano L, Vacca G. Image based detection of Kayser-Fleischer ring in patient with wilson disease. In: *IEEE International symposium on medical measurements and applications proceedings (MeMeA)*; 2013. p. 101–106.
7. Lesmana IPD, Purnama IKE, Purnomo MH. Abnormal condition detection of pancreatic beta-cells as the cause of diabetes mellitus based on iris image. In: *2nd International conference on instrumentation, communications, information technology, and biomedical engineering (ICICI-BME)*; 2011. p. 150–155. doi:[10.1109/ICICI-BME.2011.6108614](https://doi.org/10.1109/ICICI-BME.2011.6108614).
8. Acharya R et al. Computer based classification of eye diseases. In: *IEEE proceedings of EMBS international conference*; 2006. p. 6121–6124.
9. Ramlee RA, Ranjit S. Using iris recognition algorithm, detecting cholesterol presence. In: *International conference on information management and engineering. IEEE Computer Society*; 2009. p. 714–717. doi:[10.1109/ICIME.2009.61](https://doi.org/10.1109/ICIME.2009.61).
10. Ramlee RA et al. Automated detecting arcus senilis, symptom for cholesterol presence using iris recognition algorithm. *J Telecommun Electron Comput Eng.* 2011;29–39.
11. Masek L. Recognition of human iris patterns for biometric identification. Dissertation. The University of Western Australia; 2003.
12. Proenca H, Alexandre LA. UBIRIS: a noisy iris image database. In: *Proceedings of 13th international conference on Image analysis and processing*; 2005. p. 970–977.
13. Frieß T-T, Cristianini N, Campbell C. The Kernel-Adatron algorithm: a fast and simple learning procedure for support vector machines. In: *Proceedings of the fifteenth international conference on machine learning. Morgan Kaufmann Publishers Inc.*; 1998. p. 188–196.

Hospital-Based Screening for Osteoporosis in Both Sexes Aged Above 50 Years Using Prototype US Bone Densitometer

Moataz Samir and M. Anburajan

Abstract In India, an orthopedician sees many patients commonly with a complaint of bone pain and other pathological bone fracture during his/her daily clinical consulting. ‘Osteoporosis’ is the cause for bone mineral loss. It affects postmenopausal women and aged population of both sexes. Many of these people are found to be asymptomatic. A simple reliable screening device is required in a hospital to identify an individual with low areal bone mineral density (aBMD, g cm^{-2}) with good accuracy. So that, a suitable therapeutic intervention can be initiated to prevent further loss in aBMD. The dual energy X-ray absorptiometry (DXA) bone densitometer, a ‘gold’ standard device, used to measure aBMD) at the hip, spine, and forearm. In India, DXA bone densitometer is found to be costly and is restricted only in urban cities. On the other hand, quantitative ultrasound (QUS) bone densitometer is cost effective, and is widely available. Even now, the cost of QUS is not affordable by many hospitals in rural parts of India. The aim of this study was to screen subjects of both sexes, aged 50 years and above in a hospital for osteoporosis using a low cost, portable constructed prototype of QUS bones densitometer with a good accuracy. The prototype of the device was constructed using a pair of wideband, flat, composite US transducers (diameter = 10 mm) operating at a central frequency equal to 0.5 MHz. The following US parameters were measured accurately at one-third length of ulna bone using the digital storage oscilloscope (DSO): (i) Ultrasonic transmit time (ΔT , μsec) and (ii) Ultrasonic attenuation (ΔV in volt). The device was calibrated with a step bone phantom of known BMD (g cm^{-2}) values. A total number of 98 women and men, aged 50 years and above were screened for the disorder in a hospital. In each subject, the QUS parameters were measured at right side ulna bone region under standard conditions using the prototype bone densitometer. In each subject, the ulna

M. Samir (✉) · M. Anburajan
Department of Biomedical Engineering (BME), SRM University,
Kattankulathur, Chennai 603203, Tamil Nadu, India
e-mail: Moatazsamir1010@hotmail.com

M. Anburajan
e-mail: hod.biomedi@ktr.srmuniv.ac.in

aBMD was estimated with good accuracy using the measured ΔV by the prototype bone densitometer. All the obtained data were analyzed statistically. In the total women screened, aged 50 years and above ($n = 49$; mean \pm SD age = 57.8 ± 9.8 years) using the prototype bone densitometer, it was found that 57.1, 20.4, and 22.4 % of the screened women were found to be having osteoporosis, osteopenia, and normal, respectively. On the other hand, in the total men screened, aged 50 years and above ($n = 49$; mean \pm SD age = 60.8 ± 11.5 years), it was found that 36.7, 28.6, and 34.7 % of the men were found to be having osteoporosis, osteopenia, and normal, respectively. Also, it was observed that, in osteoporotic women, the percentage difference in the mean value of estimated BMD (g cm^{-2}) compared to normal was greater (71.8 %), when compared to the same measured in osteoporotic men counterpart (59.1 %). The designed prototype US bone densitometer can be used to screen an individual who is at risk for future osteoporosis, with good accuracy.

Keywords Osteoporosis • Osteopenia • Normal • US attenuation • US transmit time

1 Introduction

‘Osteoporosis’ (a condition of having low bone mineral) is one of the major health problems in India and in other parts of the world. It affects mainly postmenopausal women, and an aged population of both sexes. In postmenopausal women, the osteoclastic bone resorption would be greater due to drop in estrogen hormone than osteoblastic bone formation, and hence it results in net loss in bone mineral loss usually in trabecular component of the bone. On the other hand, in aged population, particularly 70 years and above, of both sexes, an increased osteoclastic bone resorption leads to thinning of both trabecular- as well as cortical- bone. In both cases mentioned above, a fracture of bone will occur more easily, as there is a substantial bone mineral loss. This kind of osteoporotic fractures are more common in the lumbar- and thoracic- spine, proximal femur, forearm, and humerus. It is known that, these pathological fractures are well associated with morbidity and mortality [1]. It was well known that, the areal bone mineral density (aBMD, g cm^{-2}) correlates highly with the strength of the bone, and therefore, it predicts future risk of fracture. The prevention of ‘first’ osteoporotic fracture will reduce the healthcare costs and excess mortality. It is very important to identify an individual who is at risk of future osteoporosis, before he/she gets a fracture, because, even a short-term subject specific interventions can significantly prevent further accelerated bone mineral loss [2, 3]. An ideal screening method for osteoporosis should satisfy the following criteria: (i) good accuracy; (ii) good reproducibility; (iii) cost effective; (iv) portable; and (v) no side effects [4]. In India, even the cost-effective quantitative ultrasound (QUS) bone densitometers are limited in many hospitals at rural parts of the country. Also, the accuracy as well as precision of the QUS device varies with different manufacturers. The objective of this pilot study was to screen

hospital patients, aged 50 years and above, for osteoporosis using a constructed portable QUS bone densitometer noninvasively with a good accuracy.

2 Materials and Methods

2.1 Design and Construction of Ultrasound Bone Densitometer

The prototype of QUS bone densitometer was constructed according to the technical descriptions outlined (5) by one of our earlier research study [5]. It consisted of a pair of wideband, composite US transducers (diameter = 10 mm) operating at a central frequency equal to 0.5 MHz, one acted as a single element transmitter transducer (Tt), whereas, other one as a single element receiver transducer (Rt). The device was connected to a rechargeable 12 V battery with a recharging circuit. The exciter (pulser) produced a 12 V, 500 ns pulse to excite the QUS Tt. A gel coupler placed on the transducers and the forearm was used to ensure good acoustic conduction between them. The generated US signal propagated through the ulna bone (of forearm) and it reached Rt. Finally, the received attenuated US signal was displayed in a digital storage oscilloscope (DSO) for the measurement of the following two US parameters, defined in this study: (i) Ultrasonic transmit time (ΔT), which was defined as the speed of sound (SOS) of the excited US signal reaching from transmitter transducer (Tt) to receiver transducer (Rt) and it was measured in microsecond (μsec) and (ii) Ultrasonic attenuation (ΔV), which was defined as the amplitude of the received signal and it was measured in volt (V). This device was calibrated using a bone mineral step phantom of known volumetric bone mineral densities, and the following regression equations were obtained statistically to predict areal BMD(g cm^{-2}) with good accuracy using the measured US parameters by the prototype device.

$$\text{aBMD}(\text{g cm}^{-2}) = 1840.3 (\Delta T^4) - 10585 (\Delta T^3) + 21447 (\Delta T^2) - 17622 (\Delta T) + 5170.7 (r = 0.629) \quad (1)$$

$$\text{aBMD}(\text{g cm}^{-2}) = -3.1594 (\Delta V^5) + 80.406 (\Delta V^4) - 763.98 (\Delta V^3) + 3339 (\Delta V^2) - 6687.8 (\Delta V) + 5488.3 (r = 0.836) \quad (2)$$

where ΔT and ΔV were the measured US transducer transit time (μsec) and US attenuation (volt), respectively, measured at ulna bone using the prototype QUS bone densitometer.

The prototype device was validated with the bone phantom of known aBMD value of 0.556, supplied by a pDXA manufacturer. The calculated percentage difference between the estimated aBMD values using the measured ΔT and ΔV

variables by the device and the actual aBMD value of the phantom were given as follows: +3.8 % and -2.3 %, respectively. Thus, it was found that the US parameter either ΔT or ΔV alone measured by the prototype QUS bone densitometer can estimate the aBMD of the bone phantom (pDXA) with a good accuracy. On comparison, the measured US attenuation (ΔV) parameter by the device can estimate ulna BMD with high accuracy (an error was found to be -2.3 %, when compared to bone phantom measurement studied). Further, it was found that in women studied, the estimated ulna aBMD (g cm^{-2}) using the measured ΔT and ΔV parameters by the prototype device were found to be correlated statistically with the measured forearm aBMD (g cm^{-2}) by the pDXA bone densitometer and the obtained statistical correlation coefficients were 0.504 ($p = 0.014$) and 0.508 ($p = 0.016$), respectively. Further, in men studied, the estimated ulna aBMD (g cm^{-2}) using the measured ΔT and ΔV parameters by the prototype device were found to be correlated statistically with the measured forearm aBMD (g cm^{-2}) by the pDXA bone densitometer, and the obtained statistical correlation coefficients were 0.614 ($p = 0.01$) and 0.580 ($p = 0.01$), respectively.

2.2 Hospital-Based Screening Study for Osteoporosis

A free public screening study for osteoporosis, who were aged 50 years and above of both sexes, was carried out during the second week of February 2015 at the outpatient unit of department of Orthopaedics, SRM Hospital, Research and Post-graduate Centre, SRM University, Kattankulathur, Chennai, Tamil Nadu, India. Each subject, enrolled for the study, had undergone a basic clinical assessment by a doctor. The basic characteristics of each subject were obtained using a self-explained simple questionnaire prepared for the study. According to an inclusion criteria laid down for this study, both men and women, who were aged 50 years and above were included. On the other hand, according to an exclusion criteria of the study, those who were aged less than 50 years were excluded. Also, those who were known to be suffering from secondary bone diseases and those who had old pathological bone fractures were excluded. This study was approved by our institutional ethical committee approval.

A total number of one hundred and twenty-eight subjects were enrolled in the screening camp. An informed consent was obtained from each subject, after explaining the purpose- as well as an outcome- of the study. After careful execution of both inclusion-, and exclusion- criteria defined in the study mentioned above, a total number of 98 subjects (men and women were 49 each) were included in the study analysis. As the remaining 28 subjects were not suitable for the study, they were debarred from the study.

In each subject, the right side ulna aBMD (g cm^{-2}) were estimated at standard conditions using the prototype QUS bone densitometer device. A quality assurance test for the device was performed on each day, just before the QUS measurement using the bone phantom, supplied by a pDXA manufacturer to ensure its stability.

The transducers of the prototype device were placed at a fixed anatomical location of the ulna bone of the forearm, i.e., at one-third of the forearm and the US parameters were measured. For each subject, the measurements were repeated for three times, and an average value of both ΔT and ΔV was calculated. The average value of ΔV of each subject studied was substituted in the obtained statistical equation mentioned above and their corresponding estimated ulna aBMD (g cm^{-2}) were calculated.

In each subject, aged ≥ 50 , years, a cut-off T-score value -2.0 of forearm BMD by pDXA EXA-3000, established by Marwaha and coworkers [6] was used to diagnose osteoporosis in the subjects studied with good sensitivity (6). In our earlier study [5], it was reported that, in normal young women and men studied, the peak values of estimated ulna aBMD (g cm^{-2}) using the measured ΔV value by the prototype QUS bone densitometer were found to be $0.56 (\pm 0.5)$ and $0.54 (\pm 0.7)$, respectively, (5). These estimated peak aBMD values were used (by calculating sex-specific T-score) to classify the subjects screened into normal, osteopenia, and osteoporosis. After applying these diagnostic criteria, the men and women screened in the hospital were classified as follows:

- (a) Total men screened ($n = 49$):
 - (i) Normal subjects: ($n = 17$, mean \pm SD age = 60.7 ± 9.8 years);
 - (ii) Subjects having osteopenia: ($n = 14$, mean \pm SD age = 60.8 ± 11.5 years);
 - (iii) Subjects having osteoporosis: ($n = 18$, mean \pm SD age = 50.8 ± 7.1 years).
- (b) Total women screened ($n = 49$):
 - (i) Normal subjects: ($n = 11$, mean \pm SD age = 57.8 ± 9.8 years);
 - (ii) Subjects having osteopenia: ($n = 10$, mean \pm SD age = 52.6 ± 7.1 years);
 - (iii) Subjects having osteoporosis: ($n = 28$, mean \pm SD age = 55.1 ± 7.5 years).

2.3 Statistical Analysis

The measured data were analyzed using IBM SPSS/PC statistical software version 21. The mean and SD values of all the measured parameters were calculated in each group separately. Further, the student's t-test was used to assess the statistical significance of these parameters between the groups studied in women and men separately.

3 Results

Figure 1a, b show the US parameters measurement made at ulna bone in a subject using the constructed QUS bone densitometer in a hospital. The calculated mean \pm SD values of all the parameters measured in women and men studied are

(a)



(b)

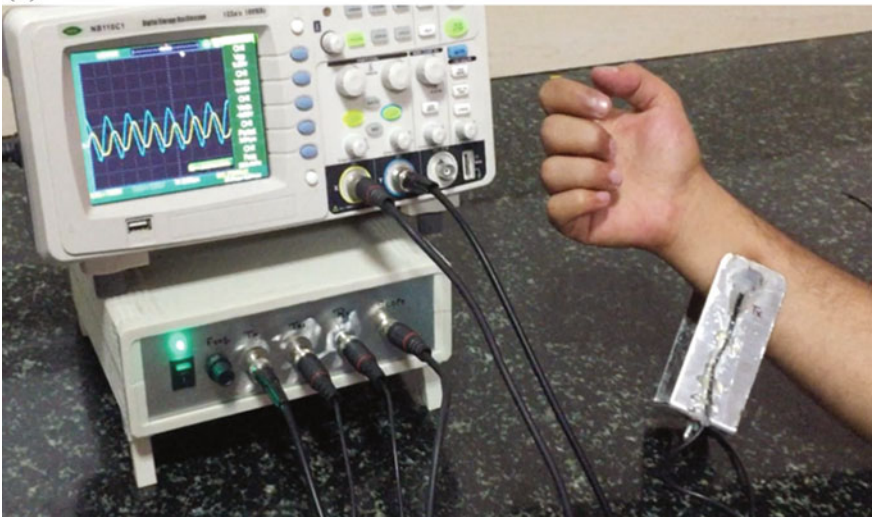


Fig. 1 a The screening a patient for osteoporosis by the first investigator (Mr. Moataz Samir) of this study in a hospital using the constructed QUS bone densitometer. b US parameter measurements at ulna bone in a subject using the constructed QUS bone densitometer

listed in Tables 1 and 2, respectively. In the total women screened, aged 50 years and above ($n = 49$; mean \pm SD age = 57.8 ± 9.8 years) using the prototype QUS bone densitometer, it was found that 57.1, 20.4, and 22.4 % of the women were found to be having osteoporosis, osteopenia, and normal, respectively. On the other hand, in the total men screened, aged 50 years and above ($n = 49$; mean \pm SD age = 60.8 ± 11.5 years), it was found that 36.7, 28.6, and 34.7 % of the men were found to be having osteoporosis, osteopenia, and normal, respectively. Thus, it was found that, the percentage of women having osteoporosis was found to be greater, when compared to the same in men counterpart studied. In osteoporotic women ($n = 28$), the calculated percentage difference in the mean value of estimated BMD (g cm^{-2}) using the prototype bone densitometer was found to be lesser by 71.8 % [$(0.85 - 0.24)/0.85 \times 100$], when compared to their normal counterpart studied and it was statistically significant at $p = 0.006$; On the other hand, in osteoporotic men ($n = 18$), the calculated percentage difference in the mean value of estimated BMD (g cm^{-2}) using the prototype device was found to be lesser by 59.1 % [$(0.66 - 0.27)/0.66 \times 100$], when compared to their normal counterpart studied, and it was statistically significant at $p = 0.002$. It was found that, in osteoporotic women, the percentage difference in the mean value of estimated BMD (g cm^{-2}) compared to normal was greater (71.8 %), when compared to the same observed in osteoporotic men counterpart.

The evaluated risk factors of the studied subjects are listed in Table 3. In osteoporotic women studied, aged 50 years and above, it was found that 75 % women obtained natural menopause, and the remaining 25 % had undergone oophorectomy. Further, 10.7 and 89.3 % of osteoporotic women were found to be vegetarian, and nonvegetarian, respectively. In osteoporotic men studied, aged 50 years and above, the smokers, alcohol drinkers, and both smokers and alcohol drinkers were found to be 16.7, 27.8, and 44.4 %, respectively. Also, 22.7 and 77.8 % of osteoporotic men were found to be vegetarian and nonvegetarian, respectively.

4 Discussion

The limitation of the study includes that those who screened as having low bone mineral mass by the prototype QUS bone densitometer was not confirmed by DXA bone densitometer, a 'gold' standard to diagnose osteoporosis. Also, the potential of the device to predict the future osteoporotic fracture risk in the population was not studied. In conclusion, in the total women screened, aged 50 years and above using the prototype bone densitometer, it was found that 57.1, 20.4, and 22.4 % of the screened women were found to be having osteoporosis, osteopenia, and normal, respectively. On the other hand, in the total men screened, aged 50 years and above, it was found that 36.7, 28.6, and 34.7 % of the men were found to be having osteoporosis, osteopenia, and normal, respectively. The constructed prototype QUS bone densitometer has a potential to screen the patients in a hospital for osteoporosis with good accuracy.

Table 1 The characteristics of the studied women subjects

Total women screened ($n = 49$, mean \pm SD age = 57.8 ± 9.8 years)						
Parameter	Normal	Osteopenia	Osteoporosis	Statistical significance		
	$n = 11$, mean \pm SD, age = 57.8 ± 9.8 years	$n = 10$, mean \pm SD, age = 52.6 ± 7.1 years	$n = 28$, mean \pm SD, age = 55.1 ± 7.5 years	Normal versus osteopenia	Normal versus osteoporosis	Osteoporosis versus osteopenia
<i>(I) Demographic characteristics</i>						
Body height (cm)	150.6 ± 10.1	147.5 ± 5.5	149.9 ± 6.4	0.446 (NS)	0.800 (NS)	0.348 (NS)
Body weight (kg)	64.0 ± 16.4	58.3 ± 13.9	58.6 ± 13.4	0.451 (NS)	0.337 (NS)	0.942 (NS)
BMI (kg m^{-2})	28.2 ± 16.7	26.8 ± 24.6	26.1 ± 32.5	0.513 (NS)	0.855 (NS)	0.956 (NS)
<i>(II) Prototype US Bone Densitometer (measured at ulna region)</i>						
Ultrasonic transmit time, ΔT (μs)	1.07 ± 0.34	0.83 ± 0.17	0.52 ± 0.36	0.006	0.001	0.013
Ultrasonic attenuation, ΔV (Volt)	0.97 ± 0.14	1.07 ± 0.17	1.23 ± 0.29	0.032	0.058	0.137 (NS)
<i>(III) Estimated ulna BMD (g cm^{-2})</i>						
Using US attenuation, ΔV	0.85 ± 0.24	0.43 ± 0.01	0.24 ± 0.03	0.000	0.006	0.000

NS—Not significant

Table 2 The characteristics of the studied male subjects

Total men screened ($n = 49$, mean \pm SD age = 60.7 ± 9.8 years)						
Parameter	Normal	Osteopenia	Osteoporosis	Statistical significance		
	$n = 17$, mean \pm SD, age = 60.7 ± 9.8 years	$n = 14$, mean \pm SD, age = 58.0 ± 7.1 years	$n = 18$, mean \pm SD, age = 60.8 ± 11.5 years	Normal versus osteopenia	Normal versus osteoporosis	Osteoporosis versus osteopenia
<i>(I) Demographic characteristics</i>						
Body height (cm)	158.2 \pm 9.0	166.5 \pm 7.3	163.9 \pm 9.3	0.016	0.097	0.426
Body weight (kg)	64.1 \pm 15.6	69.5 \pm 12.3	64.3 \pm 12.6	0.340 (NS)	0.971 (NS)	0.288
BMI (kg m^{-2})	25.6 \pm 19.9	25.1 \pm 23.1	23.9 \pm 14.8	0.213 (NS)	0.935	0.656 (NS)
<i>(II) Prototype US Bone Densitometer (measured at ulna region)</i>						
Ultrasonic transmit time, ΔT (μs)	1.8 \pm 2.6	1.45 \pm 2.6	0.78 \pm 0.12	0.699 (NS)	0.312 (NS)	0.115 (NS)
Ultrasonic attenuation, ΔV (Volt)	1.0 \pm 0.2	1.07 \pm 0.25	1.1 \pm 0.13	0.130 (NS)	0.516 (NS)	0.509 (NS)
<i>(III) Estimated ulna BMD (g cm^{-2})</i>						
Using US attenuation, ΔV	0.66 \pm 0.19	0.41 \pm 0.08	0.27 \pm 0.04	0.000	0.002	0.000

NS-Not significant

Table 3 The risk factors of the studied subjects

Risk factors	Total women studied (<i>n</i> = 49)			Total men studied (<i>n</i> = 49)		
	Normal	Osteopenia	Osteoporosis	Normal	Osteopenia	Osteoporosis
	<i>n</i> = 11	<i>n</i> = 10	<i>n</i> = 28	<i>n</i> = 17	<i>n</i> = 14	<i>n</i> = 18
Natural menopause	11 (100 %)	10 (100 %)	21 (75 %)	Not applicable		
Oophorectomy			7 (25 %)			
Vegetarian	9 (81.8 %)	2 (20 %)	3 (10.7 %)	7 (41.2 %)	5 (35.7 %)	4 (22.2 %)
Nonvegetarian	2 (18.2 %)	8 (80 %)	25 (89.3 %)	10 (58.8 %)	9 (64.3 %)	14 (77.8 %)
Nonsmoker and non-alcohol drinker	Not applicable			6 (35.3 %)	5 (35.7 %)	2 (11.1 %)
Smoker				6 (35.3 %)	4 (28.6 %)	3 (16.7 %)
Alcohol drinker				2 (11.8 %)	3 (21.4 %)	5 (27.8 %)
Both smoker alcohol drinker				3 (17.6 %)	2 (14.3 %)	8 (44.4 %)
Glucocorticoids	–	–	–	–	–	–

Acknowledgments We extend our sincere gratitude to Dr. Sundaram, Dean, SRM Medical College, Research and Post-graduate Centre, Kattankulathur, Chennai for his timely help and support. Also, the author MA thank profoundly the first author Mr. Motaz Samir and a woman patient, who have given their consent to publish their photograph while taking during the study.

References

1. Smith J, Shoukri K. Diagnosis of osteoporosis. *J Clinical Cornerstone*. 2000;2(6):22–30.
2. Overgaard K, Hansen MA, Jensen SB, Christiansen C. Effect of calcitonin given intramuscularly on bone mass and fracture rats in established osteoporosis: a dose response study. *Br Med J*. 1992;305:74–9.
3. U.S. Preventive Services Task Force: Recommendations and Rationale. Screening for osteoporosis in postmenopausal women: recommendations and rationale. *Am Fam Phys*. 2002;66(8):1430–1432.
4. Glüer CC. Quantitative ultrasound techniques for the assessment of osteoporosis: expert agreement on current status. The international quantitative ultrasound consensus group. *J Bone Miner Res*. 1997;12:1280–8.
5. Samir M, Anburajan M. A prototype of ultrasound forearm bone densitometer in validation with pDXA bone densitometer. In: Presented a paper at fifth IEEE international conference on communication systems and network technologies (CSNT-2015), Organized by Machine Intelligence research Labs, Gwalior, India, 4–6th April, 2015.
6. Marwaha RK, Tandon T, Garg MK, Kanwar R, Narang A, Sastry A, Saberwal A, Bhadra K, Mithal A. Bone health in Indian Indian population aged 50 years, and above. *Osteoporosis Int*. 2011;22:2829–2836. doi:10.1007/s00198-010-1507-8.

Real-Time ECG Acquisition and Detection of Anomalies

S. Kalaivani, I. Shahnaz, Shaikh Rizwana Shirin and C. Tharini

Abstract ECG signals occupy a vital role in the diagnosis of cardiac abnormalities. These abnormalities can be detected by the variation in the ECG parameters. This paper deals with the implementation of real-time acquisition, conditioning, and feature extraction of the ECG signal so as to monitor and detect various cardiac abnormalities. NI educational laboratory virtual instrumentation suite (NI ELVIS) is used for interfacing the acquired signal with LabVIEW. Further, LabVIEW-based virtual system is designed to create modules for conditioning and feature extraction. The detection of cardiovascular abnormalities such as bradycardia and tachycardia is based on the calculation of heart rate from extracted ECG features. Other abnormalities are detected by determining the deviation of the extracted features such as duration and amplitude, from their standard values.

Keywords ECG · Attribute extraction · Abnormality detection · LabVIEW · NI ELVIS benchtop workstation

1 Introduction

ECG is the interpretation of the electrical conductivity of the heart. ECG waveform is used to measure the regularity of the heartbeat. It can be detected with the help of electrodes attached to the surface of the skin, which can be further displayed or processed. The range of the ECG signal is (0.0001–0.0004)V. The ECG signal has P, Q, R, S, T, and U peaks. The inter-beat and intra-beat redundancy can be exploited to detect various abnormalities of the heart. In order to exploit these characteristics of the ECG signal, it has to be free of various noises. The various noises in the ECG signal are power line interference, baseline drift, and wideband noise. The bandwidth of the ECG signal is 0.1–100 Hz. However, this bandwidth of

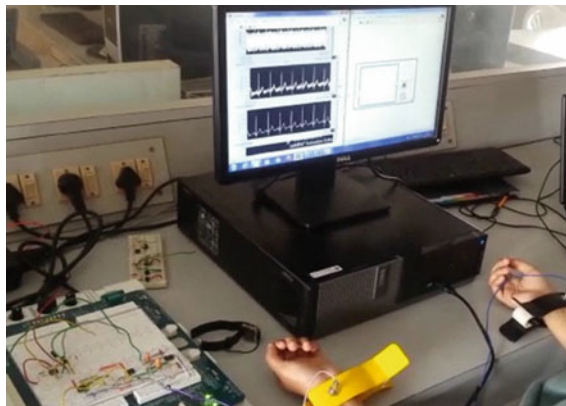
S. Kalaivani (✉) · I. Shahnaz · S.R. Shirin · C. Tharini
Department of ECE, B.S. Abdur Rahman University, Chennai, India
e-mail: skalaivani@bsauniv.ac.in

the ECG signal also includes the 50 Hz main noise along with other noises that have to be eliminated for proper interpretation of the ECG signal. As a first stage of this work, acquired real-time signal is preprocessed to remove the above noise. The preprocessed signal is suitable for feature extraction and anomaly detection. The extracted ECG features are suitable to detect various cardiovascular abnormalities. In practice, the real time raw ECG signal is acquired with electrodes and the analog ECG signal is then converted into a digital signal which can be interfaced with the personal computer (PC). For the purpose of digitization and interfacing with the PC, data acquisition card NI USB6008 [1], Bluetooth [2], Arduino, and NI ELVIS [3] can be used. In this work we have used the NI ELVIS benchtop workstation for digitization and interfacing. Moreover, the circuit is built on the NI ELVIS benchtop workstation.

2 Experimental Methodologies

The experimental setup consists of the conditioning, preprocessing, and peak detection stages through which anomalies are detected. The conditioning stage includes the hardware part of the system which is built on the NI ELVIS benchtop workstation. The input of the conditioning stage, which is the raw ECG signal, is acquired through the electrode. Here we have used a three-lead electrode. The preprocessing stage is the software part of the system executed using LabVIEW. The conditioned and preprocessed ECG signal is used for peak detection and by exploiting the correlation between the peak intervals, the anomalies are detected. The experimental setup is shown in Fig. 1. It consists of the ECG leads through which real-time ECG signal is acquired. The front panel of the LabVIEW displays the conditioned ECG. The conditioned ECG is interfaced with the preprocessing stage using the NI DAQ assistant and the noise present in the ECG signal is removed.

Fig. 1 Experimental setup



3 Algorithm Description

The algorithm can be subdivided into the following stages:

- Signal conditioning of the acquired real-time ECG signal
- Preprocessing of the conditioned signal
- Peak detection and Attribute Extraction
- Abnormality detection

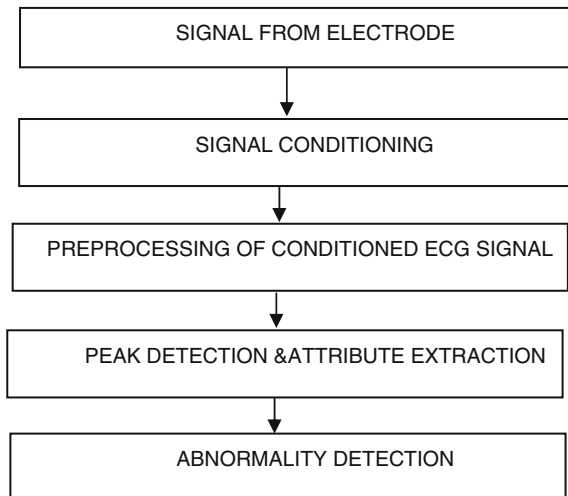
The overall flow diagram of the conditioning, preprocessing, attribute extraction, and abnormality detection is shown in Fig. 2.

3.1 Signal Conditioning Circuit

Raw ECG signals are often low in amplitude and distorted by noise sources. The recorded raw ECG signal is not suitable for analysis due to the presence of noise and artifacts that can be within the frequency band of 0.1–100 Hz, which is the frequency band of ECG and have similar characteristics as the ECG signal itself. This increases the difficulty of obtaining the physiological insights. Low signal level makes signal detection difficult and high noise level may mask out useful clinical information. A general solution to this is to build an amplification circuit to boost the raw ECG signal, preferably without boosting the noise at the same time and limiting the signal to the frequency band of 0.1–100 Hz using a band pass filter [4]. The signal conditioning circuit mainly comprises of the following two parts:

- An instrumentation amplifier circuit
- A bandpass filter circuit

Fig. 2 Overall flow diagram of the ECG signal processing



Instrumentation amplifier circuit The first component of the ECG conditioning circuit is the instrumentation amplifier. An instrumentation amplifier circuit is built using operational amplifier. The instrumentation amplifier is a popular preamplifier for signal conditioning. It offers high impedance and common mode rejection ratio (CMRR). The gain of the amplifier is determined by the resistor network based on the rules of ideal operational amplifier. The instrumentation amplifier is constructed with a typical gain of 1000 (60 dB). The instrumentation amplifier circuit is built on the prototyping board of the NI ELVIS benchtop workstation. The instrumentation amplifier comprises three operational amplifiers. Real-time ECG is acquired through the electrodes attached to the wrists of both arms and the right leg. These electrodes are further connected to the connectors on the ELVIS prototyping board (left arm to BANANA A, right arm to BANANA B and right leg to BANANA C). On the breadboard BANANA A should be connected to the positive input of the operational amplifier, BANANA B should be connected to the negative input of the amplifier, and BANANA C should be connected to ground. The schematic diagram of the ECG amplifier is shown in Fig. 3. The gain of the instrumentation amplifier is given as

$$A_v = \frac{V_{out}}{V_2 - V_1} = \left(1 + \frac{2R_1}{R_{gain}}\right) \frac{R_3}{R_2} \quad (1)$$

Band Pass Filter Circuit The second component of the ECG amplifier is the band pass filter. The lower cutoff frequency is around 0.1 Hz to minimize the baseline drift. The upper cutoff frequency is around 100 Hz. This extracts the complete ECG signal since the bandwidth of the ECG signal is 0.1–100 Hz [4]. The output of the instrumentation amplifier is connected to the input of the band pass filter. The band pass filter consists of a high pass inverting filter shown in Fig. 4, followed by a low pass inverting filter shown in Fig. 5. The output of the instrumentation amplifier is fed to the input of the high pass filter. The output of the band pass section is band limited to 100 Hz. The high pass inverting filter cut off frequency is given as

$$F_{hc} = 1/(2\pi R_1 C) \quad (2)$$

Fig. 3 ECG amplification circuit

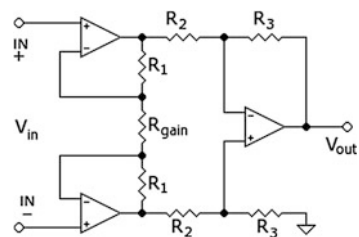


Fig. 4 Inverting high pass filter

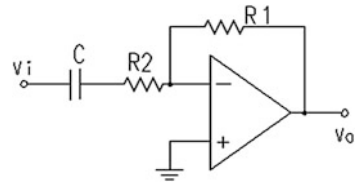


Fig. 5 Inverting low pass filter

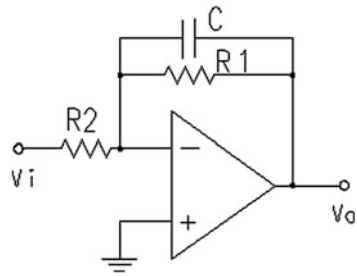
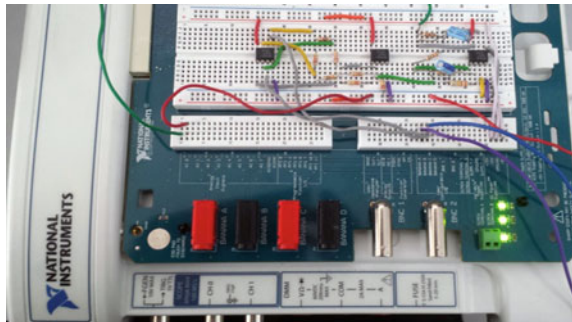


Fig. 6 Conditioning circuit built on NI ELVIS benchtop workstation



The cutoff frequency of low pass inverting filter is given as

$$F_{lc} = 1/(2\pi R_1 C) \tag{3}$$

The conditioning circuit is built on the NI ELVIS benchtop workstation as shown in Fig. 6 and the output of the conditioning circuit is interfaced with the PC using NI DAQ Assistant. The sampling frequency is also set in the NI DAQ Assistant settings. The acquisition mode used is continuous samples.

3.2 Preprocessing of the ECG Signal

The ECG signal obtained at the output of the band pass filter is contaminated with different noise sources. The most common noise sources are

- power line interference,
- baseline drift/baseline wandering, and
- wideband noise.

Removal of Power Line Interference

Improper grounding of ECG equipment and interference from nearby equipments are the major causes of power line interference. This interference can be removed by using a notch filter. This interference is more dominant and has a greater effect on the signal. The major source of such noise is the electrical activity of the muscles, i.e., the noise present due to power line interference (50 Hz) which must be removed. This can be done through appropriate filtering of the ECG signal. This is done using the 50 Hz Notch Filter VI in LabVIEW. Here the filtering type is selected as bandstop and a third order Butterworth filter is configured.

Removal of Baseline Wandering

The baseline wander is a low frequency component in the ECG signal which affects the process of ECG signal analysis. When the baseline wander takes place, ECG measurements related to isoelectric line cannot be made. The causes for baseline wander may include perspiration, respiration, muscular motions, and poor contact of electrode. The baseline wander in general is in the frequency range of 0.05–1 Hz. Wavelet transform eliminates the trend of the ECG signal [5], thus removing the baseline wander. Wavelet transform method is effective as it introduces no latency and less distortion [6]. The LabVIEW advanced signal processing toolkit (ASPT) provides the WA Detrend virtual instrument (VI) which removes the low frequency trend of the signal. The trend level means the number of levels of the wavelet decomposition, which is given by the formula:

$$\text{Trend level} = \lceil \log_2 2t / \log_2 N \rceil \quad (4)$$

where t is the sampling duration and N is the number of samples. The data used in this work have a sampling duration of 60 s and 360 samples in total, and hence the trend level is 0.8. Daubechies (db06) wavelet is used for detrending due to the similarities with the real ECG and also Daubechies wavelet being orthogonal wavelet is suitable for signal denoising.

Removal of Wideband Noise

When compared to the acquired raw ECG signal, the ECG signal obtained after removal of baseline wander is more stationary. However, the presence of some other noise makes the signal unsuitable for further analysis. For further analysis of the ECG signal, removal of wideband noise is essential. In this work, Wavelet Denoise Express VI is used to remove the wideband noise [7, 8]. By applying

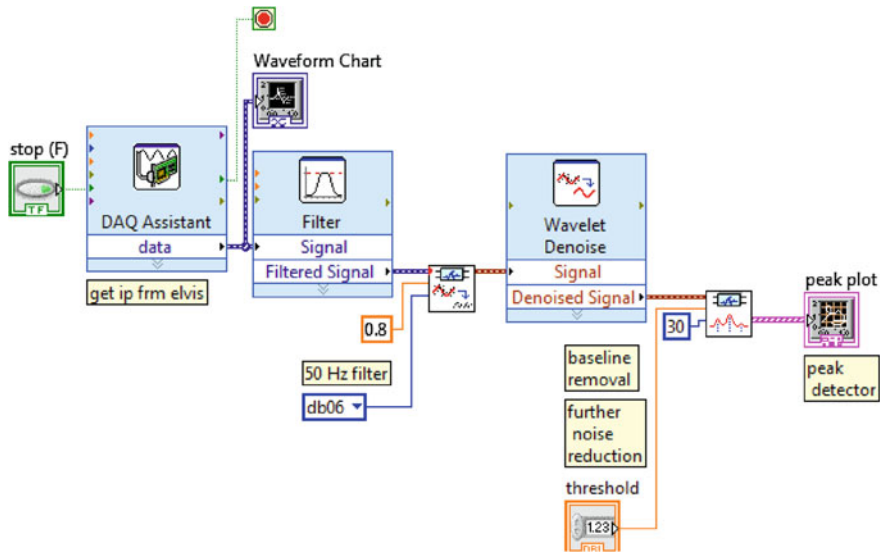


Fig. 7 LabVIEW block diagram for preprocessing stage

wavelet transform this VI decomposes the ECG signal into several subbands, which further modifies each wavelet coefficient by applying a threshold and finally reconstructs the denoised signal. Soft threshold is selected from the available threshold options and the threshold rule is selected as ‘Minimax’. The transform type chosen is undecimated wavelet transform (UWT). Compared to discrete wavelet transform, UWT provides a greater degree of smoothness and accuracy. Figure 7 shows the block diagram built in LabVIEW that is used in the preprocessing stage of the ECG signal, i.e., removal of 50 Hz noise, wideband noise, and baseline interference.

Figure 8 shows the steps involved in preprocessing of ECG. The first waveform shows the output of the conditioning stage. The second waveform shows the ECG signal with the power line interference removed. The third waveform shows the removal of baseline wander. The fourth waveform shows the preprocessed final ECG which is free from all the above mentioned noises.

3.3 Peak Detection and Attribute Extraction

Once the signal is preprocessed it can be used for further processing. First, the most prominent QRS complex is detected. The QRS complex comprises three distinct points of a single ECG heartbeat, namely Q, R, and S. Of these, the high dominated R peak is detected first. Then Q and S points are detected. The zero voltage level of the signal is found next. Finally the P and T waves are detected. Multiresolution analysis

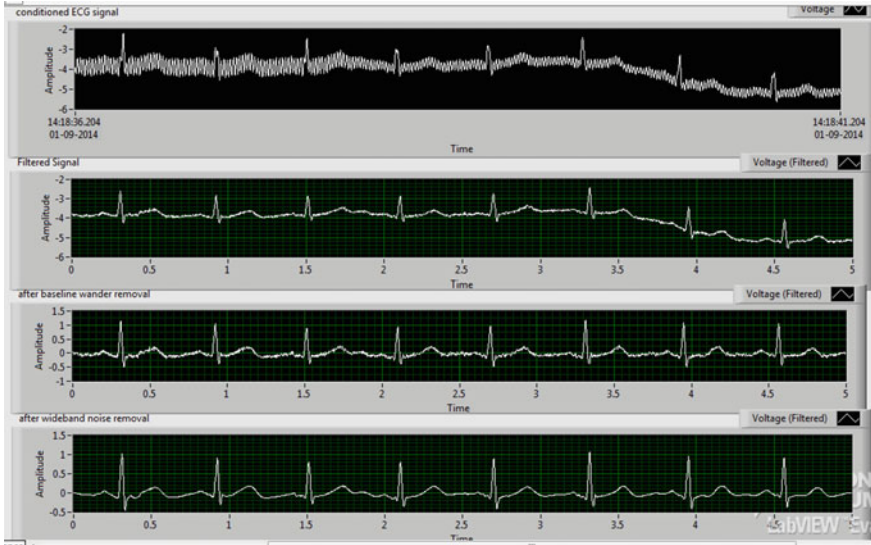


Fig. 8 Preprocessing stages of ECG signal

works as an effective tool in extracting the desired features from a signal contaminated with noise. Multiresolution express virtual instrument is used to decompose the ECG signal and then reconstruct the signal from the approximation and detail coefficients of the selected frequency bands. Here the levels are decided based on the dominant frequency components of the ECG signal and the wavelet type is chosen, which closely resembles the ECG signal. Further, depending on the frequency band of interest the corresponding coefficients are extracted for peak detection.

R Peak Detection

WA multiscale peak detection virtual instrument is used in peak detecting mode to detect the R peaks [9]. It is specified with proper width and threshold. Width specifies the width in a number of samples. Threshold specifies the value that the virtual instrument uses to reject peaks of a particular size.

Q and S Peak Detection

Once the R peaks are detected with reference to the detected peak, a window of length 0.1 s is created that scans the signal to the left of R peak to obtain the minimum value and this corresponds to Q peak. A similar window is created to scan the signal to the right and the minimum point thus found corresponds to S peak. The windows are created to extract the signal of a particular length. For this purpose extract portion of signal VI is used.

Detection of Zero Crossing Points

Once the Q and S peaks are detected, the zero crossing points are also detected in a similar manner. Here windows of appropriate width are created and the signal is

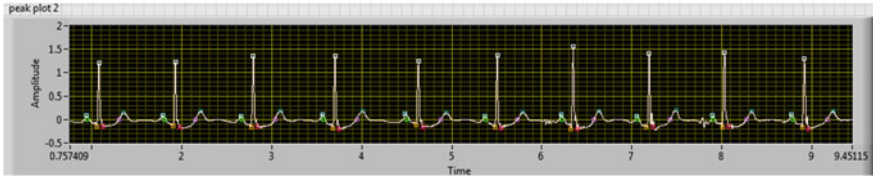


Fig. 9 Waveform indicating detection of peaks in an ECG signal

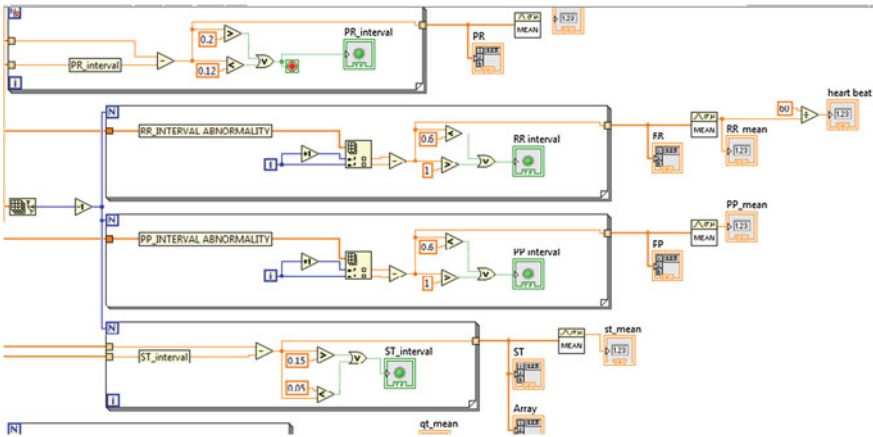


Fig. 10 Block diagram in LabVIEW for feature extraction

scanned to the left of Q and to the right of S. Using the threshold 1D array, interpolation is performed and the points crossing the isoelectric line are detected.

P and T Peak Detection

Here with reference to the zero crossing points, P and T waves are detected. Signal is scanned to the left and right of the zero crossing points using windows of appropriate width. Here, the maximum points in the window are detected as the P and T waves. Figure 9 shows the detection of the five peaks in an ECG, namely P, Q, R, S, T.

Figure 10 shows the block diagram built in LabVIEW which is used to determine the duration, amplitude, and heart rate from the detected peaks.

3.4 Abnormality Detection

With the peaks and its time of occurrence all the required attributes can be found which will help in the detection of the abnormalities. The abnormal ECG waveform detection is based on their characteristics features. The different type of

Table 1 Ecg parameters

Phase	Duration (s)
P wave	0.06–0.11
PR interval	0.12–0.2
QT interval	0.32–0.45
T wave	0.16

Table 2 Abnormality detection

Parameter	Disease
Short QT interval	Hypercalcemia
Long QT interval	Hypocalcemia
Heart rate >120	Tachycardia
Heart rate <40	Bradycardia
Increased PR interval	AV block

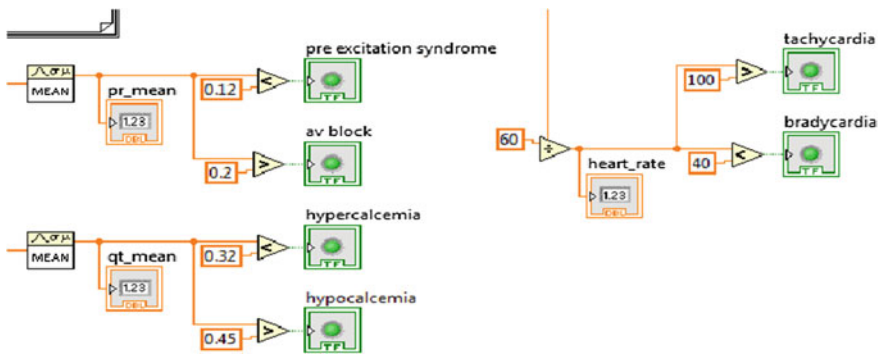


Fig. 11 Abnormality detection

abnormalities and their characteristics are shown in Tables 1 and 2. Abnormalities like Tachycardia and Bradycardia are detected using heart rate values [10]. Figure 11 displays the LabVIEW block diagram of the implementation of Table 2.

4 Results and Conclusion

For the purpose of estimating the diseases, MLII signals were taken from physionet [11]. Table 2 represents the values after the ECG attributes detection. After the preprocessing and feature extraction the attributes are determined and various abnormalities relating to the deviation from the standard values are displayed in the front panel of the LabVIEW. It emphasizes on the abnormalities in the attributes as well as the diseases corresponding to them. The GUI consists of ST, QT, RR, PR, P abnormalities. The MIT-BIH database deals with arrhythmia and is indicated as

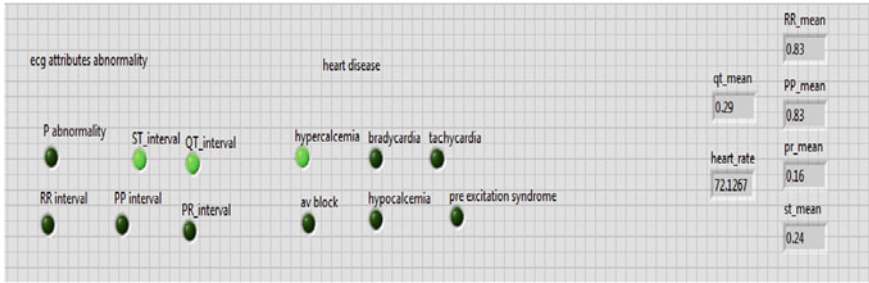


Fig. 12 Indication of abnormalities in the input signal

Table 3 Results obtained from the algorithm proposed

Features	Normal values	101	103	124
Heart rate	60–100	69.056	72.1267	50.7688
PP mean	0.6–1	0.87	0.83	0.79
PR mean	0.12–0.2	0.14	0.16	0.16
ST mean	0.05–0.15	0.25	0.24	0.24
QT mean	0.32–0.45	0.32	0.29	0.30

tachycardia, bradycardia, hypercalcemia, hypocalcemia, etc. Figure 12 shows the front panel of the MIT-BIH 103(MLII) database indicating an abnormal QT and ST levels leading to hypercalcemia. Table 3 shows the results obtained from the proposed algorithm.

References

1. Gao Z, Wu J, Zhou J, Jiang W, Feng L. Design of ECG signal acquisition and processing system. *Int Conf Biomed Eng Biotech.* 2012.
2. Patel AM, Gakare PK, Cheeran AN. Real time feature extraction and arrhythmia detection on a mobile platform. *Int J Comput Appl (0975-8887).* 2012;44(23).
3. National instruments elvis ii user guide and specification.
4. ECG signal conditioning. <http://bme.sunysb.edu/labs/wlin/BME313/>.
5. Bhyri C, Kalpana V, Hamde ST, Waghmare LM. Estimation of ECG features using LabVIEW. *Technia—Int J Comput Sci Commun Technol.* 2009;2(1). ISSN:0974-3375.
6. National Instruments Developer zone. LabVIEW for ECG signal processing; 2008.
7. Islam MK, Haque ANMM, Tangim G, Ahammad T, Khondokar MRH. Study and analysis of ECG signal using Matlab and LabVIEW as an effective tool. *Int J Comput Electr Eng.* 2012;4(3).
8. PoonamKaur, Sharma RK. Lab VIEW based design of heart disease detection system. *IEEE Int Conf Recent Adv Innovat Eng (ICRAIE-2014).* 2014.
9. Adochiei N, David V, Adochiei F, Tudosa I. ECG waves and feature extraction using wavelet multi-resolution analysis. *Int Conf E-Health Bioeng.* 2011.
10. American heart association for database. http://www.heart.org/HEARTORG/GettingHealthy/PhysicalActivity/FitnessBasics/Target-Heart-Rates_UCM_434341_Article.jsp.
11. www.phisionet.org.

Weight-Based Data Center Selection Algorithm in Cloud Computing Environment

Sunny Nandwani, Mohit Achhra, Raveena Shah, Aditi Tamrakar, Kiran Joshi and Sowmiya Raksha

Abstract Cloud computing is Internet-based computing, whereby shared and distributed resources and information are provided on demand. It involves provision of dynamically scalable and virtualized resources. Perhaps, with such high provisioning of scalability and on-demand resource availability and high computational facilities, cloud also faces many issues. Service availability on demand, unpredictability of performance, on-time availability of resources, data confidentiality, security, and privacy are the major challenges in cloud computing *e*. Different simulation tools are available to analyze and test the execution of algorithm. CloudAnalyst is one of the simulation tools used to model and analyze cloud computing environment before the actual deployment. Cloud Application Service Broker determines which data center should service the request from each user base. Service proximity-based routing selects the data center which has lowest network latency or minimum transmission delay from a user base. If there are more than one data centers in a region in close proximity, then one of the data centers is selected at random to service the incoming request. However, other factors such as cost, workload, number of virtual machines, processing time etc., are not taken into consideration. Randomly selected data center gives undesirable results in terms of response time, data processing time, cost, and other parameters. In this paper, we propose a weight-based data center selection algorithm which proves to improve the randomized service proximity-based routing in terms of processing time, i.e., performance and costs.

Keywords Cloud computing · CloudAnalyst · Data center · Service broker algorithm · Weight-based data center selection

S. Nandwani (✉) · M. Achhra · R. Shah · A. Tamrakar · K. Joshi · S. Raksha
Veermata Jijabai Technological Institute, H.R.Mahajani Marg, Matunga,
Mumbai 400 019, India
e-mail: sunnynandwani1993@gmail.com

1 Introduction

Nowadays, when almost all the applications are being provided over the Internet, the need of computational resources is shifting from the user's location to the service provider. With lower computing costs and ease of access to high powerful applications, people started switching to distributed computing [1]. Cloud computing is the technology of future which provides "IT resources as a service" on demand of the user following the "pay-per-use." It is basically increasing the utilization of IT. Cloud-based application cost is associated with two parameters: virtual machine and data transfer corresponding to the user base [2]. For experimenting the performance of cloud environment in a repeatable manner, actual deployment of cloud becomes costly and not an easier task; therefore, not preferable. For this reason, various simulation tools are used to model and analyze cloud computing environment and applications, graphically analyzing the results before the actual deployment of clouds [3].

The remainder of this paper is organized as follows: In Sect. 2, we have discussed about the related work done in the field. In Sect. 3, we have discussed about routing of user request in CloudAnalyst. In Sect. 4, we have discussed about the need for evaluating cloud performance. In Sect. 5, we have discussed about the working of service proximity-based routing algorithm in detail. Section 7 discusses about the proposed algorithm to find the solution to the problem/drawback of the existing algorithm. Section 7 discusses about the simulation configurations, results, and performance analysis, and finally we have concluded our work.

2 Related Work

It is not easy to perform experimentation in a real cloud environment because,

- It involves high purchase cost as it requires huge amount of resources for a long period of time.
- Repetition of experiments is not feasible.
- Lower flexibility of quick reconfiguration of parameters.
- Conditions prevailing in the Cloud-based environments are not in the control of developers of application services [4].

A more viable approach to use cloud simulation tools. Different simulators have been proposed for modeling of Grid-based environments [5]. It enables the Cloud providers to evaluate the different kinds of resource provisioning scenarios under varying load and pricing distribution [6]. Customers can test their services in a repeatable and controllable environment and that too free of cost and thus identify the performance issues before actual deployment on real cloud.

CloudAnalyst [7] is a graphical toolkit which separates the simulation experiment setup exercise from programming task. The modeler can focus on the simulation parameters rather than technicalities of programming. The simulator is developed using Java SE, Swing, CloudSim toolkit, and SimJava framework.

- **Region:**
The world is geographically divided into 6 Regions (0–5) which correspond with the 6 main continents.
- **Internet:**
The Internet models the Internet traffic routing around the world by introducing suitable transmission latency and data transfer delay, which can be configured.
- **Cloud Application Service Broker:**
The cloud application service broker determines which data center should service the requests from each user base. CloudAnalyst implements three types of service brokers:
 - Proximity-based routing: Selects the closest region depending upon the least network latency and from that region it selects the data center randomly.
 - Performance optimized routing: Selects the closest region and from that region it selects the data center that has best response time. It does not take cost into consideration.
 - Dynamically reconfiguring routing: This is an extension to proximity-based routing, where the routing logic is similar, but has an additional responsibility of scaling the application deployment based on the load it is facing. This policy increases and decreases the number of virtual machines allocated in the data centers.
- **User Base:**
The user base represents a group of users who are responsible to generate traffic for the simulation.
- **InternetCloudlet:**
A number of requests from the users are grouped into a single InternetCloudlet based on the ‘User Grouping Factor’
- **Data Center Controller:**
Manages VM creation and destruction and handles the routing of requests received from User Bases via the Internet to the VMs.
- **VMLoadBalancer:**
The Data Center Controller decides which VM should be allocated to a particular Cloudlet using the VMLoadBalancer. CloudAnalyst implements three types of VMLoadBalancers:
 - Round Robin Load Balancer: In this algorithm, a queue is maintained and when the request arrives, the first virtual machine is given request and is correspondingly moved to end of queue. Here, no load checking is done; so, this method fails in giving the best data processing time virtual machine.

- Active Monitoring Load Balancer: Maintains an index table which stores the number of requests handled by each VM. Initially, all the virtual machines have zero allocation. Upon request arrival, index table is parsed and the least loaded VM is assigned the request and correspondingly the table is updated regarding new allocation. But parsing the index table adds to the overhead.
 - Throttled Load Balancer: Maintains an index table which stores the availability status of each VM. When the request arrives, the index table is parsed and the first available VM is selected.
- GUI: Displays the GUI and acts as a front end interface. Enables user to define the simulation parameters, save and load simulation configuration, execute simulation, and save the results of the experiment.

3 Routing of User Request

In cloud, from user’s end, the important factors are cost optimization and provider that provides utility to the user’s need. Thus routing of user’s request is a very important aspect in cloud. Figure 1 shows the routing of user request in one of the simulation tools, i.e., CloudAnalyst [8].

1. Internet Cloudlet is created by UserBase with appropriate parameters such as application ID and name of UserBase (for routing back the RESPONSE).
2. REQUEST is sent to the Internet with zero delay.
3. Internet requests service broker to select an appropriate data center depending on the Service broker policy used.

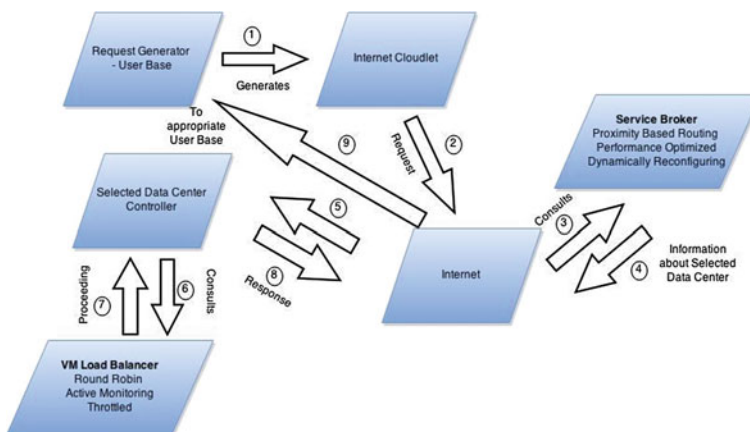


Fig. 1 Routing of user request

4. Once the Internet receives the information about which data center is to be used, Internet sends the request to that data center after adding appropriate network delay associated with that request.
5. Depending on the load balancing policy, the data center controller routes the request to suitable virtual machine for processing.
6. After processing the REQUEST, RESPONSE is sent to the Internet by selected data center.
7. Internet adds network delay to the RESPONSE and sends it to UserBase using the originator field in the Cloudlet information.

4 Need for Evaluating Cloud Performance

From the routing of the user requests it is quite evitable that many of the issues arise while:

- Selecting the appropriate data center: For selecting the appropriate data center, we have several service broker policies which affect the performance to a great extent. As it is the first step toward providing better cloud performance, properly selecting a data center by using appropriate service broker algorithm is the work of research.
- Selecting appropriate VM: After selecting the appropriate data center, Load balancing is the most important aspect in any data center. Load can be balanced only if proper VM allocation is done for a particular user request. Various load balancing techniques are present and proposed to enhance the cloud performance.

The situation may arise that all the requests may go to only one data center. As a result, only one data center is highly loaded and others are not. Other situation may arise that there is a need of migrating VM or allocating new VM for a user request. There is a lot of research work going on for providing service broker policies and load balancing algorithms which would increase/enhance cloud environment performance.

5 Working of Service Proximity-Based Routing

The step by step working of service proximity-based routing is as follows [8]:

1. ServiceProximityServiceBroker maintains an index table of all data centers indexed by their region.

2. Upon receiving the request from UserBase, Internet requests ServiceProximityServiceBroker to select a data center controller.
3. Using InternetCharacteristics, a region proximity list is retrieved by ServiceProximityServiceBroker. The list contains an ordered list of regions, arranged as per ascending order of the network latency (means lowest latency occupies first position)
4. The ServiceProximityServiceBroker picks the first data center located in the region which is at top in the proximity list. If more than one data center is located in a region, one is selected randomly.

The following are the issues present in Service Proximity-Based Routing:

- The main problem with service proximity-based routing is the random selection of data center when there are more than one data centers present in a particular region with low latency; the results are different even though configurations are kept same.
- There is a high probability that the resources that are present are not utilized to their deliverable capability. Also it is possible that the selected data center will increase the response time or might have higher workload or may be of greater cost as compared to those available in same region.

With increasing use of cloud computing, it has become much necessary to distribute the load depending upon the characteristics of data center. The random selection in service proximity technique gives poor result. The data center with poor hardware may get more number of requests while the one with good hardware may get less number of requests resulting in poor performance of the system.

With an aim of removing random selection, we thought of a solution which takes into consideration the physical characteristics of the data center. As physical characteristics vary according to the data center, we thought of assigning weights to each data center which would help distribute the load appropriately as per the potential of data center. We have assigned weights depending on number of VMs in that data center.

6 Proposed Solution

Suppose an environment is setup with three data centers DC1, DC2, and DC3 and with a number of VMs 5, 50, 100, respectively. So, proportion weights would be in ratio 5:50:100, i.e., 1:10:20. Which means a request should be forwarded to DC1, 10 to the DC2, and 20 to DC3. But when we simulated this algorithm, the results were completely inverse of what we had thought of. Average processing time of DC1 came out to be 0.4 ms, DC2 came out to be 2.5 ms, and DC3 with most number of VMs came to be 5.5 ms. From these results, we concluded that if all the hardware

characteristics of data center remain same and only number of VM varies, the data center with less number gives better performance than others with many VMs. The reason behind such result is the Time Shared VM allocation policy. This led us to the thought of taking inverse of number of VMs and assign those weights which is discussed in proposed solution.

The proposed algorithm works on the basis of service proximity service broker. Key aspects of algorithm are as follows.

6.1 Phase 1 (Initialization)

1. Assign the weights to each data center using following formula:

$$\text{Weight of a data center} = \frac{\text{LCM of number of VMs in each Data center}}{\text{Number of VMs on that data center.}} \quad (1)$$

2. Create a regionalData centerIndex map with key as region and value as list of data centers in that region.
3. Create a map with key as region and values as pointer and weightCounter that are initialized to zero.

(Pointer variable runs through the DC list and Weight Counter variable is counter for weight of a data center)

6.2 Phase 2

1. When the request arrives, the closest region is selected depending upon the proximity list.
2. Regional list (DCList) of data centers is loaded from regionalDatacenterIndex map with corresponding closest region.
3. Pointer and weightCounter values are loaded for corresponding closest region.
4. Select the data center in a circular fashion keeping into consideration the proportion weights. For example, if entry for number of virtual machines for DC1, DC2, and DC3 is 50, 30, and 10, respectively. So, the corresponding proportion weights are in the ratio 3, 5, and 15. Thus DC1 is assigned to process the first three cloudlets, DC2 is assigned to process the next 5 cloudlets and DC3 is assigned to process the next 15 cloudlets, out of first 23 cloudlets and the whole selection process is done in a repeated manner to process the entire set of workloads.

- 5. The pointer and weightCounter values are updated for selected region.
- 6. Return data center name

Note: Phase 1 runs only once during simulation. While phase 2 runs for every User request.

The following is the flowchart representation of the proposed algorithm (Fig. 2):

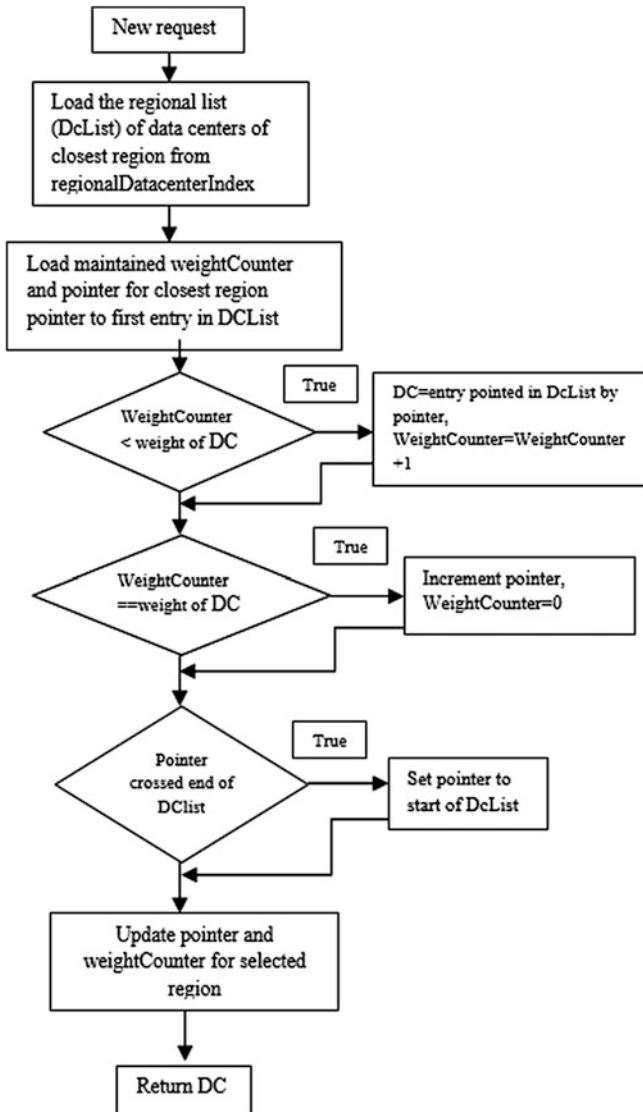


Fig. 2 Flowchart representation of proposed solution

7 Simulation and Results

7.1 Simulation Configuration

We have used CloudAnalyst tool for setting up the simulation. All the data centers are kept in one region and the user bases are spread across regions. The Configuration of simulation is as follows:

- Simulation Duration: 24 h
- Other Configurations:

The User Base configuration is shown in Table 1. Table 2 shows the configuration of application deployment for each data center. Each Data center configuration and physical hardware details of each data center are shown in figures
- User grouping factor in User Bases (Equivalent to number of simultaneous users from a single user base): 500
- Request Grouping Factor in Data Centers (Equivalent to number of simultaneous requests a single application server instance can support.): 250
- Execution instruction length per Request (bytes): 200
- Select any Load Balancing Policy across VM's in single Data Center

Table 1 Userbase configuration

Name	Region	Request per user per h	Data size per request (bytes)	Peak hours start (GMT)	Peak hours end (GMT)	Avg peak users	Avg off peak user
UB1	0	60	100	12	14	5000	500
UB2	1	60	100	14	16	1000	100
UB3	2	60	100	19	21	3500	350
UB4	3	60	100	0	2	1500	150
UB5	4	60	100	20	22	500	50
UB6	5	60	100	10	12	800	80
UB7	3	60	100	3	9	1000	100
UB8	3	60	100	3	9	1000	100

Table 2 Application deployment configuration

Data center	no. of VMs	Image size	Memory	BW
DC1	10	10,000	512	1000
DC2	50	10,000	512	1000
DC3	80	10,000	512	1000
DC4	80	10,000	512	1000
DC5	10	10,000	512	1000
DC6	50	10,000	512	1000
DC7	80	10,000	512	1000

7.2 Results

The above configuration is used one by one for both the algorithms, i.e., Proposed and Closest data center algorithm. The results produced from the CloudAnalyst is shown in the following table (Tables 3, 4 and 5):

7.3 Performance Analysis

From the outputs, as shown in Fig. 3, we can observe that proposed solution gives better overall response time than the conventional random selection. We also observe that proposed algorithm has better data center processing time than the existing service proximity-based routing algorithm. Our proposed algorithm gives 49.06 % improvement in average data center processing time and 11.47 % improvement in average overall response time. The results of the execution show that the cost of the proposed algorithm has negligible difference with random selection done in service proximity-based routing. We observe that the proposed solution yields a good amount of improvement in overall average response time and data center average processing time with the same cost. Thus, the proposed algorithm leads to better resource utilization.

Table 3 Data center configuration

Name	Region	Memory cost \$/s	Storage cost \$/s	Data transfer cost \$/Gb	Cost per VM \$/h
DC1	0	0.05	200	0.05	0.05
DC2	0	0.05	100	0.1	0.1
DC3	0	0.05	100	0.12	0.12
DC4	0	0.05	0.1	0.15	0.15
DC5	3	0.05	0.1	0.1	0.126
DC6	3	0.05	0.1	0.1	0.126
DC7	3	0.05	0.1	0.1	0.126

Table 4 Physical hardware details of each data

Id	Memory (Mb)	Storage (Mb)	Available BW	Number of processor	Processor speed
0	204,800	100,000 K	1,000,000	4	10,000

Table 5 Result table

	Closest data center (random selection)	Proposed solution
Overall response time Avg (ms)	177.8	157.4
Data center processing time Avg (ms)	37.95	19.33
Cost(\$)	1112.9	1104

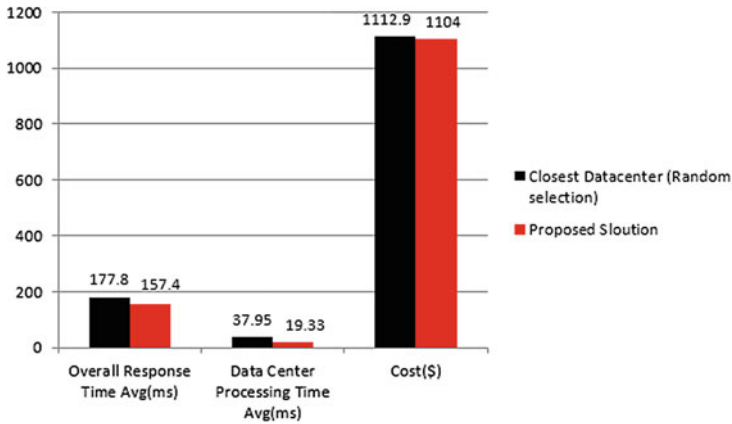


Fig. 3 Analysis of results

8 Conclusion

When it comes to efficient utilization of resource, it can be observed from the results that proposed algorithm utilizes resources well as compared to the existing random selection proximity-based algorithm. The proposed algorithm works well when it comes to overall response time and data center processing time, cost being almost the same. The proposed algorithm gives 49.06 % improvement in average data center processing time and 11.47 % improvement in average overall response time. Further work can be done to minimize the cost incurred.

References

1. Shankarwar I, Sankhe P, Patel S, Gohil R, Raksha S, oshi KK. Migrating towards data as a service in cloud computing. p. 33–9. ISBN:978-93-85225-09-3.
2. Wickremasinghe B, Calheiros RN, Buyya R. Cloudanalyst: a cloudsimsim-based visual modeller for analysing cloud computing environments and applications. In: Advanced information networking and applications (AINA), 2010 24th IEEE international conference on. IEEE; 2010. p. 446–452.
3. Nandwani S, Achhra M, Shah R, Tamrakar A, Joshi KK, Raksha S. Analysis of service broker and load balancing algorithm in cloud computing. p. 33–9. ISBN:978-93-85225-09-3.
4. <http://www.buyya.com/papers/CloudSim2010.pdf>.
5. Ranbhise SM, Joshi KK. Simulation and analysis of cloud environment. IJARCST. 2014;2(4):2347–9817.
6. Buyya R, Ranjan R, Calheiros RN. Modeling and simulation of scalable cloud computing environments and the cloudsimsim toolkit: challenges and opportunities.
7. CloudAnalyst can be downloaded from <http://www.cloudbus.org/cloudsim>.
8. Mishra RK, Kumar S, Sreenu Naik B. Priority based round-robin service broker algorithm for cloud-analyst. IEEE Int Adv Comput Conf (IACC); 2014.

Real-Time Remote Monitoring of Indoor Air Quality Using Internet of Things (IoT) and GSM Connectivity

Siva V. Girish, R. Prakash and A. Balaji Ganesh

Abstract The paper presents an indoor air quality monitoring system which comprises of real-time sensing unit that enables remote monitoring of environmental carbon-di-oxide, temperature, and relative humidity. The simple mail transfer protocol (SMTP)-based remote monitoring system employs an Internet of Things (IoT) signal processor (CC3100) interfaced on top of a low-power micro-controller (MSP430F5529). The system is also packed with a short messaging service (SMS)-based emergency alerting mechanism on the mobile network through SIM900 GSM module. The whole system when integrated with pre-calibrated non-dispersive infrared (COZIR) sensing unit showed good response in communicating the alert messages and E-mail. The information from sensing unit can be analyzed and logged for any period of time.

Keywords GSM · SMTP · Internet of Things (IoT) · SMS · Non-dispersive infrared sensor

1 Introduction

The development of good air quality monitoring and controlling systems has been recently becoming a great focus of attention due to the increased reports of health problems related to bad environmental conditions. Specifically, air quality is a major factor which affects the health condition of those who spent most of their time inside the buildings such as office and office environments. The air quality can

S.V. Girish (✉) · R. Prakash · A. Balaji Ganesh
Electronic System Design Laboratory, Velammal Engineering College,
Chennai 600066, India
e-mail: sivagirish1@gmail.com

R. Prakash
e-mail: prakash.rama121@gmail.com]

A. Balaji Ganesh
e-mail: abganesh@live.in

be affected by pollutant gases, dust particles, or decomposed food particles by microbes. In most cases, for home environment, the air quality can be affected due to decomposed food particles by microbial action. Some physical parameters like carbon-di-oxide, temperature, and humidity becomes the most important factors which affects the Indoor air quality directly or indirectly by providing a nourishing environment for the growth of microbial. The sick building syndrome is one of the best examples of the health effects caused by poor indoor air quality in a building [1]. Some of the sources of carbon monoxide inside a house are cooking activities and smoking of tobacco products or incomplete combustion of any material. As most of the pollutants are colorless, odorless, and tasteless, it is impossible to detect with our sensory system. It affects the victim by reducing the oxygen carrying capacity of the blood as it can bind easily with hemoglobin and eventually produced carboxyhemoglobin (COHb) [2, 3]. Likewise carbon dioxide is also a colorless and odorless gas which is a normally available in the atmosphere at 330–440 ppm. It affects the victim inducing headache, fatigue, burning, and irritating sensation in eye and respiratory tract. The indoor air quality monitoring devices which are available to be used for home is desktop type monitoring gadgets. Choi et al. [4] have presented a micro sensor node for air pollutant monitoring system (APOLLO) which incorporates with the off-the-shelf MEMS-based micro gas sensors. As wireless communication systems have achieved a rapid development in every aspect of day-to-day life, development of IoT-based systems becomes a common area for research. Lozano et al. [5] proposed an indoor air quality monitoring system which comprises of wireless sensor network using zigbee standard IEEE 802.15.4 integrated with sensors to measure temperature, humidity, light, and air quality.

Li et al. [6] proposed a WSN-based system comprises of three components: gateway, nodes, and software. The node interfaces with an indoor air quality (IAQ) sensor board that was specifically designed to mount on and interface through Arduino. This paper focuses on development of one such solution for real-time remote monitoring of indoor air quality and emergency alerting system for the care taker. The system has a LCD display for real-time data monitoring and IoT-enabled system for remote monitoring.

2 Experimental Procedures

2.1 Hardware

The real-time monitoring system is built using ultralow-power MSP430F5529 microcontroller for serving the interface, data processing, and controlling tasks of the system. The microcontroller can stay on standby mode with 2.1 μA at 3.0 V and shutdown mode with 0.18 μA at 3.0 V. It is also featured with 5 low-power modes making the selection optimal for the development of a power optimistic system.

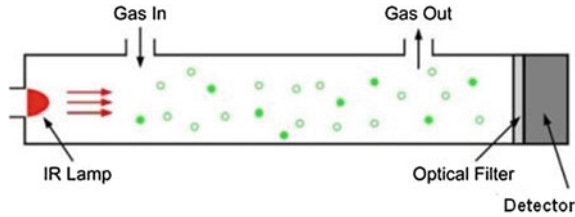


Fig. 1 Sensing mechanism of NDIR-based sensor

The system uses a NDIR-based COZIR sensor which can sense three different parameters simultaneously acts as the heart of the sensing unit [7]. The main advantage of the NDIR-based sensor is that it consumes very less power comparing all the other conventional sensors. It derives the information from the air by passing the air to be monitored through the passage of infrared rays toward its detector. The detector placed after the filter gives the output proportional to the concentration of constituents in the air. Figure 1 shown below explains the working of NDIR sensor [8, 9]. The whole setup of the NDIR sensor uses an IR lamp and detector assembly which consumes only a very less amount of power comparing the resistive element-based sensors.

The COZIR sensor when interfaced with an ultralow power microcontroller like MSP430F5529 makes the system to last longer when running on batteries. Unlike most other sensors, it is pre-calibrated with built in UART communication. It is interfaced with the MSP430F5529 using UART and polled with corresponding command of the parameter. For example, to poll for the value of CO₂, the command is $ZrVz$ which returns the most recent CO₂ measurement through UART.

The real-time monitoring of the system is achieved by interfacing a 16×2 LCD with the microcontroller for displaying the recent measurement of the parameter polled on the sensor. The microcontroller is empowered with IoT by stacking up a CC3100 signal processor on top of it, which acts as bridge for establishing communication with the internet pool for remote monitoring. The reporting system for remote monitoring is facilitated by the SMTP protocol with the recent sensor measurements on the go from any internet powered gadgets and PDA's which supports SMTP. In order to support the reporting system with conventional mobile devices, the system is interfaced with SIM900 GSM module to beep for emergency alerts about the air quality through SMS.

2.2 Emergency Alerting System

The indoor air quality monitoring system stacked up with CC3100 simple link wi-fi device which is a SOC of dedicated ARM network processor and wi-fi transceiver module over the MSP430-based ultralow power application processor. The CC3100 device is integrated with all protocols for wi-fi and internet which greatly minimizes

the software and memory requirements of the application processor, making it easy for implementing an IoT solution on a lesser cost. The system utilizes the above merits of the CC3100 device to establish communication easily with the internet backbone network wirelessly via wi-fi router installed in the indoor environment to enable SMTP protocol-based emergency alerts. The system can also be modified to do real-time data logging on the internet to achieve remote monitoring.

The proposed system also supports short messaging service-based alerting system through GSM. The SIM900 is interfaced with the application processor by UART communication protocol for the transfer of messages using AT (or) Hayes commands.

2.3 Programming Environment

In the design cycle of an embedded system development, the software development and optimizing to fit it into the hardware becomes the significant process. The selection of CC3100 network processor SOC for establishing the communication with the internet backbone reduces the time for software design cycle time as it has all its protocols needed as a bundle in its 8 MB of storage memory. The API's were called from the application processor as functions to establish communication. Here the application processor is programmed with TI's Code Composer Suite 6.0.1 version.

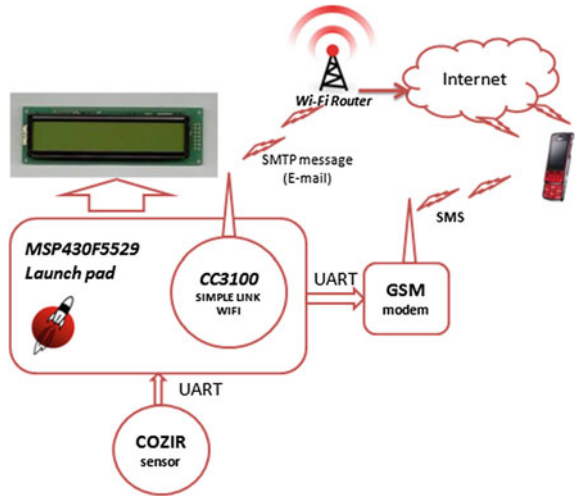
2.4 Proposed Architecture

Figure 2 shows the architecture of the proposed system. The proposed system mainly focused on development of a low power, cost effective real-time remote indoor air quality monitoring system.

The developed system shows good response with accurate environment monitoring and alerting systems. The development phase of the system involves the following stages:

- (i) Tuning and interfacing of the pre-calibrated sensor with application processor
- (ii) Interfacing LCD-based display for real-time monitoring of the vital environmental parameters
- (iii) Interfacing of MSP430 low-power controller with the predefined protocol stack of CC3100
- (iv) Establishing SMTP-based alerting system by accessing the internet backbone network with CC3100
- (v) Development of emergency alerting system using SIM900 GSM modem
- (vi) Integration of all the above units to form a low-power real-time monitoring system.

Fig. 2 Proposed architecture



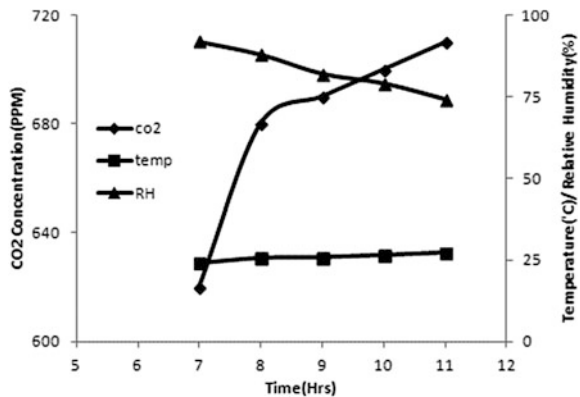
3 Results and Discussion

3.1 Real-Time Monitoring Module

The indoor air quality of the environment is evaluated by measuring the parameters like carbon-di-oxide, temperature, and relative humidity. The parameters can be monitored in real-time using an LCD display. Figure 3 shows the observed sensor data (Temperature, CO₂, and RH) of the environment for a period of 5 hours.

The whole system can be powered externally using batteries to use it as a handheld or desktop monitoring system. The display module of the system can be configured to reduce power consumption to display the recent measured value only when it is asserted externally thereby extending battery life.

Fig. 3 Response curve of monitored environmental parameters



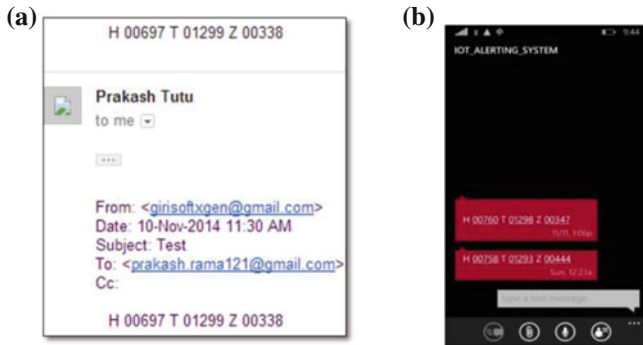


Fig. 4 Screenshots of emergency alerts with recent sensor data from **a** SMTP, **b** SMS

3.2 Emergency Alerting Systems

Figure 4 shows the emergency alerts generated through the SMTP and SMS services. The SMS was sent from the SIM 900 GSM modem and is received in the users mobile as shown in Fig. 4b.

4 Conclusion and Future Work

The paper presented a low-power real-time indoor air quality monitoring system for creating a healthy environment thereby reducing adverse health effects. The quality of the air is monitored by the NDIR sensor and evaluated for alerting the care taker to maintain the environment by taking required measures. The alerting system responded well by sending alerts when the threshold is reached. The work on this paper is limited to monitoring and reporting of environmental changes which can be extended to control the environment by interfacing HVAC system in the future.

Acknowledgments The authors gratefully acknowledge the financial support from Department of Science and Technology, New Delhi, through Instrumentation Development Program Division No: IDP/IND/2012/22 to Velammal Engineering College, Chennai.

References

1. Indoor Air Fact No.4 (revised) sick building syndrome. http://www.epa.gov/iaq/pdfs/sick_building_factsheet.pdf.
2. WHO guidelines for indoor air quality: selected pollutants. <http://www.ncbi.nlm.nih.gov/books/NBK138710/>.

3. Bono R, Piccioni P, Traversi D, Degan R, Grosa M, Bosello G, Gilli G, Arossa W, Bugiani M. Urban air quality and carboxyhemoglobin levels in a group of traffic policemen. *Sci Total Environ.* 2007;109–15.
4. Choi S, Kim N, Cha H, Ha R. Micro sensor node for air pollutant monitoring: hardware and software issues. *Sensors* 2009;7970–87.
5. Lozanoa J, Suarezb JI, Arroyoa P, Ordialesa JM, Alvareza F. Wireless sensor network for indoor air quality monitoring, *Chem Eng Trans.* 2012;319–24.
6. Li X. Applications of wireless sensors in monitoring indoor air quality in the classroom environment. *Res Experiences Teachers Program* 2012;1–33.
7. Gibson D, MacGregor C. A novel solid state non-dispersive infrared CO₂ gas sensor compatible with wireless and portable deployment. *Sensors* 2013;1–26.
8. Designing CO₂ and alcohol sensing applications. <http://www.ecnmag.com/articles/2012/04/designing-co2-and-alcohol-sensing-applications>.
9. Gardening with CO₂ explained. <http://www.novabiotique.com/hydroponics-systems/plant-555-gardening-with-co2-explained.cfm>.

Energy Conservation in Multi-storey Buildings at Indian Cities by Daylighting Control—A Study

M. Abdul Rahman Rafi and N. Albert Singh

Abstract This is a study on the scope of energy conservation in multi-storied buildings across Indian cities by employing daylighting control for the illumination needs of the building. In this study, the possibility of energy savings in a 11-storey building in various Indian cities under various conditions such as different illumination levels and different building orientations has been estimated and analyzed using EnergyPlus simulation software. It is found that 50–60 % of energy expenditure toward building lighting can be saved by adopting proper daylighting control techniques right from the time of building design to maintenance of the control system.

Keywords Energy conservation · Building energy saving · Daylighting control · EnergyPlus

1 Introduction

In order to explore the possibility of achieving energy saving in high-rise buildings through reduction of energy expenditure toward lighting needs, this study is done. A high-rise building is simulated using EnergyPlus software and daylighting is achieved by provision of windows, and consequent energy saving is achieved by dimming control of electric light fixtures. The resulting saving in different Indian cities, at different building angles and at different illumination requirements, is estimated and presented in this study.

M. Abdul Rahman Rafi (✉) · N. Albert Singh
Noorul Islam University, Kanyakumari, India
e-mail: rafi@bsnl.co.in

N. Albert Singh
e-mail: albertsingh@rediffmail.com

2 Energy Conservation Bldg. Code 2007 (India)

Bureau of energy efficiency (BEE), under the Ministry of Power, Government of India has launched the Energy Conservation Building Code 2007 (ECBC 2007) [1] and presently it is voluntary and some of the State Governments have made it mandatory.

The ECBC 2007 is applicable to buildings having a connected load of 500 kW or greater, or contract demand of 600 kVA or greater, or buildings having conditioned area of 1000 m². Hence, naturally most of the high-rise buildings will come under the purview of this code.

One of the requirements of the code is control in daylighted area. According to the code, luminaires in daylighted areas greater than 25 m² shall be equipped with either a manual or automatic control device that is capable of reducing the light output of the luminaires in the daylighted areas by at least 50 %. This ECBC requirement is applied to a simulated high-rise building in this paper and the corresponding energy saving is estimated.

3 EnergyPlus Program

EnergyPlus is a large production software branded by the Department of Energy (U.S) and is used by R&D professionals, engineers, and architects. Using EnergyPlus, buildings can be simulated along with thermal/electric loads. Air conditioning, visual and CO₂ comfort levels can be estimated using the EnergyPlus software. The software supports third-party interfaces also but simulation in this paper has been done directly with EnergyPlus software without any third-party interface.

4 Daylighting

Daylighting is the utilization of sunlight to reduce lighting energy requirements of a building and thus saving the expenditure toward lighting energy. Using the outdoor illumination, daylighting creates a visually productive environment for building occupants and reduces as much as one-third of total building energy costs [2].

A daylighting system comprises a control system that responds to the light received through the windows in the building and decreases the power input to the electric light fixtures so that the reference light level set for the particular area is met with minimum expenditure [3]. To achieve this, the location of windows in a building must be designed in such a way as to allow the sunlight into the building but not directly to the view of the occupants.

This is achieved by provision of windows with suitable glaze correction arrangements such as vertical blinds [4]. The factors involved in the successful

implementation of daylighting scheme are the climate, location of the building, orientation of the building, illumination level requirement, position and size of windows, etc. While designing a daylighting system, the adverse effects such as heat gain, glare, etc. are to be considered. It is an integrated approach and daylighting system has to be considered from the design stage of the building itself since post-construction attempts will not yield much results.

As far as Indian cities are considered, the heat gained in summer due to provision of daylighting windows is significant compared to heat loss due to the same in winter season. Control scheme has the required numbers of light sensors and a light power level control device. Lighting power control is achieved by continuous dimming or stepped control of ballasts in the light fittings or by partially switching off the selected lights [5]. Electric lighting energy expenditure for commercial buildings is 30–50 % of the total electrical energy consumption, and it varies with the occupancy/type of activity in that particular building. Moreover, there are losses in the light fittings which are to be taken care of by the air conditioning system of the building.

The reduction in heat gain due to reduced losses in the light fittings because of daylighting system is estimated to be around 10–20 %. This results in additional savings in air conditioning energy requirements of the building. People generally prefer daylight and due to its adoption, the concentration, productivity, etc. increases and there will be an overall sense of satisfaction.

Some studies conducted indicated that the focus of the students improves with daylighting and the score of students improves. Moreover, daylighting is a stimulant to human visual system and regulates circadian cycle. In order to achieve the best out of the daylighting system, proper maintenance of the components is involved in this system such as light fittings and windows, and glare reduction devices are to be cleaned periodically.

5 Simulated Multi-storey Building

Using EnergyPlus software, a 11-storey (G + 10 floors) high-rise building is simulated [6]. The overall size of the building is 49 m × 16 m. The ground floor is suitable to accommodate the transformers, engine alternator sets, and a reception which needs a high ceiling and the height of ceiling is kept at 4.5 m.

The first, second, third, and fourth floors are meant for technical equipments, and hence the ceiling height is kept at 3.6 m. The fifth to tenth floors are meant for office purpose and a normal ceiling height of 3 m is maintained. Except the ground floor, there is a corridor in all the floors.

The total areas in ground, fifth, sixth, seventh, eighth, ninth, and tenth floors are classified into two zones, i.e., non-air conditioned and air conditioned. The areas under first, second, third, and fourth floors are classified into three zones, i.e., non-air conditioned, air conditioned—technical, and air conditioned—office.

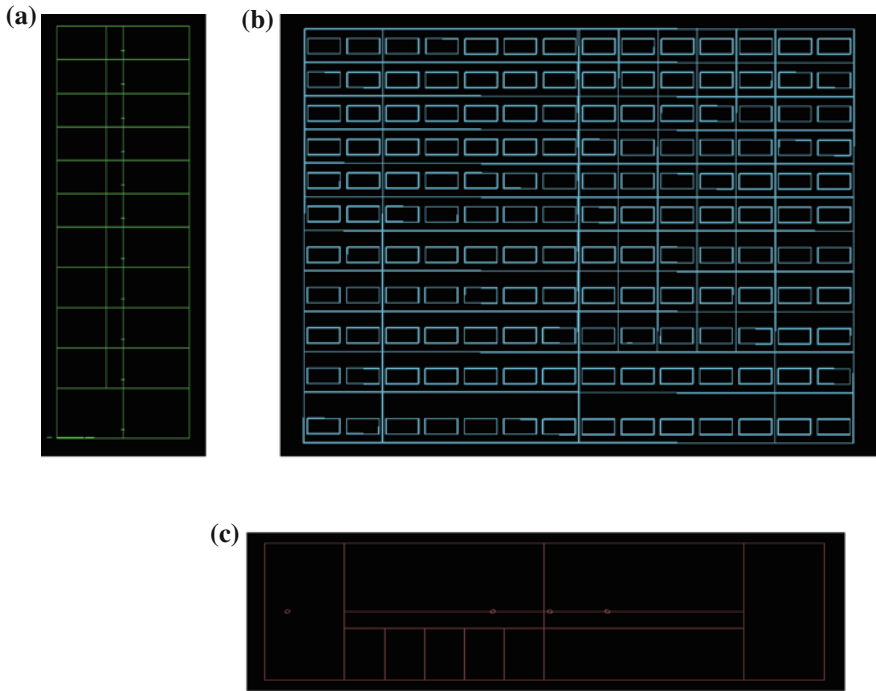


Fig. 1 Simulated building. **a** Right side view. **b** Elevation. **c** Plan

The walls on both the lengthy sides of the building have glass windows. Each bay has one window of size $0.76 \text{ m} \times 2.90 \text{ m}$. The structural members of the building such as wall, window, floor, and ceiling are defined by twelve coordinates that specify the location and extent of the member in three dimensions.

There are a total number of 532 structural members. There are 28 windows in each floor, and hence the total number of windows in the building is 308. A drawing of the building is prepared with the help of AutoCad software and the plan. Elevation and side view are shown in Fig. 1.

6 Estimation of Lighting Energy

There are a total number of 25 zones in the simulated 11-storey building. The required number of light fittings for each floor is specified. The maximum power rating of lighting fixtures in each zone is entered for simulation. Daylighting control is achieved by inclusion of daylighting control object. The daylighting control object has 14 fields and all are assigned values and some important parameters are as below:

- Zone name—Appropriate name of zone is entered.
- Total daylighting reference points—One in our case.
- X-coordinate of first reference point—25, 30, etc. according to X position of the particular zone.
- Y-coordinate of first reference point—Taken as 8 m for all zones.
- Z-coordinate of first reference point—This is the working level, i.e., desk level, taken as 0.8 m from respective floor level.
- Fraction of zone controlled by first reference point—One in our case.
- Illumination set point at first reference point—Set at 500 Lux, the optimum value for office work.
- Lighting control type—Set at 1, i.e., continuous control.
- Minimum input power fraction for continuous dimming control—Kept at 0.3
- Minimum light output fraction for continuous dimming control—Kept at 0.2.

6.1 Weather Data File

The climatic condition of a particular city is fed to the simulation program by inclusion of weather data file for simulation. The Indian Society of Refrigeration and Air-Conditioning Engineers has released the weather data file for major Indian cities. The followings are the contents of the weather data file:

- (i) Latitude and longitude
- (ii) Time zone elevation above sea level
- (iii) Standard pressure at elevation
- (iv) Monthly optical sky depth beam and diffuse
- (v) Monthly solar irradiance Wh/m²
- (vi) Monthly dry-bulb and mean coincident wet-bulb temperatures °C
- (vii) Monthly dry-bulb and wet-bulb daily ranges delta °C
- (viii) Monthly statistics for dry-bulb temperatures °C
- (ix) Monthly statistics for extreme dry-bulb temperatures °C
- (x) Monthly statistics for dew point temperatures °C
- (xi) Average hourly statistics for dry-bulb temperatures
- (xii) Average hourly statistics for dew point temperatures
- (xiii) Monthly statistics for relative humidity %
- (xiv) Average hourly relative humidity %
- (xv) Monthly indicators for precipitation/moisture (kPa)
- (xvi) Monthly statistics for wind chill/heat index temperatures °C
- (xvii) Monthly wind direction
- (xviii) Monthly statistics for wind speed m/s
- (xix) Average hourly statistics for wind speed m/s
- (xx) Average hourly statistics for wind direction °C
- (xxi) Monthly statistics for solar radiation
- (xxii) Average hourly statistics for direct normal solar radiation

- (xxiii) Average hourly statistics for diffuse horizontal solar radiation
- (xxiv) Average hourly statistics for global horizontal solar radiation
- (xxv) Average hourly statistics for total sky cover
- (xxvi) Average hourly statistics for opaque sky cover
- (xxvii) Monthly calculated “undisturbed” ground temperatures °C

6.2 Lighting Schedule

The simulated building is considered as an office building and the time period of 08:00–18:00 h is considered for simulation. The lighting schedule fraction is taken as 1.0 for the working hours of the building and it is taken as 0 for rest of the period.

6.3 Simulation Run Period

Simulation is run for a period of 1 year, i.e., from January 1 to 31, December. It is possible to generate readings for time step (4 steps per hour), hourly, daily, monthly, yearly, and run period. Monthly readings are generated for each zone and energy requirements for all zones are summed for each month and finally energy requirement for 1-year period is obtained in this study [7].

7 Simulation Results

7.1 Across Indian Cities

The annual lighting energy requirements for 10 different Indian cities are estimated [8] in the simulation run. Chennai, Delhi, Mumbai, Hyderabad, Veraval, Ahmedabad, Bhopal, Nagpur, and Dibrugarh are considered for the study. The weather data file of respective city is used for simulation.

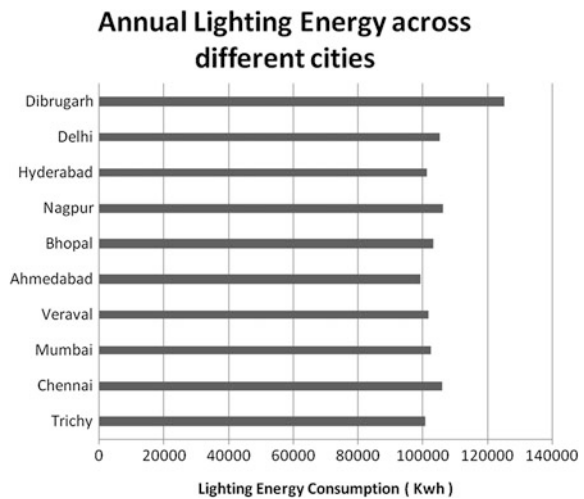
The reason for selection of different cities is that each city is geographically widely separated and their latitude and longitude are different. The estimated lighting energy in Joules and kWh without daylighting control, and with daylighting control, kWh difference, cost savings in rupees (@ Rs. 8/-per kWh), and percentage savings are listed in Table 1 and Fig. 2.

It was found that Ahmedabad city has the lowest estimated lighting energy consumption of 99,052 kWh and Dibrugarh city has the highest energy consumption of 125,034 kWh. This is because of the location of the cities: Ahmedabad is at a longitude of 72.58°E and Dibrugarh is at a longitude of 95.00°E.

Table 1 Cities’ annual lighting energy

City	Energy w/o DLC (J)	Energy w/o DLC (kWh)	Energy with DLC (J)	Energy with DLC (kWh)	kWh difference	Annual cost saving (INR)	% Energy saving
Trichy	9.1875E+11	255208	3.621E+11	100579.25	154628.75	1237030.00	60.59
Chennai	9.1875E+11	255208	3.814E+11	105950.17	149257.83	1194062.66	58.48
Mumbai	9.1875E+11	255208	3.682E+11	102278.61	152929.39	1223435.14	59.92
Veraval	9.1875E+11	255208	3.661E+11	101683.21	153524.79	1228198.36	60.16
Ahm’bad	9.1875E+11	255208	3.566E+11	99051.72	156156.28	1249250.27	61.19
Bhopal	9.1875E+11	255208	3.709E+11	103033.31	152174.69	1217397.50	59.63
Nagpur	9.1875E+11	255208	3.816E+11	106013.61	149194.39	1193555.13	58.46
Hyderabad	9.1875E+11	255208	3.644E+11	101233.06	153974.94	1231799.50	60.33
Delhi	9.1875E+11	255208	3.787E+11	105183.97	150024.03	1200192.21	58.79
Dibrugarh	9.1875E+11	255208	4.501E+11	125034.24	130173.76	1041390.09	51.01

Fig. 2 Energy consumption for different cities



Because of the longitude difference of 22.5°, Ahmedabad is utilizing the day-lighting better and operating hours of the building close during sunlit time, whereas Dibrugarh city is not utilizing the daylighting fully and operating hours of the building fall mostly in the evening. The solution to this problem is to advance the operating hours of the building by approximately 1 or 2 h.

7.2 Different Building Orientations

The light incident on a building is proportional to the angle of the building with respect to the orientation of the building [9, 10]. Hence, the annual lighting energy

Table 2 Chennai annual lighting energy versus building orientation

Angle	0°	30°	60°	90°	120°	150°
J	3.814E+11	3.982E+11	3.706E+11	3.583E+11	3.655E+11	3.8284E+11
kWh	105950.17	110606.93	102955.31	99529.83	101541.53	106345.74
Angle	180°	210°	240°	270°	300°	330°
J	4.094E+11	3.974E+11	3.583E+11	3.686E+11	3.722E+11	3.7081E+11
kWh	113714.68	110398.25	99523.43	102387.21	103380.09	103001.59

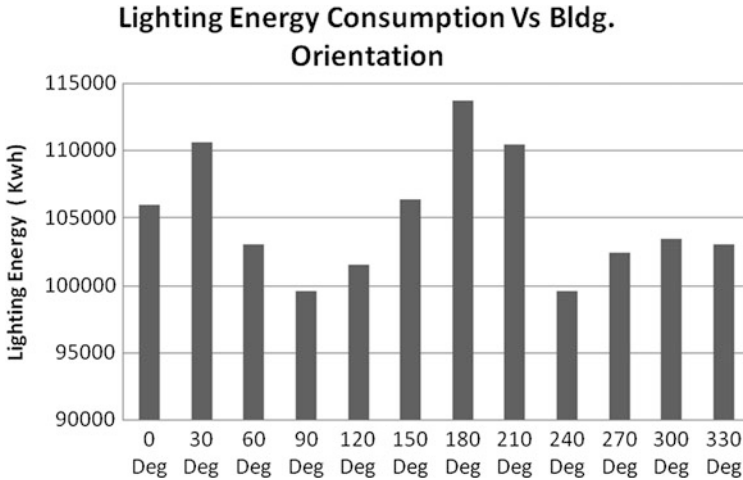


Fig. 3 Energy consumption for different angles

requirement for a building at Chennai is estimated for different angles with respect to the north and the results are shown in Table 2 and Fig. 3.

It is found that the estimated energy consumption at 90° angle and 240° angle is the lowest, i.e., 99,500 kWh, and energy consumption is highest at 180° angle, i.e., 11,371 kWh. Hence, it is advisable to take this factor into account and building orientation to be selected as 90° if other factors such as site suitability permit.

7.3 Hourly Lighting Energy

The hourly lighting energy variation is estimated with the help of a factor hourly lighting power multiplier and the power requirement is calculated for every hour of a day. It is highest, i.e., 0.879374919073515 value, at 18:00 h and it is lowest, i.e., 0.30, at 11:00 h.

The highest value of power multiplier is found to be near 1.0 (0.879) and this indicates that the total installed lighting fixtures for the building are not over

Table 3 Hourly lighting power multiplier

Time	09:00	10:00	11:00	12:00	13:00	14:00	15:00	16:00	17:00	18:00
LPM	0.534	0.383	0.300	0.302	0.351	0.326	0.410	0.425	0.658	0.879

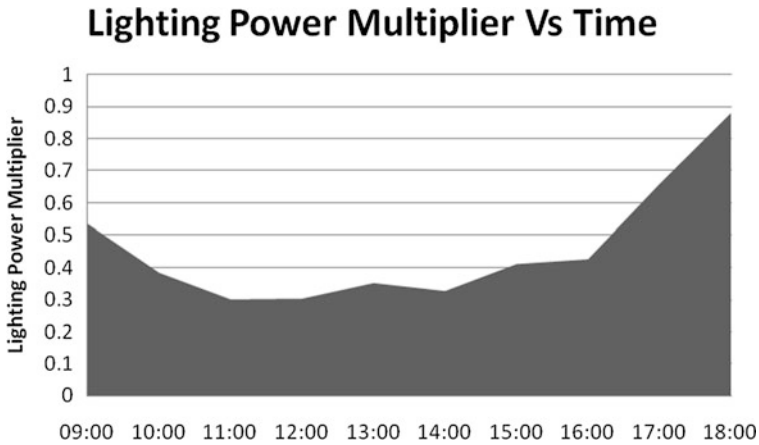


Fig. 4 Lighting power multiplier

designed. The lowest value recorded as 0.3 is due to the setting of minimum lighting input power as 0.3 in the simulation program. This lowest power multiplier indicates the saving potential available with the daylighting control scheme. The details are shown in Table 3 and Fig. 4.

7.4 Lighting Energy for Different Illumination Requirements

The general requirement for doing office task varies from 300 Lux to 600 Lux and a level of 500 Lux is adopted for the study. However, the relationship between lighting level requirement and lighting energy is also studied. The lighting level requirement is varied from 300 Lux to 600 Lux in 50 Lux steps and the energy is estimated for all the cases.

It is found that estimated energy is directionally proportional to the Lux requirement and it varies from a value of 91718.98095 kWh for 300 Lux to 116449.4775 kWh for 600 Lux. The details are shown in Table 4 and Fig. 5.

Table 4 Annual lighting energy versus lux level requirement

Lux	300 Lux	350 Lux	400 Lux	450 Lux	500 Lux	550 Lux	600 Lux
J	3.3E+11	3.403E+11	3.521E+11	3.6575E+11	3.814E+11	3.994E+11	4.192E+11
kWh	91718.98	94527.03	97809.69	101597.10	105950.17	110956.89	116449.48

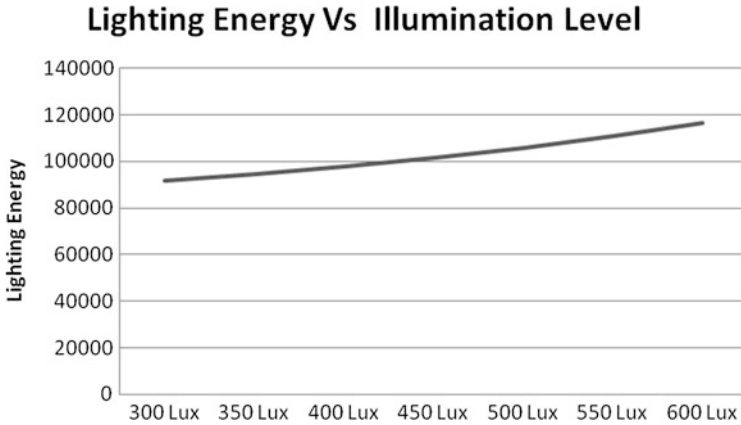


Fig. 5 Lighting energy for different Illumination levels

8 Conclusion

From the study, daylighting is a viable option from the energy conservation and mandatory compliance point of view. Since India is near the equator, there is abundance of sunlight and the scope for utilization of sunlight is large compared to other countries. From the study, we can realize that the percentage saving in lighting energy across different cities ranges from 50 to 60 %.

If we assume the lighting energy to be 30–40 %, then there is an overall energy saving of 15–25 % of total building energy consumption. In addition to the above, thermal load on the air conditioning system will be reduced due to less loss in light fixtures and consequent energy reduction is also achieved. The peak demand of the building will come down resulting saving in demand charges payable to the supply company.

Hence, we can conclude that daylighting can be adopted taking into account the economic benefits to the organization, social responsibility to tide over the power crisis prevalent in our country, and to conserve the nature by reducing the greenhouse emission.

References

1. Energy conservation building code, bureau of energy efficiency, ministry of power. Government of India; 2007.
2. Ander GD. Daylighting. National Institute of Building Sciences, Updated by U.S. Department of Energy.
3. Xu M, Weng S. Daylighting system controller and software design. Shanghai, Natural Computation (ICNC), seventh international conference on, vol. 3. 2011.
4. Mettananta V, Chaiwiwatworakulb P. Automated vertical blinds for daylighting in tropical region. International conference on alternative energy in developing countries and emerging economies; 2013.
5. Tanachaikhan L, Pathumthani. A simple control method for daylighting in passive solar design: a case study of Bangkok, Thailand. Tokyo, SICE Annual Conference; 2008.
6. Chen Y, Liu J, Peia J, Cao X, Chen Q, Jiang Y. Experimental and simulation study on the performance of daylighting in an industrial building and its energy saving potential. *Energy Build.* 2014;73:184–91.
7. Parise G, Martirano L. Daylight impact on energy performance of internal lighting. *IEEE Trans Ind Appl.* 2013;49(1).
8. Kamaruzzaman SN, Edwards R, Ahmad Zawawi EM, Che AI. Achieving energy and cost savings through simple daylighting control in tropical historic buildings. *Sci Dir Energy Build.* 2015;90:85–93
9. Verderberg RR. Lawrence Berkeley Lab., California Univ., Berkeley, CA, USA. In: Morse OC, Jewell JE, editors. Building design: impact on the lighting control system for a daylighting strategy. *IEEE Trans Ind Appl.* 1989;25(2).
10. Jovanović A, Pejić P, Djorić-Veljković S, Karamarković J, Djelić M. Importance of building orientation in determining daylighting quality in student dorm rooms: physical and simulated daylighting parameters' values compared to subjective survey results. *Energy Build.* 2014;77:158–70.

Enhancement in the Performance of Routing Protocols for Wireless Communication Using Clustering, Encryption, and Cryptography

Kanchan Dhote and G.M. Asutkar

Abstract The field of wireless communication sensor networks has been a keen area of research in the last decade. One of the crucial and important parameters for efficient operation of any wireless network is the routing algorithm. Advances in electronics and telecommunication industry in the last few decades have tremendously increased the use of wireless communication systems. However, the choice of the routing algorithm depends not only on the physical topology and geography of the network but also on the application. This paper presents enhancement in the performance analysis of various routing protocols, namely AODV, AOMDV, DSDV, and DSR. These protocols are analyzed on the basis of four quality of service parameters, namely throughput, jitter, delay, and energy consumption. After analyzing, we found that AODV is having the best overall performance. Further enhancement in the QOS parameters of AODV is done with the help of cluster-head selection, encryption, and cryptography which are applied to improve the performance of protocols and the enhanced results are shown in this paper with the help of graphs and analysis.

Keywords AODV · AOMDV · DSDV · DSR

K. Dhote (✉)

Department of Electronics Engineering, Tulsiramji Gaikwad-Patil College of Engineering & Technology, Nagpur, Maharashtra, India
e-mail: hod.etrx@tgp cet.com

G.M. Asutkar

Priyadarshani Indra Gandhi College of Engineering, Nagpur, Maharashtra, India
e-mail: g_asutkar@yahoo.com

© Springer India 2016

S.S. Dash et al. (eds.), *Artificial Intelligence and Evolutionary Computations in Engineering Systems*, Advances in Intelligent Systems and Computing 394, DOI 10.1007/978-81-322-2656-7_50

547

1 Introduction

The use of wireless devices for various commercial and noncommercial applications has increased tremendously in the last few years. Wireless communication is among technology's biggest contributions to mankind [1]. Furthermore, on-the-move internet facility and cheaply available wireless devices have added to this increase. Most organizations are potentially moving toward wireless networks today due to its obvious advantages. With the use of modern day digital image and video transmission techniques, the amount of data which is getting transmitted through these wireless networks has doubled many folds. These needs researchers have proposed various techniques to improve the efficiency and reliability of these wireless networks [2].

Routing protocol is the most critical factor determining the efficiency of these wireless networks [3, 4]. Different routing protocols have been proposed in the past and yet are getting modified to achieve better throughput and minimum delay. These routing algorithms to some extent depend on the topology and application of the network. For example, a routing algorithm may give superior performance in case of mobile ad hoc networks compared to its performance in wireless sensor networks. This paper presents a comparative performance analysis of some of the breakthrough routing protocols for wireless networks. Routing protocols are analyzed on the basis of four network parameters: delay, throughput, jitter, and energy consumption. The following section discusses these in brief by the routing algorithms, namely AODV, AOMDV, DSDV, and DSR.

2 Literature Survey

Routing protocols have been MANETs proposed so far [5]. Some of them have been a breakthrough in the field of wireless communication networks. Some most commonly used routing protocols are discussed here.

1. Ad hoc on-demand distance vector (AODV)

It is a routing protocol for other wireless ad hoc networks. It is an on-demand routing protocol, i.e., processed in a path as when process is started. In AODV protocol, the network node that needs a connection first requests for connection using broadcast which is forwarded by other nodes. Nonused routes in the routing tables are flushed after some time. In case of link failures, error is passed to its node of transmission with repetition [6].

Advantages

- (a) Established on demand.
- (b) Destination has a specified sequence in terms of its destination.
- (c) Lower delay.
- (d) In networks with light or moderate traffic requirements this protocol scales perfectly.

Disadvantages

- (a) Unnecessary bandwidth consumption due to periodic beaconing.
- (b) Is problematic for heavy traffic and high mobility networks.
- (c) Intermediate nodes can lead to inconsistent routes.
- (d) Lower BW.

2. Ad hoc on-demand multipath distance vector (AOMDV)

AOMDV computes multiple loop-free paths per route discovery. This helps the protocol to switch routes to a different path in case a path fails without the need for a new route discovery. Route discovery is initiated only when all paths to a specific destination fail.

Advantages

- (a) Routes established on demand.
- (b) Link disjoint paths are computed so that paths fail independent of each other.
- (c) Better BW compared to AODV.
- (d) Is more suited to moderate to high traffic requirements.
- (e) Delay is better compared to alternative routes compared to AODV.

Disadvantages

- (a) Requires much more overheads compared to AODV.

3. Destination-sequenced distance-vector routing (DSDV)

DSDV is a modified version of the conventional RIP protocol and is based on Bellman–Ford algorithm [7]. It adds a new attribute, and sequence number, to each route table entry of the conventional RIP. In DSDV, each node maintains a routing table containing all available destinations routes, the metric and next hop to each destination, and a sequence number generated by the destination node. Each node updates the routing table through periodic advertisement [8].

Even sequence number denotes that link is present, while the odd number denotes that link is not present or has failed. It is dispersed by smaller incremental updates more frequently.

Advantages

- (a) Solves routing loop problem efficiently.
- (b) Latency of route discovery is low.

Disadvantages

- (a) Requires frequent upgradation of various routing tables, which has its use of battery power and bandwidth.
- (b) Suffers through route fluctuation because of its criteria of frequent route updates.
- (c) Care should be taken to reduce the number of control messages.

4. Dynamic source routing (DSR)

DSR is an on-demand steering set of rules which depends upon source steering technique in which source determines the exact queuing of nodes through which packets will be propagated [9]. In DSR, every node maintains a route cache to accumulate spring routes that it has learned. When crowd wants to send a packet to some other crowd, it first checks its route cache for a source route to the destination. In case if one route is detected, the sender uses that route to propagate the packet. Otherwise, the sender lump initiates the route discovery process [10].

Advantages

- (a) It eliminates essence of flooding the network containing table messages.
- (b) Use of route cache reduces the control overhead.

Disadvantages

- (a) Requires route supervision with reliability to rectify broken link.
- (b) Connection setup delay is high.
- (c) The performance degrades rapidly with increasing mobility.

The printing area is 122 mm × 193 mm. The text should be justified to occupy the full line width, so that the right margin is not ragged, with words hyphenated as appropriate. Please fill pages so that the length of the text is no less than 180 mm, if possible.

3 Results

To analyze these routing protocols, we have implemented a wireless sensor network on NS-2 [11] consisting of 20 wireless nodes. Figure 1a–d shows all the graphs for AODV protocol. Figures 2, 3, 4, and 5 show the comparative graphs, in which the four protocols are compared on the basis of all four parameters: throughput, delay, energy, and jitter. Furthermore, the comparison is explained in Table 1 shown below.

After the comparison, we come to the conclusion that AODV protocol is the best out of four protocols. Furthermore, the cluster-head selection process, encryption, and cryptography method are applied to the AODV and the quality of service parameters are improved. It is proved through the following graph.

The cluster-head selection, compression, and encryption are applied to the AODV protocol. As in terms of the analysis, it has been obtained by the following parameters:

- (A) Run length encoding (RLE)
- (B) Elliptic curve cryptography (ECC)
- (A) Run length encoder (RLE)

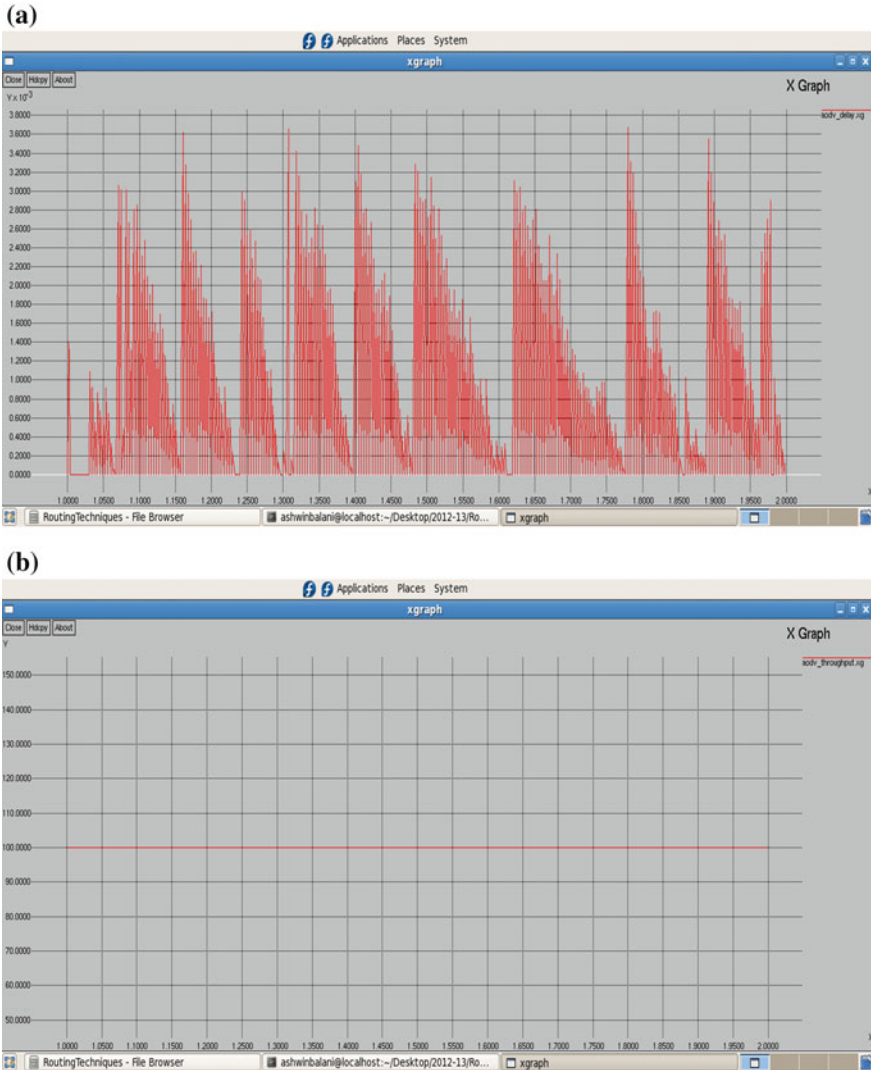
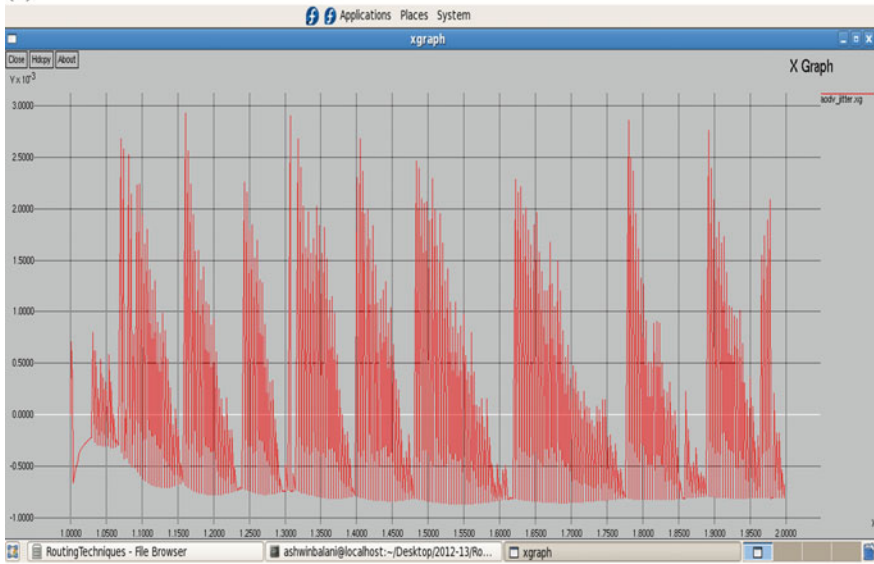


Fig. 1 a Delay graph for AODV. b Throughput graph for AODV. c Jitter graph for AODV. d Energy consumption graph for AODV

(c)



(d)

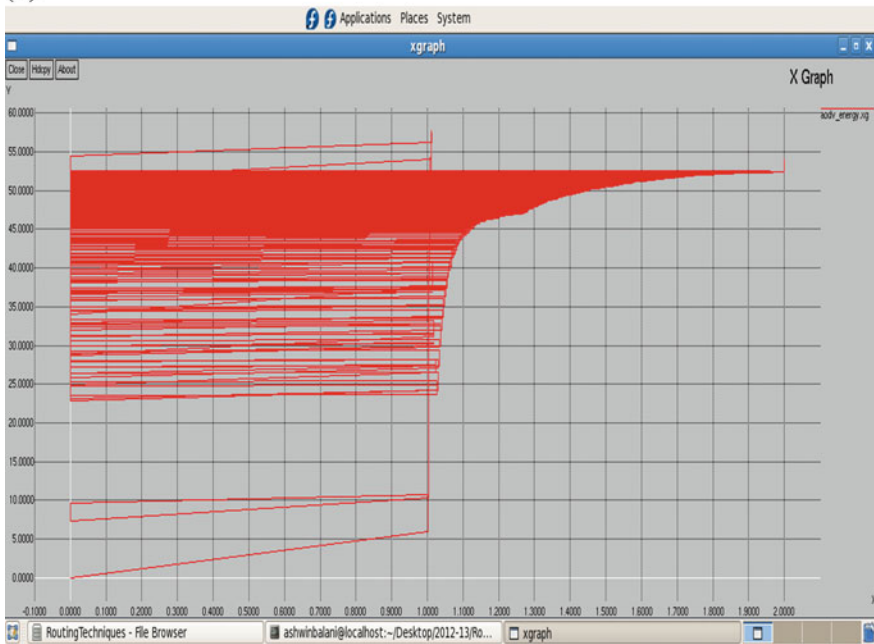


Fig. 1 (continued)

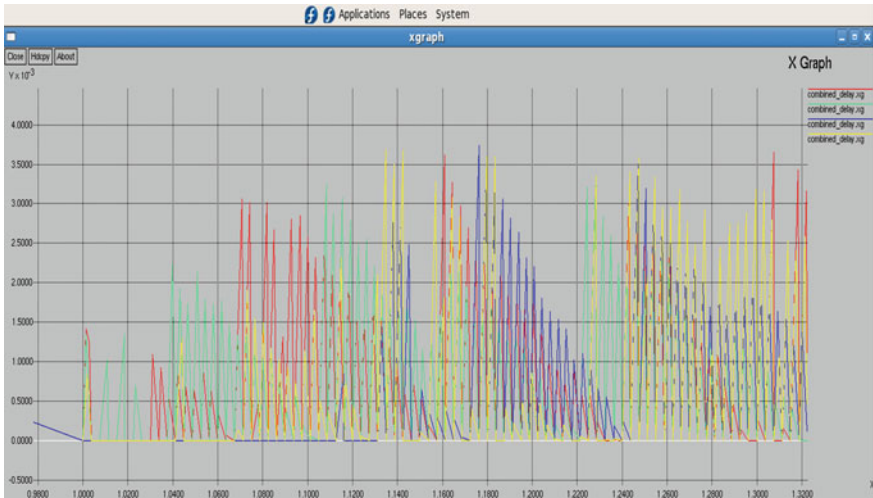


Fig. 2 Combined graphs of four protocols for DELAY

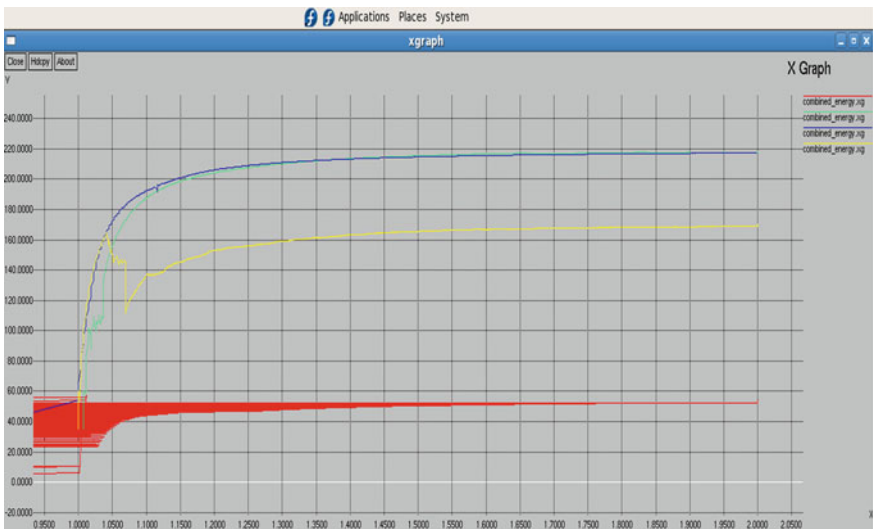


Fig. 3 Combined graphs of four protocols for energy consumption

The implementation of compression technique is used as such (Figs. 6 and 7):

1. Represents data using value and run length
2. Run length defined as number of consecutive equal values

(B) Elliptic curve cryptosystems

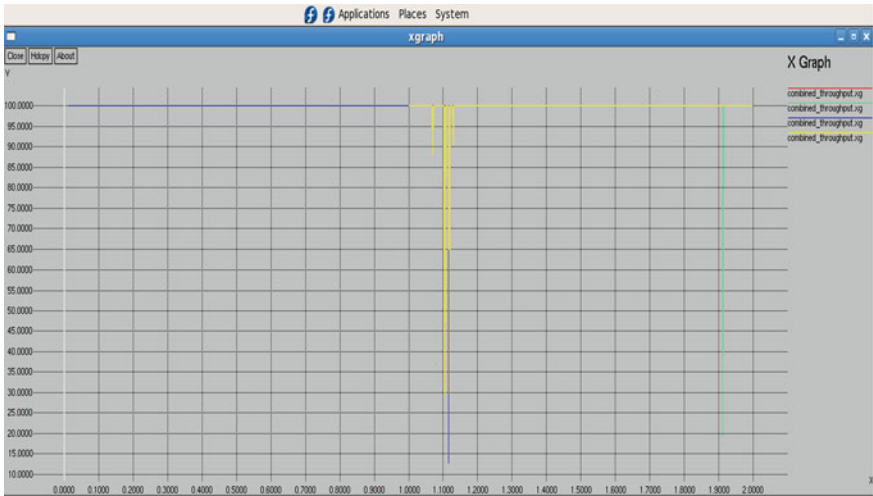


Fig. 4 Combined graphs of four protocols for throughput

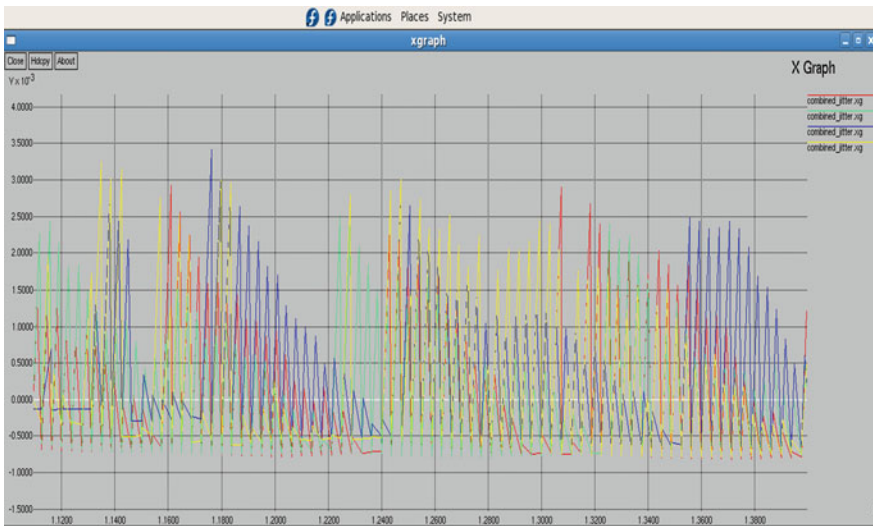


Fig. 5 Combined graphs of four protocols for Jitter (Colour figure online)

It has been seen that device consideration to be much smaller with less storage and process-based computational power.

Applications of elliptic curve cryptosystems:

- Used in varied communication devices having non-wired communications.
- Payroll enabled cards.
- Server side enrolled for web-based tasks.

Table 1 In the given graphs, red color indicates AODV protocol, blue color indicates DSDV protocol, yellow color indicates DSR protocol and green color indicates AOMDV protocol

Parameter				
Protocol	Delay	Throughput	Jitter	Energy consumption
AODV	Low	Better	Low	Lowest
AOMDV	Medium	Best	High	High
DSDV	Low	Better	Medium	Highest
DSR	Low	Good	Highest	High

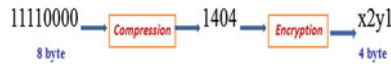


Fig. 6 Compression rate and encryption process

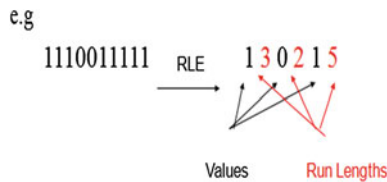


Fig. 7 Run length encoder example with process

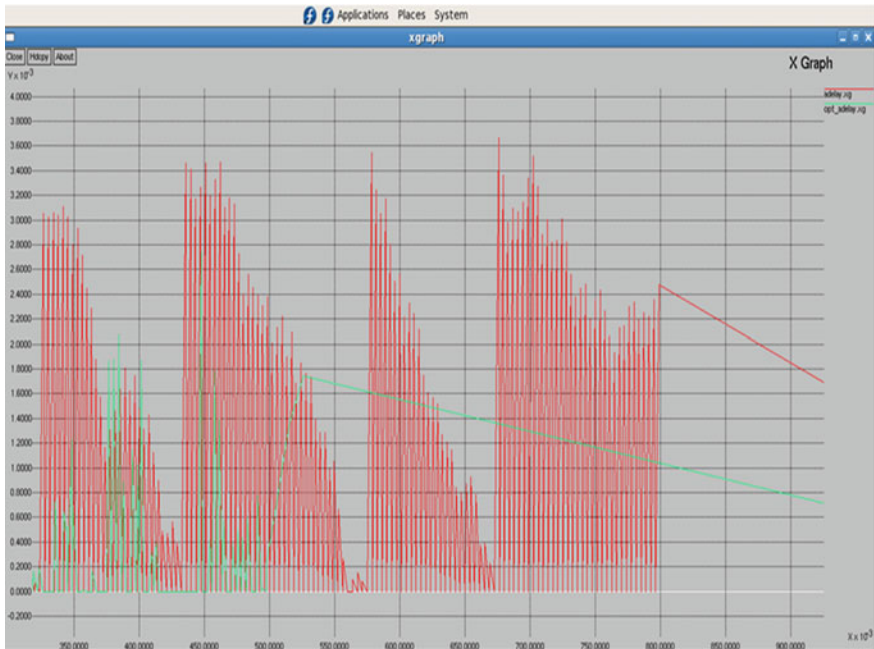


Fig. 8 Comparative graph for delay

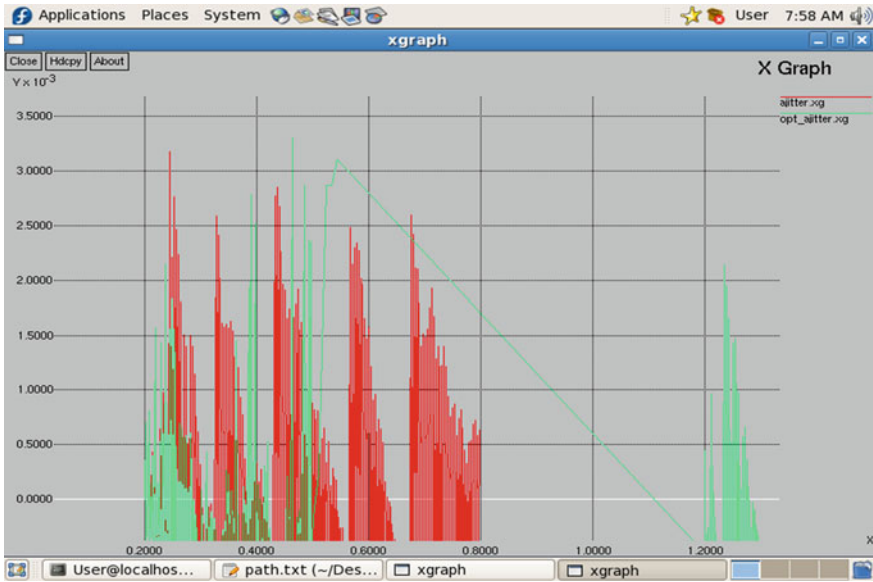


Fig. 9 Comparative graph for Jitter

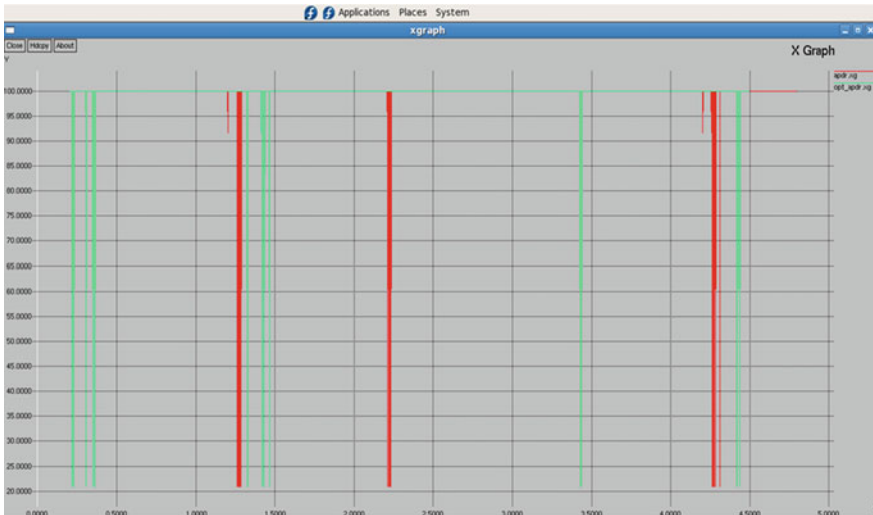


Fig. 10 Comparative graph for packet delivery ratio (PDR)

The red color in the below shown graphs (Figs. 8, 9, 10, 11 and 12) shows the performance of routing protocol before applying clustering, compression, and encryption; and the green color shows the results after the application of clustering, compression, and encryption.

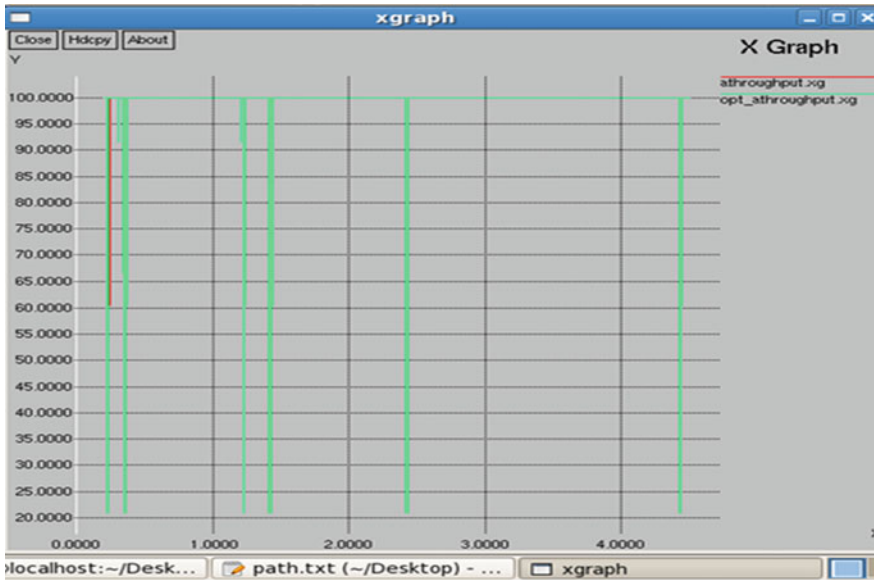


Fig. 11 Comparative graph for throughput



Fig. 12 Comparative graph for energy consumption

4 Conclusion

In this paper, we have presented an enhancement in the performance of routing protocols for wireless network communication. These protocols have been implemented in NS-2 and are analyzed on the basis of four crucial parameters: throughput, delay, jitter, and energy consumption. After analyzing the graphs, we conclude that AODV is better in comparison to AOMDV, DSR, and DSDV as it has best throughput but suffers from high jitter and energy. Furthermore, on AODV protocol clustering, encryption, and cryptography are applied and the QOS parameters are enhanced as shown in the graphs. The delay and jitter get reduced, and throughput and packet delivery ratio get improved.

References

1. Asutkar GM. Monitoring of air pollution using wireless sensors—a case study of monitoring air pollution in Nagpur city. *Int J Environ Sci.* 2012;2(2):829–38. ISSN:0976-4402.
2. Wireless lan medium access control (mac) and physical layer (phy) specifications. IEEE Standard Tech Rep. 1999.
3. Asutkar GM. Wireless sensor network for surveillance using a multichannel multi-radio approach. In: *International conference on engineering, technology & management (ICETM'12)*; 2012. ISBN:978-93-81583-52-4.
4. Yu Y, Govindan R, Estrin D. Geographical and energy aware routing: a recursive data dissemination protocol for wireless sensor networks. UCLA computer science department technical report UCLA/CSD-TR-01-0023; 2001.
5. Wang L, Liu J, Wang W. An improvement and simulation of LEACH protocol for wireless sensor network. In: *International conference on pervasive computing, signal processing and applications*; 2010.
6. Park VD, Corson SM. A highly adaptive distributed routing algorithm for mobile wireless networks. In: *Proceedings of INFOCOM*; 1997.
7. Trung HD, Benjapolakul W, Duc PM. Performance evaluation and comparison of different ad hoc routing protocols. Bangkok: Department of Electrical Engineering, Chulalongkorn University; 2007.
8. Perkins CE, et al. Highly dynamic destination -sequenced distance-vector routing (DSDV) for mobile computers. London: Published in SIGCOMM; 1994. p. 234–44.
9. Perkins C, Belding-Royer E, Das S. Ad hoc on-demand distance vector (AODV) routing. <http://www.ietf.org/internet-drafts/draftietf-manet-aodv-13.txt> (2003).
10. Johnson DB, Maltz DA. Dynamic source routing in ad-hoc ad hoc networks. In: Imielinski T, Korth H, editors. *Mobile computing*. Kluwer Academic Publishers; 1996. p. 153–81.
11. NS-2. <http://www.isi.edu/nsna>.

Design and Implementation of an Efficient Level Set Segmentation and Classification for Brain MR Images

C.M. Naveen Kumar, B. Ramesh and J. Chandrika

Abstract Nowadays, according to the fact the excess brain segmentation is one of the most prevalent diseases of human brain–body system. Further determination of the exact location of brain segmentation in the body is a big challenge. As of now, there seems to be no scientific tool which precisely determines the presence of brain segmentation. However, mammography has shortcomings which yields 34 % false negative rate which is too high. This has been overcome by digital mammography but has limitations regarding the X-ray exposure. Moreover, image cannot be altered and film processing will be slow. Brain segmentation detection rate of 7.62 % can be achieved through CAD-based techniques. Although image segmentation in CAD-based method has its advantage over spatial intensity, challenge is estimating the proper prior distribution. There are numerous medical imaging methods, viz., magnetic resonance imaging (MRI), X-ray computed tomography (CT), ultrasound imaging (US), etc., that can examine different factors of human body. The detection of brain segmentation is crucial for the doctor in order to determine the status of the brain segmentations and to visualize any abnormalities that are present in the brain segmentation. The detection of anomalies of brain segmentation inside the body is a topmost field of study in medical research using biomedical image processing. Certain defects (speckle noise) in ultrasound or MRI images or US or CT and artifacts result in wrong diagnosis that could happen by analysing the scanned image. Consequently, in this proposed work the key focus is to design the algorithm based on level set segmentation, wavelets filters and artificial neural network (ANN) architecture for real-time detection of brain segmentation using biomedical images with the help of MATLAB with maximum accuracy of 94.8 %.

C.M. Naveen Kumar (✉) · B. Ramesh · J. Chandrika
Department of Computer Science & Engineering, Malnad College of Engineering,
Hassan 573202, India
e-mail: cmnk.it@gmail.com

B. Ramesh
e-mail: sanchara@gmail.com

J. Chandrika
e-mail: jc@mcehassan.ac.in

Keywords Magnetic resonance imaging (MRI) • X-ray computed tomography (CT) • Ultrasound imaging (US) • Wavelets • Artificial neural network

1 Introduction

Brain segmentation is present in every cell of the body. It is a waxy and fat-like in appearance. Since the brain segmentation is oil based, it does not mix up with blood, which is water based. Therefore, it is spread around the body in the blood by lipoproteins. The presence of hyperbrain segmentation or high level of brain segmentation in the human body causes a significant threat to person's health, though it is not a disease but it can contribute to other forms of diseases like cardiovascular disease. Therefore, it is very important to have blood-brain segmentation level checked. The high brain segmentation is a factor of coronary heart disease and it is responsible for the heart attacks. The presence of abnormal brain segmentation might lead to the diabetes, liver or kidney disease. Also in case of polycystic ovary syndrome, pregnancy, and other conditions where there is an increase in the level of female hormones, abnormal brain segmentations are detected. The factors that may cause the brain segmentation levels are diet, weight, exercise, age and gender, diabetes, heredity, and other medical conditions. In order to detect the brain segmentation level in the human body, we proposed an artificial neural network, multilayer perceptron, and back propagation method.

1.1 Related Work

Wen-Hsuan Lai, Jiunn-Der Liao and Shyh-Hau Wang proposed nano-mechanical property of cell membrane during brain segmentation reinstatement. Depth-sensing nano-indentation method is employed to detect the LIPUS insonification and this method is useful for restoration of elastic properties of brain segmentation manipulated cells [1]. Teddy Lesmana and Wen-Yaw Chang proposed a FPGA-based dual glucose/brain segmentation metre application. This application not only provides the better performance in terms of power consumption, linearity and accuracy but also produces the glucose concentration (mg/dL) within 11 s [2]. Deano Reilly and Nicholas Bowring suggested an algorithm that processes co- and cross-polarized radar signals into a single dataset for classification. The result provides the detection rate of 80 % with a false alarm rate as small as 6 %. This scheme also improves the training regime of the ANN using PCA [3]. V. SreeHari Rao and M. Naresh Kumar proposed a novel approach for predicting the risk factors of atherosclerosis with an in-built imputation algorithm and particle swarm optimization (PSO). This approach is capable to predict the risk factor with the accuracy of 99.73 % [4]. Ali Nasir and Ella M. Atkins suggested a stochastic dynamic

programming-based framework which facilitates the implementation of collaborative fault detection through conflict resolution. This method lessens the computational complexity [5]. Ryan D. Morton and Edwin Olson described about the height–length–density terrain classifier and provided a unified mechanism for detecting both positive and negative obstacles. This method can also be estimated both in indoor and outdoor environment [6]. MdR. Ahsan and Muhammad I. Ibrahimy recommended detection of different hand movements using ANN and also uses back propagation with Levenberg–Marquardt training algorithm. The results provide an efficiency of 88.4 % of the average [7]. Sri Ram Jayakumar and Rajesh Khanna present a machine vision system based on ANN for identifying and solving the defects occurred in transistor fabrication, and this achieves 0 % PPM and provides 100 % inspection in the transistor fabrication [8]. R.A. Ramlee and S. Ranjit proposed a method for brain segmentation detection using iris recognition algorithm and iridology chart. It is not only mainly for biometric identification but it can also be implemented as a mean to detect brain segmentation presence or diagnose any other diseases [9].

1.2 Problem Statement

Brain segmentation is the most common problem that occurs in human body. This brain segmentation can be examined by many medical imaging methods such as magnetic resonance imaging (MRI), X-ray computed tomography (CT), ultra sound imaging and many others. A person suffering from brain segmentation may lead to many diseases such as cardiovascular disease, atherosclerosis and many other problems. These abnormalities are scanned using MRI, ultrasound, etc., since there is a noise in the scanned image which may lead to wrong diagnosis; so in order to overcome this problem we propose a new method which employs wavelets and multilayer perceptron (MLP) with back propagation artificial neural network which reduces error. Speed of operation can be increased using fast multiplier and adder. Matlab is used to convert the brain segmentation images to pixels (100×100) and these pixels are stored in ROM using IP core, applied to the neural network and output of MLP-BP algorithm is shown in chip scope.

2 Methodology

Figure 1 shows the overall block diagram of proposed method. It consists of the following blocks: brain segmentation image database, image preprocessing, wavelet processing and ANN classification.

Brain Segmentation Image Database

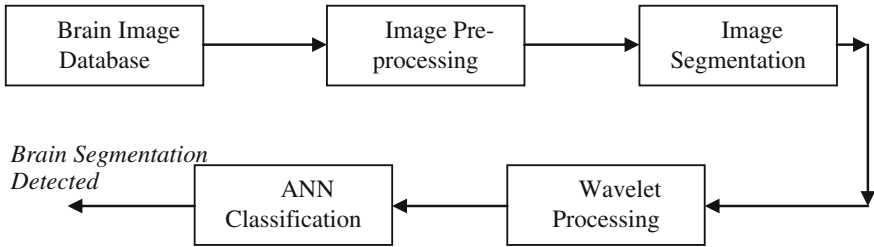


Fig. 1 Block diagram of proposed method

The 100 brain segmentation images are collected from different hospitals of different patients and are stored in database. One of the images is taken from the database and is subjected to brain segmentation detection.

2.1 Image Preprocessing

The obtained ultrasound image consists of speckle noise and is of low contrast which makes difficult for analysing. To overcome this, preprocessing of US image is done which consists of following steps:

1. Image restoration
2. Smoothing and sharpening
3. Contrast enhancement

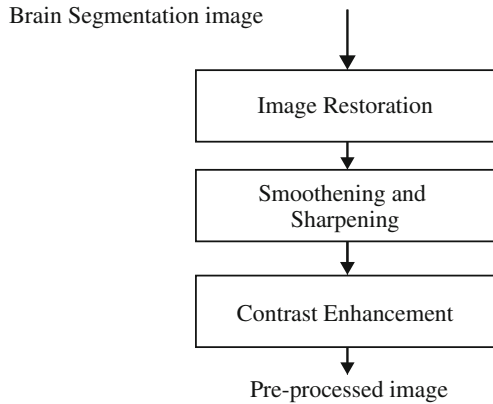
2.1.1 Image Restoration

The purpose of image restoration is to reduce the degradations that are caused during image scanning. To avoid this, we make use of level set functions for proper orientations. The shrinks can be removed using plan curve motion.

2.1.2 Smoothing and Sharpening

The Gabor filter which acts as band-pass filter is employed to get optimal resolution in both spatial and frequency domains. The degree of smoothing can be adjusted by varying the standard deviation of Gaussian function.

Fig. 2 Preprocessing of brain segmentation image



2.1.3 Contrast Enhancement

Histogram equalization is used to improve the contrast and to obtain the uniform intensity of the image. This method can be employed on the whole image or part of the image. By transforming the values in an intensity of image, the image contrast can be enhanced such that its output image matches the stated histogram image (Fig. 2).

3 Image Segmentation

Figure 3 shows the level set segmentation method used to segment the location of brain segmentation. The first method of proposed work is momentum term and second method is the resilient propagation term. The purpose of segmentation is to overcome the difficulties that exist in the energy function. These energy functions rely on image properties such as gradients, curvatures, intensities and regularization terms. The first proposed method adds momentum to the motion in solution space which is based on modification. Specific adaptive step magnitudes and signs of the gradient components are used by the R_{prop} to overcome the problems of gradient descent search.

3.1 Momentum Term

The machine learning community is adopted by spinning to gradient descent with momentum and it will choose search vector according to

Fig. 3 Segmentation of brain segmentation detection

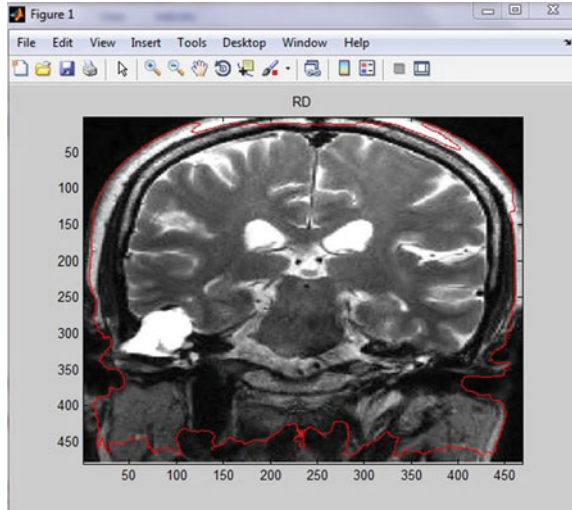
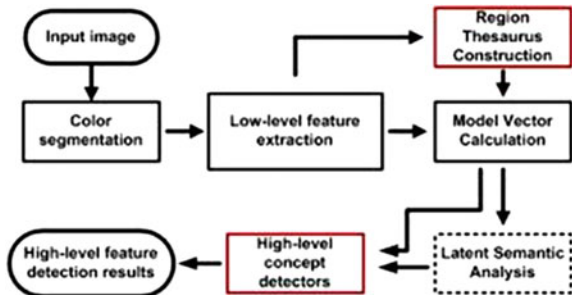


Fig. 4 Flow chart for level set segmentation



$$a_l = -\eta(1 - \omega)\nabla f_l + \omega a_l \tag{1}$$

where η is the learning rate and $\omega \in [0, 1]$ is the momentum. Note that $\omega = 0$ gives standard gradient (Fig. 4).

Descent $a_l = -\eta\nabla f_l$, whereas $\omega = 1$ gives “infinite momentum” $a_l = a_{l-1}$.

3.2 R_{prop} Method

The update values will overcome the disadvantages of standard gradient descent (SGD) and each dimension will have one update value, i.e., $\dim(\nabla_l) = \dim(x_l)$. In R_{prop} , the gradient size is not used. Partial derivatives are considered in update rule. Stoutness of R_{prop} parameters is another advantage. For R_{prop} , we choose a search vector s_k according to

$$\mathbf{a}_l = -\text{sign}(\nabla f_l) * \nabla_l \quad (2)$$

where ∇_l is a vector containing the current update values and $\text{sign}(\cdot)$ is the element-wise sign function.

3.3 Energy Optimization for Segmentation

Calculus of variations is employed to approach the segmentation problems where an energy function represents the objective of the difficulty. Gradient descent search in counter space is used as solution for the segmentation problem. Consider, for instance, the derivation of the *weighted region* described by the following functional:

$$f(p) = \iint_{\Omega_p} g(x, y) dx dy \quad (3)$$

where p is a 1D curve embedded in a 2D space, Ω_p is the region inside of p and $g(x, y)$ is a scalar function. This will maximize certain quantity given by $g(x, y)$ inside p . If $g(x, y) = 1$ for instance, the area will be maximized. Calculating the first variation of Eq. 1 produces the evolution equation:

$$\frac{\partial p}{\partial t} = -g(x, y)\eta \quad (4)$$

where η is the curve normal. Using $g(x, y) = 1$, it is a constant flow in the negative normal direction. The contour can also be represented by the zero level of a time-dependent signed distance function, which is known as the level set function. Formally, a contour p is described by $p = \{\mathbf{x}:\phi(\mathbf{x}, t) = 0\}$. The contour p is evolved in time using a set of partial differential equations (PDEs). A equation of motion for a parameterized curve $\frac{\partial p}{\partial t} = \gamma\eta$ is in general translated into the level set equation $\frac{\partial \phi}{\partial t} = \gamma|\nabla \phi|$. Equation 2 gives the familiar level set equation:

$$\frac{\partial \phi}{\partial t} = -g(x, y)|\nabla \phi| \quad (5)$$

4 Wavelet Processing

The resulting segmented image from the previous block is given as input to the wavelet processing block. It consists of Daubechies filter (Db12), Symlets filter (sym12) and Biorthogonal filter (bio3.7, bio3.9 and bio4.4). *Daubechies filter*

(*Db12*) in this the number 12 refers to the number of vanishing moments, smoother the wavelet higher is the vanishing moments (and longer the wavelet filter) and length of the wavelet filter is double the number. *Symlets filter (sym12)* extract features of brain segmentation image and analyse discontinuities and abrupt changes contained in signals. It utilizes one of the twelfth-order Symlets wavelets. *Biorthogonal filter (bio3.7, bio3.9 and bio4.4)*—The averages of horizontal and vertical coefficients details are calculated using filter wavelet energy signatures. Each filter will give different energy levels or energy features. These energy features will show significant difference, if there is any brain segmentation present in the particular region or location. The energy features show the difference.

5 Implementation and Results

Matlab2012a is used for implementation of the system. A Graphical user interface is as shown in Fig. 5. The brain segmentation images are collected from the hospitals and stored in a database. The image which is to be analysed is selected from the GUI. Z-score normalization is used to preprocess the selected image. Z-score normalized image is then applied to Wavelet filters Daubechies, Symlets and Biorthogonal. Then feature extraction option is selected to get list of the energy levels extracted from the image. In the GUI, there are two tables; one corresponds to list of energy levels of the input image. The second one corresponds to list of selected energy levels of all the images in the database.

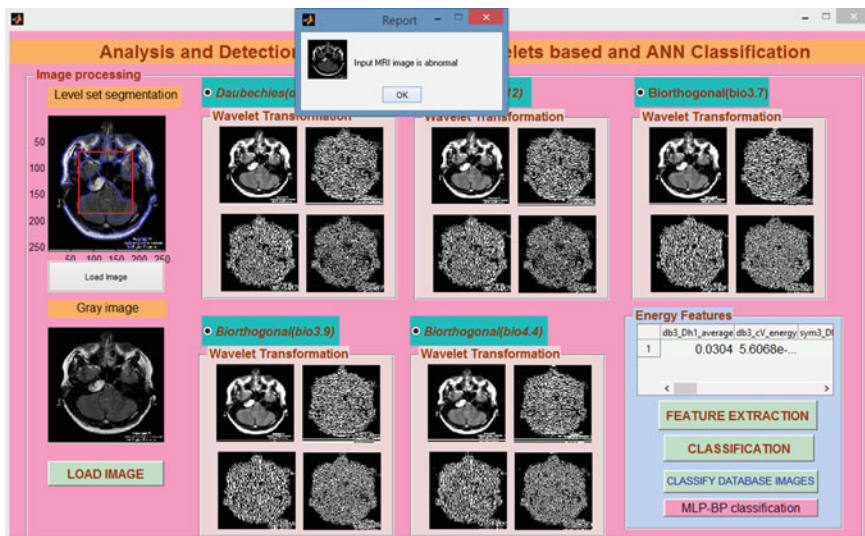


Fig. 5 GUI of wavelets, energy and classification of brain segmentation

Table 1 Enlarged energy and average values of Fig. 5

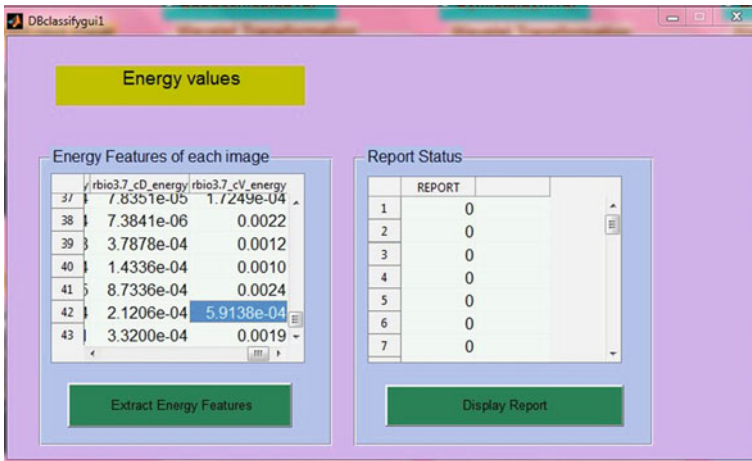
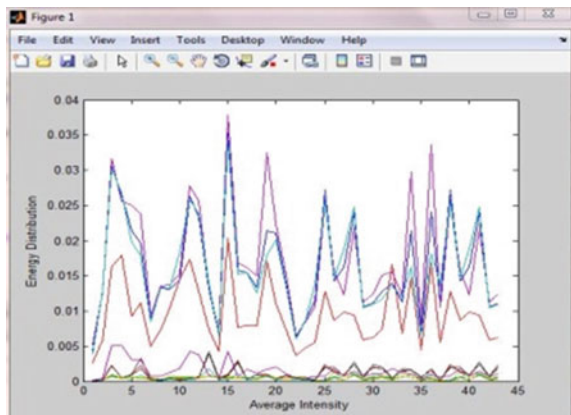


Table 1 shows the enlarged version of the second table in the GUI. The rows of the table are individual energy level of each brain segmentation image in the database. The columns of the table show energy level extracted from the images of database with respect to each wavelet filter. First two columns are corresponding to Daubechies filter, and the third and fourth columns are corresponding to symlets12. The fifth, sixth, seventh and eighth columns are corresponding to Biorthogonal filter (Bio3.7). The ninth, tenth and eleventh columns are corresponding to Biorthogonal filter (Bio3.9). The twelve, thirteenth and fourteenth columns are corresponding to Biorthogonal filter (Bio4.4) [6]. Using these energy levels, the MLP-BP ANN algorithm will classify the images based on brain segmentation levels. Table 1 shows the GUI and displays the tables corresponding to MLP-BP ANN algorithm.

Fig. 6 Plot of energy level for Table 1



MLP-BP ANN algorithm classifies the images in the database with the accuracy of 98.8 %. This GUI also shows two popup windows which are nothing but the report generated by MLP-BP ANN algorithm for the selected input image (Fig. 6).

6 Conclusion and Future Work

For the brain segmentation image, the energy levels extracted using wavelet sub-bands Daubechies (Db4), Symlets (sym4) and Biorthogonal filters (bio3.7, bio 3.9 and bio4.4) give the clear indication of difference in the energy levels compared to that of normal brain segmentation image. The ANN algorithms MLP-BP are trained and classify the images in the database with the accuracy of 89.6 %. MLP-BP ANN algorithm classifies the images in the database with the accuracy of 97.6 %. The proposed system exhibits better accuracy. This system is cost effective and can be readily used in the hospitals. This system reduces doctor's burden and overcomes human error. In future, the system can be incorporated with artificial intelligence to classify different levels of brain segmentation. It can also be designed to generate report by itself with full information of the patient so that it can be used for telemedicine purpose.

References

1. Lai W-H, Liao J-D, Wang S-H. Effect of low intensity pulsed ultrasound on the nano-mechanical properties of brain segmentation manipulated cells. IEEE international ultrasonics symposium proceedings; 2012. 10.1109/ULTSYM.2012.0149.
2. Lesmana T, Chung W-Y, Chen S-L. Dual glucose/brain segmentation meter applications based on FPGA platform. IEEE 2nd international symposium on next-generation electronics (ISNE), Kaohsiung, Taiwan; 2013. 978-1-978-1-4673-3034/13.
3. O'Reilly D, Bowring N, Harmer S. Dual signal processing techniques for concealed weapon detection by use of neural networks. IEEE 27th convention of electrical and electronics engineers in Israel; 2012. 978-1-4673-4681-8/12.
4. Sree Hari Rao V. Senior Member, IEEE, Naresh Kumar M. Novel approaches for predicting risk factors of atherosclerosis. IEEE J Biomed Health Inf. 2013;17(1):1089-7771.
5. Nasir A, Atkins EM, Kolmanovsky IV. Conflict resolution and collaborative fault detection using stochastic dynamic programming. IEEE; 2012. 978-1-4577-0557-1/12.
6. Morton RD, Olson E. Positive and negative obstacle detection using the HLD classifier. IEEE/RISJ international conference on intelligent robots and systems, San Francisco, CA, USA; 2011. 978-1-61284-456-5/11.
7. Ahsan MdR, Ibrahimy MI. Hand motion detection from EMG signals by using ANN based classifier for human comput interaction. 978-1-4577-0005-7/11/\$26.00 © IEEE; 2011.
8. Jayakuma S, Kanna R. Inspection system for detecting defects in a transistor using artificial neural network (ANN). In: Proceedings of the international conference on communication and computational intelligence; 2010.
9. Ramlee RA, Ranjit S. Using iris recognition algorithm, detecting brain segmentation presence. International conference on information management and engineering 978-0-7695-3595-1/092009 IEEE; 2009.

Robotic Imitation of Human Hand Using RGB Color Gradient Mapping

T. Thyagaraj, Kumar Abhishek, N.S. Brunda, Rakesh Ranjan
and Nikita Kini

Abstract The state-of-the-art developments in robotics reveal a scenario wherein human motion imitation has been developed through advancements in features and performance of sensors. Most of such robots uses flex sensors to acquire the information about the orientation of the body being imitated. However, these are slow and are highly vulnerable to damages and physical changes. There are image processing algorithms that are focused on a robots learning through ANN and are not into imitation without memory. This paper presents an overview of research attempts to use a robotic assembly to imitate a real object using image processing. The paper describes results in force, tactile and visual sensing, sensor-based control, and the configuration of a test-based robot integrated system for imitation of a human hand, using vision through image processing using RGB scheme; and one-on-one mapping for the acquisition of the current position of a body and orientation of the various parts of the robot in same fashion. This research has resulted in the development of a prototype capable of imitation and its applications are in the areas of medicine, defense, safety, and explorations for both research and commercial applications.

T. Thyagaraj (✉) · K. Abhishek · N.S. Brunda · R. Ranjan · N. Kini
Department of Electronics and Communication Engineering BMSIT, Visveshvaraya
Technological University (VTU), All India Council for Technical Education (AICTE),
VTU Campus Belagavi, Karnataka 590018, India
e-mail: thyagaraj_tanjavur@bmsit.in

K. Abhishek
e-mail: itsmekumarabhishek222@gmail.com

N.S. Brunda
e-mail: nsbrunda94@gmail.com

R. Ranjan
e-mail: rrrakesh265@gmail.com

N. Kini
e-mail: chinns94.nk@gmail.com

Keywords Robotic vision · Color mapping · Median filtering · Robot-arm · Embedded module image processing · Robotics · Robotic arm · Human imitation · Motion tracking · Motion sensing · Robotic vision · Sensor-based robots · Flex sensors · Embedded systems · Integrated systems · Artificial neural networks · Matlab · RGB scheme

1 Introduction

Imitation of a human body and motion capture has been an area of constant research and development since many years. It requires substantial understanding of sensation, representation, manipulation, integration, and configuration of computer processors in order to analyze, design, and evaluate the control on robotic systems [1–4]. The robotic assembly system has its pros and cons. It presents complex research issues due to the physical interactions among work pieces, their precise positioning, and complex geometry of the manipulations. Also, the vision sensing and appropriate mapping is another challenge [5]. At present, similar robots use flex sensors to acquire information about the orientation of the body being imitated [1 – 4]. The flex sensor senses the bend in the given body and accordingly produces the changes in the resistance. Depending upon the changes in the resistance of the flex sensors, a controller directs the robotic components to orient its position. There are few inbuilt drawbacks in this system of flex sensors like the degree of freedom of movement, i.e., for each degree of freedom a separate flex sensor is needed thus making the system more complex. Also, since flex sensors are expensive, the net cost increases. Deploying flex sensors in robots has another drawback which is its tendency to wear and tear with time and hence making it less reliable.

Overcoming these disadvantages of flex sensor-based robots, there are various algorithms focused on making a robot learn about its surrounding through vision and other parameters and imitation with memory [1–4]. However, meager research has been done in this field of imitation without memory in which the complete control of the body of the robot is done by the user.

The remedy to this is the use of image processing to gather the required information about the orientation of the body being imitated, map the various parts onto different colors sensed through vision using RGB scheme, and direct the controller to mimic the physical body depending upon the changes in the coordinates of the various colors. These signal processing operations are faster and more accurate than the flex sensor, thereby making it more effective [6, 7].

Prototype thus made can find its use in various defense, firefight and exploration, and other such activities. These activities, when undertaken by a human, pose a great threat to one of the most valuable resources.

For human operated robots, the person operating has to have the knowledge of computers and mechanism of operation of such robots [4]. The personnel are trained for undertaking the given job manually implying that the job would be better if done manually instead of using computers. Hence, a robot imitating their actions will come handy.

Our method combines the positives of both the above mentioned situation and hence will be more effective and safer than the present existing methods. The robot allows the user to do his job manually without being present on the scene where the potentially dangerous job is being undertaken. Hence, it eradicates the risk of the loss of human resource coupled with the efficient use of the given resource.

1.1 Robotic Vision

The robot under research uses image processing tools as a vision tool which tells the controller about the orientation of the body being imitated and the changes in it, if any.

For the purpose of demonstration, the body is taken to be a human hand. The fingers are mapped one-on-one with five different colors. Each color is assigned a different 3D coordinate axis. The coordinates of a particular color give us the position and orientation of the given colored finger. The pixels are adjusted in accordance with the size of the colored section of a given finger in order to avoid confusion with other similar colored objects in the near field of view of the camera which is used for taking the images.

1.2 MATLAB Algorithm

- Clear all the preexisting data/variables from the compiler.
- Acquire the information about the inbuilt camera, i.e., the camera which will be used to capture images of the object (object here is human hand).
- Set the properties of the video images, of the object under consideration.
- Start the video input, i.e., trigger the input.
- RGB scheme of filtering is used to make out the color composition of the object and recognize the designed colors.
- Set the interval through which the image is to be taken (here five frames per second).
- Start the video acquisition.
- Set a loop of 200 frames of acquisition, i.e., the commands repeat per 200 frames.
- Snapshot the video image.

- Track the red objects in real time by subtracting the red components from the grayscale image and extract the red components in the image.
- Track green objects in real time by subtracting the green components from the grayscale image and extract the green components in the image.
- Similarly for extracting the blue, brown, and yellow components in the image.
- Use a median filter to filter out noise.
- Median filtering [6, 7] has been analyzed by Guichard and Morel (1995)[8], who showed that in the limiting case, at points with nonzero gradients (regular points), the image evolves according to

$$L_t = \frac{L_y^2 L_{xx} - 2L_x L_y L_{xy} + L_x^2 L_{yy}}{L_x^2 + L_y^2} \quad (1)$$

- Convert the resulting grayscale image into a binary image.
- Remove all the pixels which are less than 300px, so that size of the object to be detected nears the size of detection.
- Label all the connected components in the image. Here, eight connected components are used to describe the image.
- The image blob analysis, i.e., the area of each image is calculated using

$$\begin{aligned} G(x,y) &= f(x,y) - \nabla^2 f \\ &= f(x,y) - [f(x+1, y) + f(x-1, y) + f(x, y+1) - f(x, y-1) - 4f(x,y)] \\ &= 5f(x,y) - f(x+1, y) - f(x-1, y) - f(x, y+1) - f(x, y-1) \end{aligned} \quad (2)$$

- A set of properties for each labeled region, i.e., centroid centered image is also calculated.

$$X_c = \frac{1}{M} \sum_{i=1}^n x_i m_i \quad (3)$$

- A loop to bind the desired colored objects in a rectangular box.

1.3 Robotic Imitation

The position of each finger is given by the coordinates of the associated color. Thus, the change in the coordinates gives the information about the change in the orientation of the hand or fingers in particular. Depending on the variation of the coordinates, the robot changes its orientation thus imitating the hand.

1.4 Pseudo Logic

- Clear all the data present beforehand. Reset the controller to initial stage.
- Orient the real- and robot-arm in same position to begin with.
- Get the coordinates of the arm.
- Check for the changes in coordinates.
- A relationship between the changes in coordinates of the arm and relative position has been studied and plotted.
- Check the direction of change in coordinates.
- If the change is in the negative axis.
- Depending upon the values obtained from the plots shown, the motors are turned on for a given period of time to get the orientation matched.
- If the change is in the positive axis.
- Depending upon the values obtained from the plots shown, the motors are turned on for a given period of time to get the orientation matched.
- For any change in position, the above process is repeated.
- If no changes occur, the position remains unchanged.

2 Simulation Results

The image processing simulations are done using MATLAB. The codes are given (Figs. 1, 2, 3, 4, 5, 6, 7, and 8):

As seen, code which is written as per the algorithm mentioned uses MATLAB vision tools to inform the system about the orientation of the hand and changes if any.

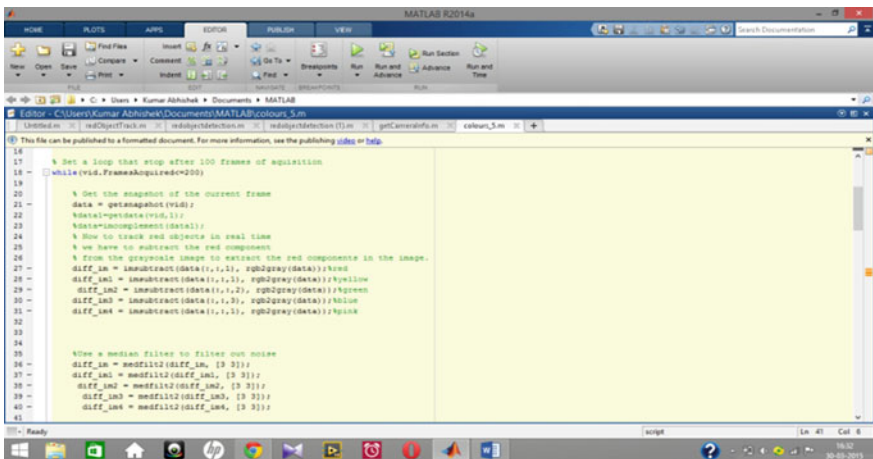


Fig. 1 MATLAB code for color detection

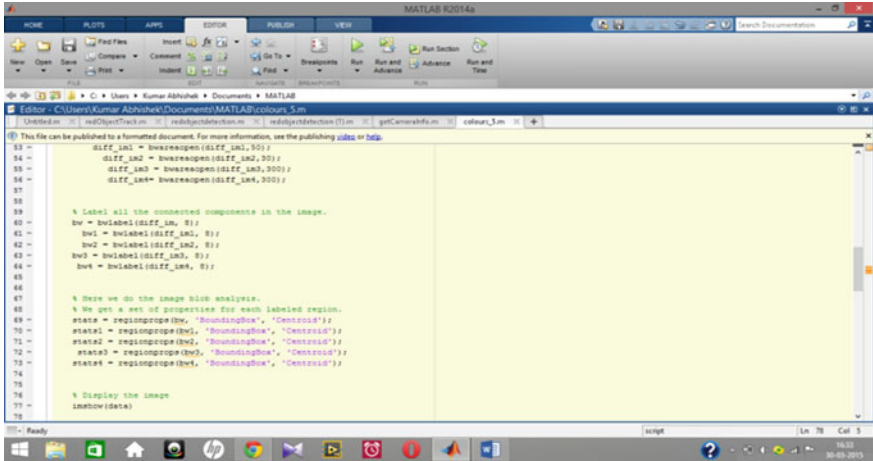


Fig. 2 MATLAB code for image acquisition

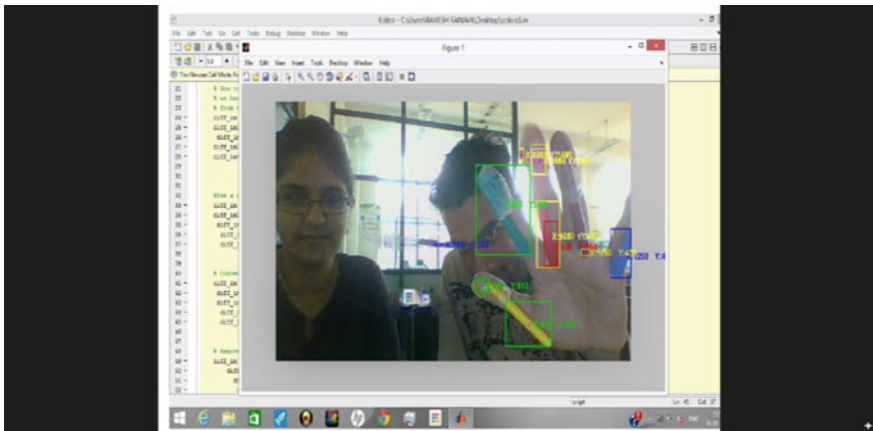


Fig. 3 MATLAB screenshot of image acquisition

And the simulation result thus obtained is as shown

As seen, the different colors associated with different fingers are recognized and their coordinates are labeled. Since the coordinates are obtained, the variation can be observed.

The embedded simulations are done using SIEMENS NX 9.0 software

The design is done as below

U-shaped joints are arranged as shown. Holes are drilled into the U(s) as above.

These parts will be a part of the assembly forming fingers.

Rectangular rods with holes on either ends are placed into the U(s) as above.

Cylindrical rods are inserted as above.

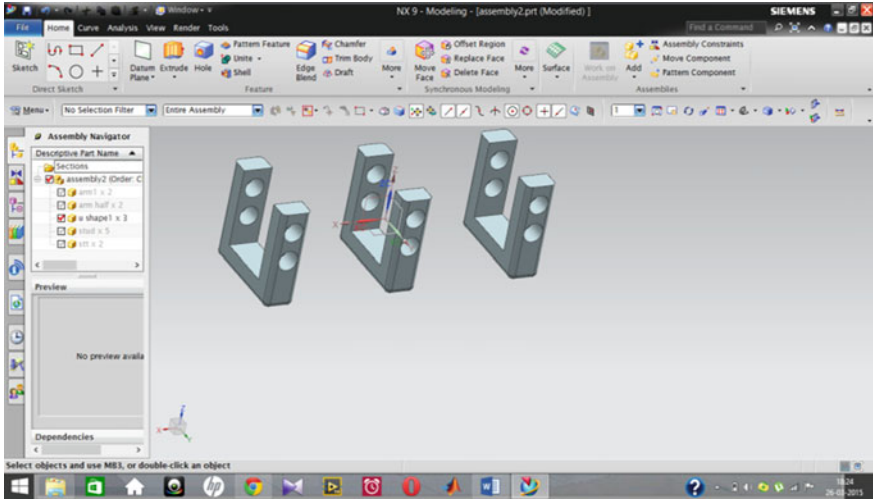


Fig. 4 Screenshot of individual robotic arm

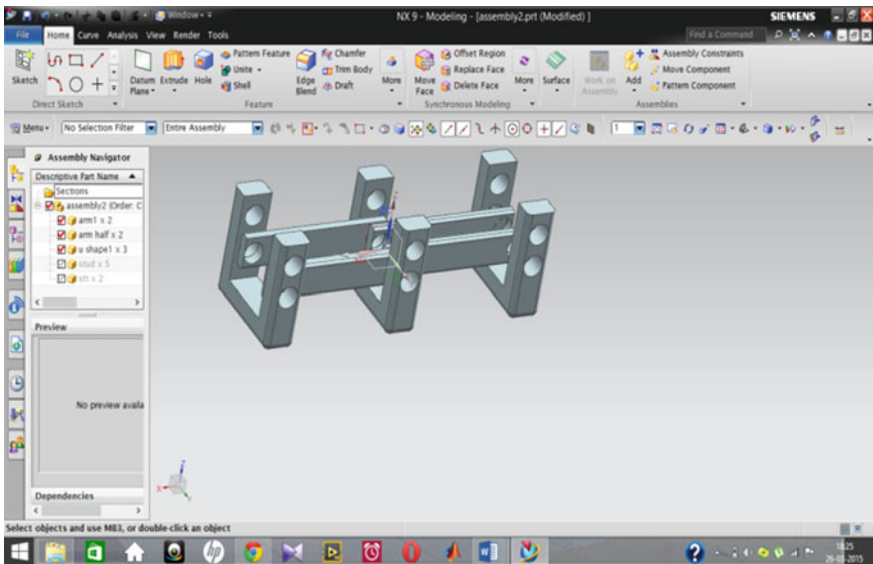


Fig. 5 Screenshot of interconnects

The friction between the rod and holes determine the motion, i.e., if the friction is practically zero, no motion takes place and rods rotate in presence of friction. A rectangular joint is placed as shown which has a cylindrical projection where motor is connected which will initiate rotation and hence desired motion. The designed assembly is now to be tested for proper motion.

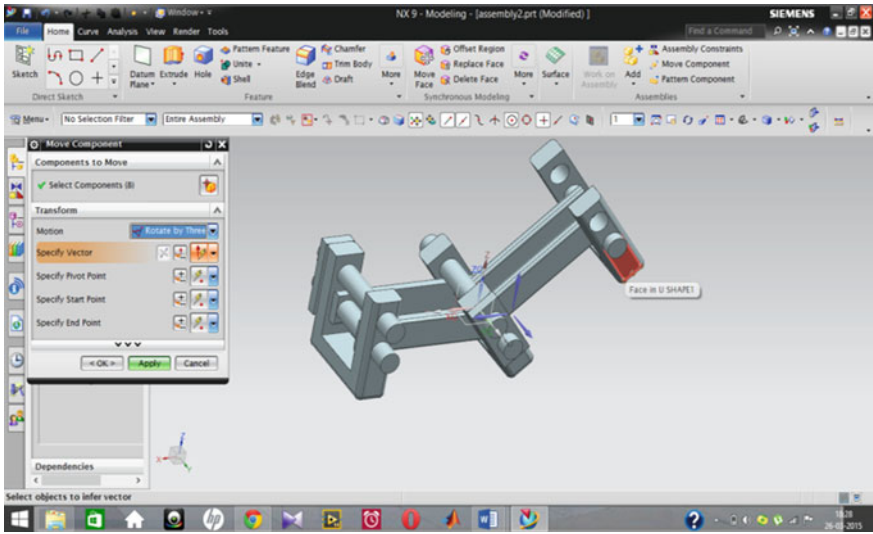


Fig. 6 Screenshot of locking interconnects

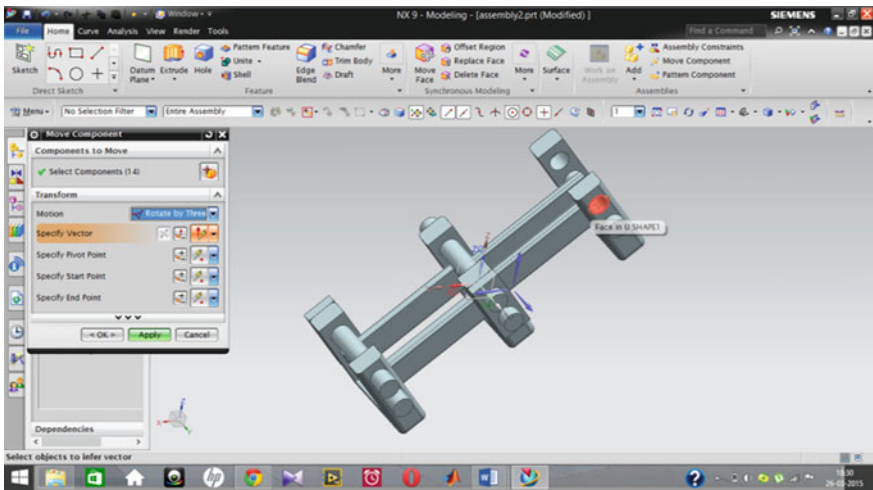


Fig. 7 Screenshot of mimicking movements

The fingers designed move without damaging the construct. Also, the entire assembly moves without any irregularities. The design, hence, overall sustains the desired motion making it a feasible design for prototype implementation.

The finger made has two degrees of freedom. Hence allowing the prototype to carry out the basic activities undertaken by a human hand.

The fingers may be placed on a chassis to resemble a human hand.

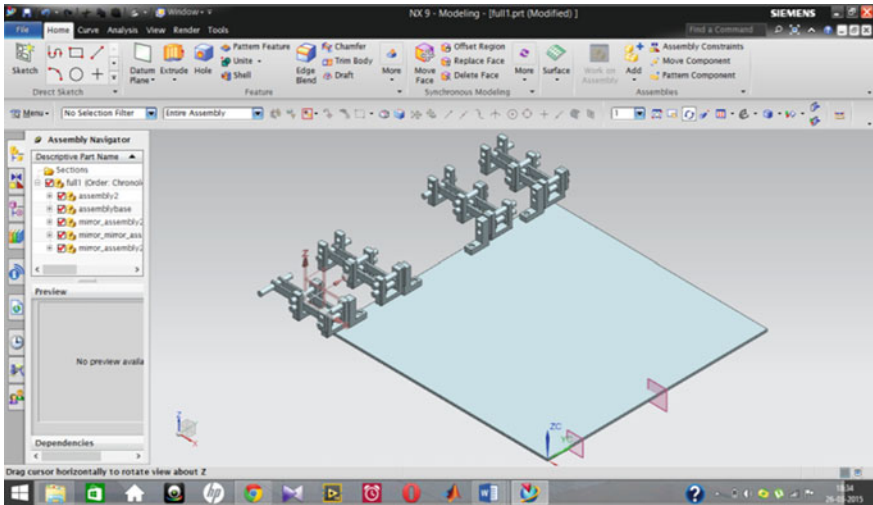


Fig. 8 Screenshot of arrangement and simulation of robotic fingers

2.1 Limitations of the Work

- The threshold value of the color has to be adjusted at times to mitigate the deviations occurring due to light intensities.
- The background, if of a similar color, may alter the results.
- In case of several hands, the result may be altered.
- The module can be used by anyone, hence causing security threat.

2.2 Scope of Future Work/Research

- A prototype is being worked upon.
- A separate and more effective pseudo logic involving correlation and use of two webcams is being developed.
- Feedback using flex sensors to give the user a sensation of the object being held by the arm can be included.
- Involve communication to enable remote control can be included.
- The module can be extended to form a complete humanoid robot rather than just arm.

3 Conclusions

The algorithms have been realized and give apt results. Thus, this theory can be practically implemented.

- The colors used are red, green, blue yellow, and brown.
- RGB is used since it is easy to detect, and yellow and brown are used because they are unaffected by intensity changes and are unlikely to be confused with other colors.
- Several different colors were considered (like black, white, gray, pink, orange, etc.) but were likely to be confused with other colors and threshold of detection varied with intensity.
- Embedded module had to be perfected in terms of friction and application of proper kinematics in absence of which the movable parts might work improperly and lead to improper results. Thus, the parts were simulated and after various different combinations finalized.
- The expected result has been obtained and is being further improvised.

References

1. Boucenna S, Anzalone S, Tilmont E, Cohen D, Chetouani M. Learning of social signatures through imitation game between a robot and a human partner. *IEEE Trans Auton Mental Dev.* 2014;6(3):213–25.
2. Calinon S, Billard A. Stochastic gesture production and recognition model for a humanoid robot. *Intell Rob Syst (IROS 2004). Proc IEEE/RSJ Int Conf.* 2004;3:2769–74.
3. Ijspeert AJ, Nakanishi J, Schaal S. Movement imitation with nonlinear dynamical systems in humanoid robots. *Robotics and automation. Proceedings. ICRA '02. IEEE Int Conf.* 2002;2:1398–1403. doi:[10.1109/ROBOT.2002.1014739](https://doi.org/10.1109/ROBOT.2002.1014739).
4. Berthouze L, Bakker P, Kuniyoshi Y. Learning of oculo-motor control: a prelude to robotic imitation. *Intelligent Robots and Systems '96, IROS 96. Proc IEEE/RSJ Int Conf.* 1996;1:376–81. doi:[10.1109/IROS.1996.570702](https://doi.org/10.1109/IROS.1996.570702).
5. Zhang X, Lee MH. A developmental robot vision system”, systems, man and cybernetics, SMC '06. *IEEE Int Conf.* 2006;3:2024–29.
6. Fitch J, Coyle EJ, Gallagher NC Jr. Median filtering by threshold decomposition. *IEEE Trans Acoust Speech Signal Proc.* 1984;32(6):1183–88. doi:[10.1109/TASSP.1984.1164468](https://doi.org/10.1109/TASSP.1984.1164468).
7. Chan RH, Ho C-W, Nikolova M. Salt-and-pepper noise removal by median-type noise detectors and detail-preserving regularization. *IEEE Trans Image Proc.* 2005;14(10):1479–85. doi:[10.1109/TIP.2005.852196](https://doi.org/10.1109/TIP.2005.852196).
8. Guichard F, Morel JM. “Introduction to partial differential equations in image processing”. *Tutorial Notes, IEEE Int. Conf. Image Proc., Washington.* 1995.

A Data Activity-Based Server-Side Cache Replacement for Mobile Devices

Kottilingam Kottursamy, Gunasekaran Raja and K. Saranya

Abstract Mobile environment allows us to access data anytime, anywhere from a wireless network in which mobile data management plays an important role. Power consumption on mobile side is a major constraint in wireless network. By reducing the access delay, we can optimize the power. Hence, one way to reduce the delay is by increasing the cache hit ratio. In this paper, to increase cache hit ratio, we introduce an AUB cache management scheme includes prefetching and ALFU cache replacement policy at server-side cache. AUB cache management scheme is designed with both access and update information and partition the cache into two zones: Active zone and Safe zone. Based on the access and update information, data is organized in their respective zone. The AUB cache management addresses the shortcomings of power consumption due to access delay and it also minimizes the workload of the main server.

Keywords Mobile data management · Access delay · Cache hit ratio · AUB cache management · Active zone · Safe zone · Power consumption · Server

1 Introduction

Mobile computing is a technology that allows transmission of data, via wireless communication [1], which involves mobile hardware, mobile software, and mobile communication. Mobile data communication has become more important, rapidly

K. Kottursamy (✉) · G. Raja · K. Saranya
Department of Computer Technology, Anna University,
MIT Campus, Chennai, India
e-mail: k.kottilingam@annauniv.edu

G. Raja
e-mail: gunamit@annauniv.edu

K. Saranya
e-mail: sksaranyakrish@gmail.com

evolving technology, and in future it allows constant contact with the internet to share data. This is a solution to the vital problem of many users with mobile devices who exchange information on the move [2]. Because mobile computer is a one that is not limited to one location, it allows access from anywhere (i.e., it allow users to transmit data from remote location to other remote or fixed locations) via internet [1]. In mobile environment, access latency is more when there is a cache miss and this latency gets reduced when there is a consistent cache hit ratio. Mobile computers are spreading faster than any other consumer technology in history and many types of mobile computers have been introduced since the 1990s including the portable computer (discontinued), personal digital assistant/enterprise digital assistant (discontinued), ultra-mobile PC (discontinued), laptop, smartphone, tablet computer, and wearable computer.

Although it has many advantages, it also has some limitations like range, bandwidth, security standards, power consumption, transmission interference, potential health hazards, and human interface with device [3]. To overcome the power consumption limitation on mobile side, cache at server side should be well organized to improve cache hit ratio [4]. It is done using a prefetching technique and ALFU scheme. Caching frequently accessed and infrequently updated data items is preferable [5]. Cache consists of two zones namely active zone and safe zone. Most of the cache algorithms are based on access rate only and it ignores the update information [6]. However, there is a possibility that access information can be made useless by update information. The proposed ALFU scheme considers two factors such as access information and update information. Active zone contains data items that have more access rate and less update rate. Safe zone contains data items that have less access rate and more update rate. Power consumption on mobile device is mainly due to factors like processor, display, and network connectivity. Data caching helps to improve the efficiency of data access [7]. Thus by prefetching, we can minimize the access latency and maximize the cache hit ratio. However, prefetching itself consumes more power and mobile clients are powered by battery, so prefetching a correct data, limited number of data is important [8]. Therefore, by prefetching and maintaining appropriate data which is evaluated with the help of access and update information, the utilization of system resources like power consumption gets reduced. Cache memory has only limited memory space [9]. So cache replacement takes places whenever the prefetching is done.

1.1 Motivation

When designing prefetching schemes, it is important to prefetch right data. For example, see Table 1, when access rate is considered, the priority will be given in the order item1, 2, 4, 5, and 3. However, item1 is updated many times compared to item2, and accordingly we can say that prefetching item2 is correct choice than item1, similarly update rate of item1 > item3 and item1 > item5, etc. When update rate is taken, the priority sequence will be as item3, 2, 5, 1, and 4. But both the

Table 1 Sample table

Item No	1	2	3	4	5
Access rate	5	5	5	5	4
Update rate	3	3	2	2	1
Data size	2	4	4	2	1
Access probability	0.208	0.208	0.208	0.208	0.167
Update probability	0.273	0.273	0.1818	0.1818	0.091
Value (i)	0.380	0.190	0.286	0.572	1.835
Priority	3	5	4	2	1

item2 and item5 have same priority if we do not consider the size of the data item, and item2 as higher priority than item5 if we consider the size of the data item. In general, the retrieval time is more when the size of item increases. So the order of priority will be as item3, 1, 5, 2, and 4. Therefore, we can conclude that considering one factor does not help us to obtain right priority.

After prefetching a valuable data, it is placed in respective zones in the cache. If cache is full, the proposed ALFU is used for replacement policy.

1.2 Contribution

To address these issues in prefetching technique, we consider three factors such as data size, access rate, and update rate. The first part of AUB cache management is to make a prefetching decision of which data item to prefetch by considering all the three factors. In the second part, the data items that must be removed are identified using the probability value calculated with the frequency rate (same as access rate), modification rate (same as update rate). Then, the third part checks the condition to decide when the prefetching should take place.

The remainder of the paper describes the related work about cache management in Sect. 2. Section 3 describes the proposed AUB cache management schemes. Section 4 describes the results of proposed work. Section 5 concludes the paper.

2 Related Work

Mobile database is a database that can be connected to a mobile computing device over a wireless mobile network which is limited by power supply, resources, mobility, restricted bandwidth of wireless networks, and disconnection. Many researches have been done on cache management, prefetching, and cache consistency. Most of the previous studies focus on the prefetching on client side. However, when the memory is issued to the user, this client side data caching will not be effective.

Yue et al. [10] developed the simulator to measure the energy efficiency of cache algorithms by considering the following four factors such as cache hit ratio which

helps to determine the energy saving, the cache populating schemes which is buffer allocation scheme before the cache is full, the cache's capacity to arrange the memory accesses temporally to the same chips, and access pattern in workload which affect the above three factors. They look at the memory efficiency at the servers' end and to attain more energy saving, the energy-aware devices must be carefully utilized on server side of the memory management scheme. The energy efficiencies of the eight different replacement algorithms are evaluated and compared under five real-world parallel workloads. The sequential assignment saves maximum energy than the random assignment.

Jin et al. [11] proposed a buffer management policy known as WIPPA (Write-intensive page preserving algorithm) for performance and stability enrichment in NAND flash memory. It keeps the write-intensive pages in the DRAM buffer, and thus it shrinks the count of write requests to NAND flash. The result was better than FARS and CFLRU.

Kang et al. [12] proposed a buffer management policy called LBM (Low-power buffer management) for various storages in mobile devices. As flash memory is high and has many good features, the flash memory and the mobile disk together are considered as secondary storage, which make huge storage available with evenhanded cost. Various storage devices need a buffer management policy to make it conscious about dissimilar input/output features of blocks, as these storages have distinct characteristics. Due to limited power supply in battery-based mobile device, power consumption rate is considered as a most important factor in designing a policy. LBM considers two parameters in the evaluation of each buffered block, namely recency and frequency. LBM is based on input/output operation type, reference potential of blocks, and dissimilar energy-consumption rate of storage devices. This policy minimizes power consumption and maximizes the input/output performance. When volatile RAM is not used as buffer cache, the consistency of file system is guaranteed.

Gomaa et al. [13] proposed the analysis model to estimate an instantaneous cache hit ratio. They consider two replacement policies such as LRU and FIFO and they proposed replacement policy known as FB-FIFO (Frequency-based-FIFO) which increases the instantaneous hit ratio within a short period of time. These three cache replacement performances are compared using the IRM to perfect LRU. They found that for the count of web objects and the popularity of object which are set for short time span, the hit ratio reaches steady state within a period which depends on object request rate, expiry rate, and cache capacity. The result states that proposed policy performs well than that of LRU and FIFO for small cache capacity and may mislead as the web server generates latest popular objects from time to time, so calculating the instantaneous hit ratio provides an appropriate hits for users.

Yin et al. [8] proposed a power-aware prefetch technique known as AVP (adaptive value-based prefetch) in cache management schemes considering power factor of the clients and other factors like size, access rate, and update rate of data items. First, VP system recognizes important data items for prefetching which must have more access probability, a less update rate, and tiny data size followed by

AVP system that determines the number of data items to be prefetched and depends on how much power has been left.

3 AUB Cache Management

Cache is divided into two zones, active and safe zone, each having an initial size of 'm.' It could be further extended by a size of 'n' on either side. Depending upon the value of each item, the item could be moved from active to safe zone and vice versa during replacement. The item in the safe zone gets deleted first, when the cache is full.

Figure 1 shows the workflow diagram of proposed cache replacement policy. The ALFU approach is a sign of both LFU algorithm and more update rate of each record. The least frequently used algorithm rejects item that has not been accessed repeatedly. As a consequence, LFU keeps the item that has high-frequency rate by removing less frequently used items. When more update rate is taken into account, it holds item with fewer changes in cache and eliminates items that get modified frequently. Thus, the LFU and Update rate together are called as ALFU. Figure 2

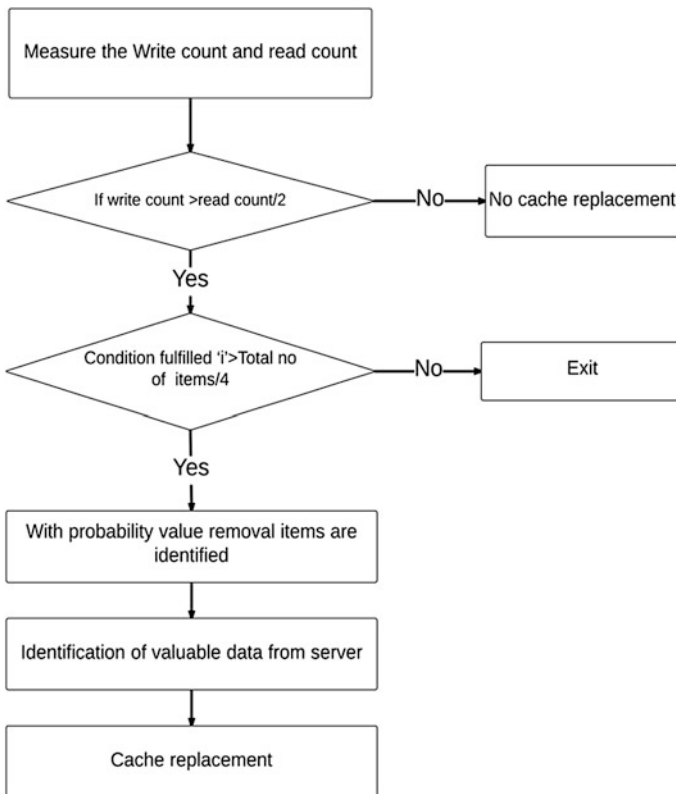


Fig. 1 Proposed ALFU cache management workflow diagram

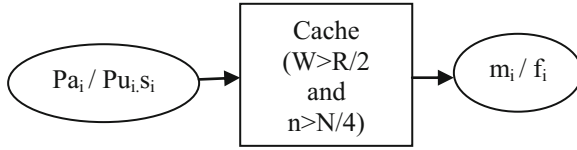


Fig. 2 AUB cache management mechanism

shows the cache management mechanism. Algorithm 1 describes the proposed ALFU policy.

The proposed method is classified into three parts. In first part, evaluation of what data has to be prefetched from server is finalized. In the second part, the data must be removed from the cache to place the prefetched data which is analyzed using ALFU scheme. The third part decides whether prefetched has to be carried out or not.

3.1 Analysis of Data to Prefetch from Server

In this subsection, value of each item is calculated to identify the ideal data item when making a prefetch decision. The data access rate (a_i), the data update rate (u_i), and the size of the data (s_i) are the factors considered for prefetching. The ideal data must have more access rate, less update rate, and a small data size. The following notations are used for calculation.

- Pa_i access probability of an item ‘ i ’;
- Pu_i update probability of an item ‘ i ’; and
- s_i size of an item ‘ i ’.

Access probability for a item ‘ i ’ is calculated by the following probability equation:

$$P\alpha_i = \frac{\alpha_i}{\alpha_1 + \alpha_2 + \alpha_3 + \dots + \alpha_k} \tag{1}$$

where i value varies from 1 to k .

Updated probability for a item ‘ i ’ is calculated by the following probability equation:

$$Pu_i = \frac{u_i}{u_1 + u_2 + u_3 + \dots + u_k} \tag{2}$$

where i value varies from 1 to k .

With these calculated probability values, the value of each item is estimated as follows:

$$\text{value}(i) = \frac{Pa_i}{Pu_i s_i} \quad (3)$$

Let a_i , u_i , represent the effective access ratio and update ratio of the item 'i.' The item which has higher value is forced to be prefetched from server. According to our assumption, access probability is indirectly proportional to update probability $Pa_i \propto 1/Pu_i$, access probability is indirectly proportional to data size $Pa_i \propto 1/s_i$, and update probability is directly proportional to data size $Pu_i \propto s_i$. The best data is known by computing $Pa_i/Pu_i \cdot s_i$. As the result, cache hit ratio is increased as the effect of prefetching a valuable data.

3.2 Analysis of Data to Remove from Cache Using ALFU Algorithm

In this subsection, the number of times each item has been accessed and the number of times each item get modified is measured. With the measured value, probability of modified rate (M) against the frequency rate (F) is calculated. In other words, amount of items going to be prefetched or amount of items to be removed is identified. The amount of items to be prefetched is directly proportional to the amount of items to be removed. The number of items to be removed is based on calculated probability:

$$P_i = \frac{m_i}{f_i} \quad (4)$$

Three cases can exist for P_i :

- (1) $0 \leq P_i < 0.5$, indicates that update rate is less than 0.5;
- (2) $P_i = 0.5$, indicates that update rate is equal to 0.5; and
- (3) $0.5 < P_i \leq 1$, indicates that update rate is greater than 0.5.

Read operation (R) and write operation (W) are collectively known as frequency rate. Write operation is alone known as update rate. The first case shows that the number of write operation is less than the number of read operation and implies that the update rate is minimum. The second case shows that number of write operation is equal to number of read operation, and implies that the updated rate is at average level. The third case shows that number of write operation is greater than the number of read operation, and implies that the update rate is maximum. The item that satisfies the third condition is removed from the safe zone of cache. Based on the amount of data removed, the equal amount of data is prefetched from the server.

Algorithm. 1. ALFU Cache Replacement

1. Select read or write operation
2. Switch (operation)
3. Case1: read
4. {Select command will be executed;
5. In cache:
 - a. $f_i = f_i + 1$, $rc_i = rc_i + 1$;
 - b. $P_i = m_i f_i$;
6. In server:
 - a. $f_i = f_i + 1$, $rc_i = rc_i + 1$;
 - b. Compute Pa_i ;
 - c. Compute Value (i);
7. }
8. Case2: write
9. {Execute the update command;
10. In cache:
 - a. $f_i = f_i + 1$, $wc_i = wc_i + 1$, $m_i = m_i + 1$;
 - b. $P_i = m_i f_i$;
 - i. Check if $(wc_i > rc_i/2)$; //first condition
 - c. {Set condition1 = TRUE;
 - d. Check if $(Truecount > 1(Falsecount)/4)$; //second condition
 - i. {Delcount = count(condition='TRUE');
 - ii. Delete items where condition1 = TRUE;
 - iii. Prefetched (delcount items) from server database;}
 - e. }
 - f. Else {Set condition1 = FALSE;}
11. In server:
 - a. $f_i = f_i + 1$, $m_i = m_i + 1$;
 - b. Compute the Pa_i and Pu_i ;
 - c. $s_i = l_1 + l_2 + l_3 + \dots + l_n$; where n = number of columns
 - d. Compute the value (i);
12. }

3.3 Analysis of Time to Prefetched Ideal Data

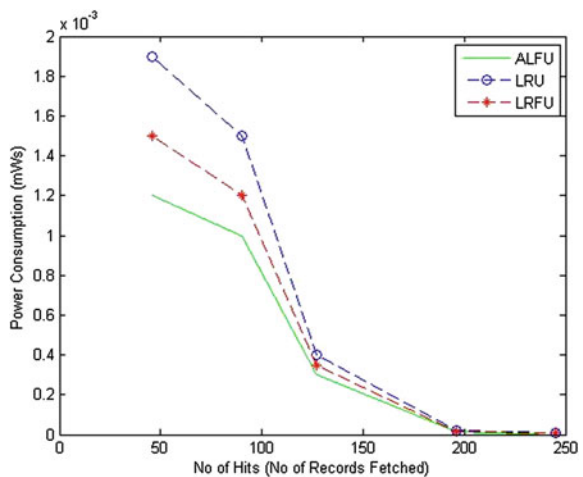
In this subsection, whether the cache replacement needs to be carried out is calculated. Once replacement requirement condition is reached, the above two subsections are executed. There are two conditions to check for items in the active zone whether replacement time is reached or not. The first condition is that write operation should be greater than half of read operation ($W > R/2$). The second condition is that number of items ‘ n ’ in safe zone should be greater than the quarter of total count of data in the cache ($n > N/4$), where n denotes the count of data satisfying the first condition, and N denotes the total count of data present in cache.

Data item with high u_i and low a_i placed in safe zone and high a_i and low u_i placed in active zone. After the replacement, the new data item is placed in the respective state (each having an initial size of ‘ m ’ and can extend till ‘ $m + n$ ’) based on the its value function during which the window size increased either upward or downward which will extend the space in active or safe zone, respectively.

4 Results and Discussion

The proposed algorithm is executed in Net beans IDE 8.0 and in oracle 11 g for computer simulation. The proposed algorithm is experimented with various read and write operations. The result shows that proposed scheme reduces query latency thereby the power consumption at client side is also reduced. When the read operation is twice the write operation and the total amount of data in the cache is four times than that of the data satisfying the read–write operation relation, the replacement take places using ALFU scheme. Thus, the performance is improved

Fig. 3 Comparison between cache replacement policies



by making the replacement to take place within a small interval of time which helps to have only valuable items in cache.

Figure 3 explains the outcome of the number of cache hits on power consumption of LRU, LRFU, and ALFU scheme. Fetching data item from the server takes more time than fetching from the cache, and indicates more access latency when we access the item from server. But when the delay increases, the power consumption also gets increases. Using ALFU, when the number of items fetched from the cache increases, the number of cache hit increases compared to LRU and LRFU; once the number of cache hit increases, the power consumption of mobile devices gets decreases. Hence, the overall performance is improved.

5 Conclusion and Future Work

We presented a new server-side AUB cache management scheme which includes ALFU and prefetching the data item from the server that aims at reducing power consumption for mobile device. Prefetching is one of the effective methods to reduce the power consumption via reducing the query latency. However, it is vital to recognize the correct data before prefetch. The several factors like the update rate, the size of data, and the access rate are taken into account to evaluate data for prefetching.

By considering both access and update information, power consumption due to access delay is reduced by increasing the cache hit ratio, as the result of prefetching an ideal data item and an appropriate server-side data activity management (i.e., by maintaining only a valuable data and eliminating remaining data) using ALFU algorithm and it also minimizes the workload of main server. The result shows that the proposed AUB cache management improves the performance of the system by reducing the server load in terms of the requested item and reduces the power consumption on client side.

In future, we can still reduce the power consumption on client side by enhancing the ALFU policy.

Acknowledgements Gunasekaran Raja, Kottilingam Kottursamy, Saranya K gratefully acknowledges support from NGN Labs, Department of Computer Technology, Anna University, Chennai.

References

1. Peng W-C, Chen M-S. Query processing in a mobile computing environment: exploiting the features of asymmetry. *IEEE Trans Knowl Data Eng.* 2005;17:7.
2. Lin C-Y, Wang S-C, Kuo S-Y, Chen I-Y. A low overhead checkpointing protocol for mobile computing systems. In: *IEEE symposium on dependable computing*, 2002.

3. Xu J, Hu Q, Lee W-C, Lee DL. Performance evaluation of an optimal cache replacement policy for wireless data dissemination. *IEEE Trans Knowl Data Eng.* 2004;16:1.
4. Wei Q, Zeng L, Chen J, Chen C. A popularity-aware buffer management to improve buffer hit ratio and write sequentiality for solid-state drive. *IEEE Trans Magn.* 2013;49:6.
5. Chen H, Xiao Y. On-bound selection cache replacement policy for wireless data access. *IEEE Trans Comput.* 2007;56:12.
6. Chen H, Xiao Y, (Sherman) Shen X. Update-based cache access and replacement in wireless data access. *IEEE Trans Mobile Comput.* 2006;5:12.
7. Tang B, Gupta H, Das SR. Benefit-based data caching in ad hoc networks. *IEEE Trans Mobile Comput* 2008;7:3.
8. Yin L, Cao G. Adaptive power-aware prefetch in wireless networks. *IEEE Trans Wirel Commun.* 2004;3:5.
9. Desai SR, Chavan H, Chitre DK. Location based services cache replacement policy for mobile environment. In: *IEEE conference 2013.*
10. Yue J, Zhu Y, Cai Z. An energy-oriented evaluation of buffer cache algorithms using parallel I/O workloads. *IEEE Trans Parallel Distrib Syst.* 2008;19:11.
11. Jin X, Jung S, Song YH. Write-aware buffer management policy for performance and durability enhancement in nand flash memory. *IEEE Trans Consum Electron* 2010;56:4.
12. Kang H, Seok J, Bahn H. A low-power buffer management policy for heterogeneous storage in mobile consumer devices. *IEEE Trans Consum Electron.* 2010;56:4.
13. Gomaa H, Messier GG, Williamson C, Davies R. Estimating instantaneous cache hit ratio using Markov Chain analysis. *IEEE/ACM Trans Netw* 2013;21:5.

Privilege-Based Scoring System Against Cross-Site Scripting Using Machine Learning

N. Shyam Sunder and T. Gireeshkumar

Abstract The attacks on the users by exploiting the vulnerabilities of the browsers have increased at an alarming rate. The existing attack prevention strategies have failed miserably in most of the situations. Moreover, users have also not taken much care of configuring their browsers securely, using available extensions and plug-ins. This proposal puts forward an advanced XSS prevention technique by introducing a new scoring system for privilege levels and vulnerability levels of the contents rendered in the browser. The java scripts rendered in the browsers are stored, classified, and analyzed using machine learning algorithms. Machine learning can also be used to predict the browser quirks and generate an attacker pattern. The security mechanisms are also implemented inside the Document Object Model (DOM) to check the execution of dynamic scripts.

Keywords Cross-site scripting · Machine learning · Document object model

1 Introduction

The cross-site scripting has emerged as the main crisis in web technology. It can affect both the client and server sides [3]. They are very much harmful to the client-side browsers. Cross-site scripting (XSS) spoils the integrity of the communication between the client and server. In the last few years, we have seen the legal websites of many famous and reputed institutions being hacked by the attackers. The attackers are stealing away the user cookies and session IDs [2]. The attackers are even hacking the plug-ins and extensions. Inability to identify and

N.S. Sunder (✉) · T. Gireeshkumar
TIFAC CORE in Cyber Security, Amrita Vishwa Vidyapeetham,
Coimbatore, India
e-mail: nshyam2911@gmail.com

T. Gireeshkumar
e-mail: gireeshkumart@gmail.com

filter the malicious javascripts is the major concern. The cross-site scripting attacks are increasing on a large scale. The vulnerability of the current browsers is a major concern [10]. The attackers are exploiting the drawbacks and shortcomings of the existing systems. The advancing web technology is also helping them to create new forms of attacks [11]. The current web browsers do not have an efficient method to identify the malicious scripts. The mismatch between the content sniffing algorithm of the browser and server is the major cause of the stored XSS attacks.

The inefficient filtering mechanism is responsible for reflected XSS attacks. The lack of security and authentication mechanisms in the browsers is the cause for DOM-based XSS attacks [15]. The attackers embed and hidden malicious javascripts into the documents. The scripts are executed once they are rendered by the browsers [13]. There is lack of prevention strategies at both the client and server sides. Cross-site scripting is the main cause for session hijacking and phishing attacks [6]. Once the attacker gains access to the browser, they may steal the session ID, cookies, local storage, passwords, etc., and later uses it for impersonating the user. The three major XSS attacks are the stored (nonpersistent) XSS, reflected (persistent XSS), and DOM (local)-based XSS [12]. The attacker can generate scripts which take the client-server communication to a non-SSL channel and can suppress the warning messages. Poisoning of cookies and injection attacks are increasing [5]. Recursive link analysis is performed during the rendering of the web page by the browser. Cross-site scripts are very difficult to find out and must be handled carefully [14].

The rest of the paper is as follows: Sect. 2 describes about the related works. Section 3 features the system design which is efficient than the existing system described in related works. Section 4 represents the results and discussion. Section 5 concludes the brief content of the paper.

2 Related Works

The cross-site scripting vulnerability has been a major threat to the browsers and web technologies for the last few years. Many prevention strategies have been applied to both the client and server sides [9]. But, with the advancement of technology, attackers have found new ways to apply the cross-site scripting. As described by Barth, Caballero, and Song in 2009 [1], the attacker modifies the files in such a way that the upload filter of the websites cannot find the vulnerabilities in it. The attacker wraps the scripts in such a way that it cannot be identified by the filters easily. The major examples of such documents are the chameleon and the bloodhound documents. The websites stores the malicious data in its server. The user enters the corresponding website and clicks the malicious documents. The server sends the file along with its MIME type and extensions identified by it. The browser's content sniffing algorithm scans the documents for vulnerability. The browser itself identifies the MIME (Multi-Purpose Internet Mail Extensions) type and extensions of the file and compares with the data sent by the browser. The major problem is the lack of mutual understanding between the server and the browser. There is no collaboration

between the content sniffing algorithms of the client and browser. The document makes the browser to believe it as a HTML document, when actually it is not. Hence, this non-HTML malicious document enjoys all the privilege levels of the HTML documents. The HTML documents have the highest privilege level in the browser.

As suggested by Ellman and Liang [7] in 2012, the byte level taint tracking approach is to detect XSS attacks. DOM-based XSS is caused mainly due to the unsafe handling of scripts and insecure flow of data within the browser. The client-side security of the browser is much difficult compared to the server-side security. The main areas in the DOM which are prone to these attacks are `location.href`, `document.write`, `document.referrer`, `windows.name`, etc. [4]. Security of communication between the source and sink must be maintained. The outgoing data from the source and the incoming data to the sink must be validated [8]. The attacker either controls part of the URL or the entire URL or causes HTTP parameter pollution.

3 Proposed System

3.1 *Secure Communication Between Browser and Server*

Contents of the webpage are passed to the user's XSS filter program. The program analyzes the documentation. It looks for a downloadable file that a webpage brings together with it. It checks for MIME type and extensions. It blocks the file if there is any mismatch between the MIME type and extensions. The program makes sure that an unknown file will not be validated as a HTML file by the browser. This prevents malicious scripts from violating the access control and privilege levels at the browsers' inner components. Content checking is performed to prevent vulnerable components from execution. The XSS filter program blocks the webpage if it encounters a stored XSS attack. It checks the white list to ensure the authenticity of the website. If a stored XSS is reported, the website is marked as blacklist. At the next stage, the webpage is passed to the string matching algorithm. Here, the request and response are compared with the matched strings. The request is monitored to check whether it is rerouted to an external domain. The domain checker inspects the DNS to ensure the same origin policy. It demands proper authentication for the cross-domain interaction. Domain checker blocks the request when it tries to connect to an external domain. The suspicious matching parts of the response when compared with the request are removed from the URL. This mechanism guarantees the prevention of the reflected XSS attacks to some extent. Figure 1 shows the architecture model of the system.

The third phase includes the static analysis part of the web page. The code is reviewed prior to the execution and the embedded javascripts are validated. Script identifier is a program which compares the javascripts of the webpage with its blacklisted strings. The program performs a grouping technique with the set of suspicious characters and symbols to verify whether a malicious script is being

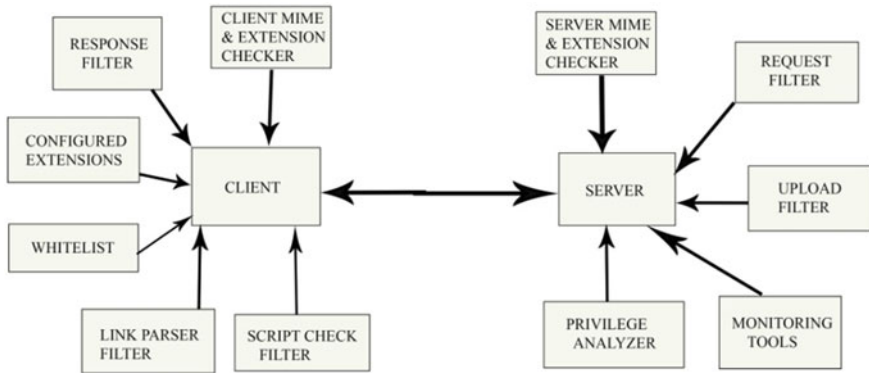


Fig. 1 Architectural model

generated. Link analysis collects all the static links, hyper links, and embedded links. It traverses through all the links to ensure authenticity. Recursive page analysis is performed to check the rerouting of connection and external domain interaction. This is a good way to prevent the DOM-based XSS. The manual network rules make sure that each and every connection is a SSL-oriented connection. Non-SSL channel blocker is integrated with the rules so that an alert is made when a nonsecure connection is being initiated. Rules can be configured to white list the sites and authenticate the server.

3.2 Machine Learning Inside the Browser Components

Figure 2 shows the machine learning algorithms applied to the browser for its internal working. The related browser information and the corresponding versions of the HTML and CSS are fed to the AdaBoost algorithm. Using these information, the AdaBoost algorithm predicts the rendering mode that should be taken by the browser. The unpredictability in the browsers’ rendering behavior and execution is exploited by many attackers. The appropriate mode is selected by the browser in rendering the document. Natural language processing is used by many browsers for parsing the HTML and CSS documents.

The contents are divided into tokens. The tokens are matched against these rule sets that are predefined in the browser. The matching tokens are added as the nodes in the DOM tree. Random forest algorithm can be used to predict the DOM tree structure. It constructs a bunch of various tree structures for making accurate decisions. The DOM tree constructed by the parser is compared with the tree set generated by the random forests. The CSS parser concentrates on the display styles and decides how the document must be presented in the web browser. The contents of the web page being rendered are divided into the HTML and CSS parts. The HTML part decides what all contents are to be displayed in the web page.

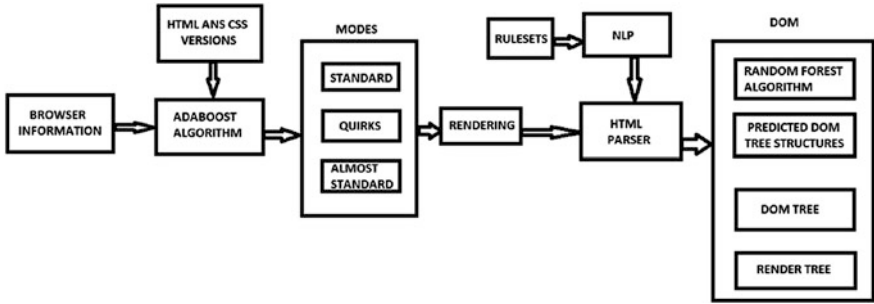


Fig. 2 Machine learning added to the browser architecture

The CSS part manages the images and selects specific places on the web page to display the contents. Context-free grammar is used to create the rule set for processing javascripts. The DOM tree is converted to render tree for the final phase of presentation. The rendering depends on the layout engines used by various browsers.

4 Results and Discussion

Major prevention strategies were taken to prevent the cross-site scripting attacks. Detailed studies were done based on the past experience and history of cross-site scripting. The attacking pattern of the XSS attacks was monitored and a detailed plan against them was made. The existing systems were studied for more information. The drawbacks on the existing systems were approached using the machine learning algorithms. Many modifications were experimented on the existing systems. Some gave positive results, whereas some yielded negative ones. It was observed from the experiments that security measures must be made on both the client as well as on the server sides. Sometimes, the weakness in the server side compromised the clients and vice versa was also observed. The fact is that there is neither mutual understanding nor collaboration between the client and the server. Hence, a thought was developed to create a system that communicates well between the server and client. Figure 3 demonstrates the performance statistics of the AdaBoost and random forest algorithms in various browsers.

Demo server was created using the NetBeans. The server used by the NetBeans was the Glassfish server. Since, both the client and server are on the same machine, we will get a good picture of the entire communication between the client and server. Filters were configured and kept for the security of the servers. One of the filters verified the malicious contents and MIME type of the uploaded contents. Second filter checked the scripts in the requests coming from the client's browser. The server ensures that a script-free response is passed to the clients. The client side is safeguarded by the securely configured extensions and tools. Some filters are

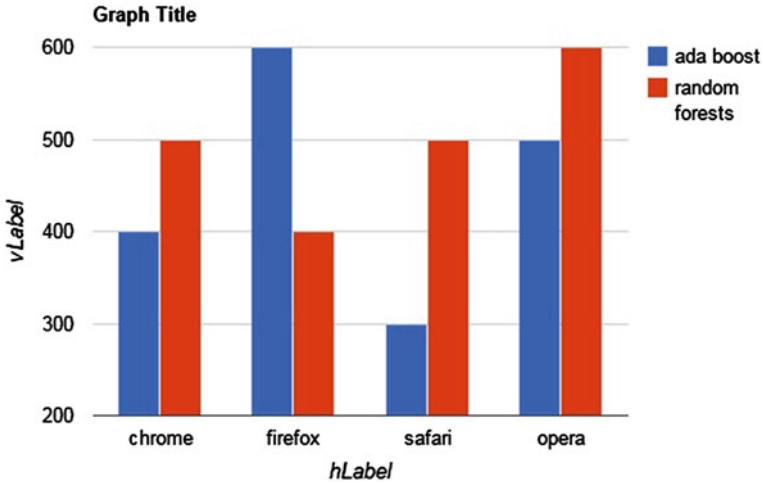


Fig. 3 Performance of AdaBoost and random forest on various browsers

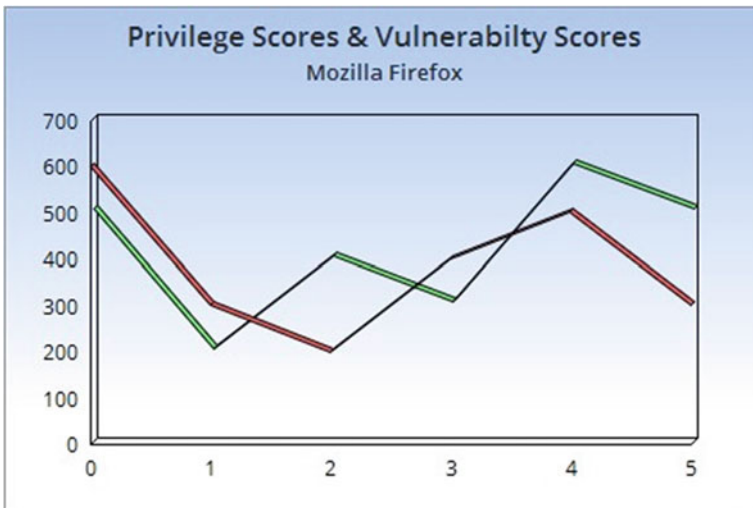


Fig. 4 Analysis of scoring systems for Mozilla Firefox

configured in the client side for security purposes. The privilege score made by both server and client helps in preventing XSS attacks and creates a better understanding between the client and server. The common vulnerability severity score is also calculated on the server-side. If the CVSS score assigned by the server exceeds the threshold value at the client, the file is marked as vulnerable and is rejected by the browser. Figure 4 shows the analysis of the privilege-based and vulnerability-based scoring systems in Mozilla Firefox.

5 Conclusion

Cross-site scripting attack is one of the topmost attacks listed in the OWASP top 10 vulnerabilities. The XSS attacks are increasing at an alarming rate in the current network. With the emergence of new web technologies, the attackers are finding out new ways and forms of XSS attacks. The attackers had understood the existing systems and their drawbacks. New prevention strategies must be developed from the attacking pattern. The proposed framework can identify all forms of XSS attacks and is capable of protecting all browsers from the attacks. Our system prevents all forms of XSS attacks like stored, protected, and DOM-based attacks. The two new scoring systems proposed in this framework will provide a new insight to the developers and security analysts.

References

1. Barth A, Jackson C, Mitchell JC. Securing frame communication in browsers. *Commun ACM*. 2009;52(6):83–91.
2. Chen, EY, Bau J, Reis C, Barth A, Jackson C. App isolation: get the security of multiple browsers with just one.” In *Proceedings of the 18th ACM conference on computer and communications security*, ACM; 2011. p. 227–238.
3. Clark J, van Oorschot PC. SoK: SSL and HTTPS: revisiting past challenges and evaluating certificate trust model enhancements. In: *IEEE symposium on security and privacy (SP)*, 2013, IEEE; 2013. p. 511–25.
4. Czeskis A, Moshchuk A, Kohno T, Wang HJ. Lightweight server support for browser-based csrf protection. In: *Proceedings of the 22nd international conference on world wide web conferences steering committee*; 2013. p. 273–284.
5. Garcia-Alfaro J, Navarro-Arribas G. Prevention of crosssite scripting attacks on current web applications. In: *On the move to meaningful internet systems 2007: CoopIS, DOA, ODBASE, GADA, and IS*. Berlin Heidelberg: Springer; 2007. p. 1770–1784
6. Jang D, Tatlock Z, Lerner S. Establishing browser security guarantees through formal shim verification. In: *Proceedings of the 21st USENIX conference on security symposium*, p. 8–8. USENIX Association; 2012.
7. Kimak, S, Ellman J, Laing C. An investigation into possible attacks on HTML5 indexed DB and their prevention. In: *13th annual post-graduate symposium on the convergence of telecommunications, networking and broadcasting (PGNet 2012)*, Liverpool, UK; 2012.
8. Luo T, Du W, Soundararaj KD. Capability-based access control for web browsers; 2011.
9. Murdoch SJ. Hardened stateless session cookies. In: *Security protocols XVI*. Berlin Heidelberg: Springer; 2011. p. 93–101
10. Nikiforakis N, et al. Cookieless monster: Exploring the ecosystem of webbased device fingerprinting. In: *IEEE symposium on security and privacy (SP)*, 2013. IEEE; 2013.
11. Pelizzi R, Sekar R. Protection, usability and improvements in reflected XSS filters. In: *ASIACCS*; 2012. p. 5.
12. Sun, F, Xu L, Su Z. Client-side detection of XSS worms by monitoring payload propagation. In: *Computer Security ESORICS 2009*. Berlin Heidelberg: Springer; 2009. p. 539–54.
13. Unger T, Mulazzani M, Fruhwirt D, Huber M, Schrittwieser S, Weippl E. SHPF: enhancing HTTP (S) session security with browser fingerprinting. In: *Eighth international conference on availability, reliability and security (ARES)*, 2013, IEEE; 2013. p. 255–61.

14. Weinberger J, Saxena P, Akhawe D, Finifter M, Shin R, Song D. A systematic analysis of xss sanitization in web application frameworks. In: Computer security ESORICS 2011, Berlin Heidelberg: Springer; 2011. p. 150–171
15. Zeller W, Felten EW. Cross-site request forgeries: exploitation and prevention. *The New York Times*;2008:1–13.

Content-Based Cricket Video Shot Classification Using Bag-of-Visual-Features

M. Ravinder and T. Venugopal

Abstract In this paper, we propose a novel method for content-based cricket video shot classification using bag-of-visual-features. Bag-of-visual-features methodology has attained huge popularity among the computer vision community. The standard steps followed in bag-of-visual-features method are unordered collection of set of local features from training images and clustering them to form a visual vocabulary which is useful for training and classification. Bag-of-visual-features technique is the best choice for content-based indexing and classification due to its simplicity and accuracy. Cricket is having huge popularity throughout the world. Cricket video consists of different types of shots (a shot can be considered as continuous sequence of frames recorded between the start and stop of a single camera. For example, different video shots present in a cricket video are close-up view shots, distance view shots, and pitch view shots. Our proposed method is based on bag-of-visual-features for classification of cricket video shots by using top 100 SIFT (Scale-Invariant Feature Transform) features selected from each frame of the training and testing video shots. We have used the dataset of cricket, made available online (Video dataset, <http://cse.iitk.ac.in/~vision/dipen/>) by Mr. Dipen Raghuvani, to evaluate our proposed framework. By using our proposed framework, we are able to achieve reasonable results compared to already existing methods.

Keywords Content • Video • SIFT • Bag-of-visual-features • Shot • Classification • Close-up view • Pitch view • Distance view

M. Ravinder (✉)
JNTUK, Kakinada, AP, India
e-mail: ravinder.rsh@gmail.com

T. Venugopal
CSE, JNTUHCEJ, Nachupally, Karimnagar, Telangana, India
e-mail: t_vgopal@rediffmail.com

1 Introduction

The fast improvements in data storing technologies have witnessed huge increase in the volumes of video data during the last ten years [1]. Video is a medium of entertainment for different broadcasting TV channels of sports, news, and others. Following the soccer game, cricket is the second popular fan-following sport throughout the world. In India, cricket has occupied the first position with huge number of fans following it. Cricket is a game played in three different popular formats and they are test, one-day, and T-20. Cricket is a game played between two teams of eleven players in each team [2]. A number of TV channels broadcasting cricket videos are facing the problem of facilitating a user to retrieve interesting parts in a video from the huge volumes of video data available with them. Indexing the big volumes of video data manually is a trivial task [1]. There is an increasing demand for efficient video indexing and retrieval frameworks.

Analysis of sports videos is an interesting field of research which has attracted the research community. The usual steps followed in analyzing a video are partitioning a video into scenes, shots, and frames and then indexing the video with the content present in them. Shot is a sequence of recorded frames between a continuous action of start and stop of a camera. Usually, a shot consists of frames with similar content [3].

Bag-of-visual-features is a method extensively used for image and video classification. Bag-of-visual-features is inspired by the popular method of bag-of-words, which is extensively used in text document analysis and text information retrieval.

Content-Based Image Retrieval (CBIR), proposed way back in the 1990s is a method of indexing an image using the color, shape, and text features and retrieving the related images accordingly. Semantic gap can be considered as the difference between the users' high-level queries and the low-level indexes assigned to the content of the image. Bag-of-visual-features, proposed by Sivic and Zisserman, is a popular option for content-based image classification. Bag-of-visual-features have shown reasonable performance in image classification tasks [4].

The main contributions of the paper are

1. Video shot classification based on bag-of-visual-features using top 100 SIFT features extracted from each frame.
2. A new algorithm based on result of frames classification to classify a video shot is proposed.

The rest of the sections of the paper are as follows: Sect. 2 introduces the concept and standard steps followed in bag-of-visual-features methodology. Section 3 discusses the proposed method, Sect. 4 demonstrates the experiments and results, and Sect. 5 concludes the paper.

2 Bag-of-Visual-Features

Bag-of-features methodology is based on an order-less collection and quantization of local descriptors of images. Bag-of-features technique has huge demand for applications like video classification, image classification, and retrieval.

Bag-of-visual-features or bag-of-visual-words is a simple and efficient framework with good performance compared to other frameworks for image classification. The term bag refers to the unordered collection of local features of an image [5].

The main steps involved in bag-of-visual-feature extraction method are

- Step 1 Locating the regions or points of interest.
- Step 2 Calculating the local features for the regions extracted in step 1.
- Step 3 Quantifying the huge amount of features extracted in step 2 into clusters of visual words which will act as the codebook of visual vocabulary.
- Step 4 Classifying a new image by calculating the occurrence histogram for local features extracted from the image by using the visual vocabulary extracted in step 3.

As discussed above, bag-of-visual-features consist of a sequence of operations in which the first step is selecting a reasonable number of training sets of images of different class types. The next step is to extract a set of local features from half of the images present in training set, after that the clustering of collected features into a set visual vocabulary, followed by training the remaining half of the images present in training set. The final step is to classify a new image by calculating occurrence histogram for the local features extracted from a new image by using visual vocabulary obtained in the previous step.

The popular and frequently used feature extractor, clustering, and distance finding techniques used in bag-of-visual-features methodology are SIFT feature extractor, k -means clustering technique, and Euclidian distance method, respectively.

The framework followed for bag-of-visual-features is as shown in Fig. 1.

3 Proposed Method of Video Shot Classification

Video shot classification plays a major role in content-based indexing of video data. Usually, the frames of a video shot contain similar content. This is the base for our proposed method.

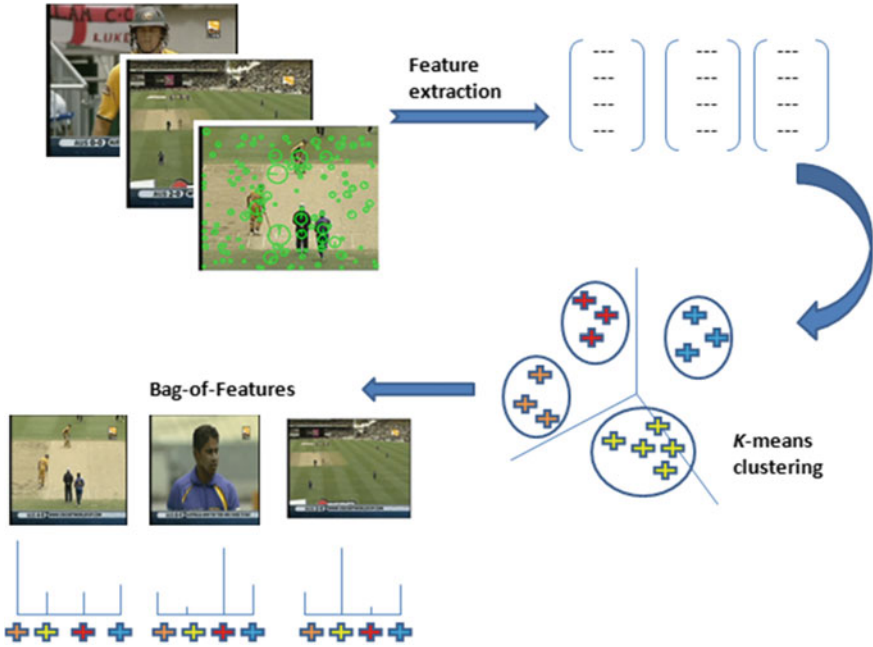


Fig. 1 Framework of bag-of-visual features

3.1 Proposed Algorithm 1

- Step 1 Collect the set of top 100 SIFT features from each frame of half of the training set of video shots of all class types. (Close-up view class type, pitch view class type, and distance view class type).
- Step 2 Cluster the collected features into a number of clusters to form visual features vocabulary.
- Step 3 Train the frames of the remaining half of the training set of video shots of all class types using the visual vocabulary extracted in step 2.
- Step 4 By using the trained data obtained in step 3, classify the frames in test set of video shots into one of the class types.

For implementing and evaluating the proposed algorithms, we have used the cricket video dataset available online at [6]. Initially, we collect a set of video shots of hundred frames in each shot. Different types of shots we have used are close-up view shots, pitch view shots, and distance view shots.

The training set consists of three different types of shots they are close-up view, pitch view and distance view.

Example frames from the three different types of video shots are as shown in Fig. 2.



Fig. 2 Example frames of different class types of video shots. **a** Close-up view. **b** Pitch view. **c** Distance view

Initial step of our proposed algorithm is collecting the top 100 SIFT features from each frame of first three shots of each class type, i.e., we collect features of three close-up view shots, three pitch view shots, and three distance view shots.

Second step is to cluster the collected features into a set of 500 clusters by using k -means clustering method which will act as the vocabulary of visual features.

Third step is to train each frame of remaining three shots present in training sets of all three classes. For this step, we have used Euclidean distance for assigning nearest visual feature for each frame in each shot by representing it with visual feature occurrence histogram.

Fourth step is to test the classification accuracy of our proposed algorithms by using the testing set of video shots of each class type.

3.2 Proposed Algorithm 2 for Shot Classification

1. Results obtained after applying Algorithm 1 on a video shot, count the number of frames in the video shot classified as close-up view type (n_c), number of frames classified as pitch view type (n_p), and number of frames classified as distance view type (n_d).
2. If $n_c > n_p$ and $n_c > n_d$
Then, the video shot is classified as close-up view type
Else, if $n_p > n_c$ and $n_p > n_d$
Then, the video shot is classified as pitch view type
Else
The video shot is classified as distance view type.
End.

4 Experiments and Results

We have selected a training set of 18 video shots (each video shot consists of 100 frames) in which six video shots are of close-up view type, six video shots are of pitch view type, and six video shots are of distance view type. In our testing set, we have 15 video shots, in which five video shots are of close-up view type, five video shots are of pitch view type, and five video shots are of distance view type.

The first step of our algorithm is collecting the top 100 SIFT features from each frame of the three video shots of each class type from the training set. By applying the first step, we have collected a set of 90000×128 SIFT features.

For extracting top 100 SIFT features, we have used VLFeat package [7].

By applying the second step, we have clustered the feature set into 500 cluster sets, i.e., we have quantized the collected feature set of size 90000×128 to feature cluster set of size 500×128 . These 500×128 feature clusters are used as the visual vocabulary in the next step.

The next step is to find out the occurrence histogram using the visual vocabulary for the features extracted from the remaining training set of video shots, three shots of close-up view type, three shots of pitch view type, and three shots of distance view type to get a trained data of size 900×500 .

The final step is classification of each frame of each video shot present in testing set, and finding out among the 100 frames of a single video shot how many number of frames belonging to which of the above-mentioned class types. That is, finding out how many number of frames among 100 frames of a video shot are classified as close-up view type, pitch view type, and distance view type.

Based on the maximum number of frames of the video shot belonging to which class type, the video shot is classified as that class type.

The results of frames classification we have obtained after applying the Algorithm 1 on the testing set of video shots is as shown in Table 1.

As shown in Table 1, consider the first video shot frames classification results are out of 100 frames—100 frames are classified as close-up view type, zero frames are classified as pitch view type, and zero frames are classified as distance view type. By using the proposed Algorithm 2, of shot classification, the first video shot is classified as close-up view type.

Consider another video shot results shown in Table 1, results of sixth video shot frames classification are out of 100 frames—14 frames are classified as close-up view type, 83 frames are classified as pitch view type, and three frames are classified as distance view type. According to the proposed shot classification algorithm, the sixth video is classified as pitch view type.

We have tested the proposed algorithm on a testing set of 15 shots as mentioned above; the testing results (percentage) of proposed shot classification algorithm are as shown in below figure.

As shown in Fig. 3, our proposed method has got hundred percent (100 %) results.

Table 1 Results of classification of frames of testing set of video shots

S. no. video shot	Close-up view	Pitch view	Distance view
1	100	0	0
2	100	0	0
3	100	0	0
4	100	0	0
5	100	0	0
6	14	83	3
7	5	93	2
8	4	96	0
9	5	94	1
10	4	96	0
11	6	1	93
12	2	0	98
13	0	0	100
14	1	0	99
15	0	0	100

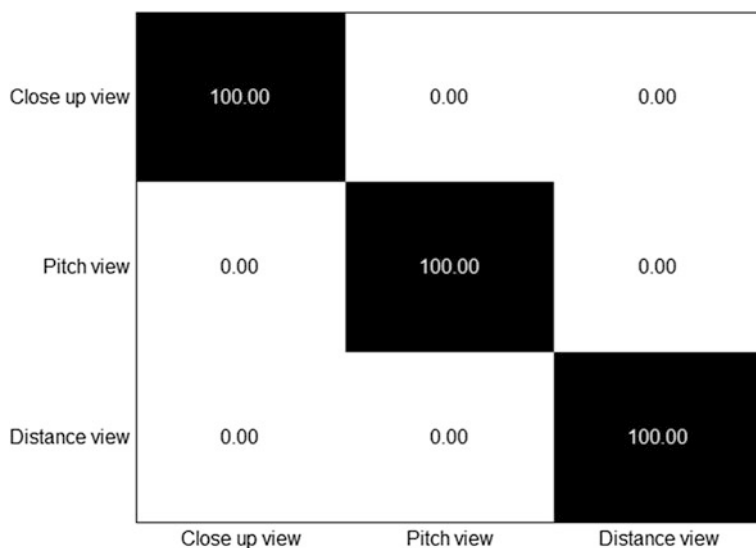


Fig. 3 Video shot classification results

5 Conclusion

We have proposed a new method of cricket video shot classification based on Bag-of-visual-features methodology; by using the proposed method we are able to classify the cricket video shots into three different class types. Our proposed method has shown reasonable performance in classifying the video shots as close-up view shot type, pitch view shot type, and distance view shot type.

Acknowledgments The Authors of want to acknowledge Ravindra Gadde [8] for the technical support, and Mr. Dipen Raghuvani for making the cricket video dataset [6] available online.

References

1. Jayanth SB, Srinivasa G. Automated classification of cricket pitch frames in cricket video. *Electron Lett Comput Vis Image Anal.* 2014;13(1):33–49.
2. Abburu S. Multi level semantic extraction for cricket video by text processing. *Int J Eng Sci Technol.* 2010;2(10):5377–84.
3. Kolekar MH, Palaniappan K, Sengupta S. Semantic event detection and classification in cricket video sequence. In: *Sixth Indian conference on computer vision, graphics and image processing*; 2008.
4. Tsai C-F. Bag-of-words representation in image annotation: a review. *International scholarly research network, ISRN Artificial Intelligence*; 2012.
5. O'hara S, Draper BA. Introduction to the bag of features paradigm for image classification and retrieval. *arXiv:1101.3354v1 [cs.CV]* 17 2011.
6. Video dataset. <http://cse.iitk.ac.in/~vision/dipen/>.
7. Vedaldi A, Fulkerson B. VLFeat: an open and portable library of computer vision algorithms; 2008. <http://www.vlfeat.org/>.
8. <https://masterravi.wordpress.com/author/masterravi/>.

HDTCV: Hybrid Detection Technique for Clickjacking Vulnerability

D. Kavitha, S. Chandrasekaran and S.K. Rani

Abstract Evolution of web technologies also brings new exploits in web applications. Attacker gains new flaws in the web application to perform wide variety of malicious tasks. These malicious tasks will compromise sensitive information of users and also makes loss in market value of the organization. Thus, the study of various types of vulnerabilities and their weakness in the web application structure is a challenging task. This paper focuses on clickjacking attack and provides an efficient detection technique to overcome this attack. The proposed technique has the features and standards to measure the attack and how much the vulnerability is being exposed with respect to the context of application in the dynamic environment. Thus, the proposed system handles clickjacking efficiently and the vulnerability of the attack can be measured by the deviation of the system state with expected state.

Keywords Malicious task · Vulnerabilities in web application · Clickjacking attack · Hybrid detection technique

1 Introduction

Web technology [1] is becoming more prevalent in commercial, corporate, and public services. All businesses rely on websites to interact with the customers, receive user aspects, and sell products. This wide range of application provides

D. Kavitha (✉) · S.K. Rani
Department of Computer Science and Engineering, Valliammai Engineering College,
Chennai, India
e-mail: dkavitha2005@gmail.com

S.K. Rani
e-mail: rsk1411@gmail.com

S. Chandrasekaran
Sri Ranganathar Institute of Engineering and Technology, Coimbatore, India
e-mail: chandrasekaran_s@msn.com

several advantages to its end users such as high reachability, high availability, and reduced business cost. Both security professionals and hackers constantly research about new flaws, which compromise on sensitive information of user.

The increasing number of new security flaws potentially cause significant risk to an organization. Although web technology has many advantages, user unawareness and the flexible nature of its structure can easily make the malicious user to perform unintentional tasks without the user consent. Providing security to these riddled vulnerabilities is an important task. Thus, web security is the most overlooked aspect of commercial viability and should be prioritized in enterprise profitability of all sizes.

This paper mainly focuses on clickjacking attack. Clickjacking [2] is a hijacking attack, which is considered as one of the topmost web attacks, where the attacker hijacks the user clicks in order to perform malicious actions. It is performed through IFrames. IFrame is an inline frame or it is a window component, which makes an HTML page that holds another HTML document. It is most commonly used by website designers to embed interactive applications in their web pages. Attacker uses these iframes by placing the malicious invisible iframe component above the clickable component. When the visitor clicks the component, the malicious component is executed than the one expected by users, which results in loss of user-sensitive information without their knowledge.

Another kind of possible clickjacking attempt through XSS attacks [3]. In XSS attack, hackers insert malicious code and infect the legitimate page. According to the Cyber Statistics report presented, clickjacking is one of the common attacks which mainly targets social sites. In these, unknown attack technique is 26.5 %, defacement has 16.4 % and it was 14 % last year, SQLi has 14.3 % down from 19 % last year, malicious iframe is 10.9 %, target attack is 10.5 %, account hijacking is 10.4 %, and malware is 6.9 %. Many of them are not aware of the clickjacking attack (Fig. 1, Table 1).

Many techniques suggested for clickjacking have been circumvented by malicious users. This paper presents a general study of various detection techniques and provides an efficient detection solution to overcome clickjacking attack.

Fig. 1 Top most attack techniques

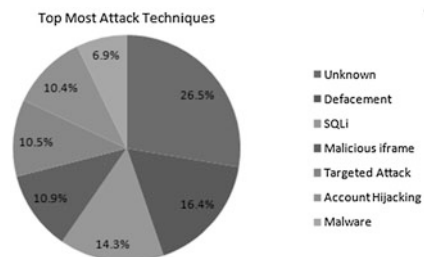


Table 1 Percentage of exploitation

Attack Techniques	Percentage of exploitation in the year 2015 (%)
Unknown	26.5
Defacement	16.4
SQLi	14.3
Malicious iframe	10.9
Targeted attack	10.5
Account hijacking	10.4
Malware	6.9

The remaining of the paper is organized as follows: Sect. 2 discusses the number of related works; Sect. 3 presents motivation and scope of this paper; Sect. 4 describes the proposed system; Sect. 5 presents implementation of the work; Sect. 6 shows the experimental evaluation; and Sect. 7 discusses about the conclusion of the work.

2 Related Works

2.1 Study of Different Web-Based Attacks

Denial-of-Service detection through TCP congestion window analysis [4]

Method: In this paper [4], proper response will be linked to the detection alarm and it is based on sequential change point detection algorithm.

Limitations: CUSUM statistic sequential change point detection algorithm added extra computational overhead to the target.

Developing a security model to protect websites from cross-site scripting attacks [5]

Method: The proposed security model provides a practical way to prevent XSS attacks using Zend framework.

Limitations: There is an added cost for implementing Zend framework validation and filtering of inputs.

Hijacking spoofing attack and defense strategy based on Internet TCP sessions [6]

Method: The attacker acts as a third party to participate in this type of attack, i.e., injection of additional information on sessions. Preventing hijacking attacks based on encryption is possible.

Limitations: Proper validation is needed to defend against this attack.

A fast and secure way to prevent SQL injection Attacks [7].

Method: The proposed algorithm uses both advanced encryption standard and Rivest–Shamir–Adleman to prevent SQL injection attacks. In this method, a unique secret key is fixed or assigned for every client or user.

Limitation: The more complex the encryption the more processing time it takes. Client-Side detection of Cross-Site Request Forgery Attacks [8].

Method: The same origin policy is defined by the scheme, host, and port of a URL. It prevents a webpage being loaded from a specific origin. This detection method is based on cross-origin policies to perform requests to a trusted website.

Limitations: if policies are specified incorrectly or undefined. This approach is ineffective.

2.2 *Pros and Cons in the Existing System of Clickjacking*

Existing defenses of clickjacking can be easily circumvented by attackers. One kind of such technique is frame-busting. This technique [9] will check if the browser's top level has the active page; if the active page is not at the browser's top level, the frame is removed by the script and it will bust the frame.

The advanced technique of frame-busting is X-Frame-Options HTTP response header [9] can be used to indicate whether or not a browser should be allowed to render a page in an iframe. Websites owners use this options in their websites while designing to avoid clickjacking attacks and ensuring that their sites are secure and it is not used by attacker to embedded their content into other sites. X-Frame-Options has DENY, SAMEORIGIN, and ALLOW-FROM values. If DENY policy is specified, the actual page does not allow the iframes to be executed either in the same sites or from different sites. The limitation of this approach is that each and every time the policies have to be defined by the designers. If any of the policies are undefined, it leads to attackers to easily implement their attack technique.

In [10] Stone, Paul describes about click; if any clicks are made in the invisible component, the browser detects and blocks the component. This protection technique targets only specific components. Another possibility of clickjacking attempt is through a webcam and a microphone [11].

In this attack, iframe is loaded by Flash Player settings manager's SWF file. Then CSS is used to make the iframe invisible and finally the attacker enticed the user to enable their webcam. The above protection technique targets only specific components and flash block technique is used to block the flash content, but it limits functionality of the websites.

Opaque Overlay Policy [12, 13] makes all iframes to be shown opaquely, but this approach causes breakdown of many genuine websites. Lundeen, Brigitte, and Jim Alves-Foss describe HTML5 sandbox implementation [14, 15]. In this technique, it prevents the execution of javascript, which is considered as one of the ways the attacker performs clickjacking.

Almost many websites entirely rely on javascript for website designing. Thus, the prevention of javascript decreases the user interface of any websites.

Onbeforeunload event [9, 16] allows you to display a message in a confirmation dialog box to inform the user whether he/she wants to stay or leave the current page.

Clear click [17] is same like the NoScript add-on; if user tries to perform clicks on an embedded element, it intercepts the user click and make the user know about the hidden embedded element.

In [18, 19], author describes automatic clickjacking detection approach; this approach consists of testing unit and detection unit. The testing unit manages the user clicks and the detection unit uses click IDS and NoScript plugin for the identification of clickjacking. This technique reports alert and warnings to the user to overcome any further ways of clickjacking attempt. The major limitation of this technique is that the testing unit focuses only on the clickable element.

In [20, 21], the author implements click-safe, which provides security against clickjacking attacks. This technique consists of detection unit, mitigation unit, and feedback unit. The limitation of this approach is that sometimes malicious user provides incorrect feedback to the victim [22].

3 Motivation and Scope

This project provides an analysis of prevalence of various web attacks and its defense strategy in the field of web security. This analysis helps us to gain knowledge about existing defense strategy for web attacks. This paper focuses on clickjacking web attack and most of them are not aware of this attack. This paper creates awareness about clickjacking.

4 Proposed System

4.1 System Architecture

See Fig. 2

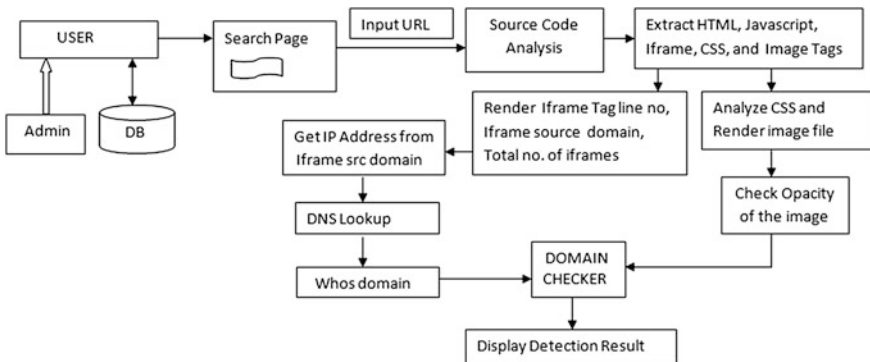


Fig. 2 Architecture for detection of clickjacking attack

5 Implementation

5.1 Implementation of Modules

5.1.1 Module 1

User authentication is needed to allow an authorized user to enter the corresponding websites. Login or logon is the process by which an individual's access to a computer system is controlled. User can log into a system to obtain access and can then logout or logoff when the access is no longer needed.

5.1.2 Search Module

Search module allows the users to search for specific URL, what they intended. It is designed to search for information on the World Wide Web. It retrieves the information about user who entered the URL (Fig. 3).

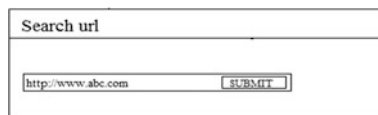
The actual input URL is placed in this module. When the user clicks the submit button, it retrieves the next module. When the user specified an inappropriate URL, it shows that the URL is invalid.

5.1.3 IFrame Tag Checker

In this module, the tag checker analyzes the source code of corresponding websites and retrieve the iframes in the HTML tags. It gets the input URL from the user and analyzes the source code for iframes using regex. First, it checks the characteristic of the input URL using preg match function of regex. Regex is also used to match the input URL with the iframe URL.

It finally displays,

- i. iframe contained tag line number
- ii. Number of iframes in the tag
- iii. iframes contained source URL



The image shows a web form titled "Search url". It contains a text input field with the value "http://www.abc.com" and a "SUBMIT" button.

Fig. 3 Search page

5.1.4 DNS Lookup

This module retrieves the iframe source domain from iframe tag checker and finds the IP address retrieved domain and it analyzes whether this module is listed in DNS lookup. If this IP address is not listed in DNS lookup it shows the results as, IP is white listed.

If the input URL is listed in DNS Lookup, the results show that the website is vulnerable and it is blocked by admin. Usually, domain is stored in DNS lookup as an array. Reverse IP function is used to reverse the IP of input URL.

5.1.5 WHOS Module

This module gets the input from the IP of DNS Lookup domain and retrieves the IP registered user details and it displays

- i. Registry Domain ID
- ii. Registrar URL
- iii. Registrar Creation and Updated Date
- iv. Registrar Organization
- v. Registrar Address Details like Street, Country, Fax, and Contact details.

5.1.6 CSS Module

Analyze the CSS file and extract the image file. And finally checks the opacity of the image file.

5.1.7 Domain Checker

This module gets the input from IP of DNS Lookup domain and retrieves the IP registered user details. It will display whether the domain is vulnerable or not based on the analysis of previous modules. It shows the results as the website is secured or vulnerable or may be secured.

5.2 Algorithms

5.2.1 Algorithm for iframe Tag Checker Using Regex

Input: Input URL

Output: Retrieve the content of iframe

Step 1: Get the input URL from User

Step 2: Analyze the URL Pattern of input URL using regex

Step 2.1: If the regex of URL matched with the input URL

Step 2.1.1: Get the domain from the matched pattern of regex

If the match is not found

Return Invalid URL

Step 3: Get the source file of input URL

Step 4: Get the domain of input URL

//Search source code of input URL for iframes

Step 5: Match regex of iframe tag with the source file

Step 5.1: Initialize framecount is equal to zero

If Match found

Step 5.2: Extract the iframesrc using regex

Step 6: Get the domain of iframesrc

Step 7: Compare the domain of iframe with input domain

If not matches

Step 7.1: Increment the framecount by one

//get the content of iframe

Step 7.2: Get line number of iframe.

Step 7.3: Get iframe domain.

Step 7.4: Get total iframe count.

If **Step 5** is false

return no iframes

5.2.2 Algorithm for White Listed and Blacklisted Using dnslookup

Input : iframe domain
Output: Whitelisted or Blacklisted
Dnsbllookup=>PredefinedDnsbllookupcontained array(“”, ””)
Type A=>”Not secured”
Step 1: Get ip of iframe domain
Step 2:
 For each ip
 Perform reverseip
 Step 2.1: Explode of ip using regex
 Step 2.2: Reverse of Explode using regex
 Step 2.3: Implode of Reverse using regex
Step 3: Check the dnsrecords of dnslookup with the output of **Step2**
 If found
Step 4: Matched with “Type A” records of dnsbllookup
 If match found
 IP is in Blacklisted
 Display vulnerable
 Else
 IP is in whitelisted

5.3 Screenshots

5.3.1 Search Page

Once the user is logged on with proper credentials, he/she is directed to the search page, where he/she can enter input URL (Fig. 4).

5.3.2 IFrame Tag Checker

When the user enters the URL, this module displays the total number of iframes and iframe tag which contains the source URL and iframe tag line number (Fig. 5).

5.3.3 IP Checker

If the user enters a vulnerable website, it gets the IP of the domain and checks with the DNS records. If the website is listed in type ‘A’ of DNS lookup, it displays the website is listed (Fig. 6).

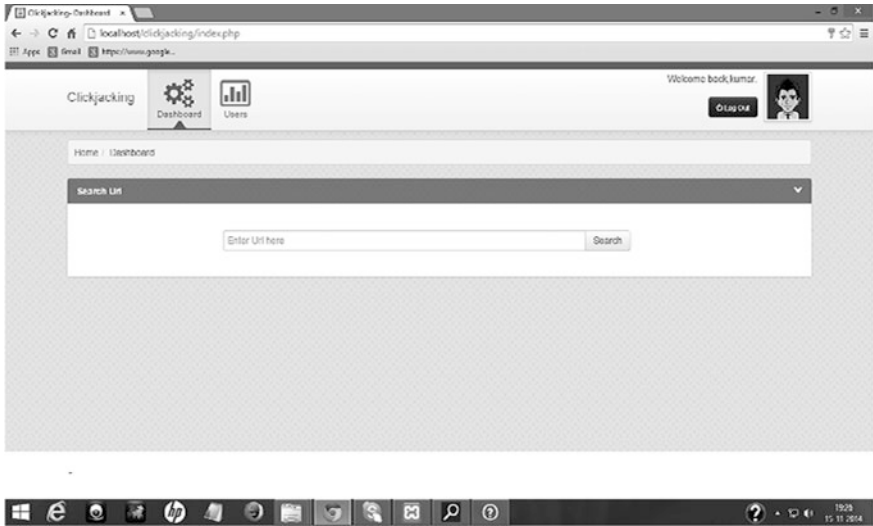


Fig. 4 Search URL page



Fig. 5 iframe tag checker

5.3.4 Whos Domain

This page retrieves the details of the vulnerable website (Fig. 7).

5.3.5 Domain Checker

In this page, the results display the website as vulnerable (Fig. 8).



Fig. 6 IP checker for vulnerable URL



Fig. 7 Whos domain for vulnerable URL

6 Experimental Evaluation

The detection result shows the highly secured websites, less secured websites, and vulnerable websites. According to the result, marketing sites are mainly targeted by attackers. In our detection method, iframe targeted attack result shows best accuracy compared to HTML, javascript, and image. This implementation is also used to find the targeted attack in other scripts also. The false positive is minimal compared to existing techniques (Figs. 9 and 10).

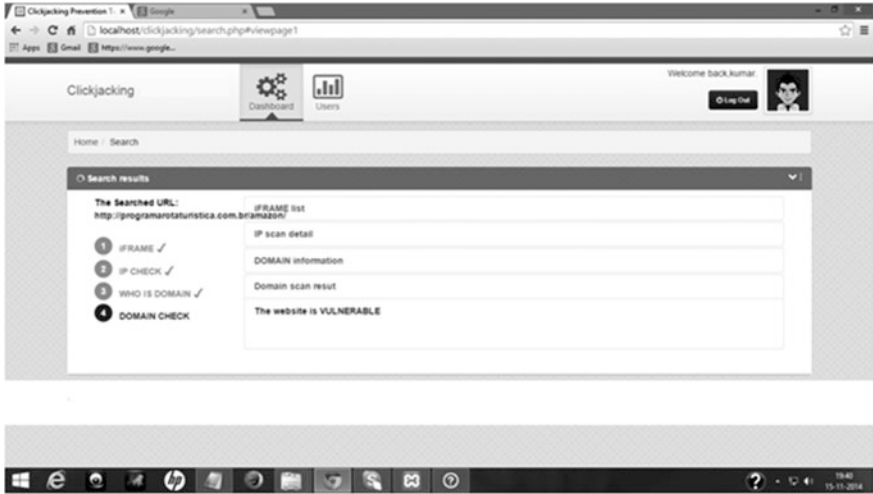


Fig. 8 Domain checker for vulnerable URL

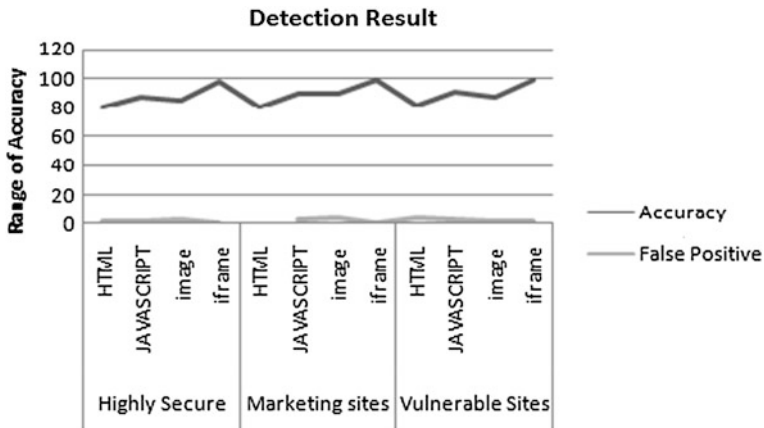


Fig. 9 Accuracy of the detection method

7 Conclusion

The analysis of clickjacking security attack was done by means of proposed detection method which uses regex for their implementation. This detection system finds the vulnerability level of clickjacking and the deviation of the system, which is from expected to the actual level of security. The proposed iframe tag checker algorithm using regex, focuses on analyzing and retrieving the iframe, and the

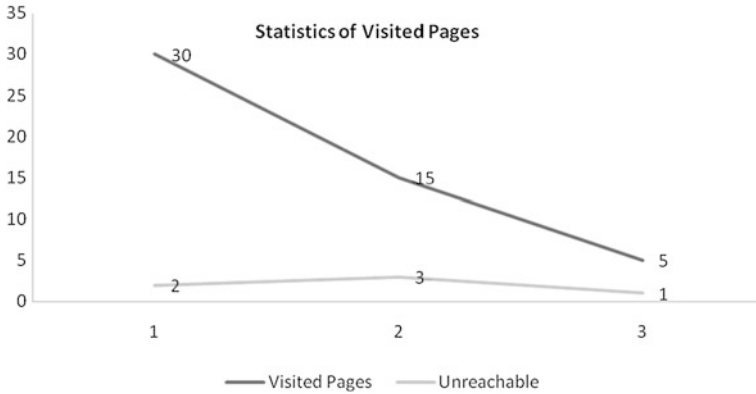


Fig. 10 Statistics of visited pages

dnslookup algorithm focuses on analyzing white listing and blacklisting. This method also detects the attack by using image files. Thus, this detection shows maximum accuracy and minimal false positive and also reduces the time spent on coding, reduces effort, and it provides efficient solution for clickjacking.

References

1. <https://msdn.microsoft.com/en-us/library/office/aa218647%28v=office.11%29.aspx>.
2. <https://www.owasp.org/index.php/Clickjacking>.
3. https://www.owasp.org/index.php/Cross-site_Scripting_%28XSS%29.
4. Alenezi M, Reed MJ. School of Computer Science and Electronic Engineering. Denial of service detection through TCP congestion window analysis. In: World Congress on Internet Security 2013.
5. Yousra Faisal Gad Mahgoup Elhakeem, Bazara I. A. Barry Developing a security model to protect websites from cross-site scripting attacks using Zend framework application. In: 2013 International Conference on Computing.
6. Yongle Wangs Xuchang ploughs the recent information science research institute Xuchang, JunZhang Chen Xuchang Vocational Technical College Xuchang, China. Hijacking spoofing attack and defense strategy based on Internet TCP sessions, 2013.
7. Proceedings of 2013 IEEE Conference on Information and Communication Technologies (ICT 2013). A fast and secure way to prevent SQL injection attacks. Piyush Mittal1, Sanjay Kumar Jena2.
8. Shahriar H, Zulkemine M. Client-side detection of cross-site request forgery attacks. In: 2010 IEEE.
9. Rydstedt G, Bursztein E, Boneh D, Jackson C. Busting framebusting: a study of click-jacking vulnerabilities at popular sites. In: Proceedings of the Web 2.0 Security and Privacy, 2010.
10. Paul S. Next generation click-jacking. BlackHat Europe. 2010.
11. US-CERT. CVE-2008-4503: adobe flash player click-jacking vulnerability. <http://cve.mitre.org/cgi-bin/cvename.cgi?name=CVE-2008-4503>. Accessed 10, 2008.

12. Wang HJ, Grier C, Moshchuk A, King ST, Choudhury P, Venter H. The multi-principal OS construction of the gazelle web browser. In: Proceedings of the 18th Conference on USENIX Security Symposium, 2009.
13. Rydstedt G, Gourdin B, Bursztein E, Boneh D. Framing attacks on smart phones and dumb routers: tap-jacking and geo-localization attacks. In: Proceedings of the 4th USENIX Conference on Offensive Technologies, USENIX Association, 2010.
14. Hickson I et al. HTML5 sandbox attribute, 2010. <http://www.whatwg.org/specs/webapps/currentwork/attr-iframe-sandbox>.
15. Sophos. "What is 'Likejacking'?" *Sophos*. [Online] <http://www.sophos.com/en-us/security-news-trends/security-trends/what-is-likejacking.aspx>. Accessed 17 Apr 2014.
16. Maone G. Noscript clearclick. <http://noscript.net/faq#clearclick>. Accessed Jan 2012.
17. Maone G. Hello ClearClick, Goodbye Clickjacking! <http://hackademix.net/2008/10/08/hello-clearclick-goodbye-clickjacking/>. Accessed 10, 2008.
18. Balduzzi M, Egele M, Kirda E, Balzarotti D, Kruegel C. Solution for the automated detection of click-jacking attacks. In: ASIACCS'10, 2010.
19. Bradbury Danny. The dangers of badly formed websites. *Comput Fraud Secur.* 2012;2012 (1):12–4.
20. Shamsi JA, Hameed S, Rahman W, Zuberi F, Altaf K, Amjad A. Click safe, providing security against click-jacking attacks. In: 15th International Symposium on High-Assurance Systems Engineering, IEEE 2014.
21. Microsoft. How to recognize phishing email messages, links, or phone calls. Microsoft. <http://www.microsoft.com/security/online-privacy/phishing-symptoms.aspx>. Accessed 17 Apr 2014.
22. Lundeen R, Jesse O, Travis R. New ways I'm going to hack YourWeb App. Blackhat AD, 2011.

QUANCE: Quality-Driven Automated Negotiation for Composite Web Services

Kanchana Rajaram and Chitra Babu

Abstract With the advent of web services, Quality of Service (QoS) serves as a benchmark to differentiate various available services and their providers. QoS characterizes the nonfunctional aspects of a web service and plays a crucial role in the area of dynamic composition of web services. There have been many works on QoS-based negotiation and service selection in deriving an appropriate web service composition. However, automated negotiation is more complex in the context of composite services. The negotiation between a service provider for a composite service and a requester has to be translated into complex one-to-many negotiations that involve the providers of the component services. In this context, this paper proposes an approach, namely, QUANCE that automates the negotiation of QoS parameter values between the service consumer and the service provider of a composite service in a service-oriented environment. This approach is tested using scenarios of an e-governance application that caters to the various operations related to vehicle registration.

Keywords Automated negotiation · SOA · QoS · SLA · Web services · Composition

1 Introduction

In the last decade, the service-oriented paradigm has emerged as a powerful solution to provide seamless integration among business organizations that expose their functionalities as web services. Web services are suitable for access from

K. Rajaram (✉) · C. Babu
Department of Computer Science and Engineering, SSN College of Engineering,
Anna University, Chennai, Tamil Nadu, India
e-mail: rkanch@ssn.edu.in

C. Babu
e-mail: chitra@ssn.edu.in

heterogeneous environments as they are interoperable across platforms and neutral to programming languages. Web services are useful for dynamically binding to services at runtime so that a business relationship with a service provider can be established or canceled on demand. Electronic contracts specify the contractual parties, service definitions, QoS parameters, guarantees, and possible penalties in case of failure to comply with the agreed guarantees. The Service Level Agreement (SLA) [5] which provides the QoS guarantees is an important aspect of the e-contract between providers and consumers.

In Business to Business (B2B) application scenarios, many organizations implement their core business alone while outsourcing other application services. For any required functionality, if it is not possible to find a single suitable service, several services can be found, which together will satisfy the requirement. The composition of web services is frequently automated to integrate cross-organizational services at runtime. An interesting challenge in such a dynamic service composition is to perform it in an environment where the services offered are accompanied by the relevant SLAs, and these SLAs are the outcome of the negotiation process. A framework for lifetime SLA management with autonomous agents that involves negotiation of QoS constraints [11, 20]. However, no prototype was built and the scenarios were only simulated and tested. Hence, a novel approach is proposed namely, **Quality-driven Automated Negotiation for Composite wEb services (QUANCE)** that follows an algorithm proposed for automated negotiation. It has roots from multidimensional auction theory [4] and is applicable to negotiation among multiple component services of a composite service and the consumer. QUANCE generates agreements that ensure closer levels of satisfaction and also maximizes the level of satisfaction for both the provider and the consumer. The approach is tested with an e-governance prototype that implements operations relevant for a road transport office.

2 Existing Work

The approach for automating the negotiation has been discussed by several authors. Negotiation has been an interesting area of research for many years [2, 6]. Different strategies and technologies such as genetic algorithms [1], game theory [3] decision models [16], and intelligent agents [7] have been applied in negotiation process. Negotiations can be bilateral (single service provider) or multilateral (several service providers) and can involve one or more parameters. A prototype system for automating negotiation called ContractBot has been proposed by [18]. There have been some frameworks that provide automated negotiations [15, 18]. Most research in web service negotiations focus on messaging and protocol languages [12, 13]. A data model proposed in [14] describes negotiation preferences and the resulting contracts. A trade-off-based automated negotiation approach described by [17], employs an iterative trade-off mechanism for evaluating the opponent's offers and generating counter-offers of mutual gain based on the selected quality of service parameters.

The PANDA approach [10] provides a mechanism for specifying a negotiation policy using a combination of rules and utility functions. A Negotiation Broker (NB) [22] facilitates a middleware framework and WS-policy specifications for an automated negotiation of SLAs for web services. A trade-off algorithm presented by [8], enables software agents to make trade-offs for the problem of distributed resource allocation. All these frameworks and algorithms proposed for automated negotiation do not consider composite services.

A framework proposed by [20] deals with automated negotiation in the context of composite web services. Algorithms for trade-off and concession have been proposed for generating counter-proposals in negotiation. However, there exists an ambiguity over when to use concessions and when to use trade-offs. In addition, the algorithm aims only to maximize utilities. The framework for lifetime SLA management with autonomous agents [11] performs negotiation to generate the contracts dynamically with QoS guarantees. This work deals with multiple agents and considers only trade-off strategy. The approach is not demonstrated with a prototype. The QUANCE approach is applicable for composite services in SOA and achieves agreements for the participants with closer satisfaction levels.

3 Proposed Approach for Automated Negotiation

The objective of the proposed QUANCE approach is to achieve automated negotiation among the component services of a composite service and the service consumer. The consumer negotiates for QoS parameters such as time and cost with many service providers of a particular service and many providers for different services in the composition. These QoS agreements of various component services of a composition should collectively fulfill the expectation of the service consumer. In a win-win business environment, the service provider(s) and the consumer exchange proposals and counter-proposals on the values of different QoS parameters until they reach a common consensus. There are two possible outcomes of a negotiation: a compromise or a disagreement. The proposed QUANCE approach adopts a bilateral conversation-oriented bargaining protocol [19] for the exchange of messages among the participating parties. According to this protocol, both the seller and the buyer can make offers. An extended version of the bargaining protocol, FIPA Iterated Contract Net Interaction Protocol [9, 20] which supports web services and SOA environment is used by QUANCE. In a service-oriented environment, an online auction can be deployed, located, and invoked by an automated negotiation system. The bargaining protocol is applied for one-to-many negotiations. In a composite service with n component services, there are n one-to-many negotiations as each component service has many providers. The negotiation coordinator instantiates n negotiators and sends the initial proposal to them. Initial proposal is computed by dividing the input QoS parameter values using aggregate functions.

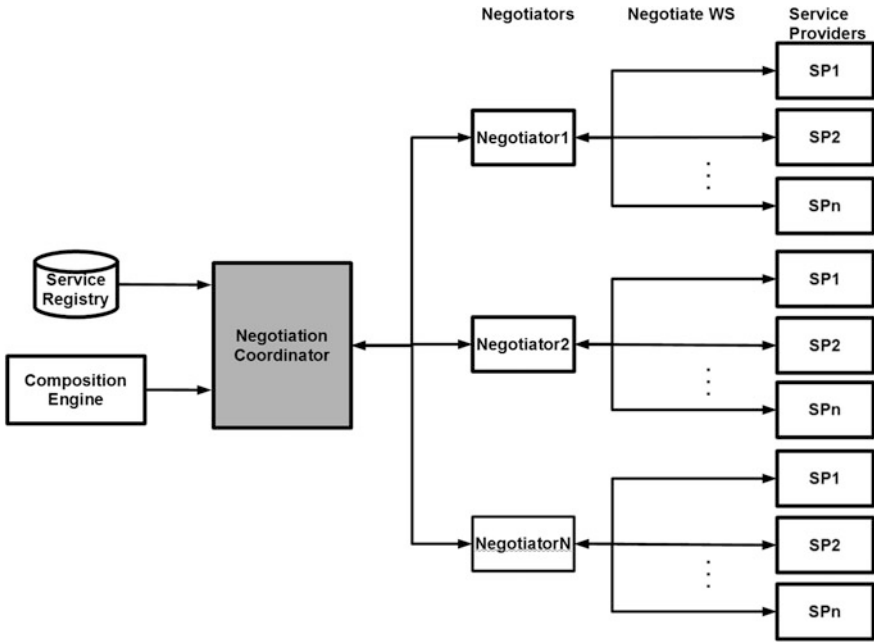


Fig. 1 Negotiation process of QUANCE

A negotiation service is deployed by each service provider of a component service to negotiate for QoS values. The negotiation between a coordinator and the negotiators of component services is depicted in Fig. 1.

3.1 Utility Function

The utility function U facilitates the evaluation of proposals received by the negotiator. It represents the satisfaction level of consumer or provider for a proposal. For two proposals with parameter values a and b , respectively, if $U(a) > U(b)$, then the proposal with value a is better than that with value b . The value of utility lies between 0 (least satisfaction) and 1 (best satisfaction). The terminologies and assumptions made in the paper are tabulated in Table 1.

Let us assume that there are t QoS parameters to be negotiated with weight W , m service providers, n types of services, and thus n negotiators. The following equations indicate how the parameter y affects the value of the proposal in the party's perspective.

$$zU_x^y = \begin{cases} \frac{z^L P_x^y - z^U P_x^y}{z^L P_x^y - z^U P_x^y} & (\text{if } y \text{ is expected to be a minimum}) \\ \frac{P_x^y - z^L P_x^y}{z^L P_x^y - z^U P_x^y} & (\text{if } y \text{ is expected to be a maximum}) \end{cases}$$

Table 1 Terminologies and assumptions

Notation	Explanation
U	Utility or satisfaction level
P	Proposal or offer
x	Type of proposal, $x \in \{\text{Ini, New, Curr, C, max, min, Avg, Prev, Best}\}$ Ini—Initial; Curr—Current; C—Counter; Prev—Previous
z	Participant of a negotiation, $z \in \{\text{SC, Co, N, SP}\}$ SC—Service Consumer; Co—Coordinator; N—Negotiator; SP—Service Provider
${}_z P_x^y$	Proposal of type x made by z on QoS parameter y
${}_z U_x^y$	Utility on the x type of proposal P made by z on QoS parameter y
${}_z U_x^T$	Total utility on the x type of proposal P made by z on multiple QoS parameters
\succ, \prec	Comparison operators to compare two proposals

For each party z , the total utility function is defined below ${}_z U_x^T = \sum_{y=1}^t ({}_z U_x^y * W_y)$ where W_y is the weight associated with a QoS parameter that reflects its importance for the party z . The sum of weights associated with all the t QoS parameters is assumed to be one.

3.2 QoS Aggregation Strategy

The negotiation coordinator shown in Fig. 1 is responsible for the overall negotiation for the composition while the negotiator is responsible for negotiating among the providers of individual services of the composition. The value of the QoS parameter (say y) of a composite service (CS) is an aggregation of expected QoS values of the CS. The NC converts composition-level requirements into service-level requirements by dividing the proposed QoS parameter values among the component services of the composition equally using the aggregation function [21] shown in Table 2. In order to facilitate automated negotiation, each provider offers a negotiation service that is deployed in the registry. The negotiator for each individual service invokes the corresponding negotiation service to establish the agreement.

Table 2 Examples of QoS aggregation functions

QoS parameter (y)	Aggregation function
Execution time, Price	$CS^y = \sum_{i=1}^n (cs^i)$
Reputation	$CS^y = \frac{1}{n} \sum_{i=1}^n (cs^i)$
Throughput	$CS^y = \min_{i=1}^n (cs^i)$

3.3 QoS Negotiation Between Negotiators and Service Providers

The negotiator receives the initial proposal from the coordinator and sends it to all the service providers. The negotiation algorithm iteratively bargains among the service providers, to generate counter-proposals and finally accepts or rejects the offer. There are two strategies for generating a counter proposal, concession and trade-off. The service providers give concessions till the average value is reached. After that they switch over to trade-offs. At any point, if the negotiator finds that the utility of incoming proposal is the same or better than the utility of the negotiator's previous proposal, the algorithm is terminated, the provider that offers such a utility is selected and the offer is accepted. Otherwise, they negotiate for *maxIterations* rounds. Concession is given for a predetermined convergence. A similar negotiation process works in the provider's side.

3.4 Agreement with Higher and Closer Satisfaction

A negotiator assigned for each component service executes the negotiation algorithm to negotiate with the individual providers of that service. The algorithm for trade-off generates random counter-proposals. Therefore, the negotiation process is repeated several times until the negotiator chooses the best offer from the agreed values. The maximum sum represents maximum satisfaction levels to both the service consumer and the provider. The minimum difference indicates that the satisfaction levels of both the participants are as close as possible. An agreement satisfying both these properties will be providing closer levels of satisfaction or utility to the consumer as well as the provider. A two-stage linear programming technique is applied to achieve this multiobjective optimization. This technique is illustrated in algorithm 4 for finding the pair of utilities with the highest sum and the lowest difference.

Algorithm 1	Agreements from QUANCE
-------------	------------------------

```

Input:      Set of utility pair (Uui, Upi) 0 < i < n, n is the number of pairs of utilities and i is the id of the pair.
Output:     i, for a set of utility pairs (Uui, Upi) where Uu and Up have maximum sum and minimum
            difference
// xID denotes i of the (Uui, Upi) pair from which x (sum or difference) is derived
Sumi • Sum(Uui, Upi);      Diffi • Difference(Uui, Upi)    for all i
Thres1 • (Max(Diffi) - Min(Diffi))/2 //Assuming equal distribution of differences
Thres2 • (Max(Sumi) - Min(Sumi))/2 // Assuming equal distribution of sums
SSum • Sumi, 0 < i < n      //sorted in descending order
SDiff • Diffi, 0 < i < n    //sorted in ascending order
for all x, (0 < x < n) do
{ for all y, (0 < y < n) do
//check if the highest sum and the lowest difference correspond to the same pair
{ if ssumxID == sdiffyID then return ssumxID
temp • ssumyID //temp holds ID of yth largest sum
FIND sdiffkID where sdiffkID = temp
FIND Ssumm where ssummID = sdiffkID
//Find the position m of SSum corresponding to xth smallest difference
if |SDiffk - SDiffxl| < Thres1 and |SSumy - Ssumml| < Thres2 then return sdiffkID}
}

```

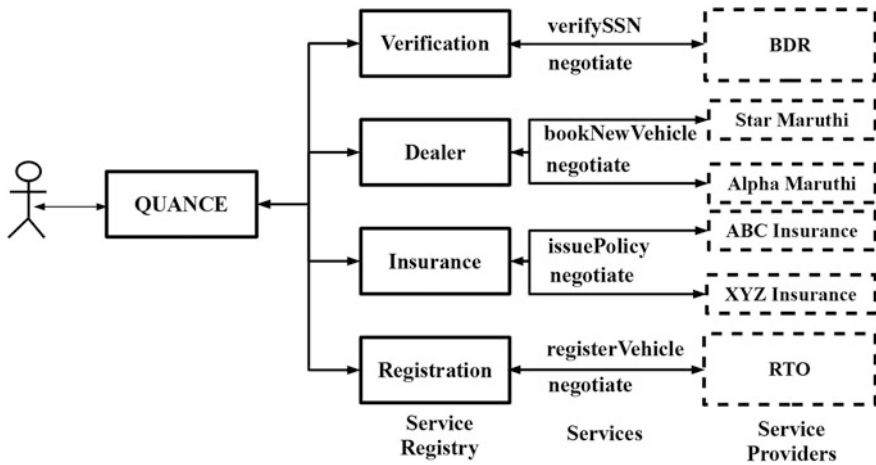


Fig. 2 Vehicle purchase and registration system—service-oriented view

4 Vehicle Registration System—A Case Study

This section introduces an e-governance application of vehicle purchase and registration system, shown in Fig. 2, to illustrate the proposed automated negotiation algorithm. Before buying a vehicle, the identity of the user has to be verified with the Birth and Death Registration (BDR) department that is responsible for issuing Social Security Numbers (SSN) to the citizens of the country. The vehicle can be selected according to the user requirements and ordered through the vehicle dealer. When the vehicle is available, the vehicle must first be insured with an insurance firm. Subsequently, the vehicle is registered in the Regional Transport Office (RTO). Finally, the vehicle is delivered to the client after receiving the payment. This requirement cannot be satisfied with a single service as it involves multiple activities from different departments. The vehicle buying service is offered as a composite service through the e-vehicle portal. There are several dealers selling vehicles and various insurance firms. Hence, negotiation among these service providers must be performed to select the one that offers the best deal in terms of QoS parameters such as execution time and price.

5 Experimental Results

The feasibility of the proposed QUANCE approach is evaluated for this case study. A prototype for the vehicle registration system is implemented using J2EE middleware and NetBeans IDE on machines with 2.4 GHz Intel Core 2 Duo processor and 4 GB RAM. The middleware services for negotiation have been deployed in the GlassFish web server.

The proposals and counter-proposals between the negotiator of BDR service and the provider are tabulated in Table 3. U_{in} denotes the utility of the incoming proposal and U_{cp} denotes the utility of the counterproposal. The negotiation with BDR service takes place for eight cycles before the provider accepts the proposal by the negotiator as shown in Fig. 3a. The negotiation between the negotiator for dealers and the providers (Star Maruthi (Fig. 3b) and Alpha Maruthi (Fig. 3c) proceeds till the fourth cycle. In Fig. 3b, the utilities clearly converge while in Fig. 3c, they do not converge and agreement is not achieved. Similarly, the negotiation between the negotiator for insurance and the service providers converges after six cycles of proposal exchanges as depicted in Fig. 3d. During the negotiation among the negotiator of RTO service and RTO Chennai as shown in Fig. 3e, none of the participants in the negotiation accepts the proposal even after 10 cycles since the number of rounds of negotiations has exceeded $maxIterations$.

All the negotiations, shown in Fig. 3, involve both concessions and trade-offs. The trade-offs are generated randomly. Hence, for the same initial proposal and the same minimum and maximum values, there may be different final agreements. To select the best agreement, the negotiation is repeated 10 times and Fig. 4 shows the sum and difference in utilities. The best set is the one having maximal sum and minimal difference which is computed using two-stage linear programming. The tenth set is selected as the desired agreement.

Sample iterations of negotiation between the service consumer and the negotiation coordinator are tabulated in Table 4. The minimum, average, and maximum values of the pair (response time and price) of all the services are assumed to be (45, 150), (50, 190), and (55, 230), respectively. The consumer is likely to select (Min(Execution Time), Min(Price)) as the initial proposal. If the four services are assumed to have equal complexity, the aggregate initial proposal would be (180, 600) shown in row 1 of Table 4. The average of difference in utilities of agreements from the consumer's perspective as well as from the provider's perspective is found to be 0.08. It is observed that the proposed QUANCE approach achieves an average of 62 % satisfaction to the negotiating participants and the satisfaction levels of different participants are closer by an average of 9 %.

Table 3 Negotiation with BDR service

Iteration	Negotiator				BDR			
	U_{in}	ET (s)	Price (\$)	U_{cp}	U_{in}	ET (s)	Price (\$)	U_{cp}
1		48.8	175	0.66	0.25	51.3	21	0.81
2	0.28	49.4	185	0.56	0.39	50.8	206	0.71
3	0.36	49.9	189	0.51	0.48	50.6	202	0.65
4	0.40	46.0	221	0.51	0.18	50.1	193	0.53
5	0.48	50.0	189	0.50	0.30	49.9	190	0.52
6	0.48	45.2	227	0.50	0.14	50.3	189	0.52
7	0.50	49.9	189	0.50	0.50	50.1	19	0.52
8	0.49	51.7	176	0.50	0.63	Accept	Accept	–

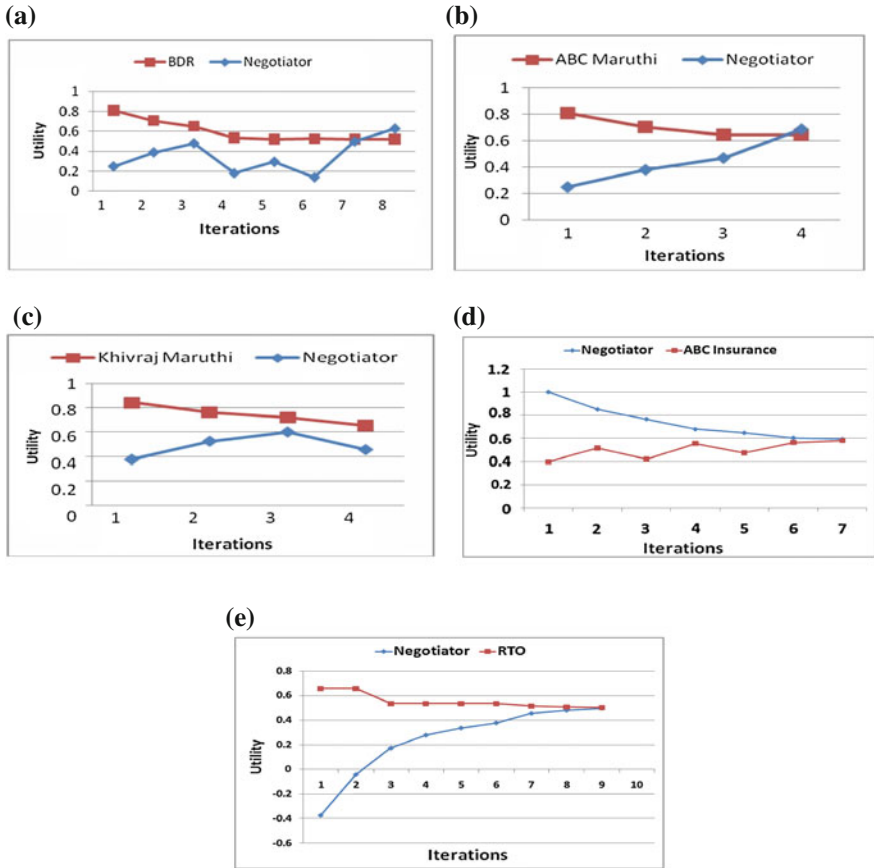


Fig. 3 Negotiation agreement. **a** Negotiation with BDR. **b** Negotiation with Dealer1. **c** Negotiation with Dealer2. **d** Negotiation with insurance. **e** Negotiation with RTO

Fig. 4 Agreement with highest and closest utility for participants

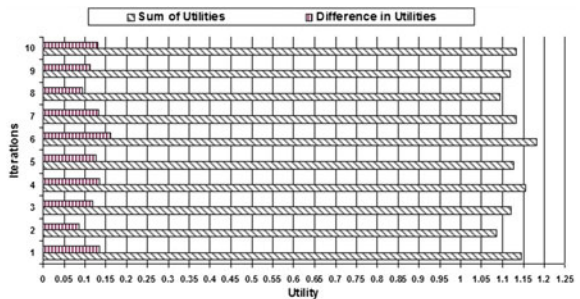


Table 4 Negotiation process proposed by QUANCE

Sl. no.	Consumer proposal		Final agreement		Consumer's utility	Providers' avg utility
	ET (s)	Price	ET (s)	Price		
1	180	600	193.23	768.20	0.52	0.51
2	185	640	202.54	710.90	0.56	0.55
3	188	660	204.33	675.36	0.65	0.53
4	190	680	201.91	722.50	0.65	0.55
5	193	700	197.44	778.59	0.67	0.58
6	195	700	204.00	718.26	0.70	0.63
7	195	720	197.35	779.70	0.76	0.61
8	200	760	201.27	753.00	0.79	0.67

6 Conclusion

The QUANCE approach proposed in this paper automates negotiation in the context of composite web services. It automates negotiation of QoS values among services of different organizations in a Service-Oriented Architecture (SOA). It uses an improved automated negotiation approach which ensures the highest satisfaction level for the providers as well as the consumers. Multiple agreements are generated in a negotiation process and the best agreement which gives the highest and the closest satisfaction to the participants is selected. More research needs to be done in automated negotiation dealing with QoS parameters other than response time and price. Contracts can be generated dynamically based on the agreements. Ongoing work focuses on automated contract generation in the context of hierarchical workflows with nested composite services.

References

1. Anderson A. An introduction to the web services policy language (WSPL). In: Proceedings of IEEE International Workshop on Policies for Distributed Systems and Networks, 2004, p. 189–92.
2. Beam C, Segev A. Automated negotiations: a survey of the state of the art. *Wirtschafts Informatik*. 1997;39(3):263–8.
3. Binmore K, Vulkan N. Applying game theory to automated negotiation. *DIMACS Workshop on Economics, Game Theory and Internet*. *Netnomics* 1999;1(1):1–9.
4. Branco F. The design of multi-dimensional auctions. *RAND J. Econ*. 1997;28(1):63–81.
5. Erl T, Karmarkar A, Walmsley P, Haas H, Yalcinalp U, Liu C, Orchard D, Tost A, Pasley J (2009) *Web service contract design and versioning for SOA*. New York: Pearson Education.
6. Faratin P, Jennings N, Lomuscio A, Parsons S, Sierra C, W M. Automated negotiation: prospects methods and challenges. *Int J Group Deci Negot*. 2001;10(2):199–215.
7. Faratin P, Sierra C, Jennings N. Negotiation decision functions for autonomous agents. *Robot Auton Syst*. 1998;24(3–4):159–82.

8. Faratin P, Sierra C, Jennings N. Using similarity criteria to make issue tradeoffs in automated negotiations. *Artif Intell.* 2002;142(2):205–37.
9. FIPA. Iterated contract net interaction protocol, 2000. <http://www.fipa.org/specs/fipa00030/>.
10. Gimpel H, Ludwig H, Dan A, Kearney R (2003) PANDA: specifying policies for automated negotiations of service contracts. In: Orłowska ME et al, editors. LNCS 2910. Berlin: Springer; 2003. p. 287–302.
11. He Q, Yan J, Kowalczyk R, Jin H, Yang Y. Lifetime service level agreement management with autonomous agents for services provisioning. *Inf Sci.* 2009;179(15):2591–605.
12. Hung P, Li H, Jeng J. WS-negotiation: an overview of research issues. In: Proceedings of the 37th Annual Hawaii International Conference on System Sciences (HICSS'04), IEEE, 2004, p. 1–10.
13. Keller A, Ludwig H. The WSLA framework: specifying and monitoring service level agreements for web services. *J Netw Syst Manage. Special Issue on E-Business Management*, 2003;11(1):57–81.
14. Lock R. Automated negotiation for service contracts. In: Annual International Computer Software and Applications Conference, vol 2, 2006, p. 127–34.
15. Maaser M, Langendoerfer P. Automated negotiation of privacy contracts. In: Proceedings of 29th Annual International Computer Software and Applications Conference (COMPSAC 2005), vol 1, 2005, p. 505–10.
16. Narayanan V, Jennings N. Learning to negotiate optimally in non-stationary environments. In: ACM Proceedings of 10th International Conference on Cooperative Information Agents, Springer, 2006, p. 288–300.
17. Patankar V, Hewett R. Automated negotiations in web service procurement. In: Proceedings of the 3rd International Conference on Internet and Web Applications and Services (ICIW2008), 2008. p. 620–5.
18. Reeves D, Wellman M, Grosz B (2001) Automated negotiation from declarative contract descriptions. In: Proceedings of Fifth International Conference on Autonomous Agents (AGENTS01), 2001, p. 51–8.
19. Rinderle S, Benyoucef M. Towards the automation of e-negotiation processes based on webservices—a modeling approach. In: WISE'05, 2005, p. 443–53.
20. Yan J, Kowalczyk R, Lin J, Chhetri M, Goh S, Zhang J. Autonomous service level agreement negotiation for service composition provision. *Future Gener Comput Syst.* 2007;23:748–59.
21. Zeng L, Benatallah ANB, Dumas M, Kalagnanam J, Chang H. QoS-aware middleware for web services composition. *IEEE Trans Softw Eng.* 2004;30(5):311–27.
22. Zulkernine F, Martin P, Craddock C, Wilson K. A policy-based middleware for web services SLA negotiation. In: Proceedings of the International Conference on Web Services (ICWS2009), 2009, p. 1043–50.

The Analysis of PQ Sequences Generated from Continued Fractions for Use as Pseudorandom Sequences in Cryptographic Applications

Jayashree S. Pillai and T. Padma

Abstract The suitability of a number theory-based novel pseudorandom sequence called Pseudorandom Partial Quotient Sequence (PPQS) generated from the continued fraction expansion of certain irrational numbers, in cryptographic applications, is analyzed in this paper. An approach to build the algorithm around a hard mathematical problem has been considered. The PPQS is tested for randomness and its suitability as a cryptographic key and one-time pad by performing randomness analysis, key sensitivity and key space analysis, precision analysis and evaluating the correlation properties is proposed.

Keywords Pseudorandom sequences · Key sensitivity · Correlation · Security analysis · Randomness analysis · Sensitivity analysis

1 Introduction

According to Kerckhoff's principle as in cryptography—*the security of the algorithm should depend on a key instead of the algorithm*. Key is a parameter that determines the output of cryptographic algorithms or ciphers and is used in encryption processes, digital signature schemes, and authentication protocols. This key may be a secret value or a random or pseudorandom sequence generated from the secret value and is used to enforce security and prevent unauthorized parties from attempting to recover or modify the original data. In order to generate random

J.S. Pillai (✉)

Mother Teresa Women's University, Kodaikanal, Tamilnadu, India

e-mail: nair.jayashree@gmail.com

T. Padma

Sona College of Technology, Salem, Tamilnadu, India

e-mail: padmatheagarajan@gmail.com

© Springer India 2016

S.S. Dash et al. (eds.), *Artificial Intelligence and Evolutionary Computations in Engineering Systems*, Advances in Intelligent Systems and Computing 394, DOI 10.1007/978-81-322-2656-7_58

633

noise to scramble sensitive information, pseudorandom numbers are commonly used. Pseudorandom number generators are a complex subject and the generators that create the most random sequence might not be the fastest or the most memory efficient.

Pseudorandom sequences are considered random if they pass certain tests of randomness [1]. If the algorithm and seed are not known, it is impractical to predict the sequence. Variations of pseudorandom sequences like decimal sequences [2, 3], M sequences [4], and Kasami sequences [5] have been researched and used in various applications requiring pseudorandom sequences.

Some of the commonly used generators for pseudorandom sequences are the Marsenne Twister (MT) [6], Linear Congruential Generators (LCGs), and Blum Blum Shub (BBS) [7].

The authors in [8] have proposed the use of continued fraction to add to the randomness of the chaotic maps and thus enhance the cryptographic properties of their encryption algorithm. In [9] the same authors have used continued fractions in [8] to encrypt images.

References [10–12] have used the concept of continued fractions to design authentication protocols, stream ciphers, and to generate e-cash. In [13], the authors have proposed the use of transcendental numbers as pseudo random generators in cryptography, but the solution has been widely criticized. That irrational numbers can be used in cryptography has been evidenced in patents [14].

This paper aims to analyze the properties of PPQS generated from infinite partial quotients of continuous fraction expansion of certain irrational numbers that are not quadratic. It is based on the difficulty of retrieving an irrational number when the information about some of the partial quotients is known and also on the fact that the continued fraction expansion of certain irrational numbers is unique. These properties make the sequences a prospective candidate that can be considered as an alternative to pseudorandom sequences generated using other means.

2 Number Theoretic-Related Concepts

2.1 Irrational Numbers

A rational number is a real number that can be represented as a ratio. For example, 1.5 is rational as it can be expressed as the ratio $3/2$. An irrational number is any real number that cannot be expressed as a ratio of two integers, i.e., as a simple fraction. The popular irrational numbers are the golden ratio— ϕ , pi— π , Euler's number— e and square root of 2, also called Pythagoras constant— $\sqrt{2}$.

2.2 Continued Fractions

In mathematics, a continued fraction is defined in [15–19] as an expression obtained through the iterative process of representing a number as the sum of its integer part and the reciprocal of another number, then writing the other number as the sum of its integer part and another reciprocal, and so on. They offer a useful means of expressing numbers and functions in mathematics and have also been used in computer algorithms for computing rational approximations to real numbers and to solve Diophantine and Pell’s equations.

A general continued fraction is represented as

$$\alpha = a_0 + \frac{b_0}{a_1 + \frac{b_1}{a_2 + \frac{b_2}{a_3 + \dots}}} \tag{1}$$

where a_i and b_i are either real or complex numbers and the terms a_i are called partial quotients. A common form of representing Eq. (1) is

$$\alpha = [a_0; a_1, a_2, a_3, \dots] \tag{2}$$

If the expression has infinite number of terms, it is an infinite continued fraction as in Eqs. (1) and (2). If the number of terms is finite, as in (3), it is a finite continued fraction and is denoted as

$$\alpha = [a_0; a_1, a_2, a_3, \dots, a_n] \tag{3}$$

If $b_i = 1$ for all i then expression (1) is a simple continued fraction and is expressed as

$$\alpha = a_0 + \frac{1}{a_1 + \frac{1}{a_2 + \frac{1}{a_3 + \dots + \frac{1}{a_n}}}} \tag{4}$$

where a_1 is the integer floor of α and a_i are the positive integers called partial quotients.

For $\pi = 3.1415926$, the continued fraction expansion is given by $\pi = [3, 7, 15, 1, 292, 1, 1, 1, 2, 1, 3, 1, 14, 2, 1, 1, 2, 2, 2, 1, 84, 2, 1, 1, 15, 3, 13, 1, 4, 2, 6, 6, 99\dots]$.

3 Generation of PPQS

A secret real number α is selected as a seed. α is an irrational number that is neither transcendental nor quadratic. The continued fraction expansion of α generates the partial coefficients. The algorithm to compute the partial coefficients of α and the PPQS is explained below.

- (1) Extract a , the integer part of α .
- (2) Subtract the integer part a from α .
- (3) If the difference is equal to zero
 - Stop and proceed to step 4
 - else
 - find the reciprocal of the difference and repeat steps 1, 2 and 3
- (4) From secret location l_1 extract n partial coefficients
- (5) Concatenate m partial coefficients and generate its binary equivalent
- (6) Use a salt after every m coefficients to eliminate any periodicity that may arise in the sequence
- (7) Repeat steps 5 and 6 until PPQS of the requires length is obtained

4 PPQS—Evaluation and Discussions

An experimental study is carried out to evaluate the PPQS to verify the suitability of the sequences as one-time pads in cryptographic applications. A nonfinite, non-quadratic, and non-transcendental irrational number is used as the seed. The partial coefficients of the continued fraction representation of the seed are extracted. From the partial coefficients array, based on a certain predetermined position, the sequence is extracted and its binary representation is used as the PPQS. A salt is added randomly to increase the randomness of the sequence. Statistical tests are applied to examine the randomness of the PQ sequences; key correlation analysis is done to examine the independence of the sequences and precision analysis is done to demonstrate the role of decimal precision of the seed in generating independent random sequences.

4.1 Randomness Analysis

4.1.1 Randomness of the PQ Sequence

Good statistical properties is the central requirement of any random or pseudo random sequence. A single statistical test is not adequate to verify the randomness of a sequence because the sequence could produce various types of nonrandomness. However, if a generator passes a wide variety of tests, then confidence in its randomness increases. The Statistical Test Suite developed by NIST [1] is an exhaustive suite looking at various aspects of randomness in a long sequence of bits and suitability of the generator for cryptographic applications. The NIST test suite comprises a suite of 15 tests—(1) Frequency test (FT) (2) Run's test (RT) (3) Longest Runs test (LROT) (4) Binary Matrix Rank test (5) DFT test (6) Cumulative Sums test (CST) (7) Random Excursions Test

Table 1 Results of statistical tests on the binary PPQS generated for $\pi = 3.141592$

Test no.	Test name		P-value	Proportion of values passing the test
1	FT	$n = 100$	0.06	978/1000
2	RT	$n = 100$	0.94	1000/1000
3	LROT	$n = 100$	0.02	940/1000
4	BMRT	$n = 38,912$	0.43	998/1000
5	DFT	$n = 1024$	0.04	999/1000
6	CST	$n = 100$	0.02	982/1000
7	RET	$n = 1,000,000$	0.23	970/1000
8	REVT	$n = 1,000,000$	0.12	983/1000
9	BFT	$n = 2000$	0.012	980/1000
10	NOTMT	$n = 1,000,000$	0.32	980/1000
11	OTMT	$n = 1,000,000$	0.12	982/1000
12	UT	$n = 400,000$	0.54	992/1000
13	LCT	$n = 1,000,000$	0.47	961/1000
14	SRT	$n = 1024$	0.93	990/1000
15	AET	$n = 1024$	0.45	989/1000

(RET) (8) Random Excursions Variants(REVT) test (9) Block frequency test (BFT) (10) Nonoverlapping template test (NOTMT) (11) Overlapping Template (OTMT) (12) Universal test (UT)) (13) Linear complexity test (LCT) (14) Serial Test (SRT) and (15) Approximate Entropy test (AET).

The NIST test suite was applied to the binary equivalent of the selected PQ sequences generated to test for randomness. The sequence passed all the tests and the result of the tests for the irrational number π and significance value of $\alpha = 0.01$ is listed in Table 1.

4.1.2 Key Correlation Analysis

PPQS is a sequence of binary bits selected from a secret random position of the generated sequence. In order to show that this position of the selection is important and deviation by even a single bit causes to key vector to represent a totally different random sequence, i.e., a different one-time pad, the correlation coefficient between sequences, one selected from position n and the other from a distance m , from the same sequence is evaluated using Pearson Correlation Coefficient (PCC). 1000 different sequences, each of length 1024, were evaluated for correlation with the original random sequence and the results are depicted in Figs. 1 2, 3, and 4.

The average correlation is -0.00075 , -0.00063 , -0.00013 , and 0.0002 , respectively, in each of the above results which is very small and shows that there is negligible correlation between the actual random sequence and the sequences generated by selecting the incorrect position. The results prove that the location of

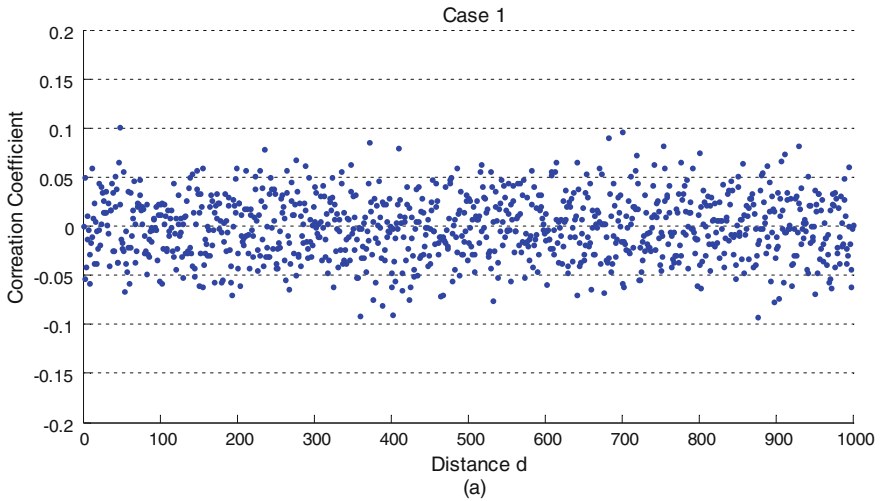


Fig. 1 Correlation coefficient of 1000 sequences of length 1024 with the original sequence chosen as the one-time random vector selected from position 1. Average correlation is -0.00075

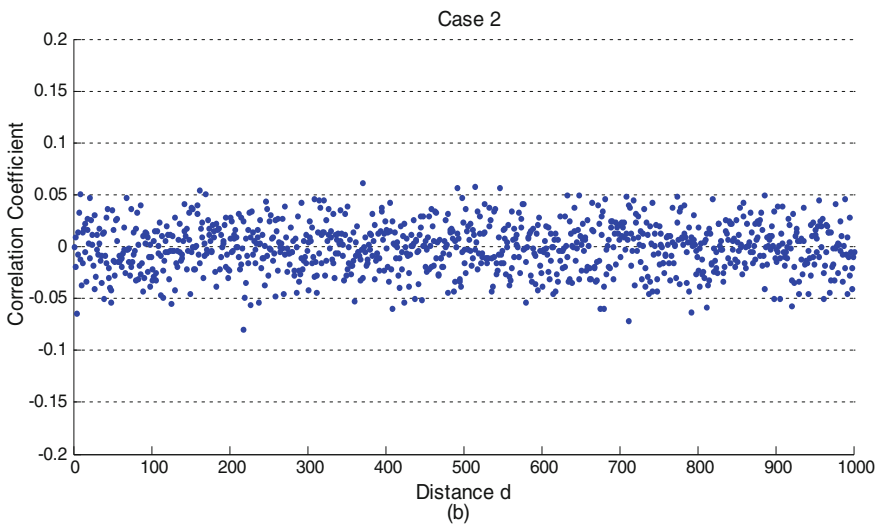


Fig. 2 Correlation coefficient of 1000 sequences of length 2048 with the original sequence chosen as the one-time random vector selected from position 85. Average correlation is -0.00063

selection of the sequences (for the one-time pad) is very precise and even a minor shift generates a totally different sequence, thus enhancing the security of its use in cryptographic solutions.

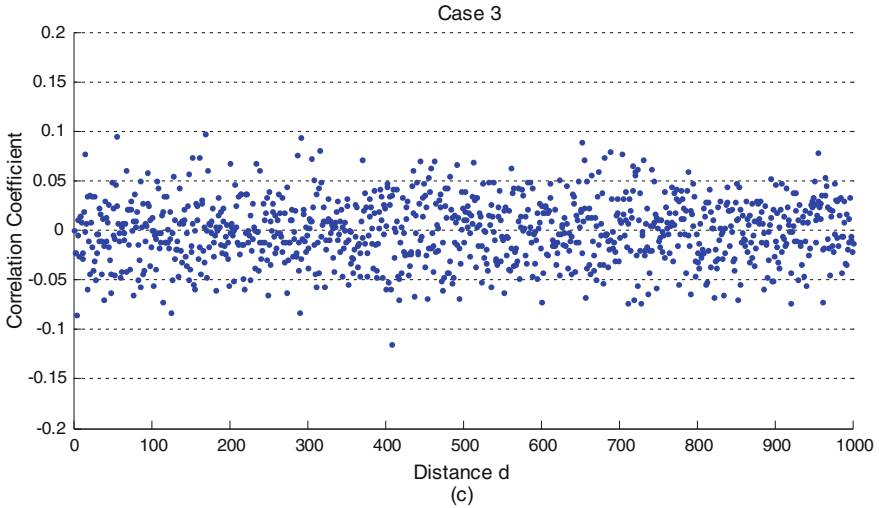


Fig. 3 Correlation coefficient of 1000 sequences of length 1024 with the original sequence chosen as the one-time random vector selected from position 315. Average correlation is -0.00013

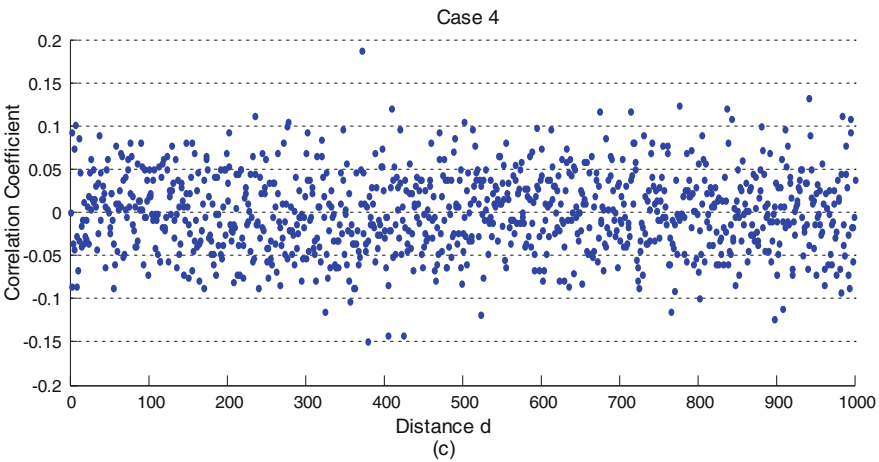


Fig. 4 Correlation coefficient of 1000 sequences of length 512 with the original sequence chosen as the one-time random vector selected from position 500. Average correlation is 0.0002

Result 1 Let α be the selected irrational number and $p_1, p_2, \dots, p_r, \dots$ be the infinite partial quotients of α . If the sequence $[p_m, p_{m+1}, \dots, p_{m+n}]$, for some secret m , say 2150, is selected, then the binary sequence of selected n coefficients can be represented as the PPQS $[pq_{250}, pq_{251}, \dots, pq_{250+n}]$. There is negligible correlation between two sequences, say $[pq_i, pq_{i+1}, pq_{i+2}, \dots, pq_t]$ and $[pq_{i+1}, pq_{i+2}, pq_{i+3}, \dots, pq_{t+1}]$.

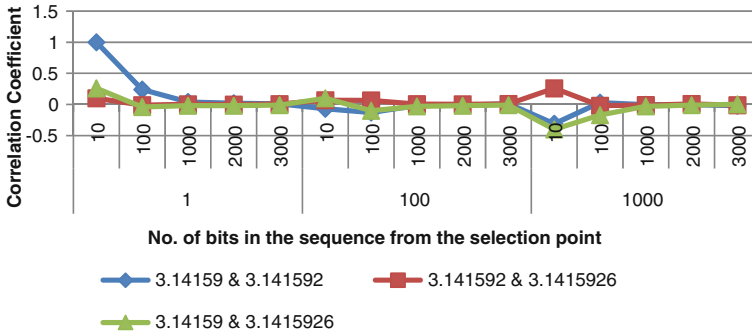


Fig. 5 Comparison of correlation of PPQS generated by the same irrational number with minor change in its precision

4.1.3 Precision Analysis

The number of digits of the irrational decimal used to generate the PPQS must follow the same precision by both the sender and the receiver. A single digit change or altering the precision by a digit can alter the partial coefficients generated. This requires exact precision of the software and architecture at the encoding and decoding ends. But this can also be considered an advantage against the attackers, because even with the exact knowledge of the software and architecture of the system used to generate the continued fractions, inaccurate precision in the choice of the seed will make cryptanalysis difficult.

The graph in Fig. 5 clearly demonstrates that a very minor change in the precision of the irrational number leads to a sequence that is negligibly correlated with the actual sequence.

It is also observed that the correlation of PPQSs is high when the sequences are selected from the start of the sequence, even for different precisions of the irrational number, which means that the correlation coefficients are very close to 1 and they are similar. For consideration as a pseudorandom sequence, it is recommended to select the sequence form a distance >100 from the start of the sequence.

The result also demonstrated that the same irrational number could be used to generate many independent sequences just by selecting a different start points for each sequence. Hence it could also be used as a one-time pad, with the location of the start of extraction of the sequence kept secret.

4.2 Security Analysis

4.2.1 Key Sensitivity Analysis

High key sensitivity is required for secure cryptosystems to ensure that the cipher text will not be able to be decrypted correctly even if there is a very minor change

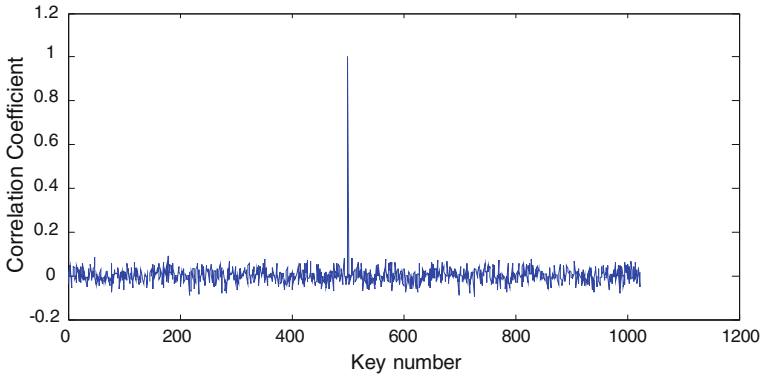


Fig. 6 Correlation of original data with decrypted data for 1024 keys, each extracted from a distance of key number bits from the original key

between the encryption and decryption keys, which means that a slight change in the key should cause a significant change in the output. Key sensitivity test is conducted by encrypting sample data using the selected PPQS and then trying to decrypt it using the same key or one-time pad, with one bit inverted. It is observed that the decryption fails completely.

On considering a random binary data, 1024 bits long, the key sensitivity analysis is done by trying to decrypt it with 1024 different keys, each differing from the original by 1 bit.

From Fig. 6 it is clear that the decrypted data correlated with the original data only when the correct key is used. For all other combinations of the 1024 keys, the correlation is negligible, implying that the decryption failed. This result confirms the sensitivity of the key to the slightest modification (1 bit) which is an essential requirement for a secure cryptosystem.

4.2.2 Prediction of the Irrational Number α or PPQS

An attack will attempt to determine the secret irrational number that is used as the seed. Theorem 1 proves that it will not be possible to predict irrational number α even with the knowledge of a part of the partial coefficients produced by the irrational number. Another attack will be to determine the remaining of the PQ sequence having knowledge of some part of the same. This is also not possible and justified from Theorem 1.

By definition, simple infinite continued fractions represent irrational numbers. If C_n denotes the n th convergent of $[a_1, a_2, a_3, \dots]$, we can define the value of the simple infinite continued fraction $[a_1, a_2, a_3, \dots]$ to be the real irrational number $\lim_{n \rightarrow \infty} C_n$, whenever the limit exists.

Theorem 1 It is not possible to find α if we have knowledge of ∂

If α is the irrational number used as the seed to generate the PPQS $[a_1, a_2, \dots a_m, a_{m+1}, \dots a_{m+n}, \dots]$, given the knowledge of a sub-sequence $\partial = [a_{m+1}, \dots a_{m+n}]$, consisting of binary sequence of length n starting from the m th quotient, it is not possible to predict α . This is because there is infinite number of irrational numbers with the same sub-partial coefficients, i.e., it is possible to find infinite irrational numbers α_p which are different from α but $[a_{m+1}, \dots a_{m+n}]$ will appear as n consecutive partial coefficients for all α_p .

Result 2 If $\partial_1 = [a_r, \dots a_{r+n}]$ is a part vector of consecutive partial coefficients of α , it need not lead to the knowledge of any other partial quotients of the continued fraction expansion of α . This results directly from Theorem 1.

4.2.3 Weak Keys

Quadratic irrationals, generating periodic continued fraction expansion and irrationals like ϕ and e with predicable expansions have to be avoided as they can create an inherent weakness in the algorithm. But this can still be circumvented as in the proposed algorithm, more than 300,000 random bits are generated and the selection of the bits for this is done from a secret position from amongst the bits, making it still secure.

4.3 Efficiency Analysis

The contributors toward the cost of signature generation in the algorithm are (1) generating the partial quotient sequences (2) conversion to binary equivalent.

Generate PQ sequences

The time taken to generate approximately 300,000 bits of the PQ sequence, which is the binary equivalent of 80,000 partial coefficient coefficients, is given in Table 2. 300,000 bits was the selected as this could be comfortably generated using the existing hardware setup, beyond which, it was necessary to increase the virtual memory.

The cost of generating the partial coefficients is evaluated to be $O(\partial^{1+\epsilon})$, where $\partial = \max(\log_2(t_1), \log_2(b_i))$ and ϵ is a very small number. If r is the number of partial coefficients to be computed and if t_1 is the number composed of the first

Table 2 Measures of time taken to generate the 3,00,000 PQ sequences

Irrational number	Time (s)
$\pi = 3.14159$	0.7
$\pi = 3.141592653$	0.8

k digits of the irrational number α , then the cost of generation of the PQ sequence is $O(r \cdot \partial^{1+\epsilon})$.

The cost of conversion of the generated coefficients to its binary equivalent can be considered as negligible.

5 Conclusion

Random numbers are an important building block in a variety of applications and its consumption is increasing rapidly with the proliferation of the gaming and e-commerce industry. Random (pseudo) numbers for cryptography applications are expected to be cryptographically secure, where the requirement is that the adversary without knowing the seed, but with knowledge of part of the sequence, cannot still identify the rest of the sequence. This paper aims to analyze the PPQS generated from the number theory-based continued fraction expansion of certain irrational numbers. The sequence so generated is verified for randomness and passes the NIST test suite. The sensitivity of the sequence toward the precision of the irrational number used and its robustness against cryptanalysis by trying to decode data using any sequence other than the correct one has also been verified. The results also demonstrate that by changing the selection position of the sequence results in a PPQS which is not correlated with any other PPQS generated from the same sequence. This property makes it suitable for use as a one-time pad in cryptographic applications. The test results also demonstrate that scrambling data using PPQS makes it robust against common cryptanalysis. The test results justify the use of PPQS, as an alternative, in cryptographic applications especially as one-time pads without much overhead.

References

1. Rukhin A, Soto J, Nuchvatal J, Smid M, Barker E, Leigh S, Levenson M, Vangel M, Banks D, Heckert A, Dray J, Vo S. A statistical test suite for random and pseudo random number generators for cryptographic applications. National Institute of Standards and Technology Special Publication, 2001, p. 800–22.
2. Parthasarathy AK, Kak S. An improved method of content based image watermarking. *IEEE Trans Broadcast*. 2007;53(2):468–79.
3. Garg S. An efficient method for digital image watermarking based on PN sequences. *Int J Comput Sci Eng*. 2012;4(09):1550–61.
4. Van Schyndel RG, Tirkel AZ, Osborne CF. A digital watermark. *Proc IEEE Int Conf Image Process*. 1994;2:86–90.
5. Mitr A. On pseudo-random and orthogonal binary spreading sequences. *Int J Inf Commun Eng*. 2008;2:27–37.
6. Makoto M, Takuji N et al. Marsenne twister: a 623-dimensionally equidistant uniform pseudorandom number generator. *ACM Trans Model Comput Simul* 1988.

7. Blum L, Blum M, Shub M. Comparison of two pseudo-random number generators. In: Rivest RL, Sherman A, Chaum D, editors. Proceedings of the CRYPTO 82. New York: Plenum Press; 1983. p. 61–78.
8. Masmoudi A. An efficient PRBG based on chaotic map and Engel continued fractions. *J Softw Eng Appl.* 2010;03(12):1141–7.
9. Masmoudi A, Bouhlel MS, Puech W. A new image cryptosystem based on chaotic map and continued fractions; 2010, p. 1504–8.
10. Kane AM. On the use of continued fractions for mutual authentication. *Int J Inf Secur Sci.* 1995;1(3):24–39.
11. Kane AM. On the use of continued fractions for electronic cash. *Int J Comput Sci Secur.* 2013;4:136–48.
12. Kane AM. On the use of continued fractions for stream ciphers. In: Proceedings of Security and Management. Las Vegas, USA; 2009.
13. Pieprzyk J, Ghodosi H, Charnes C, Safavi-Naini R. Cryptography based on transcendental numbers. In: Information security and privacy. Lecture notes in computer science. Proceedings, First Australasian Conference on Information Security and Privacy, ACISP'96, vol 1172. Wollongong, Australia, 1996.
14. Shine C. Method and apparatus of using irrational numbers in random number generators for cryptography. United States patent, Application No. 10/190455, Application Date: 3 Jul 2002.
15. Tattersall JJ. Elementary number theory in nine chapters. Cambridge: Cambridge University Press, 1999. www.cambridge.org/9780521585033.
16. Jayashree P, Padma T. Image watermarking using PQ sequences. ERCICA 2014—Elsevier Publications 2014.
17. Olds CD. Continued fractions. New York: Random House; 1963.
18. Khinchin AY. Continued fractions. Chicago: University of Chicago Press; 1961.
19. Schroeder M. Number theory in science and communication, 2nd edn. Berlin: Springer; 1986.

A Novel Approach to Adopt Scrum by an Enterprise

**B. Reddaiah, R. Pradeep Kumar Reddy, C. Nagaraju
and V. Harsha Sree**

Abstract It is very important to understand how poor quality can bring down a software project development. In the early software developing methodologies, customer requirements are ambiguous because of which specifications can be solidified. This is due to the unbending structure of old and traditional methodologies. Over the last decade, more than a few innovative software development methodologies have been developed particularly to resolve problems in the region of software quality. Such group of methodologies is called “agile.” These methodologies mostly focus on how to maximize flexibility and minimize transparency in the process of software development. These methodologies are not only based on theory, but also rather derived from experiences of successful project teams. Based on the current trend in the software industry, software developing companies are choosing agile methodologies in which scrum is widely used. In this work, the adoption process of scrum by a software company is discussed.

Keywords Adoption · Agile · Enterprise culture · Scrum

B. Reddaiah (✉) · R. Pradeep Kumar Reddy · C. Nagaraju · V. Harsha Sree
Department of Computer Science and Engineering, Y.S.R. Engineering College of Y.V.U,
Proddatur, India
e-mail: b.reddaiah@yogivemanauniversity.ac.in

R. Pradeep Kumar Reddy
e-mail: pradeepmadhavi@gmail.com

C. Nagaraju
e-mail: nagaraju.c@yogivemanauniversity.ac.in

V. Harsha Sree
e-mail: v.harshasree@gmail.com

1 Introduction

Software developing companies for the past two to three decades were using different types of software process models to develop software products effectively to meet the requirements of the customer. Reasons to use different process models to develop software products are due to change in the developing environment and mainly the change in the customer's environment. Because of these changes at both sides of the industry, new models were emerging to meet the changes. In the course of developing a successful product for the customer developing, companies are using new process models.

To use new process model in developing software, first, the new process model has to be adopted by developing organization. In this work, better and effective procedure in adopting scrum by an enterprise is discussed, because while using new process models mainly considering scrum risk factor is increasing in projects [1]. This problem arises from adoption itself. To overcome such kind of problems in adoption a new enterprise culture is required for scrum and that is discussed in this work.

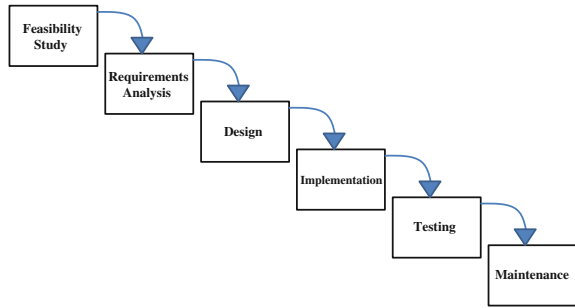
2 Traditional Software Development

The small and big companies were using traditional methods to build software, which are sequential commonly known as "Waterfall." Such sequential models begins with a detailed planning phase which means that the end product is carefully considered all the way through, designed, and documented in detail. The tasks that are needed to execute the design should be determined, and the work is organized using the tools like gantt charts. After this by the detailed estimation of individual steps involved, the team will estimate the time taken for developing the software. The team starts working only after the approval of the stockholder who has thoroughly reviewed the plan. If the specified work is completed by the team members, then it is handed over to others in the product-line fashion. After that it is delivered to the testing organization, where product is examined before delivering to the customer. This process is also known as quality assurance. Throughout the process, we have to concentrate on deviations from the plan and to control them to produce a right product (Fig. 1).

These sequential approaches have both strengths as well as weaknesses. Its great strength is that it is more logical where thinking is done before building the product, making documentation, following particular plan, and keeping everything organized. The great weakness in this approach is the involvement of human beings.

In this kind of development, all the good ideas should come at the beginning of the project where they can be easily incorporated into the process. But getting all good ideas at the beginning is almost impossible because good ideas may come at the beginning, at middle, or even at the day before the launch. At this stage, we cannot incorporate these ideas into the process. So in this approach a great idea at

Fig. 1 Waterfall model



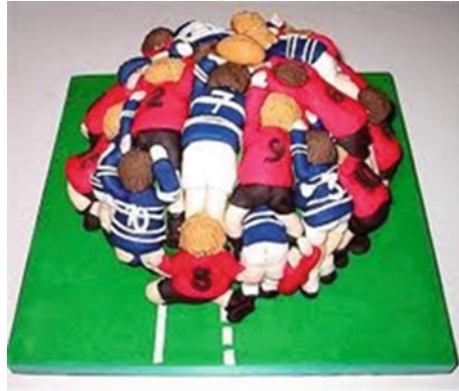
the end of the release cycle is a threat. But unfortunately, these valuable ideas often come at the end of the release cycle. At this stage of development, changes are more difficult and disruptive, when doing the right things is more expensive.

As said previously because of more human involvement in product development, when we use such products for the first time, we think that we can make it better in many ways. But we cannot able to predict the future. So some unexpected changes may occur, and some unanticipated technical problems may occur which forces us to change the direction. Apart from this, the people are particularly bad at planning uncertain things far into the future. We are planning, according to current situation and guessing about this situation. The same after 8 months or a year, it is not going to work properly, so that many gantt charts are going to fail.

Many developers of a sequential life cycle experience these flaws regularly. But it is highly logical that if we plane properly, documented well, and make it more challenging to changes then it will work properly, otherwise it fails to make a good product. Because of this many teams fails. Even though they work hard they are getting worse results. There are many management teams which will invest their reputation and many other resources in waterfall model and other sequential models. Moving from waterfall model to other fundamentally different model is clearly a mistake but scrum is fundamentally different.

3 Agile Development and Scrum

Agile development mainly concentrates on frequent changes in the requirements of customer that is not possible in traditional software life cycles. Uninterrupted requirements change can be allowed at any point of time in agile development. Such frequent change of mind by customer about their requirements is often called as requirements chum in scrum. These changes are intended to gives better results. The strength of agile team lies in its communication between team members. Frequent meetings on daily basis, weekly basis will be conducted to share the work experiences of team members, where weaknesses of team members will be rectified. Teams and team members in agile development do not follow any structural rules as

Fig. 2 Scrum cake

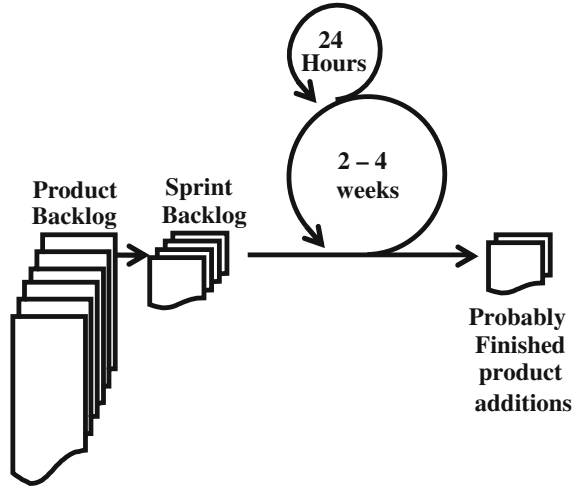
the development is least bothered about pecking order of team members and separating them by tasks. Teams in agile development are cross functional where there is no fixed role for any team member, and decision making is not confined to any particular person of the team in agile. With this type of team, innovative skills will be increased in each and every person of the team. This type of team organization is not at all possible in any other life cycle models. Effective product development up to the satisfaction of customer is supported by truly learning new things that supports innovation and enhances strengths of team members. The core structure of agile models is of iterative in nature and because of agility software product is released quickly.

Agile is a family that has various life cycle models among which scrum and extreme programming (XP) are most widely used in software industry. This paper describes the process of adapting scrum process model by an enterprise. The phrase scrum is derived from the concept of game Rugby where a self organized team progresses collectively in the course of development. The scrum team members works together called scrum cake [2] as shown in Fig. 2.

Scrum life cycle model is an empirical approach. The main focus of scrum is to increase the ability of team in developing product and delivering product to customer within specified time. In scrum, product is not released as whole instead small functional parts of software product are given to customer within specified time so that there is no need for customer to wait for final end product. If customer is asking for changes then developing team have to go as per the ideas of customer and do things according to customer. This is the reason why scrum teams are mainly focused on faster releases rather than standards in product development. These unexpected changes cannot be handled in traditional process models, because traditional process models are mainly focused on standards rather than faster releases of product.

Software product development using scrum life cycle model takes place in three main phases. The first phase is planning phase in which project development planning activity is made. Along with planning activity high-level decisions as a part of managing product development are also made. Second phase is sprint cycle phase which is considered as backbone of scrum. In this phase, actual development

Fig. 3 Scrum framework



of product is carried out in the form of sprint cycles. Sprint cycles are iterative in nature and lasts for about 2–4 weeks as shown in Fig. 3. The last and third phase is closure. In this phase development, activity is finished and the product is released to customer.

Scrum is used as an agile practice that brings software product to end users faster, better, and cooler [3, 4]. Scrum is derived from complex adaptive systems theory and was influenced by best practices in Japanese industry, particularly by lean development principle [5] implemented at companies like Toyota [6], Honda [7], knowledge management strategies development by Takeuchi, Nonaka [8], Hitotsubashi Business School in Japan and Peter Senge [9] at MIT.

4 Adopting Scrum

This first section describes how an enterprise can adopt scrum. If we did not have habit to do things differently, then learning the usage of scrum would be pretty simple and straight forward. To get the benefits of scrum changing the enterprise habits and culture is necessary.

4.1 Role of Enterprise to Adopt Scrum

Enterprise has to believe scrum as part of the game of product and software development. Scrum provides the playing field and rules for playing the game. Working with scrum is purely matched with playing game of ruby. The developing people of the enterprise are considered as players in the game who has to go on the

field given with scrum and play in opposition to the competition. If the people are skilled, it gives good results. Otherwise, it gives worse results which will be painfully obviously. This may be due to the lack of communication among team members, improper understanding of rules, or having any other defects in the capabilities of the team members. When using scrum everyone in the team can identify improvements that are essential such as more coaching, training, and better teamwork.

If scrum is used all over the enterprise, then wide game of product development throughout the enterprise is more effective. If a single team is playing, then managing issues are more important which is difficult to attain. Each and every time when product development takes place it helps everyone in the team to understand the need of further improvement as individual.

Adapting scrum by an enterprise helps the teams and team members of enterprise to grow as an individual and as a part of team with the characteristics of scrum. The main thing about scrum is that when it is used as process model, it helps in training all the people of enterprise about product development in an effective way. Scrum also guides them to work in small teams. To integrate this culture in enterprise, it takes around 6–12 months of time. After training people in developing products as small teams scrum focus on getting them better in their game of product development such that they are excellent as an individual and as a team member. This is a constant process of getting once strength to top level which may take 3–5 years of time. In this period, skills of individual and teamwork are steadily increased to higher levels. Growth of people is also observed in this period of time and the areas that are to be enhanced can be listed and sorted out.

Developing skills for an individual that helps developing team is a constant and continuous process. Unlike other software life cycles, scrum is different and has many strengths. One of the unique strength of scrum is that it represents problems that enterprise is facing. Besides finding problems it also explains the consequences that the enterprise is going to face until they are solved. This is possible in scrum because of its short iterative and increment nature, and these are referred as sprints. These sprints are easy to process as they are simple. While sprints are going on if any difference with active practice is seen which may be considered as backlogs are presented to all team members. Now the enterprise finds a solution to eliminate backlogs.

4.2 Scrum Needs a New Enterprise Culture

The scrum in theory holds changes, irregularity, and difficulty as unavoidable restrictions in all product development. These difficulties and irregularities in scrum turn into detailed long-team predictive plans worthless and waste of money. A vision of project's value is projected in baseline plane and the project moves toward the vision sprint by sprint with scrum, to optimize the possible adaptations are then made to the project.

Enterprise that is going to adopt scrum has to make a habit of working with small teams with effective communication between the team members. This is required because the team members in scrum are cross functional. The strength of the product development using scrum lies in the team. So management of the teams by the enterprise is very crucial.

4.3 Scrum Needs Huge Effort

A huge effort is required to adopt scrum, so only the enterprises with forceful reasons will make such effort. The reason for adopting scrum might be undesirable costs, missing functionality, lack of ability to delivery software in particular time the customers, developers leaving the long release cycles, or enterprise's increasing in ability to compete. The other forceful reason for using scrum is that it offers a significantly better way of building products.

Enterprise should believe that it has serious problem to fix and the scrum is the tool to help it, before an attempt is made for enterprise-wide adoption. The first step in gaining this belief is to use scrum on several projects. Scrum is very easy to understand from theory and training is also accessible. Choose some high-value, high-risk initial work, and carry out a collective iterative planning meeting which is also known as sprint planning meeting and training session, and start sprinting. At least three sprints are to be conducted, and then you can easily have room for changes. Apart from this enterprise can observe better productivity.

The above discussed are some scrum's value on simple projects. To move forward after simple project, now it is to select another project which is complicated or a project with which the enterprise is facing a problem and solve it as said above using scrum. This is started with identifying several parts of important functionality which is sufficient for get going, and this is source for product backlog. Form a scrum team and sprint them several times. By doing this, we can get required characteristics, performance capabilities, and user experience as the finished product. Calculate the cost of the functionality in the third sprint to get an estimate for the entire project. Now wait for third sprint for people on the team to know each other and the system to know that they are developing a meaningful extrapolation.

Scrum team builds several pieces of high-value, tricky functionality in the package get early information from the package whether it works according to enterprise needs or not.

4.4 Measuring the Change with Scrum

Before adopting scrum, enterprise should believe that the scrum can help the enterprise in reaching its goals and also consider the types of changes that occurred

in other enterprises. These changes are frequently more general than other predictable enterprises, because every day practices are shown as impediments.

The following are the changes and challenges that can be expected. Staff turnover will occur usually, some people just want to come to work and at the end of the day they want to go home without any worry about it. By introducing scrum the ground rules are changed, so the people are asked to solve problems in teams. Because of this some people does not like this type of work. After a period of development, changes will be particularly difficult because the problems that are more critical and present in your enterprise will be highlighted at this stage. Still they are not fixed because they are particularly well-established or difficult that the solution is hard to derive. By seeing this, some people on the project might be surprised that why they are ever boarded on the scrum process. At this point enterprise will get courage to move forward by looking back and observing the progress made. Projects are completed, software is being delivered, risks are being recognized, separated and people are working together.

Variance which is a sign of change will occur. These variations are to be expected. People will have different opinions on doing things. A new way of doing things must be considered. Because of discouraging variance by many enterprises the people are to be skilled at resolving variance. So training is need and is to be given to them to resolve this variance.

As time goes on the project management's job will vary and will be harder. Now the project managers and customers are the product owners. They are answerable for managing the projects, to maximize the values and control risk sprint by sprint. They are answerable for both success and failure of the project. If the members of senior management want to know about the running status and details of ongoing project then they have to ask the product owner but not the engineer or a project manager.

During the development process, the jobs will change. Some existing jobs will be disappeared, and the roles of the people will also be changed. For example, a project manager might become a scrum master, a functional manager will become a scrum master or product owner because functional master no longer have a function to manage contributions to the team, and the enterprise is more important than career paths.

The enterprise's primary responsibility will transfer from instruct to servant leadership. Managers are answerable for the performance of their part of the enterprise. The manager's usual strategy is to direct and instruct. They work out on what is needed to be done and express the people to do that. This development hierarchically decomposes until the underneath person is actually doing the work. The manager's responsibility is to direct and provide recourses to their staff in achieving their goals, removing complications, guiding, preparation, coaching, mentoring, and getting their people to do the work in the best they can do. The manager's responsibility in the enterprise is similar to that of a parent. Manager's role is to see that there is development in people maturity and in self-managing. These qualities can be cultured by study and experience rather than being told by someone what to be done.

Management turnover will take place. As we have seen before the management will go through significant changes and use to do outstanding difficult work. Some managers do not like the new way of working and managing, so they may go away from the enterprise. Recruiting additional people might not be a solution. When we want more work done, we often hire more people, which is not an effective strategy in reality. Adding the people to productive teams or diluting the positions of existing expert people by spreading down among new teams reduces both measured productivity and quality. Generally scrum's self-managing teams generate at least fifty percent of more productivity improvement in the first year of use and more thereafter. So, focus should be on implementing scrum fairly than adding more people.

Reimbursement strategies require to be modified. Scrum is about team brilliance but not individual brilliance. The majority of the enterprises bonus and incentive funds are allotted based on team's performance but not on individual's performance. If the team has done really good then everyone in the team is to be rewarded.

5 Limitation

Almost certainly every enterprise might have tried to put into practice new processes in the earlier period. Scrum is considered less as a process than a tool which is used to build process that is suitable for the enterprise. For every tool, there will be correct ways and incorrect ways to use it in the enterprise. The two limitations that every enterprise should keep in mind while using scrum are discussed below.

At enterprise level scrum should not be changed for any reason. Scrum is not a process which can be customized according to the way it can fit into the enterprise. It exposes every dysfunction in the enterprise. Whenever people modify scrum, it is only because that they have dashed into problem, differences that they do not want to look and fix. If they modify, the scrum it is sure that the problem remains invisible and deadly to your enterprise then you will lose the primary benefits of scrum.

The tendency of an enterprise is to plan, to wait, to over think but the tendency of scrum is to act, to build things of value and to look in and see your dysfunctions. If you have thought about these changes, consider their impact on your enterprise.

6 Conclusion

It is a better strategy for every enterprise to move according to the changes that are going on around the world in software development. Unless some important changes are made the enterprises cannot withstand the competitions in all aspects in

terms of producing successful products. Changes in the developing industry are ongoing in different areas.

In this work, successful and effective method of adopting Agile-Scrum as a new process model by an enterprise is discussed. Once if the enterprise selects scrum to use as process model the change is to be accurate and implementation is be proper. The overall change that is made by the enterprise should affect in the form of a better outcome.

Most of the software companies are seeing toward Agile methodologies because of its flexible nature. In this work, only better way of adopting Agile-scrum is discussed. It can be extended to all other methodologies which are having significant role in software product development.

References

1. Reddaiah B, Ravi SP, Movva LS. Risk management board for effective risk management in scrum. *Int J Comput Appl.* 2013;65:16–23.
2. Ravi SP, Reddaiah B, Movva LS, Kilaparthi R. A Critical review and empirical study on success of risk management activity with respect to scrum. *Eng Sci Technol: Int J.* 2012;2:467–73.
3. Schwaber K. *Agile project management with Scrum.* Redmond: Microsoft Press; 2004.
4. Schwaber K, Beedle M. *Agile software development with scrum.* Prentice Hall; 2002.
5. Poppendieck M. A history of lean: form manufacturing to software development. In: JA00 conference, Aarhus, Denmark; 2005.
6. Liker JK. *The toyota way: 14 management principles from the world's greatest manufacturer.* New York: McGraw-hill; 2004.
7. Holford WD, Ebrahimi M. Honda: approach to innovation in aerospace and automotive/pick-up truck development: a dialectical yet coherent firm. In: 40th annual Hawaii international conference on system sciences (HICSS-40) Big Island Hawaii; 2007.
8. Tekeuchi H, Nonaka I. *Hitotsubashi on knowledge management.* Singapore: Wiley; 2004.
9. Senge PM. *The fifth discipline: the art and practice of the learning organization.* Currency New York; 1990.

Review on Security Attacks and Mechanism in VANET and MANET

S. Balasubramani, S.K. Rani and K. Suja Rajeswari

Abstract Ad hoc wireless communication is an infrastructure-less network and adaptable to all environments. It is characterized by self-organizing, dynamic topology, and self-healing. These characteristics are most common for both MANET and VANET. In these networks, security is a major concern for data transmission. Ad hoc security is violated by various security attacks. In this paper, we are analyzing the common security attacks and their exploitation in various layers. The various security mechanisms and protocols are discussed in both VANET and MANET for secure data transmission.

1 Introduction

Wireless ad hoc network is one of the types in wireless communication. Ad hoc network communicates between the nodes without access point. In this communication the nodes are not present at same location, it is scattered at various location. So the routing and security in ad hoc network is a challenging one.

Ad hoc network is categorized based on the environment as, mobile ad hoc network (MANET) and vehicular ad hoc network (VANET). Based on the environmental factors these networks have different types of parameters and functionalities. MANET communicates between the mobile nodes for transmitting a packet. This network is constructed with low cost, because of the mobility and changes in dynamic topology are low compared to VANET. MANET has been used in various

S. Balasubramani (✉) · S.K. Rani · K. Suja Rajeswari
Department of Computer Science and Engineering, Valliammai
Engineering College, Chennai, India
e-mail: bala08.ap@gmail.com

S.K. Rani
e-mail: rsk1411@gmail.com

K. Suja Rajeswari
e-mail: ksrсуja@gmail.com

fields such as military applications, personal area networks, and blue-tooth, commercial sectors etc.

The communication devices (802.118.WFi) are attached to vehicles for transmitting a data in VANET. VANET has high mobility and rapid topology challenges so the construction cost of VANET is high. It is used in intelligent transport system (ITS), safety driving, collision warning, and traffic information.

Security plays an important role in an ad hoc network, some of the security goals are authentication, integrity, robustness, confidentiality, non-reputation, and anonymity.

These goals are the most challenging tasks in ad hoc networks (VANET-MANET). In an ad hoc network firewalls are not applicable, because they do not contain a boundary limit and it causes various security attacks. The vulnerability of these attacks causes droppage, tampering, modification, and hijacking, decreasing the performance of routing.

The remainder of the survey paper is presented as follows: Requirements in VANET and MANET are described in Sects. 2. Section 3 discusses about various attacks in VANET, Security mechanisms of VANET is described in Sect. 4. Section 5 discusses about various attacks in MANET, Security mechanisms of MANET described in Sect. 6 and finally the conclusion of this paper.

2 Requirements

Common requirements of VANET and MANET networks are.

2.1 Availability

At appropriate time, assets should be available to the authorized party. Some of the attacks such as denial-of-service makes use of flexible ad hoc network and prevents the information access from resources (link/path). Thus availability is a major concern which provides security to ad hoc.

2.2 Confidentiality

It is referred as privacy, i.e., the information is accessed only by the authorized parties. Confidentiality plays an important role in real-time applications such as banking, commercial, and military applications.

2.3 Integrity

During ad hoc communication, packets are transferred from source to destination, while transmission, corruption or alteration of data must be promptly detected.

2.4 Privacy

The sender identity and the personal information should not be shared with anyone else without permission.

2.5 Authentication

Authentication is an important factor to differentiate a trusted source from a malicious one. It can be provided to ad hoc network via certificates, trusted authority, etc.

2.6 Non-reputation

After the attack, non-reputation facilitates the ability to identify the attackers. This prevents the authorized node from the malicious node.

2.7 Anonymity

All the information that is used to identify the owner or current user of node should be kept private by default.

3 Attacks in VANET

Attacker uses various attacks and threats to alter and delete the data packets during the communication.

3.1 Alteration

Attacker alters the actual data within the transmission, that is, the location or position information of vehicles. The goal of an alteration attack is making the other vehicles to accept the incorrect information, which results in affecting the integrity of data and makes the vehicle to travel in a congested path.

3.2 Denial-of-Service Attack

DoS attack targets the availability of the data. In this attack, the attacker inhibits the services to a legitimate user either by blocking the communication medium or by making the resources unavailable which results in an infinite delay.

3.3 Malware

Malware is malicious software or just like viruses, which is used by attacker to disrupt the normal operation of VANET. These attacks affect the VANET environment during software updates in an on-board unit (OBU) and in a road-side unit (RSU).

3.4 Sybil Attack

Attacker creates multiple messages and sends it to other nodes and each message contains different fabricated source identity such that it creates an illusion and makes the original source unknown to other nodes. This activity forces other vehicles to take an alternative route.

3.5 Replay Attack

Replay attack is performed by non-legitimate users. In this attack, attackers fraudulently repeat the valid data transmission to take benefit of the message at the moment of its submission.

3.6 Fabrication

In fabrication attack, the attacker inserts false objects into the system. These may be a falsified position or location information to gain access to the system and ultimately degrades the authenticity of the system.

3.7 Blackhole Attack

In blackhole attack, the incoming packets are received by the malicious node, but they do not exist in the network operation. This attack happens when the actual source node drops out or refuses to participate in the network operation.

3.8 GPS Spoofing Attack

VANET maintains the location table, which contains geographic location and vehicle identities due to the global positioning system (GPS) satellite. When compared to actual satellite system, GPS satellite simulator generates stronger signal. In GPS false reading is produced by the attacker to deceive vehicles to think as if they are in different location.

3.9 Jamming

It is one of the types of DoS attack at physical level. In this attack, the attacker disrupts or jams the signal. So signal is blocked and others cannot access. This results in increased network overhead.

4 Security Mechanism in VANET

4.1 Security Using Digital Certification

This method provides secure communication between the vehicles using digital certificates. The transmission of digital certificates is done by three stages. In the first stage the communication is made between base station (BS) and road-side unit (RSU). In this process the BS has to provide certificate to RSU. In the second stage each vehicle or CAR is to be registered with RSU using regid and public key of the vehicle, finally RSU sends certificate to CAR. In the third stage vehicle-to-vehicle

communication is invoked and the corresponding vehicles transmit their certificates to each other. In this protocol the time complexity is $\theta(10)$ and also the cost is low, because the protocol uses signature, certificate, and public key.

4.2 Preventing Hole Generation Attack

This mechanism is used to prevent the hole generation attack and optimizes the routing path in three stages. Those stages are hole detection stage, hole information broadcasting stage, and secure optimal path generation stage. In hole detection stage the vehicle declares the boundaries and it is self-assigned as a boundary node. This node sends hello packet to next boundary nodes. This process continues until a hole is reached and this path is defined as a hole in the network. In the second stage the hole information is broadcasted to all other vehicles. Third stage is used to generate secure routing path. The routing path is constructed using MFR protocols until a hole is found in the network. If the hole is reached then it performs two operations. One is secure module and the other one is recovery module. Secure is used to find the genuine node and the recovery module is used to recover the malicious node from attackers. This protocol is used to recover the hole generation attack only, it does not recover other attacks.

4.3 Position-Based Routing Security

In position-based routing, security is provided using routing message protection mechanism and node evaluation mechanism. In routing message protection mechanism secure transmission of messages is done using digital signature. The signature contains the location information of the source, destination, and the data. The node evaluation mechanism is done using three steps. In the first step, it verifies the signature of the sending node. In the second stage, it records the next hop and forwards the packets. In third stage, backward evaluation is done, which is vice versa of forward evaluation.

4.4 Group-Based Authentication

This mechanism is mainly used for group-based applications like military troops. This scheme contains three phases. In the initialization phase the source is authenticated using TESLA. Initialization phase is divided into three stages that are sender setup, group membership authentication, and bootstrapping parameter transmission. In sender setup, sender secures the packet using one-way hash chain and assigns the packets according to the time interval.

In group membership authentication, group members are assigned with a group id and group certificate. These group id and group certificate are designed using MD5 algorithm. Bootstrapping transmits the packets using various parameters such as current time interval, packet encryption interval, predefined key, and commit keys. The second phase is an intra group communication. It is divided into sender operation, receiver operation and group membership update. In this communication sender sends the packets to group members and the packet is encrypted using a committed key. The receiver receives the packets and the data packet is decrypted using the committed key.

In group membership update the server generates a new keychain and multicasts it to group members so the group members are authenticated periodically with new keychain. The third phase is intergroup communication and is divided into sender operation and receiver operation. In sender operation the sender sends the packets to non-group receivers. The authentication key is signed by hash function which is known only to the receivers. The receivers receive the data packet only if the security condition is satisfied.

4.5 MAC Security

Road-side unit (RSU) aided message authentication scheme provides privacy preservation by requesting RSU for temporary ID. Temporary ID is otherwise known as pseudo ID, which is stored in RSU, is valid until the vehicle is in that particular range of RSU. Vehicles send message with private key using ECDSA signature and temporary ID. The receiver vehicle queries RSU for public key of the sender vehicle. RSU broadcasts public key of sender vehicle, after verification sender vehicle broadcasts the authenticated message. Vehicular node anonymously interacts with other nodes, so that information about the user is not known to anyone. It finds actual ID from pseudo ID and verifies it by public key certification method.

5 Attacks in MANET

5.1 Impersonation Attacks

Impersonation attacks entirely depend on authentication and confidentiality. Maintaining authentication and confidentiality is possible using a proper security mechanism. Because of the loss of these security mechanisms, here malicious node acts as a genuine node and monitors the network traffic of the sender and receiver messages.

5.2 Black Hole Attack

In this attack, routing protocol is entirely utilized by the malicious node and drops the packets instead relaying on them to claim itself being the shortest path to the destination node.

5.3 Wormhole Attack

In a wormhole attack, tunneling happens from one location to other location after the attacker records the packets at one point in the network, so routing is disrupted by the attacker indirectly.

5.4 Replay Attack

Replay attack is otherwise known as playback attack. In this attack valid data transmission is frequently repeated and sometimes maybe delayed by the attacker fraudulently. Finally it may lead to network routing traffic.

5.5 Flood Rushing Attack

Usually neighbor node receives the flood route request from the senders and only the first rushing node is forwarded to avoid duplication. This attack causes adversary reach successfully before the legitimate one. Even though proper authentication is implemented, it is impossible to prevent this attack from hackers, it may result in adversarial route from the legitimate one.

5.6 Jamming Attack

In wireless ad hoc communications valid physical transmission is interfered by the jammer. It results in blocking of legitimate traffic.

5.7 On-Off Attack

In ad hoc network, malicious entity sometimes act as good entity and sometimes act as bad entity, so it is impossible to detect this type of attack.

5.8 Modification Attacks

In this attack packet forwarding and packet integrity is modified by the malicious node by tampering its hash code or unique code, so that the receiving node discards the packet as invalid.

5.9 Selfish Behavior

An attacker depends on routing points, so that packets forwarded by sensor nodes will be dropped simply and those packets never reach the destination.

6 Security in MANET

6.1 AODV Based Security

AODV depends on distance vector routing protocol in MANET. Security in AODV protocol is based on one-way hash and two-way hash, and digital signature. To secure a AODV message an encryption algorithm with first secret key is used. In AODV protocol, first the source node generates two signs with and without key. Second, intermediate sign with and without key and then forwards to the destination node. The destination node generates sign with key and compares it with its source node. After comparison if the key value is same, destination node replies back to source node. SHA algorithm is a two-layer security algorithm which is flexible, expandable, and efficient.

6.2 Centralized Secure Routing Protocol

Centralized secure routing protocol (CSRP) considers mobile nodes (MN) and general nodes. MN in MANET architecture provide a robust secure routing protocol and acts as a third party, which provides authentication between the nodes for the purpose of communication. It creates a session key between the source and

destination. Here node sends request to MN for establishing session key with the neighbor node. Once the trusted neighbor node is found, it will reach the destination. The destination node replies back to source node through the first request accepted by neighbor. This avoids flooding and the data is secure.

6.3 Aggregate-based Path Verification

Aggregate-based path verification routing protocol (APVP) makes use of the identity-based cryptography and aggregate signature algorithm. ID-based cryptography has a private key generator (PKG) which generates a pair of keys relevant to the identity of distinct users. The PKG uses a secure channel to send private key to the owner of the identity once the generation of keys is done. The routing is secured by broadcasting the packet to its neighbor node. The secured route discovery packet (RDP) includes packet the identifier, signature, and the message with timestamp. Once the node receives RDP message and sets the reverse path, each node along with reverse path to source signs the replay (RREP). This secured routing provides the security properties of validity, authenticity, and non-impersonation.

6.4 Link-State Routing Security

In mobile ad hoc networks, optimized link-state routing is a proactive link-state routing protocol. Secured OLSR framework is designed to enhance the security in optimal link-state routing. In this framework, best MPR selection is done by means of selecting maximum reachability of the node, and threshold cryptography techniques is used to share the secret key and finally the shares can be reconstructed by using Lagrange interpolation method.

6.5 Trust Value Security

Security mechanism depends on observation-based trust value named as weight and randomized route request forwarding method. Trust value is obtained from the neighbor node and the value is stored in team leader table. Each time node sends RREQ packets to source team leader (TLS). While in secure hypercube-based team multicast routing protocol (S-HTMRP), TL selects best path based on the weight from different paths. To avoid overhead, sender node itself places in promiscuous mode after the transmission of packets. During randomized packet forwarding in on demand protocol, each route discovers the source which includes number of request

Table 1 Comparison between attacks

Attacks	Availability	Authentication	Confidentiality	Integrity	Layer
Alteration		√		√	Physical layer
DoS	√				Network layer
Malware	√				Network layer
Sybil attack		√			Network layer
Replay attack		√		√	Network layer
Fabrication		√		√	Physical layer
Blackhole	√				Network layer
GPS spoofing		√			Application layer
Jamming	√				Physical layer
Eavesdropping			√		Physical layer

(RREQ) before forwarding one long with other value and based on reply adjust parameter. To avoid attacker, place checks on the record by request messages depending on IP datagram (Table 1).

7 Conclusion

This survey provides an overview of security issues faced by ad hoc networks (MANET–VANET). Throughout the literature, we observe many security challenges still remain to be solved, to be supported, and enabled in highly secured ad hoc infrastructure and secure communication. The lack of availability, integrity, and confidentiality is due to the data packets hacked by malicious attacker. By the way, we have analyzed the security attacks in MANET and VANET.

Bibliography

1. Deng H, Li W, Agrawal DP. Routing security in wireless ad hoc networks. *Telecommun Netw Sec IEEE Commun Mag.* 2002;70–5.
2. Raya M, Papadimitratos P, Hubaux J-P. Securing vehicular communications. *IEEE Wirel Commun.* 2006.
3. Yang H, Luo H, Ye F, Lu S, Zhang L. Security in mobile ad hoc networks: challenges and solutions. *IEEE Wirel Commun.* 2004.
4. Kim Y, Kim I. Security issues in vehicular networks. *Int Conf Inf Netw (ICOIN).* 2013;468–72.
5. Kumar A, Sinha M. Overview on vehicular ad hoc network and its security issues. *Int Conf Comput Sustain Glob Dev (INDIACom).* 2014;792–7.
6. Rajakumar P, Prasanna Venkatesan T, Pitchaikkannu A. Security attacks and detection schemes in manet. *Int Conf Electron Commun Syst (ICECS).* 2014;1–6.

7. Ghosh C, Jana D, Bhaumik BB. Security challenges in reactive mobile ad hoc network. *Ann IEEE India Conf (INDICON)*. 2011;1–6.
8. Kannhavong B, Nakayama H, Nemoto Y, Kato N. A survey of routing attacks in MANET. *IEEE Wirel Commun*. 2007.
9. Varshney N, Roy T, Chaudhary N. Security protocol for VANET by using digital certification to provide security with low bandwidth. *Int Conf Commun Signal Process*. 768–72.
10. Bhoi SK, Nayak RP, Dash D, Rout JP. RRP: a robust routing protocol for vehicular ad hoc network against hole generation attack. *Int Conf Commun Signal Process*. 1175–9.
11. Hou J, Han L, Liu J, Zhao J. Secure and efficient protocol for position-based routing in VANETs. *IEEE Int Conf Intell Control Autom Detect High-End Equipment (ICADE)*. 2012;142–8.
12. Lu Y, Zhou B, Jia F, Gerla M. Group-based secure source authentication protocol for VANETs. *IEEE, GLOBECOM workshops on heterogeneous, multi-hop wireless and mobile networks*. 2010. P. 202–6.
13. Qian Y, Lu K, Moayeri N. A secure VANET MAC protocol for DSRC applications. *IEEE Global Telecommun Conf*. 2008;1–5.
14. Pandya M, Shrivastava AK. Improvising the performance with security of AODV routing protocol in MANETs. *Nirma university international conference on engineering (NUICONE)*. *Int J Comput Appl*. 2013;78(11).
15. Bhoi SK, Faruk IH, Khilar PM. CSRP: a centralized secure routing protocol for mobile ad-hoc network. *Third international conference on emerging application of information technology*. 2012. p. 429–32.
16. Wang B, Zhang J, Guo Y. APVP: an aggregate-based path verification routing protocol for the ad hoc networks. *Int Conf Comput Intell Sec*. 2008;386–9.
17. Tamil Selvi K, Kuppuswami S. Enhancing security in optimized link state routing protocol for MANET using threshold cryptography technique. *Int Conf Recent Trends Inf Technol*. 2014;1–6.
18. Dasgupta M, Choudhury S, Chaki N. A secure hypercube based team multicast routing protocols (S-HTMRP). *IEEE Int Adv Comput Conf (IACC 2009)*. 2009;1265–8.

Security of Networks Using Efficient Adaptive Flow Counting for Anomaly Detection in SDN

Gagandeep Garg and Roopali Garg

Abstract Security of network is fundamental requirement due to the rapid growth of utilization of network. SDN is nowadays the most preferred evolving networking technology. It provides higher innovation and more integration of services. Including the rapid innovation, also there lies a threat of intrusion in separate planes. Owing to open interfaces present between different planes, risks of intrusion or anonymous traffic inside the network increases. Therefore, on high-traffic networks, monitoring and measurement of traffic is a main area of concern. Several anomaly detection techniques had already been provided for this cause. But still there is a need of efficient anomaly detection methods so that network can work smoothly and intrusion-free with the proper utilization of networking resources. This paper describes a work towards enhancing the efficiency of anomaly detection method while preserving the performance of our network. Also network overhead, response time, and controller workload must be considered while applying monitoring policies. Focus will be on implementing an efficient adaptive flow counting mechanism so that anomaly can be detected dynamically, but the aggregation rules must be modified accordingly.

Keywords Adaptive flow counting · Anomaly detection · SDN traffic-aggregation · Adaptive traffic monitoring · Network measurement and management

1 Introduction

Software-defined networking provides the centralized control of network. It separates control plane from the data plane elements. With the help of different planes, it is easier to integrate new services and deploy wide number of applications on

G. Garg (✉) · R. Garg
Department of I.T., U.I.E.T., Panjab University, Chandigarh, India
e-mail: gagandeepgarg900@gmail.com

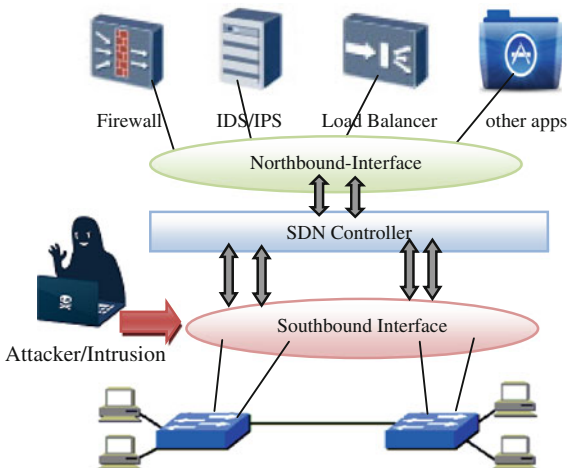
R. Garg
e-mail: roopali.garg@gmail.com

network [1]. SDN is highly flexible due to its open interfaces present for implementing higher level control programs. But, centralized control and open programming interfaces of SDN are also liable to certain level of security threats. For attackers, it is easier to apply DOS (Denial of service) attack on centralized control of SDN. Intrusion of fake packets and malicious control patterns can be inserted on open interfaces. Securing SDN from all these threats is an important task for the deployment of SDN [2]. Various techniques for security of SDN had already been proposed by different researchers. In [3], different methods for security of SDN are listed and compared. Some of these existing methods still lack in efficiency, while others lead to a very complex paradigm. Only monitoring and measurement of network traffic will be able to solve all these security concerns. Efficient set of rules for traffic measurement and monitoring must be applied for accurate monitoring. Different statistics of network traffic need to be captured and compared. These statistics can be used to detect any intrusion or anomalies in data and filter out the malicious and unauthorized packets.

SDN architecture with different planes is shown in Fig. 1 with northbound interface of SDN liable to security risks, as attacker can insert some fake traffic during the transfer of flow entries from controller to data elements. Therefore traffic monitoring must be required for security of network. Centralized control of SDN allows to implement different monitoring policies on network. In SDN, controller decides the flow paths and provides abstraction [4], so it is easier to analyze packets by applying monitoring policies. Monitoring each and every packet is also not feasible, because it will increase the overhead of the controller, and in turn response time also increases. This can lead to degradation of network performance. To overcome this problem, such a scenario is required in which proper balance between monitoring overhead and performance of network can be maintained.

For resolution of this security problem, several solutions had been provided by many researchers for monitoring the network traffic. To reduce the overhead,

Fig. 1 SDN Architecture with possible intrusion interface



analysis of packets using random sampling technique is proposed in [5]. In this work, routers selectively decide the random sample of packets from whole traffic and analyze only those packets instead of each and every packet. This method can reduce overhead, but during heavy traffic, it is likely to miss small flow entries which can lead to presence of undetected anomalies in network. Other method proposed in [6] implements the packet sampling on port scan mechanism for each and every switch. But it was still unable to reduce the complexity of monitoring policy and overhead while maintaining performance. In [7], an adaptive flow counting method for anomaly detection is proposed which provides such efficient technique to detect anomalies adaptively. Its adaptive method for updating flow counting rules for aggregation of traffic can detect anomalies while reducing the monitoring overhead.

The rest of paper is organized as follows: In Sect. 2, existing work for adaptive anomaly detection mechanism and motivation towards this technique is defined. In Sect. 3, overview of the existing algorithm and proposed method for improvement of that algorithm is provided. In Sect. 4, implementation setup used for the algorithm is discussed including results obtained by implementing rules. Finally in Sect. 5, paper is concluded by discussing the importance of adaptive technique and future works on it.

2 Motivation

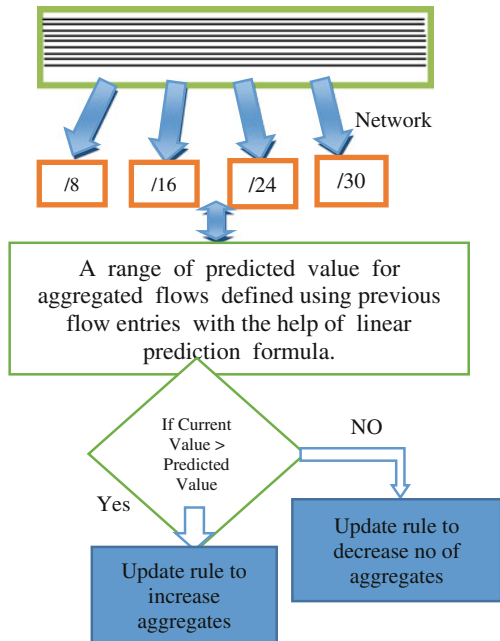
SDN dynamic flow rules updating feature motivates us towards the work of dynamically flow counting for anomaly detection. Also it draws inspiration from previously proposed methods for mitigating and detecting anomalies in our network. In [8, 9], several methods are implemented various topologies using netflow for detecting anomalies. Entropy as summarization tool is used for aggregation and classification of traffic by supervised learning for detection of DOS attack. In [10], scenarios defined for efficient anomaly detection guided us for using statistic collection for applying monitoring policies. In [11], rate-limiting and maximum entropy detection methods are used for four prominent traffic anomaly detection algorithms. In [12], tradeoff between overhead and performance is mentioned. Considering all this work, a redefined algorithm with greater efficiency and reduced complexity is defined in [13]. In this work, proposed efficient algorithm will be discussed, implemented, and evaluated.

3 Algorithmic Overview

Adaptive anomaly detection is able to maintain a proper balance between network performance and monitoring overhead. Using this technique it is easier to monitor the traffic according to the workload on the controller and also able to act dynamically according to traffic patterns. In this adaptive flow counting algorithm

for anomaly detection, initially traffic flows from the network captured on the basis of subnet prefix and aggregated accordingly. Subnet prefix can be divided into further smaller chunks according to network requirements, i.e., heavy traffic network or lesser traffic network. A range of value is predicted by using the previous network flows using the linear prediction formula. Each aggregate is then compared with its predicted value with certain parameters like packet size, header space length, etc. If current computed value of aggregate is greater than predicted value, then it is required to update the aggregation rule to increase the number of aggregates, i.e., it needs finer granularity of checking for anomalies. There can be anomalies present in that traffic so it is required to divide aggregates into smaller chunks. It increases overhead but detects anomalies accurately. It also covers the small flow entries. On the other hand, if current value is less than the range of predicted value then it means that network traffic is free from anomalies. Hence size of aggregates can be increased to reduce the controller overhead. This adaptive mechanism is presented in Fig. 2. Therefore this adaptive technique is best suited for our accuracy, performance, and overhead requirement. This mechanism will also reduce the complexity of existing adaptive flow counting algorithm given in [7] by reducing the step of setting flags on each aggregate; as in this algorithm, we are dynamically updating the rules instead of setting flags for updating rules.

Fig. 2 Adaptive flow counting mechanism for aggregation



4 Implementation and Evaluation

Owing to very large scale network traffic, it is very difficult to capture real-time aggregates for research work. Anomaly detection and dynamic rule updating model is being developed in this research. A fundamental controller-based simulator has been developed for the simulation model using the MATLAB environment. The simulator has been divided into various components such as controller, topology builder, packet generator, and data propagation.

4.1 Controller Module

The controller module is the kernel of the simulator model and handles all of the data being transferred between the nodes in the topology. The simulator nodes have been programmed to share the data via the controller module. The controller module collects the information about the datasets.

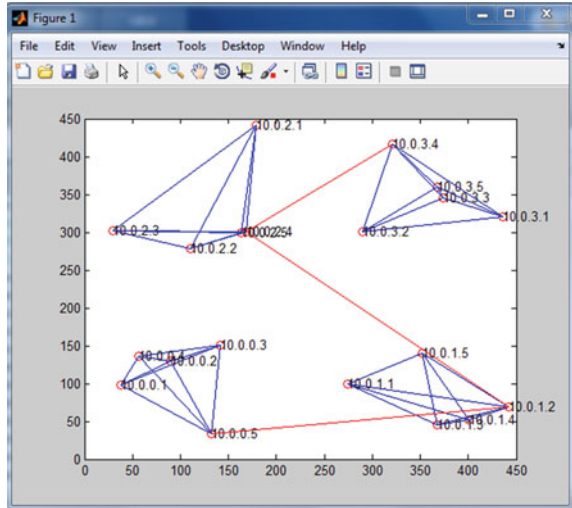
4.2 Topology Builder

This module creates different topologies for our network. It is configured for dynamically choosing different topology each time, so that it can be related to real-time network scenario. Snapshot of network topology created in MATLAB is shown in Fig. 3. Four different subnets have been created and connected to each other with different random gateways. Further inside every subnet, three node-to-node dynamic-link connections are deployed for each node. In these snapshots, a graph is plotted with 2-D plane to show different subnets in different quadrants. Only four subnets have been chosen for better representation of the network inside the graph to reduce the complexity of the understanding of connections. Red circles denote the nodes present in the created topology and each node is represented with IP address assigned to it. Blue lines represent the links between nodes in particular subnet whereas red lines represent the gateway links between different subnets. The algorithm must be applied on more complex topology with greater number of subnets.

4.3 Packet Generator

Packet generator can generate packet of any number of bytes packet size randomly, which also covers very small or very large packets. It can decide the payload size dynamically.

Fig. 3 Topology builder module



4.4 Data Propagation

In this data propagation module, data is propagated from one node to controller and then that data will be analyzed and forwarded to different nodes as shown in Fig. 4. This module encapsulates data and converts it into binary form and vice versa.

Data is transferred between two subnets by using random gateway decided dynamically. This gateway link will be created while creating topology by topology builder module. Controller gathers statistics on transfer of data as data paths are decided by the controller. Results of gathered statistics on controller for different transfers are shown with the snapshot taken using MATLAB in Figs. 5 and 6. In these statistics, number of bytes transferred per flow and number of packets transferred per flow are captured along with the source IP and destination IP address. In these snapshots, captured traffic is from source-IP 10.0.03 and 10.0.0.1. However, data from any IP address can be captured instead of these particular ones. These gathered statistics can further be used for the implementation of our algorithm.

5 Conclusion and Future Work

Security of SDN is real necessity for further deployment and expansion of software-defined networks. For securing SDN, it is required to maintain the integrity of data by ensuring that proper monitoring of network data can be done. Hence efficient anomaly detection methods need to be implemented. Such tight monitoring can still cause monitoring overhead on network and reduce the performance of network. So adaptive mechanisms need to be followed to monitor the traffic efficiently and change the behavior dynamically according to the results.

Fig. 4 Working of simulator on collected data

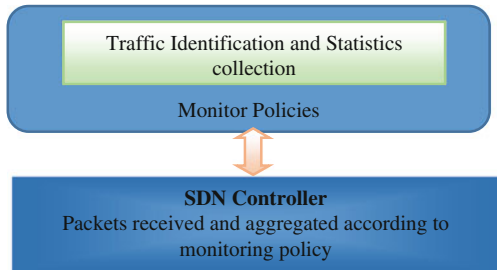


Fig. 5 Statistics gathered for Source-IP 10.0.0.3

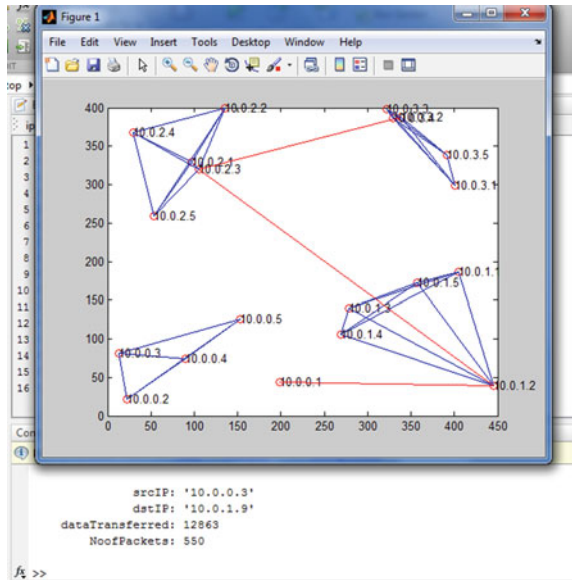
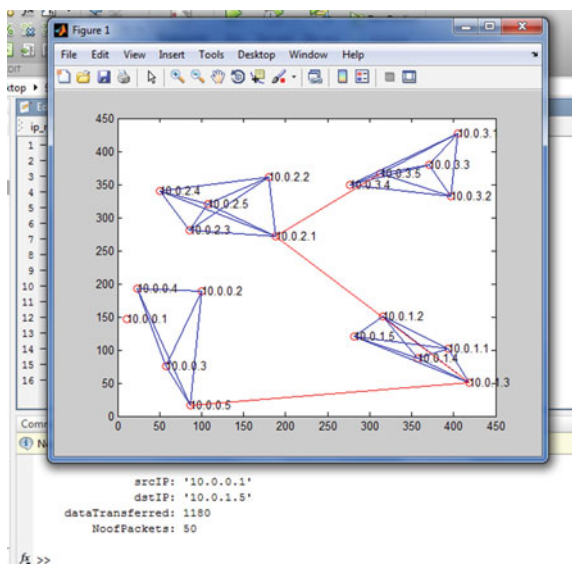


Fig. 6 Statistics gathered for Source-IP 10.0.0.1



Adaptive mechanism implemented in this work will perform with greater accuracy and also be able to maintain balance between monitoring overhead and performance of network. This efficient algorithm reduces the complexity of existing algorithms by eliminating overhead of setting flags on the aggregated data. This algorithm will cover the small flow entries as well as heavy network traffic. In future, the evaluation of its real-time results for anomaly detection on captured data can be made and can be compared to results of the existing solutions. Further some parameters like sampling rate of packets for aggregation on traffic can be considered. Also minor changes on these parameters can vastly affect the accuracy and performance.

Acknowledgments I would like to give my sincere gratitude to all the friends and colleagues who were helping me to conduct this research, without whom this research would be incomplete.

References

1. Betts M, Fratini S, Davis N, Dolin R. SDN architecture. In: Open networking foundation ONF SDN ARCH 1.0 06062014. Issue 1 (2014).
2. Akhuzada A, Ahmed E, Gani A, Khan MK, Imran M, Guizani S. Securing the software defined networks: taxonomy, requirements, and open issues. In: IEEE communication magazine. 2014.
3. Garg G, Garg R. Review on architecture and security issues in SDN. *Int J Innov Res Comput Commun Eng.* 2014;2(11):6519–24.
4. Bozakov Z, Papadimitriou P. Towards a scalable software-defined network virtualization platform. In: IEEE network operations and management symposium. 2014. p. 1–8.
5. Zseby T, Hirch T, Claise B. Packet sampling for flow accounting: challenges and limitations. In: Passive and active network measurement. Lecture notes in computer science, vol. 4979. Springer. 2008. p. 61–71.
6. Mai J, Sridharan A, Chuah CN, Zang H, Ye T. Impact of Packet Sampling on Portscan Detection. *IEEE J Selected Areas Commun.* 2006;24(12):2285–98.
7. Zhang Y. An adaptive flow counting method for anomaly detection in SDN. ACM Digital library. In: Proceedings of CoNEXT, Santa Barbara, California, USA. 2013. p. 25–30.
8. Banford P, Kline J, Plonka D, Ron A. A signal analysis of network traffic anomalies. ACM Digital library. In: Proceedings of SIGCOMM IMW'02. 2002. p. 71–82.
9. Lakhina A, Crovella M, Diot C. Mining anomalies using traffic feature distributions. ACM Digital library. In: Proceedings of SIGCOMM, Philadelphia Pennsylvania, USA. 2005. p. 217–228.
10. Giotis K, Androurlidakis G, Maglaris V. Leveraging SDN for efficient anomaly detection and mitigation on legacy networks. In: Proceedings of third European workshop on software defined networks (EWSN), Budapest, Hungary. 2013.
11. Mehdi SA, Khalid J, Khayam SA. Revisiting traffic anomaly detection using software defined networking. In: Recent advances in intrusion detection. Springer. 2011.
12. Moshref M, Yu M, Govindan R. Resource/accuracy tradeoffs in software-defined measurement. ACM Digital Library. In: Proceedings of HotSDN'13, Hong Kong, China. 2013. p. 73–78.
13. Garg G, Garg R. Detecting anomalies efficiently in SDN using adaptive mechanism. In: IEEE, International conference on advance computing and communication technologies (ACCT2015) Rohtak, INDIA. 2015.

A Novel Low Power Multiply–Accumulate (MAC) Unit Design for Fixed Point Signed Numbers

N. Jithendra Babu and Rajkumar Sarma

Abstract In the emerging technologies the low power designs play a critical role of operations. Our proposed work is on the low power MAC unit that is used to find the fixed point signed numbers. The proposed design is to achieve high throughput and low power consumption. Our proposed work has various building blocks like firstly, Wallace tree multiplier since a multiplier is one of the key part for the processing of digital signal processing systems and secondly an accumulation block. Since the output from the multiplier and adder is to be efficient, we proposed a BCD block that is used to convert the output into BCD number. The overall MAC is performed in the cadence virtuoso 90 nm technology and performance analysis of each individual block is examined using the cadence virtuoso before designing the overall MAC unit. Power, delay and power-delay product are calculated using the Cadence Spectre tool.

Keywords BCD · Fixed point · Multiply–accumulate unit · Signed number

1 Introduction

MAC refers to the multiply–accumulate unit that is the basic block in many of the digital signal processing systems for basic arithmetic operations. For any real-time processing, to achieve the high throughput and speed, the MAC unit is the basic block. From the past decades, the concentration of designers are more focused on the speed but due to technological development, low power designs have been the major considerations in designing integrated circuits. The main investigation of our work is to design a low-power and high-speed multiplier–accumulator (MAC) unit. The MAC unit is the basic consideration in any of the digital filters. Due to this, MAC unit has now become the basic and essential building block for the processing

N. Jithendra Babu (✉) · R. Sarma
Lovely Professional University, Punjab, India
e-mail: jithendra.lpu@gmail.com

systems. To design the low-power MAC unit we have considered the various architectures of the multipliers and adders. Since, the multiplier is a key element for the multiplications in the MAC unit and the accumulation unit is designed using the various considerations because the function of MAC unit is to multiply the N -bit input values from the memory location and accumulates the output of the multiplier with the previously accumulated value that is stored in the accumulator register.

Further this accumulation block is composed of various blocks as accumulation adder and accumulation register in which a register has been used for storing the data within the time synchronization, such that the register is designed using the low power hybrid flip-flop which reduces the overall power reduction of the system. This hybrid flip flop is designed using a novel ultra-low leakage CMOS circuit structure called sleepy stack. The function of mac unit is expressed as

$$Z = \sum_{i=0}^{n-1} a_i b_i$$

This paper is organized as follows. Section 2 describes the multiply–accumulate unit. Section 3 describes the proposed work of our design using the various techniques. Section 4 describes the proposed mac architecture for sign numbers. Section 5 describes the experimental analysis. Section 6 describes the power-delay analysis.

2 MAC Unit

The main concerns of the signal processing system are multiplications and additions, the multiplier and accumulator is the basic building block for any of the digital signal processing systems. For this, MAC architecture represents the various functions of the different blocks for the high speed throughout the system for an efficient processing of the signals. Basically, the MAC is a DSP processor which is used for high-speed signalling such that the different blocks of the MAC unit should also perform the high-speed operations. This can be achieved by considering the different parameters such as power, speed and area. The block diagram of the MAC architecture is represented in the Fig. 1 [1–7]. Here an N -input bits of two sets are fetched from memory and given as input to the multiplier block which performs the multiplication and produces the $2N$ -bit output as input to the register block which stores the data and sends the data to next level as input to the adder. This adder performs the adding operation by adding the output from the register block with the previously accumulated value that is stored in the accumulator register. Thus, the output from the adder is given to the accumulator register and the overall output is taken from the output of the accumulator register which is stored in the feedback register for next step. In the architecture of the MAC unit the blocks is considered to be of a high speed and low power consumption. The multiplier and

adder circuit is designed by considering the various architectures and the final MAC unit is designed by using those individual blocks.

3 Basic Blocks in Our Design

3.1 Multiplier

In any of the signal processing systems the main concern depends on the multiplication of two numbers. So, multiplier plays a vital role in such type of signal processing systems.

While designing multiplier architecture we should first consider the speed (because for any digital system the speed is the main consideration) and the second important aspect is power. Due to this we have implemented the multiplier which is

Fig. 1 Basic MAC unit [1]

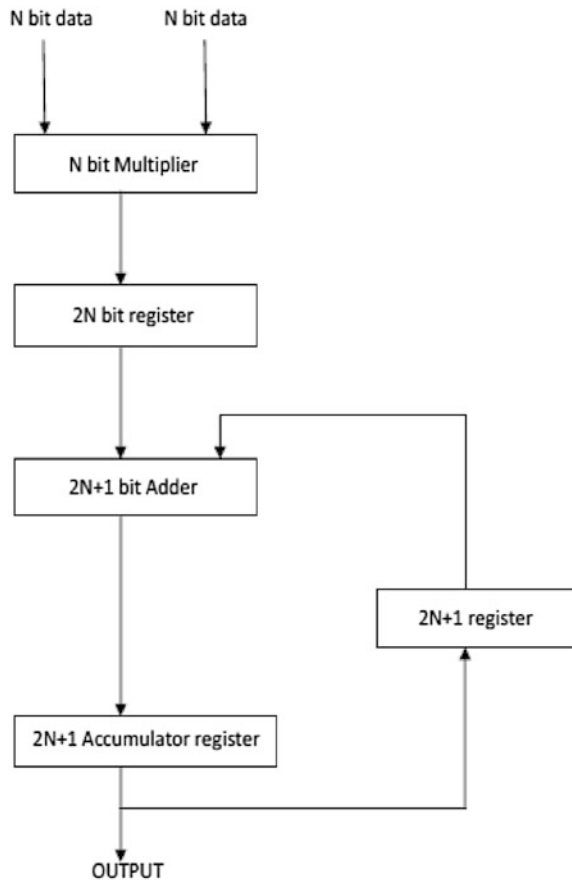
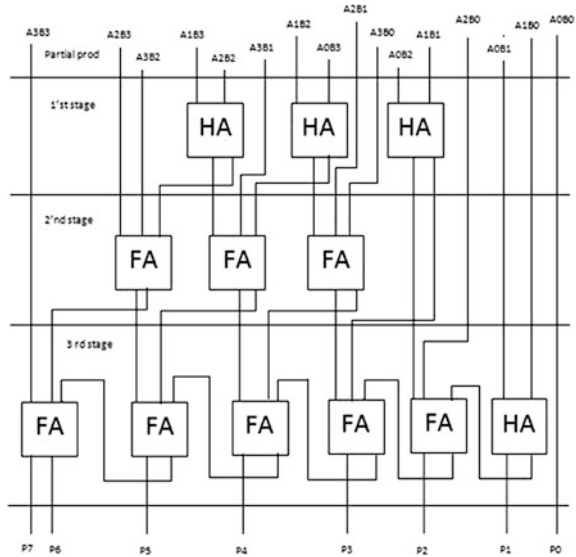


Fig. 2 Wallace tree multiplier [8]



based on Wallace tree algorithm known as Wallace tree multiplier [8]. The multiplier has efficient speed and less power dissipation when compared to other multiplier architectures. The Wallace tree multiplier architecture for a 4-bit is shown in Fig. 2 is:

1. At the very first step the partial products are multiplied by using the AND gates.
2. Half adder is used to add the two partial products.
3. At the last full adders are used which is used to produce the final result by using a simple Ripple carry architecture.

3.2 Binary to BCD

The proposed design is to convert the output of the multiplier block into the binary coded decimal format. Since, the multiplier multiplies two values that is fetched from memory and gives the output as binary format. So, there is a need for the conversion of binary values to BCD logic. The proposed designed is implemented using the basic logic gates as AND, XNOR and full adders. The output from the XNOR block passes through the AND gate whenever one of the input of XNOR gate is always high. Depending on the XNOR output the AND gate passes the BCD value as an output which are consecutively added by the full adders.

3.3 Adder

Adder is the most important part of the processing units such as arithmetic unit, signal processing unit, etc. In addition to these, the adders have important considerations in applications such as digital system architectures and processing units, etc. The basic arithmetic operations such as add, sub, multi and divide are implemented using adder as a basic building block [9].

Due to this, the design of a high-performance full adder with low power dissipation is necessary. The adder circuit is the basic block in our proposed work for adding the current output value from the multiplier block with the previously accumulated value that is stored in the accumulator register. Our adder is of 9 transistors which enhances high speed and low power dissipation throughout the circuit while compare to the other full adder architectures [9]. With the modification in W/L values of the transistors in the 9-transistor full adder circuit, provides better efficiency in the output. The modification of the W/L values in the adder circuit is done because the proposed architecture is scaled down to design in 0.9 m technology. The proposed adder is used to design our multiplier block and adder circuit that adds the output from the multiplier and previously accumulated value and is used in the design of our BCD block.

3.4 BCD Block

The proposed BCD block is to maintain the overall output of the MAC unit to be in the binary coded decimal format. The BCD block is designed using three 2:1 MUX, two 4:1 MUX, etc. The BCD block is used in two combinations in our proposed architecture as the first combination is used before our adder block which maintains the output of the first register block to be in BCD format and the second combination is used after the adder block which again helps in maintaining the overall output of the MAC unit to be in the binary coded decimal format. The proposed block diagram is shown in Fig. 3. The proposed design works according to the following combinations:

1. If the inputs i_3 and i_7 of BCD block are 0 s, then it is directly bypassed to the output of the BCD block.
2. If the i_3 bit is 1 and i_7 bit is 0 then input is converted by adding 0110 to the LSB at the first stage and OR with 1001 to the input LSB bit and considering it as a select line and adding 0110 to MSB bit at the second stage from the output of MUX block and passed to the output.
3. If the i_3 bit is 0 and i_7 bit is 1 then input is converted by adding 0110 to the MSB bit and OR with 1001 to the input MSB bit and using it as select line to MUX block and passing the output.

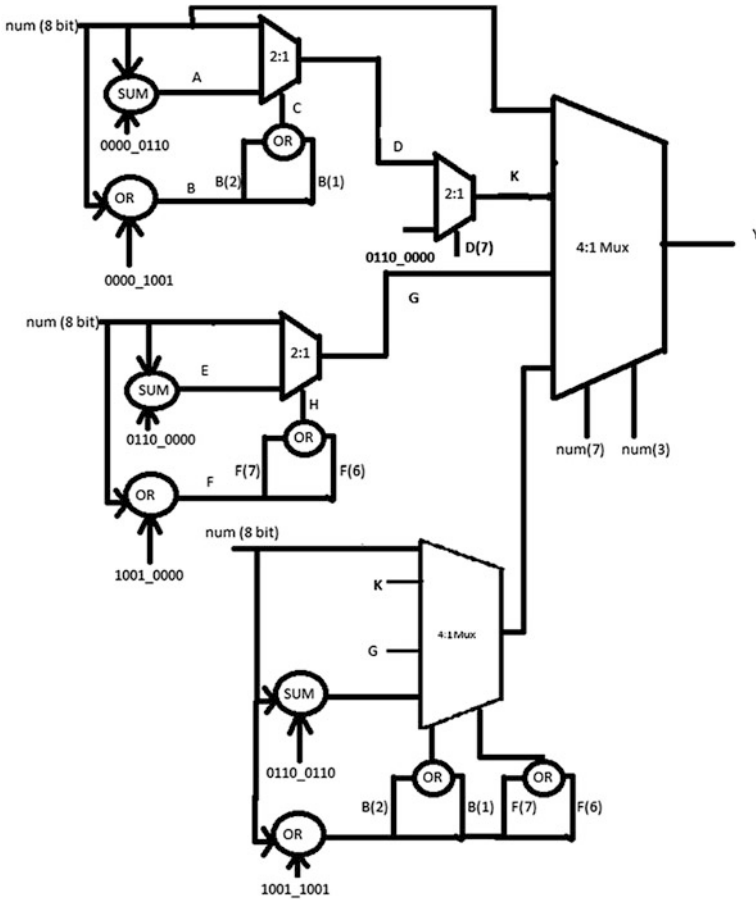


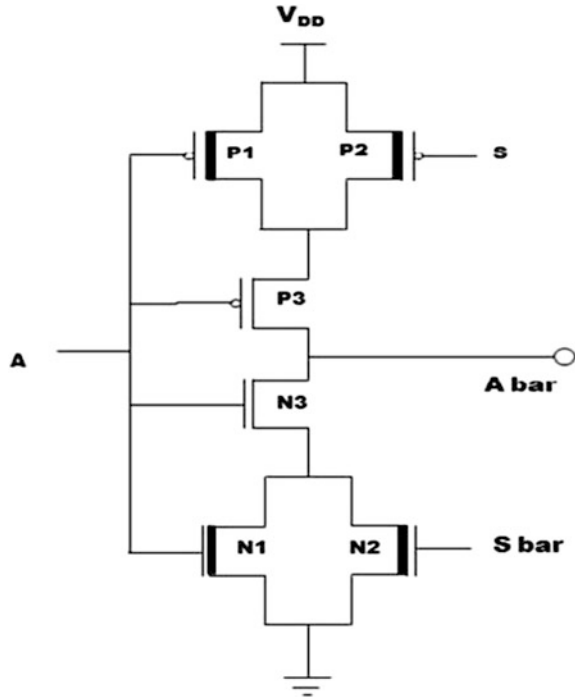
Fig. 3 BCD block

4. If the i3 and i7 bit is 1 then we are checking for all the combinations that are explained in the above steps by using a 4:1 MUX as first three inputs and last input will be by adding 01100110 to the input at the first stage and OR with 10011001 to the input and using it as a select line to pass the output.

3.5 Sleepy Stack Inverter

The sleepy stack inverter is a combination of two techniques one is forced stack and the other is sleep transistor technique [10]. As we know that for any low power design the main consideration of the work is to reduce the power dissipation and to eliminate leakage currents that occur while the transistor is in off mode.

Fig. 4 Sleepy stack inverter [11]



To eliminate this effect in our proposed design we are using the sleepy stack technique [11]. The block diagram is shown in Fig. 4.

3.6 D Flip-Flop

The D flip-flop here we are using is designed using the sleepy stack technique which enhances high switching speed and less power dissipation and low leakage currents through the register unit [11]. In the digital circuits the storing of data is done with the flip flops or latches. So, the design of D flip-flop has to be maintained at low power and high switching speed. The flip-flop design used in our architecture has two phases of operation [11]. The design is based on a conventional dual dynamic flip-flop which enhances the high switching speed throughout the circuit [12]. The function of d flip-flop is that it maintains the output which follows the input whenever our clock pulse is high. So the flip-flop designed here is a positive edge triggered hybrid node flip-flop [11]. The block diagram is shown in Fig. 5.

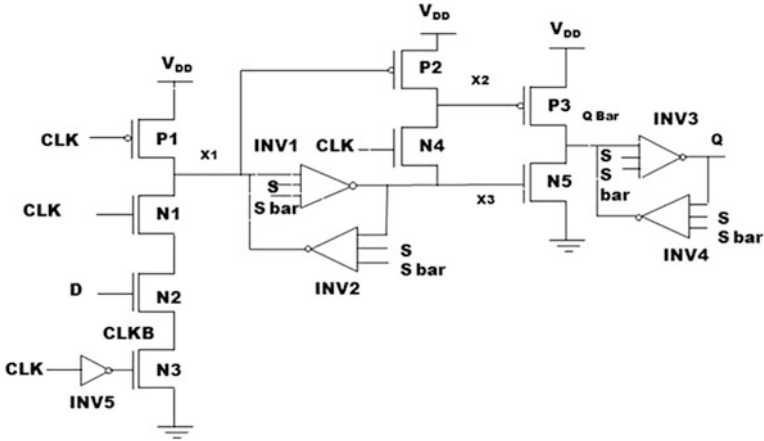


Fig. 5 Hybrid flip-flop [11]

3.7 Accumulator Register

The term accumulator or register refers to a flip-flop or latches which is used to store the one bit data. In our proposed work the accumulator register is used to store the outputs from the multiplier output which is an 8-bit and the overall MAC output which is an 12-bit used for the successive addition of the previous consecutive values with the adder circuit. The accumulator register consists of D flip-flop, basic gates that are operated by clock synchronization. The register cell has 3 inputs and 1 output. The inputs are D, Wsel and Rsel and Q will be the output. The flip-flop will store the input value when Wsel is 1, if Rsel signal is 1, then the flip-flop will pass the value that is stored using a tristate buffer to the output. In our proposed work the D flip-flop is implemented using a technique called DDFF, which is a hybrid flip-flop that uses sleepy stack technique for less power dissipation and low leakage currents which occurs during the storing of data in the register block [1]. The block diagram is shown in Fig. 6.

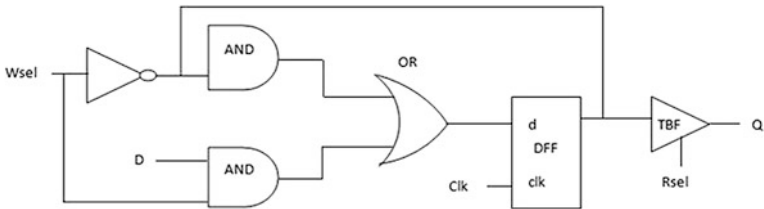


Fig. 6 1-bit register

4 Modified Architecture for Fixed Point Unsigned and Signed Numbers

4.1 *Unsigned Number Architecture*

Our proposed MAC design function is that it multiplies the two values and then adding with the previously accumulated values that is stored in the accumulator register. Here we have proposed two architectures, one is for unsigned number and the other is for signed number. The architecture for unsigned number will be as follows. The inputs of two sets of 4-bit BCD are fetched from the memory and are given to the multiplier and produce an output of 8-bit. The output from the multiplier is passed through the 8-bit register which stores the data for a certain time and reads the data to the next level during the next transition time. The output from the register block is passed to the BCD block which helps in retaining the inputs to be in BCD format and passed to the adder circuit. The adder circuit performs the addition operation with the previously accumulated values that are stored in the register and sends the data again to the second BCD block which helps in maintaining the overall output of the MAC to be in the BCD format through the output of the accumulator register. Here the BCD block, adder and the second register combination is of 12-bit. The proposed block diagram is shown in Fig. 7.

4.2 *Signed Number Architecture*

Here in the proposed design the multiplier multiplies the two sets of BCD value and passes the value to the adder at which the input for the adder circuit will be positive number or negative number. Depending on the sign bits that are taken at input sets will be ex-or with each other and defines that the product can be directly bypassed or complemented. The term 0 in the MSB indicates the positive number and the term 1 in the MSB bit indicates the negative number. So there is a need for eliminating the negative numbers and to make it as a positive number.

The modified architecture of MAC deals with the fixed point sign numbers. Our proposed modified architecture has the same architecture as if used in the fixed point representation. There is a small variation that the proposed architecture deals with the sign numbers so necessary blocks are synchronized into the fixed point architecture. The proposed architecture additionally uses a binary to BCD converter block and three multiplexer blocks which deal with the sign numbers. The function is that the product coming from the BCD block will be 10's complemented and discharged through the MUX block by using sign bit as a select line and the previous accumulated value that is stored in the register to be 10's complemented

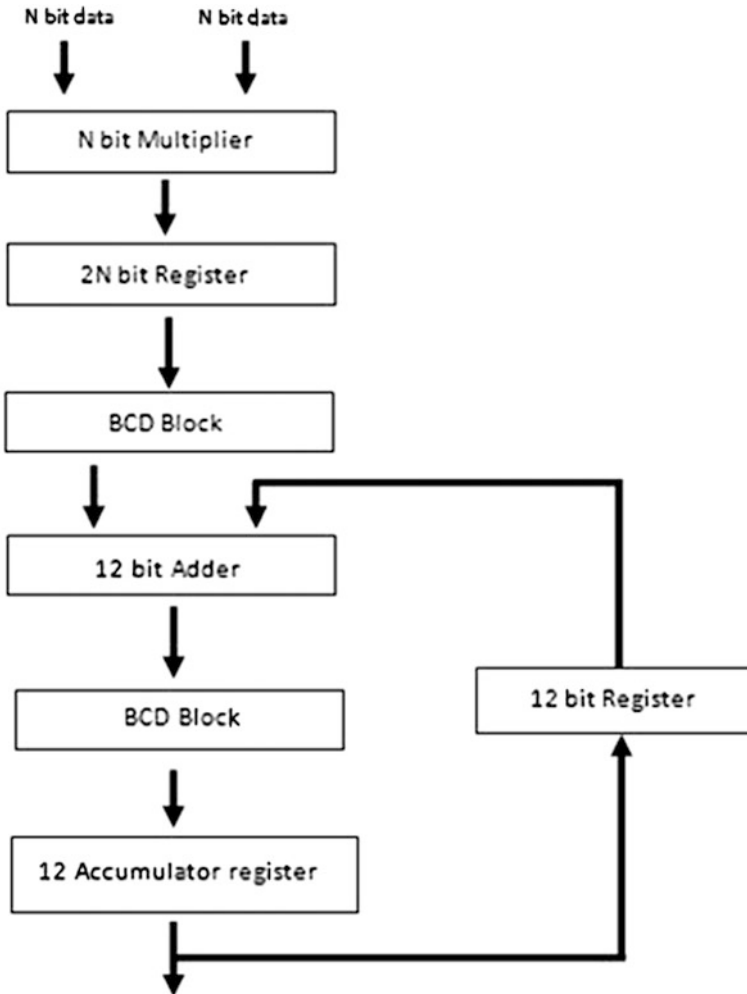


Fig. 7 Proposed MAC for unsigned numbers

and passed through another MUX by using the higher most MSB as a sign bit. The outputs from the MUX blocks are added using an adder circuit and it is passed through the MUX by taking the other input as complement of adder output by using 10's complement and sign bit from the higher most MSB bit of the adder output and the MUX output is passed to the BCD block as done in the fixed point architecture. The MAC architecture for signed numbers is shown in Fig. 8.

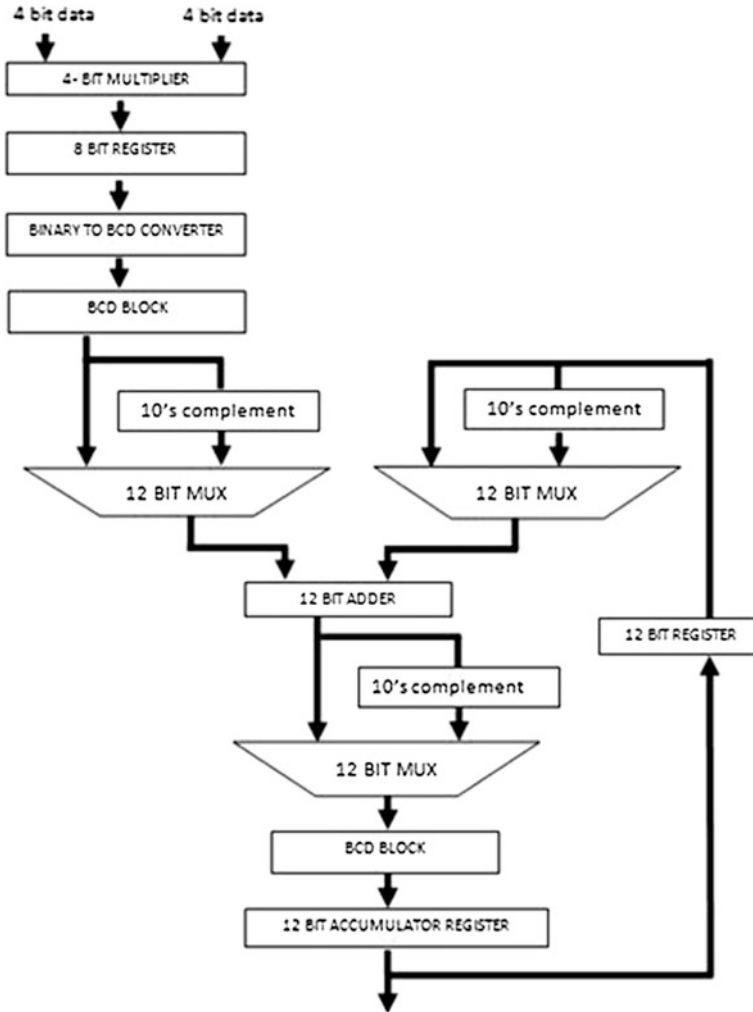


Fig. 8 Proposed MAC for signed numbers

5 Experimental Work

5.1 Unsigned Architecture

The entire MAC unit is implemented in cadence virtuoso at 90 nm technology. First the individual blocks that are the key parts of the mac unit have been designed at the virtuoso and the performance has been verified by considering the parameters power and delay. At last the individual blocks are connected according to the architecture which produces the overall architecture of our fixed point

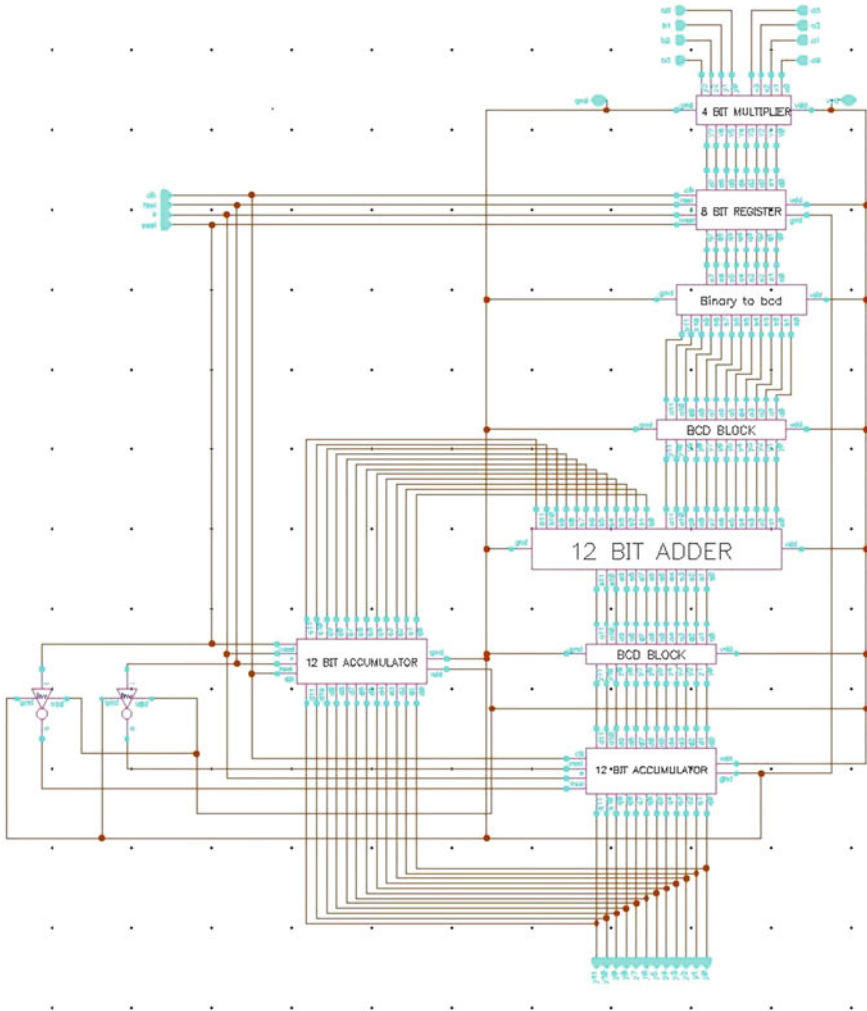


Fig. 9 MAC schematic for fixed point unsigned number

representation. The MAC unit is designed at the cadence virtuoso 90 nm technology and the following considerations are done. The overall time period of our proposed design is to be considered at 100 ns and our input bits are considered to be varied from the 40 to 20 ns and the clock gating for the register unit is taken as a positive edge clock. The Wsel and Rsel of the register unit are inverting and varying with the time response of the input bits. The working of MAC unit is as follows the multiplier multiplies the two sets of 4-bit values and produces the output as an input to the register block during the time response of 20 ns. In the register unit during the

positive edge clock $Wsel$ is taken as 1 which writes the input data to my register block at 0–20 ns after the completion of writing the data into the register block $Wsel$ is disabled and $Rsel$ is enabled which reads the data at 21–40 ns and passes the output to the binary to BCD block. The binary to BCD block converts the output of the multiplier to the BCD format where it is in binary format. The BCD block maintains the exact BCD logic and passes the value to the adder. The adder circuit adds the current input with the previously accumulated value that is stored in the register and sends to the BCD block. Here again the BCD block maintains the input to be in BCD value in the same time response and passes to the 12-bit accumulator register which reads the data from 41 to 60 ns which is the overall output of our fixed point Mac unit shown in Fig. 9.

5.2 Signed Architecture

The entire proposed MAC unit for the signed numbers is implemented in cadence virtuoso at 90 nm technology shown in Fig. 10. First the individual blocks that are the key parts of the mac unit has been designed at the virtuoso and the performance has been verified by considering the parameters power and delay. At last the individual blocks are connected according to the architecture which produces the overall architecture of our fixed point signed number representation.

The MAC unit is designed at the cadence virtuoso 90 nm technology and the following considerations are done. The overall time period of our proposed design is to be considered at 100 ns and our input bits are considered to be varied from 40 to 20 ns and the clock gating for the register unit is taken as a positive edge clock. The $Wsel$ and $Rsel$ of the register unit are inverting and varying with the time response of the input bits. The working of MAC unit is as follows the multiplier multiplies the two sets of 4-bit values and produces the output as an input to the register block during the time response of 20 ns.

In the register unit during the positive edge clock $Wsel$ is taken as 1 which writes the input data to my register block at 0–20 ns. After the completion of writing the data into the register block $Wsel$ is disabled and $Rsel$ is enabled which reads the data at 21–40 ns and passes the output to the binary to BCD block. After the conversion of binary input to the BCD output the values are sent to the BCD block. The BCD block maintains the exact BCD logic and passes the value to the multiplexer where our original product will be sent or the complement of the product will be passed through the MUX where the select line will be the AND of $B0$ and $B3$ bits of the XOR output of signed bits. At this time there will be parallel execution of the previously accumulated value whether to send the accumulated value or the complement of it through the MUX depending on the $B3$ and $B0$ of the higher MSB of the accumulated value. The outputs from the MUX are passed through the adder circuit. The adder circuit adds the outputs of the two MUX and

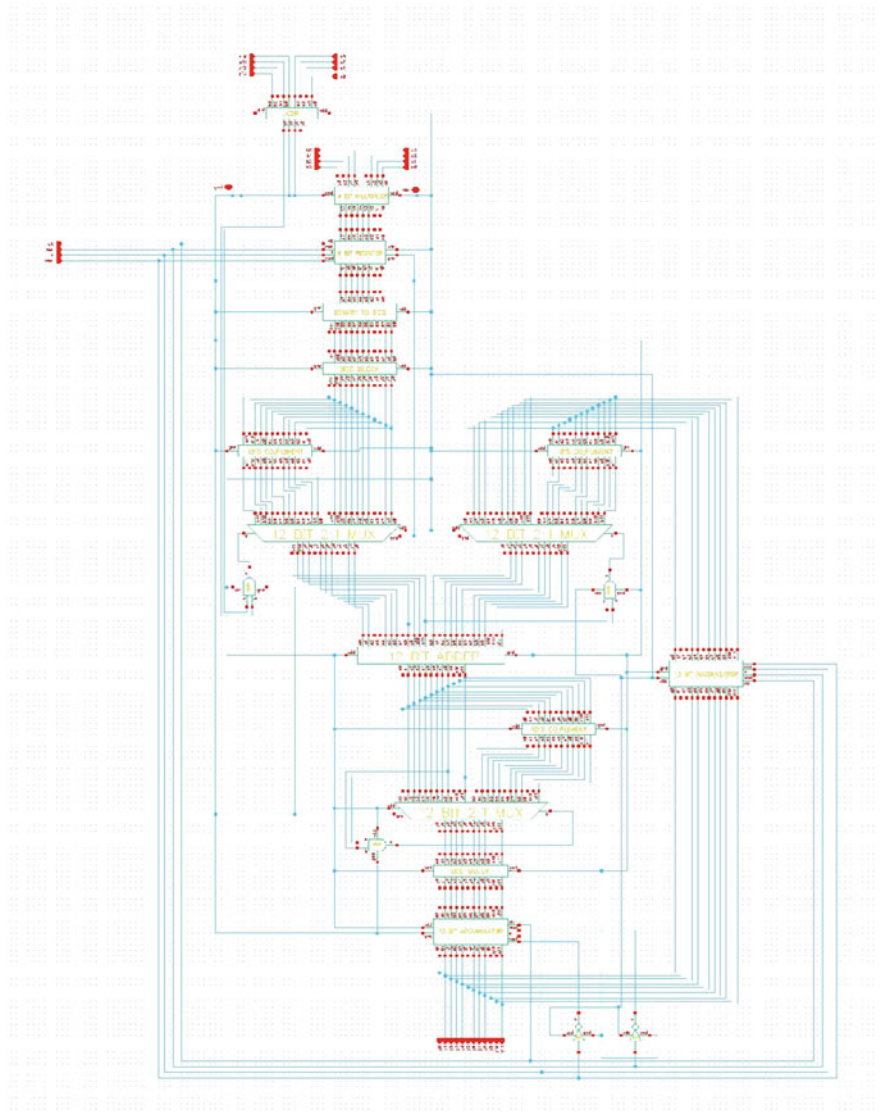


Fig. 10 MAC schematic for fixed point signed number

sends to the BCD block depending on the higher MSB bits through the MUX. Here again the BCD block maintains the input to be in BCD value in the same time response and passes to the 12-bit accumulator register which reads the data from 41 to 60 ns which is the overall output of our fixed point Mac unit.

6 Power-Delay Analysis

The MAC unit is stimulated in cadence spectre tool and analysed the power, delay and power-delay product using the spectre stimulator of each individual block and the overall MAC unit. The MAC unit is stimulated at a supply voltage of 0.9, 1.2, 1.8 V and power, delay are calculated at the three different supply voltages are shown in Tables 1, 2 and 3.

Table 1 At 0.9 V

Block	Power	Delay	PDP
4-bit multiplier	28.58E-6	20.09E-9	574.17 fs
8-bit register	7.583E-6	20.05E-9	152.03 fs
Binary to BCD	1.76E-3	5.888E-9	10.362 fs
BCD	476.5E-6	1.37E-9	652.80 fs
Adder	21.31E-6	106.3E-12	2265.25 as
12-bit register	7.11E-6	20.06E-9	142.62 fs
Unsigned MAC	1.033E-3	40.2E-9	41.52 ps
Signed MAC	5.507E-3	207.1E-12	1140.4 fs

Table 2 At 1.2 V

Block	Power	Delay	PDP
4-bit multiplier	95.1E-6	20.12E-9	1913 fs
8-bit register	16.13E-6	20.05E-9	323.4 fs
Binary to BCD	4.694E-3	1.308E-9	6.13452 ps
BCD	1.206E-3	869.8E-12	1048.9 fs
Adder	53.03E-6	75.73E-12	4015.9as
12-bit register	17.13E-6	20.05E-9	343.4 fs
Unsigned MAC	2.974E-3	80.13E-9	237.9 ps
Signed MAC	14.24E-3	40.16E-9	571.87 ps

Table 3 At 1.8 V

Block	Power	Delay	PDP
4-bit multiplier	410.6E-6	20.13E-9	8265.3 fs
8-bit register	181.1E-6	20.05E-9	3631 fs
Binary to BCD	17.17E-3	2.671E-9	45.86 ps
BCD	4.658E-3	657.9E-12	3064.4 fs
Adder	183.2E-6	58.79E-12	10770.3 as
12-bit register	143.6E-6	20.05E-9	2879.18 fs
Unsigned MAC	13.29E-3	80.1E-9	1064.5 ps
Signed MAC	51.52E-3	40.11E-9	2066.46 ps

7 Conclusion

The proposed MAC architectures for the fixed point signed and unsigned numbers are implemented at the cadence 90 nm technology. As the technology is scaled down there is a need to individually analyse the blocks of the MAC unit. The different blocks of MAC were designed and analysed to determine the power and delay. Since MAC is a digital signal processing element the design of the MAC in the cadence virtuoso environment is done successfully by varying the W/L ratios of the transistors wherever needed by doing the parametric analysis. The power, delay and power-delay products are calculated using the cadence spectre for unsigned number and signed number architecture by transient analysis. In our proposed design the inputs and output waveforms are huge and is difficult to put in the paper and the power, delay and power-delay product analyses are done based on the above waveforms. The proposed work of our paper will be on the floating point MAC architecture and the clock synchronization for the overall MAC.

References

1. Shanthala S, Kulkarni SY. VLSI design and implementation of low power MAC unit with block enabling technique. *Eur J Sci Res*. ISSN 1450-216X.
2. Kharate AB, Grumble PR. VLSI design and implementation of low power mac for digital FIR filter. *Int J Electr Commun Comput Eng*. 4(2) REACT-2013, ISSN 2249071X.
3. Sen A, Mitra P, Data D. Low power mac unit for DSP processor. *Int J Recent Technol Eng (IJRTE)*. 1(6);ISSN: 2277-3878, January 2013.
4. Abdelgawad A. Low power multiply accumulate unit (MAC) for future wireless sensor networks. 978-1-4673-4637-5/13/ 2013 IEEE.
5. Deepak S, Kailath BJ. Optimized MAC unit design. 978-1-4673-5696-1/12/ 2012 IEEE.
6. Jagadesh P. Design of high performance 64 bit MAC unit. In: 2013 International conference on circuits, power and computing technologies [ICCPCT-2013], 978-1-4673-4922-2/13/ 20 13 IEEE.
7. Francis T, Joseph T, Antony JK. Modified MAC unit for low power high speed DSP application using multiplier with bypassing technique and optimized adders. *IEEE* 31661s.
8. Shanthala S, Prasanna Raj C, Kulkarni SY. Design and VLSI implementation of pipelined multiply accumulate unit. In: *IEEE International conference on emerging trends in engineering and technology, ICETET-09*.
9. Mishra S et al. On the design of high-performance CMOS 1-bit full adder circuits. In: *International conference on VLSI, communication and instrumentation (ICVCI)*. 2011.
10. Park JC, Mooney III VJ. Sleepy stack leakage reduction. *IEEE Trans Very Large Scale Integ (VLSI) Syst*. 2006;14(11).
11. Evangelene H. A novel low power hybrid flip op using sleepy stack inverter pair. In: *Science and information conference, London, UK*. August 27-29, 2014.
12. Abdelgawad A, Bayoumi M. High speed and area efficient MAC unit for digital signal processing applications. 1-4244-0921-7/07 @ 2007 IEEE.

Optimizing Technical Ecosystem of Digital Marketing

Smitha Rao, V. Srivatsala and V. Suneetha

Abstract In recent times, marketing products has taken a new dimension and also become a greater challenge. Rapid and steep growth of technology like mobile, internet, and TV has opened new avenues for producers to advertise and market their products to have maximum and far reaching impact. Digital marketing involves the promotion of products through the digital channels and reaching the end consumer at the right time, right place through right channel. The three main pillars of digital marketing are content, data, and technology. Balanced optimization of these components results in an effective digital marketing strategy. Engaging the consumer through digital channels globally with region-specific campaigns is cost-effective, with high return on investment, thus organizations are adopting digital marketing as a priority over traditional form of targeting through print media or mails. Digital media has huge and deep impact on the people of the world. Digital marketing is as much a challenge as it is an opportunity for businesses around the globe. This paper highlights the technical components of digital marketing and various challenges and opportunities to optimize the performance of it.

Keywords Digital marketing · Balanced optimization · Real-time bidding · Opportunities · Optimization of digital marketing

S. Rao (✉) · V. Srivatsala · V. Suneetha
DSCASC, Bangalore, India
e-mail: smitha_rao_ms@yahoo.com

V. Srivatsala
e-mail: vsrivatsala123@yahoo.co.in

V. Suneetha
e-mail: sunimca@yahoo.com

1 Introduction

In today's times, marketing a product has become a greater challenge than the earlier times. The rapid and steep growth of mobiles, Internet, and TV has invariably made us dependent on the digital media to market our products. Digital media has huge and deep impact on the people of the world. It has far and global reach compared to the traditional medium of marketing. Digital media includes TV, internet, mobile phones, smart phones, iPad, PDAs, etc. Digital marketing is as much a challenge as it is an opportunity for business all over the world. More than the product, the content regarding the product has deep impact on the consumer. Content marketing is the norm of the today's digital world. How to make the content attractive and specific is one of the challenges of digital marketing. Managing huge amount of data generated on the internet due to innumerable web clicks, millions of transactions, purchases etc., is the biggest challenge the businesses face today. The producer reaches the end consumer to market his product through the marketer. How does the marketer reach the customer in an effective way, and engaging the customer, hence earn his loyalty to this/her products and in turn increasing ROI is the main concern of the digital marketer.

In this research paper, Sect. 2 briefly discusses about the concept and tools of digital marketing, Sect. 3 focuses on the opportunities and challenges in the arena of digital marketing. Section 4 discusses optimization of the technical ecosystem for an effective implementation of digital marketing, and finally conclusions are drawn in Sect. 5 (Fig. 1).

Fig. 1 Pillars of digital marketing



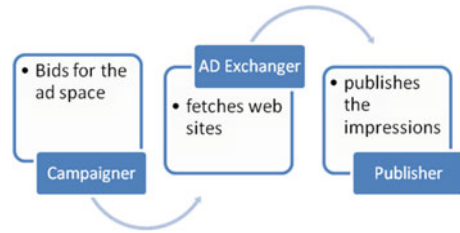
2 Concept of Digital Marketing

Digital marketing involves the promotion of products through the digital channels and reaching the end consumer at the right time and right place through right channel. The various channels are television, web, mobile phones, emails, search engines, and social media, and also through videos promotion is done. The impressions placed on these various channels albeit through various electronic devices reach the consumer. Engaging the consumer through digital channels globally with region-specific campaign is cost-effective, with high return on investment, thus organizations are adopting digital marketing as a priority over traditional form of marketing through print media or mails. Content marketing, online campaigns, social media marketing, mobile marketing, e mails, and search engine marketing are all the effective ways of digital marketing. The key players involved in digital marketing are the end consumers, the advertisers, the media companies, the ad exchange, and finally the data providers. The advertisers places the impressions on the preferred channel, the media companies make the impressions more creative, and ad exchanges bridge the gap between the advertisers and the publishers. The focus of digital marketing is content and data. “Content marketing is a strategic marketing approach focused on creating and distributing valuable, relevant, and consistent content to attract and retain a clearly defined audience—and, ultimately, to drive profitable customer action,” as mentioned in [1]. Marketing a product with content describing it attracts the consumers and holds their attention. Another very essential entity is data. Data-driven marketing is the core of the marketing strategy to engage consumers in an effective way. The voluminous data collected from various web clicks, searches, mobile apps, transactions, purchase history, enquiries etc., takes the form of ‘Big data.’

The analysis of this data helps the advertiser in targeting consumers in a more personalized way. Various demographics collected like age, race, gender, and income are used to target the consumers. There are various tools and technologies used in digital marketing.

2.1 Ad Servers

An ad server is a web server with its own database storing exclusively ads and ad-related content. These ads are rendered to the web site whenever a user visits a web page of a web site. The content of web page is refurbished with new ads, whenever the user refreshes/revisits the page. Ads and ad content are nothing but banners, images, plain text, or even animations. The motive of an ad server is multifold. First, it serves ads to the web page on request, second to manage an ad space on the web site independently and most importantly helps in providing an independent tracking system for the advertisers. There are other important functions of an ad server like report generation and keeping an track of number of clicks on a ad campaign (this will in turn assist in calculating the ROI for an advertiser for a specific web site) [2].

Fig. 2 Real-time bidding

2.2 Real-Time Bidding (RTB)

The essence of the digital marketing is the real-time bidding protocol between the campaigner (demand) and the supplier (publisher) ad exchanger as the medium between them has a huge opportunity for the digital marketer to grab the coveted ad space in coveted web sites. The bidding is real-time process happens in real time. The advertiser sets up his system with all the desired criteria. Ad exchanger tries to get the web sites that match these criteria. The advertiser bids for the space in these web sites (Fig. 2).

2.3 Data Management Platform

Data management platform or DMP is an integrated solution which is coming to the fore now, to handle the huge influx of data. Advertisers, marketers are collecting more and more data from various sources like social media, response to ad campaigns, feedback system, etc. This huge data collected has to be processed to transform it into useful information. This requires a technology-driven solution, a centralized control to collect and manage this data and that is where DMP steps in [3].

2.4 Machine Learning Algorithm

The present day marketer is looking to engage consumers in more personalized way. This has become a challenge to him as the consumer data is becoming voluminous and rapidly growing. To effectively gauge the consumers' response to their offers and engage them in a more personalized way the machine learning algorithms are used. These algorithms similar to data mining are used to search patterns in the data and thus reach consumers in a more effective and personalized way [4].

2.5 *Web Analytics*

There are millions of users visiting the web site which publishes the ad campaigns. Web analytics is a way of collecting data on the usage of web and analyzing this data to gain insights to optimize the web usage.

2.6 *Web Content Management Systems*

These web content management systems are software which aids the naïve advertiser to design their own web sites with relative ease without having the knowledge of the web development languages. This encourages an average small business owner to resort to digital marketing.

2.7 *Big Data Analytics Including Social Media Analytics*

The data created as a result of innumerable web clicks, transactions, searches, purchases, reviews, comments, likes, posts, etc., is unstructured, semistructured and also structured. This data called as 'Big data' is has large volume, grows with high velocity, and has high veracity. This data is analyzed extensively to gain insights into the consumers' behavior. Tools like Hadoop, R, SaaS are used to do so, which include collecting, filtering, storing, and finally analyzing the big data to gain insights thus helping the advertiser to make strategies.

3 Challenges and Opportunities in Digital Marketing

3.1 *Challenges in Digital Marketing*

Major challenges in Digital Marketing include:

3.1.1 *Return on Investment*

The major concern of the marketer is the ROI. The ad campaigns must be effective enough to convert the clicks into business. Whether the ad campaigns are effective enough to turn the clicks into business is the analysis the average marketer has to grapple with. Increasing the ROI is the ultimate aim of any marketer. The success or the failure of the ad campaign cannot be measured by ROI but it definitely influences (Fig. 3).

Fig. 3 Opportunities and challenges in digital marketing



3.1.2 Consumer Retention and Loyalty

Retaining a customer once he purchases a product and earning his “loyalty” is a major challenge. As the customers’ mood, habits may change frequently, it is difficult to prevent customer churning. Strategy to retain the customer and earn his loyalty to the product is a major decision the marketer has to take.

3.1.3 Consumer Behavior

Capturing and analyzing the behavior of the consumer helps the marketer to get to know the consumer and also target him in a more personalized and specific way. The marketer has to dynamically change his strategies with changing behavior and mood of the consumer. Predicting consumers’ likes and dislikes is a very difficult task.

3.1.4 Post-Sale Customer Service

Marketing a product through the ad campaigns, impressions and thus capturing the consumers’ interest are not the end of all. Once the consumer purchases the product the marketer has to also support the consumers through the customer support. Post-sale consumer service is a challenge to the marketer as it impacts the customers’ satisfaction and thus also influence his decision to keep coming back in the future to purchase the products.

3.1.5 Privacy and Security Concerns

The biggest concern for the consumer in the digital marketing world scenario is the privacy and the security of the consumer data. Legal issues in tracking the customers are being researched by the experts and protecting the consumer and the company at the same time are also the biggest concern of the digital marketing world. Consumers' demographic data including the browsing habits of the consumer is tracked constantly by marketers and thus target them with the relevant impressions. The consumers want to adopt "do-not-track" software installed in their machines to protect their data. More and more customers are installing software to block the nontargeting ads. The data collected by the companies are used in different ways such as to send the customer personalized messages, to improve their services, or market more of their products. Malicious use of this data is a hazard to the consumer. The marketer has to try to market his products and thus also ensure the data provided by the customer is secured, thus making himself more trustworthy. Consumer data once protected has potential for the marketer to be more personalized and trustworthy. The customer also has concerns over the security over the payment mode. The payment mode statistics for online shopping show that most of the online shoppers use credit card, debit cards, cash-on-delivery, e-wallets etc., for payment. All the payments made online are susceptible to fraud or other hacking issues [5].

3.1.6 Management of Data

The management of data generated by the innumerable clicks, transactions, purchases, and searches is a huge challenge. The technology as mentioned in the Sect. 2, data management platform is key to this. Various channels are the source of the data. To collect, filter, and store this data requires a platform or an ecosystem which does all this.

Campaign Response Data

The marketers' one of the concerns are the management of the campaign response data. The various reviews, opinions, likes dislikes as a part of the response to any ad campaign put out by the marketer are a major factor in gaining insights into the consumer mood and behavior. This data has to be given the utmost priority and has to be analyzed in an extensive manner. Analytics in the form of what the consumer likes about the product, dislikes about the product, improvements he would like to see in the product etc., are some of the insights a marketer could gain. The insights help the marketing team in designing a better ad campaigns and also manufacturing better products.

3.1.7 Marketing Technology

Technologies used in digital marketing have to be upgraded and constantly monitored for their performance and have to work in tandem with the analytics team and in turn marketing team. Optimizing these technologies to increase efficiency in creating better ad campaigns is the challenge.

3.2 Opportunities in Digital Marketing

The main opportunities in digital marketing, that if harnessed would have a far reaching impact are:

3.2.1 Content Marketing

Content marketing is marketing the product to the right kind of customer with relevant, useful, and attractive content regarding the product; to garner, profits are the essence of content marketing. The marketer can design the strategy to answer to the needs of customer not just providing facts about the product. Marketers can design strategies to create content using innovative language, diagrams, and pictures to market the products. To provide quicker and better understanding about the products, the content can be shown as an INFOGRAM. Info graphics are the new strategy of content marketing, which include 3D visualization of the product, top to bottom detailed view, etc.; thus new innovative strategies are an opportunity to target customers in better efficient way.

3.2.2 Hyper Personalization

“Hyper Personalization refers to the use of data to provide more personalized and targeted products, services and content,” as mentioned in [6]. Earlier times, the companies used to collect the profile data about the consumers using third parties. The advent of technologies and cross-channel platforms the advertiser can collect the data from multiple channels and target the consumer in a specific way and more personalized way. The data can be collected from mobile phones and a user profile can be created. Also the devices that have sensors fitted in them provide information like location of the device, the usage patterns of the device, even the weather can be gaged based on the location. The variety of data, i.e., location helps the advertiser to target the consumer in a specific way, i.e., he is at a station or a market or shop thus targeting him with location specific ad campaigns. The usage patterns of the consumer provide the advertiser an opportunity to target with ad campaigns related to games or technology or cooking or books etc. Even the weather at the consumers’ location could be used to target him with ad campaigns. Consumers’

data collected is grouped into segments, and these segments are analyzed in detail by studying the patterns. The marketers have to be highly alert to the conversations taking place in the various social media to gauge the mood of the consumer and thus use it to promote their brand as it is crucial. Sharing the content in the context of the consumers' needs gives the advertiser an opportunity to target the consumers' in a more personal way and thus expects a loyal consumer for a long time.

3.2.3 Customer Acquisition

Acquisition of new customers is a critical component of the digital marketing. To target the new customers, the marketer often has to gain insights into the customers' needs through specialized research, psychographic profiles, and market surveys. Analytics on the data collected from various channels help the marketers to understand who is interested in their products and thus help them to target them.

3.2.4 Divide Between Device and Physical Persona

Cross-Device Advertising

The advent of various types of devices used by consumer like the iPad, tablet, laptop, desktop, and mobile phones to search and shop for a product have posed a serious challenge to the digital marketer. The operating systems, the browsers, and the resolutions used in these devices are varied and vast thus making a marketer struggle to target audiences on these multiple platforms. The scenario of how the marketers are facing the barrier of cross-device advertising and the process of analyzing the behavior of customers who are using various digital devices is a very serious challenge. Switching between devices is the norm, posing another challenge of the tracking data from the various channels has no idea of the human behind the device used. And this challenge is more daunting, when same consumer uses varied devices to search and buy products. A challenge is to uniquely identifying the customer, to engage on more personalized way. A new technology other than cookies to identify the client can be envisaged [7].

Measuring Quality of Predictive Analysis Using Machine Learning

The data collected from the consumers is voluminous posing a challenge to advertiser in targeting a consumer in a more personalized way. The machine learning algorithms aid in this process by searching a pattern in this data and thus help in analyzing the behaviors of the consumer. The analytics are helpful to the advertiser in offering services to the consumer in a more personalized way but measuring the quality of predictions as a result of these analytics is a challenge to the advertiser and also the higher management. The failure or success of the

campaigns launched as a result of predictive analysis poses a major risk. And more often the business analyst may fail to build an appropriate predictive mode based on the data collected.

4 Optimization of Technology for Effective Digital Marketing

To effectively market a product through digital marketing, the technology used can be optimized in various aspects. This section discusses the optimization techniques.

4.1 Building Technical Ecosystem

Digital marketing involves many key players and many tools and technologies. Integrating all the technologies under one platform for effective marketing is through building ecosystems. The ecosystems aid the marketer in managing, automating, and optimizing the process of marketing to compete in the fierce world of marketing. Figure below summarizes the key technologies and players involved (Fig. 4).

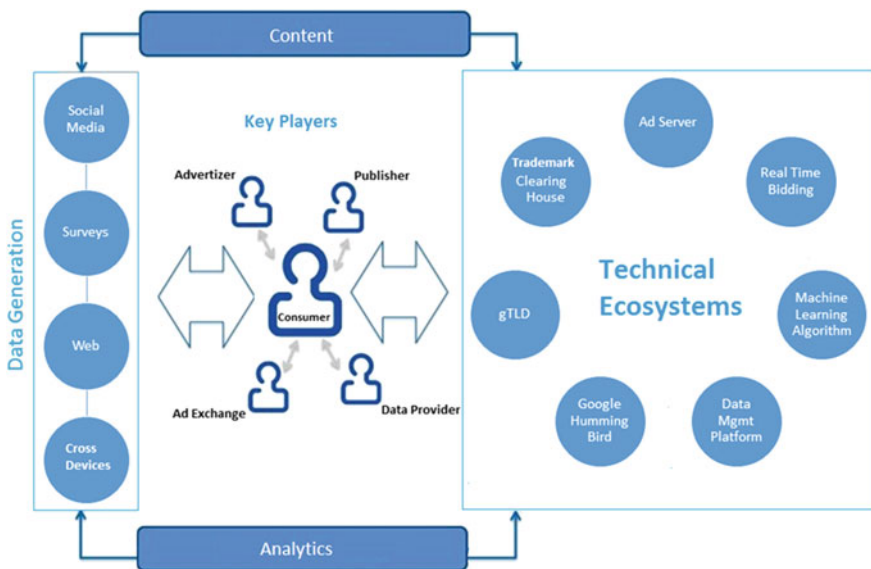


Fig. 4 Technical ecosystem for digital marketing

4.2 Optimizing Real-Time Bidding Technique

Real-time bidding protocol poses challenges like the usage of distributed systems need to be scalable, advertiser lets go of the ad exchange and directly target customer, web sites on which the ads are displayed must be of good quality, etc. To overcome the challenges the RTB process must be optimized in various ways [8].

- Adding human intuition to the protocol.
- Bid price optimization.
- Security of the user data to prevent data leakage.

4.3 Using Latest Technology to Effectively Reach the Customers

4.3.1 Generic Top-Level Domains—gTLDs

gTLDs are the most useful and unique search tool for the branding. Any brand can claim a domain name that represents it or recognizes it uniquely. The generic top-level domain helps in the expansion of the domain name system (DNS). The corporate of big and small can attract the customers through their web sites with unique names as the top-level domains. For example, the ALC Corp company can have a web site with name www.corp.ALC which will definitely stay in the minds of customers, who want to visit this website. This is one way of garnering more customers and also another unique way of marketing. This innovative technique ensures more searches by the customer and in turn more penetration into customer base [9].

4.3.2 Trademark Clearing House

The trademark clearing house (TMCH) is the rights protection mechanism, wherein the Trademark Clearinghouse protects the registered gTLDs. This also authenticates and supports the rights and claims of the companies or business which register their top-level domain. During pre-registration process, the TMCH the information collected from the rights holders are checked with the registrars and registries, so that no duplicates exist [10].

This is an opportunity and an encouragement to the small and emerging businesses to set up their own digital marketing ecosystems. And big businesses are protected and projected uniquely by their unique domain names and hence a huge opportunity for them to provide a popular and unique platform for all digital marketers.

4.3.3 Search Engine Optimization

When searching for a web site through a search engine, the tendency of the customer to look up the first ten search results and clicking the top most result is being utilized by the advertisers to target the customers by placing their ads in top ten search results. SEO which stands for Search Engine Optimization is the process of optimizing web sites (pages or the whole site) in such a way that it achieves a higher rank during search results and thus improving the chances of being noticed by the world [11, 12].

Google Hummingbird algorithm is one algorithm which helps in Search Engine Optimization; it focuses on the content or the meaning of the query rather than just keywords in the query to fetch the pages. The algorithm almost gives a human element to the query resulting in Google delivering the customer with most relevant page rather than home page or index page.

5 Conclusion

More and more marketers are adopting digital marketing over traditional marketing. The success of digital marketing lies in the reach and awareness of technology to the consumer. To target the consumer in a personalized manner to meet his needs not merely to sell him products is the aim of new age marketer. Content more than facts are presented to the consumer. Never before data collected about the consumers has taken center stage as today. Data gives insights into consumer behavior to target right kind of audience. More and more marketing solutions are being designed to help the advertisers. The marketer looks to have high ROI and research is being done to optimize technical, economical, and other aspects of digital marketing.

References

1. What is content marketing. <http://contentmarketinginstitute.com/what-is-content-marketing/>. Accessed 20 Jan 20 2015.
2. Ad Serving. http://self.gutenberg.org/articles/ad_serving. Accessed 20 Feb 2015.
3. IAB and WinterBerry Group. The data management platform: foundation for right-time customer engagement. <http://www.iab.net/DataManagementPlatforms#sthash.ZpSI5a79.dpuf>. Accessed 5 Feb 2015.
4. Sundsoy P, Bjelland J, Iqbal AM, Pentland2 AS, de Montjoye2 Y-A. Big data-driven marketing: how machine learning outperforms marketers' gut-feeling. In: Social computing, behavioral-cultural modeling and prediction lecture notes in computer science, vol. 8393, 2014. p. 367–374.
5. Arthur L. Concerns over digital privacy make us better marketers Dec 12, 2014. www.forbes.com/sites/lisaarthur/2010/12/14/concerns-over-digital-privacy-makes-us-better-marketers/. Accessed 20 Dec 2014.

6. Subramanya V. What's the hype around 'Hyper-Personalization'? <http://www.business2community.com/marketing/whats-hype-around-hyper-personalization-01045882>. Accessed 14 Oct 2014 [Feb 3, 2015].
7. eMarketer. Can marketers overcome cross-device targeting barriers? Cross-device targeting is in demand—but fragmented Dec 18, 2014. <http://www.emarketer.com/Article/Marketers-Overcome-Cross-Device-Targeting-Barriers/1011731>. Accessed 24 Jan 2015.
8. Sukornyk C. Secrets of a data scientist: five strategies for optimizing RTB Campaigns Feb 5, 2013. <http://www.chango.com/resources/articles/secrets-of-a-data-scientist/>. Accessed 20 Jan 20 2015.
9. Brands will profit from top-level domains (gTLDs). <http://www.brightlabs.com.au/page/Blog/gTLD-Top-Level-Domain/>. Accessed 20 Feb 2015.
10. TradeMark Clearing House (TMCH). <http://newgtlds.icann.org/en/about/trademark-clearinghouse>. Accessed 20 Feb 2015.
11. SEO Tutorial. <http://www.tutorialspoint.com/seo/>. Accessed 20 Feb 2015.
12. Search-engine-optimization-.starter-guide-pdf. www.google.com. Accessed 28 Dec 2015.

An Efficient Image Encryption Technique Based on Optimized Key Generation in ECC Using Genetic Algorithm

K. Shankar and P. Eswaran

Abstract Nowadays image encryption has turned into an approach to transmit interactive image information with utmost confidentiality and authenticity. In order to transmit the secret images, there are lot of image encryption techniques are available. Among these techniques, elliptic curve cryptography (ECC) is one of the fascinating techniques to maintain image information as securely and confidentially. The key generation process of the ECC method, generate the public and private key pair that is used to encrypt and decrypt an image. During the encryption process, the public key is randomly generated. In the proposed method decryption process, the private key (H) is generated by using the genetic algorithm (GA)-based optimization technique. To evaluate the performance of the image is taken as a fitness value for the optimization by using the PSNR value. Thus, the proposed method offers an optimal PSNR value compared with existing methods.

Keywords Elliptic curve cryptography · ECC · Image · Encryption · PSNR · Decryption · Genetic algorithm (GA)

1 Introduction

Information security is a significant problem to process the information over the communication medium. Because of it have some drawbacks such as illegal copying, misuses, and distribution of unauthorized multimedia contents. Cryptography is an indispensable process to protect the privacy information, which means it applies a sequence of mechanisms to enhance the security and sustain its integrity with a superior level of confidentiality and authentication [1]. In cryptography mechanism, it is used to protect private information against unauthorized

K. Shankar (✉) · P. Eswaran

Department of Computer Science and Engineering, Alagappa University,
Karaikudi, India

e-mail: shankarcrypto@gmail.com

© Springer India 2016

S.S. Dash et al. (eds.), *Artificial Intelligence and Evolutionary Computations in Engineering Systems*, Advances in Intelligent Systems and Computing 394, DOI 10.1007/978-81-322-2656-7_64

705

access. Encryption and decryption are the key concepts of the cryptographic technique. While sending an image from sender to receiver, the secrecy is protected by encrypting it. Which means the original image is converted into some unintelligible format [2]. On the receiver side the encrypted information can be decrypted into its original form by using the reverse process of encryption. The process of both encryption and decryption demands a key. Some cryptosystems uses the same key together for encryption and decryption called as symmetric key or private key cryptography and asymmetric key or public key cryptography may use different keys together [3]. The digital format of image contains some characteristics, such as redundant content of data and pixel correlation. The security of digital images attracts more consideration for its development and advantages of digital revolution [4]. Public key cryptography is based on the intractability of certain mathematical problems. ECC is one of the public key cryptographic method means that the encryption and decryption keys are different [5]. In ECC the plaintext encoding ought to be carried out before encryption and translating ought to be carried out after decoding. ECC Encryption and decryption techniques can just encrypt and decrypt a spot on the curve and not messages. The Encoding (changing over message to a point) and Decoding (changing over a point to a message) are vital capacities in encryption and decryption in ECC. It also depicts about a Koblitz's system to indicate a message to a point and vice versa [6]. A GA is the consistent and randomized search optimization technique by depending by the standard of natural assortment systems. GAs through modeling a simplified version of genetic processes used to solve complex problems [7].

2 Review of Literature

Ikshwansu et al. [8] came out with the proposal that the cryptography represents the method of concealing a message in a suitable incomprehensible design in order that the message is not visible to the naked eyes of a stranger. The safety of a public key encryption becomes stronger only if the validity of the public key is guarantee. Various Data encryption benchmarks such as the RSA and Diffie- Hellman have turned out to be incompetent on account of the necessity for a huge number of bits for the cryptographic procedure. Nowadays, the performance of ECC for encryption/decryption and authentication procedure is carried out by employing JAVA as the implementation device. It is pertinent to note that the uncivilized force ambush on ECC is impracticable on account of the discrete logarithm dilemma it contains.

Constantinopescu et al. [9] have propounded the method for a Secure E-Cash Transfer System based on the elliptic curve discrete logarithm problem. In this method, the elliptic curve discrete logarithm was used to send the secure encrypted message with their public key and receives the encrypted message which is retained by their private key.

Sindhuja et al. [10] have proposed the GA-based symmetric key cryptosystem for encryption and decryption. The basic content and the client information (key) were distorted over into content matrix and key network separately. Additive matrices were produced by including the content matrix and key network. Linear substitution capacities were connected in the additive matrix to create the transitional figure. At that point the GA capacities (hybrid and change) were connected to the transitional cipher to deliver the last cipher content. It was accomplished the symmetric key substitution strategy was utilized to guarantee secrecy in systems, which was linked and actualized with the assistance of genetic capacities to furnish included security.

Vijayakumar et al. [11] launching a novel proposition that the cryptography symbolizes the science of deploying mathematics to encrypt and decrypt the data for sheltered communication. The RSA and ECC represents the modern public key cryptography approach which is extensively employed to furnish safe data communication. A novel cryptographic technique is offered which furnished superior level of safety with minor key size and reduced computation expenditure by employing the DNA computing technique. The overall efficiency in performance of the innovative cryptography approach is assessed and contrasted with the peer cryptographic techniques.

3 Proposed Methodology

The proposed method enhances the confidentiality and secrecy of original image between the sender and receiver. From the original image the RGB (Red–Green–Blue) values are taken and create a separate matrix for each component by using their pixel values. Then the image is divided into blocks before the encryption and decryption process. Basically, the block size is 4×4 . The blocks of the each color component are encrypted by using the ECC method. The key generation process of the ECC method generates the private key randomly in the encryption and decryption process. In the proposed method decryption process, the private key is generated by applying the optimization technique which integrates the GA with it. The performance of the image is taken as a fitness value for the optimization process and here the peak signal-to-noise ratio (PSNR) value is considered. After the encryption method, the encrypted image is decrypted by using the reverse process of the encryption. When the decryption process is completed, the output image compare with the original image for evaluating their performance using the peak signal-to-noise ratio (PSNR) value, Mean square error (MSE), and correlation coefficient (CC) as quality parameters.

3.1 Elliptical Curve Cryptography

In the Asymmetric Key Cryptography, ECC algorithm is one kind of mechanism for implementing public key cryptography. In this technique, based on the curve, with specific base point and with the help of prime number function as the maximum limit an equation is evaluated, and then the encryption follows: The equation of elliptic curve cryptography is given as,

$$y^2 = x^3 + ax + b \quad (1)$$

where a, b are the integers.

In any cryptographic process, the strength of the encryption depends on the key generated. In the proposed method, there exist two types of key generation. The first process is to generate public key from the receivers end to encrypt the message and second process is to generate a private key on the receiving end to decrypt the original image.

The value “ P ” is any base point on the curve. Select a random number ‘ H ’ within the range of (1 to $n - 1$)

$$Q = H \times P \quad (2)$$

Here ‘ Q ’ is the public key and ‘ H ’ is the private key.

3.1.1 Encryption Method

In the encryption method, each color band of the input image divided into block and every block is encrypted by the encryption method. The number of blocks is represented as $F(i, j)$ where i and j are the row and column of the block of the image. The pixels $P_x(i, j)$ and $P_y(i + 1, j)$ and the point is

$$C_1 = H \times P_e \quad (3)$$

$$C_2 = (P_x, P_y) + C_1 \quad (4)$$

3.1.2 Decryption Method

In the decryption method, the private key (H) is used to decrypt the message and the point C_3 is used decrypt the pixel point.

$$C_3 = H \times C_1 \quad (5)$$

$$C_{ij} = C_2 - C_3 \quad (6)$$

The C_{ij} represents the final result of the decryption method. In this decryption process, secret key H is generated by using GA-based optimization technique. This algorithm gives best optimal key value instead of ECC method.

3.2 Genetic Algorithm (GA)-Based Optimization Technique

An algorithm starts with a set of solutions (chromosomes) called a population. Solutions from one population are taken and used to form a new population. Solutions which are selected to form new solutions (offspring) are selected according to their fitness—the more suitable they are the more chances they have to reproduce. GA optimization technique the initial solutions are finding the fitness function. Based on fitness value, the crossover is created. These individuals reproduce the offspring and after that the offspring are mutated randomly. Then the fitness value is found, and checked with the other solutions and get the optimal key to the decryption process.

.....
Steps to find Optimal Key from Genetic algorithm (GA)

Step 1: Initialize the solution H_i

$$H_i = \{H_1, H_2, \dots, H_n\}$$

Step 2: Find the fitness value (F_i)

$$F_i = PSNR + CC$$

Step 3: Cross over

Mutation (H_{new})

Step 4: Find the fitness for H_{new}

$$if (H_{new}) > f(H_i)$$

Step 5: Store the best solution so far attained

Iteration=Iteration+1

Step 6: Stop until the optimal key is attained

Then get the maximum fitness and optimal key.

$$C_3 = H_{\text{optimal}} \times C_1 \tag{7}$$

$$C_{ij} = C_2 - C_3 \tag{8}$$

The C_{ij} represents the final result of the decryption method.

4 Result and Discussions

4.1 Experimental Analysis

The experiments are conducted on a database comprising of 50 test images. The images were obtained from USC-SIPI Image Database [12]. The image results presented in this work are from the four test images, namely image 1 (Lena), image 2 (house), image 3 (peppers), and image 4 (baboon). Each image is separately encrypted and decrypted get back the original image. After the decryption process, the final output image is compared with the original image, to calculate their performance analysis by using quality parameters, such as PSNR, MSE, and CC values. The experimental result from the implementation of the proposed scheme, the original image, encrypted image and decrypted image of the image 1 (Lena), image 2 (house), image 3 (peppers), and image 4 (baboon) are represents in the Tables 1, 2, 3 and 4.

In Table 5, the row 1, 2, 3, and 4 demonstrates the analyzed results of the original images. The results of proposed method were tested with a various number of images to demonstrate that the method is more robust. The PSNR value used indicates the quality of the resultant image, whether it shows better or worse results. If the PSNR value is very high, image quality is good. Here, the PSNR qualities evolved are 58.00, 57.42, 56.68, and 58.14. It is clearly shown that the proposed method achieves the original image with the maximum PSNR value.

Table 1 Proposed method for image 1 (lena)

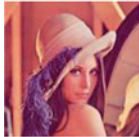





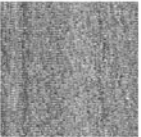


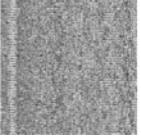

Original Image	Color Bands	Separate Bands	Encrypted Image	Decrypted Image	Final Image
	R				
	G				
	B				

Table 2 Proposed method for image 2 (house)



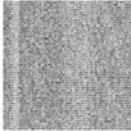






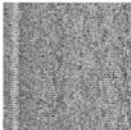

Original Image	Color Bands	Separate Bands	Encrypted Image	Decrypted Image	Final Image
	R				
	G				
	B				

Table 3 Proposed method for image 3 (pepper)










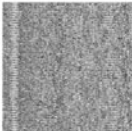







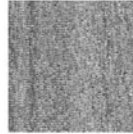


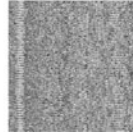

Original Image	Color Bands	Separate Bands	Encrypted Image	Decrypted Image	Final Image
	R				
	G				
	B				

Table 4 Proposed method for image 4 (baboon)

Original Image	Color Bands	Separate Bands	Encrypted Image	Decrypted Image	Final Image
	R				
	G				
	B				

Subsequently, the PSNR value maximized to 58.14 % and it's attained in 96 iterations. During the first iteration, the fitness value in GA is 46. Then the iteration is diverse while the performance besides varying with the given method, the maximum fitness of the GA projected to be 58.14. The supreme fitness of GA is 58 attained at 96 iterations. Through the GA optimization approach just specifies the perfect fitness value with the proficient results.

4.2 Comparative Analysis

The Table 6 shows the different images, performance comparison of the optimization technique is utilized to obtain the private key to the decryption process using differential evolution (DE) algorithm [13] and without optimization technique applied in the ECC. The comparison made between existing and proposed method based on significant quality parameters, such as PSNR, MSE, and CC values.

From the table above, the PSNR value of proposed method remains higher than ECC method. The image quality is improved using the proposed method. It noticeably shows that the proposed method provides the best results when compared with the existing methods.

Table 5 Performance of different images



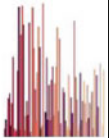


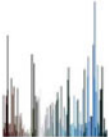
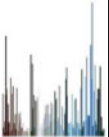



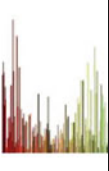





S. No	Original image	Histogram		Final mage	PSNR	MSE	CC
		Original image	Decrypted image				
1					58.00	0.10	1
2					57.42	0.11	1
3					56.68	0.14	1
4					58.14	0.09	1

Table 6 Comparison of proposed and existing methods

Images	Proposed method (ECC with GA)			ECC with DE			ECC method		
	PSNR	MSE	CC	PSNR	MSE	CC	PSNR	MSE	CC
Lena	58.00	0.10	1	50.56	1.15	1	47.81	1.42	0.97
House	57.42	0.11	1	49.16	1.11	1	46.70	1.48	0.96
Pepper	56.68	0.14	1	49.96	1.12	1	46.78	1.42	0.97
Baboon	58.14	0.09	1	50.28	1.14	1	48.90	1.33	0.99

5 Conclusion

In this paper, an efficient image encryption technique based on optimized key generation in ECC using GA has been proposed. It is clearly shown that the proposed algorithm gives better quality with average PSNR value 57.65 between original and final image. The mean square error value is minimized for all images are 0.1164; also the correlation coefficient value almost remains nearly 1 for all images. Histogram and correlation coefficient analysis extremely clear that the encryption technique without altering and maintain confidentiality of the secret image. From the proposed method, minimizing the mean square error value, the peak signal-to-noise ratio will be improved; the image quality is also improved. By using this method, the original image is shared securely and its information is maintained with the utmost confidentiality. In future, the performance of the secret image can be increased by using the any other method instead of GA.

References

1. Vinod Kumar Y, Malviya AK, Gupta DL, Satyendra S, Ganesh C. Public key cryptosystem technique elliptic curve cryptography with generator g for image encryption. *Int J Comput Technol Appl*. 2012;3(1):298–302.
2. Loukhaoukha K, Chouinard J-Y, Berdai A. A secure image encryption algorithm based on Rubik's cube principle. *J Electr Comput Eng*. 2012;2012:1–14.
3. Zhou X, Ma J, Wencai D, Zhao Y. Ergodic matrix and hybrid-key based image cryptosystem. *I J Image Graphics Signal Process*. 2011;4:1–9.
4. Kumar R, Anil A. Implementation of elliptical curve cryptography. *Int J Comput Sci*. 2011;8(4):2.
5. Gupta K, Silakari S, Gupta R, Khan SA. An ethical way for image encryption using ECC. In: *First international conference on computational intelligence, communication systems and networks*; 2009. p. 342–345.
6. Padma Bh, Chandravathi D, Prapoorna Roja P. Encoding and decoding of a message in the implementation of elliptic curve cryptography using Koblitz's method. *Int J Comput Sci Eng*. 2010;2(5):1904–1907.
7. Soni A, Agrawal S. Using genetic algorithm for symmetric key generation in image encryption. *Int J Adv Res Comput Eng Technol (IJARCET)*. 2012;1(10):137–40.
8. Nautiyal I, Sharma M. Encryption using elliptic curve cryptography using java as implementation tool. *J Adv Res Comput Sci Softw Eng*. 2014;4(1):620–5.
9. Constantin POPESCU. A secure e-cash transfer system based on the elliptic curve discrete logarithm problem. *J INFORMATICA*. 2011;22(3):395–409.
10. Pramela Devi S. A symmetric key encryption technique using genetic algorithm. *J Comput Sci Inform Technol*. 2014;5(1):414–6.
11. Vijayakumar P, Vijayalakshmi V, Zayaraz G. DNA computing based elliptic curve cryptography. *J Comput Appl*. 2011;36(4):18–21.
12. USC-SIPI Image Database. <http://sipi.usc.edu/database.php>.
13. Shankar K, Eswaran P. ECC based image encryption scheme with aid of optimization technique using differential evolution algorithm. *Int J Appl Eng Res*. 2015;10(55):1841–5.

Optimization of Fuel Consumption and Emission for Hybrid Electric Vehicle

Soham Dey, Sushma Kamlu and Sudhansu Kumar Mishra

Abstract This paper presented the application of genetic algorithm (GA) and simulated annealing (SA) for parameter optimization of parallel hybrid electric vehicle (PHEV). The proper selection of optimal size of vehicle's power train components not only improves its performance but also increases the fuel efficiency and hence enhances the cost-effectiveness. The parameter optimization of PHEV to achieve two long-range goals such as reduction of fuel consumption and toxic emission is a very challenging and interesting problem. The problem becomes a more realistic and difficult one due to the inclusion of lots of design variables, nonlinear constraints, etc. The performances of the above mentioned two optimization techniques have been compared and the simulation results demonstrate the superiority of GA over SA to solve the challenging constrained optimization problem in PHEV.

Keywords Parallel hybrid electric vehicle · Optimization · Genetic algorithm · Simulated annealing · Fuel consumption

1 Introduction

The two major problems associated with the modern transportation system are air pollution caused by emission of greenhouse gases from vehicles and continually increasing fossil fuel price. These two problems have eventually led engineers and researchers to invent an alternative vehicle propulsion system over the past two

S. Dey (✉) · S. Kamlu · S.K. Mishra
Department of EEE, Birla Institute of Technology, Mesra, Ranchi, India
e-mail: sd01041991@gmail.com

S. Kamlu
e-mail: sskadwane@gmail.com

S.K. Mishra
e-mail: sudhansu.nit@gmail.com

decades. As a result, hybrid electric vehicles (HEVs) have been emerging as the most promising solution to the above-mentioned problems so as to fulfill socio-economic demand of cleaner, eco-friendly as well as more fuel-efficient vehicle. Advanced technologies and control strategies are now being applied to decrease the fuel consumption and emission from the HEVs.

The powertrain of a hybrid electric vehicle is a very much complex system typically comprises of a conventional internal combustion engine (ICE) powered by petroleum/gasoline fuel and an electric motor powered by electrical energy storage devices such as batteries or ultra capacitors. The powertrain configurations of HEVs are mainly classified into four types, stated as follows: series HEV (SHEV), parallel HEV (PHEV), series-parallel HEV, and power-split HEV.

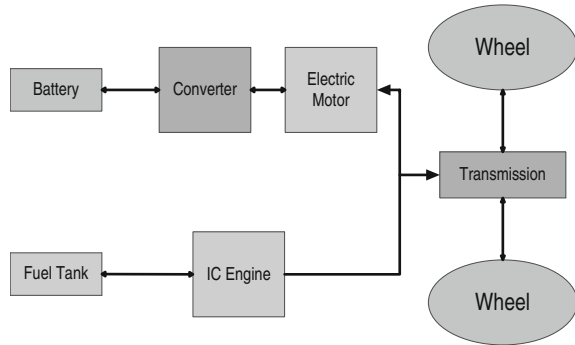
Certainly, the parameters of the hybrid electric vehicle are optimized to achieve the two long-range goals: reduction of fuel consumption and emission. But the involvement of lots of design variables, nonlinear constraints, and mutually conflicting objective functions in the optimization problem makes it very difficult as well as a challenging one [1]. Various kinds of optimization algorithms found in the recent literature have been applied to solve such a problem. Using Genetic-based methodology, Galdi et al. [2] optimized main powertrain components of HEV. Wu et al. [3] optimized the sizes of components of parallel HEVs using particle swarm optimization technique. Buerger et al. [4] used NSGA-II algorithm for multi-objective optimization of HEV parameters.

Zhengli et al. [5] suggested an optimization method based on adaptive hybrid GA for optimal sizing of series HEV. Jalil et al. [6] introduced a rule-based energy management strategy for series HEV. Lee et al. [7] proposed real-time optimization of HEVs. They have implemented fuzzy logic controller for this purpose. Wipke et al. [8] optimized the parameters of HEV using the DIRECT method and proved that DIRECT gives the best global optimal solution for HEV power control strategy. The simulated annealing algorithm was applied by Wang et al. [9] to optimize parameters of series HEV in order to enhance fuel economy and reduce emission. To minimize the equivalent fuel consumption of a power-split HEV, Liu et al. [10] implemented dynamic programming (DP) algorithm.

2 Parallel HEV Configuration

Figure 1 shows the configuration of the parallel hybrid electric vehicle (PHEV). PHEV operates with conventional IC engine and electric motor which are connected in parallel. Depending upon vehicle design and driving modes, one of the two power sources (either the electric motor or the IC engine) may be considered as the primary source of power. The battery supplies the electrical energy to the motor through a power-electronic converter. Both the electric motor and the IC engine provide mechanical energy to the transmission simultaneously and from the transmission via several mechanical coupling; energy is transmitted to the wheels which drive the vehicle. Regenerative braking is used to energize the electrical

Fig. 1 Parallel HEV configuration



power storage devices (batteries and ultra capacitors). In regenerative braking method, motor is made to act as a generator which recharges the batteries and braking torque is applied to the wheels, so that some part of the waste energy is recovered which obviously improves the efficiency of the powertrain. The electric motor and the internal combustion engine have equal importance in the vehicle’s performance. The vehicle’s maximum cruising speed depends upon the engine’s maximum power while the vehicle’s grade ability and acceleration capability is greatly influenced by the motor’s maximum power.

3 Problem Formulation

3.1 Fuel Consumption

The mathematical expression of fuel consumption (FC) is stated in Eq. (1)

$$FC = Q + \alpha(SOC_{high} - SOC_{low})^2. \tag{1}$$

where Q is the time rate of fuel consumption and can be defined as

$$Q = \frac{(P_{ICE} + P_{EM}) g_e}{1000\gamma_f}. \tag{2}$$

where P_{ICE} is the engine rated power; P_{EM} is the motor rated power; g_e is the specific fuel consumption of the engine and γ_f is the mass density of the fuel. α is a positive weighting factor; SOC_{high} and SOC_{low} are the upper and lower limits of the battery state of charge.

3.2 Emissions

The mathematical model for vehicle's emission is given below

$$\text{Emissions} = \int_{t_0}^{t_1} g_k(t) \cdot \left[\frac{P_{\text{req}}(t)}{\eta_t} - \eta_m \cdot P_{\text{batt}}(t) \right] dt. \quad (3)$$

where $g_k(k) = 1, 2, 3$ emission MAP values of HC, CO, and NO_x emissions, respectively. $P_{\text{req}}(t)$ is the vehicle demanded power; $P_{\text{batt}}(t)$ is the battery output power; η_t and η_m are, respectively, mechanical transmission efficiency and motor operational efficiency.

4 Implementation of Genetic Algorithm

One of the evolutionary-based global optimization techniques is Genetic algorithm, which implements the biological mechanism of natural selection and Darwin's theory of survival of the fittest. Genetic algorithms can effectively obtain the global optimum results and is pretty much capable of handling multimodal, non-differentiable, and noncontinuous multi-objective optimization problems with nonlinear constraints associated with it. Other than Genetic algorithm, there are many evolutionary algorithms such as particle swarm optimization (PSO) which have now become popular in solving various other engineering problems [11, 12]. The steps involved in solving optimization problems using the proposed Genetic algorithm are described below

- *Initialization*: First, all the parameters of GA considered here are initialized with predefined values. Binary coded chromosome set representing the design variables is created randomly as the initial population.
- *Fitness function evaluation*: The fitness function is evaluated for each chromosome in the initial population and the chromosome with the best fitness value is stored as an elite member.
- *Reproduction*: Reproduction operation is performed to produce the mating pool from the initial set of the population. The tournament selection method is used over here. According to this method, a tournament is conducted between the two randomly selected pair of chromosomes. This process is repeated several times unless all the members of the population are exhausted. The winners of the tournament are placed in the mating pool. The members with better fitness value have the higher possibility to get selected.
- *Crossover*: Two-point crossover method is used in this proposed GA. For each of the selected pair of parent chromosome, two crossover sites are randomly generated. As the crossover probability (pc) is 0.8, 80 % members of the total

population in the mating pool have been taken into consideration for crossover. After the crossover operation parents are replaced by the children.

- *Mutation*: To maintain the diversity in the population mutation operation is done. According to the mutation probability (pm), random mutation points are produced and the bits at the mutation points are flipped.
- *Elitist principle*: The elite member of every generation directly proceeds through next generation without any modification.
- *Finish Condition*: The algorithm stops when the maximum number of generations is attained.

5 Simulation and Results

In this paper, two different optimization techniques are adopted in order to solve the hybrid electric vehicle parameter optimization problem formulated earlier. First one is the genetic algorithm (GA) and the second one is the simulated annealing (SA). Programs for both the GA and the SA are written and simulated in MATLAB. The EPA urban dynamometer driving schedule (UDDS) driving cycle is used for real-case simulation. The specifications of the power train components of the simulated vehicle are listed in Table 1. Among the thousands of design parameters including electrical and mechanical counterparts of the PHEV power train and drive train components, it is a subject of crucial importance to choose appropriate ones that satisfy the design objectives of reduction of fuel consumption and exhaust emission. Five design variables have been selected for this research work. Those variables along with their upper- and lower- bounds are indicated in Table 2.

The above-mentioned optimization problem is solved using both the Genetic Algorithm and the Simulated Annealing. The optimization procedure is graphically represented in Fig. 2. It shows how the fitness function for fuel consumption is minimized over the progress of generations for both the GA and the SA. It is evident from the Fig. 2 that GA performs better than SA. The plot of different toxic emission versus iterations is shown in Fig. 3 for the GA. Figure 4 shows the plot of individual objective functions versus iterations for the SA. From these two plots, we

Table 1 The specifications of the power train components

Components	Specifications
Engine	1.9L SI, 41 kw/5500 rpm
AC induction motor	Max power: 75 kw Peak efficiency: 96.39 %
NiMH battery	Capacity: 60 Ah Number of modules: 20 Nominal voltage: 12 V Power density: 422.4 (w/kg)
Vehicle	Mass: 1350 kg

Table 2 The parameters and their initial values

Parameters	Lower bound	Upper bound
P_{ICE}	30 kW	60 kW
P_{EM}	60 kW	85 kW
P_{batt}	15 kW	25 kW
SOC_{high}	0.6	0.9
SOC_{low}	0.1	0.6

Fig. 2 Fuel consumption plot for GA and SA

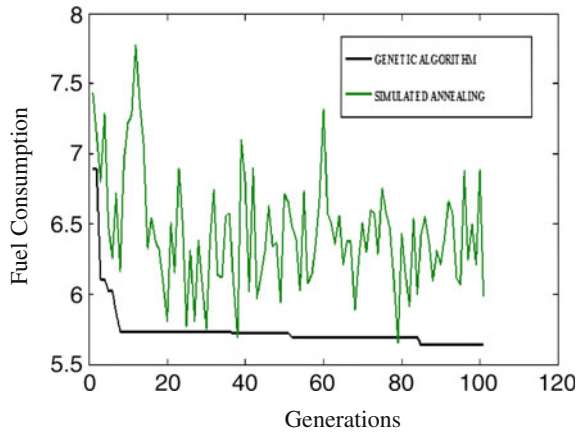


Table 3 Simulation results

Term	Items	Unit	Pre optimization values	Post-optimization values	
				Using GA	Using SA
Parameters	P_{ICE}	kW	41	30	34
	P_{EM}	kW	75	60	62
	P_{batt}	kW	19	24	24
	SOC_{high}		0.9	0.81	0.83
	SOC_{low}		0.6	0.69	0.69
Objectives	FC	L/100 km	8.04	5.64	5.98
	HC	GM/km	0.401	0.13	0.14
	CO	GM/km	3.601	1.30	0.1.32
	NO_x	GM/km	0.357	0.113	0.115

can get a much clear picture about the efficiency and effectiveness of the proposed Genetic algorithm.

The simulation results are listed in Table 3. Observing the simulation results, it can be concluded that fuel consumptions and emissions have been significantly reduced from default values while the performance constraints are still not violated.

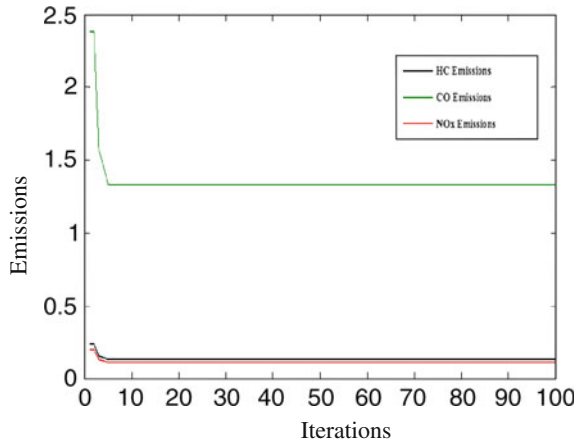


Fig. 3 Different emission plot for GA

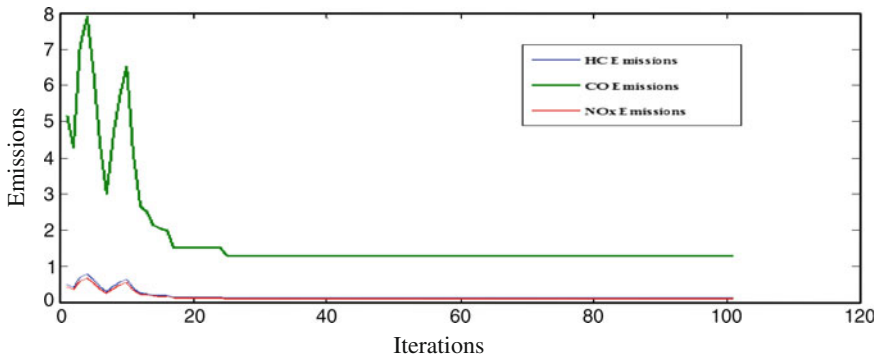


Fig. 4 Different emission plot for SA

6 Conclusion

This paper has presented the optimization of parallel hybrid electric vehicle (PHEV) parameters targeting at the reduction of fuel consumption and toxic emission. Among thousands of design variables, suitable ones are chosen which in turn have satisfied the objectives and fulfilled the performance requirements. Two different heuristic optimization techniques, genetic algorithm, and simulated annealing are applied and results are obtained accordingly. It can be observed that fuel consumption has been reduced by 42.5 % by GA and 34.8 % by SA. So, the simulation result suggests that genetic algorithm has been proved to be a better option for solving complex optimization problems constrained with nonlinear functions.

References

1. Fang LC, Qin SY. Concurrent optimization for parameters of powertrain and control system of hybrid electric vehicle based on multi-objective genetic algorithms. SICE-ICASE international joint conference. 2006. p. 2424–9.
2. Galdi V, Ippolito L, Piccolo A, Vaccaro A. A genetic-based methodology for hybrid electric vehicles sizing. *Soft Comput.* 2001;6. (Springer).
3. Wu X, Cao B, Wen J, Wang Z. Application of particle swarm optimization for component sizes in parallel hybrid electric vehicles. *IEE Congr Evol Comput.* 2008;2874–8.
4. Buerger S, Lohmann B, Vogel-Heuser B, Merz M, Hallmannsegger M. Multi-objective optimization of hybrid electric vehicles considering fuel consumption and dynamic performance. *IEEE Conf Veh Power Propul.* 2010;1–6.
5. Zhengli Z, Jianwu Z, Chengliang Y. Optimization approach for hybrid electric vehicle powertrain design. *Chin J Mech Eng.* 2005;18(1):30–6.
6. Jalil N, Kheir NA, Salman M. A rule-based energy management strategy for a series hybrid vehicle. In: *Proceedings of the American control conference, Albuquerque, New Mexico; 1997.*
7. Lee H-D, Sul S-K. Fuzzy-logic-based torque control strategy for parallel-type hybrid electric vehicle. *IEEE Trans Ind Electron.* 1998;45(4):625–32.
8. Tony M, Wipke K. Optimization techniques for hybrid electric vehicle analysis using advisor. In: *Processing of the ASME international mechanical engineering congress and exposition. New York; 2001.*
9. Wang Z, Huang B, Xu Y, Li W. Optimization of series hybrid electric vehicle operational parameters by simulated annealing algorithm. *IEEE Int Conf Control Autom.* 2007;1536–41.
10. Liu J, Peng H. Control optimization for a power-split hybrid vehicle. In: *Proceedings of the American control conference.* 2006. p. 466–71.
11. Mishra SK, Panda G, Majhi R. A comparative performance assessment of a set of multiobjective algorithms for constrained portfolio assets selection. *Swarm Evol Comput.* 2014;16:38–51 (Elsevier).
12. Gaurav K, Mishra SK. Non-linear system identification using clonal particle based functional link artificial neural network. *Springer proceedings of ICCVR-2014, vol 32.* 2015. p. 89–96.

Classification Scheme for Software Reliability Models

Dalbir Kaur and Monika Sharma

Abstract This study is mainly concerned with software reliability models where details of SGRMs model is studied. With the plethora of SRMs available, classification scheme is proposed to categorize models accordingly. Classification is based on different phases of SDLC to give a clear picture about what type of model should be used in different software development phases. This classification is meant for characterization, analysis, identification, and comparison of software reliability models and leads to selection of an optimum subclass of software reliability models. In this study, analysis and ranking of SRMs is considered, the research gaps on model usage and assumptions have been addressed, and classification of reliability models according to software development life cycle (SDLC) phases has been provided. The main objective of this study is to promote an improved understanding of software reliability model's classification and selection process.

Keywords Software reliability · SRGMs · Classification · SDLC · Models criteria · Survey · Comparative analysis · Performance evaluation

1 Introduction

The software reliability is an important part of software engineering and software quality. Analysis of reliability is now an established and important inter-disciplinary field of research. In case of measurement, management technologies, the software life cycle is very essential to maintain and produce reliable software. IEEE standard sec2.2-1 states “The reliability management program of a software constitutes the establishment of a set of balance user quality objectives and objective of

D. Kaur (✉) · M. Sharma
UIET, Panjab University, Chandigarh, India
e-mail: Dalbir1209614@gmail.com

M. Sharma
e-mail: monikahsp@gmail.com

intermediate quality identification that will force in achieving the goal of user to acquire quality objectives” ISO 9000-3 specifies “the field failures measurement is the only calculated metric of a minimum, to represent defects and field failures from customer point of view. The software product supplier needs to act and collect qualitative measures of the software product qualities.” Reliability of software is an attribute that contributes in the satisfaction of that software system to customer. Customer satisfaction about the software product performance is reduced if software failures occurs. Three activities comprise the assurance of software reliability.

- I. Prevention of Error
- II. Removal and detection of fault
- III. Reliability measurement of maximization.

Reliability of software product is the probability of nonoccurrence of product failure under particular conditions for a specified time. So, this probability is a function of the faults existence in software. This input to the software product would check either a fault is occurring or not.

2 Software Reliability Modeling

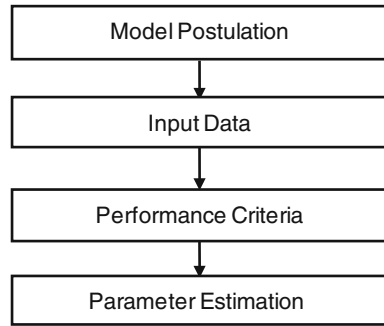
As a part of failure and fault forecasting, modeling of software reliability attracted most research attention in the field of measuring the present condition of state and prediction in order to assess the future conditions for software system. Modeling of software reliability is a very essential element of the engineering in reliability field. So, many software reliability models are developed to calculate failure data at the time of testing in forms of multiple estimates of product reliability, for example, test time function. So, many interdependent estimates may be obtained to make similar statements about the reliability of product. These estimates of reliability may give the following important information, which is very useful for the management of product quality:

- The product’s reliability at the time when testing is complete.
- The additional amount of test time needed to achieve the reliability objective of product.
- The growth of reliability as a testing result (e.g., the ratio of the failure intensity value from the start to the end of testing).
- The reliability which is predicted beyond the testing of system such as in the field the product’s reliability.

Following three are the main software reliability approaches for modeling:

- i. The approach of error tagging and seeding
- ii. The approach of data domain
- iii. The approach of time domain

Fig. 1 Software reliability model compositions



Software reliability model is a type of mathematical expression that describes the general form of the failure process for software as a function of factors like fault. It can be said that reliability models can be considered as a powerful tool for controlling, assessing, and predicting the reliability of software. A software model usually consists of the following parts, as shown in Fig. 1.

2.1 Model Postulation

Model is a form which is used for simplification or standardization of the present complicated situation, given a number of assumptions. For example, the test cases selection is on basis of the original operation, invalidation, and independent presence of different types of software.

2.2 Input Data

It can be called as software reliability data. Multiple types of models may need different forms of input data.

2.3 Performance Criteria

The outputs of the reliability model act as the measurements related to performance, which is the type of invalid intensity, the failure, and reliability cumulative number. In the field of software reliability model, measurements related to performance are usually present as a form of mathematical expression.

2.4 *Parameters Estimation*

Sometimes the original reliability value of the measurement cannot be obtained directly, such as the residual defects numbers, so it is required to find the actual value of the parameters by a particular method, consequently the actual reliability measurement value can be confirmed indirectly. For the estimate of parameters, the directly obtained value of reliability is not required.

3 *Classification Scheme*

In this section, a chronological review of different existing reliability models of software is presented through which it may be seen that there has been a large number of models studied and suggested. If their assumption and applicability's are considered, many models are too similar. In order to distinguish these models from one another and to compare two models for allocation as to which is more suitable than the other, some criteria is needed. Due to the multiple varieties of the present models, it is not a suitable task, and in literature there are many different classification techniques available. The classification used in this paper is presented according to software development life cycle (SDLC) phase.

3.1 *Classification According to Software Development Life Cycle (SDLC) Phases*

In this section, a SDLC classification system is proposed which will be used to classify the models. Software reliability models have been classified according to software development life cycle phases, based principally on the phases of software development life cycle phase to determine which model is applicable for a given product. The main characteristic of a model serves as a sub-classification. For example, it classifies the models based on the architecture, i.e., it integrates the software architecture with the behavior of failure and the failure phenomenon of software. Then, further classification of SRGM is done, as given in Fig. 2. Most of the existing models can be used during the design, implementation, and testing phase [1].

3.2 *Early Prediction Models*

For behavior prediction of software system from the time of requirement gathering to operation time, these models may use the features of development process to

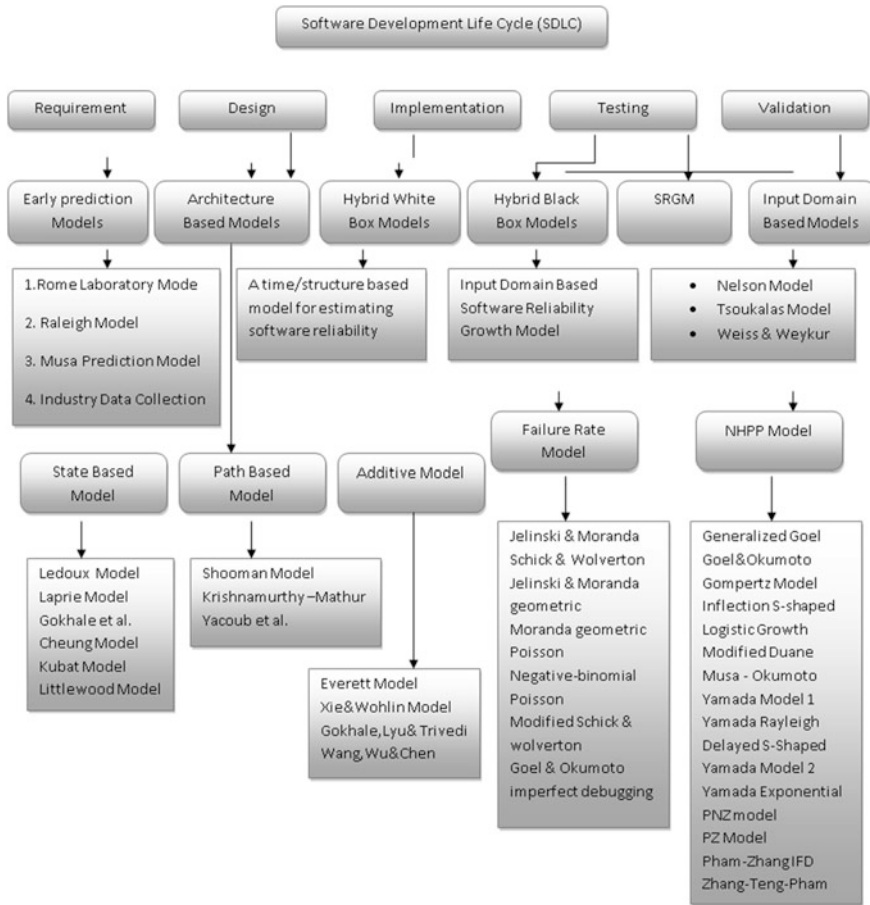


Fig. 2 Classification scheme

extrapolate and test this required information. These models mostly address the software reliability at early stage in the software life cycle at the time of requirements gathering or at the time of preliminary design phase or at the detailed design stage in a waterfall life cycle model; or at time of the first spiral in case of spiral software development. In case of predictive models under provided set of requirements, it can be used to check the risk probability of software which is under development phase and for particular personnel before the starting time of project. In case of the software which predicts the reliability earlier, software reliability models are available in less number and most models come under the category of assessment. These categories of models are seldom executable, insubstantial, insufficiently formal to be able to examine, and typically they not connected to the target system. They have modest impact on the reliability.

3.3 *Software Reliability Growth Models (SRGMs)*

For measuring reliability, software reliability growth models (SRGMs) are one of the best roots. In the literature, SRGM is the most prosperous class of models, presenting in one form or other form by hundreds of number of publications during testing; these types of models express the software's failure behavior. So, this class of models utilize information related to failure data and trends obtained to derive predictions about reliability in this failure data. Black-box models are a type of these models that consider the software system as a monolithic whole, treating only its interactions with external environment, without seeking to internal structure of model. Mostly, in these types of models, no details related to other than the failure data is required [2]. Stochastic modeling is the most common characteristic of black-box models, considering little parametric model failure which is obtained as a cumulative number over the time between failures interval or finite interval time. At the time when application is tested, failure data is acquired and then estimated model parameters are used. Mostly, SRGMs faces the biggest challenges. First of all, for testing a software operational profile, software testers are chosen and allocated to the testing process appropriately, but what is examined during testing time or how much time is taken for operational testing procedure, etc., these features might not be directly inferable. Second, when there is limited number of collected failures in a product, it is difficult to predict meaningful reliability statistically. Third, no realistic assumptions of SRGM exist, e.g., there is a most considered assumption that the fault is independent and not related to each other; however, there is one class of products in which there is a same chance of detection of each fault and no introduction of new faults occur due to the correction of old fault, but in other class of products, new faults might be introduced due to correction of old faults; so assuming that faults are independent is not a practically viable assumption. With suitable means we can overcome the above problems. Further classification of SRGM is done as NHPP model and models of failure rate. The inclination for practitioners to use a SRGM, in the concept that it has to be inexpensive and simple to collect the input data of need.

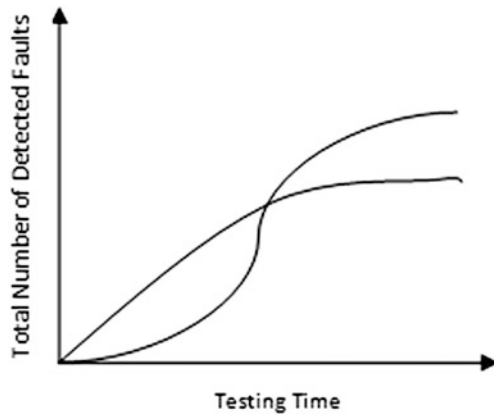
3.4 *Model Discussion*

For the last three decades, so many different model of mathematical nature are called software reliability growth models (SRGMs). They have been employed to demonstrate the phenomenon of software debugging. Failure history is used by SRGM to obtain, while testing for field behaviors predictions related to the program [3]. Mostly, the development of SRGMs were dependent on the (NHPP) non-homogeneous Poisson process, and they assumed exponential-shaped type or S-shaped type nature of them, that is the way they are called as NHPP SRGMs. NHPP SRGMs have been developed to estimate reliability of software in the

Table 1 Comparison of SRGM's

Name of model	Mean value function	Failure intensity function
1. Gompertz growth curve model	$m(t) = ake^{-bt}$	$\lambda(t) = ab \ln(k)k^{e^{-bt}} e^{-bt}$
2. Logistic growth curve model	$m(t) = \frac{a}{1+ke^{-bt}}$	$\lambda(t) = \frac{abk e^{-bt}}{(1+ke^{-bt})^2}$
3. Modified Duane model	$m(t) = a[1 - (b/(b+t))^c]$	$\lambda(t) = acb^c (b+t)^{1-c}$
4. Yamada imperfect debugging model 1	$m(t) = \frac{ab(e^{-at} - e^{-bt})}{a+b}$	$\lambda(t) = \frac{ab(ae^{-at} + e^{-bt})}{a+b}$
5. Yamada imperfect debugging model 2	$m(t) = a(1 - e^{-bt})(1 - \frac{\alpha}{b}) + \alpha at$	$\lambda(t) = abe^{-bt}(1 - \frac{\alpha}{b}) + \alpha a$

Fig. 3 Software reliability growth curve



debugging/testing phase and to predict the number of defects which remain in a software system after testing [4]. For guiding the management of testing decision making process, SGRMs are mainly used in the industry of software whether to stop or to continue to help for software release optimal policy and testing. Actually, for the assessment of reliability of software, it is very much necessary to mention the (MVN) mean value function. In the last decade, it has been proposed that many SRGM NHPP models assume the different operational environment or testing for assessment of reliability of software [5]. Five SRGM NHPP models [6] are summarized in Table 1. As mention above, the growth of reliability of software is presented as the relationship between the operation time and elapsed testing and the integrated number of faults detected, and this reliability growth curve can be shown mathematically as in Fig. 3 [7]:

4 Gompertz Growth Curve Model

Numazu and Fujitsu's work uses the model name as Gompertz growth curve model. This model is adopted mostly by Japanese software house and computer manufacturers because it is considered as an easiest S-shaped growth model for reliability of software [8].

The mean value function of this model is

$$m(t) = ake^{-bt} \quad (1)$$

Failure intensity function is

$$\lambda(t) = ab \ln(k) k e^{-bt} e^{-bt} \quad (2)$$

$$a > 0, 0 < b < \infty, 0 < k < 1$$

where "a" is the number of expected faults which is detected eventually and regression analysis are used to estimate the values of parameter k and b .

5 Logistic Growth Curve Model

At the time of testing, the reliability of software behavior comes out as growth process and it improves gradually. The faults that are fixed are responsible for growth of reliability [9]. So, we can apply the same model to estimate the growth of reliability which we apply for economic population prediction. This model is also an S-shaped curve. The cumulative number can simply fit by this model with a known form function at a given time [8].

Its mean value function is

$$m(t) = \frac{a}{1 + ke^{-bt}} \quad (3)$$

The software failure intensity is given as

$$\lambda(t) = \frac{abke^{-bt}}{(1 + ke^{-bt})^2} \quad (4)$$

$$a > 0, b > 0, k > 0$$

where "a" is the number of expected faults which is detected eventually and failure data fitting is used to estimate the values of parameter k and b .

6 Modified Duane Model

In 1962, Duane presented a report in which several systems' failure data were analyzed at the time of development [10]. He noticed that the cumulative operating time versus cumulative mean time between failures becomes near to a line that is straight if it is plotted in a log-log paper. After that he proposed a modified version of Duane model on the basis of its hypothesis and the above observation [8].

Mean value function is

$$m(t) = a[1 - (b/(b + t))^c] \tag{5}$$

The failure intensity function $\lambda(t)$ is given as

$$\lambda(t) = acb^c(b + t)^{1-c} \tag{6}$$

$$a > 0, b > 0, c > 0$$

where “ a ” is the number of expected faults which is detected eventually.

7 Yamada Imperfect Debugging Model 1

Yamada mentioned the imperfect debugging model in which rate function of detected error is constant. This model considers introduction of new errors; when detected errors are removed. In a program, the possibility of obtaining an error is directly proportional to the remaining number of errors [11]. The mean value function in equation is given as

$$m(t) = \frac{ab(e^{-\alpha t} - e^{-bt})}{a + b} \tag{7}$$

The failure intensity function is given as

$$\lambda(t) = \frac{ab(\alpha e^{-\alpha t} + e^{-bt})}{a + b} \tag{8}$$

$$a > 0, b > 0, \alpha > 0$$

where “ a ” is the number of expected faults which is detected eventually and b is the rate of detected faults; α is fault rate of constant introduction.

8 Yamada Imperfect Debugging Model 2

Yamada imperfect debugging model 2 considers that the rate function of error detection is fixed or constant [12]. When removed, the detected error may introduce many new errors. In a program, the possibility of obtaining an error is directly proportional to remaining error numbers [5]. The mean value function in equation is given as

$$m(t) = a(1 - e^{-bt}) \left(1 - \frac{\alpha}{b}\right) + \alpha t \quad (9)$$

The failure intensity is given as

$$\lambda(t) = abe^{-bt} \left(1 - \frac{\alpha}{b}\right) + \alpha a \quad (10)$$

$$a > 0, b > 0, \alpha > 0$$

9 Conclusion

SGRM models are the robust way for controlling, measuring, and predicting the reliability of software. Five non-homogenous Poisson process (NHPP) software reliability growth models were discussed. The classification scheme for software reliability models was presented. It has capacity to accommodate newly developed software reliability models. A manager can chose software reliability model from the classification scheme according to the development phase of the software being developed. It provides software reliability models for each phase of software being developed. It provides software reliability models for each phase of software development life cycle. It is very easy and straight forward for use in software industry, due to its hierarchical structure. It is also easy to modify and adjust changes due to introduction of new models and deletion of old models in practice

References

1. Pendharkar PC, Subramanian GH, Rodger JA. A probabilistic model for predicting software development effort. *IEEE Trans Softw Eng.* 2005;31(7):615–24.
2. Shanmugam L, Florence L. A comparison of parameter best estimation method for software reliability models. *Int J Softw Eng Appl.* 2012;3(5):91–102.
3. Mohan K, Krishna A, Verma K, Srividya A. Software reliability estimation through black box and white box testing at prototype level. In: *reliability, safety and hazard (ICRESH), 2010 2nd international conference on, IEEE.* 2010. p. 517–22.
4. Schneidewind NF. Software reliability model with optimal selection of failure data. *IEEE Trans Softw Eng.* 1993;19(11):1095–04.

5. Malaiya YK, Li N, Bieman J, Karcich R, Skibbe B. The relationship between test coverage and reliability. In: Software reliability engineering. Proceedings, 5th international symposium on. IEEE. 1994. p. 186–95.
6. Goel AL. Software reliability models: assumptions, limitations, and applicability. *IEEE Trans Softw Eng.* 1985;SE-11(12):1411–23.
7. Asad, Ch A, Ullah MI, Ur-Rehman MJ. An approach for software reliability model selection. In: Computer software and applications conference, 2004. COMPSAC 2004. Proceedings of the 28th annual international, IEEE. 2004. p. 534–9.
8. Mohd. Anjum et al. Analysis and ranking of software reliability models based on weighted criteria value. *I J Inf Technol Comput Sci.* 2013;2:1–14.
9. Mohd. Anjum et al. Analysis and ranking of software reliability models based on weighted criteria value. *I J Inf Technol Comput Sci.* 2013;2:1–14.
10. Yamada S, Ohba M, Osaki S. S-shaped reliability growth modeling for software error detection. *IEEE Trans Reliab.* 1983;32(5):475–84.
11. Lyu MR. Handbook of software reliability engineering, vol 222. CA: IEEE Computer Society Press; 1996.
12. Gupta A, Choudhary D, Saxena S. Software reliability estimation using yamada delayed S shaped model under imperfect debugging and time lag. *Int J Comput Appl.* 2011;23(7):0975–82.
13. Musa JD, Okumoto K. A logarithmic poisson execution time model for software reliability measurement. In: Proceedings of the 7th international conference on software engineering. IEEE Press; 1984. p. 230–8.
14. Ohba M. Software reliability analysis models. *IBM J Res Dev.* 1984;28(4):428–43.

Secure Spectrum Leasing in Cognitive Radio Networks via Secure Primary–Secondary User Interaction

Meenakshi Malhotra and Inderdeep Kaur Aulakh

Abstract Cognitive Radio Networks is an emerging technology which gives a remarkable solution to many problems that arises at the time of communication between the primary and secondary user. To affect the confidentiality and integrity of the network, many attacks come to the communication channel. In this paper, we focus on the secure communication between primary and secondary user. If the communication is not secure, then any unwanted user can pretend like a primary user or secondary user and can use that confidential data or can block the legal user. So with the help of AES and key file generation, the encryption and decryption can be done only by the legal primary and the secondary user.

Keywords Cognitive radio networks · Decryption · Denial-of-Service (DoS) attack · Encryption · Key · Primary user · Primary user emulation attack (PUEA) · Secondary user · Signals · Spectrum

1 Introduction

Nowadays, wireless technology is being used by a variety of people or in short one can say that the whole world is dependent upon the wireless technology. As the demand for wireless technology is increasing day by day, many problems come in the communication channel too.

Cognitive radio networks in wireless technology plays an important role for communication between the users. The primary user uses its allocated bands which are the licensed ones. As per the federal communication commission (FCC) information, the spectrum bands of the primary users are not being used all

M. Malhotra (✉) · I.K. Aulakh
Department of IT, U.I.E.T, Panjab University, Chandigarh, India
e-mail: meenakshi.malhotra@outlook.com

I.K. Aulakh
e-mail: ikaulakh@yahoo.com

the time, which results in underutilization of the spectrum bands. To solve such a critical problem, cognitive radio networks was introduced. Cognitive radio technique allows the unlicensed users (cognitive users) to use the available spectrum band of the primary user and this can happen only if the primary user is not using the licensed band. So in short, cognitive radio networks can be seen as the solution to the underutilization problem of the spectrum band.

Cognitive radio networks do four steps for the process: spectrum sensing, spectrum management, spectrum sharing, and spectrum mobility. The very first step in the network is the sensing process, which determines the white spaces. The sensing process basically senses the presence of primary user signal and informs the secondary user about it. After the completion of sensing process, the remaining processes do their work.

In cognitive radio networks, the secondary user (cognitive user), is considered as a serious node because with the help of this user, the underutilization problem can be dealt without any interference. In [1], the optimization of secondary user access is considered so that the sensing can be done effectively.

In [2], the optimization of secondary user access is done in the presence of probability of false alarm. The probability of false alarm gives the false indication about the availability of primary user signal whereas the primary user is not using the spectrum.

As the spectrum sensing in cognitive radio networks senses the whole environment about the availability of the primary user signal, it also increases the security challenges. In cognitive radio networks, many attacks can be introduced at the time of functionality steps like denial-of-service (DoS) attack, data modification attack, spoofing attack, primary user emulation attack, etc. The attacks may also affect the requirement of secure communication (authentication, availability, confidentiality, and integrity).

In PUE attack, the emulated user (malicious user) behaves like primary user (PU) and confuses the cognitive user with the primary user's signal identity. The PUEA results in vacating the available spectrum band by the cognitive user. So, the PUE attack degrades the performance of the cognitive radio networks as well as introduces the underutilization of the spectrum band.

In Fig. 1, the emulated user sends the same frequency as of the primary user and then after receiving the availability of the primary user signal (emulated user behaves like primary user), the secondary user 1 and secondary user 3 vacates the spectrum band.

In the DoS attack, on the other side, the emulated user after behaving like the primary user continuously send the signals or the frequencies to the secondary user. This attack may overload or block the secondary user to use the environment.

In Fig. 2, the emulated user continuously sends the signals to secondary user 1. The secondary user thinks that the signals are coming from the primary user and tries to vacate the band, but suddenly receives the frequency again. This leads to overload the secondary user and sometimes after such situation, the secondary user could not be able to use any spectrum in the network.

Fig. 1 Primary user emulation attack

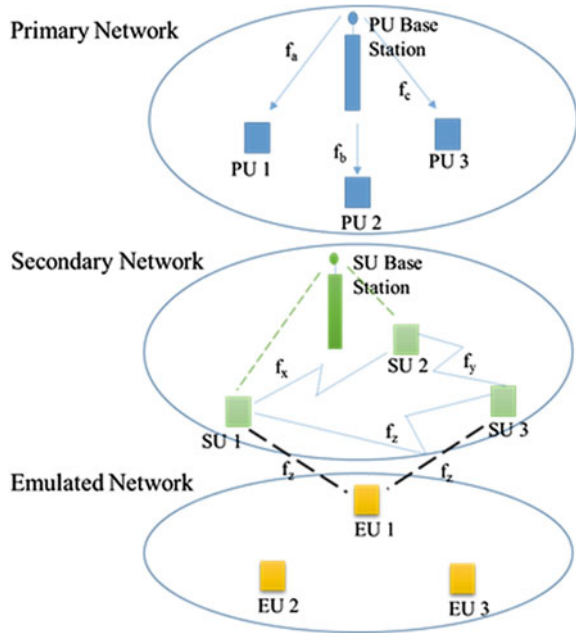
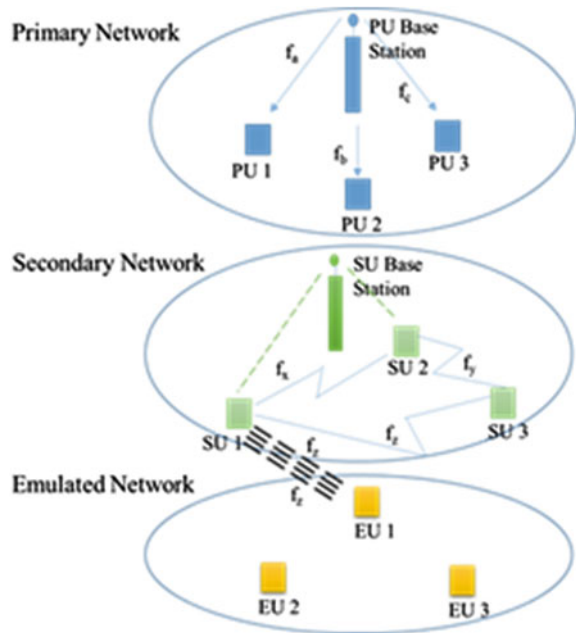


Fig. 2 Denial-of-Service attack



In the cognitive radio networks, there might be different types of attackers like the selfish attacker, malicious attacker, power-fixed attacker, power adaptive attacker, static attacker, and the mobile attacker [3]. Each attacker has its own specialty of attacking the network or harming the communication.

Attacks may also harm the bandwidth of the network, increases the interference between the primary user and the secondary one, drop in the quality of service, connection establishment, etc. These security challenges in the cognitive radio networks should be considered on a serious note.

The remaining paper is as follows: Sect. 2 contains the literature review of PUEA and DoS attack for the implementation process. Section 3 contains the result and implementation, which contains the basic algorithm for the process. Section 4 contains the simulated results and at the end the conclusion is given.

2 Literature Review

Alahmadi et al. suggested an AES-assisted DTV (Digital television) scheme [4]. In which, at the TV transmitter, the generalization of an AES-encrypted reference signal is done and that signal is then used as sync bits of the DTV data frames. With the help of shared secret among the transceiver, the reference signal can be generated again at the receiver side for achieving the result of authorized primary user identity. As a result, the difference between the primary user and the malicious user can be found with the help of the proposed AES-assisted DTV scheme. This proposed scheme gives greater accuracy in the presence of primary user emulation attack (PUEA).

Yu et al. proposed a two-level database-assisted detection scheme for the detection of PUEA. In this, the energy detection as well as the location verification is joined for reliable detection. A defense approach like admission control is introduced to eliminate the performance degradation of CR networks [3].

Xie et al. determines the collision's initial point by estimating the distance between the sender and receiver at the time of signal interference on the receiver side. With the help of interference result on many receivers, the location of an authorized primary user can be determined. To detect the PUE attack (PUEA), the comparison between the resulted location of authorized primary user and known location of primary user is done [5].

Chen et al. considers the cooperative spectrum sensing in the existence of PUEA. In this introduced scheme, at the fusion center, all the sensing information of various secondary users is joined. For increasing the probability of detection, the optimization of combined weights is done [6].

Bhunja et al. considered the honeypot theory, in which they suggested a defense mechanism named honeynet to determine the attacker in the network. The honeynet has the advantage of determining the strategy of the attacker with the past information of that attack [7].

With more than one application scenario, Soderi et al. suggested an active radio frequency fingerprinting (RFF). They encapsulate the common-control-channel (CCC) material with the help of active RFF. To interchange the public key, a node within the network can use the discussed technique [8].

3 Results and Implementation

Algorithm 1 gives the step by step process of secondary user sensing data handover. Data handover means that the secondary user sends the data to the primary user and encryption of that data is done for secure communication. By securing the communicated data, the chances of attack will be minimized.

Algorithm 1: Secondary User Sensing data handover

1. Acquire Secondary User sensing data
 2. Validate Secondary User sensing data
 3. Load key from Key File
 4. Encrypt Sensing data using AES and key provided
 5. Send data to Primary User
 6. Primary User load the data from Key File
 7. Decrypt Sensing data using AES and key provided
 8. Use the data
-

In the above algorithm, we are securing communication between primary user and the cognitive user. Encryption and decryption are done with the help of the key file stored in the database of primary user and the secondary user. This key file is generated from the AES (Advance Encryption Standard).

In the first step of the algorithm, the secondary user sensing data is received and then the data is being validated. The AES uses 16 bytes key for data encryption. In some cases, if lesser amount of data is present, then with the help of validation, padding of the data is done. The third and fourth steps do the encryption process with the help of the key file stored in the database. This key file is generated with the help of AES. After encryption, the encrypted data is sent to the primary user. Then, the primary user with the help of key file decrypts the encrypted data and at last secure communication is done.

AES does both substitution and permutation, which makes it quick in terms of hardware as well as software. Here, AES is being used for the secure encryption process. AES, in its each round contains four processing steps; in the first step the key expansion is done. In the second one, bitwise XOR is done between each byte with the block of round key. The third one contains four parts called SubBytes,

ShiftRows, MixColumns, and AddRoundKey and the last step contains the SubBytes, ShiftRows, and AddRoundKey steps.

4 Results

After working according to the algorithm defined above, secure communication between the primary user and the secondary user is achieved. The result shows that with the help of encryption and decryption process, the data is not altered and at the end we achieved the original signals.

Figure 3 contains the three figures in itself. The first one shows the secondary user signal. The second one is the secondary user sensing data, which is encrypted with the help of AES. The third one is the result of the decryption applied on the encrypted signals.

The details below show the total data size used in the implementation process and the total time taken for encryption and decryption. The result states that the time taken to encrypt and decrypt the data is in seconds. The decryption process takes lesser time as compared to the encryption time.

```
>> key_encryption_Demo
Total data size: 2812.500000 kB
The time taken for encryption : 204.739619 seconds
The time taken for decryption : 136.718552 seconds
>>
```

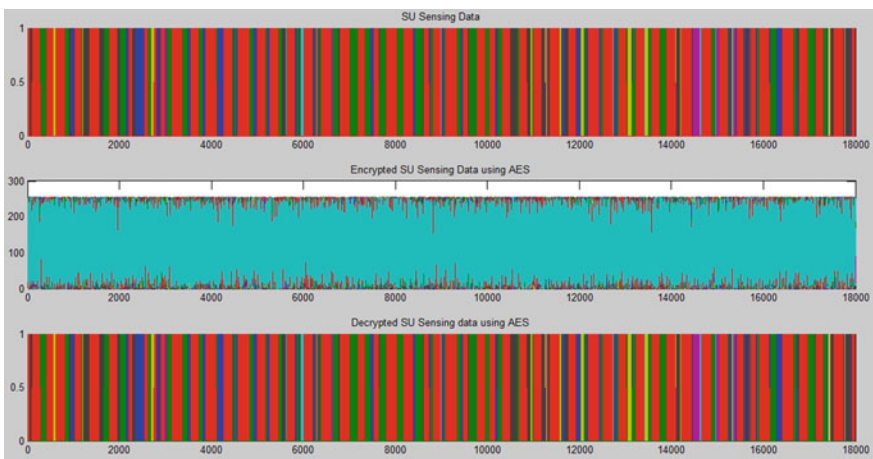


Fig. 3 Simulation results

5 Conclusion

Cognitive radio networks security is attracting the attention of many researchers. This paper gives the algorithm and simulated results, which shows that by securing the communication between the primary user and secondary user, the probability of PUE attack reduces. Only the legal primary user and the cognitive user can communicate with each other without any unexpected hurdle. After this implementation, our future work will focus on the denial-of-service attack, which affects the cognitive user and make them unavailable or overloaded with many frequencies.

References

1. Aulakh IK, Vig R. Optimization of secondary user access in cognitive radio networks. In: Proceedings of IEEE RAECS. Chandigarh, India;2014.
2. Aulakh IK, Vig R. Optimization of SU's probability of false alarm for dynamic spectrum access in cognitive radio. In: Proceedings of IEEE 8th INDIACom. New Delhi, India;2014. p. 814–9.
3. Yu R, Zhang Y, Liu Y, Gjessing S, Guizanit M. Securing cognitive radio networks against primary user emulation attacks. Emerging Technologies (cs.ET), Cornell University Library;2013.
4. Alahmadi A, Abdelhakim M, Ren J, Li T. Defense against primary user emulation attacks in cognitive radio networks using advanced encryption standard. In: IEEE transactions on information forensics and security, vol. 9, May 2014.
5. Xiea X, Wang W. Detecting primary user emulation attacks in cognitive radio networks via physical layer network coding. J Ubiquitous Syst Pervasive Networks. 2014;5:01–8.
6. Chen C, Cheng H, Yao Y. Cooperative spectrum sensing in cognitive radio networks in the presence of the primary user emulation attack. In: IEEE transactions on wireless communications, vol. 10, July 2011.
7. Bhunia S, Sengupta S, Vazquez-Abad F. CR-Honeynet: A Learning & decoy based sustenance mechanism against jamming attack in CRN. In: IEEE military communications conference (MILCOM);2014. p. 1173–80.
8. Soderi S, Dainelli G, Iinatti J, Hamalainen M. Signal fingerprinting in cognitive wireless networks. In: Cognitive radio oriented wireless networks and communications (CROWNCOM), 9th international conference;2014. p. 266–70.

Traffic Signal Synchronization Using Computer Vision and Wireless Sensor Networks

Shivani Desai and Param Trivedi

Abstract Traffic pattern analysis is an emerging field of study to understand the cardinal parameters to design the archetype of modern infrastructure projects. Understanding the rudimentary factors that affect traffic will also allow the government to deploy automated traffic signal systems. This research paper will explain a unique approach to get the traffic pattern analysis information using the combination of computer vision and wireless sensor network. To deploy the solution, artificial neural network approach is used to detect the vehicles and pedestrians. Based on training the dataset of features, it can be ported to embedded systems to detect the vehicles. Later, data is being sent to cloud infrastructure using ZigBee protocols in Leach topology. It will give traffic synchronization to traffic signal systems.

Keywords Computer vision · Artificial neural networks · Wireless sensor networks

1 Introduction

Computer vision has evolved over the period of time, but it still cannot identify the objects because of improper lighting conditions or lack of image database to accurately identify the objects. We present a unique approach to solve traffic problems with the help of computer vision and wireless sensor network. As an example, if one organization needs to assemble the interstate on a specific course it needs to recognize what kind of vehicle, in what sum, and at what recurrence goes from that point. So that they can assemble the proficient base which will be ready to support

S. Desai (✉) · P. Trivedi

Computer Science and Engineering, Nirma University, Ahmedabad, India
e-mail: shivani.desai@nirmauni.ac.in

P. Trivedi

e-mail: 12bce169@nirmauni.ac.in

© Springer India 2016

S.S. Dash et al. (eds.), *Artificial Intelligence and Evolutionary Computations in Engineering Systems*, Advances in Intelligent Systems and Computing 394, DOI 10.1007/978-81-322-2656-7_68

743

the base on the long stretch of the time. Hence, the issues like movement blockage will be disposed off the root. For this, we will be creating calculations for the computer vision which will have the capacity to get the activity designs when needed by the administration utilizing the remote sensors sent over the city and some of them on the thruways. For correspondence, we will be sending the information over the remote conventions utilizing the 802.15.4. To send the information, we will be utilizing the filter convention of the wireless sensor network.

In wireless sensor networks (WSNs), because of the constraint of nodes' vitality, vitality effectiveness is an essential variable that ought to be considered when the conventions are outlining. As a run of the mill illustrative of progressive directing conventions, Leach protocol assumes an imperative part. In light of the uneven vitality dispersion that is brought about by the irregularity of bunch head structuring, this paper proposes another enhanced calculation of drain convention (Leach-TLCH) which is planned to equalize the vitality utilization of the whole system and expand the life of the system. The new calculation is prepared by MATLAB recreation stage; the reproduction results demonstrate that both vitality effectiveness and the lifetime of the system are better than that of Leach protocol [1, 2].

2 Problem in the Current System and Solution

2.1 What Is the Current Problem?

Urban population will achieve 50 crores by 2017, which was 30.1 crores in 2012. (Arranging Commission of India, 2012) The issue is that as a result of fast advancement, urbanization, and an uncommon development rate the administrations or the foundations rendered are poorly prepared. As an aftereffect of such a state of India, we, as organizers, see that either of the administrations are not ready to adapt to the current situation (as we see with the activity issues and street framework) or the new improvement is over-arranged as it practically relies upon a great deal of suspicions. Number of urban cities is to ascend from 475 (2011) to 600 in 2011. (Anticipated) (Registration of India 2012) Seven, tier-1 urban communities face issues with transportation and versatility in their day-to-day lives which drives some issues like wastage of time and assets. Additionally, with the pattern of urbanization, these urban areas alongside 18 of the 42 level 2 urban areas are anticipated to experience a weight point on the city's foundation. One of the most pressurized foundations of the city that is being influenced by urbanization is the vehicle and versatility channel. The movement issues in the nation can be illuminated by developing a base such that it can survive the movement furthermore, vehicles for quite a while. So, the cost to remake the structure will be settled.

2.2 What Is the Current Problem?

2.2.1 Government

The legislature or the statutory bodies who are dependable for catering the transportation and versatility needs are one of the real partners as on account of sloppy, time slacked information they wind up over building the arrangements. These arrangements can be enhanced if there is exact, quick, constant information with a specific end goal to upgrade, and not over designer movement issues. The impact of the issue can be seen on both classes. Those who are at the beneficiary's end who wind up utilizing the administrations what's more, the individuals who are at the position of giving the administrations, as they wind up utilizing superfluous assets and time in arranging. 86-road transportation and parkway activities were postponed which came about into expense overwhelms of 52,445 crore.

2.2.2 Mass Populace

The aggregate populace of tier-1 urban communities is 160 million individuals, which is anticipated to be twofold by 2030. These 160 million individuals are in a roundabout way influenced with the weight of a skewed demography. These individuals, in a roundabout way put their assets in request to procure the monetary preference of a tier-1 city yet endure on account of the slack of unstructured assets.

3 Wireless Sensor Network Components

We will be utilizing the open source micro controllers like raspberry pi to process the casings and send prepared information to the base station utilizing the correspondence modules. The raspberry pi chips, away at the 400 MHz recurrence so we will need to balance the edges such that processing force of the board can be utilized basically. We will be utilizing the working framework Raspbian Debian-based Linux to process the OpenCv code and by this, we will connect the cam to the microcontroller. We will be utilizing the profundity cams with the board to process the information so that we can recognize the vehicles even at the night. This will be the strongest point to supplant yearly reviews [3, 4].

4 Computer Vision Algorithms

4.1 Object Detection

Object identification is one of the basic assignments in computer vision. A typical ideal model to deliver this issue is to prepare object locators which work on a sub-picture and apply these finders in a thorough way over all area and scales. This ideal model was effectively utilized inside a discriminatively prepared deformable part model (DPM) to accomplish condition of workmanship results on identification errands. The comprehensive pursuit through all conceivable areas and scales represents a computational test. This test gets to be significantly harder as the quantity of classes develops, since the vast majority of the methodologies prepare a different finder every class. Keeping in mind the end goal to address this issue an assortment of strategies were proposed, fluctuating from locator falls, to utilizing division to recommend a little number of article theories. In this paper, we attribute to the last reasoning and propose to prepare a locator, called “Profound Multi Box,” which produces a little number of bouncing boxes as article hopefuls. These containers are produced by a solitary deep neural network (DNN) in a class skeptic way. Our model has a few commitments. First and foremost, we characterize object discovery as a relapse issue to the directions of a few bouncing boxes. Moreover, for every anticipated box, the net yields a certainty score of how likely this container contains an article [5–8].

This is not the same as conventional methodologies, which score emphasizes inside predefined boxes, and has the point of interest of communicating discovery of items in an exceptionally conservative and effective way. The second significant commitment is the misfortune, which prepares the bouncing box indicators as a major aspect of the system preparing.

For every preparation illustration, we take care of a task issue between the current forecasts and the ground truth boxes and upgrade the coordinated box arranges their confidences, and the fundamental highlights through back spread. Along these lines, we take in a profound net custom made toward our restriction issue. We profit by the amazing representation learning capacities of DNNs, as exemplified as of late in picture order [11] and object location settings [12], and perform joint learning of representation and indicators. At long last, we prepare our item confine indicator a class-freethinker way. We consider this as an adaptable approach to empower proficient location of expansive number of item classes. We indicate in our trials that by just post-arranging under ten containers, got by a solitary system application, we can attain to aggressive recognition results. Further, we demonstrate that our crate indicator sums up over concealed classes and all things considered is adaptable to be reutilized inside other location issues.

The writing on item location is incomprehensible, and in this segment we will concentrate on methodologies misusing class-freethinker thoughts and tending to adaptability. A large number of the proposed discovery methodologies are taking into account and one section-based model which all the more, as of late have

attained to amazing execution because of discriminative learning and painstakingly created highlights. These systems, be that as it may, depend on comprehensive use of part formats over different scales and accordingly are costly. Additionally, they scale straightly in the quantity of classes, which turns into a test for cutting edge datasets, for example, ImageNet 1. To address the previous issue, Lampert et al. utilizes a limb and bound procedure to abstain from assessing all potential item areas. To address the last issue, Song et al. utilizes a low-dimensional part premise, imparted over all article classes.

A hashing-based methodology for proficient part location has indicated great results and additionally diverse line of work, closer to our own, is in light of the thought that protests can be confined without needing to know their class. Some of these methodologies expand on base up ridiculous division The portions, acquired thus, can be scored utilizing top-down criticism Using the same inspiration, Alexa et al. utilizes a modest classifier to score object theories for being an item or not and along these lines decrease the quantity of area for the consequent identification steps. These methodologies can be considered multilayered models, with division as first layer and a fragment grouping as a consequent layer. Regardless of the way that they encode demonstrated perceptual standards, we will demonstrate that having deeper models which are completely learned can prompt prevalent results. At last, we profit by the late advances in deep learning, most observably the work by Krizhevsky et al. We expand their jumping box relapse approach for discovery to the instance of taking care of numerous protests in a versatile way. DNN-based relapse connected to protest covers has been explored by Szegedy et al. This last approach accomplishes condition of craftsmanship discovery execution on VOC2007 yet does not scale up to numerous classes because of the expense of a solitary cover relapse: in that setup, one needs to execute five systems every class at induction time, which is not versatile for most true applications [9, 10].

4.2 Proposed Approach

We go for attaining to class-rationalist versatile article identification by foreseeing an arrangement of bouncing boxes, which speak to potential articles. All the more definitely, we utilize a DNN, which yields a settled number of bouncing boxes. Moreover, it yields a score for every container communicating the system certainty of this crate containing an item. Model to formalize the above thought, we encode the i -th article box and its related certainty as hub estimations of the last net layer: Bounding box: we encode the upper-left and lower-right organizes of every crate as four hub values, which can be composed as a vector $li \in \mathbb{R}^4$. These directions are standardized w.r.t. picture measurements to attain to invariance to supreme picture size. Every standardized direction is delivered by a direct change of the last shrouded layer. Certainty: the certainty score for the container containing an item is encoded as a solitary hub esteem $ci \in [0, 1]$. This quality is delivered through a

direct change of the last concealed layer took after by a sigmoid. We can consolidate the bouncing box areas, as one straight layer. Likewise, we can regard gathering of all confidences as the yield as one sigmoid layer. Both these yield layers are joined with the last concealed layers. At surmising time, our calculation produces K bouncing boxes. In our tests, we utilize $K = 100$ and $K = 200$. In the event that craved, we can utilize the certainty scores and no greatest concealment to acquire a littler number of high certainty boxes at induction time. These containers should speak to questions. All things considered, they can be grouped with a resulting classifier to attain to protest discovery. Since the quantity of boxes is little, we can manage the cost of intense classifiers. In our analyses, we utilize second DNN for arrangement [11]. For preparing an objective we prepare a DNN to foresee bouncing boxes and their certainty scores for every preparation picture such that the most noteworthy scoring boxes match well with the ground truth object boxes for the picture. Assume that for a specific preparing sample, M articles were marked by bouncing boxes $g_j, j \in \{1, \dots, M\}$. Practically speaking, the quantity of forecasts K is much bigger than the quantity of ground truth boxes M . Thus, we attempt to upgrade just the subset of anticipated boxes which match best with the ground truth ones. We improve their areas to enhance their match and amplify their confidences. In the meantime we minimize the confidences of the remaining forecasts, which are esteemed not to limit the genuine protests well. To accomplish the above, we detail a task issue for every preparation sample. Let $x_{ij} \in \{0, 1\}$ indicate the task: $x_{ij} = 1$ iff the i -th forecast is allocated to j -th genuine article. The goal of this task can be communicated where we utilize L2 separate between the standardized jumping box directions to measure the disparity between bouncing boxes. Furthermore, we need to streamline the confidences of the containers as per the task x . Boosting the confidences of allocated expectations can be communicated as

In the above target, $P_j(x_{ij} = 1)$ iff forecast i has been coordinated to a ground truth. All things considered to be c_i is being boosted, while in the inverse case it is being minimized. An alternate elucidation of the above term is accomplished in the event that we see x_{ij} as a likelihood of forecast i containing an object of investment. At that point, the above misfortune is the negative of the entropy and consequently relates to a max entropy misfortune.

4.3 Neural Network Results

The system building design for the confinement and characterization models that we utilize is the same as the one utilized by. We utilize Adagrad for controlling the learning rate η , scaled down clusters of size 128, and parallel conveyed preparing with various indistinguishable imitations of the system, which attains to quicker joining. As mentioned beforehand, we utilize priors as a part of the restriction misfortune—these are registered utilizing k -implies on the preparation set. We likewise utilize 0.3 to adjust the limitation and certainty misfortunes. The localizer

may yield organizes outside the harvest region utilized for the surmising. The directions are mapped and truncated to the last picture range, toward the end.

Boxes are further pruned utilizing non-greatest concealment with a Jaccard comparability edge of 0:5. Our second model then groups every jumping box as objects of investment or “foundation”. To prepare our localizer systems, we created roughly a large number of pictures (10–30 million, contingent upon the dataset) from the preparation set by applying the accompanying technique to every picture in the preparation set. For every picture, we produce the same number of square specimens such that the aggregate number of tests is around ten million. For every picture, the specimens are bucketed such that for each of the degrees in the scopes of 05; 515; 1550; 50100 %, there is an equivalent number of tests in which the degree secured by the bouncing boxes is in the given reach. For the examinations underneath we have not investigated any nonstandard information era or regularization alternatives. In all analyses, all hyper-parameters were chosen by assessing on a held out bit of the preparation set (10 % irregular decision of samples). The pascal visual object classes (VOC) challenge is the most widely recognized benchmark for item location calculations. It comprises essentially of complex scene pictures in which bouncing boxes of 20 differing article classes were named. In our assessment we concentrate on the 2007 version of VOC, for which a test set was discharged. We present results via preparing on VOC 2012, which contains approx. 11,000 pictures. We prepared a 100 case localizer and in addition a profound net based classifier [11].

We prepared the classifier on an information set containing 10 million products covering some item with no less than 0:5 Jaccard cover closeness. The products are named with one of the 20 VOC item classes. 20 million negative products that have at most 0:2 Jaccard similitudes with any of the article boxes. These yields are marked with the uncommon “foundation” class mark. The structural planning and the determination of hyper parameters took after that of [11]. In the first round, the localizer model is connected to the most extreme focus square yield in the picture. The harvest is resized to the system info size which is 220_220. A solitary go through this system surrenders us to hundred competitor boxes. After a, not most extreme, concealment with cover limit 0:5, the main 10 most noteworthy scoring location are kept and were grouped by the 21-way classifier model in a different goes through the system. The last recognition score is the result of the localizer score for the given box reproduced by the score of the classifier assessed on the greatest square district around the harvest. These scores are taken for the assessment and were utilized for figuring the exactness review bend.

5 Data Acquiring and Results

Information social affair will be carried out by the radio modules and portable system modems to get the information on server. There will be four hubs on every cross street. Each of them will be transmitting information to the head hub of that

range. The head hub will send the information to the base station consistently. The base station will push the information on the web and every customer will have the capacity to view the reports through the data entrance. 802.15.4 is a standard for remote correspondence issued by the IEEE (Institute for Electrical and Electronics Engineers).

The IEEE is a specialized proficient affiliation that has composed various measures to advance development and interoperability of existing and rising advances. IEEE has distributed the principles that characterize correspondence in regions, for example, the Internet, PC peripherals, modern correspondence, and remote innovation. As a couple of samples, the IEEE 802.11 standard characterizes correspondence for remote LAN and 802.16 characterize correspondence for broadband remote metropolitan area networks. While both of those remote benchmarks are concerned with higher data transfer capacity Internet access applications, 802.15.4 was produced with lower information rate, basic integration, and battery application at the top of the priority list. The 802.15.4 standard indicates that correspondence can happen in the 868–868.8 MHz, the 902–928 MHz, or the 2.400–2.4835 GHz industrial scientific and medical (ISM) groups. While any of these groups can in fact be utilized by 802.15.4 gadgets, the 2.4 GHz band is mainstream as it is open in the greater part of the nations around the world. The 868 MHz band is indicated principally for European use, while the 902–928 MHz band must be utilized as a part of the United States, Canada, and a couple of different nations and domains that acknowledge the FCC regulations. The 802.15.4 standard indicates that correspondence ought to happen in 5 MHz channels running from 2.405 to 2.480 GHz. In the 2.4 GHz band, a most extreme over the-air information rate of 250 kbps is indicated, yet because of the overhead of the convention the real hypothetical greatest information rate is give or take a large portion of that. While the standard determines 5 MHz channels, just pretty nearly 2 MHz of the channel is overcome with the possessed data transfer capacity. At 2.4 GHz, 802.15.4 determines the utilization of direct sequence spread spectrum and uses an offset quadrature phase-shift keying (OQPSK) with half-sine heartbeat forming to tweak the RF transporter. The chart beneath demonstrates the different channels at the dividing determined by 802.15.4.

6 Conclusion

Computer vision is still in the period of a work in progress regarding the matter of the application which requires exceptionally vigorous arrangements as a result of light and climate issues. In this paper, the arrangement is given with the mix of the remote sensor systems and computer vision to tackle numerous issues.

References

1. Blum JJ, Eskandarian A, Huffman LJ. Challenges of intervehicle ad-hoc networks. *IEEE Trans Intell Transp Syst.* 2004;5(4):347–51.
2. Bilstrup K, Uhlemann E, Storm EG, Bilstrup U. Evaluation of the IEEE 802.11p MAC method for vehicle-to-vehicle communication. In: *Proceedings of the 68th IEEE vehicular technology conference (VTC'08)*;2008. p. 1–5. Calgary, Canada, Sept 2008.
3. <http://standards.ieee.org/board/nes/projects/80211p.pdf>.
4. Bilstrup K. A survey regarding wireless communication standards intended for a high-speed vehicle environment. Technical Report IDE 0712, Halmstad University, Sweden, Feb 2007.
5. Stibor L, Zang Y, Reuermann H-J. Evaluation of communication distance of broadcast messages in a vehicular ad-hoc network using IEEE 802.11p. In: *Proceedings of IEEE wireless communications and networking conference*; 2007. p. 254–7. Hong Kong, China, Mar 2007.
6. Wellen M, Westphal B, Mahonen P. Performance evaluation of IEEE 802.11-based WLANs in vehicular scenarios. In: *Proceedings of IEEE vehicular technology conference*;2007. p. 1167–71. Dublin, Ireland, Apr 2007.
7. Xiang W, Richardson P, Guo J. Introduction and preliminary experimental results of wireless access for vehicular environments (WAVE) systems. In: *Proceedings of international conference on mobile and ubiquitous systems: network and services*;2013. p. 1–8. San José, CA, US, July 2007 (*International Journal of Network Security & Its Applications (IJNSA)*, vol. 5, No. 2, March 2013 169).
8. IEEE P802.11p/D3.0, Part 11: Wireless LAN medium access control (MAC) and physical layer (PHY) specifications: Amendment: Wireless Access in Vehicular Environments (WAVE);2007, Draft 3.0, July 2007.
9. Jiang D, Delgrossi L. IEEE 802.11: Towards an international standard for wireless access in vehicular environments;2007.
10. Alonso A, Sjöberg K, Uhlemann E, Ström EG, Mecklenbräuker CF. Challenging vehicular scenarios for self-organizing time division multiple access. *European Cooperation in the Field of Scientific and Technical Research*;2011.
11. Mackenzie P, Miller B, Coleman DD, Westcott DA. CWAP certified wireless analysis professional official study guide;2011.
12. Kjellberg R. Capacity and throughput using a self organized time division multiple access VHF data link in surveillance applications.

Nature-Inspired Moving Sink Energy Efficient Data Gathering Protocol for Wireless Sensor Network

Biswaranjan Swain and Siddhartha S. Satapathy

Abstract Resource constrained low-cost sensor nodes deployed in large scale are the potential source of information in wireless sensor networks (WSN). Usually, sensor nodes are equipped with a non-rechargeable battery, which is having limited power and therefore its judicious use is essential for longer network life. Data gathering protocols proposed in the research literature are elegant in terms of consumption of battery power, but suffer from basic limitations. During the initial rounds of communication, all the nodes participate in data gathering process and information is received from the entire network field. However, as the time progresses, nodes start dying due to run out of battery power and the coverage-hole area increases. This paper put forwards a moving sink-based protocol for WSNs. Our extensive simulation study showed that, our protocol not only enhanced the network life time in terms of number of rounds of communications, but also addressed the coverage-hole issue.

Keywords Wireless sensor networks · Data gathering · Energy efficiency · Moving sink · Nature-inspired · Coverage-hole

1 Introduction

Wireless sensor networks (WSNs) having varied use in numerous areas and their use in environment monitoring has been a remarkable development. WSN is a collection of power constrained, inexpensive, and battery powered sensing devices which are capable to sense certain desired phenomena from the surrounding

B. Swain (✉) · S.S. Satapathy
Department of Computer Science and Engineering, Tezpur University,
Tezpur, India
e-mail: swain.biswaa@gmail.com

S.S. Satapathy
e-mail: ssankar@tezu.ernet.in

environment and send that sensed information to a data collection center called base station (BS) over wireless medium in regular time intervals. Usually, a large number of sensor nodes are deployed in order to keep the network viable even after failure of few nodes.

One of the vital issues in WSN is to use the nodes' constrained battery power efficiently, as it is not rechargeable during its operation lifetime. Sensor nodes usually utilize a fixed amount of energy to receive one bit of information and an additional amount of energy to transmit the same. This additional amount of energy varies, depending on the transmission range. Often in a WSN, the BS happens to be located away from the sensor field, which results in dissipation of more battery power by the sensor nodes in case of direct communication with BS. Therefore, in order to increase network lifetime, several multi-hop data gathering protocols have been proposed. LEACH [1] was the first such protocol designed on cluster-based architecture. Following LEACH, many variants of it [2–4] and other similar protocols with chain-based [5–8] and tree-based [9] architectures are available in the research literature. These protocols often suffer from the hot spot problem. In every round of communication, few of the nodes such as cluster head node in LEACH, chain leader node in PEGASIS [7], and the root node in TREEPSI [9] are assigned with extra responsibilities compared to other nodes in the network and are called as the hot spots. Because of the extra responsibility, these nodes consume more battery power and die early as they run out of battery power. Although these multi-hop protocols are elegant in terms of per round of energy consumption, they suffer from some of the basic limitations. First, low-cost sensor nodes are equipped with short-range transceivers and it might be difficult to make it capable of transmitting in variable ranges. Along with the aforementioned problem, the coverage issue needs to be addressed. In the initial rounds of communication, all the nodes participate in the data gathering process and therefore data received at the BS is from the entire network field. Once a node becomes dead, the area under its surveillance remains un-sensed. In this paper, we have proposed a moving sink-based protocol, the objective of which is twofold (I) to enhance the network life time by using the limited battery power prudently, (II) to address the coverage issue for the entire network life.

Movement in a spiral track is often seen in natural phenomena. Fluid moves spirally in clock/anticlockwise direction in the phenomenon such as cyclones and hurricanes. In the rivers of hilly terrains, whirlpools are commonly observed where water flows in spiral manner. In this paper, we have also approximated a spiral track for the sink movement during the data gathering process. Moving sink approaches have also been used for data gathering process in WSN earlier. Few of them are IDGP [10], HRDG [11], IAR [12], MIHOP [13], AVRVP, and TRAIL [14]. In these protocols, sensor nodes send data to the moving sink through a multi-hop path. In our proposed protocol, by incorporating a spiral track-based moving sink approach, we presumed that the moving sink is always one hop away from the sensor nodes.

The organization of the remaining paper is as follows: Sect. 2 describes the proposed protocol. In Sects. 3 and 4, simulation setup and result analysis are presented, respectively. Finally, the paper is concluded in Sect. 5.

2 Proposed Sensor Network Architecture

A schematic architecture of the sensor network is shown in the Fig. 1. A large number of application-specific inexpensive low-power sensor nodes are distributed uniformly over the sensor field in the WSN. All the sensor nodes are of equal capability and static in nature. A special mobile node equipped with rechargeable battery power moves in a spiral track to pool data from the sensor nodes and supplies the gathered data to a remote base station.

2.1 Sensor Node

In general, each sensor node comprises of five elements [1] such as sensor unit, analog-to-digital convertor (ADC), power unit operated by battery, communication unit, and central processing unit (CPU). ADC translates the analog data sensed by the sensor to digital data and sends to CPU, and also informs the sensor unit to respond accordingly. Communication unit is entitled to receive command or query from the CPU, along with transmission data from the CPU within a fixed unit distance to the outside world. CPU is responsible for interpretation of the command or query to ADC, monitoring and controlling of power if necessary, processing of received data, etc. In addition to these basic components, there may be some other components which are specific to some applications. A special mobile node called sink pools data from these nodes in regular interval.

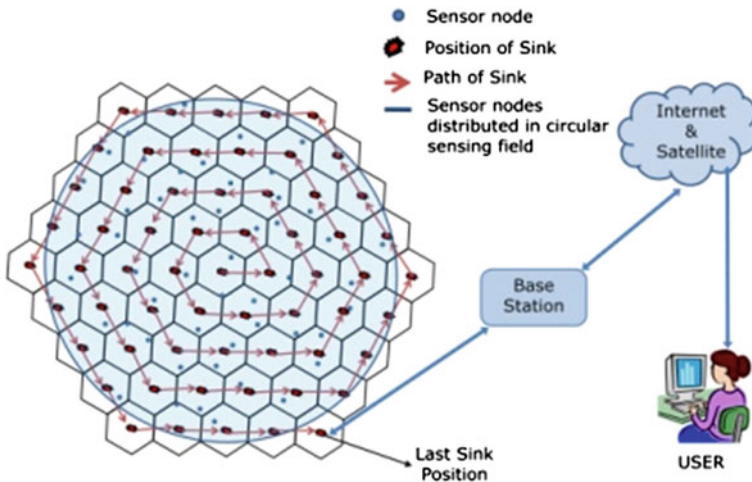


Fig. 1 Architecture of the sensor network

2.1.1 Radio Model for Energy Consumption

For estimation of energy consumption during message transmission and reception, first-order radio model [1] is commonly used. In this study, we also used the same model. In this model, energy consumed by the radio to transmit or receive data is $E_{\text{elec}} = 50$ nJ/bit and that of for transmitter amplifier is $\epsilon_{\text{amp}} = 100$ pJ/bit/m². The radios have the flexibility to go into sleep mode when required. The equations for calculating energy consumed for transmission and reception of a k -bit message within a distance d are as below:

Transmitting:

$$ETx(k, d) = E_{\text{elec}} * k + \epsilon_{\text{amp}} * k * d^2. \quad (1)$$

Receiving:

$$ERx(k) = E_{\text{elec}} * k. \quad (2)$$

2.2 Sink

Sink is a special node with mobility and a rechargeable battery. The sink node moves in a spiral track as discussed in the subsequent section and pools data from the sensor nodes at specific locations in the network field. After pooling data from the entire network, it communicates the data to the base station (BS). Finally, data can be accessed by the user from the BS either directly or through internet.

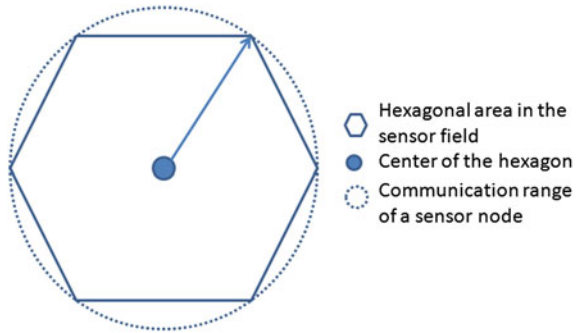
2.3 Sensor Field

The sensor field is a circular one in which sensor nodes are spread uniformly. The sensor field is divided into closely-packed hexagons of radius equal to the range of communication of a sensor node (Fig. 2). Starting from the central hexagon in the network field, the sink moves to each of the hexagons in a spiral path and gathers data from the sensor nodes which are present in their respective hexagon.

2.4 Spiral Track Generation for Sink Movement

A spiral track can be designed using several ways such as logarithmic, sine-cosine functions, and even using half-circle mathematical models. However, we observed that none of these models is suitable for modeling track of the sink in our architecture. In these models, the gap in the spiral path increases non-uniformly as we move in outward direction from the center of the sink. This uneven spacing in the spiral path exaggerates the coverage-hole issue. In our network architecture, we

Fig. 2 Hexagonal sensor field and communication range of a sensor node



assumed that the sensor nodes are capable to communicating within a fixed range and therefore many of the nodes will not be able to communicate with the sink node. We therefore divided the sensor field into hexagons and generated the spiral track (Fig. 1) for the sink node dynamically from the geometry of the hexagonal fields as explained below.

2.4.1 Layering of the Hexagons

For the purpose of implementation of the hexagonal track, the hexagons are grouped into different concentric circular layers starting from the innermost hexagon. The hexagon at the center of the area is assigned layer number 0, next layer as 1, and so on. In the layer number 0, only one hexagon is present, and in the remaining layers, number of hexagons present is six times of its layer number. Total number of layers can be calculated from the area of the sensor network field and the area of the hexagon. It is evident from Fig. 1 that the sink node changes direction in a systematic manner in the spiral track. From the orientation of the previous path, sink node changes the direction by an angle and move a fixed distance for the next position. The angle can be calculated from the algorithm FindTrack.

After reaching the last position, the sink transmits all the gathered data to the BS in that round. Then it moves back to the center of network field for the next round of data gathering process.

2.4.2 Calculate the Distance Between Two Consecutive Sink Positions

Assuming radius of the circle circumscribing the hexagonal area to be same as the communication range of a sensor node, the distance between the two consecutive sink positions is calculated as follows from Fig. 3.

$$\overline{AB} = 2 * \overline{AC} * \cos(30^\circ). \tag{3}$$

Here, \overline{AC} is the communication range of the sensor node and \overline{AB} is the distance between the center of the two neighboring hexagons or the two neighboring sink

positions. Assuming communication range of a sensor node as 1.0 unit, we have approximated \overline{AB} equal to 1.73205 unit.

Procedure FindTrack

```
/* The sink starts from the centre of the network field
called origin. For each new position, it makes certain
angle with the previous path and moves a distance of
1.73unit. After collecting data from last hexagon it
returns back to the centre of sensing region.*/
```

```
centre at 0.0;
k ← 6 ; /*number of hexagons increased per layer*/
layer ← 1;
while layer ≤ n do
/*Determination of position of sink in layer1*/
  if layer ← 1 then
    next sink at 0 deg; /*1st position in layer1. Sink
moves with 00 and 1.73unit*/
    next sink at 120 deg; /*2nd position in layer1*/
    i ← 3;
    while i ≤ k do
      next sink at 240 deg;
      i ← i+1;
    end while
    /*Determination of position of sink in layer 2 and
onwards*/
  else
    next sink at 180 deg;
    next sink at 240 deg;
    j ← 2;
    i ← 1;
    while i ≤ layer-2 do
      next sink at 180 deg;
      j ← j+1;
    end while
    while j < k do
      next sink at 240 deg;
      j ← j+1;
      i ← i+1;
      while i ≤ layer-1 do
        next sink at 180 deg;
        j ← j+1;
        i ← i+1;
      end while
    end while
  end if
  k ← k+6;
  layer ← layer+1;
end while
end procedure
```

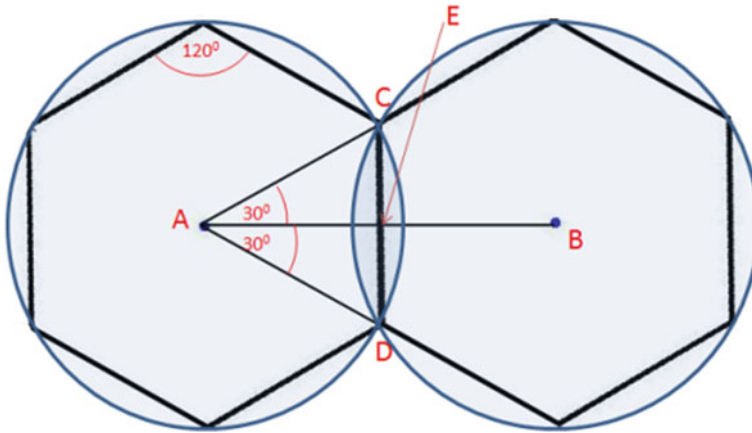


Fig. 3 Calculation of the distance between two consecutive sink positions

2.5 Data Gathering Within the Hexagonal Field

The sink after reaching the center of the hexagon broadcasts a BEACON frame, inviting response from the sensor nodes which are in the neighborhood. In response to the BEACON frame, sensor nodes send REPLY indicating their willingness to send the sensed information along with details about its residual battery power and position. After receiving REPLY message from the sensor nodes, the sink node may form a TDMA schedule for the sensor nodes and pool data from the hexagonal field. As the hexagonal field is of a unit sensing range, we can assume that the data available with each of the sensor node within the hexagonal field to be almost similar. Therefore, for optimization purpose, instead of pooling data from all the sensor nodes, sink chooses only one node based on the remaining battery power and pool data from that node.

3 Simulation Setup

We did an extensive simulation study of our proposed protocol in MATLAB. In our simulation study, we distributed five hundred sensor nodes randomly in a circular network field of radius 50 m. Each sensor was assumed to communicate within a fixed range. In our simulation setup, we assumed that a sensor can communicate within a diameter of 10 m and accordingly, the sensor field was divided into hexagons with diameter approximately equal to the communication range. In order to cover the entire circular network area maximum number of layers of hexagons is calculated as (upper-bound of (radius/(2*range)) + 1). As stated earlier, the center of the hexagonal fields are traversed in a spiral track. The sink starts from the center

of the central hexagon, which is considered as origin and moves from center to outward direction in the spiral track. Given the current sink position, next sink position was determined dynamically using the algorithm FindTrack. Initial battery power of every sensor node is assumed to be fixed as a maximum value (0.5 joule). For our simulation purpose, we assumed the size of data packets to be 3000 bits and that of the of the REPLY message to be 1000 bits. We neglected battery power consumption for receiving BEACON frame as the size of the frame was negligible compared to the data packet.

4 Result and Analysis

We did simulation study to analyze the performance of our proposed protocol. In our study, we densely deployed 500 nodes in the sensor field of radius 50 m (Fig. 4). Each node will consume a fixed amount of battery power in every round of data gathering, as the communication range of sensor node is fixed. Therefore, theoretically it was easy to calculate the life of the sensor network in terms of maximum possible round of communications. This theoretical value depends on the initial battery power of sensor node. However, sensor nodes deployed in nearby area will often sense the similar information from the environment and therefore we may think of allowing only one node to communicate to sink node from a closed area in every round of data gathering process. This would increase the network life.

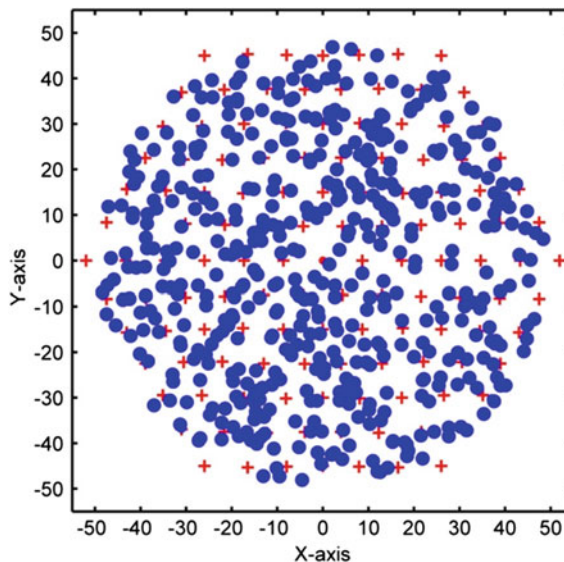


Fig. 4 Initial node distribution in the WSN

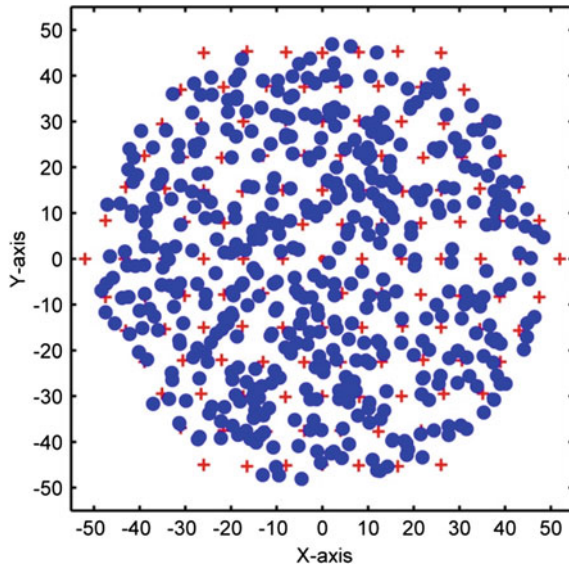


Fig. 5 Distribution of live nodes after 99.6 % of the network life in the WSN

In our simulation, the sink node determines which sensor node will send the data to the sink in a round of data gathering process. Within a hexagonal area, sink selects a node randomly from the willing nodes considering remaining battery power and participation in the previous round. We assumed battery power of every sensor node to be 0.5 J. In our network with 500 nodes, total number of data gathering rounds was found to be 2496. Out of these rounds, all the nodes were live up to the 2487th round (Fig. 5), i.e., the 1st node dies only after 99.6 % of the

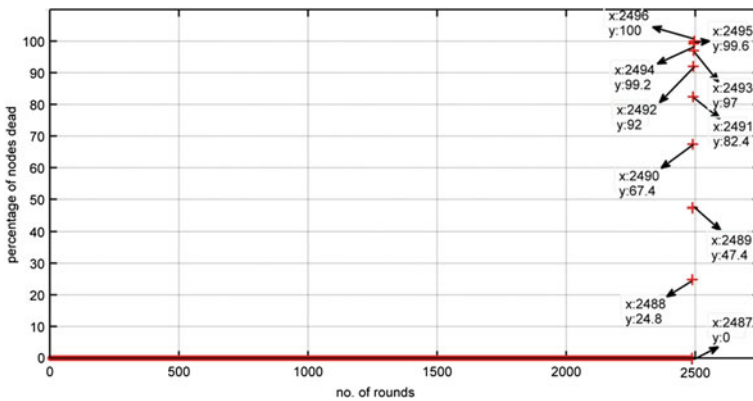


Fig. 6 Node death percentage versus life of the network in terms of number of data gathering rounds

network life. In the round 2488, 24.8 % nodes died, in round 2489, 47.4 % nodes died, and finally after round 2496 all the 100 % nodes died. Node death percentage in the data gathering process is shown in Fig. 6. From these results, it is clear that all the nodes remain active throughout larger portion of the network lifetime.

5 Conclusion and Future Works

In this article, we presented moving sink-based architecture for gathering data in a wireless sensor network. While keeping sensor node design simple and low cost, our moving sink-based protocol maximizes life of the network. As the sensor nodes communicate directly with the sink node, they consume limited battery power and that give longer life to the network. The simulation result shows that all nodes remain alive for 99.6 % of the entire sensing period. This indicated that our proposed protocol has the potential to minimize the coverage area-related issues throughout the network life. Future work lies for simulation for the proposed protocol in a network simulator.

References

1. Heinzelman W, Chandrakasan A, Balakrishnan H. Energy-efficient communication protocol for wireless microsensor networks. In: Proceedings of the 33rd annual Hawaii international conference on system sciences 2000;2000. p. 10.
2. Kumar N, Kaur J. Improved leach protocol for wireless sensor networks. In: Proceedings of 7th IEEE international conference on wireless communications, networking and mobile computing (WiCOM);2011. p. 1–5.
3. Sharma M, Sharma K. An energy efficient extended LEACH (EEE LEACH). In: Proceedings of international conference on communication systems and network technologies (CSNT);2012. p. 377–82.
4. Xiangning F, Yulin S. Improvement on LEACH protocol of wireless sensor network. In: IEEE international conference on sensor technologies and applications, SensorComm 2007; 2007. p. 260–4.
5. Chen K, Huang J, Hsiao C. CHIRON: an energy-efficient chain-based hierarchical routing protocol in wireless sensor networks. In: Proceedings of IEEE wireless telecommunications symposium; 2009. p. 1–5.
6. Jung S, Han Y, Chung T. The concentric clustering scheme for efficient energy consumption in the PEGASIS. In: Proceedings of IEEE 9th international conference on advanced communication technology;2007, vol. 1, p. 260–5.
7. Lindsey S, Raghavendra C. PEGASIS: Power-efficient gathering in sensor information systems. Proc IEEE Aersp Conf. 2002;3:1125–30.
8. Tabassum N, Mamun Q, Urano Y. COSEN: a chain oriented sensor network for efficient data collection. In: Proceedings of IEEE third international conference on information technology: new generations;2006. p. 262–7.
9. Satapathy S, Sarma N. TREEPSI: tree based energy efficient protocol for sensor information. In: Proceedings of IFIP international conference on wireless and optical communications networks;2006. p. 4.

10. Sheu J, Sahoo P, Su C, Hu W. Efficient path planning and data gathering protocols for the wireless sensor network. *Comput Commun.* 2010;33(3):398–408.
11. Huang J, Liu D. A high-reliability data gathering protocol based on mobile sinks for wireless sensor networks. In: *Proceedings of IEEE wireless and optical communication conference (WOCC)*;2013. p. 304–8.
12. Kim J, In J, Hur K, Kim J, Eom D. An intelligent agent-based routing structure for mobile sinks in WSNs. *IEEE Trans Consum Electron.* 2010;56(4):2310–6.
13. Liu D, Zhang K, Ding J. Energy-efficient transmission scheme for mobile data gathering in wireless sensor networks. *Commun China.* 2013;10(3):114–23.
14. Tian K, Zhang B, Huang K, Ma J. Data gathering protocols for wireless sensor networks with mobile sinks. In: *Proceedings of IEEE global telecommunications conference (GLOBECOM 2010)*;2012. p. 1–6.

Mining Frequent Itemsets in Association Rule Mining Using Improved SETM Algorithm

D. Kerana Hanirex and K.P. Kaliyamurthie

Abstract The Association rule mining is one of the recent data mining research. Mining frequent itemsets in relational databases using relational queries give great attention to researchers nowadays. This paper implements modified set oriented algorithm for mining frequent itemsets in relational databases. In this paper, the sort and merge scan algorithm SETM (Houtsma and Swami, IEEE 25–33 (1995)) [1] is implemented for super market data set which is further improved by integrating transaction reduction technique. Our proposed algorithm Improved SETM (ISETM) generate the frequent itemsets from the database and find its execution time. Finally the performance of the algorithm is compared with the traditional Apriori and SETM algorithm.

1 Introduction

Data mining is the process of finding the hidden information from the database. Since large amounts of information are stored in companies for decision making the data need to be analyzed carefully. This process is known as Data mining or knowledge discovery in databases. Data mining consists of various tasks such as classification, clustering, association rule mining, sequence analysis. Classification is the task of classifying the data into predefined classes where as in clustering data are grouped together based on similar characteristics.

Paper [2] proposes about an unifying frame work and the classification, association and sequence discovery were discussed in the frame work. Paper [3] proposes about the conceptual clustering algorithm in query processing and its usage were discussed. Paper [4] emphasis on INLEN architecture which integrate

D. Kerana Hanirex (✉) · K.P. Kaliyamurthie
Department of Computer Science and Engineering, Bharath University, Chennai, India
e-mail: keranarobinson@gmail.com

K.P. Kaliyamurthie
e-mail: kpkaliyamurthie@gmail.com

knowledge based machine learning algorithms with relational data bases. Paper [5] proposes association rule discovery in large databases. This system proposes association rule discovery in database systems. Paper [6] proposes technique to improve the efficiency of the association rule mining in huge databases.

In association rule mining one can find the frequent item set. An itemset is a frequent itemset if the number of occurrence is above the minimum threshold. Various work has been proposed in association rule mining. Various algorithms has been proposed for mining frequent item sets. These algorithms are feasible only for small data sets. Performance is a problem when dealing with large data sets. Paper [1] proposes set oriented approach in database systems. This set oriented approach integrate the association rule discovery with relational database systems.

In our earlier research work, paper [7] proposes mining frequent itemsets using genetic algorithm. Paper [8] implements mining frequent itemset for Dengue virus data set using Apriori algorithm. In paper [9–12] various techniques such as clustering, integration of classification with association mining techniques and various algorithms such as Apriori, Fp-growth used for mining frequent itemsets using different datasets were analyzed. In paper [13], association rule mining is implemented for distributed databases. In paper [14], Two Dimensional Transaction Reduction Approach (TDTR) algorithm is proposed. This transaction reduction technique is integrated in our proposed ISETM algorithm.

This paper describes the set oriented mining in Sect. 2. In Sect. 3 set oriented algorithm SETM which includes simple sorting and simple merge-scan join operations is given. Section 4 describes the proposed ISETM (Improved Sort and Merge Scan Algorithm). Section 5 describes about the dataset description. Section 6 describes the data preprocessing. Section 7 includes the results and discussions. Section 8 presents our conclusion.

2 Set Oriented Mining

This paper uses supermarket data set for finding frequent item sets. This data set consists of collection of transactions which involves the purchase of items by a customer. The frequent itemset can be generated by repeated joins with TRANS. TRANS is a table which stores all the transactions of the customers from the supermarket data set with the schema TRANS (trans_id,item).

An association rule is of the form $X \Rightarrow Y$ where X is the antecedent and Y is the consequent of the rule [15]. Support of an itemset can be defined as the ratio of the number of transactions supporting that transaction to the total number of transactions in the database. Confidence measure can be defined as the ratio of the number of transaction that occur together to the number of transactions in the antecedent. An itemset is a frequent itemset if the number of occurrence of an itemset is above the minimum support value. We are interested with association rules whose support value is greater than the minimum support value. For any pattern of length k , the association rules are generated by combining all possible combinations of $k - 1$

items in the antecedent. For each antecedent and consequent of the rule we have to check if the confidence exceeds the minimum confidence factor.

The frequent itemset are generated by performing repeated joins with TRANS table. To generate all pattern of exactly 2 items we can use this query

```
SELECT s1.trans_id, s1.item, s2.item
FROM TRANS s1, TRANS s2
WHERE s1.trans_id = s2.trans_id and s1.item <> s2.item
```

All patterns of 3 itemsets are generated by joining the 2 item pattern with the TRANS table. We can repeat this joining to find the largest frequent itemset. This doesn't give the good result based on its performance [1].

3 SETM Algorithm

This algorithm is proposed by Houtsma and Swami [1]. This algorithm uses two sort operations and one merge-scan join. The first sort is used to implement merge scan join and the second sort is used in order to generate support count efficiently.

Algorithm:

```
k=1;
Sort s1 on trans_id, item;
C1=Generate counts from s1;
repeat
  k=k+1;
  Sort on sk-1 on trans_id, item1, ..., itemk-1;
  sk1 := merge-scan sk-1, s1;
  Sort sk1 on item1, ..., itemk;
  Ck := generate counts from sk1;
  Sk := filter Sk1 to retain supported patterns;
until Sk = {}
```

4 Proposed Algorithm: (ISETM)

The following proposed algorithm ISETM is the improved sort and merge scan algorithm which integrates transaction reduction approach using TDTR algorithm (Two Dimensional Transaction Reduction) [14] which we proposed earlier. This transaction reduction technique delete transactions having items less

than a minimum threshold value and delete items having less than a minimum threshold value.

Algorithm:

```

Set minthreshold m;
For i=1 to n(no of transaction)
  c1[i]=Generate counts on items for each transaction;
  c2[i]=Generate counts on transactions for each item;
  Delete transactions from s1 where C1[i]< m;
  Delete items from s1 where C2[i]<m;
  i=i+1;
k=1;
Sort s1 on trans_id,item;
C1=Generate counts from s1;
repeat
  k=k+1;
  Sort on sk-1 on trans_id,item1,...itemk-1;
  sk1 := merge-scan sk-1, s1;
  Sort sk1 on item1, ..., itemk;
  Ck := generate counts from sk1;
  Sk := filter Sk1 to retain supported patterns;
until Sk = {}

```

This algorithm generates largest frequent itemset from which the subsets are generated.

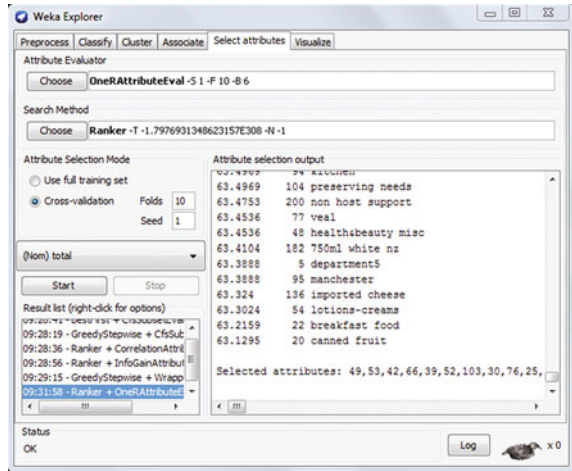
5 Data Description

This algorithm is implemented using super market dataset available in UCI data repository with 4627 instances and 217 attributes.

6 Data Preprocessing

Data need to be processed in order to improve the quality of the data. The various tasks of data mining are data transformation, data Integration, data discretization, data cleaning and data reduction. Data cleaning involves removing noisy data, incomplete data, inconsistent data. Data integration combines data from multiple sources. Data transformation task contains data aggregation, generalization, data smoothing, and normalization. Data reduction includes data aggregation, high dimensionality reduction, data compression and discretization.

Fig. 1 Selection of attributes



In this paper we have applied preprocessing using weka3.6.4 tool for this Supermarket data set. Here t represents that item present in the corresponding transaction. The data preprocessing filters such as ReplaceMissingValues, Normalization are not suitable for this data set.

Here we applying one of the data preprocessing technique called selection of attributes. Here the attributes are selected by Weka3.6.4 tool using Attribute Evaluator OneRAttributeEval and the search method we are using here is the Ranker. The following Fig. 1 shows the selection of attributes in supermarket marketdataset. Here 211 attributes are selected instead of 216 using this OneRAttributeEval.

7 Results and Discussions

In this paper the accuracy is generated by finding the number of association rules generated for different threshold values. The effectiveness of the association rule mining is measured by considering the time taken to generate the association rules from databases. The execution time and accuracy generated by ISETM algorithm is compared with SETM and traditional Apriori algorithm.

The following Tables 1 and 2 show the performance evaluation of Apriori algorithm for its efficiency and accuracy by varying its confidence and support.

7.1 Performance of Apriori Algorithm

See Tables 1 and 2.

Table 1 Execution time in secs (Apriori algorithm)

Confidence					
Support	90	80	70	60	50
10	109	115	120	121	123
20	33	34	34	35	35
30	18	18	19	20	21
40	13	14	14	15	15
50	8	9	9	10	11

Table 2 Number of association rules generated (Apriori algorithm)

Confidence					
Support	90	80	70	60	50
10	458	8071	24,570	43,580	69,369
20	–	210	759	1314	1982
30	–	1	67	148	231
40	–	–	10	30	32
50	–	–	3	4	4

7.2 Performance of SETM Algorithm

The following Tables 3 and 4 show the performance evaluation of SETM algorithm for its efficiency and accuracy by varying its confidence and support.

7.3 Performance of ISETM Algorithm

The following Tables 5 and 6 show the performance evaluation of ISETM algorithm for its efficiency and accuracy by varying its confidence and support.

From the above table we can identify that ISETM algorithm has higher efficiency and accuracy than SETM and traditional Apriori algorithm. This algorithm reveals some additional hidden rules and the execution time is less when compared with Apriori and SETM algorithm.

Table 3 Execution time in secs (SETM algorithm)

Confidence					
Support	90	80	70	60	50
10	105	110	116	118	120
20	30	31	31	33	34
30	15	15	17	19	20
40	10	12	12	13	14
50	8	9	9	10	11

Table 4 Number of association rules generated (SETM algorithm)

Confidence					
Support	90	80	70	60	50
10	464	8080	24,580	43,592	69,382
20	–	218	767	1324	1992
30	–	1	67	152	236
40	–	–	10	32	34
50	–	–	3	4	4

Table 5 Execution time in secs (ISETM algorithm)

Confidence					
Support	90	80	70	60	50
10	95	100	108	110	112
20	25	26	26	28	29
30	12	12	13	15	15
40	9	10	10	11	11
50	6	7	7	8	8

Table 6 Number of association rules generated (ISETM algorithm)

Confidence					
Support	90	80	70	60	50
10	464	8085	24,588	43,599	69,389
20	–	225	775	1342	2015
30	–	1	70	155	238
40	–	–	10	32	37
50	–	–	3	4	4

The following Fig. 2 shows the performance evaluation of Apriori and SETM with ISETM algorithm by varying confidence value with support = 10 for its efficiency.

The following Fig. 3 shows the performance evaluation of Apriori, SETM and ISETM algorithm by varying confidence value with support = 20 for its accuracy.

From the above results we can understand ISETM algorithm works well and the number of rules generated gets increased for a decreasing confidence value while with increasing support value the number of rules generated gets decreased. The execution time gets increased when the confidence value gets decreased and gets decreased with increasing support value. This algorithm reveals additionally some hidden rules.

Fig. 2 Comparison of execution time in secs between Apriori, SETM and ISETM algorithm for supermarket dataset with support = 10 and by varying confidence

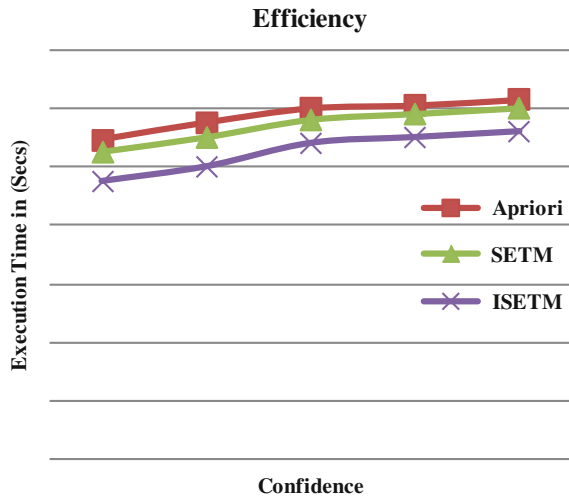
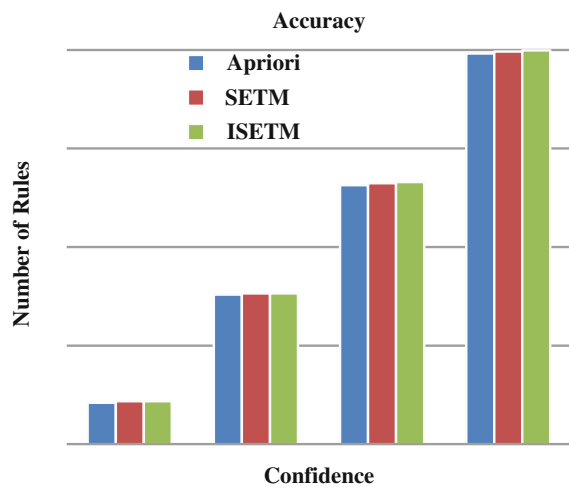


Fig. 3 Comparison of number of rules generated between Apriori, SETM and ISETM algorithm for supermarket dataset with support = 20 and by varying confidence



8 Conclusion

The ISETM algorithm has been implemented to find the frequent itemsets using super market dataset. The efficiency and accuracy of the ISETM algorithm is measured and it is compared with standard Apriori algorithm for association rule. This algorithm works well and stable and provides similar performance with the traditional Apriori algorithm. The execution time is less when compared with Apriori and SETM algorithm and it reveals additional hidden rules.

References

1. Houtsma M, Swami A. Set oriented mining for association rules in relational databases. *IEEE*;1995:25–33.
2. Agrawal R, Imielinski T, Swami A. Database mining: a performance perspective. *IEEE Trans Knowl Data Eng. Special issue on Learning and Discovery in Knowledge-Based Databases. 1993*;5(6): 914–25.
3. Anwar TM, Beck HW, Navathe SB. Knowledge mining by imprecise querying: a classification-based approach. In: *IEEE 8th international conference on data engineering*;1992.
4. Michalski RS, Kerschberg L, Kaufman KA, Ribeiro JS. Mining for knowledge in databases: the INLEN architecture, initial implementation, and first results. *J Intell Inf Syst. 1992*;1:85–113.
5. Agrawal R, Imielinski T, Swami A. Mining association rules between sets of items in large databases. In: *Proceedings of ACM-SIGMOD international conference on management of data. 1993*;207–16.
6. Umarani V, Punithavalli M. A study on effective mining of association rules from huge databases. *IJCSR. 2012*;1(1).
7. Kerana Hanirex D, Kaliyamurthie KP. Mining frequent itemsets using genetic algorithm. *Middle-East J Sci Res. 2014*;19(6):807–10.
8. Kerana Hanirex D, Kaliyamurthie KP Dr. Finding the dominating amino acids in dengue virus type1 study on mining frequent itemsets. *Int J Pharma Bio Sci. 2013*;4(3)(B):880–9.
9. Kerana Hanirex D, Kaliyamurthie KP Dr. Multi-classification approach for detecting thyroid attacks. *Int J Pharma Bio Sci. 2012*;4(3)(B):1246–51.
10. Kerana Hanirex D. A comparative analysis on mining frequent itemsets. *Int J Adv Res Comput Sci Electron Eng (IJARCSEE). 2012*;1(10):68–71.
11. Kerana Hanirex D, Kumaravel A Dr. An efficient partition and two dimensional approach for mining frequent itemsets. *Int J Technol Synth Anal (IJTSA). 2012*;1(1):14–7.
12. Kerana Hanirex D, Dorai Rengaswamy MA. Efficient algorithm for mining frequent itemsets using clustering techniques. *IJCSE. 2011*;3(3):1028–32.
13. Kerana Hanirex D. Association rule mining in distributed database system. *Int J Comput Sci Mob Comput (IJCSMC). 2014*;3(4):727–32.
14. Kerana Hanirex D. An efficient TDTR algorithm for mining frequent itemsets. *Int J Electron Comput Sci Eng. 2012*;2(1):251–6.
15. Piatesky-Shapiro G. Discovery, analysis and presentation of strong association rules. In *knowledge discovery in databases. AAAI/MITPress*;1991. p. 229–48.

An Efficient Approach for Evolution of Functional Requirements to Improve the Quality of Software Architecture

M. Sunil Kumar and A. Rama Mohan Reddy

Abstract Software architecture will be designed within the early phases combined with the development process; the huge constraints makes it possible for the achievement of certain functional requirements, quality attributes (non-functional requirements), and also business goals. Metaheuristic search algorithm performs an important role within the software architecture design to improve the performance of obtaining an optimal solution from the huge search space. This particular paper mainly focusses on balancing the combinations of “Adaptive Genetic algorithm,” which has to be applied. It has incorporated the usage of roulette wheel selection operators; this technique is implemented in java and it also finds out global minima as well as time reduction when compared with Genetic algorithm.

Keywords Software architecture • Functional requirements • Quality attributes • Responsibility • Metaheuristic search algorithms • Adaptive genetic algorithm • Simulated annealing

1 Introduction

Software plays an essential role in all the aspects of our life. The rising usage of several applications facilitating varying user’s necessities creates a sharp increase in the scale and complexity of software, which results in the decline of the software quality. As a result, the main challenges in software engineering are to measure, understand, manage, control, and lower the software complexity [1]. Software product line engineering aims at improving the productivity and reduces the realization times by collecting the analysis, design, and implementation actions of a

M. Sunil Kumar (✉)

Department of CSE, Sree Vidyanikethan Engineering College, Tirupati, India
e-mail: sunilmalchi1@gmail.com

A. Rama Mohan Reddy

Department of CSE, S.V.U. College of Engineering, SV University, Tirupati, India

© Springer India 2016

S.S. Dash et al. (eds.), *Artificial Intelligence and Evolutionary Computations in Engineering Systems*, Advances in Intelligent Systems and Computing 394, DOI 10.1007/978-81-322-2656-7_71

775

family of systems. Characteristics that vary from product to product form the variabilities. The major challenge in the context of the software product lines (PL) approach is to form and put into practice these variabilities [2]. Along with the magnitude and intricacy of the software systems varies the computational complexity of theirs. The design of the software system, the allied methodologies, and data structures play a major role in fixing the problem. The major structural concerns in the process of software system design include designing efficient communication protocols and simpler synchronization mechanisms, component formation and assessment of the components as a whole, physical placement of components on the network nodes, service distribution on the network nodes in order to support faster services to the user, etc. The design process is a spiral model, which presents the most appropriate design model given in the system requirements by considering all the possible design alternatives.

2 Problem Statement

Along with the growth of software industry, the necessity for online software systems has increased. To accommodate the enhancing technology and needs into the system on-the-fly, the architecture of the software system should be carefully designed and thoroughly analyzed. Standards, procedures, and processes to develop such system architectures need to be established. Automation up to some extent may help software architects to start from a general skeleton architecture and build on it. This leaves the architects more time to refine the architectural designs to the maximum possible extent.

This paper is only a humble beginning and there is yet an ocean of research to be done in the field. The analysis on the associated workings, which uses the genetic algorithm, has revealed that regardless of being technically sophisticated, the methods seem to be short of reduction in the computational time which further influences the excellence of the software. While designing the software, computational time is given the principal consideration. The software is considered to be quality software only when the time for computing a process is less. This has necessitated the requirement for developing better techniques for the architecture of the software with the intention of reducing the computational time and also to boost the quality of the software being designed.

Automation process may further be used to compare various possible architectural styles and designs for a given application in order to select the appropriate and best suitable combination. The idea of using the concepts of genetic science to refine the architecture model to produce the best possible automation is studied in this thesis work. The basic idea is to maintain a database of architectural styles, design patterns, and apply genetic algorithms to derive all the possible design alternatives for a given application/system, by providing the basic constraints/guidelines to be followed while generating the possibilities.

To facilitate in overcoming the disadvantages, a novel approach “An Adaptive Genetic Algorithm” has been taken in the beginning with a set of responsibilities in the class diagram. The responsibility dependency graph has been then derived which is further considered as input to the adaptive genetic algorithm, which produces suggestions for identifying the quality requirements for the architecture.

3 Metaheuristic Search Algorithm

3.1 Justification of Applicability of Metaheuristic Algorithms in Software Architecture Domain

The field of metaheuristic provides solutions to various combinatorial optimization problems like scheduling problem, integer programming, resource assignment problem, cutting stock problem, network routing problem, tree optimization problem, neural network design problem, etc. [3]. The field of Evolutionary Algorithms (EAs) had its beginning when researchers thought of using the phenomena observed in the evolution of life-form in the real world. Since then, a variety of algorithms have been developed. For example, optimization algorithms based on ant-colony behaviors have been designed. The inspiration was taken from the biological processes like population, reproduction, mutation, selection, survival of the fittest, etc. One of the advantages of evolutionary algorithms is that they can be easily modularized and hence parallel programming can be used.

For many applications or real-world problems, there does not exist exact problem-specific solutions and heuristics to be followed to find optimal and feasible solutions. In such cases, the field of metaheuristic can be helpful beyond the expectations in finding an optimal and computable solution for a given problem. The field of evolutionary algorithms along with defined problem-specific heuristics in combination with the other fields like local-search-based techniques, sampling techniques, etc., is aimed at achieving highly efficient optimization algorithms. Any problem when transformed into a combinatorial optimization problem can be solved by using metaheuristics.

3.2 Genetic Algorithms

On observing the evolution of different species of life-form, many biological principles have been found, which can be used for supporting natural evolution of a feasible solution in the process of search-based optimization [4]. It shares a commonality with the simulated annealing approach that it performs better when compared to gradient-based optimization strategy [5]. Its use is particularly appreciated when it is applied to applications or systems that show high nonlinearity. Also, it is

Table 1 Application of genetic algorithm

Some application areas by domain	Some application areas by technique
Industrial design by parameterization	Chromosomes to set membership and function optimization
Scheduling	Real valued chromosomes to function optimization
Network design by construction	Order-based binary chromosomes for optimization by construction
Routing	Tree-based chromosomes for genetic
Time series prediction	Domain-specific chromosomes for specialized solutions to particular problems

useful in situations where global optimum is to be derived from the many existing local optimums. The general working strategy of the GA algorithms can be described as follows in Table 1.

- i. A random selection of a set of initial seed points is made from the given design search space, then
- ii. Design alternatives are further improved by repeatedly applying genetic principles.

3.3 *Applicability of Genetic Algorithm in Architectural Modeling*

The dramatic improvement in the field of computing technology has given immense scope to researchers world-wide to perform deep and enhanced experimentation with their approaches efficiently and swiftly. The applicability of the newly developed approaches in specific domains could be proved. Further improvements could be effectively suggested. This has speeded up the area of research productively. As genetic algorithms need high computational power, their use after their conception was limited. As the technology grew, their use was steadily boosted up. But in the software architecture design process, the usage of genetic algorithms has been thought of and worked upon only recently. Only since the establishment of the importance of software architecture design (in handling large and complex problems efficiently) has the prospective idea of utilizing genetic principles in the design process been given a thought. Developing various design alternatives and evaluating them to extract a best design solution throws a challenge to the architects, where search-based optimization comes into picture [6]. Genetic algorithms are best suited for handling these challenges in the process of designing software architecture.

In software architecture design, genetic algorithms can be used to handle two challenges. In one way, genetic algorithms help to choose the optimal feasible

solution among the given population of the design alternatives by setting objective functions. In another way, genetic algorithms are helpful in the evolution of new design alternatives from the existing ones.

4 Proposed Methodology of Adaptive Genetic Algorithm

This paper uses adaptive genetic algorithm of software architectures to introduce varying levels of automation into design, planning, and maintenance phases. The conducted studies use UML-based representation of software architecture design. The work is in light of the perspective that software architecture is a result of a series of decisions made to incorporate the concerns of different stakeholders in the system. The decisions translate into solutions inside software architectures, where some solutions are specific to the system while others can be reused. In this work, all architectural changes resulting from architectural decisions are called architectural solutions or simply *solutions*. Software architecture can be considered as a collection of architectural solutions. A solution in its entirety enters or leaves software architecture thereby affecting some property of the system.

If we consider software architecture as a combination of solutions, then, designing a system can be understood as finding a feasible configuration of the solutions. Each solution not only resolves a functional requirement but also has an impact on quality attribute(s). The quality-related implications of the well understood solutions are usually well-documented and are known in advance. Thus, a careful selection of the solutions can be expected to lead to an acceptable architecture. This scenario can be formulated as a search problem: in principle, an algorithm can be designed which will find an optimal configuration of the solutions available in a solution database, given the architecturally significant requirements of the system. In this kind of problem, metaheuristic search methods usually outperform deterministic approaches. Adaptive genetic algorithms belong to the metaheuristic search methods family and have been employed in many studies to address software engineering problems.

In this paper, adaptive genetic algorithms have been employed to design software architectures. The adaptive genetic algorithm synthesizes software architectures and applies solutions from a solution base, thus producing improved designs. Each of the solutions is introduced through adaptive mutations employed in the adaptive genetic algorithm. The adaptive genetic algorithm is provided with an objective or fitness function to gauge the modifiability, efficiency, and complexity of the architectures. The algorithm takes an input initial design and properties of the developing organization to produce initial work distribution plans. The solutions are introduced in the architecture to ease its distribution among the teams as well as to reduce the inter-team communications during the architecture development. The difficulties in communication among the involved teams are therefore taken into account in the fitness function. The difficulties usually have their origin in the cultural, lingual, or social dissimilarities among the teams.

Consequently, the adaptive genetic algorithm favors low coupling among the components to be assigned to teams with significant overhead in communication and vice versa. Furthermore, extreme over- or under- loading of the teams are also discouraged by the fitness function. Our adaptive genetic algorithm-based maintenance is planned around some specific modification needs; instead, one or more properties, (e.g., efficiency, reliability, etc.) are targeted for maintenance. The major preplanning activities involve designing of the fitness function and selection of the solutions that have an influence on the maintained properties. Once equipped with the solutions and the fitness function, our adaptive genetic algorithm can address a wide range of future, possibly unpredictable modification needs associated with the maintained properties.

The developed genetic algorithm includes a set of solutions with an effect on the performance and reliability in distributed systems settings. The fitness function measures efficiency and reliability of architectures. The infrastructure allows run-time updating of Java classes. All the modifications, manual or automatic, are performed within the UML class diagram-based architectural representation of a running system. The software is considered to be quality software only when the time for computing a process is less. This necessitated for the requirement of developing a better technique for the architecture of the software with the intention of reducing the computational time and also to boost the quality of the software being designed. Besides the computational time, the fitness value for the solution also stays to be less which can influence the architecture of the software by and large. To overcome these disadvantages, we have designed a technique using the adaptive genetic algorithm which is proved to be a competent method for software architecture.

The alteration operation passed out is adaptive alteration in adaptive genetic algorithm which demonstrates to be further competent than the standard mutation operation in GA. Regarding its enhanced steps such as crossover, mutation, and also offers improved fitness value, the adaptive genetic algorithm is leading over normal GA. By pertaining to the adaptive alteration, the fitness value of the consequent solution for the architecture is enlarged when balanced with the algorithm utilized in the presented method, which can result in enhanced presentation of software. Consequently, the computational time has been enhanced to a larger extent when compared with the architecture produced by means of the standard GA process by utilizing the adaptive genetic algorithm for software architecture.

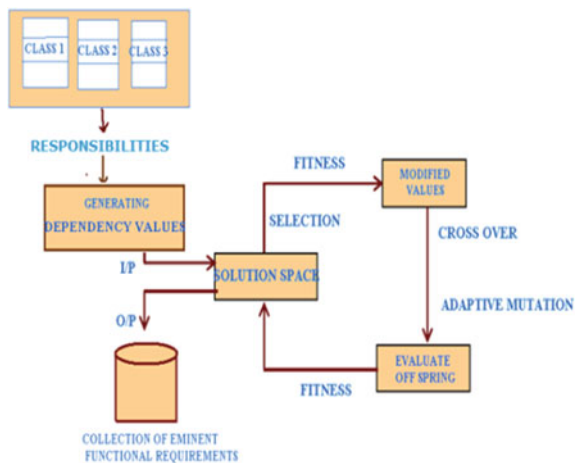
The software architecture is generally a set of decisions related to the organization of the software system and selection of the structural elements and their interfaces by which the system is composed together. Software architecture, along with the structure and behavior, is also concerned with functionality, performance, reuse, economic and technological constraints, etc. In software, its components are related to one another in a variety of ways. In order to develop good quality software, this relationship has to be represented in the architecture. The software architecture is an extremely challenging process. The functional and the non-functional necessities mostly enable the software architecture. In our proposed methodology, the responsibilities and dependency values are given as an input for finding the optimal software design.

4.1 Architecture Representation Using Adaptive Genetic Algorithm

In order to maintain variety in the course of optimization process, the chromosomes are separated into chromosomes in the recommended software architecture by means of adaptive GA. The chromosomes are similar and the folks are replaced among chromosomes, till the most excellent individuals are got through the set of chromosomes in this procedure. The substitute operation is executed by means of migration operator. Relocation of individuals among dissimilar chromosomes chased by the application of genetic operators results in the production of new individuals. To manage the level of variety, the rate of migration permits the algorithm and is continued inside the chromosomes.

To be able to elucidate that the proposed *Adaptive Genetic Algorithm* is a novel approach that has been taken in the beginning with a set of responsibilities in every class diagram shown in Fig. 1. A responsibility dependency graph is then developed for the use as input to the proposed adaptive genetic algorithm. In any field, the adaptive genetic algorithms are used to evolve best solution by performing genetic operations on the existing set of solutions. For applying adaptive genetic algorithm on a specific problem, a mapping of elements of the given problem to the elements of the adaptive genetic algorithm needs to be done—the smallest basic element of the existing solution that can be assumed as a chromosome in terms of genetic algorithm, an initial set of solutions that can be considered as the initial population, the genetic operators that should be used in the genetic algorithm, an appropriate objective or fitness function to evaluate the solutions and a selection operator to choose the survival of the fittest to be forwarded to the next generation.

Fig. 1 Conceptual model for AGA



In order to maintain variety through optimization process, the chromosomes are separated into chromosomes within the recommended software architecture by using adaptive genetic algorithm. The chromosomes have been similar as well as the individuals are replaced among chromosomes. Throughout the selection procedure, the indiscriminately generated chromosomes and also the new chromosomes are positioned in a selection pool on the basis of their fitness values. The chromosomes which contain good fitness occupy the top positions in the pool within the selection pool.

The first chromosomes which are at the top of the selection pool are selected for the next generation within the chromosomes. Here, the selection is based on the fitness and execution time for every task. This technique is repeated through the crossover with all the selected chromosomes until it reaches the termination criteria. Throughout the process, the number of iteration reaches the absolute maximum generation and then the entire process is terminated. The chromosome which can be at the top of the selection pool is selected as the best chromosome. Depending upon the identification of quality functional requirements, quality architectural design is produced.

4.2 Adaptive Genetic Algorithm

Input: Dependency values, Path coverage, Statement coverage.

Output: best chromosome after termination of condition.

- S1: Initialize population with 'n' chromosomes
 S2: Identify the fitness $f(x)$, each chromosome x in population.
 S3: For generating random population we are taking Roulette wheel selection method. [Selection] Select two parent chromosomes from a population according to their fitness
 (b) Cross over operator is used to identify new offspring (children).
 (c) Adaptive mutation, mutate new offspring (new children) at each locus
 (d) [Selection] set new offspring in new population. The new offspring will Give the quality responsibilities. Base on the responsibilities we are able to construct best software architecture.
 S4: [Replace] Use new generated population
 S5: End condition.
 S6: Go to s2

4.3 *Generating Input for Adaptive Genetic Algorithm*

In this paper, the responsibility dependency values are the inputs to the solution space. Assigning responsibilities to class is done using MH optimization algorithms. Initially, a design with responsibilities assigned to a class on differences serves as basis for applying more advanced OO mechanisms like inheritance, interfaces, abstract classes, etc.

4.3.1 **Responsibility Value**

These values are gathered from the class diagrams; assigning responsibilities to classes is among first and arguably most important step when creating object-oriented software design. This step depends greatly on human judgment and experience to automate the process of assigning responsibilities by using classes. Here is the example of retrieving the responsibilities from the class diagram.

4.3.2 **Responsibility Dependency Graph**

The concept of responsibility dependency graph is developed in order to efficiently represent the set of functional requirements of the software systems. The graph represents the functional requirements in the form of simple responsibilities. A responsibility can be defined as a job to be handled by either the complete software system or by a module or component of the software system. It can also be termed as a data object or item that has to be maintained in integrity by either the complete software system or by a module or component of the software system.

The responsibility dependency graph, as the name itself indicates, represents responsibilities and the dependency relationships between the responsibilities. Responsibilities are denoted using an oval symbol which is technically termed as a node and the dependency relationships between responsibilities is represented by using directed edges. A directed edge specifies that the fulfillment of the source responsibility is dependent on the fulfillment of the target responsibility. Using this representation format, a responsibility dependency graph for any given software system can be developed. Once this graph is developed, properties such as path coverage, dependency value, and statement coverage of the responsibilities are considered for the purpose of evaluating the software system.

The hospital management software system considered here can be divided into five major modules—new user registration and user login module, patient module, doctor module, bill entry and maintenance module, and report generation module. On the analysis of these modules, a set of functional requirements have been identified which have been modeled as 26 responsibilities having 52 dependencies relating them. A typical selection approach *assigns* the probability of selection P_j to each and every individual j according to its fitness value. A number of N random

numbers is actually generated as well as compared toward the cumulative probability $C_i = \sum_{j=1}^i P_j$ from the population. A proper individual i will be selected along with the one copied to in the new population if $C_{i-1} < U(0, 1) \leq C_i$. A variety of methods exist in order to assign probabilities to individuals: roulette wheel, linear ranking as well as geometric ranking.

Roulette wheel, may be the first selection method. The particular probability P_i for each and every individual is actually described by:

$$P[\text{Individual } i \text{ is chosen}] = F_i / \sum_{j=1}^{\text{pop size}} F_j$$

In this, F_i equals the particular fitness of individual i . The usage of roulette wheel selection limits the actual genetic algorithm in order to maximize, since the evaluation function needs to map the particular solutions in order to a completely ordered number of values on \mathfrak{R}^+ . Extensions, such as windowing as well as scaling are actually proposed to permit intended for minimization and negativity.

In roulette wheel selection, the particular individuals tend to be mapped in order to contiguous segments of the line, so that every individual's segment is every bit sized in order to its fitness. A random number can be generated as well as the individual whose segment spans the particular random number will be selected. The procedure repeats before the desired number of individuals is actually obtained (called mating population). This method is actually analogous with a roulette wheel together with each slice proportionally sized toward the fitness.

Algorithm for Roulette Wheel Selection Method

```

Step1: r := random number, where 0 =< r < 1;
Step2: sum := 0;
       for each
Step 3: individual i
       {
Step 4:     sum := sum+p(choice = i);
Step 5:     if r < sum
Step6:       {
               return i;
             }
       }
    
```

The flow diagram for our proposed adaptive genetic algorithm is shown in Fig. 2.

The software architecture is represented in terms of UML class responsibility diagrams. The optimality can be proved based on the dependencies and responsibilities of the system. Here, we have used bank management application as an example system. It contains 47 responsibilities and 94 dependencies between them. A class diagram will clearly structures the functional responsibilities, as shown in Fig. 3.

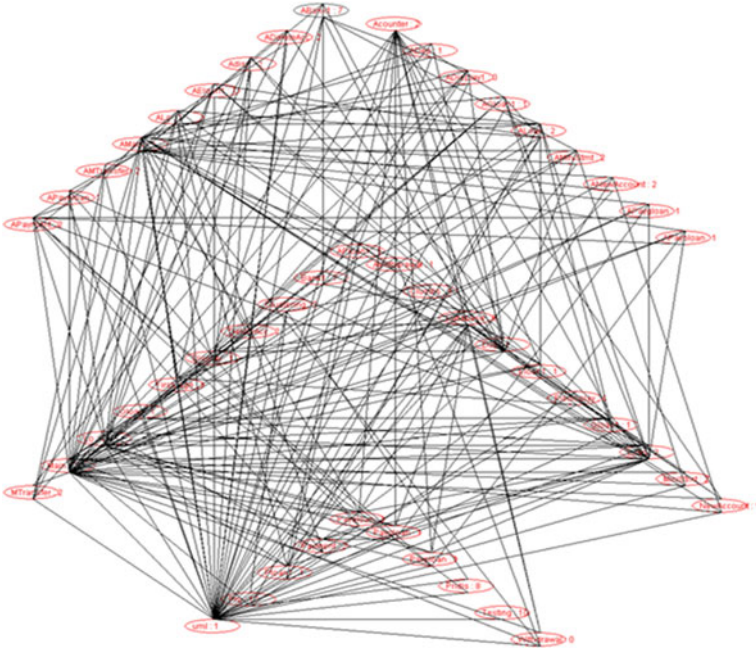


Fig. 4 Responsibility dependency graph

4.4 Generating Dependency Graph from Class Diagram

The concept of responsibility dependency graph is developed in order to efficiently represent the set of functional requirements of the software systems. The graph represents the functional requirements in the form of simple responsibilities. A responsibility can be defined as a job to be handled by either the complete software system or by a module or component of the software system. It can also be termed as a data object or item that has to be maintained in integrity by either the complete software system or by a module or component of the software system (Fig. 4).

Two basic elements are used in the responsibility dependency graph for the purpose of representation. As the name itself indicates, the graph represents responsibilities and the dependency relationships between the responsibilities. Responsibilities are denoted using an oval symbol which is technically termed as a node and the dependency relationships between responsibilities is represented by using directed edges. A directed edge specifies that the fulfillment of the source responsibility is dependent on the fulfillment of the target responsibility. Using this representation format, a responsibility dependency graph for any given software system can be developed. Once this graph is developed, properties such as path

Table 2 Responsibilities with dependency values

Responsibility number	Responsibility name	Depending value	Type
1	ABank l	48	F
2	Acounter	2	F
3	ADeleteAcc	2	F
4	ADep	2	F
5	Adisp	2	F
6	ADisplay l	2	F
7	AEloan l	2	F
8	AGloan l	3	F
9	ALo	3	F
10	ALoan	2	F
11	AMain	2	F
12	AMiniStmt	2	F
13	AMTransfer	2	F
14	ANewAccount	2	F
15	APayloan	2	F
16	APaygloan	2	F
17	APayment	2	F
18	APayloan	2	F
19	APloan l	2	F
20	AWithdrawal	3	F
21	Bank l	48	F
22	Clusdis	2	F
23	Clustering	2	F
24	Database	2	F
25	DeleteAcc	2	F
26	Dep	0	F
27	Display	2	F
28	Eloan l	0	F
29	Firstpage	2	F
30	Fisdisplay	2	F
31	Gloan	2	F
32	Gloan l	2	F
33	Lo	2	F
34	Loan	2	F
35	Main	2	F
36	MiniStmt	2	F
37	MTransfer	2	F
38	NewAccount	1	F
39	Payloan	2	F
40	Paygloan	2	F

(continued)

Table 2 (continued)

Responsibility number	Responsibility name	Depending value	Type
41	Payment	2	F
42	Payploan	2	F
43	Ploan1	3	F
44	Pridis	2	F
45	Pro	7	F
46	Testing	7	F
47	Withdrawal	2	F

coverage, dependency value, and statement coverage of the responsibilities are considered for the purpose of evaluating the software system.

For testing the given software system, identify the functional requirements in the form of responsibilities and their dependencies and having developed the responsibility dependency graph, a sample data is designed to test the system. Here, the type “F” represents the functional responsibilities. All the values are shown in the Table 2.

The bank management system contains 11 modules: login, customer, account, loan, bank, account, display, loan, clustering, transfer, and testing. These modules are independent of each other. On analysing these modules, a set of functional requirements have been identified which have been modeled as 47 responsibilities having 94 dependencies relating them. The details of the same are shown in Table 2. Effort is made to achieve a balance between complexity and structure of the graph. The parameter values are fine-tuned. Here, we illustrated path coverage, dependency values, and statement coverage values as taken from the above dependency graph.

5 Results of Final Test Case

Initial population in solution space is consisting of chromosome with length of two genes, i.e., {{23, 44}, {23, 44}, {23, 26}, {23, 26} {23, 26}}. Evaluation of fitness for each and every offspring chromosome in the solution space is show in Tables 3, 4, 5, 6, 7.

Based on the fitness values, identifying eminent functional responsibility is shown in Table 8.

From the above responsibilities, Table 8, eminent functional responsibilities are identified and represented as a class diagram as shown in Fig. 5.

After all iterations, the fitness values in the case study are constant; there is no longer generation of new offsprings. Hence, adaptive genetic algorithm is the best when compared to genetic algorithm.

Table 3 New offspring chromosome with fitness value

Iteration: 5		
Initial chromosome		Fitness values
23	44	781
23	44	781
23	26	720.5
23	26	720.5
23	26	720.5

Table 4 Crossover operation

Crossover chromosome	
23	44
23	44
23	26
23	26
23	44

Table 5 Adaptive mutation operation

Mutation chromosome		
23	2	1
23	13	1
23	44	1
23	26	1
23	44	1

Table 6 Over all fitness for all chromosome

S. no	Chromosome		Fitness values
1	23	44	781.0
2	23	44	781.0
3	23	26	720.5
4	23	26	720.5
5	23	26	720.5
6	23	44	781.0
7	23	44	781.0
8	23	26	720.5
9	23	26	720.5
10	23	44	781.0
11	23	2	551.0
12	23	13	571.0
13	23	44	781.0
14	23	28	597.5

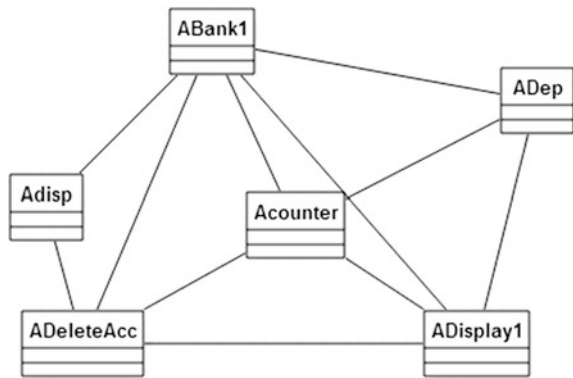
Table 7 Eminent chromosome and fitness value

Chromosome		Fitness
23	44	781
23	44	781
23	44	781
23	44	781
23	44	781

Table 8 Eminent functional responsibilities

Responsibility no	Responsibility names
1	ABank1
2	Counter
3	ADeleteAcc
4	ADep
5	Adisp
6	ADisplay1

Fig. 5 Eminent functional responsibilities for test case



5.1 Performance Analysis

The whole effort of the genetic algorithms lies on the objective functions and fitness values selected. In each generation, the chromosomes with highest fitness values are chosen. In both the GA and AGA methodologies, in each iteration, the fitness value of each of the chromosomes is calculated and the results are tabulated. By observing the information, Table 9, it is concluded that our AGA technique achieved higher fitness values when compared to the GA technique.

The results shown in Table 9 and Fig. 6 prove the efficiency of the proposed adaptive genetic algorithm in producing a quick convergence scenario when compared to the traditional genetic algorithm.

Table 9 Fitness value for adaptive GA and GA for every iteration

Number of iteration	Fitness for adaptive GA	Fitness for GA
1	978	1123
2	970.2	1110
3	870	1065
4	781	1032
5	781	996
35	781	991

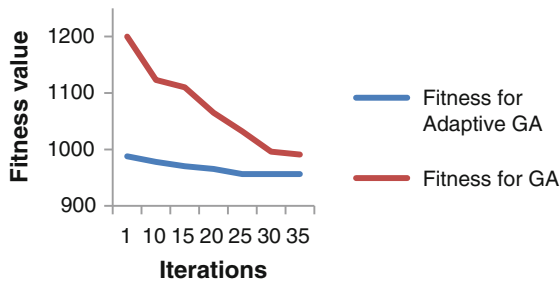


Fig. 6 Comparison of convergence between adaptive genetic algorithm and traditional conventional genetic algorithm

6 Conclusion

The implementation of the work starts from the selection of application with object-oriented approach. A UML class diagram consisting of responsibilities in generating the dependency values; these values are input for AGA. Further, this adaptive genetic algorithm has proved to be an efficient technique for software architecture. In the intended adaptive genetic algorithm, the chromosomes are separated into chromosomes to maintain assortment in the course of optimization process which demonstrated to be successful than ordinary genetic algorithm process.

Our recommended method has enhanced the computational time of the software which is the most important requirement in the software architecture. It also helps in comparing the presentation of every method which will be helpful to scheme improved software architecture. This paper has proposed one of the solutions for evaluating the fitness function dynamically to provide and identify eminent functional requirement to produce a good software architecture design.

References

1. Pan W. Applying complex network theory to software structure analysis. *World Acad Sci Eng Technol.* 2011;60:1636–42.
2. Abdelmoez M, Jalali AH, Shaik K, Menzies T, Ammar HH. Using software architecture risk assessment for product line architectures. In: *Proceedings of international conference on communication, computer and power (Icccp'09)*; 2009. Muscat, Feb 15–18, 2009.
3. Yang XS, Deb S. Engineering optimization by cuckoo search. *Int J Math Model Num Optim.* 2010;1(4):330–43.
4. Frey S, Fittkau F, Hasselbring W. Search-based genetic optimization for deployment and reconfiguration of software in the cloud. In: *2013 35th international conference on software engineering (ICSE)*; 2013, 18–26 May 2013.
5. Zitzler E, Deb K, Thiele L. Comparison of multiobjective evolutionary algorithms: empirical results. *Evol Comput.* 2000;8(2):125–48.
6. Rela L. *Evolutionary computing in search-based software engineering*, Lappeenranta University of Technology, Department of Information Technology, M.Sc. Thesis; 2004.

Pitch Frames Classification in a Cricket Video Using Bag-of-Visual-Words

M. Ravinder and T. Venugopal

Abstract We propose a method for classification of pitch frames in a cricket video based on bag-of-visual-words technique. Bag of visual words is a popular and successful technique in image classification and object-based classifications. In this paper, we demonstrate three different techniques based on bag-of-words methodology. The three different techniques use three different set of features for the classification of pitch frames in a cricket video. The three different types of features we use are SIFT (Scale-Invariant Feature Transform), LBP (Local Binary Patterns), and CTE (Color+Texture+Edge) features. We evaluate the three techniques on the dataset of cricket (<http://cse.iitk.ac.in/~vision/dipen/>), made available online by Mr. Dipen Raghuvani. Our experiments by using the above mentioned three types of features have shown significant results.

Keywords Bag-of-visual-words · Cricket · Video · Pitch frame · SIFT · LBP · Color · Texture · Edge

1 Introduction

Recent years have witnessed a huge increase in multimedia content, especially the video content. Video is a medium of entertainment for different broadcasting TV channels. Nowadays, different broadcasting channels are producing huge amounts of video repositories. One of the mediums of TV broadcasting is sports in which cricket is having more popularity throughout the world. Different sports broadcasting TV channels are facing the problem of maintaining the video repositories

M. Ravinder (✉)
JNTUK, Kakinada, Andhra Pradesh, India
e-mail: ravinder.rsh@gmail.com

T. Venugopal
CSE, JNTUHCEJ, Nachupally, Karimnagar, Telangana, India
e-mail: t_vgopal@rediffmail.com

produced by them during the past few years. There is an urgent need for a framework which is useful for indexing and retrieving the video data from the video repositories.

Cricket is the highest fan-following sport in India. Cricket is a sport which is played in different formats like one-day match, test match, and T-20 match. With the popularity of cricket, a large number of broadcasting channels are facilitating the users with live broadcasting of the matches. Due to nonavailability of efficient framework for indexing the video content produced by the broadcasting channels, the video repositories are of no use.

The primary step in content-based indexing of a cricket video is the classification of pitch frames and nonpitch frames [2].

Cricket match consists of different number of overs based on the format of the match. Each over consists of six ball deliveries by the bowler of the fielding team. In a cricket match video, pitch frame is the starting point of each ball's delivery. Pitch frame classification is useful for partitioning a cricket video as parts of ball-based segments. This is in turn useful for finding the events easily.

Few of the techniques are proposed in the literature. Sandesh Bananki et al., in their paper [2] have proposed three different techniques for classification of pitch frames in a cricket video. The three techniques proposed by them are Statistical Modeling of Grayscale values (SMoG), Component Quantization-based Region Extraction (CQRE), and a combination of those two techniques SMoG+CQRE.

M.H. Kolekar et al., in their paper [3] have proposed a method for detecting/classifying pitch frames in a cricket video by calculating the percentage of field pixels between the partitions of the image.

The main contributions of this paper are

1. Pitch frame classification using Bag-of-Visual-words based method.
2. Comparisons of three methods based on three different set of features are demonstrated.

The rest of the paper is organized as follows: in Sect. 2 we discuss about bag-of-visual-words, Sect. 3 explains about different features we use for implementing the proposed method, Sect. 4 focuses on proposed method, Sect. 5 briefs about experiments and results, and Sect. 6 concludes the paper.

2 Bag-of-Visual-Words

Bag-of-visual-words (BoVW) is based on the Bag-of-Words (BoW) methodology. BoVW considers an image as a document and local features of the image as words [4].

Indexing an image can be considered as classifying an image, i.e., classifying an image based on the low-level features present in it [5].

Bag-of-Visual-Words methodology has been used in many important computer vision applications like classification of images, retrieval of video data, and texture-based recognition.

The base for Bag-of-Visual-Features technique is an unordered collection of local image descriptors [6]. Bag-of-Words is a successful mechanism for text retrieval and which is an inspiration for Bag-of-Visual-Words based content driven image and video retrieval.

Sivic and Zisserman initially proposed the method of indexing images and video frames using Bag-of-Visual-Words mechanism [7].

The framework of Bag-of-Visual-Words consists of the following standard steps:

- Step 1: Collecting a number of local features from the sets of images of different class types (in our case pitch frames class and nonpitch frame class).
- Step 2: Partitioning/clustering the collected features from step 1 into a reasonable number of clusters which will form the visual vocabulary.
- Step 3: Train a set of new images with their local features by finding the nearest visual vocabulary words that they belong to.
- Step 4: Classifying the new test set of images using the trained data into one of the class types.

In step 1, usually the popular choice of feature extractor is SIFT (Scale-Invariant Feature Transform). In step 2, the commonly used clustering technique is *k*-means clustering. In step 3, for measuring nearest visual word the popular choice is Euclidian distance.

The frame work of Bag-of-Features is as shown in Fig. 1.

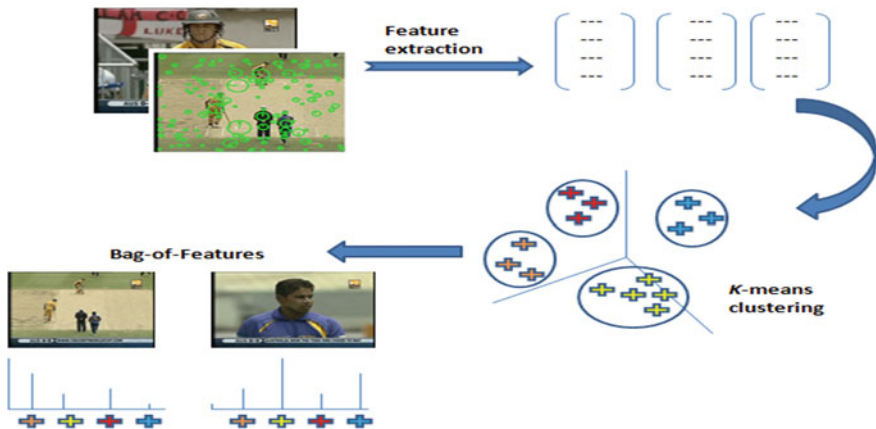


Fig. 1 Framework of implementation of the bag of features

3 Image Local Features

Different types of local image features we use in our proposed methods are discussed in this section. There are three types of features we use for implementing our proposed methods; they are SIFT (Scale-Invariant Feature Transform), LBP (Local Binary Pattern), and a CTE (Color+Texture+Edge) which is a combination of color, texture, and edge features.

3.1 Scale-Invariant Feature Transform (SIFT)

The SIFT feature extractor is a popular choice for extracting local features of an image. SIFT is a high-speed feature extractor suitable for real-time applications. The SIFT features extracted do not vary with the variation of size, rotational, and translational transformations as well as different lightening conditions. The SIFT descriptor was proposed by David Lowe (During 1999, 2004) [8]. SIFT descriptor is based on interest points selection using Difference of Gaussian Pyramids and finding the statistics from directions of local gradients around the neighborhood of the interest points as shown in the below Fig. 2.

3.2 Local Binary Pattern (LBP)

The second type of feature we have used is Local Binary Patterns, which is a popular option for texture-based image description and retrieval. LBP feature extractor is proposed by Ojala et al. [9] which is based on finding new binary code value for a given pixel based on the result of difference between the center pixel and its neighborhood pixels as shown in Fig. 3.

As shown in the Fig. 3, the thresholding process is based on the sign obtained by finding the difference between center pixel and its neighborhood.

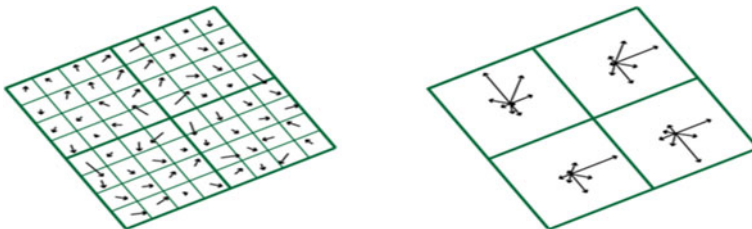


Fig. 2 SIFT descriptor, figure taken from [8]

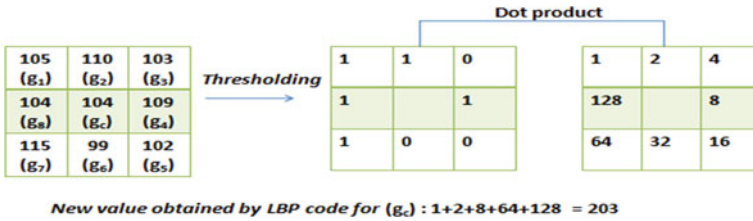


Fig. 3 LBP code-based new value calculation example

The LBP descriptor for the center pixel g_c is calculated using the following equation:

$$LBP(g_c) = \sum_{i=1}^8 2^{(i-1)} * f(g_i - g_c) \tag{1}$$

where,

$f(x)$ is 1, if $x \geq 0$
 $f(x)$ is 0, otherwise.

3.3 Color+Texture+Edge Features (CTE)

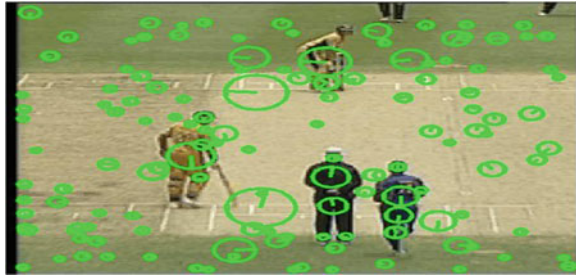
CTE is the combination of color, texture, and edge features of an image. The color features we have used are twelve bins histogram for each of red, green, blue, hue, saturation, and value components of the image.

The texture features we have used is rotational-invariant LBP histogram features. Edge features are extracted by using Sobel method of edge detection available in MATLAB. This method is useful in finding horizontal and vertical edge responses useful for finding the histogram of edge features [10].

4 Proposed Methods for Pitch Frame Classification

In this section, we propose three algorithms based on Bag-of-Visual-Words methodology for detecting and classifying the pitch frames in a cricket video.

Fig. 4 An example pitch frame with top 150 SIFT features



4.1 Algorithm 1

- Step 1: Collect a well-defined set of training images of different class types (in our case pitch frames class and nonpitch frames class).
- Step 2: Collect the top 150 SIFT features from the first half of the set of training images of all class types.
- Step 3: Cluster the features into a reasonable number of clusters (depending on user's choice) that will act as visual vocabulary.
- Step 4: Train the framework using the second half of the training set of images by finding the occurrence of visual vocabulary for the top 150 SIFT features extracted from the images.
- Step 5: By using the trained framework, classify the new testing set of images by applying the same feature extraction method used in previous steps.

As discussed in Algorithm 1, for implementation, we have extracted top 150 SIFT features from each image. We have selected only the top 150 SIFT features for effective usage of memory and time. We have used VLFeat package [11] for selecting top 150 features of each image. An example of 150 features selected for a pitch frame is as shown in Fig. 4.

4.2 Algorithm 2

- Step 1: Collect a well-defined set of training images of different class types (in our case pitch frames class and nonpitch frames class).
- Step 2: For the first half of the set of training images of all class types, divide each image into four equal parts and from each part collect the LBP features.
- Step 3: Cluster the features into a reasonable number of clusters (depending on user's choice) that will act as visual vocabulary.
- Step 4: Train the framework using the second half of the training set of images of all class types by finding the occurrence of visual vocabulary for the LBP features extracted from all the four equal parts of each image.
- Step 5: By using the trained framework classify the new testing set of images by applying the same feature extraction method used in previous steps.

As discussed in the Algorithm 2, for implementation, we partition each image into four equal parts and collect the LBP feature vectors of all the parts of the image and the same procedure is applied to all the images present in the training set and testing set.

4.3 Algorithm 3

- Step 1: Collect a well-defined set of training images of different class types (in our case pitch frames class and nonpitch frames class).
- Step 2: Collect the color, texture, and edge features from the first half of the set of training images of all class types.
- Step 3: Cluster the features into a reasonable number of clusters (depending on user's choice) that will act as visual vocabulary.
- Step 4: Train the framework using the second half of the training set of images by finding the occurrence of visual vocabulary for the color, texture, and edge features extracted from the images.
- Step 5: By using the trained framework, classify the new testing set of images by applying the same feature extraction method used in previous steps.

As discussed in the Algorithm 3, for implementation, we have used a set of feature vectors of 144 features for a single image.

The standard steps we have followed to implement the above algorithms are from the dataset we have collected; a set of 400 pitch frames and 400 nonpitch frames as our training set. As the first step, we have collected local features from each image present in first half of the training set (200 pitch frame and 200 nonpitch frame images). The second step is to cluster the collected features into a reasonable number of clusters depending on user's choice to form a vocabulary of visual words. The third step is to train the second half of the set of training images and the final step is evaluating the efficiency of proposed algorithms by classifying the test set of images using the trained framework.

5 Experiments and Results

In Sect. 4, we have proposed the three different algorithms useful for classifying the pitch frames in a cricket video. For implementing the above mentioned algorithms, we have used the cricket video dataset available at [1].

As mentioned in previous section, the standard steps followed in all the above mentioned algorithms are identical, but only the difference is the features that were used to describe an image are different.

We have evaluated all the three algorithms on a test set of images, which consists of 100 pitch frames and 100 nonpitch frames.

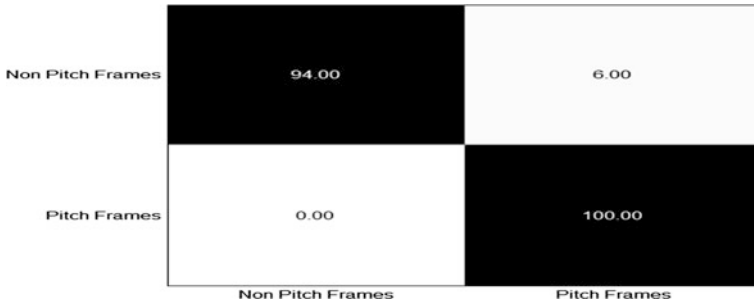


Fig. 5 Results of Algorithm 1



Fig. 6 Results of Algorithm 2

The results (percentage) that we have obtained for the three proposed algorithms are as shown in the below figures (Figs. 5, 6, and 7).

The results we have obtained by implementing the above-proposed algorithms are, by using Algorithm 1, we are able to classify all 100 pitch frames but we can classify only 94 nonpitch frames correctly. By using Algorithm 2, we are able to

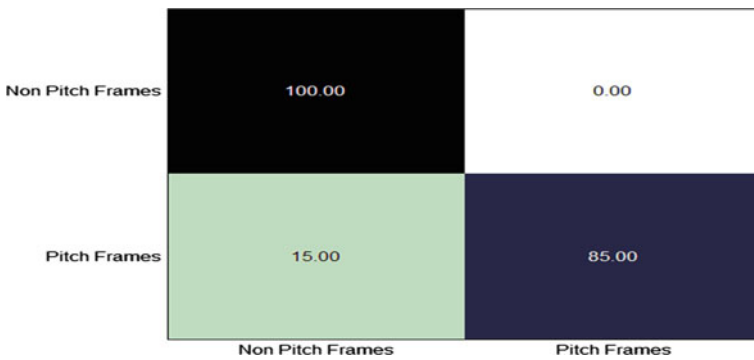


Fig. 7 Results of Algorithm 3

classify 88 pitch frames and 88 nonpitch frames correctly. And finally, by using Algorithm 3 we are able to classify 85 pitch frames and 100 nonpitch frames correctly.

6 Conclusion

In this paper, we have proposed three algorithms for classifying pitch frames in a cricket video based on Bag-of-Visual-Words methodology. We have used three different types of features and evaluated all the three methods using a testing set of 100 pitch frames and 100 nonpitch frames. With the results we have obtained, we found that we can achieve a reasonably good classification performance using SIFT features set-based algorithm (Algorithm 1).

Acknowledgments Authors of this paper want to thank Ravindra Gadde [12] and Mr. Dipen Raghurani for their technical support and for providing the cricket video dataset, and made it available online at [1].

References

1. Video dataset. <http://cse.iitk.ac.in/~vision/dipen/>.
2. Jayanth SB, Srinivasa G. Automated classification of cricket pitch frames in cricket video. *Electron Lett Comput Vis Image Anal*. 2014;13(1):33–49.
3. Kolekar MH, Palaniappan K, Sengupta S. Semantic event detection and classification in cricket video sequence. In: *Sixth Indian Conference on Computer Vision, Graphics and Image Processing*; 2008.
4. Wang X, Wang LM, Qiao Y. A comparative study of encoding, pooling and normalization methods for action. *Recognition ACCV 2012, Part III, LNCS*. 2013;7726:572–85.
5. Tsai C-F. Bag-of-words representation in image annotation: a review. In: *International scholarly research network, ISRN artificial intelligence*; 2012.
6. O'hara S, Draper BA. Introduction to the bag of features paradigm for image classification and retrieval. [arXiv:1101.3354v1](https://arxiv.org/abs/1101.3354v1) [cs.CV] 17 Jan 2011.
7. Grauman K, Leibe B, Chapter 5. Indexing and visual vocabularies. Excerpt chapter from synthesis lecture draft: visual recognition.
8. <http://www.scholarpedia.org/article/SIFT>.
9. Ojala T, Pietikainen M, Maenpaa T. Multiresolution grayscale and rotation invariant texture classification with local binary patterns. *IEEE Trans Pattern Anal Mach Intell*. 2002;24(7):971–87.
10. Lin CY, Wu M, Bloom JA, Cox IJ, Miller M. Rotation, scale, and translation resilient public watermarking for images. *IEEE Trans Image Process*. 2001;10(5):767–82.
11. Vedaldi A, Fulkerson B. VLFeat: an open and portable library of computer vision algorithms; 2008. <http://www.vlfeat.org/>.
12. <http://masterravi.wordpress.com/author/masterravi/>.

Retinal Abnormality Risk Prediction Model: A Hybrid Approach Based on Vessel Characteristics and Exudates

M. Aiswarya Raj and Shinu Acca Mani

Abstract A few systemic diseases, for example, hypertension, diabetes, and vascular disorders will first affect the retinal vessels. When affected with these diseases, the retinal vessels show some sort of vascular changes according to the severity of the conditions. So, in order to diagnose this kind of diseases an efficient system that can detect the retinal abnormalities is required. This paper presents a hybrid approach for the automatic retinal vessel classification, vascular caliber estimation, and exudate detection in retinal images. The retinal vessel classification and caliber estimation is done by exploiting both visual and geometric features that enable discrimination between vein and arteries. Exudates are identified by extracting the yellow pixel level in the retinal image. Based on these three parameters, the retinal abnormality risk prediction model predicts whether the input retinal image is normal or abnormal.

1 Introduction

Eye is the most important and sensitive part of our body by which we are perceiving thousands of beautiful and mind capturing scenes. Retina inside our eyes plays a significant role in capturing images that we see daily. Retina has numerous vessels called retinal vessels. There are of two different types. They are arteries and veins. Diseases like diabetic retinopathy, cardiovascular diseases, etc., will affect our retinal vessels first. When affected with these types of diseases, retinal vessels will show some sort of vascular disorders. These disorders in their extreme stage cause vision impairment. So, it is necessary to diagnose these types of disorders. This can

M. Aiswarya Raj (✉) · S.A. Mani
Department of Computer Science and Engineering, Nehru College of Engineering
and Research Centre, Thiruvilwamala Pampady, Thrissur, Kerala, India
e-mail: aiswaryarajm@gmail.com

S.A. Mani
e-mail: shinu.10@gmail.com

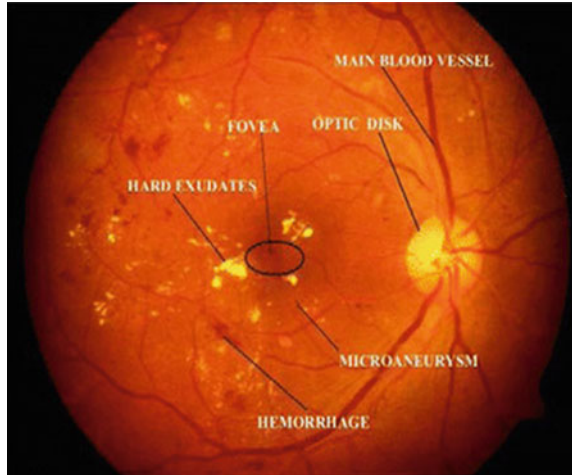
be done by taking ophthalmoscope images and analyzing it. Analyzing the retinal images for detecting diseased condition is a difficult job. An automatic strategy will be very useful in this perspective. Developing an efficient automatic approach that can predict the retinal abnormality risk is the motive of this thesis work.

Retinal abnormalities include microaneurysm, exudate, retinal hemorrhage, vascular disorders, etc. Among these abnormalities, vascular disorders, exudate, and retinal hemorrhage are the three parameters chosen for predicting the abnormality risk in this paper. These three are the most important parameters that can predict the abnormality risk in an effective manner. Vascular disorders are the changes in the diameter of retinal vessels. Due to hypertension, blood pressure increases and the retinal vessels will get damaged. This may cause rupture of retinal vessels which in turn leads to retinal hemorrhage. Exudates are the yellow or white patches seen inside the retinal vessels. This is a sort of retinal abnormality which is caused by the lipid residues of serous leakage from damaged capillaries. For estimating the vascular disorders, AVR is estimated. AVR is the arteriole-to-venule ratio which will be decreased when affected with diabetes, hypertension, and other cardiovascular diseases. So, AVR is the best parameter to predict the vascular disorder. Reduced AVR can also predict the chance of retinal hemorrhage. Arteries and veins will be affected differently by diabetes. So, before calculating AVR, there is a need to classify retinal vessels into arteries and veins. For this classification, either visual features or geometrical features can be adopted. Both of these have their own advantages as well as disadvantages. Classification using geometrical features has disadvantages of missing link, false link, etc., and classification using visual features has disadvantages of contrast variability and local luminosity in case of nonuniformly illuminated images. To eliminate these advantages in this paper, an efficient hybrid mechanism is adopted which utilizes both visual features as well as geometrical features for classification so that the disadvantages of both these methods will be complemented by the other one and thus the performance can be increased.

The remaining portion of the paper is organized as follows: Sect. 2 presents the different methods used for abnormality detection in retinal images. Section 3 discusses about the working principle of retinal abnormality risk prediction model, Sect. 4 illustrates the performance analysis table, and Sect. 5 shows the results. Finally, Sect. 6 summarizes the concludes.

2 Retinal Abnormalities and Detection Methods

In this section, we will discuss about the various methods adopted for detecting retinal abnormalities such as presence of exudates, retinal vascular changes, etc. Before getting into the methods, let us see in detail about the various retinal abnormalities.

Fig. 1 Retinal abnormalities

2.1 Retinal Abnormalities

Disorders of the optic nerve and retina are commonly termed as retinal abnormality. The following are some of the symptoms of this retinal disorder. Figure 1 shows how this appears inside the retina.

Vascular Disorders Inside the retina, there are a number of retinal vessels (arteries and veins) for carrying blood. During the diseased condition, these retinal vessels will show some sort of changes in their diameter. These changes will be different for both arteries and veins. In most of the cases, the vessels become narrower leading to the inability to carry blood which in turn leads to an increase in blood pressure. When the pressure increases, the vessels break and then leak, causing retinal hemorrhage.

Drusen or Exudate Exudates are yellowish-white stores of cellular and inflammatory debris placed inside the retina. There are both hard exudates and soft exudates. In photographs, especially red channel free-images and on fundus ophthalmoscopy, they are obvious. Occasional drusen happen regularly with aging and expanded numbers are found with a few manifestations of glomerulonephritis. Dots and flecks in the retina resemble drusen. But, they are not actually drusen as they are affecting the internal limiting membrane.

Retinal Hemorrhage It is the abnormal bleeding of the blood vessels in the retina. These blood vessels in the retina can become damaged by injury and disease, and may bleed (hemorrhage) causing temporary or permanent visual inaccuracy. Hemorrhaging is caused by the over stress of the circulatory system. Vision spots, floaters, and loss of vision are the ultimate consequences of hemorrhaging.

Microaneurysm The earliest clinical sign of diabetic retinopathy is microaneurysm. Due to pericyte loss, they appear secondary to capillary wall. They appear as small red dots in the superficial retinal layers. A tiny area of blood protruding from an artery or vein in the back of the eye is a retinal microaneurysm. These protrusions may open and leak blood into the retinal tissue surrounding it.

2.2 Detection Methods

Piecewise Gaussian Model Piecewise Gaussian model is for classifying the retinal vessels into arteries and veins which is a very important step before estimating the vessel calibers. In this model, the various characteristic properties of retinal vessels given below are exploited.

- Arteries appear lighter and narrower than the dark-red or purplish veins in the color retinal images.
- Normal width ratio of artery-to-vein is about 2:3.
- Central reflex is more apparent in arteries than in veins.
- Central reflex must be watched clearly for wide vein.

Based on these characteristic features, a mathematical model is formulated and the classification is done.

$$y = f(x) = \left\{ \begin{array}{ll} -A_1 e^{\frac{(x-m_1)^2}{2\sigma_1^2}} + I_1 & x \in \langle A, x \rangle B \\ A_2 e^{\frac{-(x-m_2)^2}{2\sigma_2^2}} + I_2 & A < x < B \end{array} \right\}$$

where, A_1 is the amplitude of the vessel; A_2 is the amplitude of the reflex. m_1, m_2 are the positions of the peaks of Gaussian functions; σ_1 and σ_2 are width distribution. I is the intensity of retinal background. A_1 represents the darkness of the vessel, which is larger for veins and A_2 stands for the brightness of the reflex, which is larger for arteries than for veins [1]. Disadvantage is that nonuniformly illuminated images exhibit problems like local luminosity and contrast variability.

Color-Based Clustering Algorithm with Vessel Tracking Method This is an intensity-based method that classifies retinal vessels into arteries and veins. First, vessel segments are detected in several circumferences centered at the optic disk. Then, clustering is done based on rotating quadrants and is applied to the vessels found in each circumference. A tracking strategy is used to link the vessel segments between circumferences. Finally, combine results obtained in each circumference [2]. As this is an intensity-based mechanism, there is the problem of contrast variability and local luminosity whenever the image is nonuniformly illuminated.

Optic Disk-Based Method This is a method that exploits structural or geometrical information for retinal vessel classification. First step is extraction of the retina

vascular tree using graph cut technique. Blood vessel information is then estimated according to location of optic disk. The markov random field (MRF) method segments optic disk by removing vessels from the optic disk region [3]. This method is purely based on optic disk detection. If this fails, automatically there is a chance of misclassification of A/V. Near the optic disk, classification is more accurate and as the distance increases classification accuracy decreases. This is not designed to consider vessels in all the zones together.

Automated Method for A/V Classification This is an automated method that uses conversion of vessel segmentation into a map of vessel segments and identifies the vessel trees using graph search for structural mapping of retinal vessels. Color features of retinal image are used for arterial-venous classification [4]. Total misclassification is introduced due to limitations in structural mapping. Limitations of structural mapping method is that when separating overlapping or parallel running vessels, there is a possibility of false vessel identification.

Retinal Vessel Segmentation Using Vessel Centerline Detection This method uses pixel processing-based approach. Initial step is combining local information with structural information (vessel length). As a next step vessel filling is done which exploits the information obtained from the initial step. The main advantage of this method is that it can adapt to intensity properties of image as the threshold set by the algorithm is computed from local or global image information. Noise segments are excluded by means of retinal vasculature skeleton [5]. There is the problem of under-segmentation in which some vessel segments are not detected due to intensity and contrast variability. Another disadvantage of this method is the small vessel branches are partially or completely missing. Rather than using vessel/nonvessel labeling if a more flexible classification process is considered for every image point, some of the above-mentioned error detections can be reduced, or even eliminated to a certain extent. Attenuated misclassification caused by the initial localization of the optic disk in this region can lead to improved global performance of the method.

Automatic Detection of Exudates in Retinal Images The intention is to detect the nonproliferative stage of DR which is exudates so that the disease can be managed appropriately to decrease the chances of vision impairment. The first step is to spot the optic disk which is done by determination of the center of optic disk, which is the lighter and brightest part in retina image. The next step is to detect all the exudates in the retinal image which is achieved by using the green channel of the retina image [6].

Most of these methods use visual information for the abnormality detection. Visual features are good parameters for identifying the disorders inside the retina. Still, there are problems associated with it. More often, retinal images will be nonuniformly illuminated due to the acquisition process and in such cases the visual features or intensity-based features will not give accurate results. Because, whenever the retinal image is nonuniformly illuminated there arise the problem of local luminosity and contrast variability. These problems may seriously influence the

diagnostic process and its result, especially if an automatic computer-based procedure is used to develop diagnostic parameters. So, whenever an automatic computer-based procedure is used, some method other than that based on intensity features should be adopted. If the geometrical features are utilized, it also has problems like missing link, false link, etc. For this reason, we are proposing a novel hybrid approach that exploits both the visual as well as geometrical features for detecting the abnormalities in retinal images so that the disadvantages of each individual approach will get complimented in the combined or hybrid approach.

3 Hybrid Approach for Retinal Abnormality Risk Prediction

The method proposed in this paper is a hybrid approach that utilizes both structural information as well as intensity information about the retinal vessels for the retinal abnormality prediction. We are using three parameters to predict whether the retinal image is normal or abnormal. They are (1) retinal vessel caliber; (2) red pixel level; (3) yellow pixel level. Figure 2 depicts the block diagram of proposed method for retinal abnormality prediction. The method first extracts a graph from the retinal image and afterward endpoints, intersection points, and splitting points are found out. Then, based on the node type all vessel segments that are elements of a particular vessel are found out. Then, intensity features like hue, saturation, etc., are used for the classification. This is done by kNN classifier. After this, the vessel thickness is estimated. Using the same intensity features, yellow pixel level and red pixel level are estimated. If the vessel thickness is lesser than normal, we will check for the red pixel level. If the red pixel level is greater than a fixed threshold, then there is hemorrhage and the retinal image is abnormal. Even if the vessel caliber is normal and red pixel level also falls in a tolerable limit we have to check the yellow

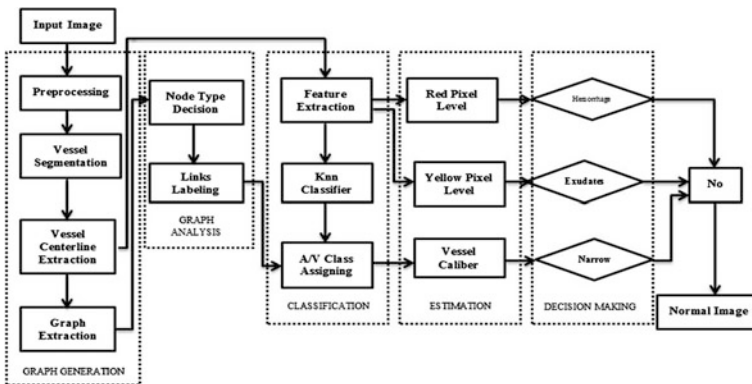


Fig. 2 Block diagram for proposed retinal abnormality prediction

pixel level. If the yellow pixel level is more than normal level, then there is the presence of exudates. This also results in the abnormality of retinal image. In the following section, we explain in detail about the proposed method.

3.1 *Image Preprocessing*

This is the first step in all image processing applications. Image preprocessing involves the correction of distortion and noise introduced during the imaging process. This process produces a corrected image that is very much similar to original image both geometrically and visually. Here, image preprocessing is done in two steps. They are explained as follows.

Preprocessing Phase Pixel preprocessing approach is used in this phase [7]. Using this approach, intensity normalization is accomplished. This is done by subtracting the estimate of image background obtained by filtering image with large arithmetic kernel from the original image. In the next step, by region growing process centerline candidates are identified and connected into segments using information obtained from a set of Gaussian filters. At last, these segments are confirmed based on their intensity and length characteristics. As the third phase, using multiscale morphological vessel enhancement and reconstruction approaches vessel segmentation is done where four different scales binary maps of the retinal vessels are generated. The ultimate image with the segmented vessels is obtained by repeatedly combining the centerline image with set of images that obtained as a result of vessel reconstruction step.

Image Enhancement Phase Image enhancement is the processing of images to bring out specific features in it. It can be used to highlight certain characteristics of the image. As an image enhancement technique channel extraction is done. Three different channels red, green, and blue can be extracted individually according to the image. Figure 3a shows the original retinal image and (b) shows the preprocessed retinal image. In this Fig. 3b, red channel is extracted.

3.2 *Vessel Segmentation*

Vessel Segmentation is implemented using multiscale morphological enhancement and reconstruction approach which generates binary maps of vessels at four different scales. In this, different morphological operations like opening and closing is done using morphological structural elements. Structural elements are used in structural analysis to split a complex structure into simple elements. Here, we are using four different structural elements namely disk, ball, square, and line. If disk is selected, the radius should be given. For ball, radius and height should be manually

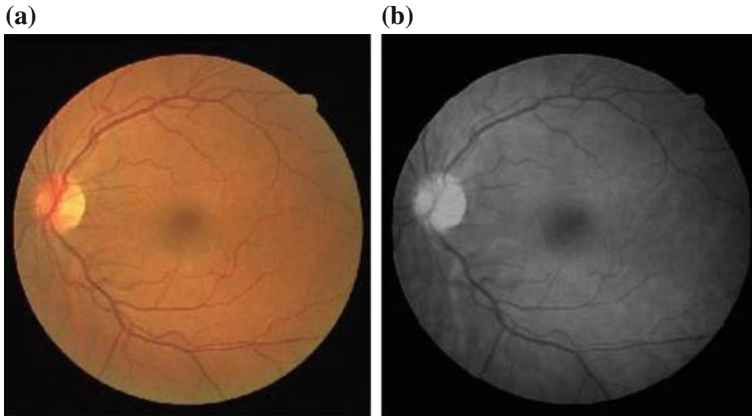


Fig. 3 a Retinal image; b preprocessed retinal image

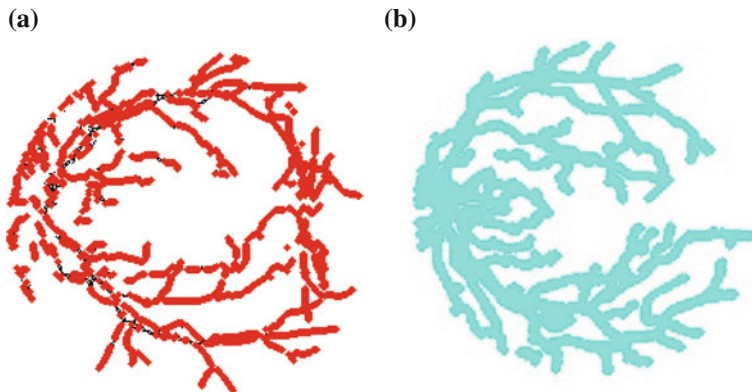


Fig. 4 Vessel segmentation results

provided and height should be 2, 4, 6, or 8. For square shaped structural element, the side of the square should be given and for line both length and angle is necessary. As a default structuring element, disk with radius three as the parameter is given which will work as an automatic segmentation structural element. This will give a better segmentation result. Figure 4a shows the vessel segmentation result using multiscale morphological enhancement and reconstruction approach.

Vessel segmentation can be done by using another method. First, convert RGB image to gray via PCA. Then, enhance contrast of gray image using contrast limited adaptive histogram equalization (CLAHE). Apply average filter and then exclude the background. Take the difference between the gray image and average filter applied image. Threshold the difference using IsoData Method. Convert the obtained result to Binary. Finally remove all small pixels. Figure 4b shows the vessel segmentation result.

3.3 Vessel Centerline Extraction

In vessel centerline extraction, border pixels are removed iteratively until the retinal image shrinks into a minimally connected stroke. This centerline extraction is done through a sequence of steps. As a first step, bottom hat filtering is done which performs morphological bottom hat filtering on gray scale or binary input image and returns a filtered image. For this, a structuring element is used. This process enhances contrast thereby limiting the effect of contrast variability. Afterward take mean of filtered image and set it as threshold. Then, remove all connected components that have pixels less than the threshold. This process is known as opening which is a morphological operation. After this, remove pixels on the boundaries but does not allow image to break apart so that remaining pixels make up image skeleton. Figure 5 shows the centerline extracted image of the retinal image shown in Fig. 3a.

3.4 Graph Extraction

After centerline extraction, nodes of the graph are pulled out from the centerline image by identifying the intersection points, splitting points, and terminal points or end points. Intersection points are the nodes with more than two neighbors. Splitting points are the nodes with exactly two neighbors and terminal or end points are the nodes with only one neighbor. For separating vessel segments we need to remove all the intersection points and their neighbors from the centerline image and the result will be image with isolated components. As a result an image with all the vessel segments and the nodes are obtained. Figure 6 illustrates the retinal image points shown in Fig. 3a.

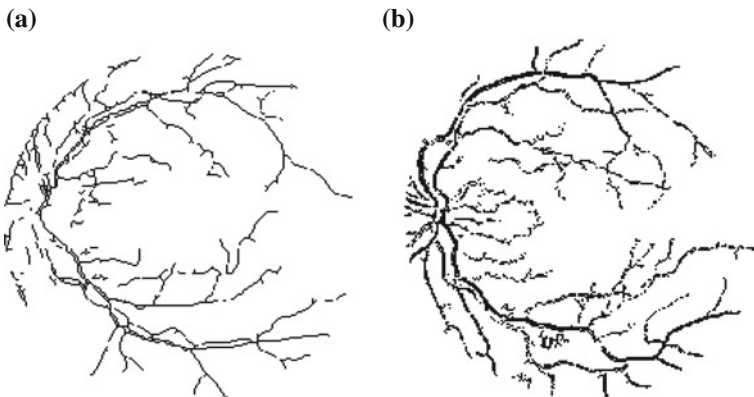


Fig. 5 Centerline extracted image

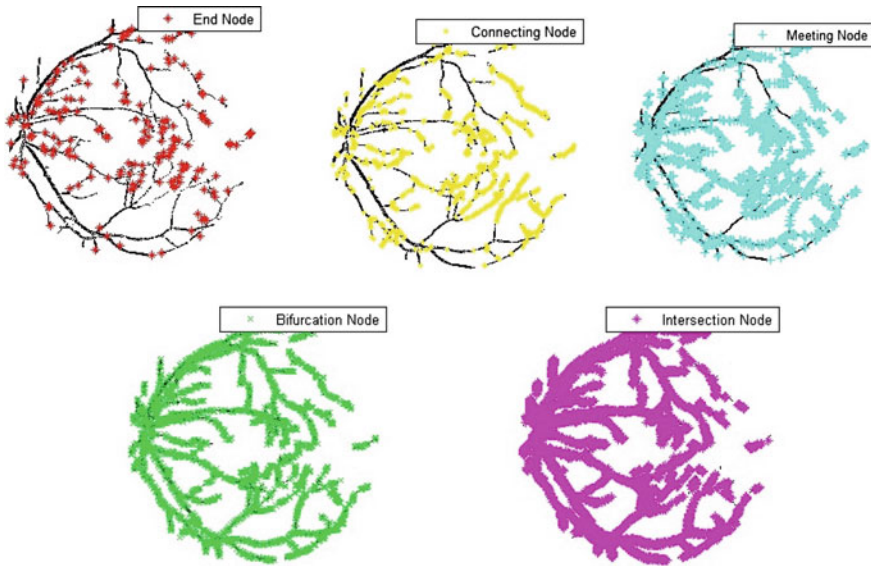


Fig. 6 Different types of nodes in retinal image

3.5 Node Type Decision

There are mainly four different varieties of nodes seen in the retinal graph. They are

1. Meeting point: Two dissimilar vessels rendezvous each other without crossing.
2. Bifurcating point: A vessel diverges into thinner vessels.
3. Crossing point: Two dissimilar vessels cross each other.
4. Connecting point: Connects different segments of the same vessel. Most of the nodes with two links fall in this category.

Node type decision step as the name indicates check the type of the node by checking the degree of the node [7]. Degree of the node is nothing but the number of links associated with a particular node. By checking the degree the method for identifying the type of the node can be found out.

Nodes of Degree 2 Degree 2 nodes can be either a connecting point or a meeting point. If at least one of the adjacent node is a terminal node, then it is a connecting point. If it is not a connecting point, check the angle between links. If the angle is an obtuse angle, then it is a meeting point.

Nodes of Degree 3 Degree 3 nodes can be either a bifurcation point or a meeting point. If at least two adjacent nodes are terminal nodes, then the point is bifurcating. If two links have different orientation then also point is bifurcating. In the event that

two connections have the same orientation then both belongs to the same vessel; also they will be considered as a primary vessel. We can choose in the event that the third connection is a branch of the same vessel or a segment of an alternate vessel by checking its edge with the thicker portion of the primary vessel. The thicker segment of the primary vessel can be found by contrasting the vessel caliber assigned with each link. In the event that the distinction between vessel caliber is little, at that point it is not solid to discover the thicker one in light of the calibers; in this circumstance, the connection associated with the closest node to the optic disk represents the thicker segment of the primary vessel, and the connection associated with the most adjacent node is the thinner part of the primary vessel. On the off-chance that the third connection makes an acute angle with the thicker fragment of the primary vessel, then it is not an extension of this vessel however a part of an alternate vessel, and the node is a meeting point; else, it is an extension and all connections have the same label [7].

Nodes of Degree 4 In this, the node can be a bifurcating point, meeting point, or crossing point. In order to find out the node type first, the four nodes are grouped into two such that the angle between them is maximal. If the two links of each of these pairs have same orientation then the node is crossing point. If the links of one pair has a different orientation then the alternate pair is selected as a primary vessel. If the angle between each one of these links and the thinner part of the primary vessel is an acute angle, then the node is the bifurcation point. If any of these links make an acute angle with the thicker segment, then the node is meeting point.

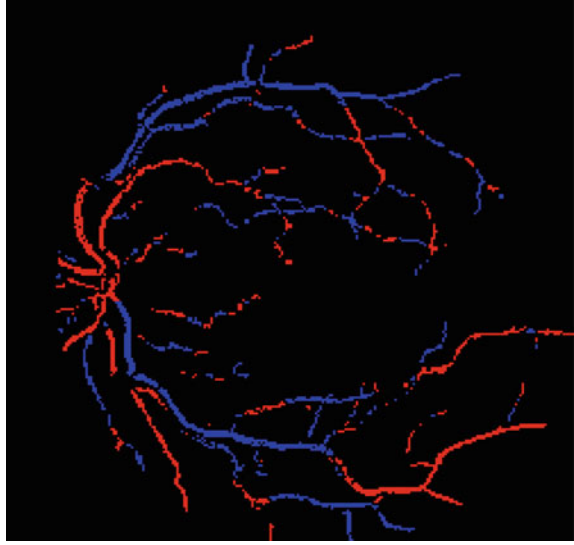
Nodes of Degree 5 This is a rare case that happens when a vessel crosses another on a bifurcation point. First, find the two vessels with the largest angle between them. These two belongs to the same vessel and the other three belongs to the alternate vessel.

After obtaining the node type, labels should be assigned to each vessel. If the point is meeting point, then assign different labels to the links. If the point is identified as bifurcating assign same label to both of the segments. And if the point is crossing point assign different labels. Else assign different labels to the links. Now, we will have a graph with two different labels.

3.6 Link Labeling

Link labeling is done by locating the optic dick [8]. Then the farthest link from optic dick is found out. And assign a label to this link. Node connected to this link is found and according to the node type assign same label or different label to the link. Repeat this process until no link is left unlabeled.

Fig. 7 Artery/vein classified image



3.7 *A/V Classification*

Now, we have to assign the links to artery class and vein class. From the above step, using graphical method itself retinal vessel class assignment is possible. But, in order to obtain a more accurate result we are using the visual or intensity features along with results from previous step. We are using intensity features or visual features like hue, saturation, intensities of red, green, and blue, their mean, standard deviation, etc. [9].

The trained kNN classifier is used for assigning A/V classes to the subgraph labels. First, each centerline pixel is classified into A/V classes. Then for every label the probability of it being an artery is calculated based on number of associated centerline pixels classified by kNN classifier. For each pair of labels in each sub-graph, the label with higher artery probability will be assigned as an artery class and the other as vein class. Figure 7 shows the classified vessels of retinal image shown in Fig. 3a.

3.8 *Estimation of Vessel Characteristics*

In this step, vascular features like the thickness of the vessel and various color pixel levels of red and blue are estimated. The color pixel level is estimated and represented as percentage. This is done on the assumption that whenever the yellow pixel

level increases beyond a certain limit, then there is the chance for occurrence of retinal exudates. And when red pixel level increases then there can be hemorrhage (blood clot or blood leakage). After calculating the thickness of retinal vessels, average thickness of artery and vein are calculated separately and then artery-to-vein ratio is calculated and checked whether it is less than 0.667 (Normal artery-to-vein ratio is 2:3). These three features can effectively predict whether the retinal image falls into normal category or abnormal category.

3.9 Decision Making and Prediction

A trained Artificial Neural Network is used for the decision making and accurate prediction. If the vessel caliber is less than a threshold value, then we have to check for the red pixel level which will help in predicting the hemorrhage presence. If both of these are showing abnormality, then there is no need to check further. Because the probability of retinal abnormality is very high and the prediction can be done. When the vessel caliber is normal, then we need not check the red pixel level as it will be normal. But the yellow pixel level should be estimated in order to detect the presence of exudates. If there is the presence of exudates (i.e., when the yellow pixel level is very high), then also the retinal image will fall into the abnormal category. If the vessel caliber is normal, and if there is no exudates present, then the retinal image can be predicted as a normal one.

4 Performance Evaluation

The summary of different features used for performance evaluation and the comparison with the related works [2–5] is listed in Table 1. From the table, it is clear that the performance of methods using visual properties alone for classification gets reduced because of nonuniformly illuminated images. This occurs due to contrast variability and local luminosity. Whereas, in methods using structural features alone the performance is average. This is because of the problem of missing link, false link, under-segmentation, etc. So, the best method is to use both these features together in a hybrid manner so that the problems can be eliminated to a certain extent and can increase the performance and efficiency of the system. Apart from the methods described in related works, retinal abnormality risk prediction model estimates the presence of hemorrhage and exudate which in turn increases the prediction accuracy.

Table 1 Comparison of abnormality detection techniques

Method	[2]	[3]	[4]	[5]	This paper
A/V classification	Color-based	Graph-based	Graph-based	Intensity-based	Hybrid approach
Features used	Visual/color	Structural	Structural	Visual	Structural and visual
Preprocessing technique	-	Illumination equalization	Channel extraction	Background normalization	Intensity normalization
Strategy	Color and tracking-based	Tracking-based	Tracking-based	Color-based	Color and tracking-based
AVR calculation	Semi-automatic	-	-	Semi-automatic	Automatic
Classification accuracy	Good	Good	Good	Excellent	Excellent
AVR accuracy	Good	-	-	Excellent	Average
Efficiency	Poor efficiency in non-uniformly illuminated images	Good	Good	Poor efficiency in nonuniformly illuminated images	Excellent
Hemorrhage detection	No	No	No	No	Red pixel level-based
Exudate identification	No	No	No	No	Yellow pixel level-based
Risk factor calculation	No	No	No	No	Yes
Abnormality prediction	No	No	No	No	Yes

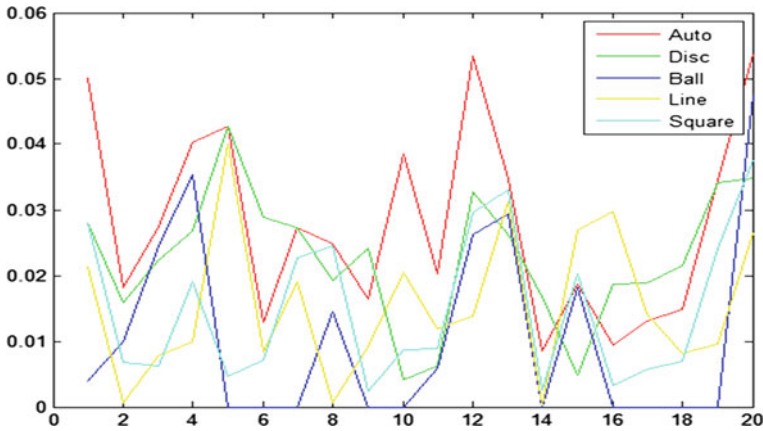


Fig. 8 Artery/vein classification performance

5 Results

The retinal abnormality risk prediction model is implemented in MATLAB. Classification accuracy is less while using multiscale morphological enhancement and reconstruction approach. Figure 8 illustrates the classification accuracy obtained when using different segmentation approaches. dick, ball, line, and square are the structural elements used for multiscale morphological enhancement and reconstruction approach and auto indicates the performance when using average filter for segmentation. The multiscale morphological enhancement and reconstruction approach will not eliminate the boundary of retinal image and so the boundary line is also classified as a retinal vessel which is a misclassification. So, average filter method outperforms the multiscale morphological enhancement and reconstruction approach in that perspective. Even small retinal vessels are obtained when average filter is used for segmentation.

Prediction performance in terms of Sensitivity, Specificity and Accuracy is calculated for DRIVE dataset. Sensitivity is 1, specificity is 0.857, and accuracy is 0.9.

6 Conclusion

Diabetes, hypertension, and vascular disorders will affect the retinal vessels first. Retinal vessels show some sort of vascular changes according to the severity of condition. To diagnose this kind of diseases Arteriolar-Venular ratio (AVR) is estimated. But for calculating this AVR, first we need to classify retinal vessels as the disease affects different retinal vessels in different ways. Hybrid approach described in this paper, helps to achieve best classification result and thereby

increases the accuracy of vessel caliber estimation and AVR ratio estimation. In this paper, along with AVR calculation hemorrhage detection and exudate identification is done which are some other indicators of retinal abnormality. This provides better retinal abnormality risk prediction results.

7 Future Work

As a future work, disease category can be identified using the results of this paper. Automatic identification of the disease class can be done with the help of unsupervised Artificial Neural Network that uses self organized mapping algorithm for training purpose and Genetic Algorithm for predicting the proper disease class.

Acknowledgments Authors would like to thank the authors of DRIVE, DERIVA, and HRIS datasets for making their image databases publicly available.

References

1. Li H, Hsu W, Lee M, Wang H. A piecewise Gaussian model for profiling and differentiating retinal vessels. *Proc Int Conf Image Process.* 2003;1:1069–72.
2. Vazquez S, Cancela B, Barreira N, Penedo M, Saez M. On the automatic computation of the arterio-venous ratio in retinal images: using minimal paths for the artery/vein classification. *Proc Int Conf Digital Image Comput Tech Appl.* 2010;599–604.
3. Kaba AD, Li Y, Liu X. Segmentation of blood vessels and optic disk in retinal images. *IEEE J Biomed Health Inf.* 2013.
4. Joshi VS, Reinhardt JM, Garvin MK, Abramoff MD. Automated method for identification and artery-venous classification of vessel trees in retinal vessel networks. *Plos One.* 2012.
5. Mendonça AM, Campilho A. Segmentation of retinal blood vessels by combining the detection of centerlines and morphological reconstruction. *IEEE Trans Med Imaging* 25(9). 2006.
6. El Abbadi NK, Al-Saadi EH. Automatic detection of exudates in retinal images. *IJCSI Int J Comput Sci Issues* 10(2). 2013.
7. Dashtbozorg B, Mendonca AM, Campilho A. An automatic graph-based approach for artery/vein classification in retinal images. *IEEE Trans Image Process.* 23(3). 2014.
8. Foracchia M, Grisan E, Ruggeri A. Detection of optic disk in retinal images by means of a geometrical model of vessel structure. *IEEE Trans Med Imaging.* 2004;23(10):1189–95.
9. Li H, Chutatape O. Automated feature extraction in color retinal images by a model based approach. *IEEE Trans Med Eng.* 2004;51:246–54.

BER and RSSI Analysis-Based Frequency Adaptive Technique for Radio Frequency Transceiver

A. Balasubramanian, A. Ahamad Meeran Mydeen and P.K. Dhal

Abstract In worldwide, the industrial, scientific, and medical applications, the specific spectrum is allotted and called ISM bands. Among these ISM bands, the 915, 868, and 433 MHz bands are popularly used by many users for different applications. Moreover, these frequency bands are declared license free in most of the countries, it encourages many users to utilize this frequency bands, which causes these bands more crowded. The advancement in technologies also enables more applications to operate in these bands. To overcome all these drawbacks and to utilize the spectrum in efficient manner, the simple adaptive method is proposed in this paper. This adaptive method is developed to identify the interference free channel and configure the RF transceiver to new channel. In this new method, the vital parameters of a RF link, like BER, RSSI, are derived and based on these parameters; the quality of service is estimated. Based on the channel quality, the frequency band of operation is selected. This adaptive technique is demonstrated here by considering Chipcon CC1010 sub 1 GHz single-chip RF transceiver. The algorithm for this technique is implemented in MATLAB. Initially the FSK RF transceiver is modeled and quality of service estimation and RSSI sampling is integrated and simulated.

Keywords Frequency bands · Spectrum utilization · Interference free channel · RF transceiver · BER · RSSI · MATLAB

1 Introduction

The frequency adaptive algorithm is developed to switch the operating frequency of the RF transceiver as and when the existing channel quality is found inoperable. The initial operating channel also selected by estimating the channel quality. The

A. Balasubramanian (✉) · A. Ahamad Meeran Mydeen · P.K. Dhal
Vel Tech Dr. RR & Dr. SR Technical University, Chennai, Tamil Nadu, India
e-mail: bala.arthanari@gmail.com

whole intension behind is to operate a RF transceiver reliable in crowded spectrum and utilize the spectrum in efficient manner which is scarce natural resource [1]. All the wireless technologies in the world use the radio frequency as medium for communication. The audio frequency which is from 20 Hz to 20 kHz can not be communicated as such because it will fade away after a short distance and need to be modulated to a higher frequency. The day by day technology advancement makes this RF spectrum source scarce. The RF spectrum which spreads between 9 kZ and 70 GHz is congested because of growing demand. The increasing demand for services like mobile phone and other services cause much crowd in spectrum. Beyond all these scenarios, through the survey conducted by international agencies reveals that most of the time the spectrum is underutilized. So as a step, the frequency adaptive technique for RF transceivers is developed [2, 3]. The direct conversion frequency shift keying (FSK) RF transceiver model is developed in MATLAB. The frequency adaptive algorithm also developed using MATLAB and integrated.

2 Architecture of Frequency Adaptive RF Transceiver

The Fig. 1 shows the architecture of BER and RSSI analysis based adaptive technique for RF transceiver.

2.1 Radio Frequency (RF) Transceiver

The RF transceiver is a radio module which has integrated transmitter and receiver. The transmitting and receiving blocks of the modem are activated in alternate time basis. The Tx/Rx switch routes the antenna between power amplifier (PA) and low-noise amplifier (LNA). The frequency adaptive technique is demonstrated using Chipcon CC1010 direct Conversion subs 1 GHz RF transceiver. Being a direct conversion RF transceiver, the frequency of operation is determined by

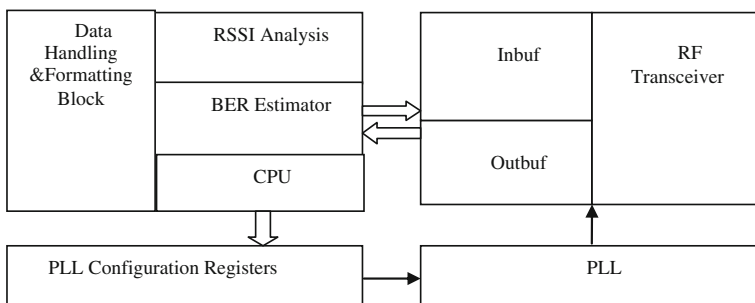


Fig. 1 Architecture of adaptive RF transceiver

PLL-based local oscillator. The frequency of a PLL can be configured through configuration registers dedicated in the RAM area of CC1010. The reference oscillator for PLL is derived from main oscillator constructed using external crystal tank circuit [4, 5]. It is proposed that to change the frequency of the RF transceiver. The PLL registers are configured using the following formula after estimating the channel quality.

$$f_{vco} = \frac{f_{ref}}{16384 (\text{FREQ} + \text{FSEP.TDATA} + 8192)},$$

where

FREQ Frequency Register
 FSEP Frequency Separation
 f_{ref} Reference Frequency
 f_{vco} VCO Frequency

By estimating the channel quality, it is proposed to shift the operating frequency between 433 and 915 MHz with respect to the above formula; Table 1 is formed for ISM bands. The input crystal frequency is assumed to be 11.0592 MHz and reference divider is fixed at 12.

2.2 Receiver Signal Strength Indicator (RSSI) Analysis

RSSI is the received signal strength indicator derived from the IF section of a RF transceiver. This signal indicates the strength of the received signal in turn it indicates whether the channel is blank or occupied. RSSI is the analog signal varies between its full ranges depending upon the received signal strength. In Chipcon CC1010, the ADC channel 2 is used to acquire the RSSI signal. The RSSI signal is acquired and stored in dedicated special function register. In a RSSI analyzer algorithm, the specific threshold range is set to determine the channel usability. The value present in the special function register is compared with the threshold value and the flags are stored in separate RAM location. This RSSI analyzer block alone is tested by applying saw tooth signal and the response is verified using Keil μ vision 4.

Table 1 Frequency value for different ISM frequency

ISM frequency	Low side/high side	Reference divider	Frequency word FREQ in hex
433.3	Low side	9	580,000
433.9	Low side	9	582,000
868.3	Low side	6	75A000
869.95	High side	6	75C000
915	High side	6	7C0000

2.3 Flow Chart for RSSI Analyzer

The Fig. 2 shows the flow chart of RSSI analyzer block and Fig. 3 shows the saw tooth response of RSSI analyzer block.

2.4 Bit Error Rate (BER) Estimator

The bit error rate (BER) is the measure, which can express the quality of channel directly. The BER is calculated normally by initiating test pattern from a master

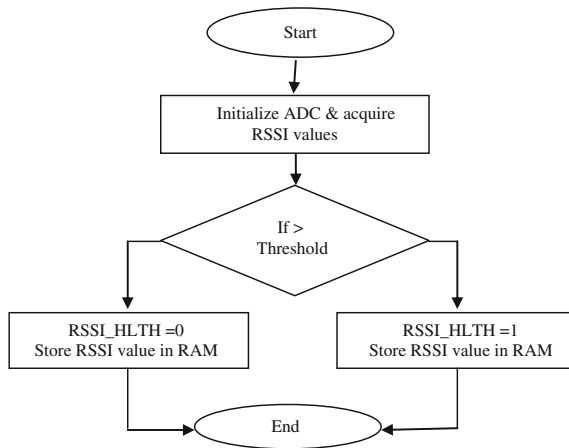


Fig. 2 Flow chart of RSSI analyzer block

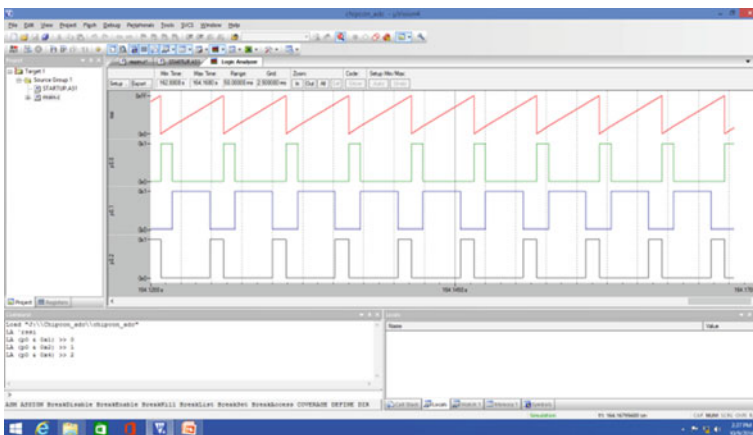
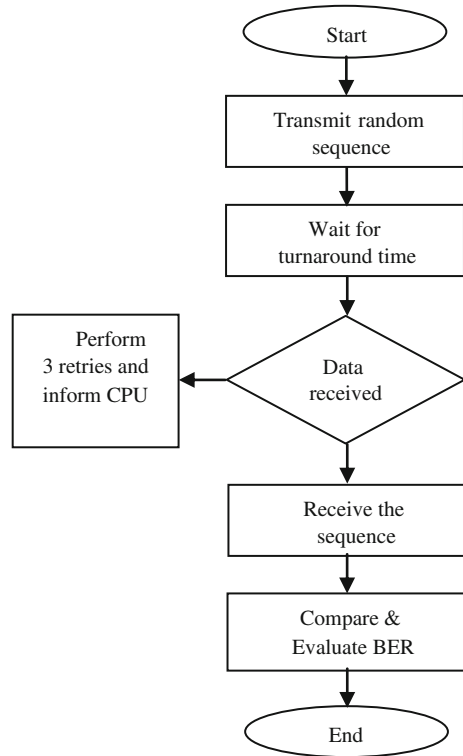


Fig. 3 Saw tooth response of RSSI analyzer block

Fig. 4 Flow chart for BER estimation



node. The same packet initiated by master node will be retransmitted by slave nodes without any modification. The master node will receive the retransmitted packet and calculate the number of errors in the packet. This exercise will be carried out periodically, and results are averaged out to calculate the effective BER. It is proposed to transmit heart beat messages which will be initiated by master [6, 7]. The addressed slave will retransmit the heart beat message. The periodicity of this activity is concluded to every 200 ms. so for every 200 ms, the number of error in the packet will be calculated and will be averaged out with the earlier result [8]. When the packet is not received from slave, the timeout error will occur. The predetermined number of repeated timeouts will be considered as a communication failure. The Fig. 4 shows the flow chart of BER estimator.

2.5 Input and Output Buffer of RF Transceiver

The input and output buffers are used to store the input data queue and output data queue. The DTEs are assumed to be faster than DCEs. In such case, these buffers are useful to match the speed between the DTE and DCE. When the data are ready

Table 2 Packet format for transmission and reception

1 Byte	1 Byte	1 Byte	1 Byte	n Bytes	2 Bytes
Header	No. of bytes	Slave address	Function code	Data bytes	CRC

with DTE it will raise a request to send (RTS) to DCE. The DCE, if its input buffer is not full, it clears the clear to send (CTS) signal. Otherwise the CTS signal will be asserted high. These buffers are normally first in first out (FIFO) kind of buffers.

2.6 Data Handling and Formatting Block of RF Transceiver

This block along with input/output buffers and with the help of hardware handshaking signals, CTS/RTS, it controls the flow of data between DTE and DCE. The data to be transmitted are encoded and packetized. The CRC code is generated and appended with the transmitting packet. Similarly the received packets are decoded and de-packetized. The Error checking is done using CRC bytes in a received packet [7]. In case of corrupted packet, the retransmission is requested.

Table 2 shows the packet format, in which the Byte header is used to synchronize the packet reception. This is the starting byte of the packet. The field 'No. of Bytes' indicates the number of bytes present in the packet excluding the header. The field 'Slave Address' defines the slave node to which the data are sent. The field 'Function Code' defines the functionality of the packet. The CRC bytes are used for error correction. The slave nodes also follow the same method to form a packet. In the case of packet initiated from slave node the field, 'Slave Address' defines the address of the slave transmits the packet.

3 Frequency Adaptive Algorithm

As explained in earlier sections, the health flag is derived from RSSI analyzer block and BER estimator block. These both parameters are used as vital parameters to decide the channel quality. The BER performance is the primary parameter considered for decision making. In cases, when BER performance is good and RSSI is weak also RF transceiver may adapt to new carrier frequency to attain better reliability [9, 10]. When these parameters are below the threshold mark, the alternate channel can be selected for the communication. The values of the frequency configuration registers are calculated for the new carrier frequency. The CPU loads the value in a PLL register `FREQ.SEP` and `FREQ` registers. The proper configuration of these registers locks the PLL to the new operating frequency, which can be detected by the lock bit of the PLL. The major challenge in shifting the operating frequency

is to synchronize master and slave nodes [11, 12]. The following is the algorithm of frequency adaptive technique for RF transceiver.

- Step 1 Read the bit error rate performance indicator flag written by BER estimator block.
- Step 2 Read RSSI indicator flag generated by RSSI analyzer block.
- Step 3 Compare the BER performance of current channel. If it goes poorer then evaluate the RSSI condition of current channel.
- Step 4 If RSSI performance is good, this means some other user has occupied the channel. Otherwise, it can be understood that attenuation is more in that particular channel.
- Step 5 Configure the PLL registers to new frequency band and transmit heartbeat message.
- Step 6 Wait for slave node to respond. Repeat the heart beat message periodically. The slave node may take 500 ms to get synchronized with master node in a new frequency channel.
- Step 7 Repeat the step 1 to step 6 for new frequency band after slave is responded to validate the channel.
- Step 8 Continue data transmission till the BER and RSSI of the new channel are within a permissible limit.

Similarly at slave side, the RF transceiver expects the heart beat message periodically from the master. It is done to ensure the intactness of the communication between the master and slave. When this heart beat message is absent for the predetermined amount of time, the slave shifts its operating frequency to next channel. In a next channel, the slave RF transceiver waits for heartbeat message and gets synchronized with the master.

4 Simulation Results and Discussions

The direct conversion FSK RF transceiver is considered here to demonstrate this proposed adaptive technique, though it can be implemented for any kind of radio. The direct conversion FSK RF transceiver is modeled in MATLAB initially. The channel quality is simulated using additive white gaussian noise (AWGN) source. By configuring EB/No of the AWGN source, we can increase or decrease the noise level in the communication channel. The GUIDE tool for MATLAB is used for better user interface. For the purpose of BER estimation, the bernault random number generator is used. Figure 5 indicates the plot of random integer generated. The random integer is generated as frame-based inputs with every frame contains 1024 bits. The initial seed for generating the random sequence is set to 32. The initial seed is the parameter decides the pattern of the random sequence.

This input random sequence is further modulated using m-ary frequency shift keying (MFSK) modulator with m-ary set to 2. The frequency separation between mark and space frequency is set to 60 Hz.

Fig. 5 Plot of random integer generators

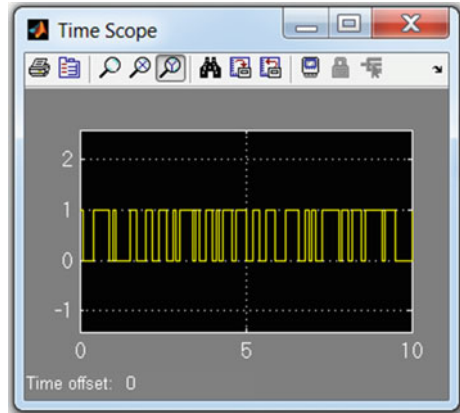


Fig. 6 Frequency spectrum of FSK modulated signal

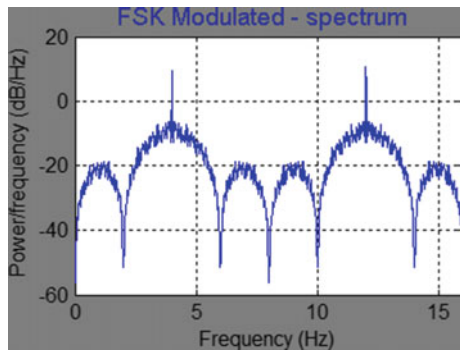


Figure 6 shows the modulated waveform of generated random sequence. This modulated signal is up converted to a carrier frequency of 433 or 915 MHz. To simulate the bit error rate performance, AWGN source is inserted in the channel. The input parameter EB/NO , the ratio of bit energy per symbol to noise power spectral density can be configured using a pull down menu given in the GUI to increase or decrease the noise level in the channel.

Figure 7 shows the waveform of FSK modulated signal at receiver when noise added to the level of $EB/NO = 10$.

It is understood from Fig. 8 the noise level is minimum in the noise added FSK modulated signal. So the carrier signal is set to 915 MHz and the BER in this condition is also very good. Since there is no error occurred in the communication.

Figure 9 shows the waveform of FSK modulated wave form with added Gaussian noise, when AWGN noise level increased to $EBNO = 0$. It can also be seen from the wave form that the noise floor compares to the case of $EBNO = 10$ are increased significantly, though the BER performance is considerably good. The BER measured under this condition is 0.1 and well manageable with error control mechanism.

Fig. 7 Spectrum of FSK modulated signal at receiver when Gaussian noise $EB/NO = 10$

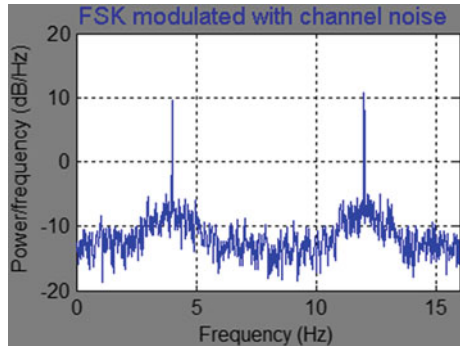


Fig. 8 Frequency spectrum of carrier signal, when $EB/NO = 10$

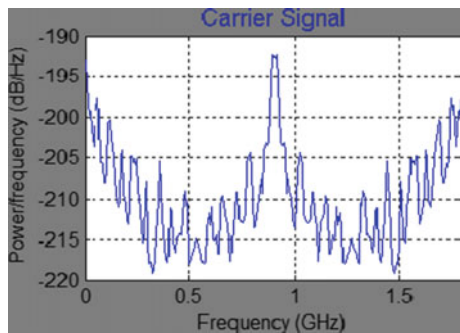
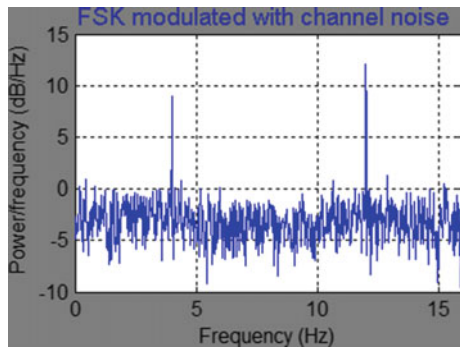


Fig. 9 Spectrum of FSK modulated signal at receiver when Gaussian noise $EB/NO = 0$



It can be seen from Fig. 10 the carrier frequency is positioned at 915 MHz unchanged. The following figures shows that the frequency domain waveforms of FSK modulated signal at receiver when Gaussian noise added to the level of $EB/NO = -10$.

It is evident from Fig. 11 that the signal is completely submerged in the noise floor and could not be distinguished. In this condition, the BER performance also goes very poor and intolerable. The channel is not usable, hence the CPU finds the

Fig. 10 Frequency spectrum of carrier signal, when $EB/NO = 0$

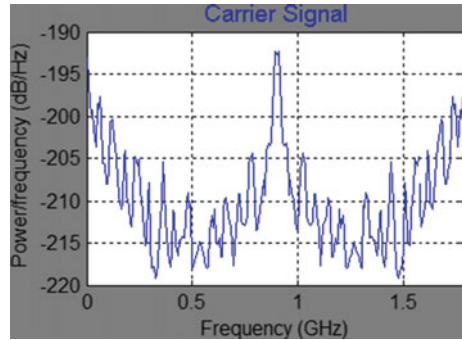


Fig. 11 Spectrum of FSK modulated signal at receiver when Gaussian noise $EB/NO = -10$

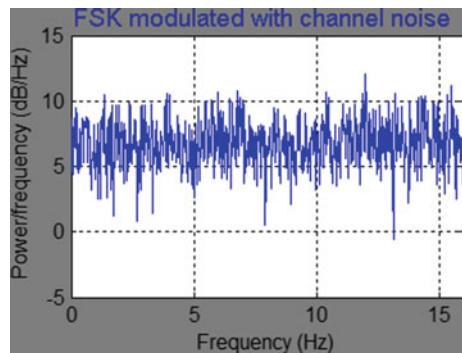
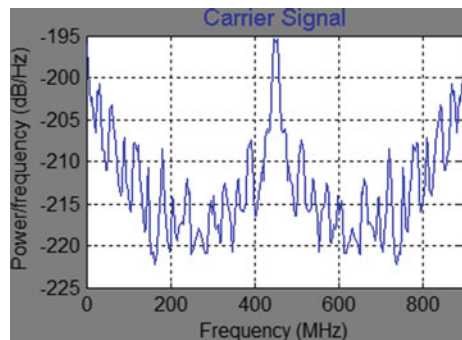


Fig. 12 Frequency spectrum of carrier signal, when $EB/NO = -10$



next better channel by shifting transmitter and receiver carriers to new frequency band, and synchronizing them as explained in the ‘Synchronization’ section.

Figure 12 shows the frequency domain plot of the carrier frequency which is shifted to 433 MHz.

Once synchronization is achieved with new channel, again the random sequence is transmitted and the whole process is repeated to estimate the BER. During this switchover time, the data received from the DTE are stored in the buffers so that

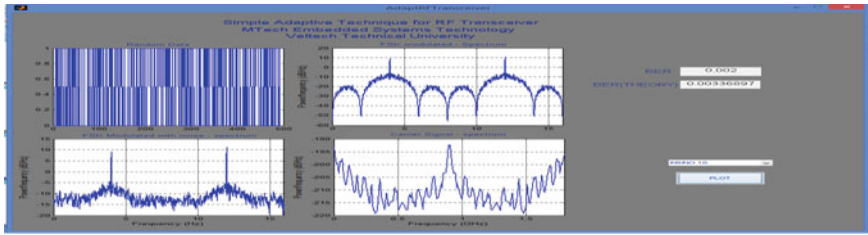


Fig. 13 Overall GUI layouts

Table 3 Carrier frequency for BER versus AWGN noise level

AWGN level	BER	Carrier frequency in MHz
10	0.0000001	915
8	0.0000001	915
5	0.0000001	915
1	0.0000012	915
0	0.0000015	915
-1	0.0000042	915
-2	0.0000159	915
-5	0.0002138	433
-8	0.0013247	433
-10	0.0152346	433

DTEs will have seamless transmission. In case of buffer overflow, as explained in ‘Data formatting and Buffer handling’ section, with the help of hand shaking signals RTS and CTS, the DTE will be requested to stop the data transmission to avoid data loss. Once the input queue is serviced again the DTE will be requested to send the data.

Figure 13 shows the overall snapshot of the GUI layout developed to simulate this proposed system. The pull down menu is given to choose the different noise levels. When the ‘plot’ button is pressed the GUI will simulate and display the result for new noise condition. The GUI also displays the theoretical and measured BER for the particular noise condition, the BER performance for the above and other test conditions are simulated and tabulated (Table 3).

5 Conclusion

It is concluded that the adaptive technique proposed here by analyzing bit error rate (BER) and received signal strength indicator (RSSI) of the channel is helpful in predicting the channel quality and then switching to the better channel available. The simulation is carried out by assuming two frequency bands 900 and 450 MHz. It is concluded that the shifting a carrier signal is used to another frequency band

when channel noise is greater, i.e., BER is poorer than 0.4. When the BER is greater than 0.4, the RF transceiver operates in frequency band of 900 MHz and otherwise it operates in 450 MHz. This technique can be further extended to frequency hopping RF transceivers also. The frequency hopping spread spectrum (FHSS) RF transceiver hops between different carrier frequency in predetermined time interval and in random sequence of frequency selection. Since most of FHSS RF transceivers uses only PLL technique to shift between frequency slots, which are close spaced in the same frequency band, this adaptive technique can also be integrated. The integration of this adaptive technique with FHSS RF transceiver will improve noise immunity to the RF link. Also this adaptive technique requires only firmware level modification to integrate with FHSS RF transceivers. This simple and affordable adaptive method can be implemented in noisy environment wherever reliability also desired.

References

1. Zhu X, Feng Y. RSSI-based algorithm for indoor localization. *Commun Netw.* 2013;5:37–42. doi:[10.4236/cn.2013.52B007](https://doi.org/10.4236/cn.2013.52B007).
2. Rasmussen A et al. Framed bit error rate testing for 100G ethernet equipment. In: Proceedings of the IEEE international conference on high performance switching and routing (HPSR), Dallas, TX, USA. 2010. p. 165–8.
3. Coelho LD, et al. Modeling nonlinear phase noise in differentially phase-modulated optical communication systems. *Opt Express.* 2009;17(5):3226–41.
4. Seconding M et al. Analytical performance evaluation of optical DQPSK systems with post detection filtering. *IEEE Photon Technol Lett.* 2009;21(13).
5. Nölle M, Seimetz M, Patzak E. System performance of high-order optical DPSK and star QAM modulation for direct detection analyzed by semi-analytical BER estimation. *J Light Wave Technol.* 2009;27(19): 4319.
6. Secondini M, Frezzini M, Forestieri E. Analytical performance evaluation of optical DQPSK systems with post detection filtering. *IEEE Photon Technol Lett.* 2009;21(13).
7. Savory S. Digital filters for coherent optical receivers. *Opt Express.* 2008;16:804–17.
8. Strobl M, Moolenaar M, Schingale A. Bit error rate testing serial communication equipment using pseudo-random bit sequences. IEEE tenth workshop on intelligent solutions in embedded systems, Klagenfurt, Austria. 2012. p. 39–44
9. Henzinger T, Sifakis J. The embedded systems design challenge. In: Proceedings of the 14th international symposium on formal methods (FM), lecture notes in computer science. Hamilton, Ontario, Canada: Springer; 2006. p. 1–15.
10. Goldfarb G, Li G. BER estimation of QPSK homodyne detection with carrier phase estimation using digital signal Processing. *Opt Express.* 2006;14(18):8043–53.
11. Richter A, Koltchanov I, Kuzmin K, Myslivets E, Freund R. Issues on bit-error rate estimation for fiber-optic communication systems. OFC/NFOEC 2005, paper NTuH3.
12. Breed G. Bit error rate: fundamental concepts and measurement issues. *High Freq Electron.* 2003;2(1):46–7.

A Two-Stage 0.18 μm CMOS Differential Low-Noise Amplifier with Integrated LC Balun for 2.4 GHz Applications

J.L. Lakshmi and Premanand V. Chandramani

Abstract This work aims at designing a two-stage 0.18 μm CMOS differential low-noise amplifier (LNA) with integrated LC balun, operating at 2.4 GHz industrial, scientific, and medical (ISM) band. A differential LNA has an advantage of common mode noise cancelation and enables a narrowband operation. The need of lossy off-chip balun in a differential LNA is overcome by a LC balun integrated at the input. The proposed two-stage differential LNA achieves a gain of 20.9 dB, noise figure of 1.7 dB, and input return loss of -39.2 dB. The proposed LNA is also observed to be stable at 2.4 GHz operating frequency.

Keywords Low-noise amplifier · ISM · Differential LNA · Gain · Noise figure · Stability

1 Introduction

The industrial, scientific, and medical (ISM) radio band is an unlicensed band used for industrial, scientific, and medical applications, which is also shared with license-free error-tolerant communication applications such as wireless local area networks (LANs), Bluetooth devices, cordless phones, or other protocol-specific devices operating in the 900 MHz, 2.4 GHz, and 5.8 GHz bands. Higher frequency bands have faster throughput and hence are favored by most of the wireless networks [1]. The 2.4 GHz band is the most common band used for wireless communications, spanning from 2.4 to 2.5 GHz. Low-noise amplifier play a major role in wireless communication. It is the first active signal processing block in the front end receiver. The importance of LNA in receiver lies in its ability to receive the

J.L. Lakshmi (✉) · P.V. Chandramani
ECE Department, SSN College of Engineering, Kalavakkam, India
e-mail: jllakshmi17@gmail.com

P.V. Chandramani
e-mail: premanandc@ssn.edu.in

smallest possible signal from the antenna, amplifying it, and at the same time limiting the noise coupled to the incident RF signal. But, the design of low-noise amplifier is critical since it involves trade-offs between parameters like gain, noise figure, input return loss, output return loss, stability, linearity, and power consumption. Noise in the front end receiver is determined by the noise figure and gain of the LNA. The gain of the LNA should be considerably high so that the noise in the subsequent stages is minimized. The overall noise figure of receiver (NF_{rec_front}) is given by the Friss Eq. (1),

$$NF_{rec_front} = \left(\frac{1}{G_{LNA}} \right) (NF_{subsequent} - 1) + NF_{LNA} . \quad (1)$$

where, $NF_{subsequent}$ is the total input referred noise factor of the components following the LNA. G_{LNA} is the gain of LNA. NF_{LNA} is the noise figure of LNA.

Different topologies of LNA exist. The common gate (CG) LNA provides a good input impedance matching but suffers from poor noise performance and low voltage gain [2]. To overcome these shortcomings, common source (CS) is used along with CG. A CS-CG (Cascode) LNA [3] provides noise and distortion cancelation, broadband impedance matching, but a trade-off exists between power consumption, noise figure, and voltage gain. A distributed amplifier [4] provides a good impedance matching, a flat gain over a wide range of frequencies, and generally high IIP3, the demand for high-quality transmission line makes it less attractive in low-cost applications. Folded cascode [5] topology possesses good bias stability, linearity, and noise figure. The major disadvantage is the lower gain. Single ended input LNA consumes less area and use less input/output (I/O) pins. On the other hand, differential signaling minimizes even order distortions, cancels out noise from the substrate [6] and power supply, and also the subsequent mixer stage is fed from a differential source. However, in case of a differential LNA, balun is required to convert the single ended signal to differential signal at the input.

In differential LNA, an off-chip balun is widely used. However, it reduces the sensitivity of LNA and increases the system cost [7]. In this paper, a common source differential LNA cascaded in two stages, integrated with a LC balun operating at 2.4 GHz ISM band is proposed. This LC balun avoids the use of lossy off-chip balun and also aids in frequency selection for a narrowband operation at the input.

2 LNA Architectural Analysis

A two-stage differential amplifier is designed with a LC balun integrated at the input of the LNA for single ended to differential signal conversion. Figure 1 shows the block diagram of the proposed two stage differential LNA. The input matching, output matching, the LC Balun design, and stability of the LNA are discussed in this section. Figure 2 shows the schematic of the proposed two-stage differential LNA.

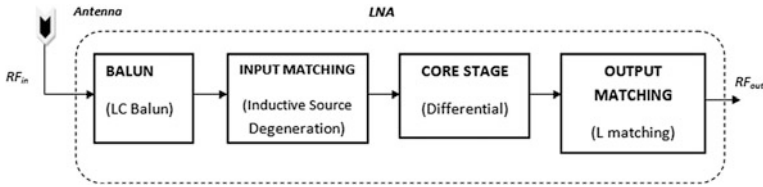


Fig. 1 Block diagram of proposed low-noise amplifier

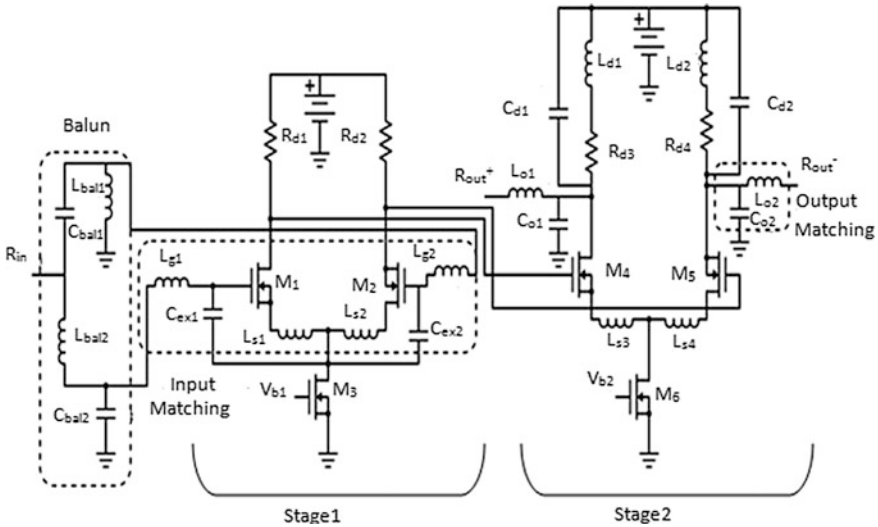


Fig. 2 Proposed two-stage differential low-noise amplifier

2.1 Gain Analysis

The half circuit small signal equivalent of the two-stage differential LNA is shown in Fig. 3. The overall gain (A_v) is given as

$$A_v = A_{v1} * A_{v2}. \tag{2}$$

where, A_{v1} and A_{v2} are the gain of the first and second stage of differential amplifier, respectively.

$$A_{v1} = \frac{V_1}{V_{in}}. A_{v2} = \frac{V_{out}}{V_1}. \tag{3}$$

$$A_{v1} = \frac{-g_{m1} \frac{r_{o1} R_{d1}}{r_{o1} + R_{d1}}}{1 + g_{m1} \frac{r_{o1} R_{d1} (S(L_{s1} + L_{g1}) + R_{on3})}{r_{o1} + R_{d1}}} \tag{4}$$

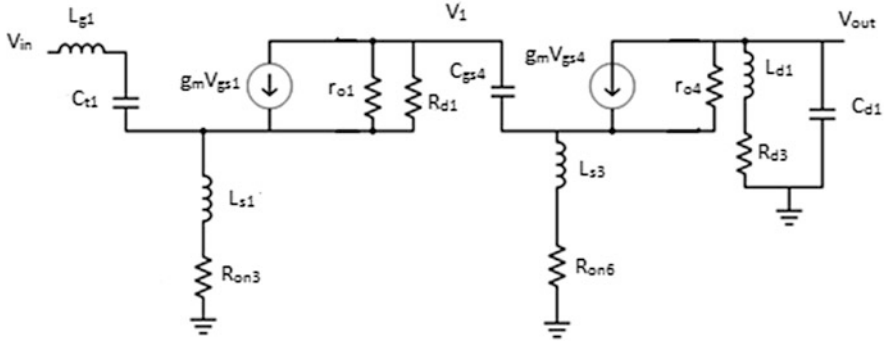


Fig. 3 Equivalent half circuit of the two-stage differential low-noise amplifier

$$A_{v2} = \frac{-g_{m4} \frac{r_{o4}(R_{d3} + SL_{d1})/SC_{d1}}{r_{o4}(R_{d3} + SL_{d1})/SC_{d1}}}{1 + g_{m4} \frac{r_{o4}(R_{d3} + SL_{d1})(SL_{s3} + R_{on6})/SC_{d1}}{r_{o4} + (R_{d3} + SL_{d1})/SC_{d1}}}. \tag{5}$$

where, g_{m1} and g_{m4} are the transconductance of M_1 and M_4 , respectively. R_{d1} and R_{d3} are the drain resistance. R_{on3} and R_{on6} are the on resistance of transistors M_3 and M_6 . L_{s1} and L_{g1} are the source and gate inductance that contribute to input matching. C_{d1} and L_{d1} are the drain capacitance and inductance of the second stage, respectively. r_{o1} and r_{o4} are the output resistance of M_1 and M_4 , respectively. V_{in} and V_{out} denote the input and output voltage, respectively and V_1 denote the voltage at the intermediate stage.

2.2 Input Matching

In [8], the input matching topologies like resistive termination [9], common gate termination, shunt-shunt feedback termination, and inductive source degeneration feedback has been investigated. The inductive source degeneration is observed to be one of the best noise performance topologies due to the absence of resistors and also helps in narrow band matching at input. Here, an external capacitance gate to source capacitance (C_{ex}) is introduced for improved input impedance matching. The half equivalent circuit of differential input matching using source inductive degeneration is shown in Fig. 4a.

The total gate source capacitance (C_t) of transistor M_1 is given as

$$C_t = C_{ex} + C_{gs}. \tag{6}$$

The input impedance (Z_{in}) given as

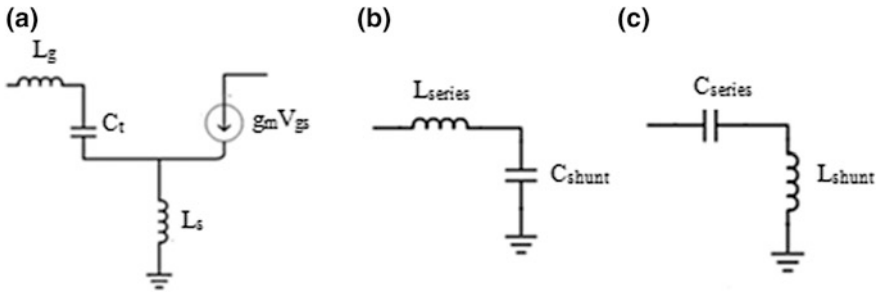


Fig. 4 **a** Equivalent half circuit of differential input matching using inductive source degeneration. **b** Output matching– L -matching network that allows DC, and **c** L -matching network that blocks DC

$$Z_{in} = \left[j\omega(L_s + L_g) + \frac{1}{j\omega C_t} + \frac{g_m L_s}{C_t} \right]. \tag{7}$$

$$R_s = \frac{g_m L_s}{C_t}. \tag{8}$$

$$\omega_o = \frac{1}{\sqrt{(L_g + L_s) * C_t}} \tag{9}$$

where, L_s is the source degeneration inductor, L_g is the gate inductance, and g_m denotes the transconductance of the transistor.

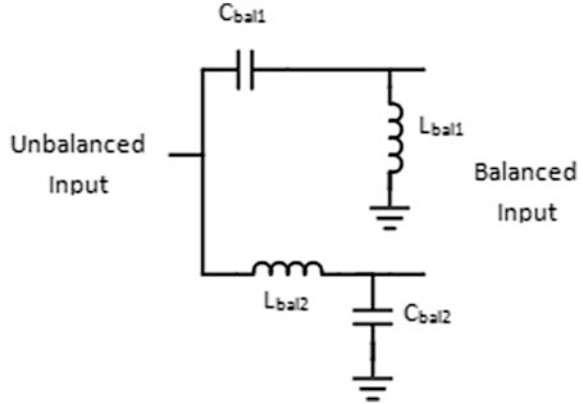
2.3 Output Matching

It is essential that the output impedance of the LNA is matched to the input impedance of the subsequent stage of the receiver. In this paper, L -matching network that allows DC is used for output impedance matching. The L -matching networks that allows and blocks direct current (DC), respectively, is shown in Fig. 4b, c.

2.4 Balun

Balun is used to convert a balanced signal to an unbalanced signal and vice versa. The LNA receives input from the antenna whose output is single ended. Since the proposed LNA has a differential input, a Balun is required to convert the unbalanced signal from the antenna to the balanced signal. In order to avoid the lossy

Fig. 5 LC balun network



off-chip balun and to achieve a narrowband operation, a LC balun is integrated at the input of the differential LNA design. Figure 5 shows the LC balun network.

2.5 Stability

Stability of the LNA is measured from the stern stability factor (K) and delta obtained from the S parameter, given by (10). The LNA is said to be unconditionally stable, if $K > 1$ and if the value of delta is less than one at the operating frequency. If the circuit does not oscillate for any load given at the input or output, then it is said to be unconditionally stable.

$$K = \frac{1 - |S_{11}|^2 - |S_{22}|^2 + |\Delta|^2}{2|S_{12} * S_{21}|} \quad |\Delta| = |S_{11}S_{22} - S_{12}S_{21}| \quad (10)$$

3 Results and Discussion

The proposed LNA is simulated using agilent advanced design systems (ADS) and analysis of S parameter is done. Gain $S(2,1)$ of 20.9 dB is achieved by cascading differential stages. The gain of two-stage differential LNA is shown in Fig. 6a. The inductive source degeneration and differential topology helps in achieving a noise figure of 1.7 dB as shown in Fig. 6b.

The inductive source degeneration (input matching) helps to maximize power transfer for the LNA without addition of noise at the input [10]. The input return loss $S(1,1)$ is observed to be -39.2 dB and the L -matching at the output of the LNA aids in maximum power transfer to the next stage. The output return loss $S(2,2)$ of LNA is -23.7 dB, as shown in Fig. 6c. Reverse isolation $S(1,2)$ determines how

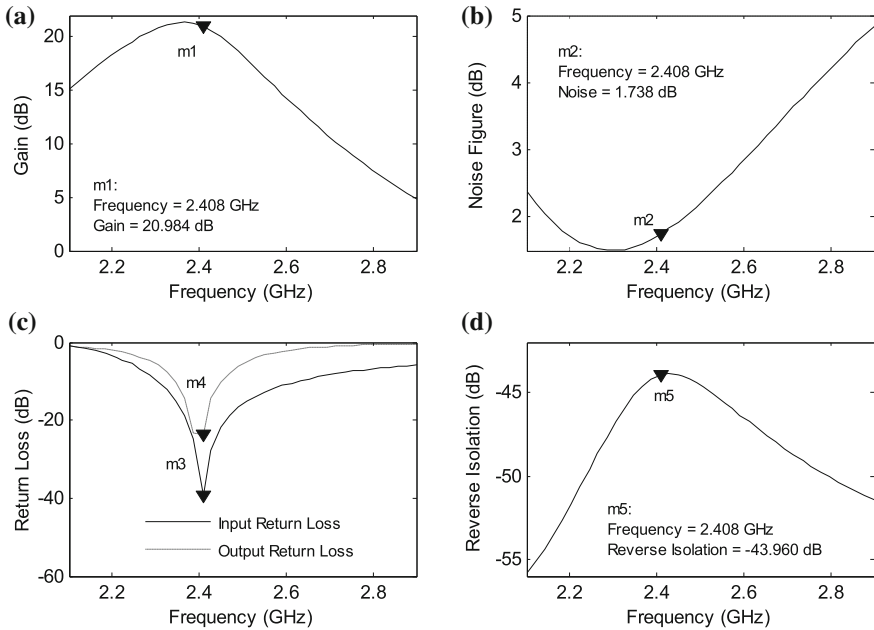


Fig. 6 a Simulated gain $S(2,1)$, b noise figure, c input return loss and output return loss, and d reverse isolation $S(1,2)$ of two-stage differential LNA

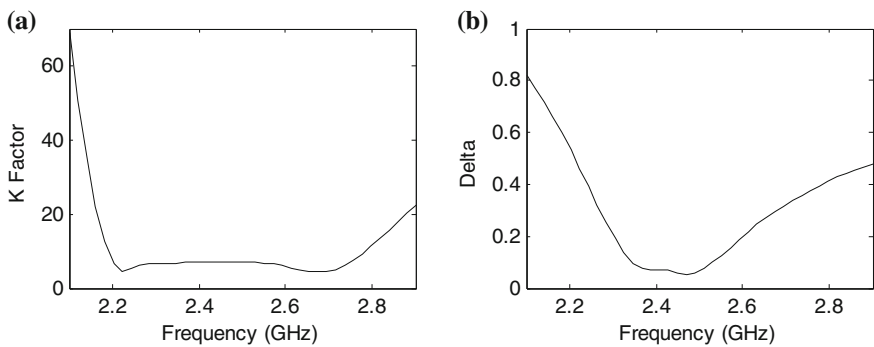


Fig. 7 a K factor and b delta of two-stage differential LNA

well the output signal is isolated from the input. It is very essential for circuit stability. In this work, the reverse isolation of the LNA is observed to be -43.96 dB as shown in Fig. 6d.

From the results shown in Fig. 7a, b, it is observed that the value of K is greater than one and the value of delta is less than one. Hence, the proposed LNA is unconditionally stable at the operating frequency. The performance of the proposed

Table 1 Performance and comparison of proposed LNA

Topology	Common gate [2]	Cascode [3]	Distributed amplifier [4]	Folded cascode [5]	Differential cascode [6]	This work
Gain (dB)	14.7	13.29	8	14.1	8.4	21
Input return loss (dB)	-18	-11	-12	-13.4	-13	-39
Output return loss (dB)	NA	-13.9	-10	-10.6	NA	-23.7
Noise figure	4.8	2.87	2.9	3.37	1.92	1.7
Power Consumption	0.58 mW	11 mW	21.6 mW	1.68 μ W	16.2 mW	10 mW

LNA (gain, noise figure, input and output return loss, and power consumption) is compared with that of the LNAs existing in literature (Table 1).

4 Conclusion

A two-stage differential LNA with integrated LC balun is designed, operating at 2.4 GHz frequency. The proposed LNA has an advantage of achieving considerable gain and minimum noise figure. The integrated LC balun at the input avoids the use of off-chip baluns which would otherwise reduce the sensitivity of LNA. The proposed LNA provides a gain of 20.9 dB, noise figure of 1.7 dB, input return loss (S_{11}) of -39.2 dB, output return loss (S_{22}) of -23.7 dB, and reverse isolation (S_{12}) of -44 dB. The two-stage differential LNA consumes 10 mW power from 1.8 V supply. Further analysis on power reduction has to be done on this circuit, and hence future study aims at exploring the techniques for reducing the power consumption of the proposed LNA so as to enhance its performance.

References

1. Coleman DD, Westcott DA. Certified wireless network administrator official study guide, 3rd ed. Sybex Publication; 2012.
2. Li Z, Wang Z, Zhang M, Chen L, Wu C, Wang Z. A 2.4 GHz ultra-low-power current-reuse CG-LNA with active-boosting technique. IEEE Microw Wirel Compon Lett. 2014;24(5):348-50.
3. Tu C-H, Juang Y-Z, Chiu C-F, Wang R-L. An accurate design of fully integrated 2.4 GHz CMOS cascode LNA. IEEE VLSI-TSA international symposium on VLSI design automation and test. 2005. 169-72.
4. Heydari P. Design and analysis of a performance-optimized CMOS UWB distributed LNA. IEEE J Solid-State Circuits. 2007;42(9):1892-905.

5. Hsieh H-H, Wang J-H, Lu L-H. Gain-enhancement techniques for CMOS folded cascode LNAs at low-voltage operations. *IEEE Trans Microw Theory Tech.* 2008;56(8):1807–16.
6. Fan X, Zhang H, Sanchez-Sinencio E. A noise reduction and linearity improvement technique for a differential cascode LNA. *IEEE J Solid-State Circuits.* 2008;43(3):588–99.
7. Peng M, Lin M, Wu T, Shi Y, Dai FF. A 2.4 GHz front-end with on-chip balun in a 0.13 μm CMOS technology. 10th IEEE international conference on solid-state and integrated circuit technology (ICSICT). 2010. 512–4.
8. Shaeffer DK, Lee TH. A 1.5-V, 1.5-GHz CMOS low noise amplifier. *IEEE J Solid-State Circuits.* 1997;32(5):745–59.
9. Joo S, Choi T-Y, Jung B. A 2.4 GHz resistive feedback LNA in 0.13 μm CMOS. *IEEE J Solid-State Circuits.* 2009;44(11):3019–29.
10. Razavi B. *RF microelectronics*. 2nd ed. Castleton: Prentice Hall; 2011.

Energy Harvesting in Wireless Sensor Networks

R. Ramya, G. Saravanakumar and S. Ravi

Abstract In recent years, wireless sensor networks (WSNs) have grown dramatically and made a great progress in many applications. But having limited life, batteries, as the power sources of wireless sensor nodes, have restricted the development and application of WSNs which often requires a very long lifespan for better performance. In order to make the WSNs prevalent in our lives, an alternative energy source is required. Environmental energy is an attractive power source, and it provides an approach to make the sensor nodes self-powered with the possibility of an almost infinite lifetime. The goal of this survey is to present a comprehensive review of the recent literature on the various possible energy harvesting technologies from ambient environment for WSNs.

Keywords Wireless sensor networks · Energy · Harvesting · Life time · Generation

1 Introduction

In recent years, with the development of microelectronics and wireless communication technology, WSNs, as one of the world's top ten technologies in the twenty-first century, are a hot research field at home and abroad for the importance

R. Ramya (✉)

Dr. M.G.R. Educational and Research Institute University, Chennai, India
e-mail: ramyarajarathinam@yahoo.com

G. Saravanakumar

Department of ECE, Vel Tech High Tech Dr. Rangarajan Dr. Sakunthala
Engineering College, Chennai, India
e-mail: shawn_pooja2003@yahoo.co.in

S. Ravi

Department of ECE, Dr MGR Educational and Research Institute University,
Chennai, India
e-mail: ravi_mls@yahoo.com

© Springer India 2016

S.S. Dash et al. (eds.), *Artificial Intelligence and Evolutionary Computations in Engineering Systems*, Advances in Intelligent Systems and Computing 394, DOI 10.1007/978-81-322-2656-7_76

841

in the national defense and military applications [1, 2], environment monitoring [3], healthcare [4, 5], traffic control [6], industrial monitoring [7], target tracking [8], structural health monitoring [9], and so on. WSNs are usually composed of many low-cost low-power microsensor nodes which are spread in a certain area aiming at collecting and processing the required data and transmitting them to a base station cooperatively by a wireless communication method [10].

At present, low power consumption has almost become a core of research in WSNs like low-power MAC protocols [11, 12], routing protocols [13, 14], transport protocols [15], and even operating systems [16] have also stressed the low power design, in order to prolong the life cycle of sensor network.

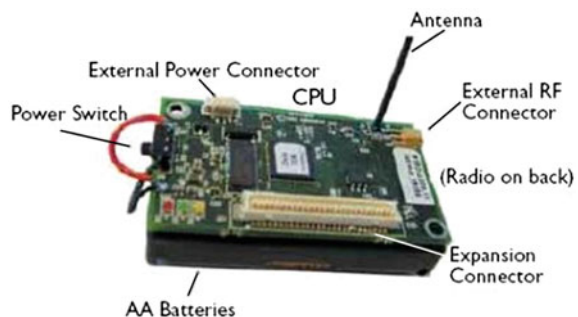
A non-rechargeable lithium battery is a promising energy storage device and the power density of it is $45 \mu\text{W}/\text{cm}^3$ for 1-year lifetime and $3.5 \mu\text{W}/\text{cm}^3$ for 10-year lifetime [17]. However, when WSNs are requested to work for a long time, the chemical battery cannot be the only energy source in many applications, where a huge number of sensors are distributed or the place is extremely difficult to access for replacing or recharging the battery is an uneconomical or impossible behavior such as biomedical field, environmental monitoring, and military applications [18, 19]. So, with the demand of exploring a new type of micro power to solve the above problems, the micro environmental energy harvesting technology has emerged.

The image of the sensor node is displayed in Fig. 1. Considering energy supply modules, the structure of wireless sensor nodes is shown in Fig. 2.

Up to now, there have been some reports that the power of WSNs was provided by energy harvesting systems. For example, the solar harvesting device was tested in the alpine valleys to supply power for wireless sensor nodes. The test system consists of storage batteries, solar panels, and various control and test circuits. The test time started from the summer of 2005 and lasted for more than 100 days. The test site was chosen in the Alps for the reason that the weather conditions there are very poor as thunderstorms and rain clouds often occur. However, experimental results showed that the solar cells were able to provide a relatively stable electric power for sensor nodes [20].

The researchers of Takenaka Corporation developed a new WSN system which contains vibration energy harvesters and wireless sensors. The system is able to run

Fig. 1 Sensor node



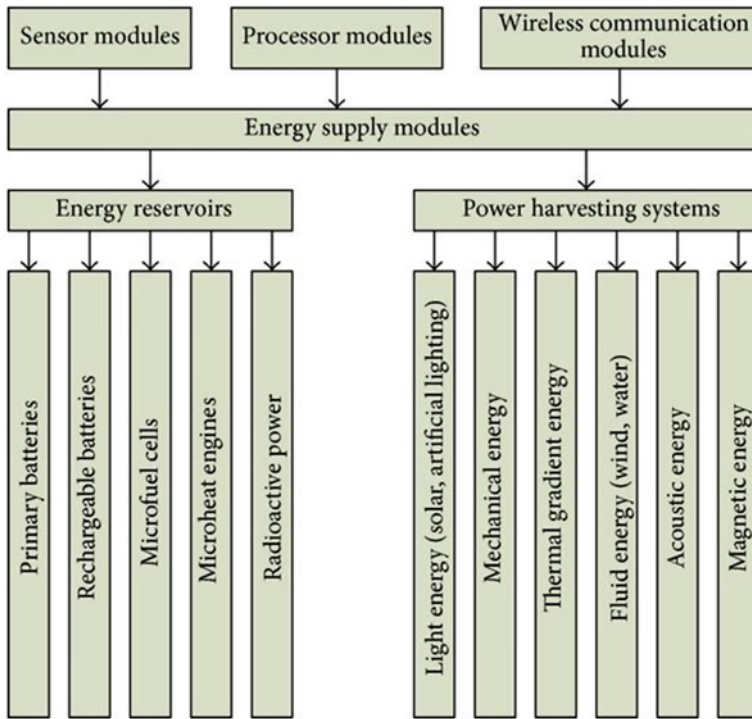


Fig. 2 The structure of wireless sensor nodes

without batteries and power lines for it can convert ambient mechanical vibration produced by the people walking around and equipment operation into electrical energy.

2 Sources of Energy Harvesting

Energy

Formula for calculating energy is

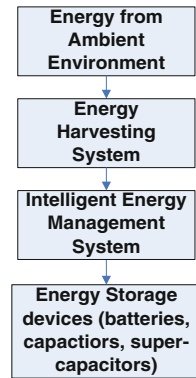
$$\text{Energy} = \text{Power} * \text{Time} \tag{1}$$

Unit of energy is kWh/h or Joule. There is a variety of methods to harvest various energies in the ambient environment. The classification of energy harvesting in this paper is organized on the basis of the different forms of energy. And the energy sources reviewed in the paper include solar, mechanical, temperature gradient, dynamic fluid, acoustic, magnetic, and hybrid energy. For comparison,

Table 1 Comparison of power outputs from energy harvesting technologies

Harvesting method	Power density
Solar energy—outdoor	15 mW/cm ³ —bright sunny day
	0.15 mW/cm ³ —cloudy day
Solar energy—indoor	10–100 μW/cm ²
Vibrations (piezoelectric—shoe inserts)	330 μW/cm ³
Vibrations (electrostatic conversion)	0.021 μW/mm ³ —105 Hz
Vibrations (electromagnetic conversion)	184 μW/cm ³ —10 Hz
	306 μW/cm ³ —52 Hz
Thermoelectric—5 °C gradient	40 μW/cm ³
Wind flow	16.2 μW/cm ³ —5 m/s
Acoustic noise	3 nW/cm ³ —75 dB
	960 nW/cm ³ —100 dB
Magnetic field energy	130 μW/cm ³ —200 μT, 60 Hz

Fig. 3 Energy harvesting system of wireless sensors



some examples of power outputs from energy harvesting technologies are listed in Table 1.

The general structure diagram of energy harvesting system of wireless sensors is shown in Fig. 3 with the purpose of achieving stable long-term operation [21].

3 Photovoltaic Power Generation

There are two methods to extract solar power at present. One is solar thermal power generation, which is suitable for large engineering systems and not applicable in WSNs for it is not available on small or nanoscale [22]. In photovoltaic system, solar cells are used to convert sunlight into electrical power directly, according to photovoltaic principle [23]. The other lights, such as fluorescent and infrared, can also be used as the power source for solar cells [22]. At present, polycrystalline

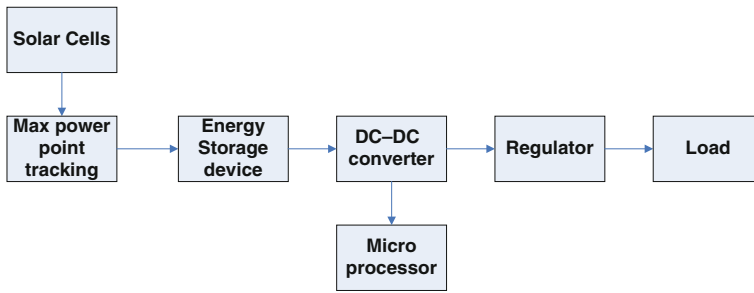


Fig. 4 Solar energy harvesting system for wireless sensors

silicon solar cells possess the largest production and market share, followed by monocrystalline silicon solar cells which are suitable for conditions of high-intensity light and outdoor spectrum [24].

The general block diagram of Solar energy harvesting system for wireless sensors is shown in Fig. 4. The energy storage device is used to store generated energy as well as buffering the power required by sensor nodes [25]. The wireless sensors can be connected to energy storage device directly for its DC characteristics. While the voltage range of each sensor node may not be the same and some sensors may be very sensitive to the change of voltage supply, then the output voltage needs to be regulated by DC-DC converter [26]. However, sometimes this method is not advisable with considering the simplicity and efficiency of energy harvesting system. The additional regulation may also be required between sensor and energy storage device to ensure that the sensor node works with a stable and safe voltage.

Solar energy has been more widely considered for WSNs which consume several mV of energy, as it is the common and accessible energy in the majority of deployment environments and can be easily tapped. While it is designed as a power source for WSNs, the first thing which we must consider is the power supply requirements of WSNs. The solar cells, power conditioning features, and the chemistry and capacity of energy storage components are used to store the harvested energy. With the cost of optoelectronic components declining, it has become a reasonable solution to utilize solar energy source for WSNs. At present, solar cells with high efficiency are available in market and have several remote sensing and wireless applications. And the photovoltaic technology has developed into particles deposition on the photosensitive substrate from the initial silicon manufacturing. Recently, researchers have made a lot of breakthroughs of micro solar cells and some of them are shown in the following.

The company of Kyosemi developed a micro spherical solar cell called Sphelear which is a revolutionary transformation compared to the previous solar cell.

Canadian scientists developed a new kind of efficient full spectrum solar cell with tandem-type connection based on colloidal quantum dots (CQD) and the theoretical conversion efficiency is as high as 42 %. This progress is helpful to develop a new battery with the thickness of only one percent of the current commercial thin-film solar cells. At present, researchers have developed a thin-film battery with thickness of a few tenth of nanometer.

Recently, the Australian and Japanese scientists invented a solar cell which is thinner than a spider web. This ultrathin solar cell is composed of electrodes which are embedded in the plastic tab and the thickness is only 1.9 μ which is equivalent to one tenth of the current thinnest solar battery. The solar panel is modular and can be utilized on any scale to achieve the power desired. It can still generate some power when there is dense cloud in sky for the ability of converting emitted light. In addition, the panels require almost no maintenance and have a typical lifetime of about 20 years [22].

4 Mechanical Energy Harvesters

The mechanical energy is generated when an object is subjected to some movement or mechanical deformation and it can be converted into electrical energy by several methods including piezoelectric, electrostatic, and electromagnetic conversion (Table 2).

The vibration is the most prevalent energy source for it is available in many environments including buildings, roads, bridges, vehicles, ships, and other kinds of production and living facilities. And in the biomedical sciences, the mechanical energy harvesters can also be utilized to provide energy for biological sensors which are used to monitor real-time parameters like blood pressure, blood-sugar levels, and so on, of human or animals by taking advantage of body pulse and blood current.

4.1 Piezoelectric Energy Harvesters

With the improvement of piezoelectric materials, piezoelectric properties and the use of highly integrated low-power electronic devices, the piezoelectric harvesting technology (Fig. 5) has received extensive attention in recent years. And it is an inherent property of piezoelectric materials that generate electricity when pressure is applied. Piezoelectric transduction is generally well suited to the reciprocating nature of the motions instead of rotating systems.

Piezoelectric materials mainly include piezoelectric monocrystal, piezoelectric ceramics, piezoelectric polymers, and piezoelectric composites. At present,

Table 2 The energy harvesting method corresponding to different vibration sources

The form of vibration sources	Energy harvesting method
Force excitation	Piezoelectric energy harvesting method
Velocity excitation	Electromagnetic energy harvesting method
Displacement excitation	Piezoelectric electrostatic energy harvesting method

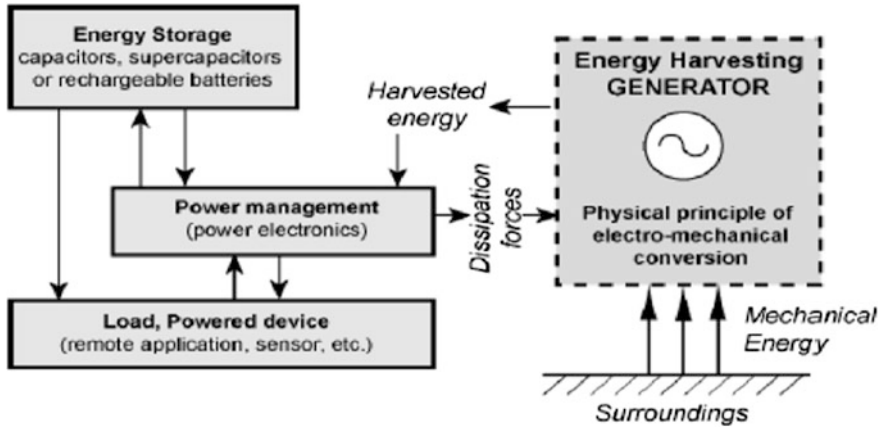


Fig. 5 Schematic of Piezoelectric energy harvesting system

piezoelectric ceramic (PZT) is the most commonly used piezoelectric material for the piezoceramics have the advantages of mature manufacturing process, low cost, large electromechanical coupling constants, and high energy conversion rate. But, piezoelectric ceramic PZT is fragile and unable to bear large strain, and it is easy to produce fatigue crack and brittle fracture on the impact of high-frequency cyclic load. Another commonly used piezoelectric material is polyvinylidene fluoride (PVDF). Compared to piezoelectric ceramic PZT, PVDF has smaller electromechanical coupling constants, but it has advantages of good flexibility, high mechanical strength, good fatigue resistance and chemical stability, and is suitable for the application under high-frequency periodic load.

4.2 Electrostatic (Capacitive) Energy Harvesting

Electrostatic harvesting is based on the principle of changing capacitance of vibration-dependent capacitors [27]. Vibrations split the plates of a charged variable capacitor, and mechanical energy is converted into the form of electrical energy. It harvesters require a polarization source to work and to change mechanical energy from vibrations into electricity. The polarization source should be in the order of some hundreds of volts; this greatly makes problem of the power management circuit. A further solution consists in using electrets, which are electrically charged dielectrics and are able to remain in polarization on the capacitor for years. It is possible to settle in structures from classical electrostatic induction generators, which also remove energy from variable capacitances, for this purpose. The resulting devices are self-biasing and can straightforwardly charge batteries, or can produce exponentially increasing voltages on storage capacitors, from which energy can be periodically pulled out by DC/DC converters.

Table 3 Performance parameters of typical magnetic materials

Material	B/mT	(BH) max/(kJ/m ³)	Hc	Tc/°C	Max. operating temperature/°C	Density/(kg/m ³)
Ceramics	100	26	High	460	250	4980
Alnico	130	42	Low	860	550	7200
SmCo (2:17)	350	208	High	750	300	8400
NdFeB (N38H)	450	306	High	320	120	7470

4.3 Electromagnetic Energy Harvesting

Electromagnetic energy harvesting is based on the well-known principle of electromagnetic induction which is defined as induced electromotive force which will be generated in a conductor when the magnetic flux is changing around it. The electromagnetic vibration energy harvesters listed in Table 3 can be simply packaged to reduce the risk of corrosion and eliminate the temperature limit.

5 Thermoelectric Generators

The temperature difference between the two ends of semiconductor PN junction is used to generate power by micro thermoelectric power generation system. Thermoelectric materials have three temperature-dependent properties: Seebeck coefficient, thermal conductivity, and electrical conductivity. There are many sources of waste heat which can be used around us such as geothermal, industrial waste heat, engine exhaust, and the heat of sun.

The conversion efficiency of current thermoelectric generators (TEGs) is commonly between 6 and 11 %. The efficiency of TEGs is approximately proportional to temperature difference when it is small while both thermoelectric materials and temperature difference have a strong influence on the output voltage, and the generated voltage is proportional to the number of thermoelectric elements and the temperature difference when the thermoelectric materials is selected. Because it is difficult to maintain a significant temperature gradient on a small device, the small available temperature difference between the surfaces of the TEG, commonly not higher than 10 °C, and the micro size of the devices make the output power and the conversion efficiency very limited.

6 Dynamic Fluid Energy Harvesting

Dynamic fluid energy includes wind and flowing water power. The kinetic energy of fluid can be harvested by two methods. The first one generates electricity by mechanical parts such as micro turbine systems.

The second one uses nonmechanical parts that work as the same as the mechanical energy harvesting technology for the flowing wind; or water induces mechanical vibration which can be converted to electricity by piezoelectric, electrostatic, or electromagnetic principles.

6.1 Micro Wind Harvester

The ambient air flow or forced convection can also be an energy source for wireless autonomous sensor nodes in outdoor, remote, or inaccessible locations. The existing methods of wind energy harvesting include micro wind turbines, micro windbelt generators, piezoelectric wind harvesters, and electromagnetic wind generators. In addition, the rotating components of conventional turbines, such as bearings, suffer from fatigue and wear.

6.2 Flowing Water Energy Harvesting

The flowing water contains kinetic energy due to the water pressure fluctuation, and it can be converted into electrical energy by energy harvesters (Fig. 6). Flowing water is a renewable, pollution-free, continuous, and dependable energy source for wireless sensor nodes. For hydropower can be developed in any size and any scale, it is applicable in WSNs [22].

Sun and Hu developed an electromagnetic vibratory generator based on impact of water current.

Pobering and Schwesinger presented two types of energy harvesters: a flag-shaped piezoelectric polymer harvester and a microstructured piezobimorph generator, to convert the kinetic energy of flowing water into electrical energy. While the flow-induced vibration energy harvester has a micro size, it needs further research to increase the conversion efficiency and optimize the generated power to be appropriate for powering wireless sensor nodes.

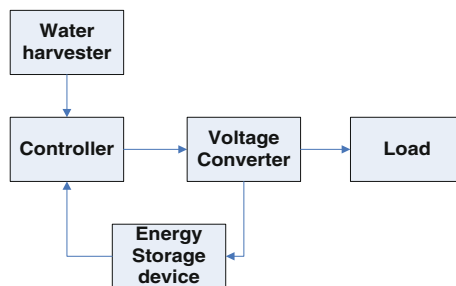


Fig. 6 The composition block diagram of flowing water energy harvesting system

7 The Acoustic Energy

The acoustic energy can be used by people like all other forms of energy. When sound wave spreads to the surface of an object, it will cause vibration of the object. It was measured that the generated power is up to 100 kW when the noise of jet is 160 dB.

The common elements of acoustic energy systems include an input mechanical power spectrum, an effective acoustic impedance matching, a piezoelectric or biased electrostrictive transducers converting the input mechanical energy into electrical energy and a matched electrical load.

8 Magnetic Energy Harvesting

Magnets vibrating on a cantilever are responsive to even small vibrations and generate micro currents by moving comparative to conductors due to Faraday's law of induction [27]. Sensors in inaccessible places can now produce their own power and transmit data to outside receivers. One of the major restrictions of the magnetic vibration energy harvester developed at University of Southampton is the size of the generator; in this case approximately one cubic centimeter, which is much too large to integrate into today's mobile technologies. The complete generator with circuitry is a massive 4 cm by 4 cm by 1 cm, nearly the similar size as some mobile devices such as the iPod nano. Additional drop in the dimensions are possible through the combination of fresh and additional stretchy materials as the cantilever beam component. In 2012, a group at Northwestern University developed a vibration-powered generator out of polymer in the form of a spring. This device was able to intention the equal frequencies as the University of Southampton groups silicon-based device, but with one-third the size of the beam component.

Business successful vibration energy harvesters have been developed from the early University of Southampton prototypes by Perpetuum. These have to be sufficiently large to generate the power required by wireless sensor nodes (WSN); but in M2M applications, this is not normally an issue. These harvesters are now being supplied in large volumes to power WSNs made by companies such as GE and Emerson and also for train bearing monitor systems made by Perpetuum. Overhead power line sensors can use magnetic induction to harvest energy straight from the conductor that they are monitoring.

9 Hybrid Power Source

In mainly the electrified transportation systems, where only batteries are operated as energy storage system, usually batteries are personalized for the power rather than energy. In recent technologies, it does not offer a battery proficient of high enough power densities without over-sizing it. Moreover, battery lifetime can reduce drastically if it is subjected to immediate charge/discharge pulses or fast variable currents. This results in increasing the size, cost, and size of the battery pack or decrease the battery life and thermal runaway troubles [28].

In order to offer more efficient propulsion, without sacrificing the performance, increasing the fuel consumption, and over-sizing the battery, more than one energy storage devices with balancing characteristics can be used in electric traction systems. In a hybrid ESS, proper power budgeting based on the specific characteristics of energy sources would result in higher efficiency, longer life time of energy sources, as well as reducing their size and cost. The energy sources should be able to store, supply, bring back high-power pulses and supply the fixed demands of the vehicle. A hybrid topology collected of a high power density component such as an ultra-capacitor (UC) and high energy density component such as a rechargeable battery offers a concession of both.

10 Conclusion

This paper gives a comprehensive introduction of the various possible environmental energy harvesting technologies and the selection of which should be suitable for the actual applications and working environments of WSNs. (1) As mentioned above, there are a lot of different forms of energy in the environment. (2) Up to now, there is a great distance between the existing energy harvesting technologies and the mass commercial production, as all kinds of environmental energy harvesting technologies are still not mature, and the output power and energy conversion efficiency are low. (3) The size of energy harvesting system should be reduced as much as possible for the strict requirements of sensor nodes in many applications.

Miniaturization is the development tendency of the future energy harvesting system. (4) It is essential to combine the structure design and key circuits with the scheduling and agreement based on power aware of wireless sensor nodes to prolong the sensor nodes life. (5) It is a necessity to integrate the energy harvesting method, power management strategy, battery recharging, and new communication standards.

References

1. Kumar KA. IMCC protocol in heterogeneous wireless sensor network for high quality data transmission in military applications. In: Proceedings of the 1st international conference on parallel, distributed and grid computing (PDGC '10). 2010. p. 339–43.
2. Jaigirdar FT, Islam MM, Huq SR. An efficient and cost effective maximum clique analysis based approximation in military application of wireless sensor network. In: Proceedings of the 14th international conference on computer and information technology (ICCIT '11). 2011. p. 85–90.
3. Padhy P, Martinez K, Riddoch A, Hart J, Ong H. Glacial environment monitoring using sensor networks. In: Proceedings of the conference on real-world wireless sensor networks. 2005.
4. Stankovic JA, Cao Q, Doan T et al. Wireless sensor networks for in-home healthcare: potential and challenges. In: Proceedings of the high confidence medical device software systems workshop. 2005.
5. Virone G, Wood A, Selavo L et al. An assisted living oriented information system based on a residential wireless sensor network. In: Proceedings of the 1st transdisciplinary conference on distributed diagnosis and home healthcare (D2H2 '0606). 2006. p. 95–100.
6. Placzek B. Selective data collection in vehicular networks for traffic control applications. *Trans Res Part C: Emerg Technol.* 2012;23:14–28.
7. Akhondi MR, Talevski A, Carlsen S, Petersen S. Applications of wireless sensor networks in the oil, gas and resources industries. In: Proceedings of the 24th IEEE international conference on advanced information networking and applications (AINA '10). 2010. p. 941–8.
8. Hubbell N, Han Q. DRAGON: detection and tracking of dynamic amorphous events in wireless sensor networks. *IEEE Trans Parallel Distrib Syst.* 2012;23(7):1193–204.
9. Elanchezian A, De Oliveira JC, Weber S. A new system for controlled testing of sensor network applications: architecture, prototype and experimental evaluation. *Ad Hoc Netw.* 2012;10(6):1101–14.
10. Yong Y-T, Chow C-O, Kanesan J, Ishii H. A survey on design of self-powered wireless sensor network. In: Proceedings of the international conference for technical postgraduates (TECHPOS '09). 2009. p. 1–5.
11. Nacef AB, Senouci S-M, Ghamri-Doudane Y, Beylot A-L. A cooperative low power Mac protocol for wireless sensor networks. In: Proceedings of the IEEE international conference on communications (ICC '11). 2011. p. 1–6.
12. Dash S, Swain AR, Ajay A. Reliable energy aware multi-token based MAC protocol for WSN. In: Proceedings of the 26th IEEE international conference on advanced information networking and applications (AINA '12). 2012. p. 144–51.
13. Mplemenos G-G, Papaefstathiou I. Fast and power-efficient hardware implementation of a routing scheme for WSNs. In: Proceedings of the IEEE wireless communications and networking conference (WCNC '12). 2012. p. 1710–4.
14. Tao L, Feng L. Power-efficient clustering routing protocol based on applications in wireless sensor network. In: Proceedings of the 5th international conference on wireless communications, networking and mobile computing (WiCOM '09). 2009. p. 1–6.
15. Bhuvanewari R, Bejoy BJ. Energy efficient reliable transport protocol for re-tasking in wireless sensor network. In: Proceedings of the national conference on innovations in emerging technology (NCOIET '11). 2011. p. 1–6.
16. Zhou H-Y, Wu F, Hou K-M. An event-driven multi-threading real-time operating system dedicated to wireless sensor networks. In: Proceedings of the international conference on embedded software and systems (ICCESS '08). 2008. p. 3–12.
17. Roundy S, Wright PK, Rabaey J. A study of low level vibrations as a power source for wireless sensor nodes. *Comput Commun.* 2003;26(11):1131–44.
18. Raghunathan V, Ganeriwal S, Srivastava M. Emerging techniques for long lived wireless sensor networks. *IEEE Commun Mag.* 2006;44(4):108–14.

19. Wu J, Zhou G. A new ultra-low power wireless sensor network with integrated energy harvesting, data sensing, and wireless communication. In: Proceedings of the IEEE international conference on communications (ICC '11). 2011. p. 1–5.
20. Alippi C, Galperti C. An adaptive system for optimal solar energy harvesting in wireless sensor network nodes. *IEEE Trans Circuits Syst I Regul Pap.* 2008;55(6):1742–50.
21. Gilbert JM, Balouchi F. Comparison of energy harvesting systems for wireless sensor networks. *Int J Autom Comput.* 2008;5(4):334–47.
22. Tabbakh SRK, Maarefdoust R, Kyun NC, Mohd Ali B. Environmental taxonomy of power scavenging techniques for autonomous self powered wireless sensors. In: Proceedings of the Asia pacific conference on circuit and system (APCCAS '10). 2010. p. 1031–4.
23. Vullers RJM, van Schaijk R, Doms I, Van Hoof C, Mertens R. Micropower energy harvesting. *Solid-State Electron.* 2009;53(7):684–93.
24. Roundy S, Steingart D, Frechette L, Wright P, Rabaey J. Power sources for wireless sensor networks, lecture notes in computer science. Springer; 2004
25. Gakkestad J, Hanssen L. Powering wireless sensor networks nodes in Northern Europe using solar cell panel for energy harvesting. In: Proceedings of the 4th IFIP international conference on new technologies, mobility and security (NTMS '11). 2011. p. 1–5.
26. Zhou G, Huang L, Li W, Zhu Z. Harvesting ambient environmental energy for wireless sensor networks: a survey. 2014.
27. https://en.wikipedia.org/wiki/Energy_harvesting.
28. <http://khaligh.umd.edu/hybrid-energy-storage-systems>.

Implementation of Z-Ternary Content-Addressable Memory Using FPGA

G.P. Mullai and C. Sheeba Joice

Abstract Ternary content-addressable memory (TCAM) is best known for its high speed lookup operation irrespective of its drawbacks like low density, slow access time, complex circuits, and high price. This paper proposes a contemporary memory design termed Z-TCAM, which imitates TCAM process in Static Random Access Memory (SRAM) and scales down the power dissipation. This improvement of the SRAM functionality includes supplement logic units, parity bit, and clock gating. Our approach is to check the most significant bit (MSB) of TCAM input by breaking the match lines into several segments using hybrid partition for search operation. The proffered architecture implements 32×16 Z-TCAM in ALTERA field-programmable gate array using QUARTUS II.

Keywords Memory architecture · Hybrid partitioning · Ternary content-addressable memory (TCAM) · Static random access memory (SRAM)

1 Introduction

The content-addressable memory (CAM) compares input search data against a table of stored data, and returns the address of the matching data. Content-addressable memory is a special type of computer memory used in certain high-speed searching applications. It is also known as associative memory, associative storage, or associative array, although the last term is more often used for a programming data structure. CAMs can be used in a wide variety of applications requiring high search speed due to its fast search capability. CAM has three operation modes: READ,

G.P. Mullai (✉) · C. Sheeba Joice
Department of Electronics and Communication Engineering,
Saveetha Engineering College, Chennai, India
e-mail: mullaipugal@gmail.com

C. Sheeba Joice
e-mail: sheebajoice@saveetha.ac.in

WRITE, and COMPARE/SEARCH. CAM is classified into two categories—binary CAM and ternary CAM. Binary CAM is used only for searching ones and zeros. It is suitable for applications that require only exact match searches. TCAM can search based on three inputs, ‘0’, ‘1’ and ‘X’ where X denotes don’t care condition or wildcard state. The state “X” also called mask can be used as a wildcard entry to perform pattern matching. To retrieve data on RAM, the operating system must provide the memory address where the data is stored. Data stored on CAM can be accessed by performing a query for the content itself, and the memory retrieves the addresses where that data can be found. RAM-based CAM uses the hash technique. It faced the problem of collisions and bucket overflow [1]. When the data contains wildcard bits in bit position, then such key is made replica into numerous buckets in turn raises capacity but the proposed design handles do not care efficiently. Due to its parallel nature, TCAM is much faster than SRAM. But expensive to build, consumes a lot of power, and generates a high level of heat that must be dissipated. TCAM is commonly found in networking systems such as high-performance routers and switches, to increase the speed of route lookup, packet classification, packet forwarding, access control list-based commands, real-time pattern matching, image processing, and virus-detection.

Field-programmable gate array (FPGA) has importance of reconfigure ability, massive hardware parallelism, and rapid prototyping capability. Since the conventional TCAM has no competency to be implementing on FPGA, the SRAM-based TCAM is flexible to implement on FPGA [2]. It can be used in many applications to achieve high speed and high throughput. Besides it has the trade-off between the value of vertical partition and the power consumption with latency. The hybrid partition SRAM-based TCAM has two SRAM access followed by logical AND operation has high energy/bit/search of 85.72FJ, because it includes the adder and counter for generating the original address [3]. In contrast, Z-TCAM reduces the power much better using clock gating. In designing the TCAM to perform search operation using match line, the critical issue is about stability with respect to noise parameter [4]. In contrast, Z-TCAM has good stability and better memory utilization.

The paper is organized as follows: Sect. 2 elaborates TCAM basics. Section 3 discusses about memory partitioning. Section 4 explains about general architecture of Z-TCAM. Section 5 involves improvising Z-TCAM operations. Section 6 provides the result and discussions of implementing Z-TCAM. Section 7 concludes the paper along with scope for future work.

2 TCAM Basics

Ternary content-addressable memory allows its memory to be searched by contents rather than by an address and a memory location. After the search operation, the matches are sent to the output in a constant time. TCAM is a specialized type of high speed memory that searches its whole contents in a single clock cycle.

The design of TCAM with low power and high speed uses various power reduction techniques that has the demerit of larger area [5]. The constant time search of TCAM makes it a suitable candidate in different applications such as network routers, data compression, real-time pattern matching in virus-detection, and image processing. The search algorithm is deterministic because of the time sensitivity of a route or forwarding lookup. It performs a wide search in TCAM memory in a very short fixed period of time, typically less than 20 ns [6]. Figure 1 shows the structure of TCAM array.

3 Existing Architecture of Z-Tcam

The global architecture is shown in Fig. 2. When the input search word of D bits is given, it is partitioned into N subword with each subword of z bits [7]. It consists of M layers and TCAM Priority encoder (TPE). Each layer gives potential match

Fig. 1 TCAM array

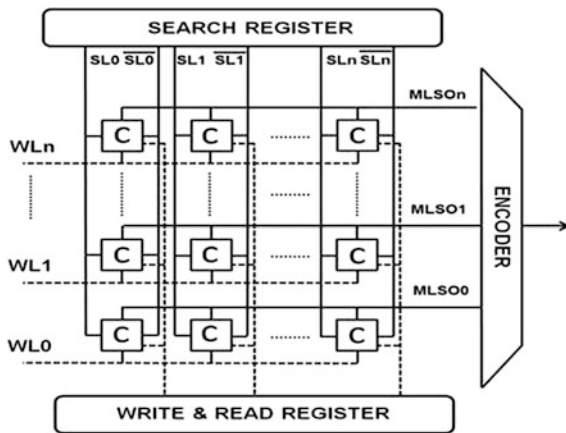


Fig. 2 Z-TCAM architecture

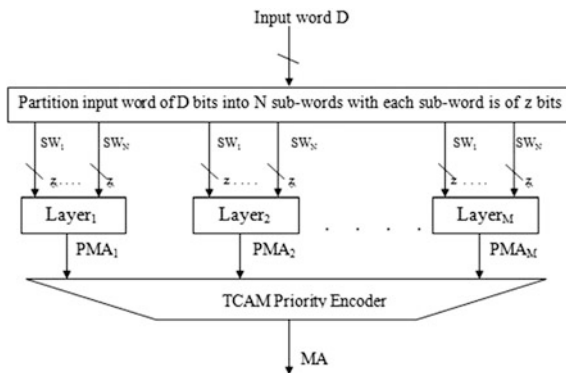
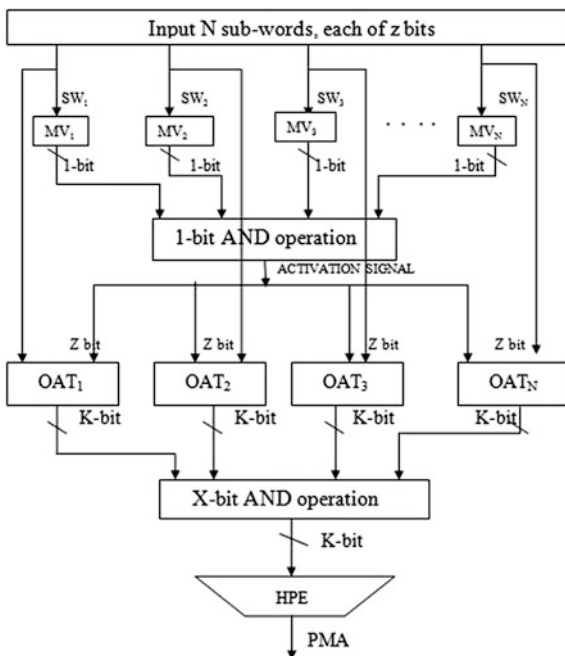


Fig. 3 Layer architecture of Z-TCAM



address as output and fed to TCPE, where the match address is selected among PMAs, assuming that it has the highest priority.

The layer architecture of Z-TCAM is shown in Fig. 3. Since the input word partitions into N subwords, then accommodation of data of N partitions requires N memory validation (MV) and N Original Address Table (OAT). For integrating the operations of TCAM, this architecture adopts 1-bit AND operation, X-bit AND operation, and horizontal priority encoder (HPE) [7].

3.1 Memory Validation

The size of each MV is $2^z \times 1$ bit, where z represents the number of bits present in each subword and 2^z shows number of rows in the memory validation. If the partitioned subword invokes the memory location, it is confirmed by corresponding VM. Further, it is used as address to OAT to read the corresponding row. This search performance is done by 1-bit AND operation. Here, the subword acts as an address to MV. If subword is present in memory location, it is justified as 1 otherwise 0. For example, consider 000, 010 are the subword fed to MV. If the subword is present, the memory location should be high and the remaining are set low. The size of MV for 3 bit is $2^3 \times 1$.

3.2 *1-Bit and Operation*

In this 1-bit AND operation, the output of all MVs undergoes AND operation. These results acts as an activation signal for further process. If the output is high, it permits the search operation else considered as mismatch in that corresponding layer.

3.3 *OAT*

The dimension of OAT are $2^z \times X$ where z represents number of bits in subword, 2^z is the number of rows and X represents number of bits in each row, where each bit represents original address. In OAT, the original address storage is considered and X is the subset of original address.

3.4 *X-Bit and Operation*

All OATs undergoes AND operation. The X -bit rows from all OATs are read by these subwords. After performing AND on them, the result is fed to HPE to select match address.

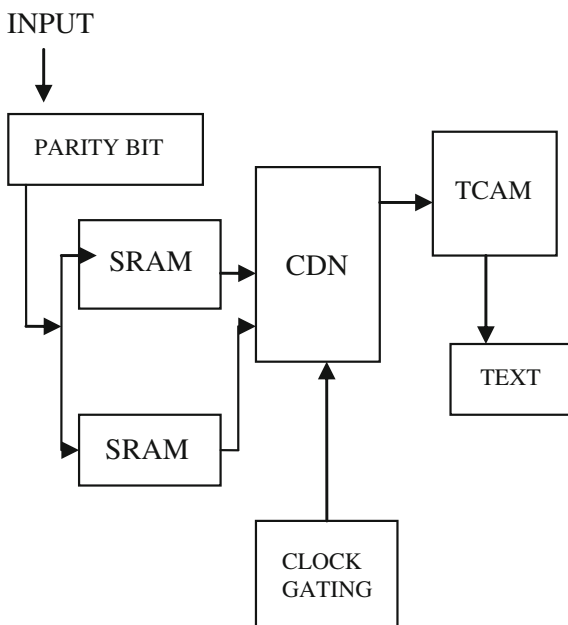
3.5 *Horizontal Priority Encoder*

The HPE selects potential match address (PMA) among the outputs of X -bit AND operation.

4 *Improvising Z-TCAM Operations*

Generally, the hybrid partitioning in a layer has its own MV and OAT which constitutes address. The input word is partitioned and validated in the memory block simultaneously. The original address is generated by which the partitions are mapped accordingly. In case of search operation, power reduction is mainly focused. When the input word is given, it undergoes partition by checking MSBs for parity in the lookup table. When address searches relevant content retrieved from the address is displayed in the ALTERA FPGA BOARD. Figure 4 shows the block diagram for the proposed method and explains the flow of algorithm followed. SRAM with TCAM along with few logic circuits form the Z-TCAM

Fig. 4 Block diagram of the proposed Z-TCAM



architecture. Clock distribution network (CDN) and clock gating kindly helps in reduction of power and delay in the design. The area is also noted using QUARTUS II 9.0 synthesis tool.

5 Clock Gating

Clock gating is a popular technique used in many synchronous circuits for reducing power dissipation. Clock gating saves power by adding more logic to a circuit to prune the clock tree and can be used to control power dissipated by clock net. The clock gating reduces the unwanted switching on the parts of the clock net by disabling the clock. RTL clock gating is the most common technique used for optimization and improving efficiency. Clock gating can save more power by not clocking the register if there is no change its state. The clock continuously consumes power. Because it toggles the registers and their associated logic the reduction of power consumption using clock gating shuts off the clock while system maintaining its current state. Based on checking the parity bit of the input word, it classifies the TCAM table by hybrid partition. For example, when the input word is of even parity, it concentrates only on even parity bits of data found in TCAM and matches their corresponding address. On the other hand, it cutoff the clock to the remaining data in the TCAM table using clock gating. It highlights on the reduction of power in the proffered design.

6 Results and Discussions

The SRAM-based TCAM memory architecture using hybrid partitioning is designed. Z-TCAM memory can be accessed in parallel to search for a given search word, providing the result as match address. The performance of Z-TCAM architecture is simulated using MODELSIM 6.4 simulator in Fig. 5. The input would be the data (say 00000101) it searches along the TCAM and gives the address as two.

Using Quartus II, synthesis is done and analyzed. The synthesis report gives the enhancement in parameter like power dissipation shown in Fig. 6.

The power dissipation is reduced when compared to the previous design and they are tabulated in Table 1.

The proposed hybrid partition scheme is used by validating operating segments of Z-TCAM, where the ideal portion should be short of to cut off region using clock gating. The maximum frequency is noted from the Fig. 7. Thus the speed is increased when compared to the previous design.

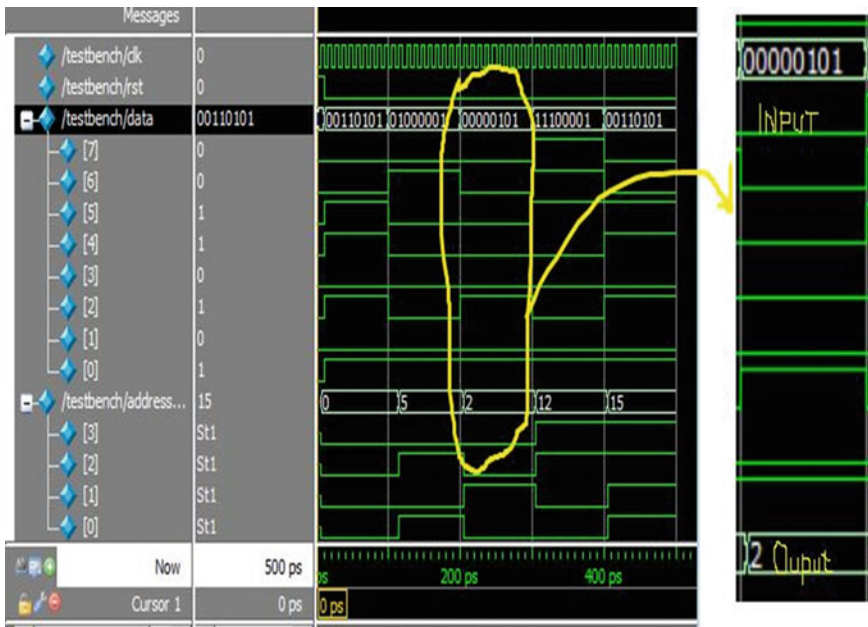


Fig. 5 MODELSIM output for Z-TCAM architecture

Fig. 6 Power output for Z-TCAM architecture

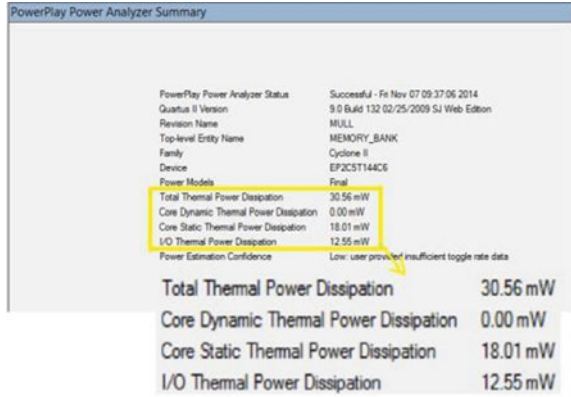
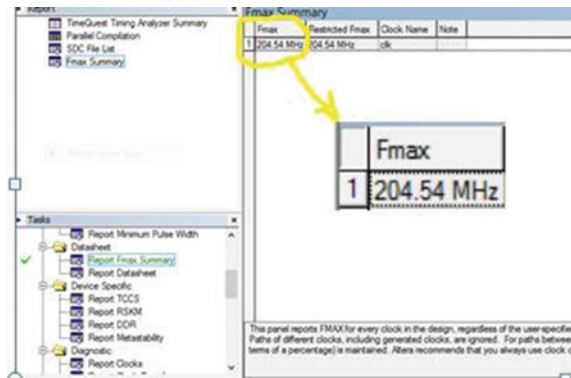


Table 1 Comparison of power and maximum frequency

Parameter	Power (mW)	Maximum frequency (MHz)
Existing method [7]	35.69	190
Proposed method	30.56	204.54

Fig. 7 Maximum frequency output for Z-TCAM



7 Conclusion

It is concluded that the Z-TCAM, an SRAM-based TCAM architecture, is designed with less power and high speed. The clock gating is used to reduce the static power consumption. The hybrid memory partition is used to divide the TCAM by checking the parity of bits. The Z-TCAM simulation is done using MODELSIM 6.4a. The future work will focus on the implementation of hardware using ALTERA field-programmable gate array.

References

1. Cho S, Martin J, Xu R, Hammoud M, Melhem R. CA-RAM: a high-performance memory substrate for search-intensive applications. In: IEEE International Symposium on Performance Analysis of System and Software, 2009, p. 230–41.
2. Ullah Z, Jaiswal MK, Chan YC, Cheung RCC. FPGA implementation of SRAM-based ternary content addressable memory. In: IEEE Conference on International Parallel and Distributed Processing Symposium, 2012, p. 383–9.
3. Ullah Z, Ilgon K, Baeg S. Hybrid partitioned SRAM-based ternary content addressable memory. *IEEE Trans Circuits Syst.* 2012;59(12):2969–79.
4. Kumar S, Noor A, Kaushik BK, Kumar B. Design of ternary content addressable memory (TCAM) with 180 nm. In: International Conference on Devices and Communication, 2011, p. 1–5.
5. Rajendra Naik B, Rao R, Shefali R. Low-area low-power and high-speed TCAMS. *Int J Comput Appl.* 2011:4–10.
6. NagaKarthik T, Ahn EH, Bae YS, Choi JR. TCAM based pattern matching technique for hand gesture recognition. *IEEE Trans Very Large Scale Integr (VLSI) Syst.* 2013;14(6):573–586.
7. Ullah Z, Jaiswal MK, Cheung RCC. Z-TCAM: an SRAM-based architecture for TCAM. In: *IEEE Transactions on Very Large Scale Integration (VLSI) Systems*, p. 1–5, 2014.

Design of Visual Aid for Blind People

Rajalakshmi Pushparaman

Abstract The proposed system is a design of visual aid for blind people. This design will help blind users to detect bank currencies and also aid them in reading printed words. It also helps them to identify human obstacles in front of them. For reading the printed texts, a combination of hierarchical optimization algorithm and pattern recognition in OCR is being used in our design. The characters from the text will be localized and isolated by pattern recognition. The resultant image of the character will be preprocessed using noise reduction filter. Text strings will be formed by grouping the identified characters from the characteristics extraction process. The output will be given as the speech for the corresponding text by converting the identified text to speech. Bank note identification is done by using the fast and efficient SIFT algorithm. It is precise and accurate. It will compare every input with the database templates and gives the highest match as output currency note for the blind user in their earphones. Obstacle identification is done using the Viola–Jones AdaBoost algorithm and using the same any obstacle can be detected and voice output is produced.

Keywords Haar feature · Obstacle identification · Pattern recognition · Jones adaboost algorithm

1 Introduction

A blind person always wants to be independent like all others. But, while reading texts they need to be dependent on others. Latest advancements in technology have made it possible to provide assistance to them by designing products that use computer vision and camera with optical character recognition (OCR) system. Reading has become an essential part in the modern world. Texts in printed form

Rajalakshmi Pushparaman (✉)
Department of Electronics and Communication, Velammal Institute of Technology,
Anna University, Chennai 600102, India
e-mail: rajalakshmi0126@gmail.com

are available in books, bills, checks, demand drafts, pamphlets, product labels, newspapers, etc. Different types of softwares such as screen reader and magnifiers are available to help blind people and people with poor eyesight to use a computer or other devices but there are less number of products that help them to read texts in the outside world. When blind people are assisted to read printed texts and products, it will improve their confidence and provide independency in this society. Recently, many devices have been developed to provide portability in text reading, but the process is a bit tedious and creates inconvenience for blind people. One such product is the barcode scanner. The basic concept behind this device is that the barcode for each product or object needs to be stored separately and all the data will be held in a database. Any time the user can scan the barcode and get the information about that object. This device has a disadvantage that blind users find it difficult to point the barcode in an object. Many softwares and mobile applications have been developed recently to give portability in reading for the blind people. "Be My Eyes" is a similar application which runs on iPhones and assists blind people by connecting them through video call to the volunteers. But it still makes them dependent on other people. All the above mentioned systems are trying to assist the blind people in reading texts, but reading texts is not the only problem faced by them in the outside world. Other major problems are recognizing the different denominations of currencies and identifying the obstacles in front of them. To detect obstacles, many devices have been developed; one such device is "The Ultra cane" for partially sighted and blind people. With this device, the users can detect the presence of an obstacle, but it is not possible to recognize the obstacle. For currency recognition, there are many systems available for office usage, but no such portable devices are available. It reduces the independency of the blind people to a greater extent. For example, while purchasing in the shops they have to depend on others to give the right amount of money and also it involves the liability of people. Some steps have been taken to resolve this issue, but it is not helping a great deal. Our prototype is mainly focused on addressing these issues for the blind people. To help blind people in reading printable text, we have connected a camera with our processing system, the camera will capture the readable texts and system will perform an OCR extraction process to extract the text information. For currency note recognition, we are using an efficient SIFT algorithm [1] to extract information and with that information we identify the correct denominations. To identify human obstacles robust face detection algorithm [2] is used and feature extraction algorithms are used to recognize other obstacles like cars, etc. After all the above process the extracted information is given to the text to speech engine and then given to the users through ear phone. With our prototype, we are trying to give them an artificial eye like camera through which they can read and identify objects and it helps them to live independently in this society like others.

2 Obstacle Identification

2.1 Human Detection Using Haar Classifier

Viola and Jones proposed the face detection algorithm. It is used as the basic concept for our system. Haar features present in a human face is used by this face detection algorithm. A face applicant is allowed to the next detection stage only when it has one of the Haar features in it. A face applicant is an original image's rectangular section called a sub-window. Usually, the sub-windows have a fixed size of 24×24 pixels. To get faces of different sizes, the sub-window is scaled often. The entire image will be scanned using this sub-window and it marks each corresponding section of a face applicant.

An integral image is used by the face detection algorithm and Haar features of a face applicant are processed using that image in constant time. The non-face applicants are eliminated by using a cascade of stages. Every stage has many different Haar features. Haar feature classifier is used to classify each feature. The output generated by Haar feature classifiers is provided to the stage comparator where it adds the Haar feature classifier's outputs and the value is compared with a stage threshold to determine whether it will pass the stage. A face applicant is concluded to be a face only if it passes all stages. Let us see the process details in the following sections.

2.2 Integral Image

The sum of the pixels of the original image is defined as the integral image. The value present at any place (x, y) of the integral image is the addition of the pixels of image to up and left side to (x, y) . Figure 1 illustrate the generation of integral image. Integral image is an intermediate representation of an image and it is used to calculate the simple rectangular features. The integral image is a group of sums of pixels; so, if $A(x, y)$ —original image and $AI[x, y]$ —integral image, then the integral image is calculated as shown below

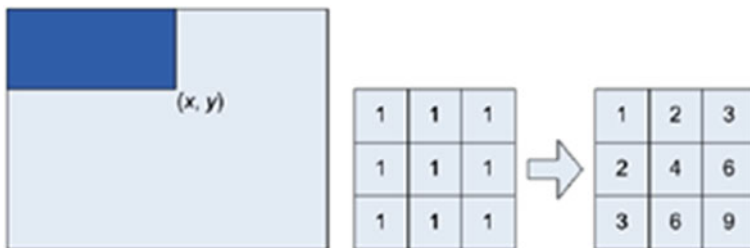


Fig. 1 Integral image generation

$$AI[x, y] = \sum_{x' \leq x, y' \leq y} A(x', y'). \quad (1)$$

The 45° rotation is given to the features and represented as an intermediate called [Rotated Sum] Auxiliary image. It is determined by the addition of the pixel (intensity) values that are presented at a 45° angle to left side and up (above) for x and down (below) for y . If $A[x, y]$ —original image and $AR[x, y]$ —rotated integral image, then the Integral image can be easily calculated. Two passes are absolutely necessary to determine both integral image arrays and one is needed for each group. Any scale feature can be determined by using the proper integral image and calculating the difference between six and eight group elements by forming two or three rectangles connected with each other. And thus, a feature is fast and efficient. The same is shown in the below equation.

$$AR[x, y] = \sum_{x' \leq x, x' \leq x - |y - y'|} A(x', y'). \quad (2)$$

It also means that finding the features of images of various sizes needs the same work as that of finding the feature for two or three pixels.

2.3 Haar Features

Haar features are made of two or three rectangles. Face applicants will be looked for Haar features of the stage where it is currently present. AdaBoost machine learning algorithm is used to generate the features and its weight and size because it generates a constant weight. Haar feature's value is calculated by using the area of rectangle, multiplying each with their weights, and then adding up the results obtained. Each rectangle's area is calculated by using its integral image. Any rectangle's corner coordinates can be used to find addition of all pixels above and to the left of that place using integral image. There are several forms of features available, as we see Fig. 2. By having the rectangle's corner, the area will be calculated as shown below. L must be added back to get correct rectangle's area, since it is subtracted for two times. The R rectangle's area, called as the rectangle integral, will be calculated as shown using the places of the integral image $L_4 - L_3 - L_2 + L_1$.

The shaded region shows the pixels addition value till place (X, Y) of image. It exhibits a 3×3 image along with its integral image representation.

2.4 Haar Feature Classifier

The rectangular integral is used by the haar classifier to find the value of a feature. The weight of each rectangle is multiplied with its area by the Haar feature classifier



Fig. 2 Calculating the rectangular area

and results are added together. Various Haar feature classifiers form a stage. All the Haar classifier results are summed by the stage comparator in a stage and this summation is compared with a stage threshold. AdaBoost algorithm will produce the threshold as a constant value and every stage will not have a set of Haar features number. Based on the training parameter data, individual stages will have variations in the Haar feature number. Viola and Jones' data set used two features in the first stage and ten in the second. Totally, there will be 6060 features for 38 stages.

2.5 Cascade

The face detection algorithm rejects face applicants using a cascade of stages. The cascade rejects applicant by making stringent requirements in each and every stage and also later stages are made more difficult for an applicant to pass that stage. Applicants exit the cascade if only they pass all stages or if they fail anyone stage. The detection of face occurs if an applicant passes all stages without any problems. This process is shown in Fig. 3.

3 Text Reading

For reading text, the video is captured from the camera fitted on the glasses of a user using Matlab. The frames are segregated and preprocessing is done. To identify texts, the captured image is binarized after the grayscale conversion. Now, the novel

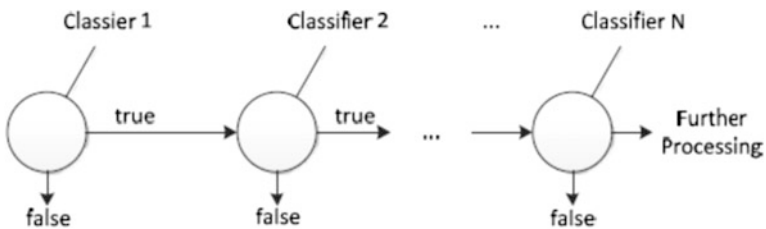


Fig. 3 Cascading of stages

hierarchical optimization method is applied along with OCR to extract the texts and then the output is given to the speech engine to generate audio output.

3.1 Hierarchical Optimization Algorithm

The normal OCR [3] will not be sufficient to detect or read text with its robustness and in its distorted form. As already explained in our previous paper [4], we are using the character recognition [pattern] and hierarchical optimization [5] to read texts in printed forms. Our Paper deals mostly with the blind persons, so the accuracy and speed are the two most important factors that should be satisfied. After considering all the requirements, it has become clear that our algorithm will suit best for our needs. The result will be obtained by comparing the given image with database patterns based on the difference (minimum) in the patterns. There is a possibility that during comparison, one of the patterns may be disturbed so the time taken to recognize depends on the amount of disturbance on the patterns. The direct pattern matching becomes obsolete when there is noise or distortions in the images. The above problems can be solved by disturbing the templates during matching and also altering the filters (Preprocess) again and again based on the last obtained results. In order to improve the searching speed during matching, we are using probability image matching. As cited in our previous paper [4] and also mentioned in [5], the algorithm will be applied.

The above mentioned algorithm will provide the best match of the quality function. The speed will be increased rapidly and search area will be reduced at the same time because of this algorithm. As already mentioned, we are going to use Powel's method (Multidimensional Optimization) in this paper also. The values that needs to be changed without dependency are tabulated below

Translations/rotations type	Points or axes
Along the axes (T)	X and Y
In the direction (T)	(X, Y)
Around the axes (R)	X and Y
Around the axis (R)	Z
Along the Z -axis (T)	Z

Based on our algorithm, the quality criterion will define the next iterations and it is shown below

$$QC_1 = \sum_{i=0}^N d_i^k. \quad (3)$$

$$QC_2 = \frac{N_e}{N_t} \cdot \frac{N_e}{N_c} \quad (4)$$

N stands for template point amounts, d_i stands for distance from i th point (template) to the nearest point of the character (recognized), k can have the value as $\frac{1}{2}$, 1, or 2. N_e stands for template point amounts coincident to the points of the character (recognized), N_t stands for the template points (Total amount), N_c stands for points amount of the image area which is covered by the template applied. Figure 4 displays the recognition algorithm (pattern) that uses matching (probabilistic). Hierarchical iterative algorithm will be used to solve the image distortion problem.

The settings change for the filter can be stopped after the required accuracy is achieved. The part of the image which is recognized is given to character recognition for further processing. The text (recognized) from OCR will be sent to the text file and it will be given as input to the speech software. Speech software transfers the text from the file and stores it in an array and then based on the comparison between it and the library files, the audio will be generated and given to the user.

4 Currency Note Detection

Currency note detection is done through SIFT [1] algorithm. SIFT (Scale-Invariant Feature Detection) is a keypoint feature descriptor which helps us to identify different types of currencies from the given image by matching its keypoint features. This descriptor is robust, distinctive, and also performs efficient feature matching. Precision and accuracy make this superior to similar descriptors. We extract the features from the image with distinctive properties which is best suited for image matching process. These features will not vary with respect to scaling or image rotation and illumination too does not show much variation. These points are not disrupted by closure, scramble, or noises because these are situated properly in frequency and spatial regions. By applying a cascade filter, complex calculations have been reduced and it reduces the time required for extraction.

4.1 SIFT Algorithm

These steps are followed in SIFT for extracting keypoints from the image.

4.1.1 Scale-Space Extrema Detection

Scale Spaces are created by removing the unnecessary details from an image. While removing those details, the false details should not be added to the image. This

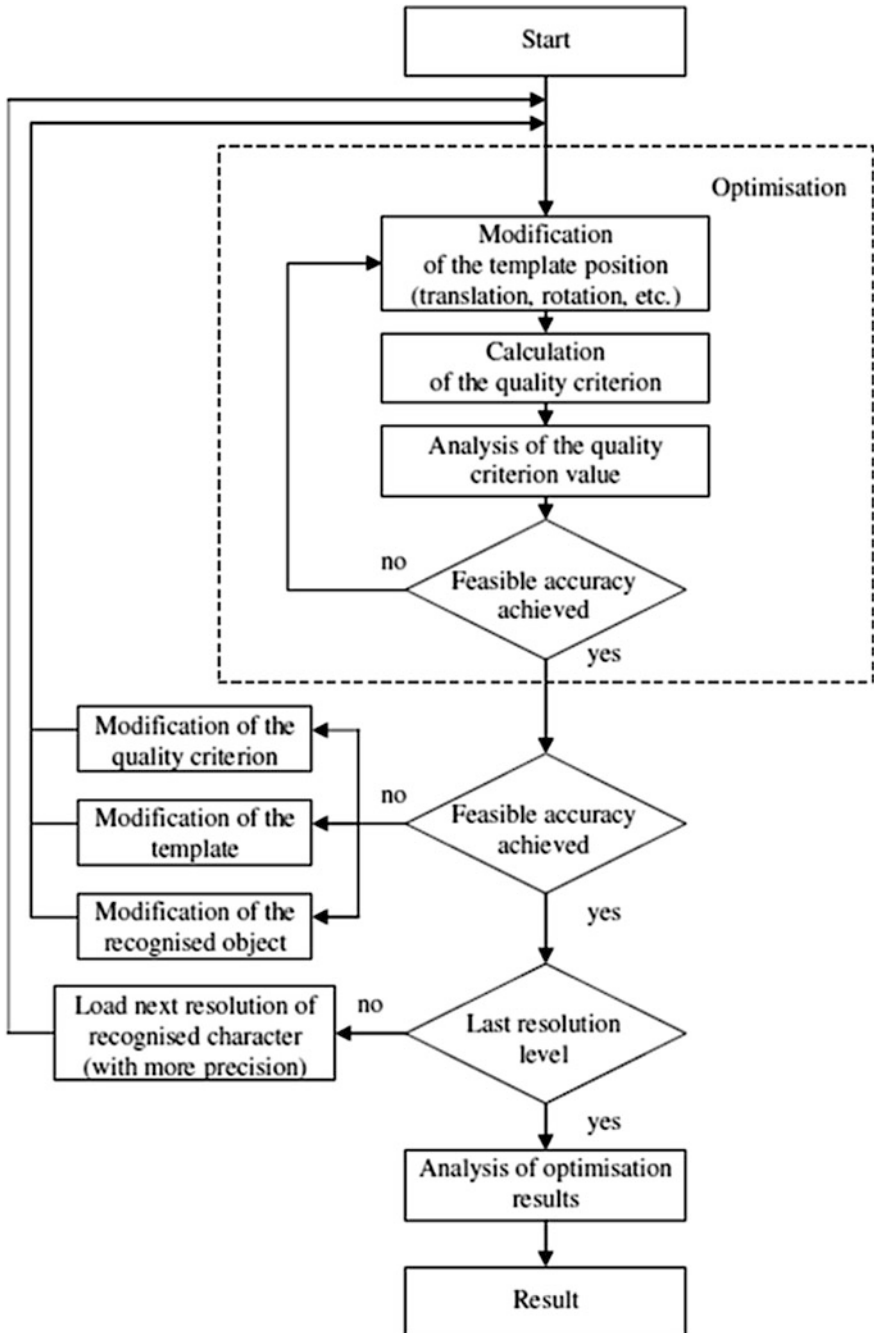


Fig. 4 Quality criterion

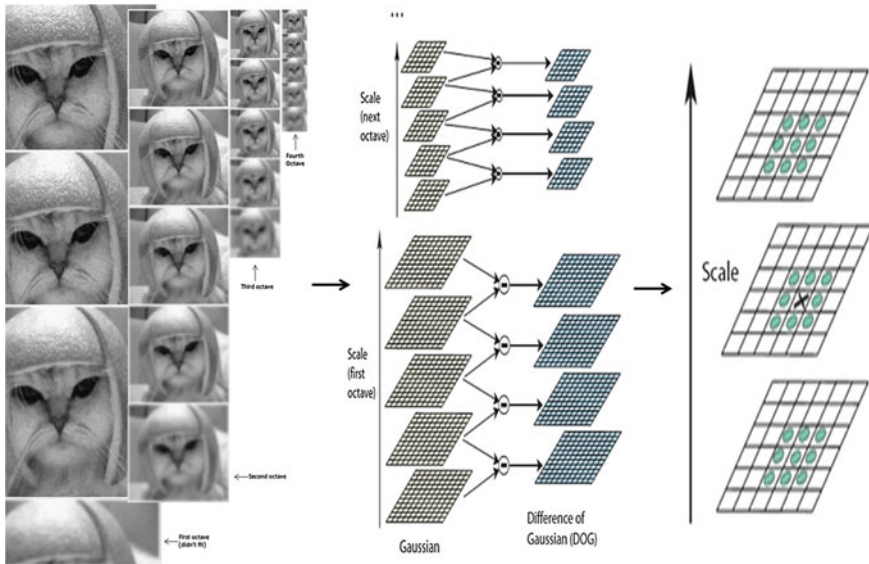


Fig. 5 Scale-space extrema detection

process is efficiently done by using Gaussian Blur. In SIFT, the scale spaces are produced by applying Gaussian blur continuously and for the next stage, the image size is reduced to half its original value and blurring is applied again. This process will be continued till acquiring the required scale spaces. Based on mathematics, “Blurring” is the convolution of the Gaussian expression and given image. Gaussian blur has an expression that is applied to each pixel and it results in image blurring.

$$L(x, y, \sigma) = G(x, y, \sigma) * I(x, y). \tag{5}$$

$$G(x, y, \sigma) = \frac{1}{2\pi\sigma^2} e^{-(x^2+y^2)/2\sigma^2}. \tag{6}$$

L—Output image (Blurred), *G*—Gaussian operator, *I*—Input image, *x*- , *y*-coordinates of the location, *σ* parameter (Scale). Amount of Blurring is based on this value, *-convolution operation to apply Gaussian blurs *G* to *I*. The above is the Original Gaussian Blur Expression. For a LOG operation, an image is taken and added with a small amount of blur and then the second order derivative is calculated for it. This will find edges and corners because these are good for locating key-points. The above mentioned derivative calculations are very complex and involves lot of computational time, so a different approach is used. To produce LOG, the Gaussian Difference method is used. It is calculated by subtracting two immediate Gaussian scales as shown in Fig. 5.

The Difference of Gaussian (DOG) is equal to the Laplacian of Gaussian, approximately. Another advantage of using DOG is that it is scale invariant. But LOG depends on the scale because of the σ^2 in the Gaussian expression. This will be eliminated by multiplying the result with σ^2 . While doing subtraction this value is automatically multiplied so it further reduces the computation time and produce scale invariance. To find the maxima and minima, iteration is done for every pixel and all its nearby pixels are checked.

4.1.2 Keypoint Localization

After finding the approximate maxima and minima, the exact keypoints will be localized. Mark the points as shown in Fig. 6, in that we need to find the green region, i.e., the exact location of extreme keypoints. From the acquired data, sub-pixel values can be found using the Taylor's formula for expansion near the approximate point. The formula is given below

$$D(x) = D + \frac{\partial d^T}{\partial t} x + \frac{1}{2} x^T \frac{\partial^2 D}{\partial x^2} x. \quad (7)$$

The extrema's can be found from the above formula by differentiating and equating it to zero. While doing so, it will improve the stableness and matching property of the algorithm. It is recommended to generate two maxima/minima images, so it requires totally four differences in Gaussian images. In order to obtain the required DOG's, totally five Gaussian images are needed. This is the reason for having five levels in every octave. Large numbers of keypoints are found from the last few steps. Some of the key points are on the edge or will have low contrast, either way they are useless features. In order to eliminate, we use two filters. One is to find low-contrast features and the other one is to find the edges. For the first filter, Taylor's formula is again used to find the intensity at key point areas, if the identified magnitude is less than the fixed value, than the key point will be eliminated. For edge detection, two perpendicular gradients are needed from the keypoint. If both gradients are large, then it is a corner and it will be accepted as a keypoint, otherwise it will be eliminated. But, in our algorithm only the ratios are calculated and thus it will increase efficiency and reduce calculation time.

4.1.3 Orientation Assignment

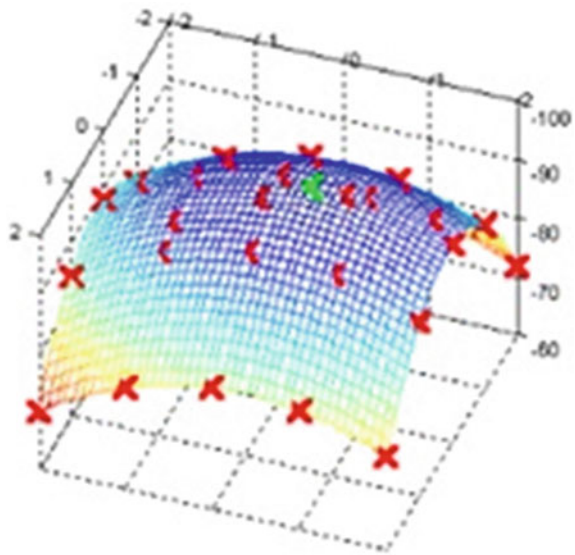
In this step, orientation is assigned to the keypoints that passed the above two filters. After the previous steps, we have stable and scale-invariant keypoints. For efficient feature matching, we need the points to show rotational invariance. This can be obtained by assigning orientation to the keypoints.

$$m(x, y) = \sqrt{(L(x + 1, y) - L(x - 1, y))^2 + L(x, y + 1) - L(x, y - 1))^2} \tag{8}$$

$$\theta(x, y) = \tan^{-1}((L(x, y + 1) - L(x, y - 1)) / (L(x + 1, y) - L(x - 1, y))).$$

where, $m(x, y)$ —Gradient magnitude, $\theta(x, y)$ —Gradient orientation. For every pixel near the keypoint, both the above gradients are calculated and a histogram is drawn for the obtained values. In the created histogram, the 360° is divided into 36 sections totally with 10° each. Certain regions of the gradients are marked as Orientation Reception Area. The pixel value that goes into each section of histogram is based on its gradient direction. For example, if it is 15.789 , then it will be put in between 10° and 19° section. The value that is added is based on its proportionality to the gradient magnitude of that point. The peak of the histogram will be at some point after plotting all the pixels around the keypoint. If the peak is between 20° and 29° , the keypoint will be assigned to orientation three, i.e., the third section. If any of the peaks are over 80 %, then it will be changed into a new keypoint with the same location as that of the original keypoint but with orientation equal to the peak. The key concept is that the images are blurred at $1.5 \cdot \sigma$, so that the size of the window kernel should be equal to the same.

Fig. 6 Keypoint localization



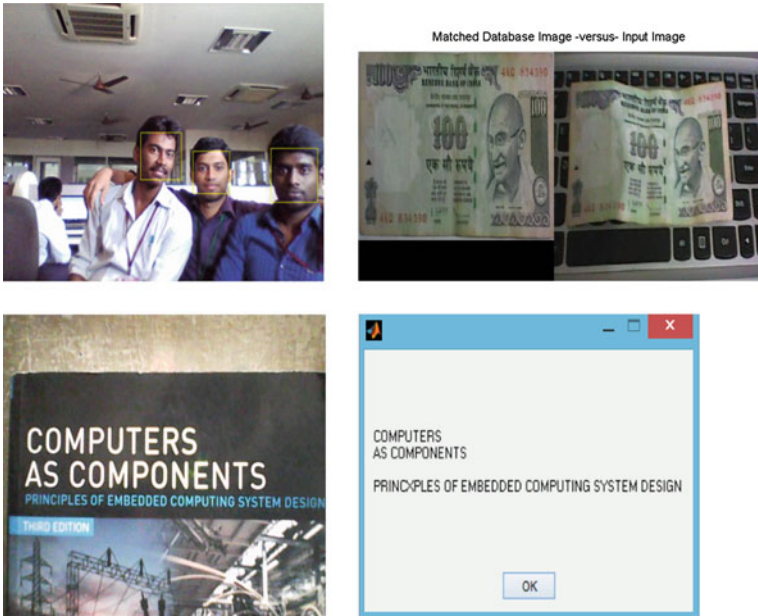
4.1.4 Keypoint Descriptor

Keypoint descriptor will describe the unique and highly distinctive fingerprint for every keypoint. In this last step, we will develop fingerprint for the keypoints obtained till this step which is invariant to scale and rotational aspects. To generate a unique fingerprint, a window of size 16×16 is taken around the keypoint. Then it will be broken into small windows of size 4×4 . In those windows, gradient magnitudes and orientations are calculated and put in an eight section histogram. Any orientation between 0 and 44 is added to the first section. Orientation between 45 and 89 is added to second section and it goes on till last section. Dissimilar to the previous step, here the amount of orientation added also depends on the distance from the keypoint. The whole process is carried out through the weighting function in Gaussian. Its main function is to create a 2D bell curve like gradient and it will be multiplied with magnitude orientations to get a weighted image. When the keypoint is at large distance, then its magnitude will be small. The same process is continued for the whole 16 pixels and we have fitted 16 completely random orientations into eighth predetermined sections. If the same process is done for all sixteen region, we will end up with $4 \times 4 \times 8 = 128$ Nos. After normalization by dividing with sum of squares, we will get the required feature vectors to uniquely identify a keypoint. Before finalization of features, two introduced problems need to be addressed. Rotational dependence is adjusted by subtraction of keypoint rotation with each orientations and lighting dependency is adjusted by keeping large thresholds before normalizations. Thus, we achieved an illumination and rotationally independent feature vector for matching. The same process is done for both templates and input images, then both the keypoints are compared to recognize the correct denomination of the input currency note.

5 Conclusion

In this paper, we have designed a prototype to support blind people in their day to day activities. The proposed prototype reads out the printable text from handheld objects to them and also helps them to identify currency notes and obstacles with ease. Here, we have confined our prototype to identify only Indian currencies and human obstacles but in future this can also be extended to read currencies of other countries also.

6 Results



References

1. David G. Lowe.: distinctive image features from scale-invariant keypoints. Int J Comput Vision. 2004;60(2):91–110.
2. Viola P, Jones MJ. Robust real-time face detection. Int J Comput Vision. 2004;57(2):137–54.
3. Tiwari S, Mishra S, Bhatia P, Km. Yadav P. Optical character recognition using MATLAB. Int J Adv Res Electron Comm Engg. 2013;2(5):579–582.
4. Rajalakshmi P, Deepanraj S, Arun Prasath M, Dinesh Kumar S. Portable camera based visual assistance for blind people. ARPN J Engg Appl Sci 2015;10:7.
5. Safronov K, Tchouchenkov I, Wörn H. Optical character recognition using optimisation algorithms. Proc. 9th Int. Workshop Comput Sci Inf Technol (CSIT'2007). 2007;1:85–89.
6. Chen X, Yuille AL. Detecting and reading text in natural scenes. Proc Comput Vision Pattern Recognit. 2004;2:366–373.

Implementing Fusion to Improve the Efficiency of Information Retrieval Using Clustering and Map Reduction

B. Gomathi and P. Sakthivel

Abstract Fusion is the concept of combining data from more than one source. Data fusion is the process of integrating multiple sources of information such that their combination yields better results than if the data sources are used individually. Retrieving the efficient and effective data from World Wide Web is very difficult because day by day the amount of data increases at a very high speed. The focus of this paper is to implement fusion of text snippets, page count, semantic similarity, k -means clustering, and map reduction to improve the efficiency of the search result. The advantage of this approach is that it provides an easy integration of web contents and data sharing.

Keywords Data fusion · k -means · Map reduction · Semantic similarity-based meta search engine · Text snippets

1 Introduction

As the World Wide Web is huge, the dependency on the existing search engines Google, Yahoo, etc. has increased tremendously. Web mining involves sequence of activities like discovering, clustering of documents, and extracting information from web documents and services. Effective retrieval and management of web information is a challenging issue.

One solution to the above problem is to narrow down the interested information space by identifying the similarities between the searched pages and developing a new information space. An alternate solution is to cluster the relevant web pages. Web page clustering uses the traditional database management approaches to create

B. Gomathi (✉)

Research & Development Centre, Bharathiar University, Coimbatore, Tamil Nadu, India
e-mail: gomathiphd2k15@gmail.com

P. Sakthivel

Department of Electronics and Communication Engineering, Anna Univeristy, Chennai, India

© Springer India 2016

S.S. Dash et al. (eds.), *Artificial Intelligence and Evolutionary Computations in Engineering Systems*, Advances in Intelligent Systems and Computing 394, DOI 10.1007/978-81-322-2656-7_79

879

index on the pages and achieves effective information storage, classification, integration, navigation, and retrieval.

In this paper, an approach for effective integration and retrieval of information from these web pages has been proposed. This approach uses SVM [1] to identify the similarities between the documents and k -means clustering is applied to cluster the relevant document. Then, map reduction is applied to k -means because now-a-days data is available in unprecedented volumes.

The rest of the paper is organized as follows: Sect. 2 presents related work, in Sect. 3 we propose the methodology for effective integration and retrieval of information from the web pages, Sect. 4 presents the results, and finally Sect. 5 concludes the paper.

2 Related Work

Data fusion is a combination more than one technique in order to prove that combination will yield better result than used as a single source. Combination of link analysis algorithm and information retrieval along with web mining algorithm improved the efficiency, thus proving that data fusion yields better results [2]. Page count fused with text snippets yielded better similarity result using support vector machine data mining technique [1, 3]. Clusters work better on frequent item sets rather than frequent concepts and this approach utilizes semantic relationship [4]. Fahim et al. [5], proved that k -means works better with dataset consisting of large number of clusters. Map reduction technique when applied to large clusters proved to be efficient [6]. The author Shihab Rahman [7] proposed a methodology for measuring the likeness among the pages.

3 Proposed Methodology

The proposed model fuses the contents from multiple sources and the contents are categorized based on their relevance to enhance the efficiency of the retrieval process. In this paper, lexical patterns are extracted from text snippets and word cooccurrence measures are defined using page counts. This similarity is based on the relationship that exists between the words queried.

Our Fusion Model follows the below steps

- Step 1: To calculate similarity between two words, say A and B.
- Step 2: Use SVM data mining technique to compute similarity.
- Step 3: Apply clustering to pattern.
- Step 4: Use k -means algorithm to clusters.
- Step 5: Implement map reduction to k -means to improve the efficiency.

3.1 Similarity Computation

The process of similarity estimation aims at describing whether two terms belong to the same category. There are several similarity measures like Cosine Similarity, Jaccard, Dice, etc. SVM (Support Vector Machine) is a data mining technique used to optimize the results.

Generally, similarity is the degree of similarity between two terms; if the value returned is 0.0 it means no similarity and if the value returned is 1.0 it means absolute similarity. For example, consider the word “crane” the results returned by Google search Engine.

In the below Fig. 1, the word “crane” returns two meanings: one is the machine and other is bird. So, in the proposed method, we use page count and text snippets returned by search engine, preferably Google search engine (Fig. 2).

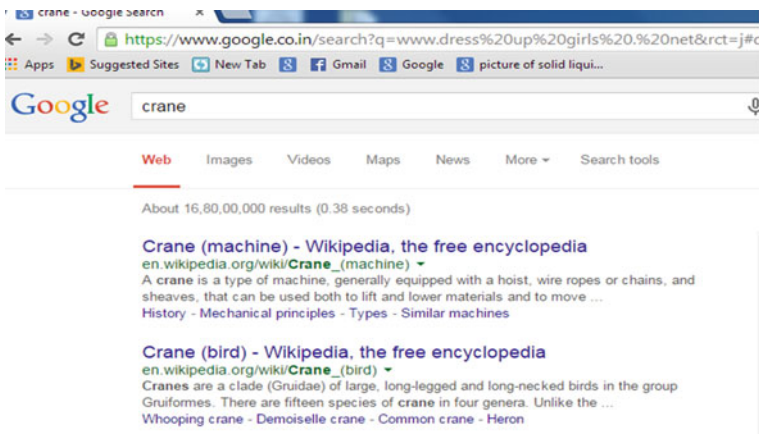


Fig. 1 Search results

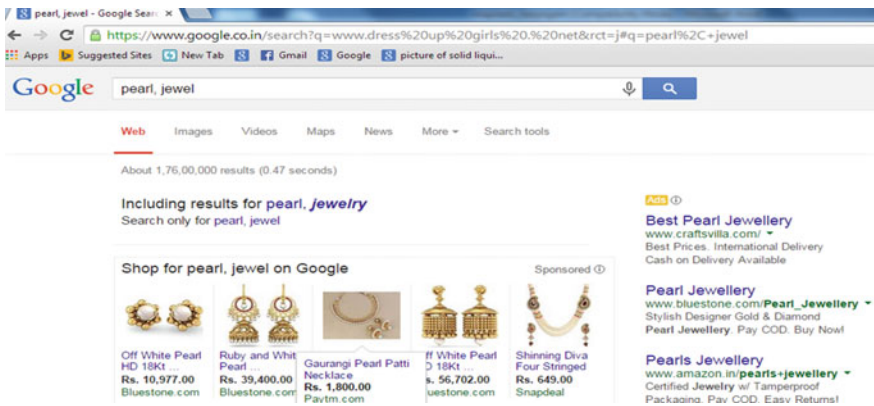


Fig. 2 Search results for words pearl, jewel

The results based on text snippets and page count given to SVM [1]. The inputs of SVM are pattern clusters and cooccurrence measure, and SVM is trained to find accurate similarity between the words.

3.2 *MapReduce*

In general, MapReduce is a framework which can be used for processing and generating large data sets. In the proposed paper, k -means is enhanced with MapReduce which in turn helps to eliminate iteration dependency. MapReduce can be applied to clusters. Here, in Map, we divide the problem into sub problems. Processing of the sub problem is done here. These results are passed to Reduce, where the evaluation of all sub problems are collected and combined which in turn gives the solution for the original problem.

3.3 *k-Means Enhanced with MapReduce*

- Step 1: The number of clusters ' k ' is initially selected.
 Step 2: Random generation of k -clusters are done to determine cluster centre.
 Step 3: Determine the distance measure

$$d(a_i, b_j) = \frac{X - m}{X}$$

where, ' X ' is the total number of words retrieved and ' m ' is the number of matches.

- Step 4: Use Map function for a finite domain set X , Weight function is

$$w : X \rightarrow R^+$$

which defines weight of every element.

- Step 5: Let $(w[x], d)$ denote weighted data.
 Step 6: Map input $[w[x], d \cdot k)$ and the output is k -partition(k -clustering) of X
 Step 7: For a finite domain set X , a distance function

$$d : X \times X \rightarrow R^+ \cup \{0\}$$

- Step 8: Calculate inter cluster distance with respect to time.
 For one cluster

$$D_r = \sum_i \sum_j \|x_i - x_j\|^2$$

for k cluster

$$W_k = \sum_{r=1}^k \frac{1}{2n_r} D_r$$

Step 9: Collect all the centre points and merge them.

Step 10: Repeat the Steps 3–8 till all the clusters are evaluated.

4 Experimental Results

Experiments were conducted using multiple words and the results are evaluated based on the relationship that exists between the words. The semantic similarity that exists between the words is shown in the below Fig. 3.

The below Fig. 4 illustrates that k -means is enhanced with MapReduce. Figure 4 shows precision and recall value of the proposed approach. The graph clearly depicts that iteration of k -means algorithm was the important factor which affected

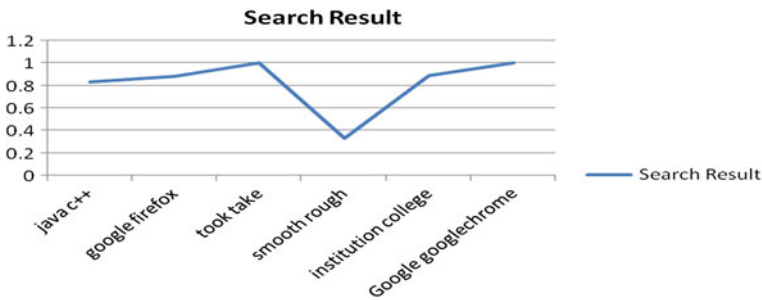
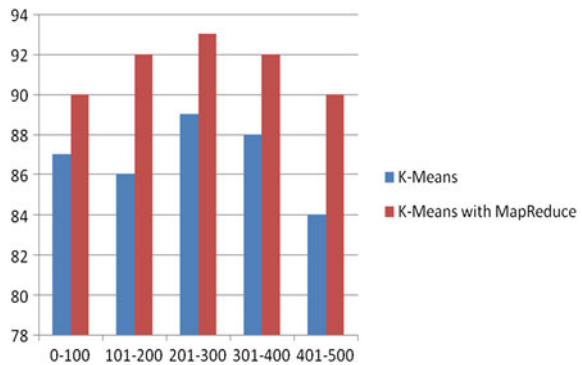


Fig. 3 Semantic similarity

Fig. 4 Precision and recall for the proposed approach



the performance of clustering. Experimental results on large real-world datasets demonstrate that the proposed k -means enhanced with MapReduce algorithm is efficient and performs better compared to the existing algorithms.

5 Conclusion

This paper applied the concept of fusion using text snippets, page count, and implemented MapReduce to k -means. The proposed approach, k -means enhanced with MapReduce, showed that efficiency would be around 91 % when compared to k -means whose efficiency comes around 88 %. In this paper, an approach for the effective integration and retrieval of information from web pages has been presented. This approach uses SVM data mining technique to measure the closeness between the terms. This is evaluated using the metrics precision and recall, and it shows that k -means enhanced with MapReduce and retrieval based on words with relations produces better results than the existing approach. The advantage of proposed approach is that it provides an easy integration of web contents and data sharing.

References

1. Manasa Ch, et al. Measuring semantic similarity between words using page counts and snippets. *Int J Comput Sci Commun Netw.* 2012;2(4):553–8.
2. Dit B, Revelle M, Poshyvanyk D. Integrating information retrieval, execution and link analysis algorithms to improve feature location in software. *Empirical Softw Eng.* 2013;18:227–309.
3. Bollegala D. A web search engine-based approach to measure semantic similarity between words; 2011, p. 977–90.
4. Baghel R Text document clustering based on frequent concepts. In: *International Conference on Grid computing*, 2010, p. 366–71.
5. Fahim AM, Salem AM, Torkey FA, Ramadan MA. An efficient enhanced k -means clustering algorithm. *J Zhejiang Univ Sci.* 2006;7(10):1626–33.
6. Dean Jeffrey, Ghemawat Sanjay. MapReduce: simplified data processing on large clusters. *Commun ACM.* 2008;51(1):107–13.
7. Rahman S, Chapa D, Kabir S. A new weighted keyword based similarity measure for clustering webpages. *Int J Comput Inf Technol.* 2014;4:693–8.

Cellular Automata-Based LDPC Decoder

C. Abisha Queen, M. Anbuselvi and S. Salivahanan

Abstract Low-density parity check (LDPC) codes are the capacity approaching codes having better decoding performance closer to Shannon's limit. The performance of the LDPC codes depends on the block length, code rate, structure of parity check matrix (H-matrix), and on the decoding process. Various code construction methods are structured including Quasi-cyclic-irregular parity check matrix to improve the performance of the LDPC codes. Cellular Automata are a computational method that realizes the complex computational blocks into simple, regular, and modular structures. In this paper, the cellular automata-based LDPC parity check matrix with hierarchical diagonal parity check matrix structure has been incorporated in the decoder design. Error performance improvement of 0.0417 dB is obtained with HDPCM-based LDPC decoder using cellular automata. Performance analysis on increased code length validates the proposed LDPC decoder with the improved decoding performance.

Keywords LDPC codes · Decoding algorithm · Cellular automata · Parity check matrix · Density · Girth

C. Abisha Queen (✉) · M. Anbuselvi
ECE Department, SSN College of Engineering, Kalavakkam, India
e-mail: abiqueenrec@gmail.com

M. Anbuselvi
e-mail: anbuselvim@ssn.edu.in

S. Salivahanan
SSN College of Engineering, Kalavakkam, India
e-mail: salivahanans@ssn.edu.in

1 Introduction

Low-density parity check codes are the class of linear block codes with sparse parity check matrix (H-matrix) [1, 2]. The advantages of LDPC codes are highly parallelizable in hardware implementation; codes are capacity approaching, efficiently decoded by parallel iterative decoding algorithm with low latency and these advantages allow LDPC codes to real-time and high-throughput application [3]. LDPC codes find application in standards such as 10GBase-T Ethernet, IEEE 802.11(WiFi), WiMAX, data storage in flash memory and Digital Video Broadcasting (DVB). LDPC decoding algorithms include functions in computation which gives complex computational blocks structures in VLSI implementation [4]. The parity check matrix gives the parity check constraints for the LDPC codes. The structure of the parity check matrix is one of the metric which determines the performance of the LDPC codes. Quasi-cyclic LDPC codes provides decoding with fast convergence rate, low error-floor, and better performance in the AWGN and BEC channel and it is close to Shannon limit [5]. Various algorithmic modifications are provided to reduce the complexity in the implementation at the cost of degradation in the performance [4, 6, 7].

The cellular automata implements the complex computational blocks into simple modular logic structures [8]. Cellular Automata (CA) is the computational method for various VLSI applications which includes error correcting codes [9, 10], design of cipher system [11], testing of circuits, authentication scheme, and compression. Cellular automata implementation provides better parallelism and it is also cost effective compared to DSP processor. Cellular automata-based LDPC structure is obtained using the cellular automata rules, which includes the modular expression for generation of the hierarchical diagonal parity check matrix.

In this paper, cellular automata-based LDPC codes have been proposed to provide better performance and reduced computational complexity. This paper includes basic concepts of cellular automata, classification of rules, and cellular automata rules for HDPCM generation.

2 Cellular Automata Concept and Classification

Cellular automata are a computational method which implements complex computational blocks into simple modular logic structures. Cellular automata (CA) are attractive due to their fine grain parallelism, simple computational structures, and local communication patterns [12]. CA consist of an infinite number of finite cells arranged on a regular lattice. Each cell in the lattice is identical and works simultaneously. The value in each cell in time $t + 1$ is a function of the value of cell in time t , the value of neighboring cells in time t , and rule associated with the cell. One-dimensional cellular automata consist of a row of cells with $r = n$ in general representation, where r is the distance from the present cell to the neighborhood

cells to which the value of the current cells depend on and n is the number of cells in the row, $n = 1$ gives $y_{i-1}(t)$, $y_i(t)$, $y_{i+1}(t)$ as the neighborhood cells. In one-dimensional cellular automata [13], the value of the cell $y_i(t+1)$ depends on the neighborhood cells $y_{i-1}(t)$, $y_i(t)$, and $y_{i+1}(t)$. $y_{i-1}(t)$ corresponds to the cell to the left of the current cell and $y_{i+1}(t)$ corresponds to the cell to the right of the current cell. The value of the present cell depends on the neighborhood cells previous values that results in 8 (i.e., 2^3) possible neighborhood combinations. The possible number of rules is 256 (i.e., 2^8).

3 Cellular Automata Rules for LDPC Decoding

Parity check matrix (PCM) is the random matrix defined in the Galois Field which determines the strength of the LDPC codes. The complexity in the computations of LDPC codes depend on the number of nonzero numbers and structure of the PCM. By increasing the sparsity of the PCM, the computational complexity is reduced significantly. The increased sparsity in the PCM is achieved by implementing the cellular automata rules. The increased sparsity of the matrix is required to reduce the complexity in the computation of LDPC codes in the implementation of the decoding algorithm. The CA-based generated PCM is sparser compared to the random PCM. PCM obtained by rule 90 is sparser compared to the random or other two CA rules. The rule 90 has a less complex function compared to all the other random CA rules.

Rule 90: A simple linear CA rule generates sparse matrix by the exclusive-or of its two neighbors [13].

$$y_i(t+1) = y_{i-1}(t) \oplus y_{i+1}(t)$$

Rule 240: Shift-right operations are performed [13].

$$y_i(t+1) = y_{i-1}(t)$$

3.1 Comparison of PCM Generated by Using Cellular Automata Rules

The sparsity comparison between the random LDPC PCM and PCM generated by the cellular automata rules are shown in Table 1. The sparse arity check matrix PCM was obtained by the Rule 90 with simple function for implementation.

The random number generation using nonuniform CA randomizer has been found to be superior to that of Rule 30 [14] and takes the same time as that of uniform cellular automata rules. The hierarchical diagonal parity check matrix is

Table 1 Comparison of CA rules

<p>Random LDPC PCM</p> $H = \begin{bmatrix} 1 & 1 & 1 & 0 & 1 & 1 & 1 & 1 \\ 0 & 1 & 1 & 1 & 0 & 0 & 0 & 1 \\ 1 & 1 & 0 & 1 & 1 & 1 & 1 & 1 \\ 1 & 0 & 1 & 1 & 1 & 1 & 1 & 0 \end{bmatrix}$	<p>PCM using CA Rule 30</p> $H = \begin{bmatrix} 1 & 0 & 0 & 0 & 0 & 0 & 0 & 0 \\ 1 & 0 & 0 & 0 & 0 & 0 & 0 & 1 \\ 0 & 1 & 0 & 1 & 0 & 1 & 1 & 0 \\ 0 & 1 & 1 & 0 & 1 & 1 & 0 & 0 \end{bmatrix}$
<p>PCM using CA Rule 90</p> $H = \begin{bmatrix} 1 & 0 & 0 & 0 & 0 & 0 & 0 & 0 \\ 0 & 1 & 0 & 0 & 0 & 0 & 0 & 1 \\ 0 & 0 & 1 & 0 & 0 & 0 & 1 & 0 \\ 0 & 1 & 0 & 1 & 0 & 1 & 0 & 1 \end{bmatrix}$	<p>PCM using CA Rule 150</p> $H = \begin{bmatrix} 1 & 0 & 0 & 0 & 0 & 0 & 0 & 0 \\ 1 & 1 & 0 & 0 & 0 & 0 & 0 & 1 \\ 1 & 0 & 1 & 0 & 0 & 0 & 1 & 0 \\ 1 & 0 & 1 & 1 & 0 & 1 & 1 & 0 \end{bmatrix}$

implemented in cellular automata by concatenating Rule 240 and Rule 90, and are represented by

$$H_{HDPCM} = [RM_{S,H,L}|IM]$$

$$H = \begin{bmatrix} 1 & 0 & 1 & 0 & 1 & 0 & 0 & 0 \\ 0 & 1 & 1 & 1 & 0 & 1 & 0 & 0 \\ 1 & 1 & 1 & 0 & 0 & 0 & 1 & 0 \\ 0 & 1 & 0 & 1 & 0 & 0 & 0 & 1 \end{bmatrix}$$

where $RM_{S,H,L}$, the single diagonal elements along with the diagonal elements both in the upper right half and lower left half of the matrix and IM, the identity matrix.

3.2 Algorithm to Generate CA-Based LDPC Codes

See Table 2.

4 LDPC Decoding Algorithm

Sum-Product decoding algorithm (SPA) of LDPC codes approach the channel capacity in the additive white Gaussian noise channel. The computational complexity of the SPA is given by $O(q)$ as it has sum and product operations for each

Table 2 Algorithm to generate CA based LDPC codes

<p>Initially the $H(m,n)$ matrix is generated by rule 240 to the first half matrix and second half matrix by specifying the initial conditions as $H(1,1)=H(1,(n/2+1))=1$.</p> <p>STEP: 1.a, Initialization for first row to apply CA rule</p> <pre> i=1 for j=1:1:n/2 If j==1 H(1,1)=1; else H(i,j)=0; end end b, Rule 240 for i=2:1:m for j=1:1:n/2 if j==1 H(i,j)=H(i-1,n/2); else H(i,j)=H(i-1,j-1); end end c, similar is done for j=n/2+1:1:n by applying the rule 240. STEP: 2. Splitting the H-matrix as H_1-matrix and H_2-matrix. STEP: 3. For H_1-matrix the rule 240 is applied by specifying $H_1(1,(n/4+1))=H_1((m/2+1),1)=1$. </pre>	<p>STEP: 4. Random matrix $H_R(m,n/2)$ is generated by using Rule 90.</p> <pre> i=1; j=1; for j=2:1:n/2 H_R(1,1)=1; H_R(i,j)=0; end for i=2:1:m for j=1:1:n/2 if j==1 H_R(1,j)=xor((H_R(i-1,n),H_R(i-1,j+1))); elseif j==n H_R(1,j)=xor(H_R(i-1,j-1),H_R(i-1,1)); else H_R(1,j)=xor(H_R(i-1,j-1),xor(H_R(i-1,j+1))); end end end STEP: 5. Matrix H_{12} is obtained by OR-operating the matrix H_R and H_1. $H_{12}=H_R \text{ or } H_1$; STEP: 6. Final HDM matrix is obtained by concatenating H_{12} and H_2. </pre>
---	--

check node processing, where q represents the cardinality of the Galois field. The SPA can also be implemented in the probability domain using fast fourier transforms (FFT) [15] and the complexity will be dominated by $O(q \log_2 q)$ as it includes sum and product operations. The FFT-based SPA (FFT-SPA) needs complicated multiplications. The hardware expensive multiplications are removed by the exponential and logarithm operation with look-up tables during the check node and variable node processing. In the max-log-SPA, the computational

complexity is given by $O(q^2)$ with sum and comparisons. Variations in the algorithm is done to reduce the complexity that includes min-sum decoding algorithm which provides reduced memory requirement and with little performance loss. Min-max decoding algorithm gives reduced number of comparisons and it degrades the performance. To provide better trade-off between computational complexity and performance, the proposed method of cellular automata-based LDPC parity check matrix is generated for the FFT-SPA decoding using the cellular automata rules. The computational complexity is reduced by the cellular automata as it implements the complex computational block to simple modular logic structures.

5 Hierarchical Diagonal Parity Check Matrix in CA-Based LDPC Codes

In the cellular automata-based LDPC codes, the hierarchical diagonal parity check matrix (HDPCM) is derived using CA rules. The information bits are encoded by using the generation matrix and modulated by BPSK modulation. The modulated information is transmitted through the channel. The Additive White Gaussian Noise (AWGN) is added to the transmitted information. The channel probability for the channel and the received bits are calculated and decoded using FFT-SPA. FFT-SPA decoding algorithm was implemented with the HDPCM derived by the CA rules as shown in Table 2. The computational complexity of the sum-product algorithm (SPA) is $O(q^2)$ and by the FFT-SPA it scales down to $O(q \log q)$.

For the code length 648, the BER for different SNR, noise variance (σ), and comparison between random LDPC codes HDPCM matrix and CA-based LDPC codes HDPCM matrix is plotted.

5.1 Analysis of HDPCM

Sparsity of the PCM is the ratio of total number of zero elements to the total number of elements in the parity check matrix structure. The sparsity of the HDPCM matrix for code length $n = 648$ is 0.9698 and for $n = 1008$ the sparsity is 0.9729.

Density of the PCM is the ratio of total numbers of nonzero elements to the total number of elements in the parity check matrix structure. The density of the HDPCM matrix for code length $n = 648$ is 0.0302 and for $n = 1008$ the density is 0.0271.

A cycle of length l is a path between the variable and check nodes of l distinct edges which closes on it. The shortest possible cycle has the length of four. The minimum cycle length is girth. Short cycles of Tanner graph have a negative influence on the performance of iterative decoding [16]. So, short cycles should be avoided when designing good LDPC codes.

5.2 Performance Analysis

BER is the ratio of number of erroneous bits to the total number of bits. Cellular automata concept is introduced in the parity check matrix generation by using the nonuniform cellular automata rules. For the code length of 648, the BER curve is plotted for different SNR dB values in Fig. 1. The BER for noise variance $\sigma = 0.8$ is obtained for different SNRs from -1 to 5 dB for 25 iterations.

The CA-based LDPC decoder error performance is improved for the increasing SNR values. The error performance is similar to the other decoder performance for the different noise variance is analyzed.

5.3 Comparison Analysis

The hybrid CA rules are used to obtain the HDM structure. The HDM structure provides better error performance compared to the random parity check matrix. For $\sigma = 0.8$ with 30 iterations, the LDPC codes comparison plot between CA derived HDPCM and random HDPCM for different SNRs is analyzed and plotted in Fig. 2. The SNR of 3 dB gives a BER of 0.0849 dB for random HDPCM and 0.0432 dB for CA-derived HDPCM. The improvement in the BER is obtained as 0.0417 dB.

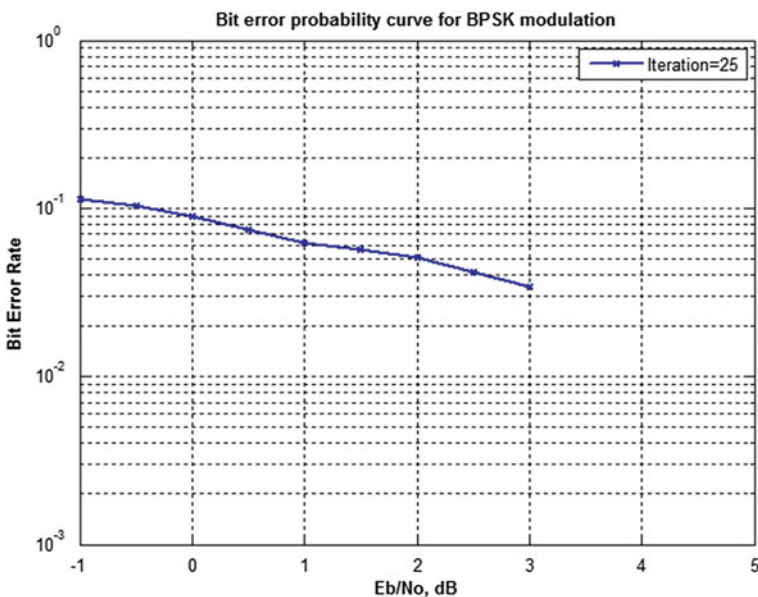


Fig. 1 BER curve for CA based LDPC codes

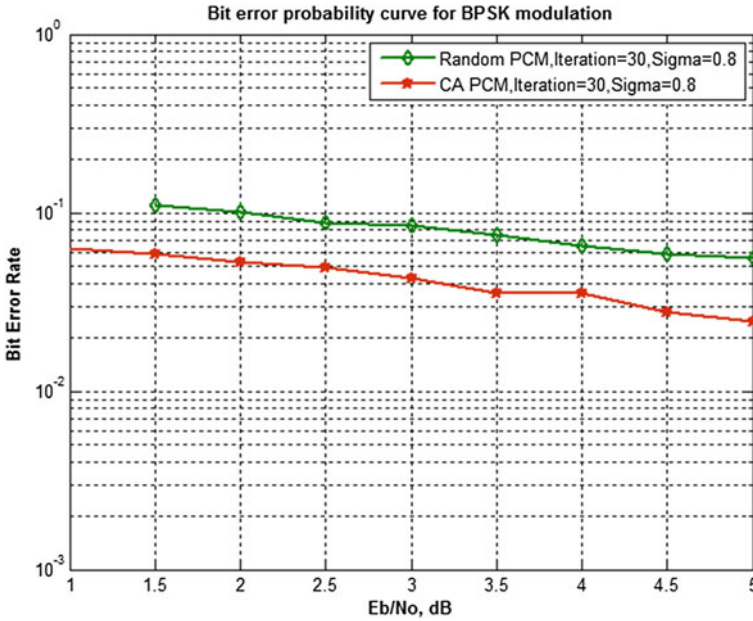


Fig. 2 Comparison between CA based and random LDPC codes

This analysis shows the error performance improvement by using the HDPCM structure in comparison with the random PCM in the LDPC decoding. The HDPCM matrix is a sparse matrix that reduces the computational complexity with the increase in the performance.

5.4 CA-Based LDPC Codes for Different Code Length

In LDPC decoding, by increasing the code length the error performance is improved. By the proposed cellular automata-based parity check matrix, the analysis for the increased code length has been done and plotted in Fig. 3. BER for code lengths 648 and 1008 was plotted for various SNR dB values with sigma = 0.8 and 25 iterations.

It has been observed that by increasing the code length, the BER performance improvement was observed. The complexity in the computation was also minimized by the increased sparsity in the cellular automata-based HDPCM. Comparing the code length $n = 648$ in the Wifi application and the underwater communication with $n = 1008$, the code length $n = 1008$ provides better error performance.

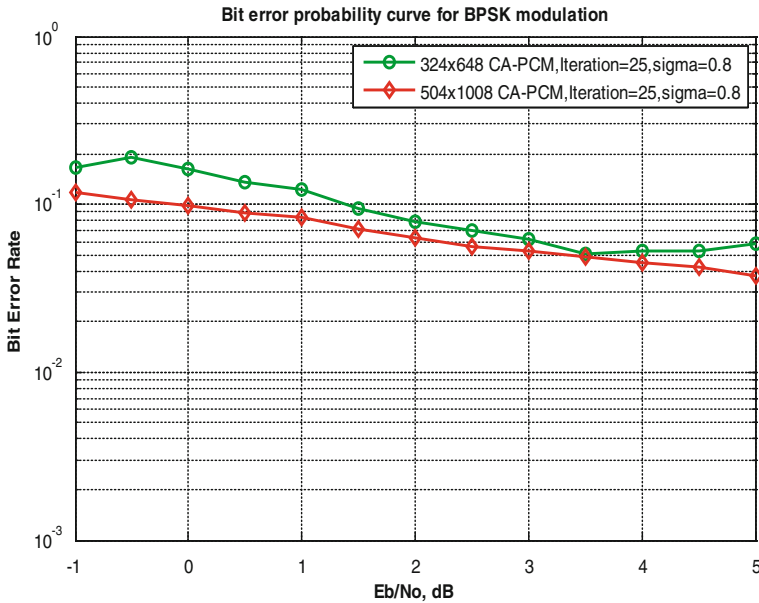


Fig. 3 BER for different code length

6 Conclusion

The cellular automata-based HDPCM is constructed and increased error performance is obtained by satisfying the girth and $\frac{1}{2}$ code rate for the decoder design. The performance analysis of the CA-based LDPC codes and the random LDPC codes provides improved error performance in the CA-based LDPC codes. Performance prompts to be increased for the increased code length. The designed decoder is evaluated for decoder parameters like BER, girth, and convergence rate. The CA-based LDPC codes provides a convergence rate of 0.0417 dB for code length $n = 324$ on comparing with random LDPC codes. The cellular automata-based LDPC decoder can be used for different channel modulations and different channels. The implication of the CA-based LDPC decoder can be used for higher order Galois Field.

References

1. Gallager RG. Low density parity check codes. IRE Trans Inf Theory 1962;IT-8:21–28.
2. Davey MC, Mackay DJC. Low density parity check codes GF (q). IEEE Commun Lett. 1998;2(6):165–7.
3. Ma X. On constructing low density parity-check codes. PhD thesis, University of Waterloo, Ontario, Canada; 2007.

4. Barnault L, Declercq D. Fast decoding algorithm for LDPC over $GF(2^q)$. *Inf Theory Workshop 2003*;2003:70–73.
5. Zhou B, Kang J, Song S, Lin S, Abdel-Ghaffar K, Xu M. Construction of non-binary quasi-cyclic LDPC codes by arrays and array dispersions. *IEEE Trans Commun* 2009;57(6):1652, 1662.
6. Song H, Cruz JR. Reduced-complexity decoding of Q-ary LDPC codes for magnetic recording. *IEEE Trans Magn*. 2003;39(2):1081–1087.
7. Hong H, Sun Z. An improved decoding algorithm of non binary LDPC code. In: 2011 International Conference on Information Technology, Computer Engineering and Management Sciences (ICM), vol 3; 2011. p. 104,107, 24–25.
8. Koroglu ME, Şiap I, Akın H. Cellular automata based byte error correcting codes over finite fields. In: American Institute of Physics Conference Proceedings, 2012, p. 183.
9. Cho S-J, Choi U-S, Heo S-H. Design of double error correcting codes based on cellular automata. *J Appl Math Comput*. 2006;21(1–2):545–53.
10. Sasidhar K, Chattopadhyay S, Chaudhuri PP. CAA decoder for cellular automata based byte error correcting code. *IEEE Trans Comput*. 1996;45(9):1003–16.
11. Das Debasis, Ray Abhishek. A parallel encryption algorithm for block ciphers based on reversible programmable cellular automata. *J Comput Sci Eng*. 2010;1(1):82–90.
12. Corsonello P, Spezzano G, Staino G, Talia D. Efficient implementation of cellular algorithms on reconfigurable hardware. In: Proceedings 10th Euromicro Workshop on Parallel, Distributed and Network-based Processing, 2002, p. 211, 218.
13. Wolfram. Theory and applications of cellular automata. In: Advanced series on complex systems, vol 1. Singapore: World Scientific, 1986. p. 485–557.
14. Tomassini M, Sipper M, Zolla M, Perrenoud M. Generating high-quality random numbers in parallel by cellular automata. *Future Gener Comput Syst*. 1999;16:291–305.
15. Carrasco RA, Johnston M. Non-binary error control coding for wireless communication and data storage. London: Wiley; 2008.
16. Tanner RM. A recursive approach to low complexity codes. *IEEE Trans Inf Theory* 1981;533–547.

A Game Theoretic Model to Detect Cooperative Intrusion Over Multiple Packets

Purbita Chakraborty, Koushik Majumder and Anurag Dasgupta

Abstract A MANET is an infrastructure-less mobile network whose principle is multi-hop relaying between nodes. They are prone to malicious attacks as no authentication or security architectures can be implemented because the nodes can continuously join or leave the network. Numerous schemes have been proposed for intrusion detection in MANETs. Recently, game theoretic approach is emerging as a major research area. The intrusion detection is a tedious task because the nodes are dynamic. A few papers have analysed the problem and provided appropriate solutions. In this paper, a game theoretic model has been developed for modelling network intrusions for colluding attacks from multiple packets. Detection is done by sampling a portion of the packets moving through the network. Depending on a sampling budget, a sampling strategy is developed and an optimal solution is found out to increase the chances of successful detection of the intrusion.

Keywords MANET · Colluding nodes · Non-cooperative model · Game theory · Intrusion detection

1 Introduction

A MANET is an automatic configuration network which lacks an infrastructure, and the nodes are free to move in all directions and change the links to the devices frequently and automatically as they move. MANETs share the wireless medium, have limited resources, lack a centralized control mechanism and have a dynamic network topology. Though these properties increase the ease of use, it also makes the system vulnerable to attack with malicious intent. Thus, MANETs must have a secure way for transmission and communication.

P. Chakraborty (✉) · K. Majumder
Department of Computer Science and Engineering, West Bengal University
of Technology, Kolkata, India
e-mail: koushik@ieee.org

A. Dasgupta
Department of Math and Computer Science, Edinboro University
of Pennsylvania, Edinboro, PA, USA

MANET is more susceptible to be attacked than a wired network. For this reason, intrusion detection is more important than intrusion prevention in MANETs. Intrusion is a mechanism in which the integrity, availability and/or the confidentiality of a resource are compromised owing to some actions. This problem can be solved using game theoretic approach. In game theory, every game played by players has a strategy associated as to how the game needs to be played or what main factors need to be considered depending on which the game is played. In network model, this strategy comes in the form of the functionalities of the network which is given prime consideration.

Modelling of ad hoc network as game components is required before the model is established. Here, *Players* are analogous to *Nodes* in the network, *Strategy* is analogous to *Action* related to the functionality being studied and the *Utility function* is to *Performance metrics* (e.g. throughput, delay and target signal-to-noise ratio). This similarity leads to a strong mapping between traditional game theory components and elements of an ad hoc network. The three main models of game theory used in this respect are (1) non-cooperative game theory model, (2) cooperative game theory model, and (3) basic Bayesian signalling game model. No work has still been done in the area of colluding nodes attacking one target node simultaneously using varied links though fragmentation and collusion has been taken separately [1, 2].

2 Related Works

The work in [3] shows that the intruder chooses a single path to attack a single node. This is the simplest model and no colluding attack is considered in this case. Another model considers distributed intrusion detection system [4] with a network of sensors. This model is very flexible and easy to implement but it considers both the intruders and nodes as a group and single node attack is not considered. This similarity leads to a strong mapping between traditional game theory components and elements of an ad hoc network. Two-player signalling dynamic game with host-based IDs [5] takes care of the trade-off and alarm rates but colluding intrusion is not considered. The non-cooperative game model in [1] takes into consideration fragmented packets attacking a single node but does not deal with collusion. Similarly, in [2] collusion is considered using non-cooperative game but no multiple attack is considered. A model [6] using two-player dynamic non-cooperative game with incomplete information deals with false alarms and is a very robust method but does not deal with collusion. Among all the six papers provided, the papers using non-cooperative game theory only deal with the collusion problem which the others do not but the papers do not have any mechanism for raising alarms. Most of the cases referenced here, analyse the presence of only a single node as the malicious node and devise mechanisms to deal with the single malicious node. Only one case of non-cooperative model and a case of cooperative model take into consideration the case of colluding nodes in which more than one

node with a malicious intent join together and create a problem in the network. So it is easily observable that the work relating to colluding activity is very less. Among all these models, only two models consider the case of raising alarm and alarming the network about the presence of a malicious node.

3 Problem Definition

This paper focuses on this area where a group of colluding adversaries send malicious packets in the network to reach the same destination using various links and various fragments. Non-cooperative game theory is used to reach to an optimal solution where the players are (1) the cooperative intruders and (2) the intrusion detection system. The game theoretic model assumes that the adversary has a full knowledge about the network and provides an optimal solution to the intrusion detection system for detecting intrusions thus minimizing the chances of attack from the colluding adversaries. The strategy in the case of the adversary will be to choose a path for successful attack to the target nodes and the strategy of the intrusion detection system will be to sample the network links so that the chances of intrusion get minimized depending on a maximum sampling budget. The model is basically divided into three main parts. First, the network is described, the adversaries are defined and then the objective of the game is described.

3.1 Network Set up Assumptions

The MANET network considered in this model is a directed graph containing N number of nodes and E number of unidirectional links. To make the intruder detection more challenging, it has been considered that the intruder as well as the service provider has the same knowledge of the network. So, the intruder can choose most frequently used paths for intrusion. The parameters chosen for describing the model are

- A. Capacity of the link, b_e , which is the maximum number of packets/fragments that can move through a link.
- B. Total number of intruders, ψ , is the measure of the number of intruders colluding together to attack the network.
- C. Sampling rate, r_e , is the rate at which the network samples the packets/fragments in the network. Sampling rate more than the capacity of the link is meaningless. Therefore, $b_e > r_e$.
- D. Sampling Bound of the network, S_B , is the maximum sampling allowed in the network. Sampling bound higher than sampling rate has no useful purpose. Therefore, $r_e > S_B$.
- E. Traffic in the network, t_e , determines the actual flow of packets at a given point of time in the network.

3.2 Introducing the Game

A non-cooperative game must at least consist of two players. Here, the two players are the set of intruders and the service provider. The set of intruders are taken together as a single intruder unit to maintain the simplicity in the calculations and understanding. The game played between the players is a zero sum game. The objective of the intruders is to send malicious packets and in this case, the malicious packets can also get divided into fragments. If majority of the fragments get detected by the central intrusion detection system and thus the service provider, the game is said to be won by the service provider and intrusion is said to have been detected. If most of the packets reach the target destination unnoticed, the game is said to be won by the intruder set and the attack is said to have been successful. The objective in this model is to provide complete network information to the intruder and still be able to detect attacks from the fragmented packets of the colluding nodes. A few terms to be used in the paper are

Malicious node is one which sends a malicious packet or disturbs the network in some way or the other. A malicious node can either behave maliciously or normally.

Normal node behaves normally.

Malicious packet is an erroneous packet sent from a malicious node to one/more than one target(s).

Normal packet is a packet sent by a normal node into the network.

Colluding attackers are a group of malicious nodes acting towards the same cause by inducing one/more than one malicious packet into the network with the intention of attacking the network.

Central Intrusion Detection System (CIDS) is a special node with added properties where the sampled packets are sent and the decision of whether intrusion is occurring or not is determined.

The game modelled above is actually a combination of two smaller cases: (1) A set of colluding nodes attacking a single node and (2) A single node attacking by fragmenting the packets using various links. Though the two individual scenarios have been dealt in the past, a combination of both has never been dealt with. For detecting intrusion, the service provider samples the links (or the nodes interchangeably, but the choice should be maintained throughout the game). The sampling is based on a sampling budget as discussed earlier which should never be more than the traffic of the network or the sampling rate of the network. The network is sampled at regular intervals and the fragments are sent to the central node for detection. The model is said to be working successfully if majority of the packets get detected, i.e. the service provider wins the game. In the Fig. 1, *A* through *G* is seven nodes in a network connected by unidirectional links. Also, *A*, *B* and *E* act as colluding nodes trying to send malicious packets to *G*. *A* fragments the malicious packet named *A* into two parts *A11* and *A12* and the similar process is applied by *B*. *E* sends a single malicious packet and does not fragment it into

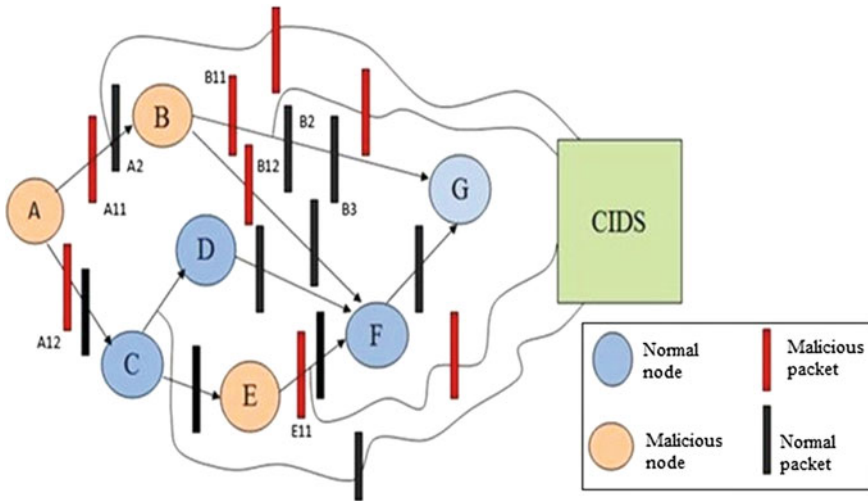


Fig. 1 A fragmented-colluding game

smaller parts. These three nodes (*A, B, E*) have common interests thus acting as colluding nodes. The CIDS receives a set of sampled packets after regular intervals and decides whether the packets are malicious or not depending on which the winner of the game is decided.

3.3 Objective and Constraints

Constraints of the system are the bounding conditions depending on which the game is played. The main constraints in the system are the sampling bound (S_B) with respect to the service provider and the fragmentation bound (F_B) with respect to the colluding nodes.

Sampling Bound is the maximum number of packets that are sampled and sent to the central intrusion detection node for checking of intrusion. The absence of any such bound will increase the chances of intrusion detection as the number of packets being sampled will increase considerably. But, at the same time, in the absence of any such bounds, the cost overhead of the system will increase. Moreover, having a sampling bound more than the actual traffic flow through the network serves no useful purpose. For this reason, a sampling bound of S_B is maintained in the network. The probability of a fragment being detected is determined by $prob_e = r_e/t_e$, where r_e is the sampling rate in the link and t_e is the traffic in the link for any link e . Now, it has already been discussed that, a sampling bound more than that of the actual sampling rate or the traffic flow is meaningless. Therefore, for any link $e \in E$,

$$\sum_{e \in E} r_e \leq S_B \Rightarrow \sum_{e \in E} (\text{prob})_e t_e \leq S_B \tag{1}$$

Though fragmentation of the packets is a main mode of attack by the intruders, fragmentation of a packet indefinitely will adversely affect the intruders in terms of energy overheads. It may happen that it loses all the energy fragmenting the packets and is left with no energy to launch attacks. To avoid such a circumstance, a fragmentation budget, F_B , is maintained by the intruders which depends on the resource availability and energy costs of the intruders.

3.4 Algorithm

In the algorithm provided in Fig. 2, a step-wise view of the overall working of the model is being presented. It starts with the sampling of the packets in the network and ends with the raising of alarm in the system.

3.5 Strategies of the Two Players

Intruders' Scenario The intruder can either use a mixed strategy or pure strategy. In a pure strategy, the intruder can pick a path $P \in \rho v u$ for each fragment to traverse

Algorithm Full_Game (SB, Val, Threshold)

Step1: Start the system.

Step2: Packets are sampled at the links of the network with the maximum sampling bound of S_B .

Step3: Each of the packets is sent to the CIDS.

Step4: A non cooperative game model is played between the intruders and the detection system.

Step5: **IF** (intrusion is doubted)
 The node is placed under doubt;
 Sent to the decision module;

Step6: **IF** (signature matches with stored pattern)
 Val = Val + 1;
 ELSE
 No action

Step7: **IF** (Val > threshold)
 Alarm is raised throughout the system;
 ELSE
 Packet is forwarded;

Step 8: **IF**(all the packets are checked)
 Stop;
 ELSE
 Goto Step4.

Fig. 2 Algorithm of the game

from u to v . In a mixed strategy, the colluding intruders have a probability distribution q_e over the set of paths $\rho v u$ such that $\sum_{P \in \rho v u} q_e(P) = 1$ where the probability vector is

$$q_{ex} = (q_e(P1)q_e(P2)q_e(P3) \dots q_e(P_x)). \tag{2}$$

Considering W_x to be a set of allowed probability allocations over a set of paths from u to v ,

$$W_x = \left\{ q : \sum_{P \in \rho v u} q(P) = 1 \right\} \tag{3}$$

Each intruder picks a path $P_a \in \rho v u$ with a probability $q_x(P_a)$ for each malicious packet and with a probability $q_y(P_a)$ for each fragment which are independent probabilistic events. So, the total probability is

$$P = q_x(P_a) \cdot q_y(P_a) \tag{4}$$

Service Provider's Scenario The service provider determines the links on which the sampling is required. Let the chosen sampling rate be r_e . To each and every sampling, the service provider also associates a sampling bound, S_B as discussed earlier. Now, the sampling rate is always less than the sampling bound. Choosing a sampling rate more than the sampling bound serves no useful purpose as the maximum number of packets sampled will be equal to the sampling bound. Using the above argument, we have

$$\sum_{e \in E} r_e \leq S_B \tag{5}$$

The probability of the detection of malicious packets is $\text{pr}_e = r_e/t_e$ or,

$$r_e = (\text{pr}_e)(t_e) \tag{6}$$

Considering Y_x to be the set of detection probability vectors of the link e ,

$$Y_x = \left\{ p_{sp} : \sum_{e \in E} (\text{pr}_e)(t_e) \leq S_B \right\} \tag{7}$$

3.6 Formulation of the Game and the Payoff Matrix

The intruder and the service provider have already chosen their respective strategies. The intruder has chosen a probability distribution q_e over the set of paths $\rho\nu u$. The service provider has picked a detection probability Y_x the links of the network.

The payoff of the system can be calculated in two different ways. The first payoff can be calculated as the number of times the malicious packet is detected while moving through the link from u to v .

If the probability of detection is pr_e , then the number of times the packet gets detected is $\sum_{e \in P} \text{pr}_e$.

The probability that the intruder selects the path is $q1(P)$.

Therefore, the number of times the packet gets detected is $\sum_{P \in \rho\nu u} q1(P) \{ \sum_{e \in P} \text{pr}_e \}$

$$\sum_{e \in P} \text{pr}_e \left\{ \sum_{P \in \rho\nu u} q1(P) \right\} \tag{8}$$

This can be represented in a matrix format as $q1^T M_p$ which can be called as payoff1.

The probability of detecting the packet is $1 - \prod_{e \in P} (1 - \text{pr}_e)$ which can be called as payoff2.

Summing up, the probability of detection is, $P_D = \sum_{P \in \rho\nu u} q1(P) [1 - \prod_{e \in P} (1 - \text{pr}_e)]$.

ψ be the total number of colluding intruders. Then, the actual probability of intrusion is $Q = P_D / |\psi|$.

Probability of sampling exactly K fractions is $Q^K x (1 - Q)^{n-K}$ where n are total number of fragments. This can be represented as (taking m to be a number of fragments greater than 1)

$$\sum_{i=m}^n Q^i * (1 - Q)^{n-i} \tag{9}$$

The strategy of the service provider is to maximize the probability, therefore,

$$S_B = \max_{p \in Y_x} \sum_{i=k}^n Q^i (1 - Q)^{n-i} \tag{10}$$

The strategy of the nodes is to minimize the probability of detection, thus,

$$\min_{W_x} \max_{p \in Y_x} \sum_{i=k}^n Q (1 - Q)^{n-i} = N_v \tag{11}$$

Optimal solution exists, if

$$SP_v = N_v \tag{12}$$

The point where this optimal solution or the Nash equilibrium exists is

$$A = SP_v = N_v. \tag{13}$$

where A is the value of the game.

3.7 Solution to the Game

It is considered where all the fragments need to be detected in order to confirm the intrusion for maintaining simplicity. In that case, it can be considered that $k = n$, where k is the number of fragments and n is the total number of fragments. If the total number of intruders are ψ , and if the sampling budget is S_B , then the budget for each of the malicious link is $S_{BM} = S_B/|\psi|$.

The min-max condition of the intruders is found to be $N_v = \min_{W_x} \max_{p \in Y_x} \sum_{i=k}^n Q^i (1 - Q)^{n-i}$

Now, taking $i = n$, we have

$$\min_{W_x} \left(\max_{p \in Y_x} \sum_{i=k}^n Q^n \right) \tag{14}$$

The inner maximization step can be written as

$$\max_{p \in Y_x} \sum_{i=k}^n Q \tag{15}$$

This means,

$$\begin{aligned} \max_{p \in Y_x} \sum_{i=k}^n q(P) \left[1 - \prod_{e \in E} (1 - pr_e) \right] &= > \\ \max_{p \in Y_x} [q(P)] - \sum_{i=k}^n \left[q(P) \prod_{e \in E} (1 - pr_e) \right] & \end{aligned} \tag{16}$$

For maximizing the Eq. 16, it is enough if the second part of the equation is minimized.

Therefore the problem reduces to

$$\min_{p \in Y_x} \sum_{i=k}^n q(P) \prod_{e \in E} (1 - pr_e) \tag{17}$$

For minimizing the above equation, it is enough to minimize the log of the equation.

$$\min_{p \in Y_x} \sum_{i=k}^n \left[q(P) \ln \prod_{e \in E} (1 - pr_e) \right] \tag{18}$$

$$= \min_{p \in Y_x} \sum_{i=k}^n \left[q(P) \sum_{e \in E} \ln(1 - pr_e) \right] \tag{19}$$

It is easier to calculate the sum of a set of terms as compared to the product. Using a log function, we can change the product to the sum which is done in Eqs. 18 and 19. It is well-known that the probability lies between 0 and 1. So,

$$0 \leq pr_e \leq 1 \Rightarrow \ln(1 - pr_e) \leq 0 \tag{20}$$

Let, $\ln(1 - pr_e) = -pa_e$. Equation 19 then becomes,

$$\max_{p \in Y_x} \sum_{i=k}^n \left[q(P) \sum_{e \in E} pa_e \right] \tag{21}$$

The budget constraint is assumed to be S_B and $S_{BM} > = r_e(pr_e)$. The relation between pr_e and pa_e is

$$pr_e = 1 - e^{-pa_e} \tag{22}$$

$$\begin{aligned} S_{BM} \geq r_e(1 - e^{-pa_e}) &\Rightarrow S_{BM} \geq \sum_{e \in E} r_e(1 - e^{-pa_e}) = \sum_{e \in E} (r_e - r_e e^{-pa_e}) \\ &\Rightarrow r_e - S_{BM} \leq \sum_{e \in E} r_e e^{-pa_e} \end{aligned} \tag{23}$$

Taking logarithm on both sides,

$$\ln(r_e - S_{BM}) \leq \ln\left(\sum_{e \in E} r_e e^{-pa_e}\right) = > \ln\left(\sum_{e \in E} r_e - S_{BM}\right) \leq \sum_{e \in E} \ln(r_e) - \sum_{e \in E} pa_e \tag{24}$$

Therefore, the game is reduced to,

$$\max_{p \in Y_x} \sum_{e \in E} \left[pa_e \sum_{p \in Y_x} q(P) \right] \tag{25}$$

where, the following constraint is applicable:

$$\sum_{e \in E} pa_e \leq \sum_{e \in E} \ln r_e - \ln\left(\sum_{e \in E} r_e - S_{BM}\right) \tag{26}$$

$$pa_e \geq 0 \tag{27}$$

Now, we associate a dual variable λ and deduce the optimization problem,

$$\begin{aligned} \min_{p \in Y_x} & \left[\sum_{e \in E} \ln r_e - \ln\left(\sum_{e \in E} r_e - S_{BM}\right) \right] \lambda \\ r_e \lambda & \geq \sum_{p \in Y_x} q(P) \end{aligned} \tag{28}$$

and

$$\lambda \geq 0 \tag{29}$$

Substituting the above obtained equations into Eq. 19,

$$\sum_{P \in Y_x} q(P) \leq r_e \lambda = > \sum_{P \in Y_x} q(P) \leq 1, \lambda \geq 0 \tag{30}$$

For a proper game, the value of lambda should be kept to a minimum. The main objective of the calculation is to find out the value of the game, A. Before finding out the value of the game, the individual flow in the network is to be determined and using the Ford–Fulkerson method, the maximum flow and the minimum cut is to be determined. Thus, the steps to be performed for finding out the value of the game are

- A. Determination of the maximum flow from the sender to the receiver, FN_{max} (using Ford–Fulkerson Method).
- B. Determination of the maximum flow among all the links, F_{max} (using Ford–Fulkerson Method).
- C. Calculation of $\lambda = FN_{max}/F_{max}$

D. Value of the game,

$$A = \ln r_e - (\ln r_e - B_{SM}) \quad (31)$$

The sampling rate of the service provider can be determined as

$$(S_{BM} * r_e) / FN_{\max} \quad (32)$$

The intruder here fragments the packets into smaller parts and sends the packets through various links. The probability of choosing a particular link by the intruder is (total number of links is n)

$$d_i / FN_{\max} \quad [\text{where } i = 1 \text{ to } n] \quad (33)$$

And

$$\sum_{i=1}^n d_i = FN_{\max} \quad (34)$$

4 Conclusions and Future Scope

The model takes both colluding nodes and packet fragmentation into account. The packets can be fragmented into smaller parts to be sent to the target. Both these have not been taken into consideration together till now. As it is well-known and discussed that colluding attacks are much more harmful than single node attacks, tackling multi-node attacks is very important. The whole formulation has been done using game theoretic approach which is an optimization tool. The value of the game is found out in the preceding section. But it has always been assumed throughout the literature that the flow through the links is fixed. The flow basically depends on the routing of the packets through the network and the traffic in between the nodes. The area where the service provider can adjust the flow through the network is not kept under consideration. As a future scope, the various routing algorithms like cut saturation algorithm and flow flushing algorithm can be applied for changing the flow through the network and the corresponding change in the value of the game can be studied.

References

1. Otrok H, Mohammed N, Wang L, Debbabi M, Bhattacharya P. A game-theoretic intrusion detection model for mobile ad hoc networks. *Comput Commun.* 2008;31(4):708–21.
2. Mehrandish M, Assi CM, Debbabi M. A game theoretic model to handle network intrusions over multiple packets. In: *Communications, 2006. ICC'06. IEEE international conference on*, vol 5. 2006. p. 2189–94.
3. Kodialam M, Lakshman TV. Detecting network intrusions via sampling: a game theoretic approach. In: *INFOCOM 2003. Twenty-second annual joint conference of the IEEE computer and communications.* IEEE Soc. 2003;3:1880–9.
4. Alpcan T, Basar T. A game theoretic approach to decision and analysis in network intrusion detection. In: *Decision and control, 2003. Proceedings. 42nd IEEE conference on*, vol 3. 2003. p. 2595–2600.
5. Patcha A, Park JM. A game theoretic approach to modeling intrusion detection in mobile ad hoc networks. In: *Information assurance workshop, 2004. Proceedings from the fifth annual IEEE SMC.* 2004, p. 280–4.
6. Paramasiva B, Pitchai KM. Modeling intrusion detection in mobile ad hoc networks as a non cooperative game. *Pattern Recogn Inf Mobile Eng (PRIME).* 2013;300–306.

Filtration of Noise in Images Using Median Filter

Vigya and Tirthadip Ghose

Abstract Image processing is one of the major aspects of signal processing. Like any other signal, images can also be hampered by noise. Filters need to be designed and implemented, to remove these unwanted signals. There could be various types of noise affecting the images and, accordingly, different types of filters need to be designed. In this paper, median type of filter is designed for different kinds of noise. Also, a study of this filter is made to determine which type of noise they are suitable for. The mean square error determines whether the designed filter is suitable for the given image and the noise or not. The estimated image is the noise filtered out from the given image. Processing is done using the MATLAB software and the image has been processed by MATLAB codes.

Keywords Image processing · Noise reduction · Median filter · MATLAB

1 Introduction

First, a signal can be defined as a function that conveys some sort of information about the behavior or the attribute of a phenomenon. Almost everything that can cause a change in time or space is referred to as a signal in this world. It is a quantity that exhibits the passing of information from one point to another. A signal gives information about a physical system and also conveys a message between the observers [1].

In this paper, the image signal is processed. Image processing on digital computers has been gaining importance in recent years. Talking about image, an image can be defined as a function of two real variables, as $A(x, y)$, where A is the amplitude or brightness of the image at some real coordinates (x, y) . It can be called as a signal that gives some visual information to the receiver. Image can be two-dimensional or multi-dimensional, and can be captured by optical devices such

Vigya (✉) · T. Ghose
Department of EEE, Jharkhand 835215, India
e-mail: k_vigya@yahoo.com

as camera, telescopes, microscopes, etc., or by natural objects such as the human eyes. In general, images can be still images (or static images) or moving images (or video). Sometimes, the image can be considered as a collection of regions to simplify the operation [2–4].

A digital image $A(x, y)$ which is described in a two-dimensional space, necessary for operation, is derived from an analog image $A(m, n)$ in a two-dimensional continuous space through a process known as sampling, often referred as digitization. The two-dimensional continuous image $A(m, n)$ is divided into ‘ Y ’ rows and ‘ X ’ columns. The value assigned to the integer coordinates (x, y) with $\{x = 0, 1, \dots, X - 1\}$ and $\{y = 0, 1, \dots, Y - 1\}$ is $A(x, y)$. The intersection of a row and a column element is termed as a pixel. There are certain values for the various parameters encountered in digital image processing. For checking the accuracy of the image, the signal-to-noise ratio is calculated [1].

The manipulation of signals, in the form of images, is referred to as image processing. For this, image analysis is carried out in such a manner that the measurements come out of the analysis. Then the image understanding takes place, where the high level description is given. Image processing involves image enhancement, image restoration, and image compression.

Image enhancement includes sharpening of image features such as boundaries, accentuation, or contrast of the image which are used to make the display more useful for analysis. Image restoration is done to reduce the degradations. It basically depicts the level of accuracy of the image being processed and observed by the receiver. Image compression is a process of minimization of the number of bits that are required to represent an image. Sometimes, the image size is much larger than it is actually required. So, to fulfill the purpose, this process is carried out [5].

In this paper, first the different types of noise are discussed, which are there in the images, and then the types of filters and the filter designed are discussed. Then, the results are discussed, followed by the conclusion of the paper.

2 Noise

During the communication of signals, various types of noise can be infuriated in the signals, which badly affect the quality of the signal at the receiving end. To eliminate noise from signals, it becomes important to know the types of noise that affect them. We know that noise is a random fluctuation in an electrical signal. It can also be called as an undesired random disturbance or an error in a useful signal in a communicating channel. If we want to know from where the noise originates, it can be said that the noise can also be referred to as a summation of unwanted energy from natural as well as man-made sources. Similarly, the noise in the image is also a random variation in the brightness or color or contrast or hue information of the images, which are the main parameters that define the image (Fig. 1).

The major causes of noise in an image are of electronic nature, such as camera, or scanner, or the sensors producing the images. The images can also be hampered by the circuitry they go through before the transition ends.

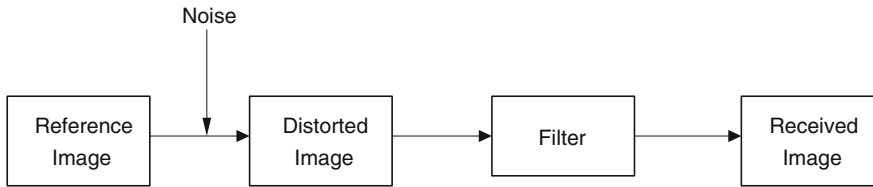


Fig. 1 Block diagram representing the basic idea

The most common effect of noise on the image could be blurriness or coloring. The image may appear either dull or blurred, or brighter or more colored, and both the cases are undesirable [6].

As regards the various types of noise in an image, some of them are listed below [6–10].

2.1 Gaussian Noise

It is one of the most common noises that occur in the image. The principal sources of this noise in digital images are noises that occur during acquisition, e.g., the noise caused by poor illumination and/or transmission, and/or high temperature, e.g., electronic circuit noise.

2.2 Salt-and-Pepper Noise

This noise has similarity to the salt and pepper sprayed to the image. The image that contains the salt-and-pepper noise will have darker pixels in the brighter regions and brighter pixels in the darker noises found in the images and generally arise by regions. This noise is generally found in the analog-to-digital converter (ADC) errors, errors in transmission, etc. It is mostly eliminated by use of dark frame subtraction and interpolation around the dark/bright pixels.

2.3 Shot Noise

It can sometimes be referred to as the dominant noise, and is seen in the lighter areas of an image. This noise is generally aroused from an image sensor which is typically caused by the statistical quantum fluctuations, i.e., some variation in the total number of photons that are sensed at some given exposure level. This noise is also known as the photon shot noise. One of the major characteristics of the shot

noise is that it has a root mean square value of intensity which is proportional to the square root of image intensity. It can also be compared with the Poisson distribution curve. Moreover, the noises at each of the different pixels are independent of each other.

2.4 *Quantization Noise*

This noise is primarily caused by the quantization of the pixels of a sensed image to a particular number of discrete levels. Unlike the shot noise, it has an approximately uniform distribution to the whole of the image. Although this noise is likely to be signal dependent, sometimes it could be signal independent if and only if the other noise sources are big enough to cause some dithering, or in cases where dithering is explicitly applied.

2.5 *Film Grain*

This type of noise is normally found in photography plates. Usually, the grain of a photographic film is the signal-dependent noise, with a nearly similar statistical distribution to shot noise. If the film grains are uniformly distributed, i.e., they possess equal number of grains per area, along with the condition that each of the grains has an equal as well as an independent probability of developing onto a dark silver grain after being able to absorb photons, then the number of such dark grains in an area will somewhat be random possessing some characteristics of a binomial distribution. In the areas where this probability is low, this distribution will turn out to be close to the classic Poisson distribution of the shot noise. Film grain is generally regarded as the nearly isotropic or non-oriented noise source. Its effect is moreover made worse by the distribution of some silver halide grains in the film which are also random.

3 **Filter**

Now, as we have an idea about the noise present in images, the next step is to know about filters that could be designed for the reduction of noises [1].

Filtering is a technique used for the enhancement or modification of an image. The filter can emphasize a certain feature and could also remove certain features. Filtering in image processing is usually a neighborhood operation, i.e., the value of the filtered pixel is found by applying some algorithm over the neighboring pixels.

There are basically two types of filters that are used for processing, viz, linear filter and nonlinear filter.

In linear filter, the output changes linearly with the change in input. Linear filtration helps in improving images in many ways [11].

Nonlinear filters do not follow the linearity condition and the linearity relationship breaks down. The median filter is a type of nonlinear filter. In applications, the nonlinear filter is used to remove outliers as well as shot noise, which is independent of magnitude.

Median filter is the most common nonlinear filter used for image processing applications [12, 13].

The filtered pixel does the required changes in the output image based on a corresponding set of input pixels. The filters for image processing involve the use of the following terms for their design [6, 9, 10]. Block operation supports that the image cannot be operated as a whole and thus has to be divided into small blocks to continue the operation. The operation in case of the median filter is the calculation of medium of the block. The edges of the image have to be given padding as the margins with zero pixel so as to not to have an effect on the operands of the block considered.

The operations in the image are basically the neighboring operations. This means that for carrying out the operation in the single pixel of the image, the neighboring pixel elements are considered and necessary modifications have to be made. In this paper, the median of the neighboring pixels is taken out and the center pixel is replaced with the median obtained. Defining center pixel, it is the pixel of the center of the neighborhood of the window considered. To find the median of the pixels, they need to be sorted first by the process called column processing.

One most important thing for operation is that the blocks should not be overlapped in the designing. They should run smoothly over the whole image, taking every pixel into consideration. However, if any extra rows or columns are also computed, then it gives a margin for overlapping of the distinct blocks over one another [12].

4 Results

Using the MATLAB code for the purpose of image processing, the median filter is implemented to the image. To serve this purpose, the inbuilt MATLAB image of a cameraman is taken. This image is infused with salt-and-pepper noise and a block size of 3×3 is created, which is used for computation purposes. A median filter basically works on the idea that a window is moved over an image (as seen in a convolution) and thereby computing the value of the output pixel as the median value of the pixels or the brightness within the considered input window. As the value selected is exactly the same as that of the existing values of the pixels, there is absolutely no round-off error involved in the computation. Figure 2 shows the original image taken. This image is an inbuilt image used for experimentation. Any other image can be taken for processing. Figure 3 shows the image infused by the salt-and-pepper noise which is put through MATLAB coding. The density of the

Fig. 2 Original image of the cameraman



Fig. 3 Image infused with salt-and-pepper noise



noise is taken as 0.01, which can also be varied. After the application of the median filter, the image is obtained as shown in Fig. 4. It is seen that the image we get after filtration is almost similar to the original image and the error in between the two images can be found by calculating the mean square error. But the image is sharp enough to be realize the attributes of the original image. The features of the image

Fig. 4 Image obtained after median filter



remain intact and thereby contribute to the fact that the median filter did its job of filtration of the image very well.

Further, the image can be infused by various other noises to check on the application and excellence of the median filter over all types of noises. It can be observed that the median filter does not work well with the Gaussian noise. It works excellently with the shot noise as well, which can be discussed later. The shot noise can be removed by the median filter nonlinearly which is very much required for systems that are more infused by this type of noise.

5 Conclusion

Figure 2 shows the original image of cameraman, Fig. 3 shows the cameraman infused with salt and pepper noise possessing a density of 0.01, and Fig. 4 shows the filtered image of the cameraman using a median filter. The image depicts clearly the conclusion of this paper that the filtered image is almost similar to the original image. The median filter uses the concept that in a window, when an element is replaced, the exact value of one of the elements of the window is used giving the final value of the pixel to be exactly the same as one of the pixels in its neighborhood, which explains that the image obtained is sharper and better than that obtained using any other operations in the same window. There is no round-off error, which lessens the whole of the error in the image.

The median filter works well with this type of noise, while it does not work accurately with the Gaussian type of noise. This filter can also be applied to systems infused with shot noises, thereby increasing its area of application. Thus the conclusion obtained is that the image from median filter is accurate and can be used in various applications.

References

1. Proakis JG, Manolakis DG. Digital signal processing, principles, algorithms and applications. Pearson Education; 2007.
2. Watanabe S. Cognition and pattern (in Japanese). Tokyo: Iwanami; 1978.
3. Bergson H. Evolution creatrice. Paris, France: Felix Alcan; 1907.
4. Wiener N. Cybernetics, 2nd ed. Cambridge, MA: MIT Press; 1962; The human use of human being, 2nd ed. Boston, MA: Houghton Mifflin; 1956.
5. Young IT, Gerbrands JJ, van Vliet LJ. Fundamentals of image processing. Digital image processing/digital image analysis. ISBN:90-75691-01-7, NUGI 841.
6. Hwang H, Haddad A. Adaptive median filters: new algorithms and results. IEEE Trans Image Process. 1995;4:499–502.
7. Chan H, Chung-wa H, Mikolova M. Salt and pepper noise removal by median type noise detectors and detail preserving regularization. IEEE Trans Image Process. 2005;14:1479–85.
8. Guo H, Xie K. An improved method of adaptive median filter. J Image Graph. 2007;12:1185–8.
9. Yuan SQ, Tan YH. The solutions of equation-based noise detector for an adaptive median filter. Pattern Recogn. 2006;39(11):2252–7.
10. Eng HL, Ma KK. Noise adaptive soft-switching median filter for image denoising. IEEE Int Conf Acoust Speech Signal Process. 2000;4:2175–8.
11. Lin HM, Willson AM Jr. Median filters with adaptive length. IEEE Trans Circuits Syst. CAS-35. 1991;675–90.
12. Weeks AR Jr. Fundamentals of electronic image processing. eISBN:9780819480439, ISBN:13:9780819421494.
13. Smith SW. The scientist and engineer's guide to digital signal processing.

PVDF Polymer-Based MEMS Cantilever for Energy Harvesting

G. Dinesh Ram and S. Praveenkumar

Abstract The ambient vibration-based MEMS cantilever is developing nowadays in terms of energy harvesting. Conventionally, battery is used as power supply for wireless devices and it should be periodically charged, which is difficult for devices in remote. MEMS cantilever-based energy harvesting is one of the solutions to this problem. The MEMS cantilever made of piezoelectric material will convert the environmental vibration into electrical energy. The structure and the material of the cantilever play a major role in producing the electric potential. In this paper, the T-shaped cantilever with PVDF is proposed and compared with the conventional structure and materials. The designed structure is simulated using COMSOL Multiphysics software and the virtual fabrication is done using the IntelliSUITE software.

Keywords MEMS · Piezoelectric · Energy harvesting · COMSOL · IntelliSUITE

1 Introduction

Conventionally, wireless network devices use battery for power supply. But the battery should be charged or changed periodically, which is difficult in remote locations. The cantilever-based energy harvester is developing at present in terms of providing solutions to battery-based problems. The cantilever made of piezoelectric material can convert the environmental vibration into electrical energy.

G. Dinesh Ram (✉) · S. Praveenkumar
Department of Electronics and Communication Engineering,
Saveetha Engineering College, Chennai, India
e-mail: dineshgram@gmail.com

S. Praveenkumar
e-mail: praveenkumarsunil@gmail.com

Mounicka Reddy et al. demonstrated that the various shapes of the cantilever beam have been analyzed for its sensitivity [1]. The different shapes such as triangular, rectangular, T-shaped and Pi-shaped structure are designed using a single crystal silicon and its sensitivity is compared. It is found that triangular shape has good deflection sensitivity.

Mateu et al. demonstrated that the rectangular cantilever made of PVDF material is presented [2], and the mode of operation selected is 31 mode, which is more efficient than the 33 mode. The configuration is unimorph, which is well suited for low frequency applications.

Salem et al. demonstrated that the conventional structure of the cantilever beam is changed to E-shape [3]. The E-shaped cantilever has three beams of varying lengths to generate energy for varying low frequencies.

Johnson et al. demonstrated that high power can be generated with the low excited frequency and load resistance. Anderson and sexton demonstrated that by varying the length of the beam and by varying the proof mask, the output power can be increased.

2 Cantilever Harvester Design

To design the cantilever energy harvester, the material, structure, and dimension should be specified.

2.1 Material Selection

Various materials can be used to build the cantilever beam for energy harvesting. The most commonly used material is piezoelectric material. The piezoelectric material has the piezoelectric property that will convert the environmental energy to electrical energy or vice versa.

Some of the properties of PVDF Kynar Flex 2800 are shown in Table 1.

Table 1 Properties of PVDF

Properties	Value
Density	1780 kg/m ³
Poisson ratio	0.18
Young's modulus	8.3 GPa

2.2 Structural Specification

Various shapes are used to build the cantilever beam. The commonly used structure is rectangular. The structure is fixed at one end and the other end is left free to get deflected. The other shapes used are triangular, T-shape, Pi-shape, trapezoidal shape, inverted trapezoidal shape, etc. Sometimes, array of cantilevers is also used to generate more electrical power. This cantilever is used to power the electronic device.

2.3 Parameter Specification

The dimension of the cantilever beam plays a major role in generating power. So the dimension should be a precise one. The force given to the cantilever beam is 0.5 N/m^2 . The material used to verify the structure is PZT (Lead, Zirconate, and Titanate). The dimension specified is given in Table 2.

3 Simulation

3.1 Simulation Using COMSOL Multiphysics Software with PZT

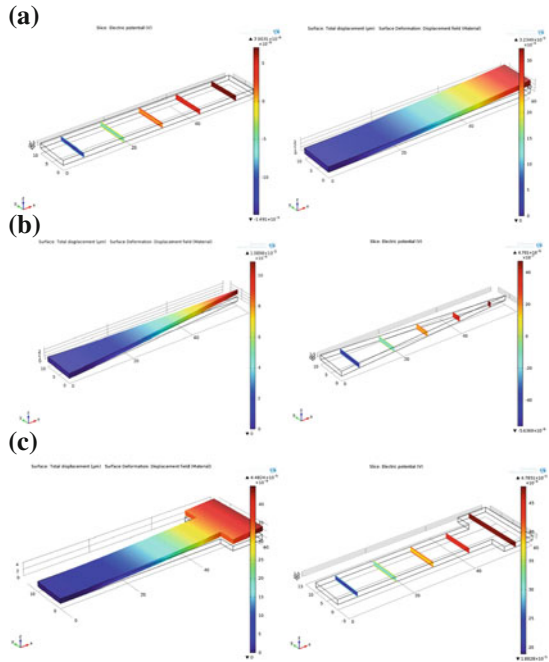
The shapes such as rectangular, triangular, and T-Shape were analyzed using COMSOL Multiphysics software and their results were compared. The steps used in COMSOL Multiphysics software is given in Fig. 1.

- Step 1 First, the dimension is selected as 3D.
- Step 2 Next in the physics selection, the structural mechanics is selected and in that piezoelectric devices is selected.
- Step 3 Then the geometry is defined (rectangular, triangular, T-Shaped, etc..) and their dimensions are also defined as length = $60 \text{ }\mu\text{m}$, breadth = $10 \text{ }\mu\text{m}$, and thickness = $1.5 \text{ }\mu\text{m}$.
- Step 4 Then the material is selected. There are many piezoelectric materials, among which PZT 4D material is selected.

Table 2 Dimension specification

Specification	In μm
Length	60
Breadth	10
Width	1.5

Fig. 1 Deflection and potential of **a** rectangular **b** triangular and, **c** T-shaped beam



Step 5 The boundary conditions are chosen. The boundary conditions such as fixed constraint and boundary load are selected. The force applied is 0.5 N/m^2 .

Step 6 Then the defined structure is meshed and simulated.

The simulation result for various shapes of cantilever beam is shown in Fig. 1. The displacement and electric potential obtained for various shapes of the cantilever beam observed using the simulation are tabulated in Table 3.

Table 3 Comparison of different structures

Structure	Force (N/m ²)	Displacement	Potential
Rectangular	0.5	3.2349×10^{-5}	1.491×10^{-5}
Triangular	0.5	1.0898×10^{-6}	5.6369×10^{-6}
T-Shaped	0.5	4.4824×10^{-5}	1.8828×10^{-5}

Table 4 Comparison of T-shaped cantilever beam with PVDF and PZT

Material	Force	Displacement	Electric
PZT	0.5	4.4824×10^{-5}	1.8828×10^{-5}
PVDF	0.5	4.6606×10^{-4}	3.2142×10^{-4}

The T-shaped cantilever beam has more deflection and generates more electric potential. So the T-shaped cantilever beam is suitable when used as a unimorph structure.

3.2 Simulation Using PVDF

The material is changed to a PVDF material and the T-shaped cantilever structure with PZT and PVDF is compared and simulated. The simulation result is shown in Table 4.

The simulation result is tabulated. The graphical representation to compare the beam with PZT and PVDF is given in Fig. 2.

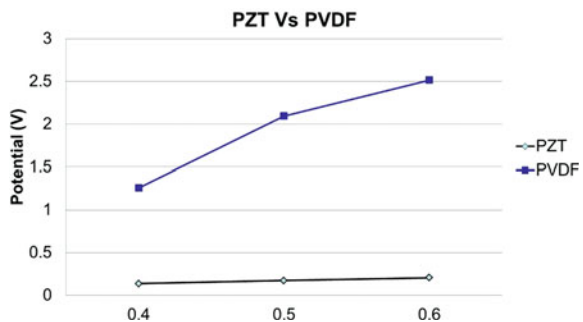
From the tabulation result and graphical representation, it is found that the cantilever beam with PVDF has more deflection and generates more electric potential compared to cantilever beam with PZT.

4 Mathematical Calculation

The end result of the energy harvester is to harvest energy from the cantilever beam. The output power depends on the material, structure, and the dimension of the beam. The various structures compared can be mathematically verified. When force is applied on the cantilever beam, deflection of the cantilever beam will occur and the deflection, δ can be

$$\delta_B = \frac{qL^4}{8EI} \tag{1}$$

Fig. 2 Graphical representation for comparison between PVDF and PZT



where

- Q is the stress applied
- E is the Young's modulus
- L is the length of the beam
- I is the moment of inertia

The resonance frequency of the cantilever beam is calculated using the following formula:

$$f = 1/2\pi\sqrt{K/M} \tag{2}$$

where

- K is the spring constant
- M is the mass

The spring constant is given by

$$k = \frac{3EI}{L^3} \tag{3}$$

where

- E is the Young's modulus
- I is the moment of inertia
- L is the length of the cantilever beam

Mass is calculated using the following relation

$$\text{Mass} = \text{density} \times \text{volume} \tag{4}$$

where density varies with different materials.

Volume depends on the structure (rectangular, triangular, trapezoidal, etc.) of the cantilever beam. Moment of inertia also depends on the structure of the beam.

Table 5 Mathematical calculation for resonance frequency of different structures

Cantilever structure	Resonance frequency (KHz)	Deflection (N/m ²)
Rectangular	94.87	4.56×10^{-6}
Triangular	77.47	1.37×10^{-5}
T-Shaped	152.13	1.525×10^{-6}

4.1 Verification

Using the PZT material, with stress applied at 0.5 N/m^2 , with length = $60 \text{ }\mu\text{m}$, width = $10 \text{ }\mu\text{m}$, and thickness = $1.5 \text{ }\mu\text{m}$, the resonance frequency and the deflection are calculated and tabulated in Table 5.

From the mathematical verification, it is found that the T-shaped cantilever beam has more deflection and generates more potential.

5 Conclusion

Thus the cantilever structure is analyzed using the COMSOL Multiphysics software and it is found that the T-shaped cantilever has more deflection and generates more potential. The PVDF which is the piezoelectric polymer material is more flexible than the PZT and this PVDF can be used to build the cantilever beam; also the rectangular cantilever fabrication process is performed in IntelliFAB software.

References

1. Mateu L, Moll F. Optimum piezoelectric bending beam structures for energy harvesting using shoe inserts. *J Intell Mater Syst Struct.* 2005;835–45.
2. Mounika Reddy V, Sunil Kumar GV. Design and analysis of microcantilevers with various shapes using COMSOL multiphysics software. *Int J Emerg Technol Adv Eng.* 2013.
3. Salem S, Othman S. Environmental vibration-based MEMS piezoelectric energy harvester (EVMPEH). IEEE Computer Society. 2011c.

Separation of Blood Cells Using Silicon-Based Microfilter

K. Swarnalatha, T. Sripriya and S. Praveenkumar

Abstract This paper reports isolation of white blood cells in a given blood sample using silicon-based microfilter. The types of silicon-based microfilters are weir, pillar, crossflow, and membrane. The membrane microfilter has been explored for the ability of grasping human blood and effectiveness in separating RBCs and WBCs. The membrane filter is embedded with crossflow microfilter design for the purpose of separating the WBCs using COMSOL software. Because the crossflow filter is superior, it can be consolidated alongside downstream constituents for on-chip genomic analysis.

Keywords RBC · WBC · MEMS · Microfilter

1 Introduction

WBCs are irregular in shape, with a nucleus and an outer buffer coat. The size exclusion principle is used for isolation of WBCs and RBCs. In human blood, RBCs are 6–8 μm in diameter and 2–3 μm in thickness. The average diameter of WBCs is 12–15 μm [1–3].

Isolating the plasma from blood samples in order to block the red blood cells (RBCs) is required for blood analysis. A weir-type microfilter is utilized for separating the plasma from the blood sample [4].

K. Swarnalatha (✉) · T. Sripriya · S. Praveenkumar
Department of Electronics and Communication Engineering,
Saveetha Engineering College, Chennai, India
e-mail: k.swarnalatha.ece@gmail.com

T. Sripriya
e-mail: priyasri81@gmail.com

S. Praveenkumar
e-mail: praveenkumarsunil@gmail.com

Acoustophoresis method is used for isolating particles based on their size and density. Isolation of lipids and red blood cells from whole blood using a single-stage acoustophoresis device was recently developed, with the eventual goal to remove the lipid [5].

Direct magnetic isolations of red blood cells from finished blood have been grasped out employing a continuous magnetic separation method [6].

This project focuses on separating the WBC from the RBC using silicon-based microfilter.

2 Designs

The silicon based microfilter has four different types of structures. The structure designs are (1) weir, (2) pillar, (3) crossflow, and (4) membrane reference [6]. In weir filter associate an individual barrier is created to block the flow path of blood sample. It can trap most of the WBCs. RBCs can pass only through a narrow slit placed on the top of the barrier. In pillar filter involves an individual barrier created in a vertical manner for obstructing the flow path of blood sample. Blood is pumped into the device via inlet port and outlet port is for collecting the components of blood that pass through the filter. A rectangular chamber is employed to house the pillar arrays. In the upstream of the pillar chamber, the main microchannel distributes the fluidic flow to uniform and parallel branches. In each branch, an array of pillars is considered for cell isolation. On the downstream side of the pillar chamber, another microchannel collects the filtered sample and directs it to outlet. RBCs can bypass across slim slits amid the pillars only. In crossflow filter involves an individual barrier crafted in horizontal manner for hindering the flow trail of blood sample. It cuts the blood clogging by sweeping the WBCs toward the filter end. Membrane filter does not use the lateral slits, it is exceptional in the sense that the slits or pores are planar starts crafted across a planar layer of substrate. It can distinct particles and molecules and above an expansive particle size scope and molecular weights. The membrane microfilter structure design is used.

3 Simulations

The microfilter was inspected by forecasting their flow velocity profile in simulation software. In this paper COMSOL Multiphysics simulation software which uses the von Mises stress Equation is applied.

Simulation steps are

Step 1: The geometry of the structure is opted as two-dimensional: 2D.

Step 2: Select the microfluidics module. Then select the laminar flow. The work plane for drawing the structure is selected from the geometry option.

Step 3: The structure is desired to thickness, then the desired material has to be selected. Silicon material is chosen for the designed framework.

Step 4: Select the laminar flow. Set the inlet 0.01 m/s.

Step 5: Select the extremely fine mesh.

Step 6: Compute the result.

This microfilter has a number of parallel pillars for WBCs separation from the blood sample. The microfilter width and height are 220, 100 μm as shown in Fig. 1. The pore size is 8 μm and the pillar size is 10 μm . The RBCs size range is below 8 μm . The WBCs size range is above 10 μm . Figure 2 shows the blood flow in the

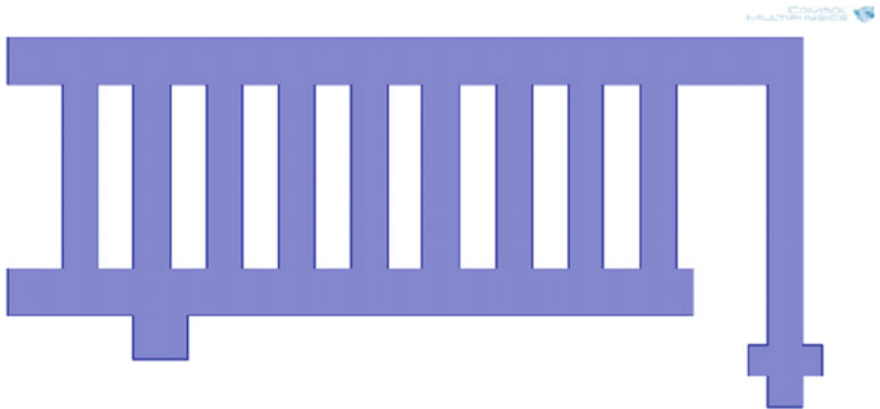


Fig. 1 Structure of a microfilter

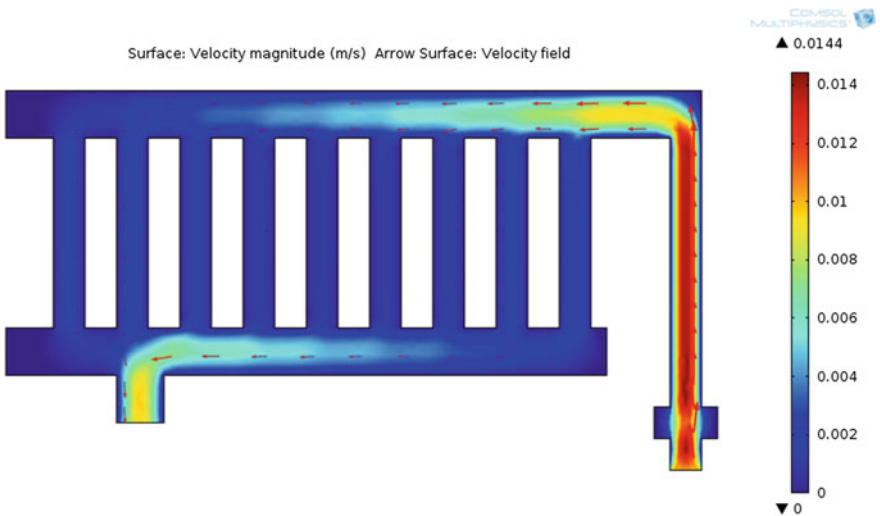


Fig. 2 Simulation output for velocity

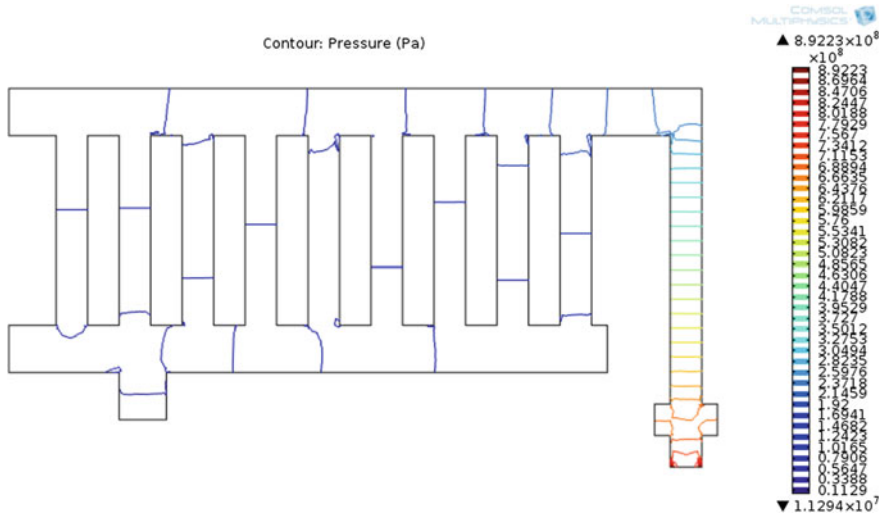


Fig. 3 Simulation output for pressure

Table 1 Measurement of velocity and pressure in microfilter

Inlet velocity (m/s)	Outlet velocity (m/s)	Total velocity (m/s)	Outlet pressure ($\times 10^8$ Pa)	Total pressure ($\times 10^8$ Pa)
0.01	0.006	0.0144	0.1412	2.2306
0.02	0.01	0.0288	0.2824	4.4612
0.03	0.015	0.0432	0.4235	6.6917
0.04	0.02	0.0576	0.5647	8.9223

microfilter and the flow velocity of the microfilter. The blood sample and buffer solution can be added to the inlet. Microfilter can efficiently trap WBCs and passes RBCs. Figure 3 shows how much pressure is present in the microfilter. Phosphate buffered saline (PBS) is a buffer solution usually utilized in biological research. The buffer helps to uphold a steady pH. Usually a pH of 7.4 is managed.

The inlet velocity is given and the corresponding outlet velocity and total velocity are increased. The inlet velocity is given and the corresponding pressure and total pressure are increased. These are shown in Table 1.

4 Theoretical Analyses

A fluid field has irrotational flow. The velocity (V) can be expressed as the gradient of the scalar quantity (ϕ). The velocity potential for incompressible flow can be expressed as [7]

$$\nabla \cdot u = \nabla^2 \phi = 0 \tag{1}$$

The potential flow can be evaluated using (1) with the appropriate boundary conditions, and the gravitational force on the cell can be calculated by [6]

$$F_g = -g(\rho_p - \rho_f)V \tag{2}$$

F_g means gravitational force on the cell, g is the gravitational constant, V represents a volume of the fluid, ρ_p represents the density of a particle, ρ_f represents the density of the fluid. Gravitational force on the RBCs is high compared to WBCs. So the microfilters can efficiently pass the RBCs through the microfilter. The hydrodynamic drag force on the cell at zero flow can be calculated as [7]

$$F_d = -6 \pi \eta bV \tag{3}$$

Hydrodynamic means dealing with the motion of fluid. F_d , represents hydrodynamic drag force on the cell at zero flow. Here ηb and V are the viscosity, radius of the particle, and particle velocity. Sedimentation velocity can be calculated as

$$U_s = (2/9) ((\rho_p - \rho_f)/\mu)g(a^2) \tag{4}$$

Sedimentation velocity means sedimentation rate for the particle of a given size and shape measures how fast the particle settles. In laminar flow, Reynolds number is less than 2000. In this project, Reynolds number of fluid flow is below 2000. So laminar flow is used in simulation of COMSOL multiphysics. Reynolds number is calculated as

$$Re = (\rho V \eta)/\eta \tag{5}$$

Maximum flow rate can be calculated as

$$\text{Maximum flow rate} = \rho \times V \tag{6}$$

Flow rate means the volume of fluid which passes per unit time. ρ and V are represented as density and velocity of the fluid.

The inlet velocity is increased when the maximum flow rate also increased. This is shown in Table 2.

Table 2 Maximum flow rate in microfilter

Inlet velocity	Maximum flow rate
0.01	15.264
0.02	30.528
0.03	45.792
0.04	61.056

5 Fabrications

IntelliSuite has many different modules. IntelliFAB is essentially to make the virtual fabrication. So IntelliFAB module is used for virtual fabrication of microfilter. It consists of four different process flows. The process flow is used to form the basis for creating the devices. The process flows are definition, deposition, bonding, and etching.

IntelliFAB is undeviatingly related alongside MEMS physical, a MEMS procedure database that accumulates physical properties for the purpose of contraption settings. Growing the fabrication procedure in conjunction alongside the scrutiny ideal, IntelliSuite enables to present extra precise mechanism, physics scrutiny, and produce manufacturable mechanisms faster.

The below steps are involved in the fabrication of microfilter,

Step 1: Defining silicon substrate (50 μm) with 100 orientations.

Step 2: Depositing the photoresist PR (AZ5214) (300 nm) using spin coating on the substrate.

Step 3: Defining the pattern on the photoresist material using UV radiation.

Step 4: Etch the photoresist material (300 nm) using wet etching.

Step 5: Etch silicon substrate (50,000 nm) using wet etching.

Step 6: Etch the photoresist material (300 nm) using wet etching.

Step 7: Deposition of SiO_2 (3000 nm) on the silicon substrate.

Step 8: Spin coating technique is used for depositing the PR (AZ5214)(300 nm) photoresist.

Step 9: Defining the pattern on the photoresist material using UV radiation.

Step 10: Etch photoresist material PR (AZ5214) (300 nm) using wet etching.

Step 11: Etch silicon dioxide using (3000 nm) wet etching.

Step 12: Etch the photoresist material PR (AZ5214) (300 nm) using wet etching.

Step 13: Depositing the photoresist PR (AZ5214) (300 nm) using Spin coating technique.

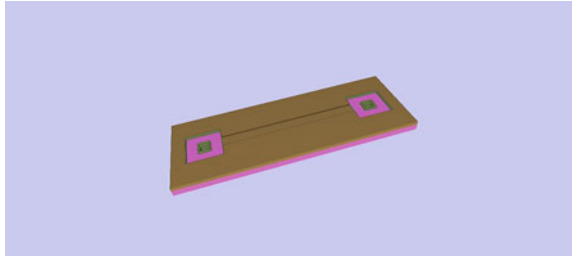
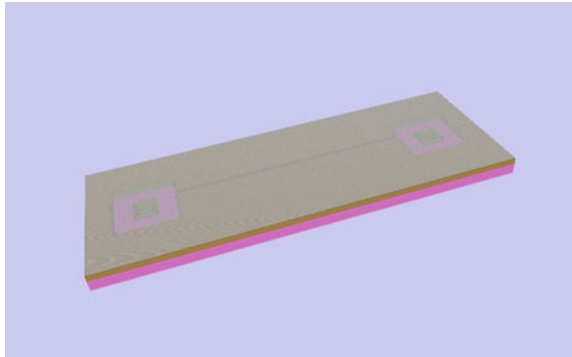
Step 14: Defining the pattern on the Photoresist material (300 nm) using UV radiation.

Step 15: Etch photoresist material PR (AZ5214) (300 nm) using wet etching.

Step 16: Etch silicon dioxide (1500 nm) using wet etching.

Step 17: Etch the photoresist material PR (AZ5214) (300 nm) using wet etching.

Figure 4 shows the microfluidic sieve. It consists of channels between the inlet and outlet. Figure 5 shows a microfluidic sieve with glass. For environmental protection, the microfluidic sieve is covered with glass.

Fig. 4 Microfluidic sieve**Fig. 5** Microfluidic sieve with glass

6 Conclusions

The microfilter is designed using COMSOL software; silicon is used as material for developing this design. The design is developed using the IntelliFAB. The microfilter is developed for separating WBCs from the whole blood. The developed design is used for application of treatment for the effectiveness of chemotherapy or radiation treatment in cancer patients, immune deficiencies, and blood disorders.

7 Future Works

The projected microfilter will be fabricated employing Intellifab module. INTELLIFAB module is utilized for adjacent fabrication. INTELLIFAB includes FAB Viewer, an easy-to-use procedure and visualization instrument that permits users to swiftly visualize a procedure flow crafted in IntelliFab. The skill to think cross serving at each slant or orientation makes it facile to debug the procedure or present a wreck analysis.

Acknowledgments I would like to take this opportunity to express my sincere gratitude to all my professors who have guided, inspired, and motivated me for my project work. It gives me immense pleasure to acknowledge their cooperation.

References

1. Kim Y, Kim K, Park Y. Measurement techniques for red blood cell deformability: recent advances. *INTECH J.* 2012. doi:10.5772/50698.
2. <http://www.healthype.com/red-blood-cells-functions-size-structure-life-cycle-pictures.html>.
3. <http://www.anatomyatlases.org/MicroscopicAnatomy/Section04/Section04.shtml>.
4. Wu C, Hong L-Z, Ou C-T. Blood cell-free plasma separated from blood samples with a cascading weir-type microfilter using dead-end filtration. *J Med Biol.* 2011;163–8.
5. Nicpon MD, Rust MJ, Lipkens B. Multi-stage acoustophoretic separation of particles from blood. In: 39th annual northeast bioengineering conference; 2013. p. 291–2.
6. Takayasu M, Kolland DR, Minervini JV. Continuous magnetic separation of blood components from whole blood. *IEEE Trans Appl Super Conduct.* 2000;10(1):927–30.
7. Ki Back M, Soon Choi H, Ki Sik L, Pack H. Numerical analysis for magnetophoretic separation of blood cells in fluid and magnetic field. *IEEE Trans Appl Superconduct.* 2012;22(3).

Optimal Image Enhancement Method Based on Histogram Analysis

S.J. Monisha Selas and E.T. Jaba Jasphin

Abstract In this paper, a generalized equalization method is proposed for image enhancement. In digital cameras, the image is stored as a raw image file, which has wider dynamic range and preserves much information about the captured image so that the bit-length will be too long for normal display. The image can be converted into suitable dynamic range by tone mapping method. This method maps a set of colors into another to approximate the high dynamic range images. Tone mapping algorithms uses two techniques, they are white balancing and contrast enhancement. The proposed method uses both white balancing and contrast enhancement method as a combined framework. This method analyzes the relationship between histogram and white balancing/contrast enhancement. The enhancement method is focused on haze images. Simulation results show better performance in image enhancement.

Keywords Image enhancement · Histogram · Tone mapping · White balancing · Contrast enhancement

1 Introduction

In day-to-day life, millions of images are being created. Sometimes, due to unfavorable climate conditions and damages in imaging devices, the captured images may not be clear. Hence, image enhancement has to be done in order to improve the quality of the image. In traditional method, white balancing and contrast enhancement method are done separately but in the proposed method, these

S.J. Monisha Selas (✉) · E.T. Jaba Jasphin
Department of Electronics and Communication Engineering,
Saveetha Engineering College, Chennai, India
e-mail: selasmoni@gmail.com

E.T. Jaba Jasphin
e-mail: jabajasphin@gmail.com

methods are combined together. In [2], a novel algorithm is proposed for restoration. The advantage of this method is its speed due to less complexity. However, this method cannot be applied to real images because there is no reference for these images. For removing a haze from an image, a dark channel prior method is proposed in [1]. A dark channel prior specifies at least one color channel has very low intensity at some pixels. This method is simple but it cannot be used for objects that are similar to atmospheric light. A pixel with highest intensity is used as atmospheric light. For restoring weak blur and strong noise images, an adaptive sharpening method is proposed in [4]. This method uses local image structure for denoising and sharpening process. In [3], optimal contrast-tone mapping is used for image enhancement which maximizes the contrast gain. The enhancement is based on contrast enhancement. This method causes tonal distortion.

2 White Balancing

White balance is one of the settings in camera that adjusts lighting in order to make white objects appear white in photos. White balancing is one of the image enhancement methods but it has a problem of color constancy. The relationship between color constancy and histogram of the image is established using this process.

An image can be considered as $f = (f_r, f_g, f_b)^T$. The dynamic range of f_c is $[0, L_c]$ where $c = r, g,$ and b and L is the upper bound of intensity. Let $\{h_c, p_c\}_{c=r,g,b}$ be the histogram of the image. Then, the histogram of original image is $\{\tilde{h}_c, p_c\}_{c=r,g,b}$ and the histogram of enhanced image is $\{\tilde{h}_c, p_c\}_{c=r,g,b}$. The distance between the adjacent intensity levels is given as $s_{ck} = h_{ck} - h_{c,k-1}$ where $k = 2, \dots, K$ and $s_{c1} = h_{c1}$ for $k = 1$. Also K is the number of intensity levels whose probability value is non-zero.

The image is expressed in Lambertian surface model as

$$f_c = \int r(\lambda)l(\lambda)m_c(\lambda)d\lambda \tag{1}$$

where, $r(\lambda)$ is the surface reflectance, $l(\lambda)$ is the light source, $m_c(\lambda)$ is the sensitivity of the camera in the channel c and λ is the wavelength of visible light.

The light source for original image can be expressed as

$$e_c(\alpha) = \frac{(p_c^T \tilde{h}_c^\alpha)^{\frac{1}{\alpha}}}{\sqrt{\sum_{c=r,g,b} (p_c^T \tilde{h}_c^\alpha)^{\frac{2}{\alpha}}}} \tag{2}$$

where, p_c is the probability of the intensity level and \tilde{h}_c is the intensity level of original image.

The histogram of white balancing can be expressed in terms of the intensity level of the enhanced image and is given by

$$\hat{h}_c = \frac{1}{e_c \alpha \sqrt{3}} \tilde{h}_c \quad (3)$$

Here, white balancing is the linear transform of histogram. Hence, it has zero nonlinearity.

3 Contrast Enhancement

Contrast enhancement can automatically brighten the image that appears to be dark or hazy. It calculates the difference between the maximum and minimum intensity of the pixel in an image. The contrast can be increased by expanding the difference in the maximum and minimum pixel values. By increasing the contrast of the image, brightness increases only in some areas and decreases in other areas; hence, light areas become lighter and dark areas become darker.

The contrast of an image can be expressed in [3] by

$$C = P_c^T s_c \quad (4)$$

where p_c is the intensity level and s_c is the distance of the adjacent intensity levels of original image.

The contrast enhancement can be done by maximizing (4) and is given by

$$\hat{s}_c = \arg \max_{s_c} P_c^T s_c \quad (5)$$

In previous work, histogram-based analysis is done for contrast enhancement. The most commonly used method in histogram analysis is histogram equalization. This method tends to make the probability density function of the enhanced image similar to uniform distribution. Hence, the intensity level of the image can be expressed as

$$h_{c1} = C \sum_{j=0}^i P_{cj} \quad (6)$$

where, C is a constant. Hence, the histogram equalization can be obtained by solving the optimization problem as follows

$$\hat{s}_c = \arg \max_{s_c} \frac{1}{\|P_C^{-1} s_c\|} \quad (7)$$

Here, the contrast enhancement is the nonlinear transform of histogram. Hence, it has strong nonlinearity. This is the major difference between white balancing and contrast enhancement.

4 Generalized Equalization Model

The main aim of the proposed method is to unify both white balancing and contrast enhancement into a single framework. The generalized equalization model can be mathematically formulated as follows:

$$\hat{s}_c = \arg \min_{s_c} \sum_{c=r,g,b} \|P_c^{-\beta} s_c\| \quad (8)$$

where P_c is the diagonal matrix of p_c , β is the parameter for nonlinearity and s_c is the distance of adjacent intensity levels of original image.

The entropy of the image can be calculated as

$$\sum_{i=0}^n p_i \log p_i \quad (9)$$

where p_i represents the pixel values and n is the total number of pixels. Along with entropy, cross-correlation is also determined. For a good quality images, the cross-correlation value is near to one.

One of the advantages of this method is its high efficiency than the existing methods. This combined method increases the quality of the image. Also decreases the tonal distortion which is a property of an image in which the contrast, brightness range or color that appear different from the original image. Tonal distortion is due to some of the following factors such as using special filters, light source which cannot be balanced by film, reciprocity failure of color balance, and so on.

5 Simulation Results

The results for the proposed method are shown in this section. The proposed method uses only three parameters for controlling the behavior and performance of the method. The parameters used are norm (n), nonlinearity (β), and color constancy (α). If the value of β is a small positive number then both white balancing and contrast enhancement can be combined into a unified framework.

The input image is a haze image which is affected by snow, fog, or smoke is shown in Fig. 1. The images are taken from the database. Haze is an atmospheric

Fig. 1 Input image

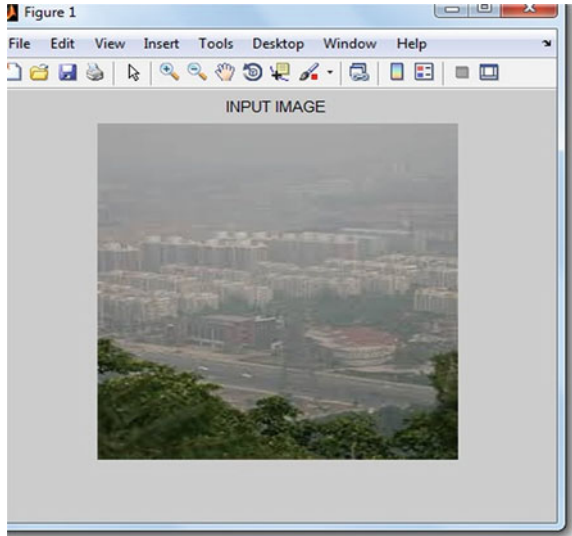
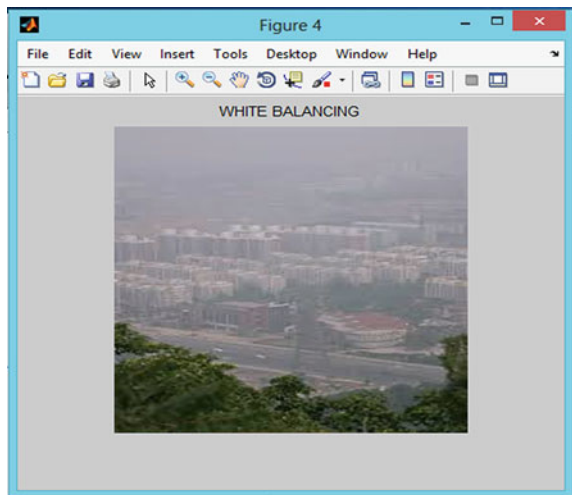


Fig. 2 White balancing output



phenomenon in which dust, smoke, and any other dry particles degrade the clarity of the image.

White balancing is a process in order to balance the color. White balancing provides many settings in different lighting conditions. The output of white balancing is shown in Fig. 2. The histogram of white balancing denotes that the intensity has been high in some areas as shown in Fig. 3.

Fig. 3 Histogram of white balancing

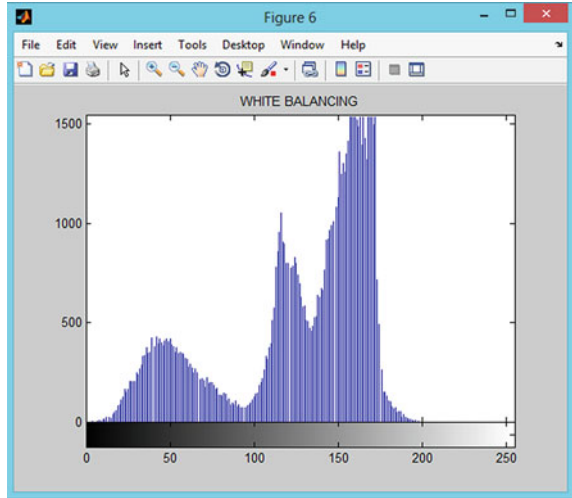
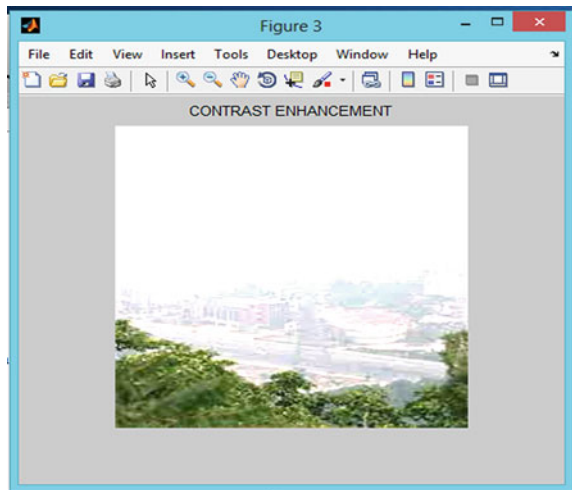


Fig. 4 Contrast enhancement output



Contrast enhancement is used to enhance the contrast of the image. Contrast is the difference between the dark and light areas of the image. By increasing the contrast, light areas become lighter and dark areas become darker as shown in Fig. 4, which is the output for contrast enhancement. Figure 5 shows the histogram of the contrast enhancement.

Fig. 5 Histogram of contrast enhancement

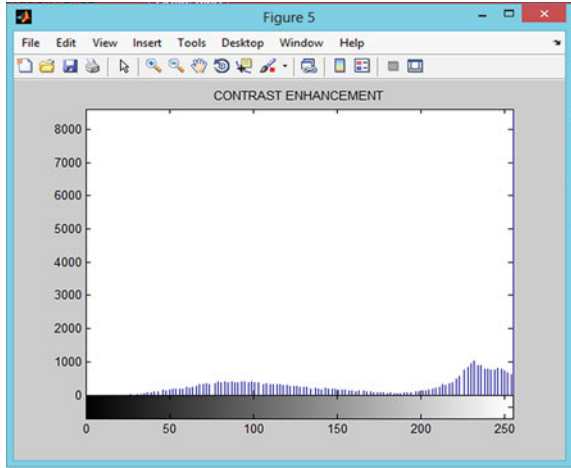
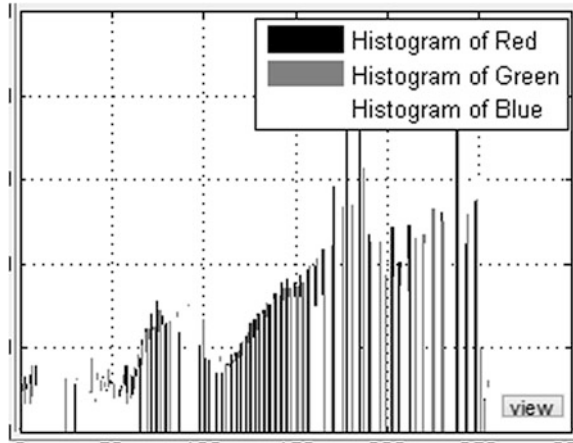


Fig. 6 Output of the proposed method



The output of the proposed image is shown in Fig. 6. The histogram of the proposed method is shown in Fig. 7 in which it has been equalized among the pixels by three components that is red, green, and blue. The proposed method shows better performance and also increases the quality of image that is degraded by haze.

Fig. 7 Histogram of the proposed method



6 Conclusion

A generalized equalization model for image enhancement is established. Thus, the relationship between image histogram and contrast/tone was analyzed. The images that are degraded due to unfavorable weather conditions such as haze images are retained by the proposed model. The proposed method can be used in many applications such as contrast enhancement, tone correction, white balancing, and for postprocessing in dehazed images.

Acknowledgments I would like to take this opportunity to express my sincere gratitude to all my professors who have guided, inspired, and motivated me for my project work. It gives me immense pleasure to acknowledge their cooperation.

References

1. He K, Sun J, Tang X, Single image haze removal using dark channel prior. In: IEEE international conference computer vision and pattern recognition; 2009. p. 1956–1963.
2. Tarel JP, Hautiere N. Fast visibility restoration from a single color or gray level image. IEEE international conference on computer vision; 2009. p. 2201–2208.
3. Wu X. A linear programming approach for optimal contrast-tone mapping. IEEE Trans Image Process. 2010;20:1262–1272.
4. Zhu X, Milanfar P. Restoration for weakly blurred and strongly noisy images. In: IEEE Workshop Applications of Computer Vision; 2011. p. 103–9.

Epileptic Seizure Characterization Using Transform Domain

Sushree Sangita Biswal, Itishree Biswal
and Mihir Narayan Mohanty

Abstract In case of epileptic seizure, the subject usually maintains silence. Sometimes it cannot be identified whether the subject is silent or has been attacked by epilepsy. In this paper, authors have taken an attempt to distinguish among these two cases. The approach is very simple and does not make any complicity by introducing the classifiers. It is based on the efficient features only. Initially, the spectral features have been obtained using Fourier transform and chirp Z-transform. Further for characterizing the specific frequency, the time-frequency analysis using wavelet transform has been done with the cepstral coefficients depicted in the result. The cepstrum of the said EEG signals shows clearly the difference among them. Fast Fourier transform (FFT), chirp Z-transform (CZT) and discrete wavelet transform (DWT) have been exploited to characterize the signals.

Keywords EEG · Characterization · FFT · CZT · DWT

S.S. Biswal · M.N. Mohanty (✉)
Department of Electronics and Communication Engineering,
Institute of Technical Education and Research, Siksha 'O'
Anusandhan University, Bhubaneswar, Odisha, India
e-mail: mihirmohanty@soauniversity.ac.in

S.S. Biswal
e-mail: sushree.in.sangita@gmail.com

I. Biswal
Department of Computer Science Engineering,
Institute of Technical Education and Research, Siksha 'O'
Anusandhan University, Bhubaneswar, Odisha, India
e-mail: iti.in.biswal@gmail.com

1 Introduction

An unexpected electrical disturbance in the brain signal may refer to the epilepsy and seizure. Generally, 1–2 % of persons will suffer from an experience of a seizure. This may lead to the occurrence of a seizure that is not predictable, totally through the progression. In the case of long recordings, visual scanning of EEG recordings for the spikes and seizures is very time consuming and complex, as biosignals are highly subjective so disagreement on the same record is possible. So the EEG signal parameters that can be extracted and analyzed using computers are highly useful in diagnostics [1, 2].

A powerful method, the wavelet transform was proposed in the late 1980s to perform time-scale analysis of signals. This method offers a theoretical account for different techniques that have been acquired for several applications. One of the useful properties of WT is that it is appropriate for analysis of nonstationary signals, which represents a major advantage over spectral analysis. Hence the WT is well, can be used to locate transient events. Such transient events such as spikes can occur during epileptic seizures [2, 3].

The silent condition in a human subject means if the person may be in a senseless condition or sleep condition [4, 5]. These conditions can be observed from the human brain signal, (i.e., EEG signals). An electroencephalogram (EEG) is a test that measures and records the electrical activity of the brain. The usual method to perform the test is to place the electrodes along the scalp that will transmit the obtained information to a recorder machine. The amplitude of the EEG is about 100 μV when measured on the scalp, and is about 1–2 mV when measured on the surface of the brain. The clinically relevant bandwidth of this signal varies from 1 Hz to around 50 Hz [6]. With this method, it is possible to determine the activity on a specific location within the brain and evaluate brain disorders that are the most common reasons to diagnose and monitor seizure disorders. EEGs can also be helpful in identifying the causes of other problems such as sleeping disorders and changes in behavior. EEGs are sometimes useful for measuring brain activity after a grievous brain injury, or before heart or liver transplantation. The patient needs to be made aware about his behavior during the process. By laying him on a bed or by making him sit on a chair, he has to be made relaxed and perhaps, he will be required to close the eyes and be still during the exam. Depending on the test there is a possibility of utilizing some character of the subject or breathe quickly [7].

There are five major brain waves that can be separated by their different frequency ranges. These frequency bands varying from low to high frequencies respectively are called alpha (α), theta (θ), beta (β), delta (δ), and gamma (γ) [8]. The higher activity of gamma wave is followed by a less strain, not on the mind. The alpha waves are active, if human is in a relaxed but aware state. The strongest brain activity is the delta wave. It is characterized by a very low frequency up to 4 Hz and an amplitude higher than 100 μV . The delta waves are usually associated with the deepest stages of sleep or meditation and aid in characterizing the depth of sleep. The theta waves are activated during a mediation, trance, hypnosis, intense dreams, and intense

Table 1 The summary of basic human brain waves

Name of the wave	Frequency (Hz)	Typical amplitude (μV)
Delta	0.1–4	100–200
Theta	4–8	Higher than 30
Alpha	8–13	30–50 or higher
Beta	13–30	2–20 or higher
Gamma	40–80	3–5 or higher

emotions. The theta state is closer to relaxation state. The difference is not much but is clear. The beta waves are responses of a human brain on the excited state [8]. Table 1 indicates the summary of different waves of EEG signals.

Over the past two decades, the use of conventional temporal and frequency analysis is used for measuring the detection of epileptic form activity in EEGs and have obtained appreciably good results. In the epileptic zone, the data obtained by analyzing the ictal EEG events in comparison with the clinical and interictal EEG features, indicates an asymmetric EEG pattern, hence indicating the localized cortical origin of the Ital. But considerable research has been progressed for alcoholic state analysis. Similarly deep meditation state has been analyzed by some authors. However, silence state belongs to all these conditions that has not been analyzed. In this work, the silence state has been considered with normal and epileptic cases.

An effort has been made to characterize the EEG signal by using the spectral methods such as fast Fourier transform, chirp Z-transform and wavelet transform. The paper has the following contents. Section 2 refers to the experimental setup for data collection. The methodology has been exploited in Sect. 3. In Sect. 4, the result has been discussed and in Sect. 5, this piece of work is concluded.

2 Experiments for Data Collection

The EEG data is acquired from the hospital using international 10–20 system as per need. Six electrodes have been applied in the EEG recordings. The signals from corresponding electrodes are taken for testing the classification with each of the above databases. There are 150,000 samples of normal/silent signal, 1400 samples of epileptic signal recorded at 512 Hz sampling frequency from each electrode for a process carrying out any of the above actions. The frontal lobe is associated with planning, reasoning, movement, emotion, and problem solving etc. The parietal lobe is associated with movement, recognition, perception of stimuli, etc. The temporal lobe is associated with recognition and perception of auditory stimuli, memory, and speech. So, as per the requirement for this study, the EEG signal is picked up from the following locations: F3, F4, T3, T4, P3, and P4 following the international 10–20 systems [9]. The signals from corresponding electrodes are required to carry the classification task. 2500 samples of the signals recorded from

each of the six electrodes for each of the above two tasks. All the signals are of silent state of human subject. The two states as silent (normal) and epileptic have been analyzed and depicted in following Sect. 3.

3 Methodology

The method is based on spectral analysis. Basically, the methods FFT, CZT, WT, and many other techniques are used for such analysis. Some of them are used in this case and is explained as follows.

3.1 Fast Fourier Transform (FFT)

The most used quantitative method for the analysis of EEG signals that is a spectral analysis based on Fourier Transform. Moreover, it is important as a diagnostic tool. Fourier Transform allows the separation and study of different EEG rhythms that refers to a task difficult for performing visually when several rhythms occur simultaneously [9, 10]. The amplitudes and phases of the sinusoidal components can be estimated using the FFT and is represented mathematically as;

$$X(k) = \frac{1}{N} \sum_{n=0}^{N-1} x(n) e^{-j(2\pi kn/NT)} \quad (1)$$

For a given biosignal $x(n)$ whose sampling period is T with N number of total samples (NT is therefore the total duration of the signal segment). The spectrum $X(k)$ is estimated at multiples of f_s/N , where f_s is the sampling frequency.

3.2 Chirp Z-Transform (CZT)

The Chirp Z-transform is commonly known as Bluestein's FFT algorithm. As it is an FFT algorithm, it computes the discrete Fourier transform (DFT) of arbitrary sizes (including prime sizes) by re-expressing the DFT as a convolution. Bluestein's algorithm can also be used for the computation of a more general transform based on the (unilateral) Z-transform [9–11]. In particular, it can be used for computation of any transform into the form:

$$X_k = \sum_{n=0}^{N-1} x_n z^{nk} \quad k = 0, \dots, M-1 \quad (2)$$

For arbitrary complex numbers and for differing numbers N and M of inputs and outputs. By observing the spectral characteristics of the signal, it can be recognized and analyzed easily.

3.3 Wavelet Transform (WT)

Wavelet transform method splits up the signal into a number of signals. It can be considered as a mathematical microscope. In the wavelet method, the same signal corresponds to different frequency bands. It only informs what frequency bands exist at what time intervals. It is developed to overcome the shortcomings of Fourier transform [12].

The continuous wavelet transform (CWT) of a function $f(t)$ with respect to some local base function (wavelet) ψ is defined as

$$W(a, b) = W_w f(b, a) \frac{1}{\sqrt{a}} \int_{-\infty}^{\infty} f(t) \psi^* \left(\frac{t-b}{a} \right) dt, \quad a > 0 \quad (3)$$

Where ψ^* is the complex conjugate of ψ . The parameter b and a are called as translation (shifting) and dilation parameters, respectively. The wavelet behaves like a window function. At any scale a , the wavelet coefficients $W(a, b)$ can be obtained by convolving $f(t)$ and a dilated version of the wavelet. To be a window and to recover from its inverse wavelet transform (IWT) $\psi(t)$ must satisfy

$$\psi(0) = \int_{-\infty}^{\infty} \psi(t) dt \quad (4)$$

Although, $W(a, b)$ provides space-scale analysis rather than space-frequency analysis, proper scale-to-frequency transformation allows analysis that is very close to space-frequency analysis. Reducing the scale parameter ' a ' reduces the support of the wavelet in space and hence covering higher frequencies and vice versa therefore ' $\frac{1}{a}$ ' is a measure of frequency. The parameter ' b ' indicates the location of the wavelet window along the space axis there by changing (a, b) enabling computation of the wavelet coefficients $W(a, b)$ of the entire frequency plane.

Scalograms are the graphical representation of the square of the wavelet coefficients for the different scales. They are the isometric view of sequence of the wavelet coefficients verses wavelength. A scalogram clearly shows more details and identifies the exact location at a particular depth, and detects low frequency cyclicity of the signal. The scalogram surface highlights the location (depth) and scale (wavelength) of dominant energetic features within the signal, say of gamma rays, bulk density, and neutron porosity of a well log. The combinations of the various vectors of coefficients at different scales (wavelengths) form the scalogram.

3.4 Cepstrum Analysis

Many clinical studies have shown that the EEG spectrum is highly related to the DoA. These results give an inspiration, the idea that the power spectral density (PSD) of the EEG signal itself can be used as a feature vector. However, using the spectrum itself as a feature vector may have some limitations [13]. The mathematical definition of cepstrum is given as follows:

$$\text{Cepstrum} = \left| \text{DCT} \left\{ \log \left\{ \left| \text{FT} \{ \text{Epoch} \}^2 \right| \right\} \right\} \right|^2 \tag{5}$$

4 Result and Discussion

4.1 Spectral Analysis

For this work first, we have analyzed the FFT of the two conditions, (i.e., silent and epileptic) by using FFT, CZT, and WT as shown. In Fig. 1 more frequency varies in between 100–130 and 210–240 samples and in Fig. 2 more frequency varies in between 130–140 samples and 250–256 samples. Figures 3 and 4 show the CZT and also find the different frequency range in two different conditions in Fig. 3. The

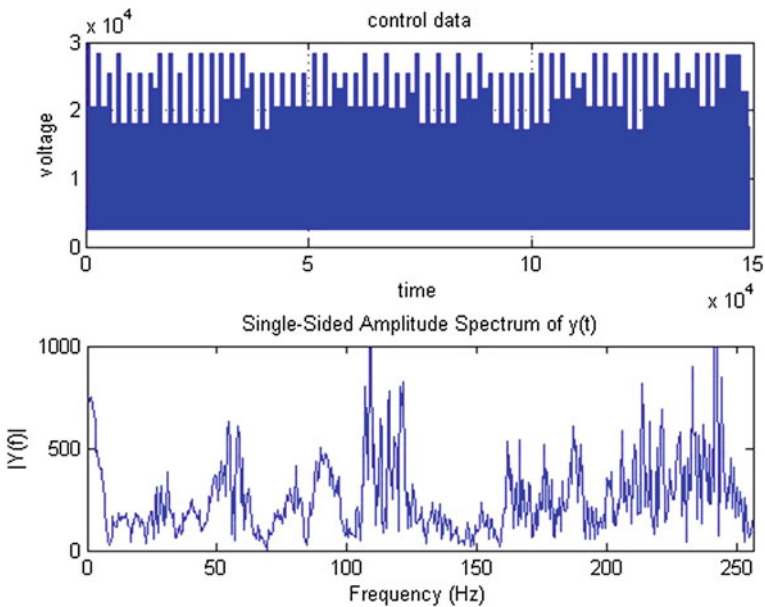


Fig. 1 FFT of the silent EEG signal

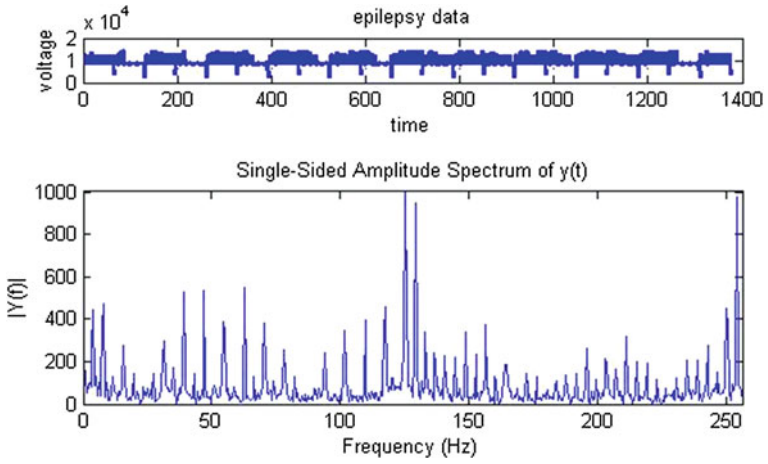


Fig. 2 FFT of the epileptic EEG signal

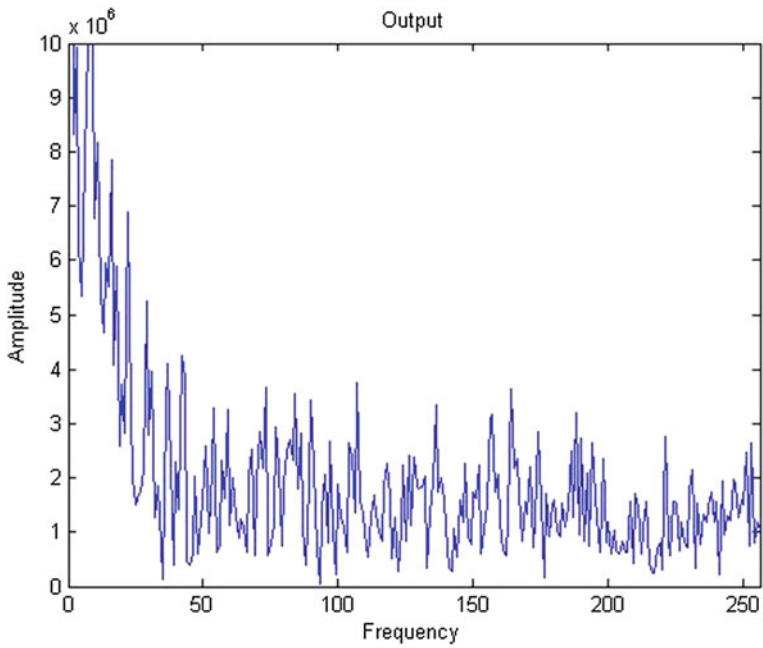


Fig. 3 Chirp Z-transform of silent EEG signal

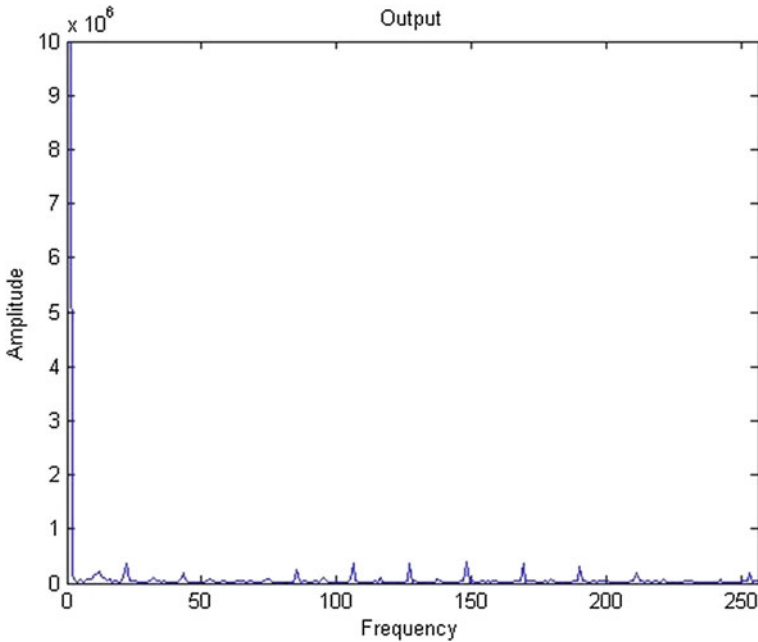


Fig. 4 Chirp Z-transform of epileptic EEG signal

frequency range varies from 0 to 30 samples. Also in Fig. 4 more frequency varies in between 0–10 and 80–90 samples.

The result of chirp Z-transform is more suitable for analyzing the spectrum than the FFT. The FFT and chirp Z-transform are not suitable to know the time information as it only gives the frequency information so we used wavelet transform for better analysis. In this case, we have found both time and frequency information as shown in the above figures. Here the WT is more suitable, because we can vary the window size. If the window size is large, then the frequency resolution is good and the time resolution is bad. If the window size is small then the frequency resolution is bad and time resolution is good. Figures 5 and 6 show the result of wavelet transform, where the frequency and time changes are clearly observable. These four figures are different for two cases.

4.2 Cepstrum Analysis

For this work, first we have analyzed the cepstrum analysis of the two conditions, (i.e., silent and epileptic) as shown; From Figs. 7 through 8 the cepstrum is shown and also found the different frequencies range in different two conditions. In Fig. 7 the amplitude of the cepstrum 0.7 at quefrequency 3 ms and also in Fig. 8 the amplitude

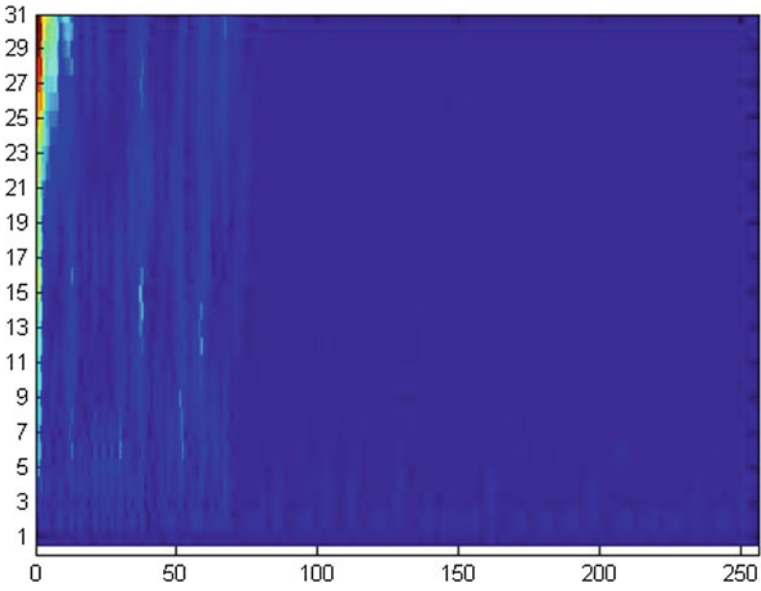


Fig. 5 Wavelet Transform of silent EEG signal

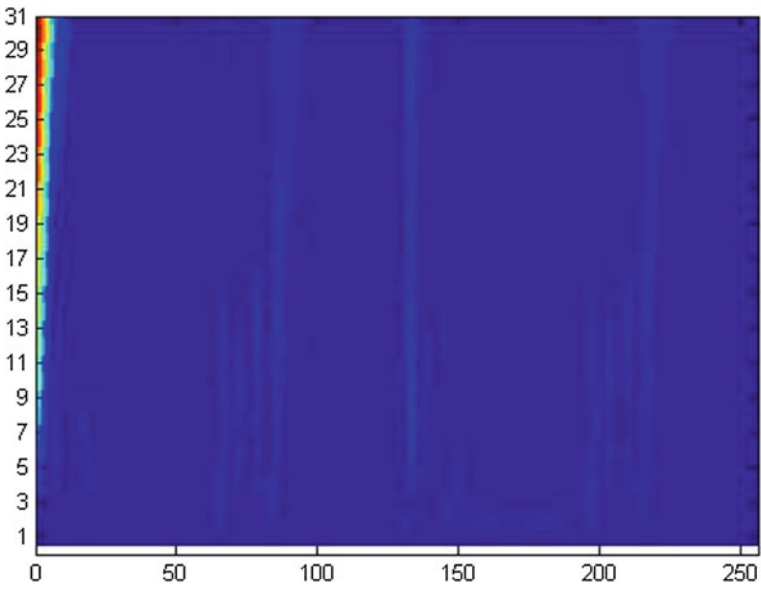


Fig. 6 Wavelet Transform of epileptic EEG signal

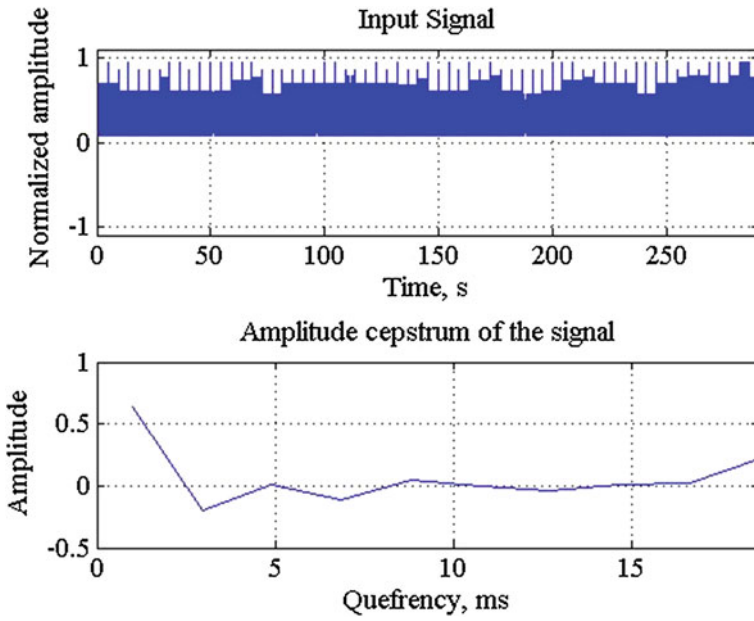


Fig. 7 Spectral analysis of silent EEG signal

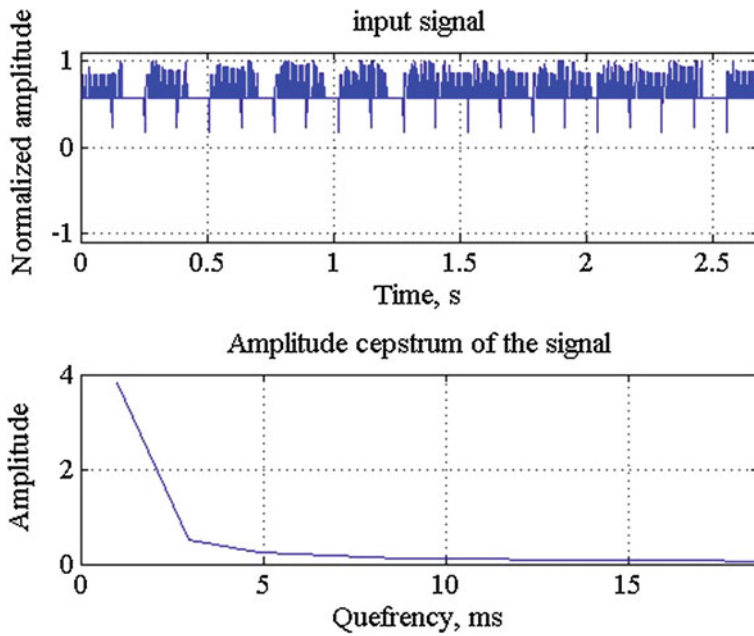


Fig. 8 Spectral analysis of epilepsy EEG signal

of the cepstrum is 3.9 at quefrequency 4 ms is found. In between these two figures, there are different in range in epileptic case but there is no much variation in cepstrum but in silent case there are many variations as shown in figures.

5 Conclusion

We have shown the frequency component based on the Fourier transform and chirp Z-transform and their comparison pictorially. Similarly, the wavelet transform is used for time-frequency analysis as the signal is non-stationary. Using the Cepstral method, the epileptic seizure is clearly visible. Therefore, the difference between silence and epileptic subjects is clearly detected. For the future work, the high frequency component as well as the sudden change in the signal may be evaluated. So, the extension of this work may help the physicians in clinical diagnosis.

References

1. Iasemidis LD, Shiao DS, Chaovalitwongse W, Sackellares JC, Pardalos PM, Principe JC. Adaptive epileptic seizure prediction system. *IEEE Trans Biomed Eng.* 2003;50(5):616–27.
2. Mohseni HR, Maghsoudi A, Shamsollahi MB. Seizure detection in EEG signals: a comparison of different approaches, Biomedical Signal and Image Processing Laboratory (BiSIPL), Sharif University of Technology, Tehran. Iran.
3. Kiyimik MK, Akin M, Subasi A. Automatic recognition of alertness level by using wavelet transform and artificial neural network. *J Neurosci Methods.* 2004;139(2):231–40.
4. Biswal SS, Mohanty MN, Sahu B, Das S. Unconscious state analysis using intelligent signal processing techniques. In: 17th Odisha Bigyan congress, national seminar on science and technology for human Development, Accepted, 2014.
5. Biswal SS, Behera R, Mohanty MN Spectral characterization of brain signal under silent state. In: IEEE sponsored 2nd international conference on electronics and communication systems (ICECS); 2015.
6. Health Library. <http://healthlibraryepnet.com/>.
7. Sanei S, Chambers JA. EEG signal processing, centre of digital signal processing Cardiff University, UK, Wiley, The Atrium, Southern Gate, Chichester, West Sussex PO19 8SQ, England; 2007.
8. Cooper R, Osselson JW, Shaw JC. EEG technology, 2nd edn. Butterworth, London; 1969. p. 275.
9. Proakis JG, Manolakis DG. Digital signal processing, 4th edn. Pearson Education 7 April 2006.
10. Mohanty MN. Bhagyalaxmi Jena: Analysis of stressed human speech. *Int J. Comput Vision Robot.* 2011;2(2):180–7.
11. Rangayam R. Biomedical signal analysis. New York:Wiley.
12. Mallat S. A wavelet tour of signal processing, Academic Press, 2008.
13. Kim T-H, Yoon Y-G, Uhm J, Jeong D-W, Yoon SZ, Park S-H. A cepstral analysis based method for quantifying the depth of anesthesia from human EEG. In: 35th Annual international conference of the IEEE EMBS Osaka, Japan, 3–7 July 2013.

WSN Backbone Formation Using Non-probabilistic Spanning Tree Algorithm

Rachita Nagpal and Roopali Garg

Abstract Wireless sensor network (WSN) consists of battery operated sensor nodes that are used to communicate information among nodes in the network. A large WSN network is often difficult to analyze due to its complexity. Analysis of such networks requires the use of graph sampling techniques. Graph sampling helps in obtaining a sample graph that has properties similar to that of the original graph. Graph sampling algorithms show biasness towards high degree nodes. For taking into account the low degree nodes, we propose to use a spanning tree protocol that helps in obtaining an efficient connected graph. Use of spanning tree protocol provides a tree-based structure to the graph which can then be used to obtain a sampled graph offering better connectivity. To analyze such networks, we implement the concept of non-probabilistic spanning tree along with default connecting dominating set (CDS) strategy. The existing solution takes into account only the construction of the backbone nodes. In this paper, we use the concept of non-probabilistic spanning tree approach that provides better connectivity, which is then used to construct the backbone resulting in energy conservation.

Keywords Spanning tree · Non-probabilistic spanning tree algorithm · Graph sampling · Connecting dominating set (CDS) strategy

1 Introduction

Wireless sensor networks (WSN) consist of sensor nodes that are arranged in the form of a network. The sensor nodes in these types of networks can vary from a few nodes to a large number of nodes. These nodes communicate with each other in

R. Nagpal (✉) · R. Garg
Department of IT, U.I.E.T., Panjab University, Chandigarh, India
e-mail: rachitanagpal1891@gmail.com

R. Garg
e-mail: roopali.garg@gmail.com

order to achieve the task they are designed for. Previously, these nodes were used to transmit scalar data from the environment but at present these sensor nodes are even used to transmit data that consist of images and video. The WSN designed for such application is known as wireless multimedia sensor network. The sensor nodes are battery operated devices so energy is utilized even when the nodes are in idle state. Achieving this objective in dense environment is complex, hence we use various graph sampling techniques to reduce the size of the network.

Graph sampling is the mathematical technique that evaluates the larger graph in the smaller samples one by one. For saving energy, the sampled graph should offer better connectivity. This is done through the implementation of spanning tree. When spanning tree is implemented on the network, a well-connected tree structure is obtained offering better connectivity. Graph sampling is then applied on this tree structure. Graph sampling algorithm gives the input to the connecting dominating sets as the sampled graphs or $G(s)$.

The WSN backbone network is the basic connectivity structure which is used to transport the data collected by the nodes to the base transceiver station (BTS), where all the data are aggregated and passed to the server.

Many works have been done to conserve energy like angled-LEACH protocol [1] in which energy efficiency is achieved by reducing traffic during communication between the nodes. Also, in [2] an enhanced version of the LEACH protocol is used to save energy.

The remainder of the paper is described as follows: Sect. 2 discusses the spanning tree techniques; Sect. 3 defines the algorithm that has been used to achieve the objective; Sect. 4 describes the methodology used; Sect. 5 provides the inference obtained, and Sect. 6 gives the conclusion.

2 Spanning Tree Techniques

Many researches have been done to increase the lifetime of the network. Long lifetime is required for efficient working of the network and also to achieve the better communication among nodes. Various graph sampling algorithms are discussed in [3] and the algorithms for construction of virtual backbone structure are discussed in [4, 5]. Apart from graph sampling and CDS technology, use of spanning tree protocol has also led to better energy usage required for communication among sensor nodes in a network.

Two spanning trees protocols based on distributive approach [6] are implemented to form spanning tree from a given network. The first protocol was used to form clusters in hierarchical structure with the destination node or the sink node as the root node. All the nodes in the network are then categorized into three types: sub root, intermediate, and leaf node. The sub roots are the dominating nodes in each cluster and the communication between the clusters takes place through these sub roots. The second protocol is manipulated to obtain a breadth-first search tree,

where a node is allowed to modify its parent node to communicate to the parent node following the shortest path.

Spanning tree has also been used to detect community structure in social networks [7]. The algorithm works in three parts; first, preprocessing is applied on the network, where weighted graph is obtained from an unweighted graph; the second step follows the process of finding the maximum spanning tree algorithm and finally the postprocessing step is performed in which the sub graphs are formed using the nodes present in the clusters.

The All Node Replacement problem and All Edge Replacement problem in social networks have been solved by constructing spanning tree from the original graph considering minimum cost [8]. Construction of spanning tree provides a better connected graph without cycles, however, when a node fails in the tree the whole tree collapses leading to disconnectivity of the nodes in the tree. Use of distributive approach creates alternative spanning trees for nodes in the network that helped efficiently in faulty environment.

An effective and efficient distributive approach for creating backbone nodes in WSN using CDS strategy has been discussed in [9]. The backbone nodes are virtually present in the network and are known as the dominant nodes. All communication between the nodes is carried out through these dominant nodes. These backbone nodes are chosen on the basis of the effective degree concept. After the construction of the dominating nodes, spanning tree algorithm is implemented to optimize the construction of these dominating nodes. It was inferred from the distributive approach that the optimized construction of backbone nodes using spanning tree gave effective results in terms of energy consumption and backbone size.

A tree structured topology that is helpful in conserving energy is discussed in [10]. A decision algorithm known as competitive decision algorithm has been used to utilize energy in an efficient and effective way. This has helped in increasing the lifetime of the network. The objective of the above stated algorithm is accomplished by dividing the load among the nodes in the WSN in a balanced way.

3 Non-probabilistic Spanning Tree Algorithm

Graph sampling along with CDS technique in sequence has been implemented in WSNs and has resulted in the construction of the backbone nodes using the CDS strategy [11]. Various graph sampling techniques [12] are used to reduce the size of the network in such a way that the obtained graph known as the sampled graph is used to represent the original graph. The sampled graph consists of nodes that have high neighbor count. This sometimes leads to bias toward nodes having high neighbor count and applying CDS strategy on this sampled graph results in a weakly connected backbone structure.

To overcome this limitation, spanning tree should be used before applying graph sampling so that we obtain a well-connected tree. Then on the obtained connected

tree, graph sampling and CDS strategy are applied in sequence. This results in an effective backbone structure as non-dominating nodes are also connected with the backbone nodes offering better connectivity and effective energy utilization. A non-probabilistic spanning tree approach is used to accomplish the objective. The algorithm is defined as under:

Algorithm 1: Non-probabilistic spanning tree protocol with connected dominating sets

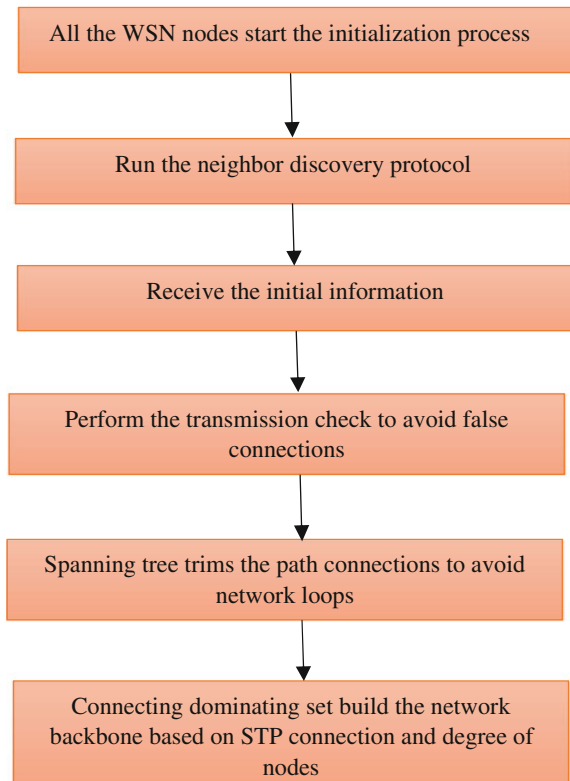
1. *WSN nodes undergo initialization process*
 2. Request the (X,Y) Coordinates to the WSN nodes from any *i*th node.
Request(N, n, broadcast) → Cluster Broadcast
 3. Receive the request replies and build neighbor information table on *i*th node
requestReply(X,Y,Node_ID) → Neighbor information table (nit)
 4. Check distance and autocorrect the neighbor table
 $\text{sqrt}((x-x')^2-(y-y')^2) < \text{Permitted Distance (Pd)} \rightarrow \text{update}(\text{nit}, \text{Node_ID}, \text{true})$
otherwise, $\rightarrow \text{update}(\text{nit}, \text{Node_ID}, \text{false})$
 5. Connect all of the nodes within transmission range
connect(nid, %any%, true) → createConnction(myID, node_ID)
 6. Non-problistic spanning tree (*nST*)fetch neighbor tables on all nodes
nST_fetch(nit(nit~=false) → nitShort(i)
 7. *trim the pathsto avoid the routing loops*
nST_trim(node_ID, nit, loopBit) → newConnectionArr, (if loopBitTrue)
 8. *connecting dominating sets evaluated the degree of each node*
nST_degree(node_ID, nit) → nitDegree(i)
 9. *Connected dominating sets (cds) selects the backbone*
cds(nitDegree) → networkBackbone
-

4 Methodology

The existing system is capable of handling the work of backbone construction for dense WSNs. The server then analyzes the data and prepares the results. The previous methodology created the backbone but did not evaluate the nodes other than the backbone nodes. Once the backbone network construction is finished after analyzing all the nodes under consideration, the algorithm terminates its operations and leaves the non-dominating nodes for the traditional connectivity protocols. The CDS algorithm evaluates the graph samples and constructs the WSN backbone structure in real time.

The major problem of the existing solution is that it does not work for the design and connectivity of the network with the nodes other than the dominating sets. Although the dominating sets or the WSN backbone structure is very important for the dense WSN working, the other nodes' connectivity with the dominating sets

Fig. 1 Non-probabilistic spanning tree flowchart



should be evaluated and connected in a tree structure along with marking the edge nodes, which can effectively mitigate the data dropping by marking the connectivity holes and edge nodes. The flowchart for non-probabilistic approach used to conserve energy is shown in Fig. 1.

5 Results

A graph with 120 nodes has been constructed in an area of 100×100 using MATLAB. The 120 nodes taken into consideration are the nodes present within a transmission radius of 10 m. The WSN network is shown in Fig. 2. The '+' symbol indicates the node and the blue lines show the connection between the two nodes. Non-probabilistic spanning tree algorithm is applied on the network shown in Fig. 2 and the resultant tree structure is obtained as shown in Fig. 3. The connections shown in the tree structure are the required connections used to carry out the

Fig. 2 Graph having 120 nodes

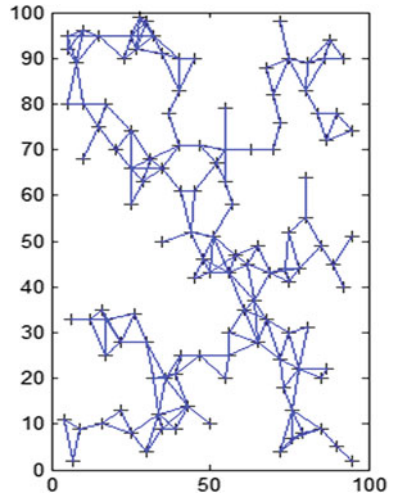
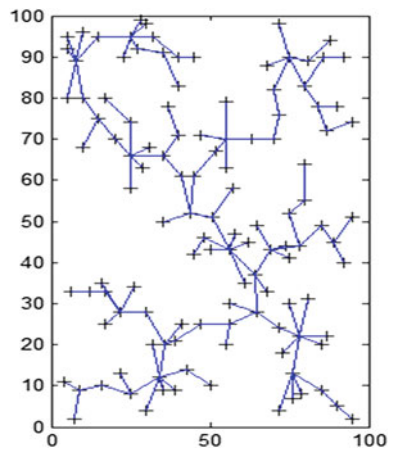
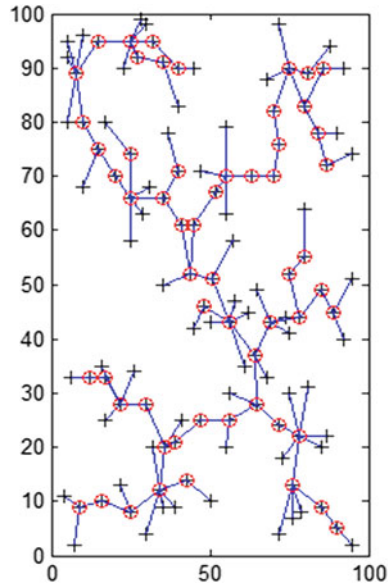


Fig. 3 Spanning tree for the graph



process of communication among nodes. After tree structure is obtained, default CDS strategy is implemented to obtain the virtual backbone network connectivity. The backbone connectivity of the network is shown in Fig. 4. The '+' symbol encircled in red depicted in Fig. 4 are the backbone nodes used to carry out the routing process.

Fig. 4 Spanning tree with backbone nodes



6 Conclusion

The method used above utilizes the spanning tree protocol to handle the tree structures for better connectivity of the non-dominating sets with the dominating sets, which is missing in the existing model. Non-probabilistic spanning tree approach along with connected dominating set (CDS) strategy is used to create a connectivity tree between the non-dominating and dominating nodes. This will offer strong connectivity for better data delivery with less power consumption, resulting in a long WSN network lifetime. The spanning tree algorithm is a popular algorithm that connects the nodes in the tree structure along with the dominating sets. This will help the WSN nodes to send the data smoothly in order to deliver the maximum collected data from the sensor nodes to the wireless base stations.

The protocol used above involves the implementation of spanning tree algorithm before the application of graph sampling and CDS technology. Spanning tree can also be applied after CDS strategy to provide pruning of connections and also to provide end node connectivity while constructing the WSN backbone.

Acknowledgments I would like to give my sincere gratitude to all the friends and colleagues who helped me to conduct this research, without which this research would be incomplete.

References

1. Garg D, Garg R. Angled-LEACH in wireless sensor networks. *Int J Adv Comput Inform Technol*. 2012.
2. Garg R, Gupta D. Improving the network lifetime in WSN through enhanced LEACH. *Int J Comput Appl*. 2013.
3. Wang T, Yang C, Zhang Z, Xu T, Jin L, Hui P, Deng B, Li X. Understanding graph sampling algorithms for social network analysis. In: *Distributed Computing Systems Workshops (ICDCSW)*. IEEE; 2011. p. 123–8.
4. Du H, Wu W, Ye Q, Li D, Lee W, Xu X. CDS-based virtual backbone construction with guaranteed routing cost in wireless sensor networks. In: *Parallel and distributed systems*. IEEE; 2013. p. 652–61.
5. Yu X, Liu X, Tang Y, Xiao J, Zhang J. A distributed algorithm for virtual backbone construction with cellular structure in WSNs. *Int J Distrib Sensor Netw*. 2012.
6. Erciyas K, Ozsoyeller D, Dagdeviren O. Distributed algorithms to form cluster based spanning trees in wireless sensor networks. In: *Computational science–ICCS 2008*. Springer Berlin Heidelberg; 2008: 519–28.
7. Basuchowdhuri P, Anand S, Srivastava DR, Mishra K, Saha SK. Detection of communities in social networks using spanning tree. In: *Advanced computing, networking and informatics*. Springer; 2014. p. 589–97.
8. Flocchini P, Enriquez TM, Pagli L, Prencipe G, Santoro N. Distributed minimum spanning tree maintenance for transient node failures. In: *Computers*. IEEE; 2012. p. 408–14.
9. Ren S, Yi P, Hong D, Wu Y, Zhu T. Distributed construction of nected dominating sets optimized by minimum-weight spanning tree in wireless ad-hoc sensor networks. In: *Computational science and engineering (CSE)*. IEEE; 2014. p. 901–8.
10. Xiong X, Ning A. Competitive decision algorithm for constructing maximum lifetime spanning tree in wireless sensor networks. In: *Computer Science & Education (ICCSE)*. IEEE; 2014. p. 1014–9.
11. Bhatt R, Datta R. Utilizing graph sampling and connected dominating set for backbone construction in wireless multimedia sensor networks. In: *Twentieth national conference on communications (NCC)*, 2014. IEEE; 2014. p. 1–6.
12. Leskovec J, Faloutsos C. Sampling from large graphs. In: *ACM*; 2006.

Design Specifications of Reversible Logic Using CMOS and Quantum Dot Cellular Automata

Shaik Shabeena and Jyotirmoy Pathak

Abstract Reversible Logic is solitary emerging technology that that promises zero-power dissipation. Multiple function generation, low-power VLSI, optical information processing, and quantum computing are the main applications of this logic. Without the reversible logic quantum computing is not implemented. This paper focuses on the designing of reversible logic gates and their design specifications using CMOS and QCA. The reversible gates are used in redesigning of intricate systems that are embedded with reversible circuits as a primal component and execute multiple sets of instruction in quantum computers. The reversible circuits shape the indispensable building block architecture of quantum-based computers as all quantum operations are destined to be reversible. These gates are implemented and results are shown in Cadence Virtuoso and QCA Designer version 2.0.3.

Keywords Reversible logic · Reversible gates · Quantum dot cellular automata (QCA) · Nanoelectronics · Cadence virtuoso

1 Introduction

In today's rising technology, power dissipation is the major issue. When high-technology circuits are implemented then some information loss will be present. Owing to this information loss, energy will dissipate. According to Landauer's theory, the amount of data loss is $k \ln 2$ joules for one bit as energy dissipation process [1]. For conservative logic schematic, every single operation dissipates some amount of heat energy in the form of information loss. This happens because of second law of thermodynamics; in any method once information is lost it cannot

S. Shabeena (✉) · J. Pathak
School of Electronics Engineering, Lovely Professional University, Punjab, India
e-mail: shabeena19912@gmail.com

J. Pathak
e-mail: jyotirmoy4ever@gmail.com

be recovered. After Landauer's theory, in the year 1973 Bennett proposed a theory to avoid the waste of information wholly; and circuits must be designed using reversibility concept [2].

This reversibility concept actuates energy solution to many upcoming fields of nanotechnology which is related to quantum computing [3]. The gates which regenerate the inputs from the available outputs are known as reversible gates. It has equal number of IN and OUT lines whereas the unused output lines in any circuit were taken as garbage signal and the fan-out must be one. The main principle behind reversibility concept is to store the cells which are having charge electrically when switching operations are done and then there is no waste of information. Then it will be able to use again through reversible computing [3].

However, the industry is besieged to make small-scale transistors and improvement in clocking speed. To overcome all the precincts of CMOS, researchers are looking for alternative emerging technology. The quantum dots are semiconductor material and the size is in nanometers. In 1993, QCA is introduced by Lent et al. QCA technology is an alternative to CMOS. This can be considered as rising technology of nanoelectronics to replace the current transistors in semiconductor design. Unlike the conservative transistor which transfers information through voltage or current, in QCA the circuits are transferring these bits of information through the cells interaction [4]. The circuit consumes extremely low power and there is no need of interconnections at all [3].

This paper is described as follows: Sect. 2 focus upon outline of reversible gates as well as QCA technology. Section 3 explains execution of reversible logic gates in 0.09 μm and QCA technology. Section 4 introduces results of reversible gates. Section 5 gives overall design specifications of reversible gates. Section 6 concludes the paper.

2 Reversibility in QCA

2.1 Reversible Gates

In a quantum system, reversible computation can be performed only when it encompasses of reversible logic gates. When a system acts as reversible then its input and output lines can be unique and input lines are generated from output lines. And there is one-to-one present between its inputs and outputs [5].

In reversible gates, power dissipation is a vital specification in circuit design. It can be minimized (theoretically zero) and by the use of these dissipation-less gates, we can achieve nil-power-dissipation circuits [6]. To achieve a nonreversible function, it must be implanted into a reversible one, and this will produce garbage outputs and constant inputs. Garbage outputs mean unused outputs in circuit that means for the outputs that are not cared. The essential reversible logic gates and their schematics are shown below [3].

1. *Feynman Gate* (Fig. 1)
2. *Toffoli Gate* (Fig. 2)
3. *Fredkin Gate* (Fig. 3)
4. *Peres Gate* (Fig. 4)

2.2 Quantum Dot Cellular Automata

In contrast to electronics which is based on transistors, QCA does not work on the transport of electrons, but by the arrangement of electrons in a small, limited area of only a few square nanometers. It is implemented by quadratic cells, therefore it is called QCA. In these small squares, precisely, four potential wells are located; one well is situated in each corner of QCA cell. In individual QCA cell, exactly two electrons are sealed. These two electrons can only reside in the potential well (Fig. 5).

There are two diagonals in a square, which means the electrons can dwell in exactly two possible variations in a QCA cell. It means each cell can be in two states. Much precisely, a high voltage is often interpreted as binary ‘1’ and a low voltage as binary ‘0’ [7].

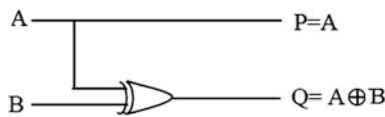


Fig. 1 Structure of Feynman gate

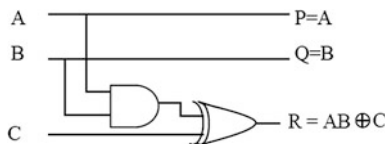


Fig. 2 Structure of Toffoli gate

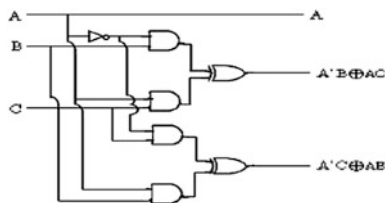


Fig. 3 Structure of Fredkin gate

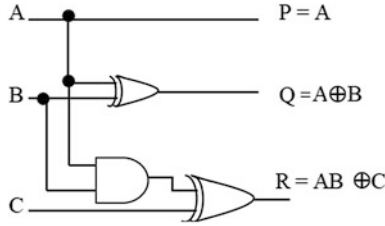


Fig. 4 Structure of Peres gate

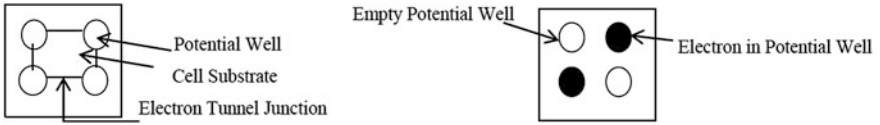


Fig. 5 Structure of QCA cell

If two QCA cells are placed side by side then there is a possibility to interchange their states. The QCA cell that has to transfer its state to a next cell must have its tunnel junctions connected, and the tunnel junctions in the side cells have to be exposed to allow the electrons to move via the tunnel junctions between the two potential wells (Figs. 6, 7, 8, 9, 10, 11, 12 and 13).

3 Implementation of Reversible Gates

Reversible gates can be implemented by using both Cadence Virtuoso and QCA Designer tool version 2.0.3 [8].

3.1 Using 0.09 μm Technology

1. Feynman Gate
2. Toffoli Gate
3. Fredkin Gate
4. Peres Gate

3.2 Using Quantum Technology

1. Feynman Gate

The implemented Feynman gate consists of two AND gates, two inverters, and one OR gates.

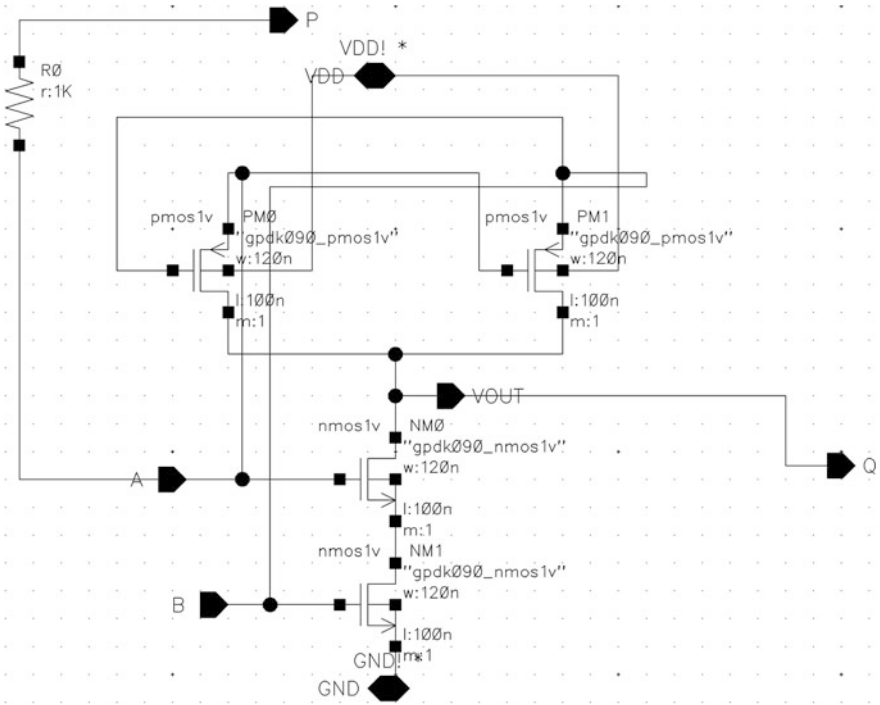


Fig. 6 CMOS-based Feynman gate

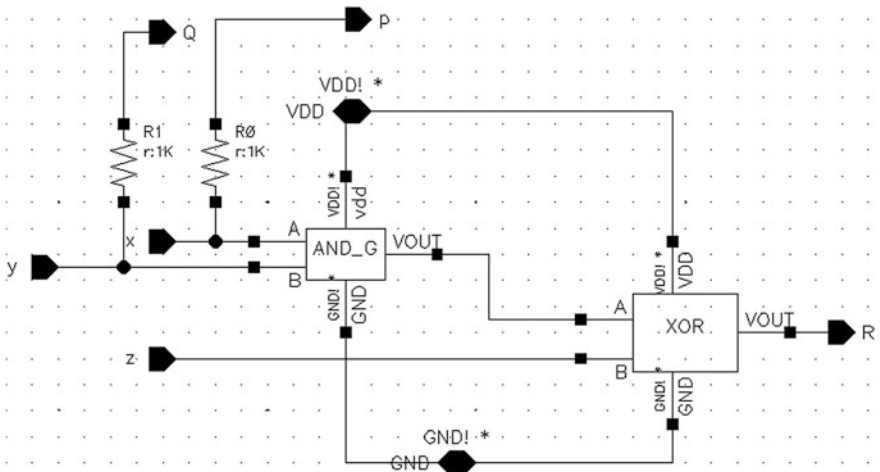


Fig. 7 CMOS-based Toffoli gate

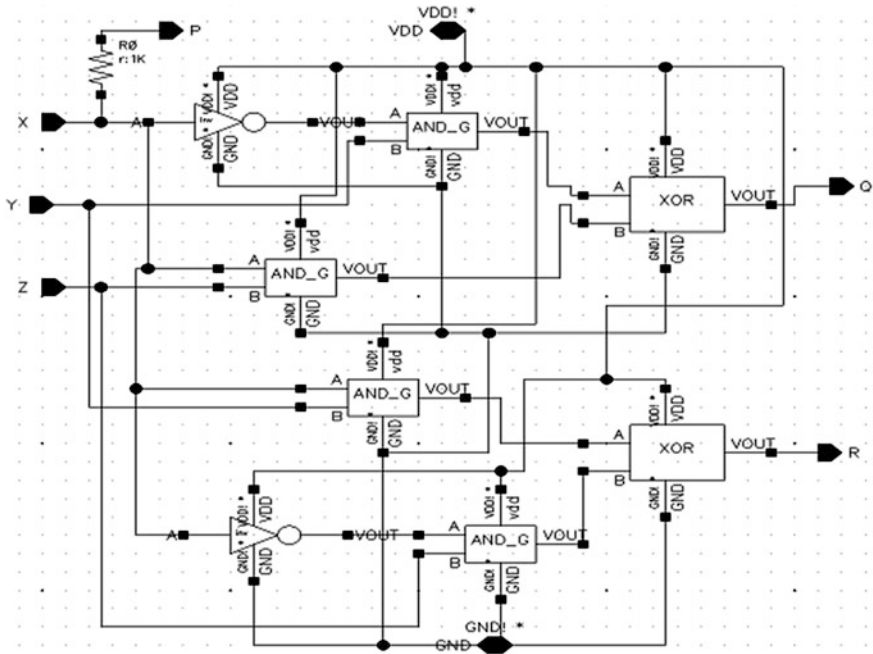


Fig. 8 CMOS-based Fredkin gate

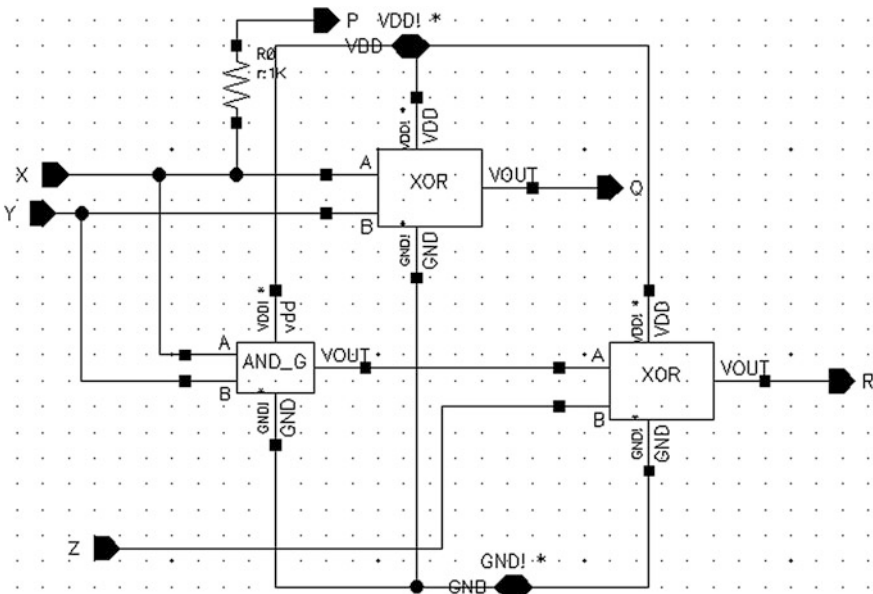


Fig. 9 CMOS-based Peres gate

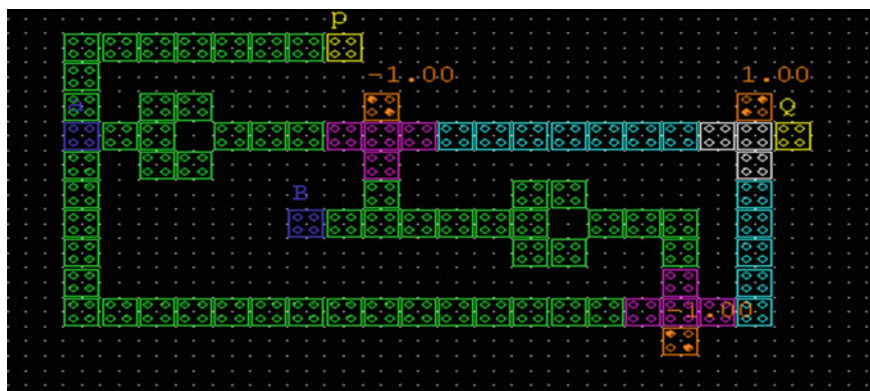


Fig. 10 QCA-based Feynman gate

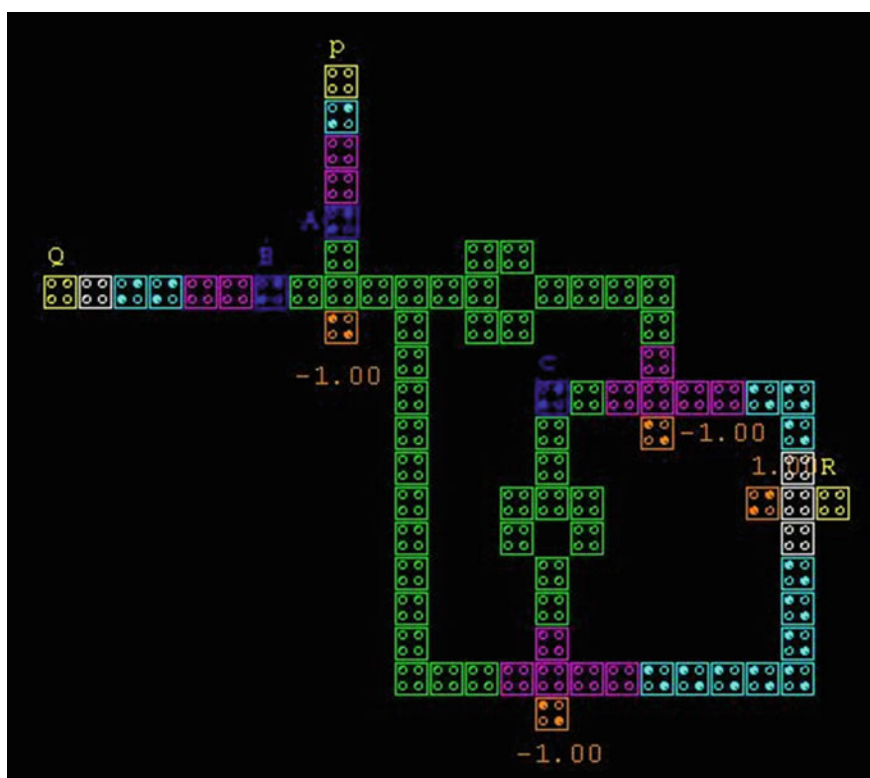


Fig. 11 QCA-based Toffoli gate

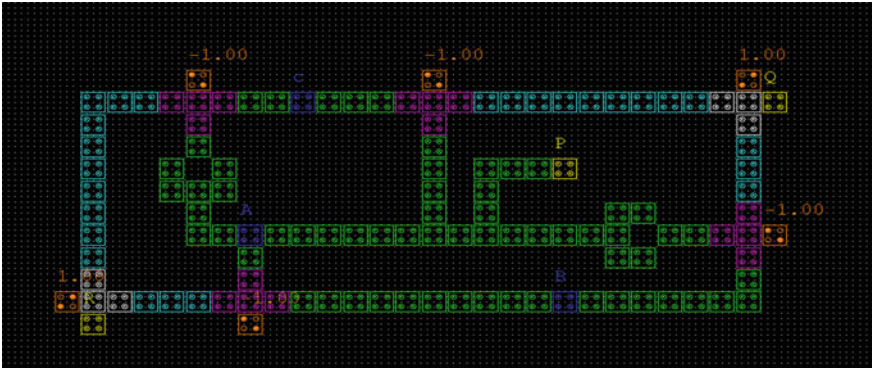


Fig. 12 QCA-based Fredkin gate

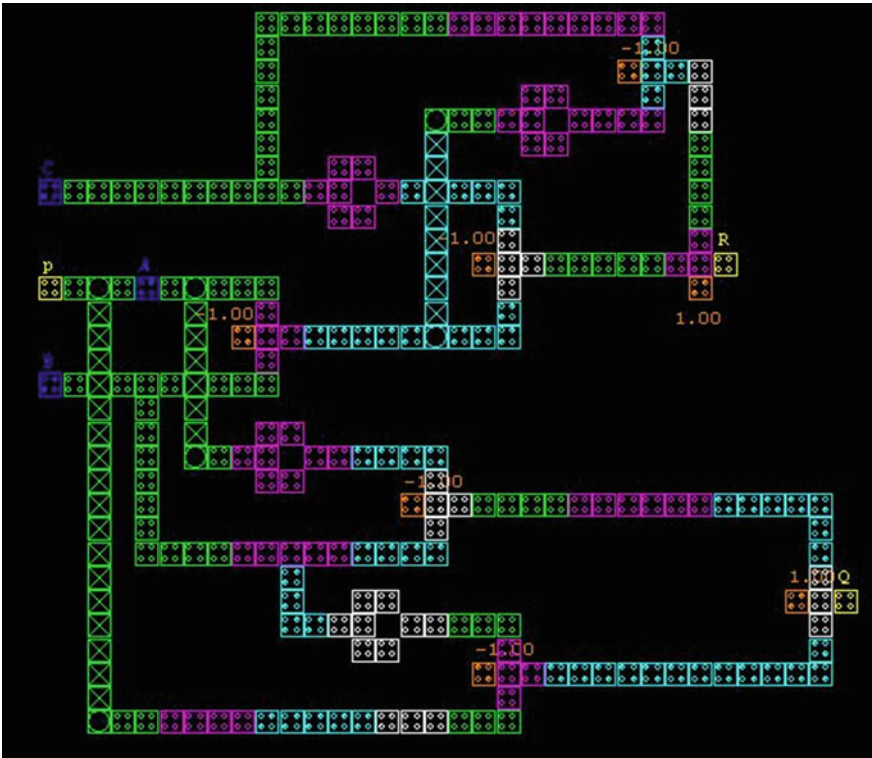


Fig. 13 QCA-based Peres gate

2. Toffoli Gate

The implemented Peres gate consists of two AND gates, two inverters, and one OR gates.

3. Fredkin Gate

The implemented Fredkin gate consists of four AND gates, two inverters, and two OR gates.

4. Peres Gate

The implemented Peres gate consists of five AND gates, four inverters, and two OR gates.

4 Output Waveforms

The results have been analyzed by summing up the graphical result attained from Cadence Virtuoso and QCA Designer V2.0.3 along with the truth table of the reversible logic gates.

4.1 Feynman Gate

See Fig. 14.

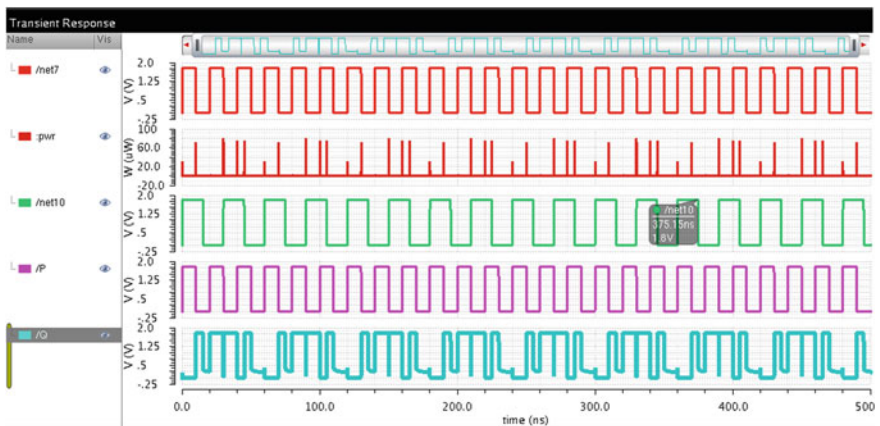


Fig. 14 CMOS output of Feynman gate

4.2 Toffoli Gate

See Fig. 15.

4.3 Fredkin Gate

See Fig. 16.

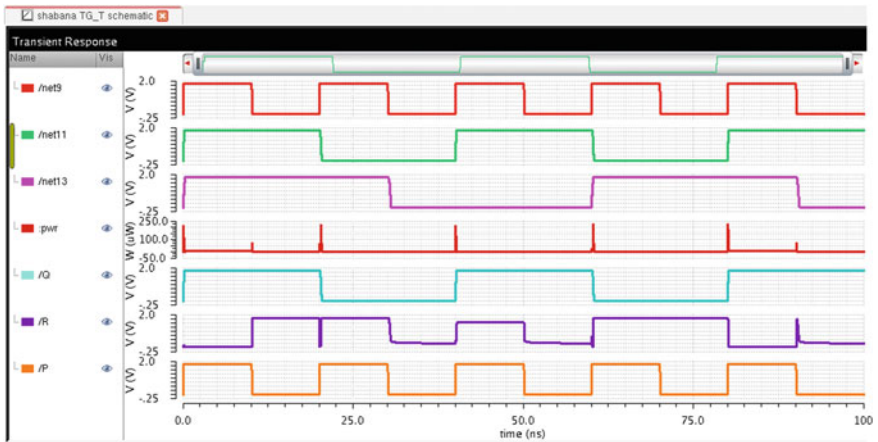


Fig. 15 CMOS output of Toffoli gate

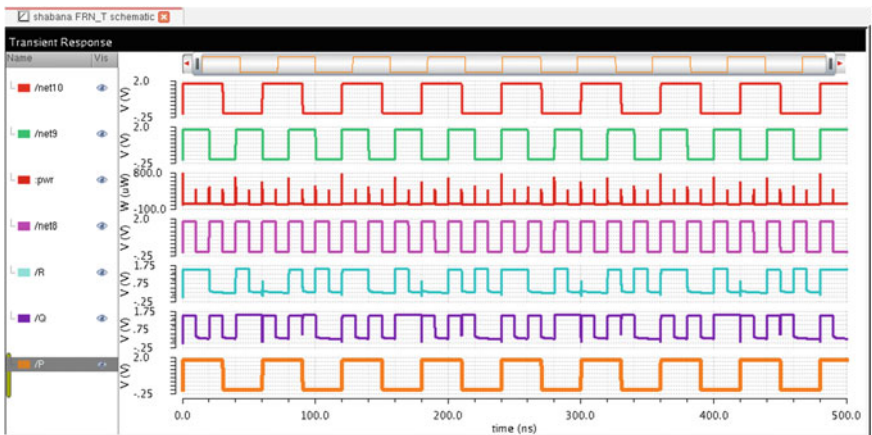


Fig. 16 CMOS output of Fredkin gate

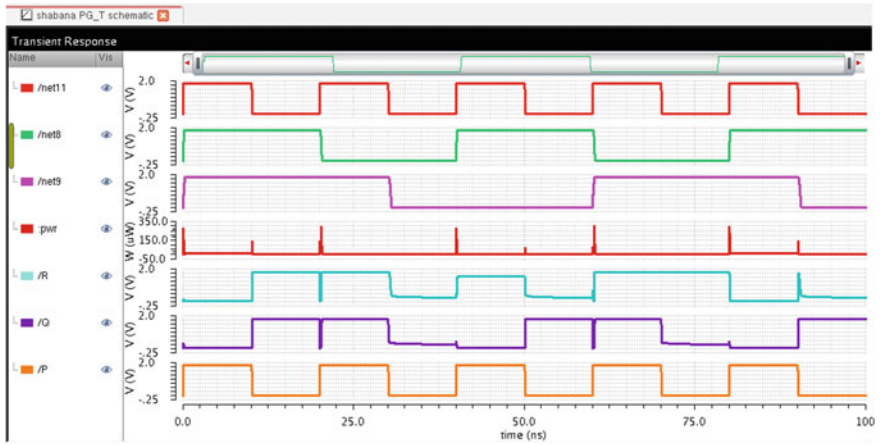


Fig. 17 CMOS output of Peres gate

4.4 Peres Gate

See Fig. 17).

5 Simulation

The four reversible logic gates are implemented and simulated using Cadence Virtuoso and QCADesigner version 2.0.3. The design specifications for reversible gates in QCADesigner for a coherence vector function having cell size must be 18 nm and remaining are as shown below.

6 Conclusion

This paper has explored the fundamental concepts of reversible logic and reversible gates. The simulations are carried using QCA tool and Cadence Virtuoso. Tables 1 and 2 gives design specifications of reversible gates. The regular reversible logic gates have been confirmed on both tools with minimum delay. Using these gates, in future we can design complex architectures as arithmetic logic unit and micro-processors, etc. The current QCA technology does not particularly set the possible operating frequency and definite latency, but it can be analyzed as an imperative parameter in forthcoming works.

Table 1 Design specifications in QCA

	Feynman gate	Toffoli gate	Fredkin gate	Peres gate
Complexity	83	81	121	284
Area	404 $\mu\text{m} \times 241 \mu\text{m}$	458 $\mu\text{m} \times 426 \mu\text{m}$	592 $\mu\text{m} \times 263 \mu\text{m}$	678 $\mu\text{m} \times 598 \mu\text{m}$
Delay (in clock pulse)	1/2	1/2	1/2	No
Clock zones	3	3	3	7

Table 2 Design specifications in 0.09 μm

	Feynman gate	Toffoli gate	Fredkin gate	Peres gate
No. of gates	XOR-1	AND-1 XOR-1	NOT-1 AND-4 XOR-1	AND-1 XOR-2
Power	516.4E-9	2.239E-6	23.13E-6	2.83E-6
Delay	15.17E-9	20.20E-9	10.13E-9	24.57E-12

Acknowledgments We thank our research scholars and faculties of Lovely Professional University for their support and guidance.

References

1. Landauer R. Irreversibility and heat generation in the computational process. *IBM J Res Dev.* 1961;5:183–91.
2. Bennett CH. Logical reversibility of computation. *IBM J Res Dev.* 1973. p. 523–32.
3. Shabeena S, Jyotirmoy P. Design and verification of reversible logic gates using quantum dot cellular automata. *Int J Comput Appl.* 2015; 114(4).
4. Chan STY, Chien FC, Ghazali AB. Design and verification of a 4 bit ripple adder using quantum dot cellular automat (QCA). In: *IEEE International conference on circuits and Systems (ICCAS)*; 2013. p. 33–8.
5. Raghava G, Madhu Kiran P, Santhosh Kumar A. A review on reversible logic gates and their implementation. *Int J Emerg Technol Adv Eng.* 2013;3(3):417–23.
6. Roohi A, Hossein K, Samira S, Keivan N. Implementation of reversible logic design in nano electronics on basis of majority gates. *ISCADS*; 2012. p. 1–6.
7. Keivan N, Mokhtar A, Samira S. A novel seven input majority gate in quantum-dot cellular automata. *IJCSI.* 2012;9(1):84–9.
8. QCA. Designer home page. www.atips.ca/projects/qcadesigner.

Effective Models for Segmentation and Shape Tracking of Cells

J. Himayavardhini and R. Ramesh

Abstract Several techniques were developed to give high efficiency for segmentation and shape tracking of cells. Owing to the large amount of data and complexity, the techniques were not suitable for analyzing both 2D and 3D data. The proposed technique deals with a fast and robust method that can be applied to time-lapse input series. In this case, the algorithm consists of four steps for the analysis of each frame in the time-lapse input series. The input frame is segmented in the first step; the cell boundaries are detected in the second step; the total cell area is determined in the third step, and then finally the cell area of each frame is compared with the results of successive frames. The robust and reliable steps in the algorithm clearly describe the variation in shapes of cells. Extensive simulation results show that the accuracy of the proposed algorithm is high and it substantially outperforms the other existing algorithms.

Keywords Cell division · Cell tracking · Level set method · Coherence · Tumorigenesis

1 Introduction

A cell is the basic, structural, and functional unit of all living organisms. They are the smallest units of all living organisms. They have the tendency to replicate and build up to form the entire structure. A cell will divide to form a tissue (a group of cells) and a group of these tissues form an organ. These well-developed organs form the human body. Abnormalities in these cells which are microscopic units can

J. Himayavardhini (✉) · R. Ramesh
Department of Electronics and Communication Engineering, Saveetha Engineering College,
Chennai, India
e-mail: himayavardhini91@gmail.com

R. Ramesh
e-mail: ramesh@saveetha.ac.in

only be analyzed using advanced techniques. These cells can have minor as well as major abnormalities. Minor abnormalities can cause small changes to the cells whereas major abnormalities can lead to cell division in an abruptly faster rate. Such cell division will lead to a tremendous change in the organ that will even hinder the function of the organ.

A normal cell will divide and produce limited number of cells, i.e., a mother cell will divide and produce only two daughter cells. These two daughter cells will further divide and produce two cells each. This rate will be stable and the cells will die after a period of time called apoptosis. But an abnormal cell division will be different. For example, a cell affected by oncogenes will divide to produce extremely large number of cells. These cells will further divide in the same manner. The cells will not die after the apoptosis period and the growth rate will be extremely large. Diagnosis of such abnormalities is tedious which is done at microscopic scale.

Image segmentation plays a vital role in the analysis of abnormal cells. It is the process of partitioning the image into two regions: a foreground region and a background region. The foreground region will consist of the region of interest (ROI) and the background region will contain all other details. Preprocessing is usually an advanced filtering technique called coherence-enhancing diffusion filtering. This kind of analysis will be used in the fields like tumorigenesis (for the detection of cancerous cell growth), or embryonic development (to study the development stages of a fetus by proper and controlled cell division).

Cell biological studies are based on the analysis of large cell populations by microscopy imaging. In many applications, the identification of each cell and the detection of its boundaries are the two major, important tasks. The complexity of performing these tasks is increasing with growing size of the image data analyzed. Manual processing of such data is not only complex and error prone but also very laborious and in many cases simply impossible creating a strong demand for automated techniques. Level sets are used as a tool for numerical analysis of surfaces and shapes. It is a great tool for modeling time-varying objects. The advantage is that it can perform numerical computations of curves and surfaces without parameterising the objects. It also makes it very easy to follow shapes that change topology. For example, when a shape splits into two, it develops holes or reverse of these operations. The main disadvantage is that the numerical analysis becomes complicated for objects that move very fast.

The drawback of the level set method is that it requires the velocities to be set for the moving objects very often. This frequent variation in velocities may lead to undesired results. Setting the velocity parameter for extremely fast moving objects was found to be very difficult [1].

Myocardial tagging is a noninvasive method for measuring the motion of heart beat. It offers a quantitative analysis of various kinetic parameters. Tags appear as dark lines which move along with the tissue and allow motion quantification of specific areas of the myocardium. The analysis of tagged MRI commonly consists of three tasks. First, the endocardial and epicardial contours of the left ventricle are defined

manually or with semiautomated algorithms. Second, tag lines are automatically segmented in every image of the sequence. Intersections are used as feature points during tracking. Third, tag line positions are used to either fit a parameterized model of cardiac displacement or to reconstruct a dense displacement field. Local tissue deformations can be captured without affecting other parts. These techniques do not require modeling of tag appearance. It requires displacement between successive frames to be small which is not practically possible. Results are prone to errors at points near myocardial boundary, where tag fading and non-myocardial background structures may cause erroneous linking of points [2].

Large amount of data sets caused the analyses of time-lapse series to rely increasingly on automated or semiautomated methods. A fast and robust approach was in demand to segment, track, and evaluate the movement tracks of cells, subcellular components and other particles. Such an approach to tracking cells in time-lapse series is presented. The proposed tracking scheme involves two steps. First, coherence-enhancing diffusion filtering is applied on each frame to reduce the amount of noise and enhance flow-like structures. Second, the enhanced cell boundaries are detected. To allow simultaneous tracking of multiple cells over time, successive frames are overlapped after segmentation. The advantage is that large amount of data sets can be analyzed [3].

It is a fast and robust technique. It is independent of the number of cells in each frame. This technique is capable of detecting objects that are not defined by a gradient. The disadvantage is that it can only be applied for 2D images [4].

2 Input Data

The input to the proposed tracking scheme is a time-lapse series of frames. The number of frames can vary from 10 to 20 depending upon the abnormality. Microscoped images of the cells, i.e., cells observed under microscope over a period of time (say 1 or 2 hours) are taken in the form of a video. This video formation is done by integrating successive images together. This video is of the range of 20–30 frames per second. When the video is converted into frames, nearly 20–30 frames will be produced for 1 second. These frames are then analyzed individually and the results are then integrated.

3 Proposed Scheme

3.1 Coherence-Enhancing Diffusion Filter

This is an advanced, spatial, nonlinear filter that will reduce noise as well as enhance the flow-like structures between the cells. During the separation stage of a

cell, i.e., when a cell starts dividing, first the cell wall and cell membrane will start dividing and the division further proceeds to the nucleus. When the nucleus divides completely, the cell separates into two with individual cell wall, cell membrane, and nucleus. At the final stage of separation, a small, slender, fiber-like structure serves as a connection between the two separated cells. This structure breaks and leaves the two cells in a separated condition. Analysis of this structure is very important during the study of cell behavior because the appearance of this structure clearly shows that the cell is in the final stage of division. CED is used in order to enhance these slender, flow-like structures between the cells which will be diffused while using other linear filters like Gaussian, mean and median filters. It will also preserve the edges in the image.

The measure of coherence is given by

$$k = \sum_{i=1}^{m-1} \sum_{j=i+1}^m (u - v)^2 \quad (1)$$

Here, ‘ u ’ and ‘ v ’ are the eigen values of two images. The value of ‘ k ’ becomes large for strongly differing eigen values, and it tends to zero for isotropic structures (Fig. 1).

3.2 Segmentation of the Initial Frame

Initial frame in the time-lapse input series is considered as the first frame or the frame of reference the result of which will be considered for comparison with the results of other frames in the sequence. The first frame is segmented, i.e., the frame is partitioned into the foreground and background regions. These two regions will be separated using a smooth, closed contour.

Consider a scalar image ‘ U ’ in the d -dimensional domain. This image is partitioned into two regions Ω_1 and Ω_2 by a closed contour ‘ C ’.

$$E(C, a, b) = \mu|C| + \lambda_1 \int_{\Omega_1} (u(x) - a)^2 + \lambda_2 \int_{\Omega_2} (u(x) - b)^2 \quad (2)$$

where ‘ a ’ and ‘ b ’ are the average intensity levels of the foreground and background regions, respectively. ‘ λ ’ and ‘ μ ’ are the positive, user-defined weights (Fig. 2).

3.3 Counting the Cell Area of Each Frame

The first frame will be considered as the frame of reference. This initial frame which is segmented in the previous step is subjected to morphological operation. The

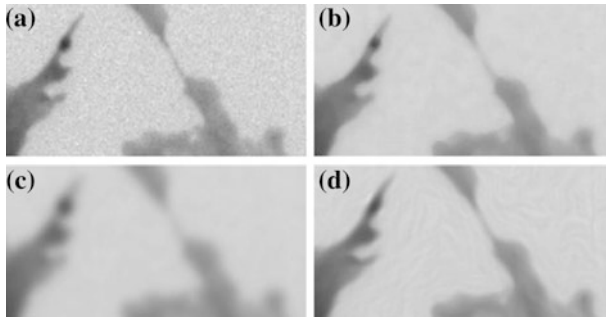


Fig. 1 Original image (a), Gaussian filter (b), median filter (c), coherence-enhancing diffusion filter (d)

Fig. 2 Segmented result of the initial frame



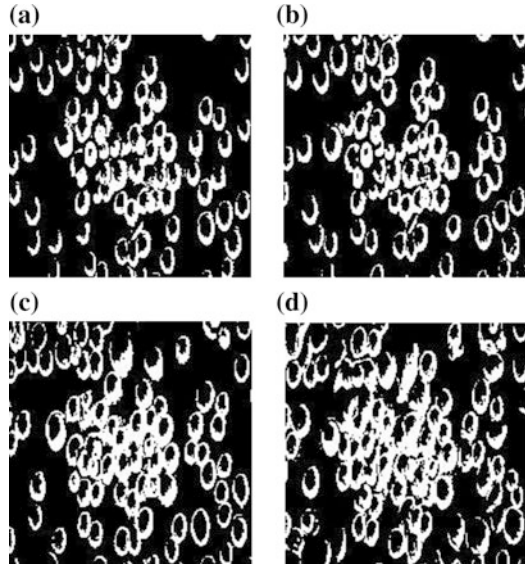
process starts with thresholding the image. After thresholding, noise will be removed from the image. The final step will include the detection of cell boundaries and will return the cell area of the frame. The cell boundaries in the initial frame are detected using erosion and dilation. Objects that are round in shape are highlighted by setting the area of circle as the threshold so that the cells that are round in shape will be detected. Thus, the first frame will be segmented into foreground which constitutes the total area of the cell and the background which contains other details of the image.

The following metric will be used to detect round objects in an image:

$$\text{Metric} = 4 * \pi * \text{area}/\text{perimeter}^2 \tag{3}$$

This metric is equal to one for circular objects and it is less than one for any other shape.

Fig. 3 Comparison of initial frame with successive frames. First Frame (a), Second Frame (b), Third Frame (c), Fourth Frame (d)



3.4 Comparing Successive Frames

After considering the cell area determined from the first frame as reference value, the second frame will be subjected to segmentation and boundary detection processes. Now, the result of the second frame is compared with that of the first frame to observe if there is any increase in the cell area or number of cells so that it can be concluded that some of the cells have started dividing. Now, the results of the first and second frames will be compared with the result of the third frame to observe the change in the cell area. In this manner, ‘n’ number of frames required for the entire analysis of the abnormality can be compared and changes can be observed (Fig. 3).

4 Results and Discussion

The frames that are obtained from the time-lapse input series are analyzed using the above tracking scheme and the following results were obtained (Table 1).

Four frames are considered for the analysis. Each frame is subjected to the above process and the results are tabulated as above. The comparison shows that the first frame consists of cells which are normal in stage. The second and third frames consist of cells which have started dividing. The fourth frame in the series consists of cells that are separated after undergoing the previous stages. This analysis can be done by observing a change in the total cell area in the subsequent frames.

Table 1 Comparison of cell area of successive frames

Frame number	Cell area	Stage
1	51	Normal stage
2	247	Dividing stage
3	307	Dividing stage
4	537	Separated stage

5 Conclusion

In this paper, an effective algorithm for tracking the shapes of cells is proposed. Simulation results show that our algorithm has outstanding ability to identify the variation in the shapes of cells. The results obtained can be used to supervise the growth of cancer cells effectively. Segmentation of each frame is accurate even when the noise intensity is high.

6 Future Work

In future work, the performance can be further improved by reducing the execution time of the Chan-Vese algorithm. Each and every frame has to be segmented, the cell area should be counted and the segmented frames have to be compared. This entire process requires an extremely larger execution time. Such a large execution time can be reduced further using a fully automated technique. Also, only the round-shaped objects were detected in the analysis. This method can be made suitable for almost all biomedical applications by detecting cells of various shapes.

Acknowledgments I would like to express my sincerest gratitude to my supervisor who has supported me throughout my work with his patience and knowledge while allowing me the room to work in my own way. I attribute the level of my masters degree to his encouragement and effort. I would also like to thank my parents for supporting me throughout all my studies.

References

1. Dzyubachyk O, Van Cappellen WA, Essers J, Niessen WJ, Meijering E. Advanced level-set-based cell tracking in time-lapse fluorescence microscopy. *IEEE Trans Med Imag.* 2010;29:852–867.
2. Smal I, Carranza-Herrezuelo N, Klein S, Niessen W, Meijering E. Quantitative comparison of tracking methods for motion analysis in tagged MRI. In: 8th IEEE International Symposium on Biomedical Imaging, 2011, p. 345–348.
3. Maska M, Danek O, Garasa S, Rouzaut A, Muñoz-Barrutia A, Ortiz-de-Solórzano C. Segmentation and shape tracking of whole fluorescent cells based on the Chan-Vese model. *IEEE Trans Med Imag.* 2013;32:995–1006.
4. Maska M, Munoz-Barrutia A, Ortiz-de-Solórzano C. Fast tracking of fluorescent cells based on the Chan-Vese model. In: 9th IEEE International Symposium on Biomedical Imaging, 2012, p. 1316–19.

Real-Time Rule-Based Scheduling System for Integrated Delivery in a Semiconductor Manufacturing Using Evolutionary Algorithm-Based Simulation Approach

V.K. Manupati, A.S. Revanth, K.S.S.L. Srikanth, A. Maheedhar and M.B.S. Sreekara Reddy

Abstract In a wafer fabrication facility, automated material handling system (AMHS) to dispatch the material flow is a critical and challenging task. This paper investigates the integrated delivery of automated material handling system (AMHS) and processing tools for a large-scale complex wafer fabrication facility. Although the dispatching rules are one of the most frequently used approach for effective semiconductor manufacturing schedule, it is necessary to adapt new techniques due to time-consuming nature of dispatching rules when the number of variables and iterations increases. There are very few studies on enhancing the rule-based scheduling system. To address this issue, we proposed an evolutionary algorithmic approach for enhancing the rule-based scheduling system. We explored the best possible genetic algorithm parameters from famous approach called Taguchi, and then, statistical analysis, i.e., regression analysis, has been conducted to find out the significance of the parameters. Later, with hierarchical rule-based scheduling approach, the combined sequential dispatching rules are formed to achieve better efficiency and effectiveness of the scheduling.

Keywords Wafer fabrication facility · Dispatching rules · Evolutionary algorithm · Rule-based scheduling

V.K. Manupati (✉)

Department of Mechanical Engineering, VIT University, Vellore, India
e-mail: manupativijay@gmail.com

A.S. Revanth · K.S.S.L. Srikanth · A. Maheedhar · M.B.S. Sreekara Reddy
Department of Mechanical Engineering, KL University, Guntur, India
e-mail: suryarevanth111@gmail.com

A. Maheedhar
e-mail: aluri.mahi0911@gmail.com

M.B.S. Sreekara Reddy
e-mail: mbssreddy@kluniversity.in

© Springer India 2016

S.S. Dash et al. (eds.), *Artificial Intelligence and Evolutionary Computations in Engineering Systems*, Advances in Intelligent Systems and Computing 394, DOI 10.1007/978-81-322-2656-7_90

1 Introduction

Semiconductor manufacturing has been considered as one of the largest, competitive, and dominating industries in the world. The prime focus of this industries is to manufacture integrated circuits which are useful for the products appear everywhere in our daily life. Their manufacturing process has been considered as one of the most sophisticated with characteristics of large processing steps, reentrant material flows, batch processing, etc. In general, most of the semiconductor manufacturing processes follow four different stages viz. wafer fabrication, wafer probe, assembly (or) packaging, and final test. Out of them, manufacturing process can be considered as the most significant step and facilitating a new fabrication unit is most expensive and time-consuming step. Therefore, proper utilization of resources through scheduling is really important.

In the past decades, dispatching decision problems for processing machine tools and material handling in wafer fabrication unit are usually investigated separately due to its modeling complexity. In order to achieve this, it is necessary to introduce an effective integrated dispatching mechanism that can fulfill the above-mentioned requirements and to enhance the performance of the semiconductor wafer fabrication system.

In recent years, many studies were focused on latest dispatching rules for scheduling semiconductor wafer fabrication systems. However, heuristic rules and mathematical programming techniques are widely used for these problems. Yang and Chang [1] developed a nonlinear multi-objective-based mathematical model for integrated circuits for sorting and testing operation. In their study, the Lagrangian relaxation approach has been used for converting nonlinear functions into linear functions. Li et al. [2] introduced a dispatching rule approach to improve on-time delivery by minimizing the throughput time and the cycle time. Wu et al. [3] proposed a line balance–starvation avoidance algorithm and then developed a simplification model for processing route for a fab with machine–dedication features. Later, they have used the shifting bottleneck heuristic approach for wafer fabrication system. Comparisons have been made among these approaches and found that dispatching rules, by far, are the most commonly used and found better for shop floor control. Another reason behind its implementation is that they are simple to use, quick in reacting to the changes encountered on the shop floor, easy to understand, and require low computational load. The contribution of this paper is twofold. First, it mainly concentrates on the combinatorial dispatching which has rarely been studied. Second, genetic algorithm (GA) parameters optimization process is developed to handle complex environments. This approach can improve the performance results by optimizing GA parameters even with the dramatically changing environments.

The remainder of this paper is organized as follows: In Sect. 2, we describe the problem and its notations. In Sect. 3, we developed a Taguchi-based experimentation for obtaining best feasible parameters. In Sect. 4, an evolutionary algorithm-based simulation experimentation is conducted for obtaining best

sequence rules. In Sect. 5, the results and their discussions are detailed. The paper concludes with Sect. 6 which suggests the directions of future work.

2 Framework of the Proposed Fab Simulation Model

The proposed methodology has the capability to integrate processing tools and AMHS for smooth functioning of the operations in a semiconductor wafer fabrication system. Here, we developed a multi-objective-based mathematical model for a real-time multiple objective scheduling problem. It mainly consists of two parts: the online real-time scheduler and off-line real-time scheduler; the online scheduler is mainly employed to monitor and convey the information between users; and it is illustrated in Fig. 1. It interacts with the off-line scheduler for accepting the combinatorial dispatching rules to optimize, and after completion of requisition, it applies the accepted combinatorial dispatching rules to the real system. Additionally, when new rules are selected, it automatically sends the information to the off-line schedule to retrieve the best results.

The off-line scheduler consists of four modules: GA parameters optimization module, simulation parameters optimization module, GA controller, and simulation module. The former two modules are used to search for better GA parameters such

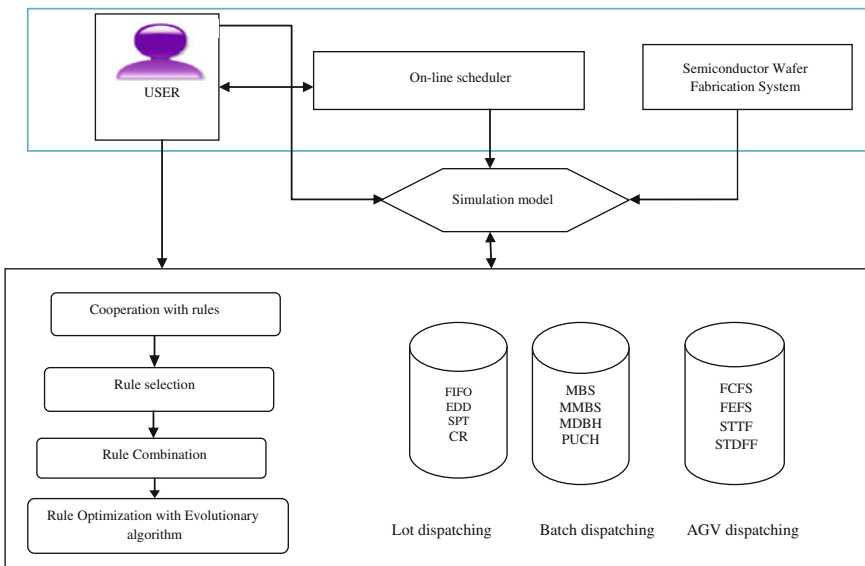


Fig. 1 GA-based simulation optimization methodology

as population size, crossover rate, mutation rate, stopping criteria, and simulation parameters, respectively. They are often conducted independently of a GA controller after receiving trigger signals from users or the online schedulers. The triggering signals mainly come from the system environment changes such as processing tool brake down or user requests.

3 GA Parameters Optimization by Taguchi Methodology

In the present study according to the Taguchi method implemented, a GA simulation procedure on a personal computer with core 2, 2.4 GHZ processor, and 2 GB RAM by using MINITAB software with a robust design and an L27 orthogonal array are employed for the experimentation. To conduct experimentation, the GA parameters such as number of population, crossover, mutation, and total number of generations are considered as controlling factors. Each of these parameters are varied with three levels, namely low, medium, and high, denoted by L1, L2, and L3, respectively, and it is shown in Table 1. The factors and their respective levels have been selected based on pilot experiments. The tabulated results given in Table 2 depict the process parameter, R_{avg} , and the variance (σ) ratio. Variance signifies higher value representing better sequence performance such as R_{avg} ‘higher-the-better,’ and inversely, the characteristics with lower value represent better sequence performance, such as variance (σ) ‘lower-the-better.’

Table 3 shows the results of two-factor regression analysis where the main effects and the interaction effect are significant for the performance measures with 95 % confidence level. As the quantity of new jobs, the level of job arrival rate and the interaction between the quantities of new jobs have a statistically significant impact on the performance measures. The considered candidate dispatching rules and the corresponding codes are shown in Table 4.

Table 1 Parameters and their levels

Factors	Levels		
	1	2	3
p/g	0.4	0.6	1.0
C	0.7	0.8	0.9
m	0.015	0.018	0.02

Table 2 Taguchi-based L_{27} experimental design

S. no	p/g	C	m	Ravg	σ
1	0.4	0.9	0.02	1.7972	0.2250
2	0.4	0.9	0.018	1.7975	0.2273
3	0.4	0.9	0.015	1.7981	0.2278
4	0.4	0.8	0.02	1.9456	0.2811
5	0.4	0.8	0.018	1.9460	0.2642
6	0.4	0.8	0.015	1.9465	0.2857
7	0.4	0.7	0.02	2.0382	0.3284
8	0.4	0.7	0.018	2.0386	0.3284
9	0.4	0.7	0.015	2.0391	0.3292
10	0.6	0.9	0.02	1.7972	0.2069
11	0.6	0.9	0.018	1.7975	0.2073
12	0.6	0.9	0.015	1.7981	0.2076
13	0.6	0.8	0.02	1.9456	0.2623
14	0.6	0.8	0.018	1.9460	0.2626
15	0.6	0.8	0.015	1.9465	0.2634
16	0.6	0.7	0.02	2.0382	0.3046
17	0.6	0.7	0.018	2.0386	0.3050
18	0.6	0.7	0.015	2.0391	0.3057
19	1.0	0.9	0.02	1.7972	0.1757
20	1.0	0.9	0.018	1.7975	0.1761
21	1.0	0.9	0.015	1.7981	0.1765
22	1.0	0.8	0.02	1.9456	0.2265
23	1.0	0.8	0.018	1.9460	0.2264
24	1.0	0.8	0.015	1.9465	0.2276
25	1.0	0.7	0.02	2.0382	0.2661
26	1.0	0.7	0.018	2.0386	0.2665
27	1.0	0.7	0.015	2.0391	0.2669

Table 3 Two-factor regression analysis

Term value	Coef	SE Coef	T-value	P-value
Constant	2.8947	0.0366	79.05	0.000
p/g	0.0000	0.0110	0.00	1.000
C	-1.2052	0.0336	-35.86	0.000
M	-0.18	1.34	-0.13	0.894

Table 4 Initial candidate dispatching rules

Lot dispatching rules		Batch dispatching rules		AGV dispatching rules	
No	Rules	No	Rules	No	Rules
1	FIFO	1	MBS	1	FCFS
2	PRI-FIFO	2	MMBS	2	FEFS
3	SPT	3	MDBH	3	CR
4	PRI-SPT	4	PUCH	4	EDD

4 Hierarchical Rule Combination

Recently, researchers are interested in developing new rule in an intuitive way that can be combined with the existing rules. However, from the literature, it is found that different rules can be combined with two approaches, i.e., hierarchical and weighted combination. In hierarchical combination, dispatching rules are applied sequentially where it is very difficult to identify single best rule for completion of the job. Chen et al. [4] used earliest duration time (EDD), first come first serve (FCFS), shortest processing time (SPT), and critical ratio (CR) rules hierarchically in a reentrant flexible job shop scheduling problem. If there is any tie exists, processing time is taken into consideration for selection, whereas in weighted combination rule, priority indices calculated by dispatching rules are aggregated through scaling of the functions. Baek et al. [5] combined rules through a linear weighted summation. They tried to determine the best weight of rules by stepwise search with orthogonal arrays. In this research paper, we have used the most prominent hierarchical combination rule for rule combination. Here, for chromosome representation, a gene can be considered as an integer value ranging from 1 to 4 representing lot dispatching rules. Batch dispatching rules and AGV dispatching rules will be represented by codes ranging from 1 to 4 and codes ranging from 1 to 4, respectively.

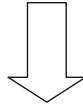
For example, if shortest processing time (SPT), critical ratio (CR), and first in first out (FIFO) rules used hierarchically for the bottleneck stations with long queue, then, for given n rules, there are $n!$ different permutations may be tested. In other words, for a small number of rules say ten in number, at least three million permutations should be tested. Further, if we want to use different hierarchical combination for different stations, the number of possible combinations will be much larger. In this case, we cannot enumerate and test all possible combinations but can rely on evolutionary algorithm simulation approach to seek for near optimal solutions. We use simple one-point or two-point crossover to exchange combined rules as a whole. Figure 2 shows where the two-point crossover exchanges the two hierarchical combinations of rules of machines 2 and 3 between two individuals. For exchanging the order of rules within a combined rule, we can use operators for permutation-based encoding like linear order crossover. Then, we apply linear order crossover to exchange the order of rules in the combined rules of machines 2 and 4. The linear order crossover exchanges the section enclosed by two random cutting points between two parents and fills the remaining positions by the unselected rules in the order they appear in the original parent. Mutation operators such as swap and insertion are available for changing the order of rules within the combined rule.

Two point crossover

4	1	2	3	2	3	1	4	2	4	1	3	1	4	2	3
---	---	---	---	---	---	---	---	---	---	---	---	---	---	---	---

2	1	3	4	4	3	1	2	3	1	2	4	1	3	2	4
---	---	---	---	---	---	---	---	---	---	---	---	---	---	---	---

Linear crossover



2	1	3	4	4	3	1	4	2	4	1	4	1	4	2	3
---	---	---	---	---	---	---	---	---	---	---	---	---	---	---	---

4	1	2	3	2	3	1	2	3	1	2	3	1	3	2	4
---	---	---	---	---	---	---	---	---	---	---	---	---	---	---	---

Fig. 2 Illustration of linear order crossover on individual with the representation scheme

5 GA Controller

Genetic algorithm can be considered as one of the best evolutionary algorithms for the computationally complex problems. It has very effective operators such as crossover, mutation, and selection which can help to obtain optimal schedule dispatching rule [6] (Fig. 3).

- Step 1: Set the parameters including population size (pop size), maximum iteration of the GA, crossover probability (p_c), and mutation probability (p_m).
- Step 2: Randomly generate pop size population. Decode each individual to obtain the fitness value. Compare them to obtain the initial solution x .
- Step 3: Set $n = 1$.
- Step 4: Generate new population for the next generations. Genetic evolution with three operations including selection, crossover, and mutation is applied to create offspring for the next population. Let $ch_i, i = 1, 2, \dots, \text{pop size}$ as the new population. The roulette wheel strategy is used to perform the selection.
- Step 5: Let each individual of the new population $ch_k, k = 1, 2, \dots, n \text{ pop size}$ as the initial solution. Repeat Step 3 to improve the quality of each individual until iteration is equal to pop size. Then go to Step 6.
- Step 6: set $j = 1$.

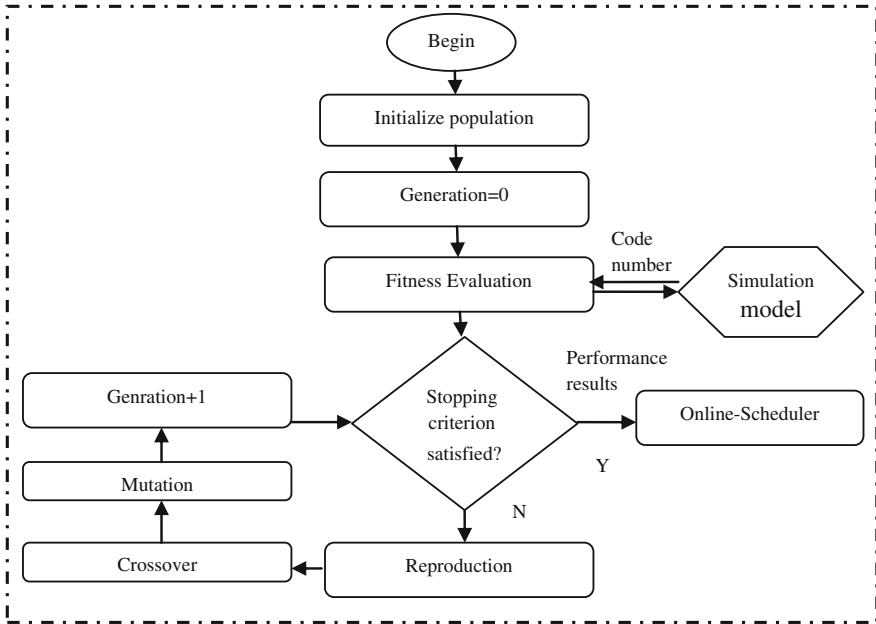


Fig. 3 The GA controller

6 Conclusions and Future Work

This paper proposes an evolutionary algorithm-based simulation optimization methodology for dispatching decision problem in a semiconductor wafer fabrication unit. We implemented a methodology that consisting of an online scheduler and off-line scheduler that can optimize the combinatorial dispatching rules including lot dispatching, batch dispatching, and AGV dispatching. The off-line scheduler phase has been conducted with four different modules such as optimization modules, simulation parameters optimization module, GA controller, and simulation module. Later, with Taguchi-based method, optimization of genetic algorithm parameters is conducted for searching better combinatorial dispatching rules. Finally, with real-time rule-based scheduling, the best combination rules are explored. In the future work, one can develop the multi-objective mathematical model with different performance measures and also try simulation approach for validation of the developed model.

References

1. Chang YJ. Multi-objective scheduling for IC sort and test with a simulation test bed. *IEEE Tran Semi Cond Manuf.* 1998;11(2):304-15.
2. Li L, Qiao F, Jiang H. The research on dispatching rules for improving on time delivery for semi conductor wafer fab. In: 8th International Conference on Control, Aero Machine, Robotics and Vision ICARCV, 2004, p. 404-4.
3. Wu MC, Huang Y, Chang VC, Yang KF. Dispatching in semi conductor with machine-dedication features. *Int J Adv Manuf Techhnol.* 2006;28(9):978-84.
4. Chen JC, Chen KH, Wu JJ, Chen CW. A study of the flexible job shop scheduling problem with parallel machine and re-entrant process. *Int J of Adv Manuf Technol.* 2008;39(3-4):344-5.
5. Baek DH, Yoon WC, Part SC. A special rule adaptation procedure for reliable production control in a wafer fabrication system. *Int J Pro Res.* 1998;36(6):147-9.
6. Can B, Hevey C. A comparison of genetic programming and artificial neural networks in meta-modelling of discrete events simulation models. *Comp OR.* 2012;39(2):424-36.

Least Square Mean Optimization-Based Real Object Detection and Tracking

Sanjay Rao, Deepak Jhanwar, Diwakar Gautam
and Anand Choudhary

Abstract In this paper, automatic real-time object detection and tracking is implemented via means of Kalman filter in which the system output is actually tracking the input canceling out any variation due to input and output noises. This paper can be used to develop a surveillance system of static camera and robotic automation visual systems. Whenever a new object comes in camera frame, system uses the concepts of frame subtraction then threshold image by Otsu's method, and later Kalman filtering is being processed to estimate the next following coordinates of its movement. The work presented here is extended to work at video processing stage. And finally, least square mean optimization technique is used to evaluate the set of system parameters for perfect tracking of forthcoming new objects, and once that parameter is evaluated it can be used to execute tracking process perfectly.

Keywords Kalman filter · Object detection · Otsu's method · Least square mean optimization · Automatic visual systems

1 Introduction

The real-time object detection and tracking has been a great field of research since emergence of field of Computer Vision and Image Processing. Earlier, many great contributions had been done by various scholars in this field. The video surveillance

S. Rao (✉) · D. Jhanwar · D. Gautam · A. Choudhary
Department of ECE, Government Engineering College Ajmer,
N.H. 8 Badliya Circle, Ajmer, India
e-mail: sanjaym.rao2012@gmail.com

D. Jhanwar
e-mail: deepakjhanwar2001@gmail.com

D. Gautam
e-mail: gdiwakar1987448@gmail.com

systems can be classified under two broad categories: static camera systems and moving camera systems. The work presented here is majorly concentrated on static systems while the presented concepts can be extended to moving camera systems by timely varying their reference frames. Background subtraction technique has been used a lot in previous works. But as technology develops, the processing time of new algorithms continues to shrink, here is too proposed a new method that is fast in processing with a fine result. Object detection can be done by two methods: (a) automatic systems and (b) manual systems. The manual system requires some human interference to locate any figure on the foreign object [1, 2], while in automated systems once the parameters have got set it can detect new foreign object by itself. In modern systems, this system can be implemented too by using color or texture information [3] of foreign objects in the frame. In previous approach, there has been a use of reference coordinates in the system to identify new objects; these coordinates can be obtained by taking edges of fixed bodies in the reference frames that restrict to perform within a certain class of surveillance systems. In advancement to that, this paper works on single- or multi-object detection by using morphological operations in the field of signal processing. The work presented here can be subdivided into various sections. Section A deals with object detection via averaging out histogram differences. Section B works with thresholding which is implemented using Otsu's threshold [4], but different methods can be used too for the same. Once the object is extracted from background, then morphological operations are used to detect number of new objects. Section C works on Kalman filter to estimate the next coordinates of object motion [5].

2 Otsu's Threshold and Class Separability

Histogram is probability representation of different gray levels in a given plane of three-dimensional images. Thus, thresholding is subdividing the whole system into two parts: foreground object and background object. There must be clear-cut valley in the histogram to easily evaluate the threshold value of gray level to subdivide our images. But this may not be the case for always, as many a times noise degrades the deep valley. In such a case, Otsu's method can be used to extract object in the image. In this method, the procedure followed in such a way that for every possible value of threshold, histogram is subdivided into classes. Then, total image variance, within the class variance and between the class variance, is used to evaluate the most exact value of threshold. This test is basically a measure of class separability. The gray image is converted into binary image using global threshold technique of Otsu's threshold [1]. If input is RGB image, result of Otsu's threshold in each plane is concatenated.

3 Object Detection and Extraction

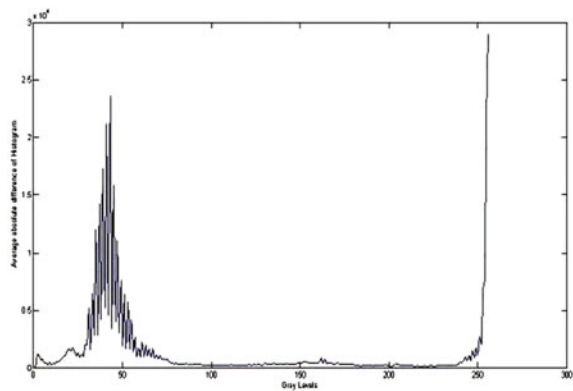
The histogram display of subsequent image sequences is frequency component, low-pass filtering will eliminate it, and result will be a more fine view of foreign labeling information of number of objects, which can be used as basic parameter to initiate Kalman filtering approach discussed later on. The detection of the foreign frames in consecutive frames is shown in Fig. 1, subtracted consecutively, and averaged out. The resultant peak at certain region of gray level indicates that the newcoming foreign object has gray scale in that particular range. The threshold image either from RGB plane or from single gray plane is first of all converted into a binary image. Then, morphological operations of image labeling are used to detect the number of objects in the image; prior to this operation, the extracted object is filtered with a low-pass filter to eliminate any noise in the image, as noise is high.

4 Discrete Kalman Filter

In order to track the moving objects, discrete version of Kalman filter is used. Kalman filter is basically estimator to follow system response irrespective of input or output and any other inherent system noises discussed later on. The detection of the foreign frames in consecutive frames is shown in the figure.

The filter predicts the next movement of object depending upon the parameters of previous and present state. Then, it measures variation of the observed value from predicted one. Thus, Kalman filter can be understood to work in two steps: (a) predictive stage and (b) measurement or correction stage analysis. As a paper is mostly concentrated on motion analysis, this paper is based on two types of error estimates: priory state estimates and posterior state estimates. Priory estimate is the prediction of next state parameters using the information of previous state, before the actual process is going to be occurred. Posterior estimate refers to state

Fig. 1 Object detection by averaging out histogram differences



estimation once the actual process or measurement has got completed. The complete module of the proposed technique is shown in the figure below:

$$x_k = Ax_{k-1} + w_k \tag{1}$$

$$x_k = \left[x, y, \frac{dx}{dt}, \frac{dy}{dt} \right]' \tag{2}$$

where A is state transition matrix relating the present state of process to its previous state and x_k represents system state at k th instance.

The state of system is represented via four important state variables: (a) x coordinate, (b) y coordinate, (c) directional velocity in x coordinate, and (d) directional velocity in y coordinate; thus, A can be represented in matrix notation as follows:

$$A = \begin{bmatrix} 1 & 0 & dt & 0 \\ 0 & 1 & 0 & dt \\ 0 & 0 & 1 & 0 \\ 0 & 0 & 0 & 1 \end{bmatrix} \tag{3}$$

where dt represents the time duration between consecutive frames. The measurement process of system response can be represented as follows:

The system inherent and measurement noise parameters are w and v , respectively. These are white noise independent of each other possessing normal probability distribution $p(w) N(0, Q)$ and $p(v) N(0, R)$. Q is variance of process inherent noise and R is that of measurement noise (error in measurement). Z_k presents the measurement at k th instance of system process. As it seems not an easy task to measure state variables, so as to convert these state variables into measurable quantities, H matrix is denoted as follows:

$$H = \begin{bmatrix} 1 & 0 & 0 & 0 \\ 0 & 1 & 0 & 1 \end{bmatrix} \tag{4}$$

In case if the effect of noises is very small, then residual signal is too small, so x_k is equal to \bar{x}_k , while this may not happen under significant effect of noises. In order to work under such circumstances, a priory state of x_k needs to be utilized represented as $\hat{x}_{\bar{k}}$. Thus, in priory state, the system and measurement equations during the priory state of x_k are expressed as $\hat{x}_{\bar{k}}$, and similarly whole system equations are represented as follows:

$$\hat{x}_{\bar{k}} = A\hat{x}_{\bar{k}-1} \tag{6}$$

$$\hat{Z}_k = H\hat{x}_{\bar{k}} \tag{7}$$

Similarly, the posterior state represents the ideal value of state variable neglecting any noise responses, x_k is represented as $\hat{x}_{\bar{k}}$ and, respectively, others. Then, the priory and posterior error estimates are expressed as follows:

$$e_{\bar{k}} = x_k - \hat{x}_{\bar{k}} \tag{8}$$

$$e_k = x_k - \hat{x}_{\bar{k}} \tag{9}$$

Associated with these errors is a mean square error, or error variance can be related as

$$\begin{aligned} P_{\bar{k}} &= E[e_{\bar{k}}e_{\bar{k}}^T] \\ P_k &= E[e_k e_k^T] \end{aligned} \tag{10}$$

As the system at a given state depends upon elements of previous state, it is vital to initialize system with some default parameters. Thus, initialization recommends null vector as starting state variables and first state covariance matrix as zero matrix. From Fig. 2, it is easy to notify that at every iteration of filtering, Kalman gain K_k varies and also error covariances Q and R (measurement noise variance). Finally, the combined function of updating and measurement can be regrouped as follows:

$$P_{\bar{k}} = AP_{k-1} + Q \tag{11}$$

$$K_k = P_{\bar{k}}H^T (HP_{\bar{k}}H^T + R)^{-1} \tag{12}$$

$$\hat{x}_k = \hat{x}_{\bar{k}} + K_k(Z_k - H\hat{x}_{\bar{k}}) \tag{13}$$

$$P_k = (1 - K_kH)P_{\bar{k}} \tag{14}$$

Fig. 2 Discrete Kalman filter model

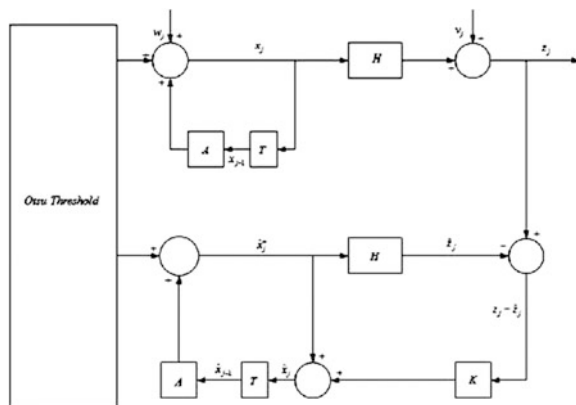
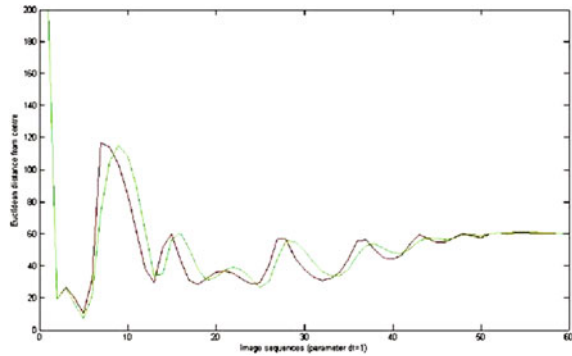


Fig. 3 Object tracking for lower values of frame occurrence rate $dt = 1$



The above equations are iterated for consecutive frames to exactly track up coordinates of moving objects. The noise variance R can be evaluated from static frames representing the noise variance executed in the measurement of the object coordinates. Thus, conclusions of Kalman filtering process can be described as follows (Fig. 3):

- (a) If the a priori error is very small, K_k is correspondingly very small, so our correction is also very small. In other words, we will ignore the current measurement and simply use past estimates to develop new estimate.
- (b) If the a priori error is very large, then in effect it tells to throw out the priority estimate and use the current (measured) value of the output to estimate the state.

5 Optimization of Frame Occurrence Timing

In actual practice, the frame extraction rate from general video sequence is 25 frames per second. But in this processing environment, it is very difficult to exactly define the time difference between consecutive frames due to above-specified conclusions of Kalman filtering process. The least mean square optimization or minimum deviation technique is implemented to evaluate the average frame occurrence rate, so that the system can track exactly moving objects, i.e., there must be a complete overlap among object centroid and tracking coordinates. One may use different notation of distance measurement such as absolute difference or Euclidean measurement to evaluate frame timing parameter by calculating mean square error between estimated measurement and actual measurement. Optimization result is figured as below.

Thus, it can be said that at higher values of frame occurrence rate, there tends to be minimum deviation between estimated and observed values.

6 Results and Conclusion

After applying the above-proposed technique on a practical video file, it seems very deterministic to detect new foreign object in image sequences or in a video file, the Red Cross represents the centroid of foreign object, and Green Square represents its Kalman filter estimated coordinates of its position at current state of system progress. The important point to be noted here is in Figs. 4 and 5, the variation in system parameter of frame occurrence timing, and Fig. 4 represents the result of unoptimized parameter and shows no overlap means moving object is not tracked perfectly while optimized result is shown in Fig. 5 where dt parameter is evaluated from whole system performance showing most perfect object tracking. Once this parameter is evaluated, it can be wholly utilized for the best result for any video or image sequences for this system. From Fig. 6, it is clearly visible that our approximation precisely matches the actual position of the object, giving us the authentication of the algorithm.

Fig. 4 Object tracking for optimized frame occurrence rate $dt = 100$

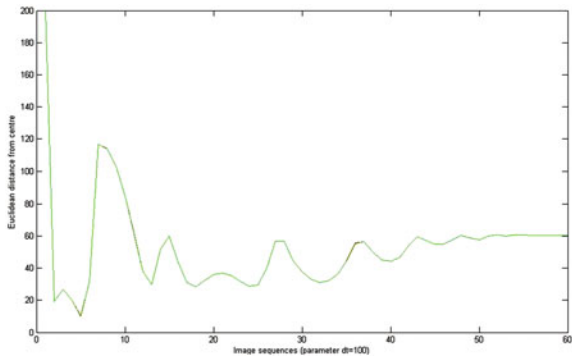


Fig. 5 Optimization of frame occurrence timing

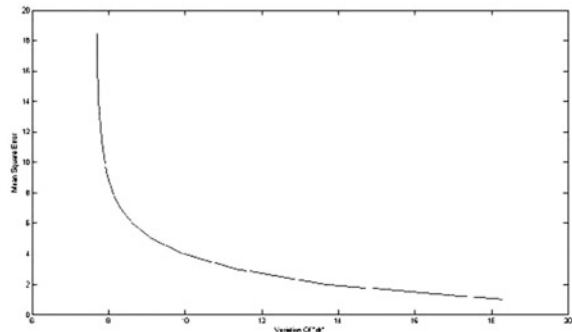


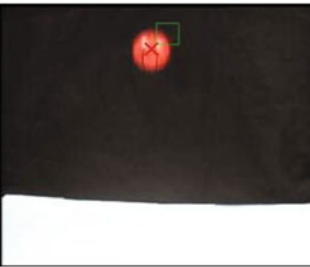







Image sequence	Frame rate(dt =1)	Frame rate (dt=100)
1.		
2.		
3.		
4.		

Fig. 6 Image sequences of real-time object tracking

References

1. Rother C, Kolmogrov V, Blake A. Grab cut interactive foreground extraction using iterated graph cuts. In: Proceedings of the SIGGRAPH, 2004.
2. Tan K-H, Ahuja N. Selecting objects with freehand sketches. In: Proceedings IEEE Computer Society Conference on Computer Vision and Pattern Recognition, 2001.
3. Ning J, Zhang L, Zhang D, Wu C. Robust object tracking using joint color-texture histogram. *Int J Pattern Recogn Artif Intell.* 2009;23:1245–63.
4. Mehta M, Goyal C. Real time object detection and tracking: histogram matching and Kalman filter approach. *IEEE Conf.* 2010;5:796–801.
5. Welch G, Bishop G. An introduction to the Kalman filter. In: Presented at Annual Conference on Computer Graphics & Interactive Techniques, ACM SIGGRAPH, 2001, p. 201–4, 2001.

Improving Efficiency and Fairness in Mobile Ad Hoc Networks

Varun Manchikalapudi and Sk. Khadar Babu

Abstract All mobile ad hoc networks (MANETs) exhibit versatile behaviour in its topology because of node mobility factor. In theory, TCP happens to be a transport layer protocol designed to provide a reliable end-to-end delivery of data over unreliable networks. But in reality, TCP encounters some challenges in multi-hop ad hoc networks especially route failures and so congestion. To address this problem previously, contention detection using congestion window adaptation (CWA-CD) procedures are designed and implemented to handle route failures. Its performance is not up to the mark because of the complexity encountered in detecting the contention variations from the round-trip time delays. So for a robust and better network performance, we propose to use candidate list generation algorithm for packet forwarding with congestion control by contention control (4C) method. The algorithm involves constant updates of location specifics for every small intervals of time and steps to sort out the forwarding list that aids communication. As a result, nearest nodes or routers participate in data transmission and this improves network performance and controls the congestion. A practical implementation of the proposed system validates the claim in terms of efficiency and fairness.

Keywords MANET · TCP · Contention · Congestion · Efficiency · Fairness

1 Introduction

mobile ad hoc networks (MANETs) are a type of unguided ad hoc network that often refers to a function of IEEE 802.11 [1] unguided network, and it has networking environment which is routable. MANETs do not require any external effort

V. Manchikalapudi (✉)

School of Computing Science & Engineering, VIT University, Vellore, India
e-mail: varunmanchikalapudi@gmail.com

Sk.Khadar Babu (✉)

School of Advanced Sciences, VIT University, Vellore, India
e-mail: Khadarbabu.sk@vit.ac.in

© Springer India 2016

S.S. Dash et al. (eds.), *Artificial Intelligence and Evolutionary Computations in Engineering Systems*, Advances in Intelligent Systems and Computing 394, DOI 10.1007/978-81-322-2656-7_92

1001

in order to control its infrastructure. They consist of end-to-end, self-making, self-recoverable network. In contrast to a mesh topological network, MANETs can configure themselves and change locations on the fly. A wireless ad hoc network is a decentralized kind of unguided network. The network is ad hoc because it does not depend on its pre-existing infrastructure, such as guided media network routers or access points in managed (infrastructure) unguided media networks. Instead, each node participates in routing by forwarding data segments for other nodes, so the determination of which node forwards the data is done automatically on the basis of connectivity of the communication network.

The flow rate is not properly given in MANETs due to many problems such as node migration, unguided link failures, channel, or bandwidth capacity variation, so it is required to find the solution for these problems. Moreover, these problems will affect the fairness and efficiency in MANETs. Fairness and efficiency are the two challenges or objectives to achieve when the flow control is come into the scene. Fairness means all the competing flows must have the equal share of the channel capacity or bandwidth and efficiency, or throughput in the form of efficiency is accumulated network traffic at the router must coincide with the available channel capacity of the outgoing links or connections.

In theory, TCP is designed to provide a reliable end-to-end delivery of data over unreliable networks, but in reality, TCP exhibits some challenges in multi-hop ad hoc networks especially route failures. Optimized TCP protocols using contention methods, i.e. contention detection using congestion window adaptation (CWA-CD) procedures, were used to handle route failures. In MANET, every node is functioned solely, and unfairly, information of one node has been accessed by other nodes in the network. Due to this, we face some problems such as network congestion, unfair bandwidth allocation, and decrease in throughput. We use "candidate list generation algorithm" to handle node mobility factor with the combination of congestion control by contention control procedure.

The candidate list will be attached to the packet header and updated hop by hop. Only the nodes specified in the candidate list will act as forwarding candidates. The lower the index of the node in the candidate list, the higher the priority it has. In proposed system, the nodes which are close together participate in the data transmission. So a better ad hoc network that is robust to node mobility is constructed using the above methods.

2 Existing System

In existing system, bandwidth delay product is calculated with congestion window adaptation and contention detection technique. In data communications, bandwidth delay product [2] refers to the product of data link capacity which is calculated in terms of bits per second and its round-trip delay time which is in seconds. Here, contention is detected by dividing or explaining the round-trip time in two ways, one is contention RTT and another one is congestion RTT. We all know that

congestion occurs due to the problem obtained by contention between the network nodes. Network performance is gradually decreased due to the overhead of capturing the contention RTT values [2].

Moreover, in MANET, every node functions independently and all the nodes try to access the links bandwidth so the packets send by one station may also be available to other stations [3], because of this, network performance is degraded and fairness is not achieved. Figure 2 represents a MANET in which all the nodes have huge number of links to other nodes in the same network, the packets send by one node are made available to the other nodes, and every node will access those packets.

As shown in Fig. 1, the MANET completely filled with congestion or unfair accessing of information in the network among the nodes. This leads to heavy traffic load and unfair data transmission and slow data transmission rate, i.e. reduction in throughput. Due to all these drawbacks in existing system, enhancements had been done and are presented in this paper.

In Fig. 2, there are 10 nodes taken for sample and these nodes are being connected to other nodes in an unfair manner, and due to this, fairness is not achieved and efficiency of network in the form of throughput will be degraded. Assume every

Fig. 1 Illustration of MANET and packet transmission with unfair data transmission

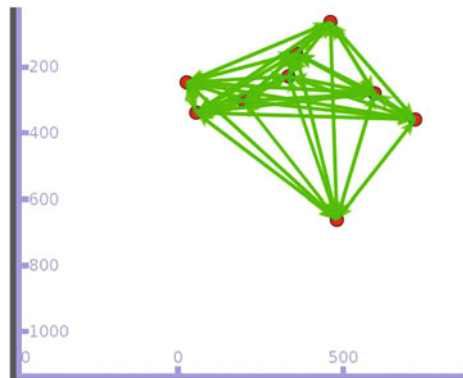
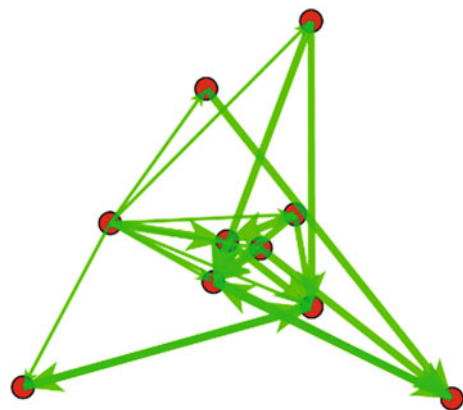


Fig. 2 Illustration of MANET and Packet transmission with better performance to some extent



individual node acts as a sender or receive. So we need to go for the further extensions to this model in order to get the efficiency and fairness among the nodes in the MANET.

3 Proposed Method

Existing mechanisms [2, 4] focused on link contentions and congestion control process. Even though, for calculating contention variation for every RTT is difficult because in the network, we keep sending so many packets from source to destination. So this process becomes very complex in order to observe the contention variation for every time interval, and bandwidth allocation is done unfairly. Link failures due to mobility are part of the main sources of link unreliability in MANETs. Among the proposed solutions to improve throughput of a network in MANET, we find a mechanism that focuses on MANET routing environment that exhibits high data transmission rates and less latency and reduces network congestion and fairness. In this paper, we propose to develop candidate list generation for packet forward algorithm along with congestion control by contention control (4C) method to handle route failures efficiently.

Algorithm

```

Algorithm      : Candidate node selection for packet forwarding
ListN         : Neighbor list
ListC         : Candidate list, initialized as an empty list
Nr            : Receiver node
Base          : Distance between current node and Nr
               If (find (ListN, Nr) then
                   Next, hop ← Nr
                   Return
               End if
               For i ← 0 to length (ListN[i], Nr)
               End for
               ListN.sort ()
               Next.hop ← ListN [0]
For i, ← 1 to length(ListN) do
  If dist (ListN[i], Nr) >= base or length (ListN)=N
  Then
    Break
  Else if dist (ListN[i], ListN [0]) < R/2 then
    ListC.add (ListN[i])
  End if
End for

```

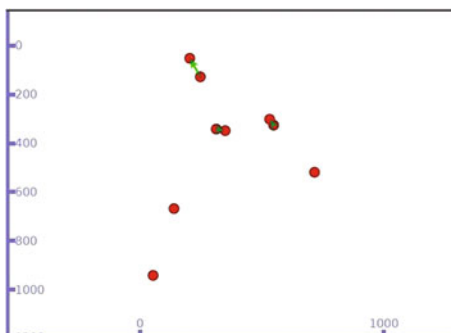
In the algorithm, ListN represents the neighbour list and ListC represents the candidate list, and the logic of algorithm verifies all the neighbours and selects candidate nodes through which data packets can be transferred to other nodes.

3.1 Congestion Control by Contention Control (4C) Procedure

Congestion and contention together degrade the network performance certainly, and one of the main reasons for congestion is simultaneous attempts to access the single network channel. So if we can control the contention problem, then obviously we can also control the congestion problem in MANET by using congestion control by contention control procedure. Every packet in the network contains a special header in which source and destination address is stored. As per the algorithm for the entire network, candidate node selection is done for packet forwarding. We all know that MANET migrates frequently from one place to another in all the way. Every nearest router checks the packet header and transfers that packet to nearest router in such a way that it reaches the target place or node.

The neighbour node verifies the special packet, and if it is not the target node, just forward to the next node and vice versa. If the target node is found with the help of acknowledgement, then it starts transferring the packets as long as the route is available. Due to mobility, if the target node goes faraway, then the link failure is occurred. Nodes in MANET continuously check the status of their neighbours by sending hello packets for every interval of time and update the routing table, and the router always stores the details according to the nearest router first. So it can easily allocate the next reliable route when link failure is identified, and due to this, continuous path will be maintained with less latency, and it also controls the packet loss and maintains high data transmission rate which causes throughput. When network haves multiple hops [5], then only the problem occurred usually is congestion, and due to this, packet loss or throughput reduction is happened. So handing route failure in multipath network is a challenge really and causes poor performance [6] of network (Fig. 3).

Fig. 3 MANET having fair bandwidth allocation and data transmission between nearest routers



4 Results and Observations

This result additionally demonstrates more change than the case in the past static situation [7], and accordingly, it outlines that the easing of blockage window overshooting still viably works in the element situation (Figs. 4, 5 and 6).

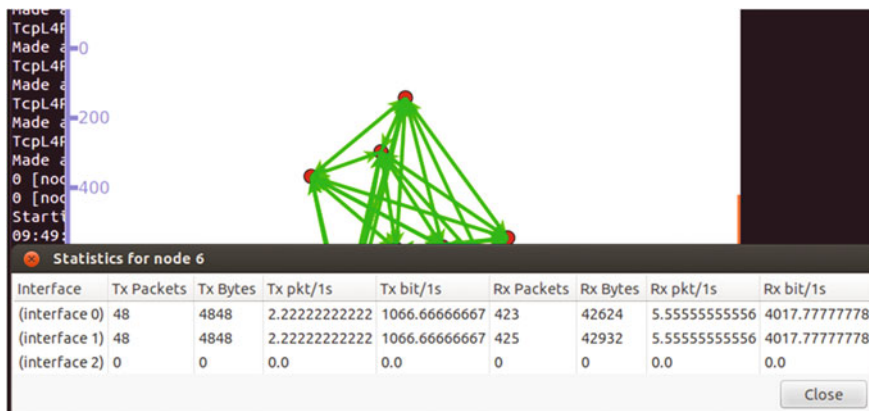


Fig. 4 Statistics for data transmission in the network

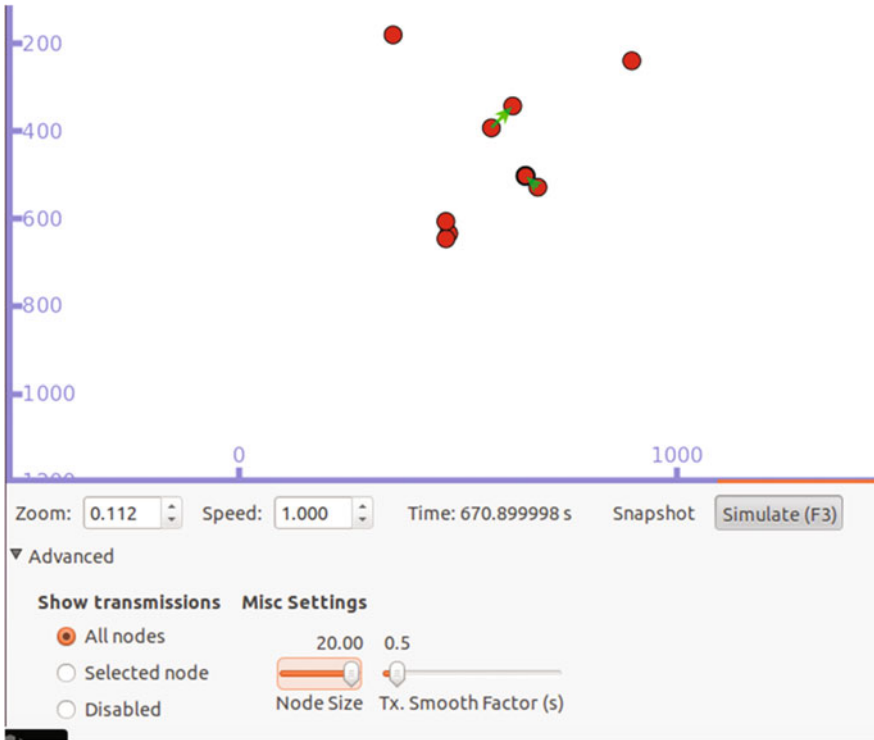


Fig. 5 Data transmission among the nearest nodes

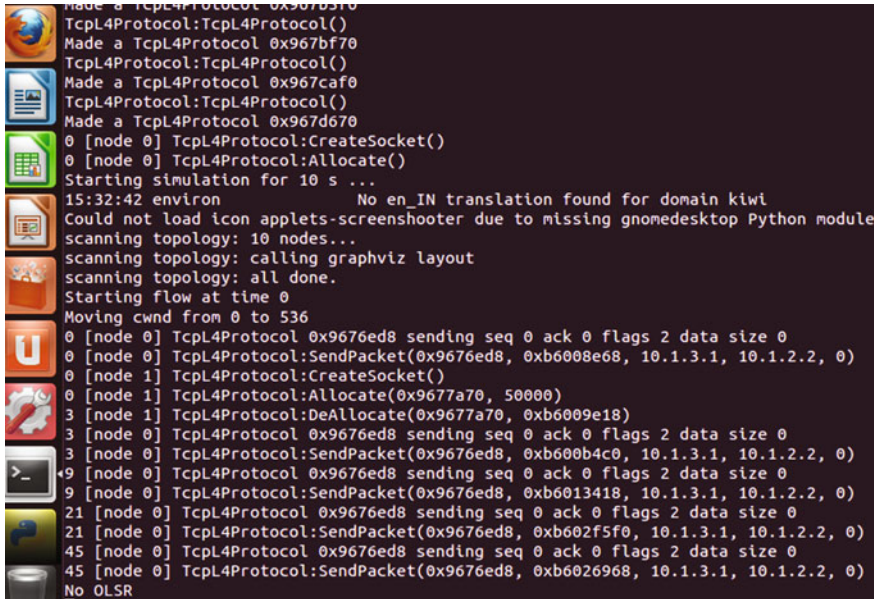


Fig. 6 Details of protocols displayed in the terminal

5 Conclusion

In this paper, we prefer to explain all data transmitting operations in order to improve the efficiency and fairness of the MANET. We present a new method called congestion control by contention control (4C) method in which contention is controlled in such a way that nearby nodes will participate in data transmission and we are using candidate node selection for packet forwarding algorithm. This algorithm keeps track of updated routing table which consists of list of nodes selected for packet forwarding and checks the status of the node in the network. Data packets are transferred as every node consists of packet header which holds source and destination address. This process reduces the contention and congestion, improves the throughput without packet loss, and maintains the fairness by allocating available bandwidth properly among several nodes.

References

1. Hoebek J, Moerman I, Dhoedt B, Demeester P. An overview of mobile ad hoc networks: applications and challenges.
2. Lakshman TV, Member, IEEE, and Upamanyu Madhow, Senior Member. IEEE: the performance of TCP/IP for networks with high bandwidth-delay products and random loss.
3. Cai DWH, Tan CW, Steven H. Low: towards reliable data delivery in MANET.
4. Chen K, Nahrstedt K, Vaidya N. The utility of explicit rate-based flow control in mobile ad hoc networks.
5. Fu Z, Zerfos P, Luo H, Lu S, Zhang L, Gerla M. UCLA computer science department: the impact of multi-hop wireless channel on TCP throughput and loss.
6. Ghosekar P, Katkar G, Ghorpade P. TCP throughput in multihop wireless networks. In: Proceedings of the of IEEE GLO.
7. Heffei CWB, Nanali DKS. TCP congestion window adaptation through contention detection in ad hoc networks by Xin Ming Zhang School of Computer Science and Technology, University of Science and Technology of China.

A Novel Content-Based Image Indexing and Retrieval Framework Using Clockwise Local Difference Binary Pattern (CWLDBP)

M. Ravinder and M. Tirupathamma

Abstract In this chapter, we propose a novel content-based image indexing and retrieval framework based on clockwise local difference binary pattern. Local binary pattern (LBP) is a popular texture content-based image indexing and retrieval framework proposed by Ojala et al. [1]. In our proposed method, we find the pair-wise difference between the pixels in clockwise direction of 3×3 neighborhood and the result of difference is used to find the binary pattern. Three novel methods such as CWLDBP1, CWLDBP2, and CWLDBP3 are proposed. The main advantage of the proposed methods such as CWLDBP1 and CWLDBP2 is the use of few binary patterns compared to LBP. That is, our proposed methods CWLDBP1 and CWLDBP2 use only sixteen binary patterns to index an image. To test our proposed method, we use Corel 1k database. Our proposed method has shown reasonable results when compared to 3×3 neighborhood-based LBP rotational invariant, LBP uniform, and LBP uniform rotational invariant methods.

Keywords LBP · Local difference · Neighborhood · Pattern · Image · CWLDBP

1 Introduction

Increase in capability of data storage technology has witnessed a huge growth of multimedia content especially image repositories. The result of which is the need for an efficient content-based image indexing and retrieval framework. Here, the content means the features of image such as color, texture, and shape. The advantage of content-based image indexing is the automatic assignment of index to

M. Ravinder (✉)
JNTUK, Kakinada, AP, India
e-mail: ravinder.rsh@gmail.com

M. Tirupathamma
Department of ECE, JNTUHCEJ, Karimnagar, Telangana, India
e-mail: tirupathamma.jntu@gmail.com

an image based on content instead of using a textual keyword. The growth of new techniques based on content of image has shown tremendous results in solving the problem of retrieving relevant image information from huge repositories of images.

Local binary pattern popularly known as LBP is a texture content-based image indexing and retrieval framework proposed by Ojala et al. [1]. LBP is a simple and efficient framework based on extracting texture features from an image using a 3×3 neighborhood. LBP operator represents an image using two hundred and fifty six binary patterns.

Other variants of LBP are rotationally invariant LBP, and uniform LBP which is useful in representing the image efficiently with less number of feature vectors is compared to normal LBP.

Due to its effectiveness and simplicity, the LBP operator has been used in number of applications such as face recognition task [2], facial expression recognitions task [3], segmentation of texture [4], and texture-based classification [5–7].

Various extensions to the standard LBP have been proposed in the literature for image and face classification applications [8–13].

An extension of the LBP operator which is used for representing a texture video using volume local binary pattern (VLBP) has been proposed [10, 11].

The rest of this chapter is organized as follows: Sect. 2 discusses the LBP in detail; Sect. 3 describes our proposed novel frameworks; Sect. 4 discusses experiments and results; and Sect. 5 concludes the chapter.

2 Local Binary Pattern

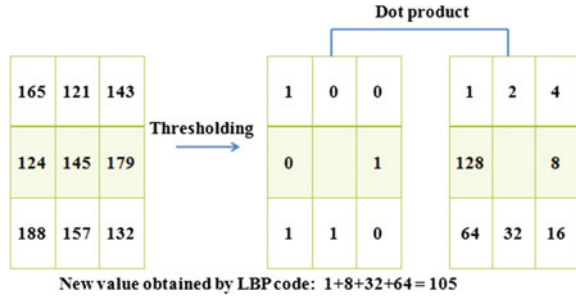
Local binary pattern operator proposed by Ojala et al. [1] is mainly used for texture-based image classification and retrieval. The standard LBP operation is based on a 3×3 neighborhood. In this chapter, we mainly concentrate on a 3×3 neighborhood for proposing the new frameworks. The standard steps in finding the LBP code for an image are given as follows:

- Step 1: After selecting a 3×3 neighborhood, threshold the eight neighbor pixels based on sign obtained by finding the difference between the neighbors and the center pixel values.
- Step 2: Multiply the thresholding result with the binary weights and sum up all the values to get the binary value code for the center pixel.

Consider $p_1, p_2, \dots, p_7, p_8$ are the neighbor pixels and p_c is the center pixel of a 3×3 neighborhood. Then, the LBP for the center pixel can be obtained by the following equation:

$$\text{LBP}(\text{Center pixel}) = \sum_{a=1}^8 2^{a-1} * f(p_a - p_c) \quad (1)$$

Fig. 1 Calculation of LBP values for center pixel of a 3×3 neighborhood



where $f(v)$ is the threshold function

$$f(v) = 1 \text{ if } v \geq 0,$$

$f(v) = 0$, otherwise. And p_c is the center pixel and p_a is the neighbor pixel.

The procedure of finding local binary pattern (LBP) is as shown in Fig. 1.

3 Proposed Method

In this section, we propose three novel clockwise local difference binary pattern algorithms meant for content-based image indexing and retrieval framework. Our framework is based on 3×3 neighborhood pixels of an image. Consider the following 3×3 neighborhood as shown in Fig. 2.

As shown in Fig. 2, P1, P2, ... P9 are the positions of pixels in a 3×3 neighborhood. As explained earlier, our proposed method mainly focused on a 3×3 neighborhood.

3.1 Algorithm 1: For CWLDBP1

Step 1: In a 3×3 neighborhood of an image, find the difference between values of pixels positioned at P1 and P7, followed by P4 and P8, by P9 and P3, and by P6 and P2. That is

Fig. 2 An example of 3×3 neighborhood

P1	P4	P7
P2	P5	P8
P3	p6	P9

- V1 = pixel value at (P1) – pixel value at (P7)
- V2 = pixel value at (P4) – pixel value at (P8)
- V3 = pixel value at (P9) – pixel value at (P3)
- V4 = pixel value at (P6) – pixel value at (P2)

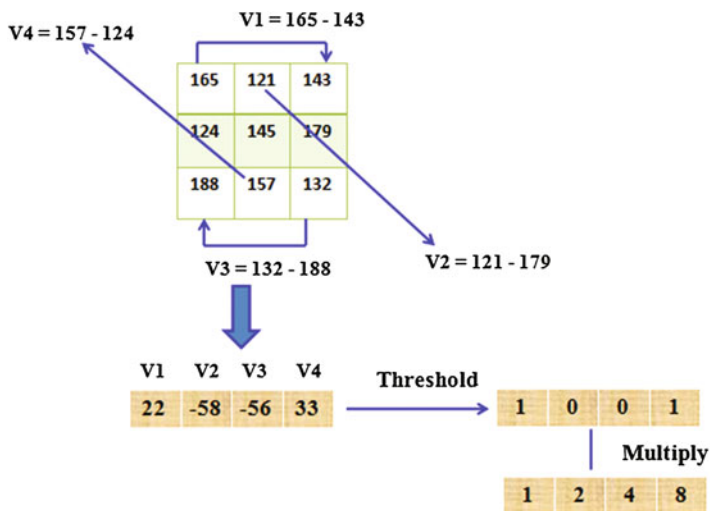
Step 2: Threshold the values V1, V2, V3, and V4 using a threshold T. In our case, value of T is 0. That is, find out whether the values V1, V2, V3, and V4 are greater than zero or not. If the value is greater than zero, then the new value will become one otherwise the new value will become zero. For example

```

If V1 > 0
V1 = 1
Else
V1 = 0
End
    
```

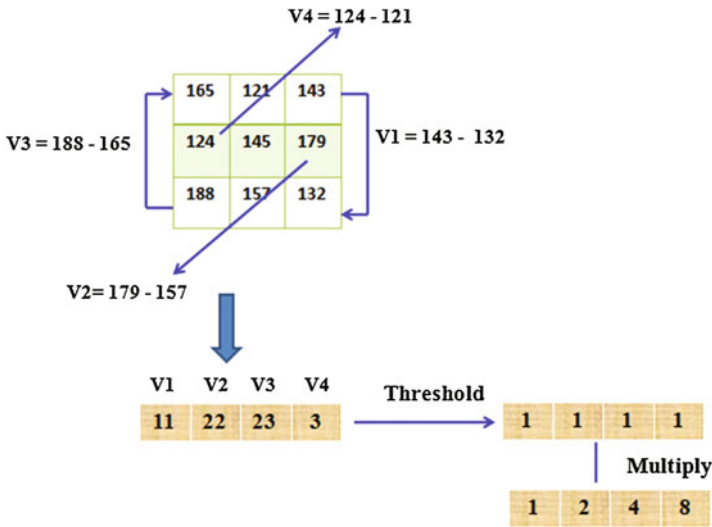
Step 3: To the threshold resultant values vector [V1, V2, V3, V4] obtained in Step 2, we perform dot product with the vector [1, 2, 4, 8] and find out the sum of all to get the binary code for the center pixel P5.

The procedure followed in the proposed Algorithm 1 is as shown in Fig. 3 with an example of calculation of new value for center pixel at position P5 (in Fig. 2).



New value for center pixel at position p5 is 1*1+0*2+0*4+1*8 = 9

Fig. 3 Example calculation of center pixel value using Algorithm 1



New value for center pixel at position p5 is $1*1+1*2+1*4+1*8 = 15$

Fig. 4 Example calculation of center pixel value using Algorithm 2

3.2 Algorithm 2: For CWLDBP2

Step 1: In a 3×3 neighborhood of an image, find the difference between values of pixels positioned at P7 and P9, followed by P8 and P6, by P3 and P1, and by P2 and P4. That is

- $V1 = \text{pixel value at (P7)} - \text{pixel value at (P9)}$
- $V2 = \text{pixel value at (P8)} - \text{pixel value at (P6)}$
- $V3 = \text{pixel value at (P3)} - \text{pixel value at (P1)}$
- $V4 = \text{pixel value at (P2)} - \text{pixel value at (P4)}$

Step 2: Threshold the values V1, V2, V3, and V4 using a threshold T. In our case value of T is 0. That is, find out whether the values V1, V2, V3, and V4 are greater than zero or not. If the value is greater than zero, then the new value will become one otherwise the new value will become zero. For example

- If $V1 > 0$
- $V1 = 1$
- Else
- $V1 = 0$
- End

Step 3: To the threshold resultant values vector [V1, V2, V3, V4] obtained in Step 2, we perform dot product with the vector [1, 2, 4, 8] and find out the sum of all to get the binary code for the center pixel P5. The procedure followed in the proposed Algorithm 2 is as shown in Fig. 4 with an example of calculation of new value for center pixel at position P5.

3.3 Algorithm 3: For CWLDBP3

Step 1: In a 3 × 3 neighborhood of an image, find the difference between values of pixels positioned at P1 and P7, followed by P4 and P8, P9 and P3, P6 and P2, P7 and P9, P8 and P6, P3 and P1, and by P2 and P4. That is

- V1 = pixel value at (P1) – pixel value at (P7)
- V2 = pixel value at (P4) – pixel value at (P8)
- V3 = pixel value at (P9) – pixel value at (P3)
- V4 = pixel value at (P6) – pixel value at (P2)
- V5 = pixel value at (P7) – pixel value at (P9)
- V6 = pixel value at (P8) – pixel value at (P6)
- V7 = pixel value at (P3) – pixel value at (P1)
- V8 = pixel value at (P2) – pixel value at (P4)

Step 2: Threshold the values V1, V2, V3, V4, V5, V6, V7, and V8 using a threshold T. In our case value of T is 0. That is, find out whether the

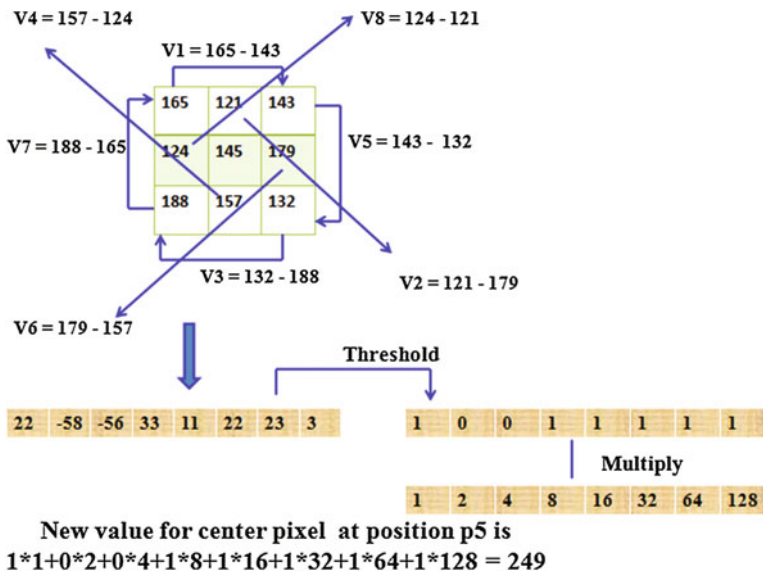


Fig. 5 Example calculation of center pixel value using Algorithm 3

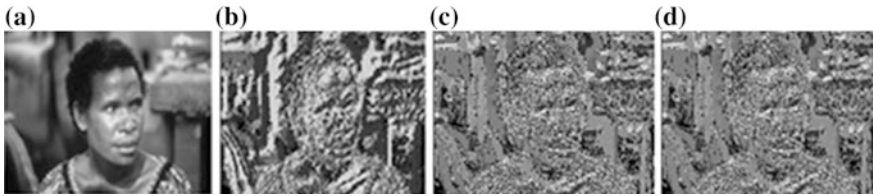


Fig. 6 **a** Gray scale image; **b** result of CWLDBP1; **c** result of CWLDBP2; **d** result of CWLDBP3

values $V_1, V_2 \dots V_8$ are greater than zero or not. If the value is greater than zero, then the new value will become one otherwise the new value will become zero. For example

- If $V_1 > 0$
- $V_1 = 1$
- Else
- $V_1 = 0$
- End

Step 3: To the threshold resultant values vector $[V_1, V_2, V_3, V_4, V_5, V_6, V_7, V_8]$ obtained in Step 2, we perform dot product with the vector $[1, 2, 4, 8, 16, 32, 64, 128]$ and find out the sum of all to get the binary code for the center pixel at position P_5 .

The procedure followed in the proposed Algorithm 3 is as shown in Fig. 5 with an example of calculation of new value for center pixel at position P_5 .

An example gray scale image from Corel-1k dataset and the resultant images after applying the proposed algorithms are shown in Fig. 6.

4 Experiments and Results

In this section, we discuss experiments and results of our proposed algorithms. To evaluate the performance of our proposed algorithms, we have used the Corel 1k dataset which consists thousands of images consisting of ten different categories of images (Hundred images of each category). We compare our proposed algorithms with already-existing methods such as 3×3 neighborhood-based LBP Rotational Invariant (**LBP-ri**), LBP Uniform (**LBP-u2**), and LBP Uniform Rotational Invariant (**LBP-riu2**).

In our experiments for finding best matches for a given query image, we have used the *k-nearest neighbor search* algorithm.

The experimental results (Precision % based on top 10 resultant images retrieved for a query image) are shown in Table 1.

The experimental results (Recall % based on top 100 resultant images retrieved for a query image) are shown in Table 2.

Table 1 Results in terms of precision ($n = 10$) (%) for various categories (S. no) of images in Corel-1k dataset

S. no	LBP-ri	LBP-u2	LBP-riu2	CWLDDBP1	CWLDDBP2	CWLDDBP1 + CWLDDBP2	CWLDDBP3
1	53.7	56.3	52.3	54.2	46.2	54.0	60.4
2	36.6	46.3	36.6	49.9	44.2	50.9	49.2
3	36.1	38.4	35	43.2	45.6	46.9	46.5
4	87.9	85.7	84.9	86.5	73.7	87.9	92.8
5	96.2	96.9	96.7	96.4	95.3	96.0	95.1
6	36.9	39.5	36.9	39.3	39.9	41.7	43.7
7	81	87	82.2	77.5	73.8	79.9	81.2
8	64.2	64.2	63.8	68.6	74.9	71.8	78.4
9	36.3	34.2	34.2	38.4	30.1	34.2	37.5
10	51.7	49.7	49.5	40.6	35.3	41.2	47.1
Avg	58.06	59.82	57.21	59.46	55.90	60.45	63.19

Table 2 Results in terms of recall ($n = 100$) (%) for various categories (S. no) of images in Corel-1k dataset

S. no	LBP-ri	LBP-u2	LBP-riu2	CWLDDBP1	CWLDDBP2	CWLDDBP1 + CWLDDBP2	CWLDDBP3
1	33.00	33.18	32.73	35.72	27.18	34.85	35.05
2	22.19	24.05	21.95	28.33	22.80	26.87	25.12
3	19.18	19.19	18.81	19.92	23.44	21.90	22.04
4	50.38	46.88	47.13	53.07	47.19	55.82	57.41
5	68.95	64.04	65.88	84.42	84.24	84.89	81.16
6	19.94	20.36	19.47	21.54	20.29	22.20	22.99
7	40.5	44.04	42.4	38.49	34.83	39.20	39.10
8	33.51	33.17	32.07	42.32	45.50	45.27	47.36
9	24.55	20.44	23.90	21.99	15.31	19.56	20.36
10	26.51	24.31	25.87	21.46	19.23	22.92	24.43
Avg	33.87	32.96	32.03	36.72	34.00	37.34	37.50

In the above tables, various categories of images in Corel-1k are 1-Africans, 2-Beaches, 3-Buildings, 4-Buses, 5-Dinosaurs, 6-Elephants, 7-Flowers, 8-Horses, 9-Mountains, 10-Food, and AVG represents average

5 Conclusion

In this chapter, we have proposed three new algorithms based on a 3×3 neighborhood in an image, meant for content-based image indexing and retrieval framework. We have evaluated our proposed algorithms using Corel-1k dataset and our proposed algorithms have shown reasonable results in terms of precision and recall. In our future work, we will try to improve the performance of above-proposed algorithms with the help of Gabor filters.

References

1. Ojala T, Pietikainen M, Harwood D. A comparative study of texture measures with classification based on feature distributions. *Pattern Recogn.* 1996;29(1):51–9.
2. Ahonen T, Hadid A, Pietikäinen M. Face description with local binary patterns: application to face recognition. *IEEE Trans Pattern Anal Mach Intell (PAMI)*. 2006;28:2037–41. doi:[10.1109/TPAMI.2006.244](https://doi.org/10.1109/TPAMI.2006.244).
3. Shan C, Gong S, McOwan PW (2005) Robust facial expression recognition using local binary patterns. In: *Proceedings of the International Conference on Image Processing (ICIP)*, 2005, p. 370–3.
4. Ojala T, Pietikainen M. Unsupervised texture segmentation using feature distributions. *Pattern Recogn.* 1999;32(3):477–86. doi:[10.1016/S0031-3203\(98\)00038-7](https://doi.org/10.1016/S0031-3203(98)00038-7).
5. Ojala T, Pietikainen M, Maenpaa T. Multiresolution gray-scale and rotation invariant texture classification with local binary patterns. *IEEE Trans Pattern Anal Mach Intell (PAMI)*. 2002;24(7):971–87. doi:[10.1109/TPAMI.2002.1017623](https://doi.org/10.1109/TPAMI.2002.1017623).
6. Topi M, Timo O, Matti P, Maricor S. Robust texture classification by subsets of local binary patterns. In: *Proceedings of the International Conference on Pattern Recognition (ICPR)*, 2000, p. 935–8.
7. Topi M, Matti P, Timo O. Texture classification by multipredicate local binary pattern operators. In: *Proceedings of the International Conference on Pattern Recognition (ICPR)*, 2000, p. 939–942.
8. Liao S, Law M, Chung A. Dominant local binary patterns for texture classification. *IEEE Trans Image Process.* 2009;18(5):1107–18.
9. Zhao G, Pietikainen M. Dynamic texture recognition using local binary patterns with an application to facial expressions. *IEEE Trans PAMI* 2007;29(6):915–928.
10. Zhang S, Yao H, Liu S. Dynamic background modeling and subtraction using spatio-temporal local binary patterns. In: *ICIP*, 2008, p.1556–9.
11. Guo Z, Zhang L, Zhang D. Rotation invariant texture classification using LBP variance (LBPV) with global matching. *Pattern Recogn.* 2010;43(3):706–19.
12. Xie S, Shan S, Chen X, Gao W. V-LGBP: volume based local Gabor binary patterns for face representation and recognition. In: *Proceedings of the ICPR*, 2008.
13. Maenpaa T, Pietikainen M. Multi-scale binary patterns for texture analysis. In: *Proceedings of the SCIA*, 2003.

Self-organization Strategies for Hierarchical Network Structure in Wireless Ad Hoc Networks: A Short Survey

Dinesh A. Kulkarni and Suhas H. Patil

Abstract Wireless Ad Hoc networks are popular for critical applications due to characteristics such as simplicity, low cost, and no central administration. These networks are infrastructure less and not comparable with traditional networks with infrastructure. Infrastructure networks are configured, managed, and administrated centrally. As no centralized administration is present, self-organization is used in wireless networks to create virtual topologies and communication among nodes of network. In this paper, we present a survey of strategies used by different researchers for achieving self-organization in wireless Ad Hoc networks and make the network robust, secure, and energy efficient.

Keywords Self-organization · Hierarchical network structure · Backbone

1 Introduction

Wireless Ad Hoc networks are playing important role in critical and home automation applications due to its simplicity and cost. Military applications, emergency services, environment monitoring, disaster monitoring, car-to-car communications [1], etc. are some real-time applications using wireless Ad Hoc networks. Wireless Ad Hoc networks are constructed using devices which are having capability to sense and communicate with other. Devices are having their own resources such as battery, radio, memory, and computational power. Devices are having finite source of energy by means of battery; otherwise in some cases, solar charging units are provided. Generally, devices are in very small size of millimeter resulting in preserving limited resources. With these limitations, it is

D.A. Kulkarni (✉)

Department of Computer Science and Engineering, JJTU, Chudela, Rajasthan 333001, India
e-mail: dineshakulkarni@yahoo.com

S.H. Patil

Department of Computer Engineering, BVP's, COE, Pune 411043, India

© Springer India 2016

S.S. Dash et al. (eds.), *Artificial Intelligence and Evolutionary Computations in Engineering Systems*, Advances in Intelligent Systems and Computing 394, DOI 10.1007/978-81-322-2656-7_94

1019

always being a challenge for researchers to construct a long life, energy efficient, and secure network of wireless devices which are used for real-time critical applications. Nodes are spread over large geographical area to collect and forward the real-time information in distributed fashion. As manual configuration and maintenance are troublesome, automatic configuration and maintenance are recommended. Automatic configuration and maintenance can simply be termed as “self-organization.”

All the nodes do not know their role at the start of network. Once network formation starts, different behaviors are assigned to nodes dynamically by the network to achieve the global role of the network. Broadcast mechanism is used by nodes to reach to all other remaining nodes of network. Runtime data is sensed by the nodes, and basic processing is done locally. This processed data is routed to base station through some intermediate nodes. Localized distributed processing is done on collected data to achieve smooth running of global network. Constructing an energy efficient, long life, maintainable, scalable, and secure [2] wireless Ad Hoc network with limited resources attracted attention of many researchers. Next section of this paper is organized into the following sections: self-organization, strategies of self-organization for hierarchical structure, and conclusion.

2 Self-organization

In wireless Ad Hoc networks, hundreds or thousands of nodes are spread over large geographical area. These nodes collect some real-time information, process it, and forward it to centralized base station. Each node will have a unique identification like IP address in the network. Nodes communicate directly or through neighbors to forward processed data. As broadcasting is the base of communication forwarding, more and more messages in the network utilize energy of nodes causing early exhaust of the node battery. Once the battery of the node is exhausted, node becomes dead and the corresponding portion of network gets disconnected from network. This makes researchers think about energy consumption and minimum broadcast of messages while designing strategies for wireless Ad Hoc networks to extend the life of network. Generally, battery of the nodes taking part in forwarding of data of their neighbors exhausts early as compared with others. As nodes do not know their role in the network at the start, by applying some policies nodes with higher energies can be chosen to work as backbone for forwarding data. These networks are self configuring and self managing; hence, self-organization can be defined as “A network is said to be self-organized if it is organized without any centralized or external control” [3]. Different strategies are suggested by researchers to minimize broadcast in the network to minimize consumption of the energy and make network long life. These strategies for self-organization are inspired from real-life self-organizations such as school of fish, ant colony, and synchronization in fireflies while emitting light. While applying these strategies, various network structures used for wireless Ad Hoc network are like the following [4, 5]:

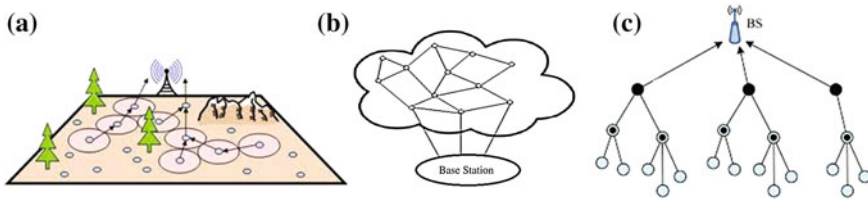


Fig. 1 Network structures of wireless Ad Hoc network

1. Location based—In location-based networks, geographical location of the node is used as an unique identification of node. Nodes are spread over large geographical area to collect real-time information, Fig. 1a.
2. Flat based—Flat-based networks are having all nodes at same level and profile. They form a mesh among them and coordinate to forward data till base station, Fig. 1b.
3. Hierarchical network—In hierarchical networks, nodes are arranged level wise and low-level nodes can communicate only with upper-level nodes. Upper-level nodes forward data to base station. Low-level nodes never communicate with base station directly, Fig. 1c.

3 Strategies of Self-organization for Hierarchical Structure

Generally, wireless Ad Hoc network is modeled using 2D Graph as $G = (V, E)$, where V is vertices (nodes) and E are edges (links) of the given network [6]. In this to minimize broadcasting of messages, maximum independent set and minimum dominating sets are formed [7, 8]. Members of independent set cannot communicate with each other directly, and members of dominating set have at least one node from independent set in reach. Members of dominating set participate in constructing virtual backbone till base station and of independent set nodes forwards messages to one of the node in the dominating set to forward it to base station.

In January 2001 [9], a long-term Terminode project was started which was one main step toward self-organization. This paper gives overview about wireless Ad Hoc networks, self-organization, and its long-term potential. Nodes in this networks were termed as terminode which is combination of terminal and node with its own sensing unit, computational unit, memory, radio frequency, and battery. It elaborates characteristics, challenges, and technical issues involved in constructing and maintaining self-organized wireless Ad Hoc network.

Toner [10] suggests a scheme for address management and merging of small networks to create a global wireless Ad Hoc network. It uses a 32-bit IP address and a 32-bit network address. A leader is selected by leader election algorithm that

maintains a list of address used by connected nodes. New node interested to join should choose a random address and make a join request. The leader assigns a valid address to this new node. As leader has complete knowledge of network, it broadcasts the table to all its neighbors with version number. In case of the absence of leader, a node with latest version of table and sufficient energy is selected as leader. When a node receives a beacon from a foreign leader, it is forwarded to its leader. Merging of two networks is done through the node who forwarded beacon, and two networks are differentiated by means of network ID. Overall, in this approach, primarily clusters are created with one leader each and then in merging clusters are connected to form a global network.

Krishnan [11] suggests an efficient clustering algorithm with maximum limit on number of nodes in a cluster called budget. This strategy consists of three algorithms:

1. Expanding ring—In this, initiator sends messages to neighbors in rounds. In each round, scope of neighbor is incremented by “1.” In some rounds, initiator gets complete list of associated nodes. If associated list of nodes is larger than budget, some nodes are dropped from cluster with a message broadcast in the network.
2. Rapid algorithm—Initiator is assigned with budget “B” including itself so with “B-1” initiator broadcasts messages to its neighbors. At each new neighbor, budget is decremented by 1. As budget is exhausted, message is not forwarded further. All nodes getting valid budget message acknowledge the initiator and become cluster member.
3. Persistent algorithm—This algorithm is recursive, and working is similar to rapid algorithm with one difference. Neighboring nodes receiving message with budget do not acknowledge initiator immediately. It waits for acknowledgment from its neighbors and checks all possibilities for further growth. If further growth is possible, it allows, and if not, it acknowledges to initiator.

Chang [12] suggests a cluster-based self-organization management protocol. While developing this strategy, 20/80 rule is followed to create upper-level nodes and low-level nodes. It uses on-demand routing to route packet in backbone. Cluster head is selected by broadcasting “Hello” message to the neighbors, but these cluster heads are just to manage cluster not involved in routing of packets. Each node of cluster maintains a routing table in which paths for desired destination nodes are present. While routing a packet source node checks in its table for destination if available packet is routed on the path, and if not, a route request is generated and is broadcasted in neighbors. This is forwarded till destination once reached new path which is updated in the table of source. In this way, every node maintains a path to destination may be in same cluster or in other cluster.

Venuturumilli [3] suggests a self-organization model for heterogeneous WSN. Heterogeneous WSN is all nodes are with different profile. It is considered that every node can choose different transmission ranges such as whisperer, shouter, and speaker. Algorithm works in three different steps: 1. initial setup, 2. basic radius updates, and 3. enhanced radius update.

1. Initial setup—At the start of network, every node in the shouter range collects information about neighboring nodes and downgrades the range to whisperer. At this collection node creates three lists one with nodes in the whisperer range, another with nodes outside whisperer range but inside shouter range, and current neighbors depending upon current transmission range.
2. Basic radius update—In this phase, each node checks whether all its ring nodes are reachable through whispering neighbor. If all its ring nodes are reachable through whisperer range of neighbors, there is no need to change transmission range from whisperer to shouter.
3. Enhanced radius update—In phase two, only one-hop neighbors are checked to reach to all ring nodes, and if not, reachable transmission range is boosted to shouter. This would be unnecessary as maybe remaining ring nodes are reachable through two-hop neighbors. This phase works in similar way but checks for two-hop neighbors to reach to ring nodes.

Lehsaini [13] suggests an efficient self-organization algorithm for clustering. In this strategy, a limit is given to maximum and minimum number of nodes in a cluster. To select a cluster head triplet metric k -density, residual energy, and mobility are used. A node with highest weight in comparison with two-hop neighbors is selected as cluster head. This leader is not permanent after specific time interval, and leader selection algorithm is executed. Each node holds information such as $Node_{id}$, $Node_{ch}$, Weight, Hop size, $Thresh_{lower}$, and $Thresh_{Upper}$. Cluster head holds information about other cluster heads such as $Node_{ch}$ and Weight. This algorithm works in two phases.

At the start, any random node initiates process of cauterization by sending “Hello” message to all its two-hop neighbors. Among receiving nodes, one node with highest weight is selected as cluster head. This new cluster head sends connection request to other neighbors if $Thresh_{upper}$ is not reached. In first phase, clusters are created but some of them may be with fewer nodes than $Thresh_{lower}$. In second phase, such clusters are merged with other clusters. Cluster heads with less nodes than $Thresh_{upper}$ broadcast a message of re-affiliation to other clusters. Result of second phase is clustered with more nodes than $Thresh_{lower}$ is formed.

Chawla [14] suggests node stability-based clustering algorithm. Node stability is mobility of the node in the network. In this approach, three parameters are used for selecting cluster head degree of node, remaining battery power, and stability. Stability of a node at the start of network is always “0.” Once a network is formed, each node keeps neighbors ID with “Hello” messages from neighbors. At next time, cycle node again gets “Hello” messages from neighbors and IDs of them. These IDs are compared to find out stability.

Algorithm starts with each node broadcasting a “Hello” message to its neighbors. Receiving nodes calculate their three factors in which stability is kept as “0.” Receiving node replies with “Hello” to the sender with this triplet. Out of collected triplets, maximum competency is calculated, and the node with maximum competency is selected as cluster head. If competency value of two nodes is matching, then the node with lower ID is selected as cluster head. Finally, each node

broadcasts a “Hello” message with cluster head ID to convey new cluster head. This process of electing cluster head is periodic and carried out after fixed amount of time. If any cluster head moves out of cluster before time expires, another node with next higher competency is selected as cluster head till timeout.

Salzmann [15] suggests a strategy to form clusters without knowing their position, and only one node of the cluster has to be active per cluster. This strategy is designed for homogenous WSN and works in three phases, namely information phase, clustering phase, and affirmation phase.

Starting node with transmission power R_w broadcasts a message “Possible Cluster Head” to all neighbors. All neighboring nodes change their mode to “Possible Cluster Head” and transmit this message with R_w . By lowering the range to 50 % (with $R_w/2$), starting node forces neighboring nodes to join cluster. They join the cluster and change mode to “Join Cluster.” At the last in Affirmation phase, all joined nodes confirm their joining to cluster and broadcast a message with $R_w/2$ to all nearby nodes to show already joined a node.

Orfanus [16] suggests an algorithm for power-law topology in self-organization. When degree of distribution followed power function, the network is called as power-law network.

It is assumed that a peer “N” with “m” links arrived in the network. “N” requests to bootstrap server for IDs for all “m” links from existing network. Bootstrap server chooses a random peer “D” with low degree to connect with “N.” “N” initiates the process by requesting ID of peer to be attached with. “D” sends its own ID or one of the neighbors ID. “N” makes connection with the node whose ID is sent by “D.” This algorithm takes care of security of network by taking all decisions in the existing network not at the new arriving peers.

Kalita [4] suggests clusterization by using triangular method for self-organization. In this, at the start of network formation, a node is chosen at random suppose “A.” Then, find another point “B” such that AB is minimum. A and B are connected and are now a live edge. Then, find third point “C” such that ABC is min triangle. Further, choose a live edge from AC and BC. This algorithm will work in loop and form a complete network till all nodes are joined. Clusters are formed by ordering procedure.

Qi [17] suggests hierarchical protocol architecture with multiple clustering. In general clustering, algorithms’ certain probability is used to choose cluster head, and all non-cluster head node should transfer data to cluster head and cluster head forwards it to base station. In the suggested MCEE protocol, cluster head sends data to super node and super node forwards it to base station. Cluster head is selected by broadcasting “Hello” messages in the neighbors, and at the same time, a super node is also selected. Super node is a functionality which is rotating or interchangeable among cluster head and other nodes of the cluster. This interchangeability is done to achieve load balancing as super node has more packets forwarding load than other nodes.

Hanchichi [18] suggests a virtual topology for routing in Ad Hoc networks. Based on virtual topology, cluster heads and gateways contribute in searching destination. In this algorithm, cluster head is chosen on preference from neighbors.

Higher choice node is chosen as cluster head by neighboring nodes. In this, one secondary cluster head is also selected per cluster. Cluster head, secondary cluster head, and normal nodes form a forest of links inside the cluster. As forest is created of links, routing become necessary to forward packets inside the cluster. Two different approaches are used while routing, inside cluster proactive routing is used, and among clusters, on-demand routing is used. Cluster head maintains a table of routes to the desired destinations. When a node of cluster is interested to forward a packet to other node, it sends a route request to the cluster head, and if the destination is in the cluster and route present in the table, then packets are forwarded through cluster head to destination. If node is not member of cluster and its route not present in the table then cluster head initiates a search in neighboring clusters. If route is present in any one of the cluster head then it is replied to source cluster head. If not present in any of the cluster, a route request is broadcasted to all its neighboring cluster heads. Replied route is updated in the table of requesting cluster head, and data is forwarded accordingly.

Heinzelman [19] suggested a Low-Energy Adaptive Clustering Hierarchy (LEACH). Two assumptions were made while developing this protocol: 1. A unique base station is present to which all nodes are interested to communicate with base station, and 2. all nodes are having capability to communicate with base station. In this protocol, cluster head is decided by self declaration by the node. Node who is interested to be as a cluster head elects himself by some probability as a cluster head and conveys its status to all its neighbors by means of broadcast message. As such many broadcast messages may be received by any node in the network, nodes decide their association with a particular cluster head by calculating minimum energy to communicate with them. Cluster head utilizes its energy at more extend as compared with other nodes to avoid cluster head battery exhaust, and selection process is done after every random time. After a random time “d,” another interested node with enough energy elects itself a cluster head.

Biradar [20] suggests a multi-hop LEACH. In this cluster formation procedure used is same as LEACH protocol, but routing is done using multi-hop technique. A message from a node reaches to the base station through a path starting from cluster head of its cluster to base station. This involves a sequence of other cluster heads (hops) rooted at the base station called as multi-hop inter-cluster operation. In intra-cluster operation, nodes that are in direct visibility of the cluster head sends messages directly to it, but nodes that are not in the visibility of cluster head can take a route to it through nodes that are in visibility.

Rauthan [21] suggests an improved multi-hop LEACH. In this, one more node is elected as vice cluster head. This node is used as backup for cluster head in case of any accidental death of cluster head. This node works as cluster head at any accidental case to avoid data loss of nodes and cluster.

Olascuaga-Cabrera [22] suggested a strategy of self-organization for a network in which all nodes are mobile nodes. They are with different constraints/profile and can enter or leave network at any time. In this algorithm, agents play multiple roles in the network such as leader, gateway, and members. Each group has at least one agent as leader, zero, or more agents as gateway and one or more agent as member.

As network starts, wake-up agents do not have any role in the network. The first role assigned is leader. Many agents may get role of leader at the start so this conflict is solved by leader election algorithm, and only one agent is elected as a leader. If an agent is visible to two or more nearby leaders, it is selected as gateway between the leaders, and remaining nodes remains as member of clusters. Leaders and gateways spend more energy as compared to other agents of the network so agents decide by their own to change their role depending upon current status of energy. Leader election algorithm is executed in the network whenever need arises like due to low energy leader changed its role to normal agent.

Routing table and its updates are broadcasted to all member agents of the cluster by the leader. To achieve optimistic energy consumption, at stable state of the network, broadcast of routing update is done with low frequency, and at unstable state, this frequency is comparatively high.

Olascuaga-Cabrera [23, 24] has done an improvement in the strategy suggested in [22]. This approach uses one or more role of Bridge other than leader, gateway, and member. This is done to solve segmentation problem discussed in [21]. Bridge is an agent which on detecting another agent from other group tries to establish a connection with them. If connection is established, agent switches its role to Bridge.

At the start of network, each agent broadcasts "Hello" messages to their neighbors, depending upon their neighbor's role of agent is decided in the network. If a node has no neighbor, it gets a role of "any" at the start. If in the neighborhood leader agent does not exist, role of leader is assigned to node, and if only one leader is detected in the neighborhood, agent becomes a member agent. When a member detects two or more than two leaders in the neighborhood, it changes its role to gateway. When a agent detects another agent from other group, it sends a Bridge request to other agent. Agent from other group first becomes Bridge and sends acknowledgment to requesting node. After receiving this acknowledgment, agent becomes a Bridge.

Shirsat [5, 25] suggested modified version for the algorithm in [23, 24] and roles of agents in the network. This approach is based on minimum spanning tree and concentrates on minimizing number of backbone links so that broadcast will be minimum and energy will be conserved.

Four different roles are identified for the agents leader, gateway, willing to act as gateway, and agent. At the start of network, first agent will get the role of leader, and if conflict arises, leader selection algorithm decides one agent as leader out of conflicting nodes. To achieve load balancing, leader selection algorithm is executed periodically. Agents who are having two or more than two leaders at the neighbor are selected as gateway, and remaining agents are members. In this way, a virtual backbone is created of cluster heads and gateways for communication of network. In the formation of network, it is possible that two or more than two agents are selected as gateway on same path. This approach tries to achieve backbone close to minimum spanning tree, but with such multiple gateways on the path, this cannot be achieved. When multiple gateways are present on the same path, only one is kept as gateway and remaining become willing to act as gateway. Willing to act as gateway works as a normal agent of the cluster but when needed can become gateway.

4 Conclusion

In this paper, the survey of various self-organization strategies is discussed. Algorithms for hierarchical network structures are studied and discussed in detail. In this survey, it is observed that hierarchical network structures of self-organization are economic in management and energy consumption. So, we want to focus on role-based cluster formation strategies/algorithms for further topic of research. Further study involves identification of efficient roles, effective formation, and maintenance of self-organized wireless Ad Hoc network such that energy consumption will be minimum. Also, we want to add a backup mechanism in case of failure of backbone network.

References

1. Aoyama M, Takeichi H. Adaptive self-organizing overlay network for car-to-car communications;2008. IEEE.
2. Prehofer C, Bettstetter C. Self organization in communication networks: principles and design paradigms. *IEEE Commun Mag.* 2005;43(7):78–85.
3. Venuturumilli A, Minai A. Obtaining robust wireless sensor networks through self-organization of heterogeneous connectivity. *Unifying Themes in Complex Systems*: Springer; 2008.
4. Kalita HK, Kar A.A new algorithm of self organization in wireless sensor network. doi:10.4236/wsn.2010.21006, <http://www.SciRP.org/journal/wsn/>.
5. Shirsat N, Game P. Role based approach for effective connections in the backbone of self organized wireless networks. In: *Proceedings of the InConINDIA 2012, AISC 132*. p. 763–8. ©Springer-Verlag Berlin Heidelberg.
6. Sanchez-Acevedo MA, Lopez-Mellado E, Ramos-Corchado F. Self organization algorithms for mobile devices;2009. IGI Global.
7. Nieberg T, Hurink J. Wireless communication graphs. In: *Proceedings of 2004 intelligent sensors, sensor networks, information processing conference*;2004. p. 367–72.
8. Funke S, Kesselman A, Meyer MSU. A simple improved distributed algorithm for minimum CDS in unit disk graphs. In *Proceedings of IEEE international conference on wireless mobile computing, networking, communications (WiMob)*, vol. 2;2005. p. 220–3.
9. Hubux J-P, Gross T, Le Boudec J-Y, Vetterli M. Towards self-organized mobile AdHoc networks: the terminodes project. *IEEE Commun Mag.* 2001;118–24.
10. Toner St, O'Mahony D. Self-organising node address management in ad-hoc networks. *Lect Notes Comput Sci.* 2003;2775:476–83.
11. Krishnan R, Starobinski D. Efficient clustering algorithms for self-organizing wireless sensor networks;2004. Elsevier.
12. Chang Y-C, Lin Z-S, Chen J-L. Cluster based self-organization management protocols for wireless sensor networks;2006. IEEE.
13. Lehsaini M, Feham M. A novel cluster-based self-organization algorithm for wireless sensor networks. In: *Collaborative Technologies and Systems*;2008. IEEE.
14. Chawla M, Singhai J, Jain S, Shrivastava A. Node stability based clustering algorithm for mobile ad hoc networks;2008. IEEE.
15. Salzmann J, Behnke R, Timmermann D. A self-organized localization-free clustering approach for redundancy exploitation in large wireless sensor networks. *GI Jahrestagung, Workshop: Adaptive und organische Systeme*, p. 747–54, Sept 2008.

16. Orfanus D, Heimfarth T, Janacik P. An approach for systematic design of emergent self-organization in wireless sensor networks. *Future Computing, Service Computation, Cognitive, Adaptive, Content, Patterns*, 2009. COMPUTATIONWORLD '09. *Computation World*. p. 92–8, 15–20 Nov 2009.
17. Qi T, Bing Q. An energy-efficient protocol architecture with multiple clustering for wireless sensor networks;2010. IEEE.
18. Hanchichi H, Chelloug S, Athmouni F. A virtual topology for routing in adhoc networks;2011. IEEE.
19. Heinzelman W, Chandrakasan A, Balakrishnan H. Energy-efficient communication protocols for wireless microsensor networks. In: *Proceedings of 33rd HICSS*;2000. Maui, HI, USA.
20. Biradar RV, Sawant SR Dr., Mudholkar RR Dr., Patil VC Dr. Multihop routing in self-organizing wireless sensor networks. *IJCSI*. 2011;8(1).
21. Rauthan JS, Mishra S. An improved cluster based multi-hop routing in self-organizing wireless sensor networks. *IJERT*. 2012;1(4).
22. Olascuaga-Cabrera JG, Lopez-Mellado E, Ramos-Corchado F. Self-organization of mobile devices networks;2009. IEEE.
23. Olascuaga-Cabrera JG, Lopez-Mellado E, Mendez-Vazquez A. Wireless network formation and maintaining for mobile devices based on self-organization strategies;2010. IEEE.
24. Olascuaga-Cabrera JG, Lopez-Mellado E, Mendez-Vazquez A, Ramos-Corchado FF. A self-organization algorithm for robust networking of wireless devices. *IEEE Sensors J*. 2011;11(3).
25. Shirsat N, Game P. An optimized approach to minimize broadcast in communication of self organized wireless networks. *Springer Adv Intell Syst Comput*. 2013;199:543–9.

Efficient-Fused Architectures for FFT Processor Using Floating-Point Arithmetic

D. Tamil Eniyan and J. Harirajkumar

Abstract In this chapter, the complex multiplier is designed using the fused dot product architecture. The floating-point number is used in this implementation for its wider range and its applications requiring the data space range from small to infinitely large. For the digital applications, the adder, subtractor, and multiplier are required at same instance. The discrete way of implementing the dot product yielded more space (in parallel implementation), high latency (in serial implementation), and power consumption. Hence, the research in fusing of the arithmetic units such as floating-point adder, subtractor, and multiplier gained interest. With the fused dot product unit, the output can be obtained in a single clock with low area and minimum latency. To further improve the performance of the fused dot product (FDP), the optimization in the architecture had been carried out and the result has been discussed. Further, the FDP unit is implemented in the complex multiplier. Thus, the performance of complex multiplier in FFT is improved and the error in computation is reduced. This optimized fused architecture can also be used in implementation in the processors and other such systems.

Keywords Fused dot product (FDP) · Floating-point adder (FPA) · Fused multiply-add (FMA) · Kogge–Stone adder

1 Introduction

Generally in computer arithmetic computation, the fixed-point numbers were being used in arithmetic unit because of its advantage of easy implementation and integration in the chip fabrication in earlier days. When the computation is made in

D. Tamil Eniyan (✉) · J. Harirajkumar
Sona College of Technology, Salem, India
e-mail: eniyannitt@gmail.com

J. Harirajkumar
e-mail: harirajkumar@gmail.com

fixed-point arithmetic, the number of bits required will be high, and hence, the high-order multiplier and adder are required. Hence, the total space required will be high and the power consumption will be more. With the development in silicon technology, the floating point is being considered as indisputable replacement [1] since the fixed-point arithmetic is error prone. Also with advancement in technology, the applications require the data space which range from the relatively small to infinitely large. A floating-point number representation can provide a wide range of numbers and a high degree of precision of the numbers [1]. As a result, a portion of the most microprocessors will be often dedicated to its hardware for floating-point computation. The floating-point unit performs the arithmetic operations such as addition, subtraction, multiplication, and division [2, 3].

For the implementation of operations such as $(X \div Y)^{1/2}$, $(X^2 + Y^2)$, $(X + Y) * (X - Y)$, floating-point unit is used. The individual use of the arithmetic in these operations will lead to more delay, large space, and high power consumption. Hence, the fusing of these arithmetics into a single unit for certain applications is much useful [4]. In this chapter, the FDP (fused dot product) unit is discussed. The dot product unit is required in applications such as complex multipliers, FFT processor [4].

2 Floating Point

The sign bit, exponent bit, and mantissa (significand) bit are put in order for floating-point representation as shown in Fig. 1. For single precision, floating point has 32 bits, where the mantissa should have 23 bits and the exponent should have 8 bits. The bias for the single precision is 127 [1].

$$N = -1^{(\text{signbit})} * (1 + \text{mantissa}) * 2^{(\text{exponentbit}-\text{bias})} \tag{1}$$

3 Complex Number Multiplication

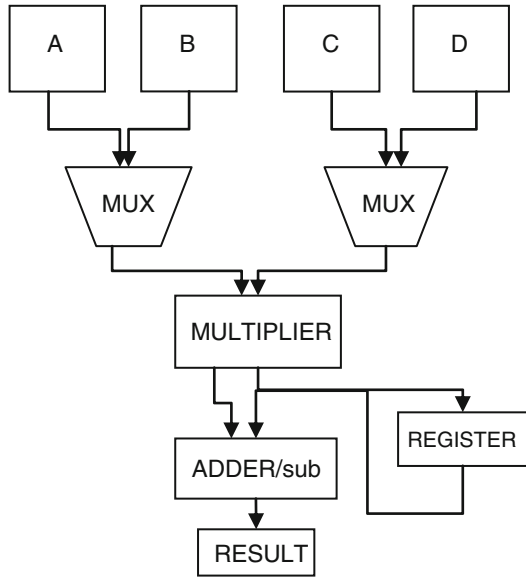
Two complex numbers $(a + ib$ and $c + id)$ are to be multiplied as shown in the equation below (Fig. 2)

$$(a + ib)(c + id) = (ac - bd) + i(ad + bc) \tag{2}$$



Fig. 1 Floating-point number representation

Fig. 2 Serial implementation of dot product



4 Dot Product

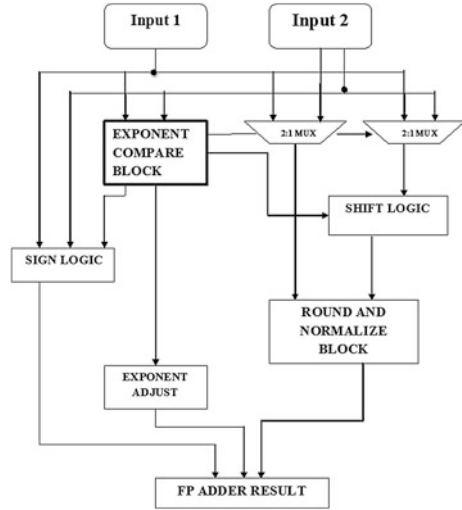
The dot product of the two complex numbers $(A + iB$ and $C + iD)$ can be determined by the following equation:

$$Z = AC \pm BD \tag{3}$$

The conventional implementation of this dot product requires two multipliers and an adder. Hence, for the larger range inputs, the implementation leads to larger computation time and the critical path being high and hence, the latency also increased. The implementation of fixed-point arithmetic dot product block requires more I/O's pin and the bit power of the input also increased due to the large number of binary bits for processing. Also the adders and multipliers required for the processing will be in higher order. Hence, using the floating-point arithmetic provides the reduced binary bit and thus low power consumption.

5 Floating-Point Adder

For addition of the floating-point numbers, a floating-point adder is required [5]. The floating-point number is unpacked into sign bit, exponent bit, and mantissa bit for the easy computation. The floating-point adder (FPA), where the two floating-point number's exponent bits are compared and the smaller exponent

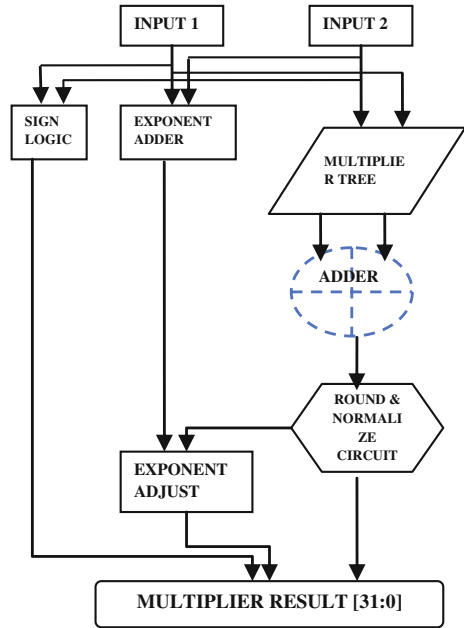
Fig. 3 Floating-point adder

number's mantissa is shifted accordingly with respect to the larger exponent number's mantissa, is shown in Fig. 3. The number of shifts is equal to the difference between the exponent bits of two numbers. This shifting of the number is done using alignment block and then addition of mantissa bit is performed. The normalization of mantissa bits is with respect to the exponent compare block. The resultant exponent is obtained through exponent computation block [6]. The sign bit of result is obtained with the EX-OR of MSB bit of the two numbers. Thus, the obtained result with the merging of the final pipelined block provides the addition result.

6 Floating-Point Multiplier

In the floating-point multiplier (FPM), initially floating-point number inputs are split into sign, exponent, and mantissa bits. The exponent bit of two floating-point numbers is added and the mantissa bit of two numbers is multiplied through the Wallace multiplier tree. The generated partial product is added through an adder and then the added result is to be rounded as shown in Fig. 4. If the mantissa bits are R-bit numbers (23 bit for floating-point single precision number), then the product can be of $2R$ bits and it should be rounded to an R-bit number [6, 7]. To obtain the result's sign bit, the EX-OR of the sign bit of two floating-point inputs is needed. The multiplier thus comprises of AND gate which is used for binary bit product, the partial product reduction unit which reduces to two number outputs, and the adder block, which sums the two outputs from partial product reduction to generate the product.

Fig. 4 Floating-point multiplier



7 Floating-Point-Fused Multiply-Add

The floating-point-fused multiply-add (FMA) executes the equation $(A * B) + C$ in single instruction. Not only the fused multiply-add improves the performance of $(A * B) + C$ instruction, but this architecture may also entirely replace the floating-point adder and floating-point multiplier [2, 3, 8]. The fused multiply-add exponent scheme requires three separate parallel calculations at the beginning of the block. The first computation is the exponent difference between $A * B$ and C to provide an alignment control to the align stage. Then, C should be aligned with respect to $A * B$ multiplier tree. Hence, three inputs are to be added (two from multiplier tree output and other input is aligned C) [3]. Thus, 3:2 compressor is used to reduce the three input to two. And then the adder will be used to add the two numbers and the obtained result is send to normalization and rounding circuit. Thus, 32 bit result of $(A * B) + C$ logic is obtained in single clock cycle using fused multiply-add (FMA) architecture. The FMA unit is also used in determining the dot product. For performing dot product, a FMA unit and a floating-point multiplier are required.

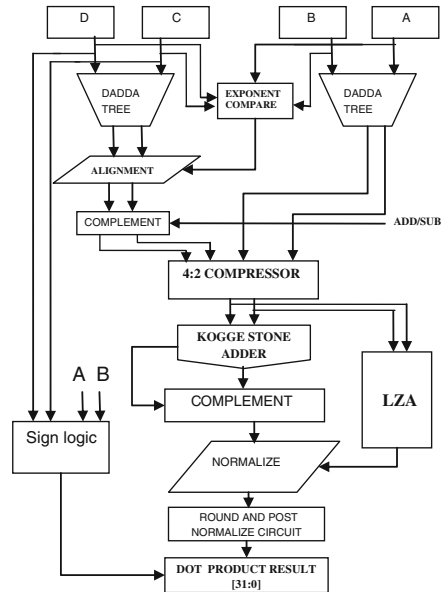
8 Fused Dot Product

By the conventional implementation, the dot product unit can be done with two multipliers and an adder. Performing dot product by using an adder and a multiplier with multiplexers (MUX) and registers provides low throughput and also that of with two independent multipliers and an adder yields expensive due to area; also the power consumption will be more. The fusing of the multiplier and adder in a single architecture thus provides the low area and power. With the single instruction, the result is obtained at low latency and at high speed [4, 9].

In the modified FDP architecture, the significand (mantissa) bit multiplier tree partial product generation is done using radix-4 booth encoding, and various tree-based multipliers had been analyzed and then the partial product reduction multiplier tree is done using the Dadda multiplier tree as shown in Fig. 5 (Figs. 6 and 7).

Since the Dadda multiplier provides the partial product result at the high speed and with less number of gates when compared to the other multiplier tree architectures. Since the floating-point number is used, the alignment scheme with respect to the exponent is important. The alignment used here in architecture considers both the input *AC* and *BD* and aligns the lower sum of the input's exponent according to greater sum of the inputs. Thus, four numbers are obtained from two multiplier trees. These four numbers are reduced into two numbers using 4:2 compressor. Then obtained two numbers from 4:2 compressor is added using an adder. The comparison of the high-speed adders with respect to ripple carry provides the result

Fig. 5 Fused dot product architecture



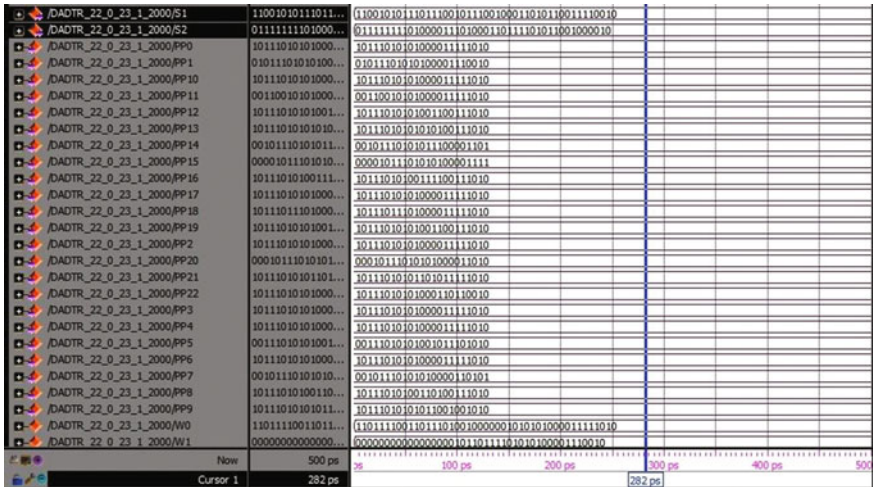


Fig. 6 23 × 23 bit Dadda multiplier tree output

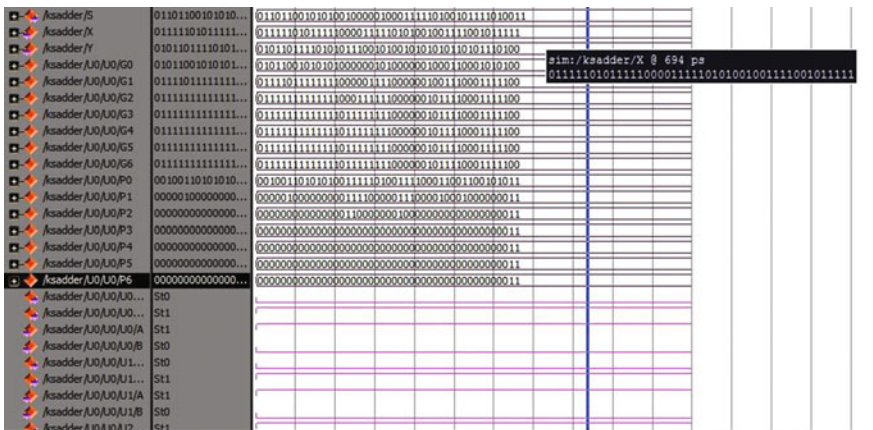


Fig. 7 48 bit Kogge–Stone adder

of higher efficiency in Kogge–Stone adder; hence, this adder is used in the proposed architecture. Then, the obtained output is to be rounded and normalized. The normalization circuit which will reduce the number of bits and result in 23 bit (mantissa bit) is shown below:

$$\text{Adder result} = (C_{out}P_{n+1}P_nP_{n-1} \dots P_1P_0GRS)$$

where G is Guard bit, R is Round bit, S is Sticky bit.

Before Normalization

$$\dots P_1 P_0 | GRS$$

Normalizing single bit (right-shift)

$$\dots P_2 P_1 | P_0 R \vee S$$

Normalizing single bit (left-shift)

$$\dots P_0 G | RS0$$

Final mantissa (after normalization)

$$\dots P_{-N+1} P_{-N} | P_{-N-1} P_{-N-2} P_{-N-3}$$

Sticky bit is OR of all the bits shifted beyond the round bit. Then, sticky bit is removed in the result. The normalizing and rounding circuit provides the final mantissa bit output with respect to exponent adjust circuit. The exponent adjust circuit will provide the exponent of the dot product result. Finally, the numbers are bundled into a single precision floating point as shown in Fig. 5. And the result is used in various applications such as complex multipliers. The design is done using Verilog RTL, and the area and delay were estimated using Xilinx Virtex 5 FPGA. Simulation is done in ModelSim and synthesis is in Xilinx XST.

8.1 Dadda Multiplier Tree

The Dadda multiplier is a parallel multiplier, where N^2 AND gates will be used for partial product generation. The partial products are arranged in a triangle manner and then the full adders and half adders are used to obtain two number outputs by reducing the partial product. The Dadda multiplier has a less delay when compared to other tree-based multiplier. The number of full adders and half adders required for an $S * S$ multiplier will be $S^2 - 4S + 3$ and $S - 1$, respectively, which is lower than the Wallace tree multiplier. Hence, the speed will be high and area required will be low.

8.2 Kogge–Stone Adder

The Kogge–Stone adder is a prefix adder and is known to be a modified form of the carry look-ahead adder [10]. Though this adder requires large area, the fan-out will be low. Thus, fan-out delay gets reduced and the speed gets increased and the

Table 1 Area and delay analysis report for different architectures

Architecture	LUT's used	Delay (ns)
Fixed-point dot product	2156	34.548
Wallace tree multiplier	787	21.097
Dadda tree multiplier	796	19.041
Ripple carry adder	328	13.726
Kogge–Stone adder	301	7.844
Carry look-ahead adder	289	10.043

routing is made easy. The carry will be generated in $O(\log(n))$ time, making it to be a fastest adder. The preprocessing stage of this adder, the generated product, and the propagate terms are produced. Also, the blocks in adder help in balancing the loading effect. This is the most preferred adder to be used in the design (Table 1, Figs. 8 and 9).

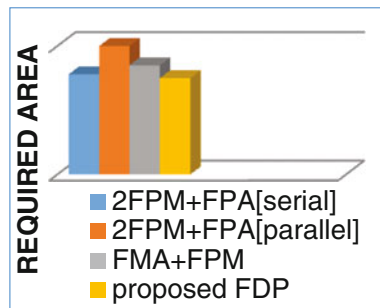


Fig. 8 Area used for implementing dot product by discrete, FMA + FPM and FDP architectures

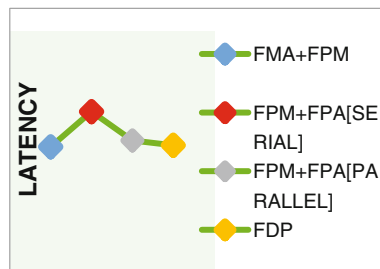


Fig. 9 Latency (Delay) comparison in implementing dot product by discrete, FMA + FPM, and FDP architectures

9 Conclusion

With the fused dot product architecture, the area and the latency for implementing the dot product is reduced to a larger extent when compared to other such architectures. Also, the power consumption for implementing the dot product using FDP has been reduced. Hence, the fusing of the arithmetic in a single unit provides the more efficient results when compared to the discrete approach. Thus, other such arithmetic operations such as sum of squares and determining the magnitude of the complex numbers can also be fused into single unit. These fused architectures will lead to low computation time with less area consumption. The future work can be implementing the fused dot product architecture in applications such as complex multipliers and FFT. And comparison of these applications with discrete way of implementation could also be performed.

References

1. IEEE standard for binary floating-point arithmetic, ANSI/IEEE Standard 754;1985.
2. Bruguera JD, Lang T. Floating-point fused multiply-add: reduced latency for floating-point addition. In: Proceedings of the 17th IEEE symposium on computer arithmetic;2005. p. 42–51.
3. Takahashi D. A Radix-16 FFT algorithm suitable for multiply-add instruction based on Goedecker method. In: Proceedings of international conference on multimedia and expo, vol. 2;2003. p. II-845–II-8.
4. Swartzlander EE Jr., Saleh HHM. FFT implementation with fused floating-point operations. *IEEE Trans Comput.* 2012; 61(2).
5. Suzuki H, Makino H, Mashiko K, Hamano H. Leading-zero anticipatory logic for high-speed floating point addition. *IEEE J Solid-State Circuits.* 1996;32:1157–64.
6. Li R-C, Boldo S, Daumas M. Theorems on efficient argument reductions. In: Proceedings of the 16th IEEE symposium on computer arithmetic;2003. p.129–36.
7. Mehta A, Bidhul CB, Joseph S, Jayakrishnan P. Implementation of single precision floating point multiplier using Karatsuba algorithm. In: 2013 International conference on green computing, communication and conservation of energy (ICGCE).
8. Hokenek E, Montoye R, Cook PW. Second-generation RISC floating point with multiply-add fused. *IEEE J Solid-State Circuits.* 1990;25:1207–13.
9. Saleh H, Swartzlander EE Jr. A floating-point fused add-subtract unit. In: Proceedings of IEEE Midwest symposium on circuits and systems (MWSCAS); 2008. p. 519–22.
10. Hoe DHK, Martinez C, Vundavalli J. Design and characterisation of parallel prefix adders using FPGAs. In: IEEE 43rd Southern symposium on system theory, March 2011.

Design, Test and Evaluation of Trace-Buffer Inserted FPGA System

R.S. Karpagam and B. Viswanathan

Abstract Integrated circuits have more functionality and complexity, and to verify that these devices working properly in all scenarios is a difficult task. For using traditional verification techniques such as software simulation, designers are taking advantage of the significantly higher clock speeds which can be achieved by using field-programmable gate-array (FPGA)-based prototypes. However, the major challenge of using FPGAs for verification and debug is observability. Designers must use special techniques to observe the values of FPGA's internal signals. In this paper, a new method has been proposed for increasing the observability of FPGAs and demonstrates its feasibility. The new method incrementally inserts the Trace-Buffers controlled by a trigger into already placed-and-routed FPGA designs.

Keywords FPGA · Verification · Debug · Incremental synthesis · Observability

1 Introduction

Now, the integrated circuits (ICs) are reaching more than a billion transistor counts which make them insignificant to design these complex devices. Verifying whether these circuits are working properly under all operating conditions (expected and unexpected) is a difficult task. To overcome this, now many designers have turned to field-programmable gate-array (FPGA)-based prototyping to improve the verification coverage more than the achievable range using the traditional software simulations. FPGAs are an attractive platform for verification and debugging because they are much faster than simulation and less costlier than fabricating an ASIC prototyping. IBM researchers stated that FPGA prototype is 100 000 times

R.S. Karpagam (✉) · B. Viswanathan
Department of Electronics and Communication Engineering, SRM University, Chennai, India
e-mail: rasiaum@yahoo.com

B. Viswanathan
e-mail: viswanathan.b@ktr.srmuniv.ac.in

faster than software simulations and 400 times slower than the fabricated application-specific integrated circuit (ASIC) [1]. An ASIC prototype could achieve even greater speeds than an FPGA, but FPGAs have other advantages over ASIC prototypes. The lead time for fabricating an ASIC can be weeks or even months and can easily cost over 1 million USD [2]. The FPGA is used to identify the sources in correct behavior. Verification and debugging both increases the device capacity and limited due to on-chip observability. These make extensive use of software simulators. The simulation is extremely slow for large design. To overcome this problem, the prototype using Trace-Buffer is to be instrumented, for recording a subset of internal signals into on-chip memory to get subsequent analysis. To do so, ChipScope Pro, Certus, and SignalTap II can be used [3–6].

Trace-Buffer is formed from a memory resource on the FPGA. Trace-Buffer records a limited size history of the signals connected to them during regular device operation. This enables the designer to run the device normally. It can extract the signal history by the Trace-Buffers with techniques such as device reed back for off-line analysis [7].

The results and challenges of using the approach may differ between architectures. However, the approach could be used on any FPGA where it is possible to incrementally insert (place and route) additional logic and memory components in an already existing circuit.

The proposed approach has some specific advantages: (1) It has no impact on the placement or routing of the user circuit. (2) It requires no additional area. (3) It enables faster turn-around time for changing the observed signals or Trace-Buffer compared to traditional flows. (4) It increases FPGA observability by taking full advantages of all leftover memory.

2 Background

2.1 *Enhancing Observability*

A limited number of signals may be observed in FPGA's pins using an external logic analyzer. But, this is often inadequate and some of the pins may be used already. Methods to observe a large number of signals can be divided into two broad categories: scan-based and trace-based.

- (1) *Scan-based*: Scan-based debug approaches are used to capture the state of an FPGA for inspection by serially shifting it out over an external pin or an interface such as JTAG. The state of the FPGA is the values in all memory elements on the chip, such as flip-flops and embedded blocks. For serially shifting out the Xilinx device uses the readback feature [7]. In [8], it was shown how readback data can be used for debugging in a combined simulation/hardware execution environment built on JHDL. However in [9], the average overhead for full scan is 84 % of additional area. A challenge with

scan-based approaches is that as devices increase in size and density, the time required to shift the entire FPGA state out proportionally increases [10].

- (2) *Trace-based:* In a trace-based approach, a designer pre-inserts Trace-Buffers controlled by a trigger, also called embedded logic analyzers, into the circuit before compilation. The Trace-Buffers allow a window of the history of the chosen signals to be recorded as the circuit operates in real time. Trace-based debug has a drawback of requiring FPGA resources which can influence the placement and routing of the circuit [11] and limit the number of signals that can observe. The circuit may go through a time-consuming recompilation if the designer wishes to change the signals being observed or parameters of the Trace-Buffers or trigger. A number of automated techniques attempted to combat this [12].

2.2 Incremental Synthesis

Incremental synthesis allows us to overcome some drawbacks of the trace-based approaches. It is because instrumentation of incremental synthesis is not included in the compilation of the original circuit. The aim of incremental synthesis is to modify the functionality of a placed-and-routed circuit while preserving as much of the original solution as possible. FPGAs are well suited as there is often unused logic and routing resources leftover after a circuit has been compiled. The main motivations behind this are (as shown in Fig. 1) to avoid a full compilation of the circuit when adding or making changes to the instrumentation, to preserve timing closure when undertaking engineering change orders, or for improved fault and defect resilience [13].

Graham et al. [14] demonstrated an approach which is more similar to this work; he put an unconnected embedded logic analysis in the FPGA prior to placing and routing, and afterward used a low-level bitstream modification to connect them to the desired signal [10]. However, their techniques relied on the Jbits API that was provided by Xilinx FPGA device, but similar APIs have not been for other

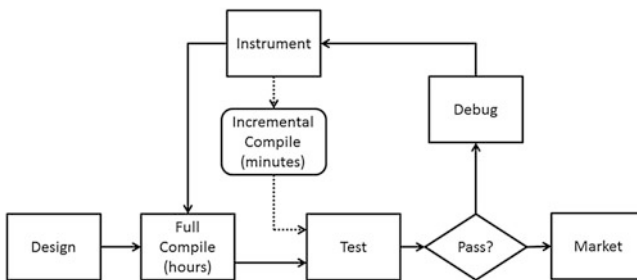


Fig. 1 Design and debug flow

commercial FPGAs. Graham system may not scale well for observing 1000s of nets, as only 128 nets were observed in their tests.

Commercial vendor tools also support the incremental compilation design. Altera's SignalTap II trace-IP solution and signal probe are specifically used to connect the I/O pins directly to the external analysis [4].

2.3 FPGA-ASIC Prototyping

FPGAs are integrated circuits fabricated to be configured by a designer after manufacturing. FPGAs are composed of reconfigurable logic, memory, and routing interconnects that can be configured to perform a huge variety of tasks. FPGAs can be used for one task and later be reprogrammed for a difficult task. They are different from application-specific integrated circuits which are typically hardwired for one task. However, the flexibility of FPGAs comes with some drawbacks. An ASIC consumes less area and power and operates faster than the equivalent circuit would on an FPGA. The specifics of FPGA architecture vary among vendors and product families. ASIC prototyping is the method to prototype ASIC design on FPGA for hardware verification. The need for verification of application-specific integrated circuit design is growing, due to the increased circuit complexity and time-to-market shrinking. Hardware platforms are becoming more prominent to test system designs at speed with on-chip bus clocks as compared to simulation clocks which may not provide an accurate reading of system behavior. These multi-gate designs usually are placed in multi-FPGA prototyping platform with six or more FPGAs, since they are unable to fit entirely onto a single FPGA. So the system RTL designs or netlist has to be partitioned onto each FPGA to be able to fit the design onto the prototyping platform.

3 Incremental Trace-Insertion

This section describes the proposed method for increasing FPGA observability to simply debug and verify. It describes how those components are incrementally inserted into the design. First, an overwrite of the proposed method that describes how it fits into Xilinx design flow is given. Then, the two major steps placement and routing are used for incrementally synthesizing the debug system.

3.1 Trace-Insertion

To increase the observability of FPGA circuits, a Trace-Buffer and a trigger unit are inserted incrementally into already placed-and-routed designs. Nets from the

original circuit shall be incrementally connected to the Trace-Buffers to be observed and recorded. The trigger unit will control the Trace-Buffers to record until it meets the specified trigger condition.

The impact on the original circuit's area, placement, routing, and timing will be reduced when incrementally inserting the debug system. From the perspective of the original circuit, the debug systems have no area overhead. The original circuit will already be placed and routed and thus will already have claimed whatever area of the FPGA it needs. The debug system is inserted into whatever FPGA area has been left unused by the original circuit. Thus, the amount of Trace-Buffers and trigger logic to insert will be influenced by the area of the original circuit.

The goal of incremental synthesis is generally to modify the functionality of an existing circuit with minimal changes to its current placement and routing. The proposed work goal is different than this "general-purpose incremental synthesis" because its only desire is to observe signals. The placement and routing of the Trace-Buffers and trigger unit are restricted to resources unused by the existing circuit. The original circuit will be left completely intact.

3.2 *Xilinx Design Flow*

The proposed work is inserted between the place and route (PAR) and BitGen stages. When inserting instrumentation, the NCD representation of the circuit produced by the PAR process is converted to a XDL file. Trace-insertion modifies the XDL file to insert the Trace-Buffers and trigger unit and creates a new XDL that includes the modifications. This XDL file can be converted back to an XCD, and the normal Xilinx flow may continue. BitGen can create a bit file that can configure the FPGA with the circuit that includes the debug system. The `ncd2xdl` and `hdl2ncd` conversions are done (as shown in Fig. 2). A XDL file representing the circuit to instrument is one of the inputs to trace-insertion. Trace-insertion requires two lists: a list of the nets to trace and a list of the nets to connect to the trigger unit inputs. There are also other parameters of trace-insertion that can be adjusted such as Trace-Buffer width, trigger width, or number of trigger unit slices.

4 Primary Results

This section describes the methodology for testing the flexibility of the proposed incremental trace-based debug system. The runtimes of the incremental insertion on a set of benchmarks and the effects on minimum period are presented. The results of the tests are presented and demonstrated that the proposed system is feasible and can observe thousands of signals.

To demonstrate the feasibility of our proposed debug system, the effects of using it to trace up to 100 % of the flip-flops and latches in three benchmark circuits

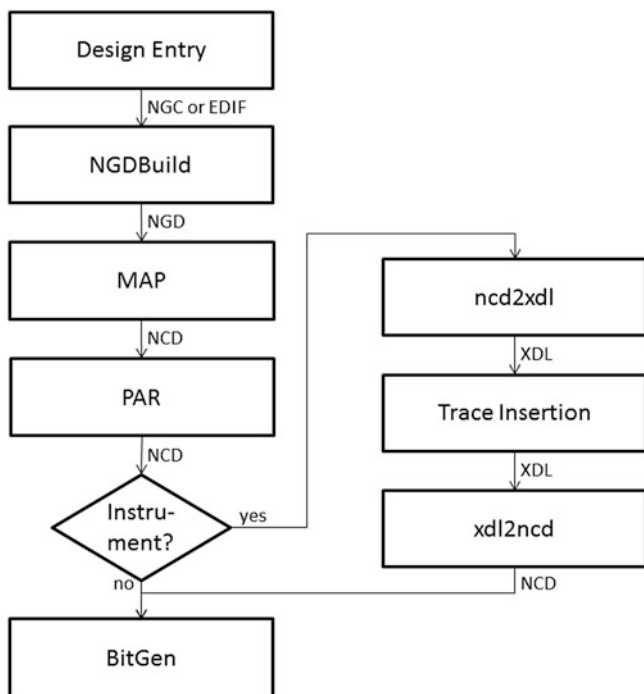


Fig. 2 Xilinx design flow

(when Trace-Buffer capacity permits). We chose to trace the flip-flops and latches because given the values of them the other intermediate values of a circuit could be calculated using techniques such as those in [15, 16].

The runtime is the time taken to place and route the Trace-Buffers and trigger unit. The time was determined by storing the current system time between major steps in the program and then comparing the times after routing has completed. The minimum period was determined by the Xilinx ISE tool, which analyses the timing of the FPGA circuit.

The important characteristics of the benchmarks are shown in Table 1. The benchmarks circuits were synthesized, and placed and routed with Xilinx ISE tools for the Virtex-2pro FG896 embedded development platform which contains a XC2VP30 FPGA. The benchmark circuits are available as part of the VTR project and represent realistic, sizable, heterogeneous designs that include Monte Carlo simulation for a financial application and linear system solvers. This table assumes a Trace-Buffer width of 16 is being used, so “Max-Traces” is calculated by multiplying the number of unused BRAMs by 16.

For the tests, there are several parameters are kept constant. The width of Trace-Buffers is fixed at 16, meaning 16 traces can be connected to each Trace-Buffer. At this width, the Trace-Buffers have a depth of 1024. The traces are routed in random order. The trigger unit is fixed at 256 inputs and 100 slices. The

Table 1 Uninstrumented benchmark summary

Circuit	LUTs	FFs	Slices	BRAMs	DSPs	IOBs	Signals traced	Max-Traces
BGM	20,511	3,672	11,708	0	44	289	3,672	4,870
Stereovision0	5,328	3,733	4,884	0	0	366	3,733	4,870
Stereovision1	9,299	9,078	7,222	0	88	278	9,078	4,870
Total available	27,392	27,392	13,696	136	136	416	–	4,870

trigger unit slices are placed in locations where the original circuits has not used any routing in the interconnect tile associated with the slices to avoid routing congestion.

The slices of the trigger unit are assumed to be placed within the same region. This ensures the trigger unit has good timing performance and its internal signals only have to be routed short distances.

4.1 Runtime Proportion

Figure 3 shows the total runtime for each of the benchmarks when the max numbers of Trace-Buffer inputs are routed. It should be noted that all benchmarks were able to successfully route all flip-flops. This is an interesting result and demonstrates that the Virtex-2pro architecture has enough routing resources to support our method. Most of the benchmarks take about a minute for the entire PAR process.

All the runtimes are less than the time it would take to recompile the entire circuit. Large and complicated circuits are known to take hours to recompile. The compile times of the benchmarks used in this work are shown in Table 2. The table also shows the average trace-insertion runtimes from Fig. 2 and the difference between the compile time and insertion runtime. None of compile times are in hours but even the shortest times are longer than all the runtime for trace-insertion, so incremental insertion decreases turnaround time for even these circuits also, if

Fig. 3 Trace-insertion runtime

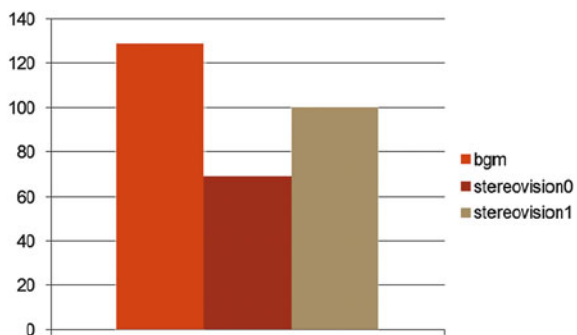


Table 2 Benchmark compile times in minutes and seconds

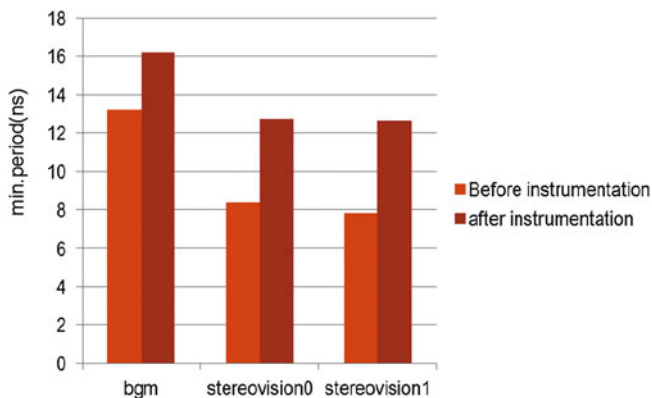
Circuit	BGM (mins:sec)	Stereo0	Stereo1
Compile time	08:55	05:10	11:06
Trace-insertion	02:05	01:25	01:43
Difference	10:50	03:45	10:23

incremental were not used then the compile time would be higher than the values shown in the Table 2 because the Xilinx tool would have to place and route the Trace-Buffer and trigger unit in addition to original circuit.

4.2 Minimum Period

The minimum period of each benchmark before and after instrumentation is shown in Fig. 4. The BGM benchmark circuit has a minimum period of 13.216 ns, and instrumentation increases this on an average by about 18 %. The stereovision benchmarks' minimum periods increase much more than other benchmarks. Stereovision0 jumps from the minimum period of 8.392–12.751 ns over 51 %. The percentage is even greater for stereovision1 which goes from 7.846 to 12.667 ns. The minimum period increases if the delay of any of the paths we insert is greater than the original minimum period. Circuits with the higher minimum are less likely to experience any increase because the inserted path may be longer without becoming a critical path.

The BGM sometimes had an increase in its minimum period and sometimes did not. The variation in period is due to the randomization in Trace-Buffer placement. The critical path is the control signal that is an output of the trigger unit and an input to the Trace-Buffers. The trigger unit is often placed near the edge of the FPGA because closer to center there are not enough free slices to place it. The

**Fig. 4** Minimum period of each benchmark before and after instrumentation

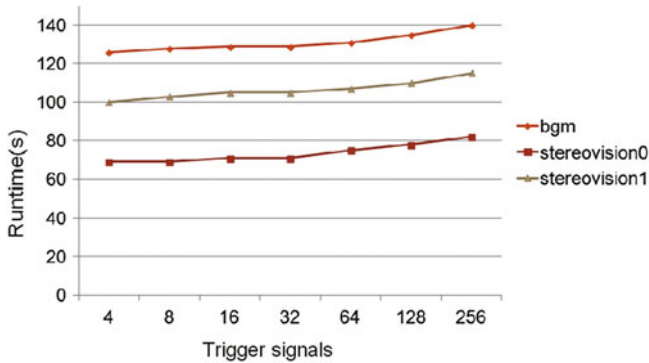


Fig. 5 Trigger signals influence on runtime

Trace-Buffers are spread throughout the FPGA. Thus, some of them are located long distance from the trigger units.

The critical path is the delay between the trigger unit and one of the distant Trace-Buffers. Figure 5 shows the runtimes for the different trigger widths. The runtime increases exponentially with the number of trigger signals, but it is mostly flat until the widths are 1024 or higher. The exponential increase comes because of the additional clock routing that is required with more slices.

Designer should avoid using trigger units that require thousands of input signals if runtime issue for the benchmarks used in our test runtime did not increase much if the runtime of input signals was 512 or below. Beyond that, the runtime increases quickly due to exponential curves. However, improving the clock router may eliminate the exponential increase in the scan time or at least keep the increase flat for even larger number of signals. Designers should also keep in mind the amount of the slices the original design uses. None of the benchmarks used here had a problem placing the trigger units of 100's of slices.

5 Conclusion

A new incremental trace-based method is used for increasing the observability of FPGAs. The method incrementally inserts the Trace-Buffers and the trigger unit in an already placed-and-routed FPGA circuits. A unique characteristic of the method is a centralized trigger unit that controls all the distributed Trace-Buffers. Advantages of this incremental method include not affecting the placing and routing of the user circuit taking full advantage of leftover BRAMs to observe more signals and decreasing turnaround time when changes are made to the debug system. The method could instrument 100 % of the flip-flops given that enough Trace-Buffer capacity exists. This was done on a commercial Xilinx Virtex-2pro FPGA further distinguishing from others. The time it takes to perform the method was less than

5 min for all benchmarks. This means that a designer could insert or change circuit instrumentation for debugging relatively fast. One drawback of our method is that it can increase minimum period for some circuits. This occurs if the delay of any of the parts we insert is greater than the current minimum period. So, the pipelining method can be used to improve the minimum period if needed.

References

1. Asaad S, Bellofatto R, Brezzo B, Haynes C, Haynes M, Kapul M, Parker B, Roewer T, Saha P, Takken T, Tierno J. A Cycle-accurate, cycle reproducible multi-FPGA system for accelerating multi-core process simulation. In: Proceedings of ACM/SIGDA international symposium field program gate arrays;2012. p. 153–62.
2. Kottolli A. The economics of structured-and standard-cell-asic designs. Open-Silicon: Technical Solutions Engineer; 2006.
3. Xilinx. Chipscope pro 12.3, software and core, user guide;2012. San Jose, CA, USA. http://www.xilinx.com/support/documentation/sw_manuals/xilinx14_4/chipscope_pro_sw_core_ug029.pdf.
4. Altera. Quartus II handbook version 11.1 vol. 3: Verification;2011. San Jose, CA, USA. http://www.altera.com/literature/hb/qts/qts_qii5v3.pdf.
5. Synopsys. Identify: Simulator-Like Visibility into Hardware Debug, Mountain View;2011. OR, USA. http://www.synopsys.com/Tools/Implementation/CapsuleModule/identify_ds.pdf.
6. Tektronix. Certus debug suite;2012. Beaverton, OR, USA. http://www.tek.com/sites/tek.com/files/media/media/resources/Certus-ASSIC-Prototyping-Debug-Solution-Datasheet_54W-28030-2_8.pdf.
7. Xilinx. Virtex-2pro fpga configuration user guide; 2012.
8. Hutchings BL, Torresen J. Unifying simulation and execution in a design environment for fpga systems. IEEE Trans Very Large Scale Integr (VLSI) Syst. 2011;9(1):201–5.
9. Wheeler T, Graham P, Nelson BE, Hutchings B. Using design-level scan to improve fpga design observability and controllability for functional verification. In: Proceedings of 11th international conference on field-programmable logic and applications, FPL'01;2001. Springer-Verlag. p. 483–92.
10. Iskander YS, Patterson CD, Craven SD. Improved abstractions and turnaround time for fpga design validation and debug. In: 2011 international conference on field programmable logic and applications (FPL);2011. p. 518–23.
11. Hung E, Wilton SJE. Incremental Trace-Buffer insertion for fpga debug. IEEE Trans Very Large Scale Integr (VLSI) Syst. 2014;22(4):850–63.
12. Hung E, Wilton SJE. On evaluating signal selection algorithms for post-silicon debug. In: Proceedings of international symposium quality electronic design, Mar 2011. p. 290–6.
13. Ko HF, Nicolici N. Algorithms for state restoration and trace-signal selection for data acquisition in silicon debug. IEEE Trans Comput-Aided Design Integr Circ Syst. 2009;28(2):285–97.
14. Graham P, Nelson B, Hutchings B. Instrumenting bitstreams for debugging fpga circuits. In: The 9th annual IEEE symposium on field-programmable custom computing machines, FCCM'01;2001. p. 41–50.
15. Prabhakar S, Hsiao M. “Using non-trivial logic implications for Trace-Buffer-based silicon debug. In: In Asian test symposium 2009, ATS'09. p. 131–6.
16. Cheng W, Chuang C, Liu CJ. An efficient mechanism to provide full visibility for hardware debugging. In: Proceedings of 2006 IEEE international symposium on circuits and systems, Iscas 2006; 2006. p. 814.

Mining-Based Device Control for Home Automation

C. Ganesh Kumar, S. Januja Josephine
and Premanand V. Chandramani

Abstract Dynamic demand response (DR) and demand side management (DSM) are the important functions that allow the customer to reduce the peak load demand. This results in the reduced energy consumption cost and better user experience. In DSM, the customers can make informed decisions regarding their energy consumption, and it helps to reshape their load profile. In this chapter, we proposed an integrated solution to predict the electricity demand and made a load shift in a locality at a given day. The system presented in this chapter expands the DR to residential loads by scheduling and controlling the appliance. The electricity demand in the home is forecasted by a decision support system, which helps the user to save energy by recommending optimal run time schedule for appliances, given user constraints and TOU pricing from the utility. The schedule is communicated to the appliance and executed by the appliance control interface.

Keywords Demand response · Demand side management · Load shift · Home automation · Data mining · Time-Of-Use pricing

1 Introduction

More electricity-consuming products are coming into our daily lives which dramatically increase the load demand and in turn impose burden on the power grid. In smart grid, to achieve high energy efficiency, load can be saved by DR and the energy

C. Ganesh Kumar (✉) · S. Januja Josephine
Department of ECE, Mohamed Sathak A.J College of Engineering, Chennai 603103, India
e-mail: cgk.1987@gmail.com

S. Januja Josephine
e-mail: januja1991@gmail.com

P.V. Chandramani
Department of ECE, SSN College of Engineering, Chennai 603110, India
e-mail: premanandc@ssn.edu.in

resources have to be well managed. The response of users to the time-varying energy prices offered by the utility defines the DR, in which the schedulable load is shifted to off-peak hours where the energy consumption cost is low. The main objective was to achieve high-quality energy service at low energy consumption cost [1].

The DSM plays an important role in electricity markets. The DSM will inform the controller about the new load schedule for the next day. Then, the controller can operate the appliance during off-peak loads. There are several demand side management system techniques and algorithms used [2].

In current regulated energy distribution system, cost of service is the norm and the electricity rate is generally averaged over the entire year. The customers pay the electricity cost based on the average electricity costs. In order to benefit both the nation and the users, the US Energy Policy Act of 2005 specifies that the pricing of electricity should be on time-based rates [3]. The requirements and needs between the energy provider and the user are coordinated by the DR strategy. This encourages the user to reduce the peak demand usage. DR can be defined as the change in the electricity usage pattern by the end-user customers from their normal pattern in order to reduce the electricity cost. In [4], the management of the system is improved by the adaptation of the Static Resource Constraint Project Scheduling Problems which satisfy the maximum power resource constraint. In [5], a linear programming scheme is presented for optimal load control of appliances.

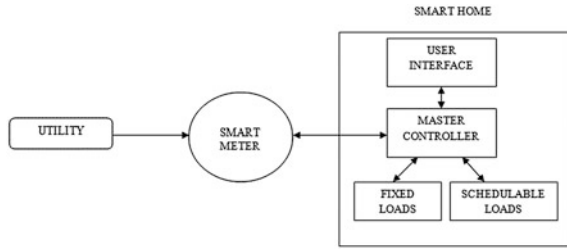
In this chapter, the energy management for the household devices is designed. The solution benefits both the residential customer and the utility company. The utility company provides the Time-Of-Use (TOU) pricing. Based on the TOU pricing, the appliance is scheduled within the user comfort zone to optimize the power consumption at lower cost. The proposed system requires no manual intervention and employs an effective heuristic algorithm. The solution presented in this chapter would enable the appliance to predict the most suitable time (based on the TOU pricing and the past utilization data) and automatically operate in that time slot, thereby scheduling and controlling the appliance to smoothen the demand. The customer is offered by the following advantages: (i) improved energy efficiency by utilizing the electricity at off-peak demand hours; (ii) maximum user comfort; and (iii) cost savings.

2 Overview of Smart Home

The smart home system alters the electricity usage pattern of the user to produce a change in the load demand. The planning objectives and the utility company change the final consumption of the appliance. The loads may be shifted to be served during appropriate times in order to reduce power blackouts during peak load hours. This in turn reduces the operational cost of energy. This in fact requires a coordinated work between the utility and the consumers.

The smart system provides feedback about the consumption habits of the appliance and making the decision autonomously. Figure 1 depicts the overall

Fig. 1 Overview of a smart home



system of a smart home. The main aim of developing a smart home was to increase the resident’s comfort level and decrease the energy consumption cost [6]. The smart home supports net metering, gets the input parameters (such as the operating time of the appliance), and the real-time electricity price and defines the optimal operating time of the appliance in every decision period. One of the most critical aspects of the smart home is the automation of demand response. The key elements of the automation are the accurate and reliable load forecasting. The appliance scheduling as well as determining the energy tariffs is based on these forecasts. The smart home system automatically learns the energy consumption pattern of the appliance under various periods.

3 Problem Formation

In residential home, if more number of appliances is operated in the low pricing period, then the peak load demand may occur in the low cost period and there is a chance for the peak load demand to occur in the low cost time period. Therefore, the operation time of the appliance should be distributed. The appliance should be turned on, not only based on the cost of electricity, but also on the most efficient time, in which the requirement of the needed appliance should be considered.

The probability for the number of occurrence of the device to be turned on in a particular time slot is given as:

$$P(X_i) = f_i/N. \tag{1}$$

where X_i denotes the occurrence of favorable time slot, f denotes the number of favorable occurrences, and N is given by $N = \sum_{i=1}^n f_i$

The user convenience level is the factor that makes this system a more efficient one.
User Convenience Level:

$$\text{Max : UCL} = \sum_{i=1}^N w_i U_{ci}(h). \quad (2)$$

where w_i denotes the weight coefficient of the significance of the task; $U_{ci}(h)$ denotes the user convenience value when the task is executed at hour h , $N = 1, 2, 3, \dots$

The power consumed by the task at hour h :

$$P_{\text{task}}(h) = E_c / L_l. \quad (3)$$

where E_c denotes the total energy consumption and L_l denotes the length of operation time.

The total power consumption of the house for a day:

$$P_D(h) = P_{D,\text{fix}}(h) + P_{D,\text{sch},i}(h). \quad (4)$$

where $P_{D,\text{fix}}(h)$ denotes the power consumed by the fixed loads and $P_{D,\text{sch},i}(h)$ denotes the power consumed by the schedulable loads.

The total power consumption of the device for a week:

$$P_w(h) = \sum_{i=1}^x P_{Di}(h). \quad (5)$$

where $P_{Di}(h)$ denotes the amount of power consumed for a day and $x = 7$

4 Scheduling Algorithm

The main goal of the algorithm was to limit the energy consumption, reduce energy costs, and provide maximum user comfort.

Algorithm for appliance scheduling

```

1. D, a database of time
2. for each time t ∈ D {
3. t1 = remove_minutes(t[0]);
4. t2 = remove_minutes(t[1]);
5. rt[] = round(t1).-.round(t2);
6. }
7. Sort(rt[],asc);
8. for each rt1 ∈ rt {
9. CT=subset(rt , rt1);
10. for each timeslot C ∈ CT {
11. C.Count ++
12. }
13. Outputk = {C ∈ rt | C.Count > 0};
14. }
15. Sort (Outputk , des);
16. for each Outputk {
17. rk= rate (Outputk[i]);
18. }
19. Subvalues (Outputk,1,5);
20. Sort (Outputk, rk, asc);
21. ON_motor (Outputk[0]);
22. Insert into D (Outputk[0]);

```

First, the usage time of the appliance is stored in a database. Each value is then rounded off to find the top most frequently used time slots. From those values, the efficient time is being found by using the daily current ratings from the utility. Each time slot is allocated with an energy price. These current ratings will be provided in advance by the utility. The database containing the schedule of the operating time of the appliance will be updated each time when the appliance is turned on.

5 Simulation and Results

In this section, we present the simulation and its results when using the appliance on a schedule basis, using TOU pricing.

5.1 Simulation

The usage times for the past few days were collected to form a database. The database for the simulation containing the past few days is shown in Table 1.

Table 1 Data set of the appliance

Data set (contains the past few days operating time)		
10:10 AM–10:45 AM	04:00 AM–04:30 AM	08:05 AM–08:30 AM
06:15 AM–06:50 AM	04:00 PM–04:40 PM	08:00 AM–08:20 AM
03:10 AM–03:20 AM	05:00 AM–05:20 AM	06:00 PM–06:10 PM
09:35 PM–09:55 PM	11:20 AM–11:50 AM	05:00 PM–05:35 PM
04:10 PM–04:30 PM	06:30 PM–06:50 PM	06:00 PM–06:45 PM

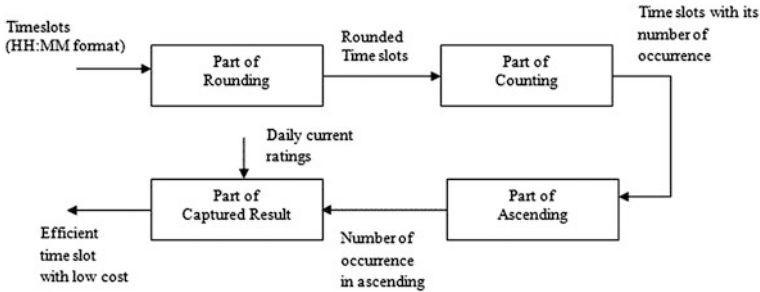


Fig. 2 Data flow in the energy management system

The simulation is carried out using LabVIEW software. The process of simulation consists of four main parts: part of rounding, part of counting, part of ascending, and part of captured result, as shown in Fig. 2.

Each part performs its operation depending on the result from the preceding part. Part of rounding rounds off the input time slot. After all the time slots have been rounded off, they are concatenated to form an array of time slots. Part of counting is used to find out the number of times the appliance is turned on in each time slot. It is followed by the process of ascending with respect to the number of counts from which gives the most frequently used time slot is obtained. In the part of captured results, the time slots will be matched with the daily ratings and the most efficient time with low cost, in which the appliance can be turned on is determined.

5.2 Result

The simulation result provides the most efficient time along with the cost of power in that particular time slot. This system not only benefits the end users, but also benefits the utility. Figure 3 shows the efficient on time of the device with user comfort and low cost.

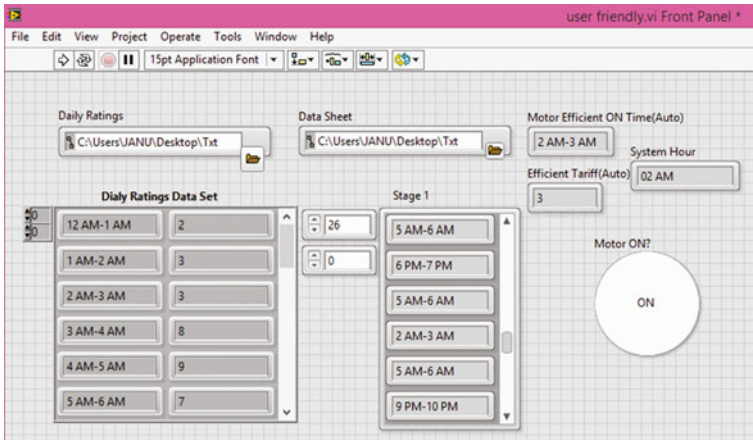


Fig. 3 Device in ON state

The obtained output efficient time is fed back to the existing database. Thus, within certain time period, a large database can be developed that makes the system more effective for further prediction.

Figure 4 shows the number of times the appliance has been used in a particular time slot. The plot is made based on the values given in Table 1. Figure 5 shows the cost for each hour, which is provided by the utility given in Table 2. Figure 6 illustrates the operating characteristic of the system to capture the most efficient time. It is observed that 02 AM–03 AM is the most efficient operating time of the appliance that satisfies both the customer and the utility.

Table 3 compares the operation of the device under different conditions. Taking the cost of electricity into account, the least cost 1 is at the time slot of 01 PM–02 PM. But this time, slot is not user friendly. When the operation of the device is considered, the most frequently used time slots are 06 PM–07 PM and 05

Fig. 4 No. of times the appliance is used

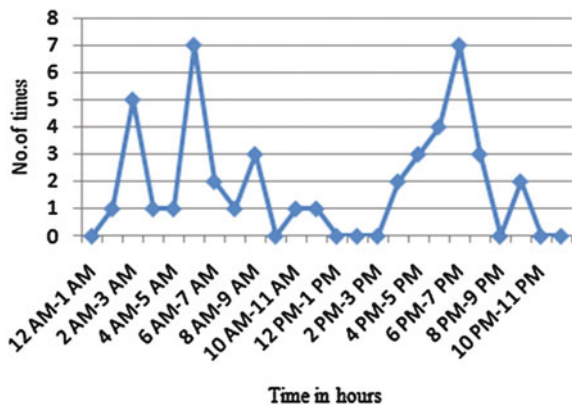


Fig. 5 Daily ratings from the utility

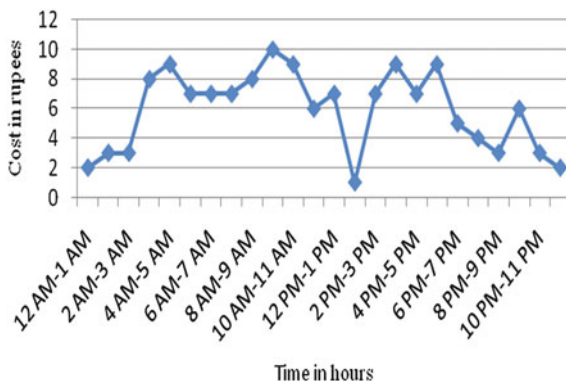


Table 2 Daily ratings from the utility

Time	Cost
12 AM-01 AM	02
01 AM-02 AM	03
02 AM-03 AM	03
03 AM-04 AM	08
04 AM-05 AM	09
05 AM-06 AM	07
06 AM-07 AM	07
07 AM-08 AM	07
08 AM-09 AM	08
09 AM-10 AM	10
10 AM-11 AM	09
11 AM-12 PM	06
12 PM-01 PM	07
01 PM-02 PM	01
02 PM-03 PM	01
03 PM-04 PM	09
04 PM-05 PM	07
05 PM-06 PM	09
06 PM-07 PM	05
07 PM-08 PM	04
08 PM-09 PM	03
09 PM-10 PM	06
10 PM-11 PM	03
11 PM-12 AM	02

AM-06 AM. But at these time slots, the cost is high, which indicates that the current generation is less at these periods. There is a chance for blackouts at these periods. Therefore, considering both the utility and the user comfort, the efficient

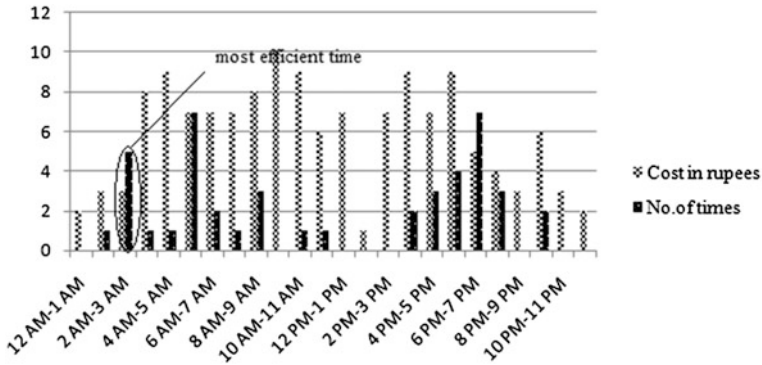


Fig. 6 Comparison between cost and no. of times

Table 3 Comparison between the customer usage and the utility ratings

Parameters	Operation time	Cost	User comfort	Comment
Electricity cost	01 PM–02 PM	01	00	Lagging user comfort
Customer usage	06 PM–07 PM 05 AM–06 AM	5	7	May lead to blackouts
Customer usage and cost	02 AM–03 AM	3	5	Satisfies both the customer and the utility

time slot is found to be 02 AM–03 AM, which has low cost and also it is one of the most frequently used time slots. This time slot benefits both the user and the utility.

6 Conclusion

This chapter provides a solution to the demand response of the users and also a more user-friendly environment can be created. The appliance will be more effectively turned on at the time slot with minimum cost and off-peak load demand. The main advantage is that the blackouts will be reduced to a greater extent. Also, the problem of inadequate power supply will be overcome. Automation process helps in the efficient usage of power which saves the cost of power, renewable, and non-renewable sources of energy and also reduces the need for man power. This process is more convenient and efficient for the people, since it does not require any manual intervention or monitoring.

References

1. Jiang B, Fei Y. Smart home in smart microgrid: a cost-effective energy ecosystem with intelligent hierarchical agents. *IEEE Trans Smart Grid*. 2015;6(1):3–13.
2. Logenthiran T, Srinivasan D, Shun TZ. Demand side management in smart grid using heuristic optimization. *IEEE Trans Smart Grid*. 2012;3(3):1244–52.
3. Ozturk Y, Senthilkumar D, Kumar S, Lee G. An intelligent home energy management system to improve demand response. *IEEE Trans Smart Grid*. 2013;4(2):694–701.
4. Ha DL, Ploix S, Zamai E, Jacomino M. Control of energy consumption in home automation by resource constraint scheduling. In: *Proceedings of 15th international conference on control systems computer science*;2005. Bucharest, Romania, 25–27 May, 2005.
5. Pedrasa MAA, Spooner TD, MacGill IF. Coordinated scheduling of residential distributed energy resources to optimize smart home energy services. *IEEE Trans Smart Grid*. 2010;1(2):134–43.
6. Anvari-Moghaddam A, Monsef H, Rahimi-Kian A. Optimal smart home energy management considering energy saving and a comfortable lifestyle. *IEEE Trans Smart Grid*. 2015;6(1): 324–32.

Methods and Materials for Adsorbing the Benzene Molecule Based on Micro Electro Mechanical System

D. Lingaraja and S. Praveen Kumar

Abstract This paper provides a review about the available adsorbent materials, the most suitable adsorbent material for coating the porous silicon for adsorbing the benzene molecule and the selection of silicon wafer type, resistivity, orientation, and thickness. Then, the basic requirements for performing electrochemical etching process (ECE) to fabricate the porous silicon and spin coating process for coating the thin layer of benzene adsorbent material on the porous silicon will be analyzed. Mathematical formulas used for estimating the adsorption amount, porosity, and pore size will be discussed.

Keywords Adsorption · Benzene · Porous silicon · Spin coating process

1 Introduction

Benzene is an organic chemical compound, the molecular size is $0.34 \times 0.60 \times 0.69$ nm, and the molecular weight is 78.11 [1]. Moreover, it is highly volatile and highly degraded in air rather than water, and the most exposure is through inhalation. The sources of benzene [2] are petroleum industry, indoor residential air, inside vehicles, food, and water. The benzene level has been raised because of petroleum industry and inside vehicles. The effect of benzene on adults, children, and pregnant women is discussed. Because of home smokers, the level of benzene in indoor air will be increased [3]. So, we need to prevent the workers and children from the exposure of benzene. If the vehicles are parked under sunlight at 60°C will have more amount of benzene, then the ventilation will provide the reduction of benzene exposure from these parked vehicles. We know that the

D. Lingaraja (✉) · S. Praveen Kumar
Department of Electronics and Communication Engineering, Saveetha Engineering College,
Chennai, India
e-mail: lingamlingamraja@gmail.com

S. Praveen Kumar
e-mail: praveenkumar@saveetha.ac.in

adsorption technique is the most available method to perform the air purification, sewage disposal, chemical industry sublimation and seawater desalting, etc. Pore size, pore distribution and surface area, and pore surface chemistry are the major factors in the adsorption process. For that, we will discuss the available benzene adsorption materials such as activated carbon fiber (ACF), granular activated carbon (GAC), and silica gel and its properties [1]. After selecting the adsorbent material, the selected adsorbent will be coated on porous silicon fiber. The porous silicon fiber will provide an additional mechanical strength to adsorbent and the porous nature that helps to coat more adsorbent into the porous silicon. The available methods for fabrication of porous silicon are chemical stain etching, chemical vapor etching, laser-induced etching, metal-assisted etching, spark processing, and reactive ion etching, electrochemical etching, and stain etching [4]. Among these methods, electrochemical etching process and stain etching process are recurrently used. Due to the stain (brownish or reddish color) that is formed on the surface of the porous silicon and the non-uniform etching outline, the electrochemical etching process is mostly used rather than stain etching process. Porous silicon is a promising material due to its suitable mechanical and thermal properties. The porous silicon which provides high specific area within a small volume, controllable pore sizes, is suitable to form dielectric multilayers.

According to IUPAC, we classified the three types of pores based on its average pore diameter. If the average pore diameter is lesser than 2 nm, then it is referred to as micropores. If the average pore diameter is 2–50 nm, then it is referred to as mesopores. If the average pore diameter is greater than 50 nm, then it is referred to as macropores [5]. The numerous parameters involved in performing the electrochemical etching process are electrolyte composition, pH, current density, etching time, wafer doping, temperature, and lighting [4]. After fabricating the porous silicon, the adsorbent material will be coated on the substrate by spin coating process [6]. The spin coating process is the most suitable form for coating the thin layer of adsorbent onto the substrate. Spin coating is a fast and easy method to generate thin and homogeneous organic films from solutions. The numerous parameters involved in performing spin coating process are fluid viscosity, speed, time, and layer thickness [6]. The four stages involved in spin coating process are as follows: (1) deposition, (2) spin-on, (3) spin-off, and (4) evaporation. The main issues in spin coating process are edge bead, geometric effect, and Bernoulli's effect.

In the next section, we will discuss the available adsorbents, the most suitable adsorbent for efficient benzene adsorption, and its reason. In the third section, we will review the needs of porous silicon for the benzene adsorption and its basic requirements. In the fourth section, we will review how the best adsorbent will be coated onto the porous silicon by spin coating process and its basic requirements.

2 Adsorbent Selection

Benzene is one of the toxic gases which cause serious effects for human beings such as cancer and leukemia. In order to absorb the benzene molecules, adsorption mechanism is the most effective technique. Based on the suitable adsorbent, the efficiency of adsorption has been improved. In this section, we will discuss the available adsorbents and the most suitable adsorbent. The mostly used adsorbents for adsorbing the benzene molecule are activated carbon fiber (ACF), granular activated carbon (GAC), silica gel, and silica aerogel [1].

2.1 Activated Carbon

Due to its high microporosity, the activated carbon will be used as a good adsorbent or it provides good application for filter. The activated carbon is also called as activated charcoal, activated coal, and carbo activates. Due to the low-volume pores, it will increase the surface area. We know that if the surface area is increased, then automatically its adsorption efficiency will be increased. The surface area of one gram of activated carbon is made 500 m² using gas adsorption method. The activated carbon is mainly used in gas purification, gold purification, metal extraction, water purification, medicine, sewage treatment, air filtering in gas mask and respirators and sound energy adsorption.

2.2 Granular Activated Carbon

GAC can be used to remove dissolved contaminants from water by adsorption due to its high particle size. The important attribute of GAC is high surface area (1065 m²/g). The preparation of GAC is similar to ACF preparation with an increasing temperature.

2.3 Silica Aerogel

Due to their nanoporous network, silica aerogel will have high adsorption performance. It also provides spongy porous structure and high porosity. The pore size of silica aerogel is in between 10 and 50 nm [1]. Silica aerogel can be of two types: hydrophobic silica aerogel and hydrophilic silica aerogel. The main attributes of silica aerogel are its high porosity (greater than 95 %) and excellent accessibility to inner surface area through open pores [8]. Three steps involved in fabricating the synthetic aerogel are as follows: (a) gel preparation, (b) aging of the gel, and

Table 1 Advantages and its reason for different adsorbents

Adsorbents	Advantages	Reasons
ACF	(i) Less diffusion	Due to the high surface area, the most of the adsorbent will be adsorbed only on the surface of the adsorbent [7]
	(ii) Less efficiency	Only 20 % of the adsorbent are used for adsorbing the adsorbent [7]
GAC	(i) Less selectivity	It will adsorb toluene and ethylene along with benzene
	(ii) Less diffusion	Due to the high surface area, the most of the adsorbent will be adsorbed only on the surface of the adsorbent
	(iii) Water adsorption	Due to the high content of carbon, it will be mostly used for removing water contaminants [9]
	(iv) Reusable	Regeneration of carbon atom is done offsite [9]
Silica aerogel	(i) High selectivity	Due to the nanoporous network, it will be able to adsorb only benzene molecule
	(ii) High diffusion	Due to the spongy-like structure and less surface area, the diffusion of adsorbent will be maximum [1]
	(iii) Reusable	By passing the inert gas at 600 °C [8]

(c) drying of the gel [5]. The precursor is the main constituent of the silica aerogel, and different molecular ratios of precursor can be used for different applications.

In Table 1, the list of available adsorbent for benzene molecule is given. Due to the nanoporous network, spongy-like structure, and its efficient reusability by passing inert gas at 600 °C, the highly suitable adsorbent for adsorbing the benzene molecule is the silica aerogel. In this section, we review the available adsorbents and the best suitable adsorbent for adsorbing the benzene.

3 Porous Silicon

The porous silicon fiber will provide an additional mechanical strength to adsorbent and the porous nature that helps to coat more adsorbent into the porous silicon. The electrochemical etching process is mostly used method for forming porous silicon. Electrochemical etching process uses numerous parameters such as type of wafer, current (AC or DC), current density, HF concentration, etching rate, platinum wire, porosity, SEM images, and TEM images. We know that the p-type and n-type wafers are available. Based on its application only, the wafer will be selected. The parameters involved in selecting the wafer are resistivity, pore size, smoothness, etc. The high-resistivity wafer will increase the hardness of the surface. The low-resistivity wafer will provide high smoothness to the surface.

Husnen et al. have researched about the efficiency of different current densities on pore morphology. And they are reported that if the HF concentration is 1:4 (HF: ethanol), then the uniformity and porosity of the porous silicon will be increased when the current density is increased [10].

Table 2 Effect of anodization parameter on the surface of the porous silicon

Anodization parameters	Porosity	Etch rate
HF concentration	Decreases	Decreases
Current density	Increases	Increases
Anodization time	Increases	Almost constant
Wafer dopant (p-type)	Decreases	Increases
Wafer dopant (n-type)	Increases	Increases

Pusendra kumar et al. have researched and proposed that if the concentration of HF is decreased, then it will increase the diameter of the pore. The other important parameters involved in electrochemical etching process are alternating current and platinum wire. The advantage of using alternating current in electrochemical etching process is (a) to exhibit higher mechanical strength and (b) avoid backside contact [11] (Table 2).

4 Spin Coating

In this section, we will analyze the compatibility of spin coating process on the porous silicon. Spin coating process is a fast and easy method for coating the thin layer on the bulk substrate. Here, this process is used for coating the silica aerogel material on the porous silicon substrate. The important parameters involved in spin coating process are fluid viscosity, speed, time, and layer thickness. In Table 3, the spin coating parameters and its suitable range are given. The maximum range of the layer thickness is 0.3–3 μm . The maximum speed limit is 6000 rpm. The trouble shooting techniques in spin coating process are air bubbles, swirl pattern pin point, uncoated areas, etc. [12].

Eswar et al. have proposed that the spin coating method is also suitable for coating the PSI fiber. They successfully deposited the ZnO particles on the PSI fiber [13].

The following stages are involved in this process (Fig. 1).

In the deposition stage, the coating fluid is deposited onto a wafer or flat substrate. In spin-on stage, the spinning has to be done at a constant rate. In spin-off stage, the spinning rate has reduced at a constant rate. In the evaporation stage, the coated solvent will start to evaporate [6].

Table 3 Spin coating parameters and its range

Parameters	Range
Fluid viscosity	1–10 Cp
Speed	500–6000 rpm
Time	Up to few minutes (it varies depending on coating fluid)
Layer thickness	0.3–3 μm

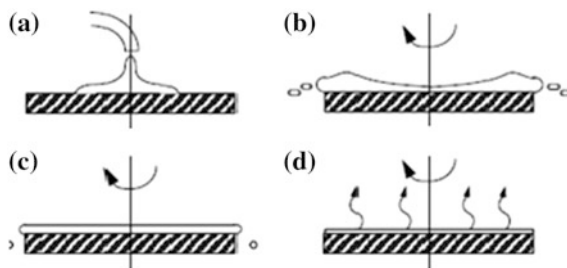


Fig. 1 Four stages in spin coating process. **a** Deposition stage, **b** spin-on stage, **c** spin-off stage, and **d** evaporation

5 Mathematical Analysis

To estimate the thickness of the porous silicon, porosity of the porous silicon, and adsorption capacity of benzene, the following formulas will be used.

5.1 Thickness (D)

The thickness of the porous silicon can be calculated using the following formula:

$$D = (m1 - m3)(\rho S)^{-1} \quad (1)$$

where $m1$ -weighted samples before samples before etching, $m2$ -weighted samples after etching and $m3$ -weighted samples after dissolution of PSI layer in a 3 % molar of aqueous KOH solution, ρ Is the density of the silicon substrate (2.3296 g/cm^3) and S is the etched surface area which can be determined by Brunauer–Emmett–Teller (BET) theory method.

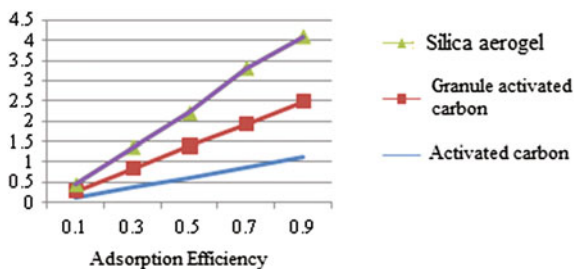
5.2 Porosity (P)

The porosity of the porous silicon can be calculated using the following formula:

$$P(\%) = (m1 - m2)(m1 - m3)^{-1} \times 100 \quad (2)$$

where $m1$ is the samples are weighted before etching, $m2$ is the samples are weighted after etching, $m3$ is the after dissolution of Psi layer in a molar 3 % KOH aqueous solution.

Fig. 2 Comparison graph



5.3 Adsorption Capacity of Benzene (B)

The gravimetric method will be used for estimating the benzene adsorption percentage,

$$B(\%) = (w(\text{sa}) \times A(\text{sa})) (w(\text{sa}) + w(\text{psi}))^{-1} \times 100 \quad (3)$$

where $w(\text{sa})$ is the weight of the silica aerogel per unit area (g/m^2), $w(\text{psi})$ is the weight of the porous silicon, and $A(\text{sa})$ is the saturated adsorption percentage of the silica aerogel (50–100 %).

6 Results and Discussion

Figure 2 shows the comparison between the silica aerogel, granular activated carbon (GAC), and activated carbon fiber (ACF). Among these, the silica aerogel has higher adsorption efficiency. So the silica aerogel can be used for adsorbing benzene which is one among the toxic gases.

7 Conclusion

This paper concludes that benzene is one among the toxic gases which cause cancer, leukemia, and other several harmful effects to human beings. The people who work in the petroleum industry would be affected seriously. In order to absorb the benzene molecule, the silica aerogel would be the effective adsorbent when compared with activated carbon and granular activated carbon. Due to the nanoporous network and spongy-like structure, it will absorb more amount of benzene. The porous silicon will be used for placing more amount of adsorbent. In Sect. 4, it is concluded that the spin coating process is also applicable to coat the porous silicon substrate.

Acknowledgments We would like to take this opportunity to express our sincere gratitude to all our professors who have guided, inspired, and motivated us for doing this project work. It gives us immense pleasure to acknowledge their cooperation.

References

1. Zhang Z, Shen J, Ni X, Li Y, Wang B, Wu G, Zhou B. Benzene adsorption properties of silica aerogel-Fiber composites. In: 2nd IEEE international nanoelectronics conference;2008.
2. Preventing diseases through healthy environment. World health organization, 20 Avenue Appia, 1211 geneva, Swizerland.
3. Benzene teach chemical summary. U.S, EPA, Toxicity and exposure assessment of children's health.
4. Haidary SM, Córcoles EP, Ali NK. Nanoporous silicon as drug delivery system for cancer therapies. *J Nanomater.* 2013.
5. Soleimani Dorcheh A, Abbasi MH. Silica aerogel; synthesis, properties and characterization. *J Mater Process Technol.* 2008;199:10–26.
6. Luurtsema GA. Spin coating for rectangular substrate. Berkeley: University of California; 1997.
7. Shivayogimath CB, Hiremath MN, Lokeshappa B. Preparation and characterization of granular activated carbon from acacia nilotica stalk. *Int J Eng Sci Innovative Technol (IJESIT).* 2014;3.
8. Novak Z, Knez Z. Silica aerogels and their application for different adsorption processes. University of Manipur, Faculty of chemistry and chemical engineering;2000.
9. Reclamation managing water in the west, U.S Department of Interior Bureau of Reclamation;2010.
10. Husnen R. Abd., Al-Douri Y, Ahmed NM, Hashim U. Alternative-current electrochemical etching of uniform porous silicon for photodetector applications. *Int J Electrochem Sci;*2013;8.
11. Kumar P, Lemmens P, Ghosh M, Ludwig F, Schilling M. Effect of HF concentration on physical and electronic properties of electrochemically formed nanoporous silicon. *J Nanaomater.* 2009.
12. Eswar KA, Rouhi R, Husari HF, Rusop M, Abdullah S. Annealing heat treatment of ZnO nano particles grown on Porous Si substrate using spin coating method. *Adv Mater Sci Eng.* 2014;138:1–6.
13. <http://www.utdallas.edu/~rar011300/CEEsSpinner/SpinTheory.pdf>.

A Multi-parametric Hybrid Cooperative Localization Scheme for Mobile Communication Network

D. Pavankumar and H.R. Mahadevaswamy

Abstract In this chapter, as proposed in the research proposal, here in this initial research phase a novel model for mobile node localization and tracking has been developed for wireless-interfaced networks for next-generation communication. In this research proposal, “A multi-parametric hybrid cooperative localization scheme for mobile communication Network” has been proposed that can be a potential solution for next-generation wireless mobile communication system functional on the basis of decentralized behavior and self-organizing nature. The proposed system can play the significant role in next-generation communication systems with ad hoc-based technologies such as MANET, VANET, VASNET, and interfaced network (LTE-based) as well as advanced sensor networks (WSNs) to be employed in interfaced communication networks (ICNs), industrial applications as well as in under sea networks (USNs).

Keywords Non-line of sight · Wireless sensor network · RSSI · Mobile node

1 Introduction

In the present-day application scenario, the highly pace increase in wireless mobile communication, there is an inevitable need of advanced and optimized communication system that could ensure quality of service (QoS) in real-time applications.

D. Pavankumar (✉) · H.R. Mahadevaswamy
Jain University, Bangalore, India
e-mail: pavidn@gmail.com

H.R. Mahadevaswamy
e-mail: hrmswamy@yahoo.in

H.R. Mahadevaswamy
Applied Inventions India Pvt Ltd., Jain University, Bangalore, India

On the other hand, optimal QoS in the wireless communication network is one of the predominant needs of the next-generation wireless communication technologies. Meanwhile, for the next-generation communication techniques such as Third-generation partnership projects (3GPP), Long-term evolution (LTE) technologies, Universal mobile telecommunication services (UMTS), and other paradigms for wireless mobile communication as well as wireless sensor-based communication systems, there is the requirement of optimization in node localization so as to increase the optimal connectivity and data delivery in real-time applications. The effective significance of node localization in the communication system makes the overall system delivering optimal results. Evolved packet core (EPC) is an IP-based communication approach which ensures QoS in real-time communication applications in LTE technologies [1]. Even in LTE communication to ensure the optimal efficiency, the handover is needed to be optimized and the effective localization of certain node can play a significant role for it. Similarly, in case of wireless sensor networks (WSNs), the exact node localization is must. On the other hand, nowadays in advanced communication systems, the static wireless nodes are being interfaced with the mobile nodes so as to ensure optimal communication performance for real-time broadband application (3G, UMTS, and LTE) [2].

This is the matter of fact that a number of researches have been done for effective node localization in wireless communication system. Considering our research-oriented literature survey (Internet resources, IEEE survey for 2011–2014), it has been found that most of the researches have been done either based on conventional node positioning approach such as Monte Carlo positioning, and GPS technologies or the conventional techniques which cannot ensure optimal performance, especially in the situation of indoor applications, under sea network, tunnels, non-line of sight (NLOS) communication scenario with higher nonlinearity, and many more [3]. Similarly, in major cases especially for WSNs, the traditional RSSI-based systems have been developed which sometime gets confined due to changes or nonlinear behavior of environmental conditions. Some of the systems have been developed based on time of arrival (TOA) or difference of angle (DOA) or some works employed the hybrid one called TDOA, but still these systems lack a proper optimized function with LOS communication as well as NLOS requirements. Therefore, considering these all limitations of the existing systems in this research proposal, a robust and efficient system has been proposed with optimized localization facility without compromising with any performance parameters. The proposed system encompasses multiple approaches for system optimization, and optimization of the better performing system has been done so as to ensure optimal behavior of the system for node tracking and positioning [4].

2 Implementation of Localization and Dynamic Triangulation Algorithm

In general, three nodes are needed for mobile user localization using dynamic triangulation-based node tracking or localization approach. Thus, taking into consideration this need, 4 nodes have been employed. Dynamic triangulation approach eliminates the weak RSSI signals that make the nodes to explore for the node having strongest RSSI. DTN also plays a significant role in selecting strongest RSSI signal to be employed for localization and mapping mobile node in communication network [5].

In this developed model, mapping circle is nothing else but the *estimation distance* d_1 existing between the master node [6] and the mobile users in the network. This can be estimated by the angle on the mapping circle using DTN and employing a novel concept of cost function or cost factor analysis that selects the optimal pair of observed distance [5].

In this system, for creating the mapping circle, the optimal localization $(x_1 + d_1 \cos \theta, y_1 + d_1 \sin \theta)$ or location estimation of the mobile user is estimated by dynamic triangulation approach by employing all feasible distances $(d_2\theta, d_3\theta)$ between the mobile user and slave nodes. Once it is done, the estimation of the mobile user distance from master node is the estimation distance and the possible error between the estimation distance and the practical location or distance is achieved by dynamic triangulation approach. Here, the cost factor analysis is accomplished where the cost function for each angle is evaluated, and finally using dynamic triangulation-based function, the minimal cost function is retrieved in terms of estimation angle on the mapping circle [8].

In this work, the angle retrieved on the mapping circle represents the estimation of the mobile node location.

The step-wise discussion for accomplishing research objective-1 is as follows:

- Step 1: Estimate the strongest RSSI parameter and then create or establish the mapping circle by equation:

$$d_1 = d_0 \frac{10 \text{RSSI}_0 - \text{RSSI}_M}{10n}$$

Then, the mapping circle was generated using the following expression:

$$(x_\theta, y_\theta) = (x_1 + d_1 \cos \theta, y_1 + d_1 \sin \theta)$$

- Step 2: Select the second and third strongest RSSI signal and estimate the distance between the mobile node and the sensor node in the deployed or considered wireless-interfaced network to be employed in the next-generation communication applications.

The derived simple expressions are

$$d_2 = d_0 10^{RSSI_0 - RSSI_1 / 10n}$$

$$d_3 = d_0 10^{RSSI_0 - RSSI_2 / 10n}$$

Step 3: Generation of the cost functions and the estimation of the minimal cost function angle

$$d_{2\theta} = \sqrt{(x_2 - d_1 \cos \theta)^2 + (y_2 - d_1 \sin \theta)^2}, \quad 0 \leq \theta \leq 360$$

$$d_{3\theta} = \sqrt{(x_3 - d_1 \cos \theta)^2 + (y_3 - d_1 \sin \theta)^2}, \quad 0 \leq \theta \leq 360$$

Error estimation

$$\text{Error}_{1\theta} = |d_{2\theta} - d_2|$$

$$\text{Error}_{2\theta} = |d_{3\theta} - d_3|$$

Step 4: Estimate the minimal cost function with associated angle

$$\text{Minimal Cost function} = \sqrt{\text{Error}_{1\theta}^2 + \text{Error}_{2\theta}^2}$$

In this model, to further optimize the accuracy and preciseness of the mobile node localization or tracking, an optimization in terms of predictive RSSI paradigm has been modeled, and for this, a gray prediction algorithm has been incorporated that employs gray system to predict the RSSI associated with the mobile node in the communication network. The dynamic RSSI of x employing the first-order equation has been developed in this work

$$\frac{dX(1)}{dt} + aX(1) = b$$

3 Simulation Results

In the specific simulation situations, when $k \geq 2$, it supposed (proposed) to employ minimal least square approach or similar algorithms which considers linear model ($yn = Ba$).

In this research phase, the implementation of dynamic triangulation approach and gray prediction scheme has exhibited better for mobile node localization in wireless-interfaced network, comprising mobile nodes and sensor transceiver terminals. These technologies can be a potential approach for future- or next-generation communication system.

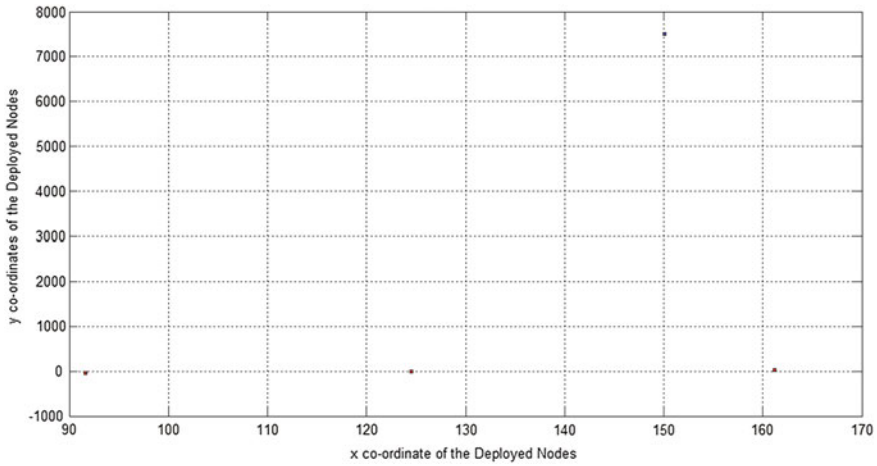


Fig. 1 With 4 numbers of cells

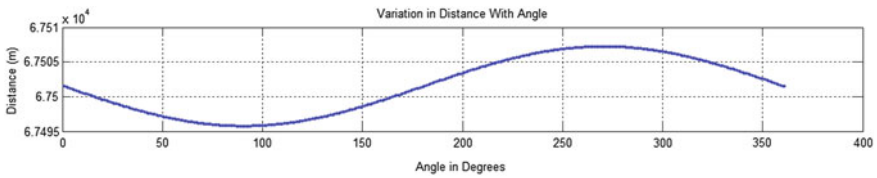


Fig. 2 Variation in distance with angle

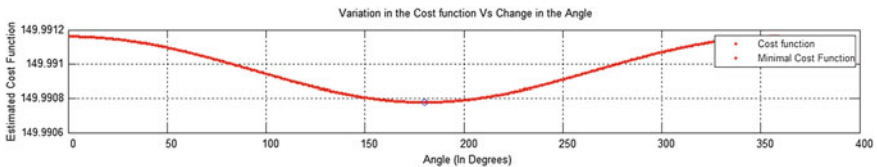


Fig. 3 Variation in cost function versus change in angle (Here, Blue circle represents the location of mobile user in the network)

The factor introduced in this research phase was the consideration of predicted RSSI estimation and associated mobile user tracking and localization along with the introduction of a unique weight-predicted scheme that exhibits better as compared to conventional localization or tracking systems in non-line of sight (NLOS) [9] communication environment (Figs. 1, 2, 3, 4 and 5).

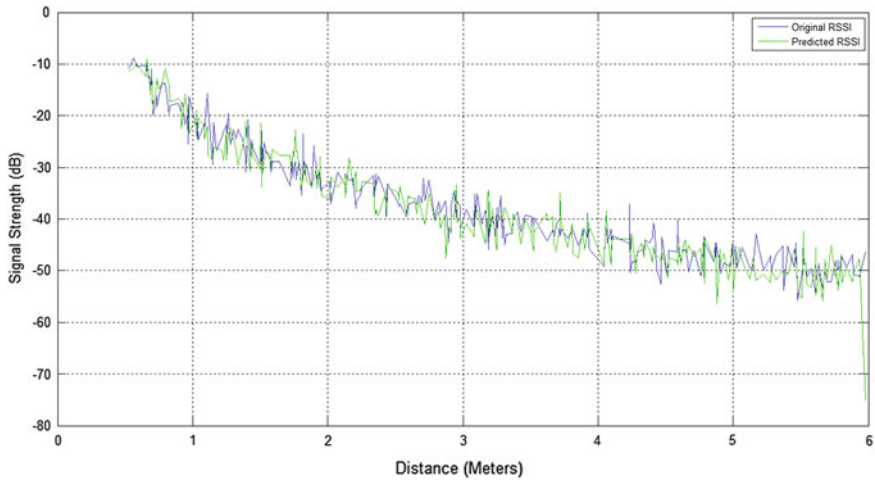


Fig. 4 Simulation result of original RSSI vs predicted RSSI

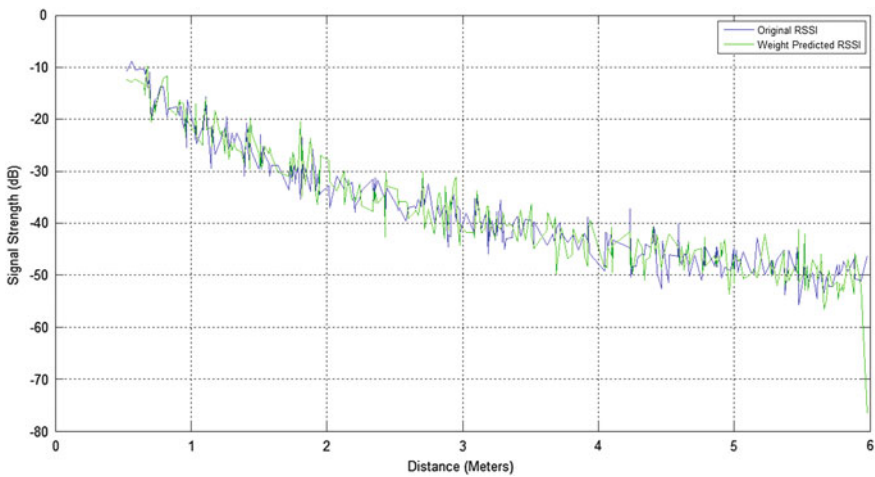


Fig. 5 Simulation result of original RSSI vs weight predicted RSSI

References

1. Farmani M, Moradi H, Asadpour M. A hybrid localization approach in wireless sensor networks using a mobile beacon and inter-node communication. In: 2012 IEEE International Conference on Cyber Technology in Automation, Control, and Intelligent Systems (CYBER), p. 269, 274, May 27–31 2012.
2. Kumar S, Tiwari SN, Hegde, RM. 3-D mobile node localization using constrained volume optimization over ad-hoc sensor networks. In: 2014 Twentieth National Conference on Communications (NCC). p. 1, 6, 28 Feb 28 2014–2 Mar 2014.

3. Zhou Z, Peng Z, Cui J-H, Shi Z, Bagtzoglou AC. Scalable localization with mobility prediction for underwater sensor networks. *IEEE Trans Mobile Comput.* 2011;10(3):335, 348.
4. Miles J, Muknahallipatna S, Kubichek RF, McInroy J, Muralidhara H. Use of radio propagation maps in a single moving beacon assisted localization in MANETs. In: 2014 International Conference on Computing, Networking and Communications (ICNC), p. 871, 877, 3–6 Feb 2014.
5. Zhu X, Huang P-C, Han S, Mok AK, Chen D, Nixon M. RoamingHART: a collaborative localization system on WirelessHART. In: 2012 IEEE 18th Real-Time and Embedded Technology and Applications Symposium (RTAS), p. 241, 250, 16–19 Apr 2012.
6. International Journal of Advanced Research in Computer and Communication Engineering, vol. 2, Issue 6, June 2013 Copyright to IJARCCCE www.ijarccce.com TRACKING the LOCATION of MOBILENODE in WIRELESS SENSOR NETWORK Vishal Garg1, Mukul Jhamb2 Department of Computer Science & Engineering, Kurukshetra University.
7. Priyadharshini C, Rubini KT. Integration of route lifetime prediction algorithm and particle swarm optimization algorithm for selecting reliable route in MANET. In: 2012 International Conference on Computing, Communication and Applications (ICCCA), p. 1, 6, 22–24 Feb 2012.
8. Amini A, Vaghefi RM, de la Garza, JM, Buehrer, RM. GPS-free cooperative mobile tracking with the application in vehicular networks. 2014 11th Workshop on Positioning, Navigation and Communication (WPNC), p. 1, 6, 12–13 Mar 2014.
9. Liu Y, Yu H, Chen B, Xu Y, Li Z, Fang Y. Improving Monte Carlo Localization algorithm using genetic algorithm in mobile WSNs. In: 2012 20th International Conference on Geoinformatics (GEOINFORMATICS), p. 1, 5, 15–17 June 2012.

Interface and Control of Appliances by the Analysis of Electrooculography Signals

S.V. Arthi and Suresh R. Norman

Abstract The movement of the eye is detected by electrooculography (EOG) technology for clinical applications to identify vestibular and ocular disorders. This technique when employed with the human–computer interface (HCI) systems can provide great benefits for the people. The main objective of measurement, analysis, and processing of these signals is to help people who are suffering with lesser motor capabilities. EOG is the technique of recording the bio-potential generated by the movement of the eyes. This is done by positioning the surface electrodes around the eyes and observing the corneo-retinal potential (CRP) between the anterior part and the posterior part of the eye. This sensed potential is linearly proportional to the movement of the eyes. The observed bio-electric signal is in terms of lower voltage, and hence, it is given to signal conditioning circuits to get a more accurate signal. The pattern is recognized for different movements of the eye and it is used for controlling the appliances.

Keywords Appliance control • Communication • Electrodes • Electrooculography • Eye movement • Human–computer interface • Signal conditioning

1 Introduction

Action is a form of communication which is more effective than words. Communication is important for a person with neural, ocular, or vestibular disorders and paralysis patients with little motor capabilities. An efficient solution for

S.V. Arthi (✉)

Applied Electronics, ECE Department, SSN College of Engineering,
Kalavakkam, India
e-mail: arthikutty5@gmail.com

S.R. Norman

ECE Department, SSN College of Engineering, Kalavakkam, India
e-mail: sureshnorman@ssn.edu.in

© Springer India 2016

S.S. Dash et al. (eds.), *Artificial Intelligence and Evolutionary Computations
in Engineering Systems*, Advances in Intelligent Systems and Computing 394,
DOI 10.1007/978-81-322-2656-7_100

1075

communicating and controlling things without speech is that hand and leg movement should be used for differently abled people. The application of using electrooculography signals to control the HCI systems is of importance in recent decades. The bioelectric potentials produced in the body are sensed directly by surface electrodes rather than by the normal pathway for communication.

The different methods used for eye movement detection are infrared oculography (IROG) [1]. This works on a light source being focused at the eye [2]. The intensity of light reflected to the detector differs proportionally with respect to the eye ball position. Here, the light source is fixed and so measuring vertical movement of the eye is difficult since the eyelids occupy more of the space in vertical movement.

The video oculogram (VOG) uses a camera to record the movements of the eye and convert it into an equivalent mouse movement on the system. Here, the person has to be seated in front of the camera. Image processing can be done for further analysis. Scleral search coil (SSC) method is an invasive method where a small coil is operated and placed inside the lens of the eye [3]. This method is useful for diagnostic purposes. When a coil of wire is moved in the magnetic field, it induces a potential in the coil which is attached to the eye.

EOG is a technique which is simple, cost-effective, and noninvasive. Here, the field of view is not restricted to a video camera or the sensors. The linear proportion between EOG and eye movement makes the waveform easier to analyze. The EOG technique can be used with HCI systems for different applications for controlling a wheelchair [4, 5], a keyboard [6, 7], or a television [8]. This paper presents the control of appliance by the analysis of eye gestures using EOG technique for the smart control of the appliances.

2 Engineering Analysis

2.1 Block Diagram

The EOG technique is used to obtain signals using electrodes at five positions around the eyes. Bio-signals are obtained in the range of 0.05–3.5 mV and have a useful frequency range from 0 to 16 Hz. So, it is amplified and filtered to remove noise. The output can be recorded or displayed using a digital storage oscilloscope (DSO). The basic block diagram of EOG signal conditioning circuit is shown in Fig. 1.

The amplified and filtered signal is analyzed using the microcontroller ATmega 328. The entire block diagram of EOG signal acquisition is shown in Fig. 2. Here, the output from the reference electrode is given to the analog reference input pin in order to get accurate digital data. The output from the signal conditioning circuit is given to the analog input pin.

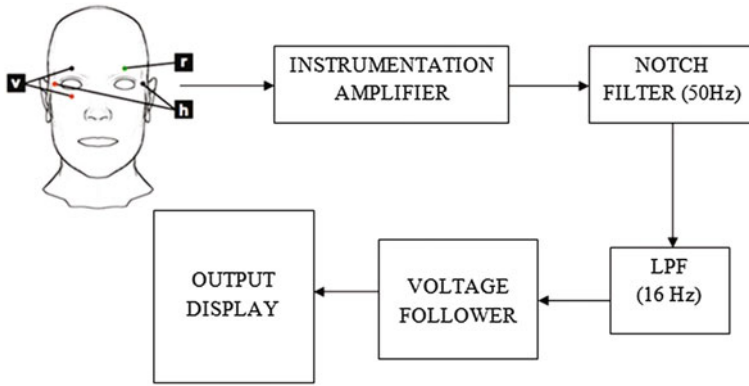


Fig. 1 Basic block diagram of EOG signal conditioning circuit

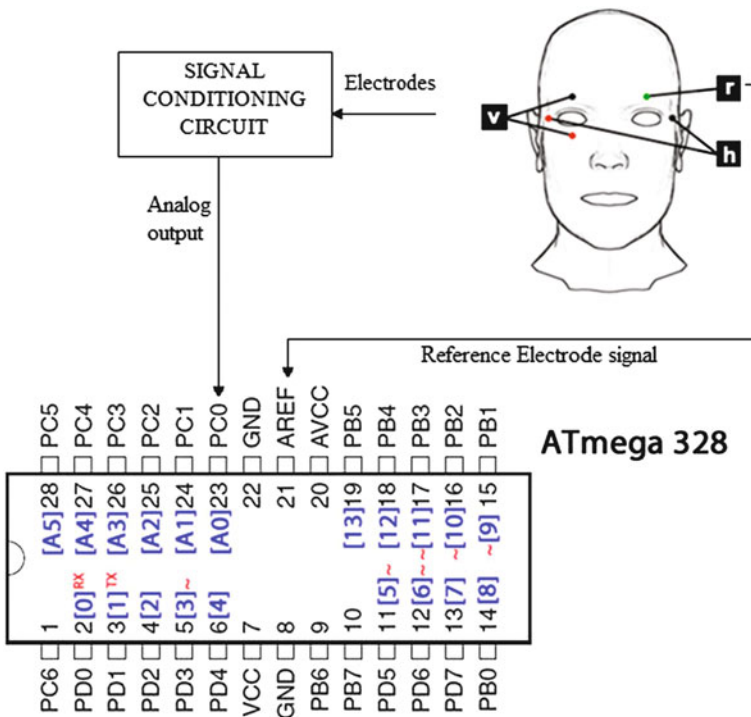


Fig. 2 Block diagram of EOG signal acquisition

2.2 Bioelectric Potentials

The chemical activity in the nerves and muscles of the body generates a variety of signals. They produce a characteristic pattern of voltage variations. This pattern is recognized for different eye movements and is used for controlling appliances. The potential difference is established in the cell and it acts similar to a tiny battery. When electrodes are placed around the eyes, they capture the resting potential between the cornea and retina, thus employed for analyzing different eye movements.

2.3 Electrodes

The medical electrodes are employed to figure the electrical activity of the body. They are used for different clinical applications including electrooculography (EOG), electrocardiogram (ECG), electromyography (EMG), electroencephalography (EEG), and electrogastrogram (EGG). The various types of electrodes used are microelectrodes, depth electrodes, surface electrodes, needle electrodes, and corneal electrodes. All these types can be used as dry electrodes or wet electrodes with an electrolytic gel for increasing the conductivity. The surface electrodes are shown in Fig. 3.

The properties of EOG signal vary depending on the positioning of the electrodes. Various configurations such as 3/4, 4/5, and 7/8 are used for different applications where the first number denotes the number of active electrodes placed and the second number denotes the total number of electrodes including the reference electrode. The 4/5 electrode configuration is used here, as the wires used in the 7/8 configuration are a disadvantage. The different measurement systems are shown in Fig. 4.

Fig. 3 Surface electrodes



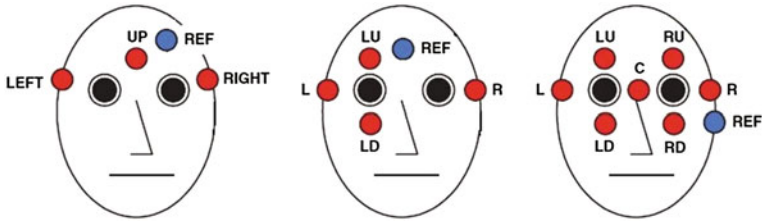
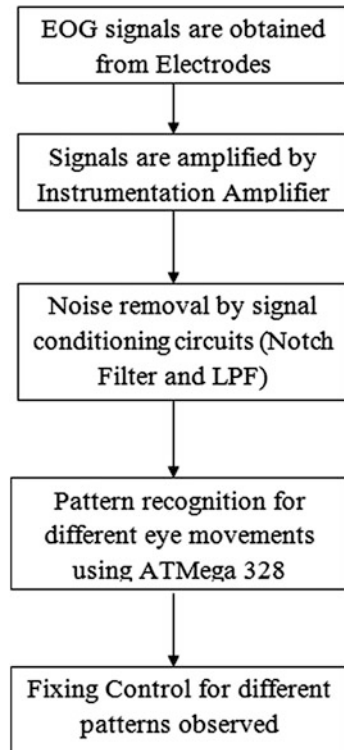


Fig. 4 Different measurement systems

2.4 Flowchart

EOG signals are obtained by 4/5 electrode configuration using the EOG technique. The signal is amplified with suitable gain using an instrumentation amplifier. The high frequency and other power line noises are removed using filters. The signal is analyzed by converting the analog data into digital data by connecting it to the microcontroller. Further, this obtained digital data are analyzed and the pattern is recognized for different eye movements. The flowchart for the entire process is shown in Fig. 5.

Fig. 5 Flowchart for EOG signal acquisition and control



3 Signal Processing

3.1 Instrumentation Amplifier

The bioelectric potential that is being sensed around the eyes is in the range of 0.05–3.5 mV. For further analysis, it must be amplified. The INA118 is a low-power instrumentation amplifier offering high gain required for the project. It is used for almost all medical applications to enhance the signal strength. It provides a high CMRR of about 110 dB and can have a gain of $G = 1000$. A single external resistor R_g sets any gain from 1 to 10000. The block diagram of an instrumentation amplifier is shown in Fig. 6.

3.2 Notch Filter and LPF

Filters are electronic circuits which are employed to extract the useful frequency range and to filter unwanted frequency components from the signal. This project requires a filter of high gain to remove power line noise of 50 Hz, and hence, twin-T notch filter is used which can tune up to 100 dB. Hence, the resistance and capacitance values are chosen appropriately to get a center rejection frequency of 50 Hz. The notch filter used is shown in Fig. 7. In general, the noises are included in high frequencies and so a LPF is used. Here, the EOG signal is obtained in the frequency of about 16 Hz or less. Hence, the cutoff frequency is chosen accordingly.

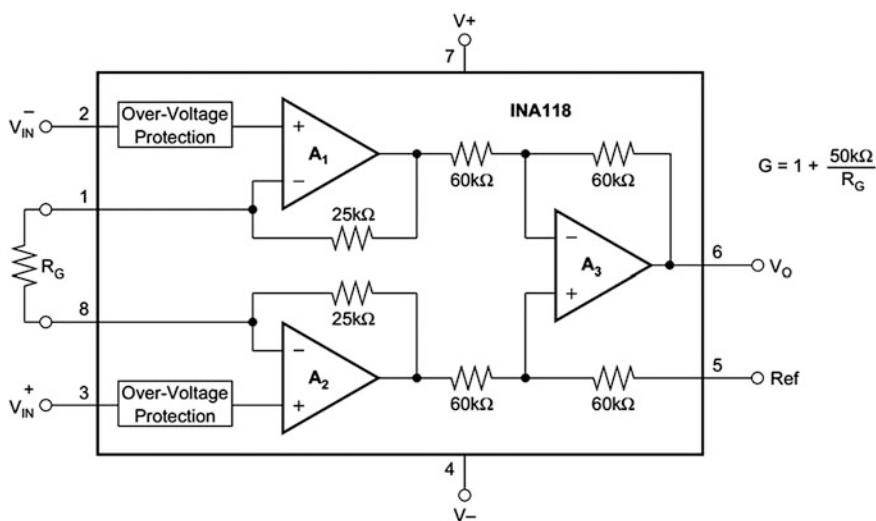
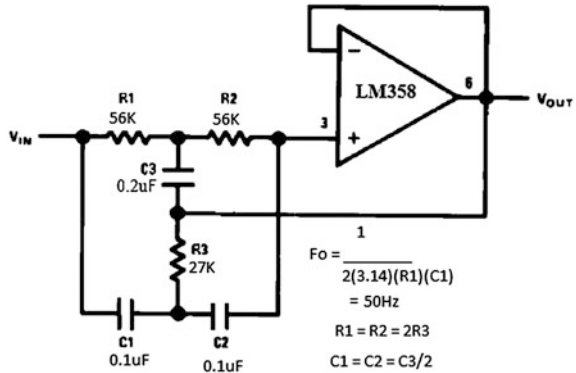


Fig. 6 Instrumentation amplifier

Fig. 7 Notch filter



3.3 Voltage Follower

A voltage follower (buffer) is added to provide electrical impedance transformation from one circuit to another. It acts as a unity gain amplifier with the gain of 1. Buffers are used in impedance matching, and the advantage is to maximize the energy transferred. It is used to connect a high output impedance source to a low input impedance device and vice versa. The buffer is added to avoid loading effects.

3.4 Microcontroller

The microcontroller used here is Atmega 328 which is a cost-effective version of Arduino. It has user-friendly open-source software and the required number of input output pins necessary to connect appliances. It has an inbuilt analog to digital convertor (ADC) which is needed for digitizing the EOG signal. Coding is done for pattern recognition, and the controls are assigned for different movements.

4 Experimental Results

The eye movement is similar to a dipole in which the anterior part, i.e., cornea, is positive and posterior part, i.e., retina, is negative. Left movement of the eye can be defined as a condition when the cornea approaches near the outer edge of the eye, thus providing a negative change in the recorded potential [9]. The EOG acquisition is done, and the waveform is obtained for a person looking straight as shown in Fig. 8.

When the electrodes are placed for detecting the vertical movements of the eye, the waveforms obtained for top movements are shown in Fig. 9 and that for downward movements of the eye are shown in Fig. 10. Blinks are more predominant in the vertical electrode placement.



Fig. 8 EOG wave of a person looking straight without moving the eye

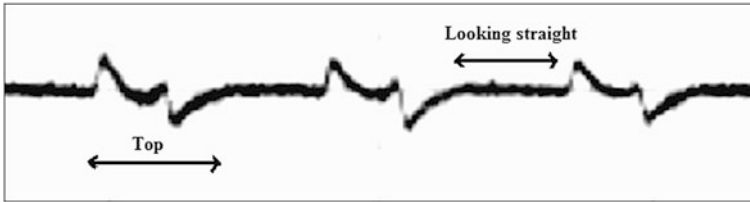


Fig. 9 EOG wave of the person moving the eye in the *top* direction

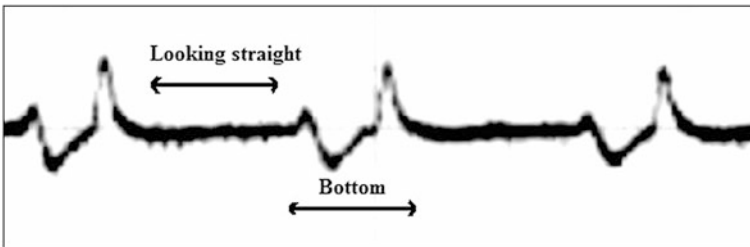


Fig. 10 EOG wave of a person moving the eye in the *bottom* direction

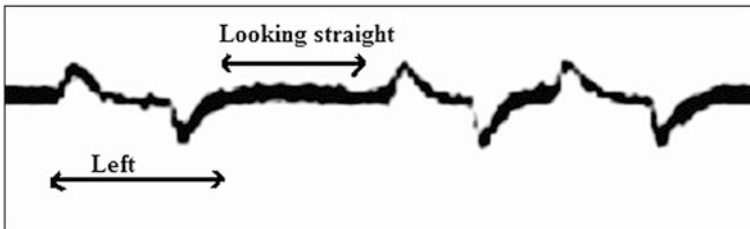


Fig. 11 EOG wave of a person moving the eye toward the *left* direction

Similarly, when the electrodes are placed for detecting the horizontal motion of the eye, the waveforms are obtained for left movement as shown in Fig. 11 and that for right movement as shown in Fig. 12.

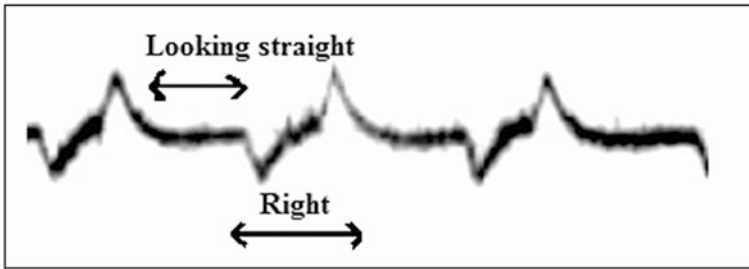


Fig. 12 EOG wave of a person moving the eye toward the *right* direction

The human eye is always active and this condition must be considered in all analysis. Therefore, validation and codification should not be performed involuntarily. The horizontal electrodes are placed, and left and right patterns of the eye are recognized. The Arduino programming is done for controlling a light. Thus, the left movement of the eye switches off the light and the right movement switches it on. Similarly, control can be assigned for the top-down movement using the vertical electrode placement. The 4/5 electrode configuration includes both the horizontal and vertical placement of electrodes. Thus, the eye movement toward top-left, top-right, bottom-left, and bottom-right can also be detected. This helps in increasing control for appliances.

5 Conclusion

The EOG technique is employed here, as it is inexpensive yet reliable human-computer interface that is used for detecting eye movements. The surface wet electrodes were used as it provides good conductivity. For this project, 4/5 electrode system worked successfully instead of 7/8 configuration which had many wires and also had the difficulty of moving the eyes. The useful EOG signal range was less than 16 Hz and also the potential was less. Thus, the obtained signal was amplified sufficiently enough using an instrumentation amplifier. Further improvements in the analysis were made by filtering the high-frequency components and removing the power line noise of 50 Hz. The resulting EOG signals were observed in the digital storage oscilloscope, and the directions of the eye movement were differentiated based on the amplitude and the time period. The results obtained were reliable. Further analyses were made by connecting the output to a microcontroller and digitizing the signal. Codification was done, and controls were assigned for different movements. Thus, the analysis of EOG signals and proper interface lets people who cannot control an object with their hands, to have more options for controlling the appliances. Further improvements can be made in placing of the electrodes around the eyes such that they are more comfortable to wear. The entire system can also be made wireless and placed in the spectacles.

References

1. Johns MW, Tucker A, Chapman JR, Crowley EK, Michael N. Monitoring eye and eyelid movements by infrared reflectance oculography to measure drowsiness in drivers. *Somnologie Schlaforschung Schlafmedizin*. 2007;11:234–42.
2. Schmitt KU, Muser MH, Lanz C, Walz F, Schwarz U. Comparing eye movements recorded by search coil and infrared eye tracking. *J Clin Monitor Comput*. 2007;21:49–53.
3. Sprenger A, Neppert B, Koster S, Gais S, Kompf D, Helmchen C, Kimmig H. Long-term eye movement recordings with a sclera search coil eyelid protection device allows new applications. *J Neurosci Methods* 2008;170:305–309.
4. Barea R, Boquete L, Mazo M, Lopez E. Wheelchair guidance strategies using EOG. *J Intell Robot Syst*. 2002;34:279–99.
5. Barae R, Boquete L, Mazo M. System for assisted mobility using eye movements based on electrooculography. *IEEE Trans Neural Syst Rehabil Eng*. 2002;10(4):209–18.
6. Dhillon HS, Singla R, Rekhi NS, Jha R. EOG and EMG based virtual keyboard: a brain-computer interface. In *Proceedings of 2nd IEEE International Conference on Computer Science and Information Technology*, 2009, p. 259–262.
7. Usakli AB, Gurkan S. Design of a novel efficient human-computer interface: an electrooculogram based virtual keyboard. *IEEE Trans. Instrum Measure*. 2010;59(8):2099–2108.
8. Deng LY, Hsu CL, Lin TC, Tuan JS, Chang SM. EOG based human-computer interface system development. *Expert Syst Appl*. 2010;37:3337–43.
9. Arthi SV, Norman SR. Analysis of electrooculography signals for the interface and control of appliances. *Int J Multi Current Res (IJMCR)* 2015;3:87–90.
10. Bulling A, Ward JA, Gellersen H, Troster G. Eye movement analysis for activity recognition using electrooculography. *IEEE Trans Pattern Anal Mach Intell*. 2011;33(4):741–53.
11. Ubeda A, Ianez E, Azorin JM. Wireless and portable EOG based interface for assisting disabled people. *IEEE/ASME Trans Mechatron*. 2011;16(5):870–3.

An Advanced Magnetic Resonance Imaging Technique for the Detection of Abnormal Changes Using Artificial Neural Network

P. Balasubramanian and S. Manju

Abstract Image Segmentation is a complicated and challenging task in detecting tumors in human brain. In diagnostic Systems, this image segmentation plays a major role for detecting brain tumors. For detecting the abnormal changes in the brain, a technique called magnetic resonance imaging (MRI) is used. MRI is based on the abundance of hydrogen nucleus in human body and there magnetic resonance activities. The proposed system consists of four stages: collecting the data by various repository systems or hospitals, preprocessing of brain images, extracting the features from the images by using k -means algorithm, and classifying the brain images with the help of neural system. In our paper, we have proposed an advanced neural network using fuzzy k -means algorithm.

Keywords Brain tumor · Classification accuracy · Specificity · Sensitivity · Fuzzy neural network · k -means algorithm

1 Introduction

Magnetic resonance imaging is widely used in medical field to examine the anatomy and physiology of the body. MRI process is recommended than other types of imaging technique because it does not use ionizing radiation. It is widely used to its neglected radiation in the application areas. In older days, brain images are analyzed manually which increases the human errors and error rate. To avoid this type of errors, various classification and segmentation algorithms are used. Though various algorithms are used, there is no standard algorithm in medical field to analyze the

P. Balasubramanian (✉) · S. Manju
Department of Electronics and Communication, Velammal Institute of Technology,
Chennai, India
e-mail: Balasubramanian.p89@gmail.com

S. Manju
e-mail: itismanju_85@yahoo.co.in

image. Hence, to analyze the different parts of human body, various segmentation and classification algorithms are used [1]. The images can then be inspected on a computer monitor, transferred electronically, printed, or reproduced to CD. Various body parts that can be examined using MRI are heart, kidneys, bowel, liver, and adrenal glands. Though MRI has several advantages, there are some disadvantages in MRI; the quality of the image is affected by the function of human during scan such as breathing and irregular heartbeats, and time and cost is also high. Abnormal cells in the brain cause brain tumor, which leads to human death or makes them unconscious. Some of the factors of brain tumor are exposure to the industrial chemicals, infection by Epstein-Barr virus as well as neurofibromatosis. There are two types of brain tumors: primary and secondary. Secondary brain tumor is common compared with primary. The various literature surveys show the average overall performance based on the segmentation and classification algorithms [2].

k -means algorithm is used in different areas to perform iterative partition. The applications of k -means algorithm are in vector quantization, fault detection, knowledge discovery, and data mining. This cluster representative is obtained using the iterative process of k -means algorithm. Mostly, fuzzy and hard k -means clustering techniques are used in many applications. Mostly, fuzzy k -means algorithm is used when compared with hard k -means algorithm. The complexity of k -means algorithm is reduced by decreasing the size of data which in turn reduces the computational complexity [3]. The outline of the paper is explained as follows: Sect. 2 describes the various literature surveys conducted to analyze the various algorithms related to the proposed system. Section 3 provides the proposed system flow. Section 4 describes about the preprocessing function of the proposed system.

2 Related Work

Warfield et al. introduce a statistical classification to improve the intensity of images by using multiparameter images [4]. Though the intensity of the images is improved, the classification accuracy is moderate. Zumray et al. improve the multilayer perceptron result for problems in biomedical image classification [5]. The learning-based unsupervised algorithm provides the improved accuracy in the classification of brain tumor, while brain abnormality classification is done using learning vector quantitation architecture. One more approach uses Hopfield neural network (HNN) which is robust in the recognition of abnormal tissues.

Solis and Perez designed ART2 network for pattern detection [6]. A modified neural network is introduced to improve the performance of the existing neural network. William Melson introduces an approach which is robust in image classification and improves the accuracy based on large data set [8]. Though it improves the accuracy, it increases dimensionality problem which raises the difficulty of the architecture. Marcelprastawa presented a system which is used to classify the brain

tumor and edema with prior probability. This classification increases the accuracy which increases the researcher’s interest. Marcin Denkowki offered a system on fuzzy logic for the organization of MRI. Yang and Zheng implemented an algorithm for image classification to improve the accuracy of image [7]. Mausumi Acharyya applied a neuro-fuzzy tool for image segmentation. In this paper, fuzzy *k*-means algorithm is used for feature extraction and classification of brain images.

3 Proposed System

The flow of the proposed system contains five major divisions which include the large set of input data, MR image preprocessing, *k*-means algorithm, segmentation, and classification. The MR image is collected from various sources such as hospital and repository sites to make the system automated. The collected database may contain different types of data sets such as normal and abnormal MR brain images [9]. Now, the obtained input set of data is fed to the preprocessing operation, comprising of the conversion of RGB to gray image, morphological operation and threshold operation. Figure 1 shows the flow diagram of the proposed system. The gray-level matrix is used to extract the features of the preprocessed images.

In this paper, abnormality of brain is proposed and the classification of MRI is analyzed and applied. The main maneuver performed in the proposed system is that MR images are alienated into subsequence structural elements, and features of these elements are extracted. The extracted features from the images are used to enumerate the symmetry, intensity, and texture properties of the brain tissues. One assumption made in processing of the image that has different texture indicating the altered physical features of image. Once the image is segmented, the next step is to perform image classification. Numerous features in brain images are identified

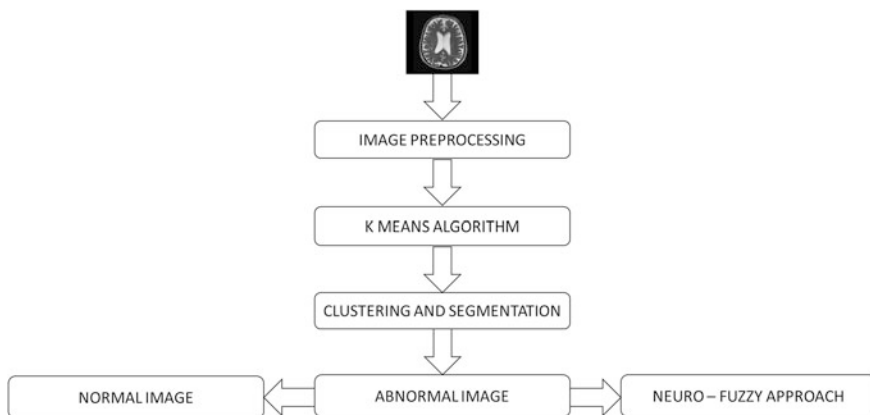


Fig. 1 Flow diagram of the proposed system

using image classification. Fuzzy algorithm is used to classify the image which identifies the abnormal and normal brain images.

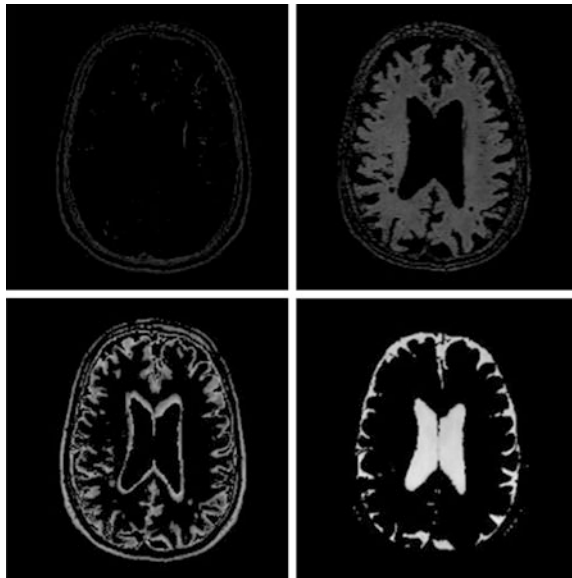
4 Image Preprocessing and Feature Extraction

A diagnosing system can be automatically implemented to form the database of numerous types of MRI images [10]. The image data can be improved to reduce the undesired distortions using image preprocessing. Figure 2 shows the extracted features of the brain image.

Image preprocessing is used to develop image which can be used for input as any other processing. Image preprocessing steps are artifact elimination using median filtering, gray conversion, and thresholding operation. Artifact elimination can be done using median filter. In median filtering, brightness of an image is used to rank the neighboring filter. The central value of the median filter is changed according to the change occurring in the neighboring filter [11]. The main advantages of the median filter are as follows:

1. Median filter is robust compared with the mean filter.
2. Median filter is not affected by the outliers.
3. The contrast of the image is retained using median filter.
4. When compared with the mean filter, median filter boundaries are not shifted from the input image.

Fig. 2 Extracted brain image



Thresholding operation is used to perform the segmentation in an image. The grayscale image is the input of the thresholding operation, and the binary image is the output. Black pixel and white pixel in the image are used to represent the background and foreground of the image. Various thresholding operations can be used to perform the segmentation, but mostly intensity thresholding is used. In intensity threshold, the intensity of the image is compared with the predefined reference value. Once the level is less than the threshold value, it is assigned to black and above that reference value is assigned as white.

5 Steps in Fuzzy— k -Means

The various clustering methods are used to minimize the error. One of the effective methods which are used to perform error minimization is sum of squared error (SSE) which uses each instance to measure the total squared Euclidean distance based on their values. This method is frequently used in clustering due to their optimized performance in isolated environment. The algorithm that is used in this method to perform the distance measure is k -means algorithm which is the most commonly used one. Based on the center or mean, the data in the cluster are partitioned into K clusters ($C_1 \dots C_K$). Each cluster center is taken, and it is assigned as mean to all instances in the cluster.

Once the algorithm starts, initially a value has to be given for center of the cluster which may be random values or values depend on heuristic procedure. Once the center value is assigned, the value of center is changed to the nearest center value in the cluster using the Euclidean distance. In reference to the Euclidean distance, the cluster center is updated. Each cluster center is taken, and it is assigned as mean to all instances in the cluster.

$$\mu_k = \frac{1}{N_k} \sum_{q=1}^{N_k} x_q$$

where μ_k is the mean of the cluster k and N_k is the number of instances in each cluster k .

There are various possible conditions to stop the algorithm. One of the most commonly used criteria to stop the algorithm is that if the new center value is increased compared to the previous center value, the algorithm is stopped because it is already optimized. The next criterion is maximum number of iterations reached.

Input: S (instance set), K (number of clusters)

Output: clusters

- 1: Initialize K cluster centers.
- 2: **while** termination condition is not satisfied **do**
- 3: Assign instances to the closest cluster center.

4: Update cluster centers based on the assignment.

5: **end while**

The clusters produced by the k -means procedure are sometimes called “hard” or “crisp” clusters, since any feature vector x either a member or non member of a particular cluster. This is in contrast to “soft” or “fuzzy” clusters, in which a feature vector x can have a degree of membership in each cluster.

The fuzzy k -means procedure is as follows:

Make initial guesses for the means m_1, m_2, \dots, m_k

Until there are no changes in any mean:

Use the estimated means to find the degree of membership.

For i from 1 to k

Replace m_i with the fuzzy mean.

End for

End until

6 Conclusion

The proposed method has proved to provide better accuracy than the existing systems. As it combines the artificial neural network and fuzzy logic, the disadvantages of both the techniques are eliminated. The proposed method detects the brain abnormalities much faster with higher accuracy, thus finding the disease in the earlier stages. The simulation results show that this fuzzy k -means algorithm has provided much specificity.

References

1. Sonka M, Hlavac V, Boyle R. Image processing, analysis, and machine vision, II edn. New Delhi: Vikas Publishing House; 2004.
2. Gonzalez RC, Richard EW. Digital image processing, II Indian edn. New Delhi: Pearson Education.
3. Bose NK, Liang P. Neural network fundamentals with graphs, algorithms, and applications. India: TMH; 2004.
4. Sivanandam SN, Sumathi S, Deepa SN. Introduction to neural networks using Matlab 6.0.
5. Rohrer J. A dramatic evolution in seeing & treating tumors. Featured Article from *Visions*, Fall/Winter, 2004.
6. Cline HE, Lorensen E, Kikinis R, Jolesz F. Three dimensional segmentation of MR images of the head using probability and connectivity. *J Comput Assist Tomogr.* 1990;14:1037–45.
7. Haralick RM, Shanmugam K, Dinstein I. Textural features for image classification. *IEEE Trans Syst Man Cybern.* 1973;3(6):610–2.
8. Vijay Kumar G, Raju GV. Biological early brain cancer detection using artificial neural network. (IJCSE) *Int J Comput Sci Eng.* 2010;02(08):2721–2725.

9. Descombes X, Kruggel F, Wollny G, Gertz HJ. An object based approach for detecting small brain lesions: application to Virchow-robin spaces. *IEEE Trans Med Imaging*. 2004;23(2):246–55.
10. Yin TK, Chiu NT. A computer-aided diagnosis for locating abnormalities in bone scintigraphy by fuzzy system with a three-step minimization approach. *IEEE Trans Med Imaging*. 2004;23(5):639–54.
11. Zhu H, Francis HY, Lam FK, Poon PWF. Deformable region model for locating the boundary of brain tumors. In: *Proceedings of the IEEE 17th Annual Conference on Engineering in Medicine and Biology*, 1995. IEEE, Montreal, Quebec, Canada, 1995, p. 411.

Implementation of a Hybrid Renewable Energy Plant with Remote Monitoring Feature

Ersan Kabalci and Ramazan Bayindir

Abstract This study is intended to present the implementation of a hybrid renewable energy plant where solar and wind energy conversion systems are installed together. The hybrid plant consists of a wind turbine with permanent magnet synchronous generator (PMSG) at 2 kW_p rated power and solar panel array at 0.64 kW_p rated power. The generated energy is coupled on the dc bus bar and is supplied to energy storage subsystem in order to ensure the sustainability of energy. The stored energy is used to meet energy requirement of a microprocessor laboratory where the left energy is supplied to the grid in spare times. The plant is developed with communication features that enable to observe the plant remotely. This is performed with the designed data acquisition card that consists of current and voltage sensors, and microprocessor communicating with computer over universal serial bus (USB) port. The user interface software that generates log files and graphs is built by using Visual C#.Net platform. The implemented system is assumed as an essential training and education plant in terms of distributed generation, renewable energy sources, smart grid, and remote monitoring.

Keywords Hybrid renewable energy · Remote monitoring · PMSG · Solar · Dc bus bar · Data acquisition · Visual C#.net

E. Kabalci

Department of Electrical and Electronics Engineering, Faculty of Engineering and Architecture, Nevsehir Hacı Bektaş Veli University, 50300 Nevsehir, Turkey
e-mail: kabalci@nevsehir.edu.tr

R. Bayindir (✉)

Department of Electrical and Electronics Engineering, Faculty of Technology, Gazi University, 06500 Teknik Okullar, Ankara, Turkey
e-mail: bayindir@gazi.edu.tr

© Springer India 2016

S.S. Dash et al. (eds.), *Artificial Intelligence and Evolutionary Computations in Engineering Systems*, Advances in Intelligent Systems and Computing 394, DOI 10.1007/978-81-322-2656-7_102

1093

1 Introduction

The shortage lived in fossil fuel reserves and environmental hesitations has given rise to researches on alternative and renewable energy sources (RES). The RESs as being the most important substitute of conventional sources allow to install distributed generation (DG) plants either on-grid or off-grid. The DG plants provide generation at or near to the load differing from central generation plants. On the other hand, the DG plants can consist of wind, solar, fuel cell, and several other RESs where the generated energy is coupled to alternative current (ac) or direct current (dc) bus bars through coupling interfaces. Furthermore, the hybrid coupling operation that is accomplished with converting ac and dc output sources on a unique bus bar is convenient to improve capacity of RESs that can be used [1, 2]. The DG plant that is built with various sources allows to obtain higher efficiency and reliability.

The energy storage subsystem (ESS) is one of the key points besides the energy sources in the low-power DG system. The ESS is considered as the buffer of DG system where the sustainability of the energy is provided by the battery bank. The ESS is mostly based on chemical storage systems as lead–acid or gel batteries [3, 4].

The implementation presented in this study is illustrated in Fig. 1. The DG part of the system is installed with a wind turbine and solar panel array where the

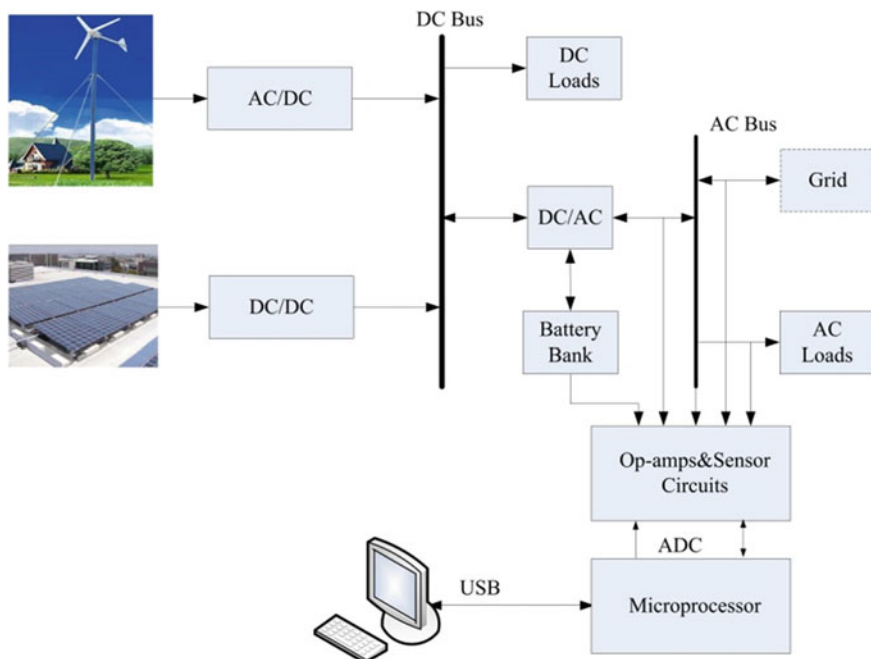


Fig. 1 Schematic diagram of the hybrid energy plant

generated energy is supplied to dc bus bar. The generator of wind turbine is a three-phase permanent magnet synchronous generator (PMSG) that generates 2 kW peak power. The solar array consists of eight solar panels that are connected in series and parallel. The dc–dc converter and ac–dc rectifier devices are used with maximum power point tracking (MPPT) features [8]. The dc bus voltage is fixed at 96 V where it is converted to ac by a single-phase grid-tied inverter. The remote monitoring system is implemented with several sensors instantly acquiring the voltage and current data. The communication infrastructure is based on PIC microcontroller where the data are inherited over analog-to-digital converter (ADC) ports and transmitted to computer over USB port. The generated and stored energy is primarily used to meet the requirement of a microprocessor laboratory in Hacı Bektas Veli Vocational High School and is supplied to the utility grid in the left periods.

2 Implemented Hybrid Plant

The wind turbines at lower power rates are mostly manufactured with three-phase PMSGs in order to decrease cost. This turbine types are controlled with a full-scale power controller that contains a rectifier and inverter. The wind turbine used in the installation of hybrid plant is selected with a simple configuration of blades and rotor. The power electronics are added externally. The converter devices of the turbine are preferred to be used as a compact box of rectifier and dc–dc converter itself. The conditioned dc power is supplied to dc bus bar as seen in Fig. 1. A dc–dc converter with MPPT feature manages the solar energy conversion part of the plant. The battery bank consists of eight 12-V/100Ah gel batteries that are connected in series. The remote monitoring infrastructure is based on voltage and current sensor located at the generation sites of solar and wind energy converters. The voltage and current sensing circuits are located at the RESs of hybrid plant and the measured data are transmitted to computer by a microprocessor. The installation levels of wind turbine are shown in Fig. 2a–d where the mechanical and electrical requirements are completed.

The wind turbine has several properties such as 3.6 m rotor diameter and 9 m hub height. The high-speed braking can be performed with electro-mechanic brake and dump load methods. The rated power speed of turbine is 3 m/s, while the cutoff speed is 20 m/s. The turbine generates ac output voltage up to 165 V at rated wind speeds. The solar panel array that is seen on the upper right-hand side of Fig. 2e is installed in parallel connection of four series solar panels. The output peak ratings of solar array is arranged to obtain 110 V and 5.8 A. The output power of solar array is connected to dc bus bar over dc–dc converter and is coupled to the output power of wind turbine. The output of dc bus bar is conditioned in order to supply several output voltages to be used in the laboratory. There is an output line supplied to adjustable switch-mode power supply (SMPS) models implemented by using LM327. The adjustable dc line of the laboratory is able to provide supply output



Fig. 2 Installation of hybrid renewable plant, **a** base concrete of WT, **b** tower connection, **c** assembling of blades, **d** building-up the turbine, **e** completed installation of plant

voltage up to 30 V and 5 A for each node. On the other hand, there is another line installed for the ac power supply in the laboratory where the output voltage supplied by hybrid plant is 220 V/50 Hz.

The integration of the completed hybrid plant to the laboratory is seen in Fig. 3. The renewable grid is constituted as an additional energy line and is connected to the utility grid over meter and controller box. The SMPS connection terminals are located at each training desk in the additional conduit. The energy control system (ECS) that is seen on the right-hand side of Fig. 3 contains the converter and inverter circuits used to energy conversion processes. The inside of the ECS is shown in Fig. 4a where the batteries are placed on the lower shelves with their connections. Figure 4b illustrates the converters that are used to stabilize the dc bus voltages with MOSFETs.

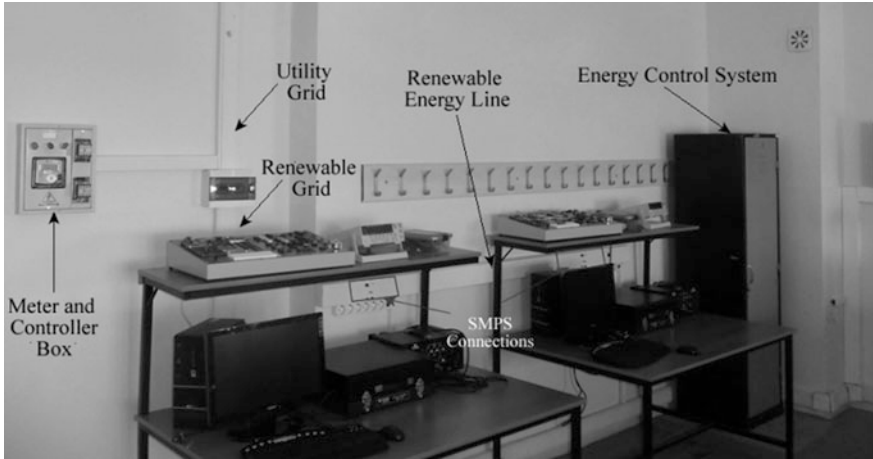


Fig. 3 Integration to the laboratory



Fig. 4 Energy control system and components, a the cabinet of batteries and converters, b converters, c inverter and controller, d SMPS assembly located in training desks

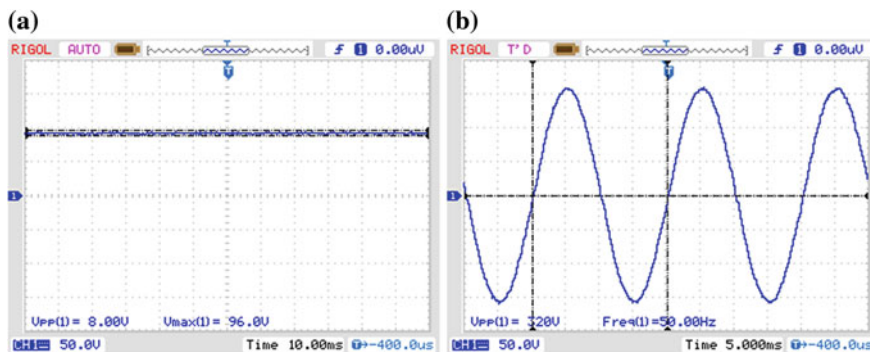


Fig. 5 Output voltages, **a** the dc line voltage of batteries, 96 V **b** inverter output voltage, 220 V_{rms} at 50 Hz line frequency

The inverter built with insulated gate bipolar transistor (IGBT) is seen in Fig. 4c that converts 96 V_{dc} voltage to 220 V_{ac} . The switching devices are controlled by using a sinusoidal pulse width modulation (SPWM) algorithm that is developed by author and introduced in detail in [5]. The algorithm is based on eliminating the side band harmonics besides the main harmonic orders as 3rd, 5th, 7th, etc. The SMPS circuits placed in the conduit is depicted in Fig. 4d. where adjusting potentiometer and fuse of the SMPS are fixed on the user side of conduit. The measurement results of the output voltages are shown in Fig. 5 as battery voltage and inverter output voltage.

3 Implementation of Remote Monitoring System

The remote monitoring system that is intended to be a key contribution of this study is based on software that is coded by using C# software development kit. Although many of the researchers cannot comprehend this requirement, the remote monitoring and observing infrastructures are well known by the researchers of power electronics and energy areas. The proposed monitoring system completely provides novelty to the implemented renewable energy systems. The user infrastructure runs a database file stored in the hard disk of the computer. The data acquisition process that builds the data log of the generated voltage and drawn current of hybrid energy plant is managed out by several electronics circuits introduced in this section. The first component located at the background of monitoring system is current and voltage sensing circuits that are illustrated in Figs. 6 and 7, respectively.

The current sensing circuit of solar array is similar to that of wind turbine where rectifier circuit is not required. Furthermore, the voltage sensing board is implemented in two ways that one contains hall-effect voltage sensors and other is with a transformer. The measured current and voltage data of hybrid plant are calibrated

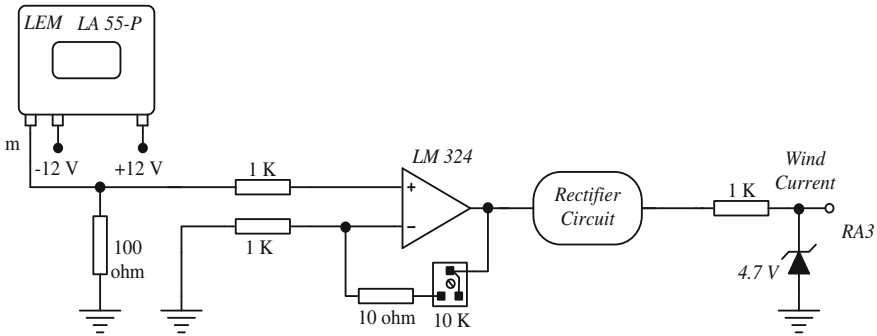


Fig. 6 Current sensing circuit of WT

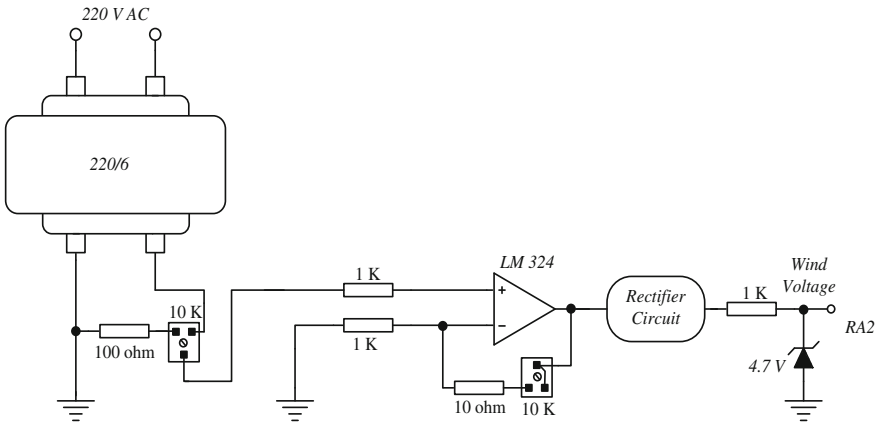


Fig. 7 Voltage sensing circuit of WT

over a card that is intended to serve as a buffer between measurement and microprocessor units. The current sensor is LA55-P of LEM that has a conversion ratio at 1/1000 [6–8]. The outputs of calibration board are supplied to ADC ports of microprocessor at a conditioned maximum value of 4.7 V that is limited to protect the ports.

The flowchart of the software run on microprocessor is illustrated in Fig. 8. It is based on the communication through the ADC to USB port where the data are processed in the required format of computer. The 18F4450 microcontroller is designed as a USB microcontroller with nanowatt technology.

Therefore, PIC18FX455/X550 device family brings a high-speed and low-speed compatible USB serial interface engine (SIE) that allows fast communication together with any USB host and the PIC® microcontroller. Besides being compatible to USB2.0 protocol, 18F4450 MCU provides 1.5 Mb/s data communication speed in low-speed mode and 12 Mb/s speed in full-speed operation mode.

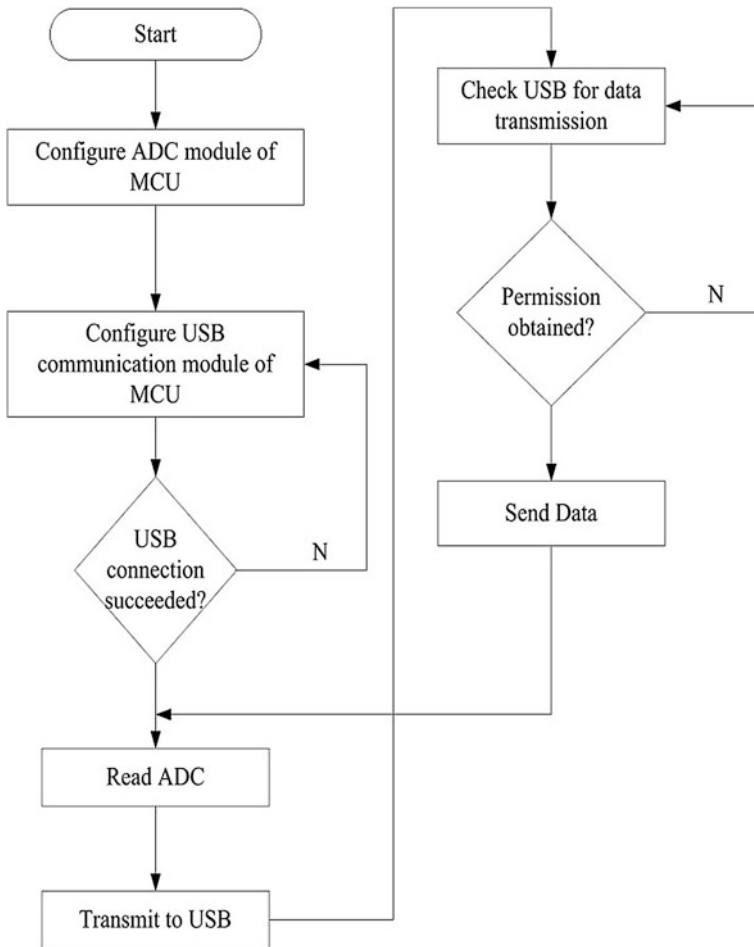


Fig. 8 The flowchart of microprocessor

There are 22 separate registers that are dedicated to USB Control Register (UCON), USB Configuration Register (UCFG), USB Transfer Status Register (USTAT) to control USB communications [8, 9]. Figure 9 illustrates the hardware of the monitoring system with their connections. The measured and processed data are transmitted to the microprocessor and are evaluated to communicate over USB.

The sensed and conditioned data are processed and are transmitted by the microcontroller to the computer. The USB controller function of the implemented interface writes the inherited data to a database (DB) file in each sensing iteration. Processor of the computer reads the written dataset of DB line by line in the second part of monitoring process. The obtained dataset lines are synchronously written in the related textboxes to inform user over interface as seen in Fig. 10. The user interface is arranged with graphs dedicated to measured values of solar array on the

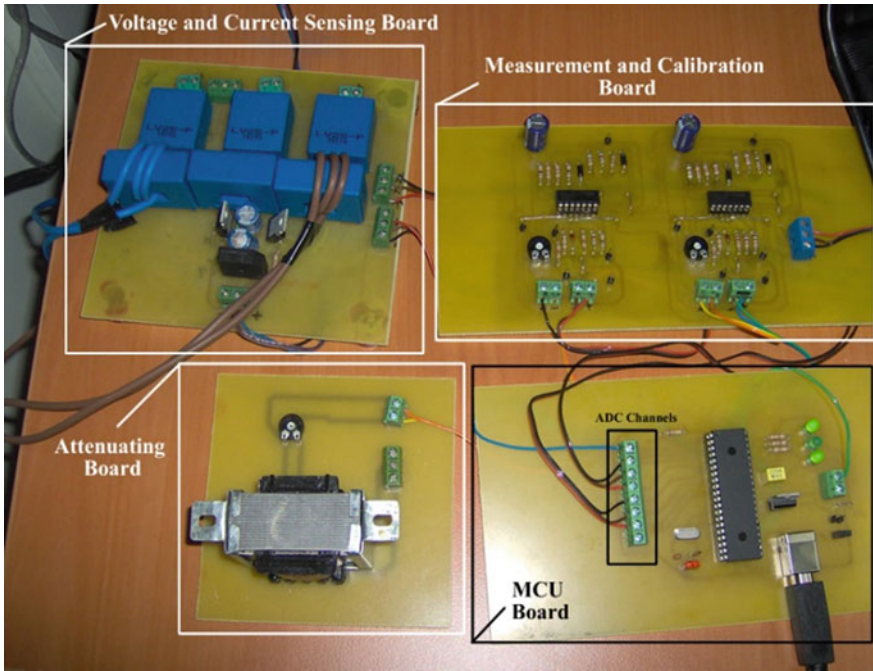


Fig. 9 Hardware of the monitoring system

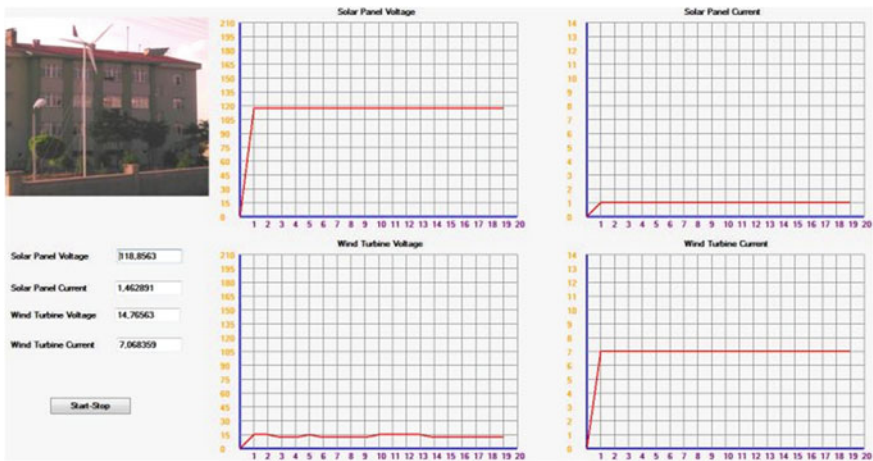


Fig. 10 User interface of monitoring tool

upper and of the wind turbine on the lower side. The experimental studies verify that the microprocessor operates the data transmission in a fast and reliable medium due to the software developed in C-based software development kit.

The time axes of the curves seen on Fig. 10 are arranged in terms of minutes where the drawn data are obtained from database. The curves illustrated in the upper line belong to solar panel while the lower curves indicate the voltage and current of wind turbine. The measured output voltage of solar array is 115.85 V and output current is 1.432 A at the last measurement point as it can be also seen on the textbox of interface on the left-hand side. On the other hand, the last measured output voltage and current of wind turbine are 14.76 V and 7.06 A at the last measurement point. The measured values are depicted in the textboxes instantly.

4 Conclusions

This study is intended to introduce a hybrid renewable energy plant installed in a vocational high school to generate the required energy of the microprocessor laboratory. The wind turbine and solar panels are coupled on a dc bus bar to integrate renewable energy sources together. The installed plant serves as a training tool for energy departments of the vocational school besides its energy generation duty. The converters and inverters are designed to supply several voltages at the desired rates and waveforms. The energy conversion devices are controlled with SPWM modulation algorithm that is improved and introduced in published articles by author where further readings can be seen in [5, 10, 11]. The remote monitoring feature that is the contribution of this study is added to the plant by the designed data acquisition and communication infrastructure. The measurement device improved provides to observe the generated energy of the renewables instantly. Therefore, the data are managed and is processed by using USB2.0 protocol that allows to transmission at 480 Mbps. The MCU board supports the energy plant with computerized measurement and monitoring features.

The implemented plant and its components are assumed as a microgrid application with its smart grid background itself. The forthcoming improvements on the system are planned to perform smart grid communication over power line.

Acknowledgments Installation of hybrid renewable plant is funded by Scientific Research Division (NEUBAP) of Nevsehir University with ref. No. 2012/13. Ersan Kabalci acknowledges to NEUBAP for the support in this study.

References

1. Kirubakaran K, Jain S, Nema RK. DSP-controlled power electronic interface for fuel-cell-based distributed generation. *IEEE Trans Power Electron.* 2011;26:3853–64.
2. Nissen MB. High performance development as distributed generation. *IEEE Potentials.* 2009;28:25–31.
3. Senjyu T, Miyazato Y, Yona A, Urasaki N, Funabashi T. Optimal distribution voltage control and coordination with distributed generation. *IEEE Trans Power Delivery.* 2008;23:1236–42.

4. Cui J, Li K, Sun Y, Zou Z, Ma Y. Distributed energy storage system in wind power generation. In: 2011 4th International conference on electric utility deregulation and restructuring and power technologies (DRPT); 2011. p. 1535–1540.
5. Çolak I, Kabalcı E. Practical implementation of a digital signal processor controlled multilevel inverter with low total harmonic distortion for motor drive applications. *J Power Sources*. 2011;196:7585–93.
6. Semikron Inc., Current Transducer LA 55-P. http://www.semikron.com/products/data/current_assets/LA_55_P_90_13_25_000_0_13950120.pdf. Accessed 24 Dec 2012.
7. Kabalcı E, Kabalcı Y. Multi-channel power line communication system design for hybrid renewables. In: 4th International conference on power engineering, energy and electrical drives; 2013. p. 563–8.
8. Kabalcı E, Gorgun A, Kabalcı Y. Design and implementation of a renewable energy monitoring system. In: 4th International conference on power engineering, energy and electrical drives; 2013. p. 1071–5.
9. Microchip Technology Inc., PIC18F2455/2550/4455/4550 Data Sheet, 2006. <http://ww1.microchip.com/downloads/en/devicedoc/39632c.pdf>. Accessed 24 Dec 2012.
10. Colak I, Kabalcı E. Developing a novel sinusoidal pulse width modulation (SPWM) technique to eliminate side band harmonics. *Int J Electr Power Energy Syst*. 2014;44:861–71.
11. Colak I, Kabalcı E. Implementation of energy efficient inverter for renewable energy sources. *Electric Power Comp Syst*. 2014;41:31–46.

Artificial Neural Network Control Strategy for Multi-converter Unified Power Quality Conditioner for Power Quality Improvements in 3-Feeder System

Karthikrajan Senthilnathan and K. Iyswarya Annapoorani

Abstract This paper presents about the power quality improvements of the 3-feeder system using the multi-converter unified power quality conditioner (MC-UPQC) based on voltage source converters in which the DC link is common. The control strategy for the converter is based on the artificial neural network (ANN) by using the Levenberg–Marquardt back-propagation algorithm for mitigation of the sag, swell, and unbalance in the system and maintaining the system voltage profile. The pulse generation is based on the hysteresis loop by comparing the error signals. The performance analysis of the MC-UPQC using neural network as control strategy is verified using the MATLAB/SIMULINK.

Keywords Artificial neural network · Unified power quality conditioner · Voltage source converter

1 Introduction

The usage of converters is used in wide range of applications in day-to-day life. The disturbance caused because of the converters is also increased rapidly and which cause major issues in the distribution system. The power quality [1–5] issues such as sag [6], swell, and unbalance [7] are the major problems in the distribution system. These problems are mitigated by using the active power filters in the configuration of shunt and series connections [8] D-STATCOM, DVR, UPQC [9–11] are the mostly used custom power devices [12–14] for the mitigation of the power quality problems. The control strategies [15] for those are done mostly by the

K. Senthilnathan (✉) · K. Iyswarya Annapoorani
VIT University, Chennai, India
e-mail: karthikrajan.s2014phd1147@vit.ac.in

K. Iyswarya Annapoorani
e-mail: iyswarya.annapoorani@vit.ac.in

conventional methods like instantaneous power theorem. The influences of artificial intelligence techniques such as neural network and fuzzy logic are more popular in current scenario.

The control techniques used for the custom power device are the major portions of the device that only finalize the performance of that device. The artificial neural network control strategy has more significant in the power converter applications. To maintain the stability of the controllers, ANN [16] has the fast dynamic response and which gives the solution for the difficult controlling problems in the wide operating range. Instead of conventional controllers, ANN used here is to mitigate the power quality problems of the multi-feeder system. ANN controller is trained offline using Levenberg–Marquardt back-propagation algorithm in MATLAB simulation, and the results for the multi-converter unified power quality conditioner are verified.

2 Multi-converter Unified Power Quality Conditioner

The multi-converter unified power quality conditioner for 3-feeder system in Fig. 1 has the common DC link and in feeder 1, the both shunt and series converters are connected. In the adjacent feeders 2 and 3, series converter alone is connected for the mitigation of the power quality problems. Voltage source converters (VSC) [17] were employed in the design of MC-UPQC, and the DC link between the converters is common.

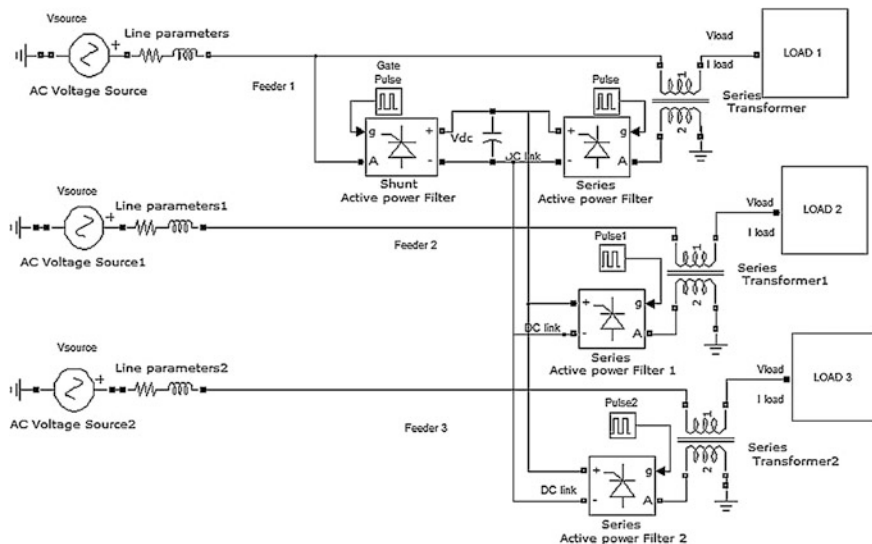


Fig. 1 Single-line diagram of MC-UPQC

The capacitor is connected in the DC link for the real power injection to mitigate the power quality problems. Figure 1 shows the single-line diagram of MC-UPQC for the 3-feeder system. The MC-UPQC design configuration is based on the left shunt in order to reduce the tracking problem, which occurs in right shunt configuration.

3 Control Strategy Based on Artificial Neural Network

The artificial neural network (ANN) [16] is the system which contains the number of artificial neurons which connected as a network with set of weights. The neuron is the processing element which gets the inputs and processes them for singular value function (activation function). The two main aspects in the ANN are that to collect the data by using the learning process and to store that collected data by using the interneuron connection strength.

The ANN is trained offline using the Levenberg–Marquardt back-propagation algorithm. It is a nonlinear optimization algorithm by using the second-order derivatives. It requires more memory for the processing, so it functions as the square of the number of weights for error calculation. It mostly works with the summed error functions so widely used for estimation (regression) applications.

The ANN is trained by offline and the number of hidden layers used here is 3 and the training algorithm used is Levenberg–Marquardt (trainlm). The performance is measured by mean-squared error (MSE) as shown in Fig. 2. The training procedure for the Levenberg–Marquardt back-propagation algorithm is as follows.

- Step 1: Initialize the weights for the network.
- Step 2: Each pattern should be present to the input of the network.

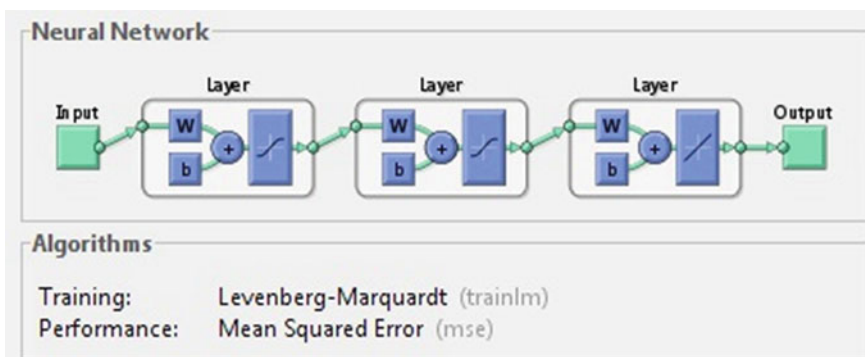


Fig. 2 Artificial neural network offline training

- Step 3: Output pattern is generated by propagating the data forward to the network and calculate the error between the target output and actual output.
- Step 4: If more patterns present in the training set, go to Step 2.
- Step 5: Calculate the error vector (e) between the target and actual output for all patterns presented by the mean-squared error.
- Step 6: Compute the Jacobian matrix (J) from the first-order partial derivatives.
- Step 7: Compute the weight update of the network.
- Step 8: Recalculate the mean-squared errors; if any new error is lower, update the weight and go to Step 9. If the new error is higher, go to Step 7.
- Step 9: If the value of gradient (g) is less than the desired amount, stop the process. If high, start from Step 1.

The product of Jacobian (J) containing first-order derivatives with error vector (e) is the gradient (g) which results in the minimized errors.

$$g = J^T e$$

The performance of the ANN training is shown in Fig. 3 which shows that the error 10^2 is reduced to 10^{-6} and achieved the best training performance at 70 epochs. The regression plot in Fig. 4 shows the training of target with output. Since $R = 1$, better training performance is achieved.

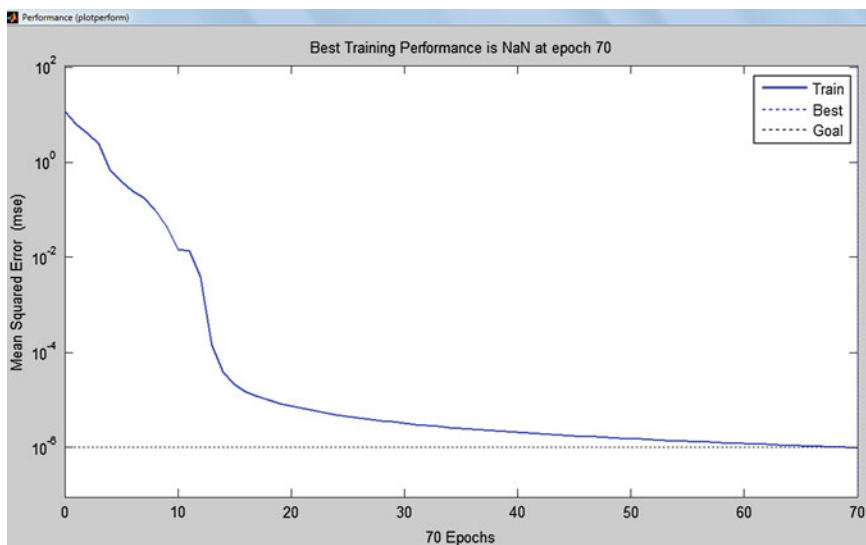


Fig. 3 Training performance plot

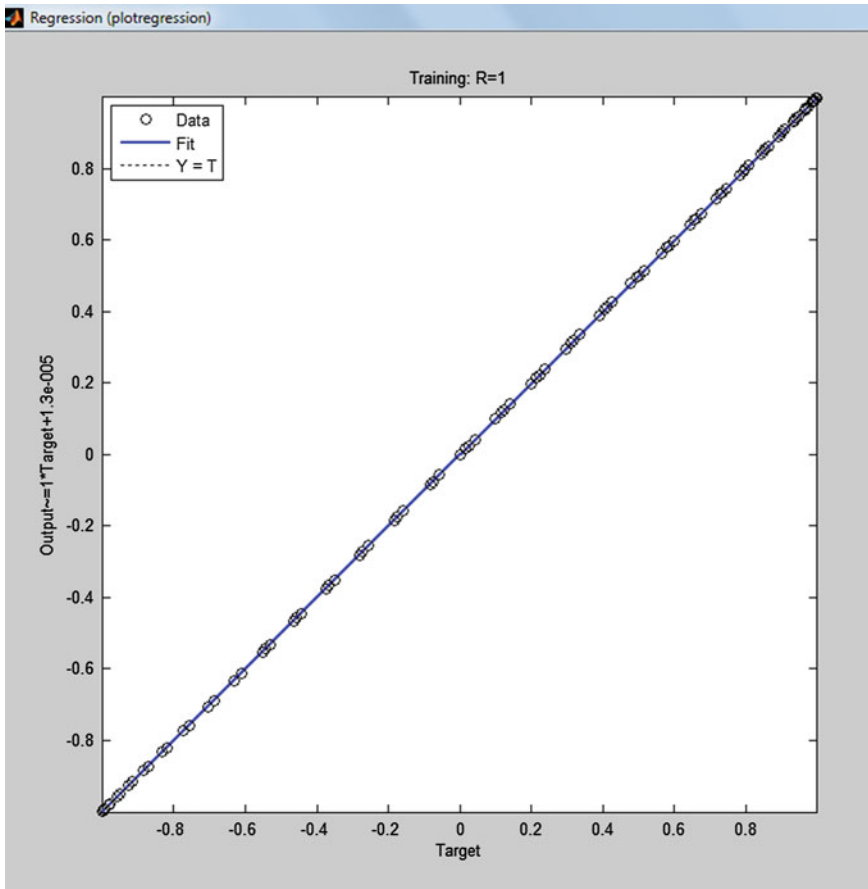


Fig. 4 Training regression plot

4 Simulation and Results of MC-UPQC with Artificial Neural Network

The simulation of multi-converter unified power quality conditioner using the control strategy as ANN Levenberg–Marquardt back-propagation algorithm is implemented for the 3Φ 415-V distribution system which is calculated in per unit system. The MC-UPQC connected with the 3-feeder system in which the feeder 1 experiences the power quality issue of voltage sag, so the voltage profile is reduced to 0.8 PU for certain period of time. The power quality issue in feeder 2 is voltage swell; hence, the voltage profile is increased to 1.2 PU. Feeder 3 experiences the problem of voltage unbalance at one phase.

The power quality issues occurred in all 3 feeders is compensated by the MC-UPQC configuration which shares the common DC link and the compensation is done by injecting the required voltage to the system. The MC-UPQC 3-feeder system was designed as shown in Fig. 1, and simulation results shown in Fig. 5 are before and after compensation of the power quality issues.

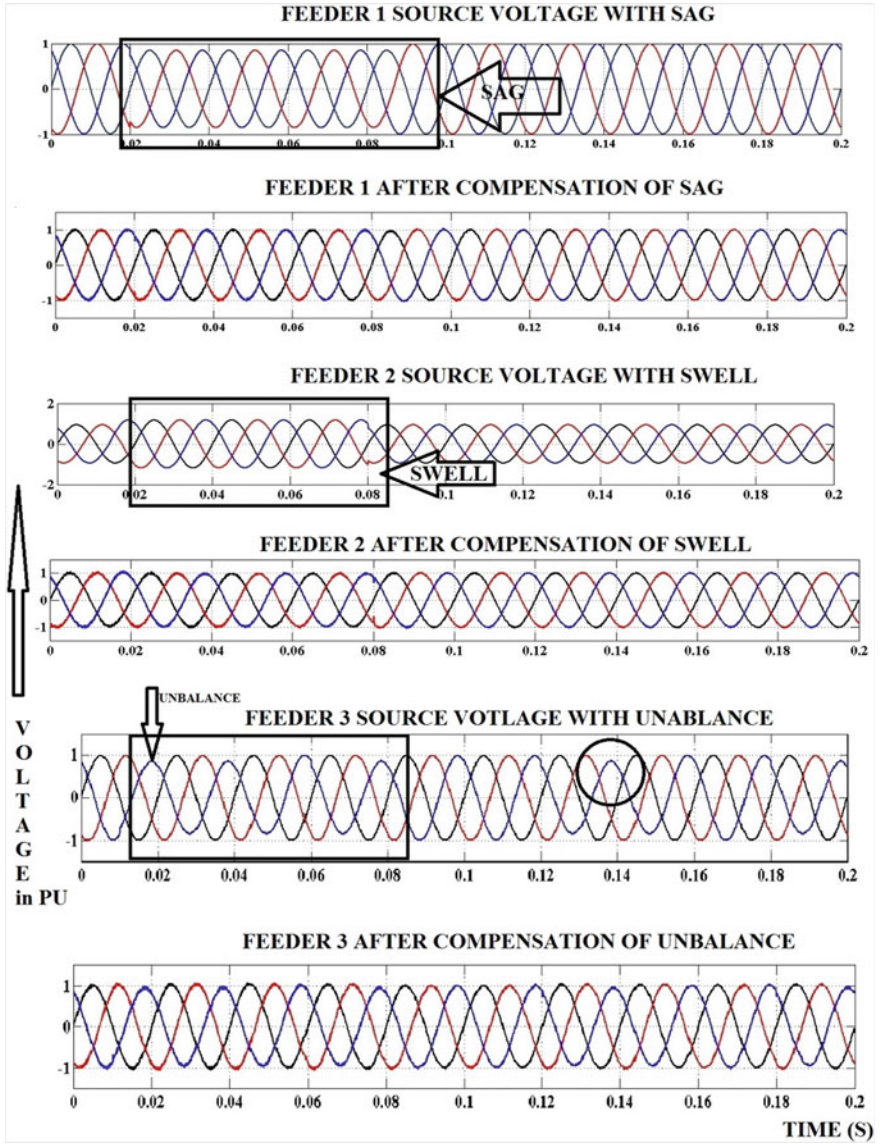


Fig. 5 Simulation results of MC-UPQC in 3-feeder system

5 Conclusion

The performance analysis of the artificial neural network control strategy for the multi-converter unified power quality conditioner is done using the MATLAB/SIMULINK. The results obtained for the 3-feeder system shows that the MC-UPQC designed using the ANN has ability to compensate the sag, swell, and unbalance simultaneously in the 3-feeder system. The design of MC-UPQC also analyzed for the compatibility of supplying the real power in common DC link for the mitigation of the power quality problems in the 3-feeder system.

References

1. Alexander K, Thompson MT. Power quality in electrical systems. New York: McGraw-Hill; 2007.
2. Arindam G, Gerard L. Power quality enhancement using custom power devices. London: Kluwer Academic Publishers; 2002.
3. Hingorani H. Introducing custom power. *IEEE Spectr.* 1995;32(6):41–8.
4. Padiyar KR. Facts controllers in power transmission and distribution. New Age International Publishers; 2007.
5. Sankaran C. Power quality. New York: CRC Press LLC; 2002.
6. Basu M, Das SP, Dubey GK. Performance study of UPQC-Q for load compensation and voltage sag mitigation. In: Conference of the Industrial Electronics Society, vol 1 2002, p. 698–703.
7. Kesler M, Ozdemir E. A novel control method for unified power quality conditioner (UPQC) under non-ideal mains voltage and unbalanced load conditions. In: 25th Annual IEEE Applied Power Electronics Conference and Exposition (APEC), 2010, p. 374–9, 2010.
8. Dugan RC, McGranaghan MF, Santoso S, WayneBeaty H. Electrical power systems quality, 2nd edn. New York: McGraw-Hill; 2004.
9. Gu J, Xu D, Liu H, Gong M. Unified power quality conditioner (UPQC): the principle, control and application. In: Conference on Power Conversion, 2002, p. 80–5.
10. Fujita H, Akagi H. The unified power quality conditioner: the integration of series- and shunt-active filters. In: *IEEE Transactions on Power Electronics*, 1998, p. 315–322.
11. Rajasekaran D, Dash SS, Senthilnathan K, Mayilvaganan AB, Chinnamuthu S. Power quality improvement by unified power quality conditioner based on CSC topology using synchronous reference frame theory. *Sci World J* 2014;2014(391975):7. doi:[10.1155/2014/391975](https://doi.org/10.1155/2014/391975).
12. Ghosh A, Amit Kumar J. A unified power quality conditioner for voltage regulation of critical load bus. In: *IEEE Conference on Power Delivery Transactions*, vol 22, 2007, p. 364–72.
13. Devaraju T, Veera Reddy VC, Vijay Kumar M. Modeling and simulation of custom power devices to mitigate power quality problems. *Int J Eng Sci Technol.* 2012;26:1880–5.
14. Anaya-Lara O, Acha E. Modeling and analysis of Cu tom power systems by PSCAD/EMTDC. *IEEE Trans Power Delivery* 2002;17:266–272.
15. Le J, Xie Y, Zhi Z, Lin C. A nonlinear control strategy for (UPQC). In: *International Conference on Electrical Machines*, 2008, p. 2067–2070.
16. Rama Rao RVD, Subhransu SD. Power quality enhancement by unified power quality conditioner using ANN with hysteresis control. *Int J Comput Appl.* 2010; 6(0975–8887):9–15.
17. Dixon JW, Venegas G, Mořan LA. A series active power filter based on a sinusoidal current-controlled voltage-source inverter. *IEEE Trans Industr Electron.* 1997;44(5):612–20.

Investigations on Multidimensional Maximum Power Point Tracking in Partially Shaded Photovoltaic Arrays with PSO and DE Algorithms

R. Sridhar, S. Jeevananthan and B. Sai Pranhita

Abstract This paper emphasizes on a multidimensional search-driven MPPT aided by particle swarm optimization (PSO) and differential evolutionary algorithm (DEA). Maximum power point trackers are crucial components in PV panels to make operate the PV panel with its maximum efficiency. Partially shaded conditions are quite common in PV panels which in turn hinder the performance of PV system. Further, the partially shaded PV panels exhibit multipower peaks which cannot be catered wisely by the conventional MPPT techniques. The entrenched evolutionary algorithms such as PSO and DEA on the hand grasp the global power peak. In this work, a multidimensional search technique embedded with DC–DC converter is proposed. By this proposed technique, during shaded conditions each panel peak is grasped rather than the cumulative GMPP. Therefore, there is an appreciable increase in extracted power. A comparison in simulation results shows the performance of PSO and DEA-aided Multidimensional MPPT.

Keywords Global maximum power point (GMPP) · Maximum power point tracking (MPPT) · Evolutionary algorithms (EA) · Particle swarm optimization (PSO) · Differential evolutionary algorithm (DEA) etc.

R. Sridhar (✉) · B. Sai Pranhita
SRM University, Kancheepuram, India
e-mail: sridharmanly@gmail.com

B. Sai Pranhita
e-mail: saipranahita178@gmail.com

S. Jeevananthan
Pondicherry Engineering College, Pondicherry, India
e-mail: jeevashree@rediffmail.com

1 Introduction

Though there is a huge encouragement for using PV systems, the technology is crippled by two prime issues. (1) conversion efficiency and (2) economic viability. The conversion efficiency is low and the economic viability is meek [1–3]. In spite of these issues, PV systems have gained substantial importance in today's power industry due to their advantages of being nonpollutant, renewable, and also available freely in nature [4]. Copious papers have been archived in the area of photovoltaic systems signifying its prominence [5]. Partial shading is an unavoidable constraint to be taken into account while investigating the characteristics of PV Arrays. The partial shading can vary based on the environmental conditions, physical structures, and the topological location of the arrays [6]. To obtain maximum efficiency from the PV panels irrespective of the partial shading, presence of a maximum power point tracking (MPPT) control is obligatory. MPPT control forces the system to operate at its maximum power rather than reducing its efficiency over time [7]. Conventional MPPT techniques like perturb and observe (P&O) and incremental conductance (INC) have failed to prove their worth under variations in temperature and irradiance [8]. The advent of soft computing techniques had given a ray of hope to deal with the uncertainty in the atmospheric conditions though they have proven to be less efficient [9, 10]. Evolutionary algorithms such as particle swarm optimization (PSO) and differential evolutionary algorithms (DEA) have proved to be suitable for various nonlinear optimization techniques. Thus, these techniques had been applied for MPPT and have also been efficacious [11–13]. When multiple arrays are present, the MPPT control becomes cumbersome and also costs more due to the complexity in its circuitry. To overcome this, multidimensional PSO and DEA were implemented leading to steep increase in the efficiency and also reduction in the cost and circuitry [14, 15]. Comparisons have been carried out for PSO and DEA embedded for different applications. It has been noticed that DEA proves to be effective during presence of erratically varying conditions [16, 17]. The multidimensional PSO- and DEA-aided MPPT are tested under extensively varying irradiance and temperature conditions to check its mettle in tracking the maximum power.

2 Partially Shaded PV Panels

The PV array possesses nonlinear characteristics which causes a major hindrance in tracking its maximum power. The amount of power extracted from the panel varies in accordance with the temperature and insolation.

To evaluate the performance of the PV Panel under partial shading conditions, the two diode model is taken into consideration. Even under very low irradiance conditions the model provides very efficient and accurate results than a single-diode model. The equivalent circuit of the two diode model is shown in Fig. 1.

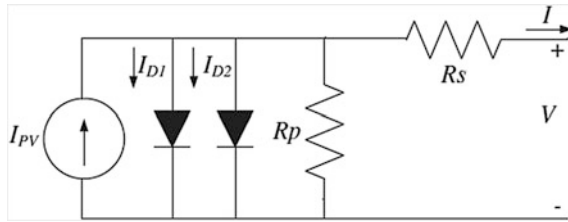


Fig. 1 Equivalent circuit of a two diode model of PV panel

The output current equation of a two diode modeled PV panel is given as

$$I = I_{PV} - I_{D1} - I_{D2} - \left(\frac{V + IR_s}{R_p} \right) \tag{1}$$

where I_{D1} and I_{D2} are the diode currents of the two diodes, respectively, given as

$$I_{D1} = I_{01} \left[\exp \left(\frac{q(V + IR_s)}{R_p} \right) - 1 \right] \tag{2}$$

$$I_{D2} = I_{02} \left[\exp \left(\frac{q(V + IR_s)}{R_p} \right) - 1 \right] \tag{3}$$

I_{01} and I_{02} are the saturation currents of the two diodes, respectively. They can be calculated as

$$I_{01} = I_{02} = \frac{(I_{SC_STC} + K_I \cdot \Delta T)}{\exp \left[\frac{V_{OC_STC} + K_V \cdot \Delta T}{\{(a_1 + a_2)/p\} \cdot V_T} \right] - 1} \tag{4}$$

- a_1 and a_2 are the diode ideality factors
- I_{SC_STC} is the short-circuit current of the cell under standard test conditions
- K_i is the temperature coefficient of current (mA/°C)
- K_v is the temperature coefficient of voltage (mV/°C)
- V_T is the thermal voltage
- V_{OC_STC} is the open circuit voltage of cell under standard test conditions
- $\Delta T = T - T_{STC}$ where; T_{STC} is the temperature at standard test conditions = 273 K.

Due to nonuniform insolation occurring as in Fig. 2, due to clouds, shadowing, and other factors, the PV panel exhibits multiple maxima, i.e., multiple local MPP and one global MPP. Under these conditions, the conventional MPPT controller may track a local MPP rather than tracking the global MPP. The partially shaded PV array and its characteristics with the shading effect in MATLAB/Simulink environment are perceived to be as in Figs. 2, 3 and 4.

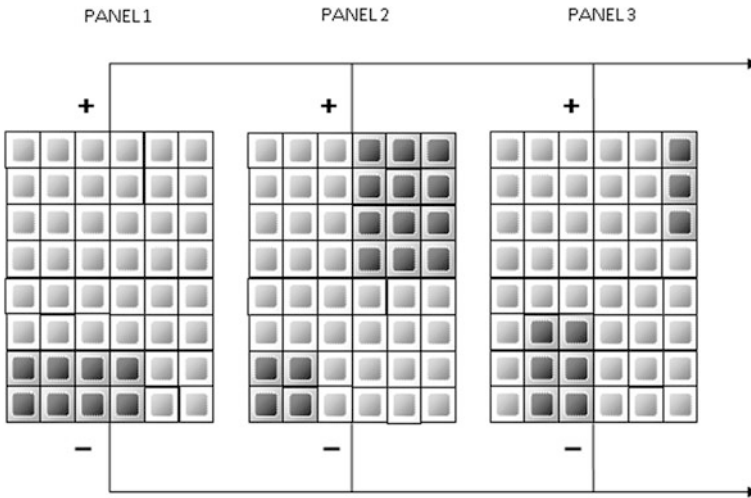


Fig. 2 Partially shaded PV panels

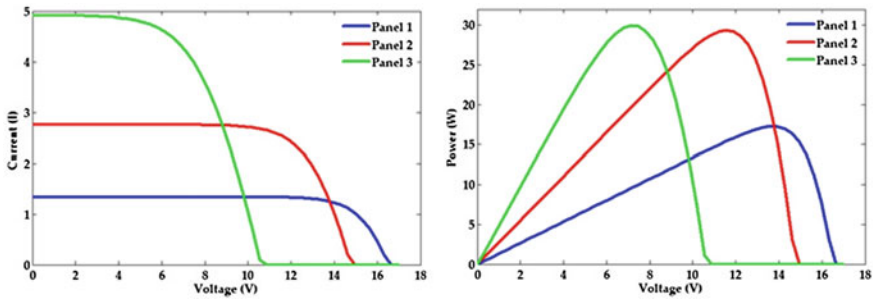


Fig. 3 PV characteristics of the array with partial shading

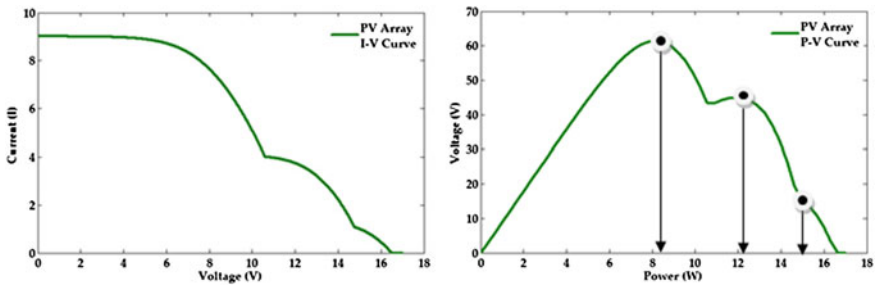


Fig. 4 Resultant PV characteristics of the array with partial shading

The partial shading effects have been realized with the effect of variations in both irradiance and temperature with panel-1 operating at $G = 1000 \text{ W/m}^2$ and $T = 75^\circ \text{C}$, panel-2 operating at $G = 750 \text{ W/m}^2$ and $T = 25^\circ \text{C}$, panel-3 operating at $G = 500 \text{ W/m}^2$ and $T = 0^\circ \text{C}$. The resultant curves after partial shading are shown in Fig. 4. Among the three peaks, one is the global power peak at 62 W and others are local peaks at 43 and 17 W, respectively. They have their operating voltages as 8.1, 12.1, and 15 V, respectively.

3 System Description

3.1 PV Panel Ratings

The system consists of three panels, each having a rating of 40 W. The specifications of each panel are given in Table 1 (Fig. 5).

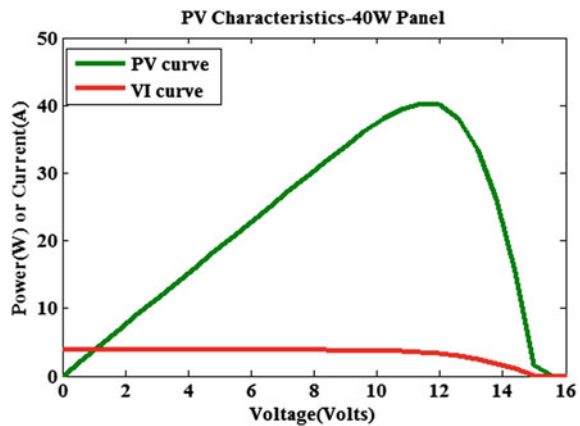
3.2 Block Diagram

See Fig. 6.

Table 1 PV panel specifications

Parameters	Values
Maximum power (P_{max})	40 W
Open circuit voltage (V_{oc})	15.08 V
Short circuit current (I_{sc})	3.8 A
Voltage at maximum power (V_{mp})	11.4 V
Current at maximum power (I_{mp})	3.54 A
Number of cells in series (N_s)	36

Fig. 5 PV characteristics of 40 W panel



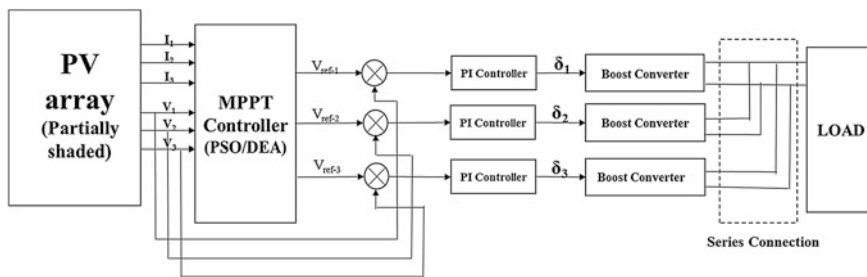


Fig. 6 Multidimensional MPPT implementation

3.3 PI Controller Values

4 PSO- and DEA-Aided MPPT for Partially Shaded PV Arrays

In this paper, a comparative study of PSO and DEA to track the maximum power of the PV array under rapidly fluctuating irradiance and temperature conditions is performed. The power of the PV array varies with respect to the temperature and irradiance variations which are responsible for the proportional variation in the voltage and current outputs of the array. In both the PSO & DEA algorithms, the population that is initialized is the operating voltage of the panel which is based on the objective function of the array is calculated. The output of the MPPT controller is the voltage at which the maximum power is obtained [11–15].

Both the optimization techniques initialize the open circuit voltage as population and the voltage at which the maximum power is obtained is optimized. The parameters for PSO and DEA are given in Tables 3 and 4.

The output of the MPPT controller outputs the reference voltage, i.e., voltage at which maximum power is obtained. The reference voltage is compared with the voltage of the PV array to produce an error signal. The error signal is processed through a PI controller which sets the duty cycle of the boost converter. Thus, the maximum power is transferred to the load. The values considered for tuning the PI controller are given in Table 2.

Table 2 Parameters for Tuning the PI Controller

Parameters	Values
K_p	0.4
K_i	500

4.1 Particle Swarm Optimization-Aided MPPT

The methodology of the particle swarm optimization-aided MPPT is illustrated in Fig. 7.

4.2 Differential Evolutionary Algorithm-Aided MPPT

The methodology of the differential evolutionary algorithm-aided MPPT is illustrated in Fig. 8.

Fig. 7 Flowchart for multidimensional PSO-aided MPPT

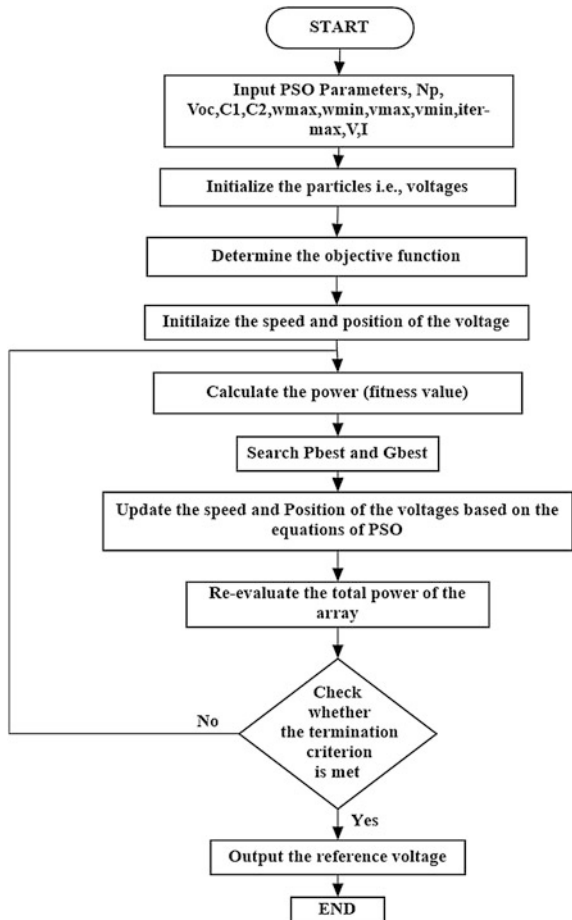
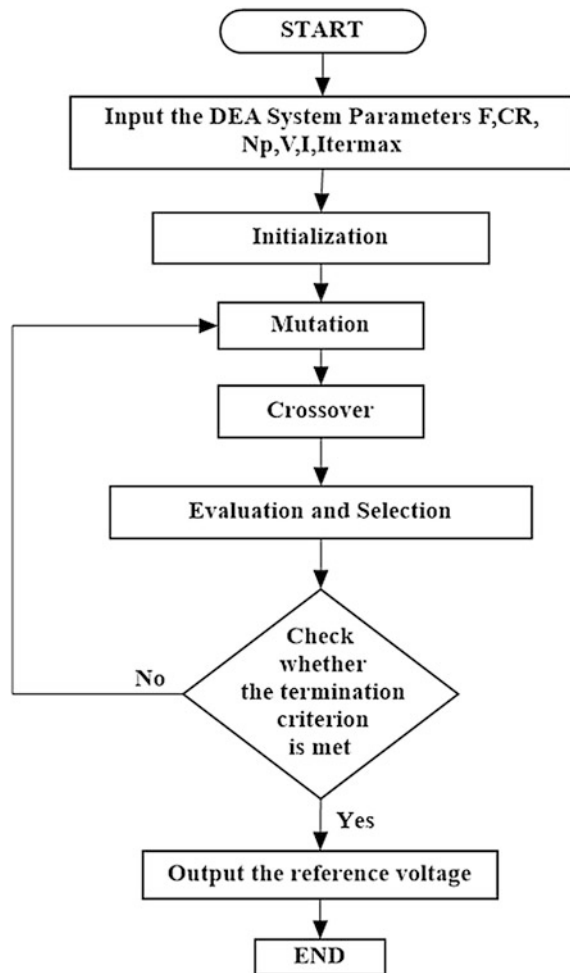


Fig. 8 Flowchart for multidimensional DEA-aided MPPT



5 Multidimensional MPPT Control

Modular connections need to be used to increase the overall efficiency of the PV array even under partial shading conditions. Considering a system with multiple PV panels, nonuniform insolation of the panels raises difficulty in finding the global MPP. When one panel is fully illuminated and another panel is partially shaded, the current in the panel reduces leading to the reduction on the power produced. As the number of panels increases, the complexity in implementing the MPPT controllers becomes more, and also the increase in the number of maxima makes it difficult for the array to operate at the global peak. It is also pragmatic that each panel possesses its own peak even under shaded conditions. But by employing the unidimensional

MPPT control, only the peak power of the panel receiving maximum insolation is obtained. Whereas, the multidimensional technique of control extracts the maximum power of the array by making each panel operate at its global maxima thereby, leading to a significant increase the overall power extracted. This mode of control captures an edge over the unidimensional control, by utilizing only a single pair of voltage and current sensors thereby reducing the complexity, area occupied and overall cost of the system.

6 Results and Discussions

The results are plotted in the MATLAB/Simulink environment. PV modules of 40 W are used for multidimensional simulation. The modules are formed into an array to give net output of 120 W, i.e., 3×1 array is employed. The buck-boost converter is mathematically modeled for simplicity and flexibility. The PSO and DEA parameters utilized for control are shown in Tables 3 and 4. To assess the performance of the methods, the system is tested with different values of irradiance and temperature. Very large variations in temperature and irradiance are set to test the proficiency of the multidimensional PSO and DE algorithms. The algorithms are tested under several test conditions containing extensive variations in irradiation and temperature to prove its efficacy. The test conditions employed are shown in Table 5. The output results were tested in terms of the following three parameters: (1) output power, (2) reference voltage, and (3) number of iterations to reach the optimum value. The obtained results are noted in Tables 6, 7, and 8, respectively.

The test conditions 1–5 show moderate shading of PV modules where utmost two panels are shaded moderately and one panel is completely unshaded. They

Table 3 Parameters of PSO

Parameters	Value
N_p	5
V_{max}	+2
V_{min}	-2
c_1	2
c_2	2
ω_{max}	0.9
ω_{min}	0.4
Iter-max	100

Table 4 Parameters of DEA

Parameters	Value
N_p	5
F	0.8
CR	0.5
G	200

Table 5 Conditions for multidimensional PSO and DEA simulation

Test condition		Panel-1	Panel-2	Panel-3
1	$G(W/m^2)$	1000	750	1000
	$T(^{\circ}C)$	25	50	75
2	$G(W/m^2)$	500	750	1000
	$T(^{\circ}C)$	0	25	50
3	$G(W/m^2)$	500	750	1000
	$T(^{\circ}C)$	0	25	75
4	$G(W/m^2)$	1000	750	500
	$T(^{\circ}C)$	25	25	25
5	$G(W/m^2)$	500	750	1000
	$T(^{\circ}C)$	25	50	75
6	$G(W/m^2)$	1000	500	250
	$T(^{\circ}C)$	0	25	75
7	$G(W/m^2)$	250	500	500
	$T(^{\circ}C)$	25	50	25
8	$G(W/m^2)$	100	250	100
	$T(^{\circ}C)$	25	0	75
9	$G(W/m^2)$	100	1000	100
	$T(^{\circ}C)$	25	75	50
10	$G(W/m^2)$	500	100	750
	$T(^{\circ}C)$	25	75	50

Table 6 Comparison of multidimensional PSO and DEA in terms of output power

Test condition	Output power through PSO(W)	Output power through DEA(W)
1	98.29	98.32
2	83.07	83.10
3	77.08	77.10
4	89.97	89.99
5	77.96	77.98
6	73.91	73.92
7	47.47	49.32
8	35.33	35.34
9	39.55	39.55
10	51.47	56.33

show large variations in temperature rather than irradiance. Test conditions 6, 8, and 9 demonstrate severe shading of the panels where the modules receive only 100 and 250 W/m^2 of irradiance. The test conditions 7 and 10 show complete shading of all three panels and wide variations in their temperature. Large variations in temperature of three modules located at the same place are not practically feasible, but the values have been considered to evaluate the performance of the algorithms with fluctuating conditions. The test of convergence is done based on the number of

Table 7 Comparison of multidimensional PSO and DEA in terms of output reference voltage

Test condition	Reference voltage through PSO(V)	Reference voltage through DEA(V)
1	28.16	28.14
2	34.65	34.64
3	32.52	32.51
4	34.65	34.64
5	28.04	28.03
6	29.95	32.36
7	30.03	31.89
8	22.82	22.59
9	23.19	23.55
10	26.93	27.63

Table 8 Comparison of multidimensional PSO and DEA in terms of iterations

Test condition	Number of iterations in PSO	Number of iterations in DEA
1	17	23
2	20	25
3	16	21
4	10	14
5	16	20
6	11	10
7	20	19
8	22	18
9	19	15
10	29	23

iterations rather than the time because, the time might vary based on the processor being used for testing.

6.1 Test Conditions 1–5

Under moderate shading conditions, i.e., under irradiance from 1000 to 500 W/m², DEA provides more efficiency in tracking the power than PSO. PSO Converges faster than DEA. These results can be studied in Tables 3, 4, and 5.

6.2 Test Conditions 6, 8, and 9

Providing severe shading to the PV panels, decreases the efficiency of the total array. When only 100 and 250 W/m² of irradiance is provided to the array,

the amount of power output reduces considerably. Even under these conditions, DEA outputs more power than PSO. The reference voltage that is set by the DEA–MPPT controller is more accurate and thus it converges faster to the maximum value. Thus, even during fluctuating environmental conditions, DEA provides higher efficiency.

6.3 Test Conditions 7 and 10

When all the three panels are shaded, it can be observed that PSO is not capable of tracking the maximum power. From Tables 6 and 7 it can be seen that there is a considerable difference in the maximum power and the reference voltage about 2 W and 3 V, respectively. Under such conditions, DEA tracks the maximum power accurately and also in lesser time.

7 Conclusion

In this paper, a comparative study of two entrenched techniques to find the most optimum solution to an optimization problem in a multidimensional approach is done. Multidimensional PSO and DEA are applied in tracking the GMPP for partial shaded PV Panels. The simulation results show that both the evolutionary algorithms-aided MPPT converge at the maximum power of the individual panels. They outperform the conventional MPPT techniques by converging at the global maxima. It can be noticed that DEA converges faster than PSO under large shaded conditions. DEA algorithm gives better accuracy than PSO in tracking the maximum power even though the irradiation is low. The right MPPT controller can be chosen based on the topological location of the plant and also its rating. Further research can be carried out in this area by modifying the existing algorithms to provide more efficiency or by developing novel algorithms.

References

1. International Energy Agency. Energy for all financing access for the poor world energy outlook; 2011.
2. Kroposki B, Sen PK, Malmedal K. Optimum sizing and placement of distributed and renewable energy sources in electric power distribution systems. *IEEE Trans Ind Appl.* 2013;49(6):2741–52.
3. Singh D, Sharma NK, Sood YR, Jarial RK. Global status of renewable energy and market: future prospectus and target. *IEEE international conference on sustainable energy and intelligent systems (SEISCON)*; 2011. p. 171–6.

4. Luque A, Hegedus S. Handbook of photovoltaic science and engineering. England: Wiley; 2003.
5. Singh GK. Solar power generation by PV (photovoltaic) technology: a review. *Energy*. 2013;53:1–13.
6. Patel H, Agarwal V. MATLAB-based modeling to study the effects of partial shading on PV array characteristics. *IEEE Trans Energy Convers*. 2008;23(1):302–10.
7. Enslin JHR. Maximum power point tracking: a cost saving necessity in solar energy systems. *Ind Electron Soc*. 1990;2:1073–7. IECON '90. 16th Annual Conference of IEEE.
8. Ishaque Kashif, Salam Zainal. A review of maximum power point tracking techniques of PV system for uniform insolation and partial shading condition. *Renew Sustain Energy Rev*. 2013;19:475–88.
9. Xu Y, Chengbi Z. Generalized dynamic fuzzy neural network-based tracking control of PV. Power and energy engineering conference (APPEEC), 2010 Asia-Pacific; 2010. p. 1–4.
10. Ishaque K, Salam Z. A review of maximum power point tracking techniques of PV system for uniform insolation and partial shading condition. *Int J Emerg Trends Electr Electron Instrum Eng*. 2013;19:475–88.
11. Liu YL, Zhou H. MPPT control method of PV system based on PSO. *Comput Eng*. 2010;36:265–7.
12. Ishaque K, Salam Z. A deterministic particle swarm optimization maximum power point tracker for photovoltaic system under partial shading condition. *IEEE Trans Ind Electron*. 2013;60(8):3195–206.
13. Tajuddin MFN, Ayob SM, Salam Z. Tracking of maximum power point in partial shading condition using differential evolution (DE). *Proceedings of 2012 IEEE international conference on power and energy (PECon)*; 2012. p. 384–9.
14. Miyatake M, Veerachary M, Toriumi F, Fujii N, Ko H. Maximum power point tracking of multiple photovoltaic arrays: a PSO approach. *IEEE Trans Aerosp Electron Syst*. 2011;47(1):367–80.
15. Sridhar R, Jeevananthan S, Dash SS, Selvan NT. Unified MPPT controller for partially shaded panels in a photovoltaic array. *Int J Autom Comput*. 2014;11(5):536–42.
16. Bakare GA, Krost G, Venayagamoorthy GK, Aliyu UO. Comparative application of differential evolution and particle swarm techniques to reactive power and voltage control. *International conference on intelligent systems applications to power systems*. ISAP; 2007. p. 1–6.
17. Abdual-Salam ME, Abdul-Kader HM, Abdel-Wahed WF. Comparative study between differential evolution and particle swarm optimization algorithms in training of feed-forward neural network for stock price prediction. *The 7th international conference on informatics and systems (INFOS)*; 2010. p. 1–8.

Study on Effect of Series Compensation on Double-Circuit Transmission Lines

S. Radha Krishna Reddy, J.B.V. Subrahmanyam
and A. Srinivasula Reddy

Abstract This paper presents a study about effect of series compensation on double-circuit transmission lines. It improves power transfer capability of a long distance transmission lines. Series capacitors connected reduce inductive reactance of transmission lines and hence reduce the losses. It controls load flow between parallel circuits and improves dynamic and transient stability. In this paper, simulations are carried out for a double-circuit transmission line for different faults and for different compensation levels using Matlab/Simulink. This study is done on double-circuit transmission line feeding both industrial and residential customers. Simulation results are shown for different levels of compensation (15, 40, and 80 %) with different faults (single-phase to ground and three phase). Voltage regulation and power generation are studied in the results to check effectiveness of series compensation. Improvement of voltage profile during transient and steady state shows the effectiveness of series compensation.

Keywords Series compensation · Transient stability · MOV · Damping reactor · SSR

S. Radha Krishna Reddy (✉)
EEE Department, JNTUH, Hyderabad, India
e-mail: rkphd2012@gmail.com

J.B.V. Subrahmanyam
EEE Department, CJITS, JNTUH, Hyderabad, India
e-mail: jbvsnm@gmail.com

A. Srinivasula Reddy
EEE Department, CMREC, JNTUH, Hyderabad, India
e-mail: svas_a@yahoo.com

1 Introduction

Main requirement of power system is to transfer power from generation to load centers efficiently and with high reliability. Voltage should be maintained within limits along the transmission lines. As much power as possible should be transmitted through the transmission lines within specified voltage limits. But with increase in line length, voltage regulation problem and charging reactive power are severe. Power transfer capability of line decreases with increase in transmission line length [1].

Maximum load carrying ability of a transmission line is function of line length. Strength of the system plays a vital role on load carrying ability of line for extra HV lines. Shunt compensation has minimum effect on load ability for high-voltage lines [2]. Reactive power compensation plays a vital role in transmission systems for an effective transmission of power. Demand for power is steadily growing for years. To meet the power demand, utilities are increasingly depending on generating units through transmission lines. But existing lines are not enough to meet the requirement of load demand [3]. To improve power transfer capability and load ability of transmission, line shunt or series compensation can be used.

Series compensation is in electrical systems since 1970s. Addition of capacitor bank in series with line improves transient performance of system and can maintain synchronism between machines connected through same line. It improves voltage profile at midpoint of line and maintains voltage to be in its limits. Reduction in inductive reactance and compensation of reactive power regulates system voltages. Power flow balance between adjacent transmission lines can be improved because of improvement transfer capability by series compensation. It improves reliability of system [4].

For protection of series capacitors used in series compensation, metal oxide varistors (MOV), bypass switch, and fast protective devices can be connected. Using metal oxide valve in surge arresters improves its protective characteristics; its over voltage reseal capability and double energy withstand capability. Rating of MOVs is the maximum power that can be applied continuously without damaging [5].

In this paper, effect of series compensation on double-circuit transmission line is studied. Simulation studies are performed on a double-circuit transmission line for different faults and different levels of compensation. Section 2 explains about series compensation and its protecting devices; Sect. 3 is about sub synchronous resonance and stability, and Sect. 4 presents simulation results for three-phase fault and single-phase fault for three levels of compensation.

2 Series Compensation

Main requirement of power transmission line is to transmit the power as much as it can be in a line with a specified voltage and to regulate the voltage within limits. By effectively regulating the voltage, power transfer capability of the line can be

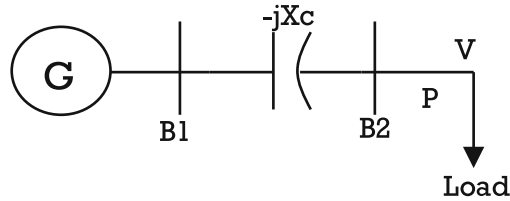


Fig. 1 Transmission system with series compensation

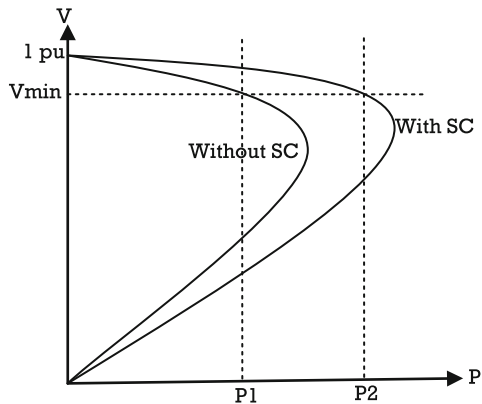
increased [6, 7]. When the line length increases, power transfer capability reduces without compensation because of problems in voltage control and charging reactive power at no load. During no load and light load conditions, consumption is less than generation and line voltage rises. And if connected load is more than surge impedance loading voltage reduces. Series capacitors in transmission line regulate reactive power flow and reduce voltage variations, and hence power transfer capability of line increases. Because of series compensation, active reactance of line reduces. Voltage across the capacitor is in proportional and in quadrature with line current. Reactive power generated across series capacitor is in proportional with square of line current. That means if the loading on the line increases, generated reactive power by series capacitor increases. In uncompensated mixed overhead cable lines exhibits peculiar behavior during single pole auto-reclosure in case of single-phase to ground faults in the overhead line section [8, 9] (Figs. 1 and 2).

Equivalent circuit of transmission line with series compensation is given in Fig. 3.

Power flow in the line is given by

$$P = \frac{U_s U_r \sin \delta}{\cos^2 \frac{\theta}{2} [2Z_n \tan \frac{\theta}{2} - X_c]} = \frac{U_s U_r \sin \delta}{Z_n \sin \theta \left[1 - \frac{X_c}{2Z_n \tan \frac{\theta}{2}} \right]}$$

Fig. 2 Power voltage curve



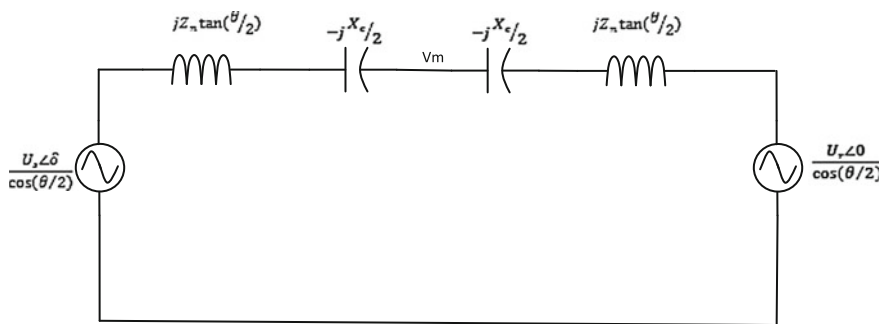


Fig. 3 Equivalent circuit of transmission line

When $U_s = U_r = U$, then midpoint current is given by

$$I_m^{se} = \frac{U \sin \frac{\delta}{2}}{Z_n \sin \frac{\theta}{2} (1 - k_{se})}$$

where

$$k_{se} = \frac{X_n}{2Z_n \tan \frac{\theta}{2}}$$

k_{se} is the degree of series compensation.

U_s, U_r are sending and receiving end voltages, δ is the phase angle between Thevenin’s equivalent voltages and receiving end voltage, Z_n is the surge impedance, I_m is the midpoint current.

From equation for a given angle δ , by increasing degree of series compensation, power transfer capability of transmission line increases. By increasing the level of compensation, the critical voltage at which voltage will collapse due to further increase in power transfer, also increases. Rating of capacitor banks depends on the level of compensation, voltage and current magnitudes, and power swing. During fault condition, magnitude of voltages and currents changes abruptly. Over voltage protection controls the voltage across the capacitors, and hence protect capacitor banks.

Metal oxide varistors can be used as over voltage protection devices in fixed series compensation [10, 11]. Varistor offers high resistance for low current and low voltages, and low resistance for high current and high voltages. At operating voltage, MOVs resistor stack behaves like pure capacitive. This capacitance causes uneven voltage distribution along the resistance of arrester which increases the effective length of resistor stack. Grading elements are required for MOVs to compensate this uneven distribution of voltage due to stray capacitance. During normal voltage, MOVs conduct very less current and during high-voltage MOVs

will conduct freely. Hence, capacitor banks are protected because of maximum current flow through MOVs. When the energy absorbed during critical conditions by MOVs is more than its limit protective devices are switched on to further protect capacitor banks and MOVs. Bypass switch is to short a series capacitor and MOV during extreme conditions. Damping reactor connected in series with bypass switch is to dampen capacitor currents [12].

3 Subsynchronous Resonance and Stability

Due to addition of series capacitance in transmission line to improve voltage stability, electrical resonance occurs in the system [13–15]. The phenomenon of electrical resonance interaction with mechanical resonance of turbine generator set is known as subsynchronous resonance. There is a possibility of limitation for level of compensation due to subsynchronous resonance.

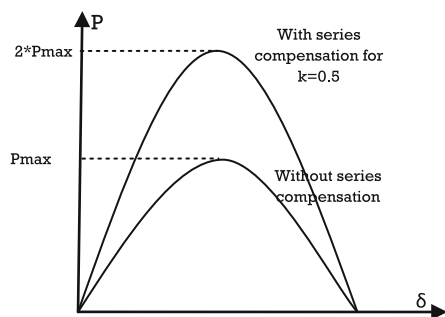
Frequency of electrical resonance in series compensated line is given by

$$\omega_R = \omega_n \sqrt{k}$$

ω_n is natural frequency of transmission line. k is the level f compensation. Frequency of electrical resonance is less than natural frequency because level of compensation is less than 1. current flow at these frequencies in stator induces MMF and hence currents through rotor. Frequency of these rotor currents is fundamental complement of frequency of stator currents.

During any severe disturbance occurred on transmission line such as faults, there is a possibility of loss of synchronism. Due to which fluctuations in rotor angles, power flows, and bus voltages occur. Transient stability to maintain synchronism during disturbances is required to maintain synchronism. By series compensation, transient stability of the system will be increased because of improvement in dynamic performance because of increase in area under power angle curve as shown in Fig. 4.

Fig. 4 Power-angle curve



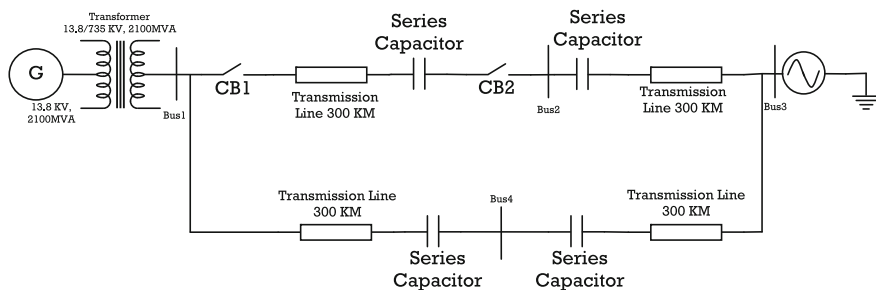


Fig. 5 Simulated system

4 Simulation Results

To study the effectiveness of series compensation on transmission line simulation is performed on double-circuit transmission line. System simulated is shown in Fig. 5. A Generating station of 2100 MVA, 13.8 kV is connected to an infinite bus through a power transformer by double-circuit transmission line. Length of transmission line is 600 km. For each line at sending end and at midpoint of the transmission line, two series capacitors are connected for series compensation. Level of compensation decides the amount of capacitors to be connected. Each capacitor bank is protected with MOV and bypass switch. Bypass switch will be operated whenever the energy across MOV is more than critical energy of it. Critical energy selected in this case is 30 MJ. A fault is created at midpoint of transmission line at bus B2, after occurrence of the fault circuit breakers of line CB1 and CB2 are opened to protect the transmission line and other devices. Simulation results are studied for three-phase fault, single-phase to ground fault and two-phase to ground fault for different levels of compensation. Amount of capacitor connected for series compensation is equal to $1/(2*\pi*f* \text{level of compensation}*X_1)$, where X_1 is inductive reactance of transmission line (Fig. 6).

a. Single-phase to ground fault

Level of compensation 15 % capacitor connected in this case is 0.16746 mF. A three-phase fault is created at 1 s and cleared at 2 s. After fault occurrence, circuit breakers are opened to isolate faulted line. Figure 7 shows midpoint voltage both transmission line, i.e., at bus 2 and bus 4. Due to low level of compensation after fault occurrence voltage at midpoint of first transmission line is reduced to 0.2 pu then after removal of faulted line, voltage is restored to its original value 1.05 pu. Voltage stabilization is done within 0.3 s after removal of faulted line. Figure 7 shows generated electrical power and stator current of phase A. Generated power is 0.85 pu during normal condition, whenever fault applied on first line and because of removal of faulted line power is reduced to 0.55 pu. After removal of fault, generated power is stabilized after 0.3 s. Figure 9 shows capacitor voltage and current and energy stored in MOV. Immediately after fault occurrence and clearance, due to

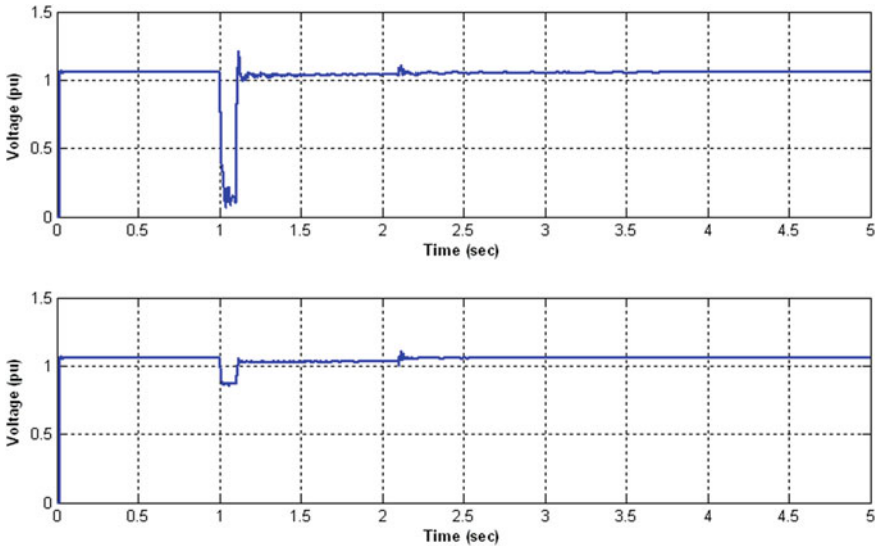


Fig. 6 Voltage magnitudes at midpoint of both lines (bus 2 and bus 4) for 15 % compensation

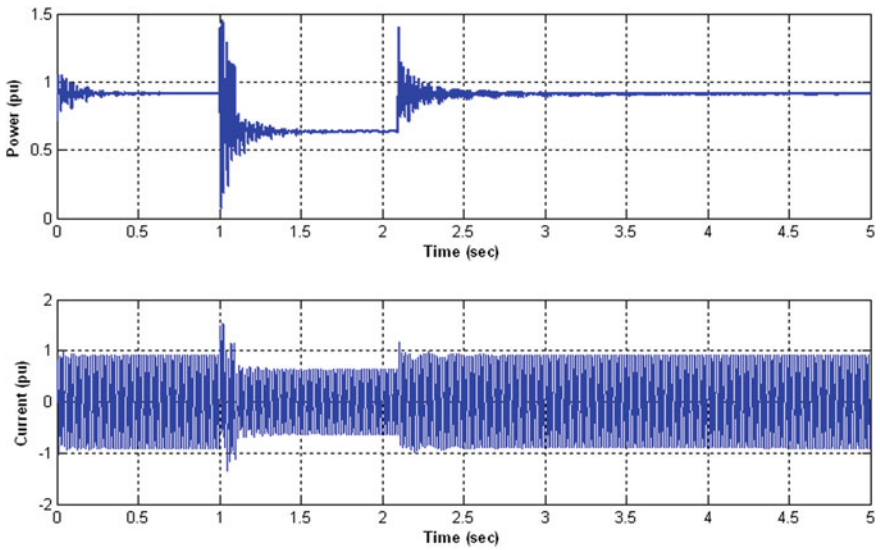


Fig. 7 Electrical power generated by generator and stator current of phase A for 15 % compensation

less amount of compensation, oscillations in bus voltages and active and reactive powers are more and will be neutralized after very less time (0.5 s for 15 % compensation) (Fig. 8).

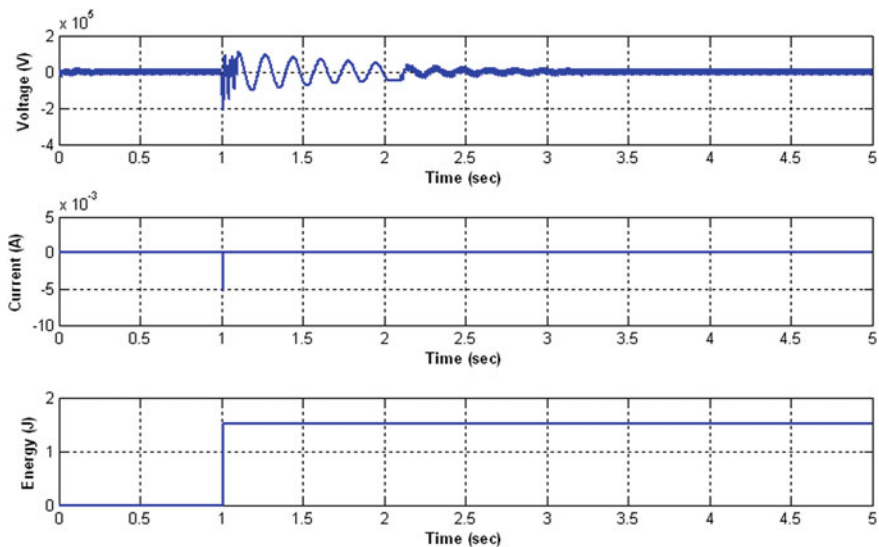


Fig. 8 Voltage and current through capacitor bank and energy stored in MOV for 15 % compensation

Level of compensation 40 % for 40 % of compensation value capacitance is 62.8 μ F. After fault reduction in voltage, magnitude at midpoint is limited to 0.5 pu because of increase in compensation level. Second line reduction in voltage is almost 0.1 pu. Both voltages at bus 2 and 4 are shown in Fig. 9. Generated electrical

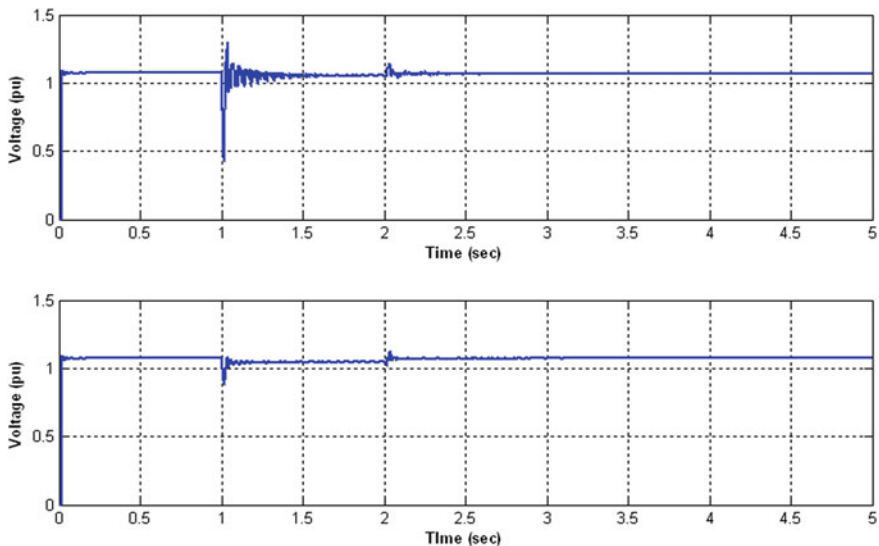


Fig. 9 Voltage magnitudes at midpoint of both lines (bus 2 and bus 4) for 40 % compensation

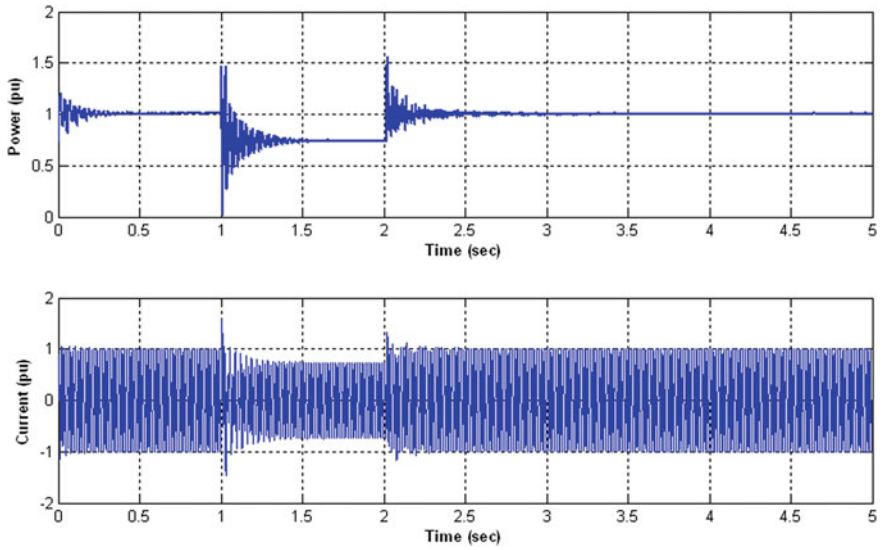


Fig. 10 Electrical power generated by generator and stator current of phase A for 40 % compensation

power is shown in Fig. 10. For 40 % compensation generated power is 1 pu. After removal of first line, power generated is reduced to 0.65 pu. Capacitor voltage, current and energy stored in MOV are shown in Fig. 11.

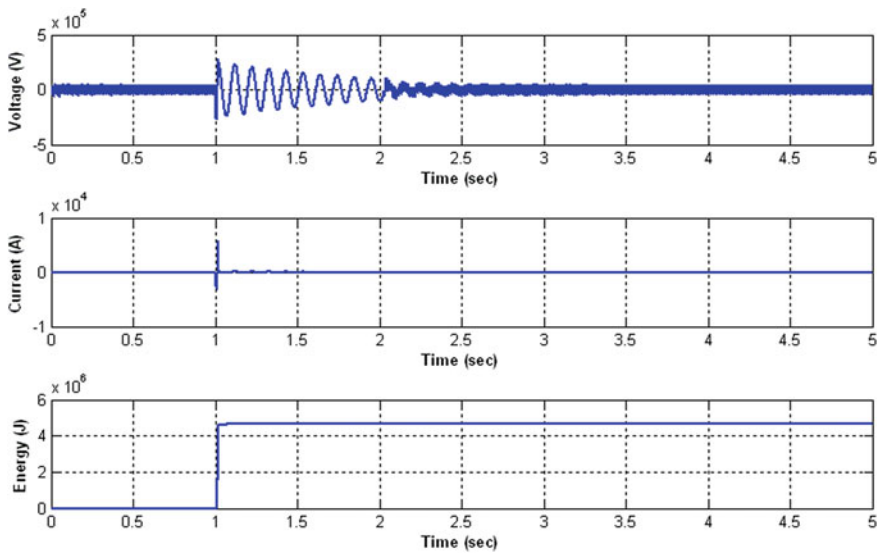


Fig. 11 Voltage and current through capacitor bank and energy stored in MOV for 40 % compensation

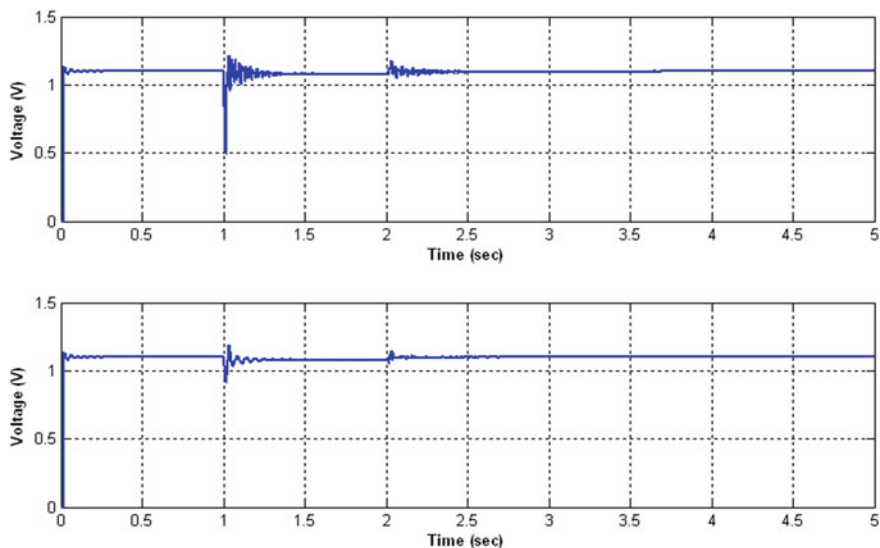


Fig. 12 Voltage magnitudes at midpoint of both *lines* (bus 2 and bus 4) for 80 % compensation

Level of compensation 80 % for 80 % compensation, capacitor connected is $31.399 \mu\text{F}$. due to increase in compensation, reduction in voltage during fault and removal is very less (0.05 pu). Generated active power for 80 % compensation is 1.2 pu. And after fault occurrence power is reduced to 1 pu. Capacitor voltage and current are shown in Fig. 14. Because of high level of compensation damping of oscillations in bus voltages and active and reactive powers is effective and time taken for stabilization is very less (0.2 s) (Figs. 12 and 13).

b. Three-phase fault

For three-phase fault simulation results are shown in Figs. 15, 16, 17, 18, 19, 20, 21, 22 and 23.

Level of compensation 15 %

See Figs. 15, 16 and 17.

Level of compensation 40 %

See Figs. 18, 19 and 20.

Level of compensation 80 %

See Figs. 21, 22 and 23.

Drop in voltage magnitude due to fault occurrence in transmission line bus B2 for different levels of compensation is shown in Table 1. Increase in level of compensation increases the voltage improvement level.

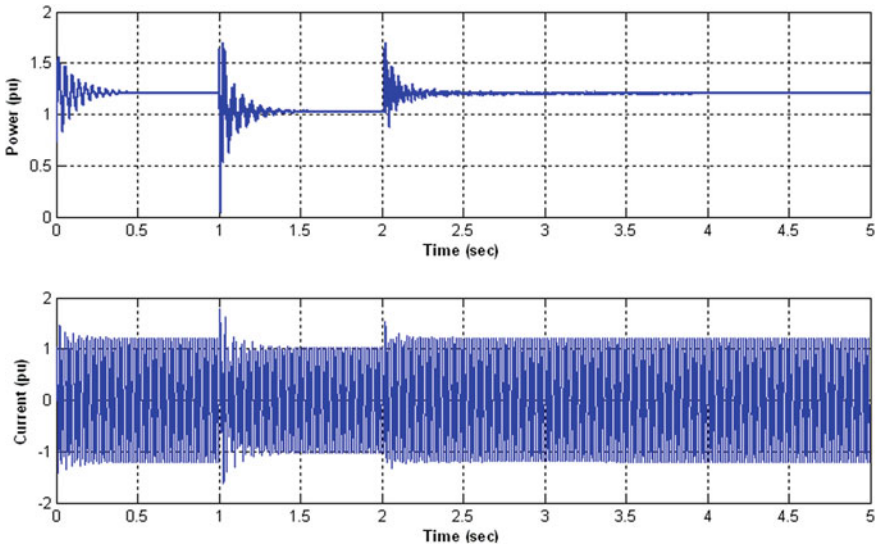


Fig. 13 Electrical power generated by generator and stator current of phase A for 80 % compensation

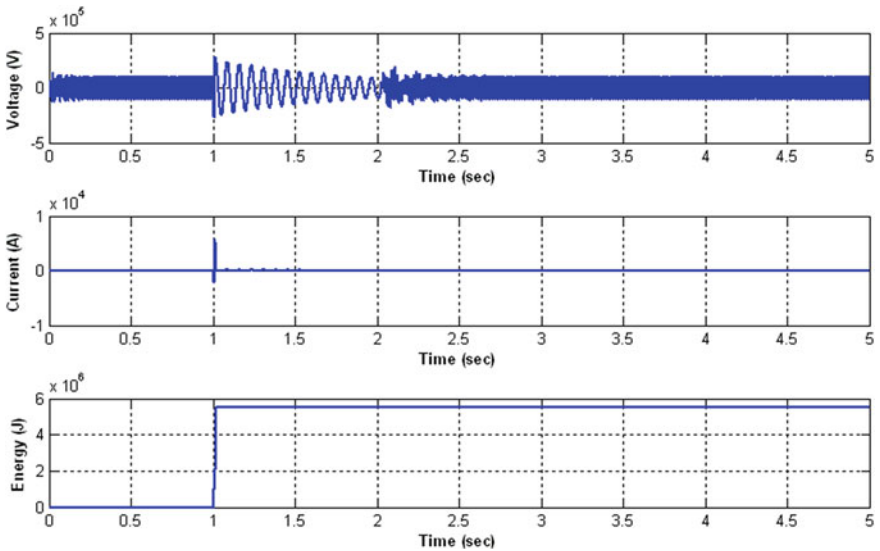


Fig. 14 Voltage and current through capacitor bank and energy stored in MOV for 80 % compensation

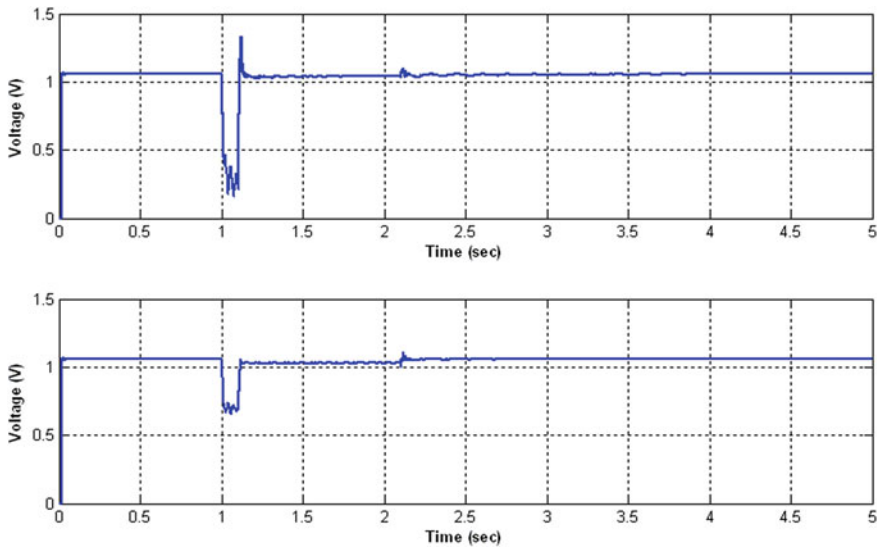


Fig. 15 Voltage magnitudes at midpoint of both lines (bus 2 and bus 4) for 15 % compensation

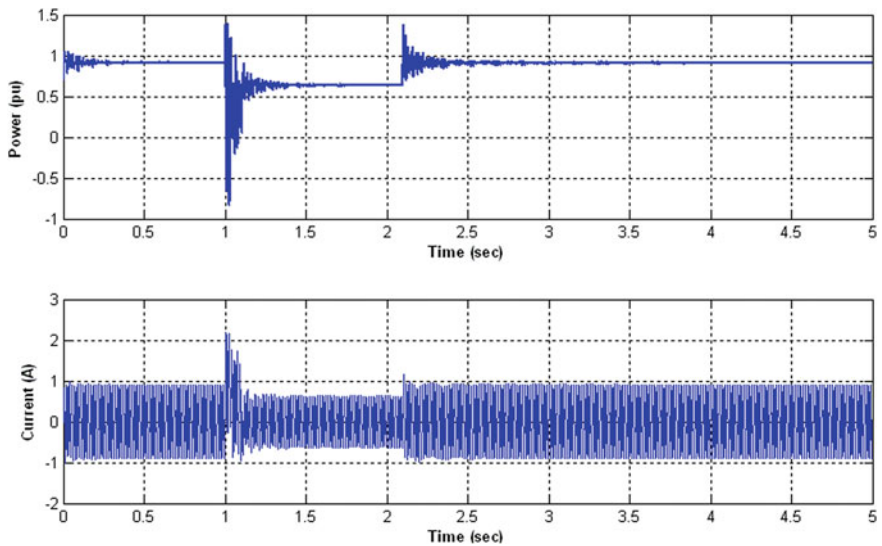


Fig. 16 Electrical power generated by generator and stator current of phase A for 15 % compensation

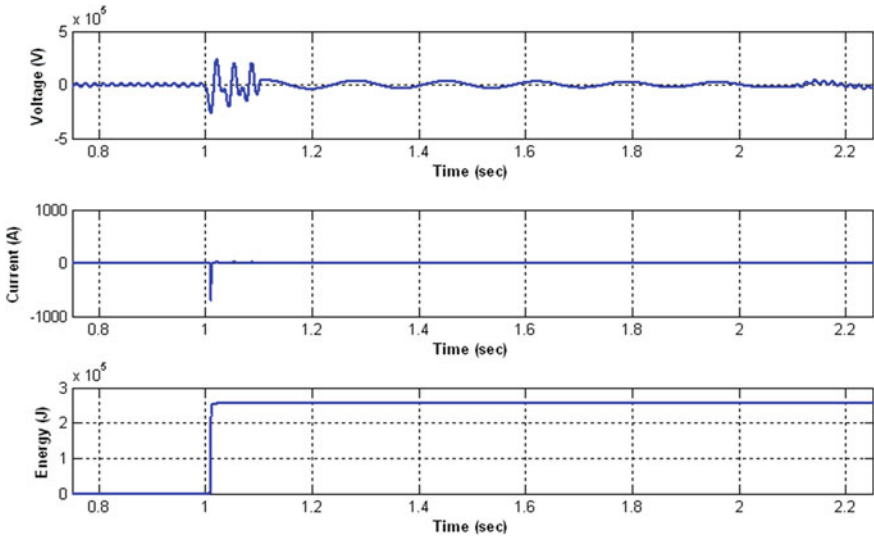


Fig. 17 Voltage and current through capacitor bank and energy stored in MOV for 15 % compensation

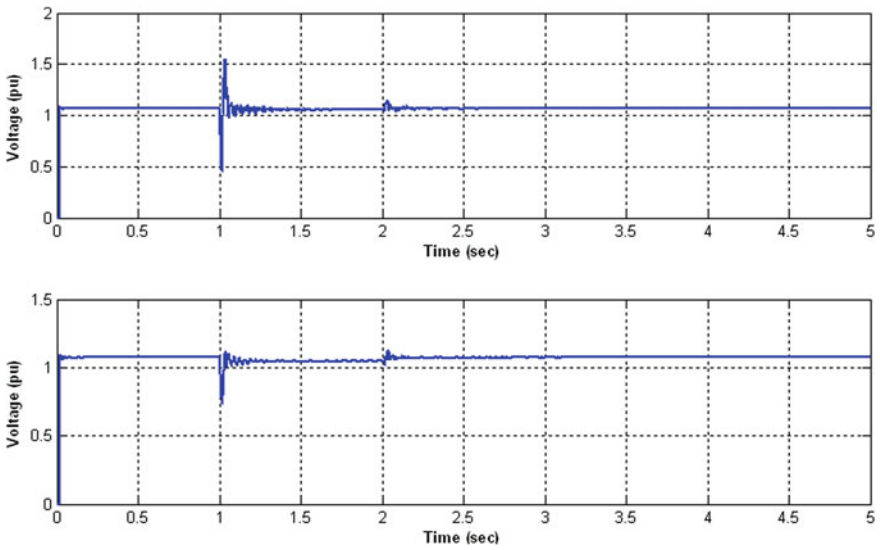


Fig. 18 Voltage magnitudes at midpoint of both lines (bus 2 and bus 4) for 40 % compensation

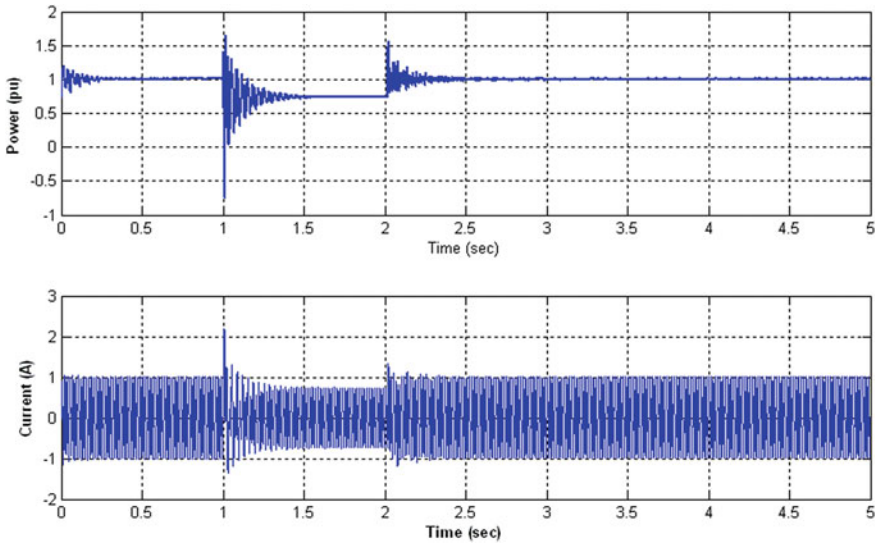


Fig. 19 Electrical power generated by generator and stator current of phase A for 40 % compensation

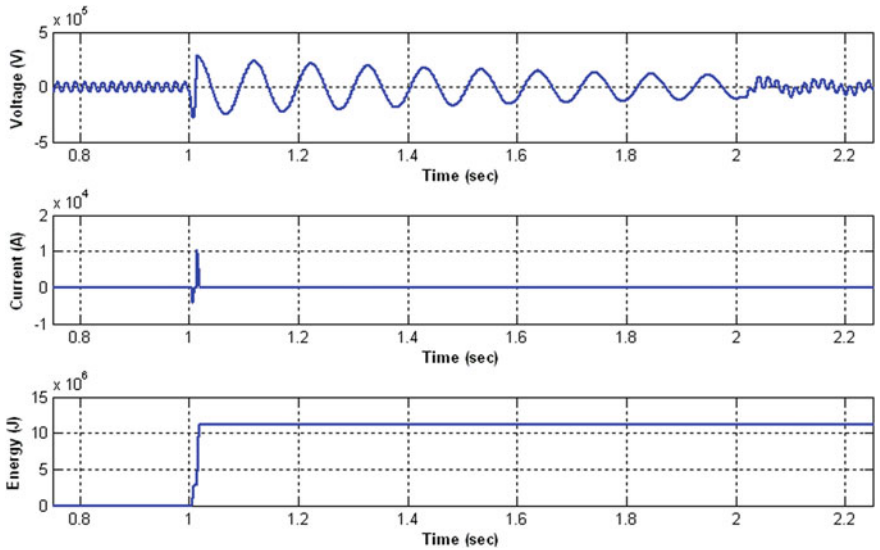


Fig. 20 Voltage and current through capacitor bank and energy stored in MOV for 40 % compensation

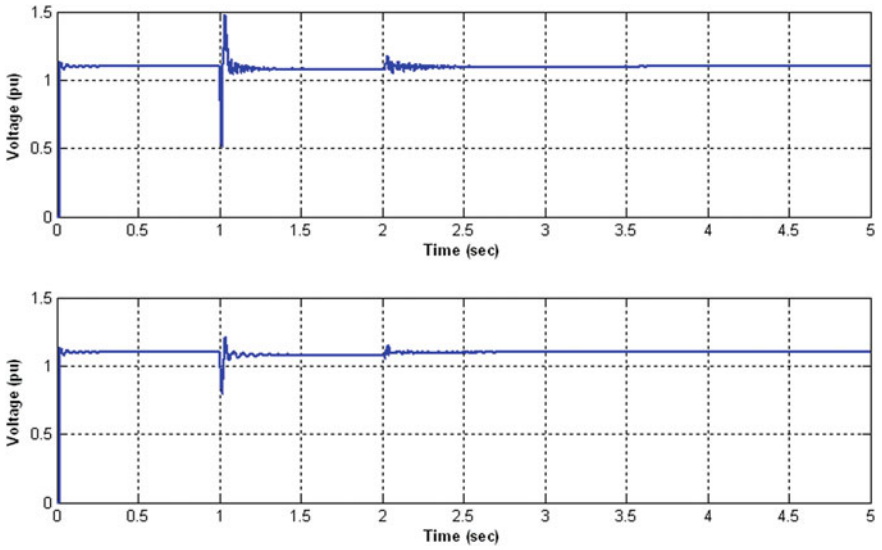


Fig. 21 Voltage magnitudes at midpoint of both lines (bus 2 and bus 4) for 80 % compensation

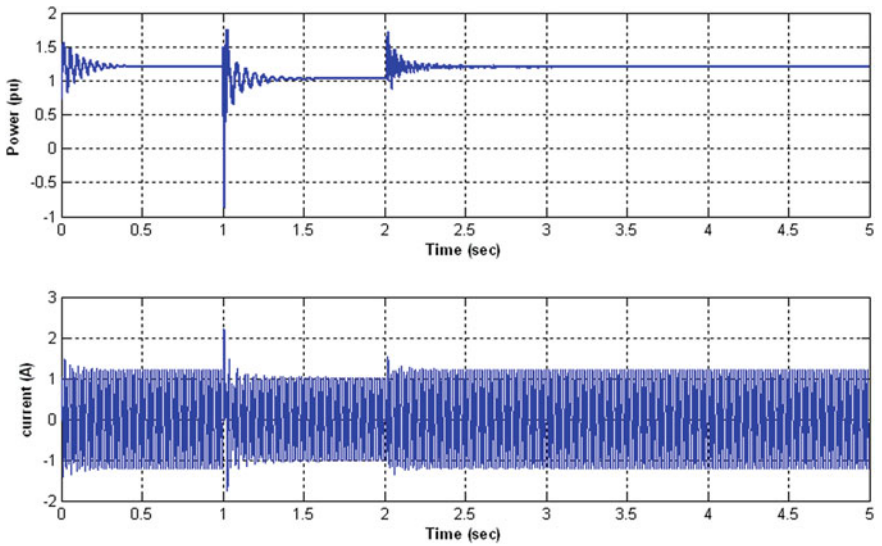


Fig. 22 Electrical power generated by generator and stator current of phase A for 80 % compensation

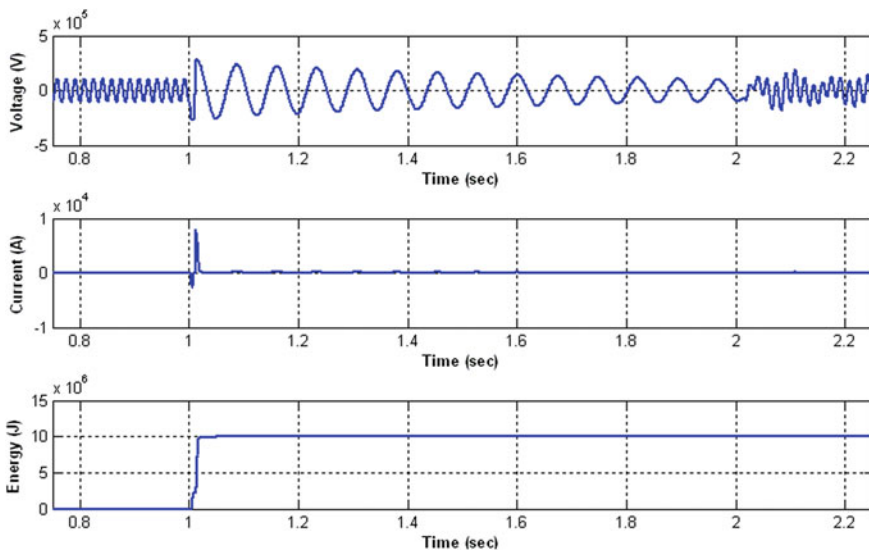


Fig. 23 Voltage and current through capacitor bank and energy stored in MOV for 80 % compensation

Table 1 COMPENSATION Vs VOLTAGE MAGNITUDE

Compensation level (%)	Voltage magnitude at bus 2 after fault (pu)	Voltage magnitude at bus 4 after fault (pu)
15	0.15	0.95
40	0.45	0.98
80	0.6	1

5 Conclusion

Simulation studies are performed on series compensated double-circuit transmission line to know effect of capacitor banks on transmission line. By adding series capacitor in line voltage regulation is done effectively. Voltage magnitudes during transient performance depend on level of compensation. With increase in the level of compensation, there is an increase in electrical power flow which shows the improvement of transfer capability. Increase in the level of compensation increases damping of oscillations in bus voltages. By effectively choosing optimal location for series compensation, performance of the system can be further improved. These simulation studies are useful to find optimal location of series compensation in the line.

References

1. Padiyar KR. FACTS controllers in power transmission and distribution. New Age International (P) Limited, Publishers.
2. Gutman R. Analytical development of load ability characteristics for EHV and UHV transmission lines. *IEEE Trans Power Apparatus Syst.* 1979;PAS-98(2).
3. Gyugyi L. Dynamic compensation of AC transmission lines by solid state synchronous voltage sources. *IEEE Trans Power Deliv.* 1994;9(2).
4. Abdelaziz AY, Ibrahim AM, Mansour MM, Talaat HE. Modern approaches for protection of series compensated transmission lines. *Electr Power Syst Res.* 2005;75:85–98.
5. Seeker SA. Protecting substation equipment with MOV surge arresters. Mc-Graw Edison Company.
6. Gatta FM, Geri A, Lauria S, Maccioni M. Steady-state operating conditions of very long EHVAC cable lines: two case studies. *Electr Power Syst Res.* 2012;83:160–9.
7. Frolov V, Backhaus S, Chertkov M. Efficient algorithm for locating and sizing series compensation devices in large power transmission grids: II. Solutions and applications. *New J Phys.* 2014;16:105016.
8. Gatta FM, Geri A, Lauria S, Maccioni M. Power frequency secondary arc current in uncompensated EHV AC mixed cable-overhead lines. *Electr Power Syst Res.* 2014;111:14–21.
9. Abdelaziz AY, Ibrahim AM, Mansour MM, Talaat HE. Modern approaches for protection of series compensated transmission lines. *Electr Power Syst Res.* 2005;75:85–98.
10. Malathi V, Marimuthu NS, Baskar S, Ramar K. Application of extreme learning machine for series compensated transmission line protection. *Eng Appl Artif Intell.* 2011;24:880–7.
11. Yusuff AA, Fei C, Jimoha AA, Munda JL. Fault location in a series compensated transmission line based on wavelet packet decomposition and support vector regression. *Electr Power Syst Res.* 2011;81:1258–65.
12. Coteli R. A combined protective scheme for fault classification and identification of faulty section in series compensated transmission lines. *Turkish J Electr Eng Comput Sci.* 2013;21:1842–56.
13. Abdelaziza AY, Mekhamera SF, Ezzata M. Fault location of uncompensated/series-compensated lines using two-end synchronized measurements. *Electr Power Compon Syst.* 2013;41(7).
14. Biswala M, Patia BB, Pradhanb AK. Adaptive distance relay setting for series compensated line. *Int J Electr Power Energy Syst.* 2013;52:198–206.
15. Moraveja Z, Khederzadehb M, Pazokia M. New combined method for fault detection, classification, and location in series-compensated transmission line. *Electr Power Compon Syst.* 2012;40(9).

Optimal Scheduling of Microgrid with Energy Storage System Considering Islanding Constraints

N. Jayalakshmi and B. Ashokvannan

Abstract This paper deals with the microgrid optimal scheduling, considering the islanding constraints with energy storage system. The main objective of this paper is to minimize the total operation cost and to optimize the power output of the microgrid by minimizing the losses of the energy storage system. The microgrid optimal scheduling problem is categorized into grid-connected operation as master problem and the islanded operation as subproblem. The scheduling decisions obtained in the grid-connected operation are examined in the islanded operation for feasible islanding. The suitable islanding cuts are generated to revise the scheduling decisions, if sufficient generation is not available. Islanding cuts generated will revise the generating units, energy storage system, and adjustable load schedules. This paper presents the numerical simulations using matlab to demonstrate the effectiveness of the microgrid optimal scheduling.

Keywords Microgrid optimal scheduling • Islanded operation • Distributed energy resources • Adjustable load • Energy storage system

Indices

- b* Index for energy storage systems
- ch* Superscript for energy storage system charging mode
- d* Index for loads
- dch* Superscript for energy storage system discharging mode
- i* Index for DERs
- s* Index for scenarios
- t* Index for time

N. Jayalakshmi (✉)

M.E. Power Systems Engineering, Anna University, CEG Campus, Chennai, Tamilnadu, India

e-mail: jayabtecheee@gmail.com

B. Ashokvannan

Dr MGR Educational and Research Institute University, Chennai, Tamilnadu, India

e-mail: ashokvannan@gmail.com

© Springer India 2016

S.S. Dash et al. (eds.), *Artificial Intelligence and Evolutionary Computations in Engineering Systems*, Advances in Intelligent Systems and Computing 394, DOI 10.1007/978-81-322-2656-7_106

1145

^ Calculated variables

Sets

DA Set of adjustable loads
 G Set of dispatchable units
 ES Set of energy storage systems

Parameters

DR Ramp down rate
 DT Minimum down time
 ER Adjustable load total required energy
 $F(.)$ Generation cost
 K_d Inconvenience penalty factor
 MC Minimum charging time
 MD Minimum discharging time
 U Outage state of the main grid line
 MO Minimum operating time
 UR Ramp up rate
 UT Minimum up time
 ss, se Specified start and end times of adjustable loads
 ρ Market price

Variables

C Energy storage system state of charge
 LD Load demand
 CDU Commitment state of the dispatchable unit
 P_{grid} DER output power
 P_{MG} Main grid power
 $C2$ Shut down cost
 VL_1, VL_2 Slack variables
 $C1$ Startup cost
 T^{ch} Number of successive charging hours
 T^{dch} Number of successive discharging hours
 T^{on} Number of successive ON hours
 T^{off} Number of successive OFF hours
 ed Energy storage system discharging state
 ec Energy storage system charging state
 mp Power mismatch
 z Adjustable load state
 α, β, γ Dual variables
 Δ_d Deviation in adjustable load operating time interval
 τ Time variables
 ΔV Differential Cost

$V(t, E)$	Value Function
$E(T)$	Energy Function
$E^*(t)$	Energy at t
$E^*(t - dt)$	Relation to a previous energy value
SOC	State of Charge
$P_1(t)$	Power at PCC
P_{total}	Total Power
P_{ES}	Storage power
J_{rated}	Storage Capacity
$\{(t + dt), E(t + dt)\}$	Two arbitrary points

1 Introduction

Microgrid is a group of interconnected loads and distributed energy resources within clearly defined electrical boundaries that act as a single controllable entity with respect to the grid. A microgrid can connect and disconnect from the grid to enable it to operate in both grid-connected or island mode. In grid-connected operation, the loads in the microgrid receive power both from the grid and from the microgrid sources depending on the customer's situation. With loss of the grid due to voltage drops, faults, blackouts, etc., the microgrid smoothly transfers to islanded operation. In addition, alarming issues related to global warming, uncertain gas prices, security of fossil fuel imports, and power blackouts have sparked additional interests in renewable energy to ensure that the electricity sector will continue to provide reliable and affordable energy to its customers [1]. Microgrids introduce a number of benefits in power system as integration of distributed generation and storage with reduced impact on existing distribution network (e.g., voltage control, congestion management), local power production, including off-grid applications, reduction of greenhouse gas emissions, sustainable power production when using renewable energy sources, enhanced security of supply (e.g., natural or grid-based events), enhanced power quality, reduction of power losses associated with power transmission and distribution, economic benefits depending also on the regulatory framework, competitive electricity price in areas where electricity prices are high. The microgrid is islanded from the main grid using upstream switches at the point of common coupling (PCC), and the microgrid load is fully supplied using local resources [2, 3].

A microgrid can be controlled in four different modes. They are: (1) Two operational modes (grid-connected and islanded); (2) Two transition modes (island forming and grid synchronization). When operating in grid-connected mode, the DERs are controlled as active and reactive power sources. So that they inject a set into the network, controllable amount of power while using the grid voltage and frequency as a reference. In islanded mode, the sources are controlled in order to

maintain the voltage and frequency within acceptable limits. The transition between grid-connected and islanded mode can be planned or unplanned. A scheduled transition is an intentional event determined by factors like maintenance or economical convenience. Unscheduled transition is usually caused by an unexpected event like a major fault in the grid. During the island-forming transition, the microgrid control has to be designed to support the system frequency and voltage. Any transients produced by this transition should be sufficiently damped in order to allow the newly formed islanded microgrid to reach a stable operation. Alternatively, island forming can be on the basis of an interruption followed by separation from the grid and then “black-starting” the microgrid. The transition between islanded and grid-connected mode (grid synchronization) is controlled so that the microgrid, with all its generation, can be safely reconnected to the grid [4, 5].

Microsource controller is an important component of the MicroGrid infrastructure. This controller responds in milliseconds and uses local information to control the microsource during all events. There are two basic classes of microsources; one is a DC source, such as fuel cells, photovoltaic cells, and battery storage, the other is a high-frequency AC source such as the microturbine, which needs to be rectified. In both cases, the resulting DC voltage is converted to an acceptable ac source using a voltage source inverter. The voltage source inverter provides control of both the magnitude and phase of its output voltage [6]. Voltage regulation is necessary for local reliability and stability. Without local voltage control, systems with high penetration of microsources can experience voltage and/or reactive power oscillations. With small errors in voltage set points, the circulating current can exceed the ratings of the microsources. This situation requires a voltage versus reactive current droop controller. Basically, as the reactive current generated by the microsource becomes more capacitive the local voltage set point is reduced. Most microsources in a microgrid are interfaced through power electronic convertors as the sources produce either DC (photovoltaic or fuel cells) or variable frequency AC (microturbines, Wind turbines). As the electrical generators are not directly connected to the 50 Hz network, they do not add any inertia to the system. This lack of inertia poses difficulties in maintaining a power balance between generation and load and the network frequency of a microgrid in islanded mode. Hence the microgrid requires careful control to maintain adequate operating reserve and to control frequency and voltage during islanded operation. It is necessary to control the power flow at the point of common coupling during grid-connected operation [7].

Energy storage is finding critical roles in powering hybrid and electric vehicles, smoothing variable generation from wind and solar systems, reducing voltage and frequency fluctuations in grid-tied systems, and enabling off-grid and rural renewable electrification systems, among others. Generation from wind, solar, and other renewable energy sources increase power supply variability which energy storage can help control by storing power when there is an oversupply of electricity and providing power when generation falls short. When power system disturbances occur, synchronous generators are not always able to respond rapidly enough to

keep the system stable. If high-speed real or reactive power control is available, load shedding or generator dropping may be avoided during the disturbance. High-speed reactive power control is possible through the use of flexible AC transmission systems (FACTS) devices [8]. In a few cases, these devices are also able to provide some measure of high-speed real-power control through power circulation within the converter, with the real power coming from the same line or in some cases from adjacent lines leaving the same substation. However, a better solution would be to have the ability to rapidly vary real power without impacting the system through power circulation. This is where energy storage technology can play a very important role in maintaining system reliability and power quality. The ideal solution is to have means to rapidly damp oscillations, respond to sudden changes in load, supply load during transmission or distribution interruptions, correct load voltage profiles with rapid reactive power control, and still allow the generators to balance with the system load at their normal speed [9].

Two factors characterize the application of an energy storage technology. One is the amount of energy that can be stored in the device. This is a characteristic of the storage device itself. Another is the rate at which energy can be transferred into or out of the storage device. In highly variable storage systems, the relationship between energy and power can become quite important as efficiency fluctuates with the range of operating powers. The objectives of energy management depend on the mode of operation: Islanded or grid-connected. In islanded mode, the main goal of power management is to stabilize the system, in terms of frequency and voltage. In grid-connected mode, typical objectives are to minimize the price of energy import at the PCC, to improve power factor at the PCC, and to optimize the voltage profile within the microgrid. The objective of this paper is to minimize the day-ahead grid-connected operation cost of the microgrid using available generation resources, energy storage systems, adjustable loads, and the main grid power, subject to prevailing operational constraints [10, 11]. It enables the microgrid to operate in the islanded mode and to provide the adequate supply to the local loads.

2 Optimal Scheduling Model of Microgrid

2.1 *Elements in Microgrid*

Distributed generation (DG) and distributed storage (DS) units are directly connected to the distribution network, together with the local loads. Often, DG and DS units are referred as distributed energy resources (DERs). The term DG is associated with renewable energy sources (RES). The new DG technologies available are microturbines, fuel cells, photovoltaic systems, and wind turbines. Typical DS units include batteries and flywheels. Dispatchable generation refers that the electricity can be dispatched at the request of power grid operators; i.e., generating plants that can be turned on or off, or can adjust their power output on demand. In general, the

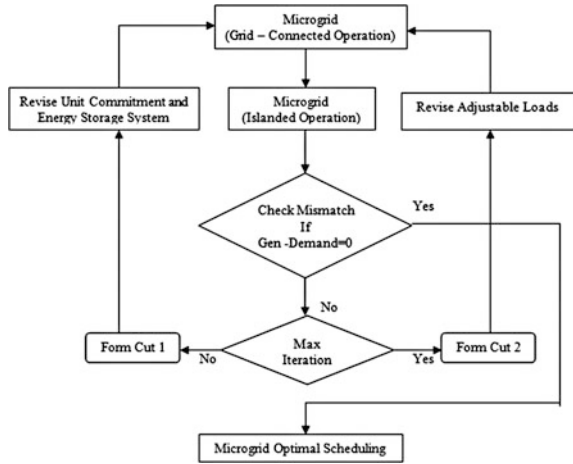
types of renewable energy which are dispatchable are biofuel, biomass, hydropower with a reservoir, and concentrated solar power with thermal storage. Dispatchable units can be controlled by the microgrid master controller and are subject to technical constraints, depending on the unit type, such as capacity limits, ramping limits, minimum on/off time limits, and fuel and emission limits. Nondispatchable units cannot be controlled by the microgrid master controller since the input source is uncontrollable. Nondispatchable units are mainly renewable resources which produce a variable, i.e., volatile and intermittent, output power. Microgrid loads are categorized into two types of fixed and adjustable loads. Fixed loads cannot be altered and must be satisfied under normal operation conditions. Adjustable loads are responsive to price variations and controlling signals from the microgrid master controller [12]. Adjustable loads could be curtailed (i.e., Curtailable loads) or deferred (i.e., shiftable loads) in response to economic incentives or islanding requirements.

2.2 Organizing of Microgrid Model

The scheduling problem is decomposed into grid-connected operation master problem and islanded operation subproblem. The master problem determines the optimal commitment and dispatch of available dispatchable units, charging and discharging schedules of energy storage systems, schedule of adjustable loads, and the power transfer with the main grid. The optimal schedule is used in the subproblem to examine the microgrid generation adequacy and confirm an uninterrupted supply of loads. If the islanding is not feasible, i.e., microgrid does not have sufficient online capacity to supply the local load, a Benders cut, i.e., Cut 1, based on the unit commitments and energy storage system schedules is generated and sent back to the master problem for revising the current solution. The benders cut indicates that power mismatches in the subproblem can be mitigated by readjusting the unit commitments and energy storage system schedules in the master problem (Fig. 1).

The revised solution will be examined in the next iteration of the subproblem for islanding. The iterative process continues until it reaches the feasible solution. Even if the change in unit commitments and energy storage system schedules does not provide required online capacity to guarantee a feasible islanding, a secondary Benders cut, i.e., Cut 2, is generated based on adjustable loads schedules. This cut would revise the adjustable loads' either by shifting or curtailing the load for feasible islanding. Day-ahead schedules are calculated for the master problem and the subproblem, i.e., a 24-h scheduling horizon is considered. The microgrid fixed load and generation of nondispatchable units are forecasted with an acceptable accuracy. The market price at the point of common coupling, i.e., the price in which microgrid purchases the main grid power and sells excess power to the main grid

Fig. 1 Proposed microgrid optimal scheduling model



are also forecasted [13]. It is assumed that microgrid components are highly reliable and are not subject to outage during the scheduling horizon.

2.3 Gradient-Based Solvers in Time Domain

An optimal solution computes powers (P, Q), voltages (V), currents (I), phase angles (δ), and stored energy (E). All quantities are time dependent. While gradient-based solvers (like Newton–Raphson) which are used to solve networks efficiently are inadequate to energy storage problems. The desired solution is a function of stored energy versus time, $E(t)$. To reach a solution, the solver must determine $E(t)$ at every time point, thus each time point is a free variable. Apparently, many time-energy functions are local minima. Due to inefficiencies of the storage device, charging and discharging are wasteful. But, this local solution does not resemble the global one, and have no desired properties, such as charging when energy is available and so forth. This local solution is unsuitable, and cannot be used in a real-power system. So the dynamic programming algorithm with time domain is used which scan all feasible solutions, to locate the global optimum. Standard charging usually involves some combination of constant current or constant voltage charging, and is traditionally designed to optimize efficiency, charge time, and/or cycle life. In renewable energy systems, batteries are charged at a non-predetermined combination of changing powers. Variable charge input has been considered as a method for improving efficiency or charge rate in certain systems. Battery charge efficiency is defined as the percent of energy stored by a battery charged at a given power for a unit of time. Batteries in off-grid renewable energy systems are subject to many

stresses [14]. These systems tend to be characterized by highly variable charging powers, deep cycling, partial cycling, and infrequent full charge.

3 Formation of Scheduling Model

3.1 Constraints of Grid-Connected Operation

The objective of the grid-connected operation master problem is to minimize the microgrid total operation cost as follows:

$$\min \sum_t \sum_{i \in G} [F_i(P_{\text{grid},it}) \text{CDU}_{it} + C1_{it} + C2_{it}] + \sum_t \rho_t P_{\text{MG},t}. \quad (1)$$

The first term in the objective is the operation cost of microgrid dispatchable units, which includes generation, startup, and shut down costs over the entire scheduling horizon. The second term is the cost of power transfer from the main grid based on the market price at PCC. When the microgrid excess power is sold back to the main grid, $P_{\text{MG},t}$ would be negative; thus, this term would represent a benefit, rather than a cost, for the microgrid. The objective is subject to generating unit, energy storage system, and load constraints, as follows:

$$\sum_i P_{\text{grid},it} + P_{\text{MG},t} = \sum_d \text{LD}_{dt} \quad \forall t. \quad (2)$$

$$-P_{\text{MG}}^{\max} \leq P_{\text{MG},t} \leq P_{\text{MG}}^{\max} \quad \forall t. \quad (3)$$

$$P_{\text{grid},i}^{\min} \text{CDU}_{it} \leq P_{\text{grid},it} \leq P_{\text{grid},i}^{\max} \text{CDU}_{it} \quad \forall i \in G, \forall t. \quad (4)$$

$$\text{LD}_{dt}^{\min} z_{dt} \leq \text{LD}_{dt} \leq \text{LD}_{dt}^{\max} z_{dt} \quad \forall d \in \text{DA}, \forall t. \quad (5)$$

$$\sum_{t \in [\text{ss}_d, \text{se}_d]} \text{LD}_{dt} = \text{ER}_d \quad \forall d \in \text{DA}. \quad (6)$$

$$T_{dt}^{\text{on}} \geq \text{MO}_d(z_{dt} - z_{d(t-1)}) \quad \forall d \in \text{DA}, \forall t. \quad (7)$$

The power balance Eq. (2) ensures that the sum of power generated by DERs (i.e., dispatchable and nondispatchable units and energy storage systems) and the power from the main grid matches the hourly load. The forecasted generation of nondispatchable units is used in (2), where it can be treated as a negative load. The power of energy storage systems can be positive (discharging), negative (charging), or zero (idle). The main grid power can be positive (import), negative (export), or zero. The power transfer with the main grid is limited by the flow limits of the line connecting microgrid to the main grid (3).

The dispatchable unit generation is subject to minimum and maximum generation capacity limits (4). The unit commitment state, CDU_{it} , is committed and is zero otherwise. Adjustable loads are subject to minimum and maximum rated powers (5). When load is consuming power, the associated scheduling state z_{dt} would be one; it is zero otherwise. Each load consumes the required energy to complete an operating cycle in time intervals specified by consumers (6). ss_d , and se_d , respectively, represent the start and end operating times of an adjustable load. Certain loads may be subject to minimum operating time which is the number of consecutive hours that a load should consume power once it is switched on (7).

3.2 Constraints of Islanded Operation

The objective of the islanded operation subproblem for an islanding scenario is to minimize the power mismatches as in (8):

$$\min mp_s = \sum_t (VL_{1,ts} + VL_{2,ts}). \quad (8)$$

$$\sum_i P_{grid,its} + P_{MG,ts} + VL_{1,ts} - VL_{2,ts} = \sum_d LD_dts. \quad (9)$$

$$CDU_{its} = \widehat{CDU}_{it} \alpha_{its} \quad \forall i \in G, \forall t. \quad (10)$$

$$ed_{its} = \widehat{ed}_{it} \beta_{its}^{dch} \quad \forall i \in ES, \forall t. \quad (11)$$

$$ec_{its} = \widehat{ec}_{it} \beta_{its}^{ch} \quad \forall i \in ES, \forall t. \quad (12)$$

$$z_{dts} = \widehat{z}_{dt} \gamma_{dts} \quad \forall d \in DA, \forall t. \quad (13)$$

Power balance Eq. (9) encompasses slack variables VL_1 and VL_2 which act as virtual generation and virtual load, respectively. Nonzero values for these variables denote a power mismatch in the microgrid. Unit commitments, energy storage charging/discharging schedules, and load schedules are obtained from the grid-connected operation master problem. These given variables are replaced with local variables for each scenario to obtain associated dual variables (10)–(13). Dual variables are later used in this section to generate islanding cuts. A zero mismatch for the islanded operation subproblem ensures that the microgrid has sufficient committed generation and energy storage to independently supply the local load; hence, it could switch to the islanded mode without interruption in the load supply. When the objective is not zero, however, islanding Cut 1 (14) is generated and added to the next iteration of the grid-connected operation master problem to revise the current microgrid schedule:

$$\begin{aligned} \widehat{\text{mp}}_s + \sum_{i \in G} \alpha_{its} (\text{CDU}_{it} - \text{CDU}_{its}) + \sum_{i \in \text{ES}} \beta_{its}^{\text{dch}} (\text{ed}_{it} - \text{ed}_{its}) \\ + \sum_{i \in \text{ES}} \beta_{its}^{\text{ch}} (\text{ec}_{it} - \text{ec}_{its}) \leq 0. \end{aligned} \quad (14)$$

where α_{its} and β_{its}^{dch} are dual variables of (10), (11), and (12), respectively. The islanding Cut 1 indicates that islanding mismatches can be mitigated by readjusting the microgrid schedule in the grid-connected operation master problem. Dual variables in the islanding cut are the incremental reduction in the objective function of the islanded operation subproblem. This cut results in a change in unit commitments and energy storage system schedules based on islanding considerations. The iterative process continues until power mismatches in all islanding scenarios reach zero. However, it is probable that after a certain number of iterations the islanding is not guaranteed, i.e., by revising unit commitments and energy storage system schedules, a zero mismatch in all islanding scenarios is not obtained. To resolve this issue, the schedule of adjustable loads would be revised using the following cut, i.e., Cut 2:

$$\begin{aligned} \widehat{\text{mp}}_s + \sum_{i \in G} \alpha_{its} (\text{CDU}_{it} - \text{CDU}_{its}) + \sum_{i \in \text{ES}} \beta_{its}^{\text{dch}} (\text{ed}_{it} - \text{ed}_{its}) \\ + \sum_{i \in \text{ES}} \beta_{its}^{\text{ch}} (\text{ec}_{it} - \text{ec}_{its}) + \sum_{i \in \text{DA}} \gamma_{dts} (z_{dt} - z_{dts}) \leq 0. \end{aligned} \quad (15)$$

where γ_{dts} is the dual variable of (15). Cut 2 enables a simultaneous change in unit commitments, energy storage system schedules, and adjustable load schedules to guarantee a feasible islanding.

3.3 Constraints of Energy Storage System

$$P_{\text{grid},it} \leq P_{\text{grid},it}^{\text{dch,max}} \text{ed}_{it} - P_{\text{grid},it}^{\text{ch,min}} \text{ec}_{it} \quad \forall i \in \text{ES}, \forall t. \quad (16)$$

$$P_{\text{grid},it} \geq P_{\text{grid},it}^{\text{dch,min}} \text{ed}_{it} - P_{\text{grid},it}^{\text{ch,max}} \text{ec}_{it} \quad \forall i \in \text{ES}, \forall t. \quad (17)$$

$$\text{ed}_{it} + \text{ec}_{it} \leq 1 \quad \forall i \in \text{ES}, \forall t. \quad (18)$$

$$C_{it} = C_{i(t-1)} - P_{\text{grid},it} \quad \forall i \in \text{ES}, \forall t. \quad (19)$$

$$0 \leq C_{it} \leq C_i^{\text{max}} \quad \forall i \in \text{ES}, \forall t. \quad (20)$$

$$T_{it}^{\text{ch}} \geq MC_i (\text{ed}_{it} - \text{ed}_{i(t-1)}) \quad \forall i \in \text{ES}, \forall t. \quad (21)$$

$$T_{ii}^{\text{dch}} \geq MD_i(\text{ec}_{it} - \text{ec}_{i(t-1)}) \quad \forall i \in ES, \forall t. \quad (22)$$

The energy storage system power is subject to charging and discharging minimum and maximum limits depending on its mode (16)–(17). When charging, the charging state ec_{it} is one and discharging state ed_{it} is zero; hence, minimum and maximum charging limits are imposed. Similarly, when discharging, the discharging state ed_{it} is one and charging state ec_{it} is zero; hence, minimum and maximum discharging limits are imposed. Since the energy storage system charging power is considered as negative, the associated limits are denoted with a minus sign. Superscripts *ch* and *dch* are used for charging and discharging modes, respectively. Only one of the charging or discharging modes at every hour is possible (18). Energy storage system state of charge (SOC) is calculated based on the amount of charged/discharged power (19) and restricted with capacity limits (20). Energy storage systems are subject to minimum charging and discharging time limits, respectively (21) and (22), which are the minimum number of consecutive hours that energy storage systems should maintain charging/discharging once the operational mode is changed.

$$V(t, E) = \int_t^T P_1(\tau) \cdot \rho(\tau) \cdot d\tau. \quad (23)$$

$$V(t, E) = \min_{E(t+dt)} \{ \Delta V(E, E(t+dt)) + V(t+dt, E(t+dt)) \}. \quad (24)$$

$$\frac{d}{dt} E \approx \frac{E(t+dt) - E(t)}{dt}. \quad (25)$$

$$\frac{d}{dt} E_i = f_i(P_i, E_i). \quad (26)$$

$$\Delta V = \left\{ \begin{array}{ll} P_1(t) \cdot \rho(t) \cdot dt, & \text{in constraints} \\ \infty, & \text{otherwise} \end{array} \right\}. \quad (27)$$

$$E^*(t) = \arg \min_{E(t)} \{ \Delta V(E^*(t-dt), E(t)) + V(t, E(t)) \}. \quad (28)$$

$$V(t, \text{SOC}) = \int_t^T (P_{\text{total}}(\tau) - \frac{R}{V_1^2} \cdot P_{\text{total}}^2(\tau)) d\tau. \quad (29)$$

$$\frac{d}{dt} \text{SOC} = -\frac{\eta \cdot P_{\text{ES}}}{J_{\text{rated}}}. \quad (30)$$

The objective is to minimize the overall cost of energy import from the public grid, determined by incoming power at the PCC (23). The optimal solution is

computed recursively by the Bellman Eq. (24). The value function $V(t, E)$ is numerically computed by backward recursion. The process starts at the final time $t = T$ where the value function is known: $V(t, E) = 0$. The process continues until reaching $t = 0$ using a backward recursion step. The first derivative of energy is evaluated by (25). Power output of the storage device, $P_i(t)$, is evaluated. The storage state (26) is solved using known values of E_t and its first derivative E_t' , revealing $P_i(t)$. The storage device is replaced with an auxiliary $P - V$ source with $P = P_i(t)$, $V = V_{S,i}$. A network power flow analysis is computed using Gauss–Seidel, Newton–Raphson, or any other method, if the power flow solution complies with all network constraints, the differential ΔV is assigned a value according to the power at the PCC, $P_1(t)$. Otherwise, it is assigned a value of infinity (27). Having computed $V(t, E)$ over all times and energies, the optimal energy $E^*(t)$ may be evaluated. This is done by a forward recursion process. Known values of $V(t, E)$ are substituted in the Bellman equation to recover the optimal solution (28). The computation process starts at $t = 0$ and continues up to the final time $t = T$. Knowing the optimal energy path, all powers, voltages, and phase angles may be computed directly. $V(\cdot)$ is evaluated using backward recursion, scanning all possible paths of SOC over time. Then, the optimal function $SOC(t)$ is constructed by forward recursion (29). The storage state Eq. (30) gives the total power.

4 Numerical Simulations

A microgrid with four dispatchable units, one nondispatchable unit, one energy storage system, and five adjustable loads is used to analyze the proposed microgrid optimal scheduling model. The fuel and coal costs are obtained from the thermal power station. The cost coefficient is calculated based upon the maximum capacity of the generating units, incremental heat rate, fuel cost or coal costs (in Rs/kwhr), no load cost, etc. The values are taken randomly for numerical simulations. The characteristics of generating units, energy storage system and adjustable loads, the forecasted values for microgrid hourly fixed load, nondispatchable units' generation, and market price over the 24-h horizon are given in above tables, respectively (Fig. 2, Tables 1, 2, 3, 4, 5, 6, 7, 8, 9 and 10).

In grid-connected mode, the economic unit 1 is committed at the entire scheduling horizon as it offers a low-cost power. Units 2–4 are committed and dispatched at the maximum capacity when the market price exceeds cost coefficient of these units. The microgrid grid-connected operation cost is Rs 13,434. A unit in the microgrid is committed only when its cost coefficient is lower than the market price. It would accordingly generate its maximum power to sell the excess power to the main grid and increase microgrid savings (i.e., to further reduce the total operation cost). The microgrid would also discharge the energy storage system at peak hours, when the market price is at its highest, for the same economic reasons. In islanded operation, the iteration schedule results in a power mismatch which

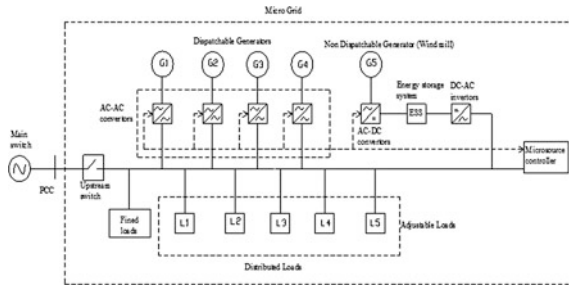


Fig. 2 Single line diagram of microgrid control system

Table 1 Characteristics of generating units

Unit	Type	Cost coefficient (Rs/Mwh)	Min-max capacity (Mw)	Min up/down time (h)	Ramp up/down rate (Mw/h)
G1	D	27.7	1–5	3	2.5
G2	D	39.1	1–5	3	2.5
G3	D	61.3	0.8–3	1	3
G4	D	65.6	0.8–3	1	3
G5	ND	0	0–1	–	–

D dispatchable
 ND nondispatchable

Table 2 Microgrid hourly fixed load

Time (h)	1	2	3	4	5	6
Load (Mw)	8.73	8.54	8.47	9.03	8.79	8.81
Time (h)	7	8	9	10	11	12
Load (Mw)	10.12	10.93	11.19	11.78	12.08	12.13
Time (h)	13	14	15	16	17	18
Load (Mw)	13.92	15.27	15.36	15.69	16.13	16.14
Time (h)	19	20	21	22	23	24
Load (Mw)	15.56	15.51	14.00	13.03	9.82	9.45

Table 3 Energy storage system

Storage	Capacity (MWh)	Min–max charging/discharging power (MW)	Min charging/discharging time (h)
ESS	10	0.4–2	5

generates Cut 1 based on the mismatch in islanding scenario for revising the obtained dispatchable unit commitment and the energy storage system schedule in the master problem. With the revised schedule, total mismatch is reduced. Since the

Table 4 Hourly market price

Time (h)	1	2	3	4	5	6
Price (Rs/Mwh)	15.03	10.97	13.51	15.36	18.51	21.8
Time (h)	7	8	9	10	11	12
Price (Rs/Mwh)	17.3	22.83	21.84	27.09	37.06	68.95
Time (h)	13	14	15	16	17	18
Price (Rs/Mwh)	65.79	66.57	65.44	79.79	115.45	110.28
Time (h)	19	20	21	22	23	24
Price (Rs/Mwh)	96.05	90.53	77.38	70.95	59.42	56.68

Table 5 Characteristics of adjustable load

Load	Type	Min–max capacity (Mw)	Required energy (Mwh)	Initial start-end time (h)	Min up time (h)
L1	S	0–0.4	1.6	11–15	1
L2	S	0–0.4	1.6	15–19	1
L3	S	0.02–0.8	2.4	16–18	1
L4	S	0.02–0.8	2.4	14–22	1
L5	C	1.8–2	47	1–24	24

S shiftable

C curtailable

Table 6 Generation of nondispatchable loads

Time (h)	1	2	3	4	5	6
G5	0	0	0	0	0.63	0.80
Time (h)	7	8	9	10	11	12
G5	0.62	0.71	0.68	0.35	0.62	0.36
Time (h)	13	14	15	16	17	18
G5	0.4	0.37	0	0	0.05	0.04
Time (h)	19	20	21	22	23	24
G5	0	0	0.57	0.60	0	0

mismatch is not zero, Cut 2 is generated which further revise the schedule of adjustable loads (Figs. 3 and 4).

If the mismatch reaches a value of zero which means that microgrid islanding criterion is satisfied and islanding is feasible to provide the optimal scheduling. Additional units are committed in each hour to ensure an uninterrupted supply of loads when the microgrid is islanded. These units are dispatched at their minimum capacity as their generation is not economical. In low price hours, the power is purchased from the main grid as much as possible, but the power purchase is reduced as the market price is increased and generation of local resources becomes

Table 10 Adjustable load schedule in islanded mode

	1	2	3	4	5	6	7	8	9	10	11	12	13	14	15	16	17	18	19	20	21	22	23	24	
L1										1	1	1	1	1	1										
L2															1	1	0	0	1						
L3																0	0	0							
L4														1	0	0	0	0	1	1	1	1			
L5	1	1	1	1	1	1	1	1	1	1	1	1	1	0	0	0	0	0	0	0	1	1	1	1	1

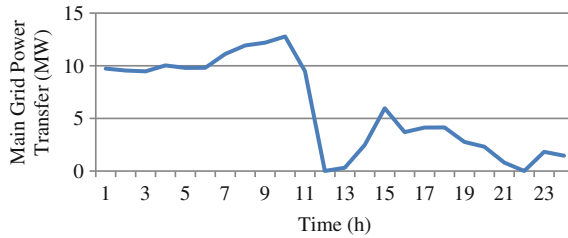


Fig. 3 Main grid power transfer in grid-connected operation

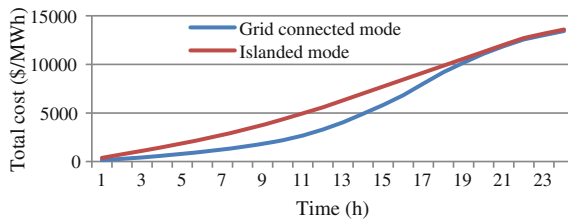


Fig. 4 Total cost of grid-connected and islanded mode operation

more economic. The minor differences in power transfer from the main grid in these two cases are a result of dispatchable units generation at their minimum capacity to enable a feasible islanding. The minimum generation of these units reduces the required power to be purchased from the main grid. The pairing of wind power with energy storage systems would serve to mitigate many of the negative characteristics of the wind which facilitates its synchronization with the power system. With renewable energy, the power fluctuations are present at different frequencies which results in distorted power output. Energy storage system (ESS) is a typical means of smoothing wind power generation fluctuations.

The energy management of the renewable energy system using ESS depends on the battery state of charge (SOC). The battery SOC needs to be controlled within a certain range as a result, the battery should be charged above valid limits for example $20 \% \leq SOC \% \leq 95 \%$ which can prevent the forced shut down of the ESS due to overcharge or over-discharge of batteries. The open circuit voltage of the battery terminal, current, power can be taken as a parameter to find optimal SOC as in (Fig. 5).

In this paper, the relationship between wind power and time is taken for calculating optimal Soc and optimal energy storage power. The optimization tool box in built with fmincon solver can be used to find the optimal scheduling for microgrid. But it finds only the local solution of the objective and not global solution. So this limits the use of the optimization tool box.

A price signal is unavailable for wind power, so a minimal price objective cannot be evaluated. So the power output of the microgrid can be maximized and the load

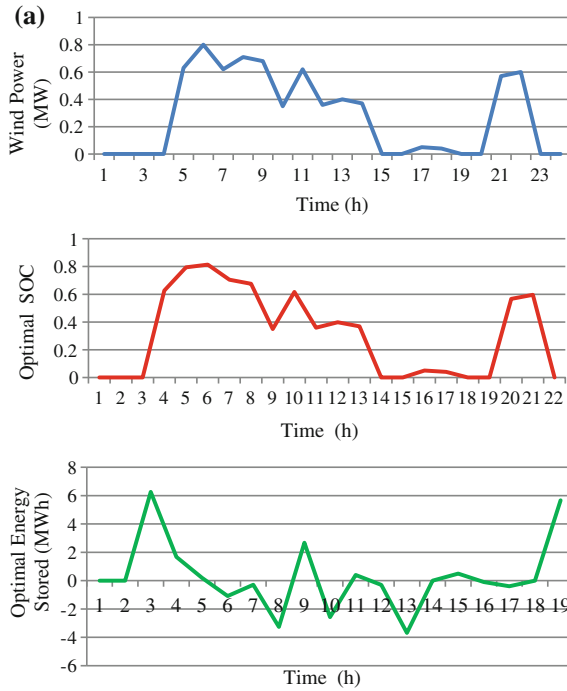


Fig. 5 Optimal SOC and optimal powers for different values of storage efficiency. **a** Storage efficiency $\eta = 1.0$. **b** Storage efficiency $\eta = 0.75$. **c** Storage efficiency $\eta = 0.5$. The graphs from *top* to *bottom*: wind power, optimal state of charge, stored energy in the battery storage system

shedding during islanding is also reduced by varying the rate of charge/discharge of energy storage system.

5 Discussions

Microgrids improve the power system economics by utilizing a variety of local generation resources, energy storage systems, and adjustable loads along with energy purchase from the main grid, and increase the reliability of local loads by ensuring an uninterrupted supply of loads when the main grid power is not available. The microgrid optimal scheduling is reinforced with islanded operation constraints to provide sufficient capacity for a smooth and uninterrupted supply of loads when switching to an islanded mode. The consumer decisions in scheduling adjustable loads are not changed unless it is required to obtain a feasible islanding solution. A dynamic programming analysis is used to provide the optimal scheduling for microgrid, to minimize the losses of energy storage system, to minimize the imported energy from the PCC when the market price is high and to

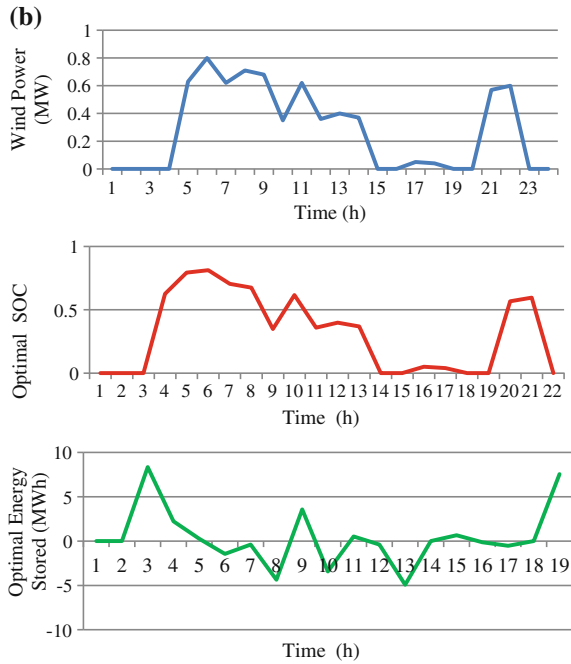


Fig. 5 (continued)

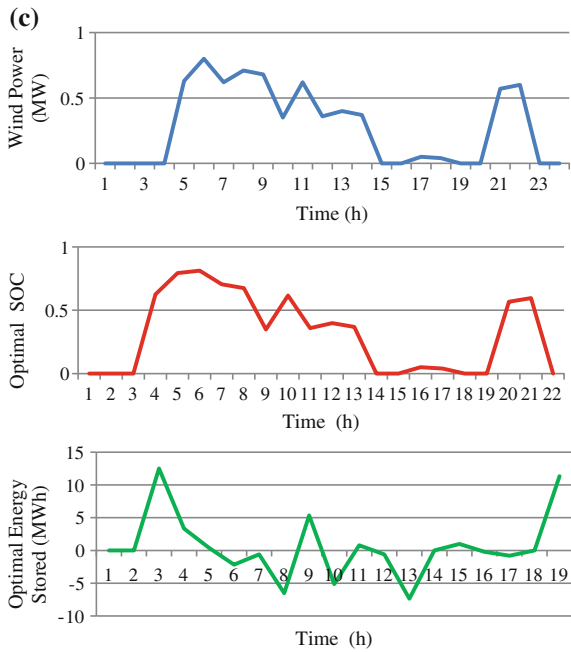


Fig. 5 (continued)

maximize the output power of microgrid. Optimal scheduling of microgrid, optimal stored energy, optimal state of energy is revealed by using forward–recursion. The cost function is evaluated by using backward recursion. The optimization tool provides only the local solution, but adding more constraints is possible. The dynamic programming approach provides global solution. But the main disadvantage is that numerical complexity grows with the number of additional components and storage devices.

6 Conclusions

This model proposes an efficient model for microgrid optimal scheduling in grid-connected mode and the islanding mode. The proposed model was analyzed through numerical simulations using matlab. The result indicates that when considering microgrid islanding, additional units, which do not necessarily offer economic merits, have to be committed and maintained online. Since the microgrid schedule is significantly changed due to additional commitments, there will be an increase in the microgrid operation cost. This small cost increase provides a huge benefit as the microgrid islanding without load interruption is ensured. The result determines the optimal schedule of dispatchable generating units, energy storage systems, and adjustable loads, along with the main grid power transfer to minimize the cost of supplying local loads.

References

1. Shahidehpour M. Role of smart microgrid in a perfect power system. In: Proceedings of the IEEE power and energy society general meeting. 2010.
2. Shahidehpour M, Clair J. A functional microgrid for enhancing reliability, sustainability, and energy efficiency. *Electr J*. 2012;25(8):21–8.
3. Hatziargyriou N, Asano H, Irvani MR, Marnay C. Microgrids: an overview of ongoing research, development and demonstration projects. *IEEE Power Energy Mag*. 2007;5(4):78–94.
4. Hou C, Hu X, Hui D. Hierarchical control techniques applied in micro-grid. *Proc. IEEE Conf. Power Syst. Technol. (POWERCON)*. Hangzhou, China;2010.
5. Tsikalakis AG, Hatziargyriou ND. Centralized control for optimizing microgrids operation. *IEEE Trans Energy Convers*. 2008;23(1):241–8.
6. Chowdhury S, Chowdhury SP, Crossley P. Microgrids and active distribution networks. *IET Renew Energy Ser*. 2009.
7. Flueck A, Li Z. Destination perfection. *IEEE Power Energy Mag*. 2008;6(6):36–47.
8. Olivares DE, Canizares CA, Kazerani M. A centralized optimal energy management system for microgrids. In: Proceedings of the power and energy society general meeting. 2011.
9. Hatziargyriou N, Contaxis G, Matos M, Lopes JAP, Kariniotakis G, Mayer D, Halliday J, Dutton G, Dokopoulos P, Bakirtzis A, Stefanakis J, Gigantidou A, O'Donnell P, McCoy D, Fernandes MJ, Cotrim JMS, Figueira AP. Energy management and control of island power

- systems with increased penetration from renewable sources. Proc IEEE-PES Winter Meeting. 2002;1:335–9.
10. Atwa Y, El-Saadany E, Salama M, Seethapathy R. Optimal renewable resources mix for distribution system energy loss minimization. IEEE Trans Power Syst. 2010;25(1):360–70.
 11. Chowdhury S, Chowdhury SP, Crossley P. Microgrids and active distribution networks. IET Renew Energy Ser. 2009.
 12. Khodaei A. Microgrid optimal scheduling with multi-period islanding constraints. IEEE Trans Power Syst. 2014;29.
 13. Kennedy S, Marden M. Reliability of islanded microgrids with stochastic generation and prioritized load. In: Proceedings of the IEEE powertech, Bucharest, Romania. 2009.
 14. Levron Y, Guerrero JM, IEEE, Beck Y. Optimal power flow in microgrids with energy storage. IEEE Trans Power Syst. 2013;28(3).

Voltage Sensitivity-Based Reactive Power Injection Using Fuzzy Inference System in Power System

Prem Pratik, Prem Prakash and R.C. Jha

Abstract Steady-state power system contingencies such as a overloading of transmission lines causes transmission line outages or generator outages, which tends to the situation of voltage instability that may lead to complete blackout. The main reason behind this instability is the inability of system to meet its reactive power requirement. This deficiency causes the bus voltage to deviate from its permissible limit at various buses in power system. Our main aim is to improve the voltage profile of the system by giving reactive power support at sensitive buses only; for this purpose, we are using fuzzy inference system (FIS) to determine the amount of reactive power to be injected at all sensitive buses by evaluating reactive power injection factor (RPIF) using sensitivity at the load buses, performance index of contingencies, and voltage at buses as *i/p*. Furthermore, we tried to reduce the number of buses by identifying most severe buses (where reactive support can be given without compromising with the voltage quality) according to the number of times of its voltage violations in each contingency. IEEE 24-Bus system is used for the simulation purpose.

Keywords Fuzzy inference system (FIS) · Performance index (PI) · Reactive power injection factor (RPIF) · Voltage profile · Voltage (V) · Reactive power (Q) · Per unit (PU)

P. Pratik (✉) · P. Prakash · R.C. Jha
BIT Mesra, Ranchi, Jharkhand, India
e-mail: Ppratik302@gmail.com

P. Prakash
e-mail: ppraksh@bitmesra.ac.in

R.C. Jha
e-mail: rcjha@bitmesra.ac.in

1 Introduction

Power system will be stable and reliable when it can withstand any kind of contingencies (outage of certain line or equipment of power system); so the security assessment has been gaining importance in present-day stressed operation of power system network. For reliable operation of power system, it is essential to maintain voltage at various buses within their stable limits under the case of increased power demand in the system, i.e., voltage stability [1–4]. So for determining system stability, reliability, and security we have to find out the severity of these contingencies which is defined as contingency ranking, where ranking of various contingencies is decided according to their severe effects on the system [5]. Various approaches are used for ranking purpose [6–13], here we have used PI ranking of contingencies [14]. Voltage sensitivity of a bus gives an idea about the weakest part of the system that is prone to voltage instability. A system is voltage stable if $V-Q$ sensitivity at all of its buses is positive and it will be voltage unstable if $V-Q$ sensitivity at any bus of the system is negative [15]. In fuzzy inference system (FIS), fuzzy rules are formed to determine the reactive power injection factor (RPIF) that would be injected at various buses. As reactive power transmission is limited when the power angle is large, even though sufficient voltage gradient is provided between sending end and receiving end, it will be beneficial to supply reactive power at the buses, also it will help to reduce transmission losses in the system [15–17]. We observed from load flow analysis that only certain buses are continuously violating the voltage limits in all cases of contingencies, so we tried to classify those buses according to the number of times of its voltage violations, i.e., more time voltage violates its permissible value more the bus will be affected in all contingencies situations and reactive support is given only on those severe buses and we will see that there will be more or less same voltage profile improvement.

The organization of present work is as follows in Sect. 2 there is the brief background of the concepts that has been used for evaluation of RIF. Section 3 discusses the steps that are taken for improvement of voltage profile. Section 4 discusses the load flow analysis that has been done on IEEE-24 bus system. Section 5 discusses the surface view and rules that are used for developing the FIS system, Sect. 6 discusses Results and Sect. 7 discusses the conclusions.

2 Theoretical Background

2.1 Contingency Ranking Based on Performance Index Ranking

It is a clear and simple analysis where an unclear setting of limit values is decided for the line flow and voltage for voltage stability analysis. Contingencies with

higher PI values will be more severe, accordingly their rank is decided, i.e., more severe contingencies will get higher rank and less severe one will have lower rank.

$$PI = \sum \text{All branches} \left(\frac{P_{\text{flow}}}{P^{\text{max}}} \right)^{2n} + \sum \text{All buses} \left(\frac{\Delta|E_i|}{\Delta E^{\text{max}}} \right)^{2m}$$

where

- P_{flow} is real power flow in line.
- P^{max} is maximum loading capacity of line.
- $\Delta|E_i|$ is the difference between voltage magnitude after load flow solution and base case voltage magnitude at bus i .
- ΔE^{max} is maximum voltage deviation allowed at any bus.
- m, n are integers, generally taken between 3 and 5.

2.2 V-Q Sensitivity

A/c to Newton Raphson load flow analysis:

$$\begin{bmatrix} \Delta P \\ \Delta Q \end{bmatrix} = \begin{bmatrix} J1 & J2 \\ J3 & J4 \end{bmatrix} \begin{bmatrix} \Delta \delta \\ \Delta V \end{bmatrix}$$

where

- $J1 = \frac{dP_i}{d\delta_i}$, $J2 = \frac{dP_i}{dV_i}$, $J3 = \frac{dQ_i}{d\delta_i}$, $J4 = \frac{dQ_i}{dV_i}$ they all are the elements of a Jacobean matrix.
- ΔP = Change in the magnitude of active power at bus i .
- ΔQ = Change in the magnitude of reactive power at bus i .
- $\Delta \delta$ = Change in the voltage angle at a bus.
- ΔV = Change in the voltage magnitude.

As ΔP is less sensitive to the change of ΔV and ΔQ is less prone to the change of $\Delta \delta$ so $J2$ and $J3$ tends to zero. The diagonal elements of $J4$ indicates the degree of weakness of the bus- i . The bus with greater value of $\frac{dQ_i}{dV_i}$ is a strong bus and weak bus will have less value of $\frac{dQ_i}{dV_i}$. To maintain stability, there is a probability of increase in voltage V as Q is increased. Reciprocal of $J4$ gives the sensitivity of the Voltage at bus w.r.t to reactive power. For certain change in voltage at the bus, we have to inject more reactive power at that bus to increase its voltage if its sensitivity is less and less reactive power if its sensitivity is high.

2.3 Fuzzy Inference System

It provides an excellent framework for modeling the uncertainty in human reasoning with the help of morphological variable with membership function. Voltage alone cannot be used to determine the voltage security as increased uses of compensating devices raises voltage to normal levels even when sufficient reactive support is absent. So FIS is developed with three *ip*, voltage at the buses for particular contingency, PI rank of the contingency, and sensitivity of the bus. Fuzzy rules are used for analyzing the severity of buses in post contingencies conditions and reactive power support factor is determined accordingly. Membership function is assigned to each of the input and output. Membership function of each set defines the fuzziness of a value to lies within particular sets.

Bus voltage

Post-contingency voltages are divided into three fuzzy sets low, medium, and high. Gaussian membership function is used which is defined as (membership width (σ), center (c)), in the range of voltage from (0.88, 1.2) where voltage membership ranges is according to Table 1.

Performance index

Performance index of contingencies is used here as second *ip* to the FIS. PI rank is given to all of the contingencies depending on their severity. Here PI rank is given for all line outages between the range of 1–33. Table 2 shows PI rank membership functions. Gaussian membership function is used here.

Sensitivity of the bus

Sensitivity of the load buses is considered for load buses only as for generator buses it will be zero. Its range is taken between (0 and 0.1). More sensitivity at the load buses guarantees more improvement in the bus voltages with less injection of reactive power. Table 3 shows membership function of sensitivity. Gaussian membership function is used here.

Reactive Injection Factor (RIF)

It is the desired output of the system. Trim membership function is used for this RIF. Its range lies between (0 and 2) (Table 4).

Table 1 Voltage membership function

Membership function	Membership width (σ)	Centre
Low	0.0672	0.89
Medium	0.06	1.02
High	0.0573	1.14

Table 2 Voltage membership function

Membership function	Membership width (σ)	Centre
High	7.23	1.423
Medium	4.32	18.14
Low	4.3	34.8

Table 3 Sensitivity membership function

Membership function	Membership width (σ)	Centre
Low	0.0136	0.00835
Medium	0.0192	0.03181
High	0.0216	0.0817

Table 4 RIF membership function

Membership function	Membership width (σ)	Centre
Low	0.4	0
Medium	0.3	1
High	0.4	2

Fig. 1 Proposed FIS algorithm

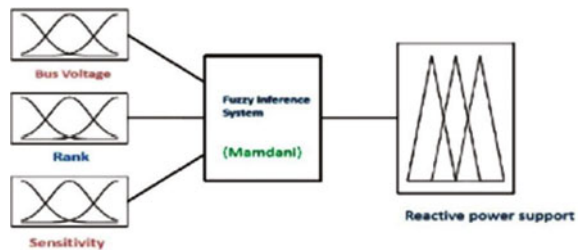


Figure 1 shows the proposed FIS algorithm where three *inp* are voltage, sensitivity, and PI rank and Reactive injection factor is the output of the FIS.

3 Proposed Methodology

- Run Newton Raphson load flow analysis for IEEE-24 bus system.
- Calculate voltage at various buses for various contingencies, PI rank of the contingencies, and sensitivity of the load buses from the load flow analysis.
- Calculate RPIF using FIS with these three *inp*, i.e., voltage, PI rank of contingencies, and sensitivity of the bus.
- Multiply RPIF with the reactive power flow at particular buses in post-contingency situations.
- Given that reactive power support at various load buses of the system and once again run the load flow, we will observe that voltage profile has been improved in later situations even for contingencies.
- Furthermore to minimize the time of operation, calculation and losses in the system we had decided to inject reactive power only at most severely affected buses in all of the contingencies.

4 Load Flow Analysis

IEEE-24 bus system is taken for study purpose. Newton load flow analysis is done for normal network and for all case of contingencies and voltages at various buses, sensitivity of load buses, and PI rank are calculated. Figure 2 shows the configuration of IEEE-24 bus system.

- 2, 7, 13, 14, 15, 16, 18, 21, 22, 23 are 10 generator buses present in this network.
- 3, 4, 5, 6, 8, 9, 10, 19, 20, 17, 24, 11, 12 are load buses in the system.
- 12th bus is taken as slack bus in the system.
- By running N-R load flow analysis on IEEE24-bus system for all contingencies, we identified that load buses are most severely affected due to Line outages also

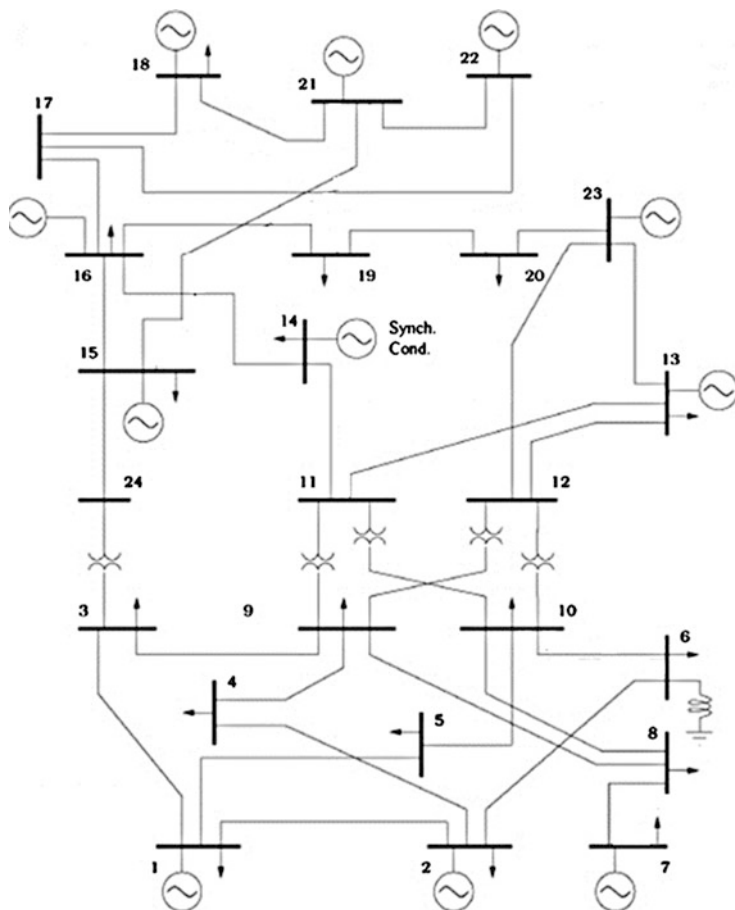


Fig. 2 IEEE-24 bus system

Table 5 Number of voltage violations at different load buses (for 33 line contingencies)

Bus number	Number of times voltage below 0.94 pu	Number of times voltage below 0.94–0.96 pu	Number of times voltage below 0.96–0.98 pu
3	32	1	0
4	1	31	1
5	1	2	30
8	0	33	0
9	1	31	1
10	1	11	21
11	1	15	17
14	9	24	0
17	0	0	1
19	1	8	23
20	0	0	2
24	16	16	16

we identified that 3, 4, 5, 6, 8, 9, 10, 11, 14, and 24 are most severely affected buses in all of the load buses.

- In Table 5, we calculated number of voltage violations for all 33 line contingencies and we identified that 17 and 20 are least severe load buses so we try to improve voltage profile of the system without giving reactive support on these buses.

5 Output Surface of Proposed FIS Algorithm

Figures 3, 4 and 5 show the same output surface obtained (with different combinations of i/p 's) from the developed FIS algorithm. From figures we see that the RPIF factor will be high for the low voltage, high sensitivity, and low rank; and

Fig. 3 Surface view of FIS (with voltage and sensitivity as i/p)

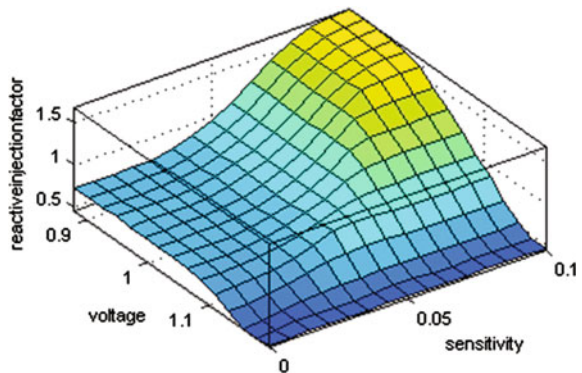


Fig. 4 Surface view of FIS (with rank and sensitivity as i/p)

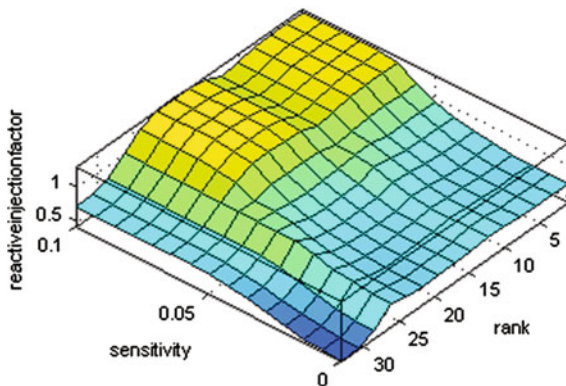
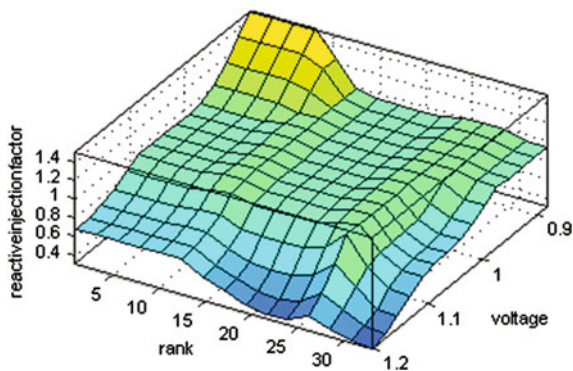


Fig. 5 Surface view of FIS (with rank and voltage as i/p)



RPIF will be low for high voltage, low sensitivity, and low rank. This surface is *a/c* to the theory that if the contingency will be severe then the voltage at the buses will go much below the acceptable limits, and accordingly we have to supply reactive power at that bus considering sensitivity of that bus. Totally, 27 rules has been formed to achieve our desired RPIF, e.g., if voltage is low and sensitivity is high and PI rank is high then RPIF will be high.

6 Results

Table 6 shows the results of the simulation done on IEEE-24 bus system in the case of line outage 6–10 which is the most severe contingency in the system, we had seen that voltage at various load buses dips down during contingency (column 3) now calculating RPIF (column 4) for various load buses using FIS and multiplying this factor with total reactive power flow on that bus during contingencies (column 6) we found our reactive support at various load buses, now by providing that

Table 6 Voltage profile improvement for line outage 6–10 (PI rank = 1)

Bus number	Voltage at the bus under normal condition	Voltage at the bus under contingency	Reactive power injection factor for contingencies	Reactive power flow at various buses under normal condition	Reactive power flow under contingencies at various buses	Reactive power injected at the buses under contingencies (RIP [®] -reactive flow at that bus)	Reactive power to be injected at the buses under contingencies (for selected severe load buses) (RIF [®] -reactive flow at that bus)	Voltage after reactive injection for all load buses under contingencies	Voltage after reactive injection for selected load buses under contingencies	Voltage after reactive injection at buses under normal condition (1.25 [®] -reactive flow at buses)
1	1.0	0.98	0	6	55.191	0	0	1.0	1.0	1.0
2	1.0	0.97	0	18	1.304	0	0	1.0	1.0	1.0
3	0.937	0.9292	1.16	37	37.00	42.92	42.92	0.975	0.975	0.984
4	0.958	0.9414	1.27	15	15.00	19.05	19.05	0.984	0.984	0.987
5	0.969	0.9559	0.996	14	14.00	13.944	13.944	0.986	0.986	0.993
6	0.954	0.7617	1.5	28	28.00	42	42	0.921	0.921	0.997
7	1.00	1.0	0	36.429	40.251	0	0	1	1	1.00
8	0.954	0.9518	1.02	35	35	35.7	35.7	0.978	0.978	0.985
9	0.957	0.9517	1.02	36	36	36.72	36.72	0.983	0.983	0.989
10	0.964	0.9578	0.986	40	40	39.44	39.44	0.984	0.984	0.997
11	0.961	0.9589	0.98	0	0	0	0	0.974	0.974	0.980
12	1.0	1	0.807	221.43	237.047	178.69	0	1.0	1.0	1.0
13	1.0	1	0	47.951	51.560	0	0	1.0	1.0	1.0
14	0.948	0.9477	0	39	39.00	0	0	0.960	0.960	0.969
15	0.970	0.9700	0	24	34.856	0	0	0.980	0.980	0.990
16	0.970	0.9700	0	10	11.241	0	0	0.980	0.980	0.990
17	0.989	0.9894	0.845	0	0.000	0	0	0.993	0.993	0.996
18	1.0	1	0	65.489	65.228	0	0	1.0	1.0	1.00
19	0.967	0.9674	0.938	37	37	34.706	34.706	0.982	0.981	0.988
20	0.984	0.9837	0.867	26	26	22.542	0	0.992	0.988	0.991

(continued)

Table 6 (continued)

Bus number	Voltage at the bus under normal condition	Voltage at the bus under contingency	Reactive power injection factor for contingencies	Reactive power flow at various buses under normal condition	Reactive power flow under contingencies at various buses	Reactive power to be injected at the buses under contingencies (for all buses) (RIF [®] -reactive bus)	Reactive power to be injected at the buses under contingencies (for selected severe load buses) (RIF [®] -reactive flow at that bus)	Voltage after reactive injection for all load buses under contingencies	Voltage after reactive injection for selected load buses under contingencies	Voltage after reactive injection at buses under normal condition (1.25 [®] -reactive flow at buses)
21	1.0	1	0	22.347	22.597	0	0	1.0	1.0	1.0
22	1.0	1	0	44.94	44.088	0	0	1.0	1.0	1.0
23	1.0	1	0	12.981	11.994	0	0	1.0	1.0	1.0
24	0.943	0.9382	1.1	0	0.00	0	0	0.962	0.962	0.974

Table 7 Active and reactive losses in the system during different situations under 6–10 line outage

Condition of system	Active loss of whole system (mw)	Reactive loss of whole system (mvar)
During line outage 6–10	85.826	172.572
When 1.25 times reactive power is injected at all buses	75.1752	70.001
When reactive power support is given only at severe buses using FIS	70.459	38.445

support on buses we find that there will be gradual improvement in voltage profile of overall system (column 9). Also by neglecting the least load severe buses (17 and 20), we get more or less same voltage profile improvement (column 10).

Table 7 shows active and reactive losses in the system during line outage 6–10 with and without reactive power support as we can see that losses increases during contingency but it considerably reduced to lower values when 1.25 when reactive support was given at various buses, also the losses particularly reactive losses gradually reduced when we give reactive support only on severe buses (using FIS).

Figure 6 shows how voltage profile improved under contingencies when reactive power is injected at selected buses. Also we can see that voltage profile is approximately similar when reactive power is given, respectively, at selected severe buses and at all load buses.

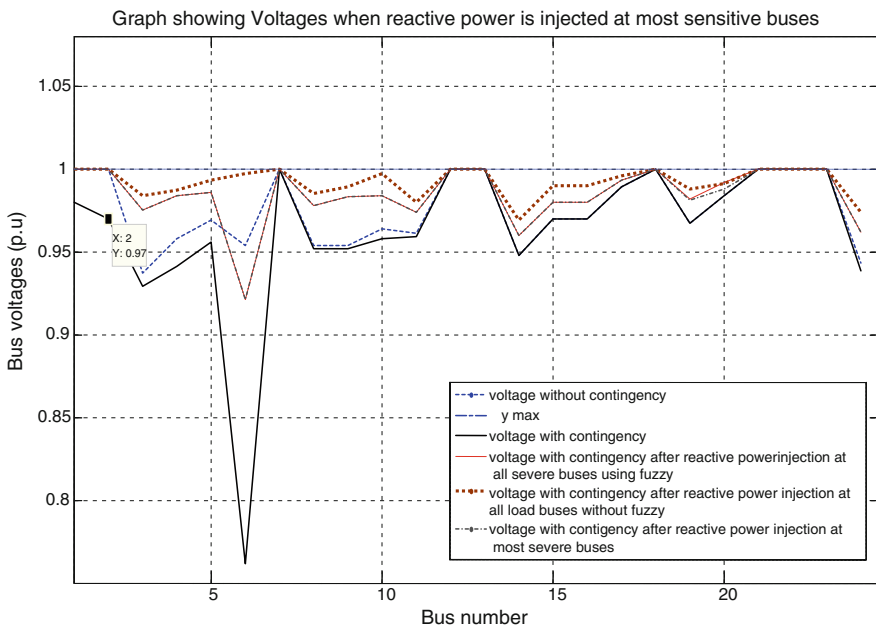


Fig. 6 Voltage profile improvement under line outage 6–10

7 Conclusion

As FIS is developed to inject reactive power at the bus depending upon the PI rank of contingencies, sensitivity of the bus and its voltage hence proposed method give minimum amount of reactive power to be injected to maintain voltage profile as seen from Fig. 6. From Table 7, we concluded that losses also reduced to lower values when reactive support was given on selective buses only furthermore by decreasing the number of buses where the reactive power being injected; we observe somewhat same voltage profile improvement so it is also tends to be economical approach.

References

1. Taylor CW. Improving grid behavior. *IEEE Spectr.* 1999;36:40–5.
2. Wadhwa CL. *Electrical power systems*. 6th ed. India: New Age International Publishers; 1983.
3. Kundur P. *Power system stability and control*. New Delhi: Tata McGraw-Hill; 1994.
4. Swe PL, Swe W, Lin KM. Effects of tap changing transformer and shunt capacitor on voltage stability enhancement of transmission networks. *World Acad Sci Eng Technol.* 2011;555–8.
5. Veenavati JPM, Khardenvis MD. Contingency analysis of power system. *International conference on emerging frontiers in technology for rural area (EFITRA)*. 2012.
6. Garg S, Prakash P, Jha RC. A new fast contingency ranking method for modern power system. *Int J Appl Eng Res.* 2013;8(6):65–8. ISSN:0973-4562.
7. Clerk Maxwell J. *A treatise on electricity and magnetism*, 3rd ed., vol 2. Oxford: Clarendon; 1892. p. 68–73.
8. Hussain Z, Chen Z, Thogersen P. Fast and precise method of contingency ranking in modern power system. *IEEE Jordan Conf Appl Electri Eng Comput Technol.* 2011;1–7 (Jordan).
9. Karbalaie F, Soleymani H, Afsharnia S. A comparison of voltage collapse proximity indicators. In: *Proceedings of international power electronics conference*. 2010. p. 429–32.
10. Srinivas TSNRK, Reddy KR, Devi VKD. Composite criteria based network contingency ranking using fuzzy logic approach. *IEEE international advance computing conference, Patiala, India; 2009*. p. 654–7.
11. Chaturvedi KT, Pandit M, Srivastava L, Bhatele RP. Voltage contingency ranking of a practical power network using hybrid neuro-fuzzy system. *Joint international conference on power system technology and IEEE power India.* 2008; p. 1–5.
12. Zhao J, Chiang HD. A enhanced contingency selection method with respect to multiple contingencies for on-line voltage stability assessment. *Int Conf Power Syst Technol.* 2006;1–6.
13. Ruhle O, Lerch E. Ranking of system contingencies in DSA systems-first experiences. *IEEE Power Energy Soc Gen Meet.* 2010;1–6.
14. Krishnakumar B, Soundarajan SK, Gnanadass R. Fuzzy based contingency assessment using performance indices with masking effect. *IEEE Students' Conf Electr Electron Comput Sci.* 2012;1–5.
15. Jayaraman J, Sekar A. Study of reactive power/voltage sensitivities in interconnected power system networks. *42nd South Eastern symposium on system theory, Tyler, Texas, USA; 2010*. p. 161–4.
16. Sul JA, Molinas M. Properties of reactive current injection by AC power electronic systems for loss minimization. *15th international conference on power electronics and motion control.* 2012. p. LS2c.3-1–LS2c.3-8.
17. Qin W, Wang P, Han X, Du X. Reactive power aspects in reliability assessment of power systems. *IEEE Trans Power Syst.* 2011;26(1):85–92.

Residential House Electrical Energy Audit Case Study with ETAP

K. Keerthi Jain, N. Kishore Kumar, S. Muralikrishanan and L. Ramesh

Abstract The economic development of a country is often closely linked to its consumption of energy. Although India ranks sixth in the world so far as total energy consumption is concerned, it still needs much more energy to keep pace with its development objectives. The power demand in India will be increased by 80 % by the year 2012–2040 and the expected demand in year 2017 would be nearly 300 GW. The government has taken new steps for the development of renewable energy sources and less consideration in conservation of electrical energy in the society. According to the current scenario of the increase in the demand, this work executed to conduct energy audit in a residential house with suitable recommendation through ETAP. The single line diagram of the house with and without recommendation is simulated in ETAP with necessary data collected from the house. There are three recommendations suggested in this paper to the consumer for implementation to reduce the tariff to 50 %.

Keywords Energy saving · Energy audit and renewable energy

1 Introduction

The energy audit is a methodology to reduce the consumption and by this method there is a benefit to the government and also to the consumers. Energy audit is a process [1] of checking how energy is used and identifying the areas where wastage

K. Keerthi Jain (✉) · N. Kishore Kumar · S. Muralikrishanan · L. Ramesh
MGR Vision 10MW, Dr. M.G.R Educational and Research Institute, Chennai, India
e-mail: keerthijain@live.com

N. Kishore Kumar
e-mail: natarajkishore11@gmail.com

L. Ramesh
e-mail: raameshl@rediffmail.com

can be minimize if not totally eradicate. Energy audit consists of several tasks which can be carried out depending up on the type of audit and the function of audit it is a periodic activity to ascertain the objective of energy usage and the amount of wastage energy can be calculated and minimized by collecting the historical data, age of equipments, efficiency of the equipments, etc. Energy management [2] is the techno-managerial activity to achieve judicious and effective energy consumption pattern to ensure maximum profit and survival in a competitive world. Literature shows that the potential of increasing energy efficiency is large, and that most of the potential has very favorable economics. It is well fact that one unit of energy saved at consumption avoids energy of three units of fresh capacity addition.

The present installed capacity of electric power generation in India is 255.012 GW and the total annual generation of electricity from all types of sources is 1102.9 TWh. The power generation and the load demand are about 300 GW by the year 2016–2017. The possible solution to match the generation and demand is by increasing power generation and energy conservation measures. As a developing country it is not possible to install the full load capacity instantly, looking over this scenario the initial work has been started on energy conservation through electrical energy audit under MGR Vision 10 MW. MGR Vision 10 MW was initiated by Dr. M.G.R Educational and Research Institute (University) to save 10 MW of energy within a period of 10 years. The team members have completed energy audit for 25 houses and 2 commercial buildings and submitted recommendation to implement. The post audit outcome achieved for two houses after 6 months of implementation.

The authors presented the comparative [3] energy audit analysis of three house with manual recommendation. This paper presents the audit recommendation of a residential house with analysis through ETAP [4].

2 Procedure

How energy audit is done in home? The answer to the question is given, the first initiative is for going for presite work, in this first we decide the location were to conduct this energy audit, for example, in home, industry, schools, etc. An execution procedure model is given below which will give a brief knowledge that how an energy audit is done and the recommendation is given to the clients as per the procedure to get an appropriate result based on the consumption and also reducing the energy tariff in electricity bills. The main vision for this auditing is to bring awareness among the society and save the demand for the nation. The government is behind the ways to generate power to reduce the demand, but we are taking initiatives to reduce the demand by electrical energy audit and this is our vision of 10 MW. The motto behind it is “Save Energy to Reduce Demand.”

We have made an executive activity to conduct this electrical energy audit and is given below:

- Collect all the load details with a maximum demand of the electrical equipment.
- Calculate the usage, load after single line diagram put the values in ETAP.
- Plot real-time load curve by taking the energy meter KWHR for 20 days.
- Calculate the connected load with respective to single line diagram.
- Plot a graph in between years and Tariff.
- Identify and calculate the unnecessary usage of power wastage in the layout with graph.
- Draw the power utilization chart with respect to the Layout.
- Calculate the daily utilization of power by all the equipments and convert to pie chart.
- Data collection of all the major equipments and find out the performance.
- Interaction about the energy usage with suitable survey.
- Identify the energy saving and conservations opportunity.
- Report on suitable recommendation with existing and implementation suggestions.
- Plot cost benefit analysis with breakeven chart.
- Check the earth resistance and report on the status of earthling in that house.
- Provide awareness on electrical safety to the person there.

Submission of suitable energy audit report with breakeven analysis chart to the customer with the above procedure to get best results. It is advisable to use the benefits of renewable energy and simulating it in the ETAP software and provide them the best recommendation to reduce electrical consumption by renewable sources.

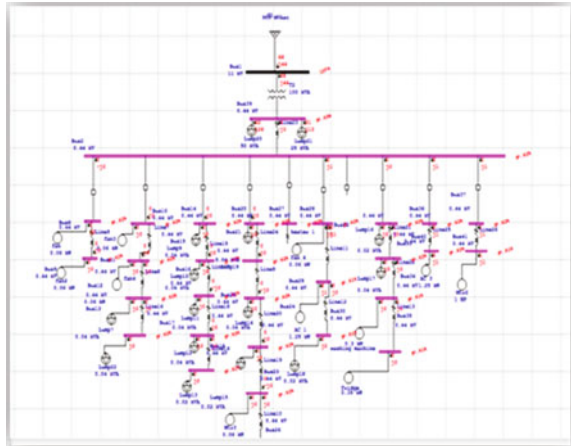
3 Data Monitoring

The following information is collected for analysis of single line diagram, age of equipments, tariff details, real-time curve, wattages, and daily utilization chart.

3.1 ETAP Single Line Diagram

The layout of the home is drawn using the ETAP simulation software as shown in Fig. 1 where all the uses are Connected to the load by which the load analysis is done. It is seen that the load is not balanced and also the consumption of the equipments is on the higher side. According to this, the recommendation is coated to reduce the electrical energy consumption and reduce the tariff bill.

Fig. 1 ETAP single line diagram



3.2 Tariff Details

The tariff details in the graph are shown below where the consumption is above 500 units and the tariff bill is higher during summer because of the use of an air conditioner as air conditioner consumption is high. Hence, the monthly consumption bill rises during the summer when compared to winter as shown in the Fig. 2.

Fig. 2 Tariff details



3.3 Daily Utilization Chart

The daily utilization chart is given in the Fig. 3 and the total consumption of the each appliance used in one single day is taken and plotted in the graph. The graph shows the utilization of each appliance that is used daily.

3.4 Age Equipments

According to each appliance in the house, the age of each appliance is also taken in which the age of the equipment is taken and plotted in the graph as shown in Fig. 4 so that we may find the equipment age and its efficiency. A graph is given below for the age of equipments.

Fig. 3 Daily utilization chart

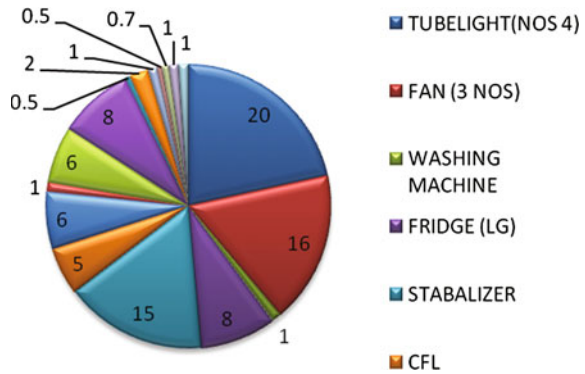


Fig. 4 Age of equipments

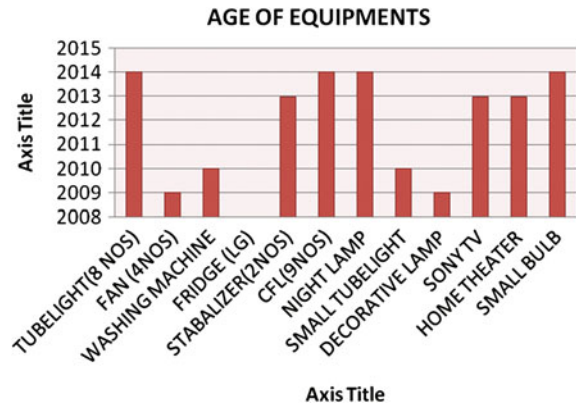
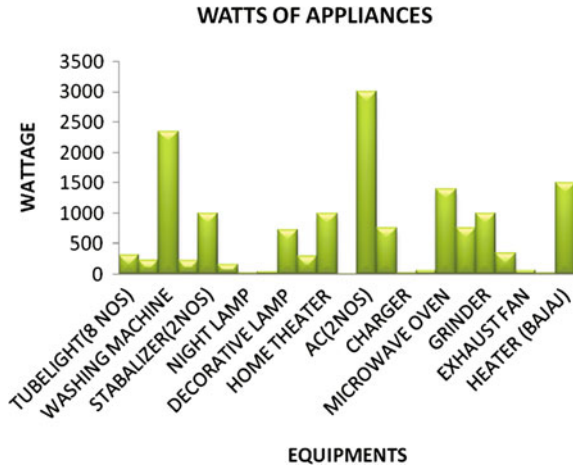


Fig. 5 Watts of appliances



3.5 Wattage of Appliance

According to a survey taken at the time of auditing, the wattage of the each appliance is taken and plotted in the graph as given in Fig. 5. The appliances given below gives the wattage of each appliance and their consumption is based according to the wattage that is given below.

3.6 Real-Time Load Analysis

From the analysis of load, it is seen that there is no balanced load on the system and due to which the power factor is also affected a lot by which the rated star appliances does not get the units that is labeled according to the BEE report.

The load analysis in the Fig. 6 shows the consumption of load and it is clear that the load is not in balanced condition.

3.7 ETAP Voltage Load Analysis

According to the ETAP simulation software, the single line diagram is drawn as shown in Fig. 7. As per this, the load flow analysis is done using the Newton-Rapson method by which the graph is drawn below where the voltage and the buses are determined.

Fig. 6 Real-time load analysis

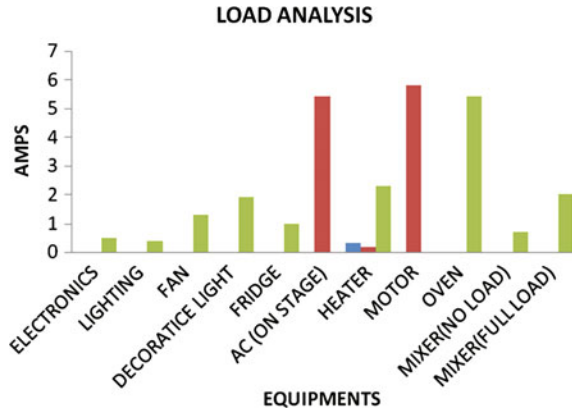
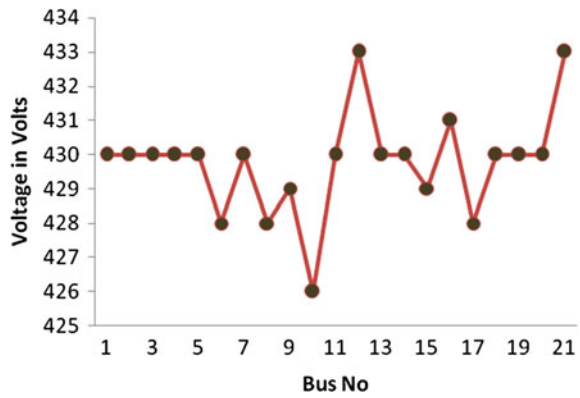


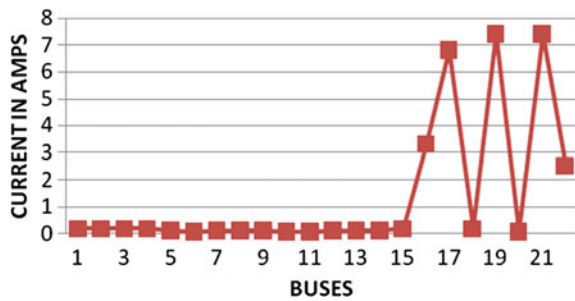
Fig. 7 ETAP load analysis by voltage



3.8 Etap Current Analysis

According to the ETAP simulation software, the single line diagram is drawn as shown in Fig. 8 as per this the load flow analysis is done using the Newton-Rapson

Fig. 8 ETAP load analysis by current



method by which the graph is drawn. The graph that is given below shows the current in amps of each equipment that is connected to the circuit breaker through buses.

4 Recommendation

According to the layout and ETAP simulation, recommendations are given below by which the client can get effective differences in their tariff bills and also in the conservation of electrical energy and a beneficial breakeven chart is represented to get the payback time for the customer.

4.1 Recommendation Without Investment

As per the ETAP simulation, layout and analysis of equipments recommendation are given below without investment by which some amount of electrical energy can be conserved.

- a. Metal cupboard should be removed from the bedroom as metal absorbs a lot of cooling due to which the power consumption of AC will be high and may also decrease the Freon level in it.
- b. As per the site visit, we saw dust particles in tube light, fans, and AC.
- c. Dust particles in fans weigh tens the fan blades due to which it starts drawing large amounts of power and causes the coil to get heated and damaged.
- d. In tube light, due to dust particles the lumens gets reduced.
- e. In AC, if the filters do not clean, cool air supply gets reduced and it also starts drawing large amount of current.
- f. In refrigerator, regular defrost manual—defrosting refrigerator and freezers; as frost builds up, it will increase the amount of energy needed to keep the motor running.
- g. Avoid putting hot and warm food and also avoid using big vessels inside the fridge.
- h. Do not open the doors of the refrigerator frequently. As it costs around 0.15 paisa.
- i. Proper dusting and cleaning of exhaust fan should be done.
- j. Using tube light in kitchen is good. Using CFL in the morning and tube light in the night is advisable.

Preventive Measures In this layout of the home, there is no preventive measure and no knowledge regarding electrical safety; so it is recommended mandatory to have preventive measure and electrical safety at the times of hazards.

- a. Allow only a qualified person to attend to your electrical repairs
- b. Service your electrical equipment at frequent intervals through a competent electrician
- c. In case of a short circuit or a fire, switch off the mains instantly. Make sure that you have easy access to switch off the supply source
- d. Make sure your extension cords are free from cuts, improper insulation, or joints
- e. Use switches of suitable current rating and preferably with indicators to indicate whether the switch is ON/OFF
- f. Use appliances with three pin plugs and connect them to three pin sockets
- g. Switch off electrical appliances when not in use.

4.2 Recommendations with Investment

Replacement of refrigerator In this home, it is seen that the most of the power that is drawn is from using AC, motor, tube light, and fridge. These are the four equipments that are used every day in home in which refrigerator is not star rated. It is highly recommended to replace the refrigerator with a star rated one since the same will consume less amount of power as given in Tables 1 and 2 (Fig. 9).

Replacement with LED According to the site review, we can see that florescent lights are used a lot, so according to that we can go for recommendation for using LED in this houses. LED has 2 years of warranty and it also saves the consumption of units compare to the CFL and tube light, this shows the results that LEsD is very much effective and also very useful in consumption of electrical energy as given in Table 3

Replacement with star rated fans It is seen that the fans used in this house are not star rated, so according to the layout the recommendation is given to change two fans that is given in Table 4 into star rated for effective reduction in power consumption and bill.

ETAP output with investment The simulation output is given below in Fig. 10 for recommendation with investment in this graph the load flow of star-rated appliances are given as per the recommendation given above by which it is seen that the power conservation is seen and reduction in tariff bills.

4.3 Recommendation with Dg

As we all know that solar energy has become an important source for generation of electricity. If the home is fully operated with solar energy by installing solar panels, the client may save money after certain period and can also sell electricity.

Table 1 Star rated refrigerator

Present energy usage	
Total number of refrigerator	1
Total number of watts	$1 * 225 = 225 \text{ W}$
Total number of watts annually	$225 * 20 * 365 = 1,642,500 \text{ W}$
Total number units consumed	$1,642,500/1000 = 1642.5 \text{ units/year}$
Cost annually	Rs. 4927.5
If the refrigerator is replaced by 3 star rated refrigerator of 250 L	
Total number of refrigerator	1
Star rated	3
Energy consumption kWh	626
Electricity cost per year	$626 * 3 = 1878$
If the refrigerator is replaced by 5 star rated refrigerator of 250 L	
Total number of refrigerator	1
Star rated	5
Energy consumption kWh	400
Electricity cost per year	$400 * 3 = 1200$
Saving for 3 star rated refrigerator	
Energy saved	$1642.5 - 626 = 1016.5 \text{ units/year}$
Money saved	$\text{Rs. } 4927.5 - \text{Rs. } 1878 = \text{Rs. } 3050 \text{ per year}$
Saving for 5 star Rated refrigerator of 250 L	
Energy saved	$1642.5 - 400 = 1242.5$
Money saved	$\text{Rs. } 4927.5 - \text{Rs. } 1200 = \text{RS. } 3727.5 \text{ per year}$
Payback time	
Energy saving star rated Refrigerator unit price	Rs. 15,000 for 250 L 3 star
	Rs. 22,100 for 250 L 5 star
Total investment	$1 * 15,000 = \text{Rs. } 15,000$
	$1 * 22,100 = \text{Rs. } 22,100$
Payback time	$(\text{Investment cost/annual saving}) * 12 \text{ months}$
$(15,000/3050) * 12 = 59 \text{ months}$	
$(22,100/3727.5) * 12 = 71 \text{ months}$	

5 Energy Saving with and Without Audit

According to the layout of the home, the recommendation is given with the ETAP simulation software and the graph is shown in Figs. 11 and 12 with audit and without audit in which it is differentiated in two parts, i.e., high-load analysis and low-load analysis by which the reduction of tariff bill is seen and also the current is reduced.

Figure 13 shows that the unit consumption is reduced to 60 % if the consumer will implement all the recommendations in a period of time.

Table 2 Replacement with LED

Present energy usage	
Total number of Tubelight need to change	3
Total number of watts	$3 * 40 = 120 \text{ W}$
Number of hours in a year	$8 \text{ h} * 365 \text{ days} = 2920$
Total number of watts annually	$120 * 8 * 365 = 350,400 \text{ W}$
Total units consumed	$350,400/1000 = 350 \text{ units/year}$
Cost annually	1050 Rs
If all the TL (3) are replaced by LEDs	
Total number of LED	3
Total number of watts	$3 * 10 = 30 \text{ W}$
Total number of watts annually	$30 * 8 * 365 = 87,600 \text{ W}$
Total number of units consumed	$87,600/1000 = 87 \text{ units per year}$
Cost annually	262 Rs
Saving	
Energy saved	$350 - 87 = 263 \text{ units per year}$
Money saved	789 Rs per year
Payback time	
LEDs	Rs. 650
Total investment	$3 * 650 = \text{Rs. } 1950$
Payback time	$(\text{Investment cost}/\text{annual saving}) * 12 \text{ months}$
$(1950/789) * 12 = 29 \text{ months}$	

Table 3 Replacement with star rated fan

Present energy usage	
Total number of ceiling fan	4
Total number of watts	$4 * 60 = 240 \text{ W}$
Total number of watts annually	$240 * 7 * 365 = 613,200 \text{ W}$
Total number of units consumed	$613,200/1000 = 613.2 \text{ units per year}$
Cost annually	$613.2 * 3 = \text{Rs. } 1840$
If all the ceiling fans (2) are replaced by energy saving models	
Total number of ceiling fan	2
Total number of watts	$2 * 40 = 80 \text{ W}$
Total number of watts annually	$80 * 7 * 365 = 204,400 \text{ W}$
Total number of units consumed	$204,400/1000 = 204.4 \text{ units per year}$
Cost annually	$204.4 * 1.5 = \text{Rs. } 306.6$
Saving	
Energy saved	$613.2 - 204.4 = 408.8 \text{ units per year}$
Money saved	$1840 - 306.6 = \text{Rs. } 1533 \text{ per year}$
Payback time	
Energy saving/unit price	Rs. 1700
Total investment	$2 * 1700 = \text{Rs. } 3400$
Payback time	$(\text{Investment cost}/\text{annual saving}) * 12 \text{ months}$
$(3400/1533) * 12 = 26 \text{ months}$	

Fig. 9 Comparisons of star rated refrigerator

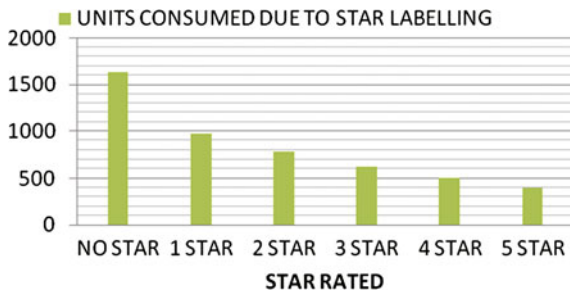


Table 4 Recommendation with DG

Solar panel capacity	1 kWp
Cost for 1 KWp solar panel	Rs. 85,000
Subsidy (30 %)	Rs. 20,000
Final investment cost	Rs. 85,000 – 20,000 = Rs. 65,000
Solar power generation	
Solar power generation Chennai	4–5 kW per day for 1 kW panel
No of working days	300 per years
Total energy production	4 * 1 * 300 units per year
	5 * 1 * 300 units per year
Cost and benefits	
Number of units of grid power substituted	1200 units per year
	1500 units per year
Cost of grid power	Rs. 3 per unit
Power saving per year	1200 * 3 = Rs. 3600
	1500 * 3 = Rs. 4500

Fig. 10 ETAP output with investment

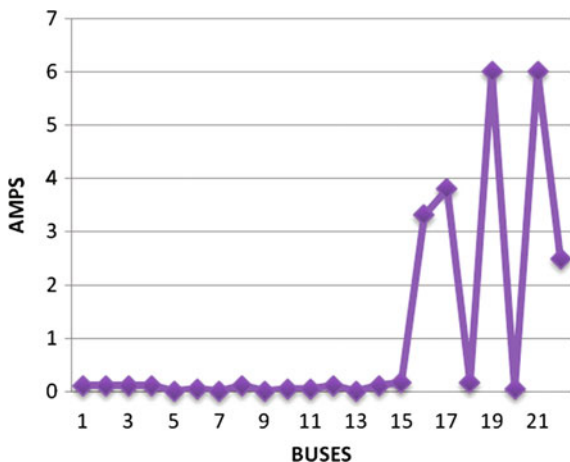


Fig. 11 Max. load analysis without and with audit

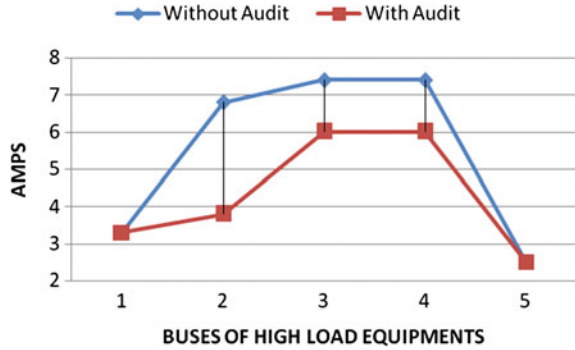


Fig. 12 Low-load analysis without and with audit

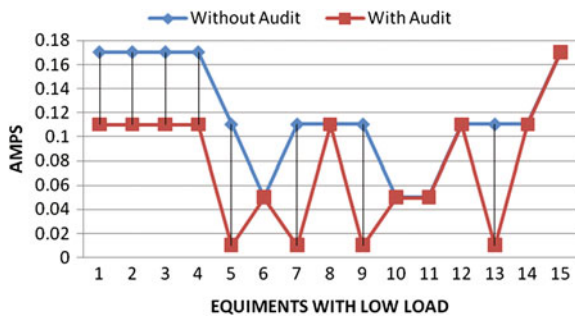


Fig. 13 Unit consumed without and with audit



6 Conclusion

This paper delivers an electrical energy audit of a residential house in Chennai with ETAP simulation and suitable recommendations to save energy as per the motto “Save Energy to Reduce Demand.” The outcome of all the recommendation clearly shows that the payback period will reach within 4 years as per today’s tariff and the client is agreed to implement all the recommendation within the span of 6 month.

References

1. Albert Thumann T, PE, CEM, Younger WJ. Hand book of energy audit. Crc Press Taylor and Francis Group.
2. Energy conservation hand book—prepared By Uttarakhand renewable energy development agency (UREDA).
3. Jain K, Kishore, Ramesh. Comparative analysis of residential houses for effective reduction in power demand. J Eng Res. 2015.
4. 2nd international conference on advances in energy engineering (ICAEE 2011) energy conservation measures in a technical institutional building in Tamilnadu in India.

Bidirectional Buck–Boost Converter-Fed DC Drive

P. Karthikeyan and V. Siva Chidambaranathan

Abstract This paper implements the regenerative braking concept with a bidirectional DC–DC converter-fed DC motor to charge the ultracapacitor and also to reduce power consumption. This paper uses the ultracapacitor power source for fast current changes and while battery responds for slow current changes which in turn increases the lifetime of the battery. Energy developed at the time of braking is not useless; it is reutilized to store the energy in the ultracapacitor. An experimental prototype is developed. The advantage is that state of charge (SOC) of the battery and ultracapacitor voltage and current and voltage are within the limits.

Keywords Bidirectional buck–boost converter · DC drive · Regenerative braking · Ultracapacitor · Fast current charges

1 Introduction

Recently, bidirectional converters are developed for various applications like battery charging and discharging of electric vehicles, and UPS systems and the converter-fed DC motor is developed for electric vehicle system (EVS) applications for both motoring and regenerative braking [1]. DC–DC converters are used to interface the electric vehicles to boost (or) reduce the voltage level. Energy storage devices vary the output with load [2]. Ultracapacitor is a newer technology to store 20 times more than the conventional electrolyte capacitor. Fast and sudden changes in the battery discharge during acceleration and (or) fast charging during regenerative braking can be avoided by using ultracapacitor [3]. Individual fuel cell can recover regenerative braking energy and storing of auxiliary source has the

P. Karthikeyan (✉) · V. Siva Chidambaranathan
EEE Department, Sathyabama University, Chennai 600119, India
e-mail: karthikeyan233131@gmail.com

V. Siva Chidambaranathan
e-mail: sivachidambaram_eee@yahoo.com

advantage of maximum power and also has reduced cost [4]. Bidirectional DC–DC converter is operated at Boost and Buck mode operation [5]. Regenerative braking is defined as the method of injecting from the running motor to the battery during braking process and at that moment the motor acts as generator, whereas it is not possible in the conventional vehicles [6]. A bidirectional control can be used for boosting control because the back-EMF generated will be lesser than the voltage of the battery and then back-EMF needs to be boosted to charge the battery [7]. The bidirectional converters are used for transferring the power from one DC source to another DC source in either direction, which is to be utilized for various applications like hybrid electric vehicle energy systems and photo voltaic hybrid power systems [8].

Bidirectional converters are utilized for stimulation of the battery charging and discharging [9]. Hybrid power sources are the combination of the fuel cells, secondary batteries for example lead–acid battery, which are combined to high energy density of the fuel cell and high power density of the battery, DC–DC converter is placed in order to balance the power flow which can able to provide the high power output [10]. High power density is the major application [11]. High efficiency is achieved [12]. Converters have no switching loss and are more suitable for high-frequency operations [13].

2 Bidirectional Converter

The bidirectional converter consists of two converters and they are boost converter and buck converter. Figure 1 shows the conventional bidirectional DC–DC boost–buck converter. The projected converter for step-up mode is shown in Fig. 2. The pulse width modulation technique is used to control the switches S_1 and S_2 simultaneously varying the duty cycle.

Fig. 1 Conventional bidirectional converter

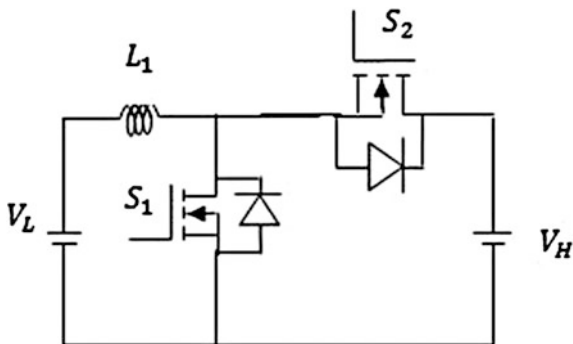
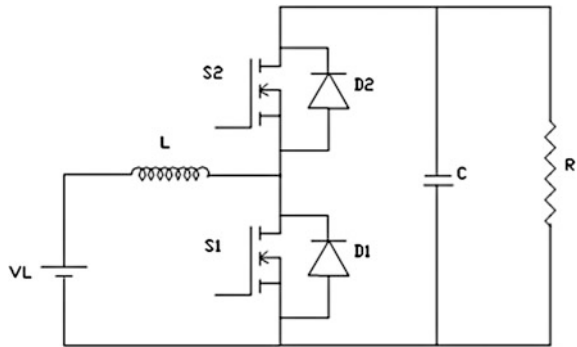


Fig. 2 Boost converter



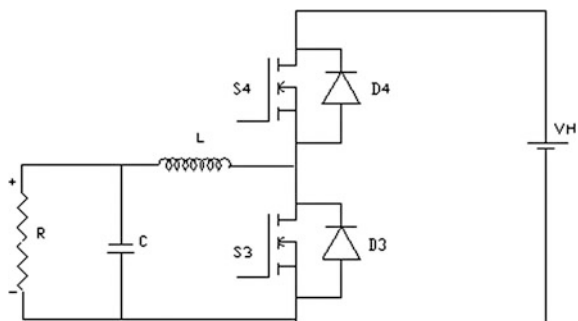
2.1 Boost Mode of Operation

During this mode, switch S_1 and diode D_2 is turned on and switch S_2 and D_1 . The energy of the low-voltage side is transferred to the inductor. The energy stored in the capacitor C is discharged to the load (motor). Thus, the boost operation takes place in forward direction of rotation of the motor.

2.2 Buck Mode of Operation

Figure 3 shows the proposed converter in buck operation, i.e., step-down mode. The PWM technique is used to control the switches S_3 and S_4 simultaneously by varying the duty cycle. During this mode of operation, switch S_4 and diode D_3 is turned on, while that of the switch S_3 and diode D_4 is turned off. Here, the energy of high voltage V_H is transferred to inductor and capacitor and then to the load (motor). Thus the buck operation takes place in reverse direction of rotation of the motor.

Fig. 3 Buck converter



3 Regenerative Braking

The regenerative braking is the method of injecting energy from the running motor to the battery for future use at the time of braking, when the vehicle force the running motor to work as a generator. Now, in this proposed system instead of battery, the voltage is restored in the ultracapacitor. Regenerative braking concept is utilized to recycle the energy in an efficient way. Usually, when power is cutoff from the supply then motor will also lose its supply, then due to kinetic energy, flywheel gets rotated for sometimes even after the power supply is cutoff then energy will be getting stored in the form of back-EMF in the motor. This back-EMF produced during the braking is again restored in the ultracapacitor for future use. Usually in the conventional electrical vehicles, regenerative braking is not utilized. The reason for going to regenerative braking is that driving range obtained is more rather than the mechanical braking. Whenever motor starts rotating in reverse direction, then motor acts as a generator getting only the kinetic energy, and then it has to be converted it into electrical energy for storing that in the ultracapacitor. Here, the voltage stored in the ultracapacitor is to be used whenever required. Compared with the mechanical braking, the efficiency obtained from the regenerative braking is more.

4 Ultracapacitor

An ultracapacitor is a charge storing device as that of the capacitor, but differs from the constructional feature with respect to the simple capacitors. It can able to store the tremendous charge. Usually the capacitance of an ultracapacitor extends up to 5000F. Ultracapacitor is also called as super capacitor (or) double-layered capacitors invented by the engineers at Standard Oil, 1966. The main advantage of ultracapacitor is having rapid, regenerative energy storage than the chemical batteries. Ultracapacitors can store 5 % as much energy as a modern lithium-ion battery. It can store nearly 20 times more energy compared to the electrolytic capacitors. The performance of specific power is better in ultracapacitor than a battery. Ultracapacitor can withstand high current pulses. Here, in the proposed system the energy obtained from the regenerative braking is again restored in the ultracapacitor by utilizing a buck converter.

5 Simulation Results

Figure 4 shows the bidirectional converter with a DC motor drive in which it consists of a DC source along with the input sensing and an inductor connected in series with a bidirectional converter acting as boost converter. Here, two MOSFETs

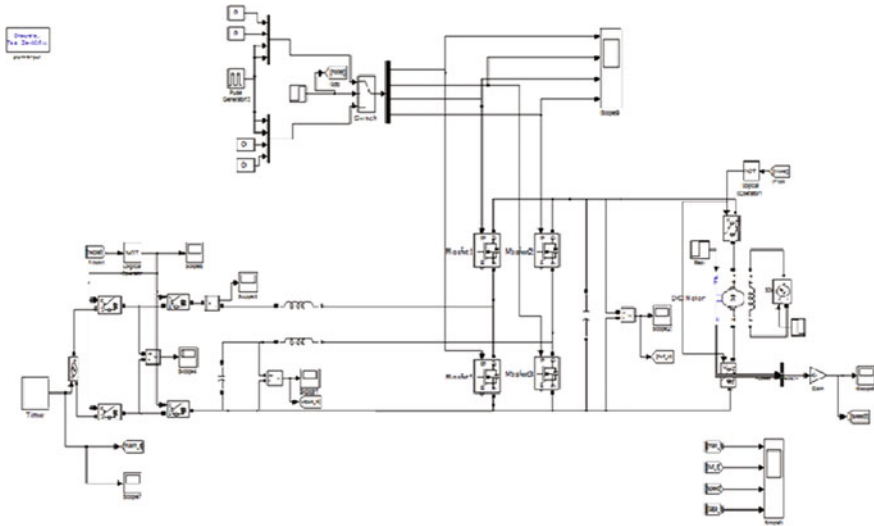


Fig. 4 Simulation diagram of the bidirectional converter with a DC motor drive

are triggered by PWM pulses generated by a PWM circuit. The scope 4 is obtained for the input voltage along the DC source. On the other hand, there is a capacitor on the left end along with the voltage sense which is connected in series with an inductor for storing the energy, which is connected in series with a bidirectional converter which consists of two MOSFET's, which are driven by the MOSFET gate driver circuit in which all the MOSFETS are triggered by the PWM pulses generated by a PWM circuit. The scope 1 can be obtained for the voltage across the capacitor. The pulse generation for whole DC–DC converter can be viewed in the scope 9. A capacitor is connected across the two bidirectional converters in which the output voltage is obtained in the scope 2. A self-excited DC motor is connected across the bidirectional converter for forward and reverse direction of the rotation. Here, the self-excited DC motor acts as a load of the circuit. The speed of the motor during the motoring and regenerative braking can be obtained from the scope 6. There are two circuit breakers, which are connected in series with DC source at the input side and another in series with the capacitor for preventing any short circuits. Again a circuit breaker is utilized to prevent any short circuit across the DC motor. A timer is attached at the input side in order generate the signal changing at specified times. Here, scope 3 is used for getting all the outputs in a single scope, i.e., the input voltage of the DC source, motor speed, ultracapacitor voltage, output voltage are available.

The bidirectional buck–boost converter-fed DC drive is simulated using MATLAB and the results are presented. The input voltage is shown in Fig. 5. The result shows that up to motoring mode of operation, voltage is constant and after regenerative braking occurs, the voltage starts reducing.

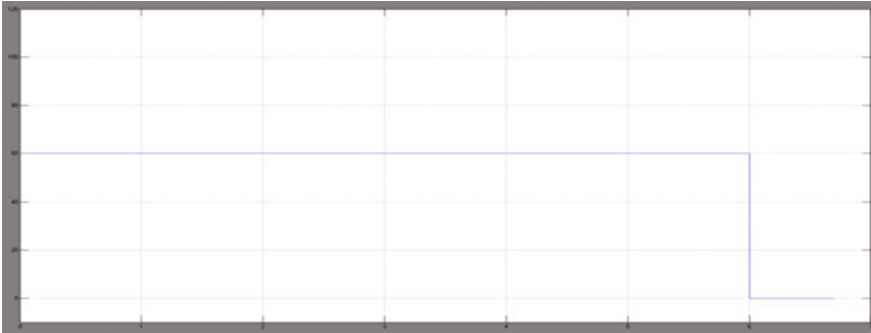


Fig. 5 Input voltage

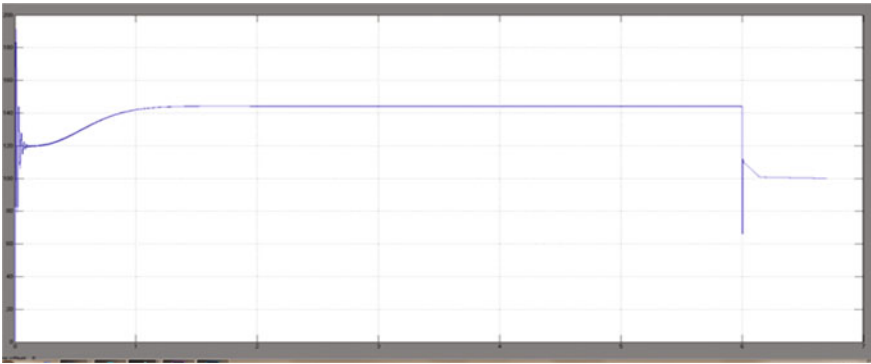


Fig. 6 Output voltage

The output voltage waveform is shown in Fig. 6. From the results it is clear that voltages starts gradually increasing from zero then attains the steady state output up to the motoring mode, then after the regenerative braking occurs, the voltage starts decreases, attains stabilized voltage after regenerative braking.

The speed of the motor is shown in the Fig. 7. The results shows that the speed of the motor starts increasing from zero speed and reaches the maximum and attains the normal speed up to motoring mode of operation and starts gradually decreasing during regenerative braking operation and after sometimes the speed of the motor reaches to zero.

The ultracapacitor voltage waveform is shown in Fig. 8. The results shows that initially ultracapacitor voltage is zero up to the motoring mode of operation and whenever the regenerative braking occurs the ultracapacitor starts charging from zero volts and attains the voltage of above 6 V to reuse it again.

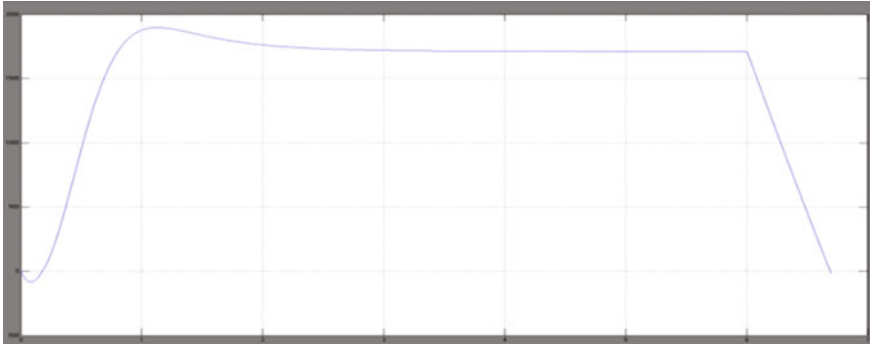


Fig. 7 Speed of the motor



Fig. 8 Ultracapacitor voltage

6 Hardware Results

To check the proposed control system, an experimental prototype had been built. A photograph of the experimental setup is shown in the Fig. 9. The hardware consists of an bidirectional converter with soft switching of four MOSFET's, The gate pulses are triggered by a MOSFET gate driver circuit IC TLP 250 is used in which it is a eight pin device used for isolation purpose and also for effective switching of MOSFET switches. A dual power supply RPS is utilized for getting two positive voltages, i.e., +12 V for driving the MOSFET gate driver circuit and again +5 V for energizing the input of the PIC microcontroller. The proposed system utilizes the PIC16F882 microcontroller for the generation of PWM pulses. An ultracapacitor is placed in series with an inductor acts as a buck converter which is utilized to store the recycled energy, which is totally different from the normal capacitor in storage manner. A DC motor is utilized as a load for the whole bidirectional converter, the main use of a DC motor is from the normal capacitor in

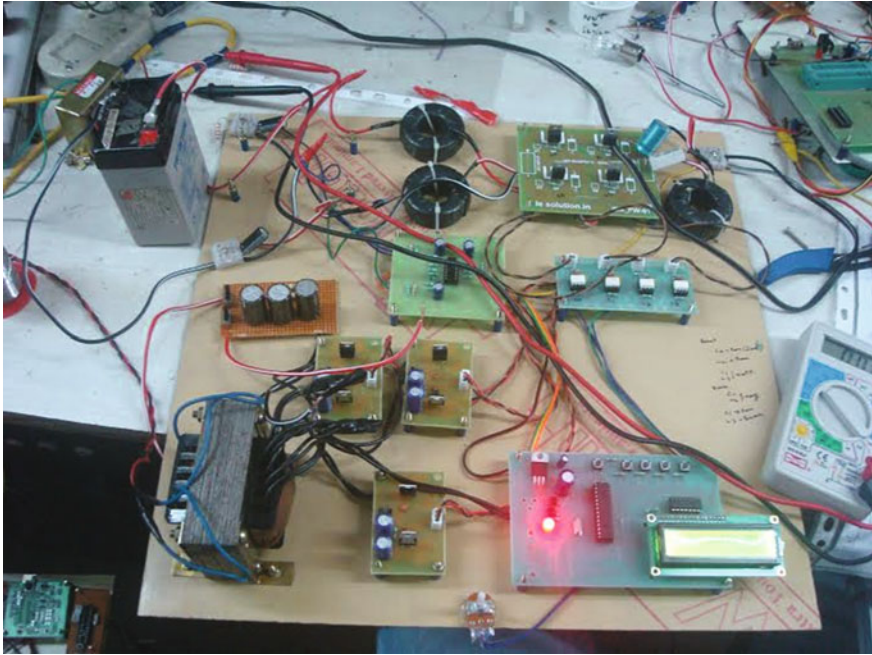


Fig. 9 Experimental setup of a bidirectional converter

storage manner. A DC motor is utilized as a load for the whole bidirectional converter, the main use of a DC motor is the regenerative braking obtained for the power supply had been removed. Another inductor is connected in series with a battery acts as a boost converter for boosting the input voltage. A signal conditioner circuit which is the combination of operational amplifier and differential amplifier is used to sense the input voltage at the input side. It is observed that the results obtained from the simulation results are matched with the hardware results.

7 Conclusion

In this paper, the bidirectional buck–boost converter is simulated using MATLAB Simulink and the results are presented. The result shows that the output voltage waveform is smooth without ripple. High efficiency is achieved with an ultracapacitor voltage. The converters have reduced switching losses, less power consumption, and recharging of ultracapacitor is achieved at the time of braking. The important advantage is all driving, charging are estimated in the single embedded system. Fast current changes reducing the lifetime of the battery can be controlled by means of ultracapacitor used. The common applications of the ultracapacitor include starting diesel trucks, railroad locomotives, used in electric/hybrid electric

vehicles for transient load level, and regenerating the braking energy. It can replace batteries in hybrid cars. A bank of ultracapacitors releases a burst of energy to help a crane to lift and at the same time it can capture the energy during the recharge. Majority of ultracapacitors are used in the military projects.

References

1. Pany P, Singh RK, Tirpathi RK. Bidirectional DC/DC converters fed drive for electric vehicles system. *Int J Eng Sci Technol*. 2011;3(3):101–10.
2. Al Sakka M, Van Mierlo J, Gualous H. DC/DC converters for electric vehicles. *Electric vehicles-modelling and simulations*. Dr. Seref Soyulu; 2011.
3. Dixon JW, Ortuzar ME. Ultracapacitors & DC-DC converters in the regenerative braking system. *IEEE AESS Syst Mag*. 2012.
4. Tsotoulidis S, Safacas A. Analysis of a drive system in a fuel cell and battery powered electric vehicle. *Int J Renew Energy Res IJRER*. 2011;1(3):31–42.
5. Lee J-H, Jung D-Y, Lee T-K, Kim Y-R, Won H-Y. Regenerative current method of bidirectional DC/DC converter for EHV/HEV applications. *J Electr Eng Technol*. 2013;8(1):97–105.
6. Cody J, Gol O, Nedic Z, Nafalski A, Mohtar A. Regenerative braking in an electric vehicle. *Magazine: Zeszyty Problemowe-Maazyny Elektryczne*. 2009.
7. Long B, Lim ST, Ryu JH, Chong KT. Energy-regenerative braking control of electric vehicles using three-phase brushless direct current motors. *Energies* 2014;7:99–114. doi:[10.3390/en7010099](https://doi.org/10.3390/en7010099).
8. Srinivas Reddy Gurrula K, Lakshmi V. A novel bidirectional DC-DC converter with battery protection. *Int J Mod Eng Res (IJMER)*. 2012;2(6):4261–5. ISSN:2249-6645.
9. Huang M-S, Yeh P-Y, Huang J-R, Liao C-H. A novel bi-directional AC-DC converter for electrical vehicle battery testing. Department of electrical engineering, national Taipei university of technology. Taiwan, national science council, Taiwan, ROC Under Grant No. NSC 98–2218-E-02-034.
10. Jiang Z, Member, IEEE, Gao L, Member, IEEE, Dougal RA, Senior Member, IEEE. Flexible multiobjective control of power converter in active hybrid fuel cell/battery power sources. *IEEE Trans Power Electron*. 2005;20(1).
11. Sivachidambaranathan V, Dash SS, Santhosh Rani M. Implementation of half bridge DC to DC converter using series resonant topology. *Eur J Sci Res*. 2012;74(3):381–8. ISSN:1450-216X.
12. Indira D, Sivachidambaranathan V, Dash SS. Closed loop control of hybrid switching scheme for LLC series-resonant half-bridge DC-DC converter. In: *Proceedings of the “second international conference on sustainable energy and intelligent system” (SEISCON 2011)*, IET Chennai and Dr.MGR University; 2011. p. 295–8.
13. Sivachidambaranathan V, Dash SS. Simulation of half bridge series resonant PFC DC to DC converter. *International conference, 2010*. p. 146–8.

Asymmetrical Multilevel Inverter Using Renewable Energy System

V. Kala and C. Bhuvaneshwari

Abstract Cascaded multilevel inverters with photovoltaic arrays are becoming famous of its application like hybrid vehicles, solar plants, etc. This paper presents cascaded asymmetrical multilevel inverter with low harmonic distortion. Photovoltaic cells are used for given inputs to the asymmetrical multilevel inverter. Thirteen-level and fifteen-level multilevel inverters with THD values are discussed. LC filters are used with less number of switches. Number of output levels is also increased in this paper. The asymmetrical multilevel inverters are simulated using Mat lab/Simulink.

Keywords Asymmetrical multilevel inverter · Renewable energy sources · Total harmonic distortion

1 Introduction

These days, multilevel inverters have more contributed for high and medium energy control. Asymmetrical multilevel inverter can give increased output levels compared to symmetrical multilevel inverter. The cost is also low for asymmetrical multilevel inverter because of less number of switches. There are different types of renewable energy sources available in the world but solar energy is more efficient and easy for installation. In solar system, the solar energy is tracked from Sun by PV cells. Electric current is directly converted from Sun. Environmental pollution can be controlled using solar energy system. Now solar panels are used for many home appliances. Solar panels are easy for installation and also small in size. Nowadays, AC PV modules are also available based on DC PV modules. AC PV modules has high flexibility.

V. Kala (✉) · C. Bhuvaneshwari
Electrical and Electronics Engineering, Sathyabama University, Chennai, India
e-mail: kala_166@yahoo.co.in

C. Bhuvaneshwari
e-mail: bhuns_sekar@yahoo.co.in

Many inverter topologies such that cascaded inverter, diode-clamped inverter, and capacitor-clamped inverters are presented [1, 2]. Capacitor-clamped voltage source of multilevel inverters generates the voltage with stepped voltage waveform. It can generate maximum power per string of 2200 W at 125–750 V by multistring inverter [3]. In multilevel inverter, the output voltage can be produced near to sinusoidal with low total harmonic distortion value [4, 5]. Less number of switches is required for asymmetrical multilevel inverter when compared to symmetrical multilevel inverter [6, 7, 8]. Modulation methods like space vector modulation, multilevel sinusoidal PWM, and multilevel selective harmonics elimination can be developed [1]. Symmetrical and hybrid asymmetrical multilevel inverters are compared by neutral-point-clamped (Diode-clamped) type.

The AC module consists of PV module and grid connected inverter [3, 4]. Switching device MOSFET is best for high frequency compared to other switching devices.

2 Multilevel Inverter

Multilevel inverter has contributed to most of the industries. Voltage source inverter can produce output current or voltage with 0 to $\pm V_{dc}$ levels by stepped waveform. Inverter which produces more than two voltage levels is called multilevel inverter.

In multilevel inverter, number of voltage levels increased, more steps are generated for the output waveform. If number of voltage levels increased, harmonic distortion of the output will be decreased. Multilevel inverter voltage source inverter allows high voltage with low harmonics without transformers or series connected switching devices.

Generally, multilevel inverter classified by three types.

- Diode-clamped multilevel inverter
- Flying capacitor multilevel inverter
- Cascaded multilevel inverter

2.1 Diode-Clamped Multilevel Inverter

Here clamped diodes are connected in series with semiconverter switching device. 8 Capacitor is also connected to DC bus. All devices are switched at fundamental frequency, so efficiency is high. For n -level inverter, $2(n - 1)$ switching devices, $(n - 1)$, $(n - 2)$ clamping diodes, and $(n - 1)$ capacitors are needed. Disadvantage of diode-clamped multilevel inverter is the usage of excessive clamping diodes that are required for more levels and difficult to control the real power for each converters.

2.2 *Flying Capacitor Multilevel Inverter*

Flying capacitor multilevel inverter is also similar to diode-clamped type of inverter but switching arrangements are different. Here capacitors are clamped with switching devices. For real-power transmission switching, frequency and switching loss will be high. So it is very difficult for the control of multilevel inverter. For high level, excessive number of storage capacitors required and high expensive.

2.3 *Cascaded Multilevel Inverter*

In cascaded multilevel inverter, H-bridge inverters are connected series. Each bridge has a separate DC source, which may be from solar cell, batteries, or fuel cells. Back-to-back connection is not possible for cascaded multilevel inverter because short circuit can occur.

Comparing with other two types of multilevel inverter, it is having less number of components to reach same number of voltage level. It does not require storage capacitors and clamping diodes. It is easy for package. These types of cascaded H-bridge multilevel inverter can further classified into.

Symmetrical cascaded multilevel inverter

Asymmetrical cascaded multilevel inverter

In symmetrical multilevel inverter, each H-bridge has same magnitude of DC input voltage source. Level of output phase voltage is defined by $2n + 1$. Here N is denoted number of DC sources.

In asymmetrical multilevel inverter, each H-bridge has different magnitude of DC input voltage source. Less number of semiconductor switches is used compared to symmetrical multilevel inverter for obtaining same level of output voltage. Output levels are increased in asymmetrical multilevel inverter compared to symmetrical multilevel inverter with the same number of bridges. 7, 9, 11, 13, 15, 17, and 21 level output voltage can be obtained by 12 switches only in asymmetrical topology but 12, 16, 20, 24, 28, 32, and 40 switches needed symmetrical topology.

3 **Renewable Energy Source**

Renewable energy sources are very popular and important for future. Solar energy, wind energy, hydropower, geothermal energy, and biomass energy are some of the renewable energy sources. Nowadays, PV-based power electronic converters are interfaced to electrical power grid.

In PV module, multiple individual solar cells are connected in series, PV module produce voltage and power above that single solar cell voltage. Generally, each

silicon solar cell has below 0.6 V under 25 °C. For PV module, mostly 12 V batteries are chosen because 12 and 9 V batteries are commonly available in the market. For a charge of 12 V battery, 12 solar cells are connected in series to produce a sufficient voltage.

In photovoltaic system, voltage and current are directly injected to the load-like DC motors, lightning system, etc. These PV cells have to work like that PN junction diode. If light is incident on the PV cells, free charges occurred by the energy from light. Voltage can be generated at the contacts, if any load connected across the solar cells current can be flow. This current is called as photocurrent (I_{ph}). It is directly proportional to the radiation intensity.

Types of photovoltaic power system:

- Stand-alone Photovoltaic system
- Hybrid Photovoltaic system
- Grid connected Photovoltaic system

4 Block Diagram

A block diagram of asymmetrical multilevel inverter is shown in Fig. 1. For asymmetrical multilevel inverter, DC input is given from battery by PV cells. In this proposed diagram, three groups of PV cells are connected to each H-bridge in

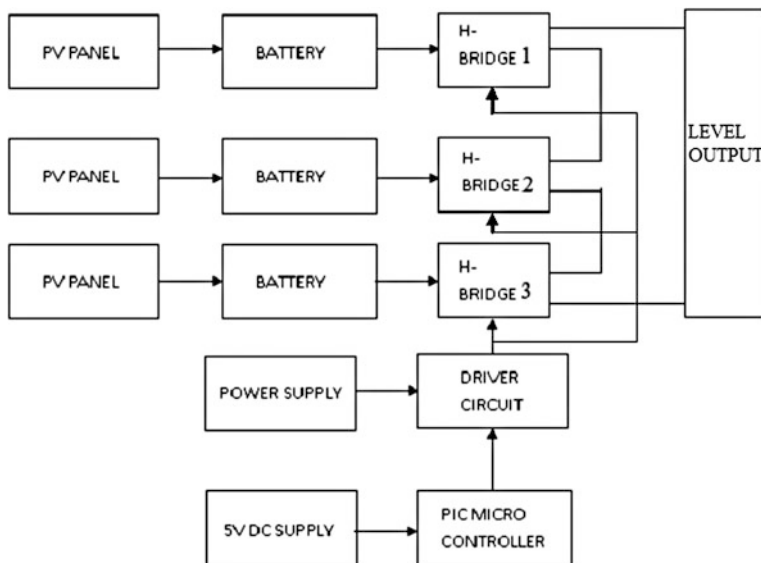


Fig. 1 Proposed block diagram

parallel. In each group, 12 solar cells are connected in series. Each H-bridge has various input from solar panels through batteries, these input are independent of the supply. In this asymmetrical multilevel inverter switching device, MOSFET used because it has high-frequency switching device and switching losses also low compared to others. 12 V supply is given to driver circuit for pulse generator by PIC controller. Filters can be used for reducing the total harmonics distortion.

5 Circuit Diagram

In proposed diagram, three H-bridge multilevel inverters are connected in series, each battery injects the various DC voltages to each H-bridge, then multilevel inverter produces the AC output. In the proposed system, 12 switches are used, 4 switches for each group. Switches S1, S2, S3, and S4 are used in bridge I. S5, S6, S7, and S8 are used in bridge II and S9, S10, S11, and S12 are used in bridge III. For each state, any two switches must ON in each H-bridges. Total AC output voltage is equal to sum of the each H-bridge inverter. When switches S1 and S2 turn ON, output voltage is positive (S3 and S4 are turn OFF), when switches S3 and S4 turn ON, output voltage is negative (S1 and S2) in first bridge. Switching states are shown in table. Expecting AC output voltage can be obtained by simulating by Matlab. Simulating diagram filter is required for pure sinusoidal output and reducing total harmonic distortion. Fifteen-level output and THD value is shown in graph (Fig. 2).

24 V is given to first H-bridge, 12 V is given to second H-bridge, and 6 V is given to third H-bridge from PV panels. Each panel consists of 36 solar cells. Each output of PV panels is given to H-bridge inverter.

Mode: 1

For "0" Level, upper or lower switches of each H bridges are ON. (i.e.) S1, S3, S5, S7, S9, S11 or S2, S4, S6, S8, S10, S12 are ON.

Mode: 2

S1, S3, S5, S7, S9, S10, switches are ON, and other switches are OFF to obtain +Vdc (6 V) level.

Mode: 3

S1, S3, S5, S6, S9, S11 switches are ON, and other switches are OFF to obtain +2 Vdc (12 V) level.

Mode: 4

S1, S3, S5, S6, S9, S10 switches are ON, and other switches are OFF to obtain +3 Vdc (18 V) level.

Mode: 5

S1, S2, S5, S7, S9, S11 switches are ON, and other switches are OFF to obtain +4 Vdc (24 V) level.

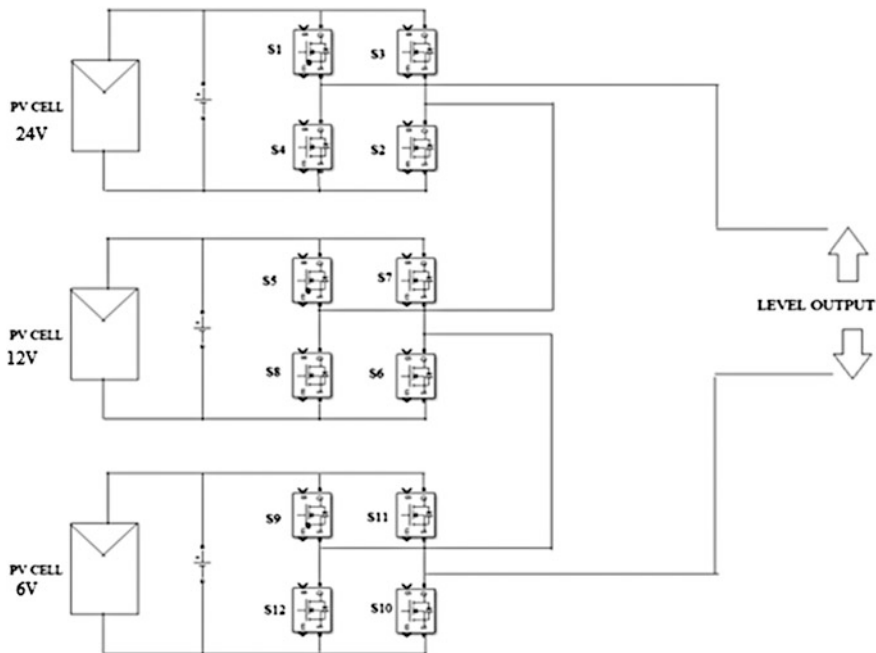


Fig. 2 Asymmetrical multilevel inverter

Mode: 6

S1, S2, S5, S7, S9, S10 switches are ON, and other switches are OFF to obtain +5 Vdc (30 V) level.

Mode: 7

S1, S2, S5, S6, S9, S11 switches are ON, and other switches are OFF to obtain +6 Vdc (36 V) level.

Mode: 8

S1, S2, S5, S6, S9, S10 switches are ON, and other switches are OFF to obtain +7 Vdc (42 V) level. For obtained negative voltage, similarly above modes operation but Switches are reversed.

6 Simulation Diagram

Fifteen-level output is obtained from simulation by Matlab. Elements from simulink library, i.e., PV panels, MOSFET switches, pulse generators are taken from simulink library. Three H-bridges are connected in series and the pulses for each H-bridge by pulse generators. PV panels connected to bridges by solar cells. In each bridge, 12 solar cells are connected for inputs. Each solar cell has 0.5 V. 6 V is tracking from each PV panel. 6, 12, 24 V are given to H-bridges for getting fifteen-level output, i.e., 7, 6, 5, 4, 3, 2, 1, 0, -1, -2, -3, -4, -5, -6, -7 Vdc. LC

filters are used for reduced total harmonic distortion. Total harmonic distortion can be obtained from simulation is 2.41 %. This is the best THD compared to thirteen-level symmetrical multilevel inverter (Fig. 3).

Switching state of fifteen-level asymmetrical multilevel inverter is illustrated in Table 1.

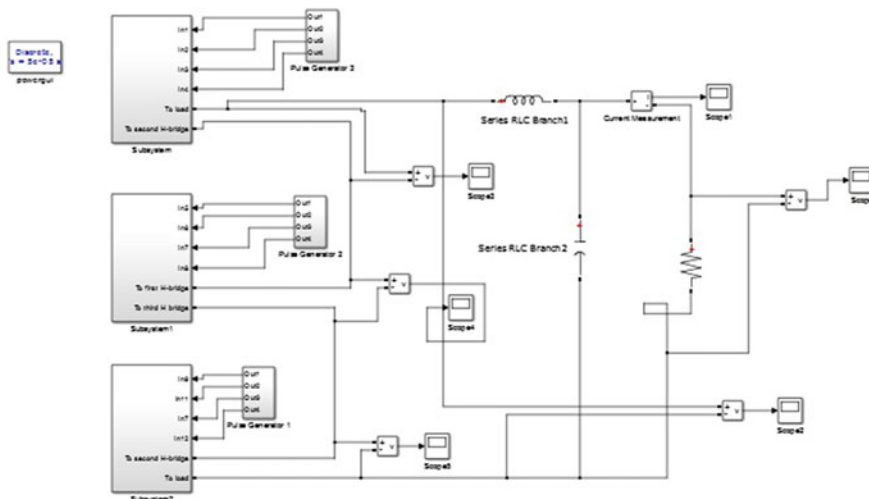


Fig. 3 Fifteen-level inverter simulation diagram

Table 1 Switching state for fifteen level

Switching states												Output voltage (Vdc)
S1	S2	S3	S4	S5	S6	S7	S8	S9	S10	S11	S12	
1	2	0	0	1	1	0	0	1	1	0	0	7
1	1	0	0	1	1	0	0	1	0	1	0	6
1	1	0	0	1	0	1	0	1	1	0	0	5
1	1	0	0	1	0	1	0	1	0	1	0	4
1	0	1	0	1	1	0	0	1	1	0	0	3
1	0	1	0	1	1	0	0	1	0	1	0	2
1	0	1	0	1	0	1	0	1	1	0	0	1
1	0	1	0	1	0	1	0	1	0	1	0	0
1	0	1	0	1	0	1	0	0	0	1	1	-1
1	0	1	0	0	0	1	1	1	0	1	0	-2
1	0	1	0	0	0	1	1	0	0	1	1	-3
0	0	1	1	1	0	1	0	1	0	1	0	-4
0	0	1	1	1	0	1	0	0	0	1	1	-5
0	0	1	1	0	0	1	1	1	0	1	0	-6
0	0	1	1	0	0	1	1	0	0	1	1	-7

Figures 4 and 5 represent the output voltage of fifteen-level multilevel Inverter without filter and with filter, respectively. Both the simulation results give an output voltage of 42 V. The THD value of the multilevel inverter has been reduced to 2.41 % as shown in Fig. 6

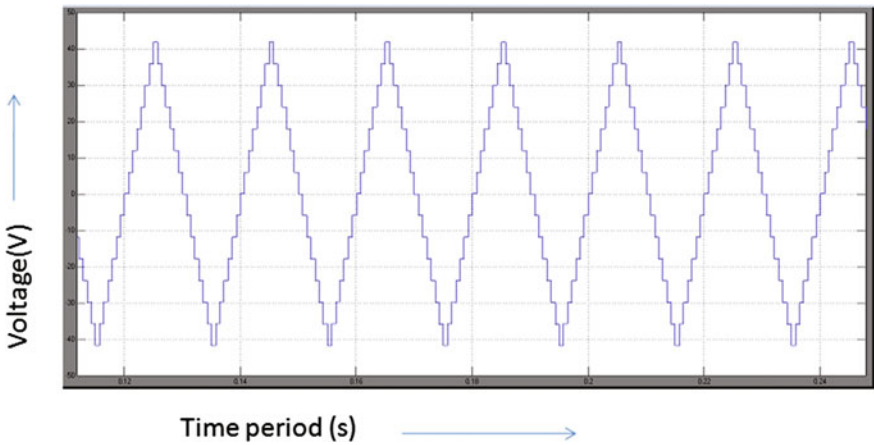


Fig. 4 Fifteen-level output voltage without filter

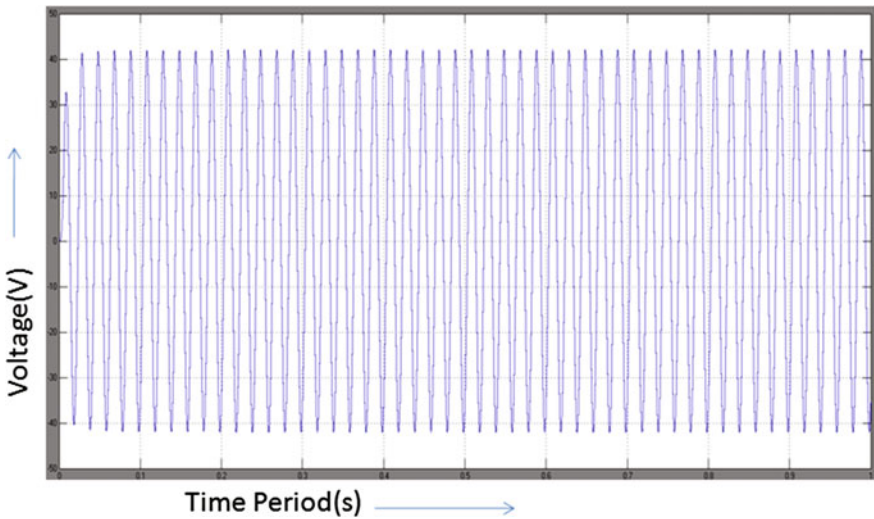


Fig. 5 Fifteen-level output voltage with filter

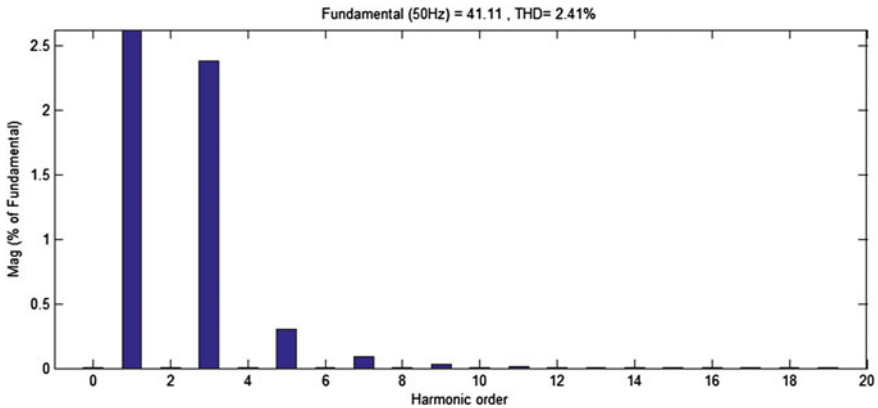


Fig. 6 THD value of output voltage

7 Conclusion

This paper proposes fifteen-level output from asymmetrical multilevel inverter, less number of switches is used, so cost is low. Number of levels is increased and THD value is reduced to 2.41 %. Number of output voltage levels is increased in asymmetrical level with low harmonic distortion. It has a good efficiency and high flexibility. Environmental pollution can be controlled by the use of renewable energy sources.

References

1. Rodriguez J, Peng FZ. Multilevel inverter: a survey of topologies, controls and applications. *IEEE Trans. Ind Electron.* 2002;49:4.
2. Nami A, Zare F, Ledwich G, Ghosh A. Comparison between symmetrical and asymmetrical single phase multilevel inverter with diode-clamped topology. *IEEE*; 2008.
3. Kjaer SB, Pedersen JK, Blaabjerg F. A review of single-phase grid-connected inverters for photovoltaic modules. *IEEE Trans Ind Appl* 2005;41:5.
4. Carbone R, Tomaselli A. Recent advances on AC PV-modules for grid-connected photovoltaic plants. *IEEE*; 2011.
5. Murali Krishna G, Muruthy VVN, Lakshmi Ganesh K. THD analysis of symmetrical and asymmetrical cascaded H-bridge multilevel inverter with PV arrays. *IJAIR*; 2012. ISSN:2278-7844.
6. Ahmed RA, Mekhilef S, Ping HW. New multilevel inverter topology with minimum number of switches. *IEEE*; 2010.
7. Ahmed RA, Mekhilef S, Ping HW. New multilevel inverter topology with reduced number of switches. In: 14th international middle east power systems conference, Cairo University, Egypt, 19–21 December 2010.
8. Patel D, Chaudhari HN, Chandwani H, Damle A. Analysis and simulation of asymmetrical type multilevel inverter using optimization angle control technique. *ISSN.* 2012;1:3.

9. Zambra DAB, Rech C, Pinheiro JR. Comparison of neutral-point-clamped, symmetrical and hybrid asymmetrical multilevel inverter. *IEEE Trans Ind Electron.* 2010;57:7.
10. Tomy MM, Krihnakumar S. Implementation of single phase 13 level inverter using single DC sources. *Int J Adv Trends Comput Sci Eng.* 2013;2(2):62–66.

High Efficient Power Supply for Ozone Generator System with Input Power Factor Correction Converter

G. Udhayakumar, M.R. Rashmi, K. Patel and A. Suresh

Abstract High-frequency switching is used to minimize the size and to improve the system performance. Most of the power supplies derived from ac mains source. The rectifier based PWM inverter has front end bridge rectifier with smoothing capacitor. As a result, the input has distorted line current and poor factor. The square wave inverter has non-sinusoidal output current. It affects the system performance and increases the switching loss and reduces the efficiency. All these problems affect the Ozone production and system efficiency. These problems are solved through proposed method. This paper presents the Power Factor Corrected (PFC) converter with parallel resonant inverter based power supply for ozone generator system. The proposed system has active power factor correction converter and Parallel resonant inverter which are used to achieve sinusoidal current and improve the supply power factor and zero-voltage switching across all switches. The active PFC converter with parallel resonant inverter fed ozone generator generates more ozone output compared to the conventional inverter. Thus the proposed system has less switching loss, less current harmonics, and better input power factor compared to the conventional system. The performance of the both inverters are compared and analyzed with the help of simulation results presented in this paper.

Keywords Active power factor correction converter • Total harmonic distortion (THD) • Ozonator • Parallel resonant inverter • Zero-voltage switching

G. Udhayakumar (✉)
St. Peter's University, Chennai, India
e-mail: udhay.eee@gmail.com

M.R. Rashmi
Amrita Vishwa Vidyapeetham, School of Engineering, Bangalore, India
e-mail: rashmi.power@gmail.com

K. Patel
International Ozone Association, Chennai, India

A. Suresh
SA Engineering College, Chennai, India
e-mail: asuresz@yahoo.com

1 Introduction

In recent years, ozone used as an oxidant element for disinfecting and bleaching applications in many industry. The ozone is generated both naturally and artificially. Artificially, it can be generated in many ways such as Corona Discharge, Electrolysis, and Radiochemical method. Corona discharge method creates higher quantities of ozone more efficiently. And much less electrical energy is required to produce the same quantity of ozone [1–3]. Therefore Corona discharge method for generating ozone is considered in the present work. Many compact inverter topologies are proposed to improve the efficiency [4–8] of the Ozone generator.

Some power supply derived from ac main supply. In this case, the front end has uncontrolled rectifier with a large DC link capacitor. This rectifier is widely used because of its simplicity and robustness. This supply has more input current distortion and poor power factor [10]. It affects the system performance and life time. These harmonics can be reduced by active PFC converter. The PFC corrector is used to improve the input side power factor, decrease cable and device rating and reduce the current harmonics. Various PFC techniques were proposed to overcome these power quality issues [11]. The boost converter topology is mostly used in various power supply conversion applications.

The low frequency to high-frequency, high-voltage power supply system has more input current distortion and poor power factor. It affects the system performance and life time of the components. These harmonics can be reduced by active PFC converter. After rectification full-bridge inverter circuit is used to convert DC to high-frequency AC voltage. The current-fed inverters are mostly used in step-up applications due to their essential low input current ripple feature [12, 13]. This type Inverter has more voltage stress. Passive snubber is used to reduce the stress but increase the conduction losses. The voltage-source inverter has low voltage stress. The phase-shift PWM inverter achieves ZVS across switches. But, it has more conduction loss due to circulating current and duty cycle loss [14, 15]. These problems are solved using parallel resonant converters. Resonant converters are mostly used due to their soft switching and high performance features [16–20].

This paper proposes PFC converter fed high-frequency parallel resonant inverter based power supply for Ozonator. Implementing power factor correction (PFC) into low frequency to high-frequency power supplies increase the current and power handling capacity of the power supply. The parallel resonant inverter is used to achieve ZVS across all power switches and reduce the switching loss.

2 Power Supply System for Ozonator

The basic boost converter topology is mostly used in various power supply conversion applications. Therefore, a boost converter is used along with the inverter as a supply unit for an Ozonator. The proposed ozone generating system is shown in

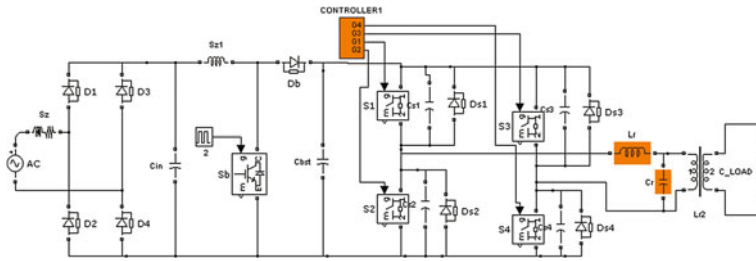


Fig. 1 Proposed system for ozone generator

Fig. 1. It consists of single-phase AC supply, uncontrolled bridge rectifier, PFC converter, and high-frequency parallel resonant inverter using power IGBTs, high step-up transformer and an electrode set up. High-frequency parallel resonant inverter operation is explained in detailed in [20]. The boost converter is used to control the input current and improve the power factor. As a result the overall system performance is improved and rating of the device is reduced.

3 Boost Converter Design

The boost converter is designed to operate at 10 kHz frequency with Duty cycle of 50 %. The output voltage V_0 is given by

$$V_0 = \frac{V_{in}}{1 - D} \tag{1}$$

where V_{in} is the input dc voltage and D is the duty cycle.

Therefore, output voltage V_0 of boost converter

$$V_0 = \frac{160}{1 - 0.5} = 320 \text{ V} \tag{2}$$

Input Inductor L is determined using this formula

$$L = \frac{(1 - D)^2 * D * R}{2 * F_s} \tag{3}$$

where

R is load Resistor = 100 Ω

F_s is the switching frequency.

Therefore $L = 630 \mu\text{H}$.

Output capacitor is determined using this formula

$$C_0 = \frac{D * V_0}{V_{ripple} * R * F_s} \tag{4}$$

where V_{ripple} is the ripple in the output voltage $C_0 = 1000 \mu\text{F}$.

3.1 Inverter Selection

The required output voltage of the inverter is 5–6 kV (peak value) which is obtained using high-frequency, high-voltage transformer and then is fed to the electrodes for ionizing the gas. The UU-80 ferrite core is used. The required frequency of currents is 6 kHz.

4 Simulation Results

The simulation is carried out in Matlab/Simulink environment. The conventional circuit which was used to supply power for Ozonator without PFC is shown in Fig. 2. The input ac supply voltage and current waveform as shown in Fig. 3. The switching pulses, current through the switches and voltage across the switches are shown in Figs. 4 and 5 for switches S2, S3 and S1, S4, respectively. Figure 6 shows the transformer primary and secondary currents. These currents are distorted. Figure 7 shows the transformer secondary side voltage and current wave form.

As observed from the simulated waveforms input current is discontinuous and the supply power factor is poor. Therefore, an active power factor correction converter based parallel resonant inverter is proposed. The simulation circuit of proposed configuration is shown in Fig. 8. It has ac source, rectifier and boost

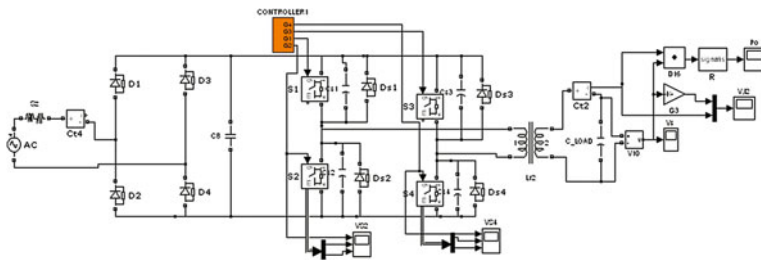


Fig. 2 Conventional power supply circuit for ozonator without PFC

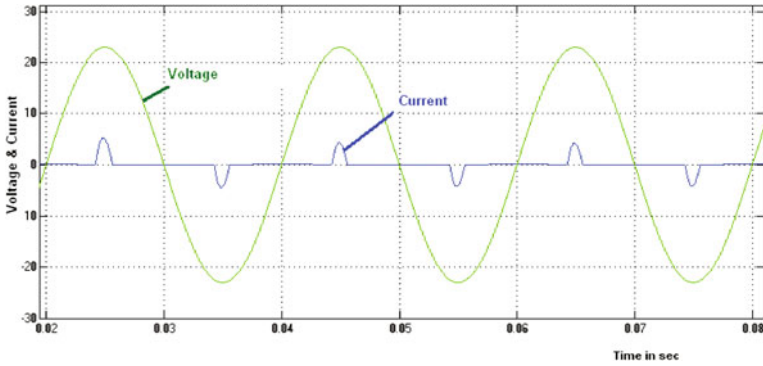


Fig. 3 Input voltage and current (scale volt one unit = 10 V)

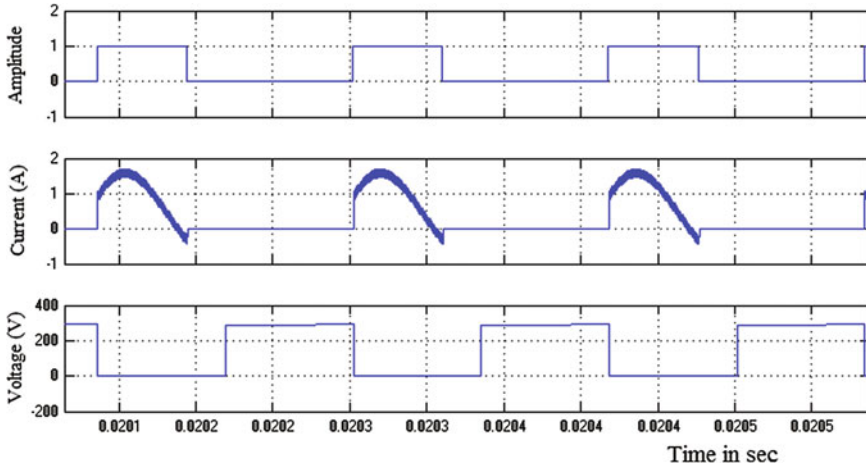


Fig. 4 Switching pulse, current through, and voltage across the switch S2 and S3

converter, smoothing capacitor, high-frequency parallel resonant inverter, high-frequency transformer, and electrodes. The input ac supply voltage and current waveform as shown in Fig. 9. The switching pulses, current through the switches and voltage across the switches are shown in Figs. 10 and 11 for switches S2, S3 and S1, S4, respectively. Figure 12 shows the transformer primary and secondary currents. Figure 13 shows the transformer secondary voltage and currents. The FFT analysis is carried out and the output current FFT spectrum is shown in Fig. 14.

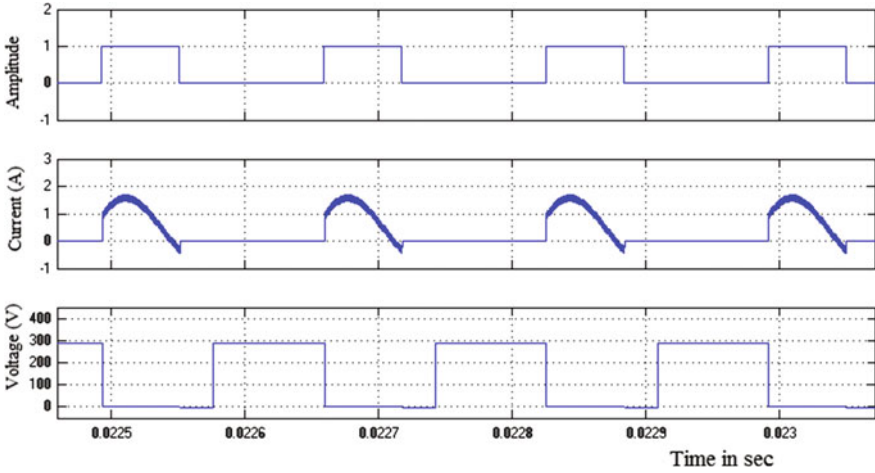


Fig. 5 Switching pulse, current through, and voltage across the switch S1 and S4

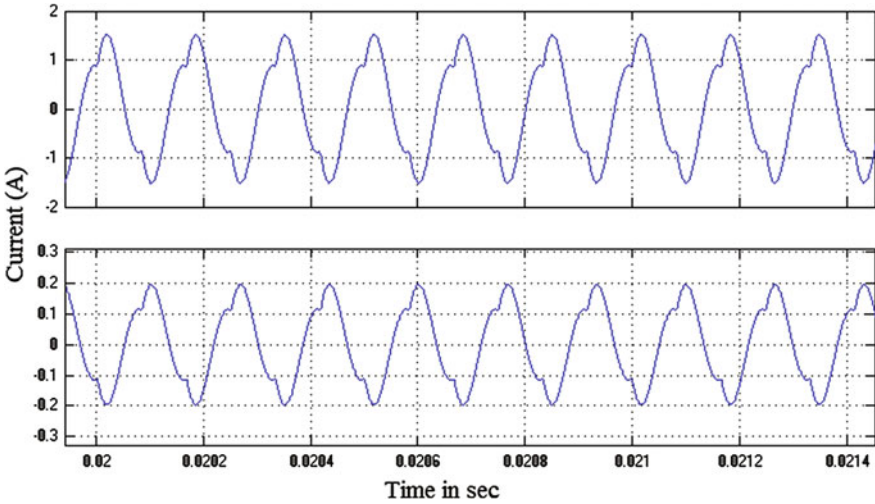


Fig. 6 Transformer primary and secondary currents

As observed from Fig. 9, the supply power factor is improved in the proposed configuration. Transformer primary side current has pure sinusoidal form as shown in Fig. 12. It has less harmonics and Zero-voltage turn on is achieved. A comparative study is been carried out between conventional inverter and proposed inverter and is given in Table 1.

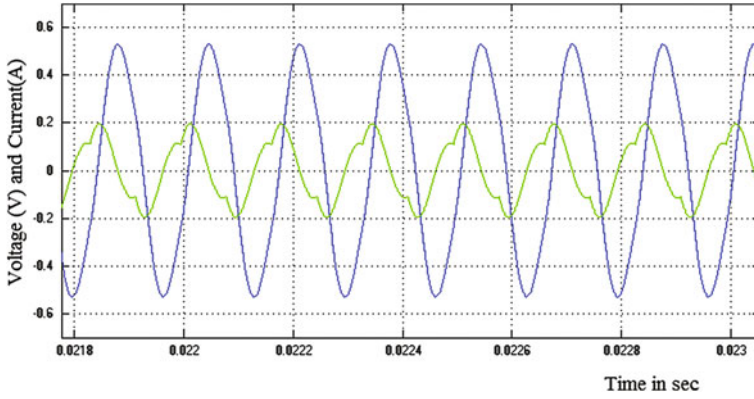


Fig. 7 Transformer secondary voltages and current

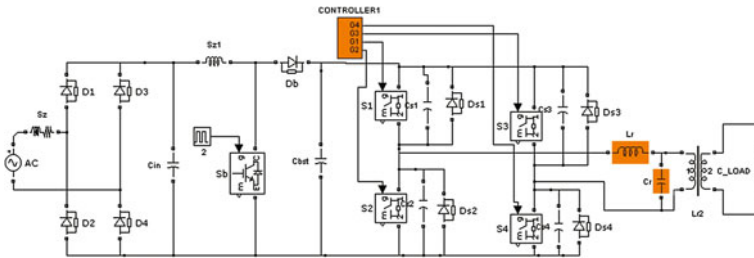


Fig. 8 Proposed power supply circuit for ozonator with PFC

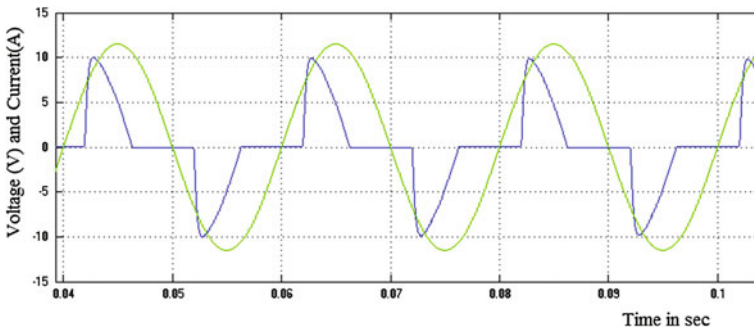


Fig. 9 Input voltage and current (scale volt one unit = 10 V)

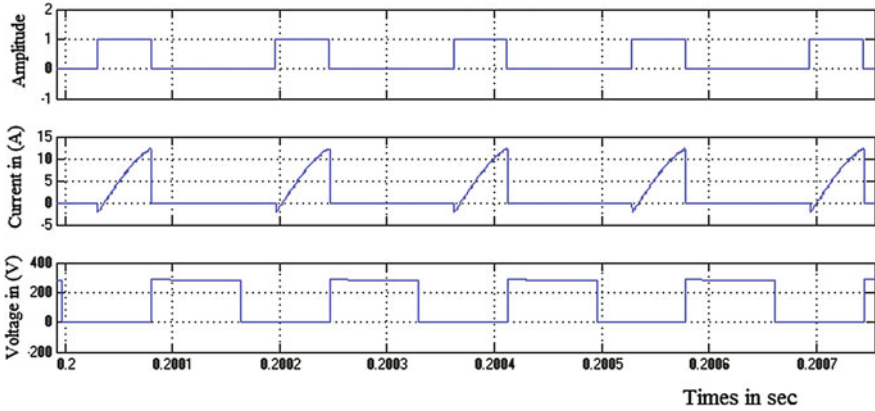


Fig. 10 Switching pulse, current through, and voltage across the switch S2 and S3

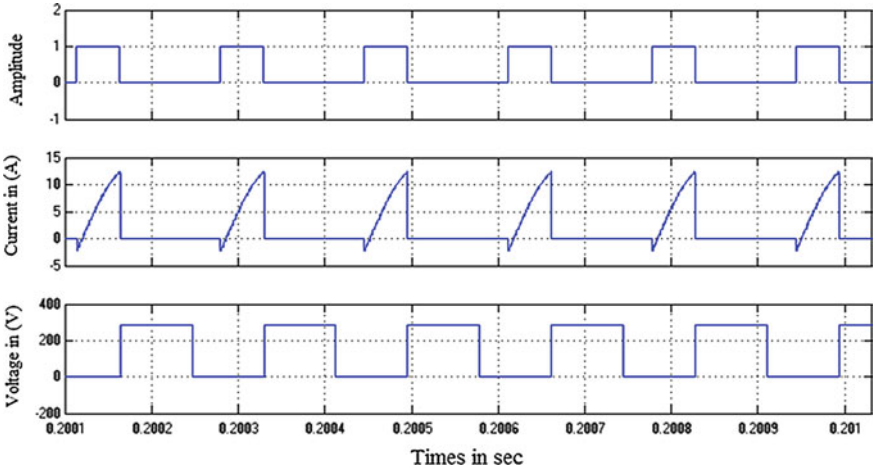


Fig. 11 Switching pulse, current through, and voltage across the switch S1 and S4

The graph in Fig. 15a shows the comparison between input and output voltage and Fig. 15b shows the comparison between input voltage and efficiency of conventional and proposed schemes. The proposed system has higher efficiency which is evident from the graph. The proposed PFC supply system has high efficiency of 89.5 % and high power factor of 0.84 compared to the conventional inverter where the efficiency was 80.7 % and the power factor was 0.31.

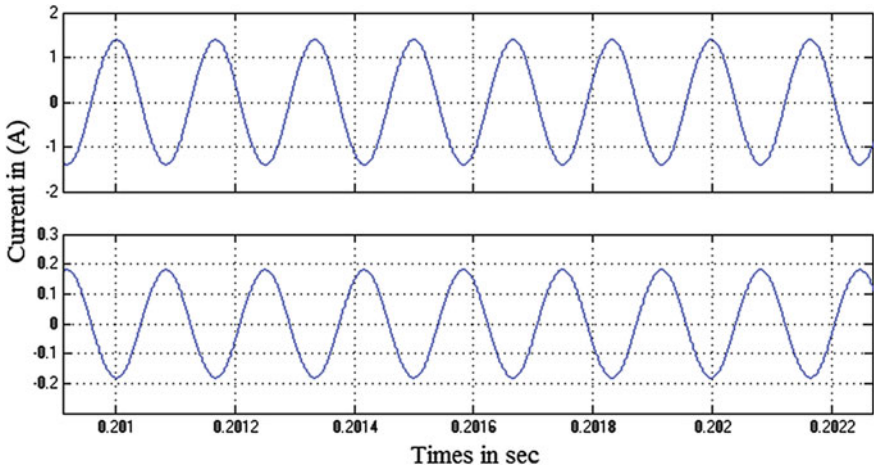


Fig. 12 Transformer primary and secondary currents

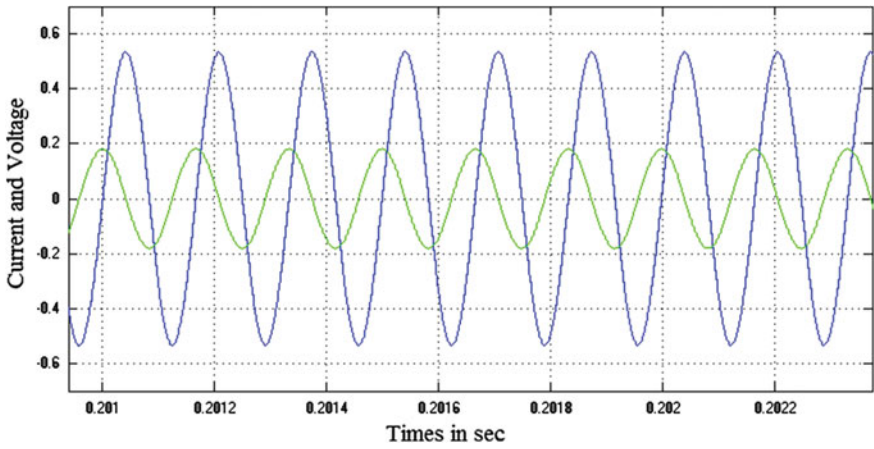


Fig. 13 Transformer secondary voltage and current (scale volt one unit=1000 V)

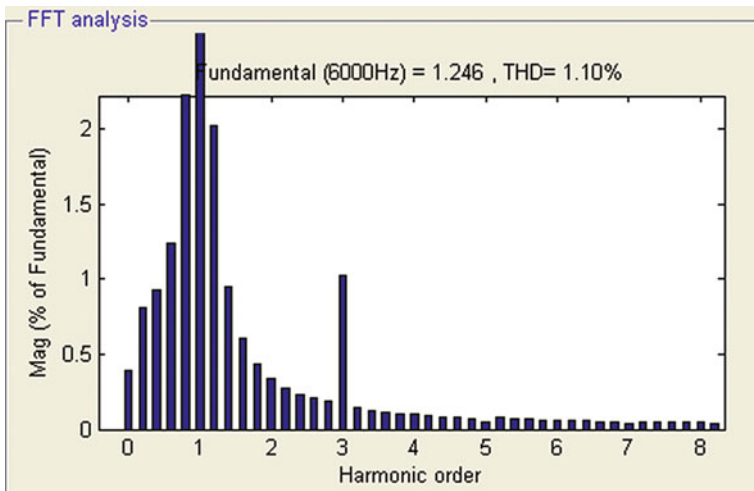


Fig. 14 FFT spectrum of the transformer primary current

Table 1 Comparative analysis of conventional and proposed inverter for ozonator

Parameter	Conventional inverter	Proposed inverter
Input DC voltage (V)	300	300
Input PF	0.31	0.844
Output voltage (peak value) (V)	5400	5680
Input power (W)	427	429
Output power (W)	345	384
Efficiency (%)	80.7	89.5
THD (%)	15.99	1.10

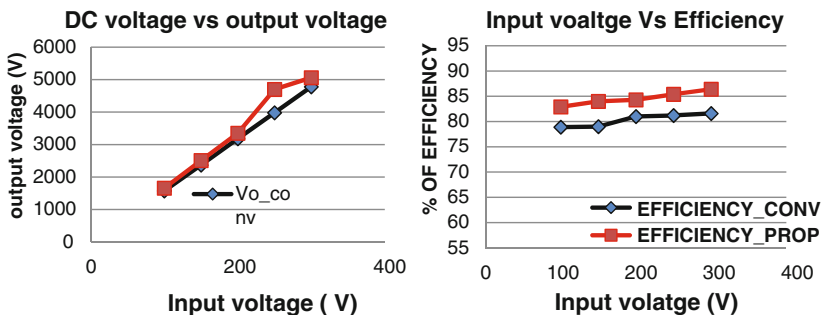


Fig. 15 (i) Input voltage versus output voltage (ii) Input voltage versus efficiency graph

5 Conclusion

Parallel resonant inverter with active PFC converter was proposed for efficient ozone generation system. Zero-voltage turn on is achieved using parallel resonant inverter as a result switching loss is reduced. From the simulation results, it is observed that the proposed configuration offer high efficiency of 89.5 % compared to the conventional configuration where efficiency was 81.7 %. It is also evident from the simulation results that the power factor of proposed supply system is 0.84, which is very much better than the conventional power supply system. Furthermore, the work can be focused on reducing the device turnoff losses.

References

1. Dascalescu L. An introduction to ionized gases. theory and applications. Toyohashi University of Technology; 1993.
2. Dimitriou MA. Design guidance manual for ozone systems. In: International ozone association (IOA). Pan American Committee; 1990.
3. Chang JS, Kelly AJ, Crowley JM. Handbook of Electrostatic processes. Marcel Dekker, Inc. 1995.
4. Alonso JM, Rico-Secades M, Corominas E, Cardesin J, García J. Low-power high-voltage high-frequency power supply for ozone generation.
5. Kinnares V, Potivejkul S, Rattanavichien P. Design of ozone generator using solar energy. In: IEEE Asia-Pacific conference on circuits and systems; 1998. p. 217–20.
6. Marcos Alonso J, García J. Analysis, design, experimentation of a high-voltage power supply for ozone generation based on current- fed parallel-resonant push-pull inverter. *IEEE Trans Ind Appl.* 2005;41:5.
7. Koudriavtsev O, Wang S, Konishi Y, Nakaoka M. A novel pulse-density modulated high-frequency inverter for silent discharge-type ozonizer. *IEEE Trans Ind Appl.* 2002;38(2):369–78.
8. Marcos Alonso J, Cardesin J, Lopez Corominas E, Rico-Secedes M, Garcia J. Low-power high-voltage high-frequency power supply for ozone generation. *IEEE Trans Ind Appl.* 2004;40(2):414–421.
9. Hothongkham P, Kinnares V. Performance evaluation of an ozone generator using a phase shift PWM full bridge inverter. In: *ECTICON2008*; 2008.
10. Athab HS, Shadhu Khan PK. A cost effective method of reducing total harmonic distortion (THD) in single-phase boost rectifier. In: *IEEE Power Electronics and Drive Systems Conference Proceedings, 2007*; p. 669–74.
11. Singh S, Bhuvaneswari G, Singh B, Khas H. Multiple output SMPS with improved input power quality. In: *IEEE industrial and information systems (ICIIS) conference proceedings; 2010.* p. 382–387. 2010.
12. Zhu L, Wang K, Lee FC, Lai JS. New start-up schemes for isolated full-bridge boost converters. *IEEE Trans Power Electron.* 2003;18:946–51.
13. Cha H, Choi J, Enjeti PN. A three-phase current-fed DC/DC converter with active clamp for low-DC renewable energy sources. *IEEE Trans Power Electron.* 2008;23:2784–2793.
14. Adib E, Farzanehfard H. Zero-voltage transition current-fed full-bridge PWM converter. *IEEE Trans Power Electron.* 2009;24:1041–1047.
15. Jang Y, Jovanovic MM. A new family of full-bridge ZVS converters. *IEEE Trans Power Electron.* 2004;19:701–708.

16. Divan DM, Skibinski GL. Zero switching loss inverters for high power applications. *Conf Rec IEEE Ind Appl Soc* 1987;1:627–634.
17. Li H-H, Kutkut NH, Divan DM. Design considerations of IGBT's in resonant converter applications. *IEEE J Solid-State Circuits*. 1996;31(1):97–105.
18. Hothongkham P, Kongkachatand S, Thodsaporn N. Performance comparison of PWM and phase-shifted PWM inverter fed high-voltage high-frequency ozone generator. In: *TENCON 2011, IEEE region 10 conference proceedings*; 2011. p. 976–80.
19. Ekemezie PN. Design of a power factor correction AC-DC converter. In: *IEEE AFRICON 2007 conference proceedings*; 2007. p. 1–8.
20. Udhayakumar G, Rashmi MR, Patel K, Ramesh GP, Suresh A. High-frequency high-voltage power supply for ozone generator system. *Int J Appl Eng Res*. 2014;9(23):18913–30.

Author Biography

G. Udhayakumar was born in Tamilnadu, India. He has received his B.E degree in Electrical and electronics engineering from Anna University, Tamilnadu , India in 2005 and M.E degree in Power Electronics and drives from Madha engineering college (Anna university) Chennai, India in 2010. Currently he is a Senior R&D engineer, Ozonetek, Chennai. He has 7 years of industrial experience in the field of power electronics. He is presently a research scholar in St. Peter's University, Chennai, Tamilnadu. He is working in the area of harmonic reduction, power factor improvement and voltage stress in high-frequency inverter.

M.R. Rashmi obtained her B.E. (EEE) degree from Mysore University in the year 2001, M.E. (Power Electronics & Industrial Drives) degree from Sathyabama University in the year 2004 and Ph.D. degree from Sathyabama University in the year 2010. She has more than a decade of academic experience and several research publications to her. She is currently working as Associate Professor for Amrita Vishwa Vidyapeetham, School of Engineering, Bangalore, India.

K. Patel Kirit Patel is managing director and Head in the R&D Department, Ozonetek Ltd, Chennai, India. He obtained his B.Tech. in Chemical Engineering from Anna University, M.Tech. from Sweden and Ph.D. in the area of Ozone field from Madras University, Tamilnadu. He has published several technical papers in National and International Conferences/Journals. He has 25 years of industrial experience. His research interests include the areas of power electronics, electrode design, and fluid mechanics for ozone injection system. Currently, he is on Board of Directors, International Ozone Association, and EA3Group.

A. Suresh obtained his M.E degree from Sathyabama University, Chennai in 2005 and Ph.D. degree from Sathyabama University in the year 2012. His area of interest is Induction Heating. He has 15 years of teaching experience in engineering college and a life member in ISTE. He has published more than 30 papers in the area of Power Electronics. He is currently working as a Professor at SA Engineering College, Chennai, India.

Performance Comparison for Feed Forward, Elman, and Radial Basis Neural Networks Applied to Line Congestion Study of Electrical Power Systems

Pradyumna K. Sahoo, Ramaprasad Panda, Prasanta K. Satpathy and Mihir N. Mohanty

Abstract This paper presents a comparative analysis of the training performance for three important types of neural networks, namely Feed Forward neural network, Elman neural network, and Radial Basis Function neural network. In order to do this analysis, the authors performed sequential training of all the three neural networks for monitoring the congestion level in the transmission lines of the power system under study. This is accomplished through neural network simulation on the IEEE 30-bus test system under various operating conditions, namely base case, higher loading scenario, and contingency conditions. The findings of this study justify two things. On one hand, the results reveal that all the three neural networks yield successful training and are capable of reducing both the complexity and computational time as compared to the conventional iterative power flow simulation. Furthermore, the comparative analysis justifies that the radial basis function neural network is the fastest of all the three neural networks considered.

Keywords Line congestion · Neural networks · Training performance comparison

P.K. Sahoo · M.N. Mohanty
ITER, S'o'A University, Bhubaneswar, Odisha, India
e-mail: pradyumnakumar_sahoo@yahoo.co.in

M.N. Mohanty
e-mail: mihir.n.mohanty@gmail.com

R. Panda
Silicon Institute of Technology, Bhubaneswar, Odisha, India
e-mail: rppanda@sify.com

P.K. Satpathy (✉)
College of Engineering and Technology, Bhubaneswar, Odisha, India
e-mail: satpathy.pks@gmail.com

1 Introduction

Congestion level in transmission lines is a measure of the closeness of actual power transferred across transmission lines to their maximum power transfer capacity. As the gap between the two power levels reduces, the line gets more congested. The reasons for increasing level of line congestion are; over utilization of generation/transmission capacities, unprecedented abnormal hike in the demand, and unforeseen contingency conditions that might occur anytime, anywhere in the system beyond the knowledge and schedule of the operators on job. The final outcome of increasing congestion level in the lines may lead to system collapse due to the cascading events such as reduction of transmission efficiency in the system, operation of the lines close to their critical transmission level, and tripping of critical lines due to overstressing. The issues related to congestion of transmission lines in electrical power systems are addressed in the literature.

Canizares et al. [1] tried to find the effect of congestion management in electricity market pricing. Antonio et al. [2] evaluated the impact of congestion for the purpose of ensuring voltage stability. Several other researchers [3–6] in their proposed work raised various key issues on the background of transmission congestion concerning to line flow control, demand response, and differential evolution based deregulation of electricity market. Yet, the problem poses serious concern for every active researcher in this area. The major trouble that surfaces in the process of evaluation of the transmission line congestion in complex systems/critical conditions is that the conventional load flow technique often suffers from either slower convergence or non-convergence. Also, it requires repeat execution of the same for each scenario/operating condition.

The major objective of this paper is to overcome these limitations of conventional load flow approach by the application of neural networks. As observed in the literature [7–9], neural networks show consistently good results in various types studies concerning to power system analysis such as power system restoration and voltage stability monitoring. During training, the neural network learns from the events, by way of experiencing the training process so that the trained network can be exposed to any set of input data in a future time for necessary validation and testing. Hence, a trained neural network reduces the operator's burden of conducting repeat execution of conventional load flow programs. In consideration of these facts, the paper is organized as follows.

Section 2 highlights the methodology adopted for evaluation of the Line Congestion Index (LCI). Section 3 presents the formulation of neural networks, namely Feed Forward Neural Network (FFNN), Elman Neural Network (ENN), and Radial Basis Function Neural Network (RBFNN) for the comparison of their training performance. In this section, the authors considered multiple layer structure of the neural network by considering various combinations of hidden layers and number of neurons in those layers. Section 4 presents a detailed case study that validates successful implementation of the proposed methodology in IEEE 30-bus test system. The study encompasses two major objectives, (i) to assess whether

these neural networks could be trained successfully to meet the specific target/goal and if so (ii) which particular neural network performs efficiently in terms of lesser computational time and robustness.

2 Line Congestion Index

The training of neural networks essentially requires an extensive set of input data and a specific target dataset. The input dataset in this paper covers the LCI values of all the lines in the test system corresponding to a diverse set of operating conditions. In order to meet this requirement, the authors performed Newton–Raphson load flow simulation, which is used once in the beginning for evaluating the LCI and formation of the input dataset. The procedure adopted in this paper for evaluation of LCI is enumerated below.

The differential voltage and current expressions over an elementary section ‘dx’ at a distance ‘x’ from the receiving end of a long transmission line with distributed parameters are represented in Eqs. (1) and (2), where ‘z’ and ‘y’ imply the impedance and admittance values per unit length of the line, respectively.

$$dV_x = (I_x z) dx \quad (1)$$

$$dI_x = (V_x y) dx \quad (2)$$

The solution of these expressions results in Eqs. (3) and (4).

$$V_x = \left(\frac{V_r + \left(\frac{\sqrt{z/y}}{2} \right) I_r}{2} \right) e^{(\sqrt{yz})x} + \left(\frac{V_r - \left(\frac{\sqrt{z/y}}{2} \right) I_r}{2} \right) e^{(-\sqrt{yz})x} \quad (3)$$

$$I_x = \left(\frac{\left(\frac{V_r}{\sqrt{z/y}} \right) + I_r}{2} \right) e^{(\sqrt{yz})x} - \left(\frac{\left(\frac{V_r}{\sqrt{z/y}} \right) - I_r}{2} \right) e^{(-\sqrt{yz})x} \quad (4)$$

The term $\sqrt{z/y}$ in the above equations represents the characteristic impedance or surge impedance (Z_c) of the line. In case of a particular power system as shown in Fig. 1, while the load impedance matches exactly with the characteristic impedance or surge impedance of the line, the line gets eventually terminated by its own characteristic impedance.

During this condition, maximum power transfer to the load takes place that eventually matches with the limiting power transfer capability of the said line. This limiting power margin is called Surge Impedance Loading (SIL) of the line, as expressed in Eq. (5).

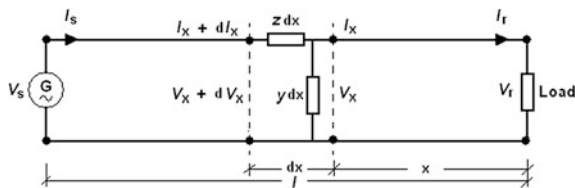


Fig. 1 Generalized representation of a long transmission line (distributed parameters)

$$SIL = \frac{|V_l|^2}{|Z_c|} \tag{5}$$

The line congestion in transmission systems has been addressed by various researchers. Aswani et al. [10] defined the transmission congestion distribution factor as a ratio of two powers at two candidate lines subject to unit change of power at one of them. However, the approach is limited to show the congestion level of the line subject to maximum change power admissible for the other line. Yingzhong et al. [11] proposed a sensitivity index for wind curtailment subject to transmission congestion as the ratio of change in curtailed wind generation to that of transmission line capacity. This index, although serves the purpose of deciding wind power generation curtailment, it suffers from determining the congestion level of individual lines from a loading perspective. The LCI proposed by Panda et al. [12] is used in this paper that takes care of both the above mentioned limitations. The proposed LCI is defined as the ratio of the actual value of real power (P_l) transmitted in a particular line to its own SIL, which serves as an indicator of the congestion level in that particular line, as shown in Eq. (6).

$$LCI = \frac{P_L}{SIL} \tag{6}$$

3 Performance Comparison for Neural Networks

Neural networks offer several applications in solving complex real world problems with ease. Such applications have been widely accepted by the researchers in the area of electrical power systems. Pandey et al. [13] performed the congestion management study using RBFNN for price prediction of electricity. Alberto et al. [14] demonstrated the possibility of applying some elementary neural network techniques for congestion analysis of a zonal market. Application of FFNN to power systems has also been reported by other researchers [15–17].

A generalized structure of these neural networks with hidden layers is presented in Fig. 2. This paper explores the possibility of applying neural network technique for monitoring the congestion level in electrical power transmission networks by

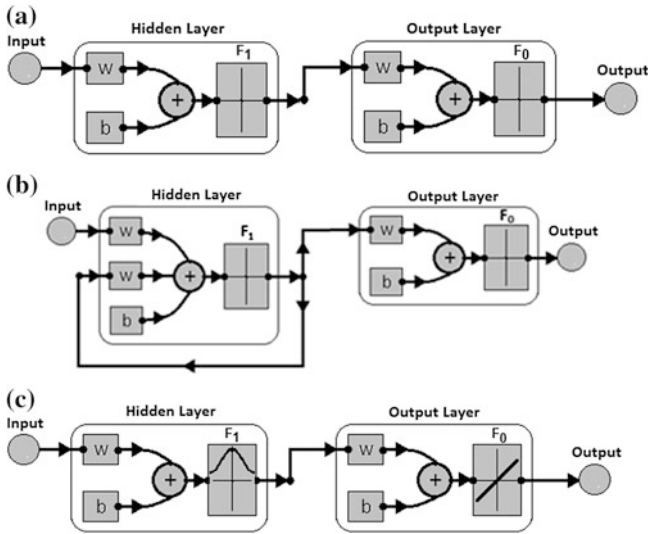


Fig. 2 Generalized structure of **a** FFNN, **b** ENN, and **c** RBFNN. **a** FFNN structure with one hidden layer. **b** ENN structure with one hidden layer. **c**RBFNN structure with one hidden layer only

considering some of the leading neural network configurations such as FFNN, ENN, and RBFNN. In case of FFNN and ENN, there could be more than one hidden layer and the function blocks (F_1 and F_0) could assume either linear or nonlinear functions. However, in case of RBFNN, there is only one hidden layer with radial basis function and one output layer with a linear function.

The hidden layers contain neuron like elements having interconnectivity. These interconnections by and large determine the network transfer function. Each connection is associated with an index called weight parameter that modulates/transforms the input in accordance with the weighting index. The transfer functions for each hidden layer may differ from one another. In this paper, the authors have made use of four types of transfer functions such as linear (*purelin*), tan-sigmoid (*tansig*), log-sigmoid (*logsig*), and radial basis function (*radbas*) as represented in Fig. 3. In this figure, the relationship between the output (a) and input (n) for a particular layer is expressed by the transfer function (f) taking into consideration the weight (w) and bias (b) associated to the neurons in that layer,

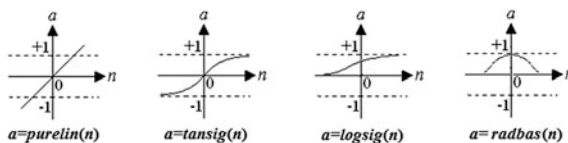


Fig. 3 Layout of various transfer functions for FFNN, ENN, and RBFNN

as shown in Eq. (7). Then, the error (e) is calculated as the difference between the specified target vector (T) and output vector (a) as shown in Eq. (8). The procedure for selection of target vector for this study is described in the next section.

$$a = f(wp + b) \quad (7)$$

$$e = T - a \quad (8)$$

4 Implementation and Result Analysis

The basic objective behind this work was to train the neural networks by exposing them to a set of input data reflecting the trend and variations in congestion level of a system pertaining to various practical situations as depicted in Table 1. In order to accomplish this goal, the authors have formulated an extensive set of input data containing LCI results obtained from conventional Newton–Raphson load flow for various operating scenario/events. These operating conditions have been simulated considering various loading level described as a function of load increasing parameter (λ) and contingency constraints. In the base case loading condition, the load increasing parameter takes a zero value, whereas higher values refer to increased loading condition.

In order to simulate the load growth in the system, the complex load demand at the buses has been increased simultaneously as a function of the base loading. This is performed with the help of a load increasing parameter (λ) that gives the loading pattern ' $S = (1 + \lambda)(S_{\text{base}})$ '. Furthermore, the line outage contingency is also considered by imposing a maximum of 15 % of existing lines taken for outage. Since the IEEE 30-bus system contains 41 lines, this paper considers a maximum of six line outage contingencies.

In the view of Table 1, 32 situations have been framed for formation of input dataset and the target dataset in order to perform the proposed training analysis. With these considerations, the proposed methodology has been tested on the standard IEEE 30-bus test system by pursuing the following steps.

Step 1: Formation of Input data: In order to form the sequential input data for training the neural networks, the N-R load flow is performed for 32 test runs and the LCI for all the 41 lines of the IEEE 30-bus test system are evaluated. When the LCI results are arranged in matrix form, the input data matrix had dimensions (32×41).

Table 1 Operating scenarios for evaluation of LCI

Nomenclature of scenario/event	Loading parameter ($\lambda = 0$ implies base case)	Contingency constraints
1–16	$\lambda = 0-1.5$ (0.1 rise per step)	No line outage
17–32	$\lambda = 0-1.5$ (0.1 rise per step)	Line outage considered (15 % of total lines out)

Step 2: *Formation of Target data:* In this step, the LCI values obtained in Step-1 are monitored for each operating scenario and a target value is formed for that scenario based on the following logic, as shown in Eq. (9).

$$T = \begin{cases} 1 & |_{m \geq n} \\ 0 & |_{m < n} \end{cases} \tag{9}$$

Here, ‘*T*’ is the target value for a particular event/scenario, which depends on two parameters ‘*m*’ and ‘*n*’ such that ‘*m*’ represents a physical count describing the number of lines with $LCI \geq 1$ as revealed from Step 1, and ‘*n*’ refers to a count described by 15 % of existing lines in the IEEE 30-bus system. In the present case, we have a fixed value for ‘*n*’ (i.e. $n = 15\%$ of $41 = 6$), whereas ‘*m*’ may vary as per the observations of Step 1. Thus, the resulting target matrix had dimensions (32×1) . The coefficient (15 %) as used in this paper for selection of line outage contingency (Table 1) and the count ‘*n*’ in this step is considered as an approximate selection that may vary from case to case.

Step 3: *Formation of Study Cases:* Different study cases are identified in this step that includes different neural network structure and conventional approach as indicated in Table 2.

Step 4: *Initialization of neural network parameters:* The authors used following parameters for imparting training to the neural networks in this study case.

- Maximum permissible Epochs per training cycle: 10
- Error tolerance limit for training convergence (ϵ): 0.001
- Number of hidden layers (FFNN, ENN, RBFNN): 1
- Number of neurons in hidden layer (FFNN, ENN): 5

Table 2 Formation of Study Cases for Performance Comparison

Study case	Type of neural network	Transfer function assigned to layers	
		Hidden layer (F_1)	Output layer (F_0)
Case-1	FFNN	Purely linear	Tan-sigmoid
Case-2	FFNN	Purely linear	Log-sigmoid
Case-3	FFNN	Tan-sigmoid	Purely linear
Case-4	FFNN	Tan-sigmoid	Log-sigmoid
Case-5	FFNN	Log-sigmoid	Purely linear
Case-6	FFNN	Log-sigmoid	Tan-sigmoid
Case-7	ENN	Purely linear	Tan-sigmoid
Case-8	ENN	Purely linear	Log-sigmoid
Case-9	ENN	Tan-sigmoid	Purely linear
Case-10	ENN	Log-sigmoid	Purely linear
Case-11	RBFNN	Radial Basis	Purely linear
Case-12	Conventional Newton–Raphson iterative load flow simulation		

Number of neurons in each hidden layer (RBFNN): same as number of Targets = 32

Step 5: *Check for convergence*: During each training cycle, the neural network uses the input dataset for calculation of the output and the corresponding error function. The error is defined as the difference between calculated output and specified target value. The training process converges if the calculated error is such that ' $e \leq \varepsilon$ ' is satisfied during a particular epoch of that training cycle. In case, the convergence criteria is not met within a desired number of training cycles, the training process is terminated and another fresh training is performed with newer settings of Step 4, till successful training is achieved.

In this paper, all the above mentioned steps have been performed to impart successful training to the neural networks through Matlab simulation. The convergence results thus obtained are presented in Table 3, and the plots are shown respectively in Figs. 4, 5, and 6.

The overall advantage of applying neural networks for monitoring congestion level is also observable from the contrasting results of Case-12 that shows a significantly high value of convergence time. A straightforward comparison between the conventional approach (Case-12) and other three cases of neural networks (Case-1 through Case-11) gives the relative speed of training convergence.

The space distribution of error vector with respect to input vector is also shown for all three types of neural network training, respectively, in Figs. 4, 5 and 6. The analysis of these figures reveals the following aspects.

Table 3 Training results showing successful training convergence

Study case	Results for successful training convergence			
	Number of training cycles	Number of epochs	Time taken in (s)	Relative speed of convergence as compared to case-12
Case-1	118	1172	49.07	8.47
Case-2	36	360	19.90	20.94
Case-3	10	98	5.39	77.18
Case-4	66	660	32.26	12.89
Case-5	93	929	41.32	10.06
Case-6	27	270	13.35	31.16
Case-7	8	80	6.52	63.80
Case-8	8	80	6.52	63.80
Case-9	11	110	8.45	49.23
Case-10	7	70	5.81	71.60
Case-11	1	1	0.07	5942.85
Case-12	NA (conventional approach)		416.00	1.00

Fig. 4 Error–input distribution obtained from a particular training convergence of FFNN

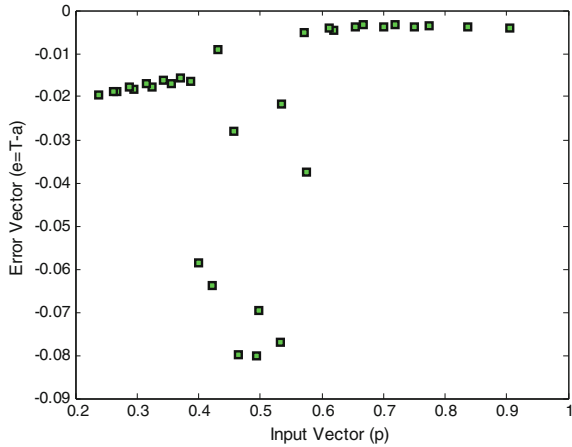
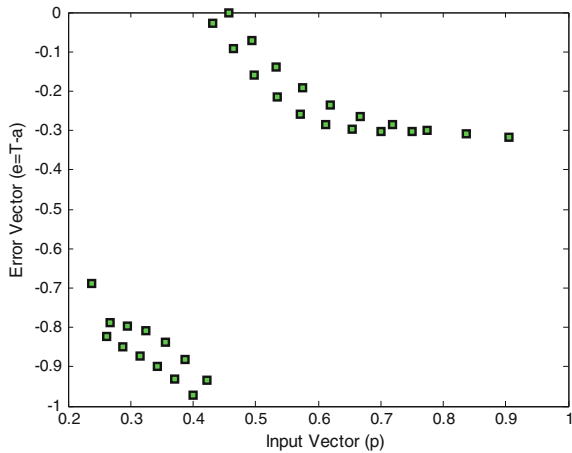


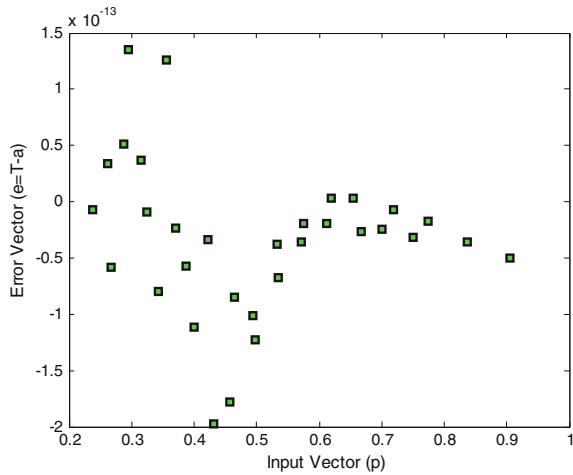
Fig. 5 Error–input distribution obtained from a particular training convergence of ENN



- (i) That the range of error is least for RBFNN (i.e., $0-3.5 \times 10^{-13}$) and highest for ENN (i.e., 0–1), while the FFNN offers a medium range for the error (i.e., 0–0.1). This also adds to the training performance in favor of RBFNN.
- (ii) That in case of Fig. 6, the overall error distribution density shows more uniform and compact distribution around the central region of the surface in the plots. This fact indicates the robustness of RBFNN as compared to the other two schemes, namely FFNN and ENN.

The results indicate that successful training convergence is achieved for all the study cases considered (Case-1 through Case-11). A further analysis based on comparison of convergence time reveals that the RBFNN (Case-11) yields the fastest convergence of all cases considered with a record timing of 0.07 s. Among the other two categories of neural networks, faster convergence is also noticed as

Fig. 6 Error–input distribution obtained from a particular training convergence of RBFNN



indicated by Case-3 for FFNN and Case-10 for ENN having convergence time of 5.39 and 5.81 s, respectively.

In view of the above analysis, it is inferred that a suitably trained neural network is capable of monitoring line congestion level in electrical power systems. Among the three types of neural networks compared in this study, it is observed that RBFNN offers best training performance.

5 Conclusions

The basic objective of this paper is satisfied through the case study conducted on IEEE 30-bus test system. The study is based on a conventional approach of load flow simulation for formulation of the input dataset consisting of LCI values for 32 situations/events. The dataset so formed are presented to three types of neural networks for imparting successful training. The study validates that all the three types of neural networks (FFNN, ENN, RBFNN) used in the study are capable of acquiring successful training showing different training performance. The training performance comparison indicates that RBFNN scheme is the most compact and robust network among the three networks that offers fastest convergence.

References

1. Canizares CA, Hong C, Milano F, Singh A. Transmission congestion management and pricing in simple auction electricity markets. *Int. J. Emerg Electric Power Syst* 2004;1(1):1–10.
2. Conejo AJ, Milano F, Raquel G. Congestion management ensuring voltage stability. *IEEE Trans Power Syst* 2006;21(1):357–364.

3. Venkatarajan SS, Thiagarajan J. A congestion line flow control in deregulated power system. *Serbian J Electr Eng.* 2011;8(2):203–12.
4. Yousefi A, Nguyen TT, Zarei H, Malik OP. Congestion management using demand response and FACTS devices. *Electr Power Energy Syst.* 2012;37(1):78–85.
5. Rajathy R, Harish K. Power Flow Tracing Based Congestion Management Using Differential Evolution in Deregulated Electricity Market. *International Journal of Electrical Engineering and Informatics.* 2012;4(2):371–92.
6. Aswani K, Srivastava SC, Singh SN. Congestion management in competitive power market: a bibliographical survey. *Electr Power Syst Res.* 2005;76:153–64.
7. Iman S, Abbas K, Rene F. Radial basis function neural network application to power system restoration studies. *Comput Intell Neurosci.* 2012;1:1–10.
8. Bahamanyar AR, Karami A. Power system voltage stability monitoring using artificial neural networks with a reduced set of inputs. *Electr Power Energy Syst.* 2014;58:246–56.
9. Zhou DQ, Annakkage UD, Rajapakse AD. Online monitoring of voltage stability margin using an artificial neural network. *IEEE Trans Power Syst.* 2010;25(3):1566–74.
10. Aswani K, Srivastava SC, Singh SN. A zonal congestion management approach using real and reactive power rescheduling. *IEEE Trans Power Syst.* 2004;19(1):554–62.
11. Yingzhong G, Xie L, Brett R, Hesselbaek B. Congestion-induced wind curtailment: sensitivity analysis case studies. In: *Proceedings of the North American power symposium*; 2011. 1–7.
12. Panda RP, Sahoo PK, Satpathy PK, Paul S. Analysis of critical conditions in electric power systems by feed forward and layer recurrent neural networks. *Int J Electr Eng Inf.* 2014;6(3):447–459.
13. Pandey SN, Tapaswi S, Srivastava L. Price prediction based congestion management using growing RBF neural network. In: *Proceedings of the annual IEEE India conference*; 2008. p. 482–7.
14. Alberto B, Maurizio D, Marco M, Marco SP, Politecnico M. Congestion management in a zonal market by a neural network approach. *Eur Trans Electr Power.* 2009;19(4):569–84.
15. Xue L, Jia C, Dajun D. Comparison of Levenberg-Marquardt method and path following interior point method for the solution of optimal power flow problem. *Emerg Electr Power Syst.* 2012;13(3):15–35.
16. Ilamathi B, Selladurai VG, Balamurugan K. ANN-SQP Approach for NOx emission reduction in coal fired Boilers. *Emerg Electr Power Syst.* 2012;13(3):1–14.
17. Keib AAE, Ma X. Application of artificial neural networks in voltage stability assessment. *IEEE Trans Power Syst.* 1995;10(4):1890–6.

Design and Analysis of PEM Fuel Cell with Multilevel Inverter Using Multicarrier PWM Techniques

M. Muthuselvi and K. Antony Samson

Abstract This project is to investigate the mathematical behavior of a PEMFC connected with different multilevel inverters. Here, multicarrier PWM technique based multilevel inverters are used to enhance output voltage with low THD. Polymer electrolyte membrane fuel cell (PEMFC) is the most preferred fuel cell for the standalone systems due to their inherent virtue of being compact with quick start-up and higher efficiencies with very low emission. In this project, various multicarrier PWM techniques of multilevel inverters are analyzed which can reduce THD for a 5 level inverter. In-phase disposition, phase opposition disposition, and alternate phase opposition disposition concepts have been employed in this project. A study is carried out by developing mathematical model of PEM fuel cell with multicarrier PWM based 5 level multilevel inverters. To obtain the desired output for the load, boost converter is connected.

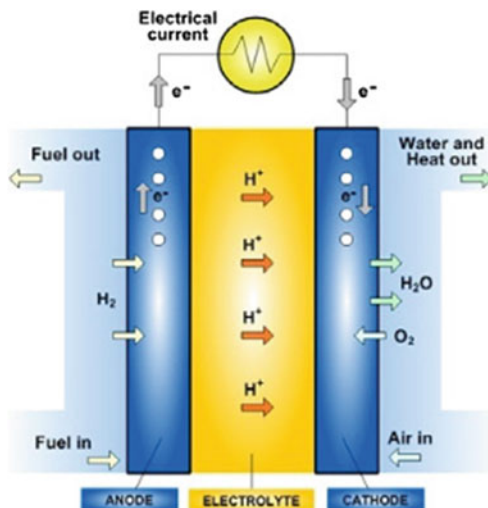
Keywords PEM fuel cell · Multilevel inverter · Pulse width modulation · Total harmonic distortion · Boost converter · Standalone systems · In phase · Phase opposition · Alternate phase opposition

1 Introduction

Fuel cell converts electrochemical energy stored in the form of gaseous molecules (fuel and oxidant) is directly converted into electrical energy. Hydrogen is used as fuel and the byproducts are water and heat. Unlike batteries which require

M. Muthuselvi (✉) · K. Antony Samson
Velammal Engineering College, Chennai, India
e-mail: eee.muthuselvi@velammal.edu.in

K. Antony Samson
e-mail: selsamk@gmail.com

Fig. 1 Structure of fuel cell

recharging, fuel cells are capable of operating continuously to produce power as long as hydrogen and oxygen are given. Typically, the fuel cell reactants consist of hydrogen on anode and oxygen on cathode. The entire process is reverse of water electrolysis. In electrolysis process, current is being supplied to water to produce hydrogen and oxygen [1].

There are many types of fuel cells available in markets. Some of them are polymer electrolyte membrane fuel cell (PEMFC), Alkaline Fuel Cell, Direct Methanol Fuel Cell, Phosphoric Acid Fuel Cell, and Solid Oxide Fuel Cell. PEM fuel cell is commonly used fuel cell because of its high efficiency. Structure of fuel cell is given in Fig. 1.

2 Proton Exchange Membrane Fuel Cell

The polymer electrolyte membrane (PEM) is a most commonly used fuel cell system that provides backup power as in standalone application such as offices, homes, hospitals, schools, vehicles, etc. The operating temperature of fuel cell stack is $80\text{ }^\circ\text{C}$ and has 40–50 % of efficiency. This cell operates at low temperature to make them suitable for standalone system. The system requires pure hydrogen as fuel and oxygen or air. When the PEM fuel cell stack is operated in a vehicle, it can operate for 2000–4000 h and for stationary application operates for about 40,000 h. Stack replacement is a major expense although it has longer lifetime and good substitute for batteries.

3 Mathematical Model of PEMFC

Generally, fuel cell modeling is done with mathematical expression. The I - V curve, otherwise known as polarization curve is used to define the characteristics of fuel cell. When these cells are series connected, it forms a stack and produce sufficient power. A PEM fuel cell generally can perform at operating temperature is around 60–80 °C with partial pressure of 3–5 atm. Electrons flow from anode to cathode to provide electrons [2]. The behavior of fuel cell depends upon a number of factors such as current density, temperature, and partial pressure. The voltage of the cell decreases with increase in current. The average voltage of a fuel cell is defined by an analytical expression:

$$V_{\text{cell}} = E - V_{\text{act}} - V_{\text{ohmic}} - V_{\text{conc}} \quad (1)$$

where, E is the Nerest voltage, V_{act} is the activation over potential, V_{ohmic} is the ohmic over potential and V_{conc} defines concentration loss. If cells are in series, the following equation is used

$$V_{\text{stack}} = V_{\text{cell}} \times N. \quad (2)$$

The energy lost is converted and stored as heat. The V - I characteristic has three regions:

1. *Region of activation polarization*, where activation over voltage takes place. The activation overvoltage occurs due to the activation of anode and cathode. The activation polarization loss is dominant at the low current density and can be described by the Tafel equation:

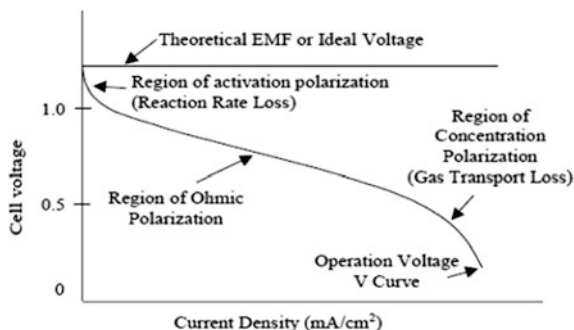
$$V_{\text{act}} = V_{\text{act},c} + V_{\text{act},a} = \frac{RT}{\alpha_c F} \ln\left(\frac{i + i_{\text{loss}}}{i_{0,c}}\right) + \frac{RT}{\alpha_a F} \ln\left(\frac{i + i_{\text{loss}}}{i_{0,a}}\right) \quad (3)$$

2. *Region of ohmic polarization*, where ohmic over voltage take place. These losses occur due to the resistance in ionic flow of the electrolyte, resistance in the flow of electrons, and the resistance at the cell terminals.

$$V_{\text{ohmic}} = (r_{\text{el}} + r_{\text{ion}}) \cdot i \quad (4)$$

3. *Region of concentration polarization*, where concentrations over voltage take place. When current exceed a particular value, the voltage collapse. These losses due to a reduction in the reactants concentrations at the electrode–membrane interface [3]. This effect can be expressed mathematically by correlating to the limiting current densities and used in the present model.

Fig. 2 V - I characteristics of PEM fuel cell



$$V_{\text{conc}} = V_{\text{conc},c} + V_{\text{conc},a} = \frac{RT}{nF} \ln\left(1 - \frac{i}{i_{\text{lim},c}}\right) + \frac{RT}{nF} \ln\left(1 - \frac{i}{i_{\text{lim},a}}\right) \quad (5)$$

In order to obtain a cell voltage v_{cell} , voltage drops caused by activation polarization loss, ohmic polarization loss, and concentration polarization loss have to be deducted from open cell voltage (Fig. 2).

4 Multilevel Inverters

The concept of multilevel inverters is to provide higher power and to use semiconductor switches to perform the power conversion by using staircase voltage waveform. Multilevel converter provides higher power rating and also enables the usage of renewable energy sources. Batteries and renewable energy sources can be used as multiple dc voltage sources. Multilevel inverters are classified into three types:

- Diode-clamped multilevel inverter (Neutral point clamped inverter)
- Flying Capacitor multilevel inverter (Capacitor clamped inverter)
- Cascaded H-bridge multilevel inverter

4.1 Diode-Clamped Multilevel Inverter

The diode-clamped inverter is used to clamp the dc voltage in order to obtain stepped output voltage. For n level diode-clamped inverter, each leg consists of $2(n - 1)$ switches, $(n - 1) * (n - 2)$ diodes and $(n - 1)$ dc link capacitor. By increasing voltage level, the output voltage can be improved and the obtained waveform is closer to sinusoidal waveform. There are five switch combinations to synthesize five-level voltages. These switching operation are given in Table 1.

Table 1 Diode-clamped five-level inverter switching states

Output VAO	Switch State							
	S_1	S_2	S_3	S_4	S_1'	S_2'	S_3'	S_4'
$V_5 = V_{dc}/2$	1	1	1	1	0	0	0	0
$V_4 = V_{dc}/4$	0	1	1	1	1	0	0	0
$V_3 = 0$	0	0	1	1	1	1	0	0
$V_2 = -V_{dc}/4$	0	0	0	1	1	1	1	0
$V_1 = -V_{dc}/2$	0	0	0	0	1	1	1	1

Table 2 Flying capacitor five-level inverter switching states

Output VAO	Switch State							
	S_1	S_2	S_3	S_4	S_1'	S_2'	S_3'	S_4'
$V_5 = V_{dc}/2$	1	1	1	1	0	0	0	0
$V_4 = V_{dc}/4$	1	1	1	0	1	0	0	0
$V_3 = 0$	1	1	0	0	1	1	0	0
$V_2 = -V_{dc}/4$	1	0	0	0	1	1	1	0
$V_1 = -V_{dc}/2$	0	0	0	0	1	1	1	1

4.2 Flying Capacitor Multilevel Inverter

The structure of this inverter is very much similar to that of diode-clamped inverter except, instead of using clamping diodes, the inverter uses capacitors for clamping. The flying capacitor involves series connection of capacitor clamped switching cells [4].

The voltage synthesis in a five-level capacitor-clamped converter has more flexibility than a diode-clamped converter. To synthesize five-level capacitor clamped multilevel output voltage, switching operation is given in Table 2.

4.3 Cascaded Multilevel Inverter

One more alternative for a multilevel inverter is the cascaded multilevel inverter or series H-bridge inverter. The cascade has been utilized in wide range of application. With its modularity and flexibility, the cascade shows superiority in high-power applications, especially shunt and series connected FACTS controllers. The cascade synthesizes its output nearly sinusoidal voltage waveforms by combining many isolated voltage levels.

To synthesize the five-level cascaded multilevel output voltage, switching operation is given in Table 3.

Table 3 Cascaded five-level inverter switching states

Output VAO	Switch state							
	S_{a1}	S_{a2}	S_{a3}	S_{a4}	S_{ab1}	S_{b2}	S_{b3}	S_{b4}
$V_5 = V_{dc}/2$	1	0	0	1	1	0	0	1
$V_4 = V_{dc}/4$	1	0	0	1	1	1	0	0
$V_3 = 0$	1	1	0	0	1	1	0	0
$V_2 = -V_{dc}/4$	1	1	0	0	0	1	1	0
$V_1 = -V_{dc}/2$	0	1	1	0	0	1	1	0

5 Multicarrier Pulse Width Modulation (MCPWM)

In multicarrier PWM, the sinusoidal reference is compared with each triangular carrier, and the output of this comparison produces two complementary signals. In this method, the frequency and the peak-to-peak amplitude of the carriers have to be same. The carrier arrangement was shown to affect THD performance. It was concluded that by increasing the modulation indices for all the MCPWM techniques, the THD is reduced [5].

The carrier-based modulations for multilevel inverters can be classified into two types. They are phase-shifted and level-shifted modulations. THD of PSM is much higher than LSM. Hence, we prefer level-shifted modulation. There are three PWM strategies with different phase relationships for the level-shifted multicarrier modulation. They are,

- i. In-phase disposition (IPD).
- ii. Phase opposition disposition (POD).
- iii. Alternate phase disposition (APOD).

5.1 In-phase Disposition

The in-phase disposition is based on a single carrier that is multiplied across the entire voltage range. These carriers have the same peak-to-peak amplitude A_c and frequency f_c and are compared with the sine wave reference to produce two complementary signals. Figure 3 represents an output waveform of IPD for a 5 level inverter [6].

5.2 Phase Opposition Disposition

The phase opposite disposition uses two carriers, one for positive voltage levels and one for negative voltage levels. The negative voltage levels are shifted by 180° with

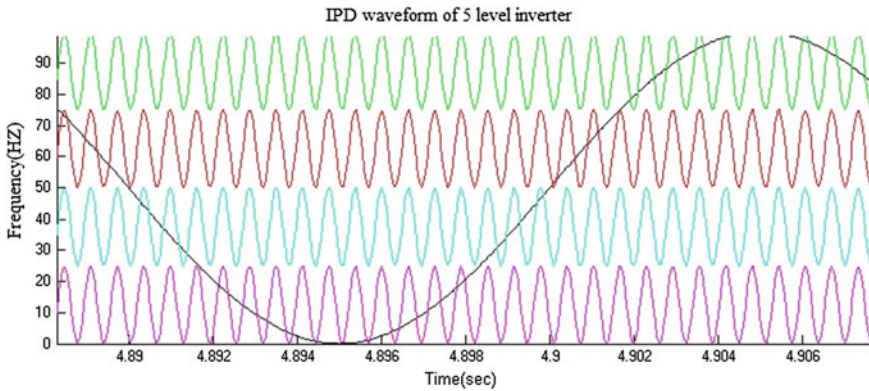


Fig. 3 In-phase disposition PWM (5 level inverter)

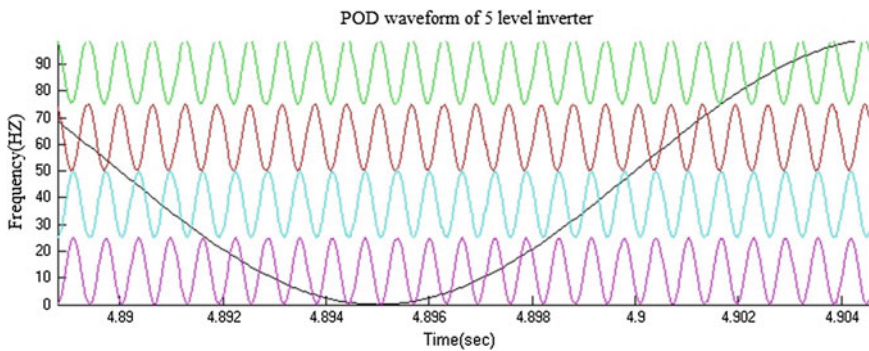


Fig. 4 Phase opposition disposition PWM (5 level inverter)

respect to the carrier for the positive voltage levels. The sign of their corresponding voltage levels in order to fill the entire voltage range then multiplies the carriers. Figure 4 represents an output waveform of POD for a 5 level inverter.

5.3 Alternate Phase Opposition Disposition

The alternative phase opposite disposition is based on two carriers that vary in the initial starting voltage level and phase. These carriers have the same amplitude and frequency. However, when these carriers are compared with the reference sinusoid a pair of complementary PWM outputs is produced. Figure 5 represents an output waveform of APOD for a 5 level inverter.

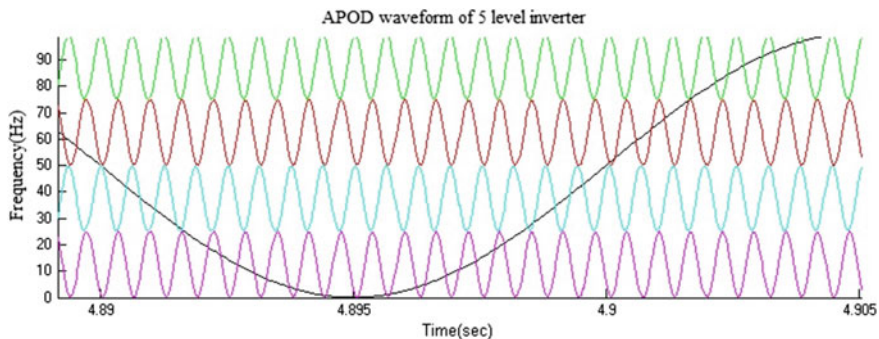


Fig. 5 Alternate phase opposition disposition PWM (5 level)

6 Simulink

The entire system has been modeled on MATLAB 2009b and Simulink. The overall block diagram is as shown in Fig. 6. A fuel cell stack connected with multilevel inverter along with the boost converter. The boost converter boosts up the output voltage obtained from fuel cell stack (Fig. 7).

Here, the input voltage obtained is 42.35 V and output voltage is approximately 85 V. It find applications in various real life scenarios like charging of battery banks, water pumping, motors etc. The simulation has been done for a resistive load and duty of 0.5. Figures 8, 9 and 10 show the simulation of five-level multilevel inverter which is using multicarrier PWM techniques.

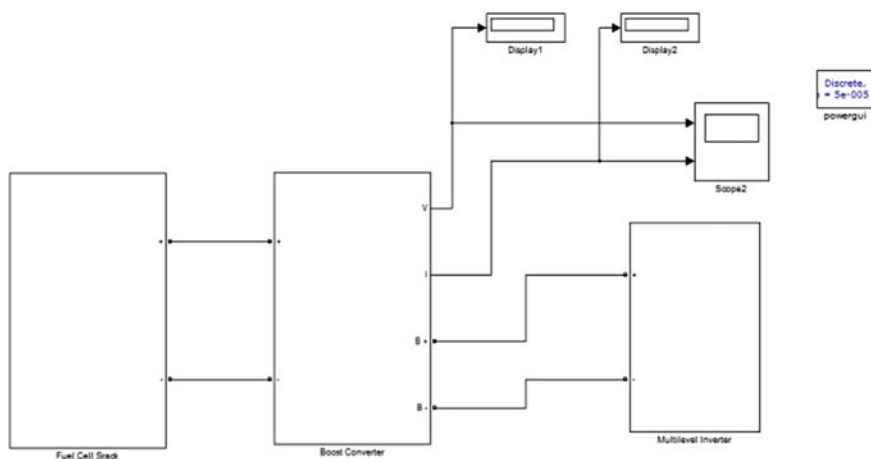


Fig. 6 Overall block diagram of fuel cell system

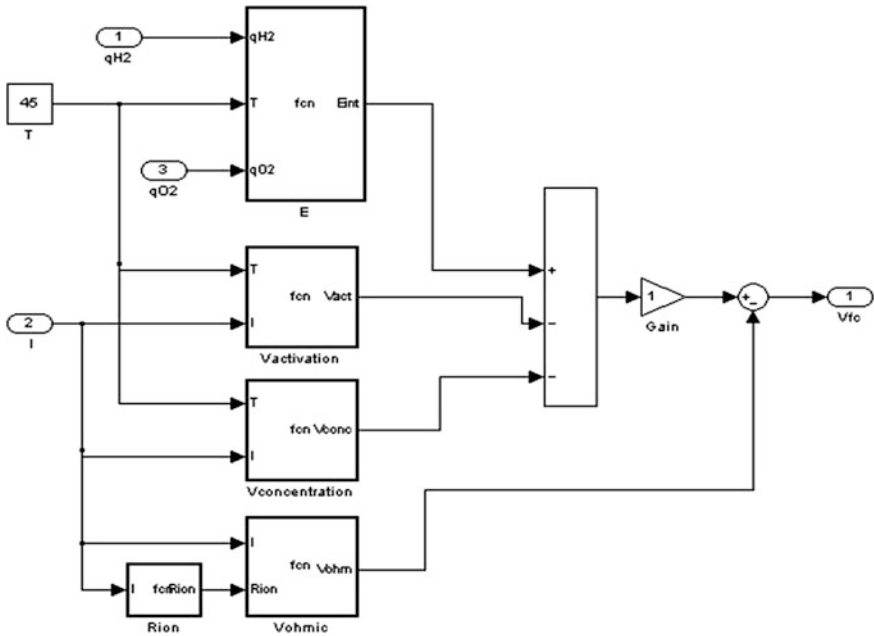


Fig. 7 Mathematical modeling of single fuel cell

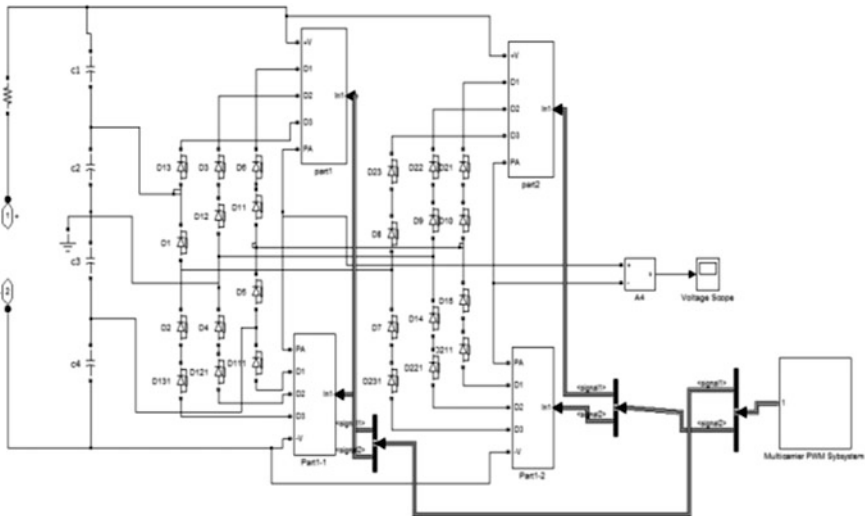


Fig. 8 Diode-clamped multilevel inverter (5 level)

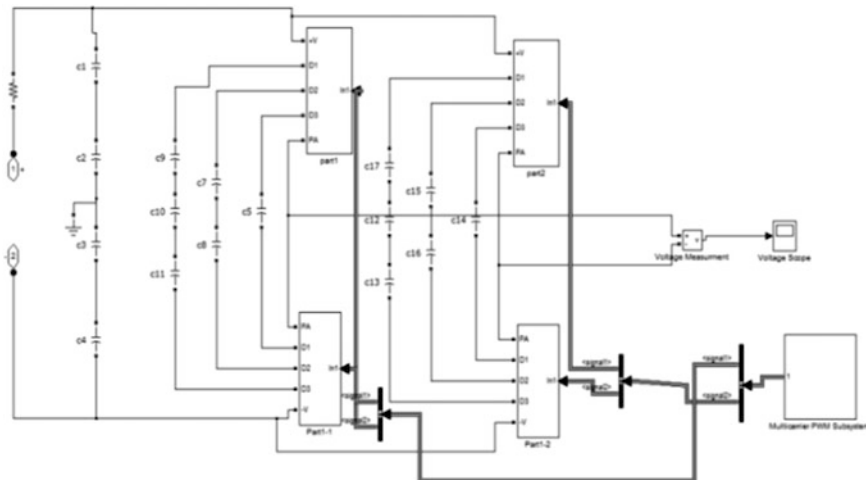


Fig. 9 Flying capacitor multilevel inverter (5 level)

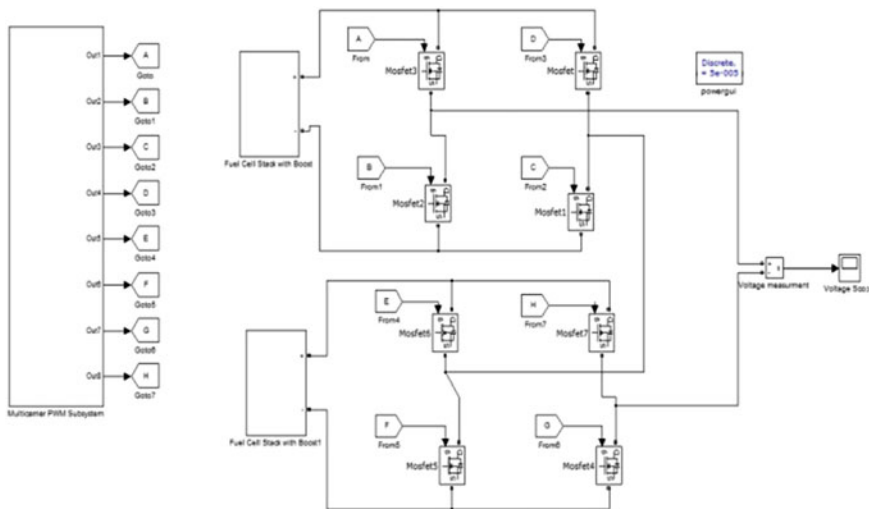


Fig. 10 Cascaded multilevel inverter (5 level)

Multicarrier PWM technique is a simple technique which uses one reference frequency and multiple carrier frequency to produce gate pulse by comparing both the frequencies. Here, one reference frequency is made to compare with four level of carrier frequency. Figure 11 shows the simulation of Multicarrier PWM [7].

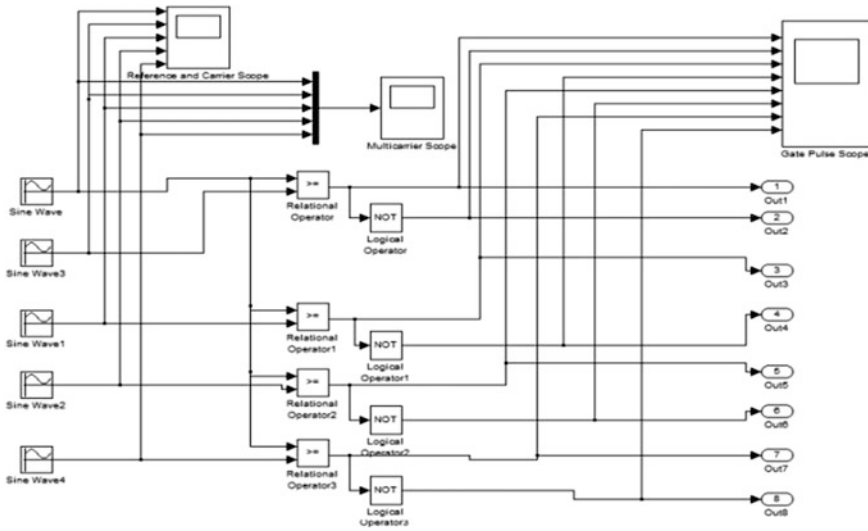


Fig. 11 Simulation of multicarrier PWM

7 Simulation Results

Single fuel cell is generating about 0.7 V with constant supply of hydrogen and oxygen at constant temperature of about 25–55 °C. In this paper, fuel cells are connected in series such that they can generate about 42.35 V. It is shown in Fig. 12. Here, only the voltage increases and the current remain constant.

The output voltage and output current waveform of boost converter is shown in Fig. 13. Thus, the boost converter steps up the stack voltage from 42.35 V to approximately 85 V.

The boost voltage is given to diode-clamped multilevel inverter and its simulation is described in Fig. 8. Here, the output voltage of diode-clamped multilevel inverter is being obtained by using three different MCPWM schemes. From the FFT analysis,

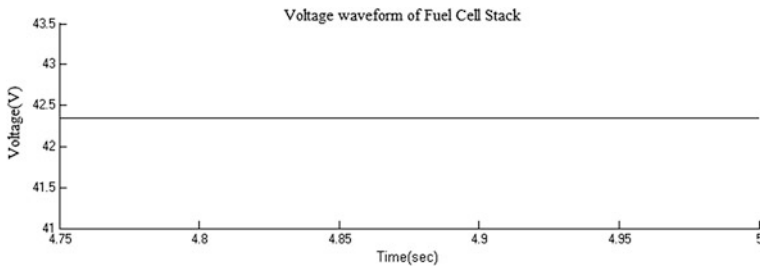


Fig. 12 Output voltage waveform fuel cell stack

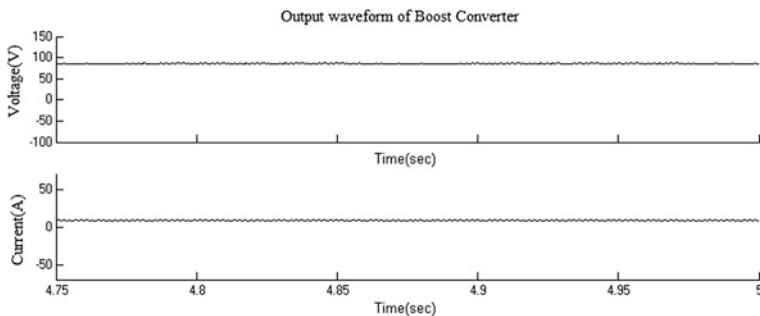


Fig. 13 Output waveforms of boost converter

it is clear that both POD and APOD produce low THD value. Figure 14 shows the output voltage waveform of 5 level diode-clamped multilevel inverter [8].

Here, the boost voltage is given to flying capacitor multilevel inverter and its simulation is described in Fig. 9. The output voltage is obtained by different types of MCPWM schemes. From the analysis, it shows that only APOD produce low THD value. Figure 15 shows the output voltage waveform of a 5 level flying capacitor multilevel inverter.

The simulation of the Cascaded multilevel inverter is being described in Fig. 10. The output voltage of cascade is approximately 85 V and is obtained by different types of MCPWM schemes. From the FFT analysis, it shows that only APOD produce low THD value. Figure 16 shows the output voltage waveform of 5 level cascaded multilevel inverter.

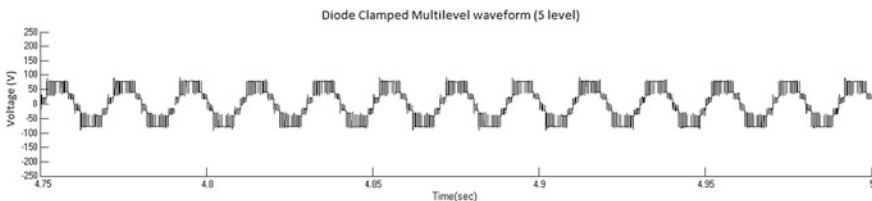


Fig. 14 Output waveform of diode-clamped MLI (5 level)

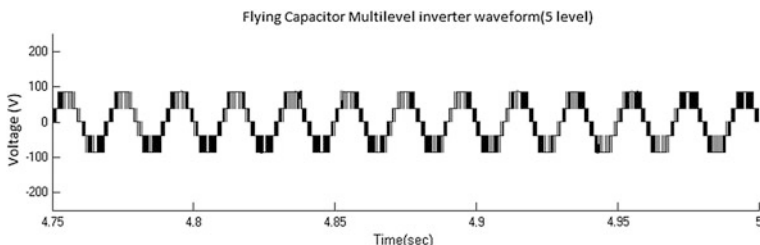


Fig. 15 Output waveform of flying capacitor MLI (5 level)

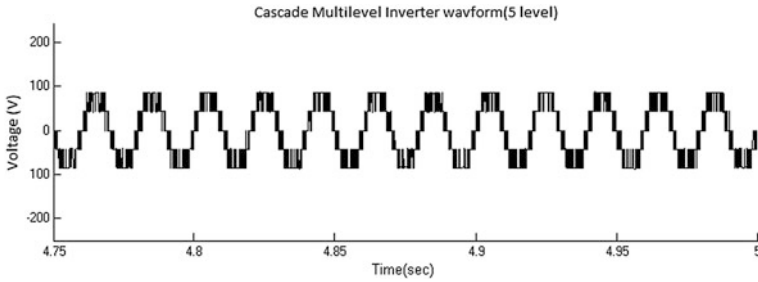


Fig. 16 Output waveform of cascaded MLI (5 level)

Table 4 Comparison of THD of three multicarrier PWM schemes

Multicarrier PWM	Diode-clamped inverter (%)	Flying capacitor inverter (%)	Cascade bridge-bridge inverter (%)
IPD	18.74	19.57	18.58
POD	18.50	19.59	18.64
APOD	18.51	19.46	18.61

A comparative study is done on various Multicarrier PWM technique. From the Table 4, the APOD schemes produce an output voltage with the lowest harmonic distortion, and are therefore likely to be the best MCPWM schemes for a 5 level multilevel inverters.

8 Conclusion

In this paper, various multilevel inverters using multicarrier PWM technique are studied and simulated. Multicarrier PWM technique is used to improve output voltage quality of the inverter. Modeling of the PEM fuel cell has successfully addressed various aspects of the fuel cell. We obtain 0.7 V for a single fuel cell and a stack of fuel cells gives 42.35 V, thus we obtain approximately 350 W. When a boost converter is connected with fuel cell stack, we obtain approximately 750 W. Three different types of level-shifted MCPWM are studied and compared in order to find the technique that gives better output voltage and produces low THD. From all these level-shifted MCPWM, alternate phase opposition disposition (APOD) provides better output voltage and low distortion.

References

1. Wang C, Nehrir, MH, Shaw SR, Dynamic models and model validation for PEM fuel cells using electrical circuits. In: IEEE transactions on energy conversion; 2005. p. 442–51.
2. Pasricha S, Shaw SR. A dynamic PEM fuel cell model. IEEE Trans Energy Convers. 2006;21(2):484–90.
3. Wang C, Hashem Nehri M. Load transient mitigation for stand-alone fuel cell power generation systems. In: IEEE transactions on energy conversion; 2007.
4. Zhao J, Han Y, He X, Tan C. Multilevel circuit topologies based on the switched capacitor converter and diode clamped converter, IEEE Trans. Power Electron. 2011;26:8.
5. Angulo M, Lezana P, Kouro S, Rodríguez J. Level shifted PWM technique for cascade multilevel inverter with even power distribution. In: IEEE transaction on power electronics, PESC; 2007.
6. Kouro S, Lezana P, Angulo M, Rodríguez J. Multicarrier PWM with DC-link ripple feed forward compensation for multilevel inverters. IEEE Trans on Power Electron. 2008;23:1.
7. Tamasas M, Saleh M, Shaker M, Hammada A. Evaluation of modulation techniques for 5 level inverter based on multicarrier level shift PWM, IEEE transaction on power electronics; 2014.
8. Tamasas M, Saleh M, Ahmed. Evaluation of modulation techniques for 5-level inverter based on multicarrier level shift PWM, In: 17th IEEE Mediterranean electro technical conference, Beirut, Lebanon, 2014;13–16.

Power Quality Enhancement in a Distribution System Using Inductive Active Filtering Technique

K. Naresh Kumar, R. Siva and S. Srinath

Abstract In this Paper a new converter transformer using inductive active filtering technique are suggested to solve the prevailing problems of the traditional converter transformer with the active filtering method in the distribution system. The distribution network provides power supply to various kinds of non-linear loads like three phase rectifier fed motor drives and high power industrial electrolysis. Generally a converter transformer is used in the rectifier and inverter station. The harmonic components from the nonlinear load flows easily into the winding of the transformer, which decreases the life time of transformer and it also brings PQ problems to the distribution network and the supply system. To overcome this problem an inductively filtering method was proposed in this paper. A tap at the connecting point of the transformer secondary prolonged winding and the secondary common winding is associated with the filter circuit. When the harmonic current goes into the secondary prolonged winding, the common winding of the new converter transformer will make the contrasting harmonic current to balance it by the zero impedance design of the secondary common winding, so there will be no induced harmonic current in the primary winding of the new converter transformer. Performance of Inductive active filtering method is very effective compared with traditional shunt active power filtering method.

Keywords Power quality · Traditional converter transformer · New converter transformer passive power filters · Inductive active filter (IAF) · Total harmonic distortion (THD) · PSCAD/EMTDC

K. Naresh Kumar (✉)

EEE Department, Velammal Institute of Technology, Chennai, India
e-mail: mail2nareshk88@gmail.com

R. Siva · S. Srinath

EEE Department, Velammal Engineering College, Chennai, India
e-mail: rsivaps@gmail.com

S. Srinath

e-mail: srinaths.1976@gmail.com

© Springer India 2016

S.S. Dash et al. (eds.), *Artificial Intelligence and Evolutionary Computations in Engineering Systems*, Advances in Intelligent Systems and Computing 394, DOI 10.1007/978-81-322-2656-7_114

1253

1 Introduction

Nowadays more power electronics based applications are being applied in distribution a network, which brings severe harmonic problems to the power system. The distribution network provides power supply to various kinds of nonlinear loads like three-phase rectifier fed motor drives and large power industrial electrolysis. Since the characteristics of power electronic devices are inherently nonlinear, it leads to power quality (PQ) problems.

The HVDC transmission system has been broadly used in long distance bulk power transmission. HVDC transmission system consists converter station at either ends, a dc link is used to connect the converter station at both ends. During conversion process, a wide-ranging harmonics will be generated by the converters. Hence, it is required to reduce the harmonics created by the converters present at either ends. The traditional converter transformer with ac filters are always located at primary side of the traditional converter transformer. So the transformer will be badly affected by harmonics, which causes some serious problems such as losses created by harmonics, noise, heat, and vibration.

To overcome these problems, a new converter transformer using inductive active power filtering method was recommended. This method can prevent a harmonic and reactive power component which flows easily into the primary winding of the converter transformer and as a result it can effectively solve the Power Quality difficulties of the power system. In principle, this method uses the balance of a transformer magnetic potential to carry out power filtering.

2 Traditional Converter Transformer

As Fig. 1 illustrate, the traditional converter transformer with passive filtering technique are normally used in HVDC system. It is clear that filters are located at the transformers primary side. Even though traditional converter transformer and passive filtering technique are commonly used in HVDC systems, these constructions still have some drawbacks

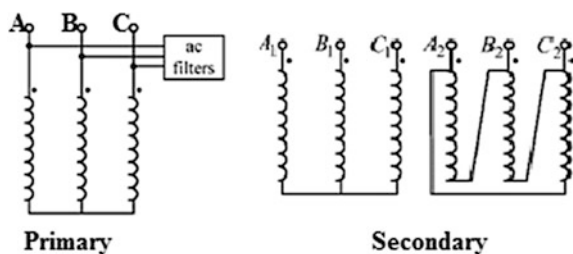


Fig. 1 Wiring method of traditional converter transformer with passive filters

1. The main harmonic-generating source is the non-linear load. The rectifier or inverter usually creates characteristic current harmonics at the ac side. The non-characteristic current harmonics can also be created due to several unbalances in system voltages, impedance, and parameters of the transformer. The entire current harmonics will flow easily in the windings of the converter transformer, as a result it increases the heat, noise and vibration in the transformer. At the end, losses, the difficulty in design of insulation, transformer capacity, and the design capability increases, which rises the overall cost of the transformer
2. The most difficult one is resonance that occur between the system impedance and the passive filters at the converter transformer primary side. This resonance condition will magnify harmonic currents and voltages, and it might damage the filters and nearest equipment. To escape from this condition, the modified frequency of filters is aimed to some extent further away from the leading harmonic frequency. But, it will damage the routine of the passive filter, and the filtering outcome of the passive filter cannot be optimum.

3 New Converter Transformer

Figure 2b illustrate the new converter transformer and the corresponding inductive filtering wiring arrangement, its secondary winding implements the prolonged-delta connection. To simplify our argument, the winding of A_i - a_i , B_i - b_i , C_i - c_i ($i = 1, 2$) is named secondary prolonged winding, and winding a_1 - b_1 , b_1 - c_1 ,

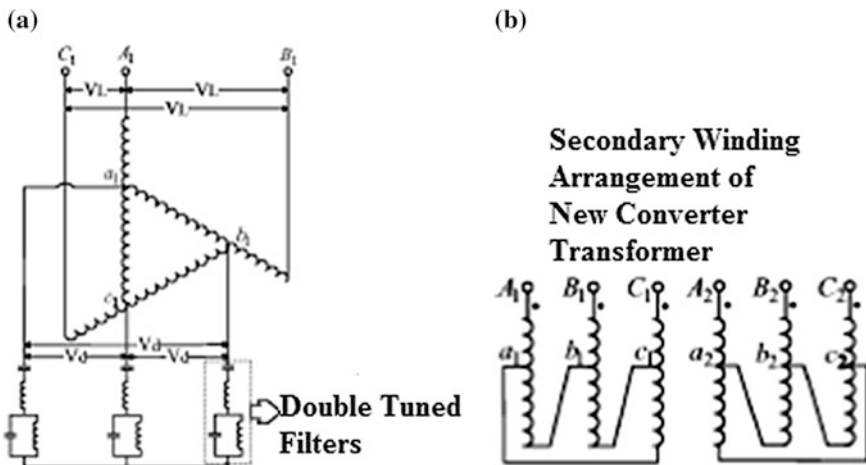
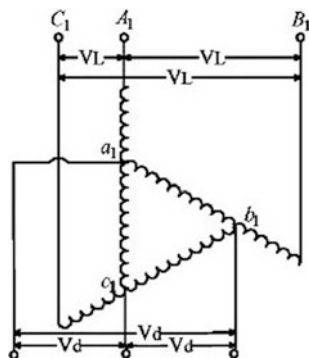


Fig. 2 Wiring method of new converter transformer

Fig. 3 Winding arrangement of new converter transformer



$c_1-a_1, a_2-c_2, b_2-a_2, c_2-a_2$ is called secondary common winding. Figure 2a indicate the arrangement of inductive filters. From Fig. 2a, we can see that double-tuned filters is connected at the linking point secondary prolonged and common winding.

Self-Coupling Action. The self-coupling accomplishment of the secondary prolonged and common winding of new converter transformer is related to the autotransformer series winding and the common winding.

Agreeing to Fig. 3, if the line-voltage is V_L , the secondary common winding voltage is V_d and secondary prolonged winding voltage is V_e . The voltage phasor diagram has been attained.

According to cosine rule, the equation for output line voltage can be stated as follows:

$$V_L^2 = (V_e + V_d)^2 + V_e^2 - 2V_e(V_e + V_d) \cos \frac{2\pi}{3} \tag{1}$$

Then, the secondary prolonged Winding voltage can be realized as follows:

$$V_e = -\frac{V_L^2}{3} + \sqrt{\frac{V_L^2}{3} - \frac{V_d^2}{12}} \tag{2}$$

The electromagnetically coupled new converter transformer’s secondary prolonged and common winding, which is related to series and common winding of autotransformer. When secondary prolonged and common windings maintains the magnetic force equilibrium, we get the following relation:

$$V_e I_e = V_d I_d \tag{3}$$

in which I_e and I_d are the RMS value of current of the prolonged and common winding respectively.

The current of secondary prolonged winding I_e and it is equal to the output current I_o , and its electromagnetic capacity can be expressed as follows:

$$S_e = 3V_e I_o \tag{4}$$

Meanwhile, the output capacity can be expressed as follows:

$$S_o = \sqrt{3}V_L I_o \tag{5}$$

Then, the coefficient ratio can be obtained as follows, which is used to analyse the material utilizing ratio of the transformer:

$$\alpha = \frac{S_e}{S_o} = \frac{\sqrt{3}V_e}{V_L} \tag{6}$$

where α is the ratio coefficient of new converter transformer.

Inductive Filtering Mechanism The single-phase harmonic model of the new converter transformer is shown in Fig. 4. This single phase harmonic model is used to analyze the inductive filtering mechanism in the new converter transformer. In this diagram, the harmonic current source is represented as I_h , which is also represents the secondary prolonged winding harmonic current. The harmonic current of primary winding and the secondary common winding is represented as I_{h1} and I_{h3} respectively. The harmonic current I_h in secondary prolonged winding will induce the harmonic currents I_{h1} and I_{h3} in the primary winding and the secondary common winding of the transformer. These currents are used to balance I_h .

According to ampere turns method, the following results:

$$W_2 I_h = W_1 I_{h1} + W_3 I_{h3} \tag{7}$$

in which W_1 , W_2 , and W_3 are the turns number of the primary winding, secondary prolonged winding, and secondary common winding, respectively.

If the turns number of the secondary prolonged winding and common winding is kept balanced then I_{h1} becomes zero. There is no induced harmonic current in the primary winding. Therefore, the harmonic currents flows only in the branch of the secondary winding of the transformer.

Fig. 4 New converter transformer's single phase harmonic model

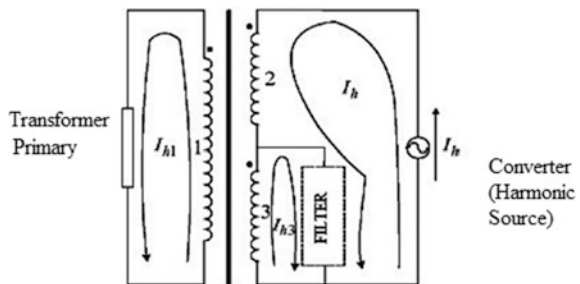




Fig. 5 Single-phase model wiring arrangement

To know the inductive filtering method, it not only needs the full tuning of the filter, but also it needs zero impedance design of common winding of the transformer. It is analyzed in the following new converter transformer single-phase model as shown in Fig. 5.

The short-circuit impedances Z_{12} , Z_{13} , and Z_{23} has been obtained from short circuit test [2]. The impedance value can be stated as follows:

$$\left. \begin{aligned} Z_1 &= 0.5(Z_{12} + Z_{13} - Z'_{23}) \\ Z'_2 &= 0.5(Z_{12} + Z'_{23} - Z_{13}) \\ Z'_3 &= 0.5(Z_{13} + Z'_{23} - Z_{12}) \end{aligned} \right\} \tag{8}$$

The winding arrangement shown in Fig. 5, the impedance of secondary common winding of new converter transformer Z'_3 is made more or less equal to zero (the resistance value is ignored in high-capacity transformers). Therefore the harmonic currents mainly flows only in the branch of the common winding, and there is no induced harmonic currents in the primary winding of the transformer.

Equivalent Circuit Model Figure 6 [1] indicate the equivalent circuit model of the IAF. In this model, the secondary side of the new converter transformer implements prolonged winding and the common winding. There is a connection point for each phase between these two windings in which tuned filter has been connected.

In order to create a balancing harmonic potential this special secondary winding design was made. Thereby, the stimulation of harmonic currents on the primary winding of the transformer has been prevented effectively.

4 System Configuration

The traditional APF and the proposed IAF topologies methods are compared in Fig. 7. The traditional APF is generally realised at the Point of Common Coupling. The coupling transformer is used to interface the shunt active filter with the power system as shown in Fig. 7a [1]. Nonlinear loads like rectifier fed DC motor drives are connected to the distribution system via converter transformer. In order to

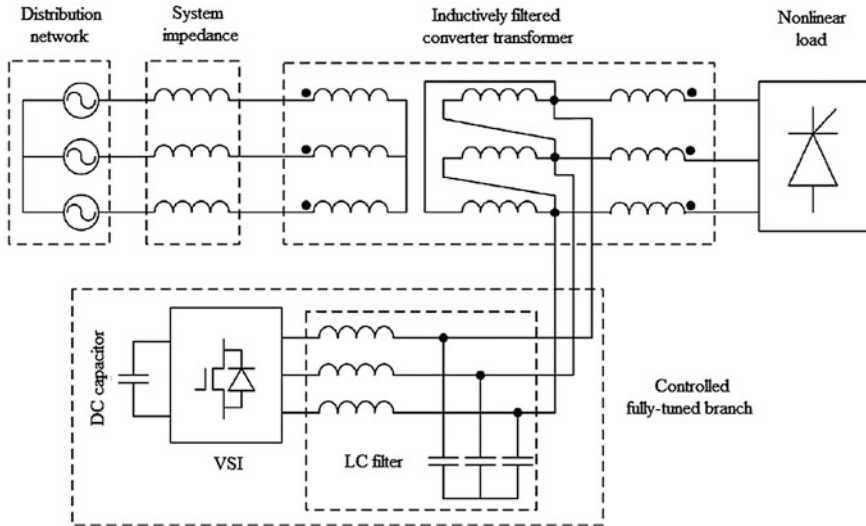


Fig. 6 Wiring scheme of IAF

separate the dc supply system from the distribution network a converter transformer is used

From Fig. 7a [1] it is obvious that the harmonic load current I_L flows into the PCC over the converter transformer. The traditional converter transformer has to suffer from all of the harmonics and reactive power components from the load current I_L . As a result it leads to added losses, increase in temperature, vibration, and noise. When APF is connected in parallel with the converter bridge, the commutation process of the rectifier gets affected by the impedance of the APF. Thus, the PQ problems cannot be avoided for the converter transformer in traditional APF method.

The proposed IAF method is shown in Fig. 7b [1]. In this figure, a new converter transformer is connected between the nonlinear load and the source. The shunt active filter is connected at the connecting point of prolonged winding and common winding of the new converter transformer. Once the commutation process starts the harmonics flows into the secondary of the prolonged winding and common winding. Since the filter is connected at the linking point of two winding the filter draws all the harmonic components on the secondary side itself. Thus, the primary winding is free from harmonics. In this way, the harmonic components are suppressed near the nonlinear load itself. It means the path of harmonic flow is restricted in a small area, which significantly reduces the effect of harmonics on the supply system.

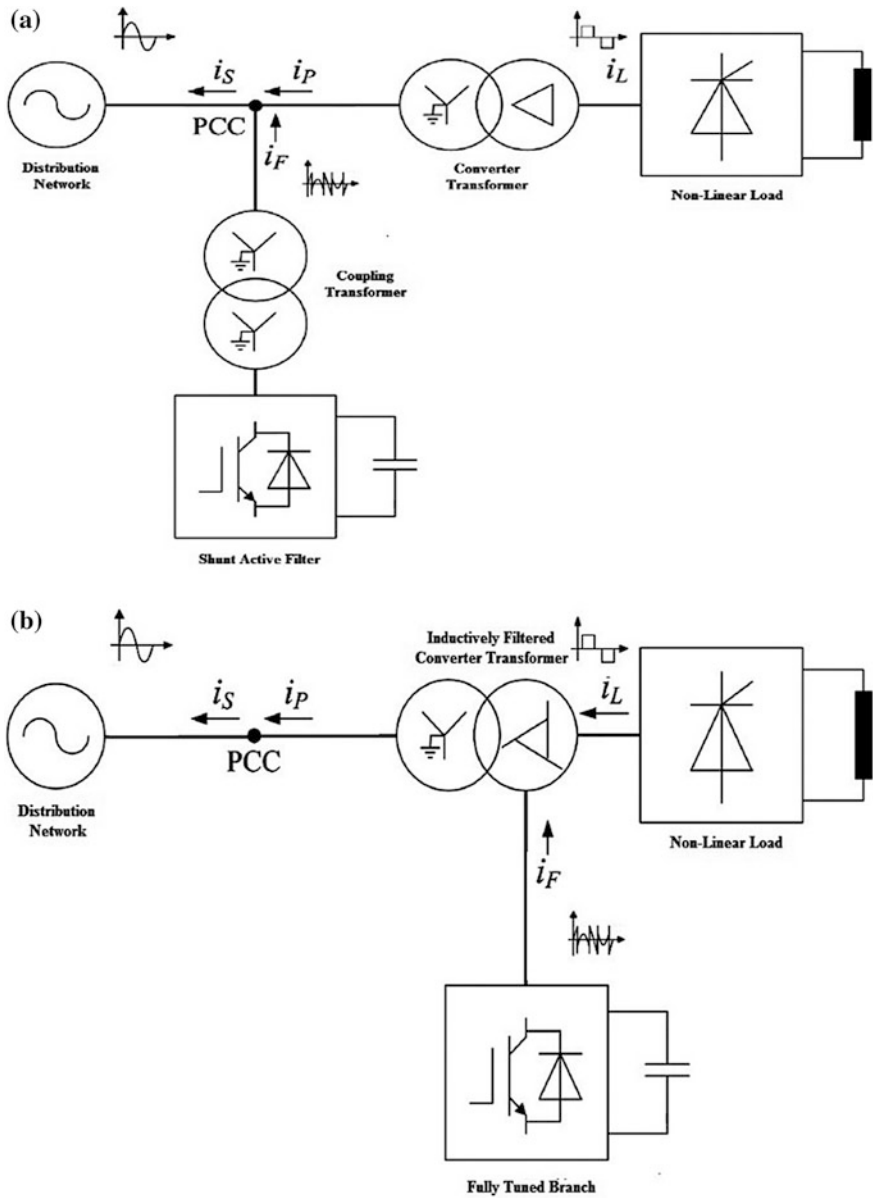


Fig. 7 Comparison of topologies: **a** traditional APF located at the PCC side, **b** proposed IAF coordinated with the converter transformer

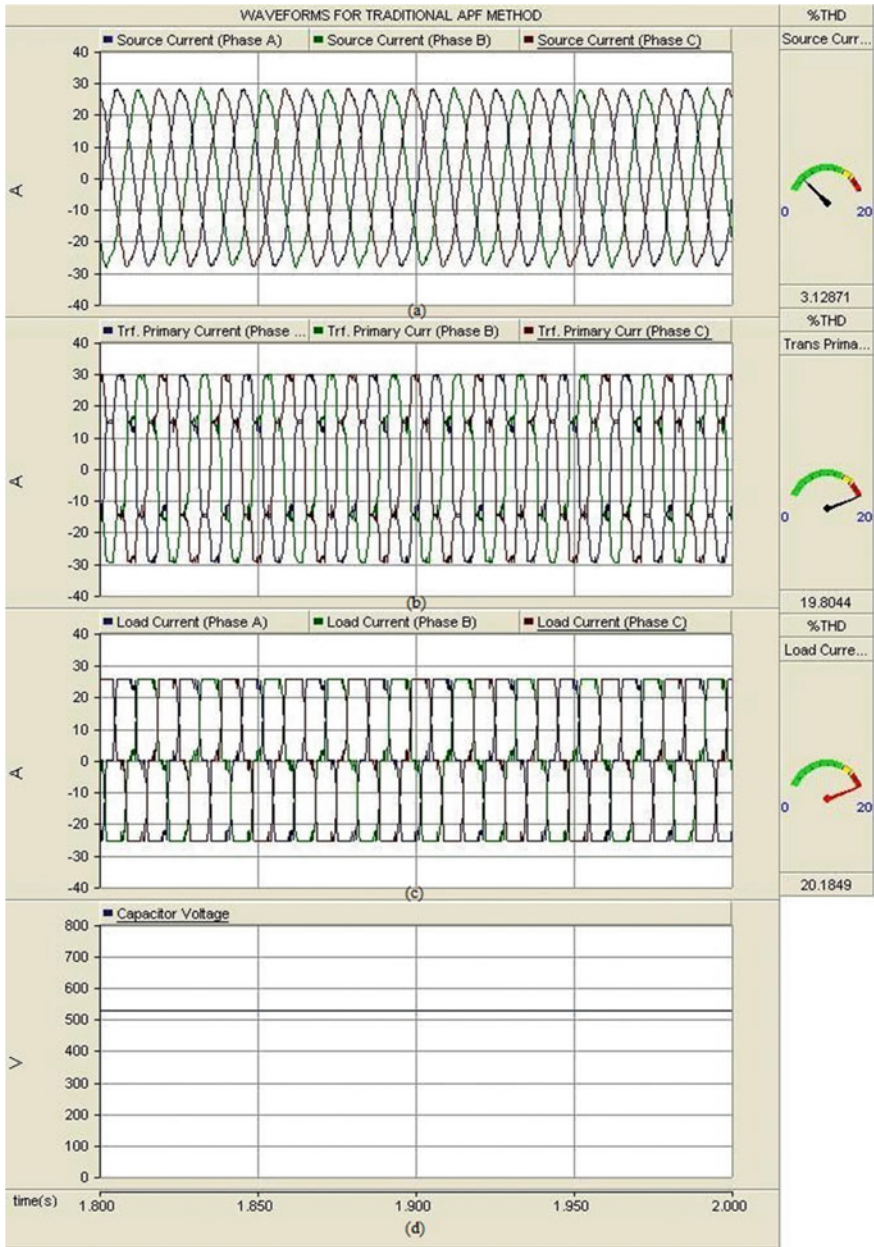


Fig. 8 PSCAD/EMTDC results of the traditional APF. **a** Current at the load side. **b** Current at the grid winding of the transformer. **c** Current at the ac side

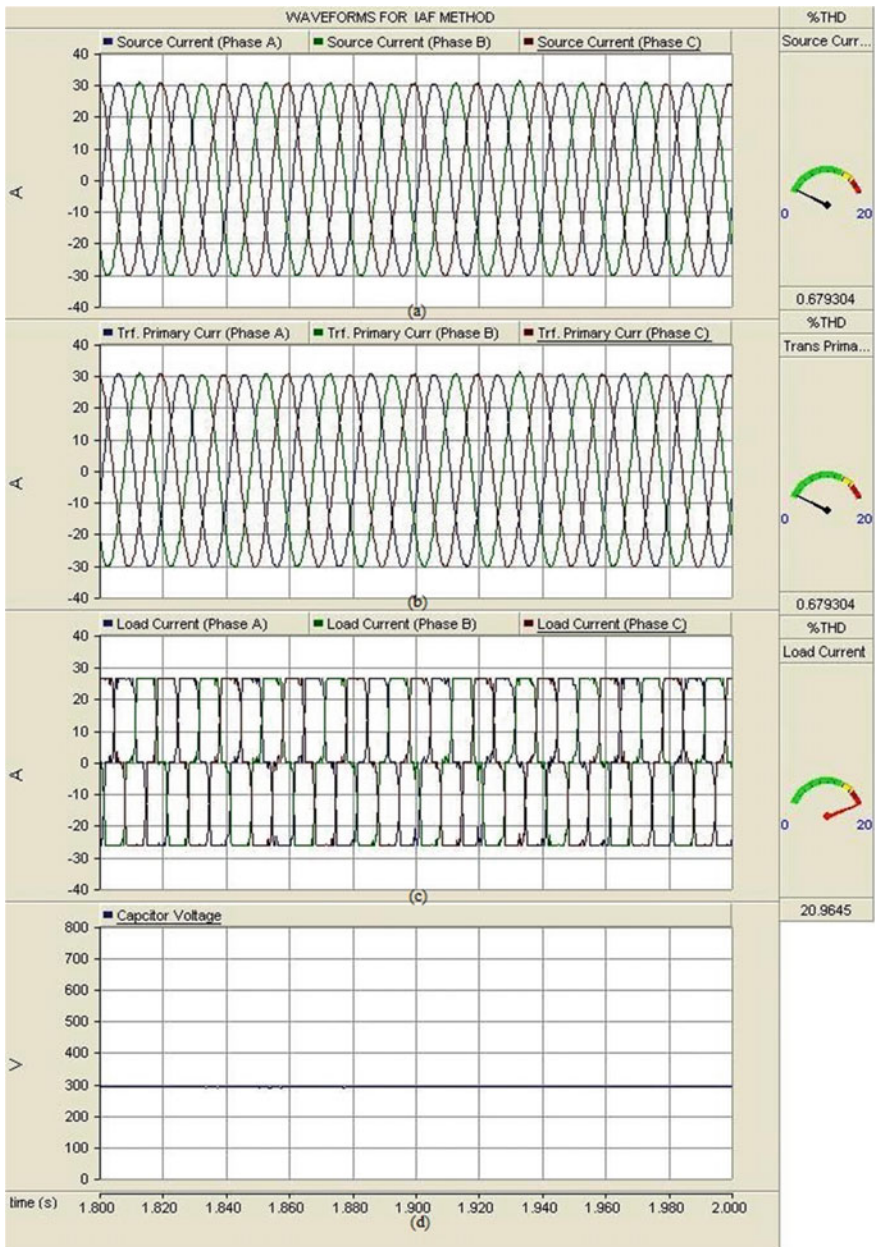


Fig. 9 PSCAD/EMTDC results of IAF method. **a** Current at the load side. **b** Current at the grid winding of the transformer. **c** Current at the ac side

5 Filtering Performance

Figures 8 and 9 shows the PSCAD/EMTDC results of the traditional APF and the IAF method, respectively. In Figs. 8a and 9b. It is seen that load current has harmonic components, which is determined by the type of nonlinear load.

It can also be seen from Figs. 8c and 9c that traditional APF and IAF methods can prevents the harmonic currents entering the source side, thus improving the power quality of the distribution network.

In Fig. 8b, it is evident that the harmonic current flows through the converter transformer. From Fig. 8b is clear that the proposed IAF method has prevented the harmonic current entering the transformer and it suppresses the harmonic component at the secondary winding itself.

Real and reactive power measurement is shown in Figs. 10 and 11. It is observed from Figs. 10a and 11a that the reactive power consumption from the source is zero MVAR. The reactive power required for the load is generated by the active filter as shown Figs. 10b and 11b (Table 1).

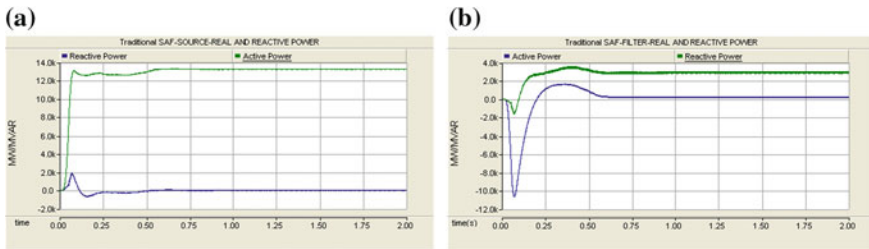


Fig. 10 Real and reactive power flow using traditional converter transformer with shunt active filter. a Source side. b Filter side

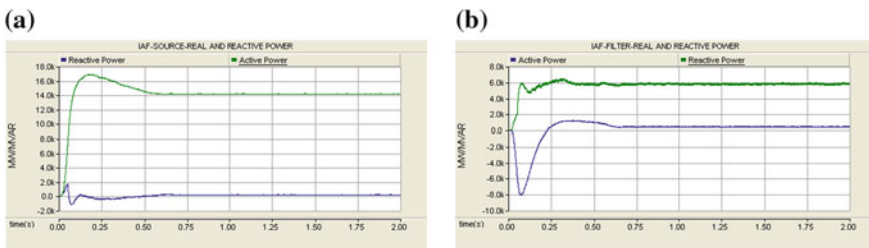


Fig. 11 Real and reactive power flow using new converter transformer with shunt active filter. a Source side. b Filter side

Table 1 Total harmonic distortion level at the primary side of new converter transformer

Filtering scheme	% Total harmonic distortion at the transformer primary winding
Traditional SAF	19.80
IAF	0.67

6 Conclusion

In this paper results of Traditional Converter Transformer and a New Converter Transformer is compared by implementing an inductively active filtering technique. It is evident from the simulation result of PSCAD/EMTDC that the New Converter Transformer with IAF method effectively reduces the harmonic component near at the harmonic source and prevents the converter transformer from the harmonics. Therefore, the transformer and the distribution network is free from the effects of harmonics.

References

1. Krause TK, Yong Li O, Saha, Rehtanz C, Cao Yijia. An Inductively active filtering method for power-quality improvement of distribution networks with nonlinear loads. *IEEE Trans Power Delivery*. 2013;2(4):2465–73.
2. Luo L, Li Y, Xu J, Li J, Hu B, Liu F. A new converter transformer and a corresponding inductive filtering method for HVDC transmission system. *IEEE Trans Power Deliv*. 2008;23(3):1426–1431.
3. Li Y, Luo LF, Rübberg S, Rehtanz C, Yang DC, Xu JZ. A class of new HVDC transmission modes improved by inductive filtering method. In: *Proceedings of IEEE PowerCon international conference*; 2010. p. 24–8.
4. Li Y, Luo L, Nakamura K, Rehtanz C, Zhang J, Xu J, Liu F. Transient response characteristics of new HVDC transmission system based on new converter transformer. In: *IEEE international conference on electric utility deregulation and restructuring and power technologies*; 2008. p. 1873–77.
5. Li Y, Luo L, He D, Rehtanz C, Yang D, Ruberg S. Study on the effects of the DC bias on the harmonic characteristics of the new converter transformer. In: *Proceedings of IEEE power and energy engineering conference*; 2010. p. 1–4.
6. Yang D, Li Y, Rehtanz C, Luo L, Xu J. Study on harmonic losses of inductive filtering converter transformer (IFCT) in HVDC system. In *Proceedings of IEEE power and energy engineering conference*; 2010. p. 1–4.
7. Zhao Z, Luo L, Li Y, Zhang J, He D, Shao P. The mathematical model of the new converter transformer based on modified node method. In: *IEEE international conference on electrical machines and systems*; 2008. p. 4379–83.

Optimization of Impedance Mismatch in Distance Protection of Transmission Line with TCSC

M. Arun Bhaskar, A. Indhirani and S. Premalatha

Abstract This paper deals with the area of distance protection that is optimization of impedance mismatch using artificial neural network (ANN). When the network is subject to various faults, voltage and current of that network will change and the other parameter impedance also will change. TCSC will make the system voltage and current to normal condition, but there is a large change in impedance value owing to impedance operation of the relay. To make the distance protection scheme to normal condition, ANN is used. ANN is designed and trained in MATLAB to eliminate the effect of impedance created by TCSC.

Keywords Distance protection · Impedance mismatch · Distance relay · Thyristor-controlled series capacitor (TCSC) · Artificial neural network (ANN) · Optimization

1 Introduction

For transmission of power, transmission lines are used. Due to environmental conditions and other parameters, it is subjected to various types of faults such as phase faults and ground faults. Due to these faults, system voltage and current get affected, so FACTS devices are used. However, it affects the area of distance protection that is normal to the operation of conventional distance relay which is affected. To avoid this, artificial intelligence techniques are used: here, artificial neural network (ANN) is used.

M. Arun Bhaskar (✉) · A. Indhirani · S. Premalatha
Department of EEE, Velammal Engineering College, Chennai, India
e-mail: m.arunbhaskar@gmail.com

A. Indhirani
e-mail: aindhirani@gmail.com

Actually, the power system parameters all are nonlinear so that ANN also can be able to handle this non-linearity, and its working operation resembles like human brain. Human brain consists of billions of neurons which are operating in parallel manner, and by means of chemical process, it transforms signals from one neuron to other neuron. Neural network consists of so many layers such as input layer, hidden layer, and output layer. It processes the information through these layers in parallel sequence.

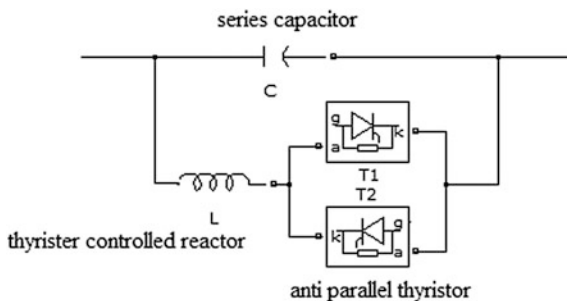
Feature of ANN is the ability to predict the future based on the present, that is, ANN is trained based on some input and output data. After training of neural network, it will predict the correct value of output for unknown inputs; because of this feature, nowadays ANN is preferred. Various types of neural networks are available based on application where particular configuration is chosen. In this paper, impedance is an important parameter, and it is based on voltage and current. The amount of impedance should be maintained within the boundary levels; to achieve this, generalized regression neural network (GRNN) is used. Training of GRNN is unsupervised learning which is used, and impedance is used as target parameter.

2 Thyristor-Controlled Series Capacitor

TCSC is one type of series compensation FACTS device; it is used to improve many system parameters such as damping of oscillations, stability, reduce the effect of sub-synchronous oscillations, and preventing from voltage collapse. TCSC configuration consists of series capacitor in parallel with the combination of two anti-parallel thyristors, and this thyristor pair is connected in series with thyristor-controlled reactor and is shown in Fig. 1 [1].

Series capacitor is generally used in the transmission line for the improvement of power transfer. For the protection of TCSC from over voltage, metal-oxide varistor is used. Anti-parallel thyristors are controlled by gate pulse, which controls the series compensation provided by TCSC. Series compensation is achieved by means

Fig. 1 Block diagram of UPFC



of changing voltage across the capacitor, which changes the reactance. Operation of TCSC is carried out by three processes:

- (a) Bypassed mode of operation;
- (b) Blocked mode of operation;
- (c) Partially conducting mode of operation.

In this first part of operation, that is, bypassed mode of operation, thyristors are fired with 180° that is fully in conduction mode. Normal sinusoidal current will pass through the thyristor and it makes the TCSC configuration as capacitor in parallel with the inductor but the net reactance is inductive only.

In second part of operation, that is, blocked mode of operation, conduction of thyristor is blocked. Gate pulses are removed and thyristor will be in off condition mode and now net reactance will be contributed only by series capacitor. In the last part of operation, partially conducting mode of operation, TCSC behaves like either controllable capacitive reactance or controllable inductive reactance. By properly varying gate pulse to the thyristor, smooth variation of capacitive to inductive can be achieved. In controllable capacitance mode of operation, thyristors are fired during voltage and current across the capacitor having opposite polarity, so that it makes the loop current. It changes voltage across the capacitor and series compensation is achieved. In controllable inductance mode of operation, only small difference is made, that is, direction of loop current is reversed and compensation is achieved [2].

3 Impedance Analysis for Various Faults

When phase faults are created in the network, to calculate the impedance value, the following equation is used [3]:

$$Z_1 = \frac{V_a}{\left(I_a + \frac{Z_0 - Z_1}{3Z_1} I_{\text{res}}\right) Z_1}$$

$$I_{\text{res}} = I_a + I_b + I_c$$

Since zero-sequence impedance is equal to three times of positive-sequence impedance, it can be written as

$$Z_1 = \frac{V_a}{I_a + \frac{2}{3} I_{\text{res}}}$$

$$Z_1 = \frac{V_a}{I_a + KI_{\text{res}}}$$

where

$$K = \frac{Z_0 - Z_1}{3Z_1}$$

When the network is subjected to ground faults, impedance can be calculated as

$$Z_1 = \frac{V_{a1} - V_{a2}}{I_{a1} - I_{a2}} = \frac{V_b - V_c}{I_b - I_c}$$

where

Z_0, Z_1 are the zero-sequence and positive-sequence impedance of the line;
 V_{a1}, V_{a2} are the positive-sequence and negative-sequence voltage of phase 'a';
 V_a, V_b, V_c are the phase voltages; and
 I_a, I_b, I_c are the phase currents.

Based on the above equations, impedance is measured by conventional distance relay [4].

4 Artificial Neural Network

Artificial neural network (ANN) is initially inspired by human neuron, and the working operation of ANN is same as human neuron. Natural neurons consist of synapse on its dendrites, and it transforms the signal from one neuron to other neuron. If the signal is strong enough, then the neuron is activated and again it transforms the signal through axon.

Now comparing to the artificial neural network, it consists of inputs like synapse and those inputs are multiplied by weights. It denotes the strength of the signal. Based on the mathematical form of activation function, neuron is activated and the layer present in the network will be in active. Output of the ANN is calculated by another mathematical operation. Weight is the important parameter of neural network, and it is adjusted to achieve the correct output. The adjustment of weight is called the training of the network. It may be positive or negative, if the weight is in higher value and strong enough mapping of input to the output will be perfect. Simple neural network is shown in Fig. 2 [5], [6], [7].

Training of network may be supervised learning or unsupervised. In supervised training, inputs and outputs are specified based on this network which is trained. In unsupervised learning, inputs are only specified, based on relationship between input and output network which is trained. The number of neurons present in the network is less, which means that training will be easy and otherwise it will be complicated. To reduce the complexity and improve the training process, different algorithms are used.

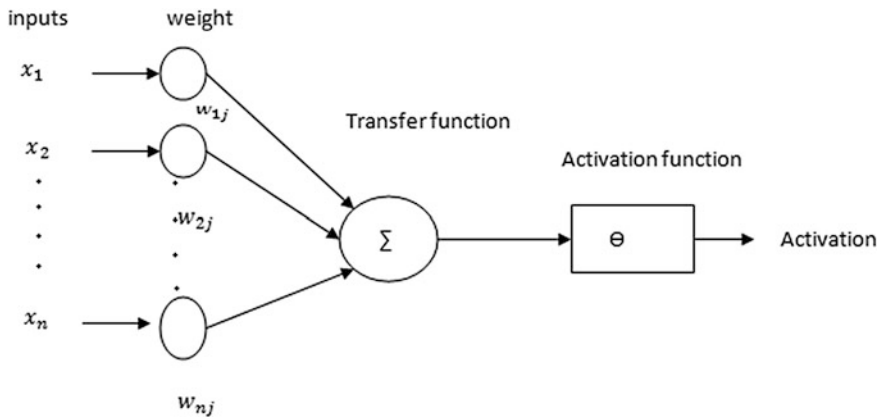


Fig. 2 Simple model of neural network

5 General Regression Neural Network (GRNN)

GRNN is a probabilistic neural network, where required training samples are very less and convergence of this network is fast compared to others. GRNN is useful for the system prediction and comparison problems. GRNN is a fast learning network because no iterative process is involved compared to back-propagation neural network and also another advantage is that it can work with both linear and non-linear data. The only disadvantage of this method is that it is not a logical or spontaneous method which is available to calculate the smoothing factor. GRNN can also be used for function approximation. The network is trained until the difference between output and target value is reduced [8], [9], [1].

Normally, it consists of three layers:

- (a) Input layer;
- (b) Hidden layer;
- (c) Output layer.

Hidden layer has two layers: pattern layer and summation layer. The arrangement of GRNN is as follows: input layer is directly connected to pattern layer and it is connected to summation layer, and finally the output layer (Fig. 3).

Input layer passes the inputs through feed forward to the pattern layer, and then this layer performs the nonlinear transformation of inputs. In this, radial basis function is chosen in pattern layer. Summation layer performs two operations: forming numerator and denominator. It forms the numerator based on the dot product between weight vector and output from the pattern layer, and for denominator weight is unity. The output layer computes the output from the summation layer, that is, quotient of those parameters. This network has only one adjusting parameter that is called smoothing factor, since there is no way of calculating this value trial-and-error method is used from the range of 0.01–0.1.

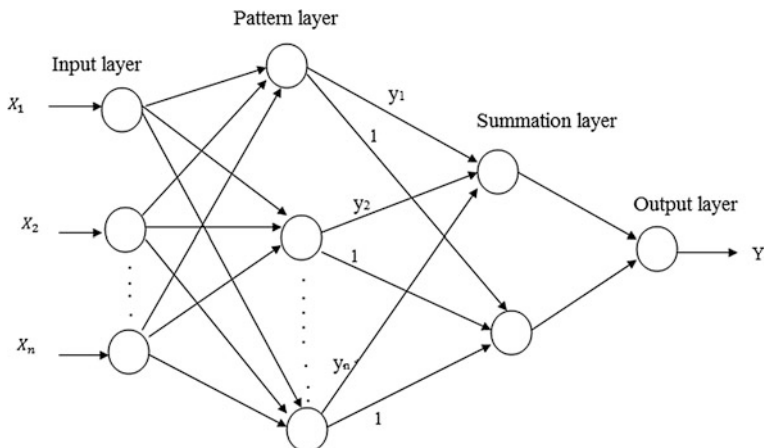


Fig. 3 Architecture of GRNN

6 GRNN Tuned Distance Relay

The conventional distance relay measures the apparent impedance for both compensated and uncompensated line, and it shows that TCSC is installed at 150th km of transmission line. Due to this, the area of protection of transmission line is affected because of real and reactive power injection or absorption. The impact of TCSC on measured impedance is high, that is, the value of resistance and reactance is high. Due to increased resistance and reactance, impedance measured by the relay is increased so that it crosses the boundary level of protection which results in mal operation of distance relay.

To measure the normal impedance of the transmission line, it is required to avoid the additional impedance caused by TCSC. Impedance of the transmission line is changing owing to the two parameters as voltage and current. Here, series compensation is provided by TCSC, which injects series voltage. The conventional distance relay will measure the apparent impedance based on series injected voltage and network current for every 0.0001 s and sends it back to summer block, where in summer block do addition or subtraction operation between impedance measured by conventional distance relay and change in impedance measured by trained neural network. Thus the conventional distance relay is trained to detect the actual transmission line impedance.

Advantage of GRNN network is speed of training and also it does not need any type of training parameters such as momentum and learning rate compared to other neural networks. The only parameter needs to adjust is the smoothing factor. For different types of faults such as single-line fault, single-line-to-ground fault, double-line fault, double-line-to-ground fault, three-phase fault, separate GRNN is tuned and used. Architecture of GRNN is same as for all faults, but the only difference is the smoothing factor. Input for GRNN is the series voltage injected by TCSC and target parameter is changed in apparent impedance.

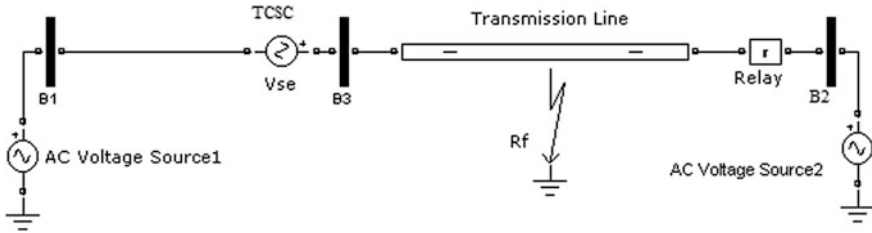


Fig. 4 Single line diagram of TCSC

7 Test System with GRNN

Single-line diagram of the test system with FACTS device TCSC is used. Here, two voltage sources, 200 km transmission line and relay, are used. Transmission line is subjected to various types of phase faults and ground faults, and it is represented in Fig. 4.

GRNN trained test system is shown in Fig. 5.

It has two voltage sources connected by the transmission line having length of 200 km. Fault is created at 150th km of the transmission line. Due to fault system, voltage gets reduced and current value gets increased. To make the system parameter to stable condition, FACTS devices are installed in the transmission line; here TCSC is used. It is a series compensation device used to inject voltage into the network. Here, some measurement blocks are used, where measured quantities are converted into digital signal by means of Fourier transformation block. Test system is simulated and those values are updated into workspace using MATLAB code. Those data are used to train the network (Table 1).

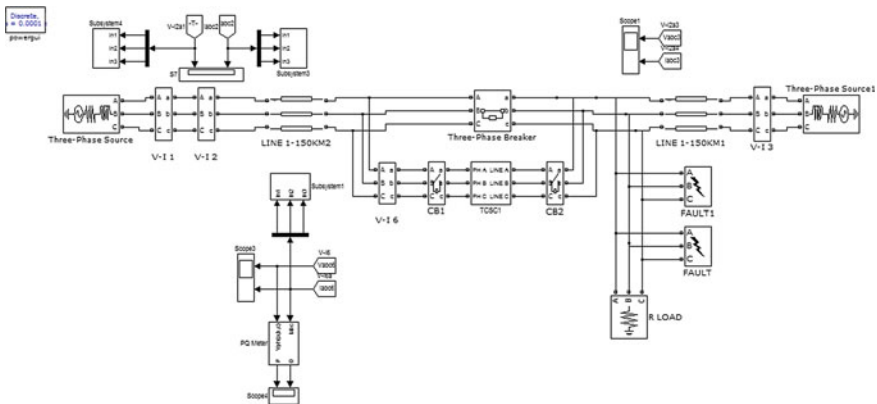


Fig. 5 GRNN tuned test system

Table 1 Test system data

Generator rating MVA, kVA	1000 MVA, 230 kVA
Source data	$Z_{S1} = 0.238 + 5.72j \Omega$
	$Z_{S0} = 2.738 + 10j \Omega$
	$Z_{R1} = 0.238 + 6.17j \Omega$
	$Z_{R0} = 0.833 + 5.12j \Omega$
Length of the transmission line	200 km
Transmission line data	$L_1, L_0 = 1.35, 3.75 \text{ mH/km}$
	$C_1, C_0 = 9.48, 6.711 \text{ nF/km}$
	$R_1, R_0 = 0.0275, 0.275 \Omega/\text{km}$
	km

8 Analysis of Test System Impedance with GRNN

Test system is simulated in MATLAB software and codings are used to train the neural network. First single-line-to-ground fault is given at 150th km of the transmission line and impedance analysis is performed and its waveform is shown in Fig. 6. It shows impedance without any training of the network.

Figure 7 shows waveform for impedance analysis for single-line-to-ground fault with trained neural network (GRNN). It shows 0–0.5 s for impedance of

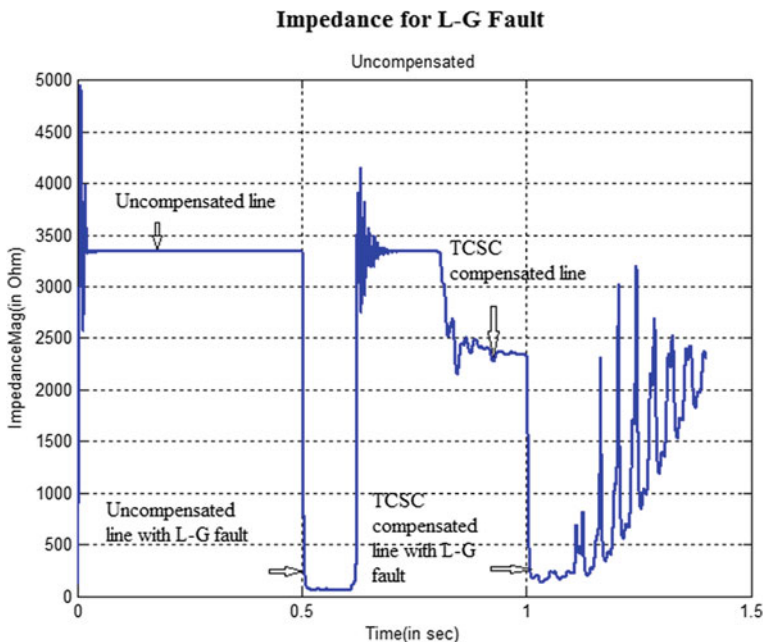


Fig. 6 Impedance for L–G fault

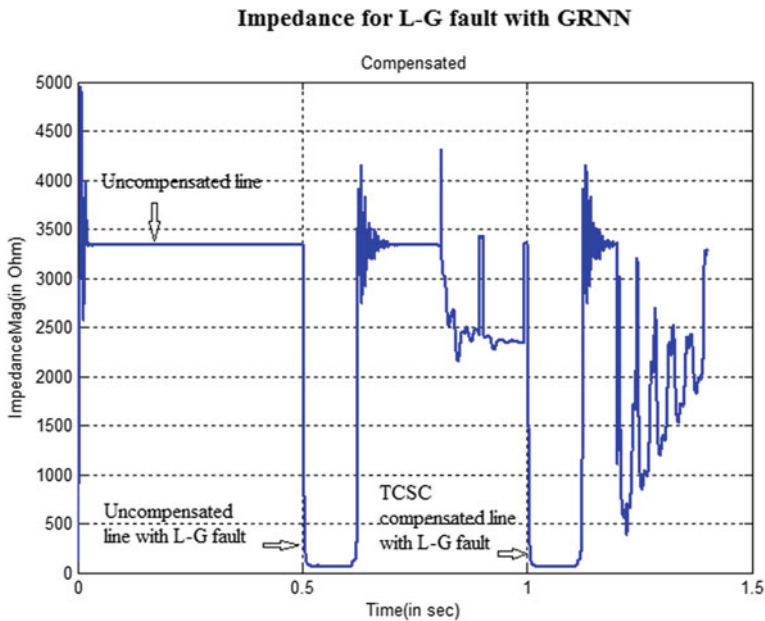


Fig. 7 Impedance for L-G fault with GRNN

uncompensated line, and from 0.5 to 0.6 s impedance is measured for the same uncompensated line with fault. From 1 to 1.1 s duration, the same type of fault is given and additional TCSC is inserted into the network and impedance is measured. The measured value of impedance is same for both uncompensated and compensated lines, so mal operation of relay is avoided.

Figure 8 shows the change in impedance, that is, impedance measured by GRNN tuned distance relay or difference between impedance of compensated and uncompensated lines. It shows that from the duration of 0–1 s, change in impedance is zero or minimum. It indicates that without TCSC there is no impact on the impedance. From 1 to 1.1 s, only GRNN generates impedance.

Now double-line fault is given for the same system to analyze about parameter impedance. Figure 9 shows impedance for double-line fault.

Duration from 0 to 0.5 s indicates the impedance for uncompensated line, and from 0.5 to 0.6 s shows impedance for uncompensated line with double-line fault and additionally TCSC is incorporated in the line during 1–1.1 s. It shows that there is a large impedance between compensated and uncompensated lines. Due to this change, relay will go to mal operation, so GRNN is used to eliminate the additional impedance caused by TCSC.

Figure 10 shows the GRNN with double-line fault. Due to neural network, added impedance is eliminated and measured value of impedance for both compensated and uncompensated lines is same.

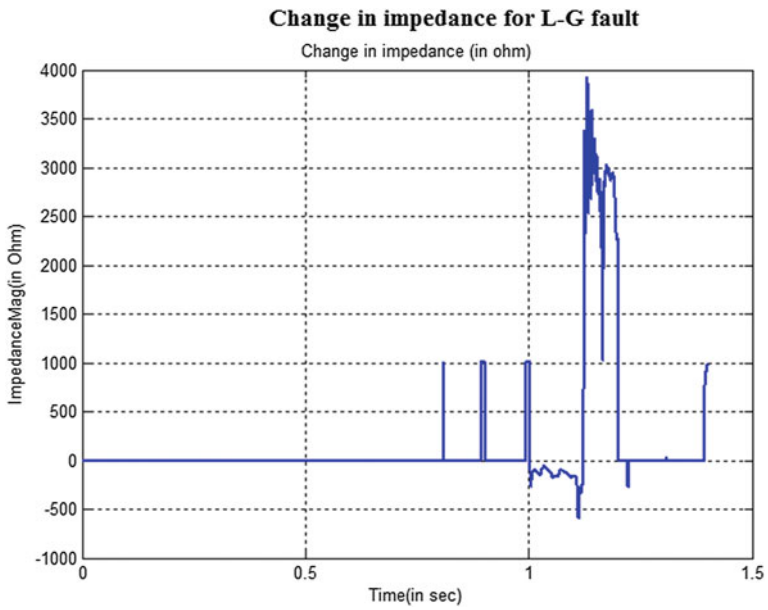


Fig. 8 Change in impedance for L-G fault

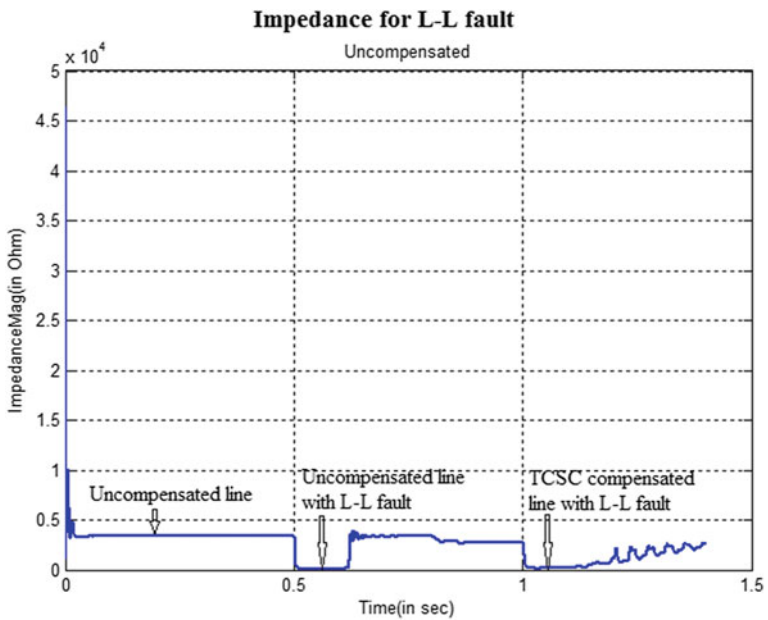


Fig. 9 Impedance for L-L fault

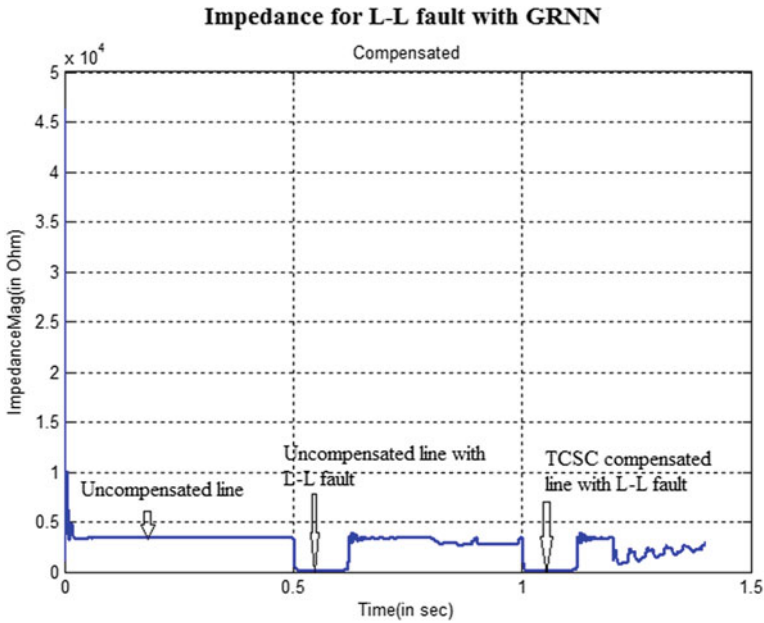


Fig. 10 Impedance for L-L fault with GRNN

The change in impedance is shown in Fig. 11. This impedance is measured by GRNN tuned distance relay and this amount of impedance is eliminated to avoid the malfunctioning of the relay.

Obtained impedances for various faults are tabulated below. It shows the impedance for uncompensated and TCSC compensated line and the change in impedance measured by GRNN tuned relay (Table 2).

Total length of the transmission line is 200 km and for zone I, protection 80 % of the line is considered and the impedance is given as follows:

Impedance for zone-1 is

$$\begin{aligned} Z_1 &= 0.0275 + 0.42411i \Omega/\text{km} \times 160 \text{ km} \\ &= 4.4 + 67.8576i \Omega \\ &= 68 \angle 86.290^\circ \Omega \end{aligned}$$

$$\text{So } |Z_{\text{set(OR)zone-1}}| = 68.03 \Omega$$

Fault is created at 150th km and the set value of impedance becomes

$$\begin{aligned} Z_1 &= 0.0275 + 0.42411i \Omega/\text{km} \times 150 \text{ km} \\ &= 4.25 + 63.6i \Omega \\ &= 63.75 \angle 86.289^\circ \Omega \end{aligned}$$

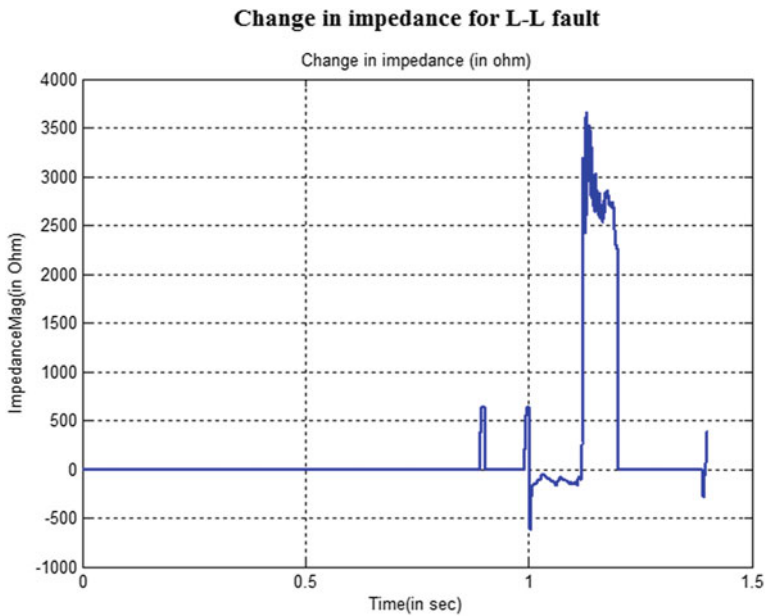


Fig. 11 Change in impedance for L-L fault

Table 2 Impedance for various faults

	Type of fault	Fault duration	Impedance measured by conventional distance relay	Change in impedance obtained by GRNN	Impedance measured by GRNN tuned distance relay
Uncompensated line	L-G	0.5-0.6	62	0	62
	L-L	0.5-0.6	63	0	63
TCSC compensated line	L-G	1-1.1	203	141	62
	L-L	1-1.1	234	171	63

Using ANN, the above impedance value is achieved, with and without TCSC, GRNN tuned distance relay measuring same amount of impedance. So the mal operation of distance relay is eliminated.

9 Conclusion

230 kV test system is designed in MATLAB software and impedance analysis is performed. In this test system, various faults are given and series compensation is provided by TCSC. Then normal conventional distance relay is designed for the

purpose of analyzing impedance of the network. Impedance results show that there is a large change in impedance due to TCSC, so that relay will mal operate. GRNN neural network is designed using MATLAB codings and the conventional distance relay is trained. The GRNN tuned distance relay eliminates the effect of additional impedance caused by TCSC. Now relay will measure same amount of impedance for both uncompensated and TCSC compensated lines, and mal operation of relay is avoided.

References

1. Khederzadeh M, Sidhu TS. Impact of TCSC on the protection of transmission lines. *IEEE Trans Power Del.* 2006.
2. Jamili S, Imani H. Dynamic analysis of the impact of tcsc on distance relay operation. *J Electr Eng.* 2011;5(7).
3. Phadke AG, Ibrahim M. Fundamental basis for distance relay symmetrical components. *IEEE Trans Power Appl Syst.* 1997;PAS-96:6354–646.
4. Paithangar YJ, Bhide SB. Fundamentals of power system protection.
5. Tarafdar Haque M, Kashtiban AM. Application of neural network in power system: a review. *Int J Electr Comput Electron Commun Eng.* 2007;1(6).
6. Comparison between artificial neural networks and neurofuzzy systems in modeling and control. *Int J Innovative Res Electr Electron Instrum Control Eng.* 2014;2(12).
7. Santosh Kumar A, Surendranath Chowdary V. Ann based protection for series compensated lines (TCSC). *Int J Adv Res Electri Electron Instrum Eng.* 2013;2(7).
8. Saha MM et al. First zone algorithm for protection of series compensated lines. *IEEE Trans Power Deliv.* 2001.
9. Elangovan S, Waikar DL. Fault Impedance estimation algorithm for digital distance relaying. *IEEE Trans Power Del.* 1994;9(3).
11. Khederzadeh M, Amir. Impact of VSC-bsaed multiline FACTS controllers on distance protection of transmission line. *IEEE Trans Power Del.* 2012.
12. Das PK, Pardhan AK, Panda G. Digital protection of power transmission line in the presence of series connected FACTS devices. In: *IEEE Power Eng. Soc. Winter Meet.* 2000.

Reconfigurable WSN Interface for Water Quality Measurement

Ajin Mathew Sam and C. Balaji

Abstract Water = Life, Conservation = Future, Safety = Prevention—the excessive advancement in the field of technology has left mankind least bothered about the water sources leading degrading the quality of water to support life. The lineage of heavy industries and chemical factories with the water sources are dumping loads of harmful wastes to the water sources. To create awareness among people, internet of things (IoT) and wearable sensors through wireless sensor networks (WSN) can be used to facilitate this task. Deployment of such sensors in remote water sources to detect the water quality is made through WSN. This paper reviews about the design of a smart WSN interface (FPGA) for water contamination measurement for the remote water resources, where human presence is very rare. Field programmable gate array (FPGA) is used, which can be programmed and used as the core controller. The proposed system is capable of detecting the chemical changes in the water source in real time by analyzing the sensors and sending the information to the default hub.

Keywords WSN · Iot · FPGA · Water quality

1 Introduction

The soul topology used for the sharing of information in an internet of things (IoT) environment is wireless sensor networks (WSN). The sensors deployed in the water sources trigger the information to the controller. The controller is where the data get processed and set for further modulations. The fragmented environmental monitoring is implemented to secure a good skeleton for streaming and to acquire

A.M. Sam (✉) · C. Balaji
Instrumentation and Control Department, SRM University, Chennai, India
e-mail: a4ajin@gmail.com

C. Balaji
e-mail: balaji.c@ktr.srmuniv.ac.in

physiological information and telecast it on real-time basis [1]. For nuclear power plants, large scale industry monitoring and controlling systems are of crucial importance with respect to safety and efficient operation. Since the system operations mainly depend on high level programming, we can extend the system without inhibitions. In this system, temperature measurement is sent to the analog channel of the controller and displayed. The performances of the channels are distinguished on the basis of its accuracy. The accuracy indicates how closely the sensor can measure the actual or real world parameter value [2]. The generic use of IoT environment in a broad class of monitoring applications for easy and low-cost applications is capable for a better communication setup [3]. The proposal for WSN systems in industries with the integration of the CPLD processors for better compatibility with the system and secure function for easy understanding and better use is adopted [4]. The proposal of WSN with a new genre by the introduction of new scheduling methods by the introduction of sleep techniques using VLSI and FPGA [5]. Since more mobile wireless communications are preferred to wired connections, WSN is gaining popularity in the world. Here, WSN is enabled with small embedded devices with wireless connectivity enabled forming a network within themselves. Tiny OS is such an embedded device to configure with the small changes and to report the subordinate systems for any environmental changes [6]. The introduction of SRAM-based devices for easy flexibility and to perform the necessary computing performance at an affordable and low-cost scheme [7]. To achieve a stable network for communication and secure transmission, a new paradigm for the IoT environment with the introduction of the RFID protocols. IoT makes all objects become interconnected and smart, which has been recognized as the next technological revolution. The methodology (ADM) for smart rehabilitation systems in IoT aids computers in further understanding the symptoms and medical resources, which helps to create a rehabilitation strategy and reconfigure medical resources according to patients' specific requirements quickly and automatically [8].

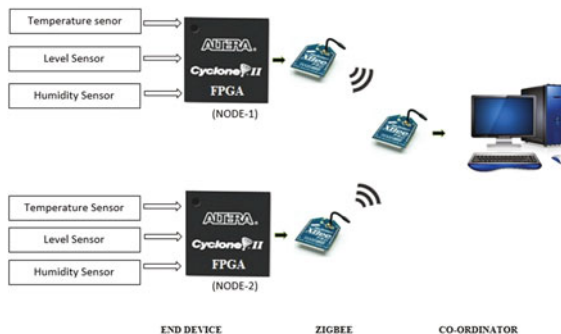
2 Overview of Related Works

Tung-Hung Lu introduced a motion-sensing based management system for smart context-awareness rehabilitation health care including various balance exercises built by the integration of the physiological sensing and feedback coaching [1]. S. Elango (2013) came up with an innovative idea for nuclear power plants and large scale industries monitoring and controlling systems with a broad class of detailed IoT established methodology [2]. Mihai T. Lazarescu (2014) addressed the phases of the practical development from scratch of a full custom WSN platform for environmental monitoring IoT applications. It starts by analyzing the application requirements and defining a set of specifications for the platform. WSN platform for easy flexibility and reusability, optimization of the sensor and gateway nodes, optimization of the communication [3]. Gerhard Griebner (2013) brought the implementation of safety functions in hardware using CPLD. This approach does

contrast to microcontroller-based systems, does not require the development of startup- and online tests for RAM and CPU. CPLD-based safety concept has been elaborated that does not require the realization of microcontroller-specific software safety integrity measures like RAM tests or CPU tests that require a lot of effort in terms of design, implementation, and verification as well as hardware resources [4]. Joyashree Bag (2013) presented about the low power sensor node processor design and its VLSI implementation in FPGA board has been presented. The overall performance, power dissipation, and hardware requirement have been described with the detail comparison of previous work [5]. K.M. Goh (2014) introduced FPGA-based wireless sensor node with a simulated chemical plant process monitoring application. The author also demonstrated the real-time processing of sensor data with WSN in order to provide self-learning, self-checking, and trending for fault detection. Additionally, he has also proposed and presented a working solution in enabling rapid creation and customization of wireless sensing applications [6]. Ali Hayek (2012) verified IP-Cores or any user implemented code in any abstract hardware description language, which makes system design more flexible [7]. Yuan Jie (2014) proposed a rehabilitation system developed using IoT-based technologies, SOA methods, and multidisciplinary optimization methods, and ontology lays the foundation for disease diagnosis and resource allocation [8].

3 Proposed System

The proposed system can detect water quality parameters namely humidity, level, and temperature in real-time environment. These sensors are interfaced with the controller. The controller used here is FPGA. The data acquired by the sensors are sent to the FPGA, the FPGA processes the data and sends it to the nearest hub by the intermediate nodes.



The transfer of data between the nodes is done by the intermediate ZigBee. The nearest router node which is at the maximum communication range with respect to the end device is considered to be the suitable neighbor node for data forwarding to

the coordinator node. The host computer connected to the coordinator is used for data analysis. Graphical user interface (GUI) is developed using LABVIEW software for the output.

4 Results and Discussion

The output of the proposed system.

The readings from the sensor are analyzed and brought to the PC. The GUI of the output is brought to the user with the LABVIEW representation. Readings at certain instances are taken and recorded (Tables 1, 2 and 3).

The information is gathered at the FPGA processor, where it is processed and further sent to the user for displaying of the details gathered.

The sensor deployed around the lake gathers the analog physiological changes in the water and sends it to the PC (base station) through the intermediate ZigBee at the other end.

Two nodes of the sensors with the FPGA are deployed around the lake. These two nodes send the data to the nearest ZigBee hubs, the nearest node receives the information and sends to the user interface which is represented on the screen with the help of the software LABVIEW (Figs. 1, 2, 3, 4 and 5).

Table 1 Humidity readings

Phase	Humidity
Morning	70
Afternoon	90
Evening	60

Table 2 Temperature readings

Phase	Time	Temperature (°C)
Morning	5.45 AM	17.54
	7.56 AM	18.81
	9.45 AM	22.12
Afternoon	12.00 PM	23.55
	01.34 PM	33.28
	02.47 PM	33.67
Evening	06.34 PM	26.45
	07.55 PM	24.54
	08.34 PM	22.65

Table 3 Water level readings

Environment	Water level
High tide	031
Low tide	018
Stagnant water bodies	024

Fig. 1 User interface graph in labview

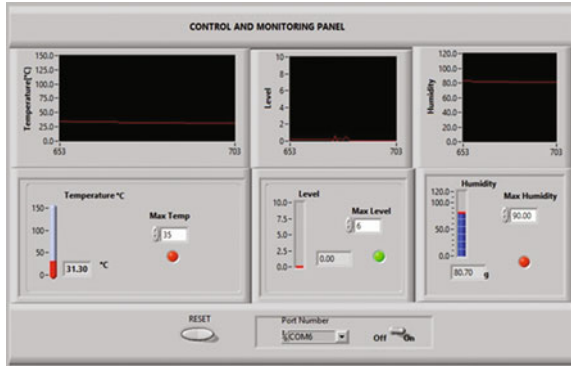


Fig. 2 Proposed system



Fig. 3 ZigBee

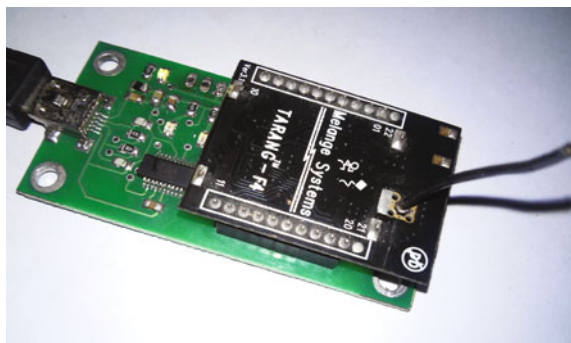
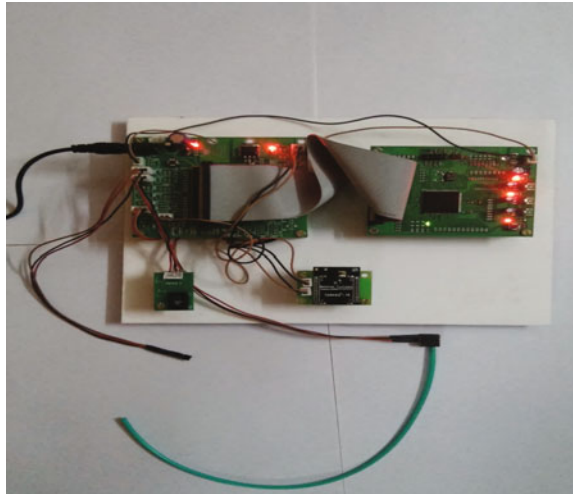
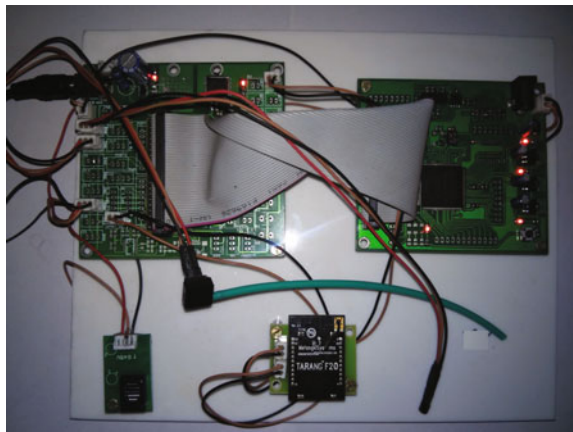


Fig. 4 Node A**Fig. 5** Node B

5 Conclusion

Various research works have been carried out in the field of WSN and enhancing the network for communication. This paper reports the introduction of a new methodology in which FPGA is the core controller, interfacing of the intermediate nodes through ZigBee for better transmission is done. A new RFID protocol and the integration of a new microcontroller Arduino are contemplated for a real-time environment. This methodology can be implemented for various sensor nodes and condition-related application using ZigBee nodes and for future works, it can be assisted with a solar-enabled power source.

Acknowledgments I would like to express special appreciation and thanks to my guide Asst. Professor. C. Balaji for being a tremendous mentor. I would like to thank you for encouraging my research. My heartfelt and solemn gratitude to my project Co-coordinator Mr. Sam Jebakumar for his help, brilliant comments, and suggestions. My sincere thanks to HoD Dr. A. Vimla Juliet for her immense help and support during the course of my project. I would like to thank my family for their love, support, and guidance to strive me towards my goal. Finally, I thank the Lord Almighty for the wisdom he has given and for all his blessings.

References

1. Lu T-H. Advances in internet of things, June 2013. In: Motion-sensing based management system for smart context-awareness rehabilitation healthcare. <http://www.scirp.org/journal/ait>.
2. Bharani M. An embedded system based smart sensor interface for monitoring industries using real time operating system (RTOS). IJAICT. 2014;1:6. <http://www.ijaict.com>.
3. Lazarescu MT. Design of a WSN platform for long-term environmental monitoring for IoT applications. In: IEEE journal of emerging and selected topics in circuits and systems. <http://mihai.lazarescu@polito.it>.
4. GrieBnig G. A CPLD-based safety concept for industrial applications. ITI, Graz University of Technology, Austria; 2012.
5. Bag J. Realization of a low power sensor node processor for wireless sensor network and its VLSI implementation. In: IEEE international advance computing conference; 2014. http://joyashree_bag@yahoo.co.in.
6. Goh KM. FPGA based wireless sensor node for distributed process monitoring. In: 7th IEEE conference on industrial electronics and applications (ICIEA); 2012. <http://kmgoh@simtech.a-star.edu.sg>.
7. Hayek A. FPGA-based wireless sensor network platform for safety systems. In: 19th international conference on telecommunications (ICT 2012). <http://hayek@uni-kassel.de>.
8. Fan YJ. IoT-Based smart rehabilitation systems. In: IEEE transactions on industrial informatics 2014;10:2. http://www.ieee.org/publications_standards/publications/rights/index.

Optimization of Micro Thermoelectric Generator for Renewable Source of Energy

Y. Jeyashree, A. Vimala Juliet, C. Prantik Barua, J. Sree Harsha and Abhilash Mallick

Abstract A micro thermoelectric generator (μ TEG) is designed for converting concentrated solar heat into electrical energy. Optimization of thermoelectric material is carried out for the operating temperature. The variation of figure of merit with temperature is considered. Optimization of the design of μ TEG is done by minimizing the electrical resistance. The source temperature is varied from 360 to 300 K. The cold side temperature is maintained at 270 K. The voltage, current, and power output of a lead telluride based single μ TEG of size $10\ \mu\text{m} \times 10\ \mu\text{m} \times 5\ \mu\text{m}$ is 0.012943 V, 9.41×10^{-6} A and 12 μW . To glow a 90 W LED matrix with a driving voltage of 30 V the drive requirements are estimated as 2307 number of devices in series and 1166 number of devices in parallel and the space required is $2.4\ \text{cm} \times 1.2\ \text{cm}$.

Keywords Figure of merit · Solar energy · Solar concentrator · Thermoelectric generator

1 Introduction

Due to the rise in energy demand and pollution control requirement, the demand for the clean energy system is increasing. Micro thermoelectric generators (μ TEGs) are the clean energy sources. They utilize waste heat and convert to electricity. It works on Seebeck effect [1–4]. When a difference in temperature exist across a material a

Y. Jeyashree (✉) · A.V. Juliet · C.P. Barua · J.S. Harsha · A. Mallick
Department of ICE, SRM University, Chennai, India
e-mail: jeyashree_christley@yahoo.co.in

A.V. Juliet
e-mail: vimlala@yahoo.co.in

C.P. Barua
e-mail: coomarprantikbarua@gmail.com

J.S. Harsha
e-mail: javvajiharsha08@gmail.com

A. Mallick
e-mail: abhilash.mallick@gmail.com

proportional voltage is developed and when a load is connected electrical power output is obtained. The μ TEGs have no moving parts. So the device is robust and maintenance free [5, 6]. This type of generation is applied for waste heat recovery in body heat. [7] developed bismuth telluride based micro thermoelectric generator and utilized the heat emitted from the person's wrist. The electrical energy generated is used to power up wrist watch of 1 μ W with a driving voltage of 1.5 V. [8] developed a poly Silicon based transparent micro thermoelectric generator and utilized the temperature difference between the inside and outside of the windows of the building. Each 60 cm \times 90 cm glass window assembled with μ TEG can generate 0.05–0.1 W of electrical power with a temperature difference of 5–10 K.

The temperature of a day varies from 305 to 313 K for a normal day at Chennai in India. When a solar concentrator is used the temperature varies from 433 to 583 K at the absorber for a normal day at Chennai in India. The electrical power output of the μ TEG depends on the temperature of the heat source. Three best known groups of thermoelectric materials are bismuth telluride, lead telluride, and silicon–germanium alloys. In this, bismuth telluride has the highest figure of merit around room temperature [9]. Lead telluride has the highest figure of merit in the temperature range (400–800 K). Silicon–germanium alloy has the highest figure of merit at 1300 K. The average heat source temperature per day is 473 K at the absorber of solar concentrator. Therefore, the suitable material for the energy conversion is lead telluride. A thermoelectric material's performance is quantified by figure of merit $ZT = \alpha^2 \sigma T / (K_E + K_L)$, where α is the Seebeck coefficient, σ is the electrical conductivity, K_E is the electronic thermal conductivity, and K_L is the lattice thermal conductivity. Commercialized single phase lead telluride has the peak ZT as 0.8. Greater performance can be achieved by compositional control and ZT reaches 1.4. Alloying PbTe–PbSe gives the peak ZT as 1.8 due to reduction in lattice thermal conductivity and increase in electrical conductivity and Seebeck coefficient [9].

2 Simulation of μ TEG Using Comsol

A single μ TEG is simulated using COMSOL. The length of TEG is 15 μ m. The cross-sectional area of μ TEG is 10 μ m \times 10 μ m. The thermoelectric material used is lead telluride. The thermoelectric properties of the materials are Seebeck coefficient of p-type lead telluride is 104.006439 μ V/K. Seebeck coefficient of n-type lead telluride is 123.5982464 μ V/K. The electrical conductivity of p-type lead telluride is 126463.7002 S/m. The electrical conductivity of n-type lead telluride is 161592.5059 S/m. The thermal conductivity of p-type lead telluride is 2.66 W/(m-K). The thermal conductivity of n-type lead telluride is 2.7 W/(m-K). The temperature of the hot side is kept at 360 K. The cold side temperature is 270 K. Figure 1 shows the design and temperature distribution of bridge type μ TEG with

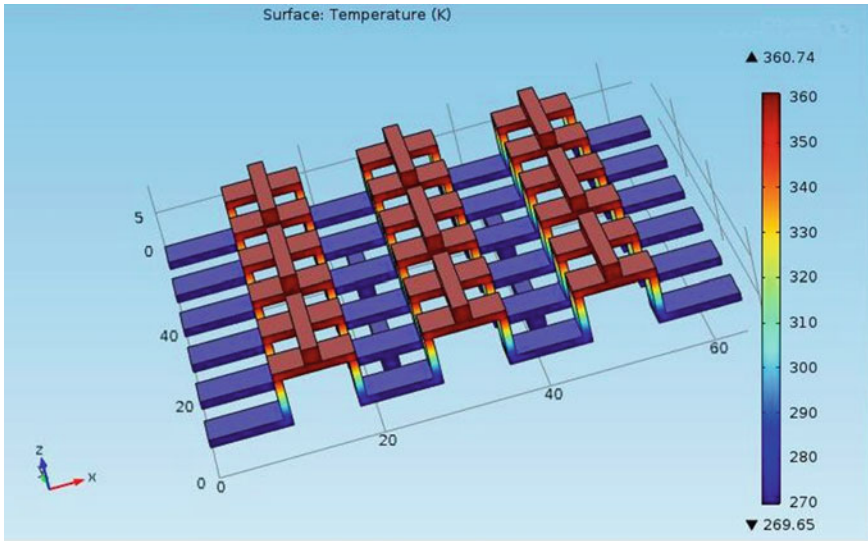


Fig. 1 Temperature distribution of bridge type μ TEG

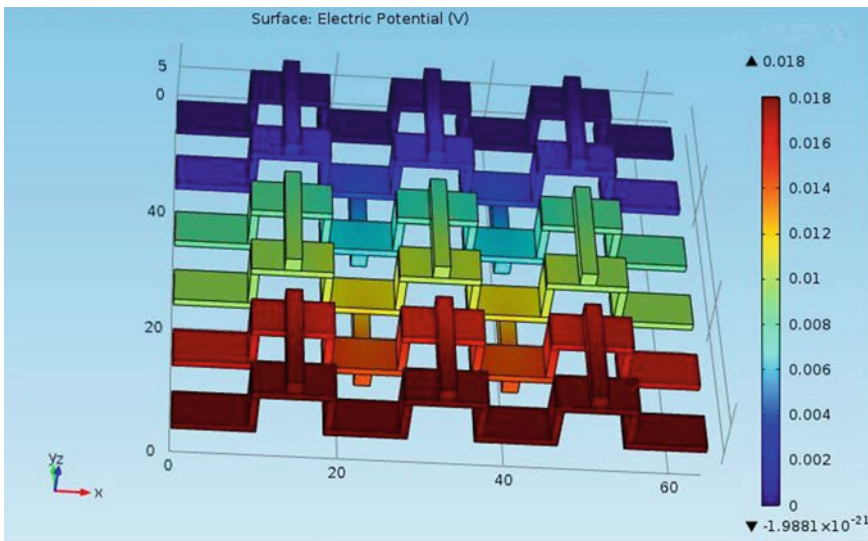


Fig. 2 Potential distribution of bridge type μ TEG

three μ TEGs connected in series and three μ TEGs connected in parallel. Figure 2 shows the design and voltage distribution of the same. The Seebeck coefficients of p- and n-type lead telluride for the temperature ranging from 360 to 300 K are given in Fig. 3. The thermal conductivities of p- and n-type lead telluride for the

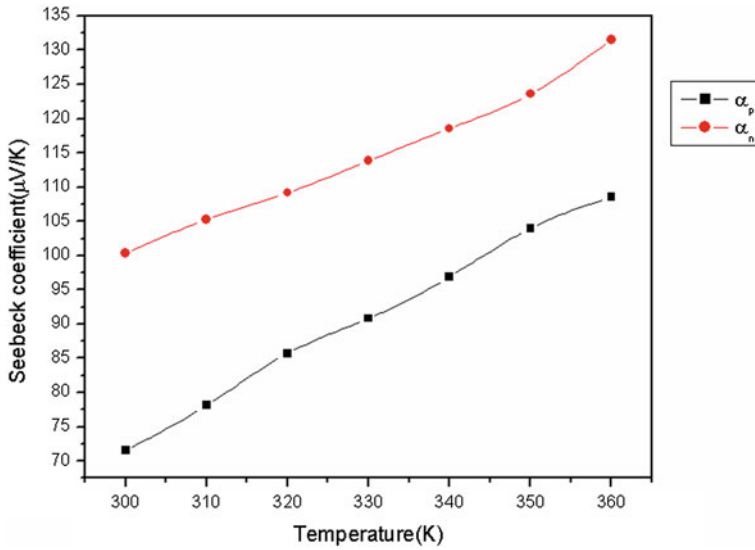


Fig. 3 Seebeck coefficient of lead telluride

temperature ranging from 360 to 300 K are given in Fig. 4. The electrical conductivities of p- and n-type lead telluride for the temperature ranging from 360 to 300 K are given in Fig. 5.

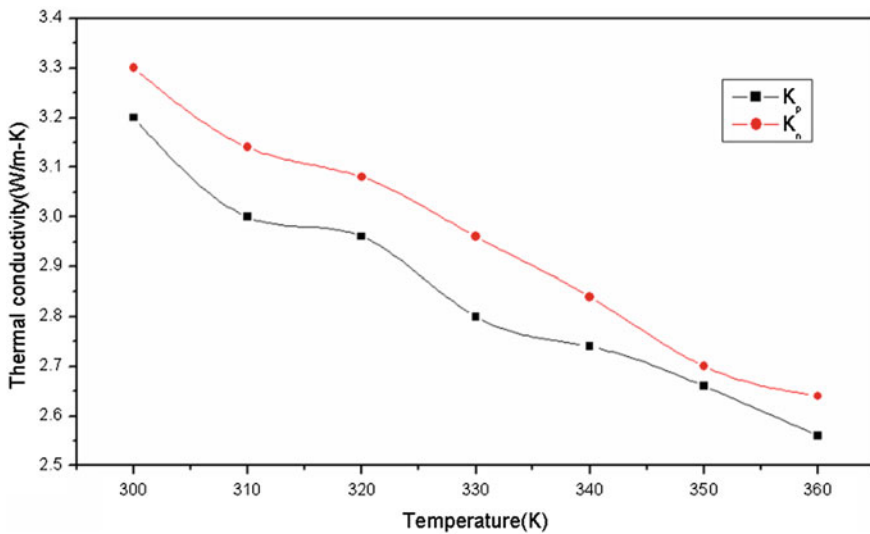


Fig. 4 Thermal conductivity of lead telluride

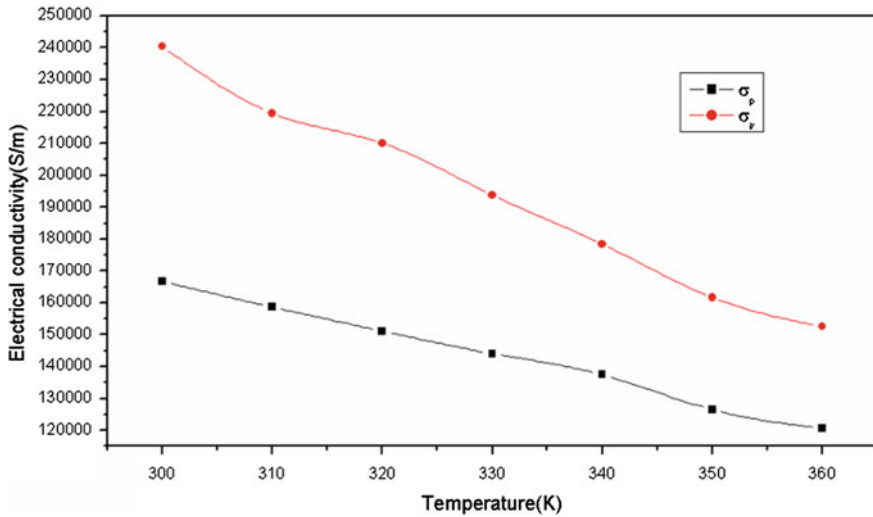


Fig. 5 Electrical conductivity of lead telluride

3 Result and Dsicussion

[5] The graph for variation of thermal conductivity of p- and n-type lead telluride with respect to temperature. From the graph, the values of thermal conductivity of p- and n-type lead telluride for various temperatures are taken [5]. It also gives the variation of lattice thermal conductivity of p- and n-type lead telluride with respect to temperature. From the graph, the values of lattice thermal conductivity of p- and n-type lead telluride for various temperatures are taken. The electron thermal conductivity of p- and n-type lead telluride is calculated using the formula:

$$K_{EP} = K_P - K_{LP} \tag{1}$$

The electrical resistivity ρ is calculated using the formula

$$\rho = \frac{LT}{K_{EP}} \tag{2}$$

The electrical conductivity σ is calculated from

$$\sigma = \frac{1}{\rho} \tag{3}$$

From the graph, the values of figure of merit of p- and n-type lead telluride for various temperatures are taken. The value of Z is calculated for various temperature.

Then, the Seebeck coefficient of p- and n-type lead telluride is calculated using the formula

$$\alpha = \left(\frac{ZK}{\sigma} \right)^{1/2} \quad (4)$$

The variation of voltage with respect to the length of the thermo leg is calculated using the formula [10]

$$V = \frac{N\alpha(T_h - T_c)}{1 + 2rl_c/l} \quad (5)$$

The variation of current is calculated with respect to the length of thermo leg using the formula

$$I = \frac{A\alpha(T_h - T_c)}{2\rho(n+1)(1 + 2rl_c/l)} \quad (6)$$

The variation of power is calculated with respect to the length of thermo leg using the formula.

$$P = \frac{\alpha^2 AN(T_h - T_c)^2}{2\rho(n+1)(1 + 2rl_c/l)} \quad (7)$$

where A is the cross-sectional area, N is the number of μ TEG, ρ is the electrical resistivity, ρ_c is the electrical contact resistivity, $n = 2\rho_c/\rho$, K is the thermal conductivity, K_c is thermal contact conductivity, $r = K/K_c$, l is the thermo element length, l_c thickness of the contact layer.

Figures 6, 7 and 8 show the MATLAB program simulation for the calculation of voltage, current, and power. The optimum length of μ TEG is 15 μm . At the optimum length the voltage generated by a single TEG is 0.012934 V. The current for a single μ TEG is 9.41×10^{-6} A. The power output for a single μ TEG is 12 μW . The temperature of hot junction is 360 K. The cold junction temperature is 270 K. The variation of voltage is calculated keeping the hot junction at different temperature ranging from 300 to 360 K. The cold junction temperature is kept at 270 K. The length of thermo leg is varied from 5 to 25 μm . Figure 6 gives the plot of voltage with respect to length.

As the leg length increases, the voltage output increases for a particular temperature. As the hot junction temperature increases for a particular length of thermo leg, the voltage also increases. The variation of current is calculated keeping the hot junction at different temperature ranging from 300 to 360 K. The cold junction temperature is kept at 270 K. The length of thermo leg is varied from 5 to 25 μm . Figure 7 gives the plot of current with respect to length.

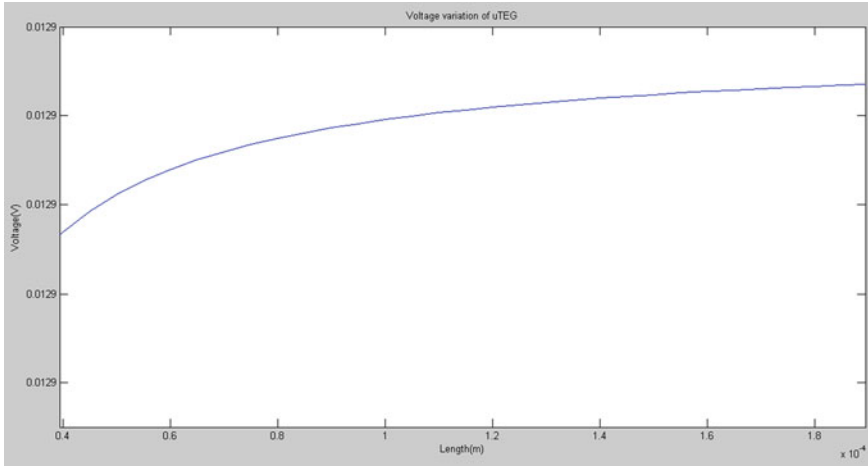


Fig. 6 Plot of voltage with respect to length

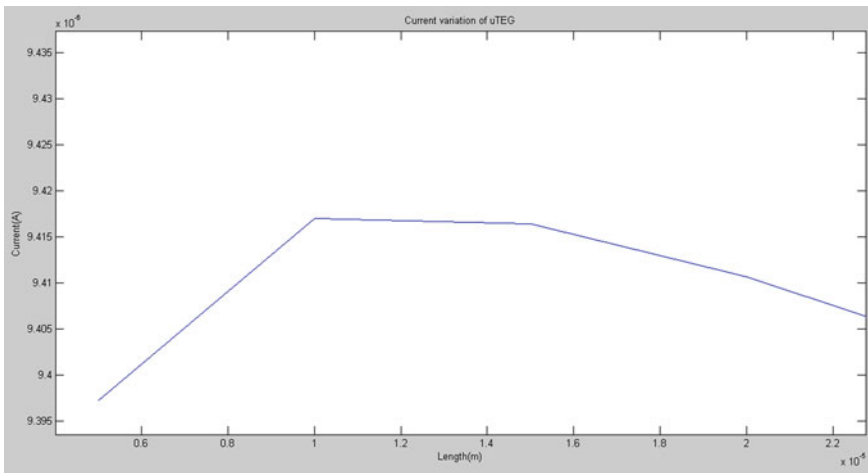


Fig. 7 Plot of current with respect to length

As the leg length increases, the power output increases initially and reaches a maximum at the optimum length of 15 μm and then decreases for a particular temperature (Fig. 8). As the hot junction temperature increases for the same optimum length of thermo leg, the power also increases. To power up a single LED matrix of 90 W, 2307 LEDs are connected in series to get an output voltage of 30 V. The number of TEGs connected in parallel is 1166 to get a current of 3 A. The space required is 2.4 cm \times 1.2 cm.

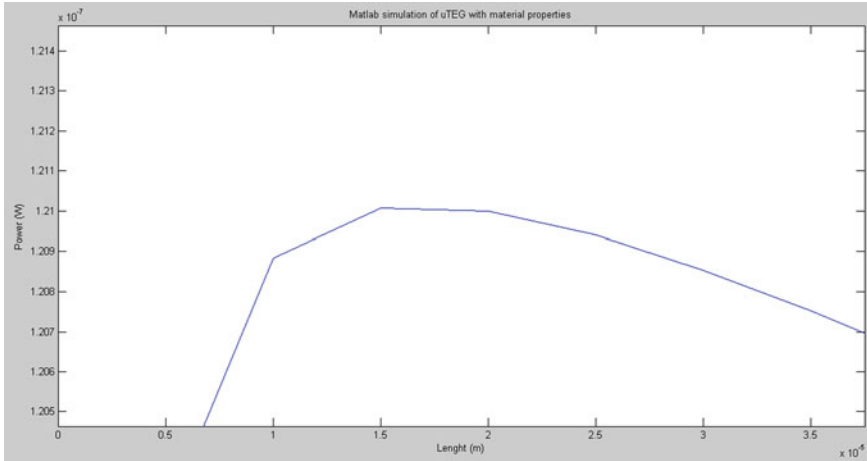


Fig. 8 Plot of power with respect to length

4 Conclusion

The thermoelectric material is optimized for the operating temperature with maximum figure of merit. The design of μ TEG is optimized for maximum power output by minimizing the electrical resistance [11]. Optimization of design for maximizing thermal resistance and addition of coolant system can be included for the future work.

References

1. Etienne Schwyter W, Durrer L, Hierold C. Bi_2Te_3 -based flexible micro thermoelectric generator with optimized design. *J Micro Electro Mech Syst.* 2009;18(3).
2. Paulo CJ, Miguel GL, Higinio CJ. Thermoelectric microconverter for energy harvesting systems. *IEEE Trans Industr Electron.* 2010;57(3):861–7.
3. Harb A. Energy harvesting: state-of-the-art. *Renew Energy.* 2011;36:2641–54.
4. Sug C-Y, Tsai Nan-Chyuan. Human powered MEMS-based energy harvest devices. *Appl Energy.* 2012;93:390–403.
5. LaLonde AD, Pei Y, Heng Wang G, Snyder J. Lead telluride alloy thermoelectrics. *Mater Today.* 2011;14(11):526–32.
6. Boniche I, Arnold DP. Micro machined radial thermoelectric modules for power generation using hot gas stream. *J Micro Electromech Syst.* 2011;20:512–21.
7. Kishi M, Nemoto H, Hamao T, Yamamoto M, Sudou S, Mandai M, Yamamoto S. Micro thermoelectric modules and their application to wrist watches as an energy source. In: *International conference on thermoelectric; 1999.* p. 301–307.
8. Chen G-M, Huang I-Y, Ma L-Y, Wu T-E. Development of a novel transparent micro thermoelectric generator for solar energy conversion. In: *IEEE international conference on nano/micro engineered and molecular systems; 2011, Taiwan.*

9. Tripathi MN, Bhandari CM. Material parameters for thermoelectric performance. *Pramana J Phys.* 2005;65(3):469–79.
10. Rowe DM, editor. *Thermoelectrics hand book: Macro to Nano*. Boca Raton: CRC Press; 2006.
11. <http://thermoelectrics.caltech.edu/thermoelectrics/engineering.html>.

Optimal Design of a Fuzzy PID Controller for Inverted Pendulum System

Sadhna Malik and Sudhansu Kumar Mishra

Abstract In this paper, a very simple and efficient technique to tune a PID controller using fuzzy logic in order to control a cart-pole type inverted pendulum system has been proposed. Due to its high non-linearity, inherent instability, and multiple outputs, controlling the inverted pendulum is a challenging task. Here, the Simulink model of the inverted pendulum system is built and then a conventional PID controller is designed. Thereafter, the fuzzy PID (FPID) controller is designed to control the angle of deviation. The efficacies of the propose technique have been demonstrated through both qualitative and quantitative analysis of experimental results. The tracking efficiency and control force are investigated to demonstrate the superiority of proposed fuzzy PID controller over the conventional PID controller.

Keywords PID controller · Fuzzy PID controller · Inverted pendulum · Tracking efficiency · SIMULINK

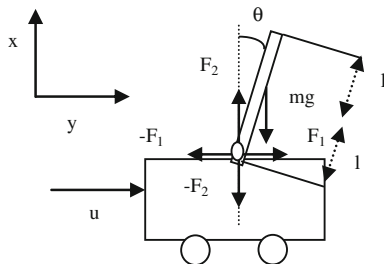
1 Introduction

The control of an inverted pendulum system is a benchmark problem in control systems, so it is widely used for testing designed controllers. The simplest of these consists of a pole mounted on a cart, where the cart moves on a horizontal track with the help of a motor attached to its wheels [1]. The pendulum is free to rotate along its axis and the cart can move forward or backward in horizontal direction as shown in Fig. 2. It is highly non-linear, multivariable, and unstable. The problem is to balance the pole or to keep it from falling by moving the cart horizontally in appropriate direction (Fig. 1).

S. Malik (✉) · S.K. Mishra
Department of Electrical and Electronics Engineering, Birla Institute of Technology,
Mesra, Ranchi 835215, India
e-mail: sadhna.malik09@gmail.com

S.K. Mishra
e-mail: sudhansu.nit@gmail.com

Fig. 1 Free body diagram of the inverted pendulum



The conventional PID controller is often the first choice among the controllers due to its simplicity, effectiveness, and ease of operation. Different PID control schemes have been proposed to control the inverted pendulum using single PID controllers and multiple PID controllers [2]. The main drawback of PID controllers is that their gains become fixed once they have been tuned. Also, they need a very precise model of the plant, which is difficult in the case of non-linear and uncertain plants. In the last few decades, researchers have seen the huge potentiality of fuzzy logic in the area of control systems. Yanchang Liu et al. discuss applications of both conventional and fuzzy tuning [3]. Asim Ali Khan and Nishkam Rapal propose a technique for tuning conventional PID controllers using fuzzy logic that results in a better performance in terms of rise time, settling time, and overshoot. However, finding the gain parameters of fuzzy PID controllers is more difficult [4]. Then, hybrid controllers are designed by combining evolutionary techniques like genetic algorithm with fuzzy logic to determine the optimal parameters of conventional PID controllers [5, 6]. Yadav et al. have done a comparison between different types of fuzzy controllers and PID controllers [7]. However, they are applicable only for linearized version of the pendulum.

The paper presents a design of the fuzzy PID (FPID) controller using the Mamdani model for an inverted pendulum system. Section 2 presents the mathematical modeling of the plant. Section 3 presents the design of the conventional PID controller for the plant. This is followed by designing the FPID controller in Sect. 4 and then comparison is made between the two using simulations in Matlab in Sect. 5.

2 Mathematical Modeling of the Inverted Pendulum System

In this section, the non-linear model of the plant is developed. Figure 1 shows the free body diagram of the inverted pendulum.

θ is the Pendulum Angle from vertical, F_1 is the horizontal Reaction Force, F_2 is the vertical reaction force, f is the frictional force of the cart wheels on the track, and u is the control force applied to the cart.

Let (x_G, y_G) be the coordinates of the center of gravity of the pendulum. where,

$$\begin{aligned} x_G &= x + l \sin \theta \\ y_G &= l \cos \theta \end{aligned}$$

Taking moments around the center of gravity of the stick, equation of horizontal motion is given by

$$I\ddot{\theta} = F_2 l \sin \theta - F_1 l \cos \theta \tag{1}$$

Equation of horizontal motion is given by

$$m d^2/dt^2(x + l \sin \theta) = F_1 \tag{2}$$

After differentiation,

$$m(\ddot{x} + l[-\dot{\theta}^2 \sin \theta + \ddot{\theta} \cos \theta]) = F_1 \tag{3}$$

Equation of vertical motion is given by

$$m \frac{d^2}{dt^2}(l \cos \theta) = F_2 - mg \tag{4}$$

After differentiation,

$$ml(-\dot{\theta}^2 \cos \theta - \ddot{\theta} \sin \theta) = F_2 - mg \tag{5}$$

Cart's motion is given by

$$M\ddot{x} = u - F_1 - f \tag{6}$$

Substituting (6) into (3)

$$m\ddot{x} + ml\ddot{\theta} \cos \theta - ml\dot{\theta}^2 \sin \theta + f = u - M\ddot{x} \tag{7}$$

Putting (5) and (6) into (1), we obtain

$$\begin{aligned} I\ddot{\theta} &= (mg - ml\dot{\theta}^2 \cos \theta - ml\ddot{\theta} \sin \theta)l \sin \theta \\ &\quad + fl \cos \theta - (u - M\ddot{x})l \cos \theta \end{aligned} \tag{8}$$

Using (7), we can write (8) as

$$I\ddot{\theta} = mgl \sin \theta - ml^2\ddot{\theta} - m\ddot{x} l \cos \theta \tag{9}$$

Let $p = \frac{1}{M+m}$

(7) can be written as

$$\ddot{x} = -mpl \cos \theta + mal\dot{\theta}^2 \sin \theta - pf + pu \tag{10}$$

Substituting (10) into (9)

$$\ddot{\theta} = \frac{mgl \sin \theta - m^2l^2p\dot{\theta}^2 \sin \frac{2\theta}{2} + mpl \cos \theta f - mpl \cos \theta u}{I - m^2l^2p(\cos \theta)^2 + ml^2} \tag{11}$$

3 Design of Conventional PID Controller

First the non-linear model of the pendulum is designed using Simulink as shown in Fig. 2. Then, the conventional PID controller is designed to get the values of gain parameters (Table 1).

The control force u is given by

$$u(t) = K_P e(t) + K_I \int e(t) + K_D de(t)/dt \tag{12}$$

where K_P , K_I , and K_D are the gain parameters.

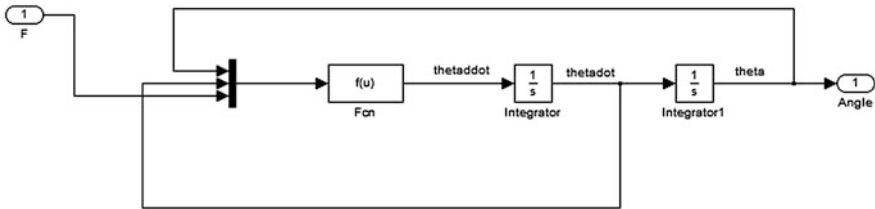


Fig. 2 Non-linear simulink model

Table 1 System parameters

S. no.	Parameter	Value
1.	Mass of cart, M	0.5 kg
2.	Mass of pendulum, m	0.2 kg
3.	Moment of inertia of pendulum, I	0.006 kg-m ²
4.	Length of pendulum, 2l	0.6 m
5.	Cart frictional force	0.1 N
6.	Acceleration due to gravity	9.8 m/s ²

Table 2 Tuning of PID controller

S. no.	K_P	K_I	K_D
1.	10	0	0
2.	50	0	0
3.	100	0	0
4.	100	1	1
5.	100	1	10
6.	100	1	30
7.	100	5	30

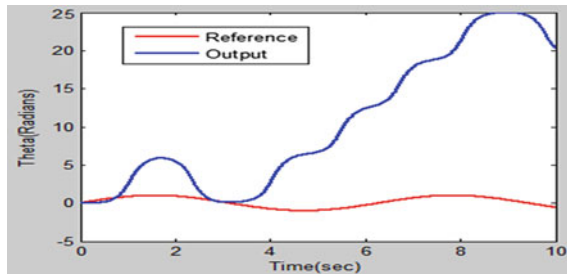


Fig. 3 Response of the uncompensated system

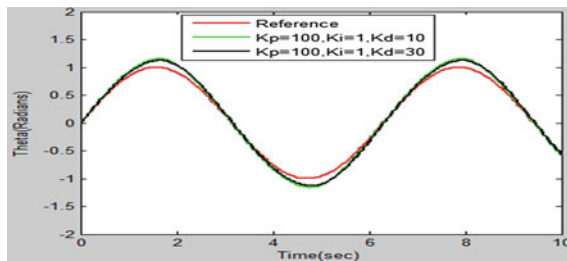


Fig. 4 Response of the compensated system with different values of K_P , K_I , and K_D

The optimum values of PID parameters are obtained by observing the response for different values of K_P , K_I , and K_D . Conventional tuning techniques like Zeigler-Nichols, Internal Model Control, etc. tuning are not applicable for this non-linear plant. Table 2 shows values used to obtain the acceptable values of gain parameters.

Figure 3 shows the response of the uncompensated system for sinusoidal input. Figure 4 shows the response of the system with three different values of K_P , K_I , and K_D . The optimum response is obtained for $K_P = 100$, $K_I = 1$, and $K_D = 30$.

4 Design of Fuzzy PID Controller

For the design of fuzzy PID controller, we first need to develop the fuzzy inference system (FIS). Figure 5 shows the block diagram of a Mamdani type Fuzzy Logic Controller.

The FIS system is designed using the Fuzzy Logic Toolbox in Matlab. Triangular membership functions are chosen for both inputs and outputs. The ranges of K_P , K_I , and K_D are decided by observing the response obtained by conventional tuning.

The range for output is taken as $K_P = 50-100$, $K_I = 1-5$, and $K_D = 15-30$. We defined seven membership functions for each input and outputs and seven linguistic variables as negative large (NL), negative medium (NM), zero error (ZO), positive small (PS), positive medium (PM), Positive large (PL) (Figs. 6, 7, 8 and 9).

Next, we designed the rule base. In Mamdani FIS, the rules are in the form of:

IF input 1 is mem_func1 **AND/OR** input 2 is mem_func2 **THEN** output is mem_func n.

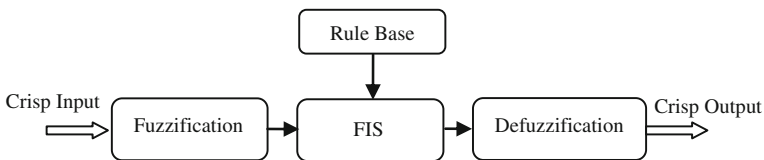


Fig. 5 Block diagram of a Mamdani type fuzzy logic controller

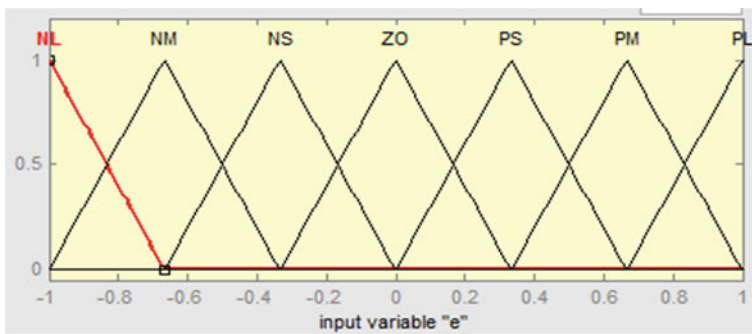


Fig. 6 Membership function of e and ec

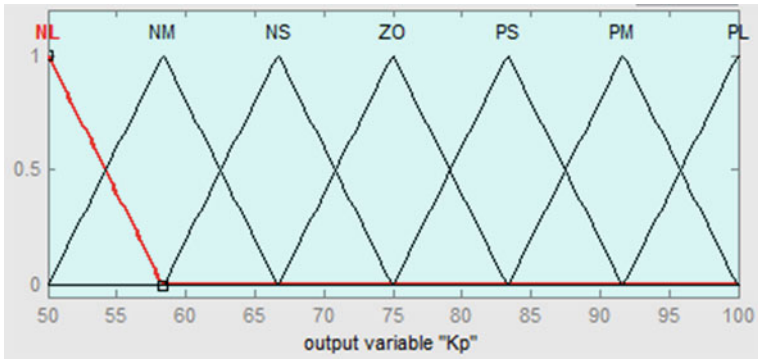


Fig. 7 Membership function of K_p

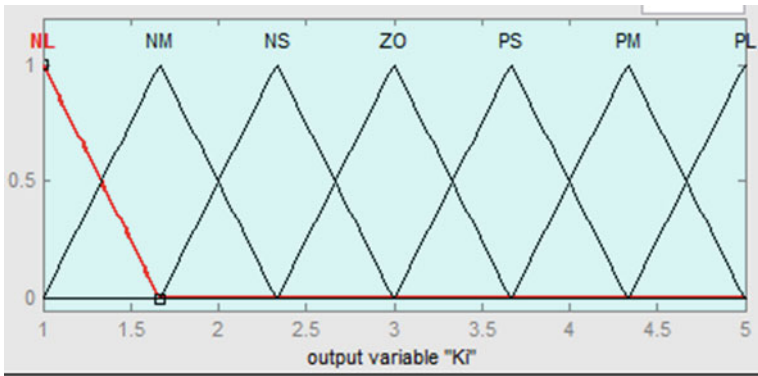


Fig. 8 Membership function of K_i

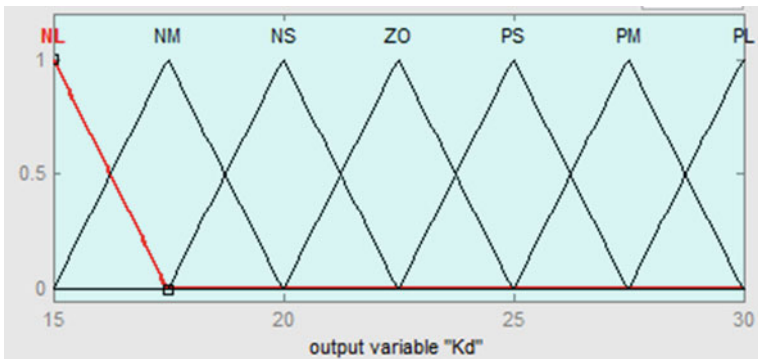


Fig. 9 Membership function of K_d

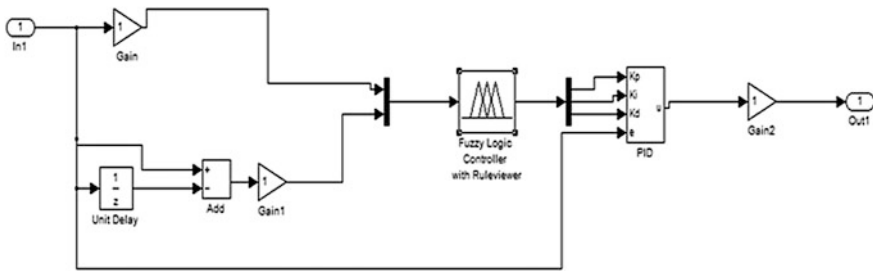


Fig. 10 Simulink model of the FPID controller

The rule base was designed after taking into consideration these points:

1. The effect of individually increasing each of the gain parameters on the output response in terms of maximum overshoot, settling time, stability etc.
2. Relationship between error (e) and the change in error (ec) with K_P , K_I , and K_D [6]
 - (a) When ' e ' is a larger value, K_P should be larger and K_D and K_I should be taken smaller.
 - (b) When both ' e ' and ' ec ' are medium values, K_P should be taken smaller.
 - (c) When ' ec ' is very small, K_D should be taken larger (Figs. 10, 11 and Table 3) .

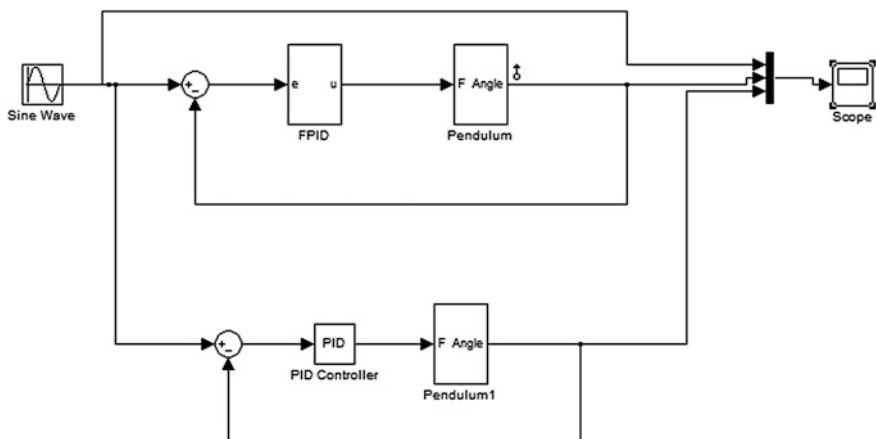


Fig. 11 Simulink model of the complete control system

Fig. 12 Response of pendulum angle(theta)

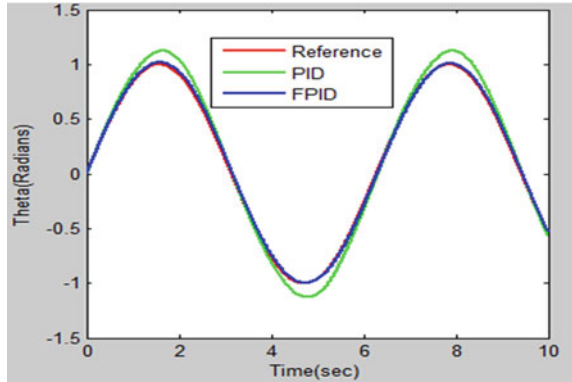


Table 3 Rule base for K_p , K_i , and K_D

K_p, K_i, K_D	NL	NM	NS	ZO	PS	PM	PL
NL	PL,PS, PM	PL,PL, PS	PL,PL, ZO	PL,PL,PS	PL,PL, PS	PL,PL, PM	PL,PL, PL
NM	PL,PM, PM	PM,PS, PS	PM,PM, PS	PM,PS, PS	PM,PM, PS	PL,PL, PS	PL,PL, PM
NS	PL,PM, PS	PM,PS, PS	PS,PS,PS	PM,PS, PS	PS,PS, PS	PM,PS, PS	PL,PM, PS
ZO	PM,PM, ZO	PS,PM, ZO	PS,PM, ZO	PM,PS, ZO	PS,PM, ZO	PS,PM, ZO	PM,PM, ZO
PS	PL,PL,PS	PL,PL, PS	PM,PM, PS	PM,PS, PS	PM,PM, PS	PL,PM, PS	PL,PM, PS
PM	PL,PL, PM	PL,PL, PS	PM,PM, PS	PM,PS, PS	PM,PM, PS	PL,PL, PS	PL,PL, PM
PL	PL,PL, PL	NL,NL, PL	NL,NL, NM	NL,NM, NS	NL,NL, NS	NL,NL, NS	NL,NL, PL

5 Simulation Results

The inverted pendulum system is simulated using Matlab Simulink for duration of 10 s. For simulation, the values of different parameters are chosen as given in Table 1.

Figure 12 shows the response of the pendulum angle for both PID and fuzzy PID controllers with sinusoidal signals as reference input. Figure 13 shows the response of error signals against time. It is clear that there is significant reduction in error due to FPID controller i.e., 89.88 %. So, the FPID controller has good tracking

Fig. 13 Response of error in theta

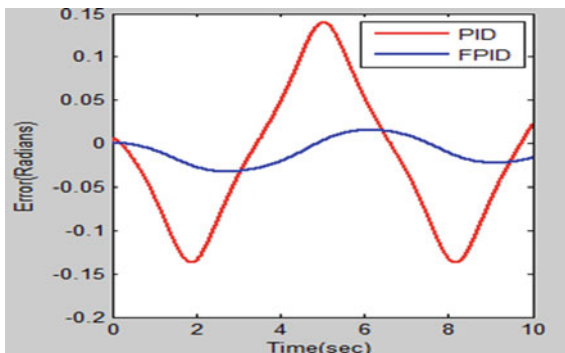
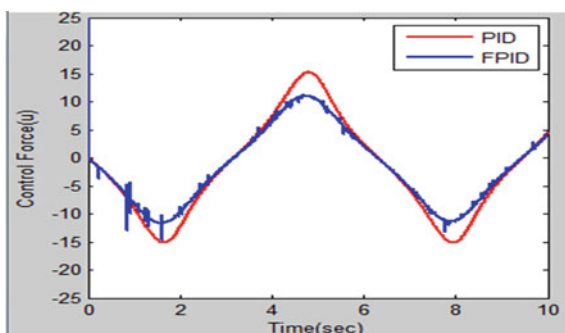


Fig. 14 Response of control force



efficiency. Figure 14 shows the response of the control force exerted by both the controllers. At time equal to zero second, the control force exerted by FPID controller is much higher than the PID controller. However, it reduces after that and remains lower than that of the PID controller for the rest of the time.

6 Conclusion

In this paper, we have proposed a technique to tune the PID controller using fuzzy logic for controlling a non-linear model of the inverted pendulum system. The proposed fuzzy based controller has been compared with the conventional PID controller. From the simulation results, it is observed that the FPID controller is superior to the PID controller in terms of error reduction. Moreover, it takes lesser effort to control the plant and also makes the tuning automatic as opposed to the conventional PID controller. Moreover, the fuzzy rule base can also be generated by using evolutionary algorithms like Genetic Algorithm, Cat Swarm Optimization etc. to test the potentiality to this challenging problem. Further research work includes

the hardware implementation of the proposed FPID controller. To assess the strength and weakness of proposed technique, it has to be investigated for other applications.

References

1. Tsoa CW, Taurb JS, Wamga CM, Chena US. Fuzzy hierarchical swing-up and sliding position controller for the inverted pendulum-cart system. Elsevier, *Fuzzy Sets Syst.* 2008;159 (2008):2763–84.
2. Wang J. Simulation studies of inverted pendulum based on PID controllers. Elsevier, *Simul Modell Practice Theory.* 2010;19(2011):440–9.
3. Liu Y, Sun S, Liu, ZH, Jiasheng, GJ (2010) Research and application of fuzzy PID controllers. In: IEEE, 2010 seventh international conference on fuzzy systems and knowledge discovery.
4. Khan AA, Rapal N. Fuzzy PID controller: design, tuning and comparison with conventional PID controller. In: IEEE international conference on engineering of intelligent systems; 2006.
5. Dr. Nandkumar MP, Nalakath R. A non linear PID fuzzy approach to inverted pendulum controller with evolutionary parameter optimisation. In: IEEE, 2012 international conference on power, signals, controls and computation; January 2012.
6. Ma Y, Liu Y, Wang C. Design of parameters self-tuning fuzzy PID control for DC motor. In: IEEE, 2nd international conference on industrial mechatronics and automation; 2010.
7. Yadav K, Anil Gaur P, Mittal A, Mittal P, Anzar M. Comparative analysis of various control techniques for inverted pendulum. In: IEEE, 2010 India International Conference on Power Electronics; January 2011.

Kalman Filter Based MPC with Dead Band for a Ball Mill

Punit Krishna, M. Guruprasath, K. Ramkumar, S. Venkatesh and G. Balasubramanian

Abstract This paper addresses the issues of regulating the fineness and mill load of ball mill by using Kalman filter and linear Model Predictive Control. The MPC is designed by various simulation results with the help of MPC toolbox. The main objective of this paper is to reduce the energy consumption during production. This can be achieved by reducing the energy used or by increasing the product units for different fineness. In this paper, two MPCs are designed, i.e., MPC with dead band type I and type II to reduce the energy consumption in different manner. Usually, normal MPC is used to take control action to force the output to reach a set point. But in this paper, the designed MPC is used in a different manner to maintain the output within a range of set point and Kalman Filter is used to estimate sensor output state as none of the sensor gives accurate measurement. Furthermore, the performance of developed methodology has been compared with the normal MPC by simulation.

Keywords Ball mill • Kalman filter • Model predictive Control (MPC) • Dead band • ECS/cemulator

P. Krishna (✉) • K. Ramkumar • S. Venkatesh • G. Balasubramanian
EIE Department, SEEE, SASTRA University, Thanjavur, India
e-mail: punitton@gmail.com

K. Ramkumar
e-mail: ramkumar@eie.sastra.edu

S. Venkatesh
e-mail: esvee@eie.sastra.edu

G. Balasubramanian
e-mail: balu_eie@eie.sastra.edu

M. Guruprasath
FLSmidth Private Limited, Thanjavur, India
e-mail: mgp-in@flsmidth.com

1 Introduction

Clinker is a very rigid, nodular material from cement kiln which can be grounded by using ball mill and vertical mill in many industries into fine grey powder is called cement. This is the final process after raw milling, pyro processing. Ball mill is commonly used by many industries due to its high reliability and easy maintenance. The efficiency of ball mill depends upon two different stages. First is the ball mill parameter and second is grinding material properties. In first stage, grinding efficiency depends upon size and number of chambers, size and number of metal balls, lifting and classifier liners, separator speed etc. In second stage, it depends upon the clinker size, feed rate, grind ability etc. Even if the ball is designed with use of designing parameters at first stage, there is a possibility of plugging due to the factors at second stage, which incurs extra penalty cost. So, maintaining the mill load is one of the most important aspects along with product quality.

The FLSmidth ball mill is divided into two chambers. The first chamber contains balls of large size and second chamber contains smaller balls called grinding media, which reduces the size of clinker from coarse powder to fine powder. Clinker feed comes through the input diaphragm and after size reduction passes to second chamber through intermediate diaphragm and finally discharged through the output diaphragm and passing through the elevator to separator. It separates the fine and coarse particle. Rejected material fed back to input and combines with fresh feed. Typical ball mill is shown in Fig. 1. This system is controlled as MIMO system, where separator speed and feed rate as input and fineness and mill load as output.

Generally, decoupled MIMO PID controllers are used to control a ball mill system.

Due to uncertainties and highly interacting loop, decoupling is very difficult and due to plant model mismatch it becomes sluggish. To address these issues, MPC has been developed.

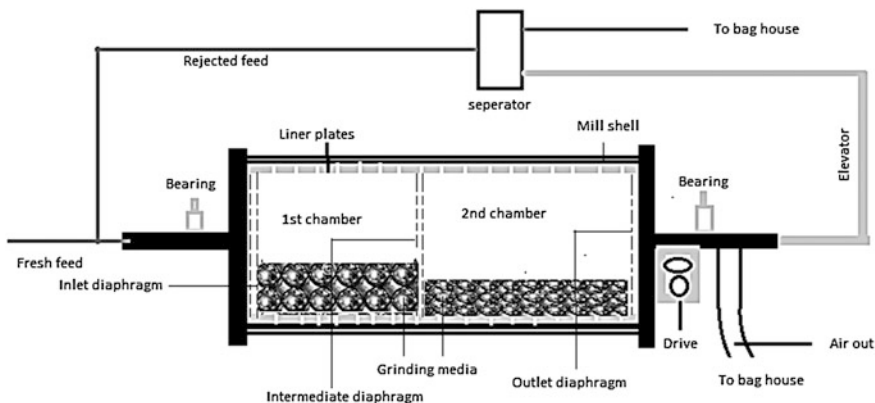


Fig. 1 Ball mill layout

The working principle of MPC is briefly explained in [5]. When the output reached in a certain range, then how the controller takes minimum control actions to reach set point is shown in [1]. A MPC is developed based on a finite response model and how plant model mismatch is investigated and solved is given in [2]. To address the problem of decoupling in PID controller, a MPC is developed for a three input, three output grinding process discussed in [3]. Modeling, sensors, measurement, and control system for a ball mill is given in [6]. The system is controlled with PI controller for decoupling, it becomes sluggish and performance comparison of constraint and unconstraint MPC by simulation as shown in [4]. A supervisory control optimizes at regulatory basis and takes action for degradation as shown in [7]. [9] describes how to reduce the energy consumption in milling process. This paper and developed controller is derived from the thesis [8], which is based on soft constraint MPC and derived MPC is with dead band.

This paper is structured as follow: in next section, ball mill control with MPC with dead band is discussed. Then principle of Kalman filter is described in Sect. 3. System implementation is given in Sect. 4 and finally conclusion in Sect. 5.

2 MPC with Dead Band

MPC is very effective control strategy to control SISO, MIMO, and highly interactive system in presence of uncertainties and plant model mismatch. Conventional MPC works on the principle of DMC (Fig. 2).

In normal MPC, reference trajectory is decided based on the single set point. The output is measured and based upon the error between reference trajectories and measured output, the future control inputs have been predicted in order to reduce the error to zero. The first control input from predicted inputs is applied and others

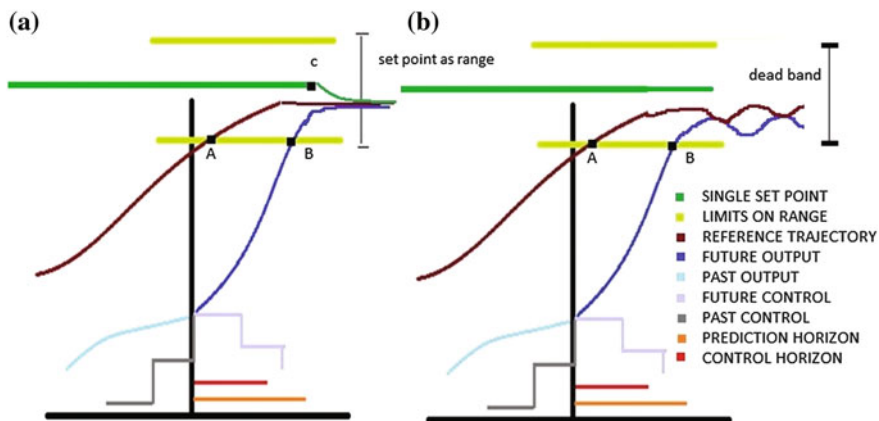


Fig. 2 a MPC with dead band: type 1. b MPC with dead band: type 2

are discarded. Same procedure is repeated until the error becomes zero. After fetching the state-space model using system identification, the model is used in MPC. Furthermore, MPC tuning is performed. MPC has some disadvantages such as tuning is based upon hit and trial method, which comes by experience. Initially to set prediction horizon and control horizon, step test is used. Generally, prediction horizon is one-third of the steady state time and control horizon is one-fifth of the prediction horizon. The output weight helps each output to reach set point with good precision. The controller estimates the deviation from set point for each output over prediction horizon and multiplies the weights; then calculates the weighted sum of squared deviations. The output weights should be set in such a manner that weighted squared sum value becomes minimal. A positive value means that the output is being forced to reach at the set point. In case of input weights, the deviation is measured from nominal value over the control horizon and further weight is multiplied with deviation from nominal value to calculate the weighted sum of squared deviation, which should be minimum. When upon increasing the output weights, it does not reach at the set point, input weights should be adjusted. There is no effect of rate weight on the steady state it only penalizes the input. The MPC tuning is briefly explained in [11].

Figure 3 shows the MPC simulation graph for output before and after tuning. The output traces the path of reference trajectory, which is given by Eqs. (1) and (2). There are many exponential paths available to reach the single point as aggressive, normal and sluggish depending upon the value of α parameter. When α becomes one, the reference trajectory is same as measured output. So, it hits the same point to reach set point which is impossible. When α becomes zero, it is equal to the set point which is also impossible to reach set point suddenly. So, its value should be in between zero and one.

$$r_i = \alpha r_{i-1} + (1 - \alpha)y_i^{SP}; i = 1, 2, \dots, p \tag{1}$$

$$i = 0, r = y_m; 0 < \alpha < 1 \tag{2}$$

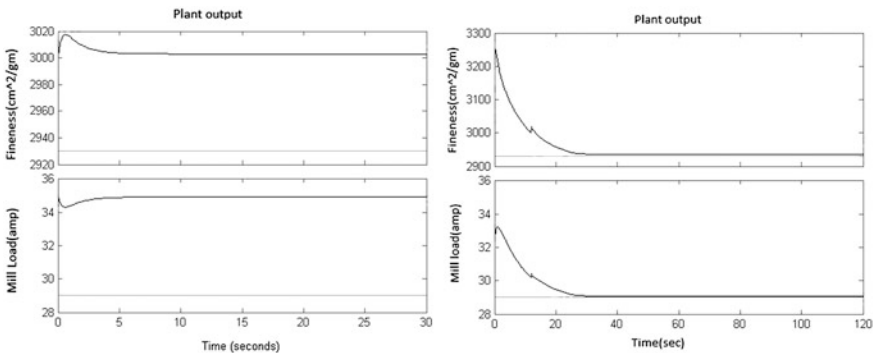


Fig. 3 Plant output before and after tuning

In order to convert the normal MPC to MPC with dead band, general parameter of DMC is used such as prediction horizon, control horizon, α , reference trajectory etc. Even if somehow a range is fixed for set point, there is infinite number of paths for reference trajectory. So, which path is to be followed is one of the most challenging issues. Two types of MPC have been developed to maintain the output within a range as it is not mandatory to reach the particular set point in many cases. Here, the example of cement fineness can be considered, i.e., within a certain range, it is acceptable.

2.1 MPC with Dead Band: Type 1

MPC uses an optimization technique in which, a single set point is required for mathematical calculation in order to decide the reference trajectory, control inputs, and outputs. So, initially a single set point is chosen for output. All mathematical calculations for predicted output, control inputs, and reference trajectory will be calculated for this single set point. Furthermore, tuned controller is connected with plant. A user defined function is used in between the output and reference port of the MPC controller. Module for reference trajectory and a range for set point is defined in the user defined function block. The output tracks the reference trajectory same as in normal MPC until it enters the predefined range. But, whenever output enters into the predefined range, the output itself assigned as a set point. As the output is assigned as the set point, the reference trajectory automatically reaches at the same point. From Fig. 2a, it is observed that the point A, B, and C all meets at the same point when output enters in the range. Hence by using this method, several control inputs to reach at point C from point B are saved, which reflects the energy point of view.

2.2 MPC with Dead Band: Type 2

Usually in normal MPC, the output changes according to the reference trajectory; where as in this proposed methodology, output tracks the reference trajectory in the same manner when it lies beyond the range. But when the output enters in dead band or predefined range, the reference trajectory has been changed according to the output to maintain the output within the range. In this controller, the reference trajectory is defined in the user defined function block in such a manner that when output enters this range, the reference trajectory at point B and output at point A becomes same. After some time, the output tries to go outside the range, because the reference trajectory has not yet reached the set point. When the output comes out of the range, the controller takes action and brings it back in the range and again reference trajectory and output meets at the same point is shown in Fig. 2b. In this method, the objective cannot be achieved simply because the deviation of output

from the specified range is undesired. So, it needs some manipulation work to maintain the output within the desired range. All possible values of output can be produced within this range. Therefore for a single set point, it is possible to generate number of products. So according to the energy point of view, no need of separate grinding circuits for each product with different fineness. Furthermore, the manipulation work is discussed in system implementation part.

3 Kalman Filter

Kalman filter is the best linear estimator. It comes under the BLUE region (Best Linear Unbiased Region). The common region of two subset linear estimator and unbiased estimator is known as BLUE region, where the Kalman filter stands. The basic structure of Kalman filter is based on the Gauss–Markov and Rao–Blackwell theorem. According to the Gauss–Markov theorem, covariance of estimated state by the least square method cannot be greater than the covariance of other possible linear unbiased estimate. According to Rao–Blackwell, non-linear estimator may estimate better than linear estimator but when the all information is associated with the Gaussian noise, the least square estimation is best including all linear and non-linear estimator. Now, let us consider that there are two pieces of information available for the state X as X_1 and X_2 with same mean and variance σ_1^2 and σ_2^2 , respectively. Initially, estimate X by linear estimator by Eq. (3) and then forcing it into unbiased region by Eq. (4) to bring into BLUE region. Variance of estimated state is found by formula Eq. (6). Objective is to find a_1 and a_2 such that variance of estimated state is minimum. So, differentiate the variance of estimated state and make it zero. Then, find the value of a_1 and a_2 to find the variance. Now, the variance of estimated state is minimum than the variance of both state X_1 and X_2 in Eq. (8). The brief explanation of Kalman filter and algorithm has followed by book [10, 12, 13].

Linear estimate:

$$\hat{X} = a_1X_1 + a_2X_2 \quad (3)$$

Unbiased estimate:

$$E[\hat{X}] = a_1E[X_1] + a_2E[X_2] \quad (4)$$

$$1 = a_1 + a_2 \quad (5)$$

$$\text{var}(\hat{X}) = a_1\sigma_1^2 + (1 - a_1)\sigma_2^2. \quad (6)$$

$$\text{var}(\hat{X}) = \frac{\sigma_2^2}{\sigma_1^2 + \sigma_2^2} \tag{7}$$

$$\text{var}(\hat{X}) < \min(\sigma_1^2, \sigma_2^2) \tag{8}$$

These two pieces of information may be the background or state equation and the observation or output equation. In this paper, the Kalman filter is connected to the process output after sensor.

4 System Implementation

4.1 Data Collection

ECS/CEMulator stands for Expert control and supervision and cement simulator shown in Fig. 4. This is a high end technology used in cement industry to train the employees.

All the equipment and features present in a real plant is available. In ECS, various parameters are available, which can be varied in order to generate the model of ball mill.

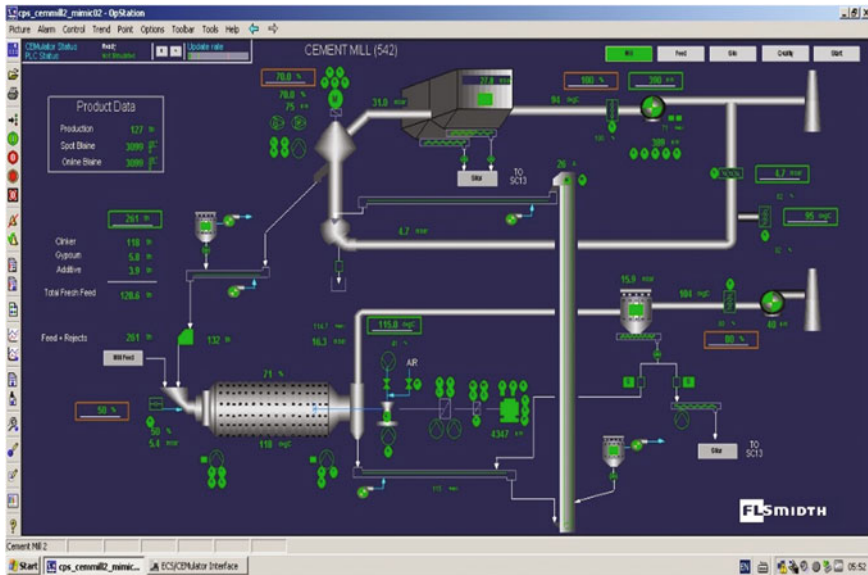


Fig. 4 ECS/CEMulator

The data are taken after performing a step that changes in feed rate and separator speed and corresponding readings of fineness and mill load have been recorded in spreadsheet.

4.2 Cross-Correlation Check

The dynamics of system should be known before start any experiment. A cross-correlation check shows how two different signals are being matched with each other and time delay after which the input signal matched with the output signal. Here, feed rate of clinker and mill load are two different signals. The maximum load associated with the maximum feed rate. It shows that these two signal are positive correlated. The Fig. 5 shows the feed rate has direct impact on mill load.

4.3 System Identification

The data recorded in spread sheet are used in system identification toolbox for modeling of the system. The input–output relationship graph is matched with the saved graph and for best fit graph model is generated. A state-space model is generated by using prediction error method and SSARX model. Best fit graphs are shown in Fig. 6.

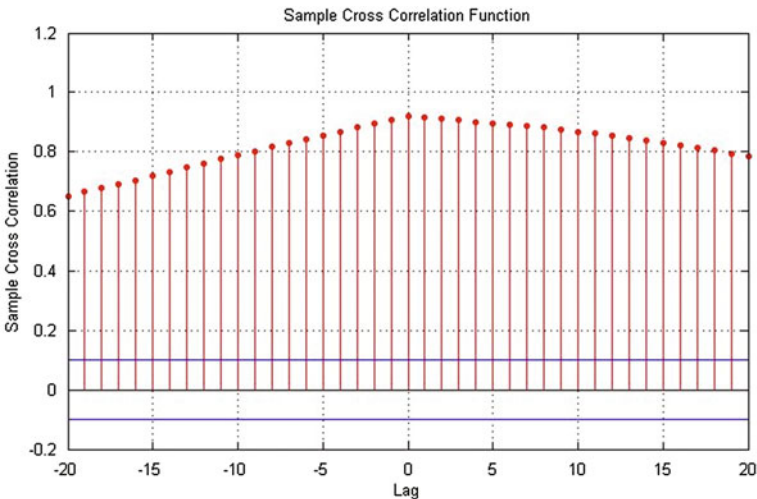


Fig. 5 Cross-correlation between feed rate and fineness

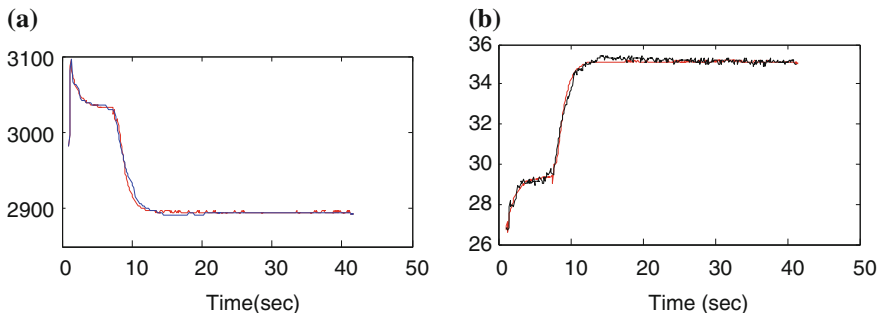


Fig. 6 a Fineness model. b Mill load model

4.4 Kalman Filter Based MPC with Dead Band

Kalman filter model is connected at the output of sensor. The simulation graph of normal MPC is shown in Fig. 7. It can be easily noticed that the output is reaching to the single set point after some time smoothly with time delay around 10 s.

MPC with dead band: type 1 is given in Fig. 8. The main objective of this paper is to replace the single set point to a viable range to maintain the quality within this range. It can be easily noticed that when output enters the range of 2800 and 2900 cm^2/gm , suddenly set point and output becomes same point. As the output is assigned as the set point, the reference trajectory automatically reaches at the same point. The output is maintained constant and within this range throughout the process. The time taken by this controller is less than the time taken by normal MPC controller

MPC with dead band: type 2 simulation graph are shown in Figs. 9 and 10. Initially, the module for reference trajectory is defined then a user defined function block is defined for the output and reference trajectory. From the Fig. 9a, main objective is to maintain the fineness within the range 2800 and 2900 cm^2/gm , but it can be noticed that there is some deviation around 20 cm^2/gm from the

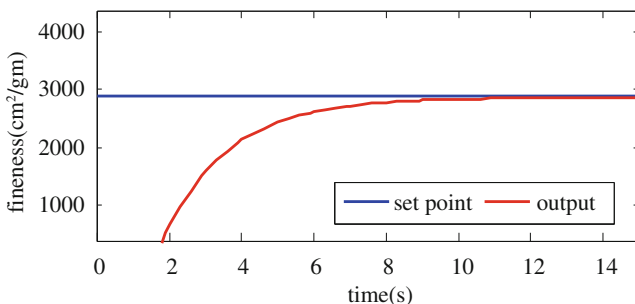


Fig. 7 Normal MPC fineness output

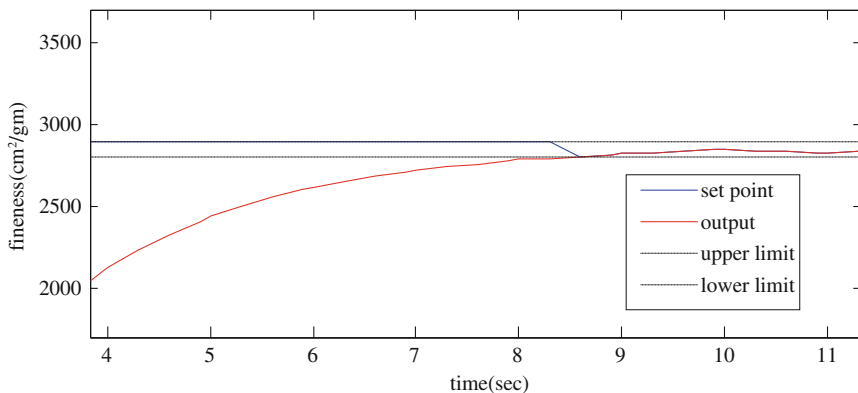


Fig. 8 Fineness output of MPC with dead band: type 1

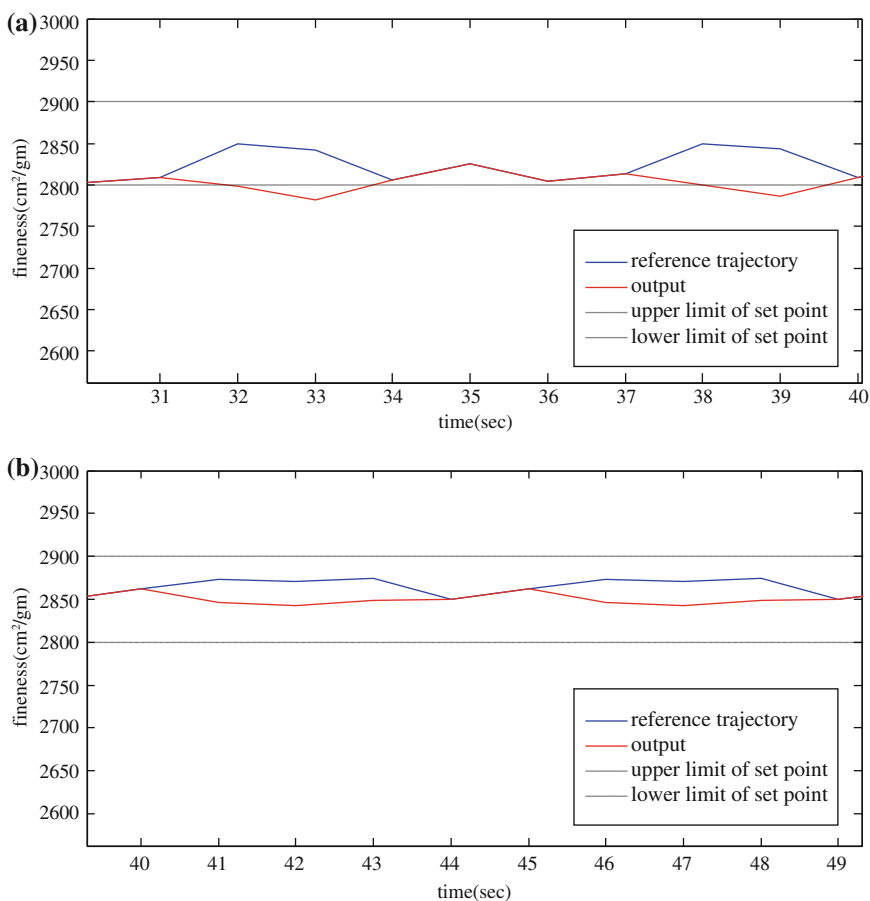


Fig. 9 a Fineness output without manipulation of MPC with dead band: type 2. **b** Fineness output after manipulation of MPC with dead band type 2

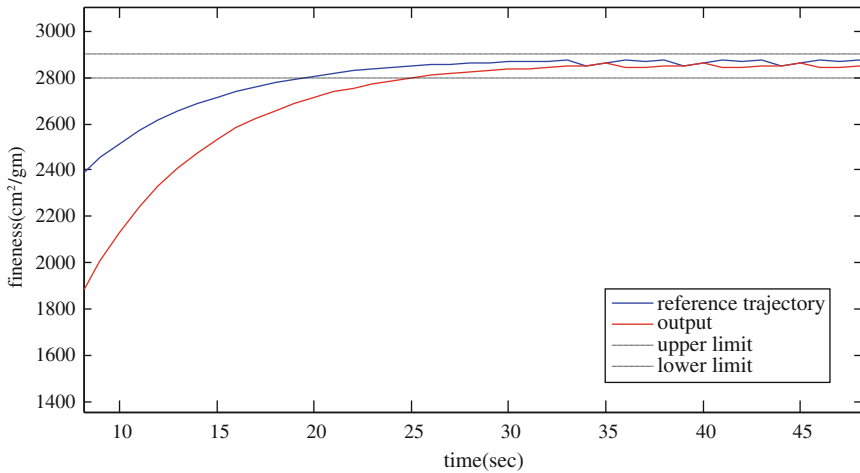


Fig. 10 Fineness output after manipulation for MPC with dead band: type 2

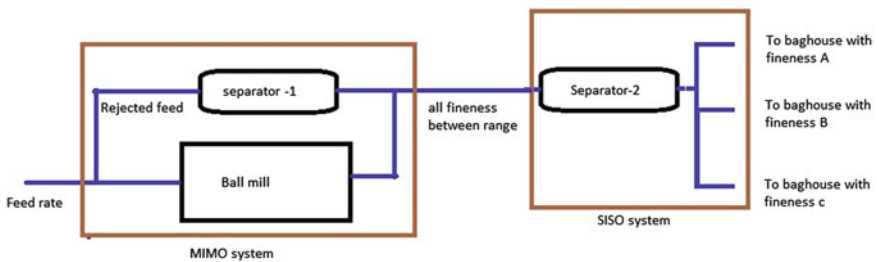


Fig. 11 Real-time implementation and application

2800 cm²/gm. Developed controller is taking action only when the output comes out from this range to bring it back in range that is undesirable, because fineness must be maintain within this range.

To achieve the objective, some manipulation works are required. From the Fig. 9a deviation is found and to maintain the fineness within this range of 2800–2900 cm²/gm, suppress the lower limit same or more than deviation. Here, the range is suppressed from 2850 to 2900 cm²/gm to maintain within the 2800–2900 cm²/gm. The fineness output after manipulation is shown in Fig. 9b.

Figure 10 shows the complete fineness output graph. It can be noticed that the controller take action in such way to maintain the fineness within the band. Cement with different sizes can be obtained by using the separator at end of process which will be a SISO system is shown in Fig. 11. There is no requirement of separate grinding circuit for each product with different size and it is easy to control a SISO system than MIMO system.

5 Conclusion

An MPC Dead Band controller with soft output constraints for reducing energy consumption of the cement mill circuit has been developed for cement grinding circuit plant by two methods. Furthermore, it has been compared with normal MPC controller with soft output constraints. In the first method, Type-I controller is taking less time to reach at the desired range than the normal MPC and in the second method, Type-II controller makes it possible to produce products with different size within a range by using the single set point. Furthermore, this can be implemented in a real cement plant with two inputs and three outputs including production rate as an output. The results indicate that MPC with Dead Band controller handles the significant uncertainties and provides very good performance.

References

1. Guruprasath M, Bodil R, Chidambaram M, John Bagterp J. Soft constraint based MPC for robust control of a cement grinding circuit. In: American control conference; 2013. p. 475–80.
2. Guruprasath M, John Bagterp J. Model predictive control based on finite impulse response model. In: American control conference; 2008. p. 441–446.
3. Chen X, Li Q, Fei S. Constraint model predictive control in ball mill grinding process. *Power Technol.* 2008;186:31–9.
4. Ramasamy M, Narayanan SS, Rao ChDP. Control of a ball mill grinding circuit using model predictive control scheme. *J Process Control.* 2005;15:273–83.
5. Rawlings JB. Tutorial overview of model predictive control. *IEEE Control System Magazine;* 2000. p. 38–52.
6. Kolacz J. Measurement system of the ball mill charge in grinding ball mill circuit. *Mineral Eng.* 2010;10(11):1471–8.
7. Radhakrishnan VR. Model based supervisory control of a ball mill grinding circuit. *J Process Control.* 1999;9:195–211.
8. Guruprasath M. Robust model predictive control of cement mill circuit. Doctor of Philosophy thesis; 2011.
9. Fujimoto S. Reducing specific power usage in cement plants. *World Cement.* 1993;7:25–35.
10. Simon S. *Optimal state estimation.* New York: Wiley; 2006. p. 263–94.
11. Garriga JL, Soroush M. Model predictive control tuning method: a review. *Ind Eng Chem Res.* 2010;49:3505–15.
12. Mendel J. *Lessons in estimation theory in signal processing, communication and control.* Prentice hall; 1995, Chapter-17.
13. Hayes Monson H. *Statistical digital signal processing and modeling.* New York: Wiley; 1996. p. 371–9.

Design of Optimal Controller for Magnetic Levitation System Using Brownian Bat Algorithm

K. Sundaravadivu, C. Ramadevi and R. Vishnupriya

Abstract This paper presents a method to design the One Degree Of Freedom (1DOF) and Two Degrees Of Freedom (2DOF) PID controllers for an unstable Magnetic Levitation System (MLS) using Brownian Bat Algorithm (BBA). Minimization of objective function (J_{\min}) is considered to guide the search towards the optimal controller parameters. A simulation study is carried to validate the performance of the proposed BBA with other successful heuristic algorithms, such as Genetic Algorithm (GA), Particle Swarm Optimization (PSO), Bacterial Foraging Optimization (BFO) and Firefly Algorithm (FA). This study confirms that the proposed method offers better result in reference tracking operation with reduced error for 1DOF and 2DOF PID structure compared with other algorithms considered in this work.

Keywords Magnetic levitation · Degrees of freedom · PID · Brownian distribution · Bat algorithm

1 Introduction

Due to its simplicity and adaptability, heuristic algorithm based Proportional+Integral+Derivative (PID) and modified forms of PID controller design is widely proposed by most of the researchers for stable [1–3] and unstable systems [4–7].

Design of traditional and advanced controllers for Magnetic Levitation System (MLS) are widely discussed in the literature. Various control techniques, such as fuzzy PID [8], sliding mode control [9], phase-lead compensation [10], H_{∞} controller [11], and heuristic algorithm-based approaches like Genetic Algorithm (GA) [12] and Bacterial Foraging Optimization (BFO) [13] are existing in the literature to achieve required performance from MLS.

K. Sundaravadivu (✉) · C. Ramadevi · R. Vishnupriya
Department of Electronics and Instrumentation Engineering, St. Joseph's College
of Engineering, Chennai 600 119, Tamil Nadu, India
e-mail: ksvadivud@gmail.com

In this paper, 1DOF PID controller design is initially proposed on the MLS system using the Bat Algorithm (BA) and the obtained controller values are then implemented on the 2DOF PID structures, such as PID controller with filter (FPID) [3, 4] and I-PD [5]. Bat Algorithm (BA) was developed by Yang [14, 15] is considered to design the optimal PID controller. This algorithm is developed by mimicking the food searching tactic of micro bats. From the recent literature, it is noted that, conventional and improved forms of BAs are extensively used to solve engineering optimization problems [16–18]. In this paper, Brownian walk strategy is used to guide the BA during the exploration of the search space. The performance of the Brownian walk based BA (BBA) is validated using the other heuristic approaches, such as GA, Particle Swarm Optimization (PSO), BFO, and Firefly Algorithm (FA).

This paper is ordered as follows: Sect. 2 discusses the model of MLS, the controller design procedure is discussed in Sect. 3 and the overview of heuristic algorithm is presented in Sect. 4. Simulated results are presented in Sect. 5 and conclusion of the proposed work is given in Sect. 6.

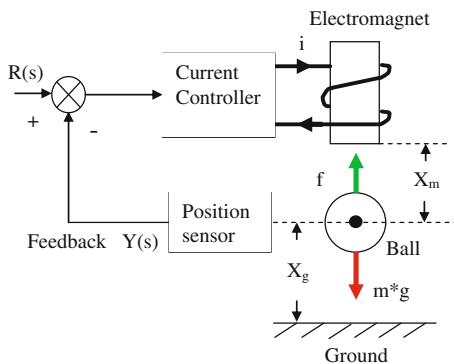
2 Magnetic Levitation System (MLS)

MLS is an electro-mechanical system and its construction detail and block diagram are shown in Figs. 1 and 2, respectively. In this system, a controller is employed to adjust the electric current until the electromagnetic force equals to the weight of the steel ball. When the above condition is reached, the ball will levitate in an equilibrium state [9, 11]. The mathematical model of the considered system is available in [9] (Fig. 1).

The mathematical model of the MLS is described below [9, 11];

$$\text{Voltage applied to the coil} : V(t) = Ri(t) + L \frac{d i(t)}{dt} \tag{1}$$

Fig. 1 Construction of MLS



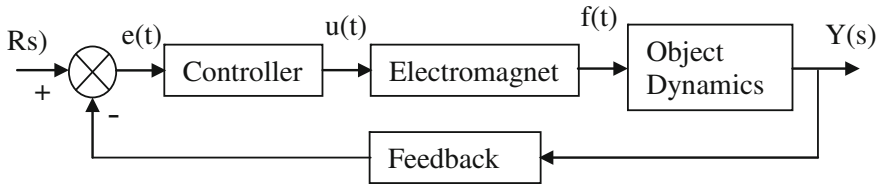


Fig. 2 Closed loop control of MLS

$$\text{Force by the electromagnet is : } f(x, i) = c \left(\frac{i}{x} \right)^2 ; \text{ and } c = \frac{L_0 X_0}{2} \quad (2)$$

$$\text{Mechanical force on the ball : } m \frac{d^2x}{dt^2} = (m * g) - c \left(\frac{i}{x} \right)^2 \quad (3)$$

where X_m is the distance between ball and magnet, i is current through coil, L is inductance of the coil, R is internal resistance of the coil, m is mass of the ball, g is acceleration due to gravity, L_0 is the additional inductance of the magnetic coil due to the ball placed at the equilibrium position x_0 .

From Eq. (1), coil inductance (L) is a nonlinear function and it is a function of ball position x .

$$\text{The approximate inductance is : } L(x) = L + \frac{L_0 x_0}{x} \quad (4)$$

Linear form of Eq. (3) can be written as:

$$m \frac{dx^2}{dt} = -c \left(\frac{i_0}{x_0} \right)^2 \left\{ 1 + 2 \left[\frac{i(t)}{i_0} - \frac{x(t)}{x_0} \right] \right\} + mg \quad (5)$$

when $c \left(\frac{i_0}{x_0} \right)^2 = m * g$, Eq. (5) can be written as:

$$m \frac{dx^2}{dt} = -\frac{2i_0 c}{x_0^2} i(t) + \frac{2i_0^2 c}{x_0^3} x(t) \quad (6)$$

In Eq. (5), $x(t)$ and $i(t)$ are the incremental displacement and incremental magnet current around their nominal values x_0 and i_0 . The linearized state model of the system around the point $x_1 = x_{01}$ is presented as:

$$\text{The state vector for the system is } X_0 = [x_{01} x_{02} x_{03}]^T \quad (7)$$

$$\text{At equilibrium, } x_{02} = 0 \text{ and } x_{03} = x_{01} \sqrt{\frac{mg}{c}} \quad (8)$$

The linearized state model of the system is:

$$A = \begin{bmatrix} 0 & 1 & 0 \\ \frac{Cx_{03}^2}{Mx_{01}^3} & 0 & -2\frac{Cx_{03}}{Mx_{01}^2} \\ 0 & 2\frac{Cx_{03}}{Lx_{01}^2} & -\frac{R}{L} \end{bmatrix}; B = \begin{bmatrix} 0 \\ 0 \\ 1/L \end{bmatrix}; C = [1 \ 0 \ 0] \quad (9)$$

In this paper, MLS parameters are assigned as $m = 0.05 \text{ kg}$, $g = 9.81 \text{ m/s}^2$, $L = 0.01 \text{ H}$, $R = 1 \ \Omega$, $C = 0.0001$, $x_{01} = 0.012 \text{ M}$, $x_{02} = 0 \text{ M/s}$, and $x_{03} = 0.84 \text{ A}$ [9]. The mathematical model of the MLS is represented in Eq. (10).

$$A = \begin{bmatrix} 0 & 1 & 0 \\ 1633.33 & 0 & -23.33 \\ 0 & 116.66 & -100 \end{bmatrix}; B = \begin{bmatrix} 0 \\ 0 \\ 100 \end{bmatrix}; C = [1 \ 0 \ 0] \quad (10)$$

From, Eq. (10), it can be observed that, the model of MLS is unstable [11].

3 Controller Tuning Procedure

A general close loop control system is depicted in Fig. 3. The controller ‘ $G_c(s)$ ’ has to help to achieve the closed loop stability, reference tracking and disturbance rejection performances [1, 6, 7].

To achieve a satisfactory reference tracking and disturbance rejection operation, the controller should have optimal values of K_P , K_I , and K_D . In this study, parallel PID controller is considered to achieve the preferred response.

The parallel PID structure is given below:

$$G_C(s) = K_P e(t) + K_I \int_0^T e(t) dt + \left(\frac{K_D}{T_f s + 1} \right) \frac{de(t)}{dt} \quad (11)$$

$$G_{PID}(s) = K_P \left[1 + \frac{1}{T_i s} + \frac{T_d s}{T_f s + 1} \right] \quad (12)$$

where $K_P/T_i = K_I$; $K_P * T_d = K_D$, and T_f is filter constant assigned as 10.

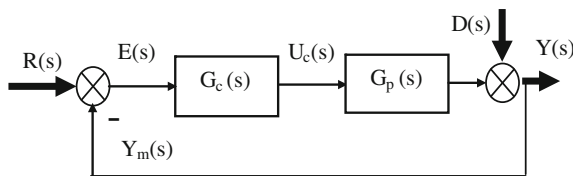


Fig. 3 Block diagram of a closed loop control system

In the proposed work, the chosen Objective Function (OF) is given below:

$$J_{\min}(K_P, K_I, K_D) = (w_1 \cdot \text{IAE}) + (w_2 \cdot \text{ISE}) + (w_3 \cdot M_p) \quad (13)$$

where $w_1 = w_2 = 1$ and $w_3 = 0.25$, IAE = Integral Absolute Error, ISE = Integral Square Error, and M_p = Peak overshoot.

4 Brownian Bat Algorithm (BBA)

The BA was developed by modelling the steering and chasing skills of bats. A detailed study of the BA algorithm can be found in [14–18].

This algorithm has the following basic equations, such as velocity update (Eq. 14), the position update (Eq. 15), and the frequency vector (Eq. 16) as presented below:

$$V_i(t+1) = V_i(t) + (X_i(t) - \text{Gbest})F_i \quad (14)$$

$$X_i(t+1) = X_i(t) + V_i(t+1) \quad (15)$$

$$F_i = F_{\min} + (F_{\max} - F_{\min})\beta \quad (16)$$

where β is a random numeral in the range [0, 1].

During the optimization search, a new solution for each bat is generated based on the following relation:

$$X_{\text{new}} = X_{\text{old}} + \varepsilon A^t \quad (17)$$

where ε is a random numeral in the range [-1,1] and A is the loudness of emitted sound by bats during the exploration of search space. The minimum and maximum values of the loudness variable A is chosen as $A_0 = 20$, and $A_{\min} = 1$ (which decay in steps of 0.05). Other related mathematical representations for loudness adjustment are allotted based on [18].

In this work, ‘ ε ’ is replaced with a Brownian walk strategy discussed in [20]. A detailed description of the Brownian distribution can be found in [15, 19, 20]. Figure 4 depicts the search traces made by ten agents in the three dimensional search space.

In this paper, the performance of the proposed BBA is validated using the GA [1], PSO [7], BFO [13] and FA [6] based methods existing in the literature. During the controller design procedure, the following values are assigned as: number of agents = 10, search dimension = 3, iteration number = 250, and stopping criteria = J_{\min} .

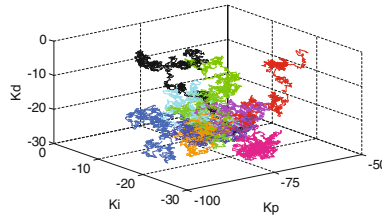


Fig. 4 Search pattern made by the agents with Brownian walk strategy

5 Result and Discussions

In the proposed work, during the heuristic algorithm-based search, search boundary of controller parameters is chosen as: $-80\% < K_P < 0\%$; $-10\% < K_I < 0\%$; $-10\% < K_D < 0\%$. The simulation is carried using Matlab 7 with a simulation time of 50 s. Initially, the BBA based search is considered to find the optimal controller values for the MLS. Later, other methods, such as GA, PSO, BFO, and FA based methods are implemented. The obtained K_P , K_I , and K_D values are then considered to implement the 2DOF controllers, such as FPID and I-PD. In FPID, the filter value T_f is chosen as K_I [4, 7].

Table 1 shows the controller values and its performance measure values for PID, FPID, and I-PD controller structures. The corresponding response is presented in Fig. 4. In Fig. 5, the images (a), (c) and (e) shows the MLS output and (b), (d), and (f) shows the controller output. From these figures and Table 1 values, it can be

Table 1 Controller values and performance measure values

Structure	Method	K_P	K_I	K_D	M_p	ISE	IAE
PID	GA	-79.8032	-4.1865	-4.0395	5.482	279.7	16.72
	PSO	-80.3204	-3.9466	-4.1773	5.109	314.7	17.74
	BFO	-83.3284	-3.6894	-3.2784	4.382	360.1	18.96
	FA	-85.0474	-3.9476	-4.5135	4.177	314.5	17.73
	BBA	-85.8475	-5.0885	-4.1773	4.045	189.3	13.76
FPID	GA	-79.8032	-4.1865	-4.0395	1.682	279.7	16.72
	PSO	-80.3204	-3.9466	-4.1773	1.764	314.7	17.74
	BFO	-83.3284	-3.6894	-3.2784	1.698	360.1	18.96
	FA	-85.0474	-3.9476	-4.5135	1.403	314.5	17.73
	BBA	-85.8475	-5.0885	-4.1773	0.914	189.3	13.76
I-PD	GA	-79.8032	-4.1865	-4.0395	0.000	5.472	2.339
	PSO	-80.3204	-3.9466	-4.1773	0.000	6.825	2.613
	BFO	-83.3284	-3.6894	-3.2784	0.000	13.03	3.610
	FA	-85.0474	-3.9476	-4.5135	0.000	14.51	3.809
	BBA	-85.8475	-5.0885	-4.1773	0.000	9.688	3.112

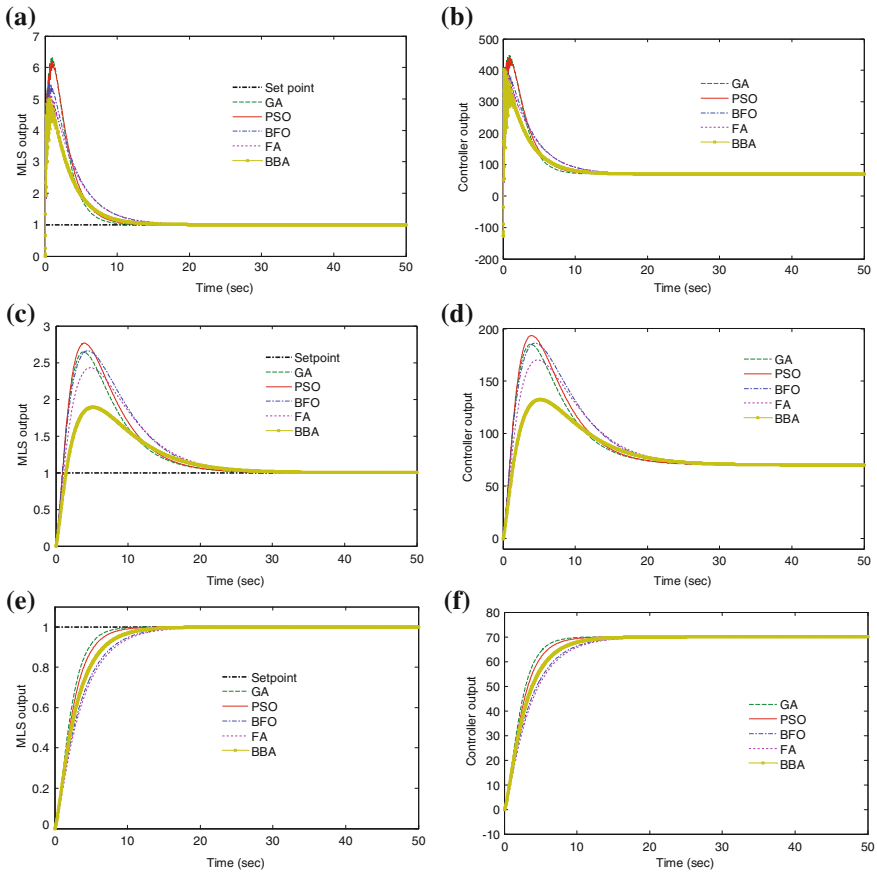


Fig. 5 Reference tracking response and controller output for 1DOF and 2DOF PID controllers. **a** MLS response with PID. **b** Controller response with PID. **c** MLS response with FPID. **d** Controller response with FPID. **e** MLS response with I-PD. **f** Controller response with I-PD

observed that, the proposed BBA offers better results in PID and FPID structures and offers satisfactory result in I-PD structure compared with the alternatives. Table 1 also confirms that, although the overshoot varies, PID and FPID structure offers similar ISE and IAE values due to the rise in settling time.

6 Conclusions

In this paper, BBA based PID controller design is proposed for MLS system and its reference tracking performance is validated with GA, PSO, BFO, and FA existing in the literature. A comparative analysis is also carried between the 1DOF and

2DOF PID controllers existing in the literature. From this study, it is concluded that, the BBA based PID and FPID offers better result than other methods considered in this study. BBA based I-PD offers satisfactory result compared with GA and PSO and better result than BFO and FA.

References

1. Sivagurunathan G, Saravanan K. Evolutionary algorithms based controller optimization for a real time spherical tank system. *Aust J Basic Appl Sci.* 2014;8(3):244–54.
2. Kotteeswaran R, Sivakumar L. A novel bat algorithm based re-tuning of pi controller of coal gasifier for optimum response. In: Prasath R, Kathirvalavakumar T (eds.) *MIKE 2013, LNAI 8284*; (2013). p. 506–17.
3. Vijayan V, Panda RC. Design of PID controllers in double feedback loops for SISO systems with set-point filters. *ISA Trans.* 2012;51(4):514–21.
4. Jung CS, Song HK, Hyun JC. A direct synthesis tuning method of unstable first-order-plus-time-delay processes. *J Process Control.* 1999;9:265–9.
5. Chen C, Hsia-Ping H, Horng-Jang L. Set-point weighted PID controller tuning for time-delayed unstable processes. *Ind Eng Chem Res.* 2008;47(18):6983–90.
6. Raja NSM, Suresh Manic K, Rajinikanth V. Firefly algorithm with various randomization parameters: an analysis. In: Panigrahi BK et al. (eds.) *SEMCCO 2013, Part.1, Lecture notes in computer science, LNCS 8297*; 2013. p. 110–21.
7. Rajinikanth V, Latha K. Internal model control-proportional integral derivative controller tuning for first order plus time delayed unstable systems using bacterial foraging algorithm. *Sci Res Essays.* 2012;7(40):3406–20.
8. Golob M, Tovornik B. Modeling and control of the magnetic suspension system. *ISA Trans.* 2003;42(1):89–100.
9. Ahmad I, Javaid MA. Nonlinear model and controller design for magnetic levitation system. In: *Proceedings of the 9th WSEAS international conference on signal processing, robotics and automation (ISPRA '10)*. University of Cambridge, UK; 2010. p. 324–8.
10. Al-Muthairi NF, Zribi M. Sliding mode control of a magnetic levitation system. *Math Probl Eng.* 2004;2004(2):93–107. doi:[10.1155/S1024123X04310033](https://doi.org/10.1155/S1024123X04310033).
11. Michail K, Zolotas A, Goodall R, Pearson J. Sensor optimisation via H^∞ applied to a MAGLEV suspension system. *World Acad Sci Eng Technol.* 2008;41:171–7.
12. Hassanzadeh I, Mobayan S, Sedaghat G. Design and implementation of a controller for magnetic levitation system using genetic algorithms. *J Appl Sci.* 2008;8(24):4644–9.
13. Rajinikanth V, Latha K. PID controller tuning for magnetic suspension system using evolutionary algorithm. *Int Rev Mech Eng.* 2012;6(5):988–95.
14. Yang X-S. A new metaheuristic bat-inspired algorithm. In: Cruz C, Gonzalez J, Krasnogor N, Terraza G (eds.) *Nature inspired cooperative strategies for optimization (NICSO 2010)*. Springer, SCI 284; 2010. p. 65–74.
15. Yang XS. *Nature-inspired metaheuristic algorithms*. Frome, UK: Luniver Press; 2008.
16. Yang XS. Bat algorithm: literature review and applications. *Int J Bio-Inspired Comput.* 2013;5(3):141–9.
17. Alihodzic A, Tuba M. Improved bat algorithm applied to multilevel image thresholding. *The Scientific World J.* 2014;2014(176718):16.
18. Rajinikanth V, Aashiha JP, Atchaya A. Gray-level histogram based multilevel threshold selection with bat algorithm. *Int J Comput Appl.* 2014;93(16):1–8.

19. Raja NSM, Rajinikanth V, Latha K. Otsu based optimal multilevel image thresholding using firefly algorithm. *Modell Simul Eng.* 2014;2014(794574):17.
20. Raja NSM, Rajinikanth V. Brownian distribution guided bacterial foraging algorithm for controller design problem. In: Satapathy SC et al. (eds.) *ICT and Critical Infrastructure: Proceedings of the 48th Annual Convention of Computer Society of India*, vol I. Springer, AISC 248; 2014. p. 141–8.

Meta-Heuristics Based Approach for Workflow Scheduling in Cloud Computing: A Survey

Poonam, Maitreyee Dutta and Naveen Aggarwal

Abstract The Cloud computing is an emerging distributed systems which follows a “pay-as-you-use” model. It is a new type of shared infrastructure able to offer several resources through the Internet. There is large number of users using the services over the cloud, which generating large volume of data. The scheduling of dependent tasks is a NP-complete problem and has become as one of the most challenging problems in cloud environment. There is a need of specifying a sequence of execution of these tasks to satisfy the user requirements in terms of QoS parameters such as cost, execution time, etc. The workflow scheduling is considered to be difficult, when it becomes a multi-objective optimization problem. In this paper, we presented a comprehensive description of the existing approaches based on meta-heuristics for workflow scheduling. On the basis of the related works, we found the Genetic algorithm as the best method for scheduling. A GA searches the problem space globally and therefore, scholars have investigated combining GAs with other meta-heuristic methods to resolve the local search problem. We feel that there is a scope of using hybrid meta-heuristics approach that combines Artificial Bee Colony algorithm and Genetic Algorithm (ABC-GA) for scheduling workflows in Cloud computing. Cross-over and mutation operators of GA can be embedded into ABC to improve scheduling strategy.

Keywords Cloud computing · Workflow · DAG · Scheduling · QoS parameters

Poonam (✉) · M. Dutta
Computer Science Department, NITTTR Chandigarh, Chandigarh, India
e-mail: poonamchalotra@gmail.com

M. Dutta
e-mail: d_maitreyee@yahoo.co.in

N. Aggarwal
UIET, Panjab University Chandigarh, Chandigarh, India
e-mail: navagg@pu.ac.in

1 Introduction

Cloud computing is an emerging research area for the past few years and it is the transformation of the computing in which all the services are being commoditized and provided similar to traditional utilities like water, electricity, gas, and telephony. The users are allowed to access the services and resources according to their usage based on some desired quality of service. These resources are distributed and accessed the basis of Pay-as-per-use model [1]. The demand for high performance computing is growing for complex and large-scale applications in science, engineering and commerce. The elasticity feature of cloud computing is suitable for such applications because of large amount of data and computation is involved. Many complex and computation intensive applications can be modeled as workflows. These workflow applications are generally described as the sequence of tasks to be processed in well defined order to accomplish a specific goal [2]. Cloud workflow system can be regarded as a platform service that facilitates the automation of distributed large-scale applications in the cloud computing. Workflows are represented as directed acyclic graphs (DAG), which consists of nodes that are linked according to their flow dependencies: $G = (V, E)$, which G represents the graph, V represents a vertex or a node that is an operation or a task, and E represents the edge that shows the relationship between two nodes [3]. Flow dependency imposed the sequence of execution as a parent node will get executed before its child nodes always. Workflow scheduling is the key problem in cloud computing. A workflow scheduling framework is needed to optimize the performance of the resource provisioning process in a cloud system that can allocate the tasks into the appropriate resources according to certain scheduling strategies. This mapping of the tasks has an impact on the performance of workflow scheduling. The goal should be to attain an optimal trade-off between performance and cost. In general, the performance of the workflow varies depending on the nature of tasks. The users may work towards different goals, such as, the shortest possible execution time, the most inexpensive execution cost, or the optimized throughput. Moreover, some users may need to create a schedule plan that satisfies more than one goal. To achieve high performance by satisfying more than one objective makes the scheduling process difficult and such problem is termed as multi-objective optimization problem [4]. There are various scheduling strategies based on heuristics and meta-heuristics methods.

Given this motivation, we investigate meta-heuristics based workflow scheduling methods capable of being applied to complex domains. This paper gives a survey of various meta-heuristics scheduling methods used in Cloud and Grid. The remainder of the paper is organized as follows. We introduce workflow scheduling algorithms for clouds and grids in Sect. 2 with Table 1 and various scheduling parameters of existing algorithms with Table 2 and Sect. 3 gives the research challenges and finally, we conclude the paper with directions for the future work in Sect. 4.

Table 1 Survey of workflow scheduling algorithms based on hybrid heuristics and meta-heuristics methods

Paper title	Nature of scheduling algorithm	Findings	Environment	Objective parameter
A multiple-objective workflow scheduling framework for cloud data analytics [5]	Artificial bee colony algorithm	In this paper, a meta-heuristics based approach is proposed which is called artificial bee colony (ABC) for scheduling workflows with multiple objectives onto a cloud system The proposed method has been compared with HEFT/LOSS and it outperforms in both the single objective optimization with the constraint, and multi-objective optimization problem for structured workflow	Java environment and Ubuntu 10.04 with Xeon E5500 CPUs	Minimizes makespan and cost
Bees life algorithm for job scheduling in cloud computing [6]	Bee life algorithm	Authors presented a swarm optimization-based bees life algorithm (BLA) has been applied to efficiently schedule computation jobs among processing resources onto the cloud datacenters	Virtual clouds	Minimizes total execution time
Honey bee behavior inspired load balancing of tasks in cloud computing environments [7]	Honey bee behavior	A honey bee behavior inspired load balancing (HBB-LB) algorithm is proposed, which balanced the load across virtual machines for maximizing the throughput. It balances the priorities of tasks on the machines in such a way that the amount of waiting time of the tasks in the queue is minimal	CloudSim	Load balancing minimum queue waiting time
Dynamic task scheduling with load balancing using hybrid PSO [8]	Hybrid PSO	Hybrid PSO is applied to dynamically schedule heterogeneous tasks on to heterogeneous processors in a distributed setup	Heterogeneous systems	Minimizing total execution time, communication cost
A particle swarm optimization-based heuristic for scheduling workflow applications in cloud computing environments [9]	PSO	PSO based approach is used which optimizes the cost of computation, based on the current network and resource conditions by updating the communication costs and also re-computes the task-resource mapping	Amazon EC2	Total execution cost load balancing

(continued)

Table 1 (continued)

Paper title	Nature of scheduling algorithm	Findings	Environment	Objective parameter
Quantum PSO technique for load balancing in cloud computing [10]	QPSO	A scheduling based on quantum particle swarm optimization technique for load balancing in cloud computing has been proposed. The work presented a load balancing algorithm in order to balance the entire load of the system. The optimal resources have been selected to perform task according to resources status and the size of given task in the cloud environment	CloudSim	Minimizes makespan and execution time Load balancing
An optimized scheduling algorithm on a cloud workflow using a discrete particle swarm [11]	PSO	To solve the problems of security threats on workflow scheduling in cloud computing environments, an optimized cloud workflow scheduling algorithm is proposed using a discrete particle swarm. This paper designed a cloud model to describe its security in the cloud workflow scheduling system	CloudSim	Minimizes completion time and cost Maximized security satisfaction
Deadline Based resource provisioning and scheduling algorithm for scientific workflows on clouds [12]	PSO	In this paper, authors developed a static cost-minimization, deadline-constrained heuristics for scheduling a scientific workflow application	CloudSim	Minimizes total Execution cost
Bacterial foraging based hyper-heuristic for resource scheduling in grid computing [13]	BFO	This paper presented a bacterial foraging optimization to schedule the resources in grid and it has been used for the practical application of protein sequence analyzer	GridSim	Minimizes makespan Resource utilization
Cloud task scheduling based on load balancing ACO 2011 [14]	LBACO	In this paper, load balancing ant colony optimization (LBACO) algorithm is proposed to find the optimal resource allocation for each task in the dynamic cloud system. The tasks are mutually independent	CloudSim	Minimizes makespan Dynamic load balancing

(continued)

Table 1 (continued)

Paper title	Nature of scheduling algorithm	Findings	Environment	Objective parameter
A novel energy efficient resource allocation algorithm based on Immune clonal optimization for green cloud computing [15]	Improved clonal selection algorithm	An effective energy efficient optimization model for resource allocation has been proposed based on artificial clonal selection algorithm	CloudSim	Minimizes response time and makespan, energy efficient
Multi-objective scheduling of many tasks in cloud platforms [16]	Ordinal-optimization workflows scheduling	The authors proposed the vectorized ordinal-optimization approach to achieve multi-objective scheduling for optimal resource allocation in the cloud computing	Virtualized cloud platform	Reduces scheduling overhead Optimizes resource allocation
Hybrid ant colony algorithm clonal selection in the application of the cloud's resource scheduling [17]	ACO-CS	Authors used a general method of clonal selection ant colony algorithm to solve the task scheduling in cloud computing. This algorithm combined global optimum advantage of the convergence of the clonal selection algorithm (CSA) into every ACO iterations	CloudSim	Improves resource utilization
Job scheduling model for cloud computing based on multi-objective genetic algorithm 2013 [18]	GA	A job scheduling algorithm based on Multi-Objective Genetic Algorithm (MO-GA) is presented in this paper that considers the energy consumption and the profits of the service providers, and provides a dynamic selection mechanism of the most suitable scheduling scheme for users according to the real-time requirements	CloudSim	Consumes less energy and higher profit
Hybrid job scheduling algorithm for cloud computing environment [19]	Modified genetic algorithm with fuzzy theory	In this paper, a hybrid job scheduling approach is presented with the aid of genetic algorithm and fuzzy theory. The idea is to assign the jobs to the resources with considering the VM MIPS and length of jobs	CloudSim	Load balancing Minimizes execution cost and time

(continued)

Table 1 (continued)

Paper title	Nature of scheduling algorithm	Findings	Environment	Objective parameter
Scheduling scientific workflow applications with deadline and budget constraints using genetic algorithms [20]	GA	This paper presented genetic algorithm based scheduling heuristic to solve performance optimization problems based on two typical QoS constraints, deadline and budget, for the workflow execution on “pay-per-use” services	GridSim	Minimizes the monetary cost while meeting user’s budget constraint Minimizes the execution time while meeting user’s deadline constraints
Immune genetic algorithm for scheduling service workflows with QoS constraints in cloud computing [21]	IGA	Authors proposed to optimize several objective functions simultaneously, depending on the requirements of the users and providers: makespan, cost, reliability, and resource utilization. When physical resources are involved, they discussed a way to monitor energy consumption. A new fitness function model for faster convergence is used and an immune genetic algorithm has been adopted efficiently to solve the constraint satisfaction problem linked with the task scheduling constraints	Amazon EC2	Optimizes makespan, cost and reliability
HSGA: a hybrid heuristic algorithm for workflow scheduling in cloud systems [22]	HSGA	This paper proposed a hybrid heuristic method based on genetic algorithm (HSGA) for scheduling workflow graph. The algorithm tried to decrease the number of GA operation iteration with starting the algorithm by an optimized initial population, considering load balancing of task on resources. The solutions are derived from two evaluation functions, one measured priority of each task in workflow, based on their influence on the others, and another function evaluate the value of the produced solutions. It focused to minimize the completion time of application as makespan and failure rate, and increasing the load balancing	CloudSim	Minimizes makespan and failure rate Load balancing

(continued)

Table 1 (continued)

Paper title	Nature of scheduling algorithm	Findings	Environment	Objective parameter
A hybrid metaheuristics algorithm for job scheduling on computational grids [23]	GGA	This research has combined the features of a genetic algorithm (GA) and the gravitational emulation local search (GELS) algorithm. As genetic algorithm is strong for global searches and GELS is a local search algorithm that imitates gravitational attraction and is therefore strong for local searches and weak for global searches. Combining the benefits of these two algorithms a static scheduling algorithm has been discussed in this paper	Java	Minimizes makespan
Simulated-annealing load balancing for resource allocation in cloud environments [24]	SA	In this paper, a simulated-annealing load balancing algorithm is presented for solving the resource allocation and scheduling problem in a cloud computing environment	CloudSim	Load balancing
Hybridization of modified ant colony optimization and intelligent water drops algorithm for job scheduling in computational grid [25]	IWD-ACO	The authors have presented a hybrid technique using Intelligent water drops with Ant colony optimization approach to solve the scheduling problem in grid environment. This method has found the optimal schedule for the job that minimized the makespan of the executing jobs and the load balancing of jobs among resources	GridSim	Minimizes makespan Load balancing Resource utilization
Hybrid ACO-IWD optimization algorithm for minimizing weighted flow time in cloud based parameter sweep experiments [26]	IWD-ACO	A hybrid meta-heuristics approach is used based on IWD and ACO algorithms for scheduling jobs. Resources are matched based on the job requirements by the IWD algorithm and then ACO is used to select the best one among the matched resources	CloudSim	Minimizes makespan Load balancing

(continued)

Table 1 (continued)

Paper title	Nature of scheduling algorithm	Findings	Environment	Objective parameter
Job scheduling in grid computing with cuckoo optimization algorithm [27]	Cuckoo optimization algorithm	In this paper, a scheduling algorithm based on COA is implemented for job scheduling problem on computational grids. This approach generated an optimal schedule that completes the jobs in a minimum time	GridSim	Minimizes execution time
A Meta-heuristic algorithm for job scheduling in grid computing [28]	CUckoo-Genetic algorithm	Authors proposed a CUckoo-Genetic Algorithm (CUGA) as a meta-heuristic algorithm to solve job scheduling problem in grid environment. CUGA is inspired by cuckoo search optimization and genetic algorithm	Matlab	Minimizes execution time Resource utilization
A Multi-objective Cat Swarm Optimization algorithm for workflow scheduling in cloud computing environment [29]	CSO	In this paper, Cat Swarm based approach is used for multi-objective optimization for workflow scheduling in cloud computing	Matlab	Minimizes execution time, cost and CPU idle time

Table 2 Scheduling parameters considered by existing workflow scheduling algorithms

References	Makespan	Cost	Scheduling overhead	Load balancing	Security	Reliability	Resource utilization	Failure rate	Energy efficient
[5]	✓	✓	X	X	X	X	X	X	X
[6]	X	✓	X	X	X	X	X	X	X
[7]	✓	X	✓	✓	X	X	X	X	X
[8]	✓	✓	X	X	X	X	X	X	X
[9]	X	✓	✓	✓	X	X	X	X	X
[10]	✓	X	✓	✓	X	X	X	X	X
[11]	✓	✓	X	X	✓	X	X	X	X
[12]	X	✓	X	X	X	X	X	X	X
[13]	✓	X	X	X	X	X	✓	X	X
[14]	✓	X	✓	✓	X	X	X	X	X
[15]	✓	X	X	X	X	X	X	X	✓
[16]	X	X	X	X	X	X	X	X	X
[17]	X	X	X	X	X	X	✓	X	X
[18]	X	X	X	X	X	X	X	X	✓
[19]	✓	✓	X	✓	X	X	X	X	X
[20]	✓	✓	X	X	X	X	X	X	X
[21]	✓	✓	X	X	X	✓	X	X	X
[22]	✓	X	✓	✓	X	X	X	✓	X
[23]	✓	X	X	X	X	X	X	X	X
[24]	X	X	✓	✓	X	X	X	X	X
[25]	✓	X	✓	✓	X	X	✓	X	X
[26]	✓	X	✓	✓	X	X	X	X	X
[27]	✓	X	X	X	X	X	✓	X	X
[28]	✓	X	X	X	X	X	✓	X	X
[29]	✓	✓	X	X	X	X	X	X	X

2 Related Work

2.1 *Workflow Scheduling in Cloud Computing: A State-of-the-Art*

Initial study has been carried out on understanding scheduling algorithms for executing workflows in cloud computing systems. A lot of work has been done in the area of workflow scheduling [2, 3]. To solve the optimization problem of scheduling, several solutions have been proposed in the literature. There are heuristic-based and meta-heuristic based scheduling strategies to achieve near-optimal solutions within polynomial time, as workflow scheduling is an NP-complete problem. The meta-heuristics based scheduling strategies can deal with massive search space and find a near-optimal solution within polynomial time for all workflow structures. Some of these approaches are based on Genetic Algorithms (GA) [18, 19]. In [20], the authors run the genetic algorithm starting with an initial population consisting of randomly generated solutions. The genetic algorithm started with an initial population consisting of a solution produced by one of the simple heuristics together with other randomly generated solutions. This proposed algorithm either minimized the monetary cost while meeting user's budget constraint, or minimized the execution time while meeting user's deadline constraints. Artificial Bee Colony algorithm for multivariable, multimodal function optimization have been used in [5, 30]. The use of Intelligent Water Drops (IWD) algorithm for solving multi-objective job shop scheduling has been discussed in [31], which optimized the makespan, tardiness and mean flow time of the schedules in job shop. Similar to this, authors in [25] has employed IWD with ACO algorithm to optimize the makespan and load balancing of the jobs in grid environment. The paper [26] showed the use of IWD as a hybrid meta-heuristics with ACO to optimize the mean flow time of the jobs in cloud systems. There is also work in which particle swarm optimization (PSO) is used for the scheduling of workflow in Cloud environment [8–11]. CSO based multi-objective optimization approach has been used in [29] to schedule workflow in a cloud computing environment. Researches show that ant colony optimization (ACO) is considered as one of the best meta-heuristic for scheduling workflow in Cloud computing [14]. Most of these researches focus only on one or two optimization objective most often cost or time.

However, current state-of-the-art studies tackle different scheduling problems in cloud workflow systems by focusing on general QoS optimization constraints as described in a Table 1. It is clear that most of the scheduling algorithms have focused on optimizing makespan and cost [5, 6, 8, 10, 11, 21]. Some of the algorithms have considered makespan and load balancing [10, 14, 16, 19, 22, 25], while others have taken care of optimizing makespan and security [11]. Optimization of resource utilization is considered in [13, 17, 25, 27] in addition to makespan and load balancing. Some have also considered the issue of reliability

along with makespan and cost [21]. Also the papers [11, 15, 18] based on meta-heuristics approaches considered the energy efficiency parameter for scheduling of the workflow tasks.

2.2 Scheduling Parameters

The scheduling decision during workflow scheduling must be guided by user’s QoS constraints [1]. There are different parameters which need to be considered when developing a scheduling algorithm for workflows. It is not possible for an algorithm to consider all the parameters in a single solution because it depends on many factors like nature or size of the job, resource availability, working environment etc. Some of the parameters considered in the existing workflow scheduling algorithms in Table 2 are explained as below:

Makespan Makespan, M , is the total elapsed time required to execute the entire workflow. The makespan of the workflow is computed as $M = \text{finish time} - \text{submission time}$. It represents the duration from the user submitting a workflow to the time it completes and receives the results.

Cost The cost is the monetary value which incurred while running a cloud workflow. It consists of the processing cost and the data transfer costs.

Security Security is an essential requirement in the cloud computing as there is a risk of sensitive data being leaked or tampered in the process of transmission or execution.

Scheduling overhead There can be the situation when numbers of tasks demand for the same resource. Such tasks then need to be queued up waiting for the desired resource which creates a problem of scheduling overhead.

Resource utilization Scheduling refers to the appropriate assignment of tasks to the resources available like CPU, memory and storage, such that there is a maximum utilization of resources.

Failure rate Many discrete events may lead to failures of an application such as non-availability of required services or overloaded resource conditions. The failure density function is defined as:

$$f(t) = \lambda e^{-\lambda t} (t \geq 0) \tag{1}$$

where λ is the failure rate of a resource [32]. If $\text{num}_{\text{fails}}$ be the number of failures within a resource during the job execution period run_{time} then the failure rate can be calculated as: $\frac{1}{\text{MTTF}} = \frac{\text{num}_{\text{fails}}}{\text{run}_{\text{time}}}$, which is the inverse of mean time to failure (MTTF).

Reliability Reliability represents the probability that the workflow will be executed successfully and it is to be maximized. A schedule is an assignment of the tasks to the virtual machine and the reliability of a schedule is defined as the probability that it finishes correctly and is given by the probability that all the VMs be functional during the execution of all their assigned tasks.

Energy efficiency Data centers consist of huge numbers of heterogeneous servers which both consume and simultaneously waste massive power to execute numerous assigned tasks due to poor task assignment optimization. So, scheduling plays a very important role in determining the efficient execution of tasks in virtualized environments. Tasks are to be mapped to the virtual machines in such a way that the energy consumption should be reduced.

3 Research Challenges

Based on the related literature, we find that the following issues have not been sufficiently solved. These issues can give the directions for future work.

Scheduling overhead There are number of resources available and it may possible that more than one user demand the same resource. This creates a scenario of multiple jobs waiting in a queue, which leads to the problem of scheduling overhead. Some mechanism needs to be discussed to reduce such overhead while generating schedules in a workflow. In [33] the authors presented different clustering techniques incorporated into the Pegasus workflow mapping system on the TeraGrid and results showed significant reduction of overall workflow runtime. Similar thing can be thought in the clouds systems also.

Scheduling with Fault tolerance There is a need of defining a method to integrate fault tolerance with scheduling algorithm based on some meta-heuristics approach. There is no evidence of such work done in the related literature. There are various fault tolerance techniques that reduce the effect of failures on application execution when the failure occurs. Check point recovery, over-provisioning or task replication and task resubmission schemes can be integrated with scheduling as discussed in [34].

Storage cost and performance trade-off workflow scheduling that takes both storage cost and execution time into consideration has not been studied as extensively. The tasks of a workflow are to be mapped to the VM-instances (Virtual Machine) in the cloud. Every available virtual machine is associated with both cost and performance related attributes like processor speed, bandwidth. Reducing the storage cost has also become a challenge for the scientists while optimizing the workflow performance [35].

4 Conclusion and Future Directions

In this paper, we have discussed various workflow scheduling algorithms in clouds and Grids. Scheduling criteria should include multiple constraints to be satisfied based on the user's requirements. There can be heuristics approach or meta-heuristics approach for optimizing the various scheduling criteria. We discussed both approaches but focus of our survey is meta-heuristics based methods. Some of the algorithms are based on Artificial Bee colony algorithms (ABC) [5, 7]. There are some work in which Genetic Algorithm (GA) is combined with other heuristic method [18–23]. Also, the use of Particle Swarm Optimization (PSO) discussed in [8, 9, 11, 12] for the scheduling of workflow in Cloud environment. Clonal selection algorithm is also being used for scheduling workflow in cloud environment [15, 17]. In [17], authors combined ACO with Clonal selection algorithm for scheduling the resources in the clouds. ACO is also combined with intelligent water drops algorithm in [25, 31] to improve the scheduling. In [27, 28], a new method based on Cuckoo Optimization has been used to generate optimal schedules in a Grid environment. Researches show that Genetic Algorithm is one of the best meta-heuristic for scheduling workflow in Cloud computing [18, 20]. In [29], Cat Swarm Optimization has been used to minimize the cost, makespan, and CPU idle time. Discrete CSO [36, 37] can also be used in combination with other heuristics method to achieve the better performance. As there is no evidence of using Discrete CSO based approach for workflow scheduling in cloud systems.

Most of the above stated researches focus only on one or two optimization objective such as cost or time and do not consider the energy efficiency and failure rate while scheduling the workflows. But, there is need to consider the failure rate and security also. The efficient scheduling will give better optimized results if energy efficiency factor is also considered. A hybrid heuristic-based scheduling [22] considered the failure rate while scheduling the tasks in workflow which is shown as in a Table 2 given. Also, the papers [15, 18] based on meta-heuristics approaches considered the energy efficiency parameter for scheduling of the workflow tasks. There is need to develop scheduling algorithms that would focus on failure rate, reliability, and energy efficient parameters.

Also, we found that the Artificial Bee Colony has not been used for optimization in workflow scheduling. The experimental results of various research works [5, 30, 38, 39] reveal that the ABC algorithm is having potential to solve optimization problems and more research is required to adapt it to other engineering problems. After getting inspiration from its successful implementation in [18] to solve Job scheduling problem in cloud computing, we feel that there is a scope of using hybrid meta-heuristics approach that combines Artificial Bee Colony algorithm and Genetic Algorithm (ABC-GA) for multi-objective optimization workflow scheduling problems. Cross-over and mutation operators of GA can be embedded into ABC to improve scheduling strategy. A hybrid meta-heuristics based energy

efficient workflow scheduling can be considered for future work, which schedules the tasks on the resources by minimizing the cost and that consider the failure rate of the resources.

References

1. Grance T, Mell P. The NIST definition of cloud computing—recommendations of the National Institute of Standards and Technology. Special Publication 800-145, NIST, Gaithersburg; 2011.
2. Buyya RK, Kotagiri R, Yu J. Workflow scheduling algorithm for grid computing. In: Meta-heuristics for scheduling in distributed computing environment, vol. 146. Berlin Heidelberg: Springer; 2008. p. 173–214.
3. Barrionuevo JJD, Fard HM, Prodan R, Fahringer T. A multi-objective approach for workflow scheduling in heterogeneous environment: cluster, cloud and grid computing. In: 12th IEEE International conference; 2012. p. 300–309.
4. Hoheisel A, Prodan R, Wiczorek M. Taxonomies of the multi-criteria grid workflow scheduling problem. In: Grid middleware and service. Springer; 2008. p. 237–64.
5. Achalakul T, Udomkasemsub O, Li XO. A multiple-objective workflow scheduling framework for cloud data analytics. In: International Joint Conference; 2012. p. 391–398.
6. Bitam S. Bees life algorithm for job scheduling in cloud computing. In: Second international conference on communications and information technology; 2012.
7. Dhinesh Babu LD, Venkata KP. Honey bee behavior inspired load balancing of tasks in cloud computing environments. *Appl Soft Comput*. 2013; 2292–2303.
8. Sivanandam SN, Visalakshi P. Dynamic task scheduling with load balancing using hybrid PSO. *Int J Open Problems Comput Math*. 2009; 475–488.
9. Buyya RK, Guru SM, Pandey S, Wu L. A particle swarm optimization based heuristic for scheduling workflow applications in cloud computing environments. In: 24th IEEE international conference on advanced information networking and applications (AINA). 2010; 400–407.
10. Sultan EI. Quantum PSO technique for load balancing in cloud computing. PhD Thesis; 2013.
11. Jianfang C, Junjie C, Qingshan Z. An optimized scheduling algorithm on a cloud workflow using a discrete particle swarm. *Cybern Inform Technol*. 2014; 25–39.
12. Buyya RK, Rodriguez MA. Deadline based resource provisioning and scheduling algorithm for scientific workflows on clouds. *IEEE Trans Cloud Comput*. 2014; 222–235.
13. Channa I, Rajni: Bacterial foraging based hyper-heuristic for resource scheduling in grid computing. In: Future Generation Computer System; 2012. p. 751–762.
14. Dong Y, Li K, Wang D, Xu G, Zhao G. Cloud task scheduling based on load balancing ACO. In: Sixth annual chinagrid Conference; 2011. p. 3–9.
15. Shu W, Wang W, Wang Y. A novel energy efficient resource allocation algorithm based on Immune clonal optimization for green cloud computing. *EURASIP J Wireless Commun Networking*; 2014.
16. Cao J, Hwang K, Khan SU, Li K, Zhanga F. Multi-objective scheduling of many tasks in cloud platforms. In: Future generation computer systems; 2013.
17. Lin J, Lin X, Lin H, Zhong Y, Zeng Q. Hybrid ant colony algorithm clonal selection in the application of the cloud's resource scheduling. In: Distributed parallel, and cluster computing (cs.DC). [arXiv:1411.2528v1](https://arxiv.org/abs/1411.2528v1); 2014.
18. Liu J, Li B, Luo XG, Zhang XM, Zhang F. Job scheduling model for cloud computing based on multi-objective genetic algorithm. *Int J Comput Sci*. 2013; 134–9.
19. Abraham A, Amendola D, Cordeschi N, Javanmardi S, Liu H, Shojafar M. Hybrid job scheduling algorithm for cloud computing environment. In: Proceedings of the fifth

- international conference on innovations in bio-inspired computing and applications IBICA 2014, vol 303. *Advances in Intelligent Systems and Computing*; 2014. p. 43–52.
20. Buyya RK, Yu J. Scheduling scientific workflow applications with deadline and budget constraints using genetic algorithms. In: *Scientific Programming Journal* IOS Press, Amsterdam; 2006. p. 217–230.
 21. Chelouah R, Nacer MA, Sellami K, Tiako PF. Immune genetic algorithm for scheduling service workflows with QoS constraints in cloud computing. *S Afr J Ind Eng*. 2013;24:68–82.
 22. Aryan Y, Delavar AG. HSGA: a hybrid heuristic algorithm for workflow scheduling in cloud systems. *J Cluster Comput*. Springer; 2013. p. 129–137.
 23. Abraham A, Pooranian Z, Shojafar M, Singhal M, Tavoli R. A hybrid metaheuristics algorithm for job scheduling on computational grids. *Informatica*. 2013;37:157–64.
 24. Fan Z, Li Y, Shen H, Wu Y. Simulated-annealing load balancing for resource allocation in cloud environments. In: *International conference on parallel and distributed computing, applications and technologies*. IEEE Computer Society, Washington, USA; 2013. p. 1–6.
 25. Mathiyalagan P, Sivanandam SN, Saranya KS. Hybridization of modified ant colony optimization and intelligent water drops algorithm for job scheduling. In: *Computational Grid. ICTACT Journal on Soft Computing*; 2013. p. 651–655.
 26. Johnson M, Preethima RA. Hybrid ACO-IWD optimization algorithm for minimizing weighted flow time in cloud based parameter sweep experiments. *Int J Res Eng Technol*. 2014; 317–321.
 27. Rabiee M, Sajedi H. Job scheduling in grid computing with cuckoo optimization algorithm. *Int J Comput Appl*. 2013;62:38–43.
 28. Rabiee M, Sajedi H. A metaheuristic algorithm for job scheduling in grid computing. *Int J Mod Educ Comput Sci*. 2014;05:52–9.
 29. Bilgaiyan S, Das M, Sagnika S. A multi-objective cat swarm optimization algorithm for workflow scheduling in cloud computing environment. In: *Proceedings of international conference on intelligent computing, communication and devices*. *Advances in Intelligent Systems and Computing*. Springer; 2015. p. 73–84.
 30. Basturk B, Karaboga D. A powerful and efficient algorithm for numerical function optimization- artificial bee colony (ABC) algorithm. *J Global Optim*. 2007; 459–471.
 31. Niu SH, Nee AYC, Ong SK. An improved intelligent water drops algorithm for solving multi-objective job shop scheduling. *Eng Appl Artif Intell*. 2013; 2431–2442.
 32. Buyya RK, Su J, Wang X, Yeo CS. Optimizing makespan and reliability for workflow applications with reputation and look-ahead genetic algorithm. *Future Gener Comput Syst*. 2011;27:1124–34.
 33. Berriman B, Deelman E, Good J, Katz DS, Mehta G, Singh G, Su MH, Vahi K. Workflow task clustering for best effort systems with pegasus. In: *Proceedings of the 15th ACM Mardi Gras conference*; 2008.
 34. Cooper K, Koelbel C, Mandal A, Zhang Y. Combined fault tolerance and scheduling techniques for workflow applications on computational grids. In: *Proceedings of 9th IEEE/ACM international symposium on cluster computing and the grid*; 2009. p. 244–251.
 35. Lin X, Wu CQ. On scientific workflow scheduling in clouds under budget constraint. In: *Proceedings of 42nd international conference on parallel processing*. IEEE; 2013. p. 90–99.
 36. Khanesar A, Sharafi Y, Teshnehlab M. Discrete binary cat swarm optimization algorithm. In: *Proceedings of 3rd international conference on computer, control and communication*; 2013. p. 1– 6.
 37. Bouzidi A, Riffi ME. Discrete cat swarm optimization to resolve the traveling salesman problem. *Int J Adv Res Comput Sci Softw Eng*. 2013; 13–18.
 38. Bahriye A, Karaboga D. A comparative study of artificial bee colony algorithm. Erciyes University, Department of Computer Engineering, Melikgazi, 38039 Kayseri, Turkey 2009.
 39. Achalakul T, Banharnsakun A, Sirinaovakul B. Job shop scheduling with the best-so far ABC. *Eng Appl Artif Intell* 2011.

Brain MRI Segmentation for Lesion Detection Using Clustering with Fire-Fly Algorithm

Pramita Manna and Tapas Si

Abstract This paper presents brain MRI segmentation for lesion detection using fire-fly based hard-clustering algorithm. First, MR images are denoised using median filter and denoised images are segmented using fire-fly based clustering algorithm. After segmentation, lesioned regions are extracted from segmented MR images. The performance of the proposed method is evaluated using quantitative measurement index. A comparative study is made with k -means and Fuzzy c-means algorithms. The experiment results demonstrate that the proposed method performs better than other two methods.

Keywords Magnetic resonance imaging · Brain · Lesion · Clustering · Fire-fly algorithm · Segmentation

1 Introduction

Multimodal Magnetic Resonance Image (MRI) [1, 2] of brain segmentation is an important medical image processing tasks for disease diagnosis. Lesion in brain's MRI detection is very much important for the diagnosis as well as treatment of the patients. There are several types modalities in MRI such as T1-weighted (T1W1), T2-weighted (T2W2), proton density weighted, Fluid Attenuated Inversion Recovery (FLAIR) etc. [1]. In brain's MRI, there are several objects like white matter, gray matter, Cerebral Spinal Fluid(CSF), bone, scalp, background, and lesions (if present) [3]. So, many research contributions are given in lesion detection

P. Manna (✉) · T. Si

Department of Computer Science and Engineering, Bankura Unnayani Institute of Engineering, Bankura, West Bengal, India

e-mail: mannapramita@gmail.com

URL: <http://www.buie.ac.in>

T. Si

e-mail: c2.tapas@gmail.com

© Springer India 2016

S.S. Dash et al. (eds.), *Artificial Intelligence and Evolutionary Computations in Engineering Systems*, Advances in Intelligent Systems and Computing 394, DOI 10.1007/978-81-322-2656-7_122

1347

during past several years. Sindhumol et al. [4] presented Multi Signal Wevelet Independent Component Analysis (MW-ICA) that is applied on Automated Brain Tissue Classification. El-Sayed et al. [5] proposed a hybrid intelligent machine learning technique for computer-aided detection system for automatic brain tumor detection using MR images. Fuzzy automatic and accurate method is suggested by Harati et al. [6] for tumor segmentation in brain images that is improved by fuzzy connectedness algorithm. Brain MRI segmentation technique based on Fuzzy C-Means (FCM) clustering algorithm proposed by Shen et al. [7] using Neighborhood attraction with neural network optimization. Hall et al. [8] segmented brain MR images using an ANN and the performance is compared with FCM. Li et al. [9] presented a knowledge-based classification and tissue labeling approach to segment magnetic resonance images brain using FCM algorithm. Si et al. [10] proposed Grammatical Swarm based clustering algorithm for detection of tumors in brain MRI. Sivaramakrishnan et al. [11] proposed an intelligent system designed to diagnose tumor through mammograms, using image processing techniques along with intelligent optimization tools, such as Fire-Fly Algorithm (FFA), Enhanced BEE Colony Optimization (EBCO), and Artificial Neural Network. In article [12], clustering and classification based approaches are applied for identifying tumor in brain's MRI. The main objective of this paper is to apply Fire-fly algorithm [13] based hard-clustering [14] technique for lesion detection in brain's MRI.

2 Materials and Methods

In this paper, a new segmentation method using Fire-fly algorithm based clustering technique for lesion detection in brain MRI is proposed. The flowchart of the proposed method is given in Fig. 1.

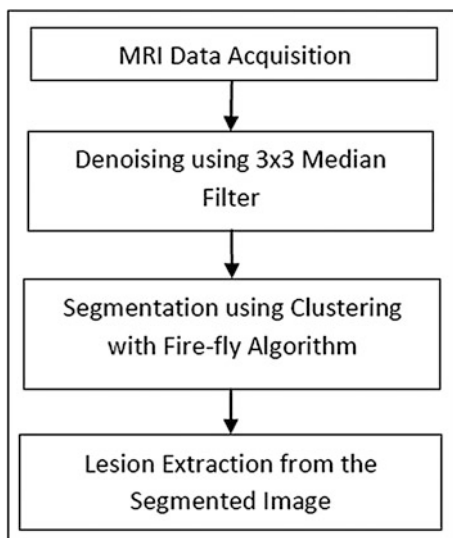
2.1 MRI Data Acquisition

Two Axial T2 MRI images of human brain have been used for application. All the images are generated by 1.5-T GE Medical MR imaging machine. The slice thickness is 5.0 mm, the gap between two slices is 1.5 mm. Each MR image has a resolution of 256×256 .

2.2 Denoising

Segmentation process faces difficulties due to presence of noise in the images and the noises are removed from images using median filter having neighborhood size

Fig. 1 Flowchart of the proposed method



3×3 . The median is calculated by first sorting all the pixel values from the window (pattern of neighbors) into numerical order, and then replacing the pixel being considered with the middle (median) pixel value.

2.3 Segmentation Using Clustering with Fire-Fly Algorithm

Clustering is a unsupervised learning method used to partition the data into groups or clusters [15]. k -means algorithm [16] is a well-known hard-clustering algorithm to partition the data into K number of clusters. Let $y_i = (y_{i1}, y_{i2}, \dots, y_{im})$ is the i th features in data set having \mathcal{N} number of data. In k -means algorithm, the initial cluster centers are randomly selected from the data set itself and the Euclidean distance of i th data point from the k th centers are calculated using the following equation:

$$\mathcal{D}_{ik} = d(y_i, m_k) = \left[\sum_{l=1}^d (y_{il} - m_{kl})^2 \right]^{\frac{1}{2}} \quad (1)$$

The data are then assigned to the closest cluster using following equation:

$$k = \arg \min_{\forall k \in \mathcal{K}} (\mathcal{D}_{ik}) \quad (2)$$

where κ is the number of clusters in the data set.

The objective function of k -means algorithm is defined as following:

$$J = \sum_{k=1}^{\mathcal{K}} \sum_{y_i \in c_k} \|y_i - m_k\|^2 \quad (3)$$

The major drawback of k -means algorithm is that it gets stuck in the local optima due to selection of the initial cluster's centers from the data itself. These drawback is overcome By using evolutionary algorithm [15] and Swarm Intelligent algorithms like Particle Swarm Optimizer [17], Fire-fly algorithm [14] in hard-clustering technique. In this work, Fire-fly based hard-clustering technique is used to segment the MR images. The Fire-fly algorithm is a nature inspired technique. Flashing light of fireflies is important to communicate (attract) their partner. Flashes are unique for a specific species. Females are attracted by male (individual) of same species. Light intensity (I) at a fixed distance (r) follows the inverse square law that means $I \propto \frac{1}{r^2}$. Fire-fly algorithm follows three rules: (a) All fireflies are unisex and they are attracted to each other by their sex. (b) Attractiveness is proportional to the brightness. Less brighter fire-fly moves toward the more brighter fire-fly one. Fire-fly will move randomly if there is no brighter fire-fly than itself (c) Brightness of a fire-fly is measured by the objective function. The distance between i th and j th fireflies at x_i and x_j respectively, is the Euclidean distance

$$r_{ij} = \|x_i - x_j\| = \sqrt{\sum_{k=1}^d (x_{ik} - x_{jk})^2} \quad (4)$$

where x_{ik} is the k th component of position x_i of i th fire-fly. The movement of a fire-fly i is attracted to another more brighter fire-fly j is measured by

$$x_i = x_i + \beta_0 e^{-\gamma r_{ij}^2} (x_j - x_i) + \alpha \left(\text{rand} - \frac{1}{2} \right) \quad (5)$$

$$\beta(r) = \beta_0 e^{-\gamma r^2} \quad (6)$$

β_0 is the attractiveness at $r = 0$ and is the light absorption coefficient.

The complete Fire-fly algorithm is given in Table 1.

Fire-fly based Clustering Algorithm (CFA) Each fire-fly x_i is constructed as $x_i = (m_{i1}, \dots, m_{ij}, \dots, m_{iN_c})$ where m_{ij} indicates to the j th cluster center of the i th fire-fly. This paper adopted fitness function from the article [17] which is comprised of three different objective functions to achieve better clustering solutions and it is defined as following:

$$f(x_i, y_i) = w_1 \cdot \bar{d}_{\max}(y_i, x_i) + w_2 \cdot (y_{\max} - d_{\min}(x_i)) + w_3 \cdot Q_{ei} \quad (7)$$

Table 1 Fire-fly algorithm

Fire-fly algorithm
1. Objective function $f(x)$, $x = (x_1, x_2, \dots, x_d)^T$
2. Generate initial population of fire flies x_i , ($i = 1, 2, \dots, n$)
3. Light intensity I_i at x_i is determined by $f(x_i)$
4. light absorption coefficient γ
5. While ($t \leq \text{Max Generation}$)
6. for $i = 1:n$
7. for $j = 1:n$
8. if ($I_j > I_i$), move fireflies i towards j in D-dimension, end if
9. Attractiveness varies with distance r via $\exp[-r]$
10. Evaluate new solutions and update light intensity
11. end for j
12. end for i
13. Find the current best
14. end while

where y_{\max} is maximum pixel value (i.e., 255) in the image set. y_i is a matrix representing assignment of pixels to clusters of i th Fire-fly. Here, w_1 , w_2 , and w_3 are user defined constants. Also, maximum average is defined by the following equation:

$$\bar{d}_{\max}(y_i, x_i) = \max_{j=1, \dots, N_c} \sum_{\forall y_p \in c_{ij}} d(y_p, m_{ij}) / |c_{ij}| \quad (8)$$

where $|c_{ij}|$ is the cardinality of the set c_{ij} .

The minimum inter-cluster distance is calculated by the following equation:

$$d_{\min}(x_i) = \min_{l_1, l_2, l_1 \neq l_2} d(m_{il_1}, m_{il_2}) \quad (9)$$

The Quantization error Q_e is defined by following equation:

$$Q_e = \frac{1}{N_c} \left\{ \sum_{j=1}^{N_c} \sum_{\forall y_p \in c_j} d(y_p, m_j) / |c_j| \right\} \quad (10)$$

The euclidean distance $d(y_p, m_j)$ is calculated as following:

$$d(y_p, m_j) = \sqrt{\sum_{k=1}^{n_b} (y_{pk} - m_{jk})^2} \quad (11)$$

2.4 Performance Measurement

Davies–Bouldin (DB) Index: The Davies–Bouldin (DB) Index [18] is the ratio of sum of within-cluster distance to between-cluster separation and it is calculated by the following equation:

$$DB = \frac{1}{\mathcal{K}} \sum_{i=1}^{\mathcal{K}} \max_{\substack{i \neq j \\ 1 \leq i, j \leq \mathcal{K}}} \left\{ \frac{S(m_i) + S(m_j)}{d(m_i + m_j)} \right\} \quad (12)$$

The DB Index minimizes the within-cluster distance $S(m_i)$ and maximizes the between-cluster separation $d(m_i, m_j)$. For a given image and κ value, low DB Index indicates better clustering.

2.5 Parameter Settings

The parameters of CFA are set as following: number of cluster (κ) = 4, population size (NP) = 50, $X_{\max} = 255$, $X_{\min} = 0$, $\alpha = \beta = \gamma = 1$, $w_1 = w_2 = w_3 = 0.33$, maximum number of iterations = 100. Total number of function evaluations = 5000. In k -means and FCM, the maximum number of function evaluations is set to 5000 to make a fair comparison with CFA.

3 Results and Discussion

The proposed method is applied on two Axial T2 MR images given in Fig. 2(a), (c). The original MR images contain noise and the noise is removed by the median filter and the denoised images are given in Fig. 2(b), (d) respectively. After denoising, the Fire-fly based clustering algorithm is used to segment the images and the segmented images are given in Fig. 3. Finally, the lesions are extracted from the segmented images and the lesions are given in Fig. 4. The quantitative performance of the CFA, k -Means and FCM methods are measured using DB Index. The lower

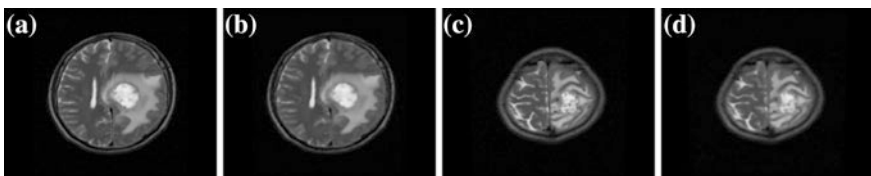


Fig. 2 Original MR images (a, c) and their denoised versions (b, d)

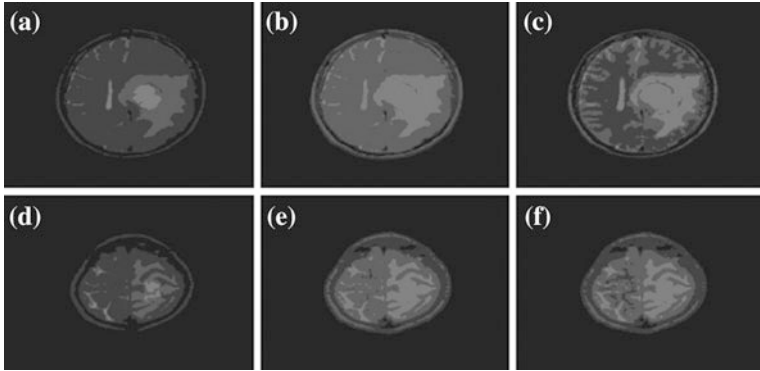


Fig. 3 Segmented MR images. *1st column* CFA, *2nd column* *k*-means, *3rd column* FCM

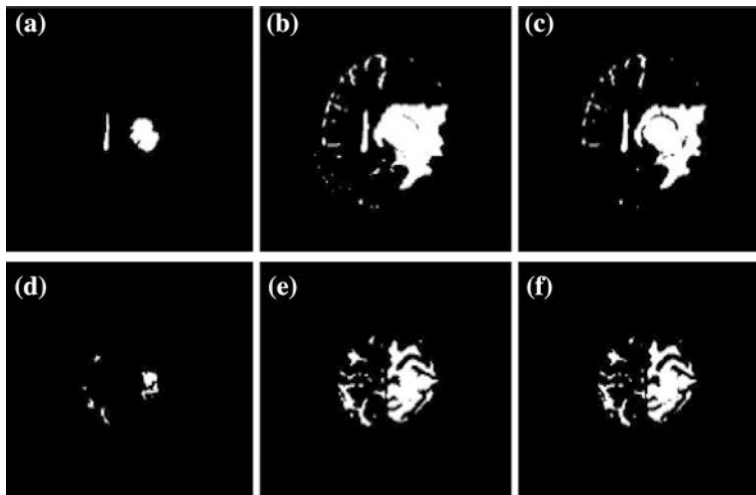


Fig. 4 Extracted lesions from segmented MR images. *1st column* CFA, *2nd column* *k*-means, *3rd column* FCM

DB-Index value indicates the good performance. The mean and standard deviation of DB-Index values over 30 independent runs are $0.1346(\pm 0.0218)$, $0.1364(\pm 0.0112)$ and $0.1548(\pm 0.0100)$ for CFA, *k*-means and FCM respectively for Fig. 2 (b) whereas $0.1317(\pm 0.0219)$, $0.1375(\pm 0.0005)$ and $0.1405(\pm 4.74e-08)$ are obtained respectively for Fig. 2(d). The mean values of DB Index achieved from CFA algorithm are lower than that of *k*-means and FCM algorithms for both images. From the visual analysis of the extracted lesions in Fig. 4, it is observed that lesions are better detected using CFA algorithm than other algorithms. In *k*-means and FCM-based segmentation methods, portions of other objects are also detected with lesions. Hence, lesions are not well detected. Whereas, very small parts of

other objects are detected along with lesions using CFA. This occurs due to similar intensities in lesions and other objects in the MR images. The experimental results show that the Fire-fly algorithm based cluster technique can be used in segmentation for lesion detection in brain MRI.

4 Conclusions

This paper presents a new segmentation method for lesion detection in brain MRI using hard-clustering technique with Fire-Fly algorithm. In the proposed method, MR images are denoised using median filter. Then, Fire-Fly based clustering algorithm is used to segment the MR images. Finally, lesions are extracted from the segmented images. The experimental results show that the proposed method can be applied in lesion segmentation in brain MRI. In future, different type of distance measures can be used in Fire-fly based clustering algorithm to improve the performance.

Acknowledgments The authors express their thanks to Associate Prof. Arunava De, Dr. B.C. Roy Engineering College, Durgapur, West Bengal, who has provided brain MR images for this work.

Conflict of Interest The authors declare that they have no conflict of interest.

Informed Consent Informed consent was obtained from all individual participants included in the study.

References

1. Parizel PM, Hauwe L, Belder FD, Goethem JV, Venstermans C, Saslgado R, Voormolen M, Hecke WV. Magnetic resonance imaging of the brain. In: Reimer P et al. (eds.) *Clinical MR imaging*. Berlin: Springer-Verlag; 2010.
2. Tonarelli, L. Magnetic resonance imaging of brain tumor. CEwebsource.com; 2013.
3. Alirezaie J, Jernigan ME, Nahmias C. Neural network based segmentation of magnetic resonance images of the brain. *IEEE Trans Nucl Sci*. 1997;44(2):194–8.
4. Sindhumol S, Kumar A, Kannan B. Automated brain tissue classification by multisignal wavelet decomposition and independent component analysis. Hindawi Publishing Corporation *ISRN Biomedical Imaging*. 2013, ArticleID 473437.
5. El-Sayed A, El-Dahshan M, Heba M, Revett K, Salem ABM. Computer-aided diagnosis of human brain tumor through MRI. *Expert Syst Appl* 2014;41:5526–5545.
6. Harati V, Khayati R, Farzan A. Fully automated tumor segmentation based on improved fuzzy connectedness algorithm in brain MR images. *Comput Biol Med*. 2011;41:483–92.
7. Shen S, Sandham W, Granat M, Sterr A. MRI fuzzy segmentation of brain tissue using neighborhood attraction with neural-network optimization. *IEEE Trans Inform Technol Biomed*. 2005 9(3).
8. Hall LO, Bensaid AM, Clarke LP, Velthuizen RP, Silbiger MS, Bezdek JC. A Comparison of neural network and fuzzy clustering techniques in segmenting magnetic resonance images of the brain. *IEEE Trans. Neural Netw*. 1992;3(5):672–82.

9. Li CL, Goldgof DB, Hall LO. Knowledge-based classification and tissue labeling of MR images of human brain. *IEEE Trans Med Imag.* 1993;12(4):740–50.
10. Si T, De A, Bhattacharjee AK. Brain MRI segmentation for tumor detection using grammatical swarm based clustering algorithm. In: *International conference on circuit, power and computing technologies (ICCPCT 2014)*; 2014. p. 1196–1201.
11. Sivaramakrishnan A, Karnan M. Medical image segmentation using firefly algorithm and enhanced bee colony optimization. In: *International conference on information and image processing (ICIIP-2014)*.
12. Jagadeesan R, Sivanandam SN. A novel clustering and classification based approaches for identifying tumor in MRI brain images. *Int J Comput Appl.* 2013; 67(8).
13. Yang, X.-S.: Firefly algorithms for multimodal optimization. In: *Stochastic algorithms: foundations and applications, SAGA 2009. Lecture notes in computer sciences, vol. 5792*, 2009. p. 169–178.
14. Senthilnath J, Omkar SN, Mani V. Clustering using firefly algorithm: performance study. *Swarm Evol Comput.* 2011;1:164–71.
15. Xu R, Donald W II. Survey of clustering algorithms. *IEEE Trans Neural Netw.* 2005; 16(3).
16. MacQueen J. Some methods for classification and analysis of multivariate observations. In: *Proceedings 5th Berkeley Symposium Mathematics, Statistics Probability*; 1967. p. 281–297.
17. Omran MGH, Engelbrecht AP, Salman A. Dynamic clustering using particle swarm optimization with application in unsupervised image classification. *World Acad Sci Eng Technol.* 2007;9:755–60.
18. Davies DL, Bouldin DW. A cluster separation measure. *IEEE Trans Pattern Anal Mach Intell.* 1979;1(2):224–7.

Author Index

A

Abdelaziz, Almoataz Y., 25
Abdul Rahman Rafi, M., 535
Abhishek, Kumar, 569
Abirami, G., 111
Abisha Queen, C., 885
Achhra, Mohit, 515
Aditya Pai, H., 345
Aggarwal, Naveen, 1331
Agrawal, Pranshu, 239
Agrawal, S.S., 173
Ahamad Meeran Mydeen, A., 819
Aiswarya Raj, M., 803
Ajith, P., 229
Albert Singh, N., 535
Ali, Mohamed, 25
Anbarasi, P.N., 193
Anburajan, M., 493
Anbuselvi, M., 885
Aneeth, T.V., 417
Anitha, T.N., 1
Antony Samson, K., 1239
Apoorva, A., 285
Arafath, Yasmeen, 453
Arathi, K., 377
Arthi, S.V., 1075
Arunan, Anjali, 135
Arun Bhaskar, M., 1265
Aryadevi, R.D., 135
Ashok, M.V., 285
Ashokvannan, B., 1145
Asutkar, G.M., 547
Atallah, Ahmed M., 25
Aulakh, Inderdeep Kaur, 735

B

Babu, Chitra, 621
Balaji, C., 1279
Balaji Ganesh, A., 527

Balakrishna, R., 1, 345
Balan, Nikhitha C., 249, 273
Balasubramani, S., 655
Balasubramanian, A., 819
Balasubramanian, G., 1309
Balasubramanian, P., 1085
Barat, Aratrika, 357
Barik, R.C., 399
Bayindir, Ramazan, 1093
Bharadwaj, D.G., 323, 459
Bharti, O.P., 25
Bhattacharya, Mahua, 239
Bhattacharya, Paritosh, 97
Bhuvaneshwari, C., 1205
Biswal, Itishree, 941
Biswal, Sushree Sangita, 941
Biswas, Prantik, 97
Brunda, N.S., 569

C

Chakraborty, Purbita, 895
Chandramani, Premanand V., 831, 1049
Chandrasekaran, S., 607
Chandrika, J., 559
Chattopadhyay, Madhurima, 357
Chethan, V., 285
Choubey, Maneesh, 49
Choudhary, Anand, 991
Chowdhury, Debjyoti, 357

D

Dasgupta, Anurag, 895
Deepa, K., 443
Deepa, R., 59
Desai, Shivani, 743
Dey, Soham, 715
Dhal, P.K., 819
Dhote, Kanchan, 547
Dinesh Ram, G., 917

Divya, P., 259
 Diwan, Tausif, 333
 Dutta, Maitreyee, 1331

E

Eswaran, P., 705

G

Gandhiraj, R., 471
 Ganesh Kumar, C., 1049
 Garg, Gagandeep, 667
 Garg, Roopali, 667, 953
 Gautam, Diwakar, 991
 George, Ria, 443
 Ghose, Tirthadip, 909
 Ghosh, Sraboni, 357
 Gireeshkumar, T., 591
 Girish, Siva V., 527
 Gomathi, B., 879
 Gubbi, Abdullah, 125
 Gunasundari, R., 209, 481
 Guruprasath, M., 1309

H

Harirajkumar, J., 1029
 Harsha Sree, V., 645
 Himayavardhini, J., 973

I

Indhirani, A., 1265
 Iyswarya Annapoorani, K., 1105

J

Jaba Jasphin, E.T., 933
 Januja Josephine, S., 1049
 Jape, Vidula S., 323
 Jayabarathi, R., 417
 Jayalakshmi, N., 1145
 Jeevananthan, S., 1113
 Jeyashree, Y., 1287
 Jhanwar, Deepak, 991
 Jha, R.C., 1169
 Jithendra Babu, N., 675
 Jose, Abinkant A., 249, 273
 Joshi, Kiran, 515

K

Kabalci, Ersan, 1093
 Kalaivani, S., 503
 Kala, V., 1205
 Kaliyamurthie, K.P., 765
 Kamlu, Sushma, 715
 Karpagam, R.S., 1039
 Karthikeyan, P., 1195

Kaur, Dalbir, 723
 Kavitha, D., 607
 Keerthi Jain, K., 1181
 Kerana Hanirex, D., 765
 Khadar Babu, Sk., 1001
 Kini, Nikita, 569
 Kishore Kumar, N., 1181
 Kottursamy, Kottilingam, 579
 Krishna, Punit, 1309
 Kulkarni, Dinesh A., 1019
 Kulkarni, HariPriya H., 459

L

Lakshmi, J.L., 831
 Lingaraja, D., 1059

M

Mahadevaswamy, H.R., 1067
 Maheedhar, A., 981
 Mahesh Kumar, S.V., 481
 Majumder, Koushik, 895
 Malhotra, Meenakshi, 735
 Malik, Sadhna, 1297
 Mallick, Abhilash, 1287
 Manchikalapudi, Varun, 1001
 Mandal, Partho, 173
 Manicka Chezian, R., 59
 Mani, Shinu Acca, 803
 Manju, S., 1085
 Manna, Pramita, 1347
 Manupati, V.K., 981
 Mathai, Nissy Sara, 471
 Mathi, Senthilkumar, 193
 Mehta, Mirav, 411
 Menon, Sreedevi K., 411
 Menon, Vrinda N., 229
 Mhetre, Sheetal B., 459
 Mishra, R., 399
 Mishra, Sudhansu Kumar, 715, 1297
 Mohan, Pournamy, 429
 Mohanty, Mihir N., 941, 1227
 Monisha Selas, S.J., 933
 Mullai, G.P., 855
 Muralikrishanan, S., 1181
 Muthuselvi, M., 1239

N

Nagaraju, C., 645
 Nagpal, Rachita, 953
 Nandi, Sarthak, 69
 Nandwani, Sunny, 515
 Naresh Kumar, K., 1253
 Naveen, K.A., 411
 Naveen Kumar, C.M., 559

Nibi, K.V., 151
 Norman, Suresh R., 1075

O

Ojha, Gaurav, 173, 185, 239

P

Padma, T., 633
 Padmavathi, S., 111
 Panda, Ramaprasad, 1227
 Pandey, Mukesh, 49
 Pandey, Ruchi, 49
 Patel, K., 1215
 Pathak, Jyotirmoy, 961
 Patil, Suhas H., 1019
 Paul, Abhisek, 97
 Pavankumar, D., 1067
 Pillai, Anju S., 377
 Pillai, Jayashree S., 633
 Pillai, Rahul R., 411
 Piyush Kumar Pareek, 345
 Prabhavathi, C.N., 11
 Pradeep Kumar Reddy, R., 645
 Pradeep, Preeja, 151
 Prakash, Prem, 1169
 Prakash, R., 527
 Prakash, Varna C., 163
 Prantik Barua, C., 1287
 Pratik, Prem, 1169
 Praveenkumar, S., 917, 925, 1059
 Premalatha, S., 1265

R

Radha Krishna Reddy, S., 1127
 Raja, Gunasekaran, 579
 Rajalakshmi Pushparaman, 865
 Rajanna, B., 295
 Rajan, Vishnu, 411
 Rajaram, Kanchana, 621
 Rajasekar, N., 79
 Rajesh, V., 39
 Rajeswara Rao, R., 295
 Rajeshwari, D.S., 39
 Rajeswari Suja, K., 655
 Raksha, Sowmiya, 515
 Ramadevi, C., 1321
 Rama Mohan Reddy, A., 775
 Ramesh, B., 559
 Ramesh, L., 1181
 Ramesh, Maneesha Vinodini, 259
 Ramesh, R., 973
 Ramkumar, K., 1309
 Ramya, R., 841
 Rani, S.K., 607, 655

Ranjan, Rakesh, 569
 Ranjith Kumar, R., 453
 Rao, P.V., 39, 125
 Rao, Sanjay, 991
 Rao, Smitha, 691
 Rashmi, M.R., 1215
 Ravikumar, K.M., 11
 Ravinder, M., 599, 793, 1009
 Ravi, S., 841
 Reddaiah, B., 645
 Revanth, A.S., 981
 Roy, Subhendu, 357

S

Sahoo, Pradyumna K., 1227
 Sai Pranahita, B., 1113
 Saket, R.K., 25
 Sakthivel, P., 879
 Salivahanan, S., 885
 Sam, Ajin Mathew, 1279
 Samir, Moataz, 493
 Sangeetha, K., 79
 Santhi, V., 69
 Saranya, K., 579
 Saravanakumar, G., 841
 Sarma, Rajkumar, 675
 Sasi, K.K., 163
 Satapathy, Siddhartha S., 753
 Sathe, S.R., 333, 365
 Satpathy, Prasanta K., 1227
 Senthilnathan, Karthikrajan, 1105
 Sethi, V.K., 49
 Shabeena, Shaik, 961
 Shabnam, Shahin, 97
 Shahnaz, I., 503
 Shah, Raveena, 515
 Shankar, K., 705
 Sharma, Monika, 723
 Sheeba Joice, C., 855
 Shet, Nagaraj, 125
 Shirin, Shaikh Rizwana, 503
 Shivayogimath, Chaitra N., 391
 Shreesha, C., 125
 Shukla, Anupam, 173, 185
 Shyam Sunder, N., 591
 Singh, Rakesh, 185
 Si, Tapas, 1347
 Siva Chidambaranathan, V., 1195
 Siva, R., 1253
 Sivraj, P., 163
 Somasundaram, K., 429
 Sree Harsha, J., 1287
 Sreekala, M., 443
 Sreekara Reddy, M.B.S., 981

Sreelakshmi, S., 307, 315
 Sridhar, R., 1113
 Srinath, S., 1253
 Srinivasula Reddy, A., 1127
 Sripriya, T., 925
 Srivatsala, V., 691
 Sruthi, N., 259
 Subrahmanyam, J.B.V., 1127
 Sudhakar Babu, T., 79
 Sundaravadivu, K., 1321
 Suneetha, V., 691
 Sunil Kumar, M., 775
 Suresh, A., 1215
 Swain, Biswaranjan, 753
 Swarnalatha, K., 925
 Syed Ibrahim, B., 89

T

Tamil Eniyan, D., 1029
 Tamrakar, Aditi, 515
 Tembhone, Jitendra V., 365
 Tharini, C., 503
 Thyagaraj, T., 569

Tirupathamma, M., 1009
 Trivedi, Param, 743

U

Udhayakumar, G., 1215
 Uma Reddy, N.V., 391
 Unnikrishna Menon, K.A., 151, 229

V

Vandana Raj, T., 307, 315
 Venkata Rao, K., 345
 Venkatesh, S., 1309
 Venugopal, T., 599, 793
 Vimala Juliet, A., 1287
 Vinothini, M., 89
 Vishnupriya, R., 1321
 Viswanathan, B., 1039
 Viswanath, K., 209

Y

Yeolekar, Dipti B., 459